ANTENNA ENGINEERING HANDBOOK

McGRAW-HILL HANDBOOKS

ANTENNA
ENGINEERING
HANDBOOK

HENRY JASIK, Editor

Fellow, The Institute of Radio Engineers
President, Jasik Laboratories, Inc.
Westbury, Long Island, New York

FIRST EDITION

New York   Toronto   London

ANTENNA ENGINEERING HANDBOOK

CONTRIBUTORS

ROGER E. AVERY, *Group Leader, Airborne Instruments Laboratory, Division of Cutler-Hammer, Melville, Long Island, New York.* (*Chapter 35*)

EDWARD BEDROSIAN, *Staff Member, The RAND Corporation, Santa Monica, California.* (*Chapter 22*)

JUDD BLASS, *Laboratory Director, W. L. Maxson Corporation, New York, New York.* (*Chapters 6 and 8*)

JOHN T. BOLLJAHN, (*deceased*) *Stanford Research Institute, Menlo Park, California.* (*Chapter 27*)

DAVID F. BOWMAN, *Engineer-in-Charge, Radio Frequency Laboratory, I-T-E Circuit Breaker Company, Philadelphia, Pennsylvania.* (*Chapter 31*)

KENNETH BULLINGTON, *Transmission Systems Engineer, Bell Telephone Laboratories, Inc., Murray Hill, New Jersey.* (*Chapter 33*)

JOHN F. BYRNE, *Manager, Systems Research Laboratory, Motorola, Inc., Riverside, California.* (*Chapter 22*)

P. S. CARTER, *Member, Technical Staff, Radio Corporation of America, RCA Laboratories, Rocky Point, Long Island, New York.* (*Chapter 19*)

SEYMOUR B. COHN, *Vice President, Rantec Corporation, Calabasas, California.* (*Chapter 14*)

GEORGES A. DESCHAMPS, *Professor of Electrical Engineering, University of Illinois, Urbana, Illinois.* (*Chapter 18*)

LORNE K. DESIZE, *Group Leader, Airborne Instruments Laboratory, Division of Cutler-Hammer, Melville, Long Island, New York.* (*Chapter 17*)

RAYMOND H. DUHAMEL, *Assistant Director of Research, Collins Radio Company, Cedar Rapids, Iowa.* (*Chapter 18*)

M. J. EHRLICH, *President, Microwave Radiation Company, Inc., Gardena, California.* (*Chapter 9*)

J. V. N. GRANGER, *President, Granger Associates, Palo Alto, California.* (*Chapter 27*)

EDWARD F. HARRIS, *President, Mark Products Company, Skokie, Illinois.* (*Chapters 7 and 11*)

v

HOWARD T. HEAD, *Partner, A. D. Ring & Associates, Washington, D.C.* *(Chapter 20)*

WILLIAM C. JAKES, JR., *Member, Technical Staff, Bell Telephone Laboratories, Inc., Holmdel, New Jersey.* *(Chapters 10 and 13)*

HENRY JASIK, *President, Jasik Laboratories, Inc., Westbury, Long Island, New York.* *(Chapters 1 and 2)*

ALAN F. KAY, *Vice President, TRG, Incorporated, Somerville, Massachusetts.* *(Chapter 32)*

KENNETH S. KELLEHER, *President, Aero Geo Astro Corporation, Alexandria, Virginia.* *(Chapters 12 and 15)*

STEPHEN W. KERSHNER, *Partner, A. D. Ring & Associates, Washington, D.C.* *(Chapter 21)*

JOHN D. KRAUS, *Director of the Radio Observatory, The Ohio State University, Columbus, Ohio.* *(Chapter 29)*

EDMUND A. LAPORT, *Director, Communications Engineering, Radio Corporation of America, Princeton, New Jersey.* *(Chapter 4)*

YUEN T. LO, *Assistant Professor, University of Illinois, Urbana, Illinois.* *(Chapter 24)*

RODERIC V. LOWMAN, *Section Head, Airborne Instruments Laboratory, Division of Cutler-Hammer, Melville, Long Island, New York.* *(Chapter 30)*

C. A. MARTIN, *Member, Technical Staff, Radio Corporation of America, RCA Laboratories, Rocky Point, Long Island, New York.* *(Chapter 19)*

ROBERT L. MATTINGLY, *Military Development Engineer, Bell Telephone Laboratories, Inc., Whippany, New Jersey.* *(Chapter 25)*

WARREN B. OFFUTT, *Manager of Engineering, Dept. of Space Technology and Research, Airborne Instruments Laboratory, Division of Cutler-Hammer, Melville, Long Island, New York.* *(Chapter 17)*

KARLE S. PACKARD, JR., *Consultant, Airborne Instruments Laboratory, Division of Cutler-Hammer, Melville, Long Island, New York.* *(Chapter 30)*

DELMER C. PORTS, *Vice President, Jansky & Bailey, A Division of Atlantic Research, Washington, D.C.* *(Chapter 23)*

HENRY J. RIBLET, *President, Microwave Development Laboratories, Inc., Babson Park, Wellesley, Massachusetts.* *(Chapter 26)*

AVERY G. RICHARDSON, *Technical Services Manager, ITT Laboratories, Nutley, New Jersey.* *(Chapter 28)*

SLOAN D. ROBERTSON, *Head, Research and Development, Goodyear Aircraft Corporation, Arizona Division, Litchfield Park, Arizona.* *(Chapter 13)*

RAYMOND E. ROHRER, *Partner, Silliman, Moffet, & Rohrer, Washington, D.C.* *(Chapter 23)*

RICHARD RUBIN, *Manager, Antenna Department, Sylvania Electronic Systems, Waltham, Massachusetts.* *(Chapter 34)*

GEORGE C. SOUTHWORTH, *Radio Consultant, Bell Telephone Laboratories, Inc., Murray Hill, New Jersey.* *(Chapter 5)*

CHEN TO TAI, *Professor of Electrical Engineering, The Ohio State University, Columbus, Ohio.* *(Chapter 3)*

WILLIAM H. YALE, *Antenna Section Group Leader, Airborne Instruments Laboratory, Division of Cutler-Hammer, Melville, Long Island, New York.* *(Chapter 17)*

FRANCIS J. ZUCKER, *Chief, Waves and Circuits Section, Air Force Cambridge Research Laboratories, Bedford, Massachusetts.* *(Chapter 16)*

PREFACE

The "Antenna Engineering Handbook" is intended to serve as a compendium of antenna design data and principles. Although it is expected that it will prove most useful to the engineer who is actively engaged in designing antennas, it will also be of considerable use to the electronic systems engineer who desires to understand the capabilities and limitations of the antenna as a component. The treatment is at the engineering level and is directed toward an understanding of antenna problems in addition to presenting an extensive collection of design data. Within its scope, it is believed that this handbook represents the most comprehensive treatment of the antenna art which has appeared in book form to date.

To keep the size of the Handbook within reasonable bounds, it has been necessary to select for presentation only those areas which are of greatest current importance to the antenna engineer and designer. Accordingly, the major part of the coverage is given to antenna types and structures that have found extensive use in practice or that have a large potential for such use. Theoretical discussions and mathematical formulations are given only where essential to understanding. Wherever possible, results have been presented in graphical or tabular form.

The Handbook is organized into four major groups of chapters, as follows:

I. Introduction and Fundamentals
II. Antenna Types and Methods
III. Applications
IV. Topics Associated with Antennas

The first group, consisting of Chapters 1 and 2, delineates those properties, fundamentals, and basic relationships which are common to all antennas. Chapter 2, which deals with fundamentals, is not intended as a substitute for the several excellent textbooks which are available. It does, however, state in very concise form many of the principles and mathematical relationships which are in continual use by antenna engineers. Certain sections of Chapter 2 have been expanded somewhat out of proportion to the rest of the chapter in order to provide supplementary background information for some of the later chapters.

The second group, consisting of Chapters 3 through 18, deals with basic

antenna types and methods.   This group of chapters treats the properties
and design relationships of many different classes of antennas, without
regard to the applications in which these antennas are used.   Although
the classification of antenna types has been made on an arbitrary basis,
it is believed that virtually every basic antenna type which is in common
use has been treated in one or another of these chapters.   Wherever
possible, design and performance data have been given.   Where this has
not been possible, qualitative information has been given along with
representative literature references on a particular structure.   No
attempt has been made to give an exhaustive bibliography since this in
itself would constitute a sizable volume.   However, many of the more
important references have been cited.   These should serve as a starting
point for those who desire to search the original literature.

The third group of chapters, 19 through 29 inclusive, treats a number
of areas of application in which the antenna art plays a significant role.
Although the applications dealt with cover a large proportion of present-
day uses, a number of military applications have been omitted for security
reasons.   The areas of application which are treated have been chosen
either to extend the information given in the second group of chapters or
to indicate qualitatively some of the important uses to which antennas
are being put.

The final group of chapters, 30 through 35 inclusive, deals with topics
associated with antennas.   These chapters have been included because
they are essential to the antenna engineer and contain a wealth of useful
information.   It is necessary for the antenna engineer to have a working
knowledge of radome problems, propagation problems, and mechanical
design problems even though he need not be an expert in all of these areas.
The areas of transmission lines, impedance-matching techniques, and
measurement problems are equally as important as the basic design of
the antenna and fully deserve the detailed treatment which they have
been given.

A limited amount of overlap between chapters will be found, although
this has been eliminated wherever possible.   In the few cases where over-
lap does exist, it has generally occurred because of the desire to make a
chapter more self-consistent or because different aspects of a subject have
been treated in the different chapters.   The reader is advised to carefully
check the index and the table of contents when looking up information in
a specific area.   For example: Yagi-Uda antennas are treated in Chapters
5, 16, and 24, while omnidirectional antenna systems are discussed in
Chapters 5, 16, 22, 23, and 26.   Similar diversity of treatment will be
found for a number of other topics.

This handbook would not have been possible without the efforts of the
many outstanding engineers who have cooperated in writing the indi-
vidual chapters.   Thanks are due also to the Institute of Radio Engineers

for its kind permission to use material from its publications.   Finally, the editor would like to express appreciation to his wife, Esther, for her continuing assistance during the preparation of this handbook.

Care has been taken to credit sources of information by reference and any omission is due to oversight rather than intention.   While diligence has been exercised in proofreading, a few errors may remain.   The editor would appreciate being advised of such errors and receiving suggestions as to how the usefulness of the book could be improved in future editions.

Henry Jasik

CONTENTS

III. APPLICATIONS

Index follows Chapter 35.

Chapter 1

PROPERTIES OF ANTENNAS

HENRY JASIK

Jasik Laboratories, Inc.
Westbury, Long Island, New York

1.1. INTRODUCTION

Antennas are basic components of any electronic system which depends on free space as the propagation medium. The antenna is the connecting link between free space and the transmitter or receiver. As such, it plays an essential part in determining the characteristics of the system in which it is used.

In many systems for navigational or direction-finding purposes, the operational characteristics of the system are designed around the directive properties of the antenna. In other systems, the antenna may be used simply to radiate energy in an omnidirectional pattern in order to provide a broadcast type of coverage. In still other systems, such as point-to-point communications, the antenna may have a highly directional pattern to achieve increased gain and interference reduction.

Regardless of the systems application, all antennas have certain basic properties which can be well defined.

The properties of an antenna which are most often of interest are the radiation pattern, polarization, gain, and impedance. For a linear passive antenna, these properties are identical for either transmitting or receiving by virtue of the reciprocity theorem.[1]

1.2. TYPES OF RADIATION PATTERNS

The radiation pattern of an antenna is generally its most basic requirement since it determines the spatial distribution of the radiated energy. The radiation pattern

1–1

is usually the first property of an antenna that is specified, once the operating frequency has been stated.

The most common types of radiation patterns are as follows:

1. Omnidirectional or broadcast-type pattern
2. Pencil-beam pattern
3. Fan-beam pattern
4. Shaped-beam pattern

The omnidirectional or broadcast-type pattern is used for many broadcast or communications services where all directions are to be covered equally well. The horizontal-plane pattern is generally circular while the vertical-plane pattern may have some directivity in order to increase the gain.

The pencil-beam pattern is a highly directional pattern which is used when it is desired to obtain maximum gain and when the radiation pattern is to be concentrated in as narrow an angular sector as possible. The beamwidths in the two principal planes are essentially equal.

The fan-beam pattern is similar to the pencil-beam pattern except that the beam cross section is elliptical in shape rather than circular. The beamwidth in one plane may be considerably broader than the beamwidth in the other plane. As with the pencil-beam pattern, the fan-beam pattern generally implies a rather substantial amount of gain.

The shaped-beam pattern is used when the pattern in one of the principal planes is desired to have a specified type of coverage. A typical example is the cosecant type of pattern which is used to provide a constant radar return over a range of angles in the vertical plane (cf. Sec. 25.4). The pattern in the other principal plane is usually a pencil-beam type of pattern but may sometimes be a circular pattern as in certain types of beacon antennas.

In addition to the pattern types just discussed, there are a number of pattern shapes used for direction finding and other purposes which do not fall under the four categories listed. Some of these patterns include the well-known figure-of-eight pattern, the cardioid or limacon pattern, split-beam patterns, and multilobed patterns whose lobes are of substantially equal amplitude. For those patterns which have particularly unusual characteristics, it is generally necessary to specify the pattern by an actual plot of its shape or by the mathematical relationship which describes its shape.

1.3. CHARACTERISTICS OF SIMPLE PATTERNS

For antennas which have patterns of simple shape, the important characteristics of the patterns can be specified by the beamwidth and side-lobe level in the two principal planes, usually taken as the E plane and the H plane. The E plane is parallel to the electric-field vector and passes through the antenna in the direction of the beam maximum. The H plane is perpendicular to the E plane and also passes through the antenna in the direction of the beam maximum (see also Sec. 34.3).

The beamwidth in a principal plane of the radiation pattern is defined by the angular width of the pattern at a level which is 3 db down from the beam maximum. This is normally called the half-power beamwidth. Although there are other definitions for the beamwidth, the above usage is almost universal in the United States. The definition of antenna beamwidth as used throughout this handbook is to be taken as the half-power beamwidth, except for a few cases where it is specifically stated in other terms.

The side-lobe level is specified with reference to the maximum of the main beam and is generally expressed in db down from the main beam. Side lobes are undesired radiation lobes which are separate from the main beam. Since they do not con-

tribute in the principal direction of interest, it is usually desirable to keep the side-lobe level reasonably low. It should be noted that since the side lobes are referred to the main beam, the smaller the magnitude of the side-lobe level the larger will be the number of db down. The first side lobes are those which are adjacent to the main beam and frequently, although not always, have the largest magnitude.

1.4. POLARIZATION

The polarization of an antenna is usually defined in terms of the orientation of the electric-field vector in the direction of maximum radiation. Thus, a vertical dipole above ground will radiate vertical polarization, while a horizontal dipole above ground will radiate horizontal polarization. Although this simple nomenclature is commonly used, it can become confusing for large angles above ground and it is more precise to define the polarization in terms of the E_θ and E_ϕ components in a polar coordinate system as shown in Fig. 34-14 (page 34–13). The direction of the polar axis of the coordinate system is generally taken as the local vertical.

In addition to linearly polarized antennas, the use of circularly polarized antennas has recently become quite common. Circular polarization can be produced by two perpendicular linearly polarized fields which have a 90° phase differential. Depending on the sense of rotation, circular polarization may be either right-handed or left-handed (see Secs. 17.1 and 34.6).

Antennas may radiate unwanted energy in a polarization which is different from the polarization in which the antenna was intended to radiate. This unwanted radiation is known as cross polarization. For linearly polarized antennas, the cross polarization is perpendicular to the intended polarization. For circular polarization, the cross polarization may be considered as the component which has the sense of rotation opposite to that of the intended sense. A more common way of specifying deviation from perfect circular polarization is in terms of the axial ratio or the ellipticity (cf. Secs. 17.1 and 34.6).

1.5. GAIN

The gain of an antenna is a basic property which is frequently used as a figure of merit. Gain is closely associated with directivity, which in turn is dependent upon the radiation patterns of an antenna.

The gain is commonly defined as the ratio of the maximum radiation intensity in a given direction to the maximum radiation intensity produced in the same direction from a reference antenna with the same power input. The reference antenna most commonly used is the isotropic radiator, a hypothetical lossless antenna which radiates uniformly in all directions. The half-wave dipole is sometimes used as a reference antenna, although present-day usage favors the isotropic radiator as a reference.

Since gain denotes a concentration of the radiated energy, high values of gain are associated with narrow beamwidths. For antennas that have no internal losses, the gain is the same as the directivity (cf. Sec. 2.6). However, while directivity can be computed from either theoretical considerations or from measured radiation patterns, the gain of an antenna is almost always determined by a direct comparison measurement against a standard-gain antenna (cf. Sec. 34.4).

The effective area of an antenna is directly related to its gain (cf. Sec. 2.7). The effective area is of interest when it is desired to compute the energy collected by a receiving antenna or to compute the transmission loss between two antennas in free space.

1.6. IMPEDANCE

The input impedance of an antenna system is of considerable importance to the systems engineer since it directly affects the efficiency of energy transfer to or from the antenna. The over-all input impedance of an antenna system depends not only on the impedance of the individual antenna elements but also on the mutual impedance between elements as well as the transmission lines and transmission-line components which are used to interconnect the antenna elements. The over-all design of a complex antenna system will therefore be governed as much by the details of the interconnecting transmission line as by the characteristics of the individual antenna elements. If a large operating bandwidth is desired, each element and component of the antenna system must have favorable impedance properties over the band of operation.

While it is possible to compute the properties of many transmission-line and wave-guide components (cf. Chaps. 30 and 31), it is extremely difficult to theoretically determine the impedance characteristics of an antenna element other than those elements which have relatively simple geometrical shapes. Even for the simple cases, many pitfalls exist, and it is generally preferable to use theoretical antenna impedance values primarily for the purpose of interpreting and guiding the experimental measurement procedure.

1.7. BANDWIDTH

Unlike some of the properties which have been treated previously, the bandwidth of an antenna or antenna system does not have a unique definition. Depending upon the operational requirement of the system with which the antenna is to be used, the functional bandwidth of an antenna may be limited by any one or several of the following factors: change of pattern shape or pattern direction, increase in side-lobe level, loss in gain, change of polarization characteristics, or deterioration of impedance characteristics. For antennas where all of the factors mentioned are important, one of the factors, such as gain or impedance, will determine the low-frequency limit while another factor, such as change of pattern shape, will determine the high-frequency limit. In general, then, the only appropriate definition for the bandwidth of a particular antenna is that band within which the antenna meets a given set of specifications.

Despite the difficulty of uniquely specifying bandwidth, it is possible to make a few observations regarding the factors which tend to limit the bandwidth of certain simple antenna structures. For antennas of relatively small dimensions (i.e., when the linear dimensions are of the order of a half wavelength or less), the limiting factor is most frequently the impedance performance. For many circularly polarized antennas, the polarization characteristics prove to be the limiting factor on bandwidth. For end-fed linear arrays, the pattern direction will deviate excessively long before the pattern shape or impedance characteristics deteriorate.

There are several situations where it is possible to make some firm estimates concerning bandwidth. One situation arises when it is necessary to face the problem of matching an antenna which has a known impedance variation over a given frequency range. By determining the equivalent Q of the antenna (see Sec. 2.14), it is possible to determine the lowest theoretically obtainable standing-wave ratio over a required bandwidth with a given number of network elements. Conversely, it is possible to determine the maximum bandwidth for a permissible value of standing-wave ratio.

It is to be noted that the bandwidth of the antenna is critically dependent on its value of Q; the higher the Q the less the bandwidth. This could be restated to

indicate that the larger the amount of stored or reactive energy as compared to the radiated energy, the lesser will be the bandwidth.

REFERENCES

1. E. C. Jordan: "Electromagnetic Waves and Radiating Systems," Prentice-Hall, Inc. Englewood Cliffs, N.J., 1950.
   J. D. Kraus: "Antennas," McGraw-Hill Book Company, Inc., New York, 1950.
   S. A. Schelkunoff and H. T. Friis: "Antennas: Theory and Practice," John Wiley & Sons, Inc., New York, 1952.
   S. Silver: "Microwave Antenna Theory and Design," McGraw-Hill Book Company, Inc., New York, 1949

Chapter 2

FUNDAMENTALS OF ANTENNAS

Henry Jasik

Jasik Laboratories, Inc.
Westbury, Long Island, New York

2.1. RADIATION FROM ELECTRIC-CURRENT ELEMENTS

One of the types of radiators frequently used in antenna practice is some form of thin wire arranged in a linear configuration. If the current distribution on such a wire is known or can be assumed with a reasonable degree of accuracy, then the radiation pattern and the radiated power can be computed. This computation is based on the integration of the effects due to each differential element of the current along the wire. It is therefore of interest to set down the complete expressions for the fields at any distance due to a differential element of current oriented along the z axis as shown in Fig. 2-1. The rms electric- and magnetic-field components are given as follows:

$$E_r = 60\beta^2 I \, dz \left[\frac{1}{(\beta r)^2} - \frac{j}{(\beta r)^3} \right] \cos \theta \, e^{-j\beta r}$$

$$E_\theta = j30\beta^2 I \, dz \left[\frac{1}{\beta r} - \frac{j}{(\beta r)^2} - \frac{1}{(\beta r)^3} \right] \sin \theta \, e^{-j\beta r}$$

$$H_\phi = j \frac{\beta^2}{4\pi} I \, dz \left[\frac{1}{\beta r} - \frac{j}{(\beta r)^2} \right] \sin \theta \, e^{-j\beta r}$$

$$E_\phi = H_r = H_\theta = 0$$

where $I \, dz$ = moment of differential current element. I is given in rms amperes and
dz is given in meters

r = distance in meters to observation point

$\beta = 2\pi/\lambda$

λ = wavelength, meters

$j = \sqrt{-1}$

E is given in volts per meter

H is given in amperes per meter

A time factor of $e^{j\omega t}$ has been omitted, since for all the cases in which we are interested it is assumed that we have a sinusoidally time-varying current of constant frequency.

For most problems of interest it is only necessary to know the components in the far field, i.e., when r is very much greater than the wavelength. Under these conditions, the field components are simply given by

$$E_\theta = j \frac{30\beta I \, dz}{r} \sin \theta \, e^{-j\beta r}$$

$$= j \frac{60\pi I \, dz}{r\lambda} \sin \theta \, e^{-j\beta r}$$

$$H_\phi = j \frac{\beta I \, dz}{4\pi r} \sin \theta \, e^{-j\beta r}$$

$$= \frac{E_\theta}{120\pi}$$
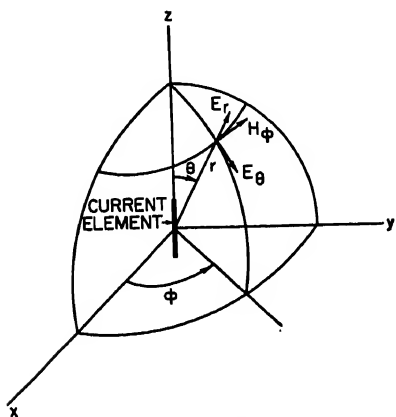
Fig. 2-1. Coordinate system for electric dipole.

These expressions apply only for a very short element of current having a constant value along its length. However, they may readily be used to determine the field from any wire having a known current distribution by integrating the field due to each of the differential current elements along the length of the antenna. Taking into account the variation of current and the phase differential due to the varying distance from the observation point to each current element, the general expression

for the field of any current distribution becomes

$$E_\theta = j\frac{60\pi \sin \theta}{r\lambda} \int_{-\ell/2}^{\ell/2} I(z)\, dz\, e^{-j\beta r(z)}.$$

where both $I(z)$ and $r(z)$ are now functions of z and the integration takes place along the length of the antenna from $-\ell/2$ to $+\ell/2$.

For very short antennas, the above expression can be simplified to

$$E_\theta = j\frac{60\pi \sin \theta}{r\lambda} I_0 L_e e^{-j\beta r}$$

where I_0 = current at center of antenna
L_e = effective length of antenna defined as

$$L_e = \frac{1}{I_0}\int_{-\ell/2}^{\ell/2} I(z)\, dz$$

The effective length is of interest in determining the open-circuit voltage at the terminals of a receiving antenna.

FIG. 2-2. Current distribution on short linear antenna: (a) With top loading. (b) Without top loading.

It is also used on occasion to indicate the effectiveness of a transmitting antenna.

For a short top-loaded linear antenna which has uniform current distribution as shown in Fig. 2-2a, the effective length is simply equal to the physical length. For a short antenna which is much less than a half wave long, as shown in Fig. 2-2b, the current distribution is essentially triangular and its effective length is one-half of its physical length.

For antennas with an over-all length greater than about a quarter wavelength, the variation of the phase term cannot be neglected and the integral must be evaluated taking this term into account. The method will be very briefly illustrated for the case of a thin half-wave radiator which can be assumed to have a sinusoidal current distribution so that $I(z)$ is given by $I_0 \cos \beta z$. The geometry for finding $r(z)$ is shown in Fig. 2-3, from which it is readily seen that

FIG. 2-3. Coordinates for computing radiation from half-wave dipole.

$$r(z) = r - z \cos \theta$$

The field for a half-wave dipole is then given by

$$E_\theta = j\frac{60\pi \sin \theta}{r\lambda} I_0 e^{-j\beta r} \int_{-\ell/2}^{\ell/2} \cos \beta z\, e^{j\beta z \cos\theta}\, dz$$

which reduces to

$$E_\theta = j\frac{60 I_0}{r} e^{-j\beta r} \frac{\cos\left(\frac{\pi}{2}\cos\theta\right)}{\sin\theta}$$

The relative-radiation pattern for a half-wave antenna is shown in solid lines in Fig. 2-4. For comparison purposes, the relative-radiation pattern of a very short dipole is shown in dotted lines. The patterns shown are those in a plane which contains the axis for the antenna. The pattern in the plane perpendicular to the antenna is perfectly circular because of symmetry.

There are a number of other properties for the half-wave dipole which are of considerable interest, such as the radiation resistance, gain, and input impedance. These properties are discussed in Secs. 2.5 and 2.6 and in Chap. 3.
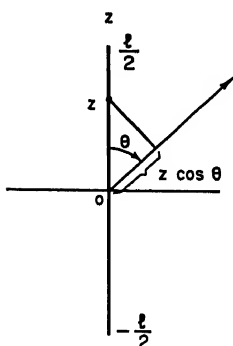
The method of computing radiation patterns for thin linear radiators is basic, regardless of the length or complexity of shape. As a matter of interest, the following formula gives the radiated field from a center-fed thin wire of arbitrary length ℓ with an assumed sinusoidal current distribution:

$$E_\theta = j\frac{60I_0e^{-j\beta r}}{r}\;\frac{\cos\left(\dfrac{\beta\ell}{2}\cos\theta\right)-\cos\dfrac{\beta\ell}{2}}{\sin\theta}$$

It will be noted that the radiated field perpendicular to the antenna continues to increase as the length is increased until the over-all length is about $1\frac{1}{4}$ wavelengths. Beyond this point the field starts falling off. When the over-all length is two wavelengths, the field is zero normal to the axis of the antenna. For this length, the radiation pattern has broken up into two major lobes which are directed off the normal to the antenna. For still longer length the antenna pattern will continue to break up into a large number of lobes whose positions depend on over-all length of the antenna (Chaps. 3 and 4).

—— HALF–WAVE DIPOLE
– – – SHORT DIPOLE

Fig. 2–4. Radiation patterns: ——
Half-wave dipole. – – – – Short dipole.

2.2. RADIATION FROM MAGNETIC-CURRENT ELEMENTS

Another basic radiator which is frequently used in antenna practice is a magnetic-current element. Although magnetic currents do not exist in nature, there are a number of configurations which produce fields identical with those which would be produced by a fictitious magnetic current. For instance, a circular loop carrying electric current whose diameter is very small in terms of wavelengths will produce fields which are equivalent to those of a short magnetic dipole. The fields for any distance are given by the following expressions:

$$E_\phi = 30\beta^3\,dm\left[\frac{1}{\beta r}-\frac{j}{(\beta r)^2}\right]\sin\theta\,e^{-j\beta r}$$

$$H_r = \frac{\beta^3}{2\pi}\,dm\left[\frac{j}{(\beta r)^2}+\frac{1}{(\beta r)^3}\right]\cos\theta\,e^{-j\beta r}$$

$$H_\theta = -\frac{\beta^3}{4\pi}\,dm\left[\frac{1}{\beta r}-\frac{j}{(\beta r)^2}-\frac{1}{(\beta r)^3}\right]\sin\theta\,e^{-j\beta r}$$

$$E_r = E_\theta = H_\phi = 0$$

where the coordinate system is as shown in Fig. 2–5, and dm is defined as the differential magnetic-dipole moment. For a small-diameter loop, the magnetic moment of the loop is equal to the electric current I flowing through the loop times its area A.

For the far field, when r is very much greater than the wavelength, the field components reduce to

$$E_\phi = \frac{30\beta^2\,dm}{r}\sin\theta\,e^{-j\beta r}$$

$$H_\theta = -\frac{\beta^2\,dm}{4\pi r}\sin\theta\,e^{-j\beta r}$$

$$= -\frac{E_\phi}{120\pi}$$

It will be noted that the field expressions for the magnetic-current element are almost exactly analogous to those for the electric-current element except for the

interchange of electric and magnetic quantities. The radiation of a short magnetic dipole or a small-diameter loop is also a doughnut pattern, as for the case of an electric dipole. For a small loop the radiation pattern in the plane of a loop is perfectly circular while the pattern in the plane through the axis of the loop is a figure of eight whose amplitude is proportional to sin θ. The expressions given are accurate for loop diameters which are considerably less than one-tenth wavelength. As a matter of fact, for very small loops the radiation pattern does not depend on the exact shape of the loop, which may be square, rectangular, or some other shape, provided the over-all circumference remains much less than a quarter wavelength.

For loops whose diameter is of the order of the wavelength, the radiation pattern can deviate considerably from the doughnut form, depending on the nature of the current distribution along the loop and diameter of the loop. These considerations are treated in Chap. 6.

Another antenna whose radiation characteristics are essentially similar to those of a magnetic dipole consists of a very thin slot in an infinitely large metallic ground plane, as shown in Fig. 2-6a. For this type of antenna, the electric field is applied across the narrow dimension of the slot. It is possible to show that field radiated by this

FIG. 2-5. Coordinate system for magnetic dipole.

slot is exactly the same as would be radiated by a fictitious magnetic dipole with a magnetic-current distribution M which is numerically equal to the distribution of electric voltage V across the slot. Thus the radiation pattern of a thin rectangular slot is identical with the radiation pattern of the complementary electric dipole which would just fill the slot, as shown in Fig. 2-6b. The only difference between the two types of radiators is the fact that the electric and magnetic quantities have been interchanged. This complementary relationship has been treated in considerable length in the literature and is briefly discussed in Chap. 8, so that it will not be elaborated on in this section.

It is pertinent to point out a few precautions concerning the application of these complementary relationships. For one thing, the complementary relationship is based on the assumption that only electric field exists within the slot and that no magnetic field is present. This is true only for vanishingly thin slots. For slots whose width is appreciable in comparison with their length, the above assumption is no longer valid and the radiation pattern will be somewhat modified as compared with the case of the very thin slot.

FIG. 2-6. (a) Thin slot in ground plane. (b) Complementary dipole.

Another assumption on which the complementary relationship is based is that the size of the conducting ground plane is infinitely large. This, of course, is never true in practice, and for finite ground planes, the size of the ground plane may exert a large influence on the radiation pattern, substantially, particularly at angles close to the plane of the sheet. Even for sheets which are fairly large in terms of wavelength, there are some minor modifications of radiation pattern, as shown in Chap. 8.

It might also be mentioned that the complementary relationship holds only when

the slot is cut in a large flat ground sheet. For slots cut in circular cylinders, the pattern can be considerably different from that predicted by the complementary relationship, particularly in the plane perpendicular to the axis of the cylinder. However, use of the complementary relationship is still very useful to the engineer as an intuitive guide, and while in many cases the results will not be exact, they will certainly give a first approximation to the actual radiation pattern.

2.3. ANTENNAS ABOVE PERFECT GROUND

The characteristics of antennas operating near ground level will be modified by the effect of ground reflections. This is particularly true of antennas operating at frequencies below 30 Mc where the height of the antenna above ground may be less than one or two wavelengths. For airborne antennas or for large-aperture, narrow-beam
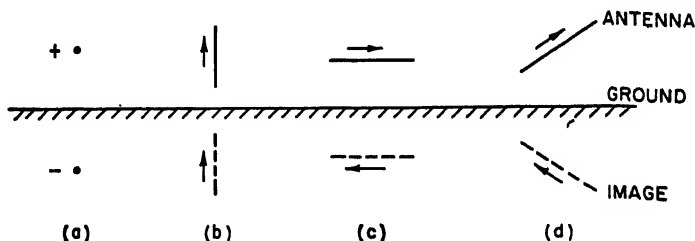
FIG. 2-7. Images above a perfectly conducting ground plane: (a) Point charge. (b) Vertical wire. (c) Horizontal wire. (d) Inclined wire.

antennas, where the main beam is elevated upward at least several beamwidths, the ground may play a relatively small role. In all cases, the ground will play a part in the propagation between transmitter and receiver and, to compute its effect, the characteristics of the ground and the geometry of the propagation path must be known, as well as the pattern characteristics of the receiving and transmitting antennas.

For antennas at relatively small heights above ground, the ground is a basic part of the antenna system and will affect not only the radiation pattern of the antenna but also its impedance properties. In order to obtain a first-order estimate of the effect of ground, simple image theory can be applied to the case of a perfectly conducting ground surface. It is well known from electromagnetic theory that the tangential field on a perfect conductor must be zero and that the electric field must be normal to the conducting surface. To satisfy this requirement, a conducting charge above a conducting plane will induce a charge distribution on the plane exactly equivalent to that which would be produced by an equal charge of the opposite sign at the same distance below the plane, as shown in Fig. 2-7a. Since current is a movement of charge, it is readily possible to deduce the direction of the images for vertical, horizontal, and inclined wires above ground, as shown in Fig. 2-7b–d. The image for any other configuration can readily be determined by using the rule that vertical components are in the same direction while horizontal components are in opposite directions.

The field in any direction above the ground plane can easily be determined by replacing the ground plane by the image and computing the resulting field due to the antenna plus its image. This is valid only above the ground plane, since for a perfect conductor the field below the ground plane is zero.

Although the above method is rigorously true only for antennas above highly conducting ground, it does give good results in many cases of interest. The same technique can be used where the ground has arbitrary values of conductivity and dielectric constant by assuming an image current which is related to the antenna

current by the ratio of the complex-reflection coefficient for the appropriate angle of incidence (Sec. 33.2).

The effect of the ground on the impedance of an antenna can also be determined by image theory. For instance, the input impedance of an antenna above perfectly conducting ground is simply the input impedance of the antenna in free space plus the mutual impedance due to the image antenna. For arbitrary ground, the same sort of relation is still true except that the mutual impedance due to the image must be multiplied by the complex-ground-reflection coefficient for normal incidence.

A special case of considerable interest occurs when one end of the antenna terminates at the ground. For this case, the input impedance of the antenna above ground is exactly one-half of the input impedance of the antenna plus its image when driven in free space. For example, the input impedance of a quarter-wave dipole above ground is exactly one-half that of a half-wave dipole in free space.

2.4. RADIATION FROM APERTURES

The computation of radiation patterns for linear-wire antennas is relatively simple if the current distribution on the wire is known. The current distribution is not usually known exactly except for a few special cases. However, physical intuition or experimental measurement can often provide a reasonable approximation to the current distribution, and for many engineering purposes a sufficiently accurate result can be obtained. In theory, of course, an exact result can be derived from a boundary-value solution if the nature of the exciting sources is known. From a practical point of view, the amount of labor involved in obtaining numerical results is excessive even for those cases where the geometry is relatively simple and a rigorous solution can be expressed in terms of a series of tabulated functions. It is therefore necessary in many situations to be able to compute the radiation pattern by alternative methods based on a reasonable assumption of the nature of the electromagnetic fields existing in the vicinity of an antenna structure.

The Equivalence Principle. One powerful technique for simplifying this type of computation makes use of an equivalence principle given by Schelkunoff.[1,2] Briefly stated, this principle supposes that a given distribution of electric and magnetic fields exists on a closed surface drawn about the antenna structure. These fields are then canceled by placing a suitable distribution of electric- and magnetic-current sheets on the closed surface such that the fields inside the closed surface are zero. The radiation is then computed from the electric- and magnetic-current sheets and, except for a difference in sign, is identical to the radiation which would have been produced by the original sources inside the closed surface. It will be noted that this principle is essentially a more rigorous formulation of Huygens' principle. If the fields on the closed surface are known exactly, then the resulting computation is also exact. The degree of approximation which can be obtained by this technique depends only on how accurately the fields across the closed surface may be estimated.

When the electric- and magnetic-field strengths are respectively given by E and H, then the equivalent densities are given by

Electric-current density: $\qquad J = n \times H$

Magnetic-current density: $\qquad M = -n \times E$

where both J and H are expressed in amperes per meter and M and E are expressed in volts per meter.

The vector cross product has been used to show that the electric current is perpendicular to direction of propagation and to the magnetic-field vector. If the

initial E and H fields are as shown in Fig. 2-8a, then the resulting electric and magnetic currents are directed as shown in Fig. 2-8b.

One way of visualizing the effect of a small portion of the wavefront is to consider the physical equivalent of the electric- and magnetic-current sheets. The electric current is equivalent to a short electric dipole, while the magnetic current is equivalent to a short magnetic dipole or a small electric-current loop, as was discussed in Sec. 2.2. The electric dipole is oriented in the direction of the electric field E, while the electric-current loop is located in the plane defined by the electric field E and the direction of propagation n, as shown in Fig. 2-8c.
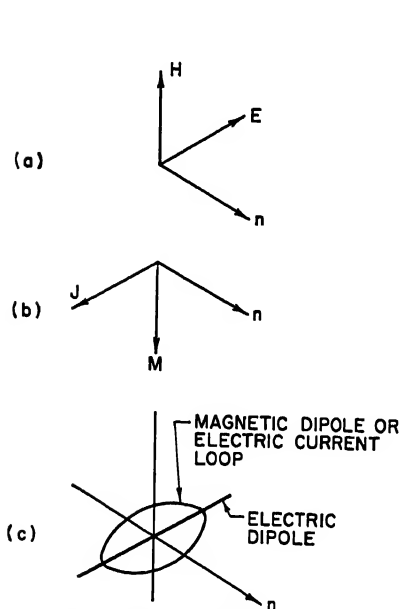
FIG. 2-8. Current sheet relations: (a) Initial E and H fields. (b) Resulting electric and magnetic currents. (c) Orientation of electric dipole and electric-current loop.
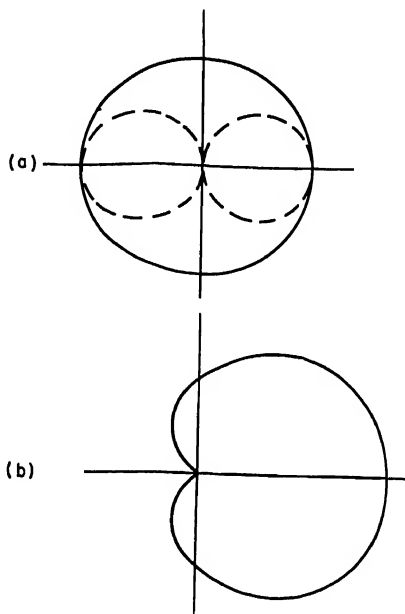
FIG. 2-9. Radiation patterns in plane of electric-current loop: (a) ———— Pattern of electric-current loop. – – – – Pattern of electric dipole. (b) Cardioid pattern due to combination of electric-current loop and electric dipole.

If we look at the radiation pattern in the plane of the loop, the component due to the electric dipole will have a $\cos \theta$ type of variation while the component due to the electric-current loop will have a circular pattern as shown in Fig. 2-9a. For a portion of wavefront in free space in which the E and H fields are related as

$$E = 120\pi H$$

then the relative amplitudes of the two components will be such that the radiation pattern of the combination is given by $(1 + \cos \theta)$ or a cardioid pattern as shown in Fig. 2-9b.

Although the concept of the electric- and magnetic-current sheets is most useful for derivation purposes and for obtaining a physical picture of radiation from apertures, it is possible to compute the reradiated field from an aperture directly in terms of the tangential electric- and magnetic-field components in the aperture itself. Referring to Fig. 2-10, the aperture lies in the xy plane with field components $E_x^{(a)}$ and $H_y^{(a)}$.

At a distant point P, the radiation components of the electric field are given by

$$E_\theta = -j[E_x{}^{(a)} + 120\pi H_y{}^{(a)} \cos \theta] \frac{\cos \phi}{2\lambda r} \, dx \, dy \, e^{-i\beta r}$$

$$E_\phi = +j[E_x{}^{(a)} \cos \theta + 120\pi H_y{}^{(a)}] \frac{\sin \phi}{2\lambda r} \, dx \, dy \, e^{-i\beta r}$$

The above is true for an aperture in which $E_x{}^{(a)}$ and $H_y{}^{(a)}$ take on arbitrary values. An important special case is that in which the field components are the same as exist in a free-space plane wave. For this case

$$E_x{}^{(a)} = 120\pi H_y{}^{(a)}$$

and the distant fields are now given by

$$E_\theta = -jE_x{}^{(a)}(1 + \cos \theta) \frac{\cos \phi}{2\lambda r} \, dx \, dy \, e^{-i\beta r}$$

$$E_\phi = jE_x{}^{(a)}(1 + \cos \theta) \frac{\sin \phi}{2\lambda r} \, dx \, dy \, e^{-i\beta r}$$

Applications of the Equivalence Principle. One typical application of these results is to the problem of determining the radiation patterns from an electromagnetic horn.[3] The tangential fields at the aperture of such a horn can be approximated by assuming that the fields at the aperture plane are the same as would be obtained if the guiding surfaces of the horn were extended to infinity. Although not exact, this assumption is quite good when both linear dimensions of the aperture are greater than one or two wavelengths. After this assumption of the electric and magnetic fields at the aperture, the far-field relationships are then formulated by taking the fields across the aperture and integrating over the aperture, taking into account the amplitude and phase variations of the field incident on the aperture and the phase differential due to the varying distance from the observation point to each area element of the aperture.

Fig. 2-10. Coordinates for current sheet computation.

The above method gives results which are good to a high degree of approximation, particularly for large-aperture horns. The equivalence principle can also be used with small-aperture horns, but caution must be exercised with regard to the assumptions of the relative values of electric- and magnetic-field strengths. In small horns, it is not true that the aperture fields are those which would exist if the waveguide were extended to infinity. For instance, in a waveguide radiator whose E-plane width is small, the field at the aperture will be predominantly electric and the magnetic field may be quite small. For this condition, the equivalent current sheet will consist mainly of magnetic current, and for a small aperture this will have a substantial effect on the radiation pattern, particularly in the E plane. For those cases where it is possible to measure the standing waves in the waveguide leading to the aperture, it is possible to estimate the relative values of electric- and magnetic-field strength at the aperture and to make a first order correction to the radiation-pattern computation.

The equivalence principle can also be used to determine the radiation from the open end of a coaxial line. For this case, the field at the aperture is predominantly electric, with only a small component of magnetic field. The field variation in the aperture

is assumed to be that of the dominant mode in the coaxial line. The problem is readily formulated in cylindrical coordinates.[4]

Another problem which can be solved using the equivalent–current–sheet method is the case of reflection from a conducting sheet such as a paraboloidal reflector or a plane reflector as used in microwave relay applications. To formulate this problem, the tangential fields that would have existed if the reflector were not present are determined. When the reflector is present, the electric field vanishes at the surface of the reflector while the tangential magnetic field is doubled. The far field is then determined by using only the magnetic-field term for the aperture field and integrating over the surface, taking into account variations of the aperture field amplitude and phase and the phase differential to the observation point.

2.5. IMPEDANCE PROPERTIES OF ANTENNAS

Self-impedance. The input impedance of an antenna is a characteristic of considerable interest to the engineer since he is concerned with the problem of supplying the antenna with the maximum amount of transmitter power available, or in abstracting the maximum amount of received energy available from the antenna. Except for the simplest types of antenna configuration, the theoretical computation of the input impedance is an extremely arduous task and for a large number of antenna types it is usually easiest to make a direct experimental measurement of the input impedance. However, for linear antennas which are relatively small in size, it is possible to make some reasonably good estimates as to the magnitude of the input resistance. It is also possible to assess, with a reasonable degree of accuracy, the mutual impedance between linear radiators for the purpose of estimating the input impedance of an individual element in an array of radiators.

In most practical cases, the input impedance of even a simple antenna is affected to a considerable degree by the terminal conditions at the point where the transmission line feeds the radiator. For most accurate results, it is therefore necessary to measure the various impedances involved and to use the calculated values primarily as a guide during the design procedure.

For very short wire dipoles, the radiation resistance is a quantity which is closely allied with the resistive component of the input impedance. The radiation resistance is normally defined as the ratio of the total power radiated by an antenna divided by the square of the effective antenna current referred to a specified point. For short antennas this is a useful quantity because it enables one to estimate the over-all radiation efficiency of the antenna by separating the radiation component of the input resistance from the loss resistance due to the ground system, or the loss resistance due to the impedance matching elements.

To compute the radiation resistance, it is necessary to know the radiation field pattern of the antenna in terms of the current flowing at the point to which the radiation resistance is referred. The total radiated power is then computed by integrating the total power density passing through a sphere surrounding the antenna. This computation will be carried through very briefly for the case of a very short dipole having an effective length L_e and carrying a current I_0. The electric-field intensity for this antenna is given in Sec. 2.1 as

$$|E_\theta| = \frac{60\pi I_0 L_e}{r\lambda} \sin \theta$$

The power density in the far field is given by the Poynting vector, which is equal to $E_\theta{}^2/120\pi$, where the electric field is given in rms volts per meter and the power density is expressed in watts per square meter. Integrating over a large sphere surrounding

the antenna, we then obtain

$$P = \int_0^\pi \frac{E_\theta^2}{120\pi} \, 2\pi r^2 \sin\theta \, d\theta$$
$$= \frac{80\pi^2 I_0^2 L_e^2}{\lambda^2}$$

Dividing this result by I_0^2, we obtain

$$R_e = 80\pi^2 \frac{L_e^2}{\lambda^2}$$

where R_e is a radiation resistance in ohms. It will be noted that the important variable is the ratio of the effective length L_e to the wavelength and that the larger this ratio the greater the radiation resistance. Thus for a short antenna of physical length l which is top-loaded so as to give a uniform current distribution, the effective length will be equal to the physical length and the radiation resistance will be $80\pi^2 l^2/\lambda^2$. For an antenna with no top loading, the current distribution will be triangular (Sec. 2.1) and the effective length will be equal to one-half the physical length, so that the radiation resistance will be $20\pi^2 l^2/\lambda^2$. It can be seen that the radiation resistance for the uniform-current case is thus equal to four times that obtained in the case of triangular current distribution, despite the fact that the radiation pattern and directivity are the same for both antennas since their length is small with respect to the wavelength.

The problem of computing the input impedance of a dipole of finite diameter whose length is of the order of a half wavelength is one that has been considered at great length by a number of writers. The subject is treated in detail in Chap. 3, where a considerable amount of measured data is presented.

For the case of very thin half-wave dipole, the input resistance may be computed by assuming a sinusoidal current distribution and integrating the total power radiated over the surface of a large sphere, in the same fashion as just described for the short current element. Using the far field for the half-wave dipole as given in Sec. 2.1 and performing the appropriate operations, the input resistance of the half-wave thin dipole is found to be 73.1 ohms. The reactive component of the input impedance cannot be determined by the far-field method since the reactance is governed primarily by the electromagnetic fields in the vicinity of the antenna itself. The input reactance is also a function of the relative diameter of the dipole and of the terminal conditions at the driving point.

Mutual Impedance. In an array of antennas, the driving-point impedance of an individual element may differ considerably from its self-impedance because of the effect of mutual coupling with other elements of the array.[5] In a multielement array, the relations between the currents and voltages are given by

$$V_1 = I_1 Z_{11} + I_2 Z_{12} + \cdots + I_n Z_{1n}$$
$$V_2 = I_1 Z_{12} + I_2 Z_{22} + \cdots + I_n Z_{2n}$$
$$\vdots$$
$$V_n = I_1 Z_{1n} + I_2 Z_{2n} + \cdots + I_n Z_{nn}$$

where V_n = impressed voltage at the nth element
         I_n = current flowing in nth element
         Z_{nn} = self-impedance of nth element
     $Z_{mn} = Z_{nm}$ = mutual impedance between mth and nth elements

The driving-point impedance for element 1, for instance, is found from the ratio of the impressed voltage to the current and is obtained from the above equations as follows:

$$Z_{1_{\text{input}}} = \frac{V_1}{I_1} = Z_{11} + \frac{I_2}{I_1} Z_{12} + \cdots + \frac{I_n}{I_1} Z_{1n}$$

It is readily seen that the input impedance or driving point impedance of a particular element is not only a function of its own self-impedance but also a function of the relative currents flowing in the other elements and of the mutual impedance between elements. In an array where the current distribution in the elements is critical because of pattern requirements, it is necessary to determine the input impedance from the above relationship and to design the transmission-line coupling system to match the input impedance rather than the self-impedance. Some examples of this are given in Ref. 6 and also in Chap. 20.

An alternative method for accurately controlling the current distribution in certain types of arrays is to use a transmission-line distribution system which forces the required current to flow in an antenna element regardless of the effect of mutual impedance. For instance, the constant-current properties of a quarter-wave line are such that the current in a load at the end of a quarter-wave line is equal to the driving voltage divided by the characteristic impedance of the quarter-wave line, regardless of the load impedance. This property is also true for a line whose length is an odd number of quarter wavelengths. Thus, for example, in order to feed an array of four dipole elements with exactly equal currents, regardless of mutual coupling, the length of transmission line from the dipole to the junction would be an odd number of quarter wavelengths. By making use of the constant-voltage properties of a half-wavelength transmission line, it is possible to build up a distribution system to feed a large number of antenna elements by means of combinations of half-wave and quarter-wave lines. It is worth mentioning, in passing, that although the uniform half-wave line behaves as a voltage transformer with a transformation ratio of 1, it is possible to obtain other transformation ratios by constructing the half-wave line of two quarter-wave sections of differing characteristic impedances.

In many situations it is not possible to sidestep the effects of mutual coupling and it is necessary to have a reasonably accurate estimate of the value of mutual impedance between antenna elements. It is possible to calculate the mutual impedance for very thin dipoles, and the results are given in Chap. 3 for several cases of interest. Although the finite diameter of a dipole does have some effect on the magnitude of the mutual impedance, the effect is a second-order one and for many computations may be neglected. This is not true for the self-impedance, whose value is very definitely a function of the dipole diameter.

Investigations have also been made of the mutual coupling between waveguide slot radiators, and a summary of these results is included in Chap. 9.

For antenna elements other than the simple dipole or slot radiator, little theoretical work is available on the magnitude of mutual-coupling effects and it is necessary to use experimental methods for determining the mutual impedance. Even in the case of dipole elements, it is frequently desirable to measure the mutual impedance, particularly for a dipole whose diameter is not small compared with its length.

Several experimental methods are available. When the antenna elements are identical and reasonably small physically, one simple method is to measure the input impedance when the element is isolated and then to repeat the measurement when a ground plane is placed near the element to simulate the effect of an image. The difference between the two impedance measurements is the mutual impedance for a distance corresponding to the distance between the driven element and its image. An alternative method when two elements are available is to measure the input

impedance when one element is isolated, and then to repeat the measurement when the second element is in place and has a short circuit across its terminals. Further details may be found in Chap. 34.

2.6. ANTENNA DIRECTIVITY AND GAIN

The directional characteristics of an antenna are frequently expressed in terms of a gain function $G(\theta,\phi)$ where θ is the angle of colatitude and ϕ is the polar angle (Fig. 2–1). The maximum value of the gain function is the gain. The gain is commonly defined as the ratio of the maximum radiation intensity in a given direction to the maximum radiation intensity produced in the same direction from a reference antenna with the same power input. If the reference is taken to be a hypothetical lossless antenna which radiates uniformly in all directions, the gain is said to be compared with that of an isotropic radiator. This definition is favored for microwave antennas and is used throughout a large part of this book. In the early development of the radio art, a half-wave dipole was used as the reference antenna, and this usage has continued for some antenna applications in communications and television. When gain figures are given, it is generally assumed that the gain is with respect to an isotropic radiator unless otherwise stated.

A quantity closely associated with gain is directivity. Directivity is defined as the ratio of the maximum radiation intensity to the average radiation intensity. For an antenna that is 100 per cent efficient and has no copper, dielectric, or mismatch losses, directivity and gain are the same. For an antenna with losses, the gain will be lower than the directivity by a factor which corresponds to the efficiency.

If the radiation pattern of an antenna is specified in terms of the electric field $E(\theta,\phi)$, as a function of the polar coordinate angles θ and ϕ, then the radiation intensity is proportional to the square of the electric field and the directivity is expressed by

$$D = \frac{E_{max}^2}{\left(\frac{1}{4\pi}\right) \iint E^2(\theta,\phi)\, d\Omega}$$

where $d\Omega$ is a differential element of solid angle. In polar coordinates this expression becomes

$$D = \frac{4\pi E_{max}^2}{\int_0^{2\pi} \int_0^{\pi} E^2(\theta,\phi)\, \sin\theta\, d\theta\, d\phi}$$

The above expression defines directivity with reference to a lossless isotropic radiator. If another radiator, such as a half-wave dipole, is used as the reference then the directivity will be less by a factor corresponding to the directivity of the reference.

Table 2–1 gives the value of directivity for a number of antennas which are sometimes used as references.

Table 2-1

Antenna type	Directivity ratio	Directivity, db
Isotropic radiator	1	0
Very short dipole	1.5	1.76
Half-wave dipole	1.64	2.15
Quarter-wave dipole above perfect ground plane	3.28	5.15

The gain is related to the directivity by the relation

$$G = kD$$

where k is the efficiency factor of the antenna and is equal to 1 if the antenna has no copper, dielectric, or mismatch losses.

For many types of antenna systems, the losses are very low and the value of gain is essentially equal to the directivity. For this reason, the two terms are often used interchangeably. However, it must be remembered that the gain is the important quantity when evaluating the systems performance of an antenna and that the value of directivity may be misleading if an antenna has substantial dissipative or mismatch losses.

The directivity figure can be evaluated theoretically from the computed radiation patterns of an antenna or evaluated experimentally by graphical integration of the measured radiation patterns. The gain figure can frequently be determined from the directivity by estimating the losses in an antenna system, but is usually measured experimentally by direct-comparison methods. The subject is treated in some detail in Chap. 34, and the only additional comment the writer can add is that the measurement of absolute gain is probably the most difficult type of antenna measurement to be made and should accordingly be approached with considerable caution.

It is occasionally of interest to obtain an approximate value for the gain when the only data available are the principal plane radiation patterns. Assuming the antenna is relatively lossless, the gain may be estimated from

$$G \approx \frac{27{,}000}{\theta_E \theta_H}$$

where θ_E and θ_H are the beamwidths in degrees between half-power points in the E and H planes, respectively. The value obtained in this fashion will generally be accurate to within 25 per cent, particularly for high-gain antennas.

2.7. THE RECEIVING ANTENNA AND EFFECTIVE APERTURE

Although much of the discussion up to now has treated the antenna for use in transmitting, it is a consequence of the reciprocity theorem[15] that the properties of a receiving antenna are identical with the properties of the same antenna when used for transmitting.

Thus the radiation patterns of an antenna will be the same whether an antenna is used for transmitting or receiving, as will be its gain and impedance. This reciprocal property of antennas is of considerable use in making antenna measurements and in making an analysis of antenna properties.

Effective Area. In considering an antenna as a receiving device, it is useful to employ the concept of effective area. If a receiving antenna is placed in the field of a linearly polarized electromagnetic wave, the received power available at the terminals of the antenna is equal to the effective area times the power per unit area carried by the wave.

$$W = PA \qquad \text{or} \qquad A = \frac{W}{P}$$

where W = available power, watts
P = power density of wave, watts/square meter
A = effective area, square meters

The power density is simply related to the rms value of the electric field by

$$P = \frac{E^2}{120\pi}$$

It should be noted that all the available power will be transferred to the receiving load only when the load impedance presents a conjugate match to the antenna impedance. For any other match condition, the transferred power will be smaller by the mismatch loss factor. However, the above definition does include the effect of dissipative losses in the antenna, so that these need not be accounted for separately.

A very useful relation exists between the effective area of an antenna and its power gain as follows:

$$A = \frac{\lambda^2 G}{4\pi}$$

The effective area of a number of simple antennas is given in Table 2-2.

Table 2-2

Antenna	*Effective area*
Isotropic radiator.........	$\lambda^2/4\pi$
Very short dipole.........	$3\lambda^2/8\pi$
Half-wave dipole.........	$1.64\lambda^2/4\pi$

The effective area of large-aperture antennas is of the same order as the physical area. For pyramidal horns, the effective area will be approximately 50 per cent of the physical area for an optimum horn and can be as high as 80 per cent of the physical area for a horn with a very long flare length. For parabolic-reflector antennas, the effective area is generally between 50 and 65 per cent of the physical area. For the case of a large mattress-type multielement dipole-reflector array, the effective area can actually be equal to, or in some cases slightly greater than, the physical area.

Transmission between Two Antennas in Free Space. The concept of effective area is useful in determining the transmission loss between two antennas in free space separated at a large distance. If the transmitting antenna has a gain G_T, then the power density in the direction of maximum gain at a distance R, expressed in meters, is simply

$$P = \frac{W_T G_T}{4\pi R^2}$$

where W_T is the power delivered to input terminals of the transmitting antenna.

The energy available at the receiving antenna whose effective area is A_R in square meters is given by

$$W_R = \frac{W_T G_T A_R}{4\pi R^2}$$

The transmission ratio between the two antennas is given by

$$\frac{W_R}{W_T} = \frac{G_T A_R}{4\pi R^2} = \frac{G_R A_T}{4\pi R^2} = \frac{A_T A_R}{\lambda^2 R^2} = \frac{G_T G_R \lambda^2}{16\pi^2 R^2}$$

It should be noted that the above relationships are valid only when the distance between antennas is large enough so that the Fraunhofer conditions are satisfied, that is, when[15]

$$R \geq \frac{2d^2}{\lambda}$$

where d is the largest linear dimension of either of the two antennas.

2.8. DIRECTIVITY PATTERNS FROM ARRAYS OF DISCRETE ELEMENTS

One of the more useful types of directive antenna systems consists of an array or arrays of discrete elements arranged in a linear configuration or in a rectangular configuration. Frequently, the discrete element will consist of a half-wave dipole or a

quarter-wave dipole over ground. For microwave applications, arrays consisting of half-wave slot elements are finding increasing use, particularly at frequencies above 3,000 Mc. The choice of a particular type of element for an array depends on a number of factors, which include the polarization desired, mechanical considerations, ease of feeding, power-handling capability, and other considerations of an engineering nature.

Regardless of the type of element used, the over-all directivity pattern for an array can be found by obtaining the array factor for the particular arrangement of point sources and multiplying it by the element factor for the element used. For broadside arrays consisting of a large number of low-directivity elements, the major factor in determining the directivity pattern is the array factor, while the element factor has only a minor effect on the pattern, other than controlling the front-to-back ratio. On occasion, the array element may consist of a medium-directivity antenna such as a

FIG. 2-11. Coordinates for two-element array.

helix or corner reflector, and for this situation the element factor will play a more important part in the over-all pattern. Use of medium-directivity elements makes it possible to use fewer elements in an array of given length and thereby reduces the complexity of the transmission-line feeding system. However, for applications where very precise control of pattern shape and side-lobe level is required, low-directivity elements are normally used and element spacings of less than three-quarters wavelength are necessary.

Two-element Arrays. The simplest form of a discrete-element array consists of two identical radiators. Although the elements may be driven with currents of arbitrary phase and amplitude, in practice the current amplitudes of the two elements are frequently equal or at least of the same order of magnitude. The general expression for the far field in the plane of the paper of a pair of discrete elements is

$$|E(\phi)| = K|I_1 + I_2 e^{j\left(\delta + \frac{2\pi d}{\lambda}\cos\phi\right)}$$

where I_1 and I_2 are the amplitudes of the current in elements 1 and 2, respectively, δ is the phase advance of element 2, and d and ϕ are as defined in Fig. 2-11. K is a constant, depending on the radiating element and the distance to the observation point. For the case where the currents are identical, the expression reduces to

$$|E(\phi)| = 2KI \cos\left(\frac{\pi d}{\lambda}\cos\phi + \frac{\delta}{2}\right)$$

Three cases are of common interest. The first case occurs when the two elements are driven in phase with equal currents. The pattern for spacings less than three-eighths wavelength is typically as shown in Fig. 2-12a. For very small spacing the pattern will be almost circular, while at spacings of a half wavelength and greater, zeros will appear in the pattern and subsidiary lobes will develop.

The second case occurs when the two elements are driven 180° out of phase with equal currents. A typical pattern for spacings less than three-eighths wavelength is shown in Fig. 2-12b. This type of pattern is commonly known as a figure-of-eight pattern and is extensively used in direction-finding applications.

The third case is when the elements are driven with equal currents and with a phase relationship such that the two currents have a phase difference equal to 180° less the element spacing expressed in electrical degrees. A typical pattern for this case when the spacing is less than three-eighths wavelength is shown in Fig. 2-12c. This type of

pattern is commonly known as a cardioid and is of considerable interest because it is a unidirectional pattern with no backward radiation. A common arrangement, with a pair of elements spaced one-fourth wavelength apart, with a phase difference of 90°, is called a unidirectional couplet. It is often used in high-frequency double-curtain broadside arrays where a large front-to-back ratio is required.

In addition to the three principal cases discussed, a wide variety of pattern shapes is available, depending on the spacing and phasing of the two elements. A series of patterns for the two-element cases may be found in Chap. 5 in Fig. 5-2.

Multielement Arrays. For three or more elements, a complete catalogue of patterns for arbitrary spacing and arbitrary current and phase relationships would be a rather bulky collection. In medium-frequency broadcast antenna arrays, configurations producing arbitrary pattern shapes are often used to obtain a required coverage pattern. Some discussion of this problem will be found in Chap. 20. An extensive collection of radiation patterns of three and four elements with arbitrary spacing and current ratios will be found in Ref. 7.

When arrays consist of large numbers of elements, the design problem is generally simplified by assuming some form of symmetry or regularity for both the element spacing and the current ratios. If this were not done, the number of parameters to be determined would make the design problem extremely unwieldy.

For this reason, the majority of multielement arrays are constructed with uniform element spacing and with a uniform progression of phase from element to element. When there is zero phase progression between elements so that all elements are in phase, the array is known as a broadside array, since the main beam will be perpendicular to the line of the array. When the phase progression between elements is equal to the element spacing in electrical degrees, the array is known as an end-fire array since the main

FIG. 2-12. Patterns for two-element array with small spacing and equal currents: (a) Elements driven in phase. (b) Elements driven 180° out of phase. (c) Elements driven with phase equal to 180° minus the element spacing.

beam is directed along the line of the array. Although the broadside and end-fire arrays are of major interest, under some circumstances it may be desirable to steer the beam, and for this condition the phase progression between array elements will have a value greater than zero but less than the element spacing in electrical degrees.

Uniform Distribution Arrays. For broadside and end-fire arrays, the radiation pattern is always symmetrical about the maximum of the main beam. For a broadside array consisting of omnidirectional elements driven with equal currents in phase,

the shape of the radiation pattern is expressed by

$$E(\phi,\theta) = \frac{\sin\left[\dfrac{n}{2}\left(S\cos\phi\sin\theta\right)\right]}{n\sin\left[\dfrac{1}{2}\left(S\cos\phi\sin\theta\right)\right]}$$

where n is the number of elements, S is the spacing in electrical degrees between elements, and ϕ and θ are as defined in Fig. 2-13. For arrays which do not have "superdirective" properties (Sec. 2.15), the maximum gain for a given length of array is obtained when the current distribution is uniform and all elements of the array are excited in phase. A typical radiation pattern for an array of 10 elements with half-wavelength element spacing is given in Fig. 2-14. For a large number of elements n, the half-power beamwidth of the array is given by $\phi_{hp} = 51\lambda/\ell$, where ϕ is in degrees, λ is the wavelength, and ℓ is the over-all length of the array expressed in the same units as the wavelength. Although the uniform distribution has the maximum gain, it also has a high side-lobe level, the intensity of the first side lobe being only 13.2 db below the level of the main beam, while the succeeding lobes are approximately 17.8, 20.8, 23.0, 24.7 db, etc., below the level of the main beam.

FIG. 2-13. Coordinate system for broadside array.

For the case of a linear array of omnidirectional elements with equal currents having a progressive phase delay equal to α in electrical degrees between adjacent
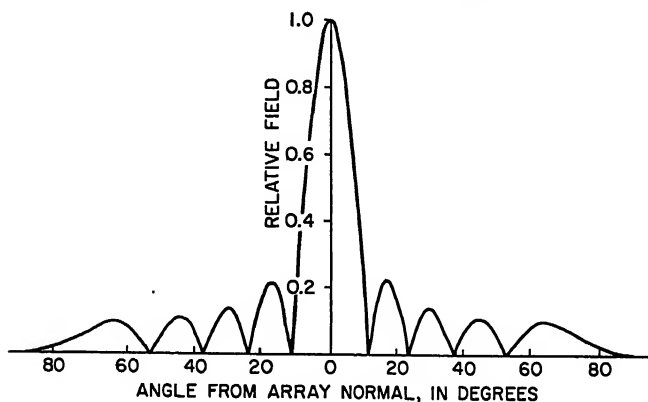
FIG. 2-14. Radiation pattern of ten-element broadside array.

elements, the shape of the radiation pattern is expressed by

$$E(\phi,\theta) = \frac{\sin\left[\dfrac{n}{2}\left(S\cos\phi\sin\theta - \alpha\right)\right]}{n\sin\left[\dfrac{1}{2}\left(S\cos\phi\sin\theta - \alpha\right)\right]}$$

This type of array is sometimes used when it is desired to steer the beam electrically by placing phase shifters in the feed lines to the individual elements. In the

principal plane of the array ($\theta = 90°$), the direction of the main beam is given by $\phi = \cos^{-1}(\alpha/S)$. When the beam is tilted from the normal to the array by relatively small amounts (i.e., less than 20°), the shape of the radiation pattern remains essentially symmetrical about the maximum of the main beam. However, if the individual elements of the array have a considerable amount of directivity, then a certain amount of asymmetry, particularly in the side-lobe levels, will appear as the beam is tilted from the normal. For large angles of scan the beam will also broaden since the apparent length of the array will be reduced by the cosine of the tilt angle.

A limiting case of the array with progressive phase delay occurs when the phase delay α is equal to the element spacing S, in electrical degrees. This is commonly known as an end-fire type of array, and in the principal plane of the array ($\theta = 90°$) the radiation pattern is given by

$$E(\phi) = \frac{\sin\left[\dfrac{nS}{2}(1 - \cos\phi)\right]}{n\sin\left[\dfrac{S}{2}(1 - \cos\phi)\right]}$$

The shape of this type of radiation pattern is characterized by a broad-nosed beam along the direction of the array. For some applications, the broad-nosed beam is desirable.

However, if maximum gain is desired from an end-fire array, it has been shown by Hansen and Woodyard[8] that the beamwidth can be reduced and the power gain be increased by a factor of 1.8 by allowing the total phase delay along the array to exceed the total electrical length of the array by 180°; that is,

$$(n - 1)\alpha = (n - 1)S + 180°$$

This increase in gain is obtained at the cost of higher side-lobe levels (Fig. 5-16), along with a possible reduction in the broadband properties of such an array.

In actual practice, end-fire arrays frequently utilize parasitically excited elements such as the well-known Yagi-Uda antenna, the dielectric-rod antenna, and other forms of surface-wave antennas. These topics are considered in Chaps. 5 and 16, where the operation of these structures is treated in some detail. It should be noted that the parasitically driven structures are less susceptible to a detailed design procedure because of the larger number of parameters, so that much of the design is of a semi-empirical nature.

Tapered Distribution Arrays. The preceding discussions have dealt primarily with discrete arrays in which the elements all carried the same value of current. Although the uniform in-phase current distribution is the one which produces the greatest gain for a given length[16], it also produces relatively high values of side-lobe levels. For many applications, high side-lobe levels are undesirable since they may be responsible for unnecessary interference or, in the case of radar, for false target returns.

It is possible, in principle, to reduce the side-lobe levels of an array to as low a level as desired by the choice of an appropriate current distribution along a linear array. This is obtained at the expense of reduced gain and a larger beamwidth. The shape of a typical current distribution is such that the current tapers from a maximum value at the center of the array to some minimum value at the edges of the array. The exact nature of the radiated field pattern is, of course, a function of the distribution, and a considerable amount of work has been done on this subject.

For arrays with large numbers of discrete elements, the current distribution is frequently represented by a continuous function and the element excitation values determined by taking the ordinates of the function. The characteristics of these continuous functions are discussed in Secs. 2.9 and 5.3. When the number of elements is relatively small, say, less than 20, then the continuous-function representa-

tion is lacking in accuracy and it is desirable to represent the current distribution by a discrete number of terms.

Dolph-Tchebyscheff Distributions. One form of current distribution which has found considerable use in recent years is the Dolph-Tchebyscheff distribution,[9,10] whose properties are optimum in the sense that it will produce the narrowest beamwidth for a given side-lobe level and vice versa. This distribution enables the designer to select a desired side-lobe level and to compute the element excitation values in terms of a parameter related to the side-lobe level. Because of the properties of the Tchebyscheff polynomial, one can be certain that the design will produce the minimum beamwidth for a given side-lobe level and for a given length of array.
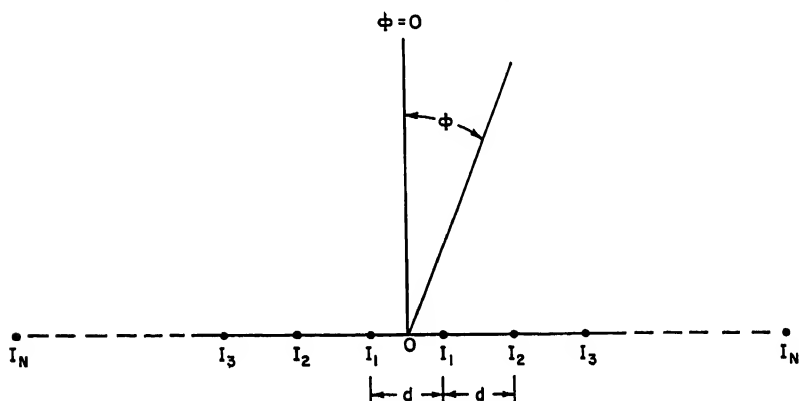
FIG. 2-15. Coordinates for broadside array of $2N$ elements.

(This excludes the so-called superdirectivity cases which are impractical from an engineering point of view; see Sec. 2.15.)

To simplify the design, the arrays discussed will consist of an even number of equally spaced elements with all currents in phase and symmetrically distributed about the center of the array, as shown in Fig. 2-15. It is also possible to carry through a similar design for an odd number of elements, but for most cases where an array is fed by a transmission-line system, the simplest feeder system results when there is an even number of elements, preferably in multiples of four.

Having chosen a number of elements equal to $2N$, the desired side-lobe ratio r is then chosen, where

$$r = \frac{\text{main-lobe maximum}}{\text{side-lobe level}}$$

The radiation pattern is then given by

$$E(\phi) = T_{2N-1}(z_0 \cos u)$$

where $T_{2N-1}(\ \ )$ is the Tchebyscheff polynomial of order $2N - 1$.

$$u = \frac{\pi d}{\lambda} \sin \phi$$

where d is the element spacing, $\lambda/2 \leq d < \lambda$, and z_0 is a parameter defined by

$$r = T_{2N-1}(z_0)$$

For purposes of computation, one convenient definition of the Tchebyscheff polynomial is as follows:

$$T_{2N-1}(z_0 \cos u) = \begin{cases} \cos\left[(2N-1)\cos^{-1}(z_0 \cos u)\right] & |z_0 \cos u| \leq 1 \\ \cosh\left[(2N-1)\cosh^{-1}(z_0 \cos u)\right] & |z_0 \cos u| \geq 1 \end{cases}$$

The parameter z_0, which is related to the side-lobe ratio, can be determined from

$$z_0 = \cosh\left[\frac{1}{2N-1}\cosh^{-1} r\right]$$

The above relationships are sufficient to derive all the radiation-pattern characteristics. A typical radiation pattern is shown in Fig. 2-16 where the side-lobe levels
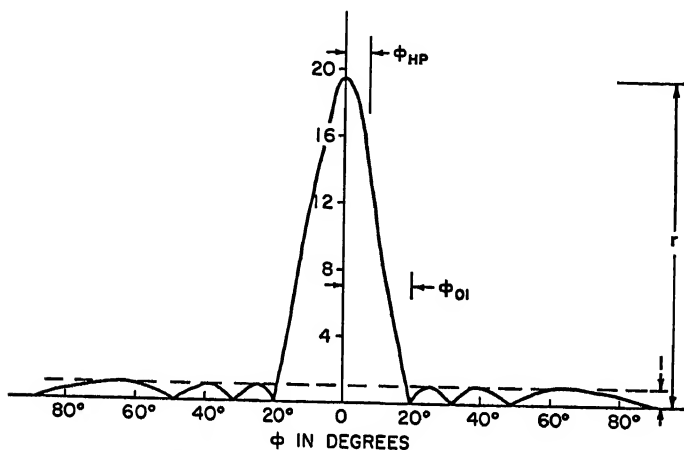
Fig. 2-16. Radiation pattern for Dolph-Tchebyscheff array.

have been normalized to unity and the maximum value of the main beam is given by r. The angles ϕ_{0k}, at which the pattern nulls occur, can be obtained by solving

$$\sin \phi_{0k} = \frac{\lambda}{\pi d}\cos^{-1}\left[\frac{1}{z_0}\cos\frac{(2k-1)\pi}{2(2N-1)}\right]$$

The first null is defined by $k = 1$, and the succeeding nulls by $k = 2, 3, 4, \ldots, N$.

The angle ϕ_{hp} at which the main beam has fallen to half power can be obtained by solving

$$\sin \phi_{hp} = \frac{\lambda}{\pi d}\cos^{-1}\left[\frac{1}{z_0}\cosh\left(\frac{1}{2N-1}\cosh^{-1}\frac{r}{\sqrt{2}}\right)\right]$$

If desired, the complete radiation pattern can also be plotted from the above relationships, although the characteristics given are the ones of major interest.

The element excitation values are readily determined once the side-lobe ratio r has been chosen and the parameter z_0 calculated. A separate set of relationships is necessary for each array consisting of $2N$ elements. Following are given the expressions for the relative current values of arrays of 4, 8, 12, and 16 elements, respectively:

4-element array:

$$I_2 = z_0^3$$
$$I_1 = 3I_2 - 3z_0$$

8-element array:

$$I_4 = z_0{}^7$$
$$I_3 = 7I_4 - 7z_0{}^5$$
$$I_2 = 5I_3 - 14I_4 + 14z_0{}^3$$
$$I_1 = 3I_2 - 5I_3 + 7I_4 - 7z_0$$

12-element array:

$$I_6 = z_0{}^{11}$$
$$I_5 = 11I_6 - 11z_0{}^9$$
$$I_4 = 9I_5 - 44I_6 + 44z_0{}^7$$
$$I_3 = 7I_4 - 27I_5 + 77I_6 - 77z_0{}^5$$
$$I_2 = 5I_3 - 14I_4 + 30I_5 - 55I_6 + 55z_0{}^3$$
$$I_1 = 3I_2 - 5I_3 + 7I_4 - 9I_5 + 11I_6 - 11z_0$$

16-element array:

$$I_8 = z_0{}^{15}$$
$$I_7 = 15I_8 - 15I_0{}^{13}$$
$$I_6 = 13I_7 - 90I_8 + 90z_0{}^{11}$$
$$I_5 = 11I_6 - 65I_7 + 275I_8 - 275z_0{}^9$$
$$I_4 = 9I_5 - 44I_6 + 156I_7 - 450I_8 + 450z_0{}^7$$
$$I_3 = 7I_4 - 27I_5 + 77I_6 - 182I_7 + 378I_8 - 378z_0{}^5$$
$$I_2 = 5I_3 - 14I_4 + 30I_5 - 55I_6 + 91I_7 - 140I_8 + 140z_0{}^3$$
$$I_1 = 3I_2 - 5I_3 + 7I_4 - 9I_5 + 11I_6 - 13I_7 + 15I_8 - 15z_0$$

For larger numbers of elements, the relationships become extremely lengthy. To conserve space the reader is referred to the original paper of Dolph[9] for the 20- and 24-element cases. For reference purposes, the relative current ratios vs. side-lobe level in decibels are shown plotted in Fig. 2-17. These curves should be used primarily as a check against an accurate computation, since for very low side-lobe levels the current values should be computed to an accuracy of at least three significant figures.

For arrays with more than 24 elements, the computations can become exceedingly laborious, since the terms in the series alternate in sign and a much greater number of significant figures is required for each term in order to end up with a final result of engineering accuracy.

An alternative method of obtaining the element coefficients for large arrays has been derived by van der Maas,[11] who showed that the envelope of the coefficients can be approximated by a continuous function, except for the current elements at the very ends of the antenna. The expression for the function is as follows:

$$f_1(\xi) = \frac{2J_1(jv\sqrt{1-\xi^2})}{jv\sqrt{1-\xi^2}} \qquad \text{for } |\xi| \neq 1$$

$$f_2(\xi) = \frac{2N-1}{v^2} \qquad \text{for } |\xi| = 1$$

where $\xi = 2x/l$

x = distance measured from center of array

l = total length of array

$2N$ = number of elements

$v = \log_\varepsilon (r + \sqrt{r^2 - 1}) \approx \log_\varepsilon 2r$

r = side-lobe ratio

$J_1(jv\sqrt{1-\xi^2})$ is the first-order Bessel function of imaginary argument for which tabulated values are available.[12,13]

In order to obtain the current amplitudes, $f_1(\xi)$ is plotted as a function of x and the value of $f_1(\xi)$ determined for the value of x corresponding to the location of an ele-
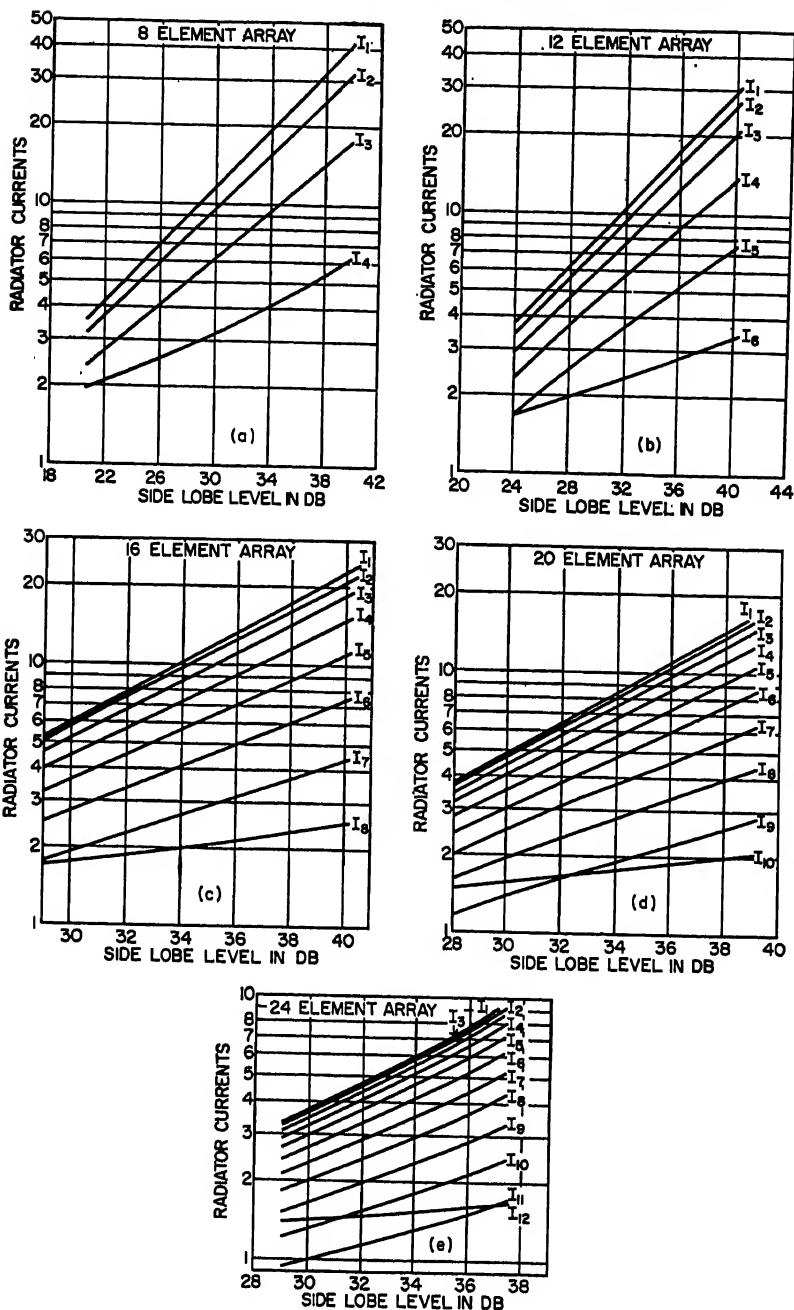
FIG. 2-17. Relative current ratio vs. side-lobe level for Dolph-Tchebyscheff array: (a) 8-element array. (b) 12-element array. (c) 16-element array. (d) 20-element array. (e) 24-element array.

ment.   This is done for each element except for the two elements on the extreme ends of the array.   The value of $f_2(\xi)$ is used for the end elements.   For arrays with side-lobe levels between 20 and 40 db down, the above expressions are good approximations even for arrays with as few as 20 elements.

It is usually of interest to know what half-power beamwidth may be expected from an array of given length and side-lobe ratio.   A good approximation for the Dolph-Tchebyscheff array has been given by Stegen,[14] which applies for arrays which are more than five wavelengths long.   The expression is as follows:

$$\phi = \frac{A\lambda}{\ell}$$

where A depends on the side-lobe level r.   Values of A are as follows:

r, db	A, deg
−20	51.1
−25	56.0
−30	60.6
−35	65.0
−40	68.7

It should be emphasized that all the preceding discussions are based on the fact that the element spacing lies between $\lambda/2$ and λ.   For element spacings shorter than $\lambda/2$, it is theoretically possible to obtain as narrow a beamwidth as desired by proper choice of the current amplitude and phase.[10]   However, as pointed out in Sec. 2.15, the so-called "supergain" case results in large amounts of stored energy along with high losses and limited bandwidth, so that little engineering use can be made of this possibility.

For element spacings as large as a wavelength, it is possible for a secondary beam to appear along the line of the array unless the individual elements have sufficient directivity to suppress the secondary beam.   Because of this problem, typical arrays generally have element spacings in the range of 0.5 to 0.75λ.

Two other points are of interest with regard to the Dolph-Tchebyscheff array. When a large number of elements are used, the current in the end elements can be considerably higher[11] than in the adjacent elements, as may be seen from the expression for $f_2(\xi)$.   This can raise serious problems with regard to feeding the end elements, particularly in the case of the waveguide-fed slot array, although the problem is by no means trivial in the case of the transmission-line-fed array.   Since the side-lobe level may be critically dependent on the end elements, caution should be exercised in choosing a design in which the values for the currents in the end elements exceed the currents in the adjacent elements by very much more than 50 per cent.

Also, for some antenna applications, it may be a disadvantage for the side lobes to remain at a constant level as the angular separation from the main beam increases. Actually, a certain amount of decrease in the side lobes will occur, depending on the directivity of the individual elements.   For applications where this rate of decrease is not sufficient, it is necessary to use a form of current distribution whose space factor is such that the side lobes do decrease at the desired rate.   Although relationships for such a radiation pattern have not been worked out for the discrete-element case in the same manner as the Tchebyscheff pattern, considerable work has been done on continuous distributions.   This is discussed in Sec. 2.9.   Although these distributions apply rigorously only for continuously excited apertures, excellent results can be obtained by dividing these distributions into discrete elements when the array contains more than 25 or 30 elements.

2.9. DIRECTIVITY PATTERNS FROM CONTINUOUS LINE SOURCES

For antenna systems which have apertures which are very large in terms of wavelength, it is frequently desirable to use a continuous type of aperture distribution because of the relative simplicity, as compared with a discrete-element type of array which requires a large number of driven elements. For instance, a common form of large-aperture antenna is a paraboloidal reflector illuminated by a point-source feed. To replace an aperture of the order of 100 wavelengths in diameter by a discrete-element array would require more than 5,000 individual radiating elements, each of which must be fed with current of the correct amplitude and phase.

It is apparent for very large apertures that a reflector type of antenna is considerably simpler than a discrete element array. In addition, the reflector can be made to operate over a wide range of frequency simply by changing the feed, while a discrete element array can operate efficiently only over a small bandwidth, on the order of 15 to 40 per cent at most. Where very low side-lobe levels are required, discrete arrays have a substantial advantage over reflector-type structures since it is possible to obtain side-lobe levels of 40 db down and greater by exercising considerable care in designing and constructing discrete element arrays. By comparison, reflector-type antenna systems have side-lobe levels in the range of 18 to 25 db down, and at the present state of the art it seems unlikely that side-lobe levels much lower than 35 db down can be achieved with a reflector system. Use of a two-dimensional folded reflector system will offer some improvement because of the elimination of blocking by the feed and its supports, but even for this type of structure special techniques are necessary to achieve side-lobe levels lower than 30 db down.

Although the continuous-aperture type of antenna has its practical limitations with regard to very low side-lobe performance, it nevertheless has found wide application because of its relative simplicity. For this reason, it is desirable to know what can be expected of various types of ideal distribution functions since these in effect place an upper limit on the potential performance of a continuous antenna. Also, for very long arrays of discrete elements, the continuous distribution may be used to obtain an excellent approximation to the element excitation coefficients.

Line-source Distributions. For line sources, the current distribution is considered to be a function of only a single coordinate. The directivity pattern $E(u)$ resulting from a given distribution is simply related to the distribution by a finite Fourier transform,[15–17] as given below:

$$E(u) = \frac{\ell}{2} \int_{-1}^{+1} f(x)\, e^{jux}\, dx$$

where $f(x)$ = relative shape of field distribution over aperture as a function of x
$u = (\pi\ell/\lambda)\sin\phi$
ℓ = over-all length of aperture
ϕ = angle measured from normal to aperture
x = normalized distance along aperture $-1 \leq x \leq 1$

The simplest type of aperture distribution is the uniform distribution where $f(x) = 1$ along the aperture and is zero outside of the aperture. The directivity pattern is given as

$$E(u) = \ell\, \frac{\sin u}{u} = \ell\, \frac{\sin\left[\left(\dfrac{\pi\ell}{\lambda}\right)\sin\phi\right]}{\left(\dfrac{\pi\ell}{\lambda}\right)\sin\phi}$$
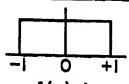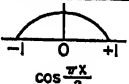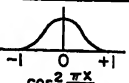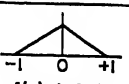
This type of directivity pattern is of interest because of all the constant-phase distributions, the uniform distribution gives the highest gain.[15] As in the case of the

discrete-element uniform distribution, it also has high side-lobe levels, the intensity of the first side lobe being 13.2 db down from the maximum.

The intensity of the side-lobe levels can be reduced very considerably by tapering the aperture distribution in such a way that the amplitude drops off smoothly from the center of the aperture to the edges. There are an unlimited number of possible distributions. However, a few simple types of distributions are typical and illustrate how the beamwidth, side-lobe level, and relative gain vary as a function of the distribution. Table 2-3 gives the important characteristics of several distributions having a simple mathematical form.

Table 2-3. Line-source Distributions

TYPE OF DISTRIBUTION $-1 \leq x \leq 1$	DIRECTIVITY PATTERN $E(u)$		HALF POWER BEAMWIDTH IN DEGREES	ANGULAR DISTANCE TO FIRST ZERO	INTENSITY OF 1st SIDELOBE db BELOW MAX.	GAIN FACTOR
$f(x)=1$	$l\,\dfrac{\sin u}{u}$		$50.8\dfrac{\lambda}{l}$	$57.3\dfrac{\lambda}{l}$	13.2	1.0
$f(x)=1-(1-\Delta)x^2$	$l(1+\chi)\dfrac{\sin u}{u}$ $\chi=(1-\Delta)\dfrac{d^2}{du^2}$	$\Delta=$ 1.0	$50.8\dfrac{\lambda}{l}$	$57.3\dfrac{\lambda}{l}$	13.2	1.0
		.8	$52.7\dfrac{\lambda}{l}$	$60.7\dfrac{\lambda}{l}$	15.8	.994
		.5	$55.6\dfrac{\lambda}{l}$	$65.3\dfrac{\lambda}{l}$	17.1	.970
		0	$65.9\dfrac{\lambda}{l}$	$81.9\dfrac{\lambda}{l}$	20.6	.833
$\cos\dfrac{\pi x}{2}$	$\dfrac{\pi l}{2}\dfrac{\cos u}{(\frac{\pi}{2})^2-u^2}$		$68.8\dfrac{\lambda}{l}$	$85.9\dfrac{\lambda}{l}$	23	.810
$\cos^2\dfrac{\pi x}{2}$	$\dfrac{l}{2}\dfrac{\sin u}{u}\dfrac{\pi^2}{\pi^2-u^2}$		$83.2\dfrac{\lambda}{l}$	$114.6\dfrac{\lambda}{l}$	32	.667
$f(x)=1-|x|$	$\dfrac{l}{2}\left(\dfrac{\sin\frac{u}{2}}{\frac{u}{2}}\right)^2$		$73.4\dfrac{\lambda}{l}$	$114.6\dfrac{\lambda}{l}$	26.4	.75

Of considerable interest is the manner in which the side lobes fall off as the angle from the main beam increases or as u increases. For the uniform distribution which has a discontinuity in both the function and its derivatives at the edge of the aperture, the side lobes decrease as u^{-1}. For the gable distribution or for the cosine distribution, both of which are continuous at the edge of the aperture but which have a discontinuous first derivative, the far-out side lobes fall off as u^{-2}. For the cosine-squared distribution which has a discontinuous second derivative, the far-out side lobes fall off as u^{-3}.

Many distributions actually obtained in practice can be approximated by one of the simpler forms or by a combination of simpler forms. For instance, suppose it were desired to find the directivity pattern of a cosine-squared distribution on a pedestal, i.e., a combination of a uniform distribution and a cosine-squared distribution as given by

$$f(x) = C + \cos^2\frac{\pi x}{2}$$

The resulting directivity pattern is then obtained directly by adding the two functions for the directivity pattern as follows:

$$E(u) = C\ell \frac{\sin u}{u} + \frac{\ell}{2} \frac{\sin u}{u} \frac{\pi^2}{\pi^2 - u^2}$$

It should be noted that the side lobes and other characteristics of the pattern must be obtained from the new directivity pattern and cannot be interpolated from Table 2-3. It is of some interest to note that by choosing the proper relative intensities of a uniform distribution and a cosine-squared distribution, it is possible to obtain a theoretical side-lobe level which is very low. For instance, if $C = 0.071$, then the intensity of the largest side lobe will be 43 db below the maximum of the main beam with a half-power beamwidth given by 76.5λ/ℓ, a value which is somewhat lower than that for the cosine-squared distribution by itself.

In recent years, work has been done on line-source distributions which produce patterns approaching the Tchebyscheff type of pattern in which all the side lobes have a constant level. As noted in Sec. 2.8, van der Maas has shown that it is possible to find the element excitations for a discrete array with a large number of elements by determining the shape of the envelope function as the number of elements is increased indefinitely.

This problem has also been investigated in detail by Taylor[18] for the case of a continuous line-source distribution. Of considerable interest is the relationship between the half-power beamwidth vs.

Fig. 2-18. Half-power beamwidth vs. side-lobe ratio for an ideal space factor.

the side-lobe ratio for the ideal space factor (i.e., the equal side-lobe type of space factor) since this relationship represents the limits of the minimum beamwidth that can be obtained for a given side-lobe level. Figure 2-18 is taken from Taylor's paper. For the details of computing the desired space factor, the reader is referred to the original paper.[18]

For many applications, the equal-side-lobe-level pattern may be undesirable and a more suitable pattern would be one in which the side lobes decrease as the angle from the main beam, or the parameter u, increases. Work on this form of distribution has been carried out by Taylor[19] in an unpublished memorandum. Basically, the approach is to represent the directivity pattern by a function of the form

$$E(u) = \frac{\sin \sqrt{u^2 - \pi^2 B^2}}{\sqrt{u^2 - \pi^2 B^2}}$$

where the ratio of the main beam to the first side lobe is given by

$$R = 4.603 \frac{\sinh \pi B}{\pi B}$$

When B is equal to zero, the directivity pattern reduces to the familiar $\sin u/u$ for the case of a uniform distribution and the first side-lobe ratio is 4.603, or 13.2 db.

As B is increased in value, the side-lobe ratio increases, and by the appropriate choice of B a theoretical side-lobe level as low as desired can be chosen. It will be noted that because of the expression for the directivity, at large values of u, the side lobes decrease as $1/u$. Hence we have a directivity pattern whose side lobes decrease in a similar fashion to that of the uniform distribution but has the property that the maximum side-lobe level can be arbitrarily chosen.

Fortunately, the aperture distribution function for this type of pattern has a relatively simple form and is given by

$$f(x) = J_0(j\pi B \sqrt{1 - x^2}) \qquad |x| \le 1$$
$$= 0 \qquad |x| > 1$$

J_0 is a Bessel function of the first kind with an imaginary argument. Tables of this function are readily available.[12,13]

Taylor has tabulated the important characteristics of this type of distribution, and some of these data have been plotted in Fig. 2-19. By comparing Fig. 2-18 with Fig. 2-19 it can be seen that for a given maximum side-lobe level, the half-power beam-width of the distribution producing a decreasing side-lobe pattern is approximately 12 to 15 per cent greater than the per cent half-power beamwidth of the distribution which produces an equal side-lobe pattern. This nominal loss in theoretical performance is a small price to pay where it is necessary that the side-lobe levels decrease as the angle from the main beam increases. When a decreasing side-lobe level which falls off inversely as the first power of the angle is desired, this type of distribution will result in a narrower beamwidth than those distributions which produce side lobes falling off as a higher inverse power of the angle.

FIG. 2-19. Half-power beamwidth vs. side-lobe ratio for space factor defined by

$$E(u) = \frac{\sin \sqrt{u^2 - \pi^2 B^2}}{\sqrt{u^2 - \pi^2 B^2}}$$

2.10. PATTERNS FROM AREA DISTRIBUTIONS

Rectangular Apertures. The directivity pattern of an area distribution is found in a similar manner to that used for line-source distributions except that the aperture field is integrated over two dimensions instead of one dimension. If the aperture distribution is given by $f(x,y)$, where x and y are the two coordinates, then the directivity pattern is given by

$$E(\theta,\phi) = \iint f(x,y)e^{j\beta \sin \theta(x \cos \phi + y \sin \phi)} \, dx \, dy$$

The difficulty of evaluating this expression will depend on the form of the distribution function. For many types of antennas, such as the rectangular horn, for example, the distribution function is separable; that is,

$$f(x,y) = f(x)f(y)$$

The directivity patterns in the principal planes are readily determined for the separable case since the pattern in the xz plane is identical with the pattern produced by a

line-source distribution $f(x)$, while the pattern in the yz plane is identical with the pattern produced by a line-source distribution $f(y)$.

For those cases where the distribution function is not separable, the integral must be evaluated either analytically or graphically.

Circular Apertures. An antenna that is frequently used in microwave application is a paraboloid having circular symmetry. The radiation pattern may be computed by projecting the field distribution on the paraboloid to a plane at the opening of the paraboloid and computing the directivity pattern due to the plane aperture.

If the field in the aperture plane is a function of the normalized radius r and the aperture angular coordinate ϕ', then the directivity pattern is given by[15]

$$E(u,\phi') = a^2 \int_0^{2\pi} \int_0^1 f(r,\phi')\, e^{jur\cos(\phi-\phi')}\, r\, dr\, d\phi'$$

where a = radius at outside of aperture
ρ = radius at any point of aperture
$r = \rho/a$
$u = (2\pi a/\lambda)\sin\theta = (\pi D/\lambda)\sin\theta$
$D = 2a$ = aperture diameter

and $f(r,\phi')$ is the normalized aperture distribution function. The coordinates are as shown in Fig. 2-20.

The simplest forms of aperture distributions to evaluate are those where the distribution is not dependent on the angular coordinate ϕ' but depends only on the radial coordinate r. The integral for the directivity pattern then becomes

$$E(u) = 2\pi a^2 \int_0^1 f(r) J_0(ur)\, r\, dr$$

When the distribution is constant, the integral becomes

$$E(u) = 2\pi a^2 \frac{J_1(u)}{u}$$

Fig. 2-20. Coordinates for circular aperture.

It is frequently desired to evaluate the directivity pattern for an illumination which tapers down toward the edge of the aperture. One function which is convenient for representing the aperture distribution is

$$f(r) = (1 - r^2)^p$$

This function behaves in a similar fashion to the nth-power distributions as discussed for the line-source case (Sec. 2.9). When the exponent increases, the distribution becomes more highly tapered and more concentrated in the center of the aperture. When the exponent decreases and approaches zero, the distribution approaches uniform illumination.

Evaluating the directivity pattern, we have

$$E(u) = 2\pi a^2 \int_0^1 (1 - r^2)^p J_0(ur)\, dr$$

$$= \pi a^2 \frac{2^p p!\, J_{p+1}(u)}{u^{p+1}} = \frac{a^2}{p+1} \Lambda_{p+1}(u)$$

Both the Bessel functions $J_{p+1}(u)$ and the Lambda function $\Lambda_{p+1}(u)$ are available in tabular form.[12]

Table 2–4.   Circular Aperture Distributions.

TYPE OF DISTRIBUTION $0 \leq r \leq 1$	DIRECTIVITY PATTERN $E(u)$	HALF POWER BEAMWIDTH IN DEGREES	ANGULAR DISTANCE TO FIRST ZERO	INTENSITY OF 1st SIDELOBE db BELOW MAX.	GAIN FACTOR
$f(r) = (1-r^2)^0 = 1$	$\pi a^2 \dfrac{J_1(u)}{u}$	$58.9 \dfrac{\lambda}{D}$	$69.8 \dfrac{\lambda}{D}$	17.6	1.00
$f(r) = (1-r^2)$	$2\pi a^2 \dfrac{J_2(u)}{u^2}$	$72.7 \dfrac{\lambda}{D}$	$93.6 \dfrac{\lambda}{D}$	24.6	0.75
$f(r) = (1-r^2)^2$	$8\pi a^2 \dfrac{J_3(u)}{u^3}$	$84.3 \dfrac{\lambda}{D}$	$116.2 \dfrac{\lambda}{D}$	30.6	0.56

The principal characteristics of the directivity patterns are given in Table 2-4 for the cases $p = 0, 1, 2$. Comparison of the patterns of the uniformly illuminated circular aperture (i.e., when $p = 0$) with the results for the uniformly illuminated line source (Sec. 2.9) shows that the circular aperture has a lower side-lobe level and a broader beamwidth. This would be expected since projection of the circular-aperture illumination on to a line would produce an equivalent line source which is no longer uniform but has some degree of tapering.

Elliptical Apertures. In some applications an elliptically shaped reflector is used in order to permit control of the relative beamwidth in the two principal planes and to control the side lobes by shaping the reflector outline. Computation of the directivity patterns for this aperture shape can be carried out from a knowledge of the Fourier components of the illumination function over the aperture. Details of the computation are given in Chap. 12, which contains a tabulation of the functions used in this computation.

2.11. EFFECTS OF PHASE ERRORS ON LINE SOURCES

The previous discussions on aperture distributions in Sec. 2.8 to 2.10 were concerned only with those aperture distributions in which the field was in phase across the entire array. In certain types of antenna systems, particularly those in which the beam is to be tilted, deviations from a uniform phase front do occur, so that it is desirable to evaluate the effects of phase errors on the directivity pattern.

For simplicity, the following discussions are limited to the case of a line-source distribution. Results will be first derived for the simple uniform amplitude distribution, and graphical results will be presented for a tapered amplitude distribution.

The most common phase-front errors are the linear, quadratic, and cubic phase errors. The linear phase error is expressed simply by

$$\Phi(x) = \beta_1 x$$

FOURIER TRANSFORMS OF EXP $(j\beta x^2)$
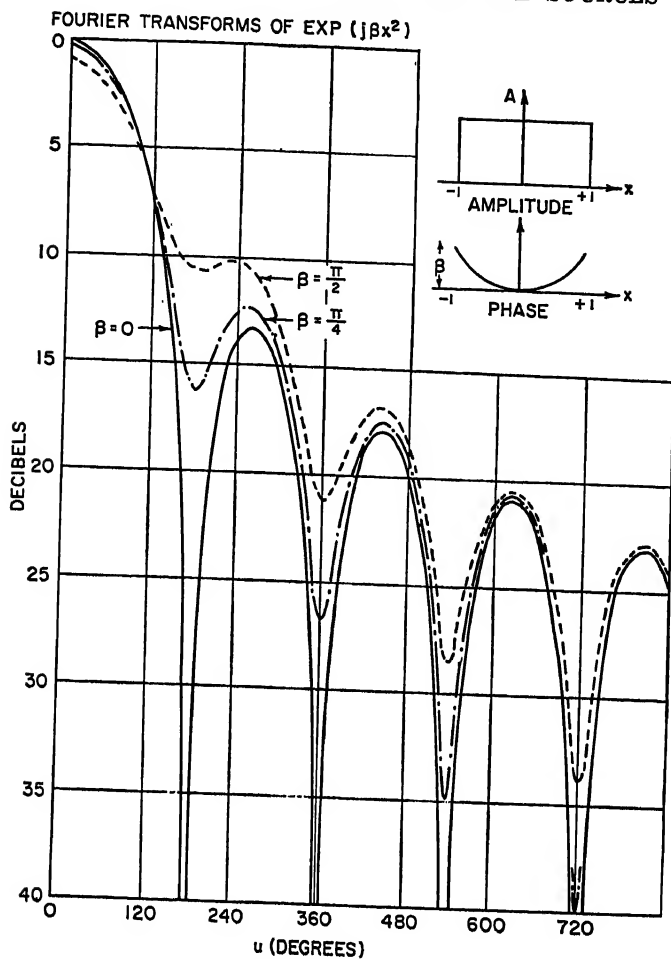
FIG. 2-21a. Effects of square-law phase error in radiation patterns for uniform aperture illumination.

where β_1 = phase departure at edge of aperture
    x = aperture coordinate as defined in Sec. 2.9
The directivity pattern is given by

$$E(u) = \frac{\ell}{2} \int_{-1}^{1} f(x)\, e^{jux}\, e^{-j\beta_1 x}\, dx$$

For a uniform illumination, the result is

$$E(u) = \ell\, \frac{\sin (u - \beta_1)}{u - \beta_1}$$

Thus the directivity pattern has the same form as for the in-phase case except that the pattern maximum is shifted in angle as defined by

$$u = \beta_1 \qquad \text{or} \qquad \sin \phi_0 = \frac{\beta_1 \lambda}{\pi \ell}$$
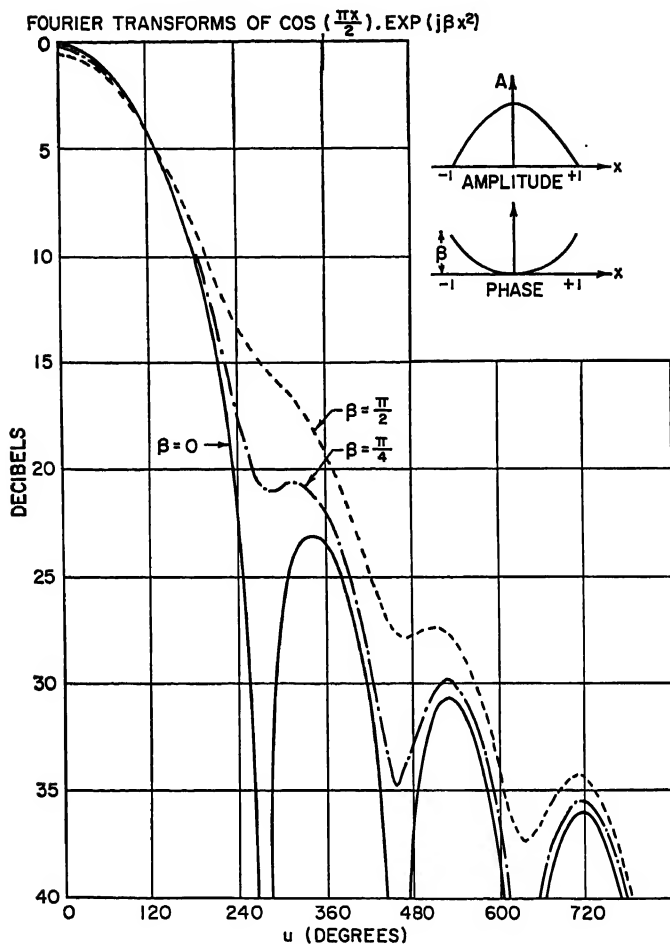
FIG. 2-21b. Effects of square-law phase error in radiation patterns for cosine aperture illumination.

For other than a uniform illumination, the patterns will also be the same as for the in-phase case, except that $u - \beta_1$ is substituted for u in the expression for the directivity.

In the vicinity of the main beam, the directivity pattern is the same as that of an aperture tilted by ϕ_0 whose length is $l \cos \phi_0$. The half-power beamwidth is increased by the factor $1/\cos \phi_0$, while the gain is decreased by $\cos \phi_0$. For small angles of beam tilt, the pattern and gain are affected by only a minor amount.

The quadratic, or square-law, phase error is inherent in flared horn antennas. It also occurs in lens-type antennas and reflector antennas when the feed is defocused along the axis of symmetry. This type of phase error also appears when the directivity pattern of an antenna is measured at a finite distance.

The quadratic phase error is expressed by

$$\Phi(x) = \beta_2 x^2$$
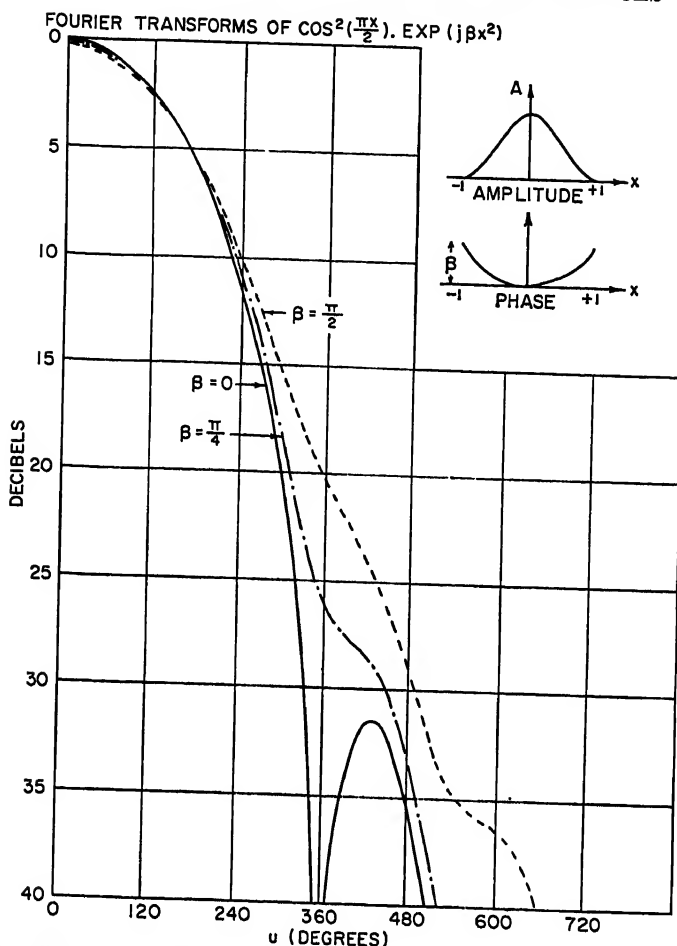
FIG. 2-21c. Effects of square-law phase error in radiation patterns for cosine-squared aperture illumination.

and the directivity pattern is expressed by

$$E(u) = \frac{\ell}{2} \int_{-1}^{1} f(x)\, e^{jux}\, e^{-j\beta_2 x^2}\, dx$$

The integral is not readily evaluated except when $f(x)$ is constant or one of the cosine distributions. For these cases, the directivity can be expressed in terms of the Fresnel integrals. The directivity pattern for the uniformly illuminated case is given by[1,2]

$$E(u) = \frac{\ell}{2} \sqrt{\frac{\pi}{2\beta_2}} \{ C(m_2) - C(m_1) - j[S(m_2) - S(m_1)] \}$$

where

$$m_2 = \sqrt{\frac{2\beta_2}{\pi}} \left(1 - \frac{u}{2\beta_2} \right)$$

$$m_1 = \sqrt{\frac{2\beta_2}{\pi}} \left(-1 - \frac{u}{2\beta_2} \right)$$
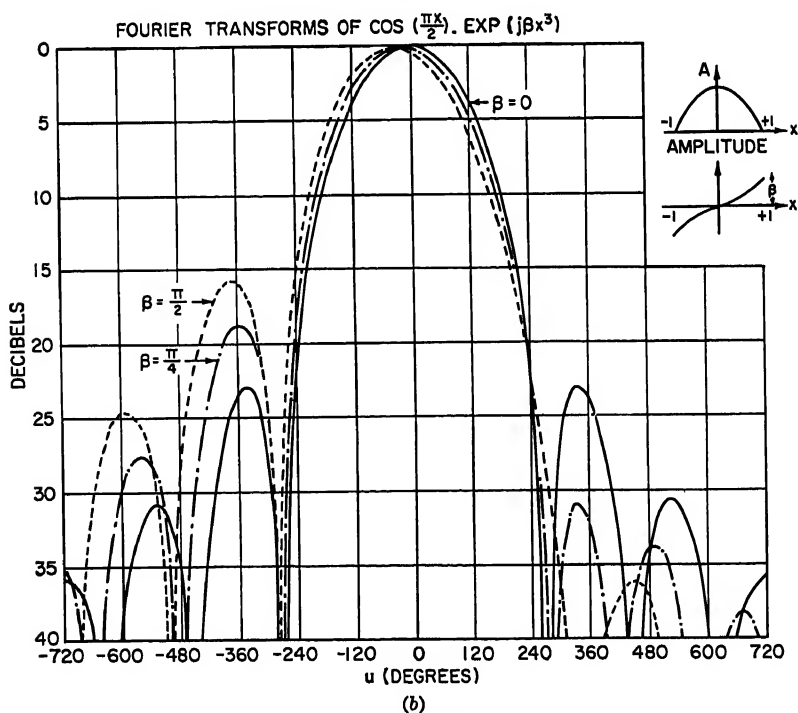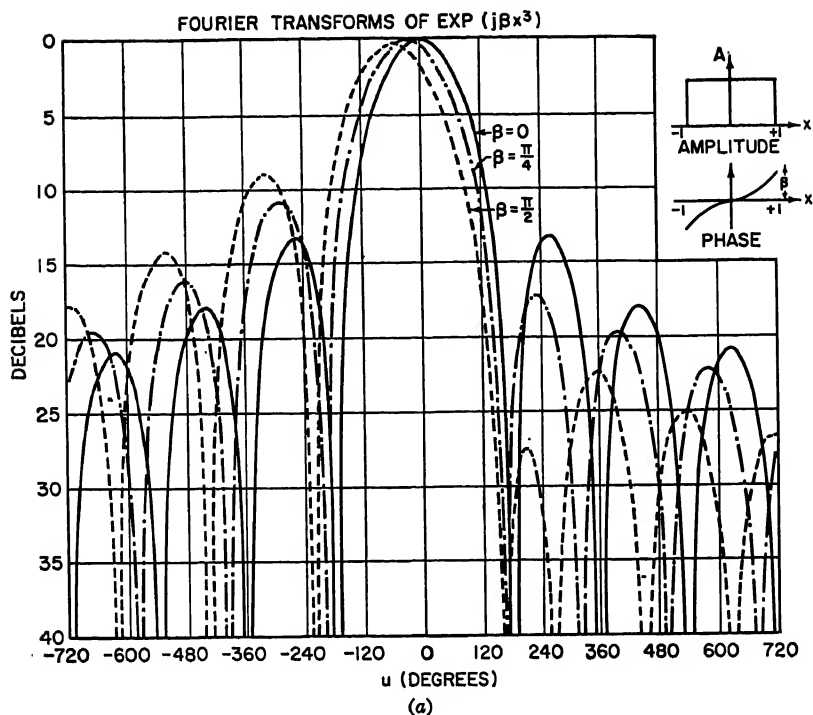
FIG. 2-22. Effects of cubic phase error on radiation pattern: (a) For uniform aperture illumination. (b) For cosine aperture illumination.

and the Fresnel integrals are defined by

$$C(m) = \int_0^m \cos\left(\frac{\pi}{2} y^2\right) dy$$

$$S(m) = \int_0^m \sin\left(\frac{\pi}{2} y^2\right) dy$$

The expressions for the cosine and higher-order cosine distributions become increasingly complicated and the problem of computation becomes exceedingly laborious. Some simplification in the computation problem can be obtained by the use of operational methods as developed by Spencer[16] and also by Milne.[20] Figure 2-21a–c is reproduced from Milne's paper.

It will be noted that the principal effects of a quadratic phase error are a reduction in gain and an increase in side-lobe amplitude on either side of the main beam. For
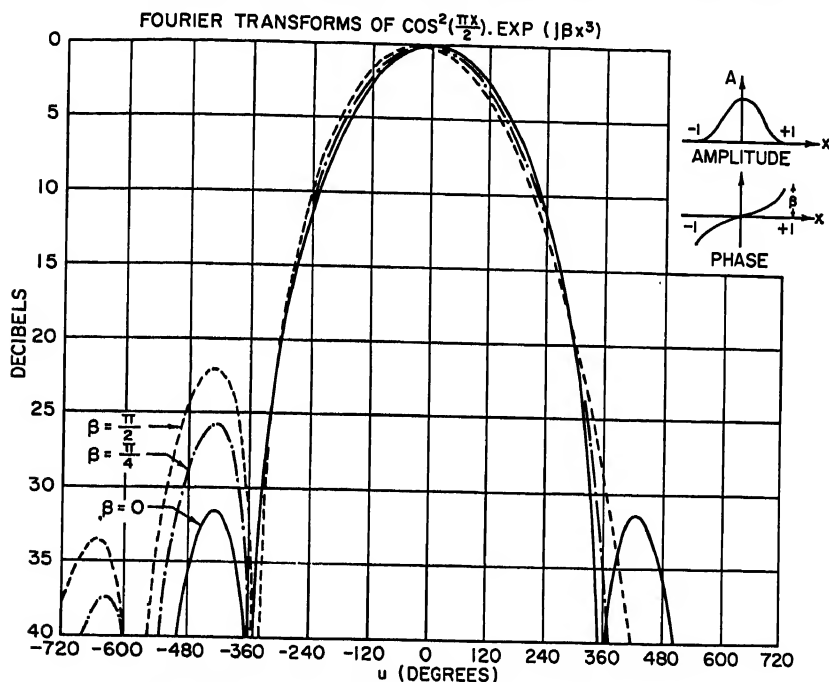
FIG. 2-22. (c) For cosine-squared aperture illumination.

moderate amounts of phase error, the nulls between the side lobes disappear and the side lobes blend into the main beam, appearing as shoulders rather than as separate side lobes.

The cubic phase error is expressed by

$$\Phi(x) = \beta_3 x^3$$

Computation of the directivity integrals for the cubic phase error becomes even more laborious than for the quadratic phase error, although the use of operational methods for computation simplifies the formal handling of the problem. Some typical results from Milne's paper are given in Fig. 2-22a–c.

It will be observed that the cubic phase error produces a tilt of the beam in addition to a loss in gain. The side lobes on one side of the beam increase in amplitude, while those on the other side diminish.

In general, when the feed is moved off axis to tilt the beam, both a linear phase term and a cubic phase term appear. The linear phase term causes a beam tilt which is a function of the geometry of the antenna system. For the case of a parabolic reflector, the cubic phase term causes a lesser amount of tilt in the opposite sense so that the resulting beam tilt is somewhat less than would be computed from geometrical considerations. For this case, the side-lobe increase appears on the side of the beam toward the axis.

2.12. EFFECTS OF RANDOM ERRORS ON GAIN AND SIDE LOBES

The previous section has discussed the effect of systematic phase errors on several different types of aperture distributions. In general, some of these errors are inherent in a given design and are a function primarily of the geometry of the antenna. In addition to systematic errors, a problem which commonly arises is that caused by random errors in both the phase and the amplitude across the aperture because of manufacturing tolerances.

An estimate of the effect of random errors can be made in at least three different ways. The first method is to measure directly the radiation performance of the antenna in question. By comparison with the computed performance, it is possible to estimate the magnitude of the errors in the field distribution across the antenna.

A second method is to measure the amplitude and phase of the field distribution across the aperture. From these data, the effect of the errors on the antenna performance can be computed.

A third method is to compute the effect of manufacturing tolerances on the desired aperture distribution and from this, in turn, to compute the effect on the radiating properties of the antenna. This method is of considerable interest to the antenna designer, who must specify what sort of tolerances are necessary in order to achieve a desired result. As is true in all fabrication work, extremely tight tolerances result in excessive costs while tolerances that are too loose can result in inadequate performance or failure of operation. It is therefore desirable to know how much accuracy is required for a given level of performance.

A theory of random errors is necessarily based on statistical considerations, so that the results predicted will not be on an absolute basis but rather in terms of a given probability level. The main use of this theory is to estimate what the effect will be on the average performance of a large number of antennas when a given tolerance level is specified.

Discrete Element Arrays. The problem of the discrete element array starts off with the premise that the ideal radiation pattern desired is specified by a uniformly spaced array of N elements, with each element carrying a specified current. If we denote the current in the nth element by I_n and the actual current by $I_n + \epsilon_n I_n$, then the radiation pattern due to the desired currents is given by

$$E(\phi) = \sum_{n=1}^{N} I_n \exp\left(j\,\frac{2\pi n d}{\lambda} \sin \phi \right)$$

where d = spacing between elements
  ϕ = angle measured from normal to array
The radiation pattern due to the error terms is given by

$$R(\phi) = \sum_{n=1}^{N} \Delta_n I_n \exp\left(j\delta'_n \right)$$

where $\delta_n' = \delta_n + (2\pi nd/\lambda)\sin\phi$

Δ_n = ratio error of nth current

δ_n = phase error

It can readily be seen that the desired radiation pattern $E(\phi)$ is altered by the addition of the error-term radiation pattern $R(\phi)$. If measured data are available for the individual element currents, then it is possible to compute $R(\phi)$ exactly, even though this may be a rather laborious process.

As is often the case, experimental data are not available beforehand and it is desirable to know what degree of precision is required in driving the array in order to achieve a given performance. For a large number of elements and for small errors, it is reasonable to assume that the individual errors are independent of one another and are distributed as a normal or Gaussian distribution. The problem has been treated on a statistical basis by Ruze,[21] who has computed the side-lobe-level probabilities in terms of the root-mean-square error in the current values.

In statistical analysis, it is not possible to predict the exact pattern of a particular array with errors but rather the average pattern of a large number of similar arrays. If $\overline{P(\phi)}$ denotes the power pattern for an "average system," $P_0(\phi)$ the power pattern for an antenna without errors, we have

$$\overline{P(\phi)} = P_0(\phi) + S(\phi)\overline{\epsilon^2}\frac{\Sigma I_n^2}{(\Sigma I_n)^2}$$

where $S(\phi)$ = a slowly varying function closely related to power pattern of a single element

$\overline{\epsilon^2} = \overline{\Delta^2} + \overline{\delta^2}$

$\overline{\epsilon^2}$ = total mean-square error

$\overline{\Delta^2}$ = mean-square amplitude error

$\overline{\delta^2}$ = mean-square phase error, radians squared

On the average, then, the effect of the random errors is to add to the pattern a constant power level which is proportional to the mean-square error. For individual arrays and in particular directions, the side-lobe radiation will differ from this constant level in a fashion governed by the probability distribution for the particular array.

It is of interest to note that the spurious radiation is approximately proportional to $1/N$, so that for a given mean-square error, lower side-lobe levels are more readily obtained with larger antennas.

Computations have been made for a Dolph-Tchebyscheff type of array consisting of 25 elements with a design side-lobe level of 29 db below the main beam. For an angular position where the no-error minor lobes have maxima, Fig. 2-23 shows the probability that the radiation will be below a specified number of decibels when a given mean error exists in the antenna currents.

As a check on the above theory, Ruze has computed the actual pattern of the 25-element antennas with a specific set of error currents. For a 0.40-rms error in each element with random phase, the radiation pattern was computed. Figure 2-24 shows the theoretical patterns for the cases with and without error. Analysis of the side-lobe magnitudes on this figure shows that their distribution compares very well with the theoretical distribution obtained on a statistical basis.

The loss in gain can also be determined from this analysis. An excellent approximation for the actual gain G with errors as compared with the theoretical gain G_0 when no errors are present is given by

$$\frac{G}{G_0} \approx \cfrac{1}{1 + \left(\frac{3\pi}{4}\right)\left(\frac{d}{\lambda}\right)^2\overline{\epsilon^2}}$$
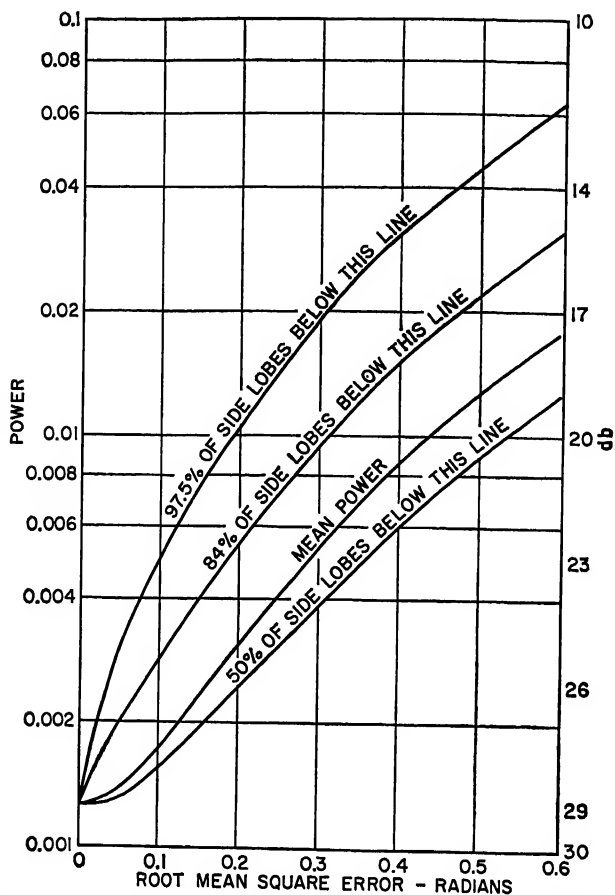
Fig. 2-23. Side-lobe distribution for 25-element broadside array. Designed for 29-db side-lobe suppression. Computed at design-lobe maxima.
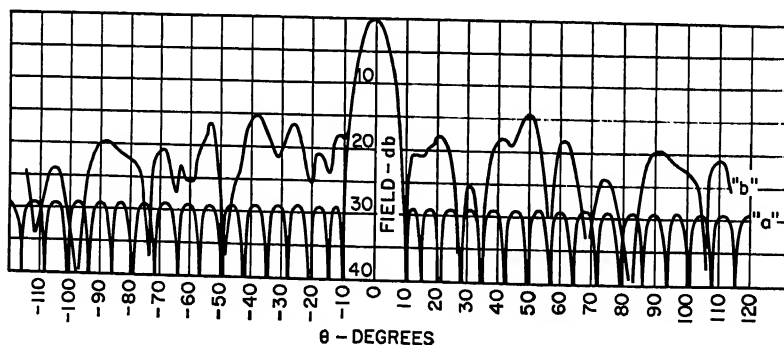
Fig. 2-24. Theoretical effect of error currents on radiation pattern of 25-element broadside array designed for 29-db side-lobe suppression: (a) No error. (b) 0.40 rms error in each element at random phase.

where d = spacing between elements

λ = wavelength

The above analysis has concerned itself only with the accuracy of the current values required for the array. To translate these results into mechanical tolerances for a given antenna system depends on the nature of the individual elements, the type of feed system used, and a variety of other factors. One particular array which readily lends itself to this type of analysis is a waveguide-fed shunt-slot linear array. Some results for an X-band waveguide array have been obtained in Refs. 22 and 23. In the latter reference, computations for the probable side-lobe level have been made for a manufacturing tolerance with a standard deviation of 0.002 in. in a Dolph-Tchebyscheff array. The effect of the design side-lobe level and the number of elements is readily shown in Table 2-5.

Table 2-5. 84 Per Cent of the Side-lobe Levels Will Be Less Than the Tabulated Value

No. of elements	Design side-lobe level, db		
	20	30	40
12	18.6	25.9	29.1
24	19.0	26.7	31.8
48	19.1	27.3	33.3

It should be noted that the figures in Table 2-5 are based on a normal distribution where the tolerances can take on all values but have a standard deviation of 0.002 in. In actual manufacturing practice, physical dimensions are not allowed to deviate from the design value by more than an arbitrary amount so that the tolerance distribution is actually a truncated normal distribution. For this condition, the deterioration in side-lobe level is somewhat less than that given.

Two conclusions can be drawn regarding the effect of random errors in discrete element arrays.

1. For a given side-lobe level, the effect of random errors becomes somewhat less critical as the number of elements in an array increases.

2. For a given number of array elements, the effect of random errors becomes more critical as the required side-lobe level is further suppressed.

As a practical matter, when designing low-side-lobe-level arrays, it is usually necessary to overdesign the array in order to be certain of achieving the desired side-lobe level in the presence of random errors. For instance, to attain a 26-db side-lobe level, it may be desirable to design the aperture distribution for a 32-db side-lobe level. Actually, the amount of overdesign required depends on a compromise between economical manufacturing tolerances and the loss in aperture efficiency due to the overdesign.

Continuous Apertures. The statistical analysis of continuous apertures, such as reflector-type antennas, is similar to that for discrete element arrays, except for two important differences. For the discrete array, the error in one element has been assumed to be independent of the errors in adjacent elements. However, for a continuous aperture array, a large error at one point implies that the error will be large in the immediate area around that point since the error could be due to warping of the reflector or a bump in the reflector. Also, the error will be purely a phase error since the amplitude distribution will be essentially unaffected by moderate changes in the reflector surface.

The fact that an error will extend over an area makes it convenient to use the

concept of a correlation interval c. c is that distance, on the average, where the errors become essentially independent of one another.   For instance, an error consisting of a bump extending over a large area implies a large value of c, while errors consisting of a number of bumps, each of which covers a small area, implies a small value of c.

In an analysis similar to that for the discrete array it has been shown[21] that the power pattern for "an average system" with small errors is given by

$$\bar{P}(\phi) = P_0(\phi) + S(\phi)\frac{4c^2\pi^2\overline{\delta^2}}{\lambda^2 G_0}\exp\left(-\frac{\pi^2c^2\sin^2\phi}{\lambda^2}\right)$$

where the symbols have the same meaning as used earlier in this section, except for c, which is defined as the correlation interval. The effects of random errors on the side lobes and gain of a circular paraboloid have been computed by Ruze. Some of his results for the case of a cosine-squared illumination are shown in Figs. 2-25 and 2-26.

The relationships for the loss in gain have also been worked out by Ruze. For small errors, simplified formulas have been obtained for the limiting cases of small and large correlation intervals, as follows:

$$\frac{G}{G_0} \approx 1 - \frac{3}{4}\overline{\delta^2}\frac{c^2\pi^2}{\lambda^2}\qquad\text{when}\ \frac{c}{\lambda}\ll 1$$

and

$$\frac{G}{G_0} \approx 1 - \overline{\delta^2}\qquad\text{when}\ \frac{c}{\lambda}\gg 1$$

Some results for the loss in gain are given in Fig. 2-27.

FIG. 2-25. Spurious radiation of paraboloid with cosine-squared illumination. Correlation interval $c = \lambda$.

Periodic Errors in Aperture Illumination. In addition to random errors introduced in the manufacturing process, certain types of antennas may also introduce periodic errors due to the particular technique used in fabricating the antenna. For instance, in certain types of reflectors using bulkhead and truss-work type of construction, mechanical stresses set up during fabrication are such that the surface has periodic errors at roughly equal intervals along the surface. This results in a periodic phase error along the aperture.

The effect of a sinusoidal phase error on the side lobes has been treated in Ref. 24, where it is pointed out that a sinusoidal phase error will produce two equal side lobes whose amplitude relative to the main-beam amplitude is equal to one-half the peak phase error expressed in radians. The two side lobes are symmetrically located on either side of the main beam at an angular distance of $m\lambda/\ell$ radians from the main beam, where m is the number of cycles of phase error along the aperture, ℓ is the total length of the aperture, and λ is the wavelength expressed in the same units as ℓ.

The effect of any type of phase error on the antenna gain has been treated by Spencer,[25] who shows that the fractional loss in gain is equal to the mean-square phase error from the least-square plane-wave approximation to the phase front. Since a periodic phase error would not alter the direction of the unperturbed phase front, the loss in gain is equal to the mean-square value of the periodic phase error. It is interesting to note that this represents the limiting case for random errors as shown in Fig. 2-27.

Another type of distribution error which can occur under certain conditions is a periodic amplitude error.[26] The side-lobe behavior of the amplitude-modulated distribution is very similar to that for the case of the sinusoidal phase error. Two equal side lobes on either side of the main beam will appear for each sinusoidal component of the amplitude modulation. For a uniform amplitude distribution with a sinusoidal ripple, the amplitude of each side lobe due to the ripple will have a value relative to the main-beam amplitude which is equal to one-half of the ratio of the
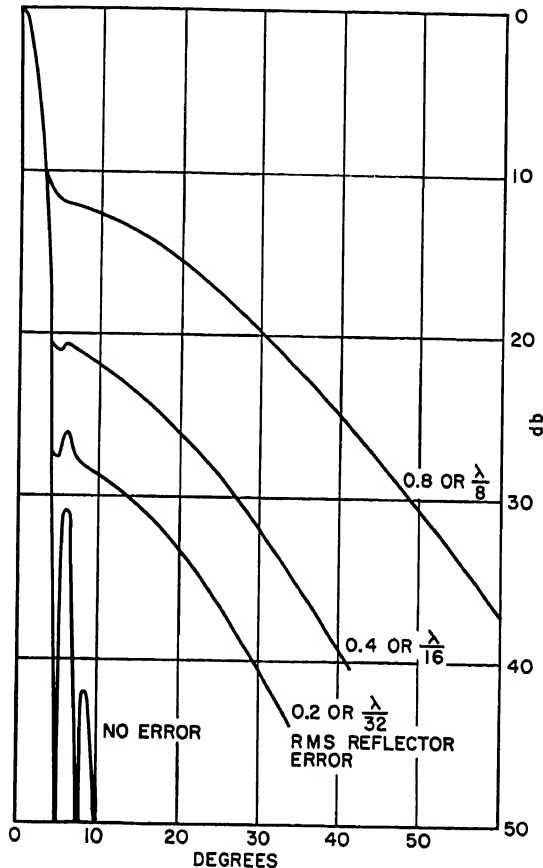
Fig. 2-26. Average system pattern for circular paraboloid with cosine-squared illumination. Correlation interval $c = \lambda$ calculated for reflector 24λ in diameter.

ripple amplitude to the amplitude of the constant term. As was true for the periodic phase error, the periodic amplitude error will produce two symmetrically located side lobes on either side of the main beam at an angular distance of $m\lambda/\ell$ radians, where m is the number of cycles of amplitude variation across the aperture whose total length is ℓ.

2.13. METHODS OF SHAPING PATTERNS

A variety of radar-system applications require that the radiation pattern of the antenna be shaped in such a fashion as to meet certain operational requirements.

One common requirement for the vertical-plane pattern is the cosecant-square pattern, which produces a uniform ground return echo from an air borne radar antenna. There are, of course, other shapes of interest, but the basic principles of obtaining shaped beams are the same for a wide variety of shapes.

Methods Useful for Linear Arrays. One of the techniques useful with slot arrays or dipole arrays is to determine what aperture distribution will produce the desired radiation pattern and then design the array feed system so as to achieve the required aperture distribution.

There are several methods in use for determining the form of the aperture distribution. Historically, the first method is based on the Fourier approximation to a given function.[27] For an equally spaced array of radiating elements, the radiated field due to the array can be represented by a finite trigonometric series with a direct relationship between the current in each element and the coefficients of the trigonometric series. If the required radiation pattern is analyzed by standard Fourier methods, the coefficients of the Fourier series then determine the current amplitudes and phase for the array elements. The accuracy with which the finite series approximates the desired function depends on how many terms are used, that is to say, how large an aperture is used. For a fixed number of terms, it is well known from the theory of Fourier series that the approximation is best in the sense that the mean-square deviation is least. It is also a property of the Fourier approximation that at a point of discontinuity, the function takes on a value that is the average of the value existing on either side of the discontinuity; i.e.,

FIG. 2-27. Loss of gain for paraboloid as a function of reflector error and correlation interval.

$$\tfrac{1}{2}[E(\phi + 0) + E(\phi - 0)]$$

A second method of approximating the desired radiation pattern is one that enables the pattern to be specified exactly at a fixed number of points. This method, which was independently proposed by Woodward[28] and by Levinson, is particularly appealing in that it gives the designer some physical insight into the way the pattern is synthesized and in addition allows some control of the pattern at points of discontinuity.

Basically, the method consists of superposing a series of uniform-amplitude, linear-phase distributions across the aperture in such a way that the sum of the patterns produced by each of the distributions adds up to the desired pattern. The required aperture distribution is then found by adding up, in proper phase, the individual uniform distributions.

To simplify matters, the following discussion will deal with the case of a continuous aperture. The extension to the case of a uniformly spaced discrete element array will be obvious from the discussion. As pointed out in Sec. 2.9, the radiation pattern for a uniform, in-phase illumination is given by

$$E(\phi) = \frac{\sin u}{u}$$

where

$$u = \frac{\pi l}{\lambda} \sin \phi$$

The pattern will pass through zero wherever $\sin \phi = n\lambda/\ell$, $n = 1, 2, 3, 4$, etc., and the pattern has its maximum when $\phi = 0$. For a case where $\ell = 10\lambda$, the pattern plotted against $\sin \phi$ will appear as in Fig. 2-28a.

It will be noted that when the pattern is plotted against $\sin \phi$, the zeros of the pattern are equally spaced except for the two zeros on either side of the main beam, which occupy two spaces. The width of one space is equal to λ/ℓ, the reciprocal of the aperture width in wavelengths.

A uniform illumination with a linear phase variation will have a field pattern given by

$$E(\phi) = \frac{\sin (u - \beta_n)}{u - \beta_n}$$

where β is one-half of the total phase variation across the aperture ℓ. The maximum of this pattern occurs when

$$\sin \phi_n = \frac{\beta_n \lambda}{\pi \ell}$$

If the phase variation is chosen such that $\beta_n = n\pi$, then the pattern will be shifted by $n\lambda/\ell$, or n spaces when plotted against $\sin \phi$. A typical pattern for $\ell = 10\lambda$ and $\beta_n = 3\pi$ is shown in Fig. 2-28b.
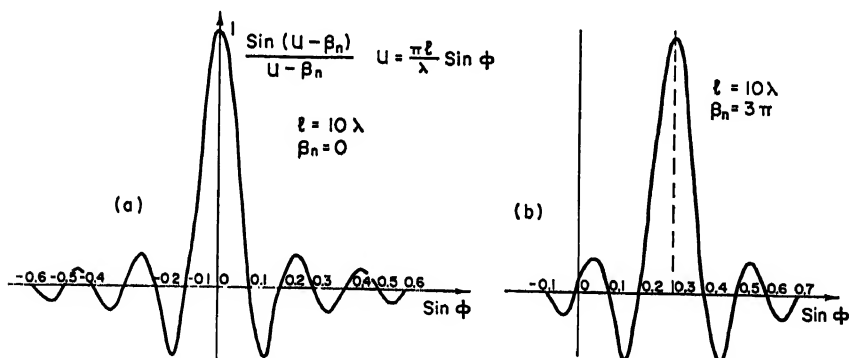
Fig. 2-28. Radiation pattern of uniformly illuminated aperture 10λ long: (a) $\beta_n = 0$. (b) $\beta_n = 3\pi$.

By combining a number of patterns shifted by integral numbers of spaces, it is possible to synthesize a pattern which can be uniquely specified at $2m + 1$ points for an aperture which is m wavelengths in extent. The total radiation pattern is given by

$$E(\phi) = \sum_n C_n \frac{\sin (u - \beta_n)}{u - \beta_n} = \sum_n C_n \frac{\sin (u - n\pi)}{u - n\pi}$$

and the corresponding normalized aperture distribution is given by

$$f(x) = \sum_n C_n e^{-i\beta_n x} = \sum_n C_n e^{-in\pi x}$$

where $-1 \leq x \leq +1$.

As an illustration of this method, let us consider the problem where it is desired to specify that the pattern have a cosecant shape over the range in $\sin \phi$ from 0.1 to 1.0 and that it have no radiation for negative values of $\sin \phi$. For an aperture length of 10 wavelengths, $\sin \phi$ is divided into spaces one-tenth wide from -1 to $+1$ and ordi-

nates erected at each division with a height equal to $E(\phi)$. For the problem at hand, $E(\phi)$ is proportional to csc ϕ. A plot of the $E(\phi)$ diagram is shown in Fig. 2-29, where at each division, an individual pattern is to be specified with a maximum value equal to each ordinate. The summation of the individual patterns is shown in Fig. 2-30, while the resulting total aperture distribution, consisting of the sum of each of the individual aperture distributions, is shown in Fig. 2-31.

For the case shown, $E(0)$ has been chosen to equal zero, and it will be noted that the resulting pattern has a fair amount of ripple in it. If the value of $E(0)$ is chosen to be 0.8, then the resulting pattern shown in Fig. 2-32 is considerably smoother although the aperture distribution is somewhat more peaked, as seen from Fig. 2-33.

This particular method of synthesis is quite useful because of the flexibility the designer has in arriving at the final radiation pattern and his ability to adjust the theoretical pattern by graphical procedures. Although the example discussed has used only real values for C_n to simplify the calculations, there is nothing in the procedure which prevents the use of complex values for C_n. It is quite possible that a judicious choice of the phase angles for the C_n's might have given as effective a control over the ripple as did the changing the value of $E(0)$.

FIG. 2-29. $E(\phi)$ pattern for cosecant shaping.
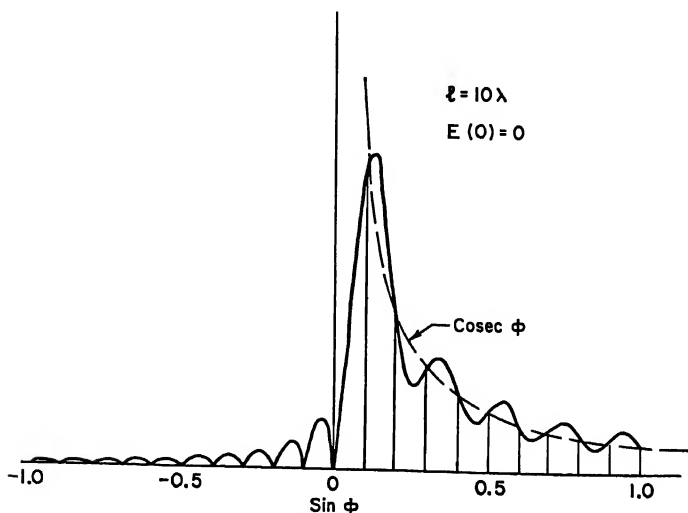
FIG. 2-30. Synthesis of cosecant pattern for $E(0) = 0$.

One note of caution should be added. Although beams can be added for values of $|\sin \phi| > 1$ in order to control the amplitude at points intermediate between the ordinates, the energy in these "imaginary beams" (when ϕ is complex) is primarily

of a reactive nature and can result in large amounts of stored energy in the aperture, with consequent reduction of bandwidth and increase of losses. It is therefore desirable to minimize or eliminate those beams which radiate in directions specified by $|\sin \phi| > 1$.

Methods Useful for Reflector-type Antennas. There are several methods useful for producing shaped patterns with reflector-type antennas. One technique, which is readily applied to a standard paraboloidal reflector, combines a number of narrow beams to form a wider beam, shaped in the vertical plane by the use of an extended feed system. In some respects, this technique has a certain similarity to the Woodward-Levinson method discussed earlier in the section.

In applying this technique, a rectangular or elliptical section of a full paraboloid is used as the reflector surface. The horizontal dimension of the reflector section is chosen to give the desired horizontal beamwidth, while the vertical dimension is chosen to control the rate of cutoff of the vertical beam. The vertical dimension also influences the feed-system problem, particularly if a small value is chosen, since the feed horn or dipole for each beam would have to have a sizable vertical dimension. The aspect ratio of the reflector commonly has a value in the range of 2:1 to 4:1.

Fig. 2-31. Aperture distribution for Fig. 2-30: (a) Amplitude distribution. (b) Phase distribution.

A considerable amount of experimental effort is necessary in the design of an extended feed system. The basic principles can be seen from Fig. 2-34. For each feed in the vertical plane, there is a corresponding vertical beam whose position is

related to the feed position. By exciting each feed with the appropriate amplitude and by choosing the feed separation and phasing, it is possible to obtain a fairly smooth vertical-plane pattern.

A number of examples of this technique are given in Ref. 15. Although most of the structures built to date have used reflector structures for collimating each beam, the same technique of combining beams is also applicable to lens-type antennas.

Another approach to the problem of generating shaped beams is the use of shaped reflector systems. One method uses a line source to feed a shaped reflector, while a second method uses a point-source feed
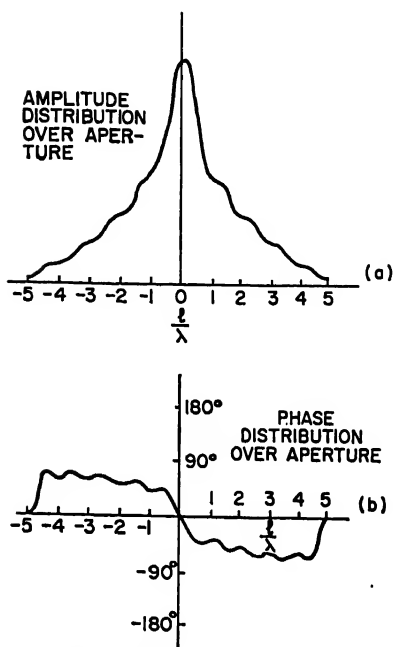
Fig. 2-33. Aperture distribution for Fig. 2-32: (*a*) Amplitude distribution. (*b*) Phase distribution.
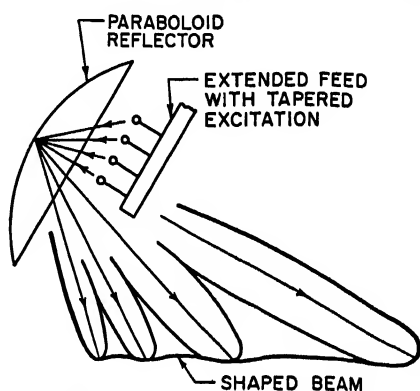
Fig. 2-34. Schematic of extended feed system for pattern shaping.

with a double-curvature reflector. The shaped-reflector approach is treated in both Chaps. 12 and 25, so that no further discussion will be given here.

2.14. ANTENNA BANDWIDTH AS RELATED TO IMPEDANCE CHARACTERISTICS

For efficient operation of an antenna system, it is necessary that the standing-wave ratio on the transmission line feeding the antenna be as close to unity as possible. High standing-wave ratios cause mismatch losses in the system and in some cases can prevent proper functioning of the equipment connected to the antenna.

In general, the input impedance of the antenna differs from that of its associated transmission line, and impedance matching networks are necessary to reduce the standing-wave ratio on the transmission line over the required band of frequencies.

For a limited number of antenna types, the input impedance may be a constant resistance over its operating band. For this special case, it is possible to transform the input resistance to any other resistance level by means of suitable matching networks (Chap. 31). By constructing a matching device with a large enough number of sections or with a long enough length, it is possible in theory to effect the required matching to as close a tolerance as desired.

The most general type of antenna input impedance will not be a constant pure resistance, but will also have a reactance component which varies over the frequency

range in addition to the variation of the resistance component. This type of input impedance cannot be matched perfectly over a large frequency band, and it is of considerable interest to determine what bandwidth can be obtained for a given tolerance in the standing-wave ratio, or conversely, what minimum standing-wave ratio is possible for a prescribed bandwidth.

The problem of the theoretical limitations on broadband matching has been considered in some detail by Fano[29] and by Tanner.[30,31] It has been shown that if
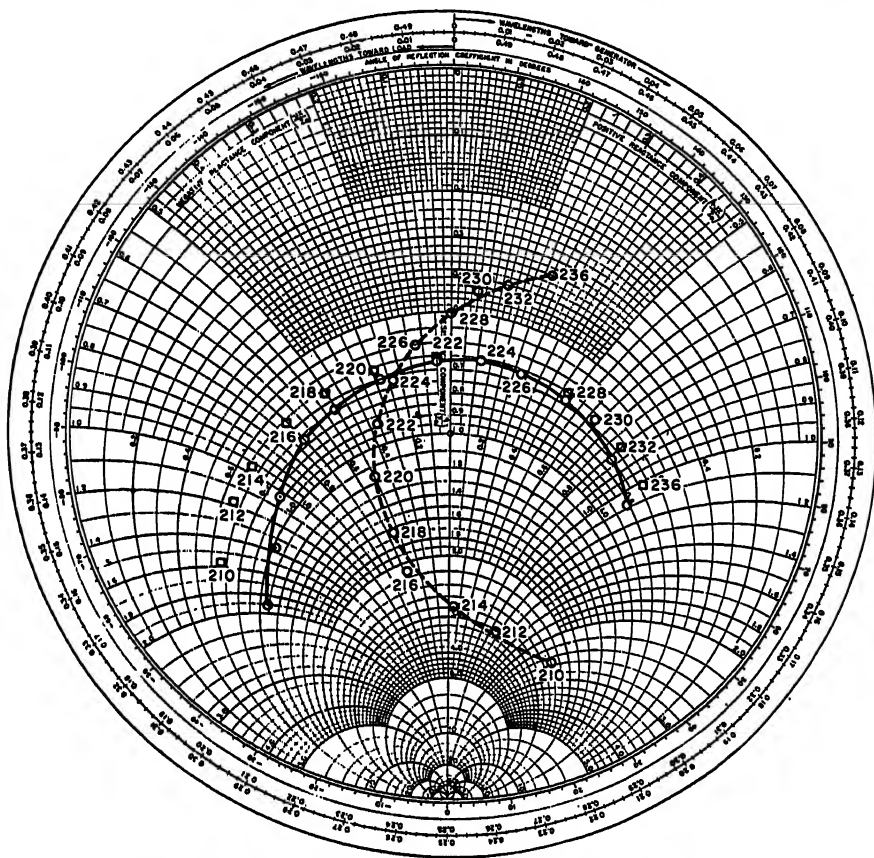
FIG. 2-35. Smith chart plot of antenna characteristics before (dashed) and after (solid) rotation.

maximum bandwidth is to be obtained, then it is necessary that the reflection coefficient be as close to a constant as possible over the bandwidth. A consequence of this is that if the reflection coefficient has a very low value at one point in the band, then the bandwidth will be lower than the theoretical maximum value for a given maximum value of reflection coefficient. Practically, this means that the impedance plot of the compensated circuit should have a shape as close to that of a circle as possible.

Some studies have been made regarding the maximum attainable bandwidth for an impedance curve which can be represented by a simple RLC circuit. Once the designer has determined the Q of the circuit to be matched, then it is possible to predict with a fair degree of accuracy what maximum bandwidth can be obtained for a given allowable value of standing-wave ratio.

At the present time, the design of impedance compensating networks is still an art rather than a science and the effectiveness of a design depends to a large part on the ingenuity of the design engineer.   It is therefore important to know the possible limits of performance beforehand in order to avoid striving for a theoretically impossible design.

The measured impedance curve of the antenna is first determined.   A typical curve is shown in the dashed line of Fig. 2-35 (taken from Ref. 30).   If this curve is rotated through a short section of 50-ohm line so that the resistive component is essentially constant, the impedance takes the form of the solid curve of Fig. 2-35.   Figure 2-36a

(a)

MATCHING NETWORK   NETWORK TO
                        BE MATCHED
(b)
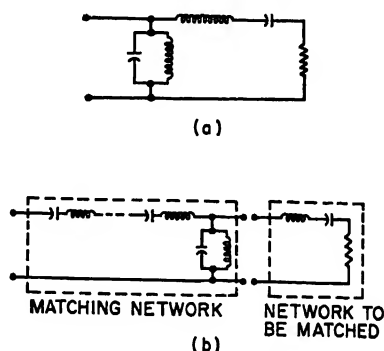
FIG. 2-36. (a) Equivalent network for impedance characteristic of solid curve, Fig. 2-35. (b) Matching network which can be used with (a).

is one representation of the equivalent circuit of this impedance.   If the susceptance of the parallel-resonant circuit is subtracted from the solid curve, the impedance is given by the square points on Fig. 2-35, which represent the series-resonant circuit of Fig. 2-36a.

The Q of the series-resonant circuit is approximately 15 as determined from

$$Q = \frac{f_r}{\Delta f}$$

where f_r = resonant frequency
    Δf = frequency difference between half-power points
The half-power points are defined by the frequencies at which the series reactance is equal to the series resistance.

Inspection of the impedance chart shows that the resonant frequency is 222 Mc, while the half-power points are 216.5 and 230 Mc, giving

$$Q = \frac{222}{230 - 216.5} = 15.3$$

An alternative method of computing Q when the reactance is not zero at the center frequency is to use the following relationship:

$$Q = \frac{f}{\Delta f} \frac{\Delta X}{2R} + \frac{|X|}{2R}$$

where f = geometric mean frequency
    Δf = frequency interval
    ΔX = absolute value of reactance change through frequency interval
    R = resistance
    $|X|$ = absolute value of reactance at geometric mean frequency

For most impedance curves, it will be possible to evaluate the Q at a particular frequency by choosing a small enough frequency interval where the resistance is essentially constant. The average Q over a frequency band can be estimated by plotting Q versus frequency.

For the equivalent circuit of Fig. 2-36a, a matching network of the form given in Fig. 2-36b can be used. It should be noted that for the matching network shown, the first element is a shunt parallel-resonant circuit. In order to obtain optimum matching, the susceptance of the equivalent parallel-resonant circuit in the antenna must be less than the required susceptance of the first element of the matching network.
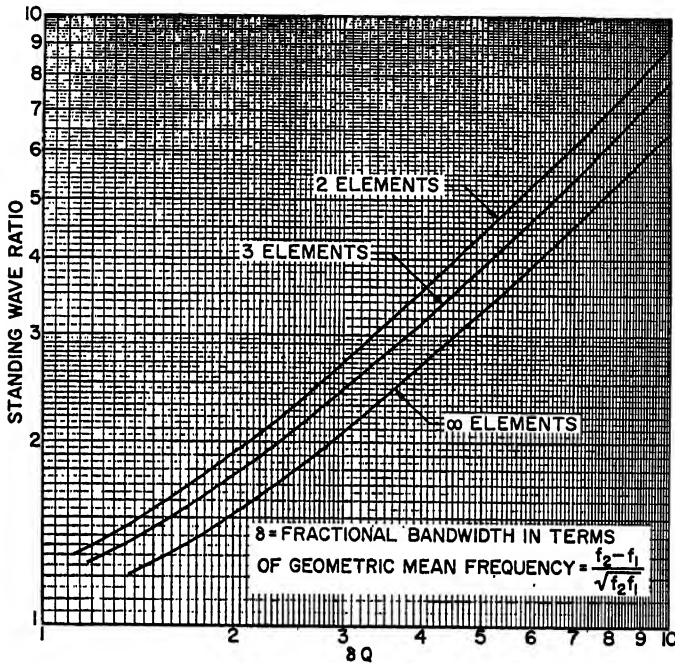
Fig. 2-37. Optimum matching to a simple resonant circuit which can be obtained with a network of n elements.

If this is the case, then the parallel-resonance circuit in the antenna impedance can be lumped with the first element of the matching network.

Having determined the approximate Q of the antenna to be matched and having specified the required bandwidth, it is then possible to determine the optimum standing-wave ratio which can be achieved with a network of N elements. Figure 2-37, which has been derived by Tanner from the results of Fano, shows the standing-wave ratio obtainable for networks of 2, 3, and an infinite number of elements versus δQ, where δ is the fractional bandwidth defined by

$$\delta = \frac{f_2 - f_1}{\sqrt{f_1 f_2}}$$

i.e., the frequency interval divided by the geometric mean frequency.

Taking the impedance curve of Fig. 2-35 as an example and assuming that the antenna is to be matched from 214 to 234 Mc, it is found that $\delta = 0.0895$ and that $\delta Q = 1.37$. Referring to Fig. 2-37 and assuming that a two-element matching net-

work is used (one shunt element and one series element), it is seen that a standing-wave ratio of approximately 1.5 can be attained over the frequency band.

Although the above theory is based on the use of the lumped-element matching networks, it is also useful in estimating the potential performance of distributed-element networks provided the bandwidths are not too large, say for values of δ considerably less than 1. It should also be mentioned that although the example considered had a series-resonant type of load, the same methods also apply where the load behaves as a parallel-resonant circuit.

2.15. GAIN LIMITATIONS FOR AN APERTURE OF SPECIFIED SIZE

It has been shown previously that the gain of a uniformly illuminated aperture-type antenna without losses is expressed by

$$G = \frac{4\pi A}{\lambda^2}$$

where A is the area of the aperture. The value of gain obtained from this expression normally represents an upper limit which can be realized with practical structures.

Certain classes of aperture distributions offer the theoretical possibility of higher values of directivity than can be obtained with uniform distribution. In general, these theoretical distributions are characterized by reversals of phase over a distance short compared with the wavelength. One common feature of these supergain distributions is the large amount of stored energy in the aperture region since very high values of field intensity are necessary in order to produce the same radiated field as would be produced by a uniformly illuminated aperture with much lower values of field intensity.

The large values of stored energy in the aperture region of a "supergain antenna" cause a number of engineering problems which are severe enough to make this type of antenna completely impractical. The first problem is that of extremely high Q's, which limit the operating bandwidth to extremely small values. For instance, it has been stated by Taylor[32] that an antenna designed within a sphere of 50 wavelengths diameter will have a beamwidth of approximately 1°. If the same beamwidth is to be maintained while the diameter of the sphere is reduced to 45 wavelengths, the Q will rise to a value of 500. If the diameter is reduced to 40 wavelengths, the Q will rise to a value of 5×10^{10}. For further reductions in diameter, the value of Q rises to astronomical values. Since the bandwidth is of the order of the inverse of Q, it can be seen that the bandwidth diminishes rapidly.

As a result of the high stored energy, large values of circulating current flow in the antenna structure and a point is very quickly reached at which the ohmic losses completely nullify any gain increase due to increased directivity.

Another concomitant of the "supergain antenna" is the extreme precision required in order to achieve any substantial increase in directivity.

There is an abundant literature on the topic of supergain antennas, and the antenna designer who may be tempted to build such antennas should consult these references.[33–35]

Lest the situation be considered completely hopeless, it should be mentioned that for certain end-fire arrays in which the values of gain are modest, some increase in gain can be achieved. Mention of the Hansen-Woodyard phasing condition has been made, in Sec. 2.8, where it has been shown that the gain can be increased by a factor of 1.8 at the expense of reduced performance. One particular design has been given in the literature[36] where a four-element end-fire array has achieved a modest increase in gain and directivity at the expense of bandwidth. However, aside from the special case of end-fire arrays, the designer is to be discouraged from attempting to construct

arrays which have gains higher than the value given for the uniform-illumination case. This caution is particularly true for broadside antennas where the aperture is large in terms of wavelengths.

2.16. SCALE MODELS OF ANTENNAS

One of the most useful tools of the antenna engineer is the ability to scale his designs. It is a direct consequence of the linearity of Maxwell's equations that an electromagnetic structure which has certain properties[37] at a given frequency f will have identically the same properties at another frequency nf, provided all linear dimensions are scaled by the ratio $1/n$. Thus an antenna design which works in one range of frequencies can be made to work at any other range of frequencies without additional redesign, provided an exact scaling of dimensions can be accomplished.

Quite aside from the ability to transfer design relationships is the ability to make radiation-pattern studies on scale models which are convenient in size. The aircraft antenna field is one in which full-size radiation studies are extremely awkward, time-consuming, and expensive. The possibility of studying aircraft antennas on a scale model[36] which may be as small as one-twentieth or one-fortieth of full size brings such studies within the realm of the laboratory rather than requiring an elaborate flight operation.

For most types of antennas, scaling is a relatively simple matter. Table 2-6 shows how the dimensions and electromagnetic properties vary as a function of the scale factor.

Table 2-6

Quality	Full-scale system	Model system
Length	L_F	$L_M = L_F/n$
Frequency	f_F	$f_M = nf_F$
Dielectric constant	ϵ_F	$\epsilon_M = \epsilon_F$
Conductivity	σ_F	$\sigma_M = n\sigma_F$
Permeability	μ_F	$\mu_M = \mu_F$

It will be noted that all the quantities can be satisfactorily scaled except for the conductivity. If the full-size antenna is constructed of copper or aluminum, then it is not possible to obtain materials which have conductivities that are an order of magnitude higher. Fortunately, conductivity losses affect the operation of most antennas to only a minor degree, so that the inability to scale the conductivity is not usually serious. This is not true for devices such as cavity resonators, where the losses may be appreciable. For a few types of antennas, such as very long wire antennas, where the conductivity losses of the antenna and of the ground may play a part in the radiating properties of the antenna, it may be necessary to proceed with considerable caution before making scale-model studies.

While it is true that an exact scale model will have exactly the same radiation patterns and input impedance as the full-scale antenna, it is not always possible to achieve perfect scaling. This is particularly so for such items as transmission lines, screw fastenings, etc. Slight discrepancies in scaling will usually affect the impedance properties much more than the radiation properties. It is therefore wise to consider scale-model impedance studies as primarily qualitative in nature, even though it is valid to consider scale-model radiation patterns as being highly accurate. Usually the general trend of the impedance characteristics is determined from the scale model but the final impedance matching work can be completed only on the full-size antenna.

REFERENCES

1. S. A. Schelkunoff: "Electromagnetic Waves," D. Van Nostrand Company, Inc., Princeton, N.J., 1943.
2. S. A. Schelkunoff and H. T. Friis: "Antennas: Theory and Practice," John Wiley & Sons, Inc., New York, 1952.
3. Reference 1, p. 360.
4. S. A. Schelkunoff: "Some Equivalence Theorems of Electromagnetics and Their Application to Radiation Problems," *Bell System Tech. J.*, vol. 15, pp. 92–112, 1936.
5. P. S. Carter: "Circuit Relations in Radiating Systems and Applications to Antenna Problems," *Proc. IRE*, vol. 20, pp. 1004–1041, June, 1932.
6. G. H. Brown: "Directional Antennas," *Proc. IRE*, vol. 25, pp. 78–145, 1937.
7. Carl E. Smith: "Directional Antennas," Cleveland Institute of Radio Electronics, Cleveland, 1946.
8. W. W. Hansen and J. R. Woodyard: "A New Principle in Directional Antenna Design," *Proc. IRE*, vol. 26, pp. 333–345, March, 1938.
9. C. L. Dolph: "A Current Distribution for Broadside Arrays Which Optimizes the Relationship between Beamwidth and Side-lobe Level," *Proc. IRE*, vol. 34, pp. 335–348, June, 1946.
10. Discussion of Ref. 9, *Proc. IRE*, vol. 35, pp. 489–492, May, 1947.
11. G. J. van der Maas: "A Simplified Calculation for Dolph-Tchebyscheff Arrays," *J. Appl. Phys.*, vol. 25, pp. 121–124, January, 1954.
12. E. Jahnke and F. Emde: "Tables of Functions," p. 227, Dover Publications, New York, 1943.
13. British Association Mathematical Tables, vols. VI and X, Cambridge University Press, London, 1950 and 1952.
14. R. J. Stegen: "Excitation Coefficients and Beamwidths of Tchebyscheff Arrays," *Proc. IRE*, vol. 41, pp. 1671–1674, November, 1952.
15. S. Silver: "Microwave Antenna Theory and Design," McGraw-Hill Book Company, Inc., New York, 1949.
16. R. C. Spencer and P. M. Austin: "Tables and Methods of Calculation for Line Sources," MIT Rad. Lab. Rept. 762-2, March, 1946; see also Rept. 762-1.
17. J. F. Ramsay: "Fourier Transforms in Aerial Theory," *Marconi Rev.*, vol. 9, 1946, p. 139, and vol. 10, 1947, pp. 17, 41, 81, 157.
18. T. T. Taylor: "Design of Line-source Antennas for Narrow Beamwidth and Low Side-lobes," *IRE Trans.*, vol. AP-3, pp. 16–28, January, 1955; see also R. J. Spellmire: "Tables of Taylor Aperture Distributions," Hughes Aircraft Co. Tech. Mem. 581, Culver City, Calif., October, 1958.
19. T. T. Taylor: "One Parameter Family of Line Sources Producing Modified Sin $\pi u/\pi u$ Patterns," Hughes Aircraft Co. Tech. Mem. 324, Culver City, Calif., September, 1953.
20. K. Milne: "The Effects of Phase Errors on Simple Aperture Illuminations," Proceedings of a Conference on Centimetric Aerials for Marine Navigational Radar, June 15–16, 1950, H. M. Stationery Office, London, 1952.
21. J. Ruze: "Physical Limitations on Antennas," MIT Research Lab. Electronics, Tech. Rept. 248, Cambridge, Mass., October, 1952; see also "The Effect of Aperture Errors on the Antenna Radiation Pattern," *Supplemento al Nuovo Cimento*, vol. 9, no. 3, pp. 364–380, 1952.
22. L. L. Bailin and M. J. Ehrlich: "Factors Affecting the Performance of Linear Arrays," *Proc. IRE*, vol. 41, pp. 235–241, February, 1953.
23. H. F. O'Neill and L. L. Bailin: "Further Effects of Manufacturing Tolerances on the Performance of Linear Shunt Slot Arrays," *IRE Trans.*, vol. AP-4, pp. 93–102, December, 1952.
24. N. I. Korman, E. B. Herman, and J. R. Ford: "Analysis of Microwave Antenna Sidelobes," *RCA Rev.*, vol. 13, pp. 323–334, September, 1952.
25. R. C. Spencer: "A Least Square Analysis of the Effect of Phase Errors on Antenna Gain," Air Force Cambridge Research Center Rept. 5025, Bedford, Mass., January, 1949.
26. J. Brown: "The Effect of a Periodic Variation in the Field Intensity across a Radiating Aperture," *Proc. IEE (London)*, pt. III, vol. 97, pp. 419–424, November, 1950.
27. I. Wolff: "Determination of the Radiating System Which Will Produce a Specified Directional Characteristic," *Proc. IRE*, vol. 25, pp. 630–643, May, 1937.
28. P. M. Woodward: "A Method of Calculating the Field over a Plane Aperture Required to Produce a Given Polar Diagram," *J. IEE (London)*, pt. IIIA, vol. 93, pp. 1554–1558, 1947.
29. R. M. Fano: "Theoretical Limitations on the Broadband Matching of Arbitrary Impedances," Research Lab. Electronics, MIT, Tech. Rept. 41, Cambridge, Mass., January, 1948.

30. R. L. Tanner: "Theoretical Limitations to Impedance Matching," *Electronics*, vol. 24, pp. 234–242, February, 1951.
31. A. Vassiliadis and R. L. Tanner: "Evaluating the Impedance Broadbanding Potential of Antennas," *IRE Trans.*, vol. AP-6, pp. 226–231, July, 1958.
32. T. T. Taylor: "A Discussion of the Maximum Directivity of an Antenna," *Proc. IRE*, vol. 36, p. 1135, September, 1948.
33. L. J. Chu: "Physical Limitations of Omnidirectional Antennas," *J. Appl. Phys.*, vol. 19, p. 1163, December, 1948.
34. P. M. Woodward and J. D. Lawson: "The Theoretical Precision with Which an Arbitrary Radiation Pattern May Be Obtained from a Source of Finite Size," *J. IEE (London)*, pt. III, vol. 95, pp. 363–370, September, 1948.
35. N. Yaru: "A Note on Super-gain Arrays," *Proc. IRE*, vol. 39, pp. 1081–1085, September, 1951.
36. A. Block, R. G. Medhurst, and S. D. Pool: "A New Approach to the Design of Super-directive Aerial Arrays," *J. IEE (London)*, pt. III, vol. 100, pp. 303–314, September, 1953.
37. G. Sinclair: "Theory of Models of Electromagnetic Systems," *Proc. IRE*, vol. 36, pp. 1364–1370, November, 1948.
38. G. Sinclair, E. C. Jordan, and E. W. Vaughan: "Measurement of Aircraft Antenna Patterns Using Models," *Proc. IRE*, vol. 35, pp. 1451–1462, December, 1947.

GENERAL REFERENCES

D. W. Fry and F. K. Goward: "Aerials for Centimetre Wavelengths," Cambridge University Press, New York, 1950.
E. C. Jordan: "Electromagnetic Waves and Radiating Systems," Prentice-Hall, Inc., Englewood Cliffs, N.J., 1950.
R. W. P. King: "The Theory of Linear Antennas," Harvard University Press, Cambridge, Mass., 1956.
J. D. Kraus: "Antennas," McGraw-Hill Book Company, Inc., New York, 1950.
E. A. Laport: "Radio Antenna Engineering," McGraw-Hill Book Company, Inc., New York, 1952.
S. Ramo and J. R. Whinnery: "Fields and Waves in Modern Radio," 2d ed., John Wiley & Sons, Inc., New York, 1953.
S. A. Schelkunoff: "Electromagnetic Waves," D. Van Nostrand Company, Inc., Princeton, N.J., 1943.
S. A. Schelkunoff and H. T. Friis: "Antennas: Theory and Practice," John Wiley & Sons, Inc., New York, 1952.
S. Silver: "Microwave Antenna Theory and Design," McGraw-Hill Book Company, Inc., New York, 1949.
J. C. Slater: "Microwave Transmission," McGraw-Hill Book Company, Inc., New York, 1942.
R. A. Smith: "Aerials for Metre and Decimetre Wavelengths," Cambridge University Press, New York, 1949.
G. C. Southworth: "Principles and Applications of Waveguide Transmission," D. Van Nostrand Company, Inc., Princeton, N.J., 1950.
J. A. Stratton: "Electromagnetic Theory," McGraw-Hill Book Company, Inc., New York, 1941.
H. P. Williams: "Antenna Theory and Design," 2 vols., Sir Isaac Pitman & Sons, London, 1950.

Chapter 3

CHARACTERISTICS OF LINEAR ANTENNA ELEMENTS

C. T. Tai

The Ohio State University
Columbus, Ohio

3.1. CYLINDRICAL DIPOLES

Impedance as a Function of Length and Diameter. The impedance characteristics of cylindrical antennas have been investigated by many writers.[1] Theoretical work

has mainly been confined to relatively thin antennas (length-to-diameter ratio greater than 15), and the effect of the junction connecting the antenna proper and the transmission line is usually not considered. Among various theories, the induced emf method[2] of computing the impedance of a cylindrical antenna based upon a sinusoidal distribution is still found to be very useful. The formula derived from this method is extremely simple. It is, however, valid only when the half length of a center-driven antenna is not much longer than a quarter wavelength. In practice, this is the most useful range. To eliminate unnecessary computations, the formula has been reduced to the following form:

$$Z_i = R(k\ell) - j\left[120\left(\log\frac{2\ell}{a} - 1\right)\cot k\ell - X(k\ell)\right] \qquad (3\text{-}1)*$$

where Z_i = input impedance in ohms of a center-driven cylindrical antenna of total length 2ℓ and of radius a

$k\ell = 2\pi\,(\ell/\lambda)$ = electrical length, corresponding to ℓ, measured in radians

The functions $R(k\ell)$ and $X(k\ell)$ are tabulated in Table 3-1 and plotted in Fig. 3-1 for the range $k\ell \leq \pi/2$. When the length of the antenna is short compared with a wavelength but still large compared with its radius, the same formula reduces to

$$(Z_i)_{\text{short}} = 20(k\ell)^2 - j120(k\ell)^{-1}\left(\log\frac{2\ell}{a} - 1\right) \qquad (3\text{-}2)$$

Table 3-1. Functions $R(k\ell)$ and $X(k\ell)$ Contained in the Formula of the Input Impedance of a Center-driven Cylindrical Antenna

$k\ell$	$R(k\ell)$	$X(k\ell)$	$k\ell$	$R(k\ell)$	$X(k\ell)$
0	0	0	0.9	18.16	15.01
0.1	0.1506	1.010	1.0	23.07	17.59
0.2	0.7980	2.302	1.1	28.83	20.54
0.3	1.821	3.818	1.2	35.60	23.93
0.4	3.264	5.584	1.3	43.55	27.88
0.5	5.171	7.141	1.4	52.92	32.20
0.6	7.563	8.829	1.5	64.01	38.00
0.7	10.48	10.68	$\pi/2$	73.12	42.46
0.8	13.99	12.73			

For antennas of half length greater than a quarter wavelength, there are a number of refined theories which provide formulas for the computation of the impedance function. None of them, however, is simple enough to be included here. As far as numerical computation is concerned, Schelkunoff's method[3] is relatively simpler than Hallén's.[4] It should be emphasized that all these theories are formulated using an idealized model where the terminal condition is not considered.

In practice, the antenna is always fed by a transmission line. The complete system may have the appearances as shown in Fig. 3-2. The effective terminal impedance of the line (often referred to as the antenna impedance) then depends not only upon the length and the diameter of the antenna but also upon the terminal condition. In cases a and b, the impedance would also be a function of the size of the ground plane. For a given terminal condition the variation of the impedance of a cylindrical antenna as a function of the length and the diameter of the antenna is best shown in the experimental work of Brown and Woodward.[5] The data cover a

---

* Natural logarithms are used in this chapter unless specified otherwise.

wide range of values of the length-to-diameter ratio. Two useful sets of curves are reproduced in Figs. 3-3 and 3-4. The impedance refers to a cylindrical antenna driven by a coaxial line through a large circular ground plane placed on the surface of the earth. The arrangement is similar to the one sketched in Fig. 3-2a. The caption of the figure indicates that the length and the diameter of the antenna are measured
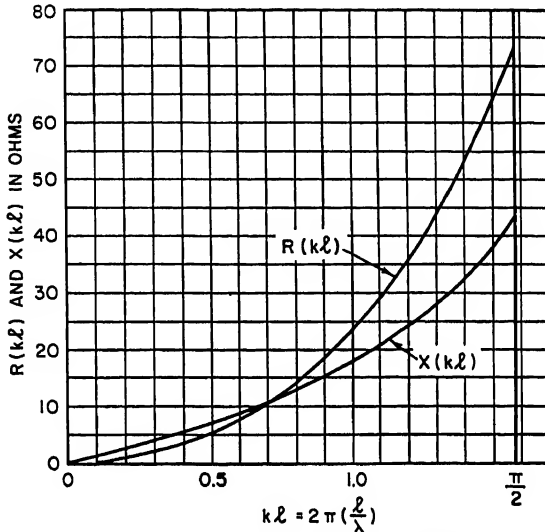
Fig. 3-1 The functions $R(k\ell)$ and $X(k\ell)$.
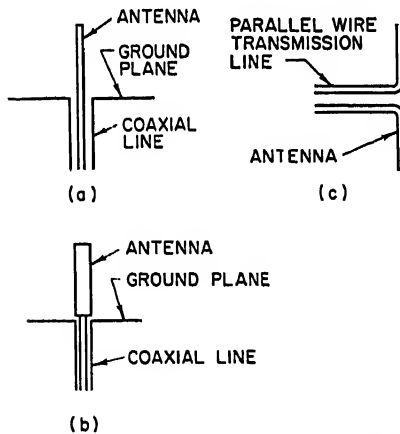
Fig. 3-2. Driving an antenna by a pair of transmission lines.

in degrees; i.e., a length of one wavelength is equivalent to 360°. If the effects due to the terminal condition and finite-size ground plane are neglected, the impedance would correspond to one-half of the impedance of a center-driven antenna (Fig. 3-2c). In using these data for design purposes, one must take into consideration the actual terminal condition as compared with the condition specified by these two authors. In particular, the maximum value of the resistance and the resonant length of the antenna may change considerably if the "base capacitance" is excessive.
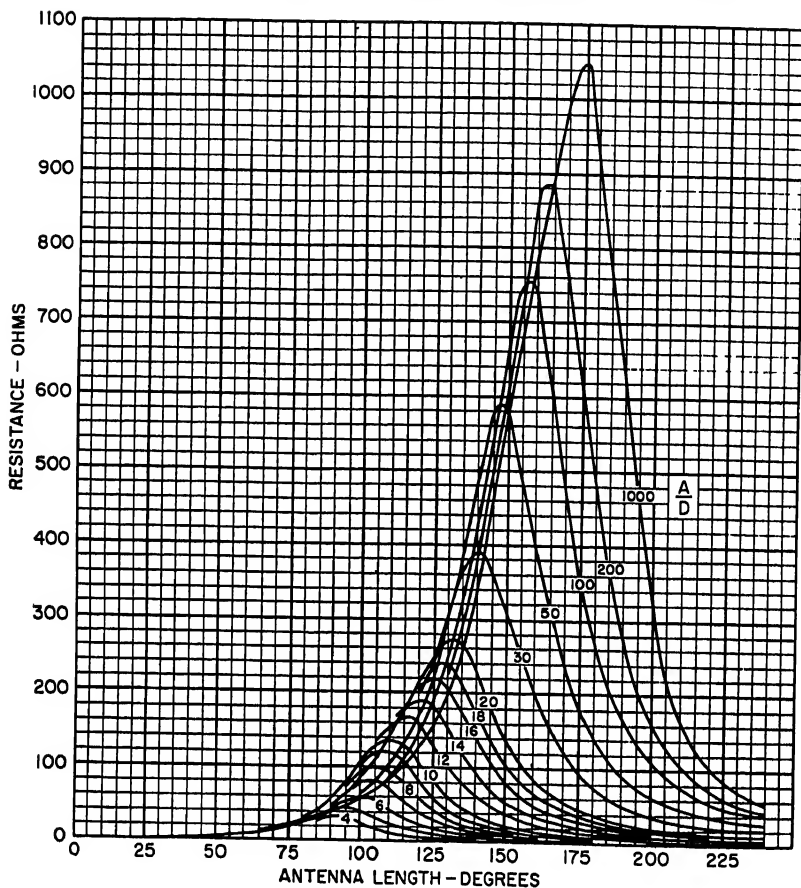
FIG. 3-3. Antenna resistance vs. antenna length A, when a constant ratio of length to diameter A/D is maintained. Here the length and diameter are held constant, while the frequency is changed.

Effect of Terminal Conditions. Many authors have attempted to determine the equivalent-circuit elements corresponding to different terminal conditions. Schelkunoff and Friis[6] have introduced the concepts of "base capacitance" and "near-base capacitance" to explain the shift of the impedance curve as the terminal condition is changed. Similar interpretations have been given by King[7] for a cylindrical antenna driven by a two-wire line or by a coaxial line and by Whinnery[8] for a biconical antenna driven by a coaxial line. The importance of the terminal condition in effecting the input impedance of the antenna is shown in Figs. 3-5 and 3-6. They are again reproduced from Brown and Woodward's paper. Because of the large variation of the effective terminal impedance of the line with changes in the geometry of the terminal junction, one must be cautious when using the theoretical results based upon isolated antennas. For junctions possessing simple geometry the static method of Schelkunoff and Friis, King, and Whinnery can be applied to estimate the shunt capacitance of the junction. The latter then can be combined with the impedance of the antenna proper to evaluate the resultant impedance. For intricate junctions, accurate information can be obtained only by direct measurement.
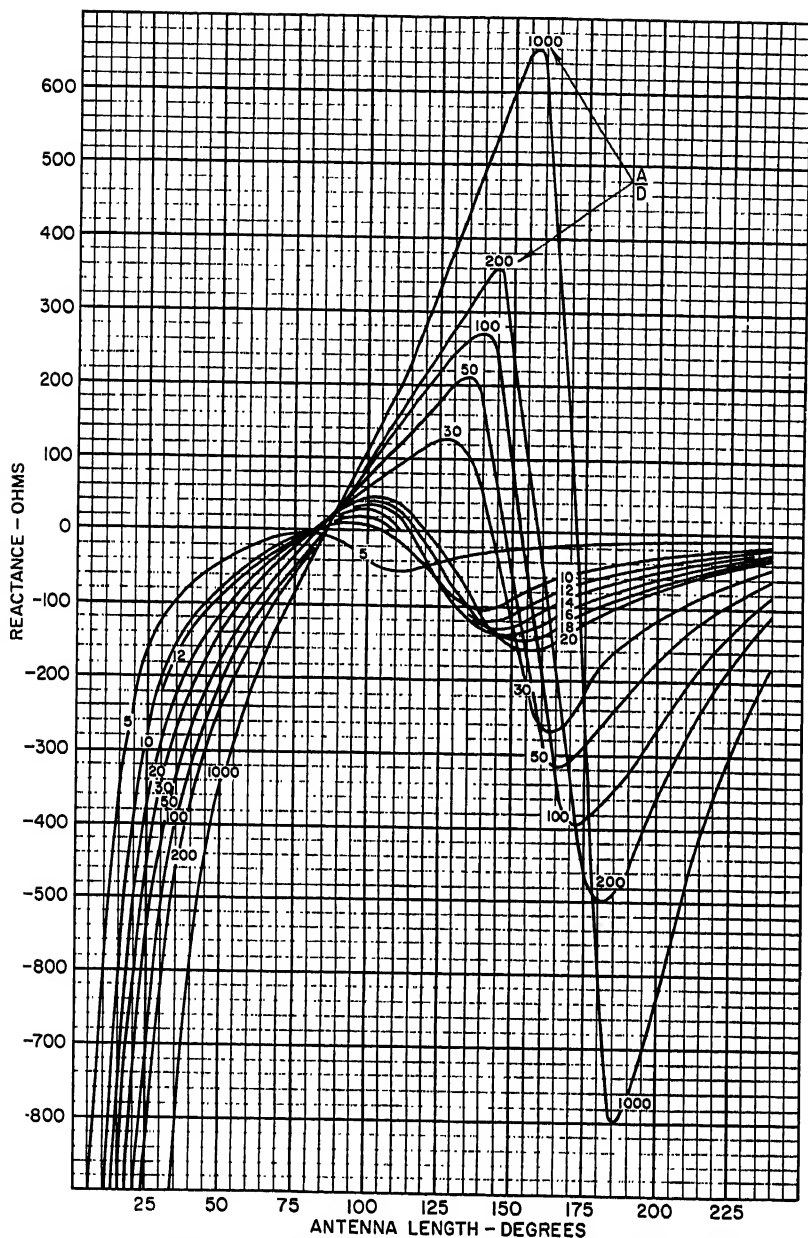
Fig. 3-4. Reactance curves corresponding to the resistance curves of Fig. 3-3.
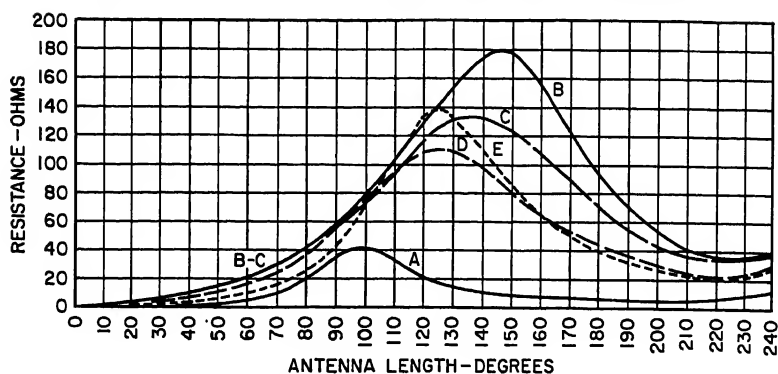
FIG. 3-5. Resistance as a function of antenna length A. The diameter D is 20.6°. Curve A: The arrangement shown in Fig. 3-2b. Curve B: the arrangement of Fig. 3-2a, with the diameter of the outer conductor equal to 74°. The characteristic impedance of the transmission line is 77.0 ohms. Curve C: The outer-conductor diameter is 49.5°, and the transmission line has a characteristic impedance of 52.5 ohms. Curve D: The diameter of the outer conductor is 33°. The characteristic impedance is 28.3 ohms. Curve E: this curve was obtained by tuning out the base reactance with an inductive reactance of 65.0 ohms.
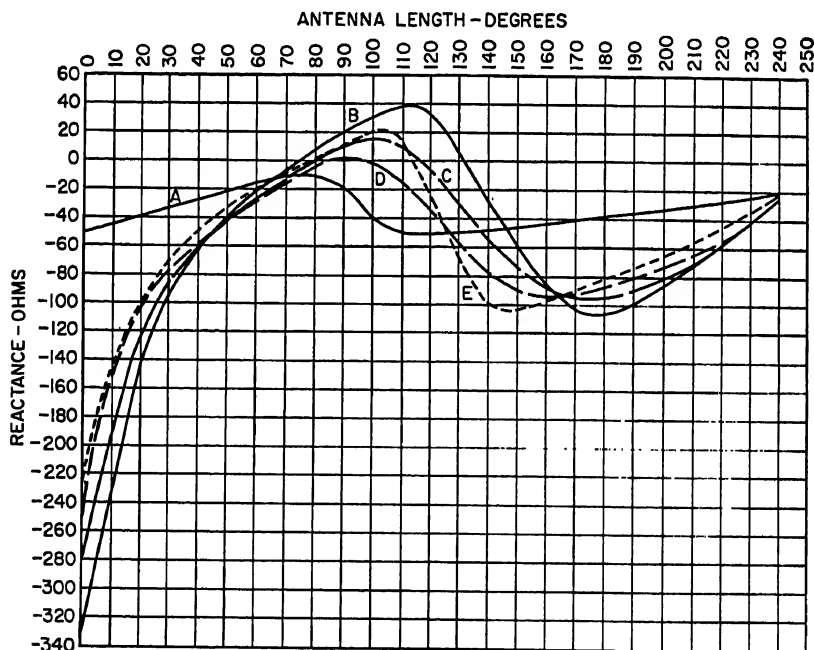
FIG. 3-6. Reactance curves corresponding to the resistance curves of Fig. 3-5.

Equivalent Radius of Noncircular Cross Sections. As far as the impedance characteristics and radiation pattern are concerned, a thin cylindrical antenna with a noncircular cross section behaves like a circular cylindrical antenna with an equivalent radius. In stating this characteristic, the terminal effect is, of course, not considered. The equivalent radius of many simply shaped cross sections can be found by the

method of conformal mapping.[9,10]   For an elliptical cross section the following simple relation exists:

$$a_{eq} = \tfrac{1}{2}(a + b) \tag{3-3}$$

where a = major axis of ellipse
    b = minor axis of ellipse

For a rectangular cross section the result is plotted in Fig. 3-7.   It is observed that
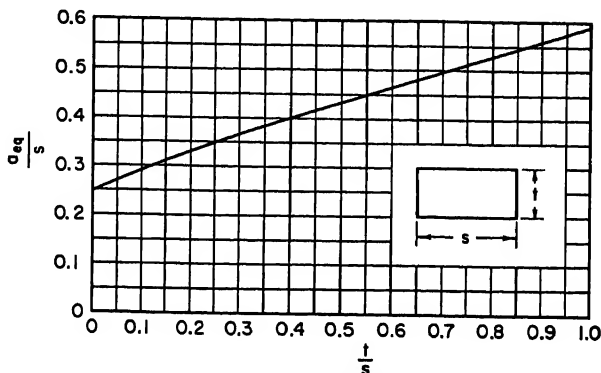
FIG. 3-7. Equivalent radius a_{eq} of a rectangle as a function of the ratio of thickness t to width s.

in the case of a strip, Eq. (3-3) and Fig. 3-7 give the identical result.   When the cross section has the form of a regular polygon, the result is tabulated in Table 3-2.

Table 3-2. Equivalent Radius of a Regular Polygon

n	3	4	5	6
a_{eq}/a	0.4214	0.5903	0.7563	0.9200

n = number of sides.
a = radius of the outscribed circle.

The equivalent radius of two parallel cylinders of radius ρ_1 and ρ_2 separated by a distance d between the centers is given by[11]

$$\log \rho_e = \frac{1}{(\rho_1 + \rho_2)^2} (\rho_1^2 \log \rho_1 + \rho_2^2 \log \rho_2 + 2\rho_1\rho_2 \log d) \tag{3-4}$$

Formulas for the equivalent radius of three cylinders and an angle strip are found in Ref. 11.

Patterns as a Function of Length and Diameter.   In this section only the radiation pattern of center-driven cylindrical antennas is discussed.   For base-driven antennas, the patterns depend very much upon the size of the ground plane.   The subject will be discussed in the section dealing with monopoles.

The radiation pattern of a center-driven cylindrical antenna in general depends upon its length and thickness.   The terminal condition which plays an important role in determining its impedance has a negligible effect on the pattern.   For thin antennas, the calculated pattern obtained by assuming a sinusoidal current distribution is a good approximation of the actual pattern.   Thus, with an assumed current

distribution of the form

$$I(z) = I_0 \sin k(\ell - |z|) \qquad +\ell \geq z \geq -\ell \tag{3-5}$$

the radiation field, expressed in a spherical coordinate system, is given by

$$E_\theta = \frac{j\eta I_0 e^{jkR}}{2\pi R} \left[\frac{\cos (k\ell \cos \theta) - \cos k\ell}{\sin \theta} \right] \tag{3-6}$$

where $\eta = (\mu/\epsilon)^{1/2} = 120\pi$ ohms
  θ = angle measured from axis of dipole, or z axis

The field pattern is obtained by evaluating the *magnitude* of the term contained in the brackets of Eq. (3-6). Some of the commonly referred to patterns are sketched in Fig. 3-8. Comparing those patterns with the actual patterns of a thin cylindrical

L=.25λ   L=.375λ   L=.5λ   L=.625λ   L=.75λ   L=.875λ

L=1.0λ   L=1.125λ   L=1.375λ   L=∞D
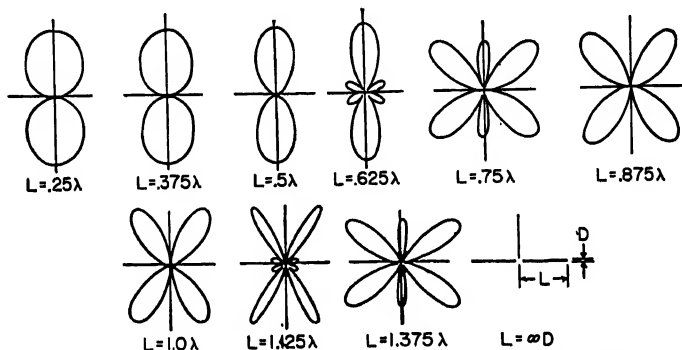
FIG. 3-8. Radiation patterns of center-driven dipoles assuming sinusoidal current distribution.

antenna obtained by measurement, one finds that the theoretical patterns based upon a sinusoidal current distribution do not contain the following information:

  1. The nulls between the lobes, except the "natural null" in the direction of the axis, are actually not vanishing.

  2. The phase of the field varies continuously from lobe to lobe instead of having a sudden jump of 180° between the adjacent lobes.

  3. The actual patterns vary slightly with respect to the diameter of the antenna instead of being independent of the thickness.

Depending upon the particular applications, some of the fine details may require special attention. In most cases, the idealized patterns based upon a sinusoidal current distribution give us sufficient information for design purpose.

When the half length ℓ of the antennas is less than about one-tenth wavelength, Eq. (3-6) is well approximated by

$$E_\theta = \frac{j\eta I_0 (k\ell)^2 e^{jkR}}{4\pi R} \sin \theta \tag{3-7}$$

The "figure-eight" pattern resulting from the plot of the sine function is not only a characteristic of short cylindrical antenna but also of all small dipole-type antennas. Equations (3-6) and (3-7) are also commonly used to evaluate the directivity of linear antennas. The directivity is defined as

$$D = \frac{\text{maximum radiation intensity}}{\text{average radiation intensity}} \tag{3-8}$$
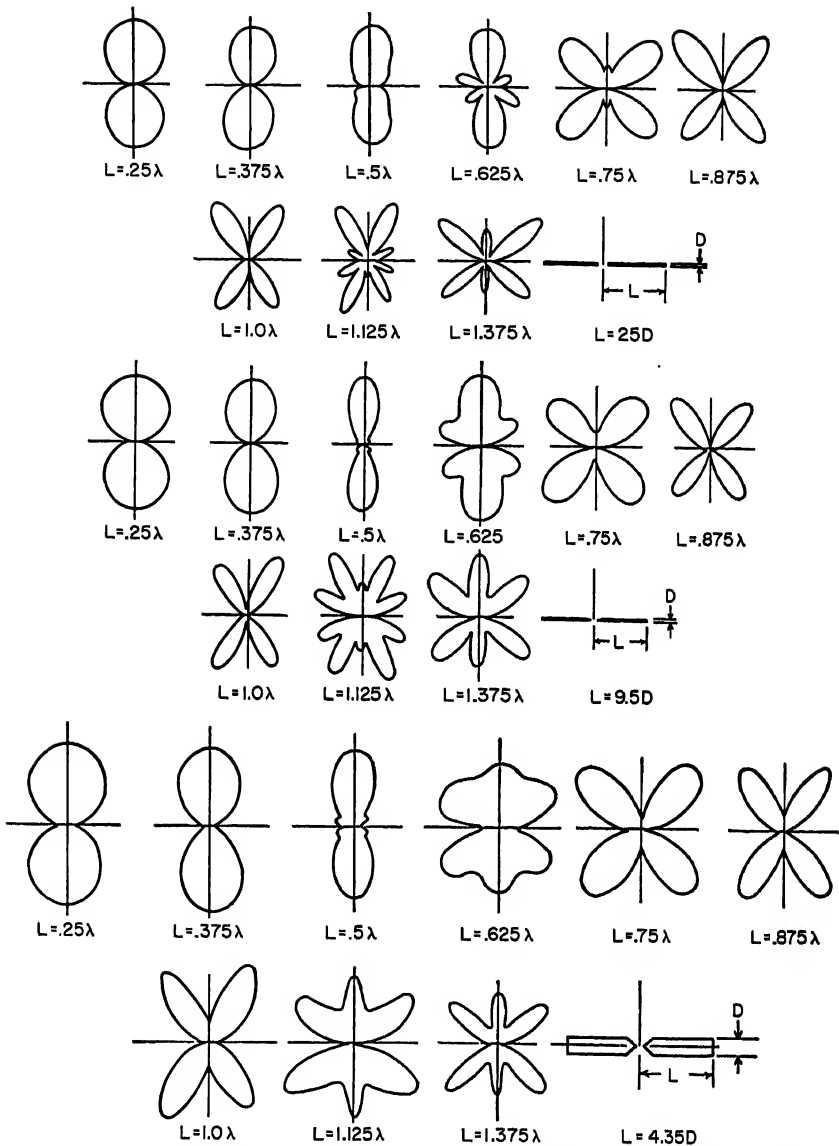
FIG. 3-9. Radiation patterns of center-driven cylindrical antenna with different length-to-diameter ratio.

For a short dipole, D is equal to 1.5. The directivity of a half-wave dipole ($\ell = \lambda/4$) is equal to 1.64. The half-wave dipole is often used as a reference antenna to describe the gain of more directive antennas, particularly arrays made of dipoles.

The radiation patterns of thick cylindrical antennas have been investigated only experimentally. Figure 3-9 shows some measured patterns corresponding to three values of the length-to-diameter ratio. The significant change as compared with Fig. 3-8 is the disappearance of the sharp nulls between the lobes.

3.2. BICONICAL DIPOLES

Impedance as a Function of Length and Cone Angle. When the angles of a symmetrical biconical antenna (Fig. 3-10) are small, the input impedance of the antenna can be calculated by using Schelkunoff's formula.[12] Some sample curves are shown in Fig. 3-11. While the biconical antenna is an excellent theoretical model for studying the essential property of a dipole-type antenna, small-angle biconical antennas are seldom used in practice. Wide-angle biconical antennas, or their derived types like the discones, however, are frequently used as broadband antennas. The broadband impedance characteristics occur when the angle of the cones, θ_0 of Fig. 3-10, lies between 30 and 60°. The exact value of θ_0 is not critical. Usually it is chosen so that the characteristic impedance of the biconical dipole matches as closely as possible the characteristic impedance of the line which feeds the antenna. The characteristic impedance of a biconical dipole as a function of the angle is plotted in Fig. 3-12. For a

Fig. 3-10. A biconical dipole.
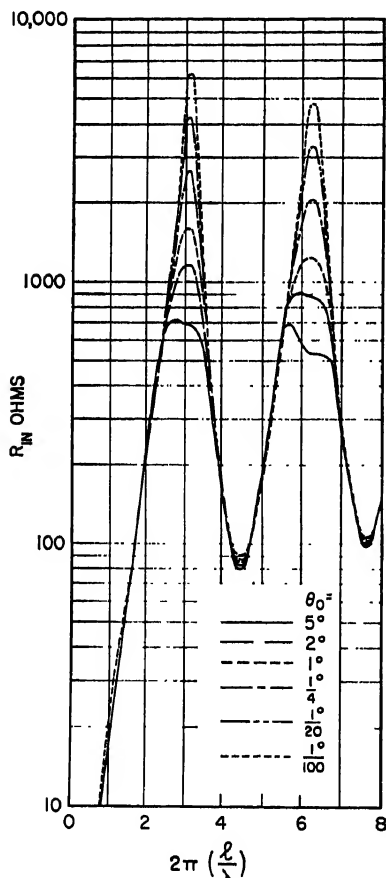
FIG. 3-11a. Input impedance of small-angle biconical antennas (resistance).
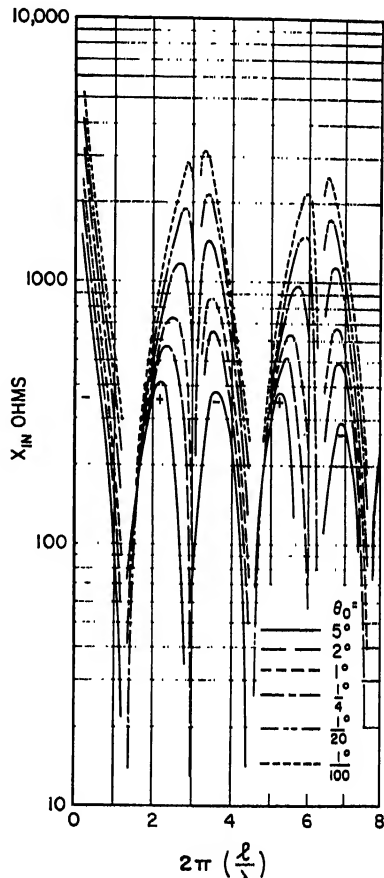
FIG. 3-11b. Input impedance of small-angle biconical antennas (reactance).

$$K = 120 \log_e \cot \left(\frac{\theta_0}{2}\right)$$
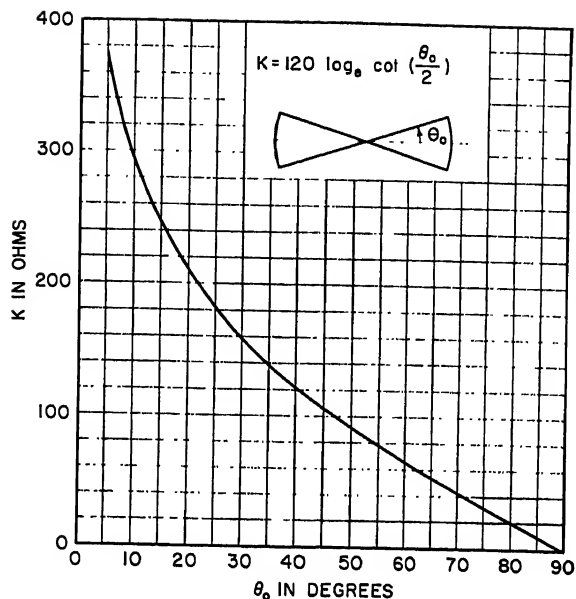
Fig. 3-12. Characteristic impedance of a biconical dipole.
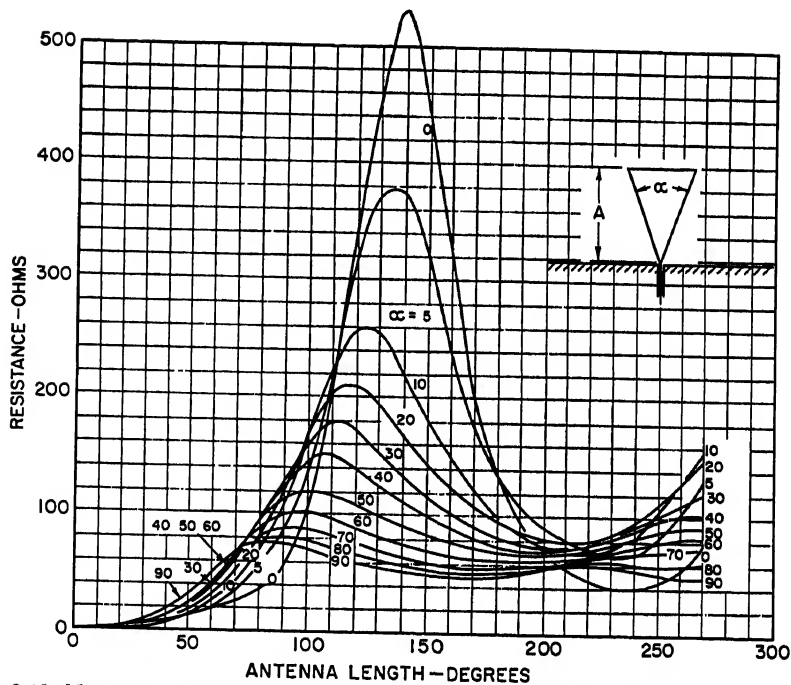
Fig. 3-13. Measured resistance curves of the conical unipole vs. length in electrical degrees for various flare angles.
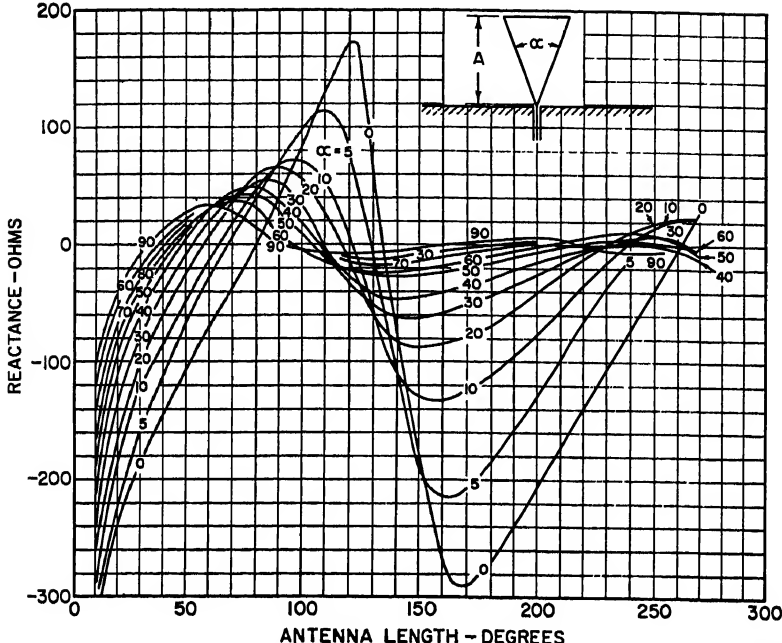
FIG. 3-14. Measured reactance curves of the conical unipole vs. length in electrical degrees for various flare angles.
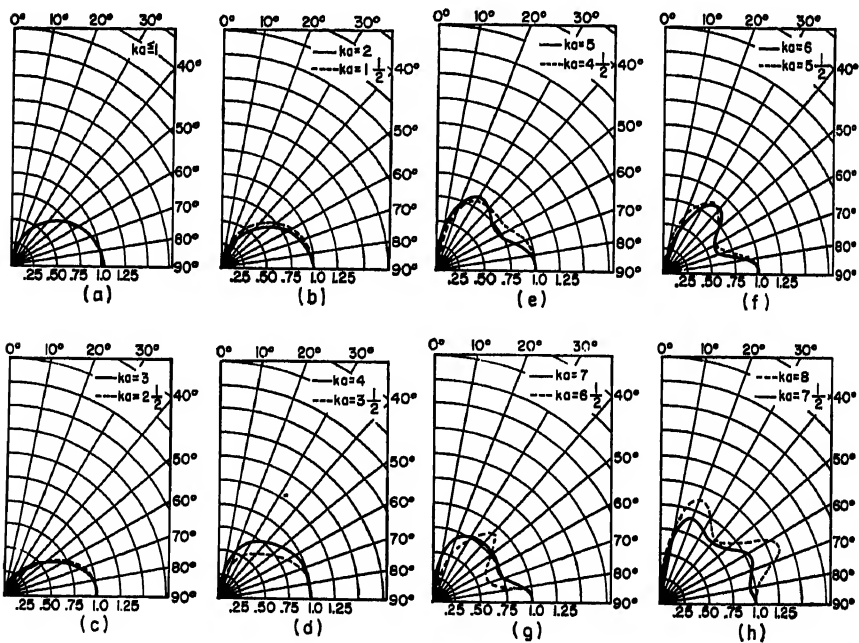
FIG. 3-15. Plots of the absolute values of the far-zone electric field as a function of the zenithal angle θ for various values of ka and with a flare angle equal to 60° ($\theta_0 = 30°$).

conical monopole driven against an infinitely large ground plane, the characteristic impedance and the input impedance of the antenna are equal to half of the corresponding values of a dipole. Several formulas[13] are available for computing the input impedance of wide-angle biconical antennas. Actual computation has been confined to a very few specific values of θ_0.[14,15] More complete information, however, is available from the experimental data obtained by Brown and Woodward.[16] Two curves are reproduced in Figs. 3-13 and 3-14. The case corresponding to $\alpha = 0°$ represents a cylindrical antenna having a diameter of 2.5 electrical degrees at a frequency of 500 Mc since the feed point was kept fixed at that diameter.

Patterns of the Biconical Dipole. The radiation patterns of biconical dipoles have been investigated theoretically by Papas and King.[17] Figure 3-15 shows the patterns of a 60°-flare-angle ($\theta_0 = 30°$) conical dipole for various values of ka, where $k = 2\pi/\lambda$ and $a =$ half length of the dipole, which is the same as the ℓ used in Fig. 3-10. Similar curves corresponding to different values of the flare angle have been obtained experimentally by Brown and Woodward.[18]

3.3. FOLDED DIPOLES

Equivalent Circuit of Folded Dipole. A folded dipole is formed by joining two cylindrical dipoles at the ends and driving them by a pair of transmission lines at the center of one arm as shown in Fig. 3-16. The diameters of the two arms can be either identical or different. A simple analysis, based upon a quasi-static approach, of the operation of a folded dipole of arbitrary dimension has recently been given by Uda and Mushiake.[19] According to their method, the excitation of a folded dipole can be considered as a superposition of two modes as shown in Fig. 3-17. The impedance of the symmetrical mode, characterized by two equal driving voltages, can be calculated by making use of the equivalent radius of two conductors as discussed in Sec. 3.1. The

FIG. 3-16. Folded dipole.

$$V_i = (1 + a) V$$

$$I_i = I_r + I_f$$

$$Z_i = \frac{(1 + a) V}{I_r + I_f}$$

$$a = \frac{\cos h^{-1} \dfrac{\nu^2 - \mu^2 + 1}{2\nu}}{\cos h^{-1} \dfrac{\nu^2 + \mu^2 - 1}{2\nu\mu}}$$

$$\mu = \rho_2/\rho_1, \quad \nu = d/\rho_1$$
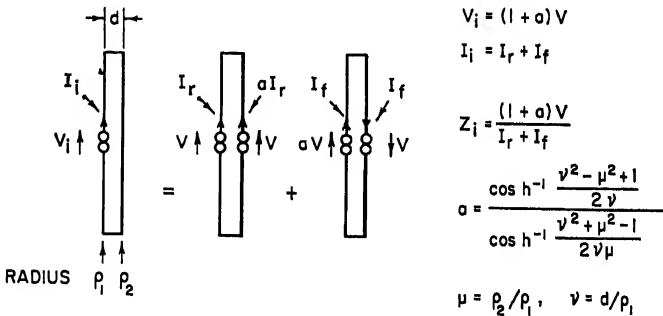
FIG. 3-17. Decomposition of the folded dipole into two fundamental modes.

equivalence is shown in Fig. 3-18. The impedance function Z_r is therefore the same as the impedance of a cylindrical dipole with an equivalent radius ρ_e given by

$$\log \rho_e = \log \rho_1 + \frac{1}{(1 + \mu)^2} (\mu^2 \log \mu + 2\mu \log \nu) \tag{3-9}$$

where the various parameters are explained in Fig. 3-18. The impedance of the asymmetrical mode, characterized by equal and opposite currents on the two arms,
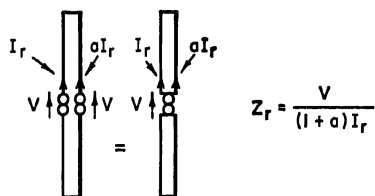
FIG. 3-18. The equivalent representation of the symmetrical mode in computing Z_r.
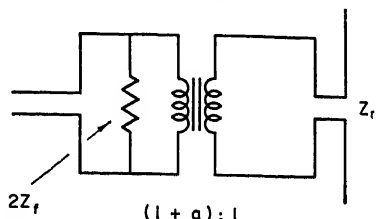
FIG. 3-19. Equivalent circuit of a folded dipole.

is the same as the shorted section of transmission line of length equal to ℓ; that is,

$$Z_f = \frac{(1+a)V}{2I_f} = jZ_0 \tan k\ell \tag{3-10}$$

where Z_0 is the characteristic impedance of the two-wire line. Expressed in terms of Z_r and Z_f, the input impedance of a folded dipole is given by

$$Z = \frac{V_i}{I_i} = \frac{(1+a)V}{I_r + I_f} = \frac{2(1+a)^2 Z_r Z_f}{(1+a)^2 Z_r + 2Z_f} \tag{3-11}$$

An equivalent circuit based upon Eq. (3-11) is shown in Fig. 3-19. For a folded dipole of length ℓ equal to $\lambda/4$, Z_f is very large compared with $(1+a)^2 Z_r$; hence

$$Z_{\lambda/4} = (1+a)^2 Z_r \tag{3-12}$$

Impedance Transformation as a Function of the Ratio of Conductor Sizes. The step-up impedance ratio $(1+a)^2$ as a function of μ and ν has been calculated by Mushiake.[20] The diagram is reproduced in Fig. 3-20 using the formula for a given
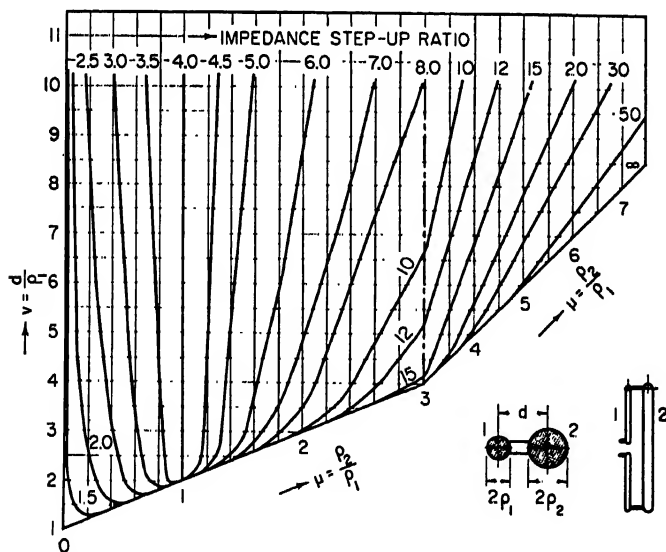
FIG. 3-20. Step-up transformation chart for a folded dipole.

in Fig. 3-17. When ρ_1 and ρ_2 are small compared with d, the value of a is given to a good approximation by

$$a = \frac{\log{(d/\rho_1)}}{\log{(d/\rho_2)}} \tag{3-13}$$

This formula was first derived by Guertler.[21] Equation (3-12) can also be used to calculate the input impedance of a Yagi-Uda array if the driving unit is made of a folded dipole as shown in Fig. 3-21a. The impedance function $Z_{\lambda/4}$ is then interpreted as the input impedance of the array shown in Fig. 3-21b.
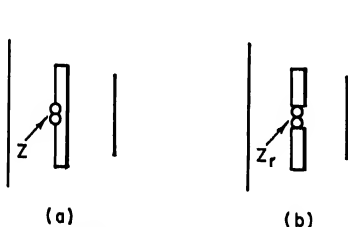
FIG. 3-21. Yagi-Uda array driven by a folded dipole.
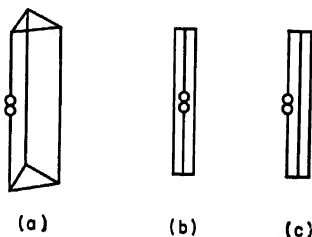
FIG. 3-22. Triply folded dipoles.

Multiple-folded Dipoles. As indicated by Eq. (3-12), the impedance level of a folded dipole can be adjusted by choosing a proper value of the step-up ratio. Another way of adjusting the impedance level is to use a multiple-folded dipole. Figure 3-22 shows several possible arrangements of a triply folded dipole. If the conductors are of the same size and a half wave long, the input impedance is approximately equal to $9Z_r$, where Z_r is the input impedance of an antenna formed by the three conductors driven simultaneously by a single generator. The equivalent radius of such a combination[22] is equal to $(\rho d^2)^{1/3}$, where d is the separation of the conductors and ρ is the radius of each conductor.

3.4. ASYMMETRICAL DIPOLES

Mean-value Formulas for the Impedance of Asymmetrical Dipoles. Asymmetrical dipoles are the prototype models of many antennas commonly used on aircrafts, like the tail-cap antennas, wing-cap antennas, and the trailing-wire antenna.[23] While no accurate formula is yet available for determining the input impedance of an asymmetrical dipole, several approximate treatments have been suggested.[24] One of them is the so-called "mean-value formula."[25] According to this formula, the impedance of an asymmetrical dipole is given approximately by

$$Z = \tfrac{1}{2}(Z_1 + Z_2) \tag{3-14}$$
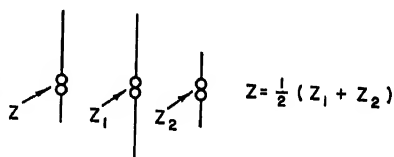
FIG. 3-23. Impedances involved in the mean-value formula.

where Z_1 and Z_2 denote the impedance of two center-driven dipoles of half length equal to ℓ_1 and ℓ_2 as shown in Fig. 3-23. The formula, which is not exact, is the simplest one to use in estimating the impedance of asymmetrical dipoles.

Patterns of Asymmetrical Dipoles. The method which leads to the mean-value impedance formula can also be used to obtain the radiation pattern of an asymmetrical

$\ell_2 = \frac{1}{4}\lambda \quad \ell_1 = 3\frac{1}{4}\lambda$

$\ell_2 = \frac{3}{8}\lambda \quad \ell = 3\frac{1}{8}\lambda$

$\ell_2 = \frac{7}{16}\lambda \quad \ell = 3\frac{1}{16}\lambda$

$\ell_2 = \frac{1}{2}\lambda \quad \ell_1 = 3\lambda$

$\ell_2 = \frac{9}{16}\lambda \quad \ell_1 = 2\frac{15}{16}\lambda$

$\ell_2 = \frac{3}{4}\lambda \quad \ell_1 = 2\frac{3}{4}\lambda$

$\ell_2 = \lambda \quad \ell_1 = 2\frac{1}{2}\lambda$

$\ell_2 = 1\frac{1}{8}\lambda \quad \ell_1 = 2\frac{3}{8}\lambda$

$\ell_2 = 1\frac{3}{8}\lambda \quad \ell_1 = 2\frac{1}{8}\lambda$

$2a$

ℓ_2

$\ell_1 + \ell_2 = 3\frac{1}{2}\lambda$

$\dfrac{\ell_1 + \ell_2}{a} = 83$

ℓ_1

$\ell_2 = 1\frac{1}{2}\lambda \quad \ell_1 = 2\lambda$

$\ell_2 = 1\frac{3}{4}\lambda \quad \ell_1 = 1\frac{3}{4}\lambda$
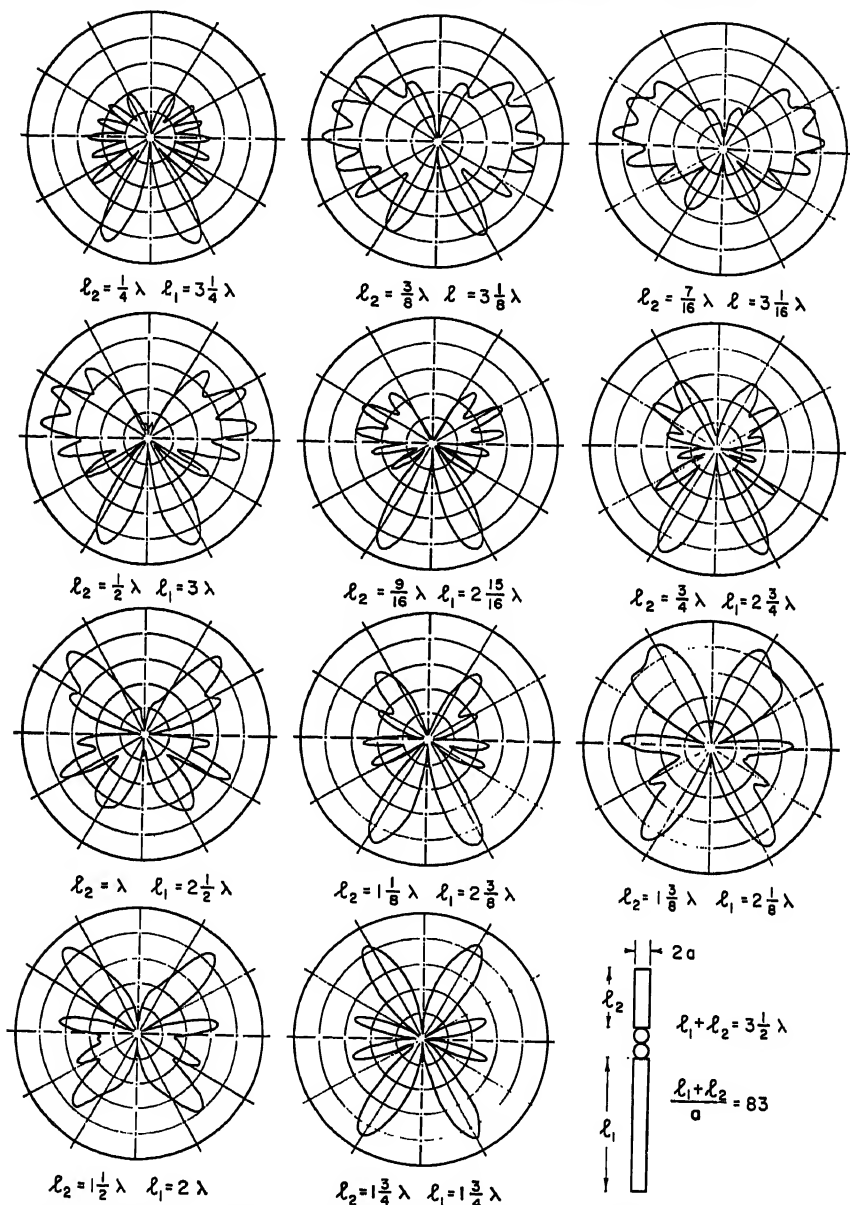
FIG. 3-24. Radiation patterns of asymmetrical dipoles with different asymmetry ratio.

dipole. No calculation, however, has actually been made to supply this information. A large amount of experimental data has been gathered at the Antenna Laboratory of Stanford Research Institute.[26] Figure 3-24 shows some typical patterns of a number of asymmetrical dipoles with various degrees of asymmetry. Figure 3-25 shows the change in the pattern as the frequency is varied while keeping the asymmetry ratio constant.
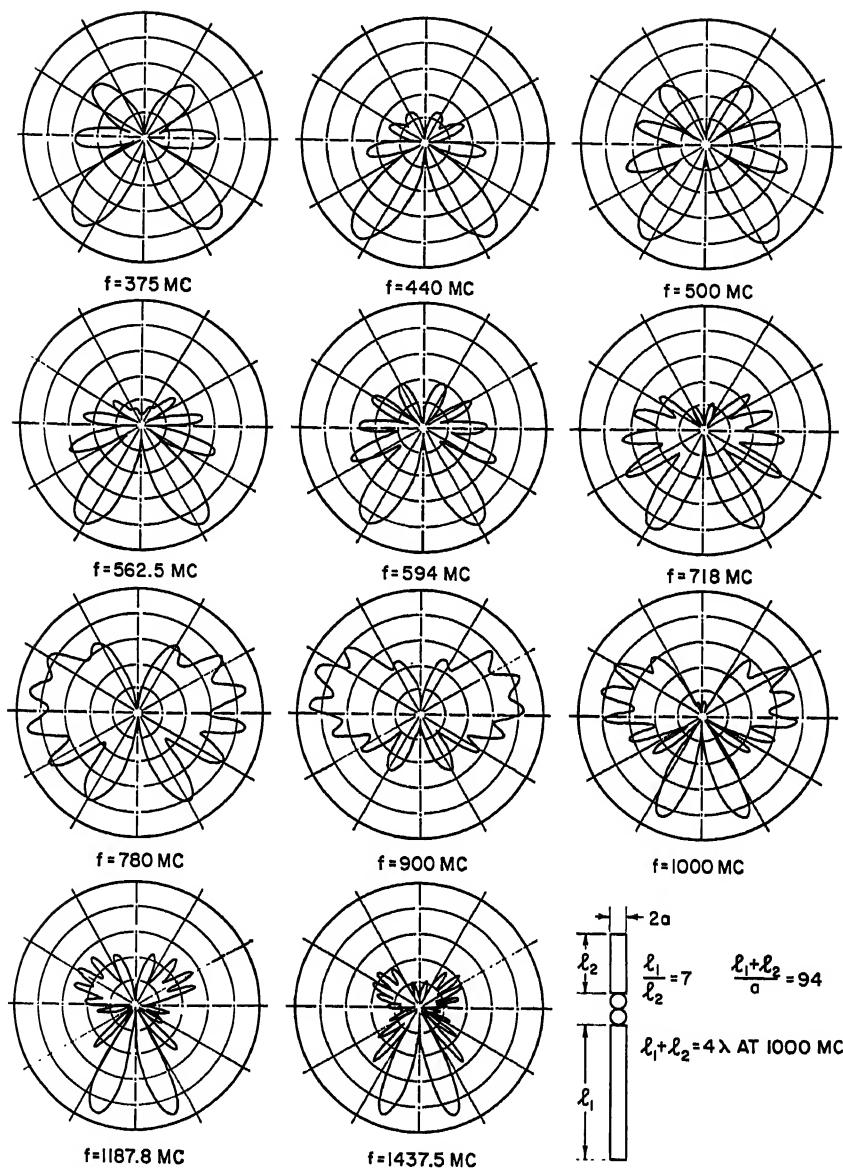
Fig. 3-25. Radiation patterns of an asymmetrical dipole at different frequencies.

3.5. SLEEVE DIPOLES

Equivalent Circuit of a Sleeve Dipole. The geometrical shape of a sleeve antenna, or a sleeve monopole, is sketched in Fig. 3-26a. If the image of the structure is included, then we have a sleeve dipole as shown in Fig. 3-26b. A sleeve dipole can therefore be considered as a doubly fed antenna where the current is a relative maximum at the center of the dipole or at the base of the monopole. Antiresonances of

the antenna impedance function take place when S is approximately an odd multiple of a quarter wavelength or L is a multiple of a half wavelength.   Theoretical analysis of the sleeve dipole has so far been limited to very restricted ranges of L and S,[27,28] and the results do not have the same degree of accuracy as the theory of a center-driven dipole.

Impedance as a Function of Length and Diameter.   The most complete experimental data on the impedance characteristics of a sleeve antenna are found in the article by Norgorden and Walters.[29]   Two sets of curves are reproduced here, Fig. 3-27a and b, showing the general characteristics of sleeve dipoles corresponding to a different ratio of L/S.   The over-all length of the antenna, the sum of L and S, is fixed at 30 in.   Similar curves, but covering a smaller range, are also found in the Radio Research Laboratory book.[30]

FIG. 3-26. The sleeve antenna.

Patterns of the Sleeve Dipole.   The radiation patterns of the sleeve antennas have also been investigated experimentally by Norgorden and Walters.[31]   Figure 3-28

SLEEVE DIAMETER...4"
RADIATOR DIAMETER..1"
RADIATOR LENGTH
SLEEVE LENGTH
CURVE 1 4
CURVE 2 2
CURVE 6 .... 1.4
CURVE 3 1
CURVE 4 .... 0.50
CURVE 5 .... 0.25
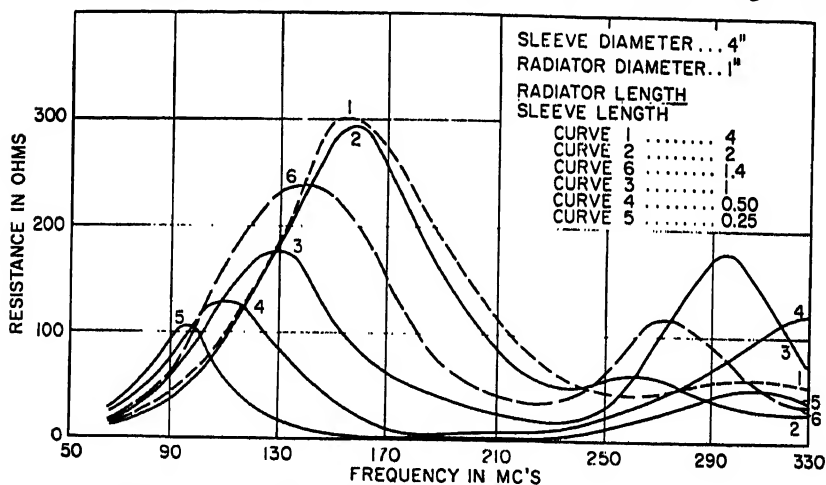
FIG. 3-27a. Input resistance of sleeve antenna as a function of frequency.

shows the change of patterns as a result of varying the frequency.   Figure 3-29 shows the change of patterns when the ratio L/S is varied.   The small fluctuations due to the size of the ground plane have been smoothed out.

3.6. COUPLED ANTENNAS

Circuit Relationships of Radiating Systems.   When several antennas are coupled to each other the input voltage and input currents to the antennas follow the same relationship as ordinary coupled circuits.[32]   For a system of n antennas, the relationships are

$$V_i = \sum_{j=1}^{n} Z_{ij} I_j \qquad i = 1, 2, \ldots, n \qquad (3\text{-}15)$$

SLEEVE DIAMETER...4"
RADIATOR DIAMETER..1"

RADIATOR LENGTH
SLEEVE LENGTH

CURVE 1	....	4
CURVE 2	....	2
CURVE 6	....	1.4
CURVE 3	....	1
CURVE 4	....	0.50
CURVE 5	....	0.25
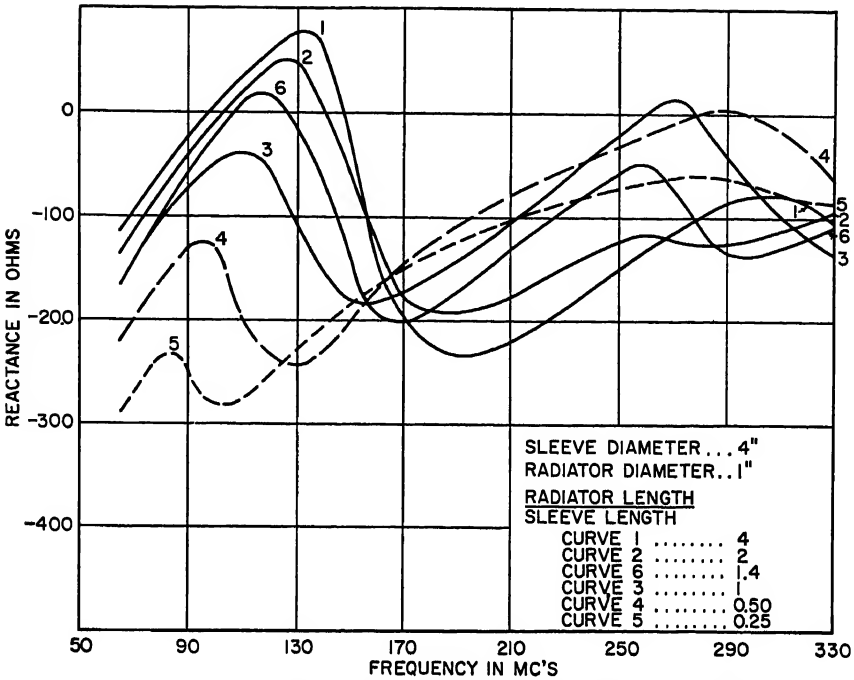
FIG. 3-27b. Input reactance of sleeve antenna as a function of frequency.
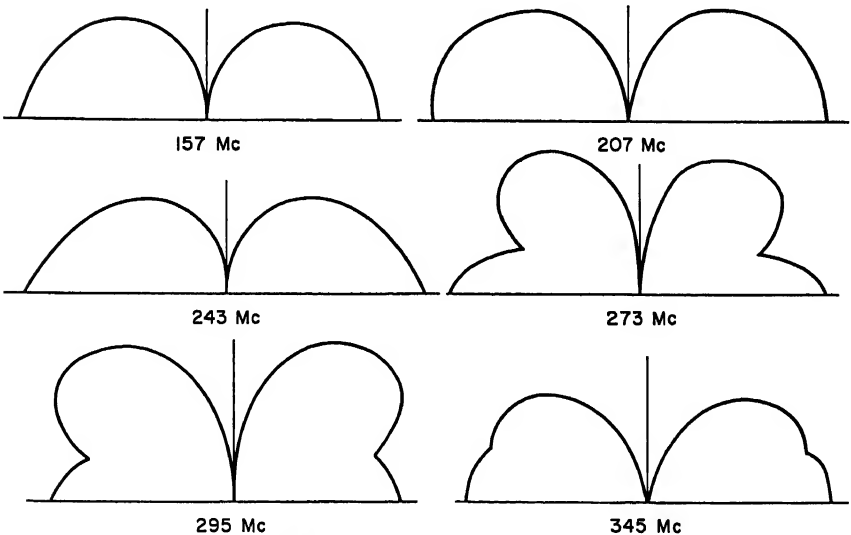
FIG. 3-28. Vertical field patterns of sleeve antennas with fixed radiator diameter (½ in.), sleeve diameter (4 in.), radiator length to sleeve length of 4, and a total length of 30 in. at frequencies as shown.
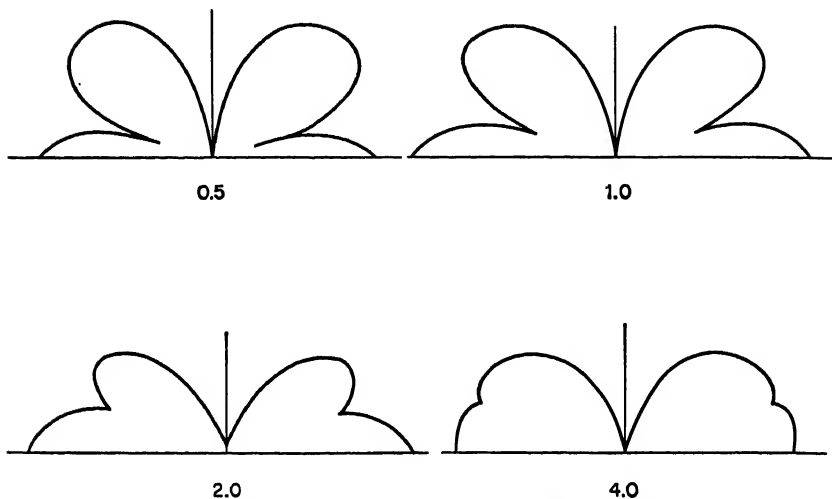
FIG. 3-29. Vertical field patterns of sleeve antennas with fixed radiator diameter (½ in.), sleeve diameter (4 in.), and total length of 30 in. at 345 Mc. Ratios of radiator to sleeve length are indicated under each figure.
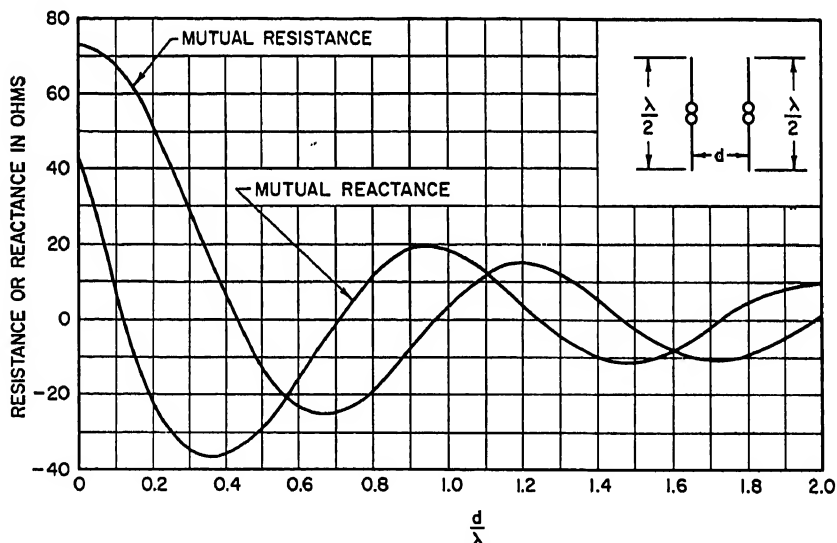
FIG. 3-30. Mutual impedance between two parallel half-wave antennas placed side by side.

where Z_{ii} is called the self-impedance of antenna i and Z_{ij} or Z_{ji} is called the mutual impedance between antenna i and antenna j.   In the case of linear radiators, Carter's method, or the induced-emf method based upon sinusoidal current distribution, is the simplest one to use in determining the various Z's.   The method applies only to antennas shorter than a half wavelength.   The self-impedance determined by this method is the same as that given by Eq. (3-1).   The formulas for the mutual impedance of two parallel antennas of equal size are found in Carter's original paper or in Kraus's book.[33]   Figure 3-30 shows the mutual impedance of two parallel half-wave

antennas placed side by side. Figure 3-31 shows the mutual impedance of two parallel collinear half-wave antennas. Mutual impedances of two parallel antennas of unequal sizes have been investigated by several authors.[34-36] The induced-emf
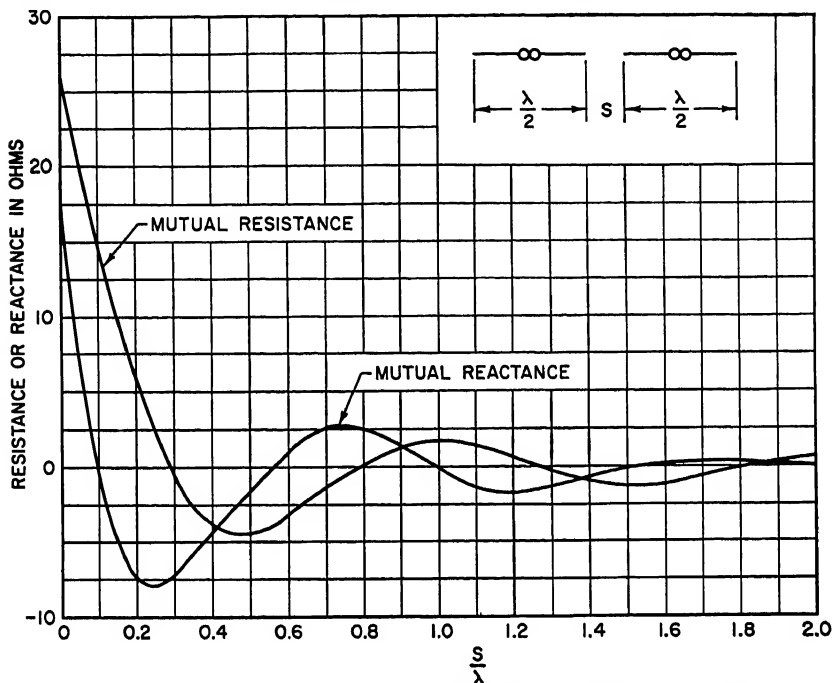
Fig. 3-31. Mutual impedance between two collinear half-wave antennas.

method has also been applied to crossed or skewed antennas[37,38] to evaluate their mutual impedance. Refined calculations based upon Hallén's integral-equation technique are found in the works of Tai,[39] Bouwkamp,[40] and Uda and Mushiake.[41] The last two authors also evaluated the self-impedance and mutual impedance of parallel antennas of unequal sizes, which ultimately applies to the design of Yagi-Uda arrays.

3.7. MONOPOLE ANTENNAS

Relationship to Balanced Antennas. When a monopole is mounted on an ideally infinite ground plane its impedance and radiation characteristics can be deduced from that of a dipole of twice its length in free space. For a base-driven monopole, its input impedance is equal to one-half that of the center-driven dipole, and the radiation pattern above the infinite ground plane is identical with the upper half of the radiation pattern of the corresponding dipole. When the ground plane is of finite size, the image theorem does not apply.

Several methods have been devised to investigate the characteristics of a monopole mounted on a finite-size ground plane. The first method is due to Bolljahn,[42] who considers the problem from the point of view of symmetrical components. The decomposition is shown in Fig. 3-32, where the ground plane is assumed of the form of an infinitely thin conducting disk. For the symmetrical mode of excitation the presence of the disk has no effect upon the radiation of the two elements. The

problem is therefore the same as if the two elements were placed in free space. The antisymmetrical pair of current elements excites equal currents on the top and the bottom sides of the disk. This mode is responsible for the variation of the input impedance of the antenna as a function of the disk diameter. It is also responsible for the asymmetry of the resultant radiation pattern with respect to the ground plane. Bolljahn's original work was developed by assuming a short monopole on a

Fig. 3-32. Monopole and finite-size ground plane and its decomposition into two modes of excitation.

disk. The entire analysis is found in Schelkunoff's book on "Advanced Antenna Theory."[43] His study of the characteristics of large ground planes was later extended by Storer[44] to monopoles of arbitrary length.

Effect of Finite-size Ground Plane on Impedance and Pattern. According to Storer, who used a variational method to formulate the problem, the change of the input impedance of a base-driven monopole erected upon a large circular ground plane can be written as

$$\Delta Z = Z - Z_0 = j\frac{60}{kd} e^{-jkd} \left| k \int_0^h \frac{I(z)}{I(0)} \, dz \right|^2 \tag{3-16}$$

where Z_0 = impedance of monopole referred to an infinite ground plane, ohms
d = diameter of circular ground plane
$k = 2\pi/\lambda$
h = height of monopole
$I(z)$ = current-distribution function of monopole
$I(0)$ = base current or input current

The function $j(60/kd)e^{-jkd}$, which is independent of the current distribution, is plotted in Fig. 3-33. The real and the imaginary parts of the function are respectively equal to $(R - R_0) \Big/ \left| k \int_0^h \frac{I(z)}{I(0)} \, dz \right|^2$ and $(X - X_0) \Big/ \left| k \int_0^h \frac{I(z)}{I(0)} \, dz \right|^2$. For a quarter-wave monopole, if we assume $I(z) = I(0) \cos kz$, then

$$\left| k \int_0^h \frac{I(z)}{I(0)} \, dz \right| = 1 \tag{3-17}$$

Thus, with a ground plane of a diameter greater than 10 wavelengths, it is seen from Fig. 3-33 that the variation of the resistance or the reactance of a quarter-wave monopole is less than 1 ohm.

While the effect of a large ground plane upon the input impedance of a monopole is not too great, the radiation pattern is affected considerably. The obvious effect of a large ground plane on the pattern is to cast an imperfect shadow at the bottom half of the plane. If the diameter of the ground plane is on the order of a wavelength, the resultant pattern can be obtained only by means of the exact solution[45] of the disk problem based upon spheroidal wave functions. For a large ground plane, the pattern distortion can be found either by Storer's analysis[46] or simply from the established solution for a half-plane sheet.[47,48] A typical pattern of a monopole over a circular ground plane obtained experimentally by Little et al.[49] is shown in Fig. 3-34. The asymmetry of the pattern is, of course, due to environmental diffraction. The position of the maximum lobe θ_m, in the case of a short monopole, can be
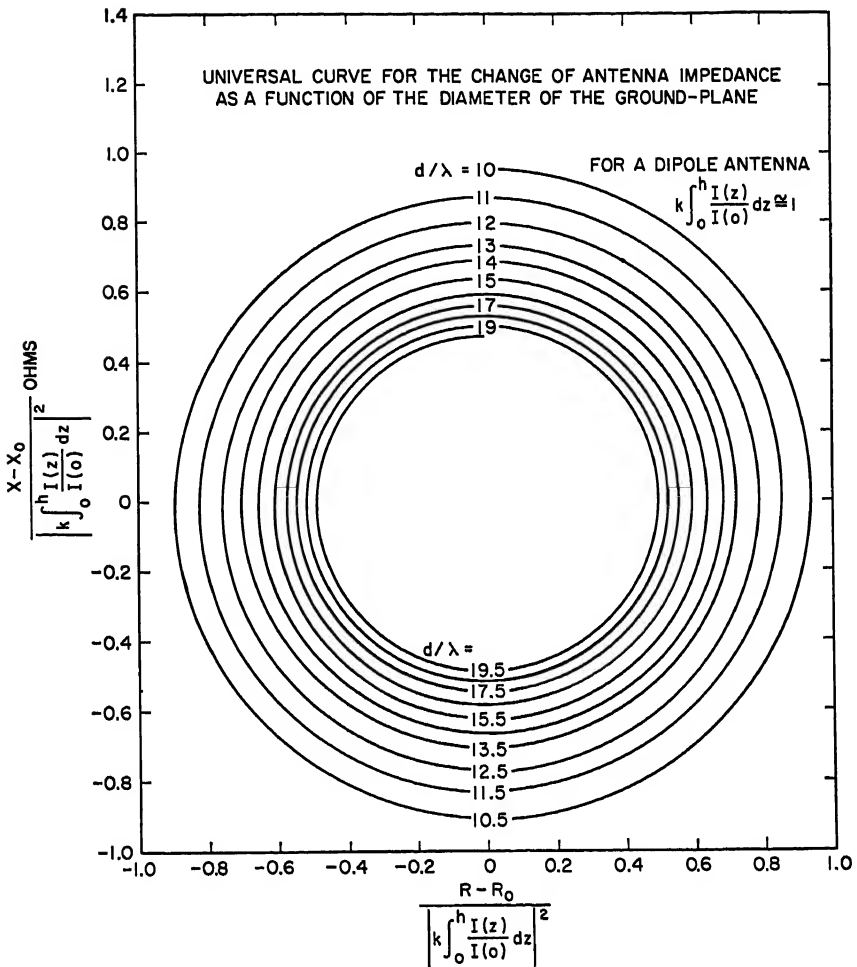
FIG. 3-33. Universal curve for the change of antenna impedance as a function of the diameter of the ground plane.
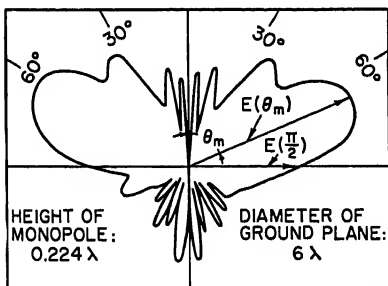
FIG. 3-34. Radiation pattern of a monopole mounted on a circular ground plane.
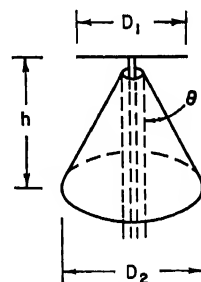
FIG. 3-35. Discone antenna.

predicted quite accurately using the formula derivable from the half-sheet problem:

$$\sin \theta_m = 1 - \frac{3\lambda}{4d} \qquad (3\text{-}18)$$

where d is the diameter of the circular ground plane. The ratio of the values of $E(\pi/2)$ and $E(\theta_m)$, on the other hand, is practically independent of the size of the ground plane. It is given by

$$\frac{E(\pi/2)}{E(\theta_m)} = 0.428$$

3.8. MISCELLANEOUS LINEAR RADIATORS

Discone Antenna.[50] The discone antenna is formed by replacing one section of a biconical antenna by a disk as shown in Fig. 3-35. Its impedance characteristic is quite similar to an ordinary biconical antenna. Best broadband impedance characteristic is obtained when the angle of the cone θ is chosen around 30°. The height h of the cone should be at least one-third wavelength at the lowest operating frequency of the band. The dimension of the disk, D_1, has a great effect upon the radiation pattern of the antenna as the frequency is changed. A large disk tends to reduce the field intensity above the horizontal direction, as indicated by the previous discussion on the circular ground plane. A too small disk, on the other hand, tends to upset the broadband impedance characteristic of the antenna and also tilts the pattern toward the cone. Some typical dimensions are found in Kandoian's paper.
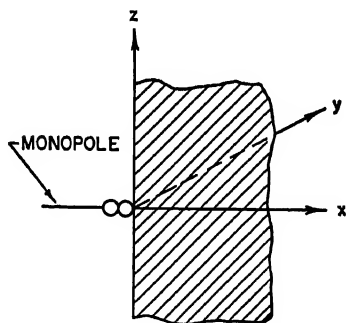
FIG. 3-36. Monopole and half-plane sheet.
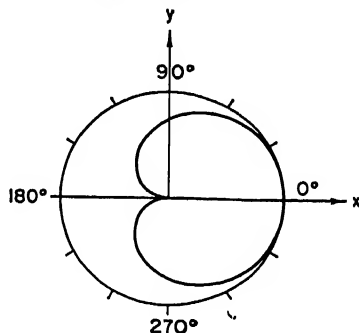
FIG. 3-37. Radiation pattern of a quarter-wave monopole mounted at the edge of a half-plane sheet.

Monopole Mounted on the Edge of a Sheet.[51] When a monopole is driven against a large conducting half-plane sheet (Fig. 3-36), its radiation characteristics and its input impedance differ considerably from the case of a monopole driven against a large ground plane. If the sheet is semi-infinite and the monopole is short, the radiation pattern of the system in the xy plane is shown in Fig. 3-37. Although there is no complete theoretical analysis on the impedance of an antenna mounted on the edge of a sheet in the case of a quarter-wave monopole, its input resistance is approximately equal to the radiation resistance calculated by means of the Poynting-vector method. This resistance is equal to 86.3 ohms.

Monopole with Radial-rod Ground Plane. When a ground plane is in contact with the earth, the latter provides a current path that modifies the characteristics of a finite-size ground plane, as previously discussed. Considering a ground system as being made of radial conductors embedded in a conducting medium, Wait and Pope[52] have
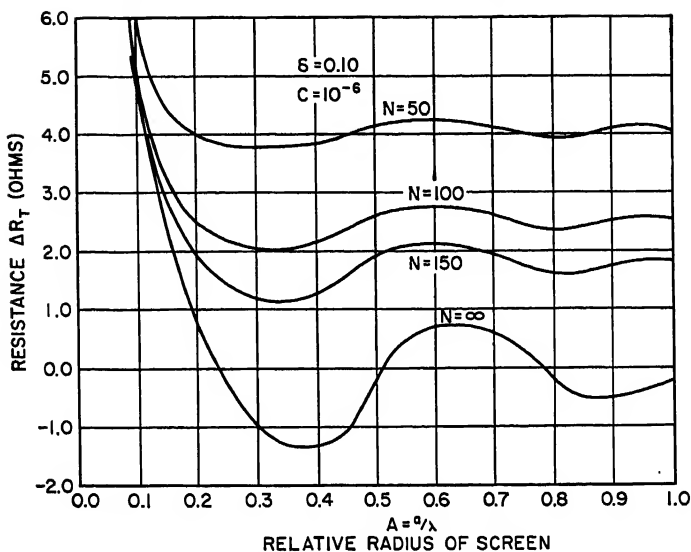
FIG. 3-38. The incremental self-resistance of a vertical quarter-wave monopole on a radial conductor ground system for a wire radius equal to 10^{-6} of a free-space wavelength.
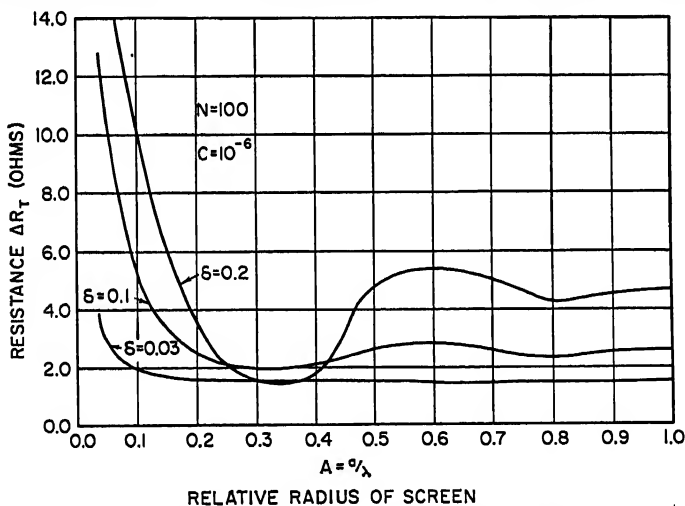
FIG. 3-39. The incremental self-resistance of a vertical quarter-wave monopole on a radial conductor ground system for a wire radius equal to 10^{-6} of a free-space wavelength.

calculated the incremental resistance of a vertical quarter-wave monopole driven against the ground system. The incremental resistance is the real part of ΔZ_T, defined by

$$\Delta Z_T = Z - Z_0$$

where Z_0 = impedance of monopole referred to an infinite perfectly conducting ground plane

Z = impedance of antenna in presence of ground system

The real part of ΔZ_T is plotted in Figs. 3-38 and 3-39 as a function of various param-

eters, which are defined as follows.

$$\delta = \left(\frac{\epsilon_0 \omega}{\sigma}\right)^{\frac{1}{2}}$$

where σ = conductivity of earth
N = number of radial conductors
C = radius of wire/free-space wavelength
A = radius of screen/free-space wavelength

Other data including the ratio of the current carried by the radial conductors to the total current are also discussed in their paper. According to their conclusion, a ground screen radius greater than about one-third wavelength is wasteful, and it is feasible to choose a large number of radials to reduce the resistance increment to a low value. For a given total weight of wire it is preferable to use a conductor of smaller diameter, say, No. 22 wire, and to employ 150 or more radial conductors. In the case of a good conducting earth, they have shown that the distortion of the pattern is of a small order of magnitude.
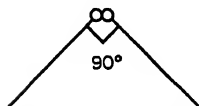
FIG. 3-40. The quadrant antenna.

The Quadrant Antenna. When two short dipoles are placed perpendicular to each other and driven in phase, the resultant pattern in the plane containing the dipoles is almost omnidirectional. Similar patterns can be produced by properly bending a single dipole as shown in Fig. 3-40. The structure is called the quadrant antenna by Wells,[53] who made an extensive study of its radiation and impedance characteristics. An omnidirectional pattern is obtained when its limbs are of the order of $\frac{1}{2}\lambda$ long.

REFERENCES

1. The theories of cylindrical antennas are discussed in several textbooks. S. A. Schelkunoff: "Advanced Antenna Theory," John Wiley & Sons, Inc., New York, 1952. This book contains the detailed information on Hallén's integral-equation method of treating cylindrical antennas and also Schelkunoff's own method by considering the cylindrical antenna as a perturbed biconical antenna. The essential steps of Hallén's method are also covered in J. D. Kraus: "Antennas," chap. 9, McGraw-Hill Book Company, Inc., New York, 1950. See also R. W. P. King: "The Theory of Linear Antennas," Harvard University Press, Cambridge, Mass., 1956. This book is by far the most comprehensive treatise on the theory of linear antennas.
2. P. S. Carter: "Circuit Relations in Radiating Systems and Applications to Antenna Problems," *Proc. IRE*, vol. 20, pp. 1004–1041, 1932; see also sec. 10-3 of Kraus' book. Carter's treatment of system of linear antennas is an important contribution to the theory and practice of linear antennas.
3. Reference 1.
4. Reference 1.
5. George H. Brown and O. M. Woodward, Jr.: "Experimentally Determined Impedance Characteristics of Cylindrical Antennas," *Proc. IRE*, vol. 33, pp. 257–262, 1945; see also Radio Research Laboratory Staff: chap. 4, "Very High Frequency Techniques," McGraw-Hill Book Company, Inc., New York, 1947. The work of Brown and Woodward demonstrates very clearly the importance of the terminal condition on the resultant input impedance of an antenna.
6. S. A. Schelkunoff and H. T. Friis: "Antennas: Theory and Practice," sec. 13.22, pp. 445-448, John Wiley & Sons, Inc., New York, 1952.
7. Ronald W. P. King: "Antennas and Open-wire Lines. Part I. Theory and Summary of Measurements," *J. Appl. Phys.*, vol. 20, pp. 832–850, 1949; "The End Correction for a Coaxial Line When Driving an Antenna over a Ground Screen," *IRE Trans. on Antennas and Propagation*, vol. AP-3, no. 2, p. 66, April, 1955.
8. John R. Whinnery: "The Effect of Input Configuration on Antenna Impedance," *J. Appl. Phys.*, vol. 21, pp. 945–956, 1950.
9. Carson Flammer: "Equivalent Radii of Thin Cylindrical Antennas with Arbitrary Cross Sections," *Stanford Research Inst., Aircraft Radio Systems Lab., Tech. Rept.* Stanford, Calif., 1950. This report contains the analysis of elliptic cross section rectangular cross section, and the Joukowsky profiles.

10. Y. T. Lo: "A Note on the Cylindrical Antenna of Noncircular Cross-section," *J. Appl. Phys.*, vol. 24, pp. 1338–1339, 1953. The paper treats the regular polygons.
11. S. Uda and Y. Mushiake: "Yagi-Uda Antennas," p. 19, Maruzen Co., Ltd., Tokyo, 1954.
12. S. A. Schelkunoff: "Theory of Antennas of Arbitrary Size and Shape," *Proc. IRE*, vol. 29, p. 493, September, 1941; see also Ref. 1, chap. 2.
13. Reference 1, chap. 2.
14. C. H. Papas and R. King: "Input Impedance of Wide-angle Conical Antennas Fed by a Coaxial Line," *Proc. IRE*, vol. 37, p. 1269, November, 1949.
15. C. T. Tai: "Application of a Variational Principle to Biconical Antennas," *J. Appl. Phys.*, vol. 20, p. 1076, November, 1949.
16. G. H. Brown and O. M. Woodward, Jr.: "Experimentally Determined Radiation Characteristics of Conical and Triangular Antennas," *RCA Rev.*, vol. 13, no. 4, p. 425, December, 1952.
17. C. H. Papas and R. King: "Radiation from Wide-angle Conical Antennas Fed by a Coaxial Line," *Proc. IRE*, vol. 39, p. 1269, November, 1949.
18. Reference 16.
19. Reference 11, chap. 10.
20. Y. Mushiake: "An Exact Step-up Impedance Ratio Chart of a Folded Antenna," *IRE Trans.*, vol. AP-3, no. 4, p. 163, October, 1954.
21. R. Guertler: "Impedance Transformation in Folded Dipoles," *J. Brit. IRE*, vol. 9, p. 344, September, 1949.
22. Reference 11, p. 20.
23. J. V. N. Granger and J. T. Bolljahn: "Aircraft Antennas," *Proc. IRE*, vol. 43, p. 533, May, 1955; see also chap. 27 of this Handbook.
24. J. V. N. Granger: "Wing-cap and Tail-cap Aircraft Antennas," *Stanford Research Inst., Aircraft Radio Systems Lab., Tech. Rept.* 6, Stanford, Calif., March, 1950.
25. R. W. P. King: "Asymmetrically Driven Antennas and the Sleeve Dipole," *Proc. IRE*, vol. 38, p. 1154, October, 1950.
26. Private communication from I. Carswell.
27. Reference 25.
28. J. Taylor: "The Sleeve Antenna," *Harvard Univ. Cruft Lab., Tech. Rept.* 128, 1951.
29. O. Norgorden and A. W. Walters: "Experimentally Determined Characteristics of Cylindrical Sleeve Antennas," *J. Am. Naval Engrs.*, p. 365, May, 1950.
30. Reference 5, "Very High-frequency Techniques," vol. 2, chap. 5.
31. Reference 29.
32. Reference 2, Carter, p. 1004.
33. Reference 1, Kraus, chap. 10, pp. 269–270.
34. C. R. Cox: "Mutual Impedance between Vertical Antennas of Unequal Heights," *Proc. IRE*, vol. 35, p. 1367, November, 1947.
35. G. Barzilai: "Mutual Impedance of Parallel Aerials," *Wireless Engr.*, vol. 25, p. 347, November, 1948.
36. R. G. Medhurst: "Mutual Impedance of Parallel Aerials," *Wireless Engr.*, vol. 28, p. 67, February, 1951.
37. L. Lewin: "Mutual Impedance of Wire Aerials," *Wireless Eng.*, vol. 28, p. 352, December, 1951.
38. R. G. Medhurst: "Dipole Aerials in Close Proximity," *Wireless Engr.*, vol. 28, p. 356, December, 1951.
39. C. T. Tai: "Coupled Antennas," *Proc. IRE*, vol. 36, p. 487, April, 1948.
40. C. J. Bouwkamp: "On the Theory of Coupled Antennae," *Philips Research Repts.*, vol. 3, p. 213, June, 1948.
41. Reference 11, chap. 4.
42. J. T. Bolljahn: "Antennas Near Conducting Sheets of Finite Size," *Univ. Calif., Dept. Engineering, Rept.* 162, December, 1949.
43. Reference 1, p. 83.
44. J. E. Storer: "The Impedance of an Antenna over a Large Circular Screen," *J. Appl. Phys.*, vol. 12, p. 1058, August, 1951.
45. A. Leitner and R. D. Spence: "Effect of a Circular Ground-plane on Antenna Radiation," *J. Appl. Phys.*, vol. 21, p. 1001, October, 1950.
46. J. E. Storer: "The Radiation Pattern of an Antenna over a Circular Ground Screen," *Harvard Univ., Cruft Lab., Tech. Rept.* 126, June, 1951.
47. B. B. Baker and E. T. Copson: "The Mathematical Theory of Huygens' Principle," chap. 4, Oxford University Press, London, 1950.
48. C. T. Tai: "Radiation from Current Elements and Apertures in the Presence of a Perfectly Conducting Half-plane Sheet," *Stanford Research Inst., Radio Systems Lab., Tech. Report.* 45, Stanford, Calif., June, 1954.

49. D. W. Little, D. R. Rhodes, W. P. Summers, and A. S. Meier: "Measured Impedance of Vertical Antennas over Finite Ground Plane," *Ohio State Univ. Research Foundation Tech. Rept.* 233-3, Columbus, Ohio, October, 1946.
50. A. G. Kandoian: "Three New Antenna Types and Their Applications," *Proc. IRE*, vol. 34, p. 70W, February, 1946.
51. Reference 48.
52. J. R. Wait and W. A. Pope: "The Characteristics of a Vertical Antenna with a Radial Conductor Ground System," *Appl. Sci. Research*, ser. B, vol. 4, p. 177, 1954.
53. N. Wells: "The Quadrant Aerial," *J. IEE (London)*, pt. III, vol. 91, p. 182, December, 1944.

Chapter 4

LONG-WIRE ANTENNAS

Edmund A. Laport

Radio Corporation of America
Princeton, N.J.

4.1. INTRODUCTION

Long-wire radiators are used as elements in certain types of radiating systems commonly called "long-wire antennas." A long wire means a straight conductor from one to many wavelengths long having natural current distributions. The current

distributions may be standing waves or traveling (progressive) waves on the conductor. Practical long-wire antennas are the V and rhombic types or their derivatives.

The radiation patterns of long-wire antennas are typically complicated, in theory as well as in practice. Practical engineering design is based on the simplest theoretical concepts which give an acceptable first approximation, according to prevailing views. It must be understood that a precise proof of performance of a long-wire antenna is so formidable an undertaking that it is seldom attempted even on a scale model. A substantial body of experimental data has been taken in the region of the main lobe where interest centers; and on this evidence the first-approximation approach to design gives adequate accuracy for situations where long-wire antennas are applied.

As in any branch of engineering where empirical methods are used, one must develop a sense of significant values and understand certain limitations of good engineering practice.

Regardless of theoretical complications, long-wire antennas have practical value because of their structural simplicity and relatively low cost.

4.2. SINGLE LONG WIRE AS A UNIT RADIATOR

Radiation Patterns. The following basic facts about the radiation patterns of long wires isolated in free space with idealized natural current distributions will be useful for reference:

1. There is a lobe in the radiation pattern for each half wavelength of wire length. Each lobe is a cone of radiation centered on the wire.

2. With respect to the middle of the wire as center of the polar radiation pattern, half of the lobes are tilted forward and half of them backward. If the wire is an odd number of half wavelengths long, there is an odd number of lobes, so one of them will be normal to the wire.

3. The direction of the electric field reverses in each successive lobe. This is analogous to the reversals of phase of the currents in successive half-wavelength portions of the wire.

4. Between successive lobes are regions of little or no radiation, called nulls, or zeros. Practically, these are minima because the field strengths at these angles never actually go to zero. These zeros are related analogously to the current zeros in the standing-wave current distribution or to the phase reversals in a traveling-wave distribution.

5. The angles of the *zeros* are symmetrically distributed about the plane normal to the middle of the wire.

6. For a given electrical length, the angles of the *zeros* are the same for both standing- and traveling-wave current distributions.

7. In the first quadrant the angles of the maxima for both current distributions are virtually coincident. The only exception applies to the direction of the main (first) lobe for wire lengths less than three wavelengths, as may be seen in Fig. 4-1.

8. The largest lobe in the radiation pattern is the one forming the smallest angle (θ_1) to the wire. For the traveling-wave case, this lobe is in the direction of current flow only. For the standing-wave case the radiation pattern is symmetrical with respect to the middle of the wire, and so has a complementary major lobe toward the other end of the wire.

9. With a standing-wave current distribution an integral number of half wavelengths long, the envelope of the polar plot of the field-strength distribution pattern is a straight line parallel to the wire, or more correctly, a concentric cylinder. For a nonintegral number of half wavelengths, the middle lobes are further decreased in amplitude. The maximum depression of inner lobes occurs when the current distribution consists of an odd integral number of quarter wavelengths (Fig. 4-2).
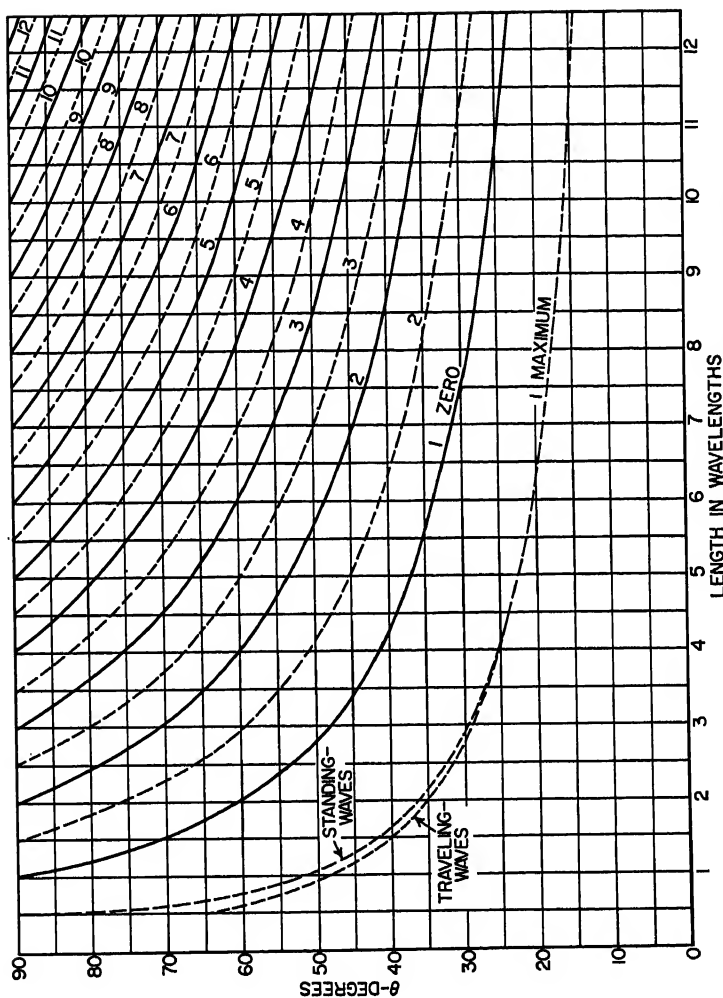
Fig. 4-1. Angles of maxima and zeros in the radiation patterns for isolated long wires with natural current distribution.

RADIATION PATTERN
7 3/4 λ WIRE
(SINUSOIDAL CURRENT
DISTRIBUTION)

RADIATION PATTERN
8 λ WIRE
(SINUSOIDAL CURRENT
DISTRIBUTION)

WIRE AXIS

ENVELOPE PARALLEL
TO WIRE
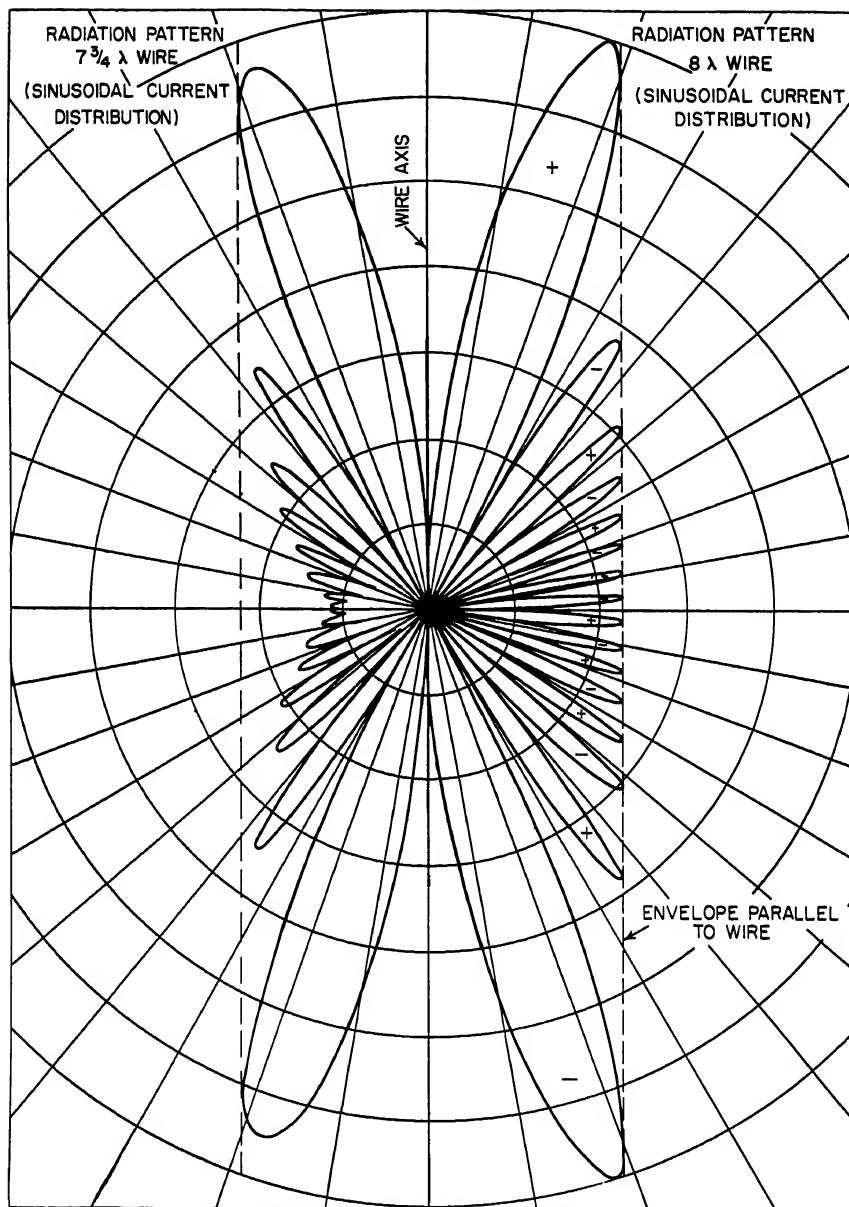
FIG. 4-2. Comparison between the polar radiation patterns of a 7.75λ- and an 8λ-long wire with standing-wave current distribution, in terms of relative field strength.

10. With traveling waves, the field-strength pattern has lobes of diminishing amplitude, the smallest being in the direction opposite to that of current flow.

11. Typical deviations from idealized current distributions modify the relative lobe amplitudes slightly and fill in the zeros slightly, but do not affect the *angles* of the maxima or the zeros in the radiation pattern.

12. The ratios of the amplitudes of successive lobes are higher for a traveling-wave system than for the equivalent standing-wave system (compare Figs. 4-3 and 4-4).

Example of a Measured Standing-wave Current Distribution. Figure 4-5 shows a long-wire standing-wave current distribution measured by P. S. Carter. It is seen that the true distribution is not well approximated by using an attenuation constant and transmission-line theory. Curve *a* is the current envelope for the antenna as measured, and *t* is the envelope for a transmission line having the same total attenuation as the antenna.
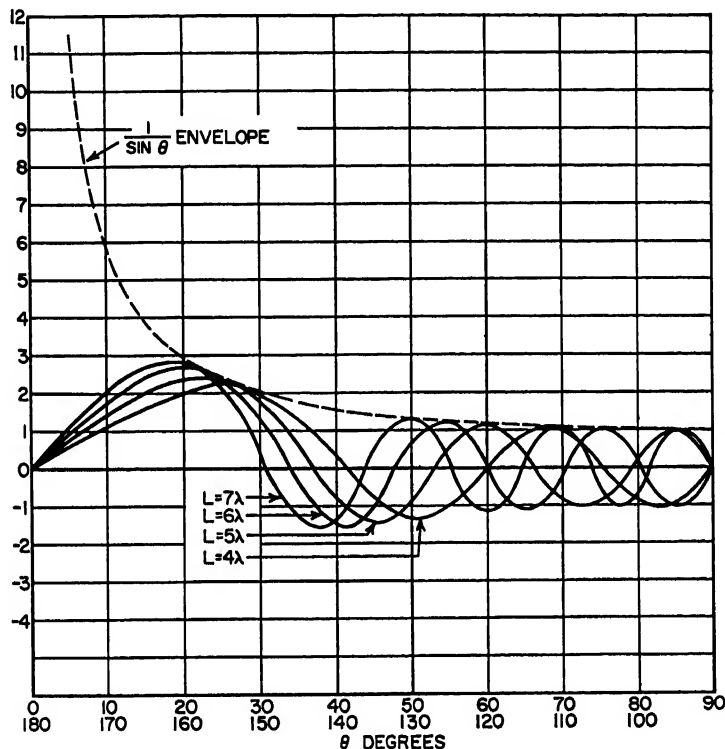
Fig. 4-3. Field-strength radiation patterns for standing-wave current distributions.

Equations for the Field-strength Patterns. The far-field pattern for a long straight wire in free space with pure sinusoidal (standing-wave) current distribution is expressed by

$$E_\theta = \frac{60I}{r} \left[\frac{1}{\sin \theta} \cdot \frac{\cos}{\sin} \left(\frac{\pi L}{\lambda} \cos \theta \right) \right] \qquad \text{volts/meter} \qquad (4\text{-}1)$$

$$(A) \quad (B) \qquad\quad (C)$$

(Cosine or sine in factor *C* is used when the number of half wavelengths is odd or even, respectively.)

The coefficient (factor *A*) relates field strength to the antinode current *I* in amperes and the distance *r* in meters from the center of the wire. If *I* is expressed in rms values, the field strengths will also be expressed in rms values. The factor *B* by itself gives the envelope for the pattern lobes, θ being the angle to the wire axis. Factor *C* by itself oscillates from $+1$ to -1 and contains the information about the angles of the zeros in the pattern. *B* and *C* together describe the *shape* of the pattern. The
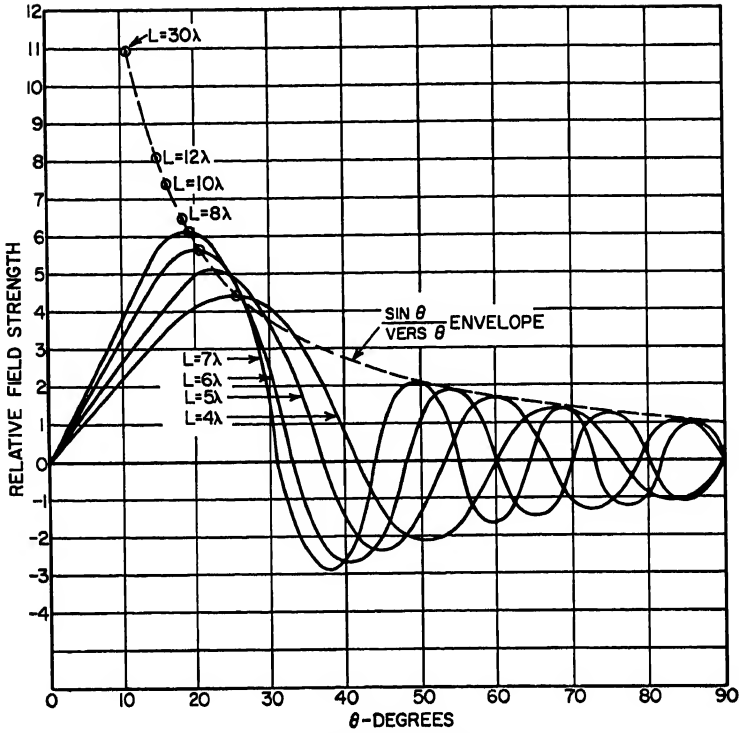
FIG. 4-4. Field-strength radiation patterns for traveling-wave current distributions.
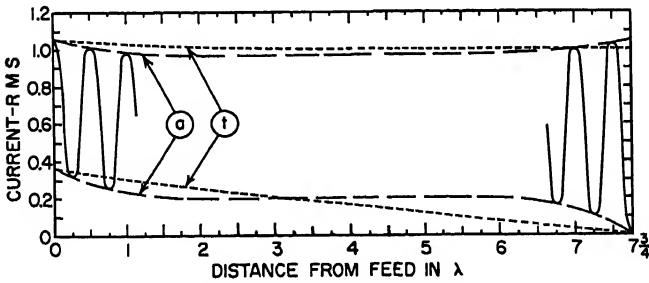
FIG. 4-5. Measured standing-wave current distribution on a long wire and comparison with transmission-line theory.

power flow at any angle θ is given by

$$W = \frac{E_\theta{}^2}{377} = \text{power density, watts/meter}^2$$

For the case of a perfect unattenuated traveling-wave current distribution of any length,

$$E_\theta = \frac{60I}{r} \frac{\sin\theta}{\text{vers }\theta} \sin\left(\frac{\pi L}{\lambda} \text{ vers }\theta\right) \qquad \text{volts/meter} \qquad (4\text{-}2)$$

$$(A) \quad (B) \qquad\qquad (C)$$

As before, A is a scale factor.   Factor B is the envelope factor, with vers $\theta \equiv 1 - \cos \theta$. Factor C ranges in value from $+1$ to -1 and contains the information on the locations of the lobes and zeros. B and C together describe the complete *shape* of the pattern.

In these equations L is the wire length in meters and λ the wavelength in meters. Although the C factors in both equations are not identical, they do in fact have identical zeros, and the first quadrant maxima are virtually coincident, with the exception noted above.

The following equations are more convenient for the determinations of the angles of maxima and zeros in the far-field radiation patterns for long straight wires with traveling-wave current distributions.

For the angles of the series of maxima of diminishing amplitude starting with the largest at θ_{m1} nearest to the forward axis of the wire,

$$\theta_{mm} = \text{haversine}^{-1} \frac{K}{2L/\lambda}$$

where K has successive values of 0.371, 1.466, 2.480, 3.486, and 4.495; then $m - \frac{1}{2}$ in order.

For the angle θ_{0m} for the mth zero with respect to the wire axis, from θ_{01} to $180°$,

$$\theta_{0m} = \text{haversine}^{-1} \frac{m}{2L/\lambda}$$

Haversines $[\equiv (1 - \cos \theta)/2]$ are tabulated in Handbook of Chemistry and Physics, Chemical Rubber Publications Company, Cleveland, and in many navigation handbooks.

Comparisons between standing-wave and traveling-wave field-strength patterns can be seen in Figs. 4-3 and 4-4, which plot the relative values of E_θ from Eqs. (4-1) and (4-2), using factors B and C only.   They illustrate some basic differences between the two current distributions.

These functions are tedious to compute and apply to antenna designs, so it is fortunate that it is not necessary to use more than the angles of maxima and zeros in engineering practice.   These can be conveniently displayed in stereographic coordinates to simplify the computations needed to design V and rhombic antennas. Figure 4-1 gives these angles for all lobes and zeros in the first quadrant to $L = 12.5\lambda$. If a complete function is wanted, a fair approximation can be made to the Figs. 4-3 and 4-4 plots by locating the zeros and the maxima with their amplitudes in accordance with the envelope functions and sketching in the intermediate values.   It is interesting to note that there is a virtually linear rise in the value of the first lobe almost to its peak when plotted in rectangular coordinates.

An alternative way of obtaining the lobes and zeros is to use the stereographic method as discussed in Sec. 4.4 and as shown in Fig. 4-7 for the cases $L = 2$, 4.5, and 8λ.

4.3. LONG WIRES IN THE PRESENCE OF GROUND

Any practical antenna must be located somewhere above the earth surface, be it ground or water.   The free-space field concept has to be modified to take into account the wave interference between the direct field of the wire and that reflected from the ground where it is illuminated by the radiator.   The resulting radiation pattern at any point in the half space above the ground is the phasor sum of the direct and reflected waves arriving at every point on the enclosing hemisphere.

If the ground were everywhere a plane surface of infinite conductivity, the field

strength at every point would be the resultant of two equal phasors with a phase difference equal to the angular difference in the direct and reflected path lengths, provided the wire is *vertical*. In this case the field is everywhere vertically polarized.

When the long wire is horizontal, or inclined from the vertical, the combined pattern is greatly complicated because the wave reflected from any portion of the ground will depend for its amplitude and phase upon the orientation of the electric vector of the direct incident field. If the electric vector E is horizontal, there will be a reversal of phase at reflection and the resultant field will be horizontally polarized. When the incident field has an obliquely oriented E vector, its vertical component will be reflected without phase reversal (except at very low angles) while the horizontal component will be reversed. At the space point where the direct and reflected waves combine, the resultant field is obliquely polarized and composed of the direct and the two differently polarized reflected components.

Another order of complication is introduced by the nature of physical ground, which is not perfectly conducting but is a complex dielectric. The conductivity and inductivity of the ground vary with its location, depth, and humidity or wetness; also, the complex-reflection coefficient at any location varies with frequency and the angle of incidence of the impinging field. It is therefore evident that an exact solution of the complete antenna pattern is practically unrealizable in any circumstance. One cannot ignore the ground, but its properties can be idealized for design purposes and the study of the resulting radiation pattern can be limited to those zones of greatest importance. With this simplification, the computations for an antenna design can be made manageable.

4.4. CONSTRUCTION OF DESIGN CHARTS IN STEREOGRAPHIC PROJECTION

One of the ways to project a sphere onto a plane is that called stereographic projection. It is conformal, meaning that all angles on the sphere are correctly preserved in its two-dimensional representation; and as a consequence, all lines that are circles on a sphere, including great circles, become circles, or arcs of circles, in this projection. This property is very useful for long-wire-antenna design where we deal with angles.
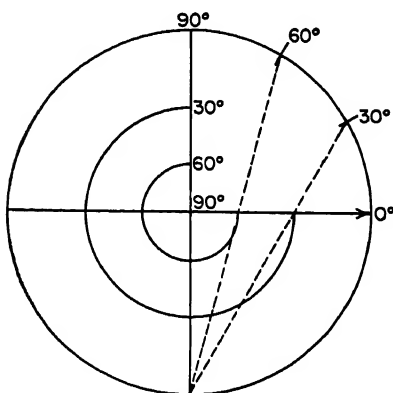
FIG. 4-6a. Derivation of stereographic elevation angles from circular azimuth angles.

The construction of the stereographic projection of the hemisphere is illustrated in Fig. 4-6a; and in this way a set of stereographic coordinates are generated, such as Fig. 4-6b.

If we assign the direction of a long-wire radiating element to a diameter of the stereographic field, the angle of a cone of radiation (lobe) can be shown by the following. The angle of the first maximum is θ_1. It will intersect the equatorial circle at angles plus and minus θ_1 and cross the wire axis at θ_1 in the stereographically projected third dimension (along the wire axis or diameter) of the chart. The locus of this conical lobe maximum will then be correctly located at all other azimuth and elevation angles by the arc of a circle drawn through these three points and centered on an extension of the wire axis. In the same way all other cones of maxima and zeros centered on the wire can be constructed. The three examples of Fig. 4-7 were con-

structed this way. Although they show the complete set of maxima and zeros for each wire length, it suffices to draw only the first three or four maxima and their related zeros.

A pair of transparent charts of this kind can be overlaid to show the effect of combining the fields from two such long wires in a V arrangement by cocentering them and setting them at the same angle as the angle between the wires. By this method, the
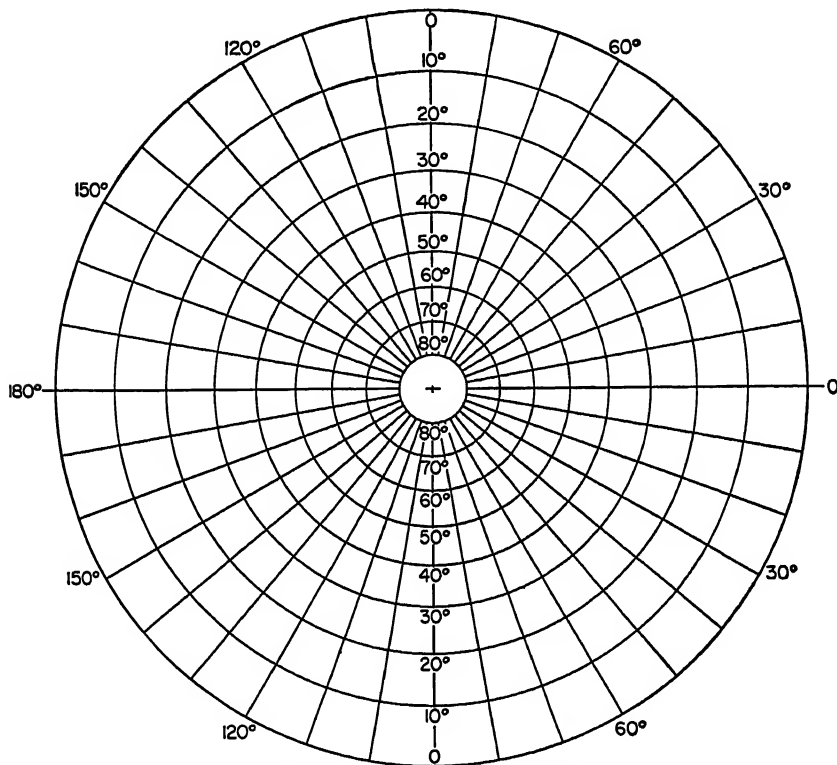
FIG. 4-6b. Stereographic coordinate system for the projection of a sphere.

two chart patterns multiply each other. Where there is a zero in one pattern, there is a zero in the pattern of the combination.

To avoid cluttering the charts, the altitude angles are indicated as small cross lines on the wire axis, in 10° steps starting from 0 at the equatorial plane and progressing to the pole at 90°, at the center.

In Fig. 4-8 is shown another chart of identical size on which different height factors are drawn stereographically. Eight height factors, from 0.6λ to 2.0λ height above ground, are included and can be used with the two other charts to show the complete pattern for a horizontal V or rhombic antenna. The maxima and zeros in each height factor are shown, obtained from the values in Fig. 4-9. Here again the height factor multiplies with the array factors, giving zeros in the final pattern wherever there is a zero in one of the charts.

In all these charts and related curves such as Figs. 4-1 and 4-9, the maxima are shown as broken lines and the zeros as thin full lines. (There is an exception to this convention in Fig. 4-16 because these diagrams are reproduced from another source.)

In the charts, the maxima are numbered in order as M_1, M_2, etc., and the zeros as 0_1, 0_2, etc. The zero in the direction of the wire is identified as 0_0; likewise for the zero at ground level in the height factor.

(a)
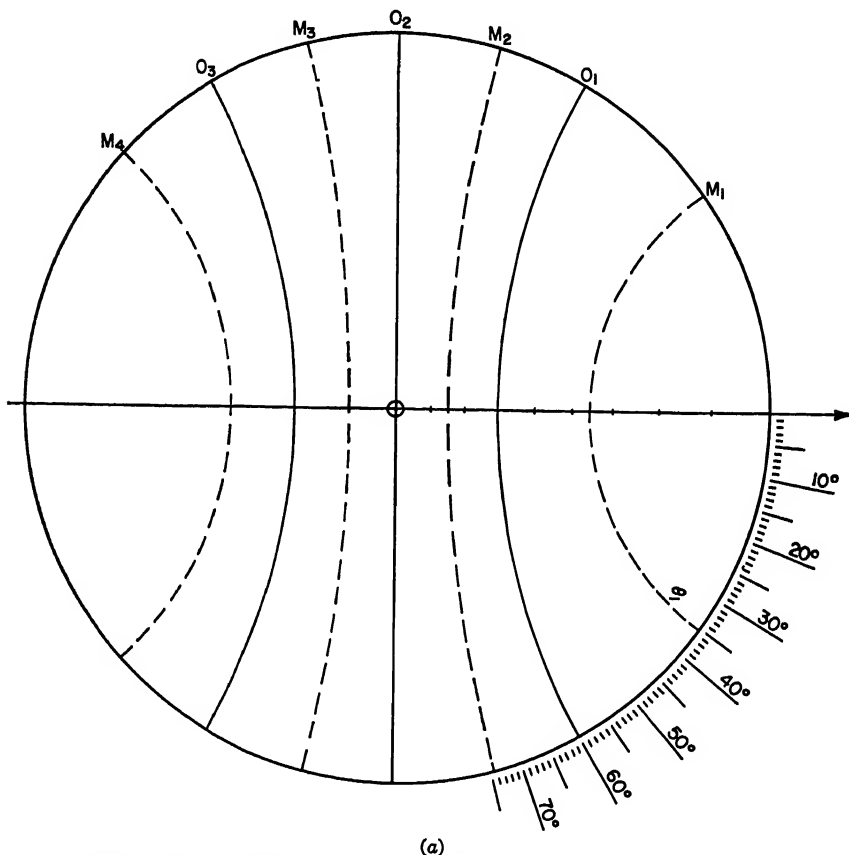
FIG. 4-7. Stereographic representation of the radiation patterns for isolated straight wires with traveling-wave current distributions: (a) $L = 2\lambda$. (b) $L = 4.5\lambda$. (c) $L = 8\lambda$.

4.5. ARRAYS OF LONG WIRES

A single long wire is not a desirable antenna, because of its many radiation lobes of rather large values. The best use of long wires is realized in those antennas where the main lobes from two or more long wires add in phase and other lobes are reduced or eliminated by destructive wave interference. The basic fact that the long-wire radiation patterns have their main lobes at small angles relative to the wire restricts the number of configurations that yield the desired main-beam reinforcement to the V arrangements.

Practical long-wire antennas have been developed in the following forms, though time has filtered out most of these.

Vertically Polarized Main Beams

1. Single sloping wire, one end near ground, which with its electrical image forms a V (Fig. 4-10a).

2. Two long wires in series forming an inverted V, with each end near ground and maximum height obtained with one central support. This, together with its electrical image, forms a vertical rhombic. The antenna is frequently called a vertical half rhombic for that reason (Fig. 4-10b).

Horizontally Polarized Main Beams

1. Two long wires in a V arrangement starting from a common apex, both parallel to ground. This is called a horizontal V antenna (Fig. 4-10c).
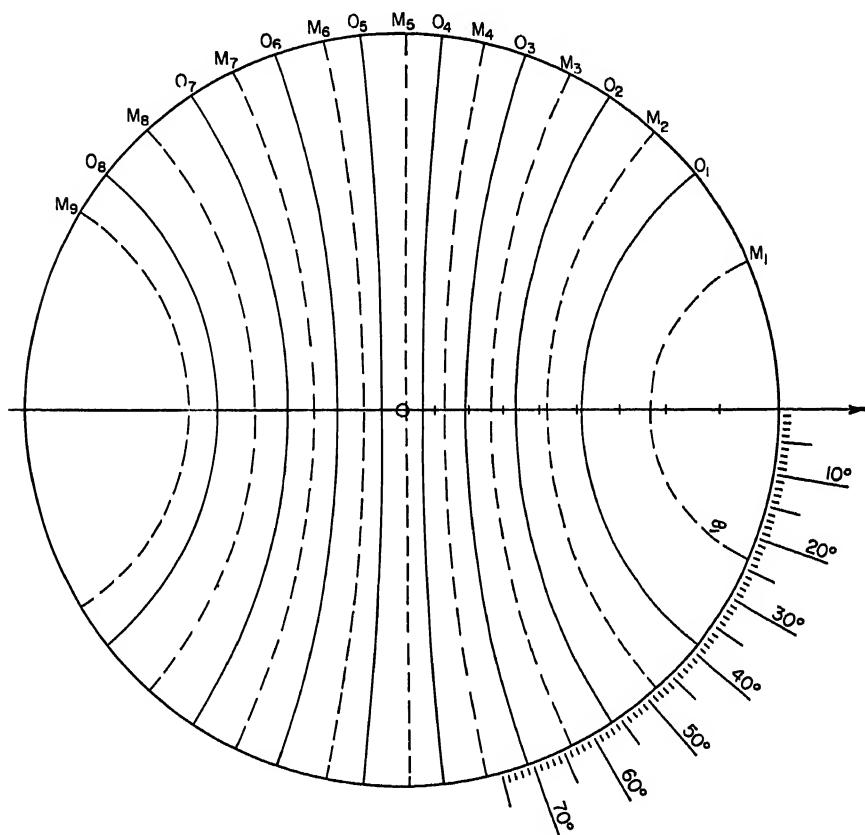
(b)

FIG. 4-7. (Continued)

2. Arrays of two or more V antennas spaced in height, laterally or axially, or combinations of these. One such type is shown in Fig. 4-10d.

3. Sloping V traveling-wave antenna elevated at the apex (Fig. 4-10e).

4. A rhombic array of four long wires in a common horizontal plane, called the horizontal rhombic antenna. This popular type is illustrated in Fig. 4-11a. It may also have its plane tilted with respect to ground, in which case it is called a sloping or inclined rhombic antenna.

5. Arrays of rhombic elements, displaced laterally, axially, or in height, or combinations of these (Fig. 4-11b–d). All these forms have sides of equal length to obtain

Certain obsolete types of long-wave antennas have used long wires in parallel in a common horizontal plane. Practically all standing-wave long-wire antennas have gone out of use with preference for the traveling-wave types. For that reason only the horizontal rhombic antenna will be discussed here.

If θ_1 is the angle of the maximum for the largest lobe with respect to each wire of a V, it is evident that the main lobe of the combination will be a maximum in the plane
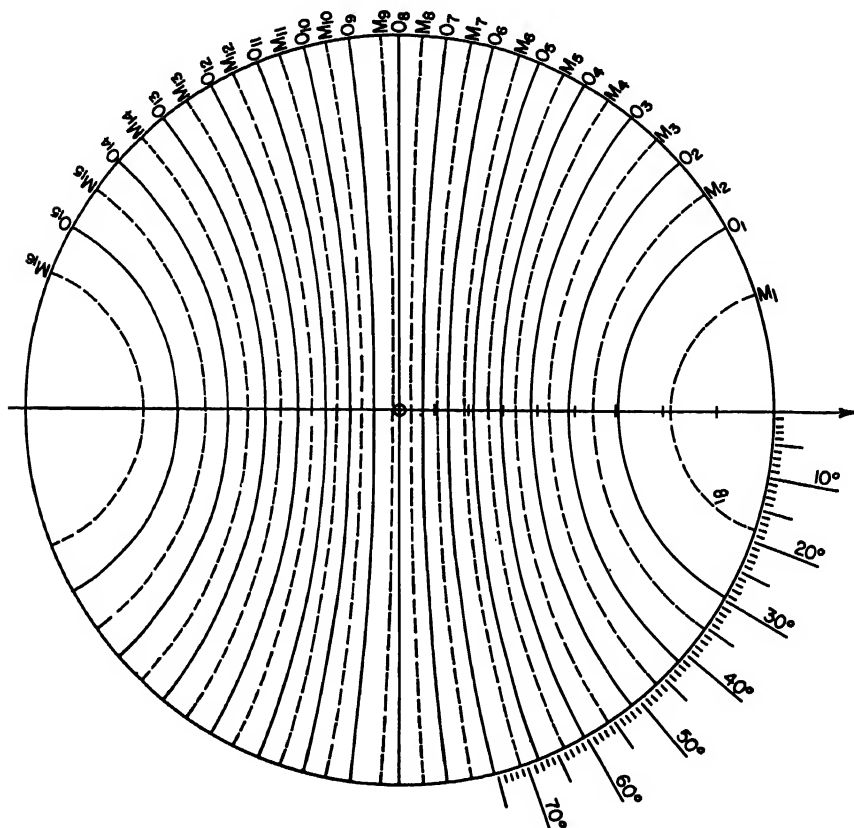
(c)

FIG. 4-7. (*Continued*)

of the V (or rhombus) when the apex angle is $2\theta_1$. For apex angles less than $2\theta_1$, the main beam for the combination will occur at some angle α with respect to the plane of the wires and approaches $\alpha = \theta_1$ as the apex angle A approaches zero. The mode of variation of α with A is seen in Fig. 4-12 for wires of various electrical lengths.

With a pair of stereographic charts overlaid and cocentered, the effect of varying A is readily demonstrated, as shown in Fig. 4-13.

4.6. RHOMBIC ANTENNA IN FREE SPACE

A rhombus is an equilateral parallelogram, usually with two opposite acute angles. It can also be regarded as two identical but reversed V's in series at their outer ends. These acute angles are designated A and the side lengths by L. The two parameters
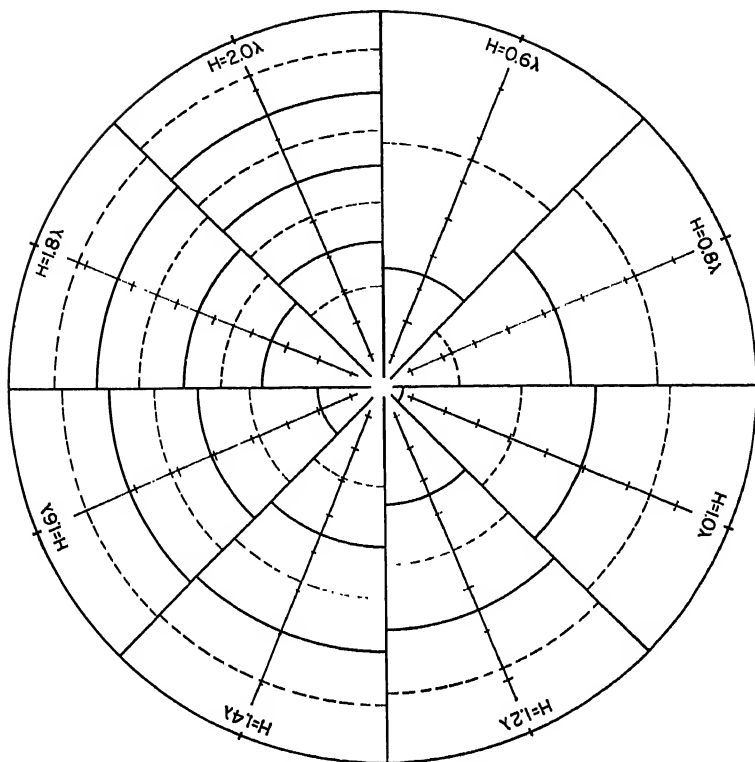
Fɪɢ. 4-8. Stereographic representation of the height factor for horizontal polarization for H from 0.6λ to 2.0λ.
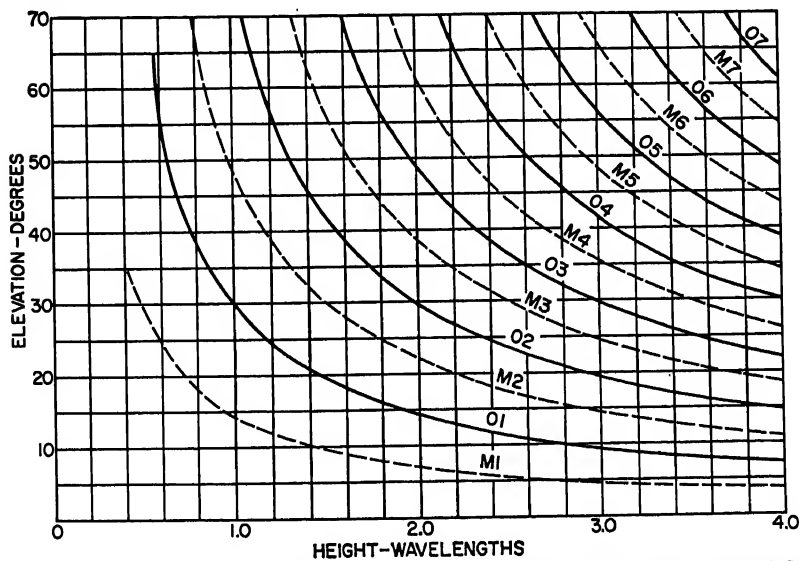
Fɪɢ. 4-9. Angles of maxima and zeros in the height factor for horizontally polarized fields.

(SIDE VIEW)

VERSION I. SLOPE ANGLE S SAME AS θ_1
VERSION 2.   "   "   S   "   "   ANGLE OF IST ZERO FROM WIRE

(a)

FEED   (SIDE VIEW)

TERMINAL RESISTOR

SLOPE ANGLE S = θ_1

(b)

MATCHING NETWORK

PLAN VIEW

A

(c)

35°

$\dfrac{A}{2}$ = 17.5°

INSULATORS
$7\frac{3}{4}\lambda$ V-REFLECTOR
$7\frac{3}{4}\lambda$ V-RADIATOR

RADIATOR FEEDER
UPPER & LOWER VEES
CONNECTED
IN PARALLEL
REFLECTOR
FEEDER

$2\frac{1}{4}\lambda$

(d)

(ISOMETRIC VIEW)

FEEDER

TERMINAL RESISTOR

S

S

TERMINAL RESISTOR
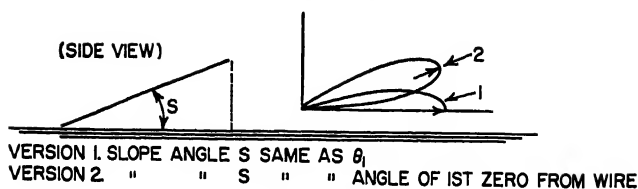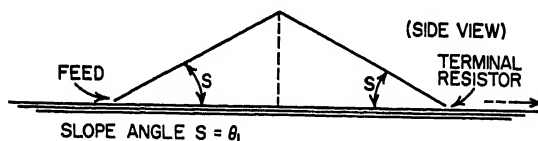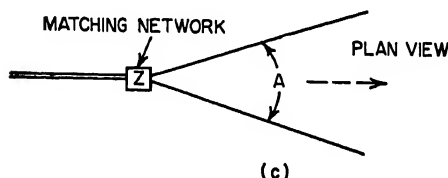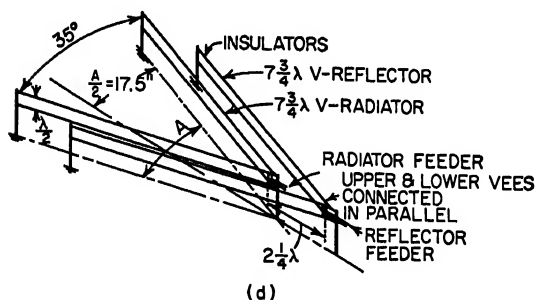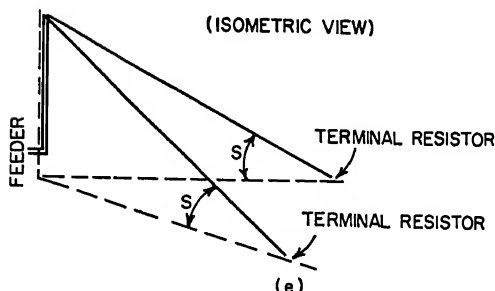
(e)

FIG. 4-10. Long-wire antenna configurations: (a) Sloping single-wire antenna. (b) Inverted-V antenna. (c) Single-element horizontal V antenna. (d) V array, RCA Model D. (e) Sloping V antenna.

completely describe the physical form and size of the rhombus as a radiator. Its electrical size is determined by the length of each side in wavelengths, radians, or degrees. Typically, the sides are electrically very long.

Since the two V portions of a rhombus are identical, even though reversed, and the directions of the currents are the same, they will each have identical radiation patterns, with the same angles for all corresponding maxima and zeros. However, because of wave interference between these two V's, due to their spatial separation, the lobe amplitudes for the rhombus will not be the same as for a single V.
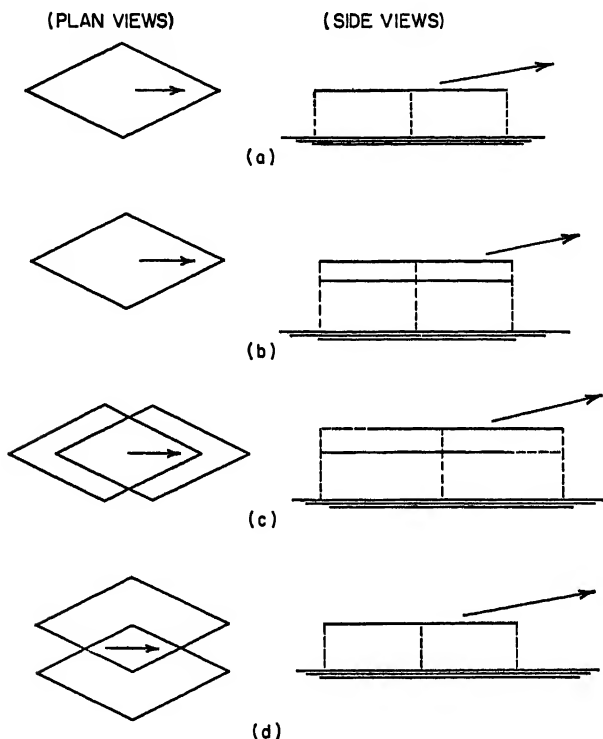
FIG. 4-11. Rhombic-antenna arrangements: (a) Single-element horizontal rhombic antenna. (b) Two-layer horizontal rhombic antenna. (c) Two-layer axially displaced horizontal rhombic array. (d) Broadside array of two horizontal rhombic antennas.

When $A < 2\theta_1$ the major lobe for the array will lie in the major axial plane normal to the plane of the rhombus. All fields in this plane have their E vectors parallel to the rhombic minor axis. Fields in all other directions have E vectors having various degrees of obliquity.

It is desirable or necessary to know the coordinates of the various minor lobes of radiation from a rhombus. Their coordinates can be found from the stereographic charts for any L/λ and A. Tables 4-1 to 4-6 list their coordinates as L/λ varies from 2 to 7 in integral steps and values of A from 35 to 71°. Their relative amplitudes in decibels, normalized on the main beam in each case, are listed in Table 4-7 for cases where the main beam satisfies the condition that $A \leq 2\theta_1$.

Horizontal Rhombic Antenna. The effect of ground on the pattern for an actual rhombic antenna is to produce additional wave interference between the rhombus and its image. The primary parameter due to the presence of ground is the electrical
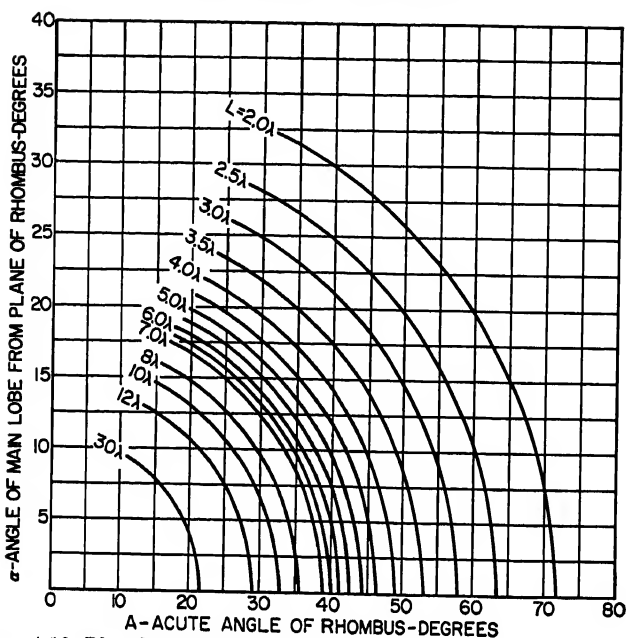
FIG. 4-12. Rhombus main-lobe orientation as functions of A and L/λ.

(a)
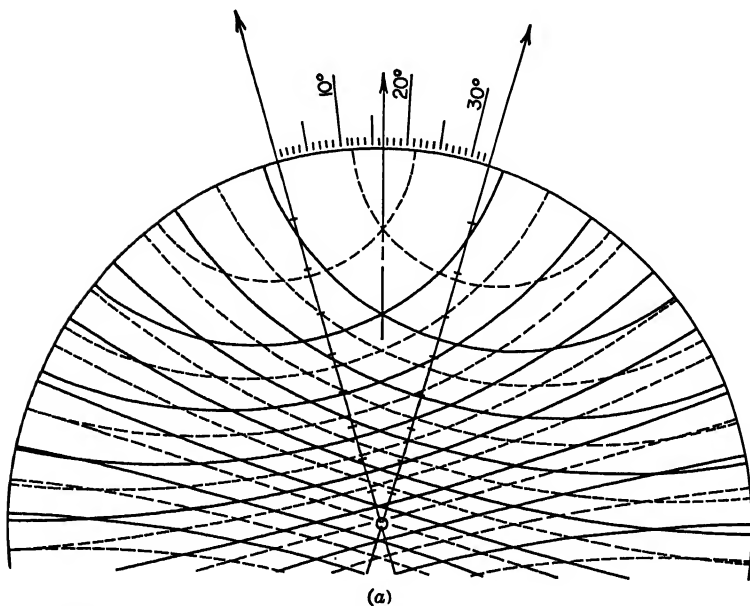
FIG. 4-13. Radiation patterns for a 5.5λ rhombus as A is varied: (a) $A < 2\theta_1$. (b) $A = 2\theta_1$. (c) $A > 2\theta_1$.

(b)

(c)
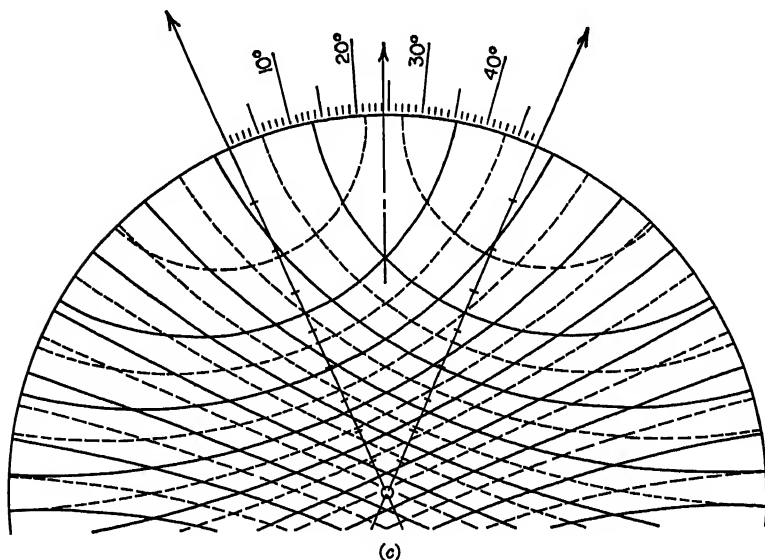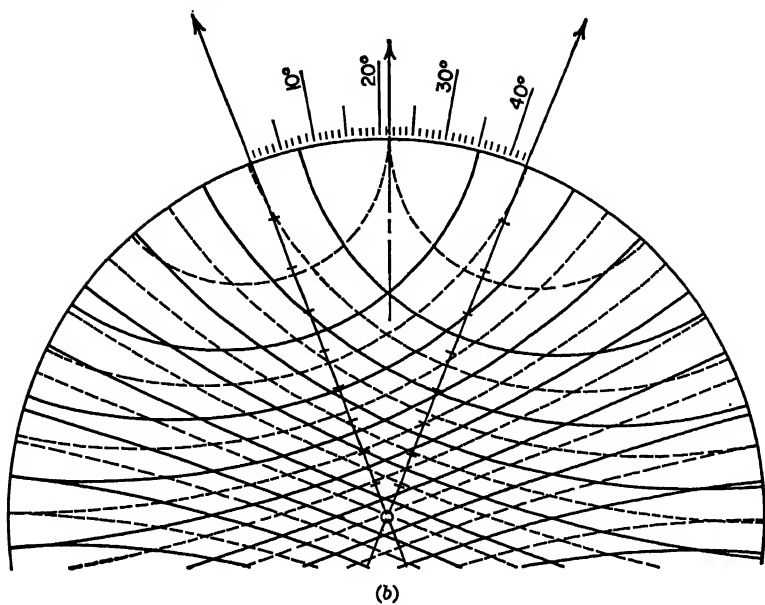
FIG. 4-13. (*Continued*)

height of the primary radiator. For the *horizontally polarized* field components the height factor is, ideally,

$$f_h(H) = \sin\left(\frac{2\pi H}{\lambda} \sin \alpha\right) \tag{4-3}$$

which applies rather adequately to all practical situations.

Table 4-1. Orientation of Pattern Lobes for Free-space Rhombus When $L = 2\lambda$, in Degrees

For first side (orders 1–4), each with β and α:

$A=$	Order of maxima for second side	1 β	1 α	2 β	2 α	3 β	3 α	4 β	4 α
71°	1	0	0	34	36	71	8	108	24
	2	...	...	0	70	88	04	146	43
	3	...	...	...	...	180	107	...	...
	4	...	...	...	...	...	...	180	155
65°	1	0	16	38	36	...	...	107	9
	2	...	...	0	71	88	82	142	43
	3	...	...	...	...	180	107	...	...
	4	...	...	...	...	...	...	180	30
60°	1	0	20	41	35	...	...	...	...
	2	...	...	0	72	88	59	...	...
	3	...	...	...	...	180	107	140	42
	4	...	...	...	...	...	...	180	33
55°	1	0	24	43	33	...	...	...	...
	2	...	...	0	72	89	56	...	...
	3	...	...	...	...	180	107	138	41
	4	...	...	...	...	...	...	180	34
50°	1	0	27	47	29	...	...	...	...
	2	...	...	0	72	89	52	...	...
	3	...	...	...	...	180	106	134	38
	4	...	...	...	...	...	...	180	37
45°	1	0	28	50	24	...	...	...	...
	2	...	...	0	73	89	47	...	...
	3	...	...	...	...	180	106	131	35
	4	...	...	...	...	...	...	180	38
40°	1	0	30	53	13	...	...	...	...
	2	...	...	0	73	89	40	...	...
	3	...	...	...	...	180	105	127	29
	4	...	...	...	...	...	...	180	39
35°	1	0	32	...	...	...	...	...	...
	2	...	...	0	73	89	26	...	...
	3	...	...	...	...	180	105	124	19
	4	...	...	...	...	...	...	180	40

NOTE: In Tables 4-1 to 4-6, α is the elevation angle measured vertically from the plane of the rhombus, β is the azimuth angle from the axis of the rhombus. $\alpha = 0 = \beta$ is the forward projection of the major axis of the rhombus or V.

The vertically polarized height factor involves the use of Fresnel equations of reflection from a complex dielectric and will not be included here because it is seldom used in design. Values of $f_h(H)$ in Eq. (4–3) have their maxima and zeros plotted in Fig. 4-9.

Optimum Design Parameters for Horizontal Rhombic Antenna. The best performance of a horizontal rhombic antenna is obtained when the first maximum in the

Table 4-2. Orientation of Pattern Lobes for Free-space Rhombus When $L = 3\lambda$, in Degrees

A =	Order of maxima for second side	1 β	1 α	2 β	2 α	3 β	3 α	4 β	4 α	5 β	5 α	6 β	6 α
65°	1			22	27	46	26	71	49	89	21		
	2			0	52	38	59	89	73	107	49		
	3					0	78						
	4							180	79	141	60	133	31
	5									180	53	158	32
	6											180	7
60°	1			24	28	49	22	73	46	90	0		
	2			0	53	41	58	89	72	106	46		
	3					0	78						
	4							180	79	137	59	130	27
	5									180	55	157	33
	6											180	15
55°	1	0	9	27	29	52	17	74	42				
	2			0	54	44	57	89	69	104	42		
	3					0	78						
	4							180	80	135	58	127	22
	5									180	56	154	33
	6											180	19
50°	1*	0	15	29	29	29	0						
	2			0	55	47	57	86	36	103	36		
	3					0	79	89	68				
	4							180	80	132	57	125	14
	5									180	57	152	33
	6											180	22
45°	1	0	19	32	27								
	2			0	56	50	54	78	28	102	28		
	3					0	79	89	65				
	4							180	80	128	56		
	5									180	57	148	33
	6											180	25
40°	1	0	22	36	25								
	2			0	57	54	52	79	5	110	5		
	3					0	79	89	62				
	4							180	80	125	53		
	5									180	57	145	30
	6											180	27
35°	1	0	23	40	20								
	2			0	57	58	48	89	58				
	3					0	80	89	58				
	4							180	80	122	48		
	5									180	58	142	27
	6											180	28

* Optimum.

Table 4-3. Orientation of Pattern Lobes for Free-space Rhombus When $L = 4\lambda$, in Degrees

A =	Order of maxima for second side	For first side											
		1		2		3		4		5		6	
		β	α	β	α	β	α	β	α	β	α	β	α
60°	1	...	...	17	21	35	24	52	11				
	2	...	...	0	42	23	50	48	48	69	36		
	3	...	...	...	...	0	63	40	67	74	58	90	41
	4	...	...	...	...	...	...	0	81	88	76	105	58
	5	...	...	...	...	...	...	...	...	180	82	140	68
	6	...	...	...	...	...	...	...	...	...	...	180	64
55°	1	...	...	18	23	37	23						
	2	...	...	0	44	25	50	51	46	71	30		
	3	...	...	...	...	0	64	42	67	75	56	90	36
	4	...	...	...	...	...	...	0	81	88	74	104	56
	5	...	...	...	...	...	...	...	...	180	82	137	67
	6	...	...	...	...	...	...	...	...	...	...	180	65
50°	1	...	...	21	24	41	19						
	2	...	...	0	45	27	50	54	44	73	20		
	3	...	...	...	...	0	64	45	66	77	52	90	27
	4	...	...	...	...	...	...	0	81	88	73	102	52
	5	...	...	...	...	...	...	...	...	180	82	134	60
	6	...	...	...	...	...	...	...	...	...	...	180	65
45°	1	0	10	23	25	44	12						
	2	...	...	0	46	30	50	57	40				
	3	...	...	...	...	0	65	48	65	78	47	99	10
	4	...	...	...	...	...	...	0	81	89	70	101	47
	5	...	...	...	...	...	...	...	...	180	82	130	65
	6	...	...	...	...	...	...	...	...	...	...	180	66
40°	1	0	14	26	24								
	2	...	...	0	47	34	48	61	34				
	3	...	...	...	...	0	65	52	63	80	41	100	42
	4	...	...	...	...	...	...	0	81	89	68		
	5	...	...	...	...	...	...	...	...	180	82	127	64
	6	...	...	...	...	...	...	...	...	...	...	180	66
35°	1	0	17	29	22								
	2	...	...	0	48	37	47	64	24				
	3	...	...	...	...	0	65	55	61	81	31	98	33
	4	...	...	...	...	...	...	0	81	89	64		
	5	...	...	...	...	...	...	...	...	180	82	123	61
	6	...	...	...	...	...	...	...	...	...	...	180	66

height factor has the same elevation angle as that of the main beam of the rhombus. This condition obviously depends upon an interrelated set of values for L, A, and H for a particular operating frequency. At other operating frequencies there will be some compromise in the performance because all the factors do not vary synchronously with frequency.

A further objective in designing is to maximize the main lobe at some desired vertical angle α and to minimize all other lobes. Optimum design parameters are given

Table 4-4. Orientation of Pattern Lobes for Free-space Rhombus When $L = 5\lambda$, in Degrees

A =	Order of maxima for second side	For first side											
		1		**2**		**3**		**4**		**5**		**6**	
		β	α	β	α	β	α	β	α	β	α	β	α
60°	1	...	...	13	15	27	22	42	19	53	0	67	29
	2	...	...	0	36	17	44	35	45	52	41	69	50
	3	...	...	...	...	0	54	24	59	49	58	74	66
	4	...	...	...	...	...	...	0	69	42	72	74	66
	5	...	...	...	...	...	...	...	...	0	84	90	78
	6	...	...	...	...	...	...	...	...	...	...	180	84
55°	1	...	...	15	18	30	22	44	15			69	22
	2	...	...	0	38	18	44	38	45	54	38	71	47
	3	...	...	...	...	0	55	27	60	52	57	76	64
	4	...	...	...	...	...	...	0	70	45	72	91	78
	5	...	...	...	...	...	...	...	...	0	84	180	84
	6	..	...	...	...	...	...	...	...	...	...		
50°	1	...	...	16	20	32	22	48	0			71	0
	2	...	...	0	39	20	45	41	43	58	34	71	0
	3	...	...	...	...	0	50	28	60	54	55	73	43
	4	...	...	...	...	...	...	0	71	47	72	77	62
	5	...	...	...	...	...	...	...	...	0	84	91	77
	6	...	...	...	...	...	...	...	...	...	...	180	84
45°	1	0	0	18	22	36	18			61	27		
	2	...	...	0	41	22	45	44	41	58	52	75	36
	3	...	...	...	...	0	57	32	59	58	52	78	58
	4	...	...	...	...	...	...	0	71	50	70	78	58
	5	...	...	...	...	...	...	...	...	0	84	91	76
	6	...	...	...	...	...	...	...	...	...	...	180	84
40°	1	0	10	21	22	39	12			64	14		
	2	...	...	0	42	25	45	48	37	64	14	77	25
	3	...	...	...	...	0	57	35	58	61	48	80	54
	4	...	...	...	...	...	...	0	72	54	69	80	54
	5	...	...	...	...	...	...	...	...	0	84	90	74
	6	...	...	...	...	...	...	...	..	...	...	180	84
35°	1	0	14	24	22	40	0			64	43		
	2	...	...	0	42	28	44	52	32	64	43		
	3	...	...	...	...	0	58	39	57	64	43	82	48
	4	...	...	...	...	...	...	0	72	58	67	82	48
	5	...	...	...	...	...	...	...	...	0	84	90	71
	6	...	...	...	...	...	...	...	...	...	...	180	84

in Fig. 4-14, applicable to single frequencies only. From a study of stereographic charts corresponding to changes in operating frequency, the maximum tolerances in frequency departure from the design frequency were estimated and are indicated at the top of Fig. 4-14. Beyond these limits the performance can be regarded as intolerable because the minor lobes are excessively large and the main beam has seriously deteriorated. The compromise in performance often depends upon the conditions of a particular application, so the tolerances indicated should not be accepted without inquiry. Figure 4-15 illustrates such a case.

Table 4-5. Orientation of Pattern Lobes for Free-space Rhombus When $L = 6\lambda$, in Degrees

A =	Order of maxima for second side	For first side											
		1		2		3		4		5		6	
		β	α	β	α	β	α	β	α	β	α	β	α
60°	1	...	...	10	7	22	19	34	20	45	14		
	2	...	...	0	28	13	37	27	40	41	39	55	32
	3	...	...	...	...	0	46	17	52	35	53	53	49
	4	...	...	...	...	...	...	0	61	23	65	50	63
	5	...	...	...	...	...	...	...	...	0	72	45	74
	6	...	...	...	...	...	...	...	...	...	...	0	85
55°	1	...	...	11	13	25	20	37	18	47	0		
	2	...	...	0	31	14	38	29	40	43	37	57	28
	3	...	...	...	...	0	47	19	52	37	52	56	47
	4	...	...	...	...	...	...	0	62	26	65	53	62
	5	...	...	...	...	...	...	...	...	0	73	46	64
	6	...	...	...	...	...	...	...	...	...	...	0	85
50°	1	...[	...	13	17	26	21	39	15				
	2	...	...	0	33	15	39	32	40	47	15	60	21
	3	...	...	...	...	0	48	21	53	41	51	59	44
	4	...	...	...	...	...	...	0	62	28	65	56	60
	5	...	...	...	...	...	...	...	...	0	73	49	74
	6	...	...	...	...	...	...	...	...	...	...	0	85
45°	1	...	...	14	19	28	20	43	6				
	2	...	...	0	34	17	40	35	38	50	30	63	5
	3	...	...	...	...	0	49	23	53	44	50	62	40
	4	...	...	...	...	...	...	0	62	30	64	59	58
	5	...	...	...	...	...	...	...	...	0	73	52	72
	6	...	...	...	...	...	...	...	...	...	...	0	85
40°	1	0	5	16	20	32	17						
	2	...	...	0	36	20	40	39	36	54	23		
	3	...	...	...	...	0	60	26	53	47	47	65	33
	4	...	...	...	...	...	...	0	63	34	64	63	55
	5	...	...	...	...	...	...	...	...	0	74	57	71
	6	...	...	...	...	...	...	...	...	...	...	0	85
35°	1	0	11	18	21	35	10						
	2	...	...	0	37	22	40	43	33	57	2		
	3	...	...	...	...	0	51	29	52	51	44	67	22
	4	...	...	...	...	...	...	0	63	38	64	66	50
	5	...	...	...	...	...	...	...	...	0	74	60	69
	6	...	...	...	...	...	...	...	...	...	...	0	85

The optimum efficiency design at the frequency where $L = 4\lambda$ is seen in Fig. 4-15b. Here we note the near coincidence of the $M1$-$M1$ lobes with a maximum in the height factor to form the main beam along the major axis bisecting the angle of the V. The next largest rhombus lobes would be the $M1 = M2$ intersections, but note that a zero in the height factor suppresses these. The third largest lobes would be the $M1$-$M3$ intersections, but they occur at zero elevation, also a zero in the height factor. However, vestigial lobes of this order appear at the angle of the first maximum in the height factor because the $M1$-$M3$ lobes separate slowly with elevation angle. Table

Table 4-6. Orientation of Pattern Lobes for Free-space Rhombus When $L = 7\lambda$, in Degrees

$A=$	Order of maxima for second side	For first side											
		1		2		3		4		5		6	
		β	α	β	α	β	α	β	α	β	α	β	α
60°	1	...	...	...	...	18	15	28	19	48	17	48	8
	2	...	...	0	23	10	32	21	37	33	37	45	35
	3	...	...	...	...	0	42	12	47	27	49	41	48
	4	...	...	...	...	...	...	0	54	16	58	34	59
	5	...	...	...	...	...	...	...	...	0	64	24	68
	6	...	...	...	...	...	...	...	...	...	...	0	75
55°	1	...	...	10	7	20	18	31	19	42	14		
	2	...	...	0	27	11	34	23	37	36	36	48	32
	3	...	...	...	...	0	43	14	47	29	49	44	47
	4	...	...	...	...	...	...	0	55	18	58	37	59
	5	...	...	...	...	...	...	...	...	0	65	27	68
	6	...	...	...	...	...	...	...	...	...	...	0	76
50°	1	...	...	11	13	22	19	33	17	45	0		
	2	...	...	0	29	13	36	26	37	39	35	51	27
	3	...	...	...	...	0	44	15	48	31	49	47	46
	4	...	...	...	...	...	...	0	56	20	59	41	58
	5	...	...	...	...	...	...	...	...	0	66	29	68
	6	...	...	...	...	...	...	...	...	...	...	0	76
45°	1	...	...	12	16	24	19	37	13			54	20
	2	...	...	0	31	14	36	28	37	42	33	50	43
	3	...	...	...	...	0	45	17	49	34	48	43	67
	4	...	...	...	...	...	...	0	56	22	59	43	67
	5	...	...	...	...	...	...	...	...	0	66	32	68
	6	...	...	...	...	...	...	...	...	...	...	0	76
40°	1	...	...	13	18	27	17						
	2	...	...	0	32	16	37	32	36	47	27	57	0
	3	...	...	...	...	0	46	20	49	38	36	54	38
	4	...	...	...	...	...	...	0	57	24	59	48	55
	5	...	...	...	...	...	...	...	...	0	67	35	67
	6	...	...	...	...	...	...	...	...	...	...	0	76
35°	1	0	8	16	19	31	14						
	2	...	...	0	33	18	37	36	33	50	19		
	3	...	...	...	...	0	47	22	49	42	44	57	32
	4	...	...	...	...	...	...	0	48	27	58	52	52
	5	...	...	...	...	...	...	...	...	0	67	40	66
	6	...	...	...	...	...	...	...	...	...	...	0	76

4-7 shows the fourth largest maximum lobes to be the $M1$-$M4$ pair, but these do not occur in this configuration. Next, the $M2$-$M2$ lobe on the axis at high angle does not coincide with a height-factor maximum by a large margin, so is largely suppressed. Other possible small lobes of higher order are indicated by dots. The main beam is fully reinforced, while all the other lobes except the $M2$-$M4$ and the $M3$-$M5$ are well suppressed; and these lobes are naturally small. This case illustrates the cleanest possible radiation pattern for a horizontal rhombic antenna of this size.

Table 4-7. Amplitudes of Secondary Lobes, in Decibels, Relative to a Fully Formed Main Beam, for Free-space Rhombus

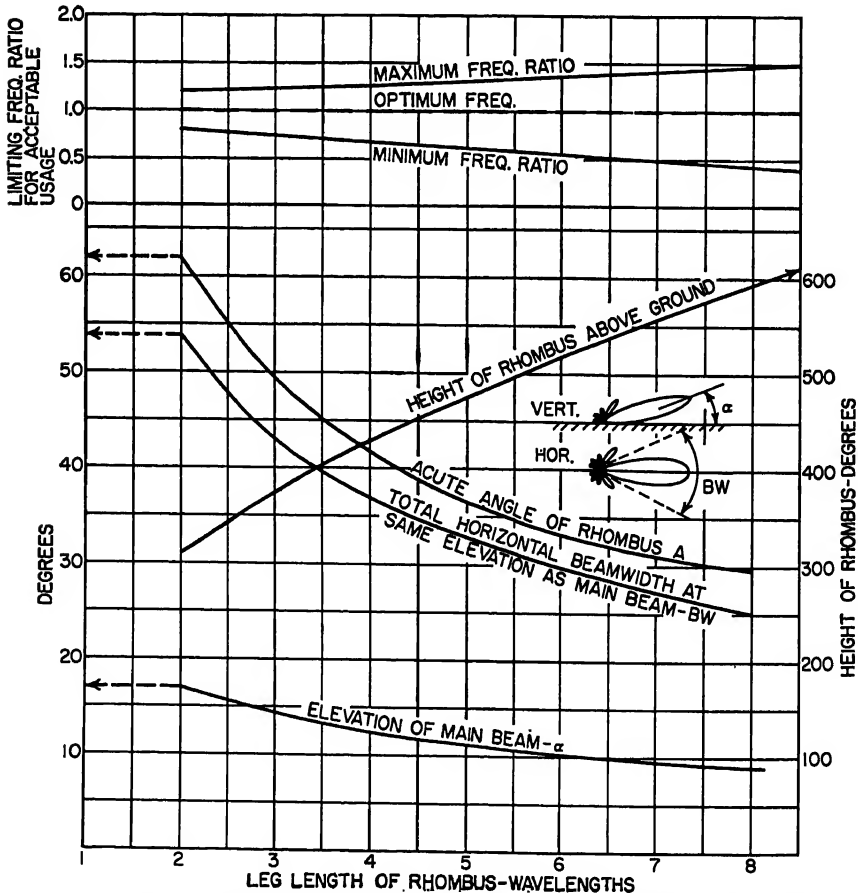| Order of maxima for first side	Order of maxima for second side								
	1	2	3	4	5	6	7	8	9
1	0								
2	−5.27	−10.6							
3	−7.7	−12.8	−15.6						
4	−9.0	−14.3	−16.5	−18.0					
5	−10.1	−15.4	−17.6	−19.1	−20.2				
6	−11.0	−16.3	−18.5	−20.0	−21.1	−21.9			
7	−11.7	−17.0	−19.2	−20.7	−21.8	−22.7	−23.4		
8	−12.3	−17.6	−19.9	−21.3	−22.3	−23.3	−24.0	−24.6	
9	−12.9	−18.1	−20.4	−21.9	−23.0	−23.8	−24.6	−25.2	−25.7

FIG. 4-14. Optimum-design parameters for high-frequency horizontal rhombic antennas.

(a)

(b)
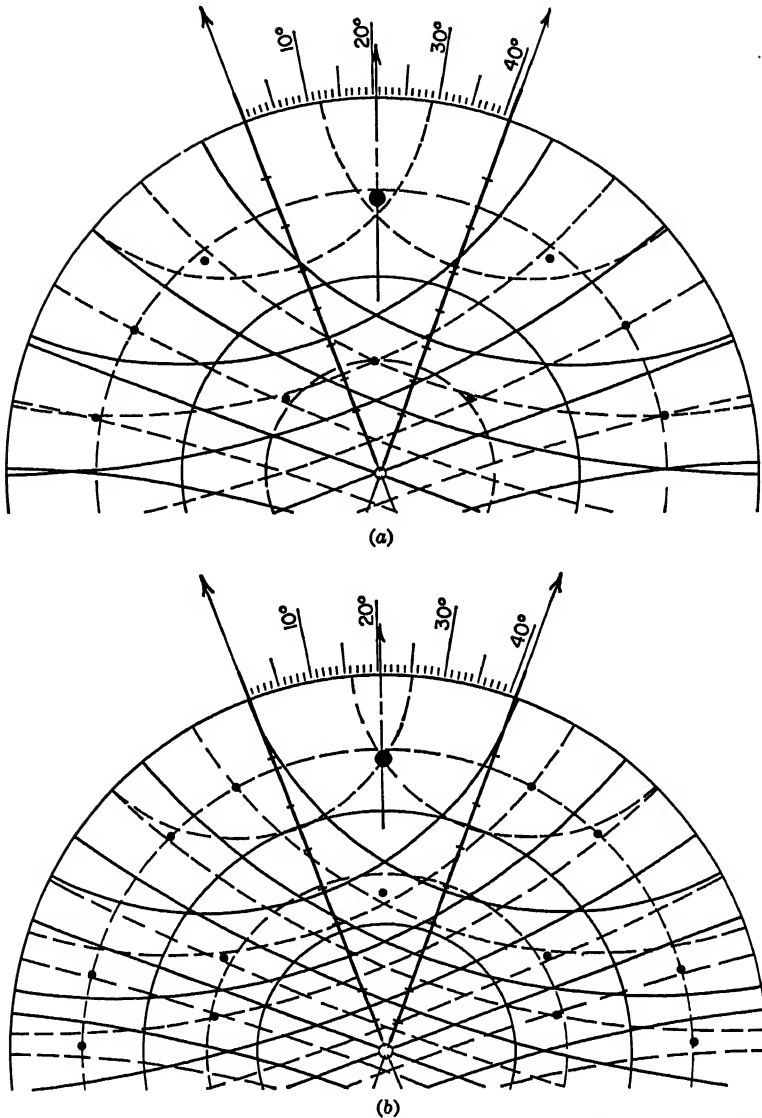
FIG. 4-15. Radiation patterns for a horizontal rhombic antenna of fixed physical size as the working frequency is changed: (a) $L = 3\lambda$ at frequency $0.75f_0$.   (b) $L = 4\lambda$ optimum design for frequency f_0.   (c) $L = 5\lambda$ at frequency $1.25f_0$.

Figure 4-15a and c shows the patterns for the same antenna when operated at a lower frequency where $L = 3.0\lambda$ and at a higher frequency where $L = 5\lambda$, respectively. It is immediately apparent from these that the conditions for the minor lobes are such that some of them are fully reinforced by the height factor, or only slightly reduced.   None is fully suppressed except the $M2$-$M2$ lobe in Fig. 4-15c.   Dots indicate the coordinates of the secondary lobes.   Each lobe is bounded by its enclosing

zero lines, from which the orientation of the cross section of each lobe can be estimated by inspection.

Wherever a maximum in the height factor coincides with a rhombus lobe maximum its field strength will be twice that of the rhombus alone (for the same antenna current) *provided* that the main beam is also maximized. The ratios then remain as in Table 4-7 for such lobes. For lobes not coinciding with maxima in the height factor, their relative values will be reduced. Where a side lobe is maximized but the main beam is not, the relative strength of the side lobe will exceed that given in the table.
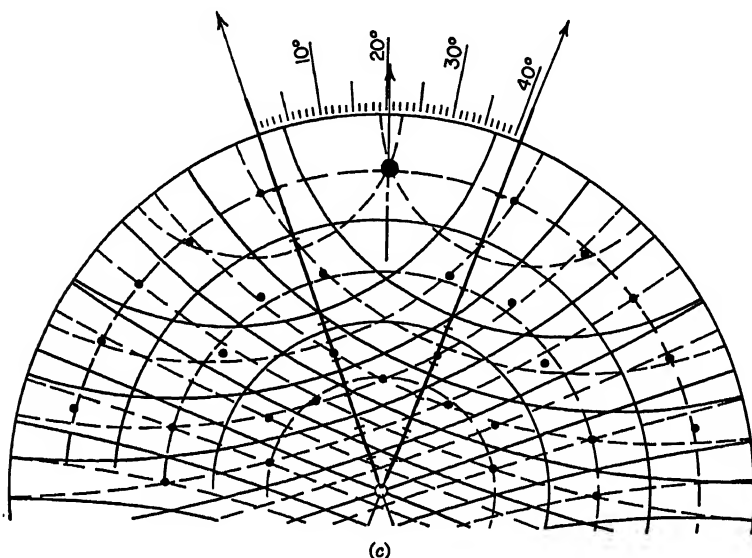

(c)

FIG. 4-15. (*Continued*)

It often is desired to design a rhombic antenna for minimum radiation or response in the back direction, at the design frequency. This is accomplished by choosing a side length that is an integral number of quarter wavelengths long, rather than one with an integral number of half wavelengths. This places a zero for the rhombus in the backward direction, where otherwise there will be a lobe, often favored by coherence with the first maximum in the height factor.

By means of stereographic charts for computation, the situation where the main beam splits because $A > 2\theta_1$ (Fig. 4-13c) is easily avoided. The highest working frequency is thereby limited for a particular antenna size and shape. These charts also demonstrate that the V and rhombic antennas are best used for the lower angles of radiation. Where high-angle radiation is wanted, the gain of a horizontal rhombic antenna is so low that equal or better performance can be had from simpler and far less expensive dipole antennas.

Sloping Rhombic Antenna. This type of antenna, as in Fig. 4-17, and the sloping V of Fig. 4-10e cannot be analyzed with the same stereographic charts, though special charts for sloping wires can be constructed. A set of charts would be needed for each different angle of slope of the wires with respect to ground. The principal vertical patterns and the parameters for sloping V and sloping rhombic antennas can be computed for any slope angle S for the plane of the antenna with respect to ground by rotating the antenna free-space pattern by the angle S and multiplying it by the height factor $f_h(H)$ [Eq. (4-3)], H being the mid-height. In this process use is made
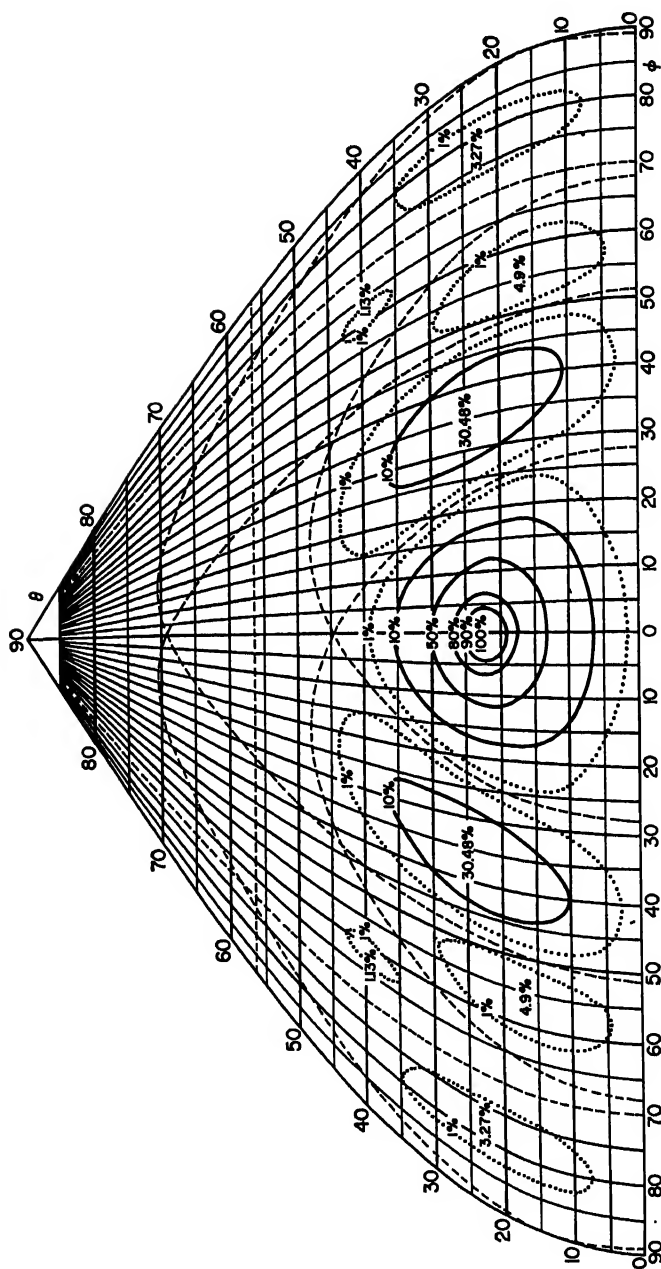
(a)

Fig. 4-16. C.C.I.R diagrams of relative power distribution through the forward half of the hemisphere from a horizontal rhombic antenna of fixed physical size with nonoptimum parameters, as they change with frequency: (a) $A = 40°, L = 3\lambda, H = 0.6\lambda$. (b) $A = 40°, L = 4\lambda, H = 0.8\lambda$. (c) $A = 40°, L = 5\lambda, H = 1.0\lambda$. (Note: In these diagrams the zeros in the patterns are shown by thin broken lines. Power contours relative to the main beam are shown in heavy broken lines. From C.C.I.R. Antenna Diagrams.)
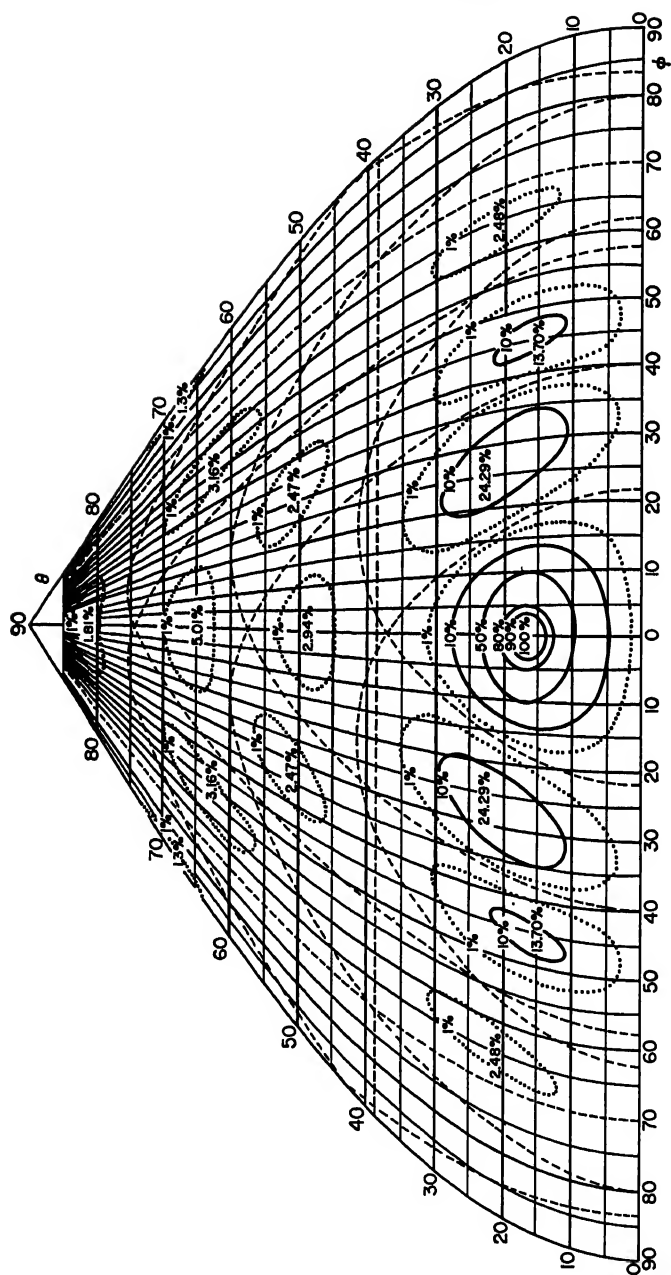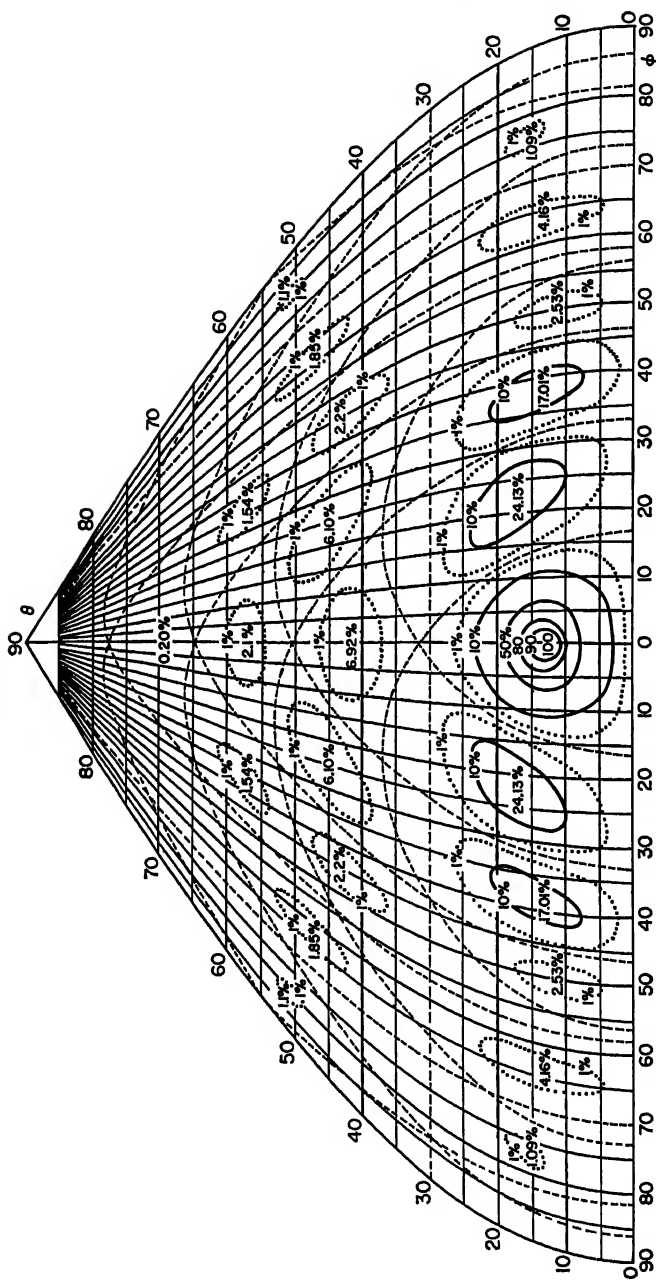
Fig. 4-16. (*Continued*)

Fig. 4-16. (Continued)

of the fact that the pattern of the rhombus or V is symmetrical with respect to its plane.

Land-saving Arrangements of Rhombic Antennas. The large land area occupied by the larger rhombic antennas raises the question of multiple usage in certain situations. There is successful experience with smaller antennas for the same direction within the area of the larger, with negligible interaction. Quantitative evaluation of this practice is lacking.
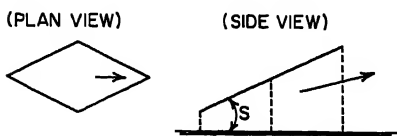
(PLAN VIEW)   **(SIDE VIEW)**

FIG. 4-17. Sloping rhombic antenna.

Rhombic Antennas for VHF and UHF. In VHF and higher-frequency applications where the best response is desired as nearly as possible in the direction of the horizon, the rhombus is designed with $A = 2\theta_1$, and its height above the effective reflection plane is made as high as feasible to get the first maximum in the height factor at the lowest angle.

An effective two-layer rhombic antenna for such applications where minimum size is a controlling factor is shown in Fig. 4-18. The measured characteristics are summarized in Table 4-8 over a 1.8:1 frequency range.
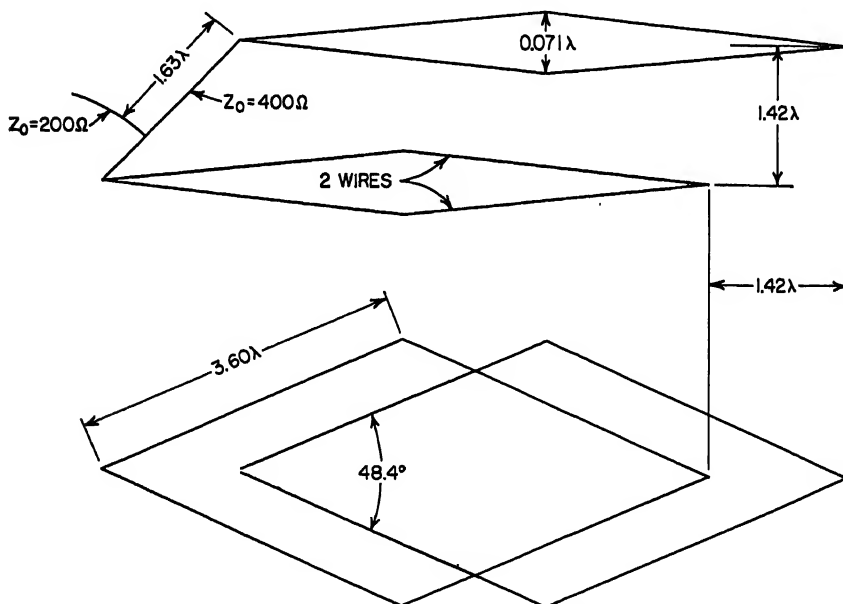
FIG. 4-18. Double rhombus optimized for ultrahigh-frequency reception over 1.8- to 1-frequency range.

Side-lobe Reduction in Rhombic Antennas. Single rhombic elements can be arrayed in various ways, in height, width, and length, to reduce side lobes and enhance the gain of the main beam. Figure 4-18 is an example of one method of combining two rhombic elements into an array.

Another is that shown in Fig. 4-19, where two coaxial rhombics having different configurations, but in the same plane, have common input terminals. The double rhombic of Fig. 4-19a and the double rhomboid of Fig. 4-19b are radiationally equivalent when the side lengths and apex angles are equal as shown. By this method, the principal lobes for four pairs of sides are made coherent to form the main beam, while

throughout the side-lobe areas there is generally incoherence between the component lobes. Side lobes are also reduced by the larger number of zero lines throughout the side-lobe areas, which either diminish or extinguish many of the side lobes. The resultant pattern contains a larger number of very much smaller lobes when the parameters for the antenna are carefully chosen. This can be done with stereographic

Table 4-8. Measured Values for Antenna, Fig. 4-18, Where Electrical Dimensions
Are at Frequency f_0

Frequency	Half-power beamwidth		Gain relative to half-wave dipole, db	Relative amplitude of largest secondary lobe in antenna plane, db	Front-to-back-ratio horizontal plane, db
	Vertical	Horizontal			
$0.714f_0$	28.4°	15.5°	9.6	−8	20
$0.856f_0$	.....	16.1°	11.6	−10	
f_0	19.0°	13.0°	13.0	−16.5	20
$1.14f_0$	.....	13.2°	14.7	−16.0	
$1.285f_0$	13.8°	11.0°	17.0	−14.0	>30

Terminal resistance for each rhombus, 470 ohms.
Paralleling feeder characteristic impedance, 400 ohms.
Common feeder characteristic impedance, 200 ohms.

charts, as illustrated in Fig. 4-20, together with measured azimuthal and main vertical patterns in terms of field strength. This method of arraying rhombics, or their equivalent in rhomboidal elements, can be carried to higher orders than 2, with further reduction of side lobes.

Radiation Patterns for Vertical-V Antenna. A vertical-V (inverted-V) antenna supported by one central mast is a half rhombic, with the major axis lying along the
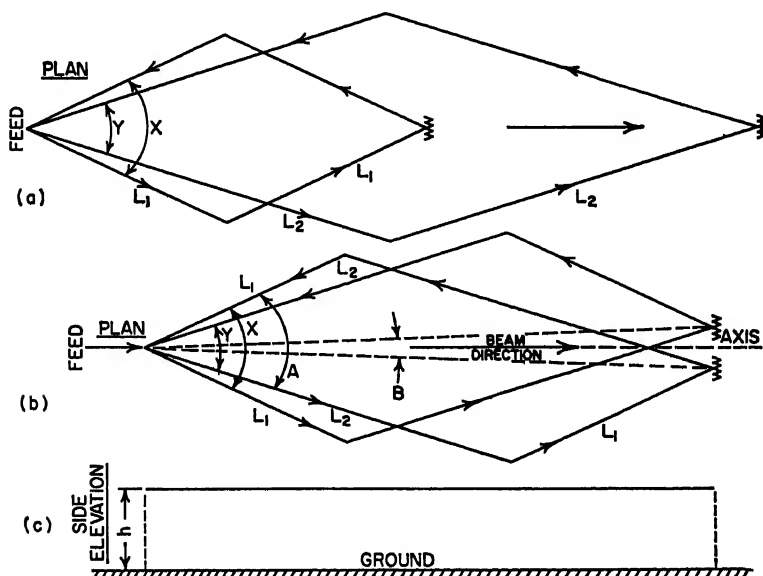

FIG. 4-19. Double rhombic and double rhomboid antennas having same radiation patterns.

ground.   The angle of each of the two wires with respect to ground is θ_1, so that the main lobe maximizes in the plane of the V along the ground.

The resulting radiation pattern can be read from the stereographic charts by simply interchanging the designations for elevation and azimuth angles on the charts.   The

MEASURED MAIN AZIMUTHAL RADIATION PATTERN

MEASURED MAIN VERTICAL RADIATION PATTERN
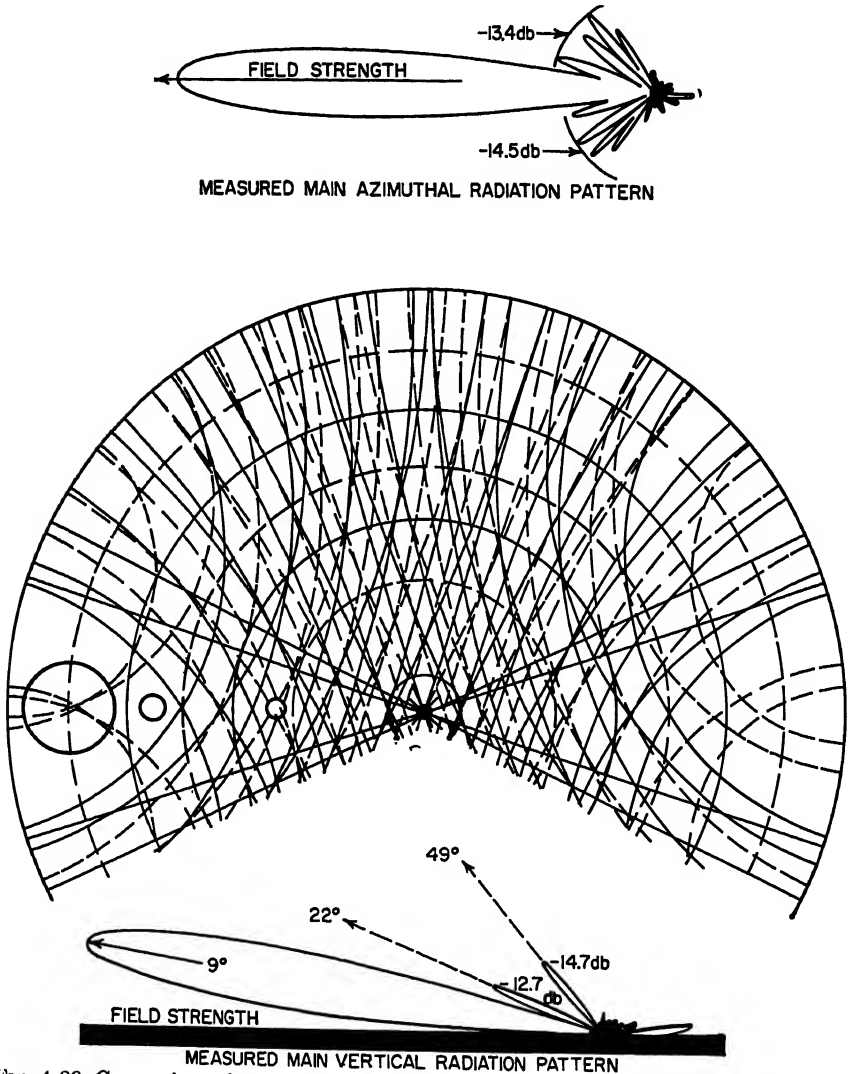
Fɪɢ. 4-20. Comparison of measured and stereographically computed radiation patterns for array of Fig 4-19b when $L_1 = 3.5\lambda$, $L_2 = 6.0\lambda$, $X = 50°$, and $Y = 35°$.

azimuth angles are now represented stereographically, while the vertical angles are normal (peripheral) circular angles.

Beam Reversal in a Rhombic Antenna.   The direction of the main beam of a horizontal rhombic antenna can be reversed by switching the feeder and also the terminal load resistance to opposite ends of the antenna.

Feeders from both ends of the antenna can be connected to separate receivers for simultaneous reception from opposite directions, provided that the impedance remains matched to the feeder at all frequencies. This is best accomplished by using a resistance termination of the correct value and having a receiver with a well-balanced, high-impedance input bridging the resistor, at each end. This requires, of course, that all radiation from the receivers be very low so that they do not mutually interfere.

Importance of Electrical Balance (Symmetry). The performance of symmetrical antennas depends largely on maintaining electrical balance and mechanical symmetry of the antenna and its feeder system. There must be a minimum of radiation coupling between the antenna and its feeder, which is best realized by the feeder being in line with the major axis of the antenna. Where this is not possible throughout its length, that part of the feeder nearest the antenna should always be so oriented. Radiation coupling introduces unbalanced potentials, so that there is a component of current returning in the ground. This affects the antenna performance unfavorably. A transmission line can be balanced by means of a parallel-wave drain circuit, but this does not remove the radiation effect of unbalance.

Cross Talk between Feeders. Broadband antennas of the rhombic type have no frequency selectivity. Any stray power induced into the feeder from the fields of other antennas, or by cross coupling between feeders, will be radiated spuriously. Care must be used in the design of large plants to ensure the highest practicable degree of isolation between feeders and from all antennas to all feeders. Coaxial feeders with balance-to-unbalance transformers near the antenna are often used to avoid this effect.

4.7. CIRCUITAL PROPERTIES OF LONG-WIRE ANTENNAS

Antenna design involves, first, the attainment of radiation distributions that satisfy the needs for most favorable wave propagation and reception. The second aspect of design concerns the circuital properties of the antenna at each working frequency. It is here that matters of impedance, voltage, and current are considered and the methods for coupling antennas to transmitters and receivers.

Radiation Resistance. That component of input resistance due to power lost by radiation is called the radiation resistance referred to some point. In elementary antennas this quantity has practical as well as academic significance. In the more complicated arrays, including all the long-wire antennas, radiation resistance is virtually meaningless to the engineer. Radiation efficiency, the ratio of power radiated to the total power input to the system, must be determined by indirect methods such as field-strength measurements or left unknown.

Feed-point Impedance (Rhombic Antennas). The input impedance of an antenna at any working frequency is a quantity of prime interest, either directly or indirectly. It is of direct interest when antenna and feeder are to be self-matched at a frequency or over a range of frequencies. The transmission line can sometimes be designed to have a characteristic impedance the same as that of the antenna input resistance, or vice versa in some cases. Alternatively, transformers or passive networks can be designed for use when two unequal impedances are to be matched.

If the match is to be at a single frequency, the antenna impedance can be unknown and the impedances matched by making standing-wave measurements on the feeder, followed by the application of various techniques for suppressing the return wave on the feeder. The method used, the required precision of the impedance match, the range of frequencies over which the match must be obtained within allowed tolerances, the variations of the antenna input impedance, and the transmission-line impedance with weather and time are all dependent on the nature of the problem at hand.

The rhombic antenna is one where it usually is desired to have the antenna input

impedance match that of the feeder over a wide range of frequencies without any additional devices or networks. The resistive component of antenna impedance and the characteristic impedance of a balanced two-wire open transmission line are made to meet at about 600 ohms. A matched single-wire rhombus has a median resistance over a range of frequencies of 750 to 800 ohms; but by using three wires in parallel starting from the apex, spreading out until they arrive at the side poles, and converging again at the other apex, the median resistance is made to be about 600 ohms, with relatively small reactive components. A 600-ohm two-wire balanced feeder gives a line of reasonable cross section, but becomes less reasonable for higher values of impedance. For this reason, rhombic antenna and feeder are designed for a unique value of 600 ohms for the majority of applications.

For arrays of rhombics and for open-wire balanced feeders operating at very high power, it is sometimes impracticable to make the antenna system and the feeder self-matching. Wideband impedance-matching networks, such as exponentially tapered lines, are sometimes used for this purpose. Where it is desired to use a coaxial feeder with a balanced antenna, the coupling is made through a network capable of matching the impedances properly and also transforming from unbalanced to balanced potentials (Chap. 31).

Terminal Resistance for Rhombic Antenna. The rhombic antenna is made to perform as a traveling-wave antenna by absorbing and dissipating in a resistance at the far end all the energy of the system that is not radiated or lost in heating the antenna and ground. For best performance the terminal load for this purpose must also match the far-end impedance over a range of frequencies, because any reflected energy is propagated backward through the antenna, decreasing its front-to-back ratio of radiation. For low-power use a resistor of uniform frequency-resistance characteristics is connected directly across the two sides at the apex. The resistor must in any case be capable of handling high impulses, electrically and mechanically, due to induction from lightning.

For transmitting applications where the resistor must have a large dissipation capacity, common practice is to use another transmission line of the same characteristic impedance but with high losses. This is called a dissipation line and is a balanced open-wire line made of high-loss material such as iron or some alloy of stainless steel having appreciable magnetic permeability. The dissipation line should have an attenuation length of about 20 db if the end is to be short-circuited and grounded. The reflected wave reaching the antenna is then attenuated 40 db, so that the reflected voltage is 1 per cent and therefore negligible. Most of the power is lost in the input end of the line, so the line length can be shortened at that distance where a resistor can be substituted for an extension of the line. This is usually an economy. Grounding the center of the shortening resistor provides a static drain circuit, as does the grounding of the end of the 20-db-line length.

The power to be dissipated in the terminal resistor varies from about 50 per cent of the input power when the sides are of the order of two wavelengths to 15 per cent for rhombics five wavelengths or more per side.

There are techniques for conducting the excess energy arriving at the far end back to the input end where, if it is properly transformed in voltage and phase, the two circuits can be paralleled and the excess power radiated. Methods for accomplishing this are frequency-selective so that it can be adjusted for only one frequency. Because the principal appeal of the rhombic antenna usually is its broad-frequency capability, this technique of re-using the excess power has found very little application.

Feed-point Impedance (Standing-wave Antennas). Standing-wave antennas, often called resonant antennas, have the common characteristic of large changes of impedance with frequency, with resistance and reactance values varying over very

wide ranges. Such antennas are usually designed for particular working frequencies so that the antenna to feeder match is also frequency-selective.

Potentials and Currents. The limiting potential on any part of the antenna and feeder system occurs when the potential gradient is sufficient to ionize the air to form a standing arc (plume) or to damage the insulation. The limiting current is that value which overheats the conductors sufficiently to cause damage or to compromise their mechanical strength.

Traveling-wave antennas are similar to matched transmission lines in the nature of their potential and current distributions, which are relatively uniform. In this respect they are superior to standing-wave antennas for high-power transmission for a given conductor size and insulation rating. A 600-ohm rhombic, fed with a 600-ohm transmission line, has substantially the same current and potential throughout the length of the system. Relatively very much larger potentials and currents exist at antinodal points along a standing-wave antenna with the same power input.

4.8. LONG-WIRE ANTENNAS WITH MODIFIED CURRENT DISTRIBUTIONS

It is possible, and sometimes desirable, to use long-wire antennas with unnatural or modified current distributions. Of the many possible ways to do this, a few have found extensive practical use because of the desirable radiation distributions thus achieved.

One useful configuration is an end-to-end series of cophased half-wave dipoles. A natural standing-wave current distribution can be converted to this distribution by reversing the relative phase of the current in alternate half-wavelength sections. This can be done by inserting antiresonant networks every half wavelength, or its equivalent, a quarter-wave nonradiating transmission line, the latter being wound up into a mechanically reasonable form. Antennas of this general class are known as Franklin antennas, after the inventor. Figure 4-21 shows three arrangements of Franklin vertical omnidirectional antennas.

Further evolutions of the Franklin antenna provide current distributions more nearly approaching a continuous, uniform cophased distribution. One of these (Fig. 4-21c) places the successive current maxima less than one-half wavelength apart by using a series capacitor for power-factor correction at locations midway between the successive maxima. At these locations the antenna current is a fairly large percentage of the antinodal current, and not zero (ideally) as in Fig. 4-21b. Another version is a folded wire, or "zigzag" type, shown in Fig. 4-21d. The parameters for the latter are somewhat frequency-dependent because of insulator capacitance and effects of rigging, but the approximate electrical dimensions are given in the caption for preliminary guidance.

The E-plane radiation patterns for vertical long-wire Franklin antennas are approximated by the following.

For the type of collinear cophased dipoles shown in Fig. 4-21b, with equal antinodal currents and with n dipoles in series in free space,

$$E_\theta = \frac{60I}{r} \frac{\cos\left(\frac{\pi}{2}\sin\theta\right)}{\cos\theta} \frac{\sin\left(\frac{n\pi}{2}\sin\theta\right)}{\sin\left(\frac{\pi}{2}\sin\theta\right)} \quad \text{volts/meter} \quad (4\text{-}4)$$

The field strength of the main lobe normal to the wire ($\theta = 0$) is $60nI/r$ volts/meter at distance r meters.

When this array is placed vertically over perfectly conducting ground the antenna

radiation pattern is expressed by

$$E_\theta = \frac{120I}{r} \frac{\cos\left(\dfrac{\pi}{2}\sin\theta\right)}{\cos\theta} \frac{\sin\left(\dfrac{n\pi}{2}\sin\theta\right)}{\sin\left(\dfrac{\pi}{2}\sin\theta\right)} \cos(h\sin\theta) \qquad (4\text{–}5)$$

where $h = 2\pi H/\lambda$ is the electrical height above ground of the mid-point of the radiator.

The radiation pattern for Fig. 4-21c and d depends upon the design proportions, but one can assume for instructive purposes that they approximate the uniform
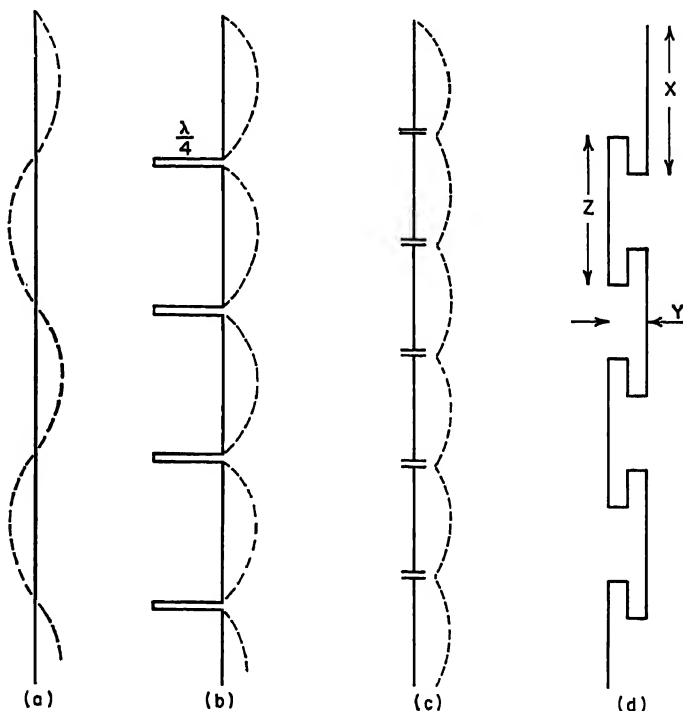
FIG. 4-21. Franklin antennas: (a) Natural standing-wave current distribution. (b) Cophased standing-wave current distribution. (c) Phase-compensated current distribution. (d) Zigzag, with $X \doteq 0.6\lambda$, $Y \doteq 0.11\lambda$, and $Z \doteq 0.7\lambda$.

cophased current distribution, producing a radiation pattern in free space of the sin x/x type. When such a current distribution exists in a vertical antenna of physical length L and has an electrical height h from a perfectly conducting ground to its mid-point, the shape of the field-strength pattern (E plane) is expressed approximately by

$$f(\theta) = \frac{\sin x}{x} \cos(h\sin\theta)\cos\theta \qquad (4\text{–}6)$$

where $x = (\pi L/\lambda)\sin\theta$.

Antennas of this class have relatively small bandwidth because of their resonant nature, even though these types have considerable radiation damping. The attainment of performance close to that expected ideally is critical; and once attained, a small frequency change will cumulatively change the current-amplitude distributions and phase distributions progressively throughout such long systems.

REFERENCES

1. P. S. Carter: "Circuit Relations in Radiating Systems and Application to Antenna Problems," *Proc. IRE*, vol. 20, p. 1004, June, 1932.
2. Colebrook, F. M.: "Electric and Magnetic Fields for Linear Radiator Carrying a Progressive Wave," *J. IEE (London)*, vol. 89, p. 169, February, 1940.
3. C. W. Harrison, Jr.: "Radiation from Vee Antennas," *Proc. IRE*, vol. 31, p. 362, July, 1943.
4. C. W. Harrison, Jr.: "Radiation Field of Long Wires with Application to Vee Antennas," *J. Appl. Phys.*, vol. 14, p. 537, October, 1943.
5. J. D. Kraus: "Antennas," pp. 148–153, McGraw-Hill Book Company, Inc., New York, 1950.
6. J. A. Stratton: "Electromagnetic Theory," pp. 439–448, McGraw-Hill Book Company, Inc., New York, 1941.
7. E. M. Wells: "Radiation Resistance of Horizontal and Vertical Aerials Carrying a Progressive Wave," *Marconi Rev.*, no. 83, October–December, 1946.
8. C. F. Booth and B. N. MacLarty: "The New High-frequency Transmitting Station at Rugby," *J. IEE (London)*, pt. B, vol. 103, October, 1955. Rhombic antenna layouts, two rhombic antennas on one set of masts, and feeder cross-talk measurements.
9. E. Bruce: "Developments in Short-wave Directive Antennas," *Proc. IRE*, vol. 19, p. 1406; *Bell System Tech. J.*, vol. 10, p. 656, October, 1951. Evolution of the vertical-V antenna.
10. E. Bruce, A. C. Beck, and L. R. Lowry: "Horizontal Rhombic Antennas," *Proc. IRE*, vol. 23, p. 24, January, 1935. Development of the rhombic antenna.
11. P. S. Carter, C. W. Hansell, and N. E. Lindenblad: "Development of Directive Transmitting Antennas by RCA Communications," *Proc. IRE*, vol. 19, p. 1733, October, 1931. Evolution of standing-wave long-wire antenna development.
12. CCIR Antenna Diagrams, International Telecommunications Union, Geneva, 1954.
13. W. N. Christiansen, W. W. Jenvey, and R. D. Carmen: "Radio-frequency Measurements on Rhombic Antennae," *AWA (Australia) Tech. Rev.*, vol. 7, no. 2, p. 131, 1946. Instrumentation and measuring techniques for determining current distributions on two-tier rhombic arrays.
14. W. N. Christiansen: "Directional Patterns for Rhombic Antennae," *AWA (Australia) Tech. Rev.*, vol. 7, p. 1, 1946. Study and pattern computations for horizontal rhombic antennas and four types of rhombic arrays. A basic paper on rhombic arrays. Some of the diagrams are reproduced in Ref. 18.
15. Jean Dufour: "Diagrammes de réception d'antennes rhombiques dans un plan vertical: resultats experimentaux," *Bull. Tech. PTT* (Bern, Switzerland), vol. 31, p. 65, March, 1953. Measurements of vertical-plane patterns with aircraft, including effects of rough terrain.
16. Donald Foster: "Radiation from Rhombic Antennas," *Proc. IRE*, vol. 25, p. 1327, October, 1937. A classic in rhombic antenna theory and design. Foster's stereographic technique is featured in this chapter.
17. A. E. Harper: "Rhombic Antenna Design," D. Van Nostrand Company, Inc., Princeton, N.J., 1941. An old but still useful reference on rhombic antenna engineering, electrical and mechanical.
18. E. A. Laport: "Radio Antenna Engineering," McGraw-Hill Book Company, Inc., New York, 1952. Pages 301–339 treat long-wire antennas from the designer's viewpoint.
19. E. A. Laport: "Design Data for Horizontal Rhombic Antennas," *RCA Rev.*, vol. 13, p. 71, March, 1952. Sets of translucent stereographic design charts were supplied on request; now out of print.

Chapter 5

ARRAYS OF LINEAR ELEMENTS

GEORGE C. SOUTHWORTH

Bell Telephone Laboratories, Incorporated
Murray Hill, N.J.

5.1. INTRODUCTION

A practical objective of directive radio is an improvement in received signal as measured relative to the prevailing noise. More particularly, directivity improves the *signal-to-noise ratio*. This improvement may be accomplished either by using at the transmitter an antenna that projects the transmitted wave power in the form of a concentrated beam toward the distant receiver, or it may be accomplished at the receiver by using a similar antenna, which in this case intercepts a maximum of passing wave power. It is interesting that these seemingly different functions are entirely reciprocal, and except for minor details they are altogether equivalent. Thus any signal improvements desired may theoretically be taken either at the transmitter

or at the receiver or be shared between the two. In either case the improvement increases as the measured beam becomes progressively sharper.

The above principles apply at the receiver only if atmospheric noise arrives with equal intensity from all directions. If the noise should be highly directive and should unfortunately arrive from the same direction as the signal, no improvement would result. On the other hand, if it should arrive from a direction toward which the antenna is particularly discriminant, then more than the usual improvement could be expected.

One of the more common methods of obtaining directive gain is an arrangement of several individual antennas so spaced and phased that their individual contributions add in one preferred direction while canceling in others. Such an arrangement is known as an *array of antennas*. Bearing in mind that the several antennas may be arranged in various configurations such as straight lines, rectangles, circles, or triangles of possibly three-dimensional configurations and may bear radiated amplitudes differing both in phase and amplitude, it is easily seen that there is an unlimited number of possible combinations. Fortunately, years of experience have reduced the number that are thoroughly practicable to a relatively few.

As pointed out in Sec. 2.6, signal improvements resulting from directivity may be specified in a variety of ways. Sometimes this specification takes the form of a plotted pattern which shows at a glance the relative signal level in various directions. In other cases the over-all improvement is measured relative to some accepted standard such as an isotropic source, a short dipole, or a half-wave antenna. Table 2-1 gives specific data relating to these various standards. For purposes of this section, all gains specified will, unless otherwise noted, be measured relative to a single element of the specific array under consideration, regardless of whether the element be an isotropic source, a dipole, a half-wave antenna, or a small current loop. We sometimes refer to these relative gains as *test ratios* and designate the same by the letter T. If questions arise, as for example in connection with certain vertical directional patterns, we shall assume, unless otherwise noted, that each element of the array is a short dipole. It is to be noted that the directive beam of an array of half-wave antennas is only slightly sharper than that of the corresponding array of short dipoles, and for many purposes the difference can be neglected.

Representative Forms. As we shall later see, one of the more important arrays used in practice consists of a number of identical parallel antennas set up along a line drawn perpendicular to their respective axes. In one preferred arrangement, the individual currents are identical both in magnitude and phase. In this case, radiation proceeds both forward and backward in directions perpendicular to the line of the array. Such an antenna is said to be *broadside* and *bidirectional*. It may be made essentially unidirectional by erecting a second identical array a quarter wave to the rear of the first and driving the same by currents leading in phase by a quarter period. The directivity of this type of array usually increases with its length or *aperture*. In a second arrangement, the individual currents are again equal in magnitude, but this time their phase varies progressively along the line in such a way as to make the over-all arrangement substantially unidirectional. Since in this case the direction of optimum signal lies along the line of elements, it is referred to as an end-fire array. In a third arrangement, the single line of antennas is arranged collinearly, often with one antenna above another (*stacked*). In this case the currents are, as in the first case, identical both in magnitude and phase. This provides a symmetrical pattern with its main lobe everywhere perpendicular to the principal axis. Accordingly, it is referred to as a *broadcast*, or *omnidirectional*, array. Often two-dimensional combinations of the first and last of these three arrangements are used.

In some instances it may be desirable to depart from the plan of using currents of equal magnitude in the several antennas. Indeed, very desirable directional charac-

teristics may sometimes be obtained by *tapering* the amplitudes of currents progressively along the line. Examples of all these arrangements will be discussed below.

Applications. Antenna arrays have a wide range of application. They are often used in simplified form at frequencies as low as 1 Mc (λ = 300 meters) or lower, while at the other extreme they are sometimes used at frequencies as high as perhaps 1,000 Mc (λ = 30 cm) or even higher. Though the principles of antenna arrays have been known in an abstract way for many decades, their use did not become general until about thirty years ago, when the pressure of commercial radio led to the use of the higher frequencies where such arrays became feasible. It is a general rule that the higher the operating frequency, the more feasible will be antennas of high directivity.

It is significant that interest in arrays is not confined to the particular structures known by that name. We find that the general philosophy of arrays becomes applicable also to other very different kinds of antennas. More particularly, it may be convenient to regard the radiating aperture of certain horn antennas described in Chap. 10 as equivalent to an array of individual sources. Similarly, we may prefer to think of certain dielectric antennas as the equivalent of an end-fire array. Finally, in certain scanning antennas to be described later, we may like to regard the whole as made up of an array of arrays where each individual array consists of a group of individual radiators. Thus in reading the present section, we should consider it in part a preparation for the practical array designs to follow and in part the basic fundamentals of certain other antennas to be described later. In applying these fundamentals, we are perhaps merely invoking Huygens' principle, a concept that has been useful in optics for more than two and a half centuries.

5.2. TWO-ELEMENT DRIVEN ARRAYS

As a suitable introduction to the subject of antenna arrays, we shall consider, first, some of the more common combinations of two antennas. For the case of two short dipole antennas spaced along the X axis by A wavelengths and differing in phase by B periods of oscillation, the radius of the space pattern is given by

$$r = \cos \pi (A \cos \varphi \sin \theta + B) \sin \theta \quad (5\text{-}1)$$

where φ and θ are the angles designated in Fig. 5-1.

If the XY-plane pattern is desired, the angle θ is made $\pi/2$. If the XZ-plane pattern is desired, $\varphi = 0$. Figure 5-2 shows representative XY-plane patterns for various values of $A\lambda$ and BT. In this type of diagram directive gain is roughly proportional to the ratio of the area of the circumscribed circle to that of the pattern inside. In practice, these are often horizontal-plane patterns. The practical-minded engineer will readily identify various configurations that may perform useful functions. A case of special practical importance is that in which the two antennas

FIG. 5-1. Three-dimensional polar coordinate system.

are spaced by a quarter wavelength and are driven by currents of the same magnitude but the phase of one lags the other by a quarter period. Thus $A = \frac{1}{4}$ and $B = -\frac{1}{4}$. For this particular case, the corresponding patterns are shown in Figs. 5-2b and
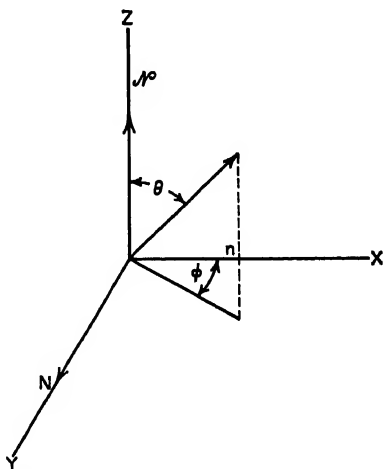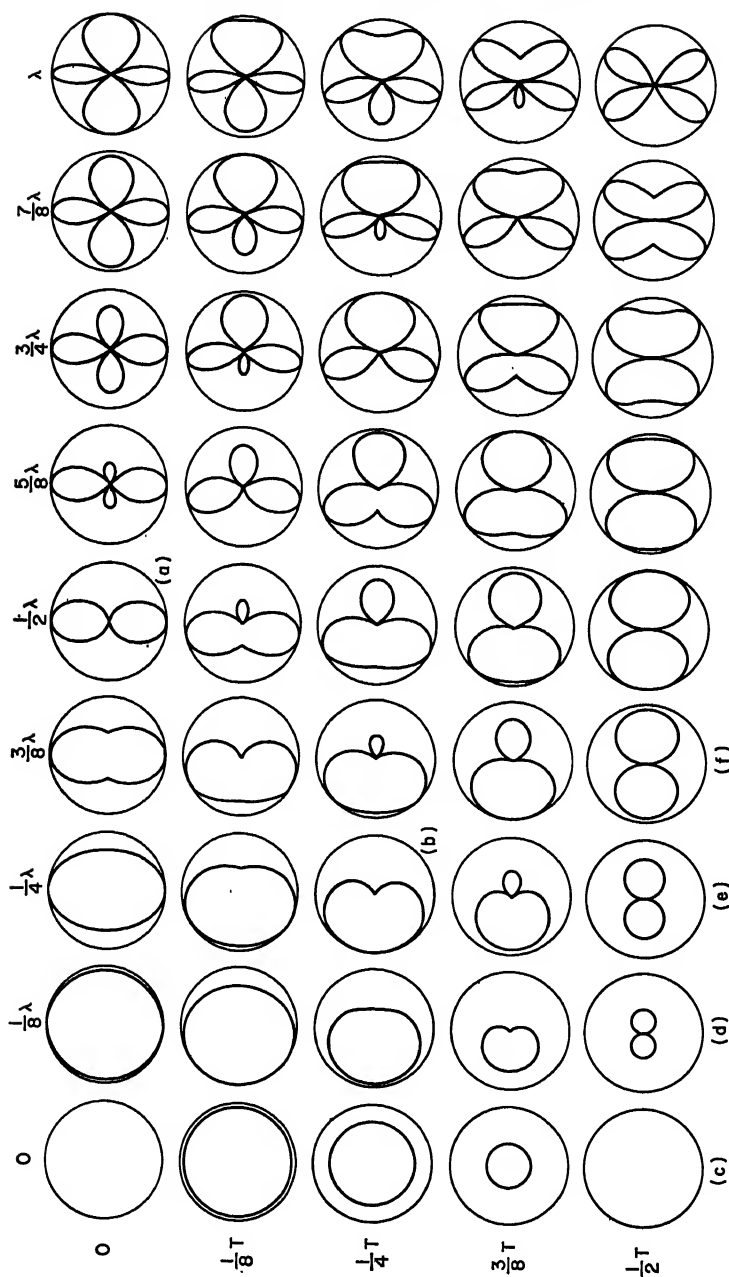
FIG. 5-2. Directive amplitude diagrams for an array of two antennas driven by currents of equal amplitude. Separation in wavelengths (λ) along the top. Phase difference in periods (T) at left.

5-3a. This arrangement, which is often referred to as an *end-fire couplet*, is of importance, for it is one of the fundamental building blocks from which other more elaborate arrays may be constructed. There are other patterns nearby to Fig. 5-2b which may perform similar functions. It is to be noted that whereas this particular directional pattern is only moderately sharp, there is at its rear a direction in which the intensity is zero. Thus this arrangement has an infinitely high *front-to-back ratio*. In practice, such high ratios are often very advantageous. For example, at a receiver, they may aid materially in discriminating against a nearby transmitter or other source of interference.

A second example of some practical importance is that in which the spacing between the two antennas is one-half wavelength but the corresponding currents are in the same phase. Representative patterns are shown in Fig. 5-2a and also in Fig. 5-3b. In this case, the pattern is somewhat sharper than before but there is equal power transmitted both forward and backward. More accurate calculations show that the directive gain relative to a single element resulting from the use of either arrangement

g=3db	g=3db	g=6db
(a)	(b)	(c)
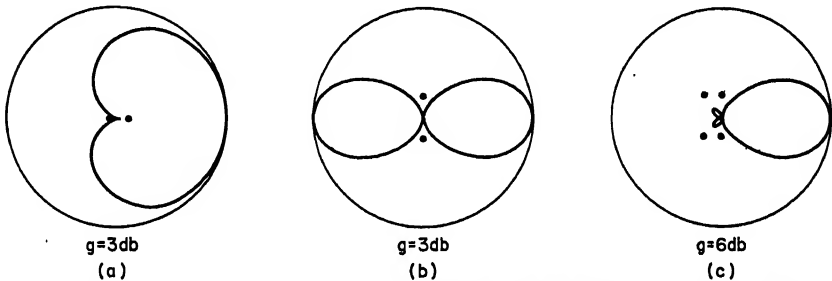
Fig. 5-3. Representative directive patterns and gains to be expected from antennas driven by currents of equal amplitude: (a) Antennas spaced by one-fourth wavelength, currents differing in phase by one-fourth period—the end-fire couplet. (b) Antennas spaced by one-half wavelength, currents in the same phase—the broadside couplet. (c) A combination of (a) and (b).

is substantially the same* (3 db), but in one case the front-to-back ratio is theoretically infinity, while for the other it is unity. Alternatively, there may be used in place of pattern a in Fig. 5-2 such compromises as that to the left and right of pattern a or perhaps pattern d, e, or f, or possibly some intermediate between patterns c and d. Patterns of the latter kind are typical of *superdirectivity*, a subject to be discussed later.

The inquiring engineer will naturally ask if we may not advantageously combine the two schemes shown in Fig. 5-3a and b. This is indeed the case, and it gives the very desirable directional pattern shown in Fig. 5-3c. In this case, the front-to-back ratio is again high, the directive pattern is even sharper than that shown in Fig. 5-3b, giving now a combined gain equal substantially to the sum (6 db) of those represented in Fig. 5-3a and b. Most antenna arrays are elaborations of the arrangement shown in Fig. 5-3c.

The simple configurations shown in Fig. 5-3 are favorite forms used particularly where moderate directivity is acceptable. At the longer wavelengths where antenna lengths would be inordinately large and their supports would be correspondingly expensive, the individual antennas may be grounded and therefore be a quarter wave or less in height. At somewhat shorter wavelengths, it may be feasible to use half-wave antennas and possibly elevate them to strategic heights above the earth. As is

* It is interesting that for broadside spacings greater than one-half wavelength, the gain from two elements may be appreciably more than 3 db.

well known, reflections from the earth may at various elevations combine to add or subtract from the effects obtained from antennas located in free space. The results to be expected from earth effects are in most practical cases involved functions of frequency, dielectric constant, and conductivity of the earth. These effects are considered more at length in Chap. 33. They should be taken into account particularly in cases where gain and vertical directivity are of interest. The reader is referred to that chapter for the necessary correction factors.

Feed lines for interconnecting the several antennas shown in Fig. 5-3 must, of course, be arranged so that their respective driving voltages appear at the antennas in the proper amplitude and phase. Details of such interconnecting lines are given in Chaps. 20, 21, 30, and 31. As we shall see, the spacings between individual antennas are often deliberately chosen with a view to simplifying the feed-line problem, and were it not for feed-line considerations, it might often be advantageous to use other spacings. As we shall later see, the feed-line problem in most cases calls for considerably ingenuity, and accordingly it occupies an important place in antenna design. Again the reader is referred to these sections for the necessary information.

5.3. SIMPLE ARRANGEMENTS INVOLVING PARASITIC ANTENNAS

Because of the feed-line problems already mentioned, it is sometimes desirable to feed certain antennas of an array parasitically. In these cases, the currents appearing in the several parasitic antennas are derived by radiation from a nearby driven antenna. A particularly simple case is a driven antenna together with a single parasite. Together the two may be considered as a kind of two-element array. Because the current flowing in the parasite is often less than that in the driven antenna, patterns considerably different from those illustrated in Fig. 5-2 may be expected. As will be appreciated, the magnitude of the current in the parasite falls off rapidly with separation from the driven element. Hence there is a tendency toward small separations. On the other hand, the phase of the parasitic current relative to the driven element increases with separation. So in order to obtain the desired phase change, it may be necessary to operate with considerable spacing, perhaps a quarter wave or even one-half wavelength. Often there is a need to compromise between these two variables, thereby making their separations somewhat less than might ordinarily be expected. In addition to the phase change due to separation, it is possible to alter the phase of the parasite, sometimes as much as $\pm \frac{1}{8}$ cycle, merely by altering its length. Though this is usually at the expense of current, it is an additional dimension of compromise and it is very useful. Together these several aspects make the problem of parasitic antennas rather involved. In fact, it is far too involved for adequate consideration in the limited space here available. As might be expected, much of the existing technique of parasitic antennas is based on experiment. Representative data are given below in graphical form.

Parasitic antennas are of interest over a wide range of frequencies. At moderately low frequencies, perhaps one or two megacycles, and particularly in cases in which only moderate directivity is needed, it may be expedient to add to the primary radiator one or more parasites. At the other extreme, perhaps at frequencies of several hundred megacycles, they are used in places where the numerous interconnecting feed lines would become unwieldy. In these cases, also, it is more advantageous to use a single driven antenna together with a multiplicity of parasites. At these higher frequencies both the driven antenna and its parasites are often nominally one-half wavelength long and are operated so as not to be affected materially by the earth. At these higher frequencies, too, it is sometimes desirable, in order to get certain phase relations, to depart appreciably from the nominal half-wave relationship.

Representative Spacings. As might be expected, an infinite number of combinations may be made of a driven antenna and a single parasite. One, sometimes used at the lower frequencies, is the quarter-wave combination shown in Fig. 5-4a. It is the counterpart of the end-fire couplet shown in Fig. 5-3a, but since the current flowing in the parasite is much smaller than that in the driven antenna, the front-to-back ratio is usually low. Measured gains ranging up to 3.6 db or even more have been reported. Combinations involving more than one parasite are shown in Fig. 5-4b and c, together with representative patterns. That of Fig. 5-4b is largely of academic interest and may be regarded as a rough counterpart of Fig. 5-3b. It is shown here with a view to illustrating the part played by the two lateral elements in the final parabolical form shown in Fig. 5-4c.

g_c = 3.6db
g_m = 3.6db
Z_0 = 60.2 + i132.6Ω
(a)

g_c = 4.6db
g_m = 4.2db
Z_0 = 87.2 − i122.8Ω
(b)

g_c = 5.6db
g_m = 4.8db
Z_0 = 73.8 + i143.8Ω
(c)
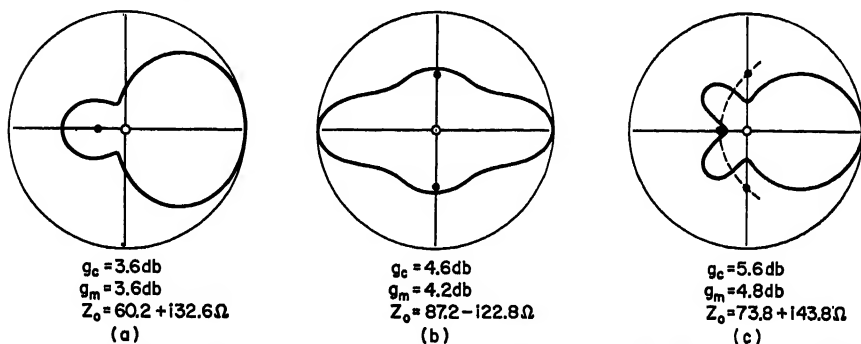
FIG. 5-4. Representative patterns, gains, and input impedances to be expected from a single driven antenna together with: (a) A single parasite spaced approximately by a quarter wavelength. (b) Two parasites spaced laterally approximately one-half wavelength. (c) A combination of (a) and (b) to form the rudiments of a parabola.

A little reflection will show that in the arrangement of Fig. 5-4c, the three parasites there shown fall on a parabola. This suggests that if we were to fill in the intervening spaces with an infinite number of similar reflectors and perhaps extend them along the dotted line shown, we would have the cylindrical parabola described in Chap. 12. It will be seen from Fig. 5-4b and c that the effect on gain of the two lateral parasites is comparable with the effect of the driven antenna and the quarter-wave reflector alone. The presence of a parasite tends to reduce slightly the input resistance of the driven antenna for quarter-wave spacings and to increase it slightly for half-wave spacings. It is of interest that as a result, the combined input resistance of the driven antenna and its three parasites is not very different from that of the driven antenna alone.

In addition to the nominal quarter- and half-wave spacings between a driven antenna and its parasite already discussed, an especially interesting result may be obtained from relatively close spacings, especially when we detune the parasite relative to its normal free-space resonant length. Typical results are shown in Fig. 5-5. In Fig. 5-5a we show representative directional patterns both in the plane of the two antennas and at right angles thereto for the particular case of a separation of 0.04λ, assuming that both are resonant. At this close spacing, the current in the parasite is substantially that in the driven element, and since they are oppositely phased, there is a null along the Y axis as well as the expected null along the Z axis. Though the front-to-back ratio is unity, there is nevertheless a directive gain of 3 db relative to a single element.

By increasing the length of the parasite by 5 per cent, still keeping the spacing the same, the symmetry characteristic of Fig. 5-5a is destroyed as shown by Fig. 5-5b.

The parasite now acts as a *reflector*, giving a directive gain approaching 6 db. The front-to-back ratio is much improved, but the null along the Y axis is now lost. By detuning the parasite an approximately equal amount in the opposite sense, the pattern will be essentially the same but will be reversed in direction (Fig. 5-5c). In this case the parasite is now called a *director*. As might be expected, both a reflector
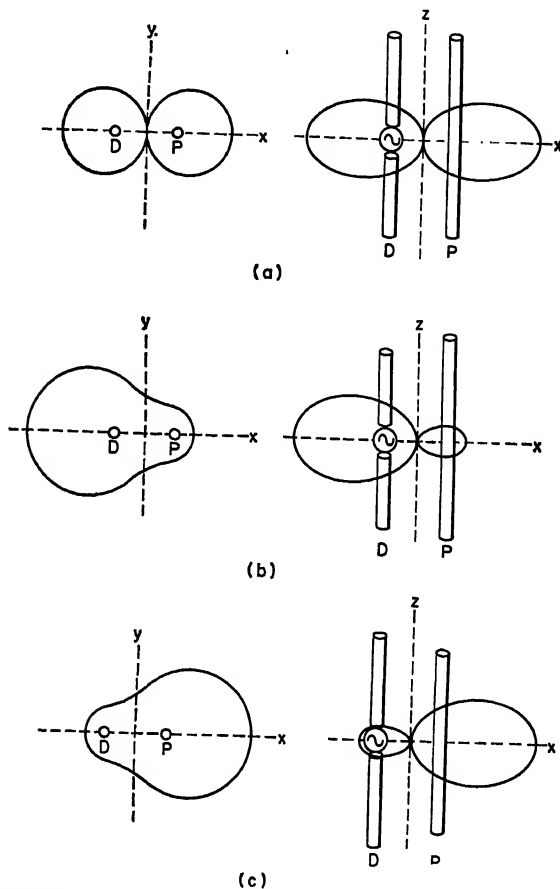

(a)

(b)

(c)

FIG. 5-5. Representative patterns to be expected from a driven antenna together with a single closely spaced (0.04λ) parasite: (a) Both elements are resonant. (b) Parasite lengthened by 5 per cent to act as a reflector. (c) Parasite shortened by 5 per cent to act as a director. (Reference 4.)

and a director may be combined with a driven antenna to form a three-element array, but because of interaction between elements, the gain now falls somewhat short of that to be expected. A gain of 8 db is regarded as representative. As we shall see, the particular adaptation of parasitic radiators just cited is in rudimentary form the Yagi-Uda antenna.*

* For a good discussion of parasite antennas and their behavior, the reader is referred to "TV and Other Receiving Antennas" by Arnold B. Bailey, John Francis Rider, Publishers, Inc., New York.

Closely spaced radiators oppositely phased belong to a class of antennas which are said to be *superdirective*. Being closely spaced, their over-all dimensional apertures are
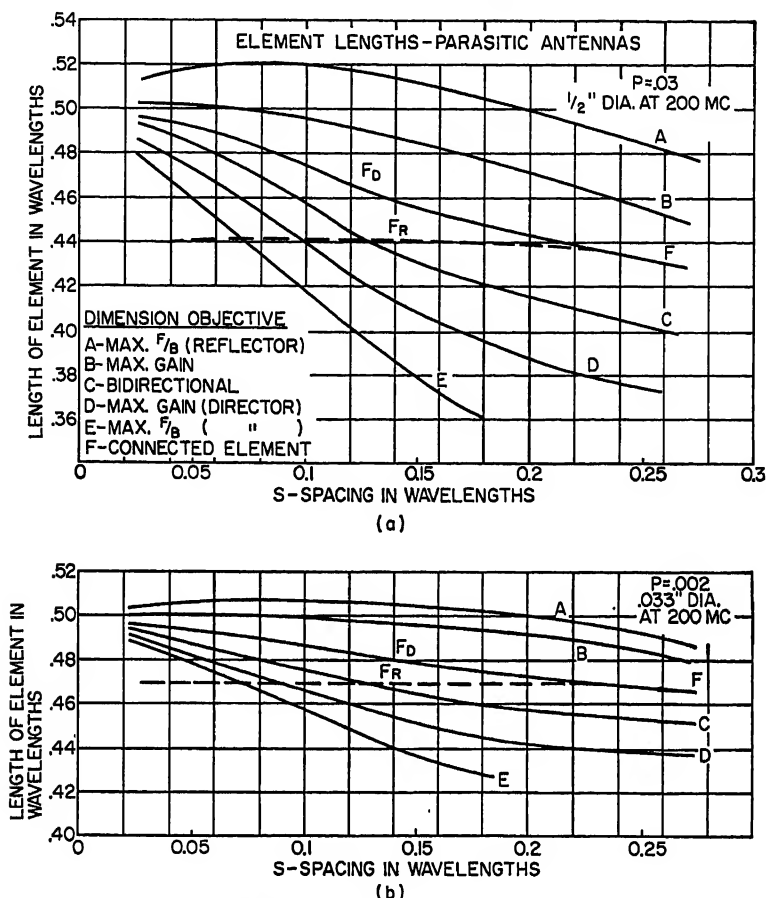
Fig. 5-6. Required parasitic lengths to meet objectives noted. Case A (upper), diameter = $\frac{1}{2}$ in., f = 200 Mc. Case B (lower), diameter = 0.033 in., f = 200 Mc. (Reference 4.)

A driven antenna together with a single parasite may be used advantageously in a variety of ways, depending on the ends to be accomplished. Representative results given in the text by Bailey already referred to are shown in Figs. 5-6 and 5-7. The lettered curves there shown refer to the various objectives as follows:

1. To obtain maximum front-to-back (F/B) ratio for a reflector-type parasitic
2. To obtain maximum gain for a reflector-type parasitic
3. To obtain equal gain in opposite directions (cf. Fig. 5-5a)

small and they seemingly violate a well-known rule of antenna arrays which says that directivity should be proportional to the width or aperture of the array. It is for this reason that they are said to be *superdirective*. Representative patterns appear in the lower left-hand corner of Fig. 5-2. Superdirectivity is not limited to the case of two antennas. It may be extended to almost any number of antennas with a corresponding increase in gain. Since the spacing is small, the dimensional aperture is likewise small. The limitations of such arrangements rest in their inherent low radiation resistance and the corresponding difficulties of feeding power into such sharply tuned arrangements, as well as into the medium outside.

4. To obtain maximum gain for a director-type parasitic

5. To obtain maximum front-to-back ratio using a director-type parasitic

In the above, top signal T in the ratio F/T refers to the signal received in a direction perpendicular to the plane of the two antennas. The quantity P is the periphery of the conductor measured in wavelengths; thus $P = 2\pi a/\lambda$, where a is the radius of the conductor. The two cases cited correspond to diameters of $\frac{1}{2}$ and 0.033 in. at 200 Mc. Curve F in Fig. 5-6 has two possible values, F_R or F_D, depending on whether it is associated with a reflector or with a director.
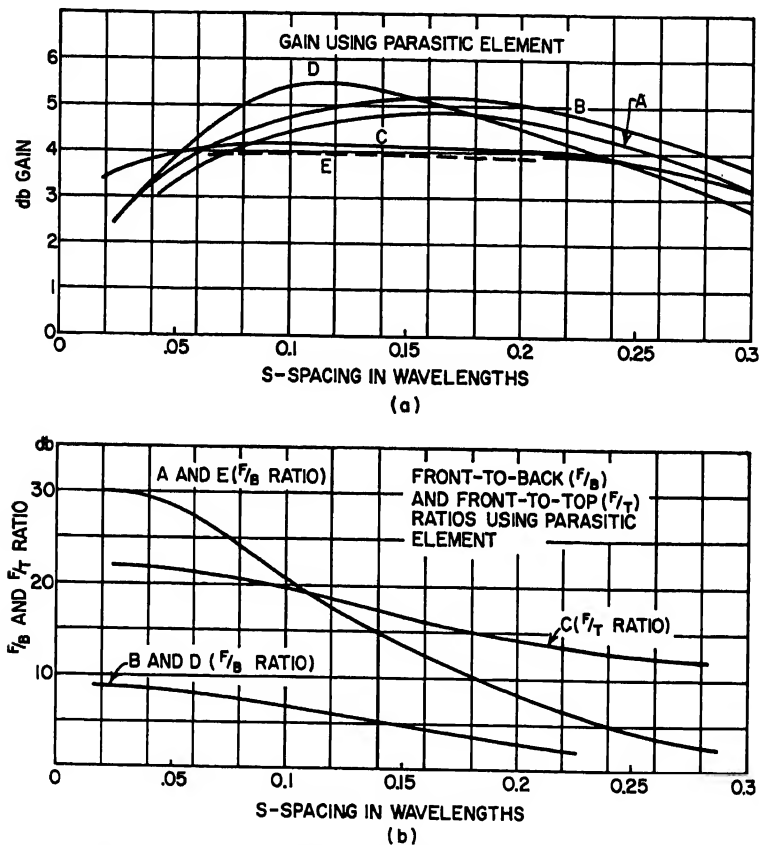
FIG. 5-7. Case A (upper): Expected gains (over a half-wave dipole) from parasitic antennas while meeting certain stated objectives. Case B (lower): performance ratios, F/B front-to-back and F/T front-to-top. (Reference 4.)

The combination of a driven antenna and a closely spaced parasite in which the respective currents are nearly equal but oppositely phased appears to the source as a high-Q load. Such a load is very unstable, for only at resonance is it a *pure resistance.* Slightly off frequency the resultant impedance may include a very substantial reactance component. Thus the bandwidth is limited. Bandwidths of 1 per cent and mid-band load resistances of 2.5 ohms are representative. The latter may be compared with 72 ohms as the mid-point feed resistances of a half-wave antenna at resonance. It may also be compared with an impedance of 300 ohms, which is the standard characteristic impedance of one of the

favored feed lines used in television-receiving-antenna practice. Thus the use of closely spaced antenna combinations of this kind presents serious impedance matching as well as bandwidth problems. To alleviate this difficulty wider spacings are often used. Often, too, the dipole to be fed is folded so that the coupling is made to the open ends, thereby affording a better approximation to the 300 ohms characteristic impedance of the line. The reduction in resistance of a radiator in the presence of a parasitic element is shown in Fig. 5–8.
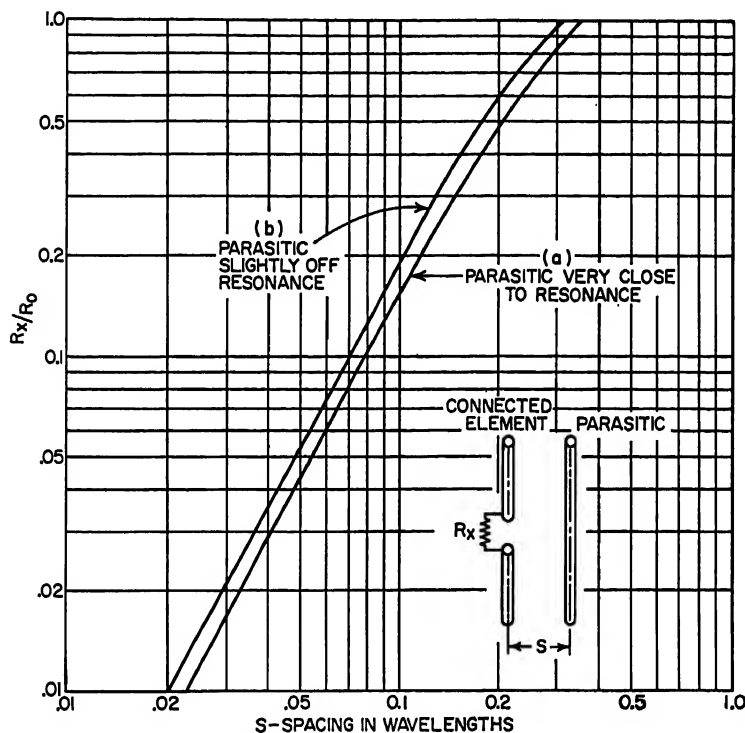
Fig. 5–8. Reduction in resistance of a radiator in the presence of a parasitic element. (Reference 4.)

5.4. MULTIELEMENT BROADSIDE ARRAYS

The arrangement of two antennas as shown in Figs. 5-2 and 5-3 may be regarded as the first step in forming a more highly directive antenna array. Arrangements in the same straight line of more than two elements become far more significant. An example is shown in Fig. 5-9, which gives the XY-plane patterns (often horizontal-plane) for the particular case of 16 elements. These patterns were calculated by the formula applying to this case:

$$r = \frac{\sin N\pi(A \sin \varphi \sin \theta + B)}{N \sin \pi(A \sin \varphi \sin \theta + B)} \tag{5-2}$$

where N is the number of individual elements in the linear array. If the above formula is to be applied to an array of dipoles and the YZ pattern is desired, it should be multiplied by $\sin \theta$. Equation (5-1) above is a particular case of this equation in which $N = 2$.
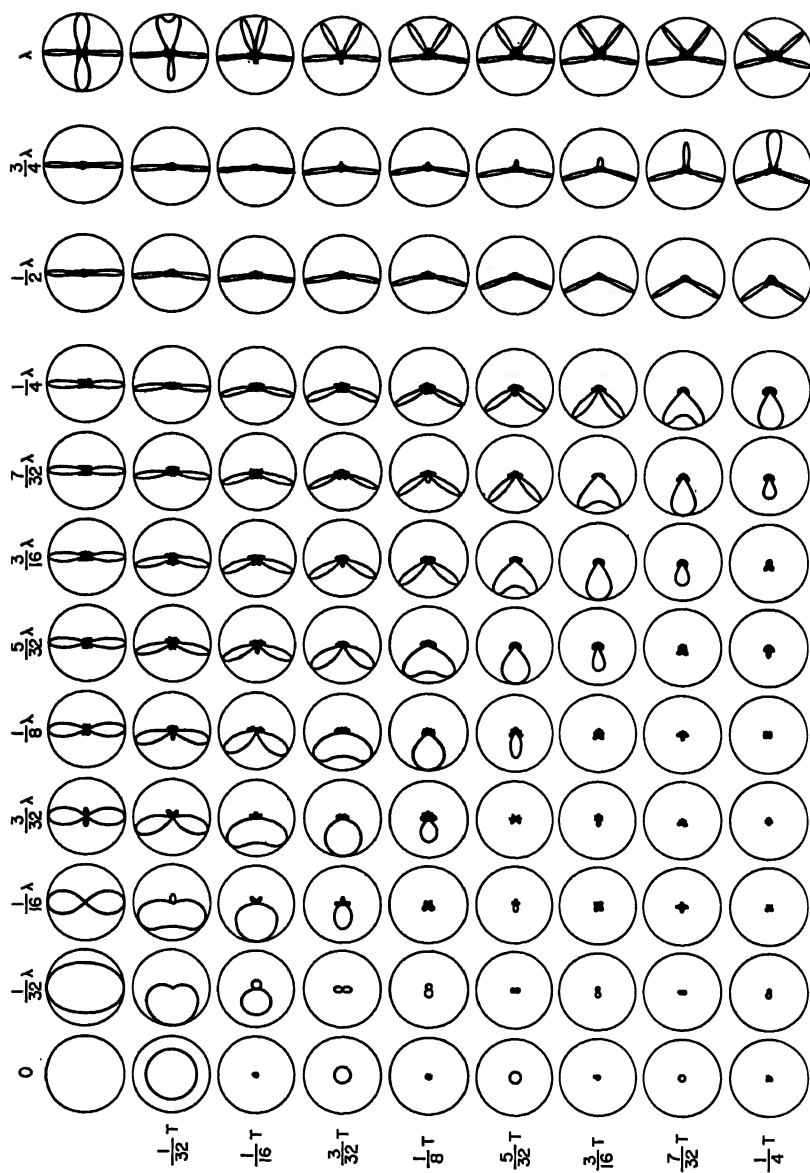
FIG. 5-9. Representative plots of Eq. (5-2) for particular case of 16 elements of equal amplitude, all for various spacings and phasings. Diagonal extending from 0, 0 to $\frac{1}{4}T$, $\frac{1}{4}\lambda$ corresponds to end-fire array. Top row corresponds to broadside arrays.

Of considerable interest is the series of patterns corresponding to the case where the space factor A and the phase factor B are numerically equal. An example is that corresponding to $\frac{1}{8}\lambda$ and $\frac{1}{8}T$. It is of interest that in this case sharpness increases with spacing simultaneously both in the XY and YZ planes. It is of interest also that though the illustration suggests that directive gain increases indefinitely, as A and B are simultaneously increased, there comes a limit, approaching $A = B = \frac{1}{2}$, not shown in the illustration, when the pattern becomes bidirectional. The arrangements above are known as end-fire arrays, and more will be said about them in Sec. 5.5. The practical engineer will probably regard most of the remaining patterns of Fig. 5-9 as being largely of academic interest, but naturally of help in establishing a proper sense of magnitudes.

Of particular interest to the case at hand is the top row of diagrams, which corresponds to a broadside array of elements. In this case all elements are driven in the same phase ($B = 0$). It is to be noted that like the corresponding case of two elements, the main oppositely lobed pattern increases with sharpness with spacing. However, as before, an optimum in gain is reached after which extraneous lobes become appreciable. In this case the limit occurs at a spacing somewhat greater than three-quarters wavelength.

Pattern and Side-lobe Considerations. Equation (5-2) when restricted to the case of equiphased elements ($B = 0$) defines the condition for broadside operation. Examination of this equation shows that whereas $r = 1$ when $\sin \varphi = 0$, assuming $\theta = \pi/2$, $r = 0$ when $\sin \varphi = 1/NA$, $2/NA$, $3/NA$, etc., and between these successive zeros, that is, where $\sin \varphi = 3/2NA$, $5/2NA$, etc., there are minor lobes of the kind shown in Fig. 5-9. The amplitude of the first and largest of these minor lobes is

$$r_1 = \left(N \sin \frac{3\pi}{2N} \right)^{-1} \tag{5-3}$$

For cases where N is fairly large, $r_1 \doteq 0.212$. This corresponds to about 13.5 db. Often this level is acceptable, but for certain purposes it may not be ignored. The zeros defined above are truly zero only if the magnitudes of the several currents are equal. Otherwise they are mere minima and the lobes between may be rather ill defined. Indeed, it is possible by an orderly arrangement of currents, referred to as tapering, to greatly reduce or even eliminate the amplitudes of minor lobes.

As already pointed out, the sharpness of a pattern increases with the spacing of the elements which make up the array, suggesting thereby that the total length of the array, *aperture*, is a very important dimension. This is indeed true. It is to be noted again, however, that with extremely wide spacings, extraneous lobes make further directive gain impossible. Calculated gains vs. spacing for specified numbers of elements are shown in Fig. 5-10. Certain feed-line problems to be discussed later often make it desirable to use spacings between adjacent elements of one-half wavelength. It will be noted that these latter spacings are well within the limits of safety. It seems very reasonable, however, that there may arise cases of practice where in the interests of simplicity it may be desirable to minimize the number of radiators for a given aperture, and in such cases it may be desirable to use spacings near the optimum.

Tapered Amplitudes. Of considerable importance in antenna practice is the principle of tapering already mentioned. This may assume a large variety of forms, but one especially significant is that in which the amplitudes of the individual radiators, in a linear array, vary in accordance with a cosine function beginning with a maximum at the center of the array and decreasing progressively to some finite value a at each end. It may be shown that where this special distribution is applied to an array in which N is large and A is relatively small with $\rho = NA$, then

$$r = a \frac{\sin (\pi\rho \cos \varphi)}{\pi\rho \cos \varphi} + (1 - a) \frac{\cos (\pi\rho \cos \varphi)}{1 - 4\rho^2 \cos^2 \varphi} \tag{5-4}$$

The significance of a will be evident from Fig. 5-11. This illustration in addition shows representative patterns plotted in rectangular coordinates for an array six wavelengths wide ($\rho = NA = 6$). Two examples are shown for comparison purposes: pattern b, the broadside case here under discussion, and pattern a, the end-fire case to be discussed later. It will be noted that reduction in minor lobes is at the expense of sharpness of pattern. In certain practical cases, power fed to an array is introduced
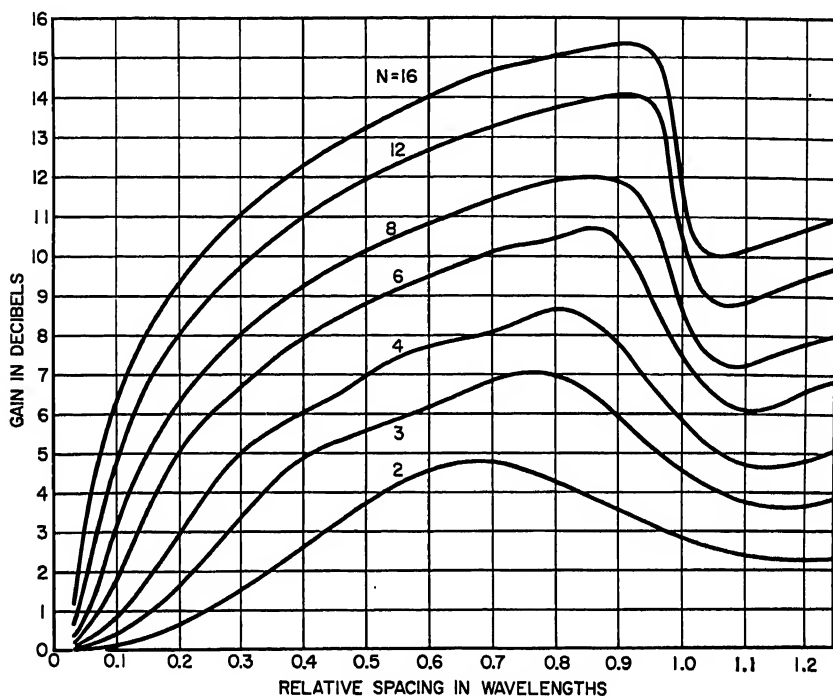

Fig. 5-10. Gains* to be expected from a single array (no reflector) of broadside elements.

at its center with equal portions flowing both to the right and left progressively from one element to the next. Because there is a loss in each element, there is a measure of tapering in their respective amplitudes, and hence a corresponding reduction in minor lobes.

Arrays of Couplets. Discussions in connection with Fig. 5-3 suggest that the bidirectional diagram typical of the single broadside array may be rectified by replacing it by an array of couplets. This is equivalent to erecting one-fourth wavelength to the rear of the array, a second identical array to be driven by identical currents lagging in phase by a quarter period. Typical XY-plane patterns for arrays of couplets differing in number of elements and their spacings are shown in Fig. 5-12. Since sharpness increases, both with numbers of elements and their spacings, we again see that the total width of the array (aperture) is an important dimension in establishing directive gain. The gain* to be expected from arrays of end-fire couplets may be obtained from Fig. 5-10 by adding 3 db to the values there given. For many practical cases this follows the relation

$$g = 5.4 \frac{\ell}{\lambda} \tag{5-5}$$

* Note that the gain is relative to that of a single element.

$$\text{REL. AMP.} = a\frac{\sin \pi (\rho\cos\theta+\beta)}{\pi(\rho\cos\theta+\beta)} + (1-a)\frac{\cos \pi (\rho\cos\theta+\beta)}{1-4(\rho\cos\theta+\beta)^2}$$
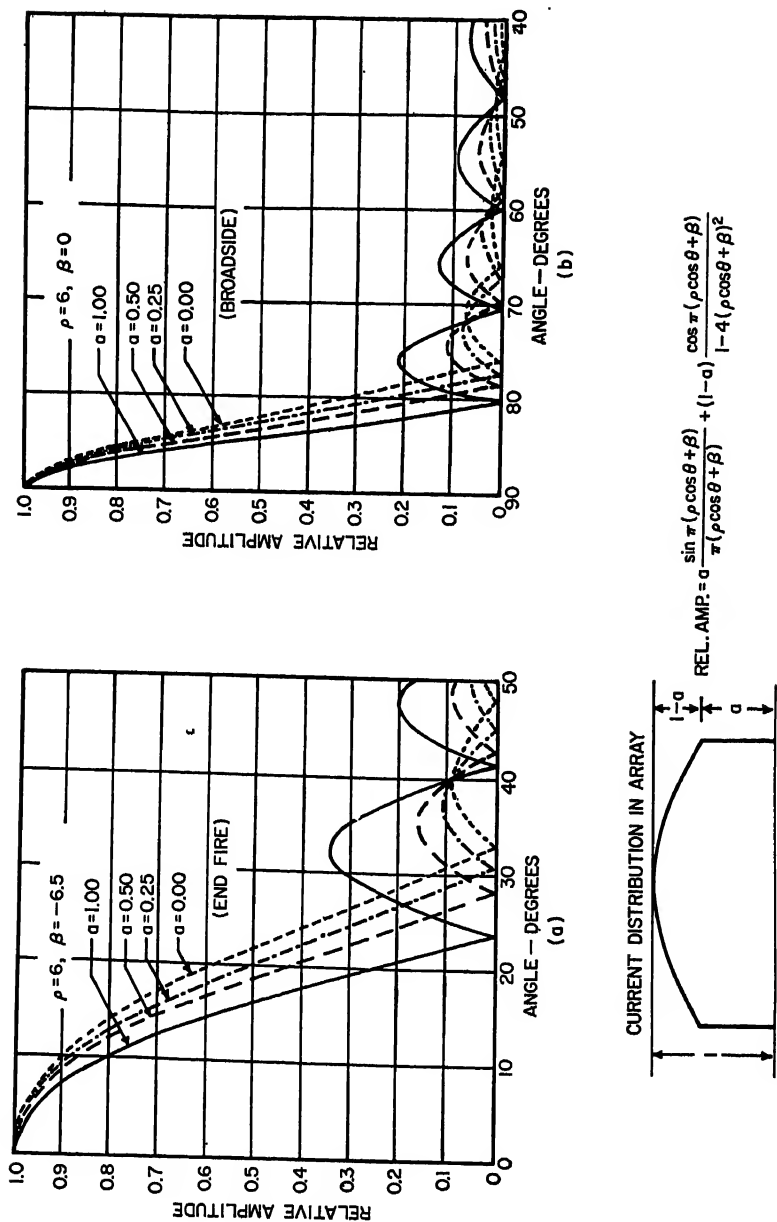
FIG. 5-11. Effect of tapering on patterns of a linear array of radiating elements: (*a*) End-fire array. (*b*) Broadside array.

FIG. 5-12. Representative patterns from arrays of end-fire couplets.
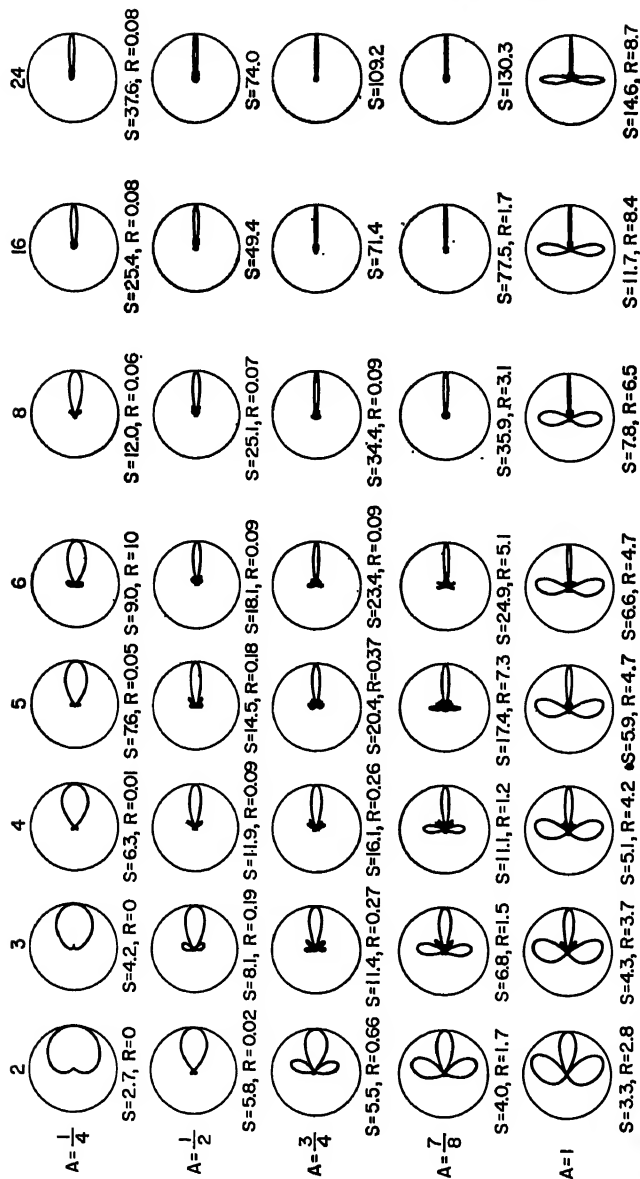
NOTES

S = RATIO OF AREA OF UNIT CIRCLES TO THAT OF DIRECTIONAL DIAGRAM

R = RATIO OF AREA OF SUBORDINATE LOOPS TO THAT OF MAIN LOOP

A = FRACTION OF WAVELENGTH SPACING BETWEEN ELEMENTS IN SAME COLUMN

EQUATION OF DIAGRAM

$$r = \frac{\sin(N\pi A\sin\phi)}{N\sin(\pi A\sin\phi)} \cdot \cos\frac{\pi}{4}(\cos\phi - 1)$$

ARRANGEMENT OF ARRAY

DIRECTION OF TRANSMISSION

Arrays of Arrays. It often happens in practice that it is desirable to place in array individual radiators each having a substantial measure of directivity. Each radiator, for example, may be a horn, or perhaps another rudimentary array such as a Yagi-Uda antenna. Since each directive radiator may be approximated by an array of elements, it is convenient to regard the whole as an array of arrays. To exemplify the limitations as well as the advantages of such a procedure, we shall cite two typical cases.

It may be shown that when a number of identical arrays are placed in array, the resultant pattern is given by the product of an array factor r characteristic of the directional pattern of each individual array times other factors representing the relative position and phase of the individual array in the array of arrays. For the simple case of arrays along the Y axis, the equation takes the form

$$R = r \frac{\sin N'\pi(A' \sin \varphi + B')}{N' \sin \pi(A' \sin \varphi + B')} \tag{5-6}$$

where A' is spacing between centers of individual arrays, B' is the relative phase, and r is the factor representing the pattern of each individual array.

d=0
R=0.174

d=λ
R=0.462

d=2λ
R=1.00

d=3λ
R=1.304

ARRANGEMENT
OF ARRAYS

· EQUATION OF SPACED ARRAY

$$r = \frac{\sin(3\pi \sin\phi)}{6 \sin(\pi/2 \sin\phi)} \cos \pi/4 (\cos\phi - 1) \cos\left[(3+d)\pi \sin\phi\right]$$

NOTES

R — RATIO OF AREA OF SUBORDINATE
LOOPS TO THAT OF MAIN LOOP

d — SEPARATION BETWEEN TWO
SIMILAR ARRAYS

A — FRACTION OF WAVELENGTH
SPACING BETWEEN ELEMENTS
IN SAME COLUMN
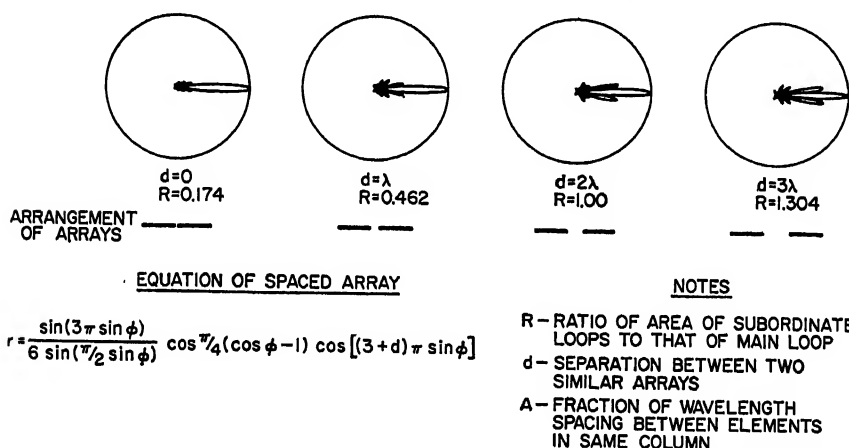
FIG. 5-13. Directional diagrams in horizontal plane of two equiphased arrays spaced laterally as noted ($N = 6$ and $A = \frac{1}{2}$).

In the first of the two cases cited, we shall assume two adjacent arrays, each consisting of six unidirectional couplets, as shown in Fig. 5-13. The change in resulting pattern as the spacing between adjacent ends of the two arrays is increased from $d = 0$ to $d = 3\lambda$ is obvious. Spacings of this kind may, for example, result from the introduction of a supporting tower between two bays of a single array. Another representative problem arises below in Sec. 5.6 on arrays of Yagi-Uda antennas.

As a second example we show in Fig. 5-14 a configuration made up of eight arrays of two couplets each. In this case we keep the spacings A' constant but vary the relative phase B' between adjacent groups of couplets. The pattern of one of the unit arrays is shown dotted. The resultant pattern is shown solid. It is to be noted that as the phase constant varies from $B' = -\sin 25°$ to $B' = 0$ to $B' = +\sin 25°$, the principal pattern rotates in space, always staying within the confines of the pattern of the unit array. Representative methods of introducing phase are described elsewhere.

Stacked Antennas. The discussion thus far has centered around the horizontal pattern of the array where the respective axes of the various elements are perpendicu-

lar to the line of array.   It is of course possible to array antennas with their respective axes coaxial with the line of array.   The equation for this case is

$$r = \frac{\sin (n\pi a \cos \theta)}{n \sin (\pi a \cos \theta)} \sin \theta \qquad (5\text{-}7)$$

The corresponding pattern for such a coaxial array differs from the case already discussed only in minor respects.   Thus there are in addition to the major lobe the usual number of minor lobes.   Like the previous case, the pattern is perpendicular to the line of elements, but in this case it is symmetrical with respect to the principal axis.   Such an arrangement is sometimes referred to as the *broadcast*, or *omnidirectional*, type.   Sometimes such arrangements are referred to as *stacked antennas*. Their characteristics will be discussed more fully in Sec. 5.7 below.

$$\frac{\sin 8\pi (\sin\phi + B')}{8\sin\pi(2\sin\phi + B')} \cdot \frac{\sin(\pi\sin\phi)}{2\sin(\frac{\pi}{2}\sin\phi)} \cos \frac{\pi}{4}(1-\cos\phi)$$
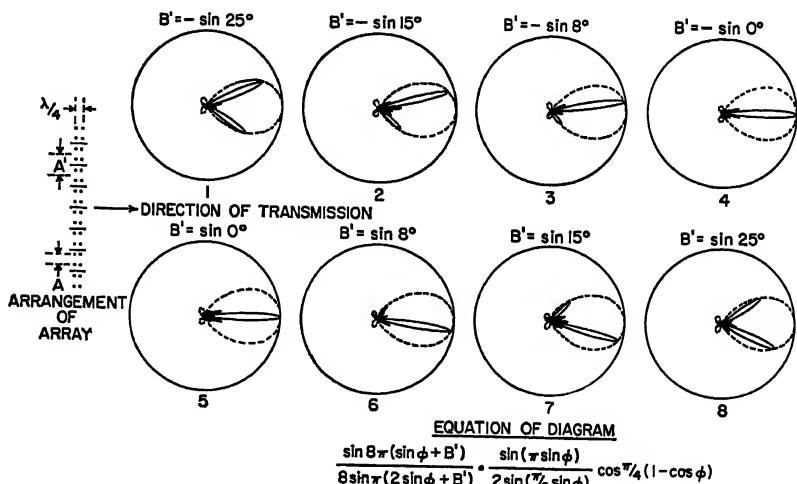
FIG. 5-14. Illustrating how the directional pattern of an array of elemental arrays may be rotated in space by changing the phase between individual sections.

Curtains of Antennas.   It is obvious that arrays of coaxial antennas each of the kind just described may be arrayed along the Y axis to form a two-dimensional array. This provides a simultaneous directivity both in the XZ and XY planes.   The two-dimensional patterns so formed are specified approximately by the product of Eqs. (5-2) and (5-7).   Since the array of elements is a single plane, the resultant pattern is bidirectional, with its principal axis perpendicular to the plane of the array.   Antennas of this kind are frequently suspended from catenaries supported by towers.   For this reason they are sometimes referred to as *curtains of antennas*.   Also, since the currents flowing in the several antennas of the array are equal in magnitude and are in the same phase, it is easy to see that if spacings are not too great, the whole is roughly equivalent to a *uniform current sheet*.   The latter is a term that appears frequently in antenna theory.

From what has been said in connection with Fig. 5-3, it is obvious that the bidirectional feature of the single-curtain broadside array may be corrected by erecting at a quarter wave to the rear of the array another identical array (reflector) driven with a phase leading by a quarter period.   This combination may be regarded as a two-dimensional array of unidirectional couplets.   Two-curtain arrays have been used extensively in overseas telephone and telegraph services at frequencies of the order of 20 Mc.   The method is, however, often used at frequencies up to 1,000 Mc or even

more. At the lower frequencies the reflector curtain is often fed in a manner similar to that of the main array, but in some instances, particularly with large arrays, the reflector may derive its power parasitically. At the highest frequencies at which arrays are used, the reflector is invariably fed parasitically, and it usually takes the form of a mesh screen or simply a sheet of metal. Closely meshed reflectors may be expected to be efficient provided the dimensions of the interstices are small compared with the wavelength and the over-all area is as large as or larger than the corresponding driven curtain.

Quantitative Considerations. Textbooks on antennas show that certain approximations may be made in the equation for the directive pattern that permit the radiated power to be integrated over a sphere surrounding the antenna. This makes possible an expression for power input P in order to produce at a given distance a signal of specified level. Such an equation was derived many years ago. (Ref. 7, Appendix). Further simplifications, warranted only in the case of a fairly large number of couplets, permit a formula of the form

$$P = K \frac{\lambda^2}{ab} \tag{5-8}$$

where a and b are now the over-all dimensions of the array, and λ is the wavelength. If we wish to compare this with the power P' necessary to produce the same signal from a nondirective or isotropic source, the comparison must be made with

$$P' = K \iint d\Omega = K4\pi \tag{5-9}$$

The corresponding gain of a short dipole is $g' = \frac{3}{2}$, and for a half-wave antenna it is 1.64. The gain of the current sheet measured relative to an isotropic source is accordingly

$$g = \frac{P'}{P} = \frac{4\pi ab}{\lambda^2} = \frac{4\pi S}{\lambda^2} \tag{5-10}$$

where S is the area of the antenna. Gains measured relative to an isotropic radiator are referred to as *absolute gains*. If we wish to specify the gain of an array relative to a single half-wave antenna, Eq. (5-10) should accordingly be divided by the factor 1.64. If it is to be measured relative to a short dipole, the factor is $\frac{3}{2}$.

Equation (5-10), when applied to measured gains, defines a quantity of S, known as the *effective area* of a directive device. In most devices, as for example horns and parabolas, the effective area is somewhat less than the dimensional area. In other devices, as for example a broadside array of couplets, it may be slightly larger.* In still other devices, as for example a single radiating doublet or possibly the end-fire array, to be discussed presently, the difference may be very large indeed. In the receiving case we interpret this to mean that such a device is able to reach out for a considerable distance to bring in passing wave power.

In applying the above formula to a broadside array of couplets, each made up of half-wave antennas spaced laterally at intervals of one-half wavelength and spaced vertically one-half wavelength between centers, we may, with sufficient accuracy, call the effective area $Nn\lambda^2/4$. Thus the effective height is regarded equal to the dimensional height and the effective width is larger than the dimensional width by

---

* Though the reciprocal relationships between transmitting and receiving antennas are easily accepted, there would seem to be a special significance to the effective area of a broadside receiving array as compared with its counterpart among transmitting antennas. More particularly, it is especially easy to see that the received power from an advancing plane wavefront is greater when intercepted by a large broadside array than when intercepted by a small broadside array. It is not quite so easy to see that at the transmitter more power will be directed toward a distant receiver by a large antenna than by a small antenna. Reciprocity shows that the latter must be true.

the quantity $\lambda/2$. It is a convenient rule to say that the absolute gain of an array is about 12.5 per square wavelength. If the gain is to be measured relative to a half-wave antenna, the corresponding gain is about 7.6 per square wavelength.

5.5. END-FIRE ARRAYS

Upon referring to Fig. 5-9, one observes a series of sensibly unidirectional patterns which lie along a diagonal corresponding to the spacing factor a equaling numerically the phasing factor b. Somewhat attractive also is the diagonal that lies immediately below. Since the direction of optimum signal lies parallel to the line of antennas, this arrangement is often referred to as *end fire*. It is to be noted that as the spacing is increased, thereby increasing the total length of the array, the corresponding XY-plane patterns (often horizontal) become progressively sharper. It is of special

(a)   (b)
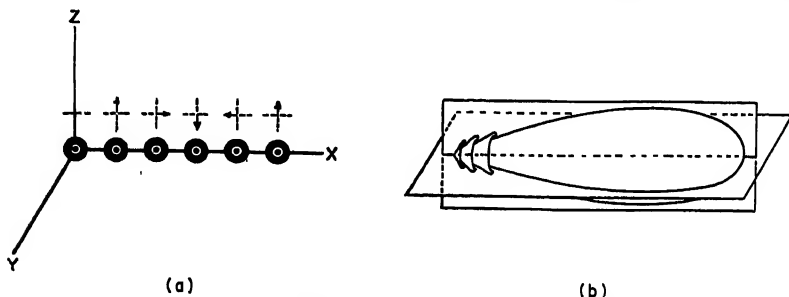
Fig. 5-15. (a) Schematic representation of an end-fire array of isotropic sources. (b) Typical directional pattern.

interest that this increase in sharpness occurs also in the XZ plane (vertical). All this occurs with a single line of antennas. No reflector is required. These seeming advantages notwithstanding, end-fire arrays have certain limitations, particularly when high gains are desired. The equation for the polar diagram for an end-fire array of isotropic sources aligned along the X axis is

$$r = \frac{\sin n\pi a(\cos \varphi \sin \theta - 1)}{n \sin \pi a(\cos \varphi \sin \theta - 1)} \qquad \frac{\pi}{2} > \varphi > -\frac{\pi}{2}$$
$$r = \frac{\sin n\pi a(\cos \varphi \sin \theta + 1)}{n \sin \pi a(\cos \varphi \sin \theta + 1)} \qquad \frac{\pi}{2} < \varphi < \frac{3}{2}\pi \qquad (5\text{-}11)$$

For short dipoles the above equations should be multiplied by $\sin \theta$. Like Eq. (5-2), which referred specifically to the broadside pattern, Eq. (5-11) specifies a main lobe together with various minor lobes. A schematic end-fire array and its corresponding two-dimensional pattern are shown in Fig. 5-15. In an end-fire array where the spacing factor is numerically equal to the phasing factor, it is possible to interpret the behavior in terms of a wave that sweeps progressively along the array. End-fire arrays, like broadside arrays, are of interest not only for the particular structures which they represent, but because they afford a good explanation for the behavior of certain other antennas quite different in structure.

Continuous End-fire Arrays. More light on the behavior of end-fire arrays can be had from a slightly different approach. In this, we assume that the number n of elements becomes large as a and b each become very small. At the same time, we assume that $\rho = na$ represents the total length of the array measured in wavelengths and $\beta = nb$ represents the total over-all phase delay between the two ends. For the end-fire condition, $\beta + \rho$ approximates zero, but somewhat improved results may be

obtained from departing from this relationship. In general,

$$r = \frac{\sin \pi(\rho \cos \varphi \sin \theta + \beta)}{\pi(\rho \cos \varphi \sin \theta + \beta)} \tag{5-12}$$

represents the equation corresponding to an infinite number of infinitesimally spaced sources phased as specified above. This arrangement is referred to as a *continuous end-fire array.* If we measure θ relative to the axis of the line of radiators and bear in mind that the radiators are here assumed to be symmetrical, then

$$r = \frac{\sin \pi(\rho \cos \theta + \beta)}{\pi(\rho \cos \theta + \beta)} \tag{5-13}$$

In Fig. 5-16 are illustrated directional patterns for varying values of phase differences corresponding both to end-fire and to broadside arrays each six wavelengths long. An
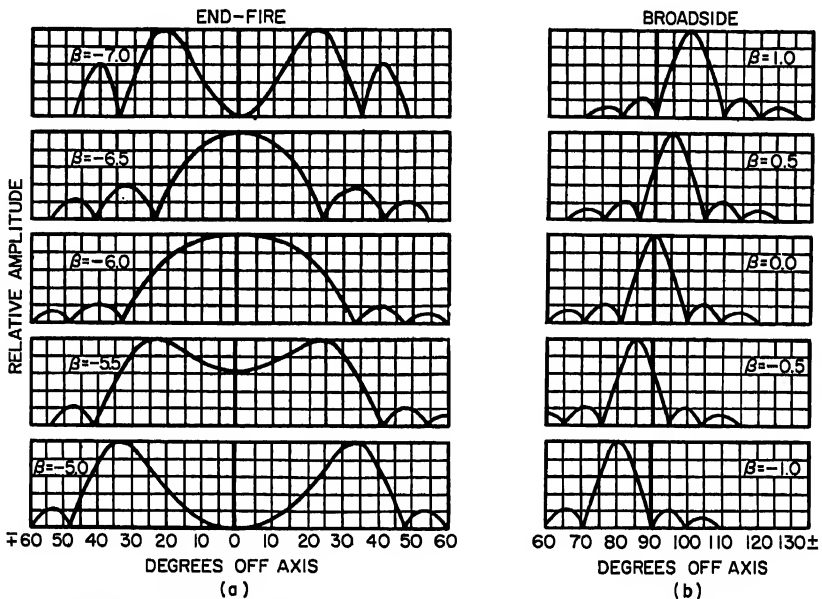
FIG. 5-16. Effect of phase velocity on the directional characteristics of continuous arrays.

inspection of Fig. 5-16a shows that the pattern for the case $\beta = -6.5$ is somewhat sharper than that for $\beta = -6.0$, suggesting that the gain is somewhat greater when the quantity $-(\beta + \rho)$ is about 0.5. It will be observed that the case where $\beta = 0$ corresponds to broadside operation is discussed in Sec. 5.4. An inspection of Fig. 5-16b, which represents the broadside case, shows a rotation of the beam with phase difference, as already suggested by Fig. 5-14.

The gain of an end-fire array of isotropic elements has been calculated. For the particular case in which $\beta + \rho = 0$, $g = 4\rho$. For cases in which $\beta + \rho \neq 0$, the gain (relative to an isotropic radiator) can be written

$$g = 4A\rho \tag{5-14}$$

where the factor A may be read from the calculated graphs shown in Fig. 5-17. It is evident from the graphs that the gain is optimum when the quantity $-(\beta + \rho)$ is a number slightly less than 0.5. This may be interpreted to mean that for best gain,

the phase lag between the two ends of the end-fire array should be roughly one-half period. As already suggested, it is sometimes simpler to interpret β in terms of a wave traveling along the array with a velocity v_z, such that $-\beta = \rho(v/v_z)$, where v is the velocity in free space. The electrical length of the antenna measured in terms of the velocity along the antenna will then be one-half wave greater than that measured in free space. For the particular case cited above ($\rho = 6$, $-\beta = 6.5$), v_z is about 92.3 per cent of v. It is evident that in an end-fire array, the effective area is very much larger than the actual area. This suggests that, as a part of the receiving process, wave power is fed in from the sides as well as at the end of the array. It is not difficult to see that a velocity of propagation within the array that is somewhat less than that without could aid in this receiving process. It follows, from Eq. (5-14), that the optimum gain of this particular uniform end-fire array is about 7.5 times its length measured in wavelengths. It is evident that if substantial gains were needed, perhaps 30 db ($g = 1,000$), the length of the array would need to be about 133 wavelengths. For many cases of practice this might seem large. Perhaps more attractive from the engineer's point of view would be a broadside array, possibly nine wavelengths on a side.

FIG. 5-17. Relation between factors A and $\beta + \rho$ in an end-fire array [see Eq. (5-14)].

It has been pointed out that uniform end-fire arrays, like their counterpart broadside arrays, have minor lobes. Also like their broadside counterparts, these minor lobes may be reduced by judicial tapering of the currents in the individual elements. Figure 5-11 above shows the effect of tapering in end-fire arrays as compared with the corresponding case of broadside arrays. It is evident that here, as in the broadside case, reduction in minor lobes comes at the expense of a broadening of the principal beam.

Fishbone Antennas. Two structures known generally as the fishbone and comb antennas have been devised by H. O. Peterson of the Radio Corporation of America. As regards dissipation, these adaptations are relatively inefficient compared with the ordinary broadside array; they are nevertheless very effective as receiving antennas in discriminating against noise. Also, they function well over a band of frequencies, differing by as much as 2:1. Because of their inefficiency, they are seldom, if ever, used at transmitting stations. Thus far their use even for receiving has been rather limited, and for the most part this use has been confined to frequencies between 10 and 20 Mc.

The fishbone antenna (Fig. 5-18) consists essentially of a two-wire transmission line, perhaps four wavelengths long, to which are attached at closely spaced intervals horizontally disposed lateral wires each of the order of a quarter wave in length. Often these wires are coupled to the transmission line by small capacitances, as shown schematically in Fig. 5-18. The proportioning gives rise to a wave propagated along the structure with a velocity v_z, which is about 90 per cent of that in free space. This, it will be noted, is one of the features of an end-fire antenna. In a modification of the fishbone antenna used currently in England, the wires are made one-half wavelength and the capacitances are eliminated. This leads to a velocity of propagation approaching that of light in free space and to a much restricted bandwidth.

One physical picture of the behavior of the fishbone antenna as a receiver depicts power from the advancing wavefront picked up by the individual wires and fed

progressively to the transmission line as wave power along the latter moves onward. By this means, wave power advancing from the right is impressed on the receiver at the left to produce a usable signal, while wave power, perhaps in the form of noise,

FIG. 5-18. The fishbone receiving antenna.

advancing from the left, is dissipated in the termination z_0 at the right. Good front-to-back ratios therefore depend on the extent to which the line may be perfectly terminated. In the transmitting case, it is easy to conceive of each radiating wire as being a discrete source and the whole as an end-fire array of sources of the kind already discussed.

The gain relative to an isotropic radiator of a fishbone antenna of length ℓ is given approximately by [10]

$$g = 4\rho A B \qquad (5\text{-}15)$$

where the factor A is identical with that shown in Fig. 5-17, and B is read from the graph of Fig. 5-19. In this case ρ is the length of the antenna measured in wavelengths, and β is the total phase delay between its two ends measured in complete periods. Thus $\rho = \ell/\lambda$, and $\beta = -\ell/\lambda'$. For long antennas, B is roughly unity and Eqs. (5-14) and (5-15) are essentially equivalent. The horizontal-plane pattern of a fishbone antenna is given by

$$r = \frac{\sin\,[\varphi'/2 + \pi\rho(1 - \cos\theta)]}{\varphi'/2 + \pi\rho(1 - \cos\theta)} \qquad (5\text{-}16)$$

where $\varphi' = 2\pi(\rho + \beta)$.

The Comb Antenna. The comb antenna is essentially one-half of a fishbone antenna set up on edge above a suitable ground mat so as to receive vertically polarized waves. Since antennas of this general class have been used mainly for reception and since

FIG. 5-19. Relation between the factor B in Eq. (5-15) and the length measured in wavelengths of a fishbone antenna.

noise, particularly from local sources, is generally greater when signals are received on vertical antennas than when received on horizontal antennas, the comb type has thus far found little practical use.

5.6. END-FIRE PARASITIC ARRAYS (YAGI-UDA ARRAYS)

The combination of a single driven antenna and a closely coupled parasitic which may function either as a reflector or as a director, as was discussed in Sec. 5.3, strongly suggests an array of such elements. Such structures are not only feasible, but they have a rather important place in antenna practice, particularly in the frequency range between 100 and 1,000 Mc. Arrays of this kind were first described in Japanese by S. Uda,[12] professor at the Tohoku Imperial University in Japan. Subsequently, it was described in English by one of his colleagues, H. Yagi.[13]* This type of directional antenna is an interesting example of compactness accomplished at the expense of bandwidth. It therefore possesses a measure of the superdirectivity referred to in Sec. 5.3 above. This antenna also has many of the characteristics of the end-fire array described in Sec. 5.5. For example, one may identify in such an array a wave propagated parasitically from one element to the next with an effective velocity that is somewhat less than the velocity characteristic of free space.
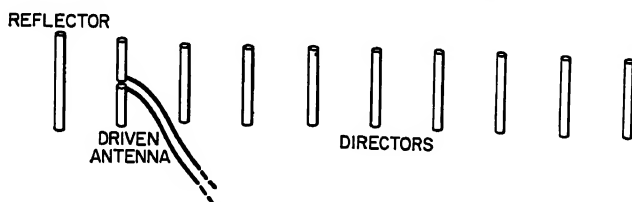
FIG. 5-20. Schematic arrangement of the Yagi-Uda array.

In practical Yagi-Uda arrays, experiment shows that little is gained by adding to the driven antenna more than one reflector but considerable gain results from adding numerous directors. However, since each director receives its power parasitically from the next preceding director and each in its turn radiates a portion of its power, the respective currents are progressively less as we proceed along the array and there is a measure of tapering. Also, there is a practical limit to the total number of elements. Though arrays of thirty or forty elements have been built, the practical engineer will probably stop at a dozen or even less. A total antenna length of 6λ has been mentioned as a reasonable limit.[14] Figure 5-20 shows in schematic form a Yagi-Uda array consisting of a driven antenna together with a reflector and eight directors. The gain factor to be expected from such an antenna ranges from 5 to 9 per unit length, where in this case the gain is measured relative to an isotropic source and the unit of length is one wavelength.

The lengths of the reflector and the various directors, as well as their respective spacings, are for the most part compromises with such factors as gain, input impedance, front-to-back ratio, magnitude of minor lobes, and bandwidth. Though a theory[3] has been developed applicable to the case of a very few elements, best proportioning for most practical cases depends on experiment. Representative data taken largely from experiments by Fishenden and Wiblin are given below.[14] The progressive reduction in current amplitudes mentioned above implies tapering. Ordinarily this would tend to reduce minor lobes, but the desire for optimum gain from a given

---

* It is of interest that the Yagi paper[13] described the short-wave work then in progress in Japan and made Professor Uda's work but one of its several features. However, because Yagi's paper was in English and was widely read, it became the custom to refer to this new array as the Yagi antenna. This occurred in spite of the fact that Yagi was quite clear about the part that had been played by Professor Uda. In view of accepted practices, it should be in order to adopt the name Yagi-Uda antenna. We understand that this is also the desire of Mr. Yagi.

structure encourages the engineer to increase the over-all length of the array, and hence its individual spacings. This has the effect of increasing minor lobes. Spacings ranging from 0.15λ to 0.30λ, or even 0.40λ, are representative. This is in contrast with the spacing of 0.04λ mentioned in connection with Fig. 5-5. In the region of wider spacings, front-to-back ratios of perhaps 30 (15 db) may sometimes obtain, though front-to-back ratio is sometimes sacrificed for other desirable features.

The authors mentioned above obtained gains from Yagi-Uda antennas as shown in Table 5-1. In this case, the director spacing was 0.34λ. The director length conformed in a general way with the data given in Table 5-2. In this case, the lengths were chosen to provide side-lobe ratios of 30 per cent or less. The reflector was one-half-wave long and was spaced one-fourth wave to the rear of the driven element.

Table 5-1. Representative Gains of Yagi-Uda Arrays

Number of directors	Beamwidth,* deg	Power gain over half-wave element	Gain per element
30	22		
20	26	21	0.95
13	31	15	1.00
9	37	13	1.18
4	46	8	1.33

* Beamwidth in this case is measured relative to 6-db points on the directive pattern.

Table 5-2. Variation of Optimum Director Length with Number of Directors

(Periphery $P = 2\pi r = 0.019\lambda$)

Number of directors	Director length, λ
42	0.385
30	0.40
20	0.407
13	0.414
10	0.42
7	0.423
5	0.434

It has already been suggested that one of the limitations of the Yagi-Uda array is its low input impedance and its relatively narrow bandwidth. Both of these quantities may be compromised against other factors to moderate the difficulty. Representative input impedances as measured at the center of the driven antenna are given in Table 5-3. In all cases the length of the driven antenna was adjusted to provide a nonreactive load at the mid-band frequency. Bandwidths of 2 per cent are representative.

Figure 5-21 shows three horizontal patterns corresponding to three possible director lengths. It will be noted that the pattern is rather critical as regards director length, and arrangements that provide a favorable forward pattern may lead to unfavorable front-to-back ratios.

Arrays of Yagi-Uda Arrays. Since the gain from a single Yagi-Uda array is often limited by length to about 30 (15 db), arrays of such arrays are suggested as a means of providing further gain. Ideally two such arrays should provide a total gain of 18 db and four arrays should provide 21 db. However, numerous difficulties lie in the way of obtaining these high directivities. In arraying antennas the following two objectives may need to be considered.

Table 5-3. Input Impedance of a 13-director Antenna
(Reflector length 0.5λ, director spacing 0.34λ)

Reflector spacings, λ	Director length	
	Spacing 0.406λ, ohms	Spacing 0.42λ, ohms
0.25	62	50
0.18	50	43
0.15	32	27
0.13	22	
0.10	12	
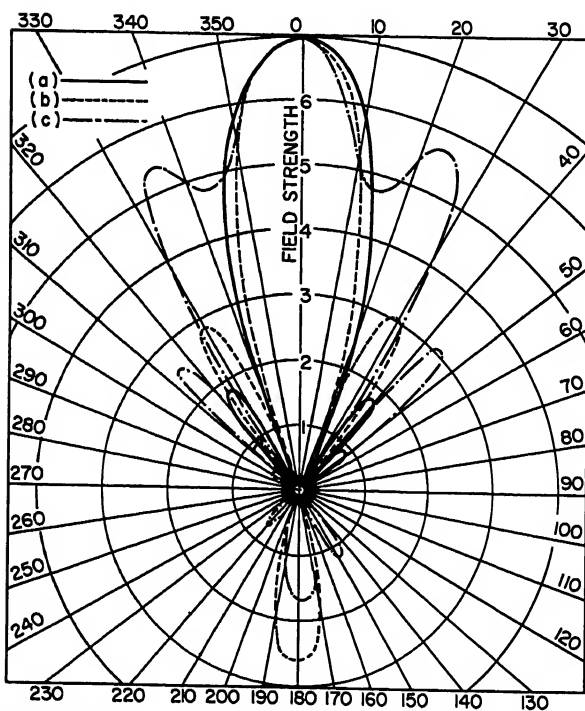
FIG. 5-21. Horizontal polar diagrams of a 13-director Yagi-Uda array.   (Reference 14.)

Small Side Lobes May Be Desired.   In this case the first minimum incidental to the interunit spacing should preferably be arranged to coincide with the first side-lobe maximum of a single array.

A Narrow Beam May Be Desired.   In this case the first interference minimum is made to lie immediately inside the main lobe, but not so far inside as to give rise to a substantial minor lobe.   The reader is referred to Figs. 5-3 to 5-6 as an aid in fixing ideas.

In arraying Yagi-Uda antennas, the engineer may in the interests of compactness prefer to accept a total gain of perhaps 15 db and obtain the same by means of an

array of Yagi-Uda antennas, each of perhaps 10 db.   One possibility is an arrangement discussed by Fishenden and Wiblin.[14]

5.7. OMNIDIRECTIONAL COLLINEAR ANTENNAS

As has already been pointed out, it is entirely feasible to array linear antennas coaxially.   Such an array provides a directional pattern which, when viewed in any plane through the major axis, closely resembles that of the simple broadside array already discussed.   However, such a pattern has circular symmetry, and accordingly it is said to be *broadcast*, or *omnidirectional*.   As already suggested, the several elements may in the general case be spaced or phased in an infinite number of possible ways.   In the case of short-dipole elements fed in phase, the polar diagram is specified by Eq. (5-7).   This also gives with moderately good accuracy the diagram for a collinear array of equiphased half-wave elements.*
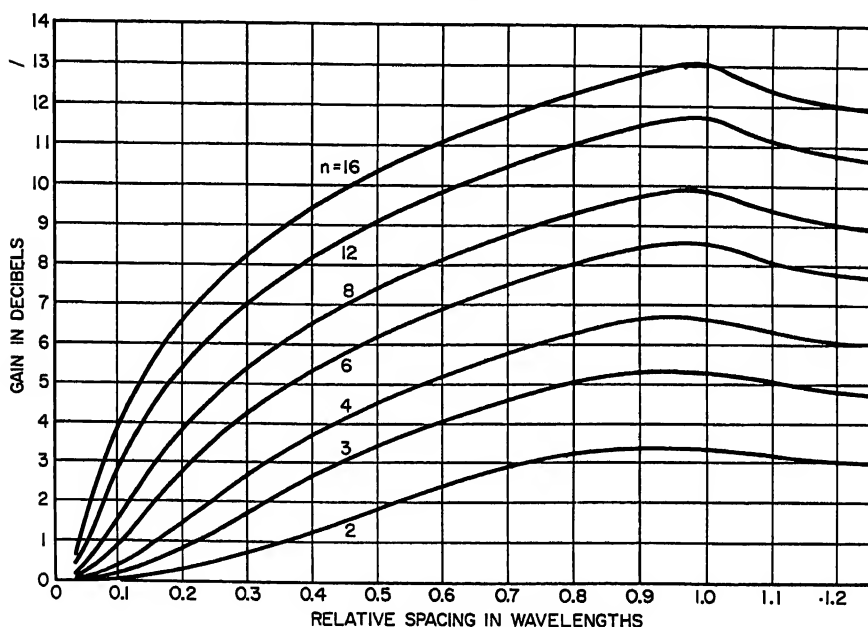
FIG. 5-22. Gains to be expected from a collinear (omnidirectional) array of short-dipole elements.   The gain is relative to that of a single element.

In many practical cases the spacing is fixed by the physical arrangement of antennas at about one-half wavelength, but in others it is made greater than one-half wavelength.   As already pointed out, Eq. (5-7) has a maximum of unity when $\theta = \pi/2$.   This corresponds to the major lobe of the pattern.   Also, there are minor lobes with minima between, very similar to those discussed in connection with Fig. 5-9.   The corresponding patterns are also similar to those shown in the top row of Fig. 5-9, their differences being so small as to hardly justify additional illustrations.

As in the previous cases, the total length (aperture) of the collinear array is an important dimension in determining gain.   For a given aperture, the spacing between elements is relatively unimportant provided minor lobes do not become appreciable.

* It also gives with good accuracy the pattern for an array of small-loop antennas each with its plane perpendicular to the axis of the array.

Figure 5-22 shows how the gain expected from a collinear array of antennas varies with spacing. Though applicable specifically only to short antennas or to small loops, these data are applicable with reasonable accuracy to half-wave antennas as well. Comparing Fig. 5-22 with Fig. 5-10, it will be noted that arrays of collinear antennas permit of somewhat wider spacings than do the corresponding arrays of transverse elements.

For a number of applications, the element spacing of the array is sometimes made greater than one-half wavelength. This is done in the interests of saving fittings and otherwise simplifying the construction and reducing the weight of the antenna structure. In other structures, the half-wave elements are placed approximately end to end and are therefore spaced by one-half wavelength between centers. The half-wave elements may of course be overlapped, thereby making the effective spacing substantially less than one-half wavelength. This is a possible expedient in the case of low-frequency antennas.

It should be obvious that principles of tapering already discussed in Sec. 5.3 apply to collinear antennas. Also, it should be possible, if the occasion should arise, to vary slightly from zero the phase between adjacent elements of the array, thus moving the beam up or down slightly. These are some of the variables at the engineer's disposal.

REFERENCES

1. R. M. Foster: "Directive Diagrams of Antenna Arrays," *Bell System Tech. J.*, vol. 5, p. 307, 1926.
2. G. C. Southworth: "Certain Factors Affecting the Gain of Directive Antenna Arrays," *Proc. IRE*, vol. 18, pp. 1502–1536, September, 1930.
3. W. Wilkinshaw: "Theoretical Treatment of Short Yagi Aerials," *J. IEE (London)*, pt. III, vol. 93, p. 598, 1946.
4. Arnold B. Bailey: "TV and Other Receiving Antenna," John Francis Rider, Publisher, Inc., New York, 1950.
5. G. H. Brown: "Directional Antennas," *Proc. IRE*, vol. 25, pp. 78–145, January, 1937.
6. A. Wheeler Nagy: "An Experimental Study of Parasitic Wire Reflectors," *Proc. IRE*, vol. 24, pp. 233–254, February, 1936.
7. S. A. Schelkunoff and H. T. Friis: "Antennas: Theory and Practice," John Wiley & Sons, Inc., New York, 1952.
8. R. M. Wilmotte and J. S. McPetrie: "A Theoretical Investigation of the Phase Relations in Beam Systems," *J. IEE (London)*, vol. 66, pp. 949–954, September, 1928; see also two papers by Wilmotte alone, *ibid.*, pp. 956–967.
9. G. C. Southworth: "Principles and Applications of Waveguide Transmission," chap. 10, D. Van Nostrand Company, Inc., Princeton, N.J., 1950.
10. Reference 7, chap. 15.
11. H. H. Beverage and H. O. Peterson: "Diversity Receiving System," *Proc. IRE*, vol. 19, pp. 531–561, April, 1931.
12. S. Uda: "Wireless Beam of Short Electric Waves," *J. IEE (Japan)*, no. 452, pp. 273–282, March, 1926; no. 472, pp. 1209–1219, November, 1927. Written in Japanese with English abstract.
13. H. Yagi: "Beam Transmission of Ultra Short Waves," *Proc. IRE*, vol. 16, pp. 715–741, June, 1928.
14. R. M. Fishenden and E. R. Wiblin: "Design of Yagi Aerials," *Proc. IEE (London)*, pt. III, vol. 96, p. 5, January, 1949.
15. S. Uda and Y. Mushiake: "Yagi-Uda Antenna," Maruzen Co., Ltd., Tokyo, 1954. In English.
16. R. A. Smith: "Aerials for Meter and Decimeter Wavelengths," Cambridge University Press, London, 1949.
17. D. G. Reid: "The Gain of an Idealized Yagi Array," *J. IEE (London)*, pt. IIIA, vol. 93, p. 564, 1946.
18. G. H. Brown: "Critical Study of the Characteristics of Broadcast Antennas as Affected by Antenna Current Distribution," *Proc. IRE*, vol. 24, pp. 48–81, January, 1936.

Chapter 6

LOOP ANTENNAS

Judd Blass

*W. L. Maxson Co.
New York, New York*

6.1. INTRODUCTION

The loop antenna is a radiating coil of one or more turns.   Both ferrite and air-coil loops are commonly used in radio receivers.   There is also wide application in direction finders, aircraft receivers, and UHF transmitters.

6.2. RADIATION PATTERN

The radiation pattern of a small loop is identical with that of a small dipole oriented normal to the plane of the loop with the E and H fields interchanged.   If the normal
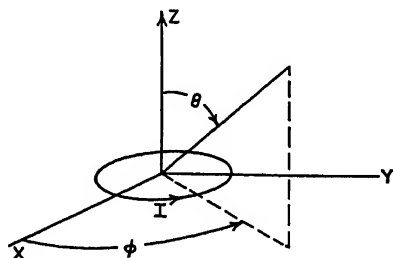
Fig. 6-1. Coordinates for loop antenna.

direction to the plane of the loop is the polar axis of a spherical coordinate system (see Fig. 6-1), the radiated electromagnetic fields are given by

$$E_\phi = \frac{120\pi^2 N}{r} \frac{A}{\lambda^2} I \sin \theta \qquad (6\text{-}1)$$

$$H_\theta = \frac{\pi N}{r} \frac{A}{\lambda^2} I \sin \theta \qquad (6\text{-}2)$$

where r = distance from antenna
     I = antenna current
     N = number of turns
     A = area of loop
     λ = wavelength

Equations (6-1) and (6-2) are valid, for arbitrary loop cross sections, provided that the current is uniform and the loop diameter is uniform and the loop diameter is small (i.e., loop radius $a < \lambda/6$). The radiation pattern of the loop is shown in Fig. 6-2.
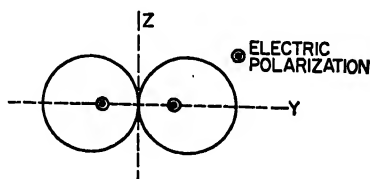
FIG. 6-2. Principal plane pattern—small loop.

The voltage induced in a small-loop receiving antenna is

$$V = \frac{2\pi}{\lambda} NAE_\phi \sin \theta$$

where θ is measured from the axis of the loop, and E_ϕ is the ϕ component of the incident field.

If a uniform current is maintained around a single-turn circular loop of radius a, the radiated field is

$$E_\phi = \frac{120\pi^2 aI}{\lambda r} J_1 \left(\frac{2\pi a}{\lambda} \sin \theta\right) \tag{6-3}$$

$$H_\theta = \frac{\pi aI}{\lambda r} J_1 \left(\frac{2\pi a}{\lambda} \sin \theta\right) \tag{6-4}$$

where J_1 is the Bessel function of the first kind and first order. These patterns have identically the same shape as those of an annular slot of large diameter (Sec. 8.6).

6.3. RADIATION RESISTANCE

The radiation resistance of a small air loop is

$$R_{\text{rad}} = \frac{320\pi^4 A^2 N^2}{\lambda^4} \tag{6-5}$$

For a circular loop of diameter D ($D = 2a$),

$$R_{\text{rad}} = 19{,}000N^2 \left(\frac{D}{\lambda}\right)^4 \tag{6-6}$$

In order to be below resonance, the diameter of a simple loop fed from a single point must be less than $\lambda/2$. If $D = 0.1$, $R_{\text{rad}} = 1.9$ ohms.

In the case of a radio receiver, if $N = 50$ and $D/\lambda = 10^{-3}$, it follows that

$$R_{\text{rad}} = 50 \text{ microohms,}$$

which is far less than the ohmic resistance of the wire. However, in this case the loop is feeding a high impedance input and the induced voltage is the quantity of greater interest.

Several techniques are possible for increasing the diameter of the loop while still maintaining approximately uniform current distribution. The radiation resistance for square loops whose dimensions are comparable with the wavelength is given by Eq. (6-6).

$$R_{rad} = 320N^2 \left(\sin \frac{\pi \ell}{\lambda} \right)^4 \tag{6-6}$$

where ℓ is the length of the side of the square. For $\ell = \lambda/4$, $N = 1$, $R_{rad} = 80$ ohms.

For the case of the Alford loop design (Type 1) shown in Fig. 6-3, there are two
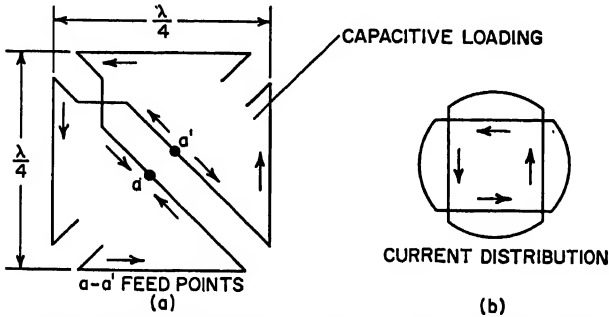
FIG. 6-3. One-wavelength-circumference Alford loop: (a) Schematic. (b) Current distribution.
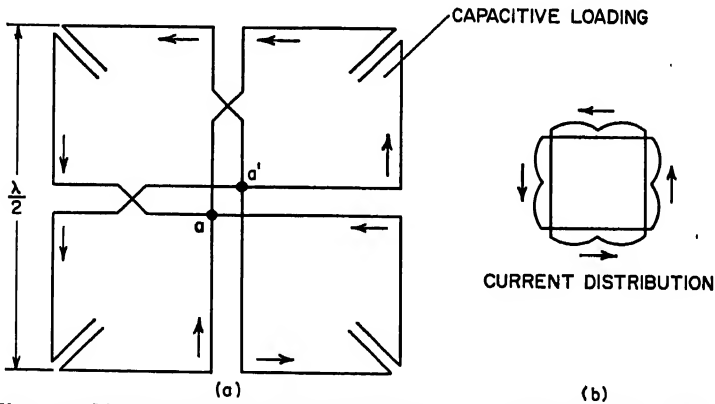
FIG. 6-4. Maximum-gain loop: (a) Schematic. (b) Current distribution.

feed points on the loop. Capacitive loading of the corners opposite from the feed result in maximum currents at the centers of each side of the loop. The loop circumference is approximately one wavelength. Figure 6-4 illustrates a design for a four-feed two-wavelength-circumference design ($\lambda/2$ circumference per feed point). This design is close to maximum gain since spacing between opposite sides is $\lambda/2$.

REFERENCES

1. J. D. Kraus: "Antennas," chap. 6, McGraw-Hill Book Company, Inc., New York, 1950.
2. D. Foster: "Loop Antennas with Uniform Current," *Proc. IRE*, vol. 32, pp. 603–607, October, 1944.

3. J. B. Sherman: "Circular Loop Antennas at UHF," *Proc. IRE*, vol. 32, pp. 534–537, September, 1944.
4. A. Alford and A. Kandoian: "Loop Antennas," *Trans. AIEE*, Supplement, vol. 59, p. 843, 1940.
5. G. Glinski: "Circular Loop Antenna with Non-uniform Current Distribution," *J. Appl. Phys.*, vol. 18, pp. 638–644, July, 1947.
6. L. L. Libby: "Special Aspects of Balanced Shielded Loops," *Proc. IRE*, vol. 34, pp. 641–646, September, 1946.
7. J. E. Browder and V. J. Young: "Design Values for Loop Input Circuits," *Proc. IRE*, vol. 35, pp. 519–525, May, 1947.
8. N. Marchand: "Loop Antennas for FM Broadcasting," *Communications*, vol. 27, pp. 34–35, April, 1947.
9. G. Bramsler: "Loop Aerial Reception," *Wireless World*, vol. 58, pp. 469–472, November, 1952.
10. J. R. Wait: "Receiving Properties of a Wire Loop with Spheroidal Core," *Can. J. Technol.*, January, 1953, pp. 9–24.

Chapter 7

HELICAL ANTENNAS

Edward F. Harris

Mark Products Co.
Skokie, Illinois

7.1. AXIAL-MODE HELICAL ANTENNAS

A very thorough study of the basic concepts of the axial or beam mode of helical antennas has been made by John D. Kraus, and a great deal of information appears in print prepared by Kraus and his associates.[1-6] Of necessity, the material herein, which covers the end-fire types of helical antennas, draws heavily from the works of Kraus.

The helical beam antenna, or axial-mode helix, possesses a number of unusual characteristics. It operates as an end-fire beam antenna generating waves that are circularly polarized. Perhaps the most remarkable property of the axial-mode helix is that this type of radiation persists over about a 1.7:1 range in frequency, with the directivity or gain close to maximum at all frequencies in that range. This results from a natural adjustment of the phase velocity of wave propagation along the helix to approximately the proper value required at each frequency for

Fig. 7-1. Axial, or beam mode, of helical antenna as contrasted with the omnidirectional, or perpendicular, mode.

making the directivity of the antenna a maximum; that is, a given helix automatically produces about the highest directivity possible for an antenna of its size and does this over a considerable bandwidth. Figure 7-1 shows the axial, or beam, mode of operation as contrasted with the omnidirectional, or broadside, mode obtained with other dimensions.

The axial, or end-fire, mode of radiation of the helix is most simply generated by the coaxial-line and ground-plane arrangement shown in Fig. 7-2, with the inner conductor connected to one end of the helix and the outer conductor terminated in a ground plane. The ground plane may be made of sheet, of screen, or of a number of radial and concentric conductors.

The following symbols are used to describe the helix and ground plane (Fig. 7-2):

D = diameter of helix

S = spacing between turns (center to center)

α = pitch angle = $\tan^{-1}(S/\pi D)$

L = length of one turn

n = number of turns

A = axial length (nS)

d = diameter of helix conductor

g = distance of helix proper from ground plane

G = ground-plane diameter

If one turn of a helix is unrolled on a flat plane, the circumference (πD), spacing (S),

Fig. 7-2. Helix and associated dimensions.

turn length (L), and pitch angle (α) are related by the triangle shown in Fig. 7-2.

In Fig. 7-2 the coaxial line is coincident with the helix axis and the feed wire (between a and b) lies in a plane through the helix axis. Beyond point b the conductor lies in the surface of the imaginary helix cylinder. This is the helix proper of axial length A. The component of the feed-wire length parallel to the axis is g, which is about equal to $S/2$. The antenna terminals are considered to be at the point of connection with the coaxial line, and all impedances are referred to this point a. It is sometimes more convenient to place the coaxial-line terminals at a point which is $D/2$ from the axis, as indicated by point c.

As the frequency varies, the helix diameter D_λ and spacing S_λ in free-space wavelengths change, but the pitch angle remains constant. The relation of D_λ, S_λ, and α as a function of frequency is conveniently illustrated by a diameter-spacing chart as in Fig. 7-3. The dimensions of any uniform helix are defined by a point on the chart. Let us consider a helix of pitch angle equal to 10°. At zero frequency, $D_\lambda = S_\lambda = 0$. With increase in frequency, the coordinates (S_λ, D_λ) of the point giving the helix spacing and diameter increase, but their ratio is constant so that the point moves along the constant-pitch-angle line for 10°. Designating the lower- and upper-frequency limits of the frequency range of the beam mode by F_1 and F_2, respectively, the corresponding range in spacing and diameter is given by a line between the points for F_1 and F_2 on the 10° line. The center frequency of the range is F_0 and is taken arbitrarily such that $F_0 - F_1 = F_2 - F_0$, or $F_0 = (F_1 + F_2)/2$.

Pattern and impedance data are available in the literature[3] for helical antennas of fixed physical length with pitch angles ranging from 6 to 24°. The antennas are about 1.6 wavelengths long at the center frequency of the beam-mode range with half-power beamwidths of about 40°. An optimum helix may be determined by comparing pattern and impedance data[2,3] on a D-S chart, as in Fig. 7-4. The pattern contour in Fig. 7-4 indicates the approximate region of satisfactory patterns. A satisfactory pattern is considered to be one with a major lobe in the axial direction and with relatively small minor lobes. Inside the pattern contour of Fig. 7-4 the pat-

terns are of this type and have beamwidths of from 30 to 60°. Inside the impedance contour the terminal impedance is relatively constant (between 100 and 150 ohms) and is nearly a pure resistance. A third contour in Fig. 7-4 is for the axial ratio measured in the direction of the helix axis. Inside this contour the axial ratio is less than 1.25. From a consideration of the three contours it is apparent that too small or too large a pitch angle is undesirable. An "optimum" pitch angle appears to be about 14°. Since the properties change slowly as a function of α in the vicinity of 14°, there is nothing critical about this value. In fact, the properties of helices of pitch angles of $14 \pm 2°$ differ but little. Referring to Fig. 7-4, a line is indicated for $\alpha = 14°$, with upper and lower frequency limits for satisfactory operation. Although
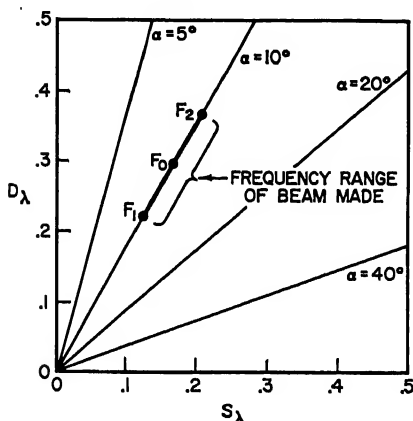
Fig. 7-3. Diameter-spacing chart showing range of dimensions associated with an operating band.
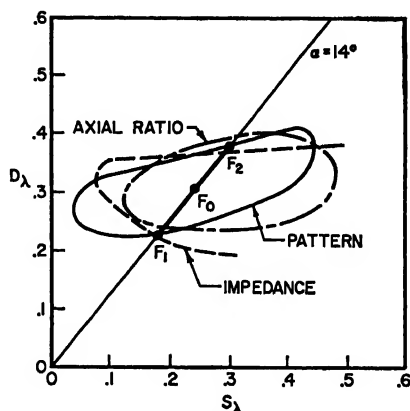
Fig. 7-4. Diameter-spacing chart with contours showing regions of stable performance for pattern, impedance, and low axial ratio.

the exact location of these limits is arbitrary, it is relatively well defined by the close bunching of the contours for the three properties near the frequency limits. The frequency range between F_1 and F_2 is 1.67 to 1. Although the optimum pitch angle of 14° associated with this frequency range applies specifically to a helix with an overall axial length of about 1.65 wavelengths and a conductor diameter of 0.017 wavelength at the center frequency, it is probable that 14° is close to optimum for helices that are considerably shorter or longer or are of somewhat different conductor diameter. An optimum helix has been constructed and measured.[4] Since $S = 0.24$ wavelength at the center frequency for the 14° helix, the number of turns n is approximately 6. Thus the optimum helix is chosen as a unit with six turns and 14° pitch angle for general-purpose wideband applications.

Figures 7-5 and 7-6 show a summary of field pattern, axial ratio, and standing-wave ratio measurements performed on a six-turn 14° helix. It is evident from these data that the axial mode of radiation occurs for frequencies between about 290 and 500 Mc. For general design applications of the helical antenna the following dimensions may be used; all dimensions are expressed in terms of the free-space wavelength at the center frequency of operation:[5]

Diameter: $D = 0.32\lambda$
Spacing: $S = 0.22\lambda$
Ground-plane diameter: $G \geqq 0.8\lambda$
Conductor diameter: $d = 0.02\lambda$
Spacing from ground plane to first turn: $g = S/2 = 0.12\lambda$

The only remaining quantity which must be specified is the number of turns n, and this is determined by the desired beamwidth or gain.
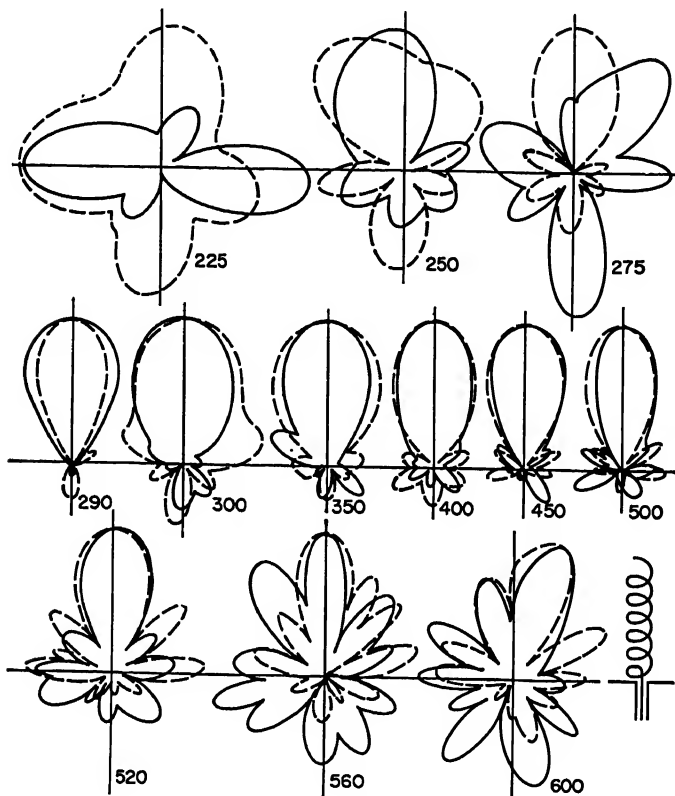
FIG. 7-5. Measured azimuthal electric-field patterns of the six-turn, 14° helix. The solid patterns are for the horizontally polarized, and dashed patterns for the vertically polarized field component. Between 290 and 500 Mc the patterns are characteristic of the fundamental beam mode of radiation.

Based on the measured patterns of a large number of helical-beam antennas,[5] it is found that the beamwidth (β) between half-power points is given quite closely by

$$\beta = \frac{52}{\frac{C}{\lambda}\sqrt{\frac{nS}{\lambda}}} \quad \text{deg} \tag{7-1}$$

where λ = free-space wavelength
S = spacing = $C \tan \alpha$
C = circumference
n = number of turns

It is assumed that the pitch angle is between 12 and 15°, that n is at least 3, and that the circumference is between three-quarters and four-thirds wavelengths. Half-power beamwidths are illustrated graphically in Fig. 7-7 as a function of the axial length of the helix nS and of the circumference C in free-space wavelengths. The number of turns n for the center frequency and a pitch angle of 12.5° is also indicated

in Fig. 7-7 by the lower scale for the abscissa.   Thus for a 37° beamwidth at the center frequency, a 12.5° helix requires nine turns.

If the shape of the main lobe of the radiation pattern is desired, it can be drawn
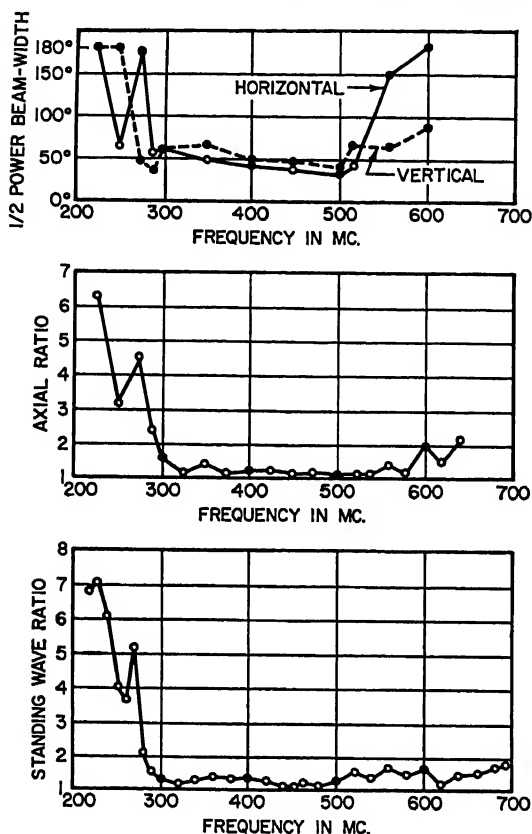
FIG. 7-6. Summary of measured performance of the six-turn, 14° helix.

approximately with the aid of the half-power points (β) and the beamwidth δ between first nulls of the pattern as given by

$$\delta = \frac{115}{\frac{C}{\lambda}\sqrt{\frac{nS}{\lambda}}} = 2.21\beta \quad \text{deg} \tag{7-2}$$

An approximate expression for the power gain of a helical beam antenna, with respect to an isotropic circularly polarized source, can be obtained by dividing the square of the beamwidth into the number of square degrees in a sphere (41,253). Thus

$$\text{Gain} \cong 15 \left(\frac{C}{\lambda}\right)^2 \frac{nS}{\lambda} \tag{7-3}$$

or as a decibel ratio:

$$\text{Gain} \cong 11.8 + 10 \log_{10}\left[\left(\frac{C}{\lambda}\right)^2 \frac{nS}{\lambda}\right] \quad \text{db} \tag{7-4}$$

These formulas neglect the effect of minor lobes, and the gains may in some cases be

slightly high, but usually not by more than 1 or 2 db. A graph giving the power gain of helical beam antennas as a function of axial length nS and circumference C in free-space wavelengths is presented in Fig. 7-8. The number of turns n for the center frequency ($C = 1.0\lambda$) and a pitch angle of 12.5° is also indicated in Fig. 7-8 by the lower scale for the abscissa. For example, if a gain of 12 db is desired at the center frequency, a 12.5° helix with about 4.8 turns is required.
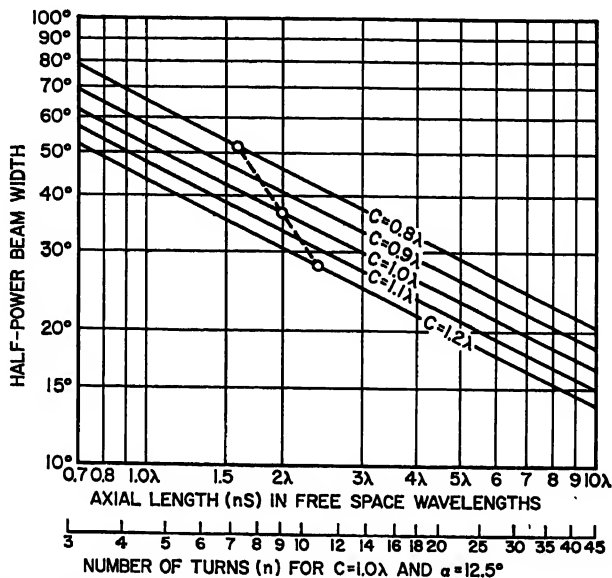
FIG. 7-7. Half-power beamwidth of helical beam antenna as a function of the axial length and circumference in free-space wavelengths, and also as a function of the number of turns when $C = 1$ wavelength and $\alpha = 12.5°$.

Assuming that the relative phase velocity of wave propagation on the helix fulfills the *maximum* directivity conditions,[6] the ellipticity, or axial ratio AR, of the polarization in the direction of the helix axis can be stated approximately by

$$\text{AR} = \frac{2n + 1}{2n} \qquad (7\text{-}5)$$

There are two kinds of circular polarization, right-hand and left-hand. Either type may be generated by a helical beam antenna, depending on the manner in which the helix is wound. A helix wound like a right-hand screw radiates or receives right-hand circular polarization. It is important for maximum signal over a direct path between circularly polarized transmitting and receiving antennas that both be of the same type, that is, both helices be right-hand or both be left-hand.

A helix of more than three turns, with a pitch angle between 12 and 15°, has a terminal impedance which is nearly a pure resistance. If the feed arrangement is as in Fig. 7-2, the terminal resistance tends to increase as a function of the frequency over the frequency range of the axial mode.[5]

From impedance measurements on a large number of helical beam antennas with this feed arrangement and of at least a few turns, it was found that in the frequency range of the axial mode (circumference between three-fourths and four-thirds wavelengths) the terminal resistance R was within about ±20 per cent when the following expression was used:

$$R = \frac{140C}{\lambda} \qquad \text{ohms} \qquad (7\text{-}6)$$
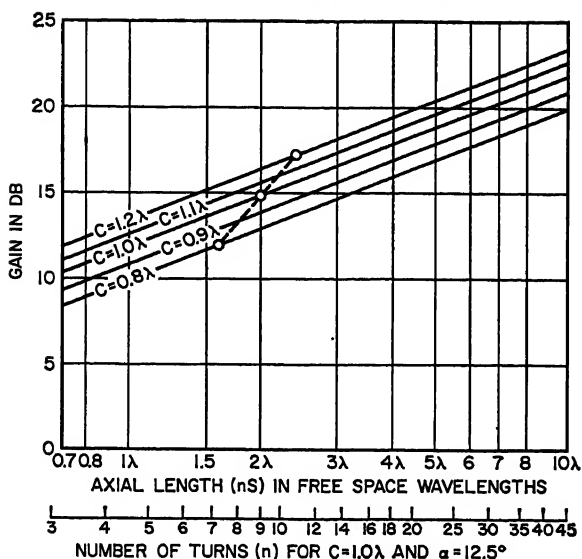
FIG. 7-8. Power gain of helical beam antenna with respect to isotropic circularly polarized source.

In general, the terminal-resistance variation with frequency will be less for a large number of turns than for a small number.

7.2. ARRAYS OF HELICAL ANTENNAS

Circularly polarized antennas of considerably greater directivity than is provided by the single helix can be obtained with helical beam antennas in a variety of arrangements.[4,13] Three methods are illustrated in Fig. 7-9, showing broadside arrangements. In Fig. 7-9a a helical beam antenna acts as the primary antenna to illuminate a sheetmetal reflector of parabolic or other shape. By adjustment of the illumination of the reflector by the primary helical beam antenna, control of both the beam shape and the size of minor lobes is afforded.

In Fig. 7-9b a helical beam antenna is used to excite a circularly polarized TE_{11} mode in a cylindrical waveguide connected to a cylindrical horn. The area of the aperture of the horn for a given gain will be approximately the same as for the reflector arrangement.

In Fig. 7-9c a broadside array of helices is shown as an arrangement for obtaining a circularly polarized antenna with high gain. With this configuration linear polarization may be obtained with suitable arrangement and phasing of left-hand and right-hand helices in the array.
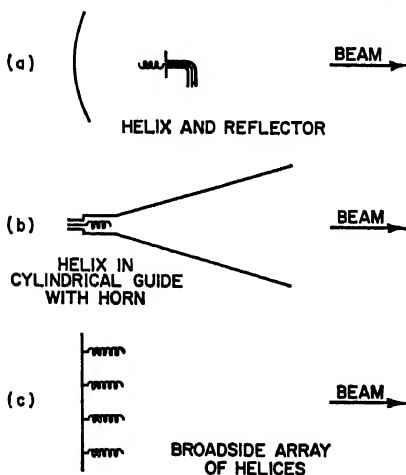
FIG. 7-9. High-gain antenna systems using helical beam antennas.

Figure 7-10 gives the dimensions for a broadside array of four helical beam anten-

nas.[4] Each helix is of the six-turn 14° type. Dimensions are given in free-space wavelengths at the center frequency. The helices are mounted on a flat square ground plane of 2.5 × 2.5 wavelengths. All helices are oriented in the same manner and are energized with equal, in-phase voltages. The helices are symmetrically
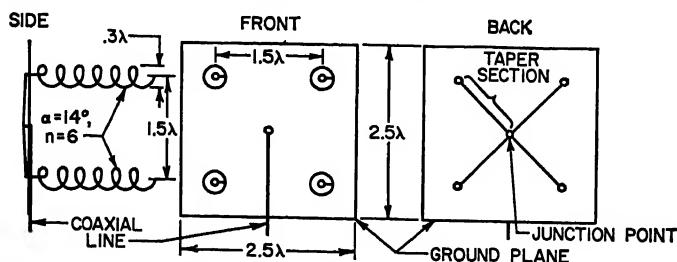
Fig. 7-10. Constructional details for broadside array of helices with four six-turn 14° units. Dimensions are in free-space wavelengths at the center frequency.

placed and spaced 1.5 wavelengths between centers. All the helices are wound in the same direction, and the radiation is circularly polarized. If two of the helices were wound left-hand and the other two right-hand, the radiation would be linearly polarized.

To energize each of the helices with equal, in-phase voltages and, at the same time, provide a broadband transformer between the antennas and a 53-ohm line, the following arrangement is employed. Each antenna is connected by a "single-wire vs. ground-plane" transmission line which tapers gradually from about 130 ohms characteristic impedance at the antenna to about 200 ohms at the center of the ground plane. The four lines from the four helices connect in parallel at this point, yielding 50 ohms.

The ground plane of the antenna is 94 × 94 cm, and the center frequency is 800 Mc. Figure 7-11 shows the half-power beamwidths, the axial ratio, and the

Fig. 7-11. Summary of measured performance of four-helix array shown in Fig. 7-10.
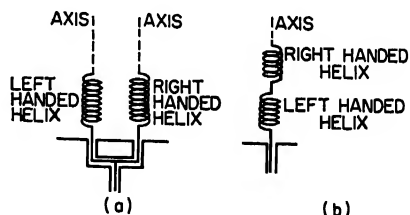
Fig. 7-12. Helical-antenna configurations for producing linear polarization.

SWR on a 53-ohm line as a function of frequency for the array.

Figure 7-12 shows helical-antenna configurations for producing linear polarization. Two helices, one wound left-hand and the other right-hand but otherwise identical, are mounted as shown in Fig. 7-12a. The right and left circular polarization combine on the axis to give linear polarization. If the resulting field is vertically polarized,

then rotating one helix 180° on its axis turns the plane of polarization to horizontal. Another method of obtaining linearly polarized radiation in the axial direction is by connecting a left- and a right-hand helix in series as in Fig. 7-12b.

Mutual coupling between helical beam antennas is of interest,[11] especially where they are to be employed on two adjacent communication circuits. Measurements have been made on two right-hand helical beam antennas at 400 Mc where the spacing between units on the same tower was varied. The two helical antennas were oriented

FOR A GAIN
G, AND N TURNS
EACH SIDE OF
FEED:

$G \cong N$

$d = \sqrt{\dfrac{(2\lambda)^2 - (P)^2}{\pi^2}}$

$P = \dfrac{\lambda}{2}$

$S \cong \dfrac{\lambda}{6}$
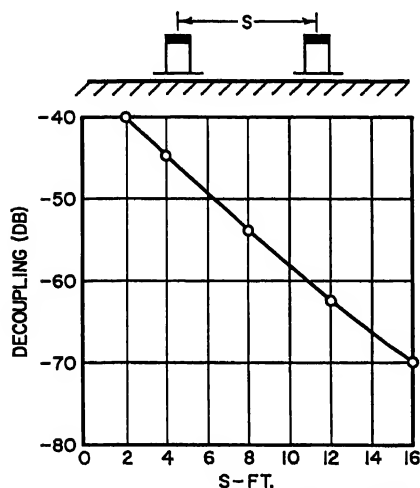
FIG. 7-13. Measured decoupling between two helices at 400 Mc.
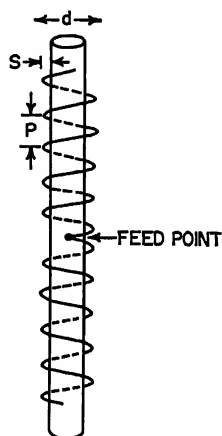
FIG. 7-14. Winding arrangement of single-bay side-fire antenna composed of concentrically disposed helical conductor and conducting cylinder.

in the same direction for these measurements, and the vertical spacing varied. Reference level (0 db) was established by directly connecting the signal generator to the input terminals of the receiver. For subsequent readings the signal generator was connected to one helical antenna and the receiver to the other. The relative signal levels at various spacings are shown in the curve of Fig. 7-13.

7.3. BROADSIDE-TYPE HELICAL ANTENNAS

The broadside-type helical antenna uses the traveling-wave principle to excite a large portion of the aperture from a single feed.[14,15] Figure 7-14 shows the winding arrangement of a single-bay side-fire (broadside) antenna composed of concentrically disposed helical conductor and conducting cylinder. In such a configuration each helix and its associated conducting cylinder may be considered much the same as a single-wire transmission line, using the cylindrical surface as the return path. As is well known, such a line tends to radiate energy in increasing amounts as the spacing between conductor and return surface is increased. Hence the relative diameter of the helix and the cylinder constitute an effective control over the radiation of energy per turn. This spacing can be used to accomplish a proper balance between aperture illumination and standing wave present on the helix. By choice of the helix diameter so that one turn of the helix constitutes a length equal to an integral number of wavelengths, the currents in all conductors of the antenna possess a coherent phase relationship at a given azimuth and consequently radiate as a broadside array to concentrate the radiation in a vertical plane.

Figure 7-15 shows the calculated results for vertical patterns for modes up to and

including the fifth (mode numbers correspond to numbers of wavelengths per helix turn). Note that the one-wavelength mode radiates rather uniformly in most directions, better along the axis than in its plane. This is the mode commonly used in the end-fire helices.

The one-wavelength mode does not lend itself to practical mast support. The
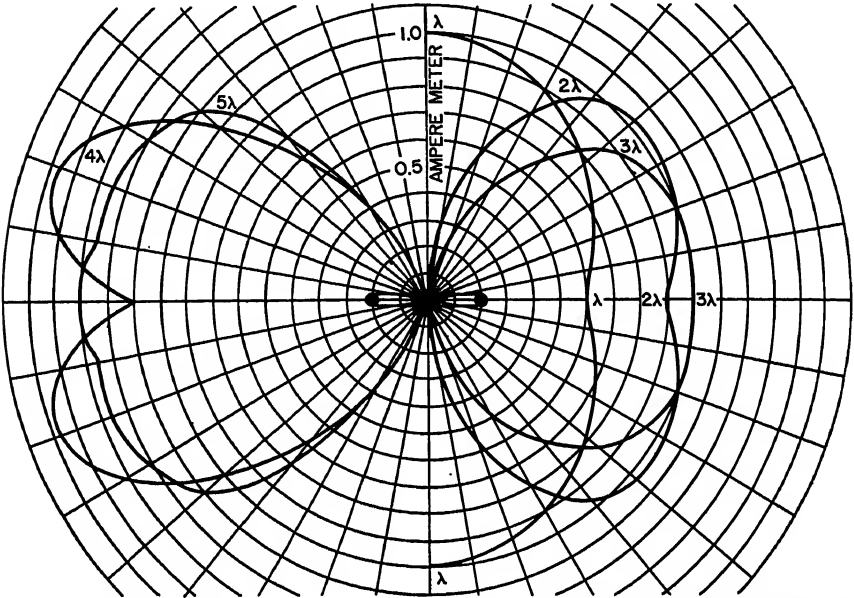
Fig. 7-15. Vertical patterns from one turn of integral-mode helix with zero pitch angle and attenuation. Patterns are shown up to the fifth mode.
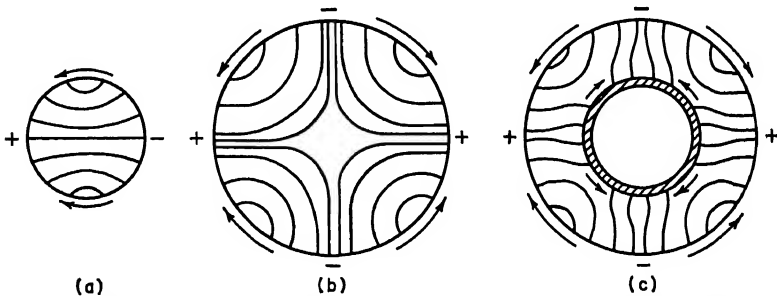
Fig. 7-16. Partial instantaneous fields. (a) In first-mode helix without mast. (b) In second mode without mast. (c) In second mode with mast.

strong loop field passes directly through the center of the loop, and a large metallic member causes serious disruption of normal operation. By using a higher-order mode, where the field at the center is zero and where the diameter per turn is large enough to permit a sufficiently strong support without seriously disturbing operation, the desired radiation characteristics can be obtained.

Figure 7-16a and b shows a sketch of the instantaneous fields existing in one turn of a first- and second-mode helix. Figure 7-16c shows the second-mode-helix field after a mast has been inserted along the axis. Naturally, there is some component of vertically polarized radiation from the helix because of the helix pitch. The percentage of this component is appreciable when based on the analysis of a single turn.

MEASURED HORIZONTAL PATTERN,
ONE BAY, 500 MC. MODEL
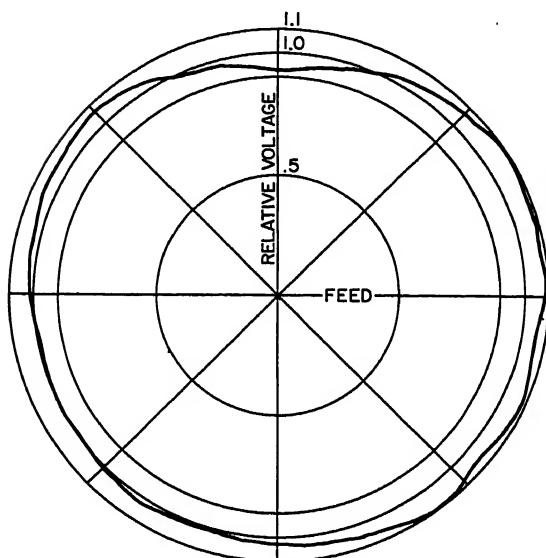
FIG. 7-17a. Measured horizontal pattern, one-bay, 500-Mc model.
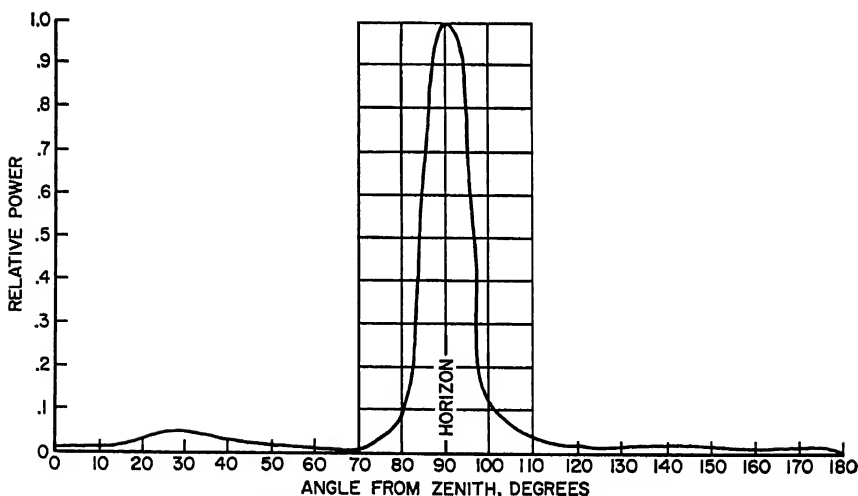
FIG. 7-17b. Measured vertical pattern, one-bay, 500-Mc model.

However, by making use of a right-hand and a left-hand helix, placed end to end and fed in the center, the vertical components can be made to cancel, while the horizontal components are reinforced. In the normal design the power gain per bay is of the order of 5. The design center for radiation loss per turn is chosen as 4 db per turn so that the energy remaining at the ends is down more than 20 db. Thus the far end of the conductor of the helical current may be left open or shorted rather than terminated, with negligible effects from the reflections occurring at the unterminated ends, since only a small amount of energy remains in the wave at this point. Higher-

gain antennas are made by stacking and properly feeding identical bays.   Arrays of vertically stacked bays up to five have been developed, and various patterns are shown in Fig. 7-17.
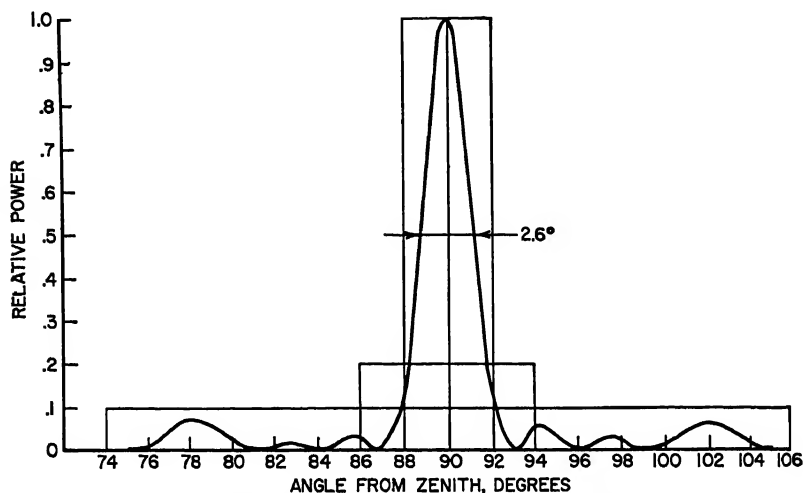
FIG. 7-17c. Measured vertical pattern, four-bay, 1,000-Mc model.

The feed-point impedance at the junction located at the center of a single bay is of the order of 100 ohms and is essentially resistive over a large percentage of the band because of the nonresonant characteristic of the antenna.

REFERENCES

1. J. D. Kraus: "Helical Beam Antenna," *Electronics*, vol. 20, pp. 109–111, April, 1947.
2. J. D. Kraus and J. C. Williamson: "Characteristics of Helical Antennas Radiating in the Axial Mode," *J. Appl. Phys.*, vol. 19, pp. 87–96, January, 1948.
3. O. J. Glasser and J. D. Kraus: "Measured Impedances of Helical Beam Antennas," *J. Appl. Phys.*, vol. 19, pp. 193–197, February, 1948.
4. J. D. Kraus: "Helical Beam Antennas for Wide-band Applications," *Proc. IRE*, vol. 36, no. 10, pp. 1236–1242, October, 1948.
5. John D. Kraus: "Helical Beam Antenna Design Techniques," *Communications*, September, 1949, p. 6.
6. John D. Kraus: "The Helical Antenna," *Proc. IRE*, vol. 37, no. 3, pp. 263–272, March, 1949.
7. H. A. Wheeler: "A Helical Antenna for Circular Polarization," *Proc. IRE*, vol. 35, pp. 1484–1488, December, 1947.
8. C. C. Cutler: "Experimental Determination of Helical-wave Properties," *Proc. IRE*, vol. 35, pp. 230–233, February, 1948.
9. G. H. Brown and O. M. Woodward: "Circularly Polarized Omnidirectional Antenna," *RCA Rev.*, vol. 8, pp. 259–269, June, 1947.
10. J. D. Kraus: "Antennas," chap. 7, McGraw-Hill Book Company, Inc., New York, 1950.
11. E. A. Blasi: "The Theory and Application of the Radiation Mutual-coupling Factor," *Proc. IRE*, vol. 42, no. 7, pp. 1180–1183, July, 1954.
12. J. D. Kraus and Edward Ksiazek: "New Techniques in Radio Astronomy," *Electronics*, vol. 26, no. 9, pp. 148–152, September, 1953.
13. Edward F. Harris: "Helical Beam Antenna Performance," *Commun. Eng.*, July–August, 1953, p. 19.
14. Lloyd O. Krause: "Sidefire Helix UHF-TV Transmitting Antenna," *Electronics*, August, 1951, p. 107.
15. H. G. Smith: "High-gain Side Firing Helical Antennas," *AIEE Trans.*, pt. I, Communication and Electronics, vol. 73, pp. 135–138, May, 1954.

Chapter 8

SLOT ANTENNAS

Judd Blass

W. L. Maxson Co.
New York, New York

8.1. INTRODUCTION

This chapter deals with the characteristics of small slot antennas. The metal surfaces in which the slots are cut will be large compared with a wavelength, but the slots themselves are less than one wavelength in extent. Such slots may be excited by means of an energized cavity placed behind it, through a waveguide, or by a transmission line connected across the slot.

The simplest example of such an antenna consists of a rectangular slot cut in an extended thin flat sheet of metal with the slot free to radiate on both sides of this sheet, as shown in Fig. 8-1. The slot is excited by a voltage source such as a balanced parallel transmission line connected to the opposite edges of the slot, or a coaxial transmission line.
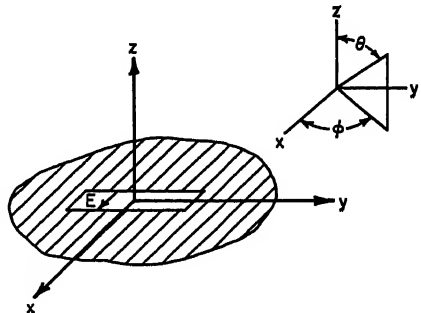
Fig. 8-1. Rectangular slot.

The electric-field distribution in the slot can be obtained from the relationship between the slot antennas and complementary wire antennas as established by Booker.[1] It has been shown that the electric-field distribution (magnetic current) in the slot is identical with the electric-current distribution on the complementary wire. In the case of the rectangular slot illustrated, the electric field is perpendicular to the long dimension and its amplitude vanishes at the ends of the slot.

The electric field is everywhere normal to the surface of the slot antenna except in the region of the slot itself. The theoretical analysis of this configuration shows that the radiation of the currents in the sheet can be deduced directly from the distribution of the electric field in the slot. Consequently, the radiated field of an elementary magnetic moment within the slot boundaries should include the contributions of the electric currents flowing on a metal surface.

In general, a slot-antenna design will require that the slot be cut in other than an extended flat sheet surface. Whatever the surface is, the electric field will be everywhere normal to it except in the region of the slot. The field due to the electric currents on this metal surface can be deduced from the exciting magnetic currents[2] in the slot, just as in the case of the flat metal sheet. This field can be combined with the exciting field so that the resultant is the total field due to a magnetic current on the given boundary surface. Thus the field of a thin rectangular slot cut in a circular cylinder differs from that of a slot cut in a flat metal sheet since the distribution of electric currents is different for the two cases. Sections 8.2 to 8.7 discuss the radiated fields of slot antennas cut in a variety of surfaces.

In general, the slot antenna is not free to radiate on both sides of the surface on which it is cut since one side is either completely enclosed, e.g., the slotted cylinder antenna, or it is desired that the radiation on one side be minimized. In these cases, the influence of the enclosed cavity region on the excitation and impedance of the slot antenna is significant to the antenna design. Aspects of this problem are discussed in Sec. 8.9 for the rectangular slot.

8.2. SMALL RECTANGULAR SLOT IN INFINITE GROUND PLANE

The theoretical properties of a radiating slot in a flat sheet can be obtained from Booker's extension[1] of Babinet's principle, which shows that the field of the slot can be deduced from those surrounding a dipole of the same dimensions by interchanging the electric and magnetic vectors. Alternatively, the field can be found from the equivalence principle, as discussed in Sec. 2.4. The radiation field of a small rectangular slot such as shown in Fig. 8-1 is given by

$$E_\theta = -jE_x^{(a)} \frac{\cos \phi}{2r\lambda} dx\, dy\, e^{-jkr} \tag{8-1a}$$

$$E_\phi = jE_x^{(a)} \frac{\cos \theta \sin \phi}{2r\lambda} dx\, dy\, e^{-jkr} \tag{8-1b}$$

where $E_x^{(a)}$ is the x component of the electric field in the slot, $k = 2\pi/\lambda$, r is the distance from the slot, θ and ϕ are as defined in Fig. 8-1, and it is assumed that the electric field is parallel to the x axis. The principal plane radiation patterns of this magnetic-current dipole are presented in Fig. 8-2. It is seen that the radiation pattern in the xz plane is omnidirectional, and the pattern in the yz plane varies as $\sin \theta$. It is important to observe that the phase of the radiated field reverses on the two sides of the ground plane even though the patterns are identical.

8.3. HALF-WAVE RADIATING SLOT IN INFINITE GROUND PLANE

Radiation Field. A rectangular slot cut in a flat sheet of metal will be resonant when it is a half wavelength long. As in the case of the complementary wire antenna,

the magnetic-current distribution for the thin slot is approximately sinusoidal. The radiation pattern of the half-wave slot in the xz plane is the same as that given in Fig. 8-2. In the yz plane, however, the radiation pattern is given by Eq. (8-2).

$$E_\phi = E_\phi(0) \cos\left(\frac{\pi}{2}\sin\theta\right)\sec\theta \qquad (8\text{-}2)$$

where $E_\phi(0)$ is the field strength at the peak of the pattern.

Near Field. The near field of a slot antenna is of interest in determining the coupling of antennas to each other. Although the radiation pattern of a slot antenna is dependent upon the shape of the metal surface at large distances from the slot, the
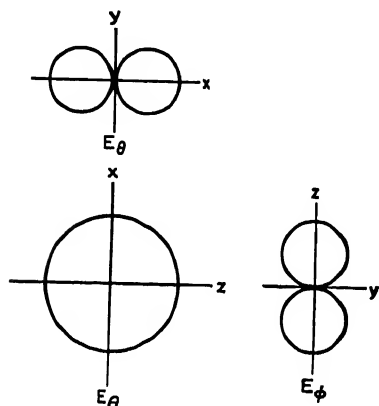
Fig. 8-2. Principal plane field diagrams for thin rectangular slot.
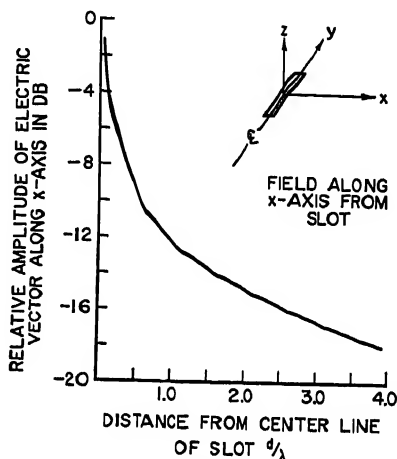
Fig. 8-3. Field attenuation near half-wave slot.

near fields attenuate rapidly for relatively short distances from the source. The near field of a half-wave slot antenna in a flat ground plane is thus approximately equal to the near field in any surface of large curvature. The fields due to a half-wave slot in an infinite conducting sheet are given by Eqs. (8–3a) to (8–3c):

$$H_z = -j\frac{E_0}{2\pi\eta}\left(\frac{e^{-jkr_1}}{r_1} + \frac{e^{-jkr_2}}{r_2}\right) \qquad (8\text{-}3a)$$

$$H_\rho = j\frac{E_0}{2\pi\eta}\left(\frac{z-\lambda/4}{\rho}\frac{e^{-jkr_1}}{r_1} + \frac{z+\lambda/4}{\rho}\frac{e^{-jkr_2}}{r_2}\right) \qquad (8\text{-}3b)$$

$$E_\phi = -j\frac{E_0}{2\pi}\frac{1}{\rho}\left(e^{-jkr_1} + e^{-jkr_2}\right) \qquad (8\text{-}3c)$$

where (ρ,ϕ,z) are the coordinates of a cylindrical coordinate system in which the slot is coincident with the z axis. r_1 and r_2 are the distances from the ends of the slot to the point of observation. $\eta = 120\pi$ is the impedance of free space. E is expressed in volts per meter, and H in amperes per meter.

These theoretical expressions indicate that the electric field in the plane of the slot is zero along the axis of the slot inversely proportional to distance from the center along the x axis. Surfaces of equal phase are ellipsoids of revolution about the x axis.

The experimental work carried out by Putnam, Russell, and Walkinshaw[3] indicates that the distribution in a half-wavelength slot with a length-to-width ratio of 14:1 is closely sinusoidal but that within 20 per cent of the resonant frequency there is a considerable departure from the sinusoidal distribution. Figure 8-3 illustrates the

measured attenuation of the electric field along the sheet on the x axis. Figure 8–4a is a plot of the phase front of a half-wave slot at resonance, and Fig. 8–4b is a plot of the amplitude distribution at resonance. It should be noted that the phase velocity is greater than the free-space velocity near the center of the slot.

8.4. RADIATION CHARACTERISTICS OF HALF-WAVE SLOT IN A FINITE FLAT SHEET

An important slot-antenna configuration is one in which a slot is free to radiate on one side of a flat sheet only. Calculations for this configuration are generally difficult and at best approximate. Measured results[3] for patterns of a half-wave slot in a circular ground plane of diameters 2λ, 3λ, and 10λ are shown in Fig. 8–5a, b, and c, respectively. It is seen that an interference pattern results in the illuminated region which corresponds to sources located approximately a half diameter apart, with the center at the slot. The radiation in the shadow zone immediately behind the slot is appreciable even for the 10-wavelength diameter. Figure 8–5d is a polar diagram in the yz plane for a diameter of 10 wavelengths. (See also Ref. 22.)

FIG. 8–4. Phase and amplitude contours near a half-wave slot.

8.5. AXIAL SLOT IN A CIRCULAR CYLINDER

A cylinder of radius a is shown in Fig. 8–6, which is coaxial with a cylindrical coordinate system (ρ,ϕ,z). The radiation field of a slot cut along the z axis consists of E_ϕ and H_θ components referred to the indicated spherical coordinate system. If V_0 is the voltage across the center of a half-wave resonant slot,

$$E_\phi = V_0 \frac{e^{-jkr}\cos\left(\dfrac{\pi}{2}\cos\theta\right)}{r\sin\theta} M(ka\sin\theta,\ \phi-\phi_0) \tag{8-4a}$$

and

$$H_\theta = -\frac{E_\phi}{120} \tag{8-4b}$$

The cylinder space factor $M(x,\phi)$ is given by

$$M(x,\phi) = \frac{1}{\pi^2}\sum_{m=0}^{\infty} \frac{\epsilon_m e^{jm\pi/2}\cos m\phi}{xH_m^{(2)'}(x)} \tag{8-5}$$

where

$$\epsilon_0 = 1,\ \epsilon_m = 2 \qquad m \neq 0$$

For a small-diameter cylinder, that is, $x = ka\sin\theta \ll 1$,

$$M(ka\sin\theta,\phi) = \frac{1}{2\pi}e^{j\pi/2} \tag{8-6}$$

FIG. 8-5. Polar diagrams of half-wave slot on finite ground plane: (a) xz-plane pattern for 2λ-diameter ground plane. (b) xz-plane pattern for 3λ-diameter ground plane. (c) xz-plane pattern for 10λ-diameter ground plane. (d) yz-plane pattern for 10λ-diameter ground plane.
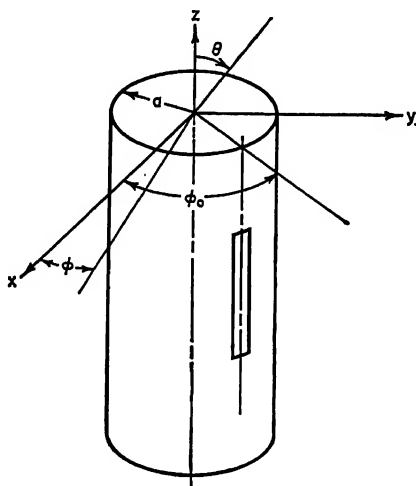
FIG. 8-6. Axial slot on a cylinder.
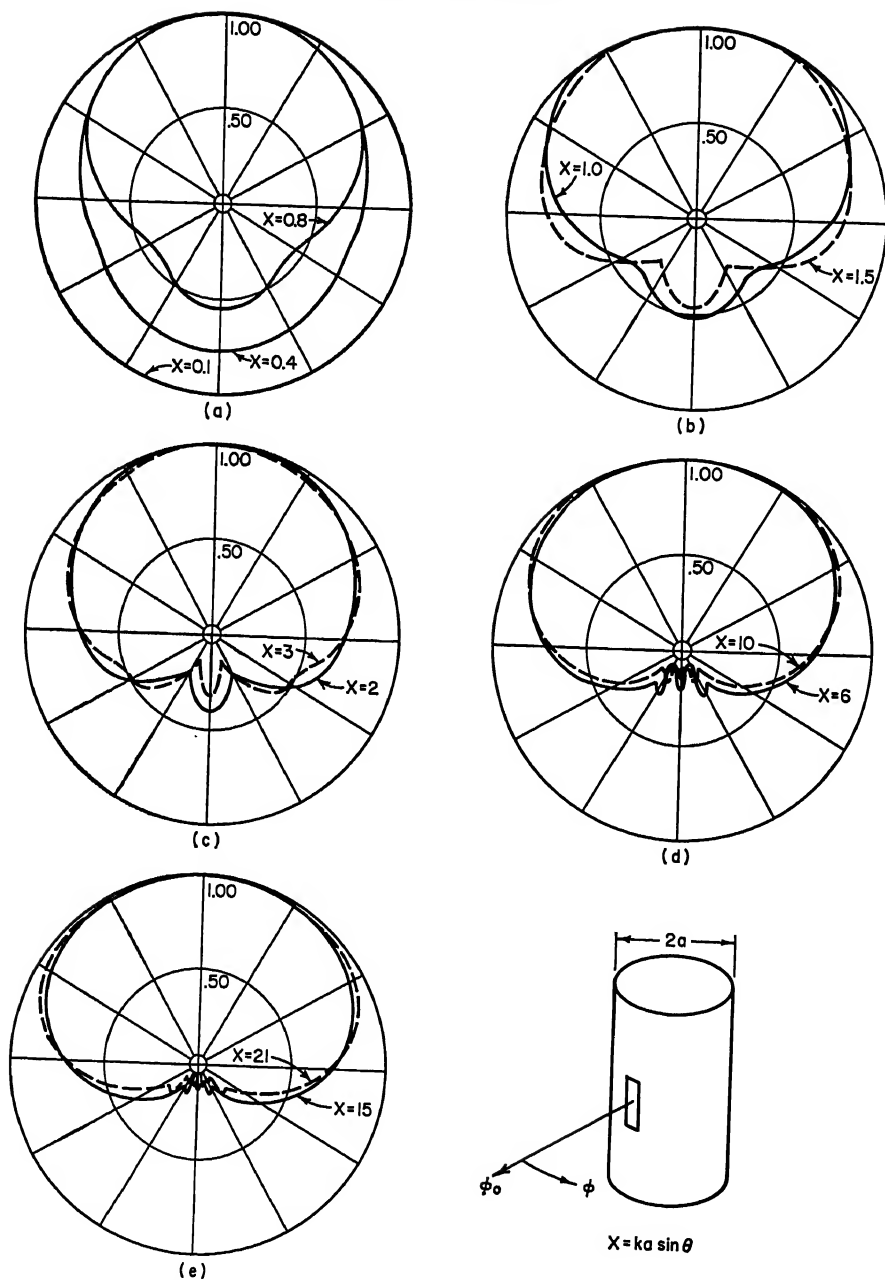
FIG. 8-7. Azimuth patterns of axial slot on a circular cylinder: (a) $x = 0.1, 0.4, 0.8$. (b) $x = 1.0, 1.5$.   (c) $x = 2, 3$.   (d) $x = 6, 10$.   (e) $x = 15, 21$.
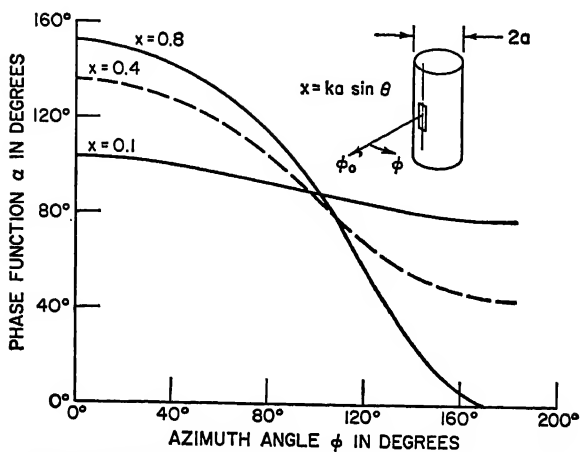
FIG. 8-8. Phase of cylinder space factor, $x = 0.1, 0.4, 0.8$.
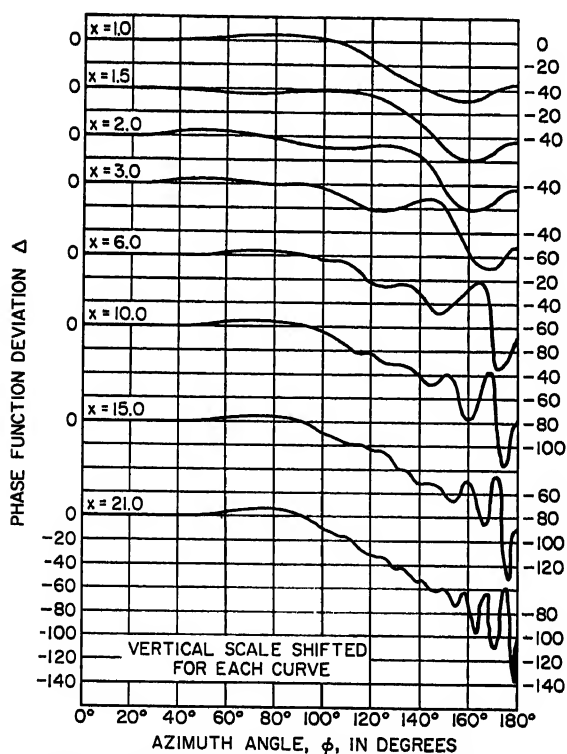
FIG. 8-9. Phase of cylinder space factor, $x = 1.0, 1.5, 2, 3, 6, 10, 15, 21$.

The radiation pattern is omnidirectional, with phase 90° relative to V_0.

The cylinder space factor $M(x,\phi)$ contains all the information pertinent to the radiation characteristic for a slot on a cylinder of any diameter. The relative amplitude of M is plotted as a radiation diagram in Fig. 8-7a to e as a function of ϕ with $ka \sin \theta$, that is, x, as a parameter.[7] x takes on values between 0.1 and 21 in these graphs.

The phase of M is α, which is given by

and

$$\alpha(x,\phi) = \alpha(x,0) - 57.3°x(1 - \cos \phi) + \Delta(x,\phi) \qquad \text{for } \phi \le 90° \qquad (8\text{-}7a)$$

$$\alpha(x,\phi) = \alpha(x,0) - x(57.3° + \phi - 90°) + \Delta(x,\phi) \qquad 90° \le \phi \le 180° \qquad (8\text{-}7b)$$

α is plotted directly in Fig. 8-8 for $x = 0.1$, 0.4, and 0.8. Note that this is the phase of the radiation pattern relative to V_0 for $kr = 2N\pi$. Figure 8-9 is a family of graphs of Δ with x as a parameter between 1.0 and 15.0. The curves are displaced to avoid overlap.

8.6. ANNULAR SLOT

Radiation Characteristics. The radiation characteristics of an annular slot (cut in an infinite ground screen) are identical with those of a complementary wire loop with electric and magnetic fields interchanged. In the case of the small slot the radiation diagram is close to that of a small electric stub in the ground screen.

Consider a thin annular slot, as shown in Fig. 8-10. The polar axis of a spherical coordinate system being normal to the plane of the slot, the magnetic component of the radiated field is

(a)

PLANE OF SLOT
RADIATION DIAGRAM
(b)

FIG. 8-10. Annular slot: (a) Coordinate system. (b) Vertical-plane pattern for small-diameter slot.

$$H_\phi = \frac{aVe^{-jkr}}{120\pi\lambda r} \int_0^{2\pi} \cos (\phi - \phi')e^{jka \sin \theta \cos (\phi - \phi')} \, d\phi' \qquad (8\text{-}8)$$

where a = radius of slot
V = voltage across slot
$k = 2\pi/\lambda$

(a)

(b)
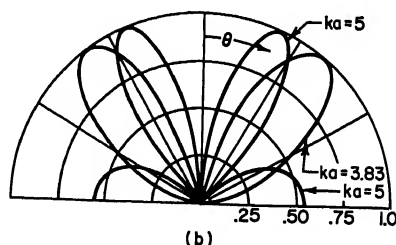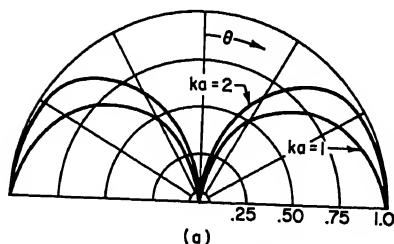
FIG. 8-11. Vertical-plane patterns of annular slot on infinite ground plane: (a) $ka = 1, 2$. (b) $ka = 3.83, 5$.

For small values of a, that is, $a < \lambda/2\pi$,

$$H_\phi = j \frac{Ve^{-jkr}}{60r} \frac{A}{\lambda^2} \sin\theta \qquad \text{amp/meter} \qquad (8\text{-}9)$$

where $A = \pi a^2$ is the included area of the annular slot. Equation (8-9) is valid for small slots of arbitrary shape.

The integral in Eq. (8-8) can be evaluated exactly as[14,15]

$$H_\phi = j \frac{aVe^{-jkr}}{60r} J_1(ka \sin\theta) \qquad (8\text{-}10)$$

where J_1 is the Bessel function of the first kind and the first order. Figure 8-11a and b illustrates the vertical-plane patterns through the polar axis for values of $ka = 1, 2,$ 3.83, 5. It will be noted that a null in the plane of the slot results for $ka = 3.83$, the zero of the Bessel function J_1.

The radiation characteristics on a large but finite ground screen are closely approximated by Eqs. (8-9) and (8-10). There are slight perturbations because of edge effects which result in energy radiated into the shadow region plus modulation of the main radiation pattern. For small-diameter annular slots, the effect on the radiation pattern is essentially the same as discussed in Sec. 3.7.

8.7. NOTCH ANTENNA

The notch, or open-ended slot antenna shown in Fig. 8-12, has been described by Cary[18] and Johnson.[19] It is a broadband radiator which is often used to excite the empennage of aircraft as radiators. For example, the leading edge of a wing or rudder can be used. The theoretical field patterns of a notch in a semi-infinite screen[19] are plotted in Figs. 8-13 and 8-14 in the xz plane
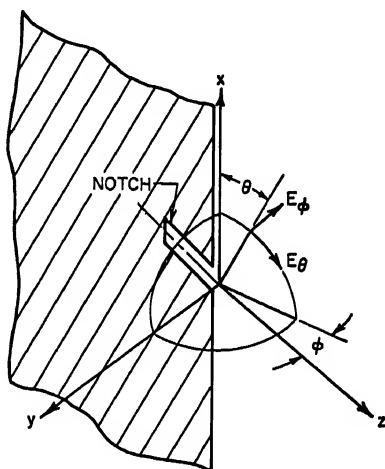
FIG. 8-12. Open-ended slot antenna (notch antenna). (E_θ lies in plane through x axis; E_ϕ lies in plane perpendicular to x axis.)
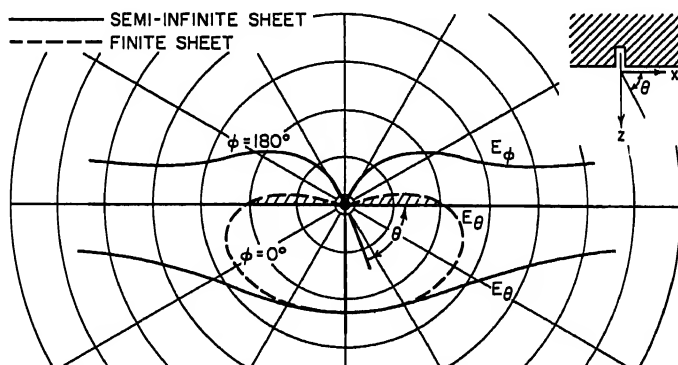
FIG. 8-13. Radiation pattern in xz plane for notch antenna.

of the screen and the plane normal to the screen (*yz* plane), respectively. The dotted graph is an estimate of the pattern in a large but finite sheet. Figure 8-15 shows
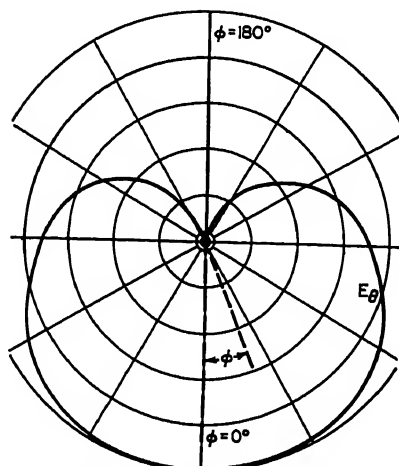
FIG. 8-14. Radiation pattern in *yz* plane for notch antenna.
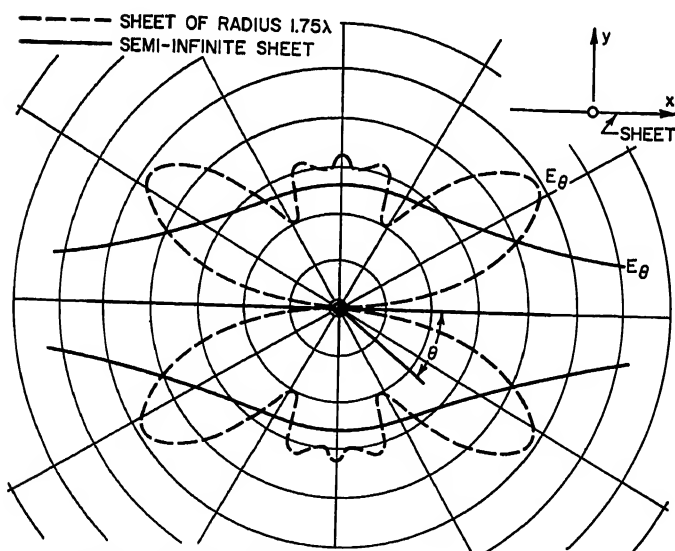
FIG. 8-15. Radiation pattern in *xy* plane for notch antenna.

the field pattern in the *xy* normal plane, which includes the edge for a semi-infinite screen and a semicircular screen of 1.75λ radius.

8.8. IMPEDANCE OF SINGLE SLOT IN FLAT METAL SHEET

The impedance of a slot antenna, in a flat metal sheet, which is free to radiate on both sides, can be obtained directly from the impedance of the complementary wire

antenna using Babinet's principle.[1]   Equation (8-11) gives this relation:

$$Z_{\text{dipole}} Z_{\text{slot}} = \frac{1}{4} \eta^2 = \frac{(120\pi)^2}{4} \tag{8-11}$$

For the specific case of a thin half-wave dipole, we obtain

$$Z_{\text{slot}} = 363 + j210 \tag{8-12}$$

Figure 8-16 shows the measured impedance of a parallel wire-feed rectangular slot with spacing between the feed lines equal to 0.08λ.   Available data with 0.15λ spacing indicate that the fixed feed separation introduces only a small error.   Resonance
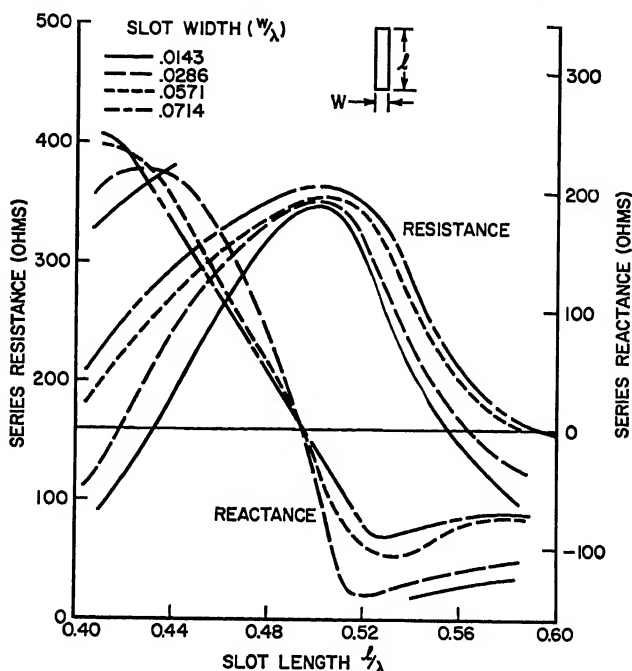
FIG. 18-16. Impedance of thin rectangular slot.

occurs at the frequency for which the slot length is within 2 per cent of a half wavelength.   Measured results show that the resonant frequency is independent of the slot width, for width-to-length ratios as large as 1:5.   It is significant that this resonance phenomenon does not compare exactly with the results of Booker's extension of Babinet's principle.   It is further seen from Fig. 8-16 that the resistance measured with the parallel feed line is fairly close to that obtained from complementary wire antenna impedance [Eq. (8-12)].   Equation (8-11) can be used to obtain the admittance of a short slot antenna in a flat metal sheet and, in particular, the radiation conductance.   The radiation resistance of a short complementary wire dipole with no end loading is given as (Sec. 2.5)

$$R_d = 20\pi^2 \left(\frac{\ell}{\lambda}\right)^2 \tag{8-13}$$

where ℓ is the total length of the short dipole.

It follows that the radiation conductance of the short slot is given by

$$g_s = \frac{1}{180}\left(\frac{\ell}{\lambda}\right)^2 \tag{8-14}$$

The resistance of the center-fed resonant slot antenna is a high impedance (363 ohms). The characteristic impedance of a coaxial feeder is approximately 50 ohms, so that the bandwidth of a coaxial-fed rectangular slot is limited by the impedance transformer design.
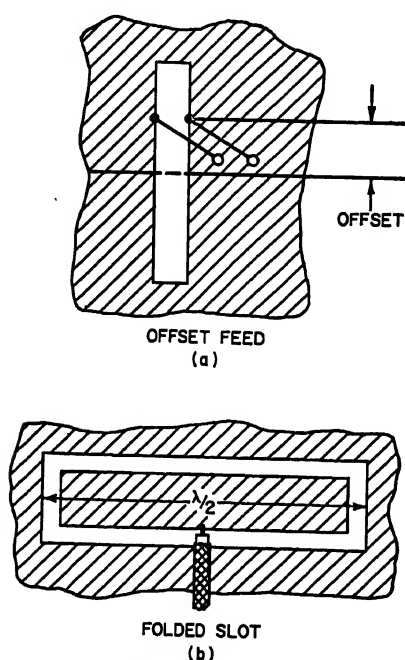
FIG. 8-17. Methods for lowering slot resistance.
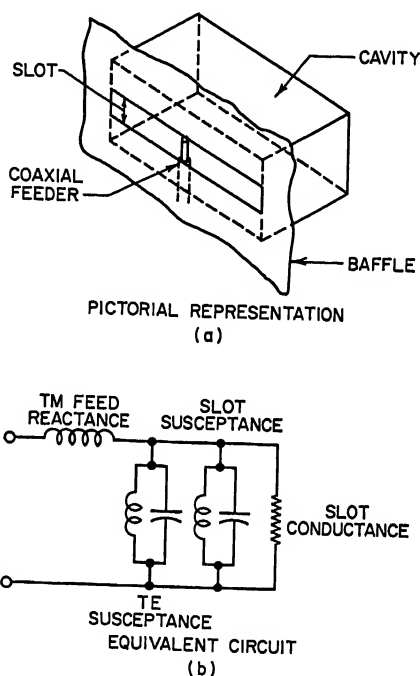
FIG. 8-18. Cavity-backed rectangular slot.

It is possible to transform the slot impedance by feeding the slot at some point off center as shown in Fig. 8-17a. The voltage distribution along the slot is approximately sinusoidal when fed at any point on it, so that the radiation patterns are unaffected. The impedance behavior can be determined from the complementary asymmetrical dipole (Sec. 3.4). Folding the slot as shown in Fig. 8-17b is another method for reducing the slot impedance. The impedance of the complementary wire antenna is quadrupled, so that the impedance of the slot is reduced by a factor of 4 to a value of approximately 100 ohms.

8.9. CAVITY-BACKED RECTANGULAR SLOT

The electric field along cavity-backed rectangular slot (Fig. 8-18a) is not necessarily sinusoidal or related to a complementary wire antenna. The boxed slot antenna can be treated as a cavity resonator which is energized by some transducer and free to radiate out of the slot. The field distribution in the slot therefore is dependent on the relative excitation of the principal and higher-order cavity modes. The equivalent

circuit of a cavity antenna is shown schematically in Fig. 8-18b. The shunt conductance is the radiation conductance of the slot for the given distribution. In the case of the resonant half-wave slot, the conductance is halved by the presence of the cavity since the slot radiates only into half space so that the shunt resistance is approximately 800 ohms. The parallel susceptance is a sum of the shunt susceptance of the slot and the TE mode susceptance of the cavity. The series-resonant circuit is the result of the energy stored in the TM modes in the cavity and feed structure. Alternatively, the energy stored in the shunt circuit and the energy stored in the series circuit correspond to the stored energy in the TE and TM modes, respectively.

In order to obtain a radiation conductance which is commensurate with the dimensions of the slot, a uniform, or at least sinusoidal, distribution of magnetic current must be obtained. This will be the case when the energy stored in the cavity in the vicinity of the slot is primarily in the principal TE mode. It can be achieved by making the cavity dimensions sufficiently large so that the dominant mode is above cutoff, or in the case of the small cavity by means of a distributed edge loading such as a highly capacitive slot. An important design parameter is the antenna Q, the ratio of the dominant-mode stored energy per cycle to the radiated power. The Q will be a minimum when the stored energy is in the dominant mode only. The Q limits the inverse VSWR bandwidth product and for a small cavity is

$$Q = \frac{3}{4\pi^2} \frac{\lambda^3}{V} \tag{8-15}$$

where V is the volume of the cavity expressed in cubic wavelengths. This Q is obtained only if the series reactance shown in Fig. 8-18b is substantially eliminated by proper feed and cavity design. In the case of the capacitive slot-loaded cavity similar to the one shown in Fig. 8-18a, a simple transverse mode does not exist in the cavity. In general, it is extremely difficult to predict accurately the admittance of a cavity antenna.
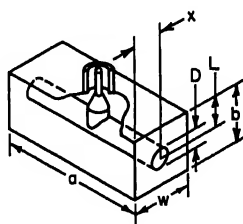
	ANT. I	ANT. II
a	0.62λ	0.65λ
b	0.20λ	0.14λ
w	0.20λ	0.18λ
x	0.073λ	0.070λ
D	0.073λ	0.055λ
L	0.10λ	0.07λ

ANTENNA PARAMETERS
(a)
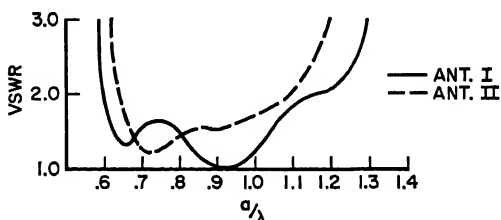
VSWR PERFORMANCE
(b)
FIG. 8-19. T-fed slot antenna.

Some rather wide band designs have been obtained by measuring the input impedance of a waveguide-fed slot antenna and then designing a suitable waveguide to coaxial line transition. One such technique utilizes a T-bar transition[22] as shown in Fig. 8-19a, which gives the dimensions for two such designs. The impedance match which can be obtained with this technique is shown in Fig. 8-19b.

8.10. ADMITTANCE OF ANNULAR SLOT

The optimum excitation of an annular slot, i.e., least stored energy and lowest Q, results when the magnetic-current distribution is uniform around the slot. One

CONDUCTANCE OF ANNULAR SLOT

(a)

SUSCEPTANCE OF ANNULAR SLOT

(b)
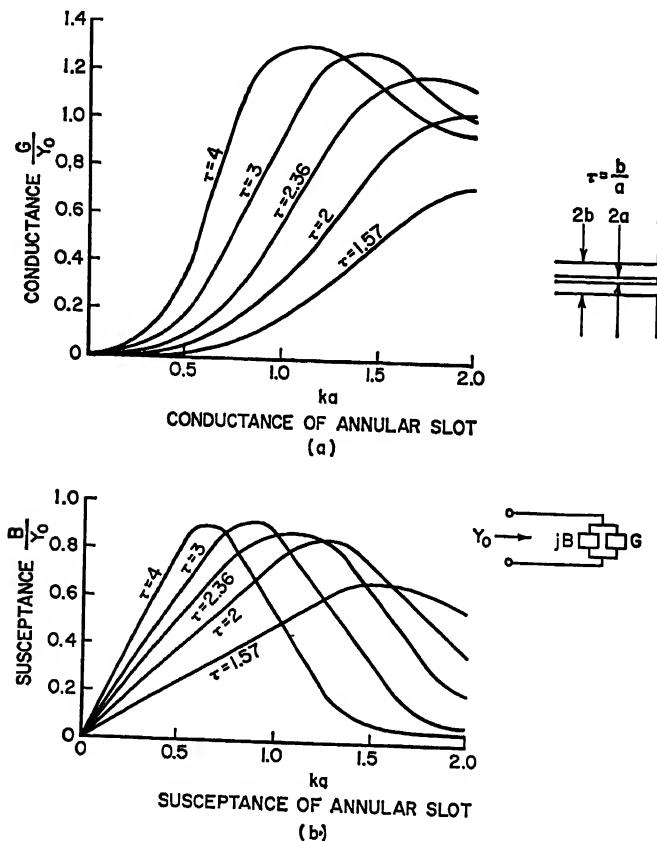
FIG. 8-20. Admittance of coaxial-fed annular slot in infinite ground plane.

method for obtaining this result is to feed the annular slot by a coaxial transmission-line structure which has the same inner and outer diameter as the annular structure. Figure 8-20a and b consists of graphs of the conductance and susceptance in the plane of the aperture relative to the characteristic admittance of the feed line as a function of the radian length ka of the inner radius a. It is seen that the slot is at all times nonresonant and has a capacitive susceptance.

One rather successful design of a cavity-backed annular slot antenna has been developed by Dorne.[16] Some of the details of this design are discussed in Chap. 27.

8.11. NOTCH-ANTENNA IMPEDANCE[19]

The radiation resistance of a notch antenna at the top of the notch is

$$R = \frac{2\eta}{3[C(k\ell) - \cot k\ell \, S(k\ell)]^2} \tag{8-16}$$

where $\eta = 377$ ohms
C and S = even and odd Fresnel integrals, respectively
The reactance appearing in shunt across the mouth of the notch is given by

$$X = jZ_\ell \tan k\ell \tag{8-17}$$

where Z_ℓ, the characteristic impedance of the notch transmission line, is given by

$$Z_\ell = \frac{60\pi^2}{\log_e \dfrac{16\ell}{w} - 1} \tag{8-18}$$

ℓ is the length of the notch, and w its width. Figure 8-21 is a plot of the radiation resistance as a function of ℓ/λ.
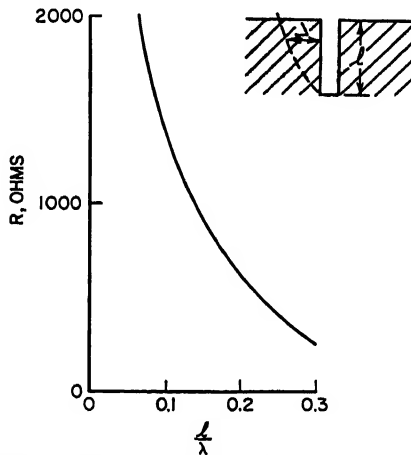
FIG. 8-21. Radiation resistance of notch antenna referred to top of notch.

REFERENCES

1. H. G. Booker: "Slot Aerials and Their Relation to Complementary Wire Aerials," *J. IEE (London)*, pt. IIIA, vol. 93, pp. 620–626, 1946.
2. J. A. Stratton: "Electromagnetic Theory," p. 437, McGraw-Hill Book Company, Inc., New York, 1941.
3. J. L. Putnam, B. Russell, and W. Walkinshaw: "Field Distributions Near a Center Fed Half-wave Radiating Slot," *J. IEE (London)*, pt. III, vol. 95, pp. 282–289, July, 1948.
4. N. E. Lindenblad: "Slot Antennas," *Proc. IRE*, vol. 35, pp, 1472–1479, December, 1947.
5. G. Sinclair: "The Patterns of Slotted Cylinder Antennas," *Proc. IRE*, vol. 36, pp. 1487–1493, December, 1948.
6. S. Silver and W. K. Saunders: "The External Field Produced by a Slot in an Infinite Circular Cylinder," *J. Appl. Phys.*, vol. 21, pp. 153–158, February, 1950.
7. S. Silver and W. K. Saunders: "The Radiation from a Transverse Rectangular Slot in a Circular Cylinder," *J. Appl. Phys.*, vol. 21, pp. 745–749, August, 1950.

8. J. R. Wait: "Radiation Characteristics of Axial Slots on a Conducting Cylinder," *Wireless Engr.*, pp. 316–323, December, 1955.
9. J. Y. Wong: "Radiation Conductance of Axial and Transverse Slots in Cylinders of Elliptical Cross-section," *Proc. IRE*, vol. 41, pp. 1172–1177, September, 1953.
10. J. R. Wait: "Field Produced by an Arbitrary Slot on an Elliptic Cylinder," *J. Appl. Phys.*, vol. 26, pp. 458–463, April, 1955.
11. J. R. Wait: "Electromagnetic Radiation from Sources on and Near Cylindrical Surfaces," *Natl. Bur. Standards (U.S.) Rept.* 5553, January, 1958.
12. A. Alford: "Long Slot Antennas," *Proc. Natl. Electronics Conf.*, vol. 2, pp. 143–155, 1946.
13. S. A. Schelkunoff: "Some Equivalence Theorems of Electromagnetics and Their Application to Radiation Problems," *Bell System Tech. J.*, vol. 15, pp. 92–112, January, 1936.
14. A. A. Pistolkors: "Theory of the Circular Diffraction Antenna," *Proc. IRE*, vol. 36, pp. 56–60, January, 1948.
15. H. Levine and C. R. Papas: "Theory of the Circular Diffraction Antenna," *J. Appl. Phys.*, vol. 22, pp. 29–43, January, 1951.
16. A. Dorne: "Recessed Slot Antenna," U.S. Patent No. 2,644,090, June, 1953.
17. W. S. Lucke: "The Admittance of an Open-ended Coaxial Line in an Infinite Ground Plane," *Stanford Research Inst. Rept.* 11 of *Project* 188, Palo Alto, Calif., June, 1950.
18. R. H. J. Cary: "The Slot Aerial and Its Application to Aircraft," *Proc. IEE (London)*, pt. III, vol. 99, pp. 187–196, July, 1952.
19. W. A. Johnson: "The Notch Aerial and Some Applications to Aircraft Radio Installations," *Proc. IEE (London)*, pt B, vol. 102, pp. 211–218, March, 1955.
20. J. L. Putnam: "Input Impedances of Center Fed Slot Aerials near Half-wave Resonance," *J. IEE (London)*, pt. III, vol. 95, pp. 290–294, July, 1948.
21. N. A. Begovich: "Slot Radiators," *Proc. IRE*, vol. 38, pp. 803–806, July, 1950.
22. Radio Research Laboratory Staff: "Very High Frequency Techniques," chap. 7, McGraw-Hill Book Company, Inc., New York, 1947.

Chapter 9

SLOT-ANTENNA ARRAYS

M. J. Ehrlich

Microwave Radiation Co., Inc.
Gardena, California

9.1. INTRODUCTION

The use of linear arrays as line sources to provide shaped broadside beams or end-fire beams has been treated in considerable detail in previous chapters, and the reader's familiarity with the material is assumed in the following sections of this chapter. The topics of interest covered in the foregoing material are (1) arrays of linear elements (Chaps. 2 and 5), (2) pattern synthesis techniques (Chap. 2), (3) pattern analysis (Chap. 2), and (4) slot antennas (Chap. 8).

The use of line-source radiators has been greatly extended with the expanded use of microwave frequencies. Line sources have been used as (1) primary feeds to illuminate large cylindrical reflectors, (2) vertically disposed radiators to obtain omnidirectional patterns in the azimuthal plane for beacon requirements, (3) flush-mounted, end-fire radiators for high-speed air-borne applications, and (4) flush-mounted, two-dimensional arrays to obtain shaped-broadside or near-broadside patterns for airborne use. These are but a few of the many applications that have been made of line-source arrays.

The material presented in this chapter is primarily concerned with the design of line-source arrays for use at microwave frequencies, wherein slots cut in the walls of a rectangular waveguide are used as individual radiating elements to form the array.

If the slots are very closely spaced so that mutual-coupling effects dominate the

design problem, it is sometimes advantageous to discard the idea of an array of individually excited elements and use instead the notion of a traveling or surface wave along a periodic interface. This type of slot array is treated in Chap. 16 on Surface-wave Antennas.

9.2. WAVEGUIDE-FED SLOT RADIATOR

A cylindrical waveguide in which a single mode is propagated may be represented by an equivalent two-wire transmission line whose phase velocity and characteristic impedance*[1] can be specified as a function of frequency and waveguide dimension.

The surface current flow along the inner walls of the waveguide that is associated with the propagation of the TE_{10} mode in rectangular waveguide is shown in Fig. 9-1.

———— ELECTRIC FIELD

------ MAGNETIC FIELD

— — — CURRENT LINES
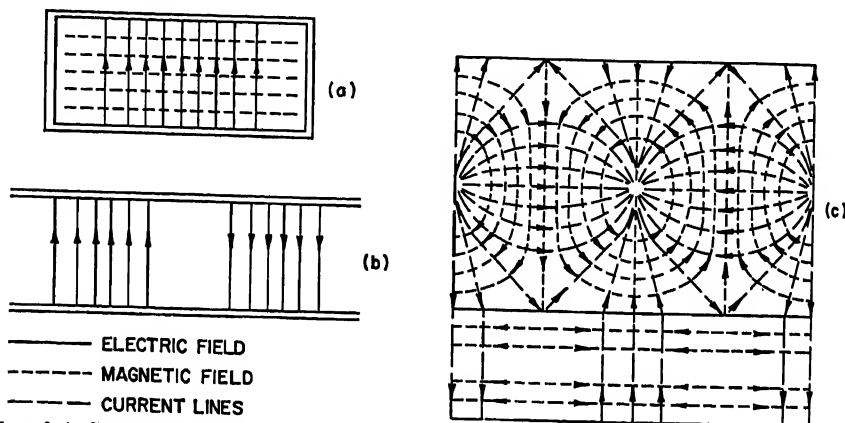
FIG. 9-1. Surface current distribution for rectangular waveguide propagating TE_{10} mode: (a) Cross-sectional view. (b) Longitudinal view. (c) Surface view.

The surface current J at the inner surface of the waveguide is given by the

$$\bar{n} \times \bar{H} = \bar{J}$$

where $\bar{n}$ = inner surface normal

$\bar{J}$ = surface current

$\bar{H}$ = magnetic field at surface

The distribution of electric and magnetic field within the radiating thin half-wave slot has been discussed in Chap. 8, and it is evident from an examination of the fields in the slot that a slot cut into a wall of a waveguide will perturb the current distribution and couple energy out of the waveguide, if it is so aligned that a transverse component of surface current flow exists across it. When the slot is cut into the waveguide as shown in Fig. 9-2, it interrupts the flow of transverse current and couples energy from the waveguide mode to free space. Examples of nonradiating slots cut in rectangular waveguide, i.e., aligned parallel to the surface current vector, are shown in Fig. 9-3.

The magnitude of the coupling of the slot to the waveguide mode is a function of the component of the slot length perpendicular to the current lines, current density at the center of the slot, slot dimensions, waveguide transverse dimensions, waveguide wall thickness, and frequency. The equivalent representation and impedance characteristics of the slot radiators are presented in the following sections.

* The characteristic impedance of a waveguide cannot be uniquely specified and may be specified by any one of a number of definitions.
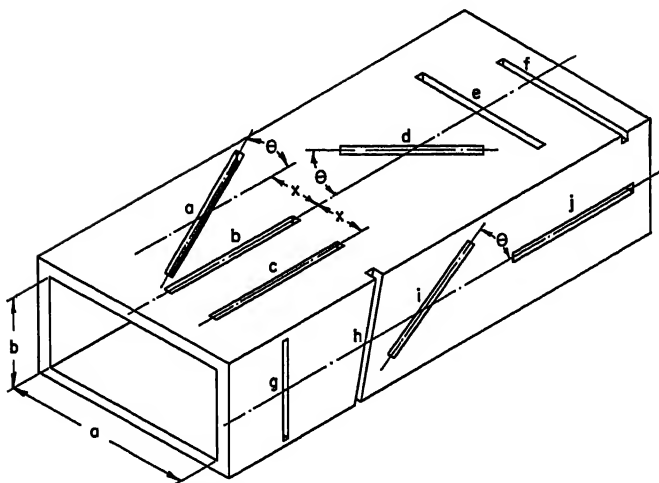
FIG. 9-2. Radiating slots cut in the walls of a rectangular waveguide.
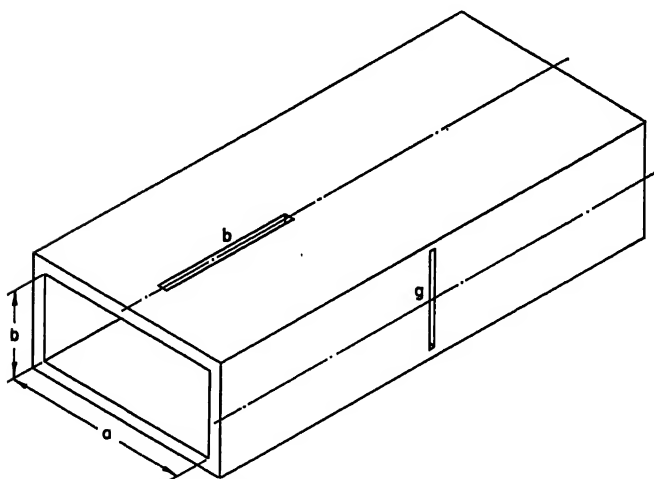
FIG. 9-3. Nonradiating slots cut in the walls of a rectangular waveguide.

9.3. SLOT IMPEDANCE CHARACTERISTICS AND EQUIVALENT REPRESENTATION

The current flow lines interrupted by slots at several different locations are shown in Fig. 9-2. Slots c, h, i, and j are coupled to the transverse current flow only and may be represented as simple two-terminal shunt elements. Slot d is coupled to the longitudinal and transverse currents. However, the transverse currents are in opposite directions on either side of the centerline, and their net contribution is zero. Slot d may then be represented as a simple two-terminal series element. Slot a is coupled to both transverse and longitudinal currents and cannot be represented by a simple series or shunt network. Slots e and f couple only to the longitudinal currents and

are represented as simple two-terminal series elements. The equivalent representation of some of the slots is shown in Fig. 9-4.
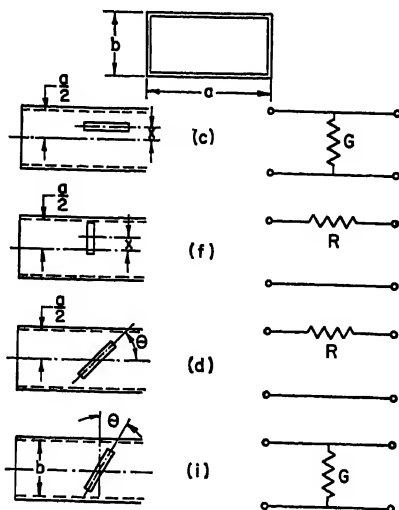
FIG. 9-4. Equivalent-network representations of slot radiators.

The values of the resistance and conductance for the various slots have been determined by Stevenson[2] when the slots are at the first resonance, i.e., when the reactance or susceptance is zero. Stevenson's results give:

1. Conductance of the longitudinal shunt slot in the broad face (slot c in Fig. 9-4):

$$g = g_1 \sin^2 \frac{\pi x}{a} \tag{9-1}$$

$$g_1 = 2.09 \frac{\lambda_g}{\lambda} \left(\frac{a}{b}\right) \cos^2 \frac{\pi \lambda}{2\lambda_g} \tag{9-2}$$

where λ = free-space wavelength

    λ_g = guide wavelength for the TE_{10} mode

2. Resistance of a centered inclined series slot on the broad face (slot d of Fig. 9-4):

$$r = 0.131 \left(\frac{\lambda}{\lambda_g}\right) \frac{\lambda^2}{ab} \left[I(\theta) \sin \theta + \frac{\lambda_g}{2a} J(\theta) \cos \theta \right]^2 \tag{9-3}$$

$$\left.\begin{array}{c} I(\theta) \\ J(\theta) \end{array}\right\} = \frac{\cos (\pi \xi / 2)}{1 - \xi^2} \pm \frac{\cos (\pi \eta / 2)}{1 - \eta^2} \tag{9-4}$$

$$\left.\begin{array}{c} \xi \\ \eta \end{array}\right\} = \frac{\lambda}{\lambda_g} \cos \theta \mp \frac{\lambda}{2a} \sin \theta \tag{9-5}$$

3. Conductance of the short slot on the narrow face (slot i of Fig. 9-4):

$$g = \frac{30}{73\pi} \left(\frac{\lambda_g}{\lambda}\right) \frac{\lambda^4}{a^3 b} \left[\frac{\sin \theta \cos \left(\frac{\pi \lambda}{2\lambda_g} \sin \theta\right)}{1 - \left(\frac{\lambda}{\lambda_g}\right)^2 \sin^2 \theta} \right]^2 \tag{9-6}$$

4. Resistance of the transverse displaced series slot on the broad face (slot f of Fig. 9-4):

$$r = r_0 \cos \frac{\pi x}{a} \tag{9-7}$$

$$r_0 = 0.523 \left(\frac{\lambda_g}{\lambda}\right)^3 \frac{\lambda^2}{ab} \cos^2 \frac{\pi\lambda}{4a} \tag{9-8}$$

These results were derived by the use of several assumptions, among which are those of (1) perfectly conducting, infinitely thin waveguide walls and (2) no radiation on the half space behind the plane containing the slotted waveguide wall. The assumptions are not realized in a physical waveguide, and hence the measured values of g and r depart slightly from the calculated values. In practice, the measured data are used for design purposes and the theoretical results are used primarily to provide a basis for scaling data to frequency regions and/or to waveguide sizes where measured data are not available.

9.4. EXPERIMENTAL DATA ON WAVEGUIDE-FED SLOT RADIATORS

Longitudinal Shunt Slots. Extensive experimental studies of the impedance characteristics of a waveguide-fed slot radiator have been performed since 1943, and the data primarily used for design are given in Figs. 9-5 to 9-16.

The conductance and susceptance of a displaced longitudinal shunt slot are shown in Fig. 9-5, and agreement with the theoretical results is quite good.
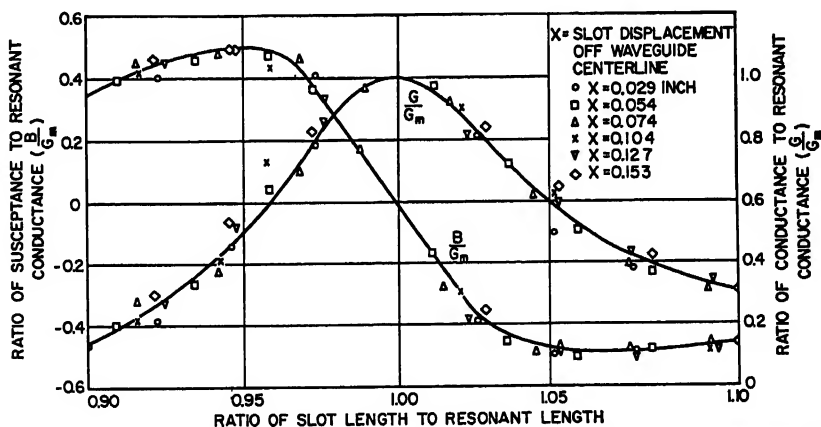
Fig. 9-5. Admittance of a longitudinal shunt slot as a function of frequency: $f = 9,375$ Mc, slot width = 0.0625 in. RG52/U waveguide.

The variation of the slot admittance with frequency is shown in Fig. 9-6 for several values of slot width as measured in a larger waveguide in the 3,000-Mc region. It is seen that an increase in the width of the slot increases the usable bandwidth of the slot. The increase in slot bandwidth thus obtained is analogous to the increase in bandwidth of an electric dipole that is achieved by an increase in the dipole width.[3] It will be pointed out in a later portion of this chapter that it is usually not feasible to obtain bandwidth by increase of slot width when the array is more than several wavelengths in extent.
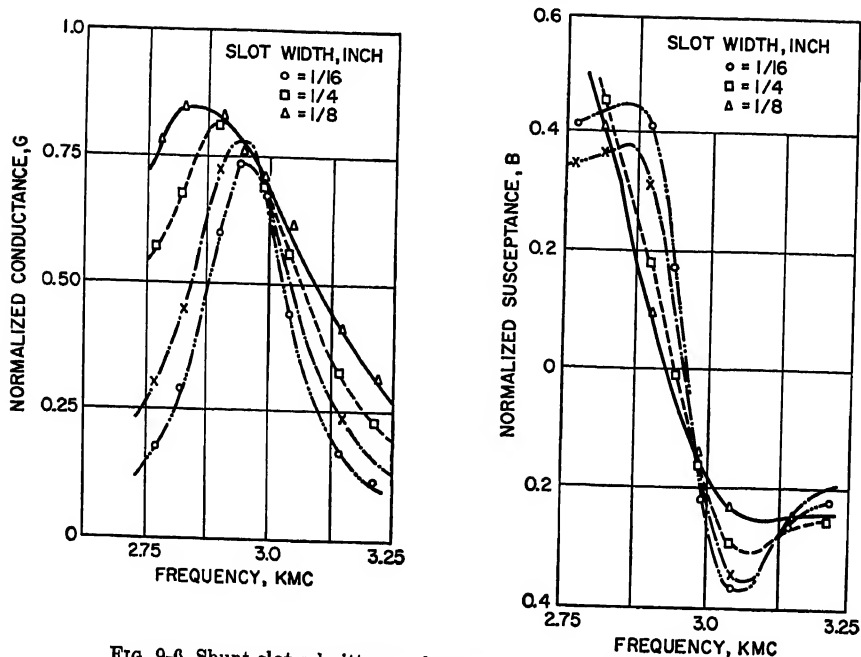
Fig. 9-6. Shunt-slot admittance characteristics: RG48/U waveguide.
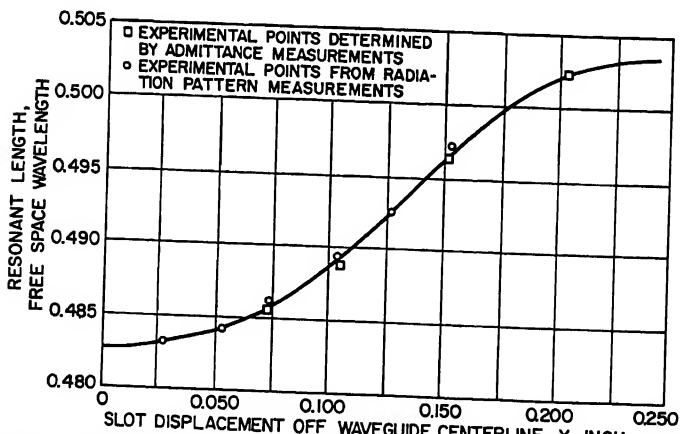
Fig. 9-7. Shunt-slot resonant length as a function of displacement off waveguide centerline: slot width = 0.0625 in.   RG52/U waveguide.

The resonant length of the longitudinal displaced shunt slot has been found to be a function of its displacement from the center of the waveguide,[4] and the data are shown in Fig. 9-7.   The variation of resonant length with frequency for a fixed value of displacement is given in Fig. 9-8.   The resonant length for any value of displacement at a particular frequency in the range of Fig. 9-8 is then readily obtained from Figs. 9-8 and 9-9.
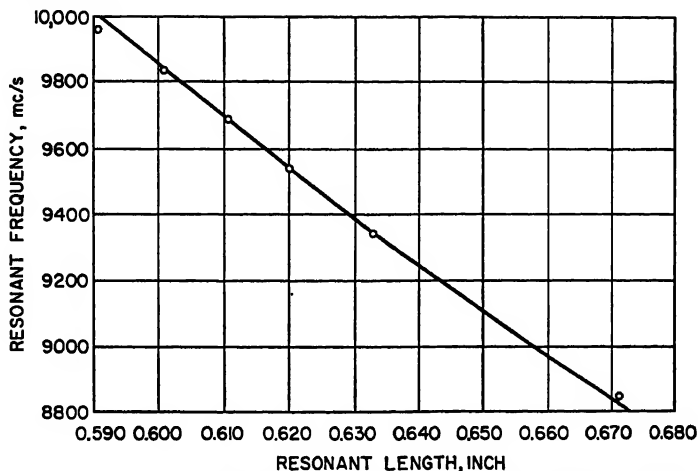
FIG. 9-8. Shunt-slot resonant length as a function of frequency (points are measured; curve is semiempirical): Slot width = 0.0625 in., slot displacement x = 0.2040 in.   RG52/U waveguide.
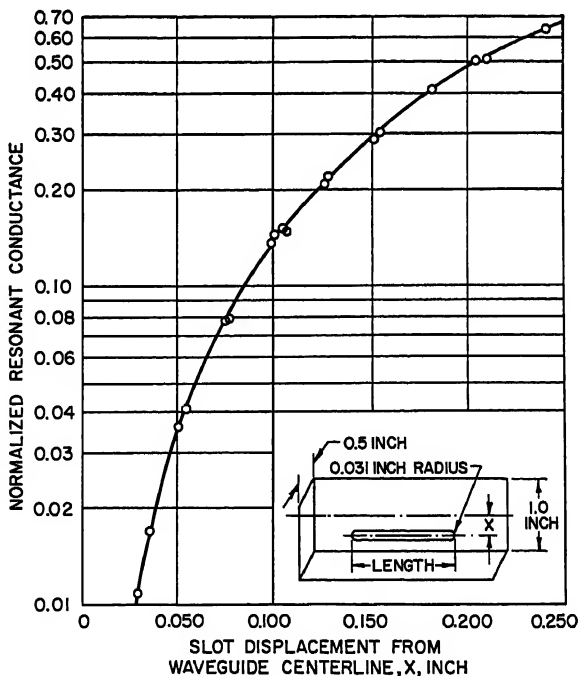
FIG. 9-9. Resonant conductance of longitudinal shunt slot as a function of slot displacement (points are measured; curve is semiempirical): f = 9,375 Mc, slot width = 0.0625 in. RG52/U waveguide.

It is noted from (Eq. 9-2) that the conductance at resonance of a longitudinal shunt slot is a function of frequency and waveguide transverse dimensions. The conductance obtainable from a resonant slot falls off quite rapidly with an increase in frequency. The variation of conductance with frequency for a resonant longitudinal shunt slot cut in standard RG-52-U rectangular waveguide is shown in Fig. 9-10. It may prove difficult in the design of a short linear array, which contains a small number of high-conductance slots, to obtain the specified conductance values when the waveguide is operated at the high end of its specified frequency range.

It is a simple matter to extend the data for a slot from one frequency where data are available to a new frequency where data are unavailable. The resonant conductance G is determined from Fig. 9-10, which is plotted for one specific value of displacement, 0.1833 in. Then

$$G = A \sin^2 \frac{\pi x}{a} \qquad (9\text{-}9)$$

where x = displacement of slot.

The equation thus determines the constant of proportionality which relates resonant conductance to displacement for the new frequency in waveguides of the same a/b ratio. The resonant slot length is then determined from Figs. 9-8 and 9-9. When the new guide has an a/b ratio different from that of the waveguide of Fig. 9-8, the constant A of Eq. (9-9) is multiplied by the old b/a ratio times the new a/b ratio.

FIG. 9-10. Resonant conductance of longitudinal shunt slot as a function of frequency: Slot width = 0.0625 in., slot displacement $x = 0.1833$ in. RG52/U waveguide.

It is evident from an examination of Figs. 9-1 and 9-2 that the phase of the radiated field is changed 180° by moving the slot across the centerline of the waveguide. Hence, two slots one-half wavelength apart along the guide can be made to radiate in phase by being placed on opposite sides of the centerline.

The resonant conductance of a longitudinal shunt slot as a function of frequency has been measured by several investigators, notably Watson,[5] Cullen,[6] and Stegen,[7] and a spread of approximately 10 per cent exists between the various results. Essentially equivalent-array performance is obtained when the array is designed utilizing any one set of available data. This is particularly true in the larger arrays wherein small conductances, i.e., small displacements, are used and dimensional tolerances introduce random variations which tend to smooth out small performance differences that exist between arrays designed on the basis of the various sets of slot data.

Edge Slots. The great majority of linear, waveguide-fed slot arrays designed to date have used either longitudinal shunt slots on the broad face or shunt slots on the narrow face. Designs using the former somewhat outnumber designs using the latter. Edge slots are used when a polarization parallel to the long axis of the waveguide is desired. Longitudinal slots are used to provide a polarization perpendicular to the long axis of the waveguide. When the polarization may be either horizontal or vertical, the choice of slot is controlled by fabrication difficulties, number of slots in the array, cross-polarization requirements, off-axis lobes, etc.

The conductance of an edge slot may be expressed as

$$G \approx G_0 \sin^2 \theta \qquad \theta < 15° \qquad (9\text{-}10)$$

Since the narrow dimension of the waveguide is substantially less than a half free-space wavelength, the slot is wrapped around the broadsides to obtain the required length for resonance. The small-angle, that is, $\theta < 15°$, edge slot is shown in Fig. 9-11.

The series component added to the equivalent-network representation of the slot by the presence of the portions of the slot on the top and bottom faces is usually
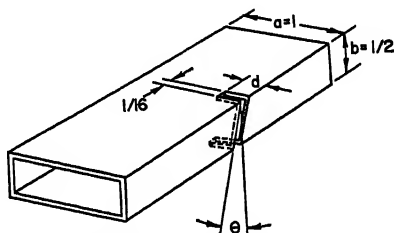
FIG. 9-11. Edge slot in rectangular waveguide (all dimensions are in inches): RG52/U waveguide.
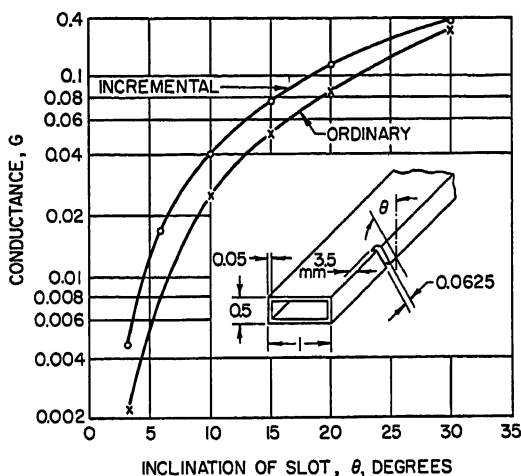
FIG. 9-12. Incremental and single-slot conductances (unmarked dimensions of waveguide section are in inches): $f = 9,375$ Mc. RG52/U waveguide.

neglected in design. The phase of the radiated field of the slot may be changed 180° by inclination on the other side of the vertical centerline. Two slots one-half guide wavelength apart in the guide can be made to radiate in phase by being inclined on opposite sides of the vertical centerline.

The edge slots in a long array, that is, $\theta < 15°$, are aligned nearly parallel to one another, and strong mutual coupling exists between the slots. Hence the conductance value for a single edge slot differs markedly from that of an edge slot in the presence of neighboring edge slots. Since the edge-slot array has many slots, the value of slot conductance used in design must take mutual-coupling effects into account. Stevenson[8] has defined an incremental conductance, i.e., the increase in the conductance of a group of resonant, half-wave-spaced, parallel edge slots when another slot is added to the group, as the value for use in array design. The single-slot data and incremental-conductance data are shown in Fig. 9-12. It is evident upon consideration that the incremental-conductance data are valid, in a design sense, only for slots well removed

from the ends of the array. The conductance of the slots near the ends of the array lies somewhere between that of the single slot and that of the incremental slot. In a long array, errors introduced by the uncertainty as to the exact values of the end-slot conductances are negligible. In a short array, serious error is introduced. A cut-and-try procedure is recommended for a short array when performance is to be optimal.

Relatively little data are available for the design of edge-slot arrays, and considerable use of scaling techniques must be employed. The conductance curves are closely approximated by Eq. (9-10). The variation of resonant length with frequency is quite small and is usually neglected. The slot admittance is insensitive to variation in the depth of cut. Hence, if the incremental conductance is obtained by experiment for one value of θ at the specified frequency for a particular waveguide, a $\sin^2 \theta$ curve may be fitted to the point to obtain a reasonably accurate design curve of conductance vs. angle of inclination. This scaling technique has been employed with considerable success in design in the past. The over-all edge-slot length, including the portion on the broad faces, is adjusted to be approximately one-half free-space wavelength to obtain the resonant length. The variation of slot admittance with depth of cut into the broad faces is shown in Fig. 9-13.
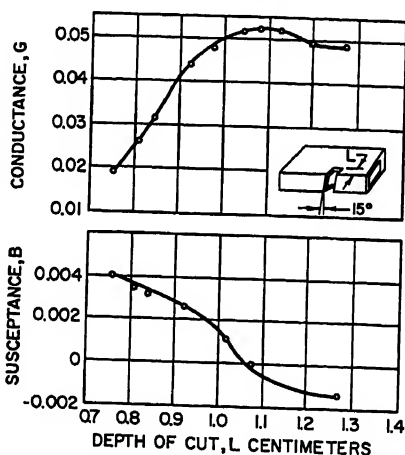
Fig. 9-13. Variation of slot admittance with depth of cut: $f = 2,800$ Mc, $\lambda = 10.7$ cm. RG48/U waveguide.

The incremental conductance is a function of the narrow dimension of the waveguide. Relatively slight changes in thickness cause large changes in the conductance, and considerable caution is to be exercised in scaling data to a waveguide of different a/b ratios. An experimental study of one slot, at an angle of 10 or 15° in the new waveguide, is recommended as the basis for obtaining a design curve for the new waveguide. The principal difficulties encountered in the use of edge slots in arrays are (1) lack of accurate slot data for slots near the end of the array and (2) excessive cross-polarization components. The first difficulty has been discussed previously, and the second is treated in Sec. 9.7.

Series slots in the broad face radiate a wave whose polarization is essentially transverse to the longitudinal axis of the waveguide. However, the slot also radiates a component polarized parallel to the long axis of the waveguide. The cross-polarization component is usually an undesirable feature of the array, and a substantial design effort is necessary to completely remove the unwanted component.

The resonant length and normalized resistance of series slots for three different angles are given in Fig. 9-14. The agreement with the theoretical values is quite good.

The phase of the radiated field can be changed 180° by rotation of the slot across the longitudinal axis of the waveguide. Two slots one-half guide wavelength apart along the waveguide may be made to radiate in phase by being rotated in opposite senses across the longitudinal axis of the waveguide.
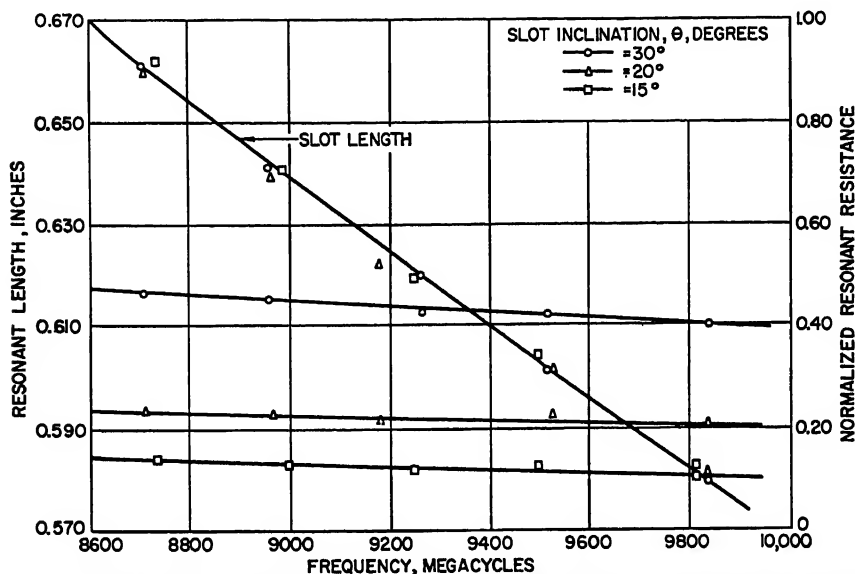
FIG. 9-14. Resonant length and normalized resistance as a function of frequency for series-inclined slot on centerline of waveguide. RG52/U waveguide.

9.5. DESIGN OF WAVEGUIDE SLOT ARRAY

The array design requirements are usually specified in terms of desired beamwidth, side-lobe levels, gain, polarization, cross-polarization levels, power-handling capability, input VSWR, size and weight, and not infrequently, allowable aerodynamic configuration. The design problem consists of (1) determination of the excitation coefficients of the individual slots to achieve the required performance and (2) determination of the slot dimensions and spacings or angles of inclination to achieve the required excitation coefficients and input VSWR. The first problem has been treated in Chap. 2, and more detailed treatments are listed in the bibliography.[9–12] The problem of concern here is to specify slot dimensions, etc., when the excitation coefficients have been determined.

The design techniques herein presented are basically as developed by Stegen.[13] The array design is predicated upon the assumption of negligible external mutual coupling between the slot radiators forming the array. This assumption is valid for longitudinal shunt slots on the broad face of the waveguide[14] and series slots on the broad face of the waveguide when the angle of inclination is small; that is, $\theta < 15°$. It is valid in a special sense for edge shunt slots in that the use of the incremental-conductance data has perforce taken mutual coupling into account.

An array of longitudinal shunt slots on the broad face of a rectangular waveguide is represented by a two-wire line and shunt loads as shown in Fig. 9-15. The Y_i are the normalized admittances of the various elements. Y_i^+ and Y_i^- are the normalized admittances looking toward the load end of the array, on the right and left sides of
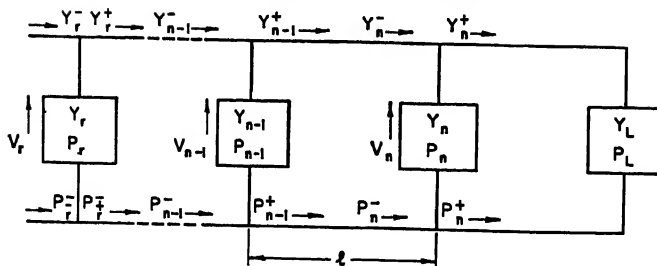
Fig. 9-15. Equivalent-network representation of a shunt slot array.

the ith element, respectively. P_i is the power radiated by the ith element, and l is the interelement spacing, a constant along the array in most designs. Then

$$V_{n-1} = V_n(\cosh \gamma l + Y_n^- \sinh \gamma l) \tag{9-11}$$
$$V_{n-2} = V_{n-1}(2 \cosh \gamma l + Y_{n-1} \sinh \gamma l) - V_n \tag{9-12}$$
$$V_i = V_{i+1}(2 \cosh \gamma l + Y_{i+1} \sinh \gamma l) - V_{i+2} \tag{9-13}$$

where $\gamma = \alpha + j\beta$, the complex propagation constant of the unloaded line. The conductance required at the ith element is

$$G_i = G_i^+ \frac{P_i}{P_i^+} \tag{9-14}$$

where

$$P_i^+ = P_{i+1} \left[e^{2\alpha l} + \frac{2|\Gamma_{i+1}|^2 \sin 2\alpha l}{1 - |\Gamma_{i+1}|^2} \right] \tag{9-15}$$

$$Y_i^+ = G_i^+ + jB_i^+ = \frac{Y_{i+1}^- \cosh \gamma l + \sinh \gamma l}{\cosh \gamma l + Y_{i+1}^- \sinh \gamma l} \tag{9-16}$$

$$Y_i^- = Y_i - Y_i^+ \tag{9-17}$$

and $|\Gamma_i|$ = absolute value of the reflection coefficient at the ith element.

The ratio of the field across a longitudinal shunt slot to the total field across the waveguide has been found to be

$$\frac{E_S}{E_T} = \frac{jAY}{\cos (\pi x/a)} \tag{9-18}$$

where A = positive real constant

Y = slot admittance

Values are chosen for Y_L and Y_n. In a long array, Y_L, the waveguide termination, is chosen to be 1.0. In a short array or a narrow-band array, Y_L is usually 0, that is, a short circuit spaced one-quarter wavelength from Y_n.

The phase of the slot admittance ϕ is given by

$$\phi = \tan^{-1} \frac{B}{G} \tag{9-19}$$

The value of G_{n-1} is calculated using Eq. (9-14), and Y_{n-1} is calculated using Eqs. (9-11), (9-16), (9-18), (9-19), and the phase of radiation specified by the excitation coefficient. The remaining Y_i are then computed in a similar manner. The expressions are much simplified when a lossless waveguide is assumed. The simplified equations yield good design data when the array is not too long. When the waveguide attenuation loss becomes a significant fraction of the total input power, the original equations must be used.

Previous design experience has indicated that it is desirable to use resonant slots and to avoid beam-shaping techniques where the phase of the nonresonant slot is changed from slot to slot in order to obtain a specific beam shape. It is customary to utilize a constant phase difference between consecutive slots in the design of arrays.

A somewhat unfortunate confusion* has arisen in the use of the terms "resonant array" and "nonresonant array." The term resonant array is used to describe an array whose elements are spaced one-half guide wavelength apart, and the term non-resonant array is used to describe an array whose elements are spaced slightly greater or smaller than a half guide wavelength apart. The design of a nonresonant array will be considered first.

A nonresonant spacing is used to achieve a large bandwidth for the array, both for the radiation pattern and input VSWR. Since there is a constant phase difference between elements, resulting in a progressive phase shift along the array, the phase front is inclined at an angle θ' to the normal to the waveguide where θ' is given by the relation

$$\sin \theta' = \frac{\lambda}{\lambda_g} - \frac{\lambda}{2\ell} \qquad (9\text{-}20)$$

where λ_g = guide wavelength
      ℓ = interelement spacing

As the frequency is increased, the beam moves in angle toward the load end. Hence the beam peak position is frequency-dependent. As the frequency is reduced to a point where the beam peak is very close to the broadside position; that is, $\theta' \approx 0$, an increase in VSWR, will result. The nonresonant array achieves its large impedance bandwidth by virtue of the phase differences between the reflections from the various slots. The phase differences which arise from the nonresonant spacing cause the resultant sum of all the reflected waves to be quite small; that is, the input VSWR is near unity. The termination must be a matched load and will absorb a fraction of the input power. The amount of power absorbed in the load is a function of the bandwidth, realizable slot conductance, etc. It is usually chosen to be about 5 to 10 per cent of the input power at mid-band. The design of a nonresonant spaced array using resonant slots is presented in the following:

1. Y_L is chosen to be 1.0 by use of a matched load.
2. Y_n is chosen to be less than 0.1.
3. Then $Y_n^- = Y_n + 1.0$.
4. Y_{n-1}^+ is calculated from Eq. (9-16).
5. G_{n-1} is calculated from Eqs. (9-14) and (9-15) where the P_i are specified by the squares of the excitation coefficients.
6. The remainder of the G_i are calculated in a similar manner.

It may develop during the course of the calculation that the computed conductances for the slot in the middle of the array are too large to be achieved. If such is the case, more power must be dissipated in the load, that is, Y_n made smaller and the G_i recomputed. A design criterion is given by

$$G_{\max}^2 \csc^2 \beta\ell \leq 0.2 \qquad (9\text{-}21)$$

where $G_{\max}$ is the largest slot conductance in the array $\beta = 2\pi/\lambda_g$ and ℓ is the element spacing. If series slots are used, currents replace voltage and impedances replace admittances.

---

* This confusion has arisen because resonant slot elements are used in both types of array. Actually, the resonant array derives its name from the similarity of its input impedance behavior to that of a resonant circuit in the vicinity of frequencies where the slot spacing is exactly a half wavelength.

A resonant spaced array may be regarded as a special case of a nonresonant spaced array. The resonant array has a very small bandwidth of the order of $\pm 50\%/n$, where n equals the number of slot radiators in the array. In an n-element array, where the slots are spaced one-half guide wavelength apart, with adjacent elements on opposite sides of the longitudinal axis so as to radiate in phase, Eq. (9-13) simplifies to

$$V_i = V_n \left(1 + \alpha l \sum_{s=1}^{n} s\, Y_{i+s} \right) \tag{9-22}$$

If attenuation is neglected,

$$V_i = V_n$$

Then $$P_i = |V_i|^2 G_i \tag{9-23}$$

and $$G_i = G_n \frac{P_i}{P_n} = \frac{P_i \displaystyle\sum_{m=1}^{n} G_m}{\displaystyle\sum_{m=1}^{n} P_m} \tag{9-24}$$

The input admittance Y_{in} is

$$Y_{\text{in}} = \sum_{i=1}^{n} Y_i \tag{9-25}$$

The procedure used for the design of a resonant spaced array is as follows:

1. Choose the desired value of input admittance when the termination load is an open circuit. Usually Y_{in} is chosen to be 1.0, or

$$\sum_{m=1}^{n} G_m = 1.0 \qquad \sum_{m=1}^{n} j\beta_m = 0$$

2. Determine the relative power P_i to be radiated by each slot; i.e., determine the excitation coefficients.

3. Determine G_i from Eq. (9-24).

If series slots are used, the resistance of each slot is determined in an identical manner.

9.6. LONGITUDINAL-SHUNT-SLOT ARRAY DESIGN

The basic technique for the determination of the individual slot conductances has been presented in the foregoing sections. Once the operating frequency has been determined and bandwidth requirements have been specified, the slot resonant length and slot displacement are obtained from the curves presented in Figs. 9-5 to 9-9. The design of the slot array is then complete. However, the design problem has been presented in a simplified manner and some of the complications that may exist in an actual shunt-slot array design will now be treated.

One of the difficulties in the design of a shunt-slot array is that the designer may obtain the required side-lobe level in the principal planes of the antenna without obtaining the required side-lobe level over the full hemisphere. It has been experimentally and theoretically determined[15,16] that side lobes exist off the principal planes, approximately at the 45° angles, which usually are considerably larger than the side lobes in the principal planes. These off-axis, or "squint," side lobes arise from the fact that the shunt slots are not in one straight line but are staggered on either side

of the longitudinal centerline of the waveguide. Thus a region exists wherein these contributions add in phase off the principal axes of the pattern to form large secondary lobes. It is possible to define a new exit aperture for the longitudinal-shunt-slot array by fitting a long E-plane horn to the array, i.e., providing a pair of flared sheets, one on either side of the waveguide. In the new aperture thus delineated by the exit face of the horn, the distribution is essentially uniform in the transverse direction and the largest side lobes will be encountered in the principal planes. However, the use of a horn or parallel-plate media to achieve the new exit aperture will modify the conductance values obtained from the slots as compared with the values obtained when the horn plates are absent. Thus the slot conductances must be measured for slots, for several different values of displacement over the operating frequency band, in the presence of the horn plates, to obtain data from which design curves can be scaled with a reasonable degree of accuracy. Further complications arise from the use of the parallel-plate media in that the mutual coupling between the individual slots is markedly increased by the presence of the plates, and conductance values are again altered. These phenomena do not produce severe pattern deterioration in the long array, but do alter the performance in a short array.

It has been noted in the measurements of the radiation pattern of a single slot on a waveguide[17] that the peak of the radiation pattern of a single slot is shifted off the normal as the slot is displaced with respect to the longitudinal axis of the waveguide. Hence the contributions of the large conductance slots, i.e., large displacement slots, to the radiation pattern of the total array are not quite in agreement with what is to be anticipated in theoretical calculations since the peak of their radiation is not directed in the principal plane but is slightly skewed in angle.

A further factor which causes additional discrepancy between measured and calculated results is the change in slot conductance arising from the departure of the slot dimensions from the theoretical dimensions.[18] The variation in slot dimensions from the computed values arises from the requirements for manufacturing tolerances on all dimensions. The variation of performance as a function of manufacturing tolerances has received considerable theoretical treatment and experimental verification in the last few years,[19-21] and good agreement is obtained between theoretical calculations and measured results as to the deterioration in array performance (see also Sec. 2.12).

The foregoing comments relative to the deterioration of measured pattern performance as compared with the calculated values have been given to forcibly impress upon the designer the necessity for an overdesign of the array in order to achieve specified levels. The problem may be restated in a more succinct form. Relatively little overdesign is required to obtain the calculated half-power beamwidth value, but the smaller the side-lobe level that is required, the greater the overdesign that must be allowed in the array distribution to achieve the specified value of side-lobe level. An example will serve to illustrate the point. If, for the moment, the effect of manufacturing tolerances alone is considered and the performance of a 24-element array is examined, it is found that an array designed for 20-db side-lobe level has a very high probability that one side lobe will be approximately $-18\frac{1}{2}$ db. An array designed for -30-db side-lobe level will display a -26-db side lobe, and an array designed for a -40-db side lobe will have a high probability of side lobes of the order of -32 db. The overdesign requirement increases in magnitude as the side-lobe level requirement is increased, and the second-order effects that can be safely neglected in the design of a -20-db side-lobe-level array are factors of paramount interest in the design of a -30-db side-lobe array.

A further difficulty that arises in the use of longitudinal shunt slots in a waveguide slot array is found in the design of a very long array, i.e., one which contains many slots, the bulk of which have relatively small conductances. It is not simple to

fabricate slots whose width is much smaller than $\frac{1}{16}$ in. by the use of conventional techniques, and fabrication costs play an important role in the design problem. In a long slot array where the conductances are small, the displacement of the centerline of a small conductance slot off the longitudinal centerline of the waveguide is so small that the slot, because of its finite width, actually overlaps the centerline of the waveguide. The currents which feed the slot are out of phase with respect to the centerline of the waveguide, and it has been experimentally determined that the phase and conductance of the slot undergo radical changes as one edge of the slot moves across the waveguide centerline. It is far better in the design of a long slot array to accept deviations in conductance values which will result in not having the slots cross the centerline, rather than design for the specified values and have the actual values undergo marked change as a consequence of the slot overlapping the centerline of the waveguide. Power-breakdown considerations, as well as fabrication considerations, preclude the use of slots of very small widths in an effort to circumvent the difficulties arising from the use of low-conductance elements.

9.7. EDGE-SHUNT-SLOT ARRAY DESIGN

The measured performance of an edge-shunt-slot array will also be found to be poorer than the calculated performance. The chief sources of the discrepancies are the uncertainty as to the exact values of conductances of the slots near the input and termination ends of the array and the variations in slot dimensions arising from manufacturing tolerances. The edge-shunt-slot array radiates a field whose polarization is parallel to the waveguide. In addition, it also radiates a fairly strong cross-polarized component which has maxima at approximately $\pm 45°$ in the H plane of the waveguide array. When the design requirements are such that the cross-polarization components must be removed, two separate techniques may be employed to achieve this end. The first is to use the array to feed a parallel-plate media, as in the longitudinal-shunt-slot array, and to fit a polarizer grid across the exit aperture so that only the desired polarization component is radiated. An increase in the input VSWR and change in the mutual coupling between the slots are produced by the reflected cross-polarized component. It is difficult to obtain successful designs by the use of this outwardly simple technique.

A more suitable but more complicated design technique is to have each individual edge shunt slot feed into a separate section of rectangular waveguide, which is aligned so that its a dimension is parallel to the b dimension of the main feed waveguide. Each small section of waveguide then acts as a separate horn whose electric vector is aligned parallel to the longitudinal axis of the waveguide. The conductance of the edge shunt slot is of course different under these conditions of coupling, and design data for waveguide-to-waveguide slot coupling are presented in Fig. 9-16. The mutual coupling between the individual horns formed by the exit apertures of the short sections of individual waveguide stubs is negligible in design, and a much closer agreement between measured and computed array performance is achieved by the use of this type of edge-shunt-slot array.

9.8. SERIES-SLOT ARRAY

A series-slot array does not have the off-axis lobes of the longitudinal shunt-slot array, nor does it have the strong mutual-coupling difficulties of the edge-shunt-slot array. However, it does suffer from the presence of cross-polarized components with maxima at approximately $\pm 45°$ in the H plane of the radiation pattern. As in the edge-shunt-slot array, the use of a polarization suppressor causes severe performance change. It is possible to fit the array with an E-plane horn whose b dimension is

reduced to a point below cutoff for the unwanted polarization component. It is necessary to measure the resistance of the series slot in the presence of the specific horn to be used in order to obtain slot data adequate for design purposes.
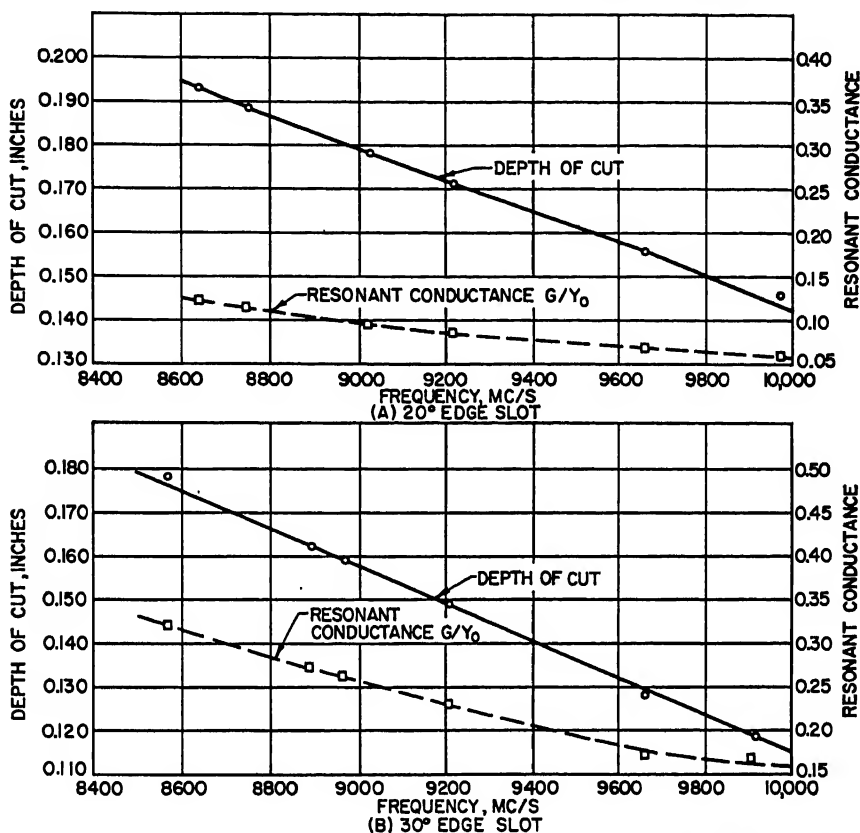
FIG. 9-16. Conductance and depth of cut as a function of frequency for edge slots. Shunt-series coupling between waveguides. Auxiliary guide terminated by Z_0. Wall thickness = 0.050 in. RG52/U waveguide.

9.9. POWER-HANDLING CAPABILITIES OF WAVEGUIDE-SLOT ARRAYS

In many applications of waveguide-slot arrays, it is necessary that the array operate at high-power levels. The slot array can handle high power without undue difficulty at normal atmospheric pressures. In air-borne applications, it is not readily possible to obtain atmospheric pressure and the array must either be sealed by the use of individual covers over each slot or be wholly encapsulated in a pressurized housing. The construction and fabrication difficulties of the pressurized housing are severe, but its use is by far to be preferred.

The use of a complete capsule with a window or radome for the entire array also introduces a reflected wave back into the array. There are several simple techniques to circumvent changes in VSWR arising from these reflections.[22] The simplest in a narrow bandwidth operation is to utilize the reflections from the pressurization window or radome to cancel the reflected wave in the waveguide when the window is

not present, and thus obtain a better input match. In broadband operation, it will be necessary to reduce the magnitude of the reflection from the window or radome to a minimum and also to skew the array with respect to the window so that the reflected rays essentially arrive at an angle corresponding to one of the side lobes of the antenna, and hence are not readily transmitted back down the feed waveguide.

The impedance characteristics of a resonant slot are modified by the presence of dielectric material in the immediate vicinity of the slot. A dielectric cover immediately on top of the slot or in the slot proper can shift the resonant frequency many per cent and greatly change the conductance values. A cover removed just a small fraction of an inch away from the slot produces a smaller perturbation. However, considerable care must be taken to minimize the reflections from the individual cover or to utilize the reflections for matching purposes. The tolerance requirements on individual slot covers are severe, and the covers are costly to fabricate. Small variations in position, thickness, etc., will cause large performance changes. The use of separate slot covers therefore requires a substantial amount of experimental effort to ensure correct spacings and to determine allowable dimensional tolerances.

REFERENCES

1. G. L. Ragan: "Microwave Transmission Circuits," MIT Radiation Laboratory Series, vol. 9, chap. 2, McGraw-Hill Book Company, Inc., New York, 1948.
2. S. Silver: "Microwave Theory and Design," MIT Radiation Laboratory Series, vol. 12, chap. 9, McGraw-Hill Book Company, Inc., New York, 1949.
3. Radio Research Laboratory Staff: "Very High Frequency Techniques," vol. 1, McGraw-Hill Book Company, Inc., New York, 1947.
4. I. Kaminow and R. F. Stegen: "Waveguide Slot Array Design," *Hughes Aircraft Co. Tech. Mem.* 348, 1954.
5. W. H. Watson: "Resonant Slots," *J. IEE* (London), pt. IIIA, vol. 93, pp. 747–777.
6. A. L. Cullen: "Laterally-displaced Slot in Rectangular Waveguide," *Wireless Eng.*, pp. 3–10, January, 1949.
7. R. J. Stegen: "Longitudinal Shunt Slot Characteristics," *Hughes Aircraft Co. Tech. Mem.* 261, November, 1951.
8. A. F. Stevenson: "Theory of Slots in Rectangular Waveguides," *J. Appl. Phys.*, vol. 19, pp. 24–38, 1948.
9. Reference 2.
10. C. L. Dolph: "A Current for Broadside Arrays Which Optimizes the Relationship between Beamwidth and Sidelobe Level," *Proc. IRE*, vol. 34, pp. 335–348, 1946.
11. P. M. Woodward: "A Method of Calculating the Field over a Plane Aperture Required to Produce a Given Polar Diagram," *J. IEE* (London), pt. IIIA, vol. 93, p. 1554, 1946.
12. T. T. Taylor and J. R. Whinnery: "Applications of Potential Theory to the Design of Linear Arrays," *J. Appl. Phys.*, vol. 22, pp. 19–29, 1951.
13. Reference 4.
14. M. J. Ehrlich and J. Short: "Mutual Coupling Consideration in Linear Slot Array Design," *Proc. IRE*, vol. 42, no. 4, June, 1954.
15. H. Gruenberg: "Second Order Beams of Slotted Waveguide Arrays," *Can. J. Phys.*, vol. 31, pp. 55–69, 1953.
16. H. Gruenberg: "Theory of Waveguide-fed Slots Radiating into Parallel Plate Regions," *J. Appl. Phys.*, vol. 23, p. 733, 1952.
17. Reference 7.
18. L. L. Bailin and M. J. Ehrlich: "Factors Affecting the Performance of Linear Arrays," *Proc. IRE*, vol. 41, pp. 235–241, 1953.
19. H. F. O'Neill and L. L. Bailin: "Further Effects of Manufacturing Tolerances on the Performance of Linear Shunt Slot Arrays," *IRE Trans.*, no. PGAP-4, pp. 93–102, December, 1952.
20. J. Ruze: "Effect of Aperture Distribution Errors on the Radiation Pattern," U.S. Air Force, Cambridge Research Center, January, 1952.
21. L. L. Bailin: "Fundamental Limitations of Long Arrays," *Hughes Aircraft Co. Tech. Mem.* 330, October, 1953.
22. D. W. Fry and F. K. Goward: "Aerials for Centimeter Wave-lengths," pp. 115, 117–125, Cambridge University Press, London, 1950.

Chapter 10

HORN ANTENNAS

WILLIAM C. JAKES, JR.

Bell Telephone Laboratories, Incorporated
Holmdel, New Jersey

10.1. TYPES OF HORNS AND THEIR USES

Electromagnetic horns in general are characterized by their ability to effect a transition from a medium supporting a small number of propagating modes, such as a waveguide, to one supporting a large or infinite number of modes, such as free space. They represent another means of approximating the ideal wavefront needed for good

directivity, with the additional advantage of being able to accommodate an exceptionally broad band of frequencies. Horns are constructed in a variety of shapes in order to control one or more of their three major electrical properties: gain, radiation patterns, and impedance. In addition, the choice of a particular type of horn may be governed by its ability to transmit certain desired modes or polarizations.

The radiation characteristics of horns having aperture dimensions greater than one wavelength may usually be calculated by using Huygens' principle, assuming the aperture field to be known.[18] The calculation becomes accurate enough for most

(a) PYRAMIDAL

(d) CONICAL

(b) SECTORAL H-PLANE

(c) SECTORAL E-PLANE

(e) BICONICAL
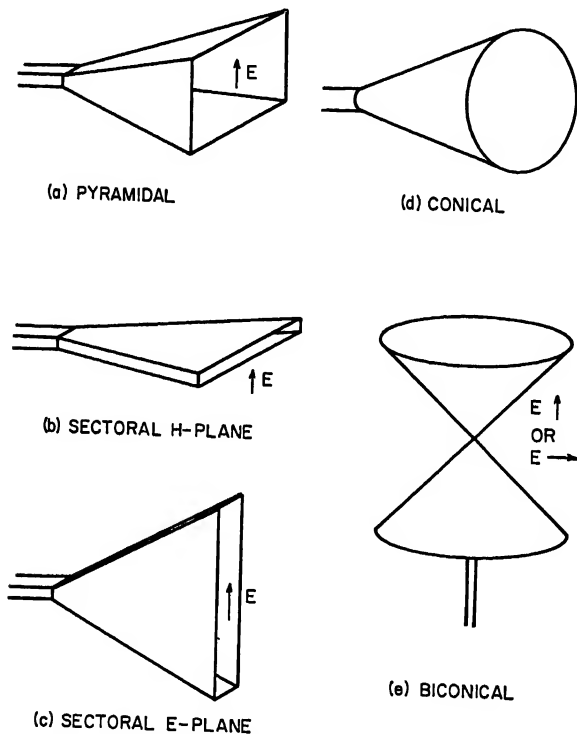
FIG. 10-1. Commonly used horn types.

purposes as the aperture size increases beyond one or two wavelengths. The radiated field is directly related to the field over the horn aperture, which may usually be predicted from the geometry of the horn and mode excitation. Wherever calculated properties are given in the following sections, the phase distribution over the aperture in question has been assumed to be parabolic, exp (imx^2), where m is the maximum phase deviation in radians and x is a normalized aperture variable. This type of phase distribution is a result of the curvature of the wavefront produced by the flare of the horn sides. In addition, the modes excited in these horns are usually such as to produce an amplitude distribution which allows expression of the radiation properties in terms of known functions. Calculated radiation patterns and gain curves are given here in universal form. The maximum phase deviation for the particular horn in question is first calculated, and then reference to the appropriate curve gives the desired property.

The more frequently used types of horns are illustrated in Fig. 10-1.

The pyramidal horn of Fig. 10-1a is commonly used as a primary gain standard,

since its gain can be calculated to within a tenth of a decibel if it is accurately constructed.[23]   This type of horn can also be used to obtain specified beamwidths independently in the two principal planes.

The sectoral horns shown in Fig. 10-1*b* and *c* are special cases of the pyramidal horn.   They are generally used only to obtain "fan-shaped" beams of specified sharpness in the plane containing the flare.   The pattern is very broad in the other plane and is essentially the same as that of an open-ended waveguide.

(a) COMPOUND HORN   (b) BOX HORN

(c) POINTED WAVEGUIDE

(d) ROUNDED WAVEGUIDE

(e) SYMMETRICALLY BEVELED WAVEGUIDE WITH POST

(f) WAVEGUIDE WITH DISK

(g) WAVEGUIDE WITH DIELECTRIC

(h) ASYMMETRICALLY BEVELED WAVEGUIDE

(i) HOG HORN   (j) ASYMMETRIC HORN
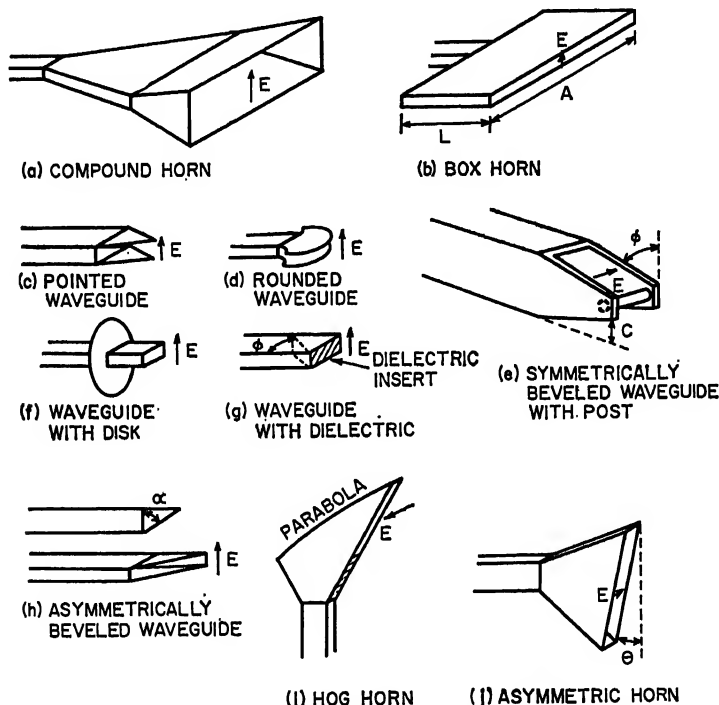
Fig. 10-2. Miscellaneous horn types.

The conical horn is shown in Fig. 10-1*d*.   By virtue of its complete axial symmetry it can handle any polarization of the dominant TE_{11} mode.   The radiation pattern is completely determined by the flare angle and length for a given mode excitation; thus the beamwidth can be arbitrarily specified in only one plane.   The gain of conical horns can be calculated to good accuracy, and thus they may also be used as primary gain standards.

The biconical horn finds use where an omnidirectional horizontal radiation pattern is desired.   Control of the vertical radiation pattern may be easily effected by choosing a suitable flare angle and length of side.   This type of antenna thus finds frequent use in the VHF-UHF band for broadcasting purposes.   By use of the appropriate feeding arrangement, either horizontal or vertical polarization may be employed.

In order to obtain characteristics not possible with the common types of horns just described, the horns shown in Fig. 10-2 have been used.

The compound horn with a long *H*-plane flare but a short *E*-plane flare, as illustrated in Fig. 10-2*a*, may be used to achieve a good broadband impedance match to free space by properly proportioning the *E*-plane flare length and angle.   The box horn of Fig. 10-2*b* gives a narrower pattern in the *H* plane than a sectoral horn of the same

aperture. The various types of horns in Fig. 10-2c–h result in H-plane patterns either broader or narrower than that of an open-ended waveguide.

The hog horn shown in Fig. 10-2i has been frequently used for illuminating "cheese," or "pillbox," antennas. In one element it combines a 90°-direction change, aperture enlargement in the H plane, and phase correction in the H plane.
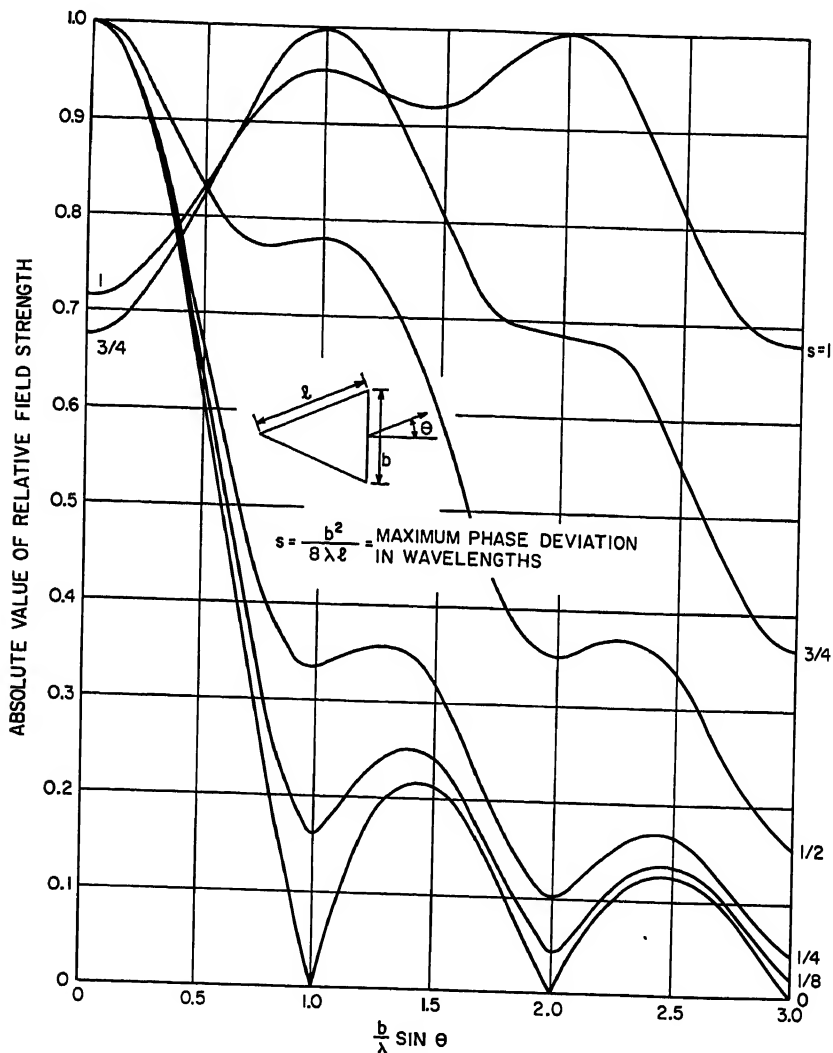
Fɪɢ. 10-3. Universal radiation patterns of horns flared in the E plane (applies to sectoral, pyramidal, and biconical horns).

The asymmetrical horn of Fig. 10-2j has been used as an offset feed for parabolic cylinder antennas.

In the sections that follow, the important characteristics of the above types of horns will be treated in more detail. In all cases gain, where mentioned, is referred to that of an isotropic radiator.

10.2. SECTORAL HORNS

Radiation Patterns. The radiation patterns of sectoral horns may be calculated in the plane containing the flare. It is assumed that the horn is fed by a rectangular waveguide supporting only the dominant TE_{10} mode. For the H-plane horn (flare in

$t = \dfrac{a^2}{8\lambda\ell}$ = MAXIMUM PHASE DEVIATION IN WAVELENGTHS
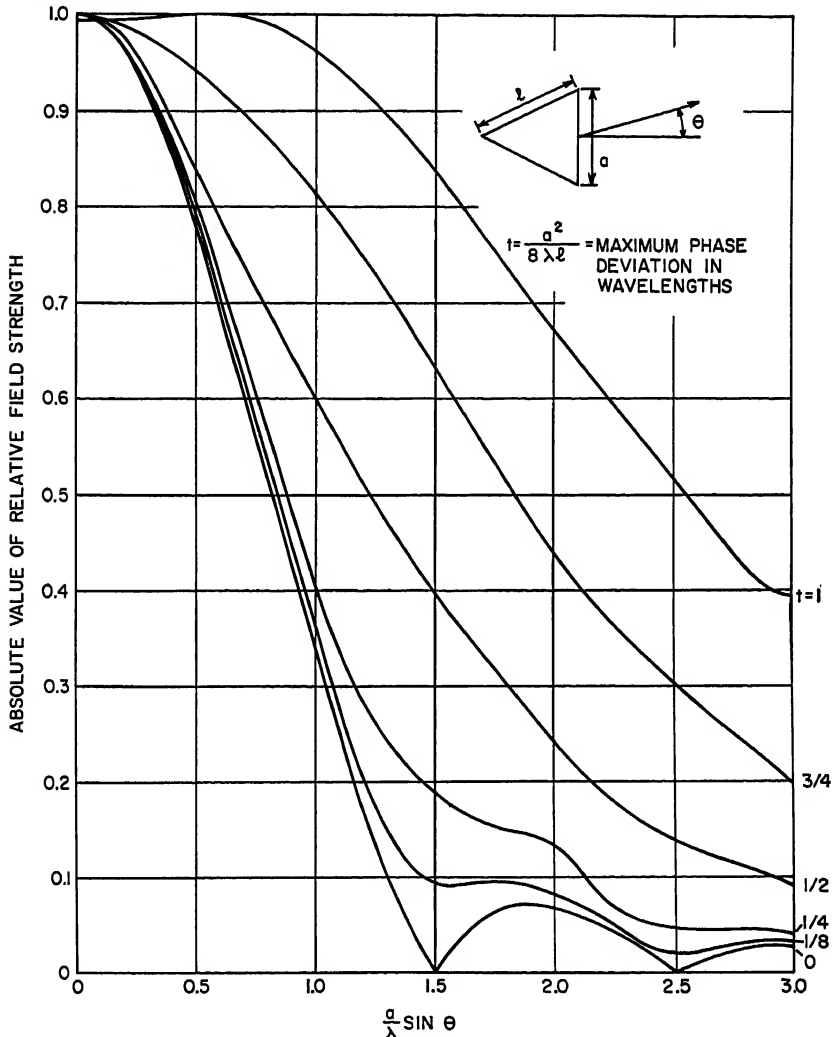
FIG. 10–4. Universal radiation patterns of horns flared in the H plane (applies to sectoral, pyramidal, and biconical horns).

the plane containing the magnetic field) the amplitude of the electric field thus varies sinusoidally over the large dimension of the aperture, while for the E plane horn it is constant. In both horns the phase of the aperture field varies essentially parabolically over the aperture with maximum deviation $2\pi a^2/8\lambda\ell$ radians,* where a is the aperture

* This assumes that the total flare angle of the horn is less than about 60°, so that $\ell - [\ell^2 - (a/2)^2]^{1/2} \approx a^2/8\ell$.

width and l the slant length of the flare. Figures 10-3 and 10-4 show the far-field radiation patterns for E-plane and H-plane sectoral horns, respectively, as functions of the dimensionless quantity $(b/\lambda) \sin \theta$ or $(a/\lambda) \sin \theta$, with the maximum phase deviation in wavelengths, s or t, as parameters. Note that in general the minor lobes are much more pronounced for the E-plane horn. These curves have been amply verified experimentally and are valid for apertures greater than several wavelengths in extent. For smaller apertures, down to about one wavelength, the values of relative field strength obtained from the curves should be multiplied by the factor $0.5(1 + \cos \theta)$.
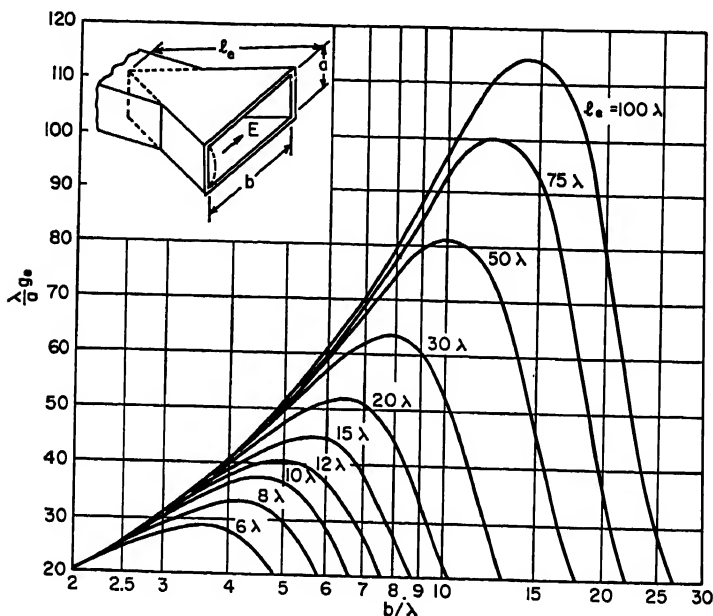
Fig. 10-5. Gain for an E-plane sectoral horn ($a \geqq \lambda$).

Gain. The gain of sectoral horns may be calculated[19] from the curves of Figs. 10-5 and 10-6 provided the narrow aperture dimension is at least one wavelength. Measurements made on typical horns show that the theoretical gain values can be relied on to a fraction of a decibel. It is of interest to note that the maximum gain for an H-plane sectoral horn with a slant length of 12λ occurs when the aperture is 6λ wide, and for an E-plane sectoral horn with a slant length of 15λ it occurs when the aperture is 5.5λ wide. These values correspond to a phase deviation in the aperture wavefront of $\frac{3}{8}\lambda$ and $\frac{1}{4}\lambda$, respectively. The 3-db total beamwidths for these horns are about 13 and 10°, respectively.

Impedance. The impedance characteristics of sectoral horns depend on the mismatch between the horn mouth and free space, the length of radial guide between the horn aperture and throat, and the mismatch at the junction between the uniform guide and the throat. The input VSWR of an E-plane horn in general varies periodically between 1.05 and 1.5 as the horn slant length is varied, with minima occurring every half guide wavelength.[2,14] (The guide wavelength in the E-plane sectoral horn is equal to that in the rectangular waveguide.)

The input impedance of an H-plane sectoral horn differs somewhat from that of the E-plane horn in that the mismatch at the junction of the horn and rectangular wave-

guide is much smaller than that at the horn aperture. The result is that the input VSWR to an H-plane sectoral horn is essentially constant in magnitude and varies only in phase as the length of the horn is changed.[2]

A broadband match is best obtained in the E-plane sectoral horn by treating the two discontinuities separately. The mismatch at the junction of the waveguide and horn may be eliminated with a reactive window (usually inductive) at the junction. The horn aperture is frequently matched to free space by using a plastic weather
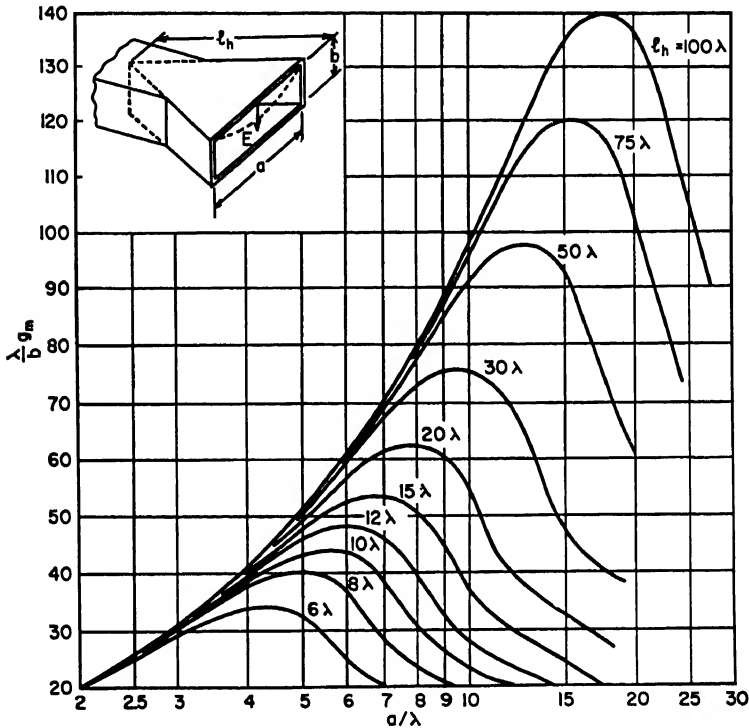
FIG. 10-6. Gain for an H-plane sectoral horn ($b \geqq \lambda$).

cover of proper thickness and dielectric constant. If no weather cover is used, a match may be obtained by use of small reactive discontinuities at the aperture.

The problem of obtaining a broadband match with the H-plane horn is somewhat easier, because of the small discontinuity at the horn throat. Generally, only the aperture needs to be matched, and the same techniques mentioned for the E-plane horn may be employed.

10.3. PYRAMIDAL HORNS

Gain. As mentioned in Sec. 10.1, the pyramidal horn is frequently used as a standard horn of known gain in making gain measurements of other antennas. Its gain in decibels over an isotropic radiator may be accurately calculated from the curves of Figs. 10-7 and 10-8 and the following relationship:

$$\text{Gain in db} = 10\left(1.008 + \log\frac{a}{\lambda}\frac{b}{\lambda}\right) - (L_e + L_h) \qquad (10\text{-}1)$$

where L_e and L_h are the decibel loss figures obtained from the curves. (*Note:* The log is to the base 10.)

The gain may also be calculated by multiplying the product of the gains obtained from Figs. 10-5 and 10-6, $(\lambda g_m/b)$ $(\lambda g_e/a)$, by $\pi/32$.

Optimum Horn. A horn is said to be optimum when the aperture dimensions are adjusted to give maximum gain for given slant lengths of flare in the H and E planes.
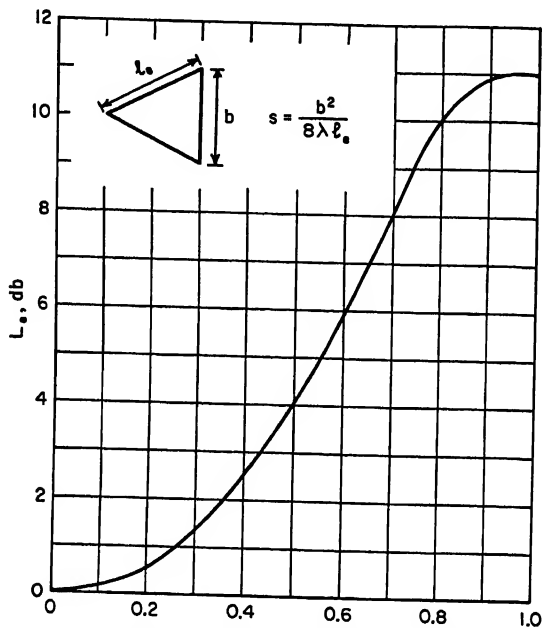
Fig. 10-7. Gain-correction factor for E-plane flare.

This occurs when the maximum aperture phase deviations in the H and E planes are $\frac{3}{8}\lambda$ and $\frac{1}{4}\lambda$, respectively, or

$$a = \sqrt{3\ell_h\lambda} \qquad b = \sqrt{2\ell_e\lambda} \qquad (10\text{-}2)$$

where a and b are the H- and E-plane aperture dimensions, respectively, and ℓ_h and ℓ_e are the H- and E-plane slant lengths, respectively. λ is the free-space wavelength. The effective area of an optimum horn is almost exactly 50 per cent of its actual area, its gain being given by

$$\text{Gain}_{\text{opt}} \text{ in db} = 10\left(0.808 + \log\frac{a}{\lambda}\frac{b}{\lambda}\right) \qquad (10\text{-}3)$$

Radiation Patterns. Radiation patterns for any type of pyramidal horn may be obtained by the same method used for the sectoral horns, as described in Sec. 10.2. Figure 10-3 gives the E-plane patterns, and Fig. 10-4 those for the H plane. For apertures greater than one wavelength in extent the patterns in the two planes may be controlled independently by adjusting the horn proportions. Designing a horn to have specified beamwidths in the E and H planes is a matter of trial and error because of the necessity of fitting the horn to the waveguide. The curves of Figs. 10-3 and

10-4 are used to select possible values of a, ℓ_h, b, ℓ_e. These values must then satisfy the relation

$$(a - a_0)^2 \left[\left(\frac{\ell_h}{a} \right)^2 - \frac{1}{4} \right] = (b - b_0)^2 \left[\left(\frac{\ell_e}{b} \right)^2 - \frac{1}{4} \right] \tag{10-4}$$

for the horn to be physically realizable. Here a_0 and b_0 are the H- and E-plane waveguide dimensions, respectively.

Impedance. The impedance characteristics of pyramidal horns are somewhat more complicated than for sectoral horns. However, horns having a gain of 20 db
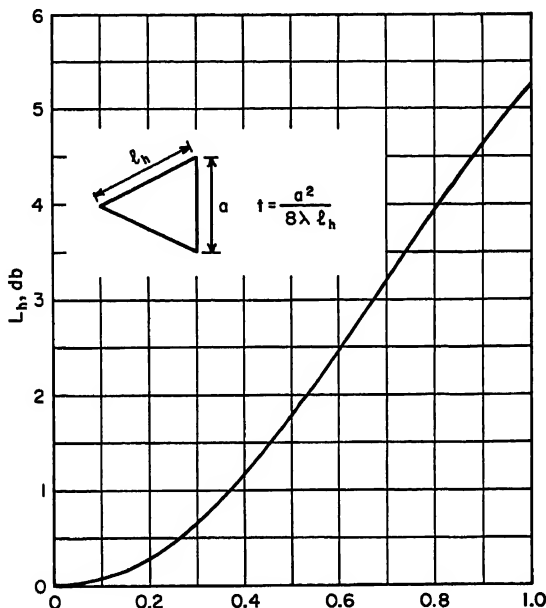
t, MAXIMUM APERTURE PHASE DEVIATION IN WAVELENGTHS

FIG. 10-8. Gain-correction factor for H-plane flare.

or more and moderate flare angles, such as optimum horns, are usually well matched by a rectangular waveguide supporting only the dominant mode. For example, an optimum horn with 28 db gain at 3,000 Mc fed by 1½- × 3-in. waveguide has an input VSWR of about 1.03. In cases where the over-all match must be improved, techniques similar to those described for sectoral horns may be used.

Practical Design Considerations. In designing a standard horn one generally knows the desired gain, wavelength, and dimensions of the feeding waveguide. If the horn is also to be optimum, these quantities, together with the restrictions discussed above, completely determine the final dimensions of the horn. Let a_0 and b_0 be the H- and E-plane waveguide dimensions, respectively. Then the following equation must be satisfied if the horn is to be physically realizable (that is, fit the feeding waveguide), optimum, and have numerical gain G:

$$\left(\sqrt{\frac{2\ell_e}{\lambda}} - \frac{b_0}{\lambda} \right)^2 \left(\frac{2\ell_e}{\lambda} - 1 \right) = \left(\sqrt{\frac{3K\lambda}{\ell_e}} - \frac{a_0}{\lambda} \right)^2 \left(\frac{4K}{3} \frac{\lambda}{\ell_e} - 1 \right) \tag{10-5}$$

where $K = (G/15.7497)^2$.

This equation may be easily solved by trial and error for l_e. A rough approximation which can serve as a first trial is $l_e = \lambda \sqrt{K}$. After l_e has been determined, l_h is given by

$$l_h = \frac{K\lambda^2}{l_e} \tag{10-6}$$

Knowing l_e, l_h, the quantities a and b may then be calculated from Eq. (10-2).

It has been pointed out* that a pyramidal horn may be designed to have almost constant gain over a fairly broad band of frequencies by sacrificing about 2 db of gain
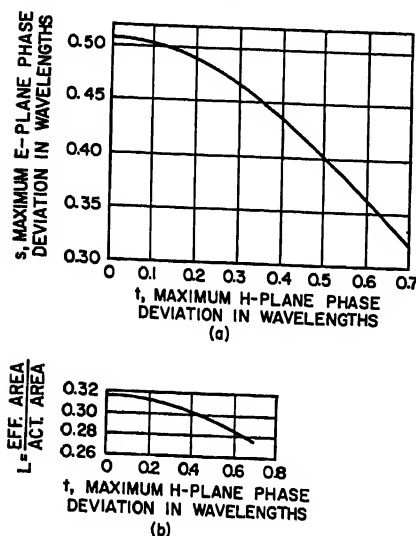
FIG. 10-9. Design curves for flat gain pyramidal horn.
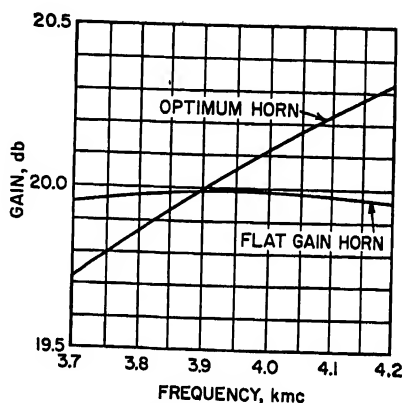
FIG. 10-10. Comparison of calculated gain of an optimum pyramidal horn and gain of horn designed for minimum gain variation over a 10 per cent band.

compared with an optimum horn of the same aperture dimensions. Design of such a horn proceeds along lines similar to that of an optimum horn. The equation which must be satisfied to make the horn physically realizable is

$$\left(\sqrt{\frac{8sl_e}{\lambda}} - \frac{b_0}{\lambda} \right)^2 \left(\frac{l_e}{2s\lambda} - 1 \right) = \left(\sqrt{\frac{8tM\lambda}{l_e}} - \frac{a_0}{\lambda} \right)^2 \left(\frac{M\lambda}{2tl_e} - 1 \right) \tag{10-7}$$

where s and t are related as shown in Fig. 10-9a and $M = \frac{1}{st}\left(\frac{G}{32\pi L}\right)^2$. The ratio of effective to actual area for this type of horn is equal to L and is given as a function of t in Fig. 10-9b. Note that the maximum efficiency is 31 per cent, whereas it is 50 per cent for the optimum horn. The parameter t may be chosen somewhat arbitrarily, but in general values of t greater than about 0.2 are preferable since the horn will then have flare angles more nearly equal in the two planes, usually a desirable feature. The proper value of t may be found by working out designs for several different values. The gain of this type of horn will be constant to better than ± 0.02 db over a ± 5 per cent bandwidth centered at the design frequency.

As an example of horn design the curves in Fig. 10-10 show the calculated variation

---

* P. R. Wickliffe of Bell Telephone Laboratories.

of gain vs. frequency for an optimum horn and a flat-gain horn, each designed for a gain of 20 db at a frequency of 3,900 Mc.

10.4. CONICAL HORNS

Gain. The properties of a conical horn excited in the dominant TE_{11} mode are similar to those of the pyramidal horn in many respects. The gain in decibels may
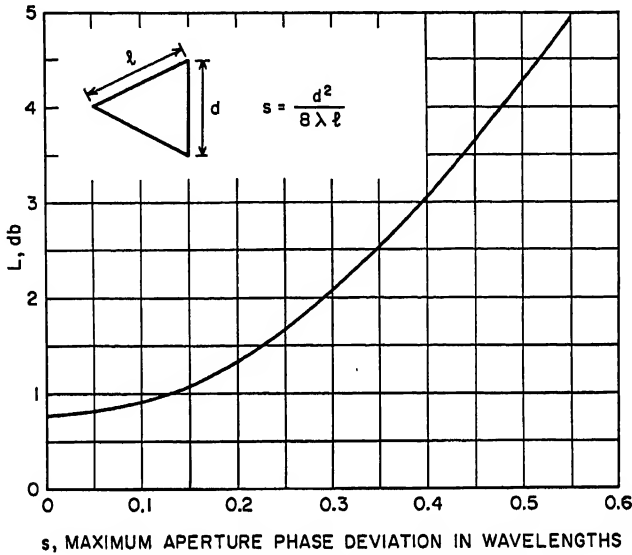
s, MAXIMUM APERTURE PHASE DEVIATION IN WAVELENGTHS
FIG. 10-11. Gain-correction factor for conical horn.

be calculated from the curve of Fig. 10-11 and the following relationship:

$$\text{Gain in db} = 20 \log \frac{C}{\lambda} - L \tag{10-8}$$

where C is the circumference of the horn aperture, and L is the decibel loss figure obtained from the curve.

The gain is optimum for a given slant length of flare ℓ when the diameter of the aperture d is related to ℓ by the equation

$$d = \sqrt{3\ell\lambda} \tag{10-9}$$

This corresponds to a maximum phase deviation of $\tfrac{3}{8}\lambda$ in the aperture wavefront and is the same criterion as for the H-plane flare in a sectoral or pyramidal horn. The effective area of an optimum conical horn is approximately 52 per cent of its actual area, 2 per cent more than that of the optimum pyramidal horn. The gain of an optimum conical horn is thus

$$\text{Gain}_{\text{opt}} \text{ in db} = 20 \log \frac{C}{\lambda} - 2.82 \tag{10-10}$$

Radiation Patterns. The radiation pattern of a conical horn is difficult to calculate because of mathematical complexity. Experimentally measured patterns are available,[8] however, and Fig. 10-12 gives representative results for various horns. Horns a
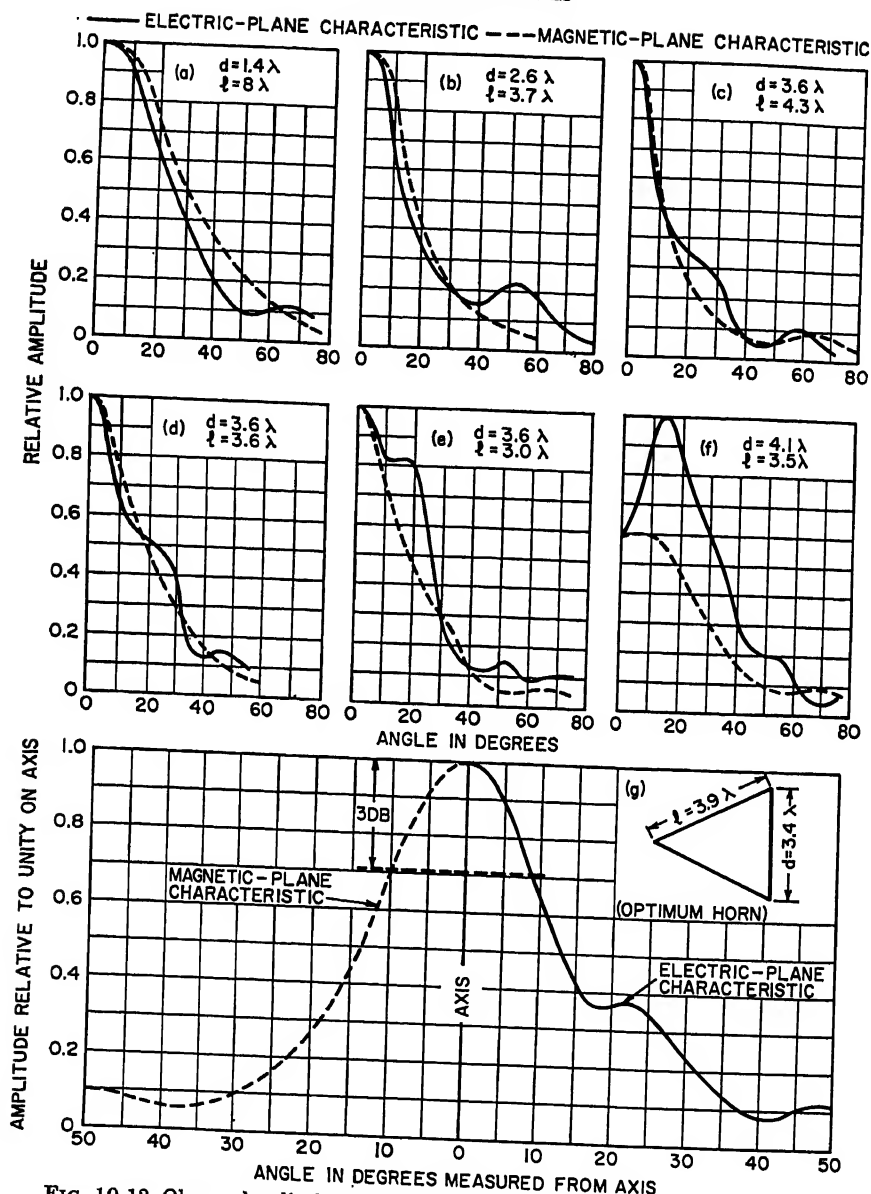
Fig. 10-12. Observed radiation patterns for conical horns of various dimensions.

and *b* have aperture diameter *d* less than optimum, horn *c* is very close to optimum, and horns *d*, *e*, and *f* have *d* greater than the optimum value. Figure 10-12*g* gives the pattern in somewhat more detail of an optimum horn having slightly different proportions than horn *c*. Note the general similarity to pyramidal horn patterns in that the *H*-plane patterns are relatively free of minor lobes. These curves may also be used for horns having dimensions different from any of those shown but proportioned to have the same phase deviation as one of the given horns, provided the

proper change is made in the abscissa scale. For example, suppose the patterns of a horn with slant length $\ell_1 = 7\lambda_1$ and diameter $d_1 = 5.8\lambda_1$ are desired. Calculating the phase deviation, one obtains

$$m \approx \frac{2\pi}{\lambda_1} \frac{d_1{}^2}{8\ell_1} = 0.6(2\pi),\ \text{or } 0.6\text{ wavelength}$$

$$(10\text{-}11)$$

This is the same phase deviation as that for horn f in Fig. 10-12; thus the horn under consideration will have the same radiation patterns. The angular position θ_1 of the distant field is related to θ in Fig. 10-12f as follows:

$$\sin\theta_1 = \frac{\lambda_1 d}{\lambda d_1}\sin\theta = \frac{4.1}{5.8}\sin\theta \quad (10\text{-}12)$$

Impedance. Very little information is available on the impedance properties of conical horns. It appears likely, however, that dominant-mode horns of 20 db or more gain and moderate flare angle, such as optimum horns, will be reasonably well matched to the waveguide feed. The two sources of reflections are at the throat and the aperture of the horn. If it is desired to improve the over-all impedance match, the proper reactive components to place at these two locations may be determined experimentally.

10.5. BICONICAL HORNS

Methods of Excitation. As mentioned in Sec. 10.1, a biconical horn[5] may be excited in either vertical or horizontal polarization by use of the appropriate feeding system. (The axis of the cones is taken to be vertical.) Possible feeds are shown in Fig. 10-13. If the waveguide in Fig. 10-13a is propagating the TE_{01} (circular electric) mode, the resulting field in the horn will be horizontally polarized and will be zero at the sides of the horn and maximum in the horizontal plane through the apex. This is the TE_{01} mode in the horn. If the TM_{01} (circular magnetic) mode is used, the resulting field in the horn will be ver-

(a) WAVEGUIDE FEED SYSTEM FOR VERTICAL POLARIZATION (TM_{01} IN GUIDE) OR HORIZONTAL POLARIZATION
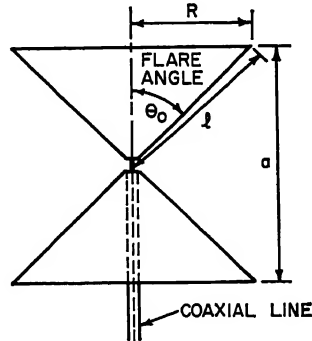
(b) COAXIAL FEED SYSTEM FOR VERTICAL POLARIZATION
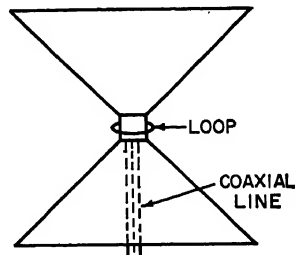
(c) LOOP FEED FOR HORIZONTAL POLARIZATION

Fig. 10-13. Methods of feeding biconical horn.

tically polarized with uniform field amplitude in the vertical direction. In this case the field in the horn is a TEM mode. The coaxial feed in Fig. 10-13b will also excite the vertical polarization and is more commonly used than the waveguide feed. The loop feed of Fig. 10-13c may be used to excite the horizontal polarization.

Gain. If the radius R of the biconical horn is greater than two wavelengths, the gain in decibels may be calculated from
Vertical polarization (TEM):

$$G_{db} = 10 \log \frac{2a}{\lambda} - L_s \qquad (10\text{-}13)$$

Horizontal polarization (TE$_{01}$):

$$G_{db} = 10 \log \frac{2a}{\lambda} - (L_h + 0.91) \qquad (10\text{-}14)$$

where L_s and L_h are the decibel loss figures given in Figs. 10-7 and 10-8. The quantities s and t of these curves (the aperture field phase deviation in wavelengths) are both equal to $a^2/8\ell\lambda$ in the case of the biconical horn. As for sectoral and pyramidal horns, there exist values of a for which the gain of the biconical horn is maximum for given ℓ and λ. These values depend on the polarization and are given by
Vertical polarization (TEM):

$$a_{opt} = \sqrt{2\ell\lambda} \qquad (10\text{-}15)$$

Horizontal polarization (TE$_{01}$):

$$a_{opt} = \sqrt{3\ell\lambda} \qquad (10\text{-}16)$$

The gain for optimum proportions is then given by
TEM:

$$\text{Opt } G_{db} = 5 \log \frac{\ell}{\lambda} + 3.57 \qquad (10\text{-}17)$$

TE$_{01}$:

$$\text{Opt } G_{db} = 5 \log \frac{\ell}{\lambda} + 3.45 \qquad (10\text{-}18)$$

Radiation Patterns. The radiation pattern of the biconical horn is uniform (omnidirectional) in the horizontal plane for either vertical or horizontal polarization. In the vertical plane the pattern is given by the universal curves of Fig. 10-3 for vertical polarization and Fig. 10-4 for horizontal polarization. By proper choice of flare angle θ_0 and slant length ℓ, a desired beamwidth in the vertical plane may be obtained by use of these curves.

Impedance. The impedance characteristics of biconical horns have been studied both experimentally and theoretically for various lengths and flare angles. Most of the work done has been for the TEM horn mode, very little information being available for the TE$_{01}$ case. For horns with slant length greater than two wavelengths and flare angle greater than about 20°, the input impedance (vertical polarization) is essentially equal to the characteristic impedance:

$$K = 120 \log_e \cot \frac{\theta_0}{2} \quad \text{(TEM case)} \qquad (10\text{-}19)$$

For shorter horns the input impedance becomes complex and varies both with slant length and flare angle.[3,4]

10.6. MISCELLANEOUS HORN TYPES

Compound Horn. The impedance properties of sectoral horns suggest the possibility of obtaining a good broadband match with the compound horn of Fig. 10-2a, where the H-plane dimension is considerably larger than that of the E plane. Because

of the negligible mismatch at the junction of the waveguide with the H-plane flare, the over-all impedance characteristics depend only on the mismatch at the throat and aperture of the *E*-plane flare. By proper choice of the flare angle and length these two reflections may be made to cancel each other. The frequency band over which a match may be obtained depends on the *E*-plane flare length and is greater the shorter the length. The exact impedance characteristics of *E*-plane flares are probably best obtained experimentally for this purpose.[2]

The gain- and radiation-pattern characteristics will be essentially the same as for pyramidal horns of the same flare angles and lengths.

Box Horn. The box horn shown in Fig. 10-2*b* consists of a dominant-mode rectangular waveguide coupled to a length *L* of rectangular waveguide of the same *E*-plane height but whose *H*-plane width *A* is large enough to support the TE_{30} mode. The field over the horn aperture is thus a combination of the TE_{10} and TE_{30} modes, the exact distribution depending on their relative phase and amplitude. The length of the box determines the relative phase of the two modes, and the ratio of the *H*-plane dimensions of the two waveguides determines their relative amplitude. Usually the length is adjusted so that the two modes are 180° out of phase, or

$$L = \frac{\lambda/2}{[1 - (\lambda/2A)^2]^{1/2} - [1 - (3\lambda/2A)^2]^{1/2}} \qquad (10\text{-}20)$$

Under these conditions the amplitude distribution over the *H* plane of the aperture is a closer approximation to uniform than is the cosine variation associated with the TE_{10} mode. This results in an increased efficiency, together with a somewhat narrower major-lobe and higher minor-lobe levels. Optimum efficiency is realized when *A* is about $1\frac{1}{2}$ times the *H*-plane width of the smaller waveguide. In this case the amplitude of the TE_{30} mode is about 35 per cent that of the TE_{10} mode. The first minor lobe is about 13 db down from the major-lobe peak for $A > 2\lambda$.

The principal advantage of the box horn lies in its ability to produce narrower beams than a sectoral horn of the same over-all length and aperture width. It is not used to produce beamwidths between tenth-power points of less than 36°, however, because this would require that *A* become so large that modes of higher order than TE_{30} could appear. Thus the box horn finds use in producing *H*-plane beamwidths between tenth-power points of about 36 to 70°.

Further details on the box horn may be found in Ref. 2, pp. 377–380, and Ref. 12.

Waveguide Radiators. One of the simplest types of horns is an open-ended rectangular waveguide supporting the dominant TE_{10} mode. The radiation patterns of such a horn are generally narrower than would be expected from simple Huygens theory because of the presence of currents flowing on the outside walls of the waveguide. Also because of this effect the gain is higher than might be expected, to the extent that the effective area may be greater than the actual area. The presence of these currents makes exact calculation of the radiation properties of waveguides very difficult. As a result, most small horns of this type are usually studied experimentally.

Figure 10-14 gives the *E*- and *H*-plane patterns that have been obtained for a rectangular waveguide with dominant-mode excitation and inside dimensions 0.9 in. in the *H* plane and 0.4 in. in the *E* plane at 9,375 Mc.[2,9] Figure 10-15 gives experimental patterns for a 2.81-in.-ID round waveguide at 4,087 Mc for the dominant TE_{11} mode.

In order to modify the patterns from open-ended waveguides, a number of methods have been used. The waveguides shown in Fig. 10-2*c* and *d* have had their ends shaped, in pattern *c* to a point with 90° included angle and in pattern *d* to a semicircle of 0.7-in. radius. At 9,375 Mc the *H*-plane patterns of Fig. 10-16 were obtained.[9]

Broader *H*-plane patterns may also be produced by the waveguide of Fig. 10-2*e*.[2,11] Here a conductive post has been placed across the waveguide (parallel to the electric

field) on the axis and immediately back of the aperture. The corners of the wave-guide are removed symmetrically at an angle ϕ with respect to the normal to the wave-guide axis. The cuts begin a distance c from each edge. For values of $c = 0.4\lambda$ and $\phi = 45°$ the H-plane pattern may be broadened to a total beamwidth between
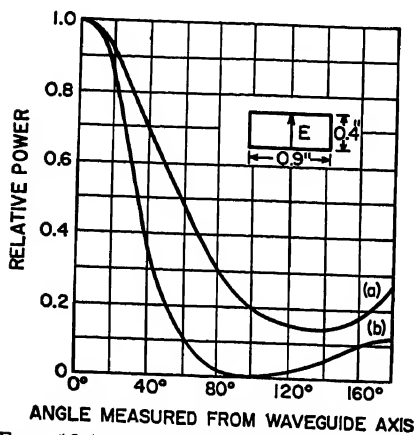
FIG. 10-14. Observed radiation patterns from rectangular waveguide at $\lambda = 3.2$ cm: (a) E-plane pattern. (b) H-plane pattern.
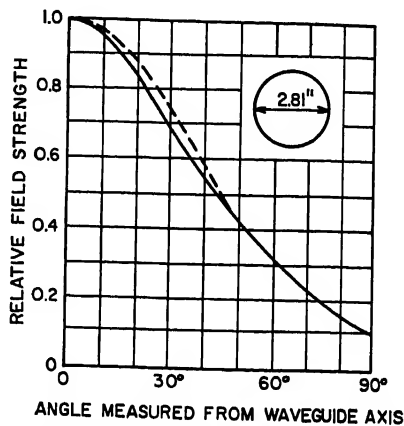
FIG. 10-15. Observed radiation patterns from round waveguide with TE$_{11}$ mode at $\lambda = 7.35$ cm: ——— E-plane pattern. – – – – H-plane pattern.

tenth-power points of over 300°, compared with about 120° for an open-ended waveguide.

An open-ended waveguide equipped with a disk a short distance behind the aperture such as shown in Fig. 10-2f will have radiation patterns significantly different from those of a waveguide alone.[9,15] As the disk is moved along the waveguide away from the aperture, the H-plane patterns become alternately broader and narrower than that of the open-ended waveguide. The broad patterns may have a double hump with a minimum in the direction of the waveguide axis. A disk about two wavelengths in diameter apparently is as effective as one much larger. The broadest pattern obtained with a disk of this size was 145° between tenth-power points when the disk was 2.0 cm behind the aperture of a 0.9- × 0.4-in.-ID wave-guide at a frequency of 9,375 Mc.

FIG. 10-16. Observed H-plane radiation patterns at $\lambda = 3.2$ cm of rectangular wave-guide with shaped ends (TE$_{10}$ mode).

Waveguide radiators with dielectric slugs in the waveguide at the aperture, have also been experimentally studied.[9] In order to produce an effect, the slug must be asymmetric with respect to the guide axis. The action of the slug is twofold: the asymmetry provides a disconti-nuity which excites higher-order TE$_{no}$ modes, and the dielectric loads the waveguide to the extent that some of these higher-order modes can propagate to the aperture. The aperture field may thus be markedly different from the dominant TE$_{10}$ mode

configuration, with a consequent effect on the radiation pattern. A triangular slug of polystyrene, as shown in Fig. 10-2g, cut to an angle $\phi = 40°$, resulted in an H-plane pattern with peak intensity shifted 25° to one side and an increase in minor-lobe level to about 12 db below the peak.

A dominant-mode rectangular waveguide with the end obliquely cut off as in Fig. 10-2h displays certain interesting beam shifting and shaping properties in the H plane.[10] There is practically no effect, however, on the E-plane pattern. As the angle of inclination of the end plane α increases, the beam is progressively shifted away from the guide axis in a direction toward the normal to the plane of the aperture and the width of the major lobe progressively decreases. These effects can be predicted rather well by assuming a uniform amplitude field distribution over the aperture (accounting in an approximate way for the presence of higher-order modes) and a linear phase distribution calculated along the line of the cut but assuming it to be the same as though the waveguide had not been cut.

Hog Horn. The hog horn of Fig. 10-2i has been used principally as a feed horn for pillbox or cheese antennas. These antennas are characterized by use of a section of a cylindrical parabola bounded by two parallel conducting plates. The separation between plates may be very small (less than $\lambda/2$), in which case the TEM mode is used with waveguide or dipole feed at the focus of the parabola. For larger separations it is possible to use the TE_{10} mode with the electric field parallel to the plates. If this mode is used for plate separations larger than the wavelength, the problem of exciting only the one mode becomes important. The hog horn fills this need very well and has been used successfully for plate separations up to 30 wavelengths.[7,12,16]

Fig. 10-17. H-plane array of asymmetrical horns.

The hog horn accomplishes this because the field distribution in its aperture is plane, because of the parabolic reflecting surface, and varies in amplitude essentially as the TE_{10} mode in the parallel plate region because of the use of the dominant TE_{10} mode in feeding the horn. The H-plane pattern of the hog horn is essentially the same as the curve for $t = 0$ in Fig. 10-4. The E-plane pattern is quite broad, corresponding to that of an open-ended waveguide in the E plane.

The impedance match of the hog horn depends mainly on the match of the aperture, since the H-plane flare of the throat and the parabolic reflector produce little reflection. A frequently used matching technique at the aperture is to use a dielectric weather cover of the proper spacing and thickness.

Asymmetric Horn. The horn of Fig. 10-2j is simply an H-plane sectoral horn whose aperture plane is cut at an angle to the axis of the waveguide. The main lobe of the H-plane pattern is deflected somewhat toward the normal to the aperture plane, following Snell's law. In other respects the pattern will be similar to those of an H-plane sectoral horn. Asymmetric horns have been used as feeds for cylindrical parabolas[7,12] and in stacked arrays. In the latter application the horns are placed side by side in the H plane with the short side of one horn adjacent to the long side of the next as shown in Fig. 10-17, in order to locate the apertures of the horns closer together.

REFERENCES

1. G. C. Southworth: "Principles and Applications of Waveguide Transmission," chap. 10, D. Van Nostrand Company, Inc., Princeton, N.J., 1950. Experimental and

theoretical data on radiation patterns and gain of various types of horns. Also a good bibliography on horns, p. 669.

2. Samuel Silver: "Microwave Antenna Theory and Design," MIT Radiation Laboratory Series, vol. 12, chap. 10, McGraw-Hill Book Company, Inc., New York, 1949. Radiation patterns, gain, and impedance data for various types of horns, especially sectoral.

3. C. T. Tai: "Application of a Variational Principle to Biconical Antennas," *J. Appl. Phys.*, vol. 20, pp. 1076–1084, November, 1949. Impedance calculation for biconical horns of large angle.

4. "Input Impedance of Wide-angle Conical Antennas," *Harvard Univ. Cruft Lab.*, *Tech. Rept.* 52, 1948. Experimental study.

5. W. L. Barrow, L. J. Chu, and J. J. Jansen: "Biconical Electromagnetic Horns," *Proc. IRE*, vol. 27, pp. 769–779, December, 1939. Theoretical and experimental study. Corrected gain curves published in *ibid.*, vol. 39, pp. 434–435, April, 1951.

6. M. G. Schorr and F. J. Beck: "Electromagnetic Field of the Conical Horn," *J. Appl. Phys.*, vol. 21, pp. 795–801, August, 1950. Calculation of radiation patterns for moderate values of aperture phase deviation.

7. Proceedings of a Conference on Centimetric Aerials for Marine Navigational Radar, June 15–16, 1950, H.M. Stationery Office, London, 1952.

8. A. P. King: "The Radiation Characteristics of Conical Horn Antennas," *Proc. IRE*, vol. 38, pp. 249–251, March, 1950. Experimental results of measurements of patterns and gain for various conical horns.

9. R. E. Beam, M. M. Astrahan, and H. E. Mathis: "Open-ended Waveguide Radiators," *Proc. Natl. Electronics Conf.*, vol. 4, pp. 472–486, November, 1948. Experimental radiation patterns of waveguides with shaped ends, dielectric slugs.

10. G. S. Sanyal: "Radiation Properties of the Open End of a Rectangular Waveguide When the End Plane Is Inclined to the Guide Axis," *Indian J. Phys.*, vol. 27, pp. 465–475, September, 1953. Experimental and theoretical study.

11. C. S. Pao: "Shaping the Primary Pattern of a Horn Feed," *MIT Rad. Lab. Rept.* 655, January, 1945. Experimental study of various small horns and waveguide radiators.

12. S. J. Mason: "Horn Feeds for Parabolic Reflectors," *MIT Rad. Lab. Rept.* 690, January, 1946. Experimental and theoretical study of various types of feeds.

13. G. A. Woonton, D. R. Hay, and E. L. Vogan: "An Experimental Investigation of Formulas for the Prediction of Horn Radiator Patterns," *J. Appl. Phys.*, vol. 20, pp. 71–78, January, 1949.

14. L. Lewin: "Advanced Theory of Waveguides," Iliffe & Sons, Ltd., London, 1951. Theoretical analysis of waveguide tapers, chap. 5. Also an excellent bibliography on horn antennas, p. 171.

15. A. R. G. Owen and L. G. Reynolds: "The Effect of Flanges on the Radiation Patterns of Small Horns," *J. IEE (London)*, pt. IIIA, vol. 93, no. 10, pp. 1528–1530, 1946.

16. A. B. Pippard: "The Hoghorn: An Electromagnetic Horn Radiator of Medium-sized Aperture," *J. IEE (London)*, pt. IIIA, vol. 93, no. 10, pp. 1536–1538, 1946. A short study of various types of hog horns and some experimental results on one model.

17. D. R. Rhodes: "An Experimental Investigation of the Radiation Patterns of Electromagnetic Horn Antennas," *Proc. IRE*, vol. 36, pp. 1101–1105, September, 1948.

18. H. T. Friis and W. D. Lewis: "Radar Antennas," *Bell System Tech. J.*, vol. 26, pp. 219–317, April, 1947. Theoretical study of radar antennas, with some material on horns, and experimental results for certain types of radar antennas.

19. S. A. Schelkunoff and H. T. Friis: "Antennas: Theory and Practice," chap. 16, John Wiley & Sons, Inc., New York, 1952. Theoretical study of horns.

20. J. D. Kraus: "Antennas," chap. 13, McGraw-Hill Book Company, Inc., New York, 1950. Horn theory.

21. E. II. Braun: "Gain of Electromagnetic Horns," *Proc. IRE*, vol. 41, pp. 109–115, January, 1953.

22. E. H. Braun: "Some Data for the Design of Electromagnetic Horns," *IRE Trans.*, vol. AP-4, no. 1, pp. 29–31, January, 1956.

23. W. C. Jakes, Jr.: "Gain of Electromagnetic Horns," *Proc. IRE*, vol. 39, pp. 160–162, February, 1951.

Chapter 11

CORNER-REFLECTOR ANTENNAS

EDWARD F. HARRIS

Mark Products Co.
Skokie, Illinois

11.1. INTRODUCTION

The corner-reflector antenna[1,2] consists of a driven radiator, normally a half-wave element, associated with a reflector constructed of two flat conducting sheets (or their equivalent) which meet at an angle to form a corner. Figure 11-1 shows the antenna configuration and coordinate system. As in the horn type of antenna, the most useful radiation patterns of the corner-reflector antenna are those in the two
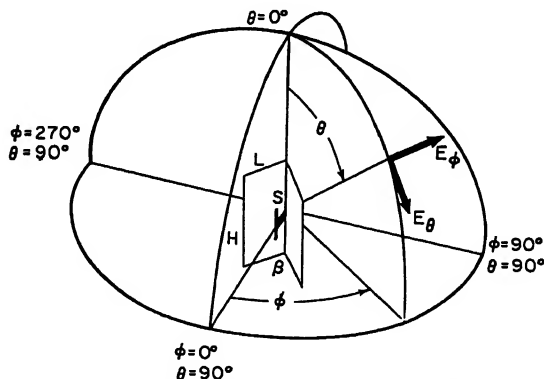
FIG. 11-1. Corner-reflector antenna and coordinate system.

principal planes, usually designated by the terms E plane and H plane because they are parallel to the electric- and magnetic-field intensities, respectively.

When the corner angle β is $180/n$ and n is an integer, the effect of the corner reflector can be taken into account by the method of images. For a 90°corner it is necessary to postulate three images as shown in Fig. 11-2. A 60° corner requires five images, a 45° corner seven images, etc.
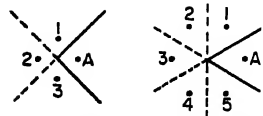
(a) 90° CORNER   (b) 60° CORNER

FIG. 11-2. Image system for corner-reflector antennas. *A* represents the exciting antenna, and the numbered antennas are images. The antenna *A*, in conjunction with its images, produces the same field in the direction of the reflector mouth as does the system consisting of *A* and the corner reflector.

11.2. EFFECT OF SPACING FOR GIVEN CORNER ANGLE

The principal effect of a corner reflector is to concentrate the radiation in the direction of the bisector of the corner, with the maximum concentration taking place in the H plane. There is a wide latitude of spacings possible for the dipole within the corner, and the forward gain goes through maximum and minimum values as the spacing is increased. The principal region of operation for the corner reflector is that in the region of the first maximum, and this may be termed the first-order mode of operation. There are advantages in operation at the second maximum if physical size can be tolerated, and in general at the higher modes of operation both the H-plane and E-plane patterns are concentrated to a great extent.

For best results there is an optimum spacing S between the antenna and corner for each angle. If the spacing becomes too large in the first mode of operation, the
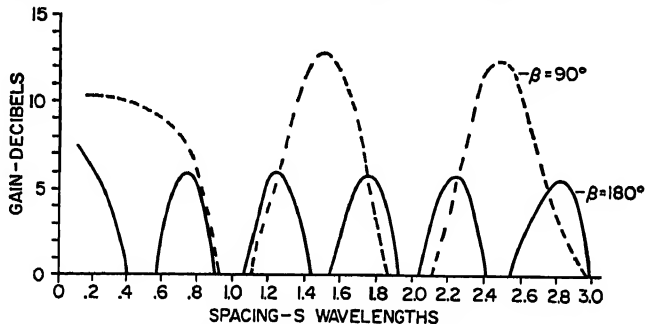
FIG. 11-3. Gain vs. spacing for $\beta = 90°$ and $\beta = 180°$, direction $\phi = 0°$, $\theta = 90°$.

directional pattern begins to show multiple lobes, the gain drops off, and the arrangement also becomes large physically. On the other hand, as the spacing becomes small, the radiation resistance is reduced and incidental loss resistances then consume an increasingly large fraction of the energy. The relationship between spacing and gain for a corner reflector with infinite sides is shown in Figs. 11-3 and 11-4 for various corner angles. The radiation resistance is shown in Figs. 11-5 and 11-6. It will be noted that power gains of the order of 10 to 13 db (10 to 20 times), as compared with an isolated half-wave antenna, are readily obtainable in a relatively simple, compact arrangement having a reasonable radiation resistance.

11.3. DETERMINATION OF SIZE OF CORNER REFLECTOR

Neglecting edge effects, a suitable value for the length of sides may be arrived at by the following line of reasoning.[3] An essential region of the reflector is that near
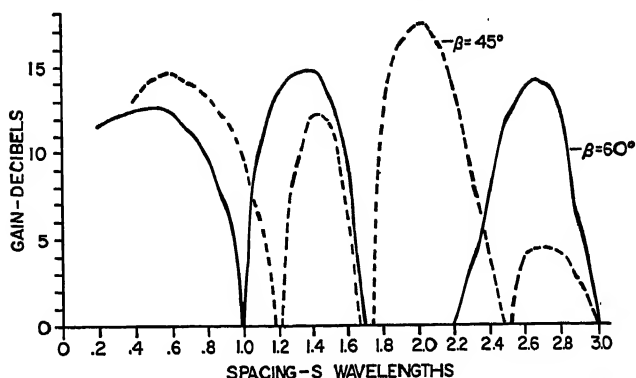
FIG. 11-4. Gain vs. spacing for $\beta = 45°$ and $\beta = 60°$, direction $\phi = 0°$, $\theta = 90°$.
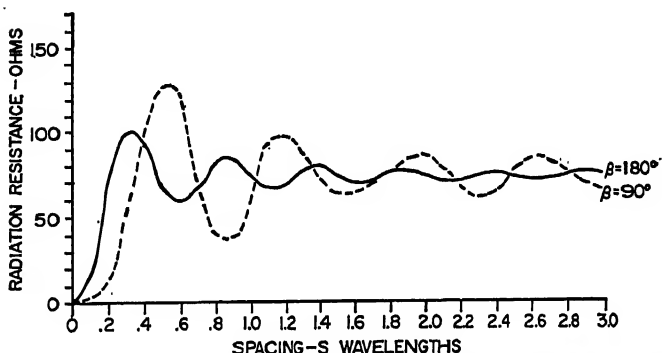
FIG. 11-5. Radiation resistance of driven $\lambda/2$ dipole vs. spacing for $\beta = 90°$ and $\beta = 180°$
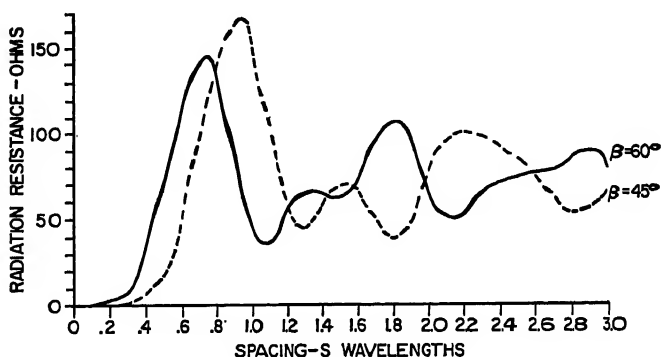
FIG. 11-6. Radiation resistance of driven $\lambda/2$ dipole vs. spacing for $\beta = 45°$ and $\beta = 60°$.

the point at which a wave from the driven antenna is reflected parallel to the axis. For example, point A of the 90° corner reflector shown in Fig. 11-7 is at a distance of $1.41S$ from the corner C, where S is the antenna-to-corner spacing. If the reflector ends at point B at a distance $L = 2S$ from the corner, as in Fig. 11-7, the reflector ends approximately $0.6S$ beyond A. With the reflector ending at B, it is to be noted that the only waves reflected from infinite sides, but not finite sides, are those radiated

in the sectors η. Furthermore, these waves are reflected with infinite sides into a direction that is at a considerable angle ϕ with respect to the axis. Hence the absence of the reflector beyond B should not have a large effect. It should also have relatively little effect on the driving-point impedance. The most noticeable effect with finite sides is that the measured pattern is broader than that calculated for infinite sides
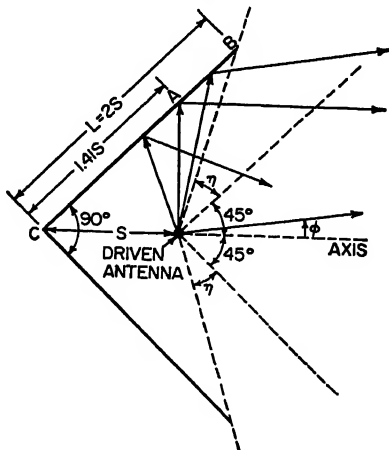
Fig. 11-7. Square corner reflector with sides of length L equal to twice the antenna-to-corner spacing S.

and a null does not occur at $\phi = 45°$ but at a somewhat larger angle. If this is not objectionable, a side length of twice the antenna-to-corner spacing $(L = 2S)$ is a practical minimum value for the 90° corner reflector.

Although the gain of a corner reflector with infinite sides can be increased by reducing the corner angle, it does not follow that the gain of a corner reflector with finite sides will increase as the corner angle is decreased. To maintain a given
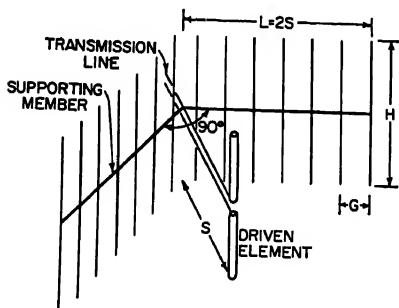
Fig. 11-8. Grid-type reflector.
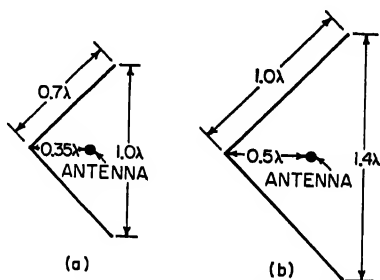
Fig. 11-9. Dimensions for square-corner-reflector antennas.

efficiency with a smaller corner angle requires that S be increased. Also on a 60° reflector, for example, the point at which a wave is reflected parallel to the axis is at a distance of $1.73S$ from the corner as compared with $1.41S$ for the square-corner type. Hence, to realize the increase in gain requires that the length of the reflector sides be much larger than for the square-corner reflector designed for the same frequency. Usually this is a practical disadvantage in view of the relatively small increase to be expected in gain.

To reduce the wind resistance offered by a solid reflector, a grid of parallel wires or conductors can be used as in Fig. 11-8. The supporting member joining the midpoints of the reflector conductors may be either a conductor or an insulator. In general, the spacing G between reflector conductors should be equal to or less than 0.1λ. With a half-wavelength driven element the length H of the reflector conductors should be equal to or greater than 0.6λ. If the length H is reduced to values of less than 0.6λ, radiation to the sides and rear tends to increase and the gain decreases.
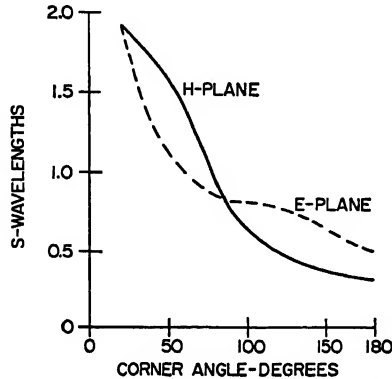
FIG. 11-10. Region of first-order-mode operation.

Two square-corner reflectors of practical dimensions are illustrated in Fig. 11-9. The design a with $S = 0.35\lambda$ and the side length $L = 0.7\lambda$ can be used where the physical size of the antenna must be a minimum. If physical size is not a restriction, design b may be used, with the advantage of a greater bandwidth. The type of driven element is also a factor in determining bandwidth. A fat cylindrical element or a biconical element gives more bandwidth than a thin driven element[4] (see also Chap. 3).

11.4. EXPERIMENTAL RADIATION PATTERNS

Experimental-pattern data* are shown for various corner configurations in Figs. 11-11 to 11-21. Several interesting trends may be observed by close examination of the H-plane patterns. For any particular corner angle, $\beta = 60°$ for example, the
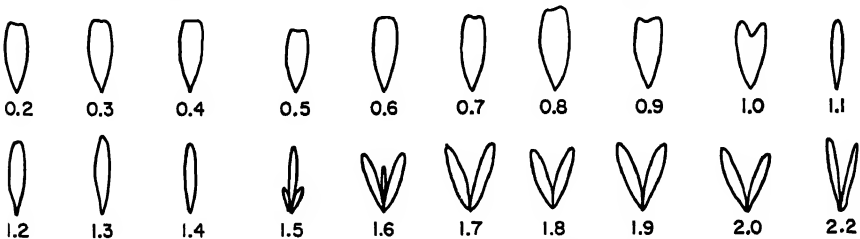
FIG. 11-11. 60° corner, H plane, S_λ variable.

magnitude of any particular set of minor lobes relative to a major lobe may be traced from its origin. At a spacing of 1.4 wavelengths the single-lobe condition is still in existence, but at 1.5 wavelengths the first set of minor lobes begin to appear. Continuing, somewhere between 1.5λ and 1.6λ the amplitudes of the minor and major

* The patterns were taken with sides of dimensions 4×6 wavelengths. These values approximate semi-infinite sheets for the measurements involved.

lobes become equal, and then through a series of spacings during which the minor lobes become larger in relation to the major lobe, until at $S = 1.8\lambda$ the center lobe has entirely disappeared. It is this growth of secondary-lobe structure that represents the higher-order modes of operation and is responsible for the divided characteristic of the beam at larger spacings.

This same evolutionary process may be observed by tracing any one of the other secondary lobes in other configurations through its various stages of development.
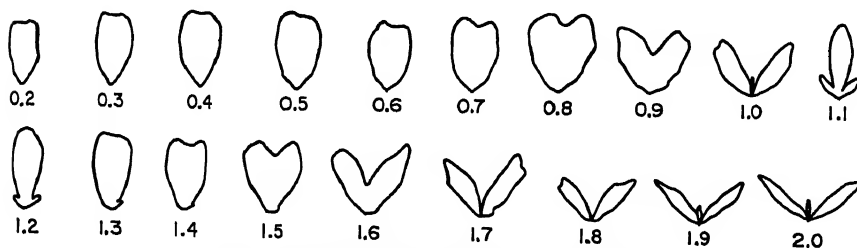
FIG. 11-12. 60° corner, E plane, S_λ variable.
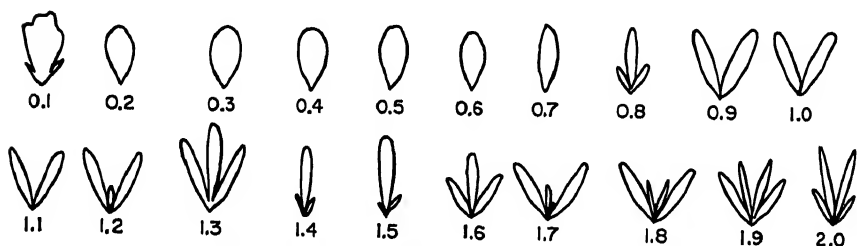
FIG. 11-13. 90° corner, H plane, S_λ variable.
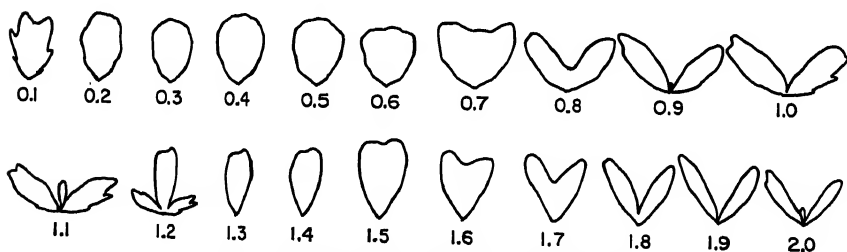
FIG. 11-14. 90° corner, E plane, S_λ variable.

As the spacing becomes of large magnitude, the pattern has a large number of lobes of comparable size. Figure 11-10 is an empirical set of curves which depicts the region over which the spacing may be carried for any particular corner angle in order to maintain first-order-mode operation. The data for the preparation of these curves were obtained from direct observation of the measured patterns.[2]

In an effort to extend the methods of the corner reflector beyond the case of the flat-sheet reflector, the configuration employing an angle of 270° was investigated. The patterns are shown in Fig. 11-19. An immediate application may be seen from inspection of the patterns with spacings around 0.3 wavelength. This configuration provides a perfectly uniform distribution of radiated field over 180° of azimuth. Beyond this the field drops rapidly to zero. At greater spacings the pattern becomes

elongated, and finally multilobes appear. For services requiring coverage diagrams of 180° this is a very useful device and might conceivably be mounted at the corner of a building in order to take full advantage of structural conditions.

11.5. TILT OF MAIN BEAM

It is of interest to investigate methods of tilting the main beam off the centerline of the corner angle. Figure 11-20 shows the effects on pattern of setting the dipole
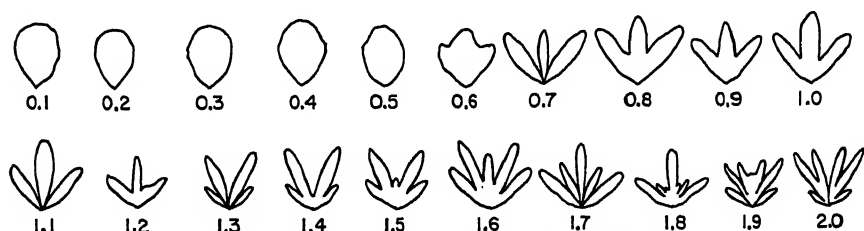
Fig. 11-15. 120° corner, H plane, S_λ variable.
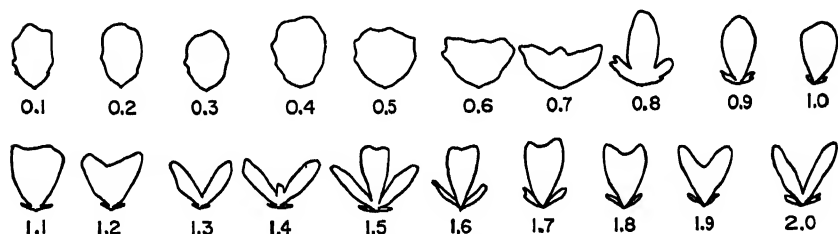
Fig. 11-16. 120° corner, E plane, S_λ variable.
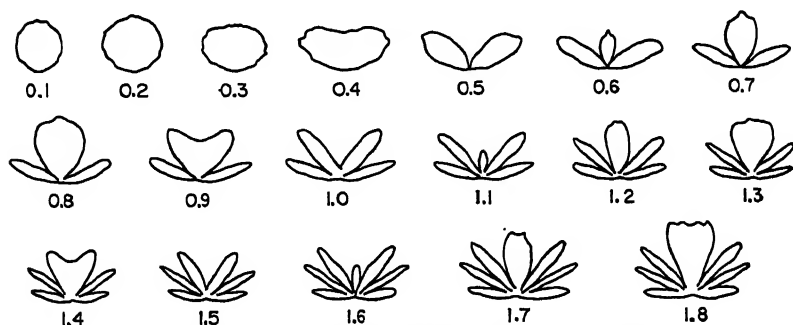
Fig. 11-17. 180° corner (flat sheet), H plane, S_λ variable.

15° and 25° off the centerline as the apex-to-corner spacing is varied. In the 15° case the beam is single-lobed for small spacings and the tilt condition begins to appear at 0.5λ. This tilt is in a direction opposite to the offset of the dipole, and the maximum angle of about 15° occurs at $S = 0.6\lambda$. Beyond this the beam becomes multilobed. At a spacing of 1.0 wavelength a single tilted lobe reappears at an angle of about 20° in the direction of the dipole offset. At greater spacings the breakup becomes severe and the operation is no longer practical. In the 25° offset, operation is similar except that the second single lobe occurs around 1.5 wavelengths with a deflection

somewhat greater than before. Designs utilizing two dipoles in lobe-switching applications are possible using this property of the 90° corner-reflector antenna. However, these data do not include the effects of the passive dipole.

11.6. CORNER REFLECTOR USING SPINE CONSTRUCTION

Of practical interest is the operation of the array using spine construction. Figure 11-21 shows several cases of spine construction, with the 90° corner. The first set using 0.1λ spine spacing and a 6λ reflector substantially reproduces those patterns
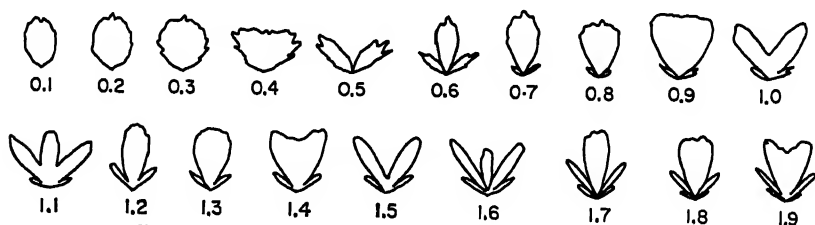
FIG. 11-18. 180° corner (flat sheet), E plane, S_λ variable.
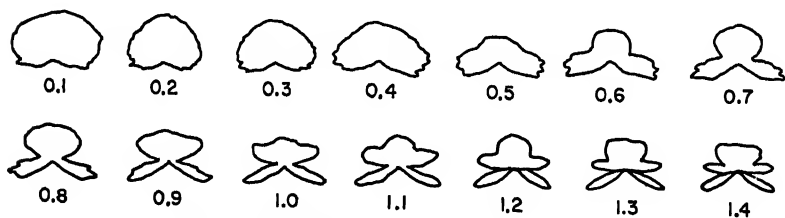
FIG. 11-19. 270° corner, H plane, S_λ variable.
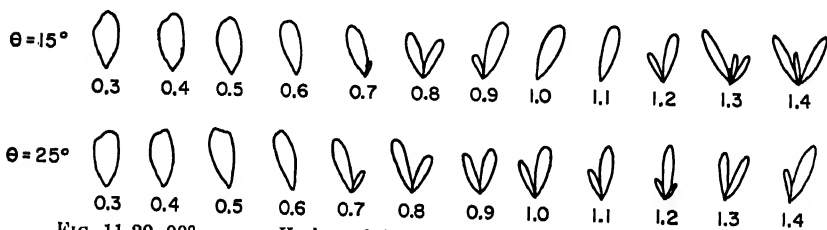
FIG. 11-20. 90° corner, H plane, λ/2 dipole located off bisector, S_λ variable.

taken with semi-infinite sheets. When the length of the reflector is reduced to 2 wavelengths, there is a tendency to broaden some of the lobes and to lose the definite minimum ($S = 1.0λ$). However, the agreement is still quite good. When the spine spacing is increased to 0.2 wavelength the patterns hold up quite well, but when it is further increased to 0.3 wavelength there is quite an increase in radiation through the reflector sheets although the main lobes hold up quite well. The last set of patterns shows the condition of 0.1λ spine spacing and reflector length of one wavelength. The one-wavelength reflector seems capable of maintaining the pattern at spacings as large as 0.6λ, and although the general shape of the pattern is recognizable at greater spacings, the diffraction around the reflector is so great as to make for very poor operation.

G=0.1λ H=2λ L=6λ

0.4 0.6 0.8 1.0 1.2 1.4 1.5

G=0.1λ H=2λ L=2λ

0.4 0.6 0.8 1.0 1.2 1.4 1.5

G=0.2λ H=2λ L=2λ

0.4 0.6 0.8 1.0 1.2 1.4 1.5

G=0.3λ H=2λ L=2λ

0.4 0.6 0.8 1.0 1.2 1.4 1.5

G=0.1λ H=2λ L=1λ

0.4 0.6 0.8 1.0 1.2 1.5
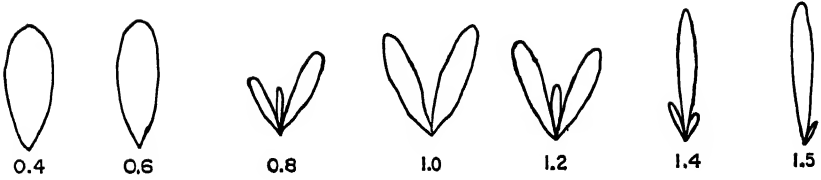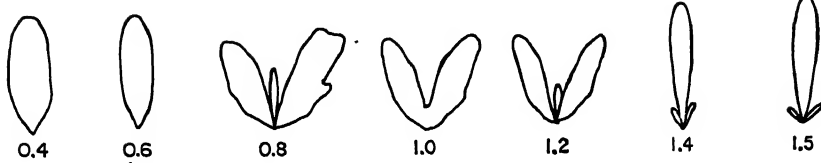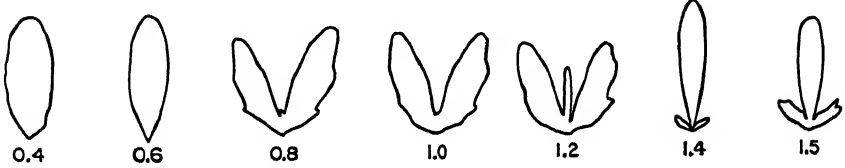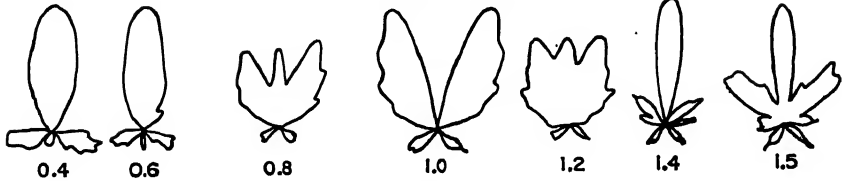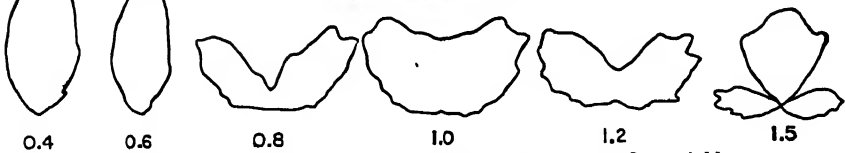
FIG. 11-21. 90° corner, H plane, spine construction, S_λ variable.

REFERENCES

1. John D. Kraus: "The Corner-reflector Antenna," *Proc. IRE*, vol. 28, p. 513, November, 1940.
2. Edward F. Harris: "An Experimental Investigation of the Corner-reflector Antenna," *Proc. IRE*, vol. 41, p. 645, May, 1953.
3. John D. Kraus: "Antennas," p. 334, McGraw-Hill Book Company, Inc., New York, 1950.
4. Radio Research Laboratory Staff: "Very High Frequency Techniques," vol. I, p. 129, McGraw-Hill Book Company, Inc., New York, 1947.
5. S. G. Brown: "Systems of Wireless Telegraphy," U.S. Patent No. 741,622, Oct. 20, 1903.

6. Hidetsugu Yagi: "Directive Projecting System of Electric Waves," U.S. Patent No. 1,745,342, Jan. 28, 1930.
7. John D. Kraus: "The Square Corner Reflector," *Radio*, March, 1939.
8. John D. Kraus: "Corner Reflector Antenna," U.S. Patent No. 2,270,314, Jan. 20, 1942.
9. John D. Kraus: "Broad Band Antenna," U.S. Patent No. 2,452,767, Nov. 2, 1948.
10. J. L. Putnam and W. B. Macro: "Experiments with Slot Aerials in Corner Reflectors," *J. IEE (London)*, pt. IIIA, vol. 93, no. 10, p. 1539, March–May, 1946.
11. E. B. Moullin: "Radio Aerials," Oxford University Press, New York, 1949.
12. James Jeans: "Mathematical Theory of Electricity and Magnetism," 5th ed., p. 188, Cambridge University Press, London, 1933.
13. G. H. Brown: "Directional Antennas," *Proc. IRE*, vol. 25, p. 122, January, 1937.
14. F. Schroter: "Short Wave Aerial," U.S. Patent No. 1,830,176, Nov. 3, 1931.
15. TV Receiving Antennas, chap. 24 of this Handbook.
16. O. M. Woodward, Jr.: "A Circularly-polarized Corner Reflector Antenna," *IRE Trans.*, vol. AP-5, pp. 290–297, July, 1957.
17. R. W. Kloppenstein: "Corner Reflector Antennas with Arbitrary Dipole Orientation and Apex Angle," *IRE Trans.*, vol. AP-5, pp. 297–305, July, 1957.
18. H. V. Cottony and A. C. Wilson: "Gains of Finite-size Corner-reflector Antennas," *IRE Trans.*, vol. AP-6, pp. 366–369, October, 1958.
19. A. C. Wilson: "Impedance of a Corner-reflector Antenna as a Function of the Diameter and Length of the Driven Element," *Journal of Research*, National Bureau of Standards, vol. 64 D, no. 2, pp. 135–137, March–April, 1960.
20. A. C. Wilson and H. V. Cottony: "Radiation Patterns of Finite-size Corner-reflector Antennas," *IRE Trans.*, vol. AP-8, pp. 144–157, March, 1960.

Chapter 12

HIGH-GAIN REFLECTOR-TYPE ANTENNAS

Kenneth S. Kelleher

Aero Geo Astro Corp.
Alexandria, Virginia

12.1. BASIC DESIGN PRINCIPLES

Introduction. The antennas to be considered in this section are used with systems for communication or for radar purposes in which a large value of gain is necessary.

The basic antenna has two components: a relatively small feed and a large reflecting surface. Since the design of the feed has been considered in other sections, a discussion of this element will be carried out here only when necessary to clarify a particular reflector design. The greatest part of the material will consider reflectors utilizing the properties of a parabola. Since these reflectors have been found to be satisfactory in very many different applications, the fundamentals of their design are of greatest importance. However, some consideration will be given to the general reflector problem, so that, with additional effort on the part of the designer, reflector surfaces having novel properties can be devised.

Some general statements can be made concerning the relationship of the reflector-type antenna to other elements used for producing directive beams. At UHF frequencies and above, where directive beams become practical, the designer has the choice of end-fire or broad-side arrays, corner-reflector antenna, or a reflector using a curved surface for focusing incident energy. A careful design of the end-fire, or Yagi, antenna, will produce an economic unit yielding about 15 db gain. However, this element has a relatively narrow band, over which it satisfactorily matches the transmission line, so that it is limited in application. The broad-side array can be used to produce gains greater than that of the end-fire element and equal to that of a reflector antenna. However, the broad-side arrays are limited, from a practical standpoint, by the number of elements required to approximate the reflector antenna. Since at least four array elements must be placed in each square wavelength of the aperture, the number of elements required to approximate the pattern of the reflector-type system may be of the order of a few thousand, so that the feed system becomes unreasonably complex. Few operational array-type antennas have produced gains greater than about 30 db, so that, in general, this antenna compares unfavorably with a high-gain reflector system.

The final directive radiator considered, the corner-reflector antenna, has a basic limitation in that after a certain point an increase in the size of the flat surfaces forming the corner reflector produces no corresponding increase in the antenna gain. Successful corner reflectors have produced gains as high as 14 db with a single feed element; it is doubtful if any greater improvement can be achieved.

In general, the basic advantage of the reflector-type antenna over the other elements mentioned lies in the ease with which a high gain can be achieved. For gains less than 20 db, however, other elements should be considered, and for very low gain antennas, the reflector type is virtually useless, since the curved surface can be replaced by a flat surface with little or no change in antenna performance.

Reflector Geometrical Optics. The high-gain reflector antenna offers an excellent opportunity for the application of geometric optics to antenna problems. The feed horn for such an antenna can be considered as a point source producing a spherical wavefront. This wavefront, upon reflection, is converted into a plane wave or a wave of any desired shape. Reference 1 shows that a general-incident wavefront, reflector wavefront, and a reflector surface can be related so that, given any two of the three, the third can be determined. For the particular case of a spherical wavefront incident upon a reflector, let the origin of the coordinates be at the center of the sphere. Consider a virtual reflected wavefront as the constant phase surface whose phase is equal to that of the center of the sphere, the source point. This "zero wavefront" is indicated in Fig. 12-1 to be given by the vector $Y = 2n(n \cdot R)$, where R is the vector describing the reflector and n is the unit normal to the reflector. It should be noted that this simplification occurs only for the zero wavefront obtained by moving a distance R behind the reflector in the direction of the reflected ray. Any other wavefront can be conveniently obtained from this zero wavefront by analytical or geometrical ray tracing.

For the case of the parabola with focal point at the origin, the reflector R is given

by $(\tan^2 \varphi/2 - 1)i + (2 \tan \varphi/2)j$, where i and j are unit vectors along the x and y axes, respectively. The normal n is $(\cos^2 \varphi/2)i - (\sin^2 \varphi/2)j$ so that the zero wavefront, $Y = 2 \sec \varphi/2 [(\cos \varphi/2)i + (\sin \varphi/2)j]$, is a straight line. This indicates the well-known fact that the wavefront reflected by a paraboloid is a plane.

Another useful formula, which can be applied to the problem of a general ray reflected from a general surface, is obtained by considering the plane of incidence, that is, the plane containing the incident vector and the normal to the surface. In
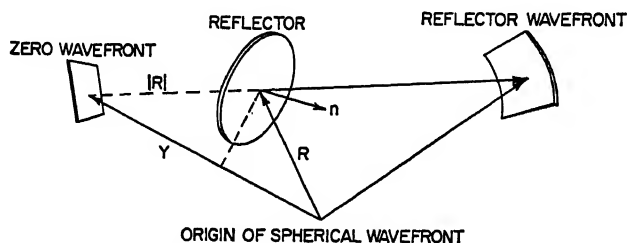
FIG. 12-1. Vector representation of wavefront and reflector surfaces.
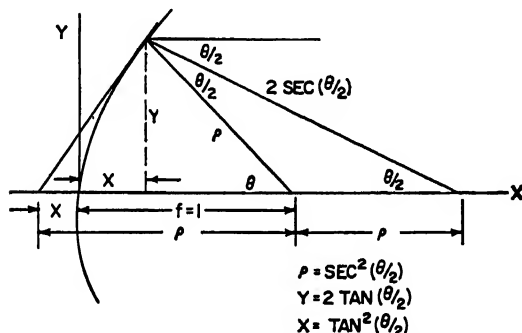
FIG. 12-2. Geometric relationships in parabola with unit focal length.

polar coordinates, the radius vector $\rho(\theta)$, given in the terms of the angle θ, can be related to the angle of incidence i as $\tan i = \rho'/\rho$, where the prime denotes differentiation. In order to indicate the utility of this formula, we can consider the example of surfaces having a plane intersection given by the curve $\rho = \sec^n \theta/n$ with the feed source at the origin. An incident vector in this plane then has an angle of incidence given by $i = \theta/n$. Particular examples of this curve include the straight line for which n equals unity and the parabola for which n is equal to 2. Using this formula for $n = 2$, one can obtain the values of parameters related to the parabolic arc, as are displayed in Fig. 12-2.

The previous discussion has been concerned with wavefronts which give the phase characteristics of a reflector radiator; an analysis can also be made of the signal amplitude in the reflected wave. The flow of ray energy between points P_1 and P_2 can be evaluated from conservation-of-energy principles. If Δs is the area of a surface cutting the ray bundle orthogonally at P_1 and ΔS is the corresponding area at P_2, then the divergence of energy is given by

$$D = \lim_{\Delta s \to 0} \frac{E_1^2}{E_2^2} = \lim_{\Delta s \to 0} \frac{\Delta s}{\Delta S}$$

where E_1 and E_2 are the fields at P_1 and P_2, respectively. Using this formula, it can

be seen that there is no divergence in a ray bundle of a plane wave ($D = 1$) and a divergence of $1/d$ for a cylindrical wave, where d is the distance from the point under consideration to the line source producing the cylindrical wave. For a spherical wave, the divergence is $1/d^2$, where d is measured from the source.

An expression has been derived for the energy divergence of a reflected wave.[2] It is limited to an incident spherical wave and so is not as general as the result obtained in Ref. 1 for the phase of the reflected wave:

$$\frac{1}{D} = \frac{4d_1{}^2d_2{}^2}{\rho_1\rho_2} + (d_1 + d_2)^2 + 2d_1d_2\left(\frac{\sin^2\theta_1}{\rho_2} + \frac{\sin^2\theta_2}{\rho_1}\right)\left(\frac{d_1 + d_2}{\cos i}\right)\ .$$

where d_1 is the distance from the source to the reflector point, d_2 is the distance from that point to the point of observation, and i is the angle of incidence. The ρ's and θ's are related to the principal directions on the reflector;* the ρ's are the radii of curvature in those directions, and the θ's are the angles between the incident ray and those directions.

For the simple paraboloid with feed on focus, we do not need the complex expression above, but instead remark that for a spherical wave the power falls off as $1/d^2$, or as [$\cos^4(\theta/2)$] (see Fig. 12-2 for notation). For the parabolic cylinder fed by a cylindrical wave, the divergence becomes [$\cos^2(\theta/2)$].

12.2. PARABOLOIDAL-TYPE REFLECTORS

The most useful of the high-gain reflector antennas utilizes the paraboloidal surface, which is formed by rotating the arc of a parabola about the line joining the vertex and the focal point. The geometrical relations for such a reflector can be obtained from Fig. 12-2, which represents a typical cross section through the reflector in a plane containing the axis. The major problems associated with this reflector antenna are related to obtaining an efficient combination of reflector and feed. If it is assumed, for convenience, that the typical feed pattern can be described as a cosine function of the angle measured away from the peak of the beam, some general conclusions can be found. The first is that the reflector cannot intercept all energy from the feed, as might be desirable for maximum gain. A second consideration is that in attempting to intercept all this energy, the reflector size becomes large and its outer portion, which represents a considerable amount of the reflector area, receives a low-intensity field from the feed. This tends to minimize the abrupt field discontinuity at the reflector edges and so minimizes side lobes. Since reflector size is limited from the mechanical design standpoint, it is often desirable to minimize the reflector regions of low intensity. A compromise must therefore be reached between making the reflector sufficiently large to capture the feed energy and making it too large to be useful from a mechanical standpoint.

In a typical design, the reflector size is chosen to be as large as practical, and then the feed is designed for efficient illumination. Normally, the design is based on obtaining either the maximum gain from the antenna or a reduction in side lobes at the expense of a slight decrease in gain. For maximum gain, it has been found that the energy reflected should be distributed so that the field at the reflector edges is approximately 10 db below that of the center; for good side-lobe performance, the field at the edge should be about 20 db down.

It has been found useful in feed design to employ a set of curves which will indicate the beamwidth of the feed necessary to produce the desired edge illumination on a particular reflector. One of the curves utilized is a normalized feed pattern (Fig.

* For discussion of principal directions, see L. P. Eisenhart, "An Introduction to Differential Geometry," Princeton University Press, Princeton, N.J., 1940.

12-3). This pattern was obtained through a comparison of many experimentally measured data points. It can be closely approximated over all but the lower intensity regions of the beam by a simple quadratic function. The beamwidth at any point is proportional to the square root of the decibel reading at that point. For example, the beamwidth is doubled when the decibel reading is increased by a factor of 4. This
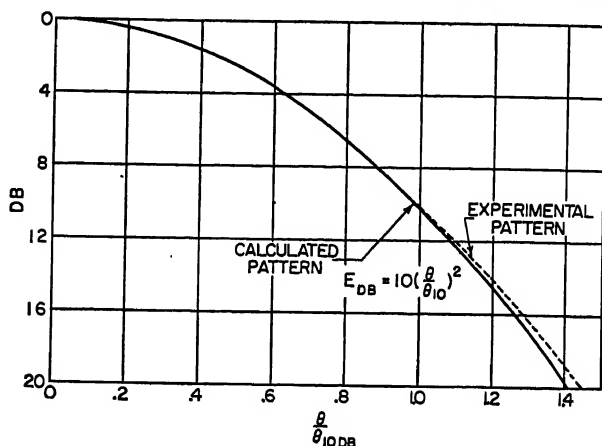
FIG. 12-3. Universal feed-horn pattern.
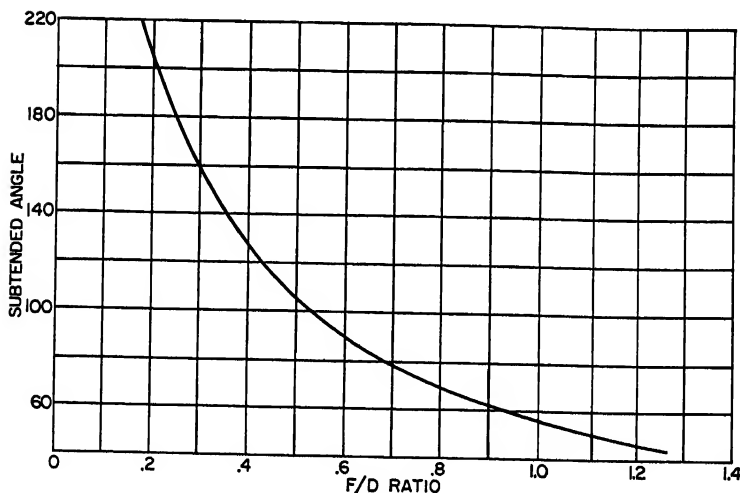
FIG. 12-4. Ratio of focal length to aperture diameter vs. subtended angle at focal point.

curve is necessary because of the fact that beamwidth information is normally available only at a particular decibel value, such as 3 or 10 db, whereas in actual application one is interested in the beamwidth at the points where rays are directed to the edges of the reflector.

In order to relate the reflector geometry to the pattern beamwidth, a second curve is necessary. Normally, the information available on the paraboloidal reflector surface is its focal length and aperture dimension, so that one can immediately use the ratio of these quantities, designated by f/D. From the information of Fig. 12-2,

it is possible to produce a curve relating the f/D ratio to the feed angle θ. This relationship is given graphically in Fig. 12-4.

Once the feed angle corresponding to the reflector edges has been determined, it would appear possible to utilize Fig. 12-3 directly in order to obtain a value of edge illumination. However, one additional factor must be considered, the divergence factor of Fig. 12-1 ($\cos^4 \theta/2$). This function can be converted to decibels and plotted in Fig. 12-5. It is evident from the figure that the space-attenuation factor is negligible for small values of feed angle and becomes relatively large for feed angles of the order of 90°.
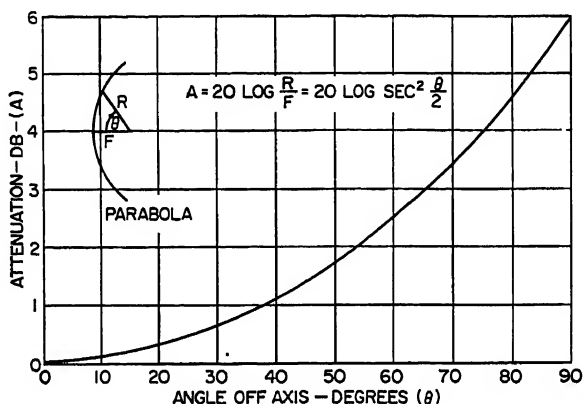
FIG. 12-5. Space attenuation vs. feed angle.

In order to understand the use of Figs. 12-3 to 12-5, a typical problem can be solved. If it is required that the edge illumination should be 20 db in a reflector whose f/D ratio is 0.5, one first enters the curve of Fig. 12-4 and finds that the total feed angle is 106°. From Fig. 12-5, the space attenuation at this angle (53° degrees from the axis) is 1.9 db. The desired edge illumination can then be found by noting that the feed horn should have a signal 18.1 db down at an angle of 53° from the peak of the beam. Since the feed-horn design curves are given in terms of the 10-db beamwidth, it is necessary to determine what 10 db width is associated with 18.1 db at 53°. Since, as previously stated, the beamwidth ratio is proportional to the square root of the decibel ratio, the desired width is given by $(10/18.1)^{1/2} \times 53° = 39.5°$, so that the total 10-db width is equal to 79°.

Some slight improvement in accuracy might be obtained if the quadratic nature of the beamwidth is ignored and the standard pattern of Fig. 12-3 is used. From this figure, it is found that the ratio in beamwidth between 10 and 18.1 db is equal to 0.73, which corresponds to a feed whose 10-db width is 77.5°. Because of the negligible difference between these two answers, it can be seen that, for most practical applications, the quadratic approximation to the standard pattern can be employed.

Interaction between Reflector and Feed. From the considerations of the previous section, it is evident that the design of the reflector cannot be entirely divorced from that of the feed. An even more significant relationship arises when one considers interaction between these two elements. Because of this interaction, the feed disturbs the radiation pattern of the reflector and the reflector affects the match of the feed. A third problem of considerable significance in smaller reflectors is the contribution of the backward radiation from the feed to the pattern formed by the reflector. This effect tends to raise the side-lobe level of the radiation pattern as the reflector aperture is decreased below an aperture of 10 wavelengths.

The effect of the horn on the radiation pattern of a large reflector can be analyzed in a very simple manner. The horn, with its associated waveguide, represents an obstacle in the radiating aperture. The final radiation pattern can be shown to consist of the pattern from the unobstructed aperture minus the pattern of the obstruction. This very simple analysis has been shown to be satisfactory and to compare very closely with measured experimental results. Since, in general, the feed design is determined from mechanical considerations and from the reasoning of the previous section, a minimization in the effect of feed blocking is obtained only as the aperture size in wavelengths increases. This is due to the fact that the feed geometry depends primarily on the angular sector of the dish and so is unchanged as the reflector size in wavelengths is increased. It should be noted that the feed obstruction, that is, the feed horn plus waveguide, is normally limited to a single plane. The effect of this obstruction on side-lobe performance is then most pronounced in the plane perpendicular to the feed obstruction where the obstruction pattern is very broad. In the other plane, the obstruction pattern has a much narrower beamwidth, which approaches that of the reflector and so is relatively weak in the regions where it might contribute an increase in side-lobe level.

The above discussion of feed obstruction assumes that the dimension of this obstruction in the direction of propagation is relatively small; however, if this dimension becomes appreciable, then the effect of the obstruction on the feed pattern becomes more complex and, in almost every case, a further increase in side-lobe level is found. Experimentally, it has been determined that the minimum value of side-lobe level is obtained if the feed structure in the direction of propagation is "streamlined." This has been accomplished by enclosing all parts of the feed structure, with the exception of the feed horn itself, in a thin cylinder whose cross section approximates an ellipse of large ratio between major and minor axes.

The effect of the reflector on the match of the feed horn can be analyzed in a simple manner if it is understood that most of the energy reflected back into the feed comes from the region in the neighborhood of the reflector vertex. Since the incident wave was divergent, a focal length large in wavelengths would tend to minimize the amount of signal reflected back to the feed. For a given reflector, an increase in the gain of the feed, which corresponds to an increase in peak signal compared with signals from other directions, will result in greater energy incident upon the reflector vertex and therefore a greater reflected wave and a greater mismatch. From these considerations it can be shown[3] that the reflection coefficient introduced by the presence of the paraboloid is given by $\Gamma = g\lambda/4\pi f$, where g is the gain of the feed in the direction of the vertex.

It is of interest to determine the proper value of focal length for minimum mismatch if the reflector aperture and illumination are held fixed. Since for a circular aperture the feed gain is inversely proportional to beamwidth squared, it can be replaced in the formula by the square of an angle, which except for space attenuation is directly related to the angle θ, subtended by the aperture at the focal point. Since the aperture diameter is given by $D = 2f \tan (\theta/2)$ (Fig. 12-2), we can write $\Gamma \propto [\tan (\theta/2)]/\theta^2$, which indicates a smaller value of reflection coefficient for large θ, that is, for short focal lengths. The minimum reflection is limited by the decreased value of reflector gain realized when a short focal-length reflector is used.

Asymmetrical Cut Paraboloids. In order to reduce the effects of the feed-horn blocking on the radiation pattern and of the reflector mismatch on the feed horn, the paraboloid with vertex in the aperture center can be replaced by one whose vertex lies off center or, in the extreme case, completely outside of the reflector aperture. This departure from the previous symmetrical aperture introduces no change whatsoever in the aperture-phase characteristics. The phase, determined by geometrical-optics ray tracing from feed to reflector, and hence to an aperture plane, is a constant

for any ray position. The use of any selected region of the paraboloidal surface does not affect the ray-path length, and so leaves the phase characteristics unaltered.

The amplitude of the signal across the aperture is affected by the change to an asymmetrical surface. It is evident that the feed horn must be repositioned so that it points its peak intensity toward the reflector surface. In general, it is not centered on the reflector surface but is moved past the reflector in the direction away from the vertex. This noncentering arises from the fact that there is usually a considerable difference between the space attenuation at the two reflector edges. Since this attenuation is greater at the edge farthest from the vertex, the feed horn is positioned to compensate for the difference in space attenuation.

The effect of the feed system on the radiation pattern can be analyzed by projecting the reflector surface and the outlines of the feed horn upon the aperture plane. If the feed horn does not lie on the projected surface area, then it will not affect the radiation pattern. For cases in which it lies on this projected area, its effect is a direct function of amplitude of the aperture field at that point.

The improvement in match obtained from an asymmetrical reflector can be evaluated by determining the reflection coefficient corresponding to the asymmetrical surface. Since the reflected signal which enters the feed horn still originates at the vertex, the only change in the previous formula for reflection coefficient would be a modification in the gain figure to account for the fact that the tilted feed has reduced gain in the direction of the vertex.

Feed Horn off Focus. The problem of the radiation patterns to be expected when the feed-horn phase center does not correspond with the focal point of the paraboloid can be analyzed in two steps. The first, and simplest, occurs when the feed remains on the paraboloid axis. As the feed is moved toward the vertex or away from the vertex, it can be seen that the wavefront becomes convex or concave. For reasonable displacements of the feed, the corresponding phase error across the aperture can be represented by a quadratic function. With such a phase error, the pattern to be expected can be conveniently analyzed through use of the Cornu spiral.[4] If the displacement from the focus is given as p, the phase error is $px^2/(2f^2 - 4fp)$, where f is the focal length. The resulting pattern, for a uniformly illuminated aperture, is given by the integral below:

$$E(\theta) = \int_a^b \exp\,(jt^2)\,dt$$

where $a = -q(D/2) - (2\pi/q\lambda)\sin\alpha$, $b = q(D/2) - (2\pi/q\lambda)\sin\alpha$, $q^2 = p/(2f^2 - 4fp)$, and D is the aperture dimension in the plane of the pattern. In order to evaluate this pattern, one computes the values of the limits for various pattern angles α. These values represent arc lengths along the Cornu spiral. The straight-line distance between the limit points corresponds to the radiation field at the pattern angle used to compute that value of a and b. From the nature of this pattern computation, it can be seen that it is very difficult to obtain pattern angles at which the field disappears. Therefore a general characteristic of feeds displaced from the focal point is the absence of deep nulls in the radiation pattern. The presence or absence of nulls can therefore be used to indicate the correct feed positioning at the focus of a reflector which satisfies mechanical tolerances. Other characteristics of the defocused radiation pattern are a reduction in gain and a tendency for the side lobes to increase and to merge into the minor beam as "shoulders." These effects can be evaluated in a particular instance by using the Cornu spiral (see also Sec. 2.11).

The radiation patterns which are found when a feed moves away from the axis are considerably more complex. For small displacements from the focal point in a plane normal to the axis and containing the focal point, the phase error has a cubic form (see also Sec. 2.11).

If the aperture illumination is represented by $\exp(-\beta^2 x^2)$, the pattern for small feed displacement p can be given by[5]

$$E(\theta) = e^{vw} \int_0^\infty \cos\left[\frac{y^3}{3} + (w + v^2)y\right] dy$$

where

$$v = \beta^2 / (3\pi f p / 2\lambda)^{2/3}$$

$$w = \frac{2\pi f \sin\theta/\lambda}{(3\pi f p / 2\lambda)^{1/3}}$$

This expression is known as the "Airy integral"; values of this integral for various values of $w + v^2$ are tabulated.[6] A plot of this function shows that the cubic phase error produces an asymmetrical pattern. On the side of this pattern nearest the reflector axis, a series of side lobes appear which decrease as one leaves the main beam. On the other side of the beam, the signal decreases without exhibiting any pronounced lobe structure. It has been customary to designate the side lobes in this pattern as "coma" lobes. These lobes represent the basic limitation in the use of the paraboloid with feed displaced from the axis, since they are excessively high before any reduction in antenna gain is apparent.
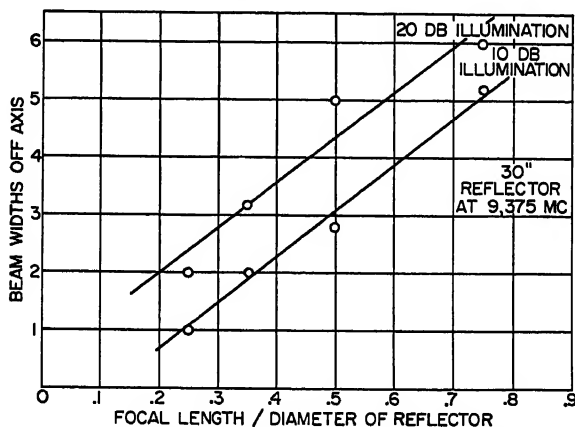
FIG. 12-6. Beamwidths off axis as a function of f/D ratio.

For small displacements of the feed from the axis, it can be shown[5] that for a given position off axis, the patterns can be improved by increasing the focal length of the reflector relative to the aperture dimension and by increasing the illumination taper at the reflector edges. The number of wavelengths in the aperture has little effect on the side-lobe level, and this factor can be removed from an analysis of the problem by expressing the off-axis position in terms of "beamwidths off axis." Figure 12-6 shows the beamwidths off axis which can be scanned before side-lobe level of 15 db is reached. The two curves correspond to edge illuminations of 10 and 20 db.

Beam Factor. When a beam is scanned off axis in a paraboloid, its angular position is smaller than the angular displacement of the feed horn. The ratio between these two angles was studied[5] and was found to depend on edge illumination and on f/D ratio. This dependence is shown in Fig 12-7. The points for zero displacement are calculated points, while the remaining ones are experimental. It can be seen that for large f/D ratios, the beam factor approaches unity.

Radiation Patterns from Paraboloidal Reflector. The problem of the analysis of radiation patterns from the simple paraboloidal reflector has been considered many

times by many different investigators. The most satisfactory work[7] compared computed patterns with measured ones. This work considered a reflector whose edges formed an ellipse; a particular case would be the circular aperture. Other work considered rectangular or circular apertures which have less general application.
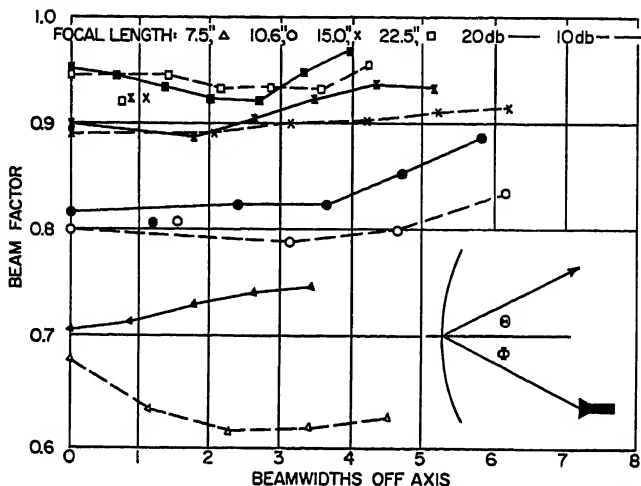
FIG. 12-7. Beam factor vs. f for $D = 30''$.   (Data taken at 9,375 Mc.)

Since the side-lobe level is dependent on the outline of the reflector aperture, the elliptical aperture yields closer agreement with experiment.

When an elliptical aperture has an illumination function

$$A(x,y) = \left(\Sigma a_r \cos \frac{r\pi x}{a} \right) \left(\Sigma b_s \cos \frac{s\pi y}{b} \right)$$

and a and b are the semimajor and semiminor axes of the ellipse, an accurate pattern can be obtained from the expression below:

$$F(u) = \pi a b \sum_{r=0}^{2} \sum_{s=0}^{2} a_r b_s G_{rs} \qquad u = ak \sin \alpha, \text{ or } bk \sin \beta$$

The G functions are tabulated in Table 12-1 for the pattern in the plane of the major axis (aperture dimension of $2a$). For the pattern in the other principal plane, the indices of G in the tabulation must be interchanged. An implicit assumption in this calculation is that the field amplitude at any point can be found from the product of the field at corresponding points on the x and y axes. This assumption was investigated experimentally and found to be satisfactory. The patterns obtained from the formula above closely matched experimentally measured patterns, particularly as regards gain, beamwidth, and first side lobe. The position, but not the amplitude of other side lobes, was correctly predicted. It is well known that the side-lobe level in one principal plane depends on the edge illumination in that plane; however, Ref. 7 reveals the little-known fact that the edge illumination in the other plane will also influence the side-lobe level. Figure 12-8 shows the side lobes computed, using measured primary patterns. It can be noted that in the plane of varying illumination the level decreases with increasing illumination taper, while in the other plane a slight increase in side-lobe level is found.

Table 12-1. Table of Functions Used to Compute Radiation Pattern

u	πG_{00}	πG_{01}	πG_{02}	πG_{10}	πG_{11}	πG_{12}	πG_{20}	πG_{21}	πG_{22}
0.00	3.1416	0.5688	−0.2124	0.5688	−0.3042	0.0032	−0.2124	0.0032	0.1820
0.25π	2.9042	0.6753	−0.1882	0.4764	−0.2369	−0.0224	−0.1980	0.0042	0.1576
0.50π	2.2674	0.9460	−0.1032	0.2366	−0.0637	−0.0808	−0.1522	0.0069	0.0934
0.75π	1.4112	1.2569	0.0686	−0.0606	0.2029	−0.1319	−0.0864	0.0020	0.0126
1.00π	0.5692	1.4646	0.3435	−0.3042	0.2855	−0.1332	0.0032	−0.0152	−0.0584
1.25π	−0.0606	1.4590	0.7028	−0.4132	0.3148	−0.0652	0.0948	−0.0424	−0.1019
1.50π	−0.3754	1.2182	1.0834	−0.3640	0.2195	0.0565	0.1690	−0.0687	−0.1117
1.625π	−0.4154	1.0259	1.2478	−0.2912	0.1366	0.1239	0.1918	−0.0766	−0.1069
1.75π	−0.3904	0.8045	1.3901	−0.1980	0.0444	0.1850	0.2020	−0.0780	−0.0975
2.00π	−0.2124	0.3435	1.5312	0.0022	−0.1332	0.2649	0.1820	−0.0584	−0.0746
2.25π	0.0141	−0.0331	1.4536	0.1532	−0.2415	0.2571	0.1132	−0.0113	−0.0552
2.50π	0.1690	−0.2380	1.1679	0.2024	−0.2438	0.1600	0.0178	0.0504	−0.0430
2.75π	0.1978	−0.2572	0.7491	0.1494	−0.1512	0.0093	−0.0096	0.1024	−0.0326
3.00π	0.1178	−0.1448	0.3124	0.0378	−0.0184	−0.1350	−0.1200	0.1126	−0.0139
3.25π	−0.0056	0.0085	−0.0311	−0.0698	0.0955	−0.2180	−0.1174	0.1004	0.0163
3.50π	−0.1006	0.1187	−0.2129	−0.1236	0.1429	−0.2122	−0.0682	0.0435	0.0546
3.75π	−0.1240	0.1424	−0.2279	−0.1064	0.1143	−0.1296	0.0030	−0.0242	0.0869
4.00π	−0.0772	0.0867	−0.1274	−0.0390	0.0360	−0.1034	0.0632	−0.1755	0.0980
4.25π	0.0030	−0.0036	0.0076	0.0378	−0.0463	0.0841	0.0876	−0.0898	0.0791
4.50π	0.0684	−0.0755	0.1041	0.0834	−0.0920	0.1243	0.0692	−0.0640	0.0339
4.75π	0.0870	−0.0857	0.1246	0.0792	−0.0838	0.0992	0.0212	−0.0126	−0.0204
5.00π	0.0556	−0.0598	0.0758	0.0342	−0.0340	0.0313	−0.0310	0.0386	−0.0625
5.25π	−0.0016	0.0021	−0.0032	−0.0228	0.0264	−0.0401	−0.0622	0.0663	−0.0753
5.50π	−0.0504	0.0538	−0.0060	−0.0604	0.0648	−0.0801	−0.0598	0.0596	−0.0549
5.75π	−0.0654	0.0692	−0.0829	−0.0612	0.0641	−0.0733	−0.0282	0.0250	−0.0121
6.00π	−0.0424	0.0447	−0.0525	−0.0290	0.0295	−0.0302	0.0140	−0.0180	0.0317
6.25π	0.0012	−0.0012	0.0018	0.0150	−0.0166	0.0211	0.0450	−0.0477	0.0564
6.50π	0.0392	−0.0409	0.0472	0.0462	−0.0485	0.0507	0.0500	−0.0507	0.0520
6.75π	0.0514	−0.0536	0.0609	0.0490	−0.0507	0.0565	0.0288	−0.0277	0.0231
7.00π	0.0338	−0.0351	0.0395	0.0248	−0.0252	0.0204	−0.0050	0.0071	−0.0141
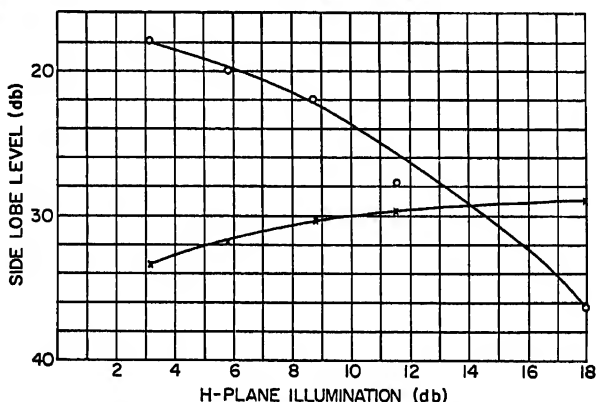
FIG. 12-8. Side-lobe level as a function of illumination.

It should be noted that side-lobe levels are independent of the polarization characteristics of the feed and so cannot be predicted to be higher or lower in the E or H planes. These lobes depend instead on the feed-horn pattern and on the reflector outline. The role of the reflector outline can be understood if it is realized that the principal plane pattern is made up of contributions from weighted elements across

the corresponding line in the aperture; for example, a diamond-shaped reflector which has its greatest dimension in the horizontal plane will produce a pattern in that plane with very low side lobes. This is due to the fact that with given feed illumination the weighted illumination across the horizontal line in the aperture produces a taper considerably greater than that for a corresponding rectangular aperture. From these considerations it is evident that design information involving side-lobe levels will require an analysis of the contribution of every point in the reflector to a given principal plane pattern, rather than a consideration only of the points lying along the aperture line corresponding to the given principal plane.

The analysis of Ref. 7 and other similar work predicted a gain for the paraboloid of 74 per cent of that obtained from a uniformly illuminated aperture. This is some 0.6 db greater than that which has been obtained experimentally and is probably due to a neglect of back radiation from the feed horn or to the existence of cross-polarized energy. Experimental gain measurements have shown that with a large reflector a gain of 65 per cent of uniform-illumination gain could be achieved.

The beamwidth predicted by the elliptical-aperture analysis can be expressed in a simple form. When an optimum in side lobes and gain is obtained, the pattern in either principal plane has a 3-db width given by $\alpha = 65°\lambda/D$, where D is the aperture dimension in that plane. This formula has also been found satisfactory for use with an aperture of rectangular outline; however, some deviation is experienced in a reflector with a diamond-shaped outline, so that some thought must be given before applying this formula to any paraboloidal reflector. It should be noted that this beamwidth is obtained in a good design; an average paraboloidal antenna might have a pattern width given by $70°\lambda/D$.

The side-lobe level to be expected from the reflector depends on the illumination, both in amplitude and phase, and on the reflector outline. Minimum side-lobe levels are obtained from a simple feed horn, a reflector with precision surface, and low edge illumination. Major variations in the reflector outline are not generally available to the antenna designer; if the outline can be modified, best performance is obtained when the reflector edge is distorted to form an acute angle.

Gain of Paraboloidal Reflector. The reflector gain is less than that which could be obtained from a uniformly illuminated aperture. The reason for this is twofold. First, with conventional feed it is impossible to produce an illumination at the reflector edges equal to that at the center. Second, some energy from the feed system must spill over past the edges of the reflector so that it does not appear in the focused wave leaving the reflector. Many different analyses can be made on this decrease in gain; the final results depend on the approximations employed in mathematics. The best mathematical work predicts a gain of 74 per cent of that for the uniformly illuminated aperture, while careful experimental measurements indicate an optimum-gain figure of 65 per cent. At the present time, this difference is attributed to radiation from the feed horn in the form of back lobes and to the existence of cross-polarized energy.

Early work on reflector gain considered systems utilizing dipole feeds. Because of the difficulty in controlling the amplitude and phase throughout a reflector aperture illuminated by a dipole feed, and because of the high back-lobe characteristic of these feeds, they see limited use in present applications. If such a feed system must be used, maximum gain is obtained only by a cut-and-try procedure on the dipole dimensions and position. In general, maximum gain might be obtained with the dipole displaced from the focal point so that a phase error exists over the aperture. It can be expected that the gain of this system would be somewhat less than that employing a horn at the focal point to give no aperture phase error.

It is interesting to relate the reflector gain to its beamwidth. A useful gain formula based on experimental results is $G = 27,000/\alpha\beta$, where α and β are the 3-db beamwidths in the two principal planes. If we substitute into this formula the value of

α and β in terms of wavelength and aperture dimension, as given in the previous section, we find that for a circular aperture, the gain becomes

$$G = \frac{6.4D^2}{\lambda^2} = \frac{0.65(4\pi)(\pi D^2/4)}{\lambda^2} = 0.65\frac{4\pi A}{\lambda^2}$$

This final expression for gain represents 65 per cent of the gain from a uniformly illuminated aperture, indicating that the experimental gain figure is consistent with the experimental beamwidth figure.

For a given reflector, maximum gain is usually obtained with an edge illumination of about 12 db; however, this value can change with f/D ratio of the reflector. Moreover, for small f/D ratio, that is, for reflector subtending large angles at the local point, it is difficult to obtain a gain figure as great as 65 per cent. The reason for this can be understood by considering the twofold loss in gain described previously. For small values of f/D ratio, large space-attenuation factors are introduced in the edge illumination (Fig. 12-5). This means that for edge illumination of 12 db, the feed pattern in this direction might be down only 6 db (for $f/D = 0.25$). All the energy below the 6-db point is spilled over past the edge of the reflector and is lost. Larger values of f/D ratios yield less space attenuation, so that only energy below the 10-db level will be lost past the reflector. Table 12-2 shows measured gain variation with f/D ratio.

It should be mentioned that phase errors across the aperture affect the pattern gain. In a good design, these will be minimized by using a precision-surface reflector and a simple feed horn positioned at the focus. If some phase error must be accepted, gain can be optimized only by cut-and-try techniques.

Table 12-2. Antenna Gain vs. f/D (10-db Illumination)

f/D...........	0.35	0.50	0.75
Gain..........	34.8	35.6	35.6

12.3. PARABOLIC-CYLINDER REFLECTORS

Another useful type of reflector is a parabolic cylinder whose elements are all perpendicular to the plane containing a parabolic arc. Because this is a singly curved surface, the problems of construction and maintaining tolerances are somewhat easier than those encountered in the case of the paraboloid. It can be constructed of tubes or slats which are straight-line elements of the cylinder, or it can use identical parabolic arcs formed of tubes or slats and positioned so that their corresponding planes are perpendicular to the elements of the cylinder.

The feed system for this type of reflector can be either a line source or a point source. The line source generates a cylindrical wave which becomes a plane wavefront upon reflection. The point source generates a spherical wave which becomes a cylindrical wavefront upon reflection, so that the effective combination produces a line source which is normal to the cylinder elements. If desired, an additional parabolic cylinder could be so positioned as to convert this cylindrical wavefront upon reflection into a plane wavefront; that is, a point source and two parabolic-cylinder reflectors will produce the same wavefront as a point source and a single paraboloid.

Line-source Feeds. The more conventional use for the parabolic-cylinder reflector is in conjunction with a line-source feed. This source can assume many different forms, each of which can be analyzed as a linear radiating aperture. In practice, this aperture is made to coincide with the locus of the focal points of the parabolic arcs, which is a line parallel to a cylinder element.

The early line sources utilized waveguide transmission line which energized a linear array of dipole elements. The design characteristics of such arrays have been considered in Chap. 5. Another system utilized slot antenna arrays, such as those considered in Chap. 9. A third technique employed the pillbox-type antenna, which will be described in Sec. 12.4.

An important characteristic of these feeds is that they need not produce only cylindrical waves, but, as a feed for the parabolic cylinder, will prove just as effective when they generate a conical wavefront. It can be shown that a line source which has a linear variation in phase along its length produces a conical wavefront. This wavefront, upon reflection from the parabolic cylinder, becomes a plane wave propagated from the antenna at an angle whose direction is related to the angle of the cone. If the direction normal to the line source is used as a reference, then the reflected wavefront makes an angle with this direction equal to the half angle of the cone.

The illumination problems of a line-source feed used in connection with a parabolic-cylinder reflector are quite similar to those encountered when a point source is used with the paraboloid. The two-dimensional analyses of the two antenna systems are identical; however, the space-attenuation factor and the minor-lobe problems are different. Since the decrease of energy in the cylindrical wave is inversely proportioned to the distance, whereas that in the spherical wave is inversely proportioned to the square of the distance, the space-attenuation factor for the line source is given by the square root of the figure for the point source. In decibels, one uses values of one-half those given in Fig. 12–5.

The side-lobe problem for a line source feeding the parabolic cylinder presents the difficulty that the relative difference in gain between the source and the focused wave is not sufficient to depress the lobes from the source. This problem is particularly acute for a system in which the polarization of the line source is normal to the line of the source aperture. The radiation pattern in the plane normal to this is of the E-plane type, so that high side lobes are normally found. These lobes may be only 10 db down from peak intensity. If the relative gain of the reflector is 10 db more than that of the source, the side lobes in the source pattern are only 20 db down in the final radiation pattern. Some success in reducing these side lobes has been achieved by adding choke sections to either side of the horn aperture. The design is achieved by experimental techniques.

The feed-blocking problem for a parabolic-cylinder reflector is much more serious than in the case of the paraboloid because of the increase in feed size with respect to the size of the radiating aperture. This blocking will produce the pattern distortion described in Sec. 12.2. It is most significant in the plane normal to the line source. For this reason, an asymmetrical reflector is used so that the feed can be removed from the path of the reflected radiation.

The size of the feed has indirectly restricted the f/D ratio of the parabolic-cylinder antennas. From a consideration of the earlier material on paraboloids, it can be seen that larger feed-horn structures are required to correctly illuminate reflectors of large f/D ratio. Therefore, in order to minimize the size of the line-source feed, smaller values of this ratio are chosen. A further advantage in the choice of small focal length lies in the fact that the structure supporting the feed and the reflector is minimized. The only apparent disadvantage lies in the fact that it is sometimes difficult to correctly illuminate reflectors of small f/D ratio. A very broad feed pattern is required, and for a given edge illumination a greater amount of energy is lost in "spillover."

Parabolic Cylinders Fed by Point-source Feeds. The simple feed horn used with the paraboloid can also be employed with the parabolic cylinder. In such a case, the illumination considerations for the plane normal to the cylinder elements are the same as those considered for the paraboloid. In the other plane, the illumination

should be low enough so that spillover is minimized. It is interesting to note that the value of space attenuation as a function of angle in this plane is obtained from the square root of the value for the parabolic plane. For the parabolic plane, the decibel data of Fig. 12-5 can be used directly; for the other plane the value in decibels at twice the feed angle is halved.

The wavefront produced by the point source and cylindrical reflector is a cylinder whose elements are normal to the elements of a parabolic cylinder. The radiation pattern to be expected from this combination will be a reproduction of the essential features of the source pattern in one plane and a directive, paraboloid-type pattern in the other plane.

The best work on the parabolic cylinder fed by a point source is included in Ref. 8. Here low side-lobe level is achieved by removing the feed horn from the radiating aperture through use of a parabolic cylinder tilted forward, as shown in Fig. 12-9. Focusing is obtained in the horizontal plane, while the feed-horn pattern is reproduced in the other plane. The height of the cylinder and the aperture of the feed horn are chosen to minimize spillover in the vertical plane. With this design, it was found that

Fig. 12-9. Tilted parabolic-cylinder reflector.

the maximum side lobes were not adjacent to the main beam but occurred at greater angles. These side lobes were 28 db down over a 200-Mc range at X band. The reflector used had an aperture of 5 by 1 ft with a focal length of $1\frac{1}{2}$ ft; the angle of tilt of the parabolic cylinder was 12°. A brief study of variations in the aperture outline indicated that no appreciable improvement could be obtained by replacing the rectangular shape by an elliptical shape.

In some applications, the size of the feed horn necessary to minimize spillover in the vertical plane may produce a vertical pattern narrower than desired. In this case, the surface used should depart from the cylindrical surface and permit some pattern divergence in the vertical plane. The problem becomes one requiring beam-shaping techniques. Some experimental work on such a system indicated that the side-lobe level (26 db) in the region of the main beam was greater than that obtained from the tilted parabolic cylinder. The vertical-plane pattern of this reflector showed some distortion without an appreciably greater beamwidth; it is possible that some further improvement in the design would produce the desired beamwidth.

Double Parabolic-cylinder Antennas. Since the antenna combination of the preceding section generated a cylindrical wave and since the parabolic cylinder is normally fed by a cylindrical wave, the addition of a second parabolic cylinder to the system described in the previous section will produce a combination of reflectors generating a plane wave. The use of a point-source feed and two parabolic-cylinder antennas then produces a final wavefront identical with that which could be obtained from a paraboloidal reflector.

If the equation of the first cylinder is given by $y^2 = 4fx$, with f the focal length, the second cylindrical surface is given by $(x + f)^2 = 4f(z + f)$ and the final rays are all parallel to the z axis.[9] The curve of intersection between the two surfaces is given in parametric form by $x = t^2/2$, $y = t$, $z = (t^2 + 1)^2/8 - \frac{1}{2}$. The curves of intersection, resulting when the two cylinders are developed into a plane, can be obtained from Ref. 9.

Since the first cylinder produces a line source, existing design techniques can be used to obtain a second cylinder which will produce a shaped beam. Another use for this antenna system arises when it is desired to minimize the cross-polarization component of the radiated field. If the polarization of the feed horn is parallel to the

elements of the first reflecting cylinder, the final field across the aperture plane has only this component.

Experimental data on this antenna indicated that good patterns could be obtained in the H plane but that a side lobe of about 15 db appeared on one side of the E-plane pattern. It is not known whether this is a basic limitation on the antenna; presumably some work on the feed horn will reduce this lobe.

Typical Pattern and Gain Performance. The patterns and gain obtained from the parabolic-cylinder reflector can be predicted from physical reasoning based on the pattern discussion of Sec. 12.2. The pattern in the plane of the cylinder elements is a reproduction of the feed pattern in that plane, with the addition of some diffraction effects. If the intensity of the field at the reflector edges is small, these effects are minimized. In the other plane, since the weighted illumination is no different from the illumination in any cross section, and since there is no shaping of the reflector outline, the side-lobe level will be slightly higher than can be obtained from a paraboloid.

Two different side-lobe problems arise in considering the symmetrical and asymmetrical cylinders. In the symmetrical case, the side lobes are increased by the presence of the feed structure blocking the reflecting radiation. In the asymmetrical reflector, the illumination across the aperture is not symmetrical, which results in a reduction in the null between the main beam and first side lobe, as well as a slight increase in the side-lobe level.

The gain which can be achieved in practice from the two reflector types is limited by feed blocking in one case and asymmetrical illumination in the other, so that some difficulty occurs in trying to obtain the gain factor (80 per cent of uniform illumination) predicted from analytical considerations. The value of gain which can be realized is of the same order as obtained from a paraboloid of equal size, namely, 65 per cent of uniformly illuminated aperture gain.

12.4. REFLECTORS FOR PRODUCING LINE SOURCES

The reflector-type antenna offers a very simple means of obtaining a line source because of the relative feed simplicity when compared with the feed configuration of an array antenna. The basic reflector system which has seen the greatest use is the pillbox antenna, or as it is called in England, the cheese antenna.[10] There are three principal types of pillbox antennas, namely, the simple pillbox, the half pillbox, and the double pillbox. These will be considered in turn in the following subsections.

Simple-pillbox Antenna. The pillbox antenna is made up of two parallel plates connected by a parabolic-cylinder reflector whose height is equal to the plate spacing. The feed is placed in the focal region of the reflector so that it lies in the middle of the radiating aperture.

Many different feed configurations have been utilized in an attempt to minimize the inherent problems of feed blocking and of reflector mismatch. Since these problems were mentioned previously in connection with other reflectors (Sec. 12 2), they will not be discussed further. The simple waveguide feed has proved to be the device with the most bandwidth and the best system for dependability. The next most popular feed system involves a unipole or stub-type antenna with a reflector. Such a feed is useful for UHF pillboxes, but does not have the front-to-back ratio which can be obtained from the waveguide feed.

One system considered in an effort to minimize feed blocking involves a waveguide feed for a slot radiator in one of the parallel plates. Improved front-to-back ratio is obtained by introducing a quarter-wavelength stub in the parallel plates at a distance one-quarter wavelength away from the slot feed (Fig. 12-10). Unfortunately, no great success has been achieved with this system, since the slot which is intended to

serve as the reflecting element for the primary radiation also has some effect on the secondary radiation focused by the reflector.

Another feed problem of some interest is that of adequately illuminating the reflector surface. For mechanical convenience, many pillbox antennas have utilized the parabolic arc out to the point where the feed angle is ±90°. This corresponds to a focus-in-face reflector in which the focal point lies in the aperture. As can be noted from the previous discussion of reflector illumination (Sec. 12.2), the feed system should provide a very broad primary pattern, broader than is normally achieved with an unflared waveguide. If such a reflector type must be used, a broad-beam horn can be used for *H*-plane beam broadening and a simple waveguide of small *E*-plane width can be used to obtain *E*-plane broadening.

Many pillbox antennas have been of the *H*-plane type, in which the electric-field vector is perpendicular to the parallel plates. In such an arrangement, no close tolerances on plate spacing are introduced. Some success has been achieved in the *E*-plane-type pillbox where the electric field is parallel to the plates. One advantage of this pillbox lies in the ease of obtaining satisfactory illumination from a horn with thin *E*-plane dimension. Such a horn also introduces less feed blocking. Closer tolerances on plate spacing are required. However, metallic pin supports can be introduced throughout the region between the parallel plates without harmful effect, since such pins are normal to the electric field.

Fig. 12-10. Slot feed for pillbox antenna.

It should be noted that the presence of the feed in the aperture not only introduces the well-known shadow effect, which effectively removes a portion of the radiating aperture, but it also introduces reflected radiation due to the finite dimension of the feed in the direction of propagation. This second effect is independent of polarization and appears in both the *E*-plane and *H*-plane pillboxes. Experimental investigation showed that these reflections can be reduced by coating the outer surface of the feed structure with an absorbent material. With such absorbing material, deeper nulls and more symmetrical side lobes were found, so that the radiation pattern approached the theoretical prediction.[10]

One problem encountered in simple pillboxes has been the effect of the back lobe of the feed on the pillbox pattern. Some improvement in back-lobe radiation from the feed horn can be obtained by use of flanges of various shapes and orientations in the region of the feed-horn aperture. However, in the pillbox, the use of flanges increases the shadow area and so alters the aperture distribution even more, with a resulting increase in side-lobe level.

Half-pillbox Antenna. A considerable improvement in pillbox performance can be obtained if the feed system is removed from the aperture. This is accomplished, as in previous cases, by using an asymmetrical reflector. The reflector which has seen the greatest use in this application consists of the parabolic arc, one end of which is the vertex point while the other end corresponds to a point at a feed angle of 90°.

The problems arising in the half-pillbox antenna are not severe, but they must be considered in the design. The first of these is the asymmetrical illumination, which has been mentioned in connection with previous asymmetrical reflectors. A careful study of this problem by Kiely[10] has indicated that little general improvement could be obtained by introducing a more complex feed structure which might result in a symmetrical illumination. A problem of more importance is related to the spillover radiation from the edge of the aperture at the 90° point. Because of the relatively low gain of pillbox antenna compared with its feed, direct radiation from the feed horn can give rise to wide-angle side lobes about 90° away from the main beam. It was
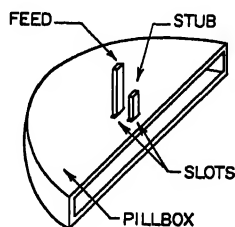
found in one application that these side lobes could be maintained below 26 db by tilting the horn to reduce the illumination in the 90° region. Too great a horn tilt reduces the effective aperture and hence the pillbox gain. Thus a compromise must be made between low spillover, which gives rise to wide-angle side lobes, and acceptable performance in the region of the main beam. As a rule of thumb, the horn axis should bisect the 90° angle subtended by the reflector edges at the focal point. With this type of design, the side lobes in the region of the main beam can be maintained at a 28-db level. It was found that these side lobes, unlike those of the simple pillbox (17 to 25 db), were relatively independent of frequency.

Double-pillbox Antenna. Another possibility for minimizing feed blocking is obtained if the pillbox is formed as two sets of parallel plates, one containing the incident field and the other the reflected field. The reflector can be one of two forms,
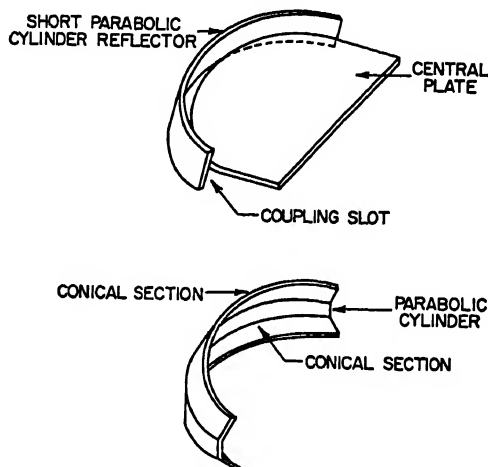
FIG. 12-11. Transition regions in double-layer pillbox.

the simple parabolic cylinder with an adjacent coupling slot or the more complex reflector whose center section is the parabolic cylinder but whose upper and lower sections are parts of conical surfaces (Fig. 12-11). A considerable amount of the work has been done on the reflector system used with the double-pillbox antenna. Early work assumed that the pillbox regions could be replaced by simple waveguide. With this assumption, information was obtained as to the slot width in terms of the total reflector height. Some brief experimental work indicated that this technique was satisfactory. The following is one formula for the slot width in the region adjacent to the simple parabolic cylinder: slot width equals 0.7 spacing between plates (for septum plate thickness approximately one-tenth the plate spacing).

For the more complex reflector, a study was made of the desired configuration as three plane reflectors instead of the cones and cylinder. These results were not applied directly to the problem of the double pillbox, but they did indicate that the optimum configuration depended on the angle which the incoming rays made with the reflector surface. Since in the pillbox this angle varies across the reflector, it appears that the reflector cross section should not be the same for all feed angles. A rigorous solution of this type of reflector can probably be obtained from a consideration of the geodesic paths followed by the rays on a mean surface (Chap. 15).

The experimental double pillboxes have been found to give satisfactory performance with side lobes of the order of those obtained in the half pillbox if the correct mechani-

cal configuration is maintained. The biggest problem in this type of pillbox is that of supporting the central region. This is particularly severe in the case of the *H*-plane pillbox where simple metal pin supports cannot be used. Some work has been done on metal supports which are tuned, so that over a limited frequency band they introduce little interference in the radiation pattern. However, as yet, no pillboxes with low side-lobe levels have been constructed using the tuned metallic supports.

Typical Patterns and Gain Performance. The gain which can be achieved from a pillbox is approximately 60 per cent of the gain from a uniformly illuminated aperture equal to the pillbox aperture. This gain figure is reduced in the simple pillbox if the feed horn is large compared with the pillbox aperture. It is reduced for any type of pillbox if the aperture in the plane perpendicular to the parallel plates is made excessively large. A large aperture in this plane is usually obtained at the expense of a quadratic phase error which quickly reduces antenna gain. If a large aperture must be used, this phase error should be corrected by a lens mounted in the aperture.

The side-lobe levels which have been achieved with the simple pillbox are as low as 24 db; however, this low level is obtained only over a narrow frequency band where the back radiation from the feed and the side lobes from the aperture can be made to cancel. With a 2 per cent variation in frequency, the side lobe may increase to as much as 14 db down.

The side lobes from the half cheese can be held to 28 db in the neighborhood of the main beam. However, a lobe of the order of 26 db appears 90° away from the main beam. For the double-cheese antenna, side-lobe effects at the present time appear to be associated with the reflector connecting the two sections of the pillbox. No extensive work has been done on this system, so that, as yet, side-lobe levels as good as those of the half cheese have not been obtained.

12.5. SHAPED-BEAM ANTENNAS

The design of reflectors which produce shaped beams can be based on the concepts of geometrical optics, whereas patterns of high-gain, pencil-beam reflectors cannot be predicted by geometrical optics. The reason behind this difference can be traced to the reflected wavefronts produced in the two cases. In other high-gain antennas, the reflected wavefront is a plane and the radiation pattern is obtained from the Kirchhoff diffraction theory of physical optics. In the shaped-beam antenna, a limited section of the wavefront may be a plane, but in the region where the beam is shaped, the wavefront has much greater curvature and geometrical-optics techniques can be applied.

In a curved wavefront, the region in the neighborhood of a ray tends to be in phase at the far-field direction corresponding to that ray, whereas energy in the neighborhood of other positions on the wavefront has more rapid phase variations for this far-field point. These phase variations cause field cancellation, so that the contribution from most of the wavefront is small. Therefore the radiation pattern is determined as a point-to-point geometrical relation in which each pattern point corresponds to a point on the curved wavefront. Because this correspondence is not exact and because some energy at each pattern point is contributed by other sections of the wavefront, slight amplitude variations, not predicted by geometrical optics, appear in the radiation pattern. These variations are minimized only by maximizing phase variations across the wavefront, which, for a particular wavefront, corresponds to increasing the number of wavelengths in the radiating aperture. For this reason, when a particular beam shape is required, a minimum deviation is obtained through use of the largest permissible reflector surface.

Singly Curved Reflectors.[11] This problem is essentially two-dimensional, so that ray paths can be restricted to a plane and the cylindrical-reflector surface can be

obtained from its plane-curve generator. The basic concepts for the design of a singly curved reflector are simple; the desired shaped-beam pattern is obtained, point by point, from the primary feed pattern. The problem presented is that of forming the reflector to make any particular segment of primary-pattern energy appear at the desired point in space. Two basic conditions must be satisfied. First is that of the energy correspondence between primary $I(\phi)$ and secondary pattern $P(\theta)$, which can be expressed as

$$\frac{\int_{\theta_1}^{\theta} P(\theta) \, d\theta}{\int_{\theta_1}^{\theta_2} P(\theta) \, d\theta} = \frac{\int_{\phi_1}^{\phi} I(\phi) \, d\phi}{\int_{\phi_1}^{\phi_2} I(\phi) \, d\phi}$$

where ϕ and θ are the primary- and secondary-pattern angles and the subscript values correspond to the reflector limits. The second condition, obtained from the geometrical optics of Sec. 12.1, relates the angle of incidence to the radius vector defining the surface:

$$\frac{\rho'}{\rho} = \tan i = \tan \frac{\phi - \theta}{2}$$

The relationship between θ and ϕ obtained from the first expression can be substituted in the second expression so that a differential equation is obtained between the radius vector ρ and the feed angle ϕ; this relationship defines the desired reflector curve.

The most difficult part of the shaped-beam problem is that of computing the desired curve from the above expressions. Quite often the first expression must be solved graphically so that the differential equation also requires a graphic solution. If the functions $P(\theta)$ and $I(\phi)$ are integrable, then the first expression can be solved for $\theta(\varphi)$ and the second expression becomes

$$\ln \frac{\rho}{\rho_1} = \int_{\varphi_1}^{\varphi} \tan \frac{\varphi - \theta(\varphi)}{2} \, d\varphi$$

and the integral is evaluated by numerical methods. If the pattern functions are not integrable directly, numerical methods are used. First, a plot is made of the pattern functions. Next, the four integrals in the first expression are evaluated by obtaining the corresponding areas under the curves. For the integrals with variable upper limits, many different values of the area must be found, corresponding to different values of the variable. With this information,[12] it is possible to obtain the two curves of Fig. 12-12. These curves are used to obtain the desired value of θ for
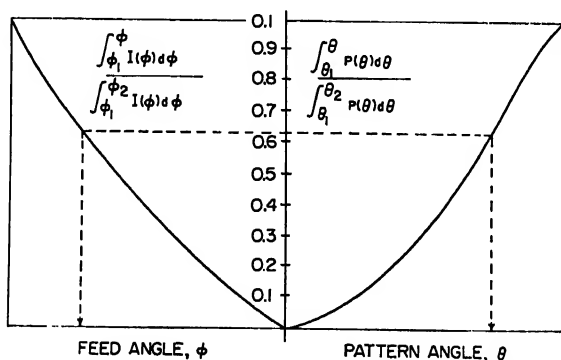
FIG. 12-12. Relationship between feed angle and pattern angle in shaped reflector.

any given value of ϕ. Knowing this, $\tan\{[\varphi - \theta(\varphi)]/2\}$ is plotted and the integral evaluated so that $\rho(\varphi)$, the desired curve, can be obtained.

Doubly Curved Reflectors.[11,12] The problem of beam shaping becomes somewhat more complicated when it is desired that the reflector should shape the beam in one principal plane and focus it in the other plane. Since the problem is a three-dimensional one, the possibility also exists that the feed might not produce a simple spherical wavefront but might also yield a cylindrical surface, a football-type surface, or any one of a number of other surfaces. Fortunately, all feed systems of interest have a circular wavefront in the plane of beam shaping, so that techniques similar to that employed in the previous section can be utilized to determine the surface cross section in that plane. The existing techniques consist of forming the reflector surface from the plane-curve cross section, which serves as a "spine," and a series of other plane curves which are attached as "ribs" to the spine. Some question has arisen regarding this general technique, but it has been found to produce satisfactory experimental results for cases in which the beam shaping is desired over a limited angle. This problem may be studied more carefully for application to beam shaping over wider angles.

The plane curve, identified as a spine above, has been called the central-section curve. This curve is found in a manner quite similar to that described in the preceding section. The design equations for the feed with spherical wavefront are obtained, using the same quantities as before:

$$\frac{\int_{\theta_1}^{\theta} P(\theta)\,d\theta}{\int_{\theta_1}^{\theta_1} P(\theta)\,d\theta} = \frac{\int_{\phi_1}^{\phi} \frac{I(\phi)}{\rho}\,d\phi}{\int_{\phi_1}^{\phi_1} \frac{I(\phi)}{\rho}\,d\phi}, \qquad \frac{\rho'}{\rho} = \tan\frac{\phi - \theta}{2}$$

The major difference between these expressions and the previous ones occurs in the presence of ρ under the integral sign. The integration can be carried out as before if first ρ is assumed to be a constant over the shaped portion of the central-section curve; then follow a parabolic arc $[\rho = \sec^2(\phi/2)]$ over the region which produces the main beam. With this assumption, the procedure is identical with that of the last section for obtaining the function $\rho(\varphi)$. This function represents a closer approximation to the correct value than the original assumption. When it is used as the value under the integral sign and the entire procedure is repeated, a new value of $\rho(\varphi)$ is obtained which is as close to the true value as necessary in any practical case.

A discussion of the rib curves will indicate the limitations in the present techniques. In order to obtain the ribs, it is customary to consider an incoming bundle of rays from the secondary pattern angle θ. For beam shaping in the vertical plane, this bundle of rays is confined to a plane making an angle θ with the horizontal plane. It is required that the reflector surface direct these rays to the feed position. Figure 12-13 shows two parallel rays in this plane which intersect the reflector in the
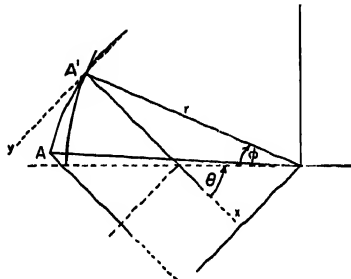
Fig. 12-13. Geometry of three-dimensional shaped reflector.

curve AA'. The rays between the points A and A' are reflected to lie on a conical surface with apex at the feed.

If we considered the transmit case and a plane sheet of rays emanating from the feed point, they would intersect the reflector in a curve AA' and the reflected rays would lie on a cylindrical surface tilted at an angle of θ with the horizontal plane. It should be apparent that although they have the same end points, the plane curves AA' are not the same for the transmit and receive cases. This can be understood since it is known that, if focusing is desired, the reflector surface in the neighborhood of the points of ray incidence must be a paraboloid. The plane curve cut by this paraboloid will be different if we consider the intersection caused by the transmit plane passing through a focal point and that caused by the receive plane inclined at an angle θ to the horizontal. It is difficult to make a choice between the two curves, although the great majority of existing efforts has chosen the receiving-plane case. A compromise solution might be the plane bisecting the angle formed by the transmitting and receiving plane. The parabolic curve for the receive case mentioned above is

$$y^2 = 4z\rho \cos^2 \frac{\theta + \varphi}{2}$$

Here z is the coordinate measured from the point A' away from the reflector and y is the orthogonal coordinate. It should be noted that each of the rib curves is a parabola lying in a different plane; when the reflector surface is formed, the planes of various parabola ribs must be inclined at the corresponding angles.

All the previous expressions yield only normalized coordinates for the surface; these must be converted to usable dimensions before the reflector can be constructed. It is desirable to make the central-section curve as large as possible in order to minimize the diffraction effects on the shaped-beam pattern. In the other plane, the reflector size is chosen to produce the desired beamwidth. The feed angles associated with the reflector are chosen in a manner similar to those of the simple paraboloid. It is desirable that the aperture illumination be 10 db down at the reflector edges.

It is possible that the feed system utilized may not produce a spherical wavefront, so that the point-source analysis already described may not apply. One incident wavefront which has been of interest is a football-type surface, which is produced by a short horn with large-aperture dimension in the plane of focusing; in the beam-shaping plane, this feed has a normal aperture. The football surface arises from the fact that the center of phase in the plane of beam shaping is at the aperture whereas the center of phase in the plane of focusing occurs at the input waveguide to the short horn.

The football-type wavefront surface can be handled by modifying the integral relationship between ϕ and θ and the parabola ribs. In the integrals, ρ will be replaced by $\rho + b$, where b is the dimension from the waveguide input to the horn aperture. The parabolic ribs for this case are altered so that they are given as

$$y^2 = 2z\rho \cos(\theta + \phi) - 2b\sqrt{\rho^2 + z^2 - 2z\rho \cos \beta} + 2[(\rho + b)z + \rho b]$$

The parameters here are identical with those given previously, b is the horn length previously described, and $\beta = \theta + \phi$.

For a general-incident wavefront surface, no formulas are available; however, the design can be carried out if it is realized that the final wavefront should be a cylinder whose generating curve can be found once the central-section curve is known. If the wavefront is circular in the plane of the desired central-section curve, this curve is obtained by the techniques used for the singly curved reflector. Once this curve on the reflector is known, simple ray tracing would indicate the reflected wavefront obtained from an incident circular wavefront. Another means of obtaining this wave-

front would be to use the analysis of Sec. 12.1 to obtain the reflected curve in terms of the incident wavefront and the reflector surface. Once the reflected curve is known, the corresponding cylinder can be found, and using the techniques of Ref. 1, the reflector surface can be obtained.

Paraboloids with Extended Feeds. It has been indicated above that beam shaping is obtained by producing a cylindrical reflected wavefront. In general, this wavefront was produced by a simple point-source feed and a variation in the reflector curvature. However, from what has been said about the relationship between incident-wavefront reflector surface and reflector wavefront, it is evident that the reflector could be chosen as the simple paraboloid and the incident wavefront could be tailored to give the desired reflected wavefront. The problem of shaping the incident wavefront is somewhat more difficult than that of shaping the reflector because of certain inherent physical limitations. It has been found experimentally that the wavefront in the neighborhood of a feed system varies somewhat with distance from the feed in a very complex manner. For this reason, and because of the fact that the desired wavefront can be obtained only from a very complex feed system, most shaped-beam antennas have represented only a limited approximation to the desired incident wavefront. This approximation can be achieved by utilizing three separate feeds, in other words, the continuous feed is replaced by three discrete elements. The amplitude and phase of these elements are chosen so as to approximate the desired pattern. In general, one source provides the main beam; the second source, of reduced intensity, produces a beam whose peak is displaced from the main beam; and the third source, of even less intensity, completes the coverage with a third beam. Another feed system which has been used involves an array of slots, or of dipoles, arranged to approximate a desired incident wavefront. The design of this array has been found to be even more difficult than that of normal arrays because of the fact that some experimental variations were necessary in order to obtain the desired beam.

One further technique which has been studied involves a feed system in a parallel-plate region. The incident wavefront in the plane of the plates can be conveniently obtained by shaping a reflector between the plates. Energy from a simple feed is introduced between the plates, reflected, and appears at the plate aperture with the required phase and amplitude distribution.

Typical Pattern and Gain Performance. The patterns which can be achieved with a single curvature reflector are dependent, in the shaped-beam plane, on the size of the reflector in wavelengths and, in the other plane, on the basic pattern from the feed structure. Since most line-source feeds can be designed to give side lobes better than 25 db, it can be expected that these lobes will be obtained in the plane of focusing. No analysis has been made of the degree of ripple obtained in the shaped-beam pattern as a function of aperture width; however, with low illumination taper at the reflector edges and with an aperture width at least 15 wavelengths across, the pattern ripple can be held to less than 2 db from the desired curve.

The patterns which can be expected from the doubly curved surface are quite similar in the plane of beam shaping but vary in the other plane. The side-lobe level in the plane passing through the main beam is as good as 25 db; however, in all other planes, the side lobes are higher and they tend to increase with increasing angles. Up to 30°, these lobes can be held between 18 and 20 db; from 30 to 60°, these lobes will get as high as 15 db. Somewhere in this region, the cross-polarization lobes rise to about 15 db; these lobes are diminished by using long focal-length systems. All these side-lobe values are referred to the peak signal in the elevation plane under consideration.

The gain of the shaped-beam antenna depends on the degree of beam shaping required, since the energy in the region away from the main beam must be subtracted from the main-beam energy. In most designs, this results in a gain reduction of the

order of 2 db. No great change in this gain figure occurs in conventional shaped-beam antennas as one goes to greater angles; since relatively low signal is required at these angles, very little intensity must be subtracted from the main beam to provide this coverage.

12.6. MISCELLANEOUS REFLECTOR TYPES

Most of the discussion up to the present time has been based on the simple paraboloidal reflector. However, many other reflector types have been used in the past, and it can be expected that even more will be found in the future. Every known type of microwave reflector has a design which is based on geometrical optics techniques, so that consideration of these types can be facilitated by the use of the information in Ref. 1 concerning general reflectors and wavefronts. For simple systems, the complexity of this treatment is not necessary, but instead normal plane geometry can be used.

Shielded Reflectors. One very successful reflector system, which is very useful in reducing wide-angle radiation, is the horn paraboloid, shown in Fig. 12-14. Its
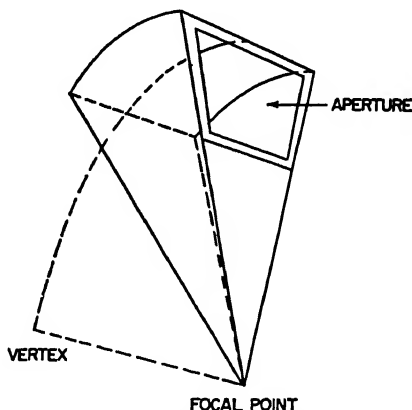
Fig. 12-14. Horn-paraboloid reflector system.

action can be understood by noting that the paraboloidal section is far removed from the vertex point, but it nevertheless accurately focuses the energy incident from the focal point. Stray radiation is minimized by extending the sides of the feed until they touch the paraboloid surface on three sides. On the fourth side, an opening is left for the reflected rays. Although this type of structure is very useful in minimizing wide-angle side lobes, it has no significant effect on the close-in side lobes caused by the normal diffraction effects.

The design of this reflector normally involves a horn length at least as great as the aperture dimensions. If a wide flare angle is used in an attempt to reduce the horn length, poor pattern characteristics are found. This is undoubtedly due to the fact that the geometrical-optics approximations, normally used to relate the feed-horn radiation to the aperture illumination, are no longer valid. The reflector portion of the assembly is not in the far field of the horn aperture, so that the system cannot be examined on the basis of standard feed-horn and reflector techniques.

Another possibility for reducing wide-angle radiation involves the use of a cylindrical shield around the reflector and the feed to reduce lobes associated with direct radiation from the feed horn. The shielded assembly minimizes this direction radiation, but

it is not as satisfactory as the horn paraboloid discussed above. Energy across its aperture is made up of fields reflected from the antenna, as well as direct radiation from the feed, whereas the energy across the aperture of the horn paraboloid consists primarily of reflected energy. The principal advantage of the shielded reflector over the horn paraboloid lies in its compact configuration.

Point-source to Point-source Reflectors. For some applications, it is desirable to produce a virtual source from a given real source. For example, it may be desirable to position a real source at the vertex of a paraboloidal reflector and utilize some surface between the vertex and the focal point which images the real source into a virtual source located at the focal point. The resulting antenna system, a counterpart of the optical Cassegrain system, will then have a focused beam, since the paraboloid is energized by a source which is apparently at the focal point.

It is first obvious that the reflector surface desired must be symmetrical about the axis joining the two sources. If a cross section of the reflector is known, the complete surface can be formed by rotating this reflector arc about the axis. Figure 12-15
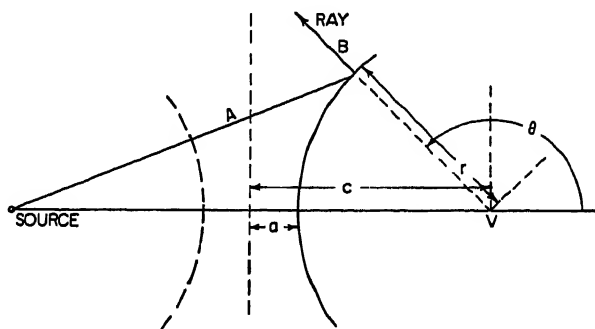
Fig. 12-15. Geometry of hyperbola reflection.

indicates the geometry of the two-dimensional problem. The reflected rays should appear to originate at the point v, or in other words, rays from the real source shall be reflected to form a spherical wavefront with center at v. Since in the figure we require that $A + B$ be a constant and $r + B$ should be a constant, we find that the surface is determined by the fact that $A - r$ is a constant. From analytic geometry, it is known that the locus of points satisfying this condition is a hyperbola. This curve can then be written as

$$r = \frac{c^2 - a^2}{a \pm c \cos \theta}$$

The quantities here are indicated in the figure. The plus-or-minus sign corresponds to two possible reflector surfaces, one concave and one convex.

Another possible reflector for translating a point source into a point source is an ellipsoid. The ellipse cross section is given by

$$r = \frac{a^2 - c^2}{a + c \cos \theta}$$

where the quantities are the same as in Fig. 12-15.

For application to the paraboloidal reflector mentioned in the first paragraph above, three surfaces are possible, namely, the ellipsoid and the two hyperboloids. For practical application, the ellipsoid, which must be mounted at a greater distance from the reflector, is not satisfactory. Of the two hyperboloid surfaces, the one which

can be mounted farther from the reflector illuminates typical reflectors better than the nearer, which requires a paraboloid with large f/D ratio. When the real source is moved from one focal point of the hyperboloid system, the image source will move away from the other focal point but will, at the same time, become distorted. Any great motion of the real source produces a poor image.

Point-source to Line-source Reflectors. It has already been mentioned that the parabolic-cylinder reflection will convert a point source into a line source. However, this property is not unique for this reflector. Other surfaces[13] capable of accomplishing the same result have been designated as hypar and elpar surfaces. These have principal plane sections which are hyperbolas, parabolas, and ellipses. It can be seen that in the plane of the parabola, rays from the feed source can be focused to be parallel, whereas in the plane of a hyperbola (or ellipse), the rays can be reflected so that they appear to come from a virtual source point. This does not prove that the reflected wave is a cylindrical wavefront, but only indicates that the cross sections of this wave in the two principal planes correspond to those of a cylindrical wave. A general reflector can be obtained by assuming that the point source lies at the coordinate value $(d, 0, 0)$ and that the line source coincides with the z axis as in Fig. 12-16.
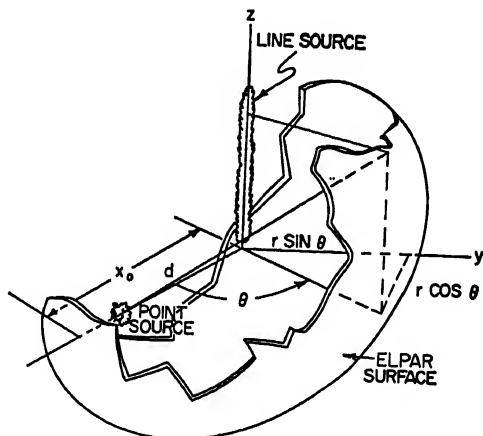
Fig 12-16. Geometry of Elpar surface.

By taking a general ray not lying in either principal plane and requiring that it have a constant path length between the point source and the line source, it can be shown that the reflector surface is given by the following expression:

$$\sqrt{(r \sin \theta)^2 + (r \cos \theta - d)^2 + z^2} + r = 2x_0 - d$$

or

$$\sqrt{(x - d)^2 + y^2 + z^2} + \sqrt{x^2 + y^2} = 2x_0 - d$$

All quantities in this expression are shown in Fig. 12-16. If one sets θ equal to a constant, it can be shown that all such sections of the reflector are parabolas, whereas setting z equal to a constant yields ellipses in those planes.

A reflector directly related to that indicated above involves cross sections which are hyperbolas rather than ellipses. The mathematics is similar. Using the quantities of Fig. 12-16, we have the expression

$$\sqrt{(r \sin \theta)^2 + (r \cos \theta - d)^2 + z^2} - r = \pm(2x_0 - d)$$

The plus-or-minus signs indicate two possible surfaces, one concave and one convex. Here it can be shown that the planes θ equal constant intersect at the surface in parabolas and the planes z equal constant intersect it in hyperbolas.

Wide-angle Reflectors. In recent years, a considerable amount of interest has been expressed in stationary reflectors which produce a scanned beam obtained by a motion of the reflector feed. Such beams are not perfectly focused for all positions of the feed, but by proper design of the reflector surface, it is possible to obtain pattern characteristics which vary only slightly with feed motion or beam scanning. Most of these reflectors are based on the use of a circular arc in the plane through which the feed moves. The surface itself is formed by rotating a plane curve which intersects the circular arc about some axis perpendicular to the plane of the arc. These surfaces are all similar to the torus and therefore can be designated as toroidal surfaces.

One particular example of the toroidal surface is the sphere. Here a circular arc is rotated about an axis to generate a spherical surface for wide-angle scanning. It is shown in Ref. 5 that a spherical reflector of the same general configuration as a paraboloidal reflector had off-axis characteristics similar to those of the paraboloid. Therefore the spherical surface is useful for wide-angle performance only when a limited sector of the surface is illuminated at any one time. This illumination of a limited sector is associated with the toroidal surfaces used for wide-angle performance. If a limited portion of the spherical reflector is energized, the feed should be close to the half-radius point. However, where greater portions are illuminated, it is necessary that the feed be brought nearer to the reflector. An expression for the distance from the feed position to the center of a unit radius sphere is:

$$d = (1 - \sqrt{1 - r^2})/r^2$$

where r represents the normalized radius of the effective aperture. This aperture is determined by the fact that energy striking the spherical surface at wider angles cannot be focused. It has been found experimentally that values of d much greater than 0.55 yield an inefficient aperture.

More satisfactory wide-angle toroids than the sphere are the parabolic torus[14] and the elliptic torus.[15] It is evident that the substitution of a parabolic curve as the generator yields a surface which is a compromise between the paraboloid and a sphere. This compromise results in improved pattern performance in one principal plane and so is very desirable from a practical standpoint. A satisfactory design was achieved by utilizing a parabola whose focal length was 45 per cent of the radius of the circular arc. The sector of a parabolic arc utilized subtended a total angle at the focal point of approximately 90°. Two versions are possible, namely, one in which the angle lies entirely to one side of the parabola axis, so that an asymmetrical reflector is obtained, and the symmetrical reflector in which the axis bisects the subtended angle. The most satisfactory reflector proved to be the asymmetrical one. Good pattern performance was obtained in both principal planes, but high side lobes were found in other planes.

Another asymmetrical toroidal surface which has been considered proved to be based on an ellipse as the generating curve. This configuration was arrived at by a computational technique in which many reflectors were investigated and one chosen which minimized aperture phase errors. It was found that the curve which most closely fit the computed points was an ellipse with eccentricity of 0.985, that is, an ellipse which closely approaches the parabola. Here the focal length was 44 per cent of the radius of the circular arc, and the near focal point of the ellipse was at 45 per cent of the radius.

It is characteristic of all toroidal surfaces that a certain geometrical-optics phase error is inherent in the reflected wavefront; the paraboloid is the only surface which

focuses a point source into a plane wave. Because of this phase error, a basic limitation on beamwidth arises. In attempting to obtain narrower beams, the physical amount of geometric phase error measured, perhaps in inches, increases rapidly. For example, in attempting to go from a beamwidth of 4° to one of 2°, a phase error which is originally $\lambda/4$ becomes $\lambda/2$. This increase in phase error means that one cannot scale directly from a 4° beam to a 2° beam, but must rather expect that a direct scale will produce a beamwidth between $2\frac{1}{2}$ and 3°. This effect becomes even more pronounced as one attempts to obtain beamwidths less than 2°. Based on existing experimental information, it can be said that aperture efficiency decreases below a 4° width and that for any applications in which aperture efficiency is an important factor, the toroidal surfaces will probably be unsatisfactory for beamwidths less than 2°.

REFERENCES

1. K. S. Kelleher: "Relations Concerning Wavefronts and Reflectors," *J. Appl. Phys.*, vol. 21, no. 6, pp. 573–576, June, 1950. A geometrical-optics treatment of the phase characteristics of arbitrary wave reflected from arbitrary reflectors.
2. H. J. Riblet, and C. B. Barker: "A General Divergence Formula," *J. Appl. Phys.*, vol. 19, no. 1, pp. 63–70, January, 1948. A geometrical-optics treatment of energy distribution after reflection of a spherical wave from an arbitrary surface.
3. S. Silver: "Microwave Antenna Theory and Design," pp. 157 and 454, McGraw-Hill Book Company, Inc., New York, 1949. A derivation of the formula for reflection coefficient of an antenna feed introduced by the presence of a paraboloid.
4. H. T. Friis and W. D. Lewis: Radar Antennas, p. 785, in "Radar Systems and Components," D. Van Nostrand Company, Inc., Princeton, N.J., 1949. A discussion of patterns from an aperture with quadratic phase error.
5. K. S. Kelleher and H. P. Coleman: "Off-axis Characteristics of the Paraboloidal Reflector," *Naval Research Lab. Rept.* 4088. A consideration of patterns obtained from an aperture with primarily a cubic phase error.
6. "The Airy Integral," British Association for Advancement of Science and Cambridge University Press, London, 1946. A discussion and tabulation of a function useful in evaluating diffraction integrals containing cubic phase errors.
7. R. J. Adams and K. S. Kelleher: "Pattern Calculations for Antennas of Elliptical Aperture," *Proc. IRE*, vol. 38, no. 9, September, 1950. Abstract of an unpublished paper which accurately related experimental patterns to derived formulas.
8. D. G. Kiely: "Parabolic Cylinder Aerials," *Wireless Eng.*, p. 73, March, 1951. Investigation of the parabolic-cylinder antenna for obtaining a fan beam pattern from a reflector fed by a point source.
9. R. C. Spencer, F. S. Holt, H. M. Beauchemin, and J. L. Sampson: "Double Parabolic Cylinder Pencil Beam Antenna," IRE Convention Record, pt. I, Antennas and Propagation, 1954. Discussion of the use of two parabolic-cylinder reflectors to produce a pencil beam.
10. D. G. Kiely, A. E. Collins, and G. S. Evans: "Cheese Aerials for Marine Navigational Radar," *Proc. IEE (London)*, pt. III, vol. 98, no. 51, January, 1951. Investigation of the pillbox, or "cheese," antenna aimed at minimizing side lobes.
11. Reference 3, chap. 13. A discussion of beam-shaping techniques using a reflector.
12. A. S. Dunbar: "Calculations of Doubly Curved Reflectors for Shaped Beams," *Proc. IRE*, vol. 36, pp. 1289–1296, October, 1948. Techniques for computing shaped-beam reflectors together with experimental data on such reflectors.
13. G. Stavis and A. Dorne: Horns and Reflectors, chap. 6, in "Very High Frequency Techniques," vol. 1, McGraw-Hill Book Company, Inc., New York, 1947. Discussion of the elpar reflector surface.
14. K. S. Kelleher: "A New Wide-angle Microwave Reflector," p. 98, Tele-Tech and Electronic Industries, June, 1953. A discussion of the parabolic-torus reflector.
15. G. D. M. Peeler and D. H. Archer: "A Toroidal Microwave Reflector," IRE Convention Record, pt. I, Antennas and Propagation, 1956. A discussion of the elliptic-torus reflector.
16. L. P. Eisenhart: "An Introduction to Differential Geometry," Princeton University Press, Princeton, N.J., 1940.

Chapter 13

PASSIVE REFLECTORS

William C. Jakes, Jr.*

*Bell Telephone Laboratories, Incorporated
Holmdel, New Jersey*

and

Sloan D. Robertson†

*Goodyear Aircraft Corp.
Litchfield Park, Arizona*

13.1. SINGLE-SURFACE REFLECTORS USED FOR MICROWAVE RELAY SYSTEMS

Single- and Double-mirror Systems. Reflectors are often used in microwave relay systems for the purpose of redirecting the incident energy. Several simple schemes for accomplishing this are shown in Fig. 13-1, where the reflector system is in the distant (Fraunhofer) field of the transmitting and receiving antennas in each case. The single-mirror type of passive repeater shown in Fig. 13-1a is useful when the transfer angle α is greater than about 40°. For values of α less than this, the length of the mirror becomes excessively large for a given projected area and the double-mirror system of Fig. 13-1b should be used. The incident and exit rays in each system

---

*Sec. 13.1.
†Sec. 13.2

define a plane, and the projected area of the passive repeater is referred to this plane in the cases illustrated.

Generally, passive repeater systems of these types have dimensions of many wavelengths; thus several simplifying assumptions may be made for the purpose of calculating their transmission properties. The reflection is specular,* so that the angle of

(a) SINGLE MIRROR PASSIVE REPEATER USEFUL FOR LARGE VALUES OF α.

(b) DOUBLE MIRROR PASSIVE REPEATER USEFUL FOR SMALL VALUE OF α.
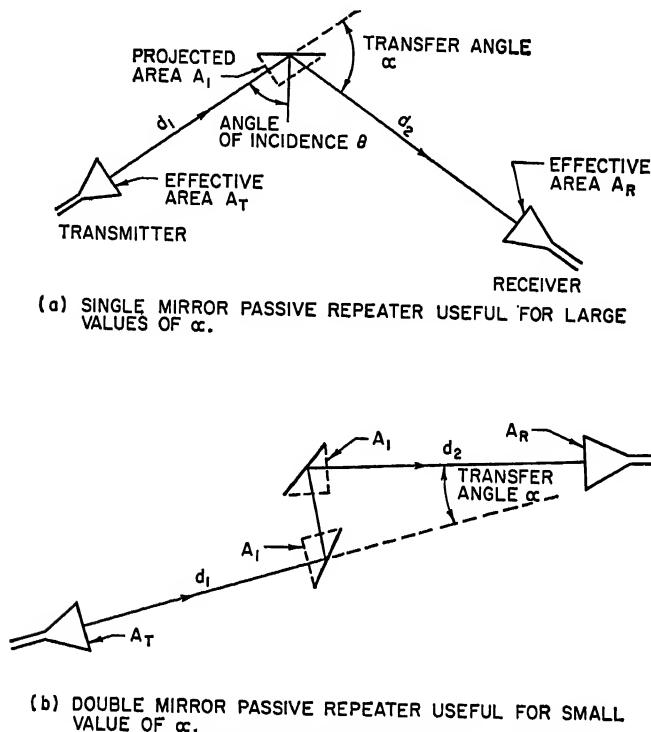
FIG. 13-1. Types of microwave passive repeaters.

incidence equals the angle of reflection; except for heat loss (usually negligible) the reflectors are 100 per cent efficient, so that all the power incident is reflected and the radiation patterns are those of a uniformly illuminated aperture. The two reflectors in the repeater system of Fig. 13-1b are assumed to be so close together that the energy travels in a perfectly collimated beam between them. Furthermore, their sizes are such that the projected area for the incident ray is the same as that for the final exit ray.

Provided that the passive repeater is in the far field of the transmitting and receiving antennas, the total transmission loss in decibels for either of the systems shown in Fig. 1 is given by[2]

$$10 \log \frac{P_T}{P_R} = 10 \log \frac{\lambda^4 d_1^2 d_2^2}{A_T A_1^2 A_R} \tag{13-1}$$

This may be written as

$$10 \log \frac{P_T}{P_R} = 10 \log \frac{\lambda^2 (d_1 + d_2)^2}{A_T A_R} + 20 \log \frac{\lambda d_1 d_2}{A_1 (d_1 + d_2)} \tag{13-2}$$

* The reflector surface must be flat to within $\pm \lambda/16$.

where λ = free-space wavelength

A_T = transmitting-antenna effective area

A_R = receiving-antenna effective area

A_1 = projected area of passive repeater in a plane normal to incident or reflected ray

d_1, d_2 = distances from repeater to transmitting and receiving antennas

P_T, P_R = transmitted and received power, respectively

The first term in Eq. (13-2) is simply the free-space transmission loss between two antennas separated by a distance $d_1 + d_2$. The second term is the additional loss due to the passive repeater.

It may happen that more than one repeater is necessary over a given path in order to get around certain obstacles. Suppose there are n repeaters having projected areas $A_1, A_2, \ldots , A_n$ and the ith one is separated a distance d_i from the previous, $i - 1$ one. The total transmission loss in decibels is, then,

$$10 \log \frac{P_T}{P_R} = 10 \log \frac{\lambda^{2n+2}(d_1 d_2 d_3 \cdots d_{n+1})^2}{A_T A_R (A_1 A_2 A_3 \cdots A_n)^2} \tag{13-3}$$

which may also be written

$$10 \log \frac{P_T}{P_R} = 10 \log \frac{\lambda^2 (d_1 + d_2 + \cdots + d_{n+1})^2}{A_T A_R}$$
$$+ 20 \log \frac{\lambda^n (d_1 d_2 d_3 \cdots d_{n+1})}{(A_1 A_2 A_3 \cdots A_n)(d_1 + d_2 + \cdots + d_{n+1})} \tag{13-4}$$

where d_{n+1} is the distance from the nth repeater to the terminal antenna. Again the first term in Eq. (13-4) is the free-space loss between two antennas separated a distance $(d_1 + d_2 + \cdots + d_{n+1})$. The second term is the additional loss due to the passive repeaters.

Each antenna or repeater system must be in the Fraunhofer region of the one adjacent to it in order for the above formulas to be valid to 0.5 db or better. This imposes the following approximate restriction on the spacing between systems:

$$d > \frac{0.9}{\lambda} \sqrt{A_1^2 + 6A_1 A_2 + A_2^2} \tag{13-5}$$

where A_1, A_2 are the effective areas of the two elements in question (antenna and repeater, or two repeaters) and d is the distance between them.

The double-mirror repeater has an extra degree of freedom in its physical design. Taking advantage of this it is possible to minimize the total length of mirrors required and to design the system so that it occupies the smallest possible amount of space. Referring to Fig. 13-2, the following quantities are of interest:

w = projected length of each mirror

α = transfer angle

ℓ_1, ℓ_2 = actual length of each mirror

θ = angle of incidence at mirror 1

h = mirror separation, measured between their centers

L = length of a single mirror equivalent to double-mirror system

Assuming that α and w are given, the variations of $\ell_1 + \ell_2$ and h as functions of θ may be calculated. The mirrors are assumed to be as close together as possible, so that the line joining their inner ends ($\overline{AB}$ in Fig. 13-2) makes an angle α with the incident ray.

The total length of the two mirrors, $\ell_1 + \ell_2$, varies with α and θ as shown in Fig. 13-3, together with the variation of the length L of an equivalent single mirror for
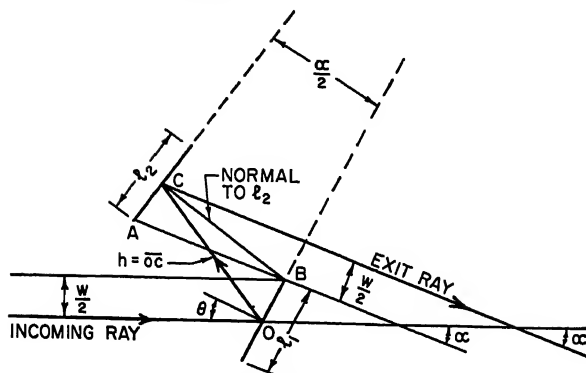
FIG. 13-2. Layout of double-mirror passive repeater.
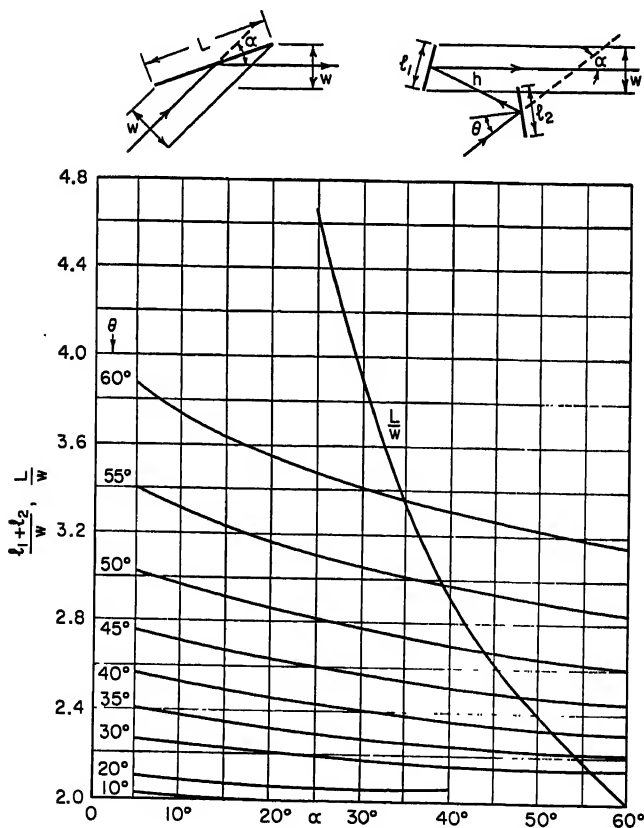
FIG. 13-3. Variation of (normalized) mirror length with α and θ for single- and double-mirror passive repeaters.

comparison.   The values of θ for which the total mirror length for the double repeater is less than that for a single one can be obtained by inspection.   For example, if $\alpha = 40°$, $\ell_1 + \ell_2 < L$ for $0 \leq \theta \leq 53°$.

Figure 13-4 gives the variation of the mirror separation h with θ and α.   For a given α it will be noted that a value of θ can be found for which h is a minimum.
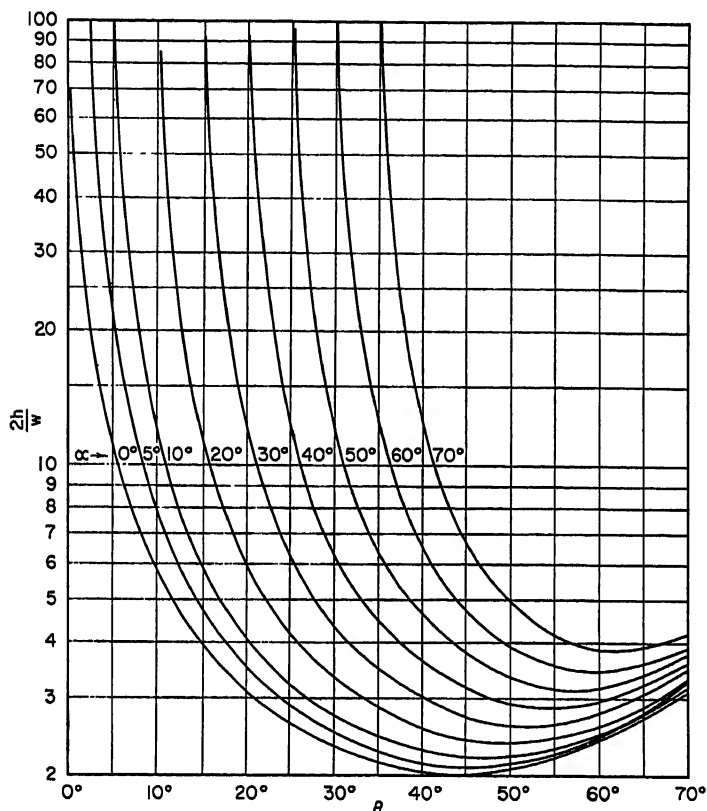
Fɪɢ. 13-4. Variation of (normalized) separation between the two mirrors of a double-mirror passive repeater with θ and α.

Having selected a value of θ for a given w and α, the design may be completed with the help of the relations

$$\ell_1 = \frac{w}{\cos \theta} \qquad \ell_2 = \frac{w}{\cos (\theta - \alpha/2)} \qquad (13\text{-}6)$$

Furthermore, the angle included between the two mirrors is $\alpha/2$ and the normal at C to mirror 2 passes through the inner end of mirror 1, point B, as shown in Fig. 13-2.

Periscope Antenna Systems.   Another important use for reflectors is shown in Fig. 13-5.   This arrangement differs from the passive repeater discussed above in that the reflector is located in the Fresnel or near-Fraunhofer region of the antenna, with separations between the two seldom exceeding several hundred feet.   For this reason the combination is more appropriately thought of as an antenna *system** rather

---

* The name "periscope antenna" has been suggested, for obvious reasons.

than a combination of antenna and reflector with independent radiation properties, as for the passive repeaters described above. The main advantage in microwave repeater antenna systems of this type is that the final radiating element may be located at a considerable elevation so that nearby obstructions are cleared without using long lengths of waveguide. The terminal equipment may also be located at ground level for convenient maintenance. The price paid for these advantages is the considerably increased difficulty of alignment and higher values of unwanted coupling to similar nearby systems. This coupling generally will not be much less than −50 db,
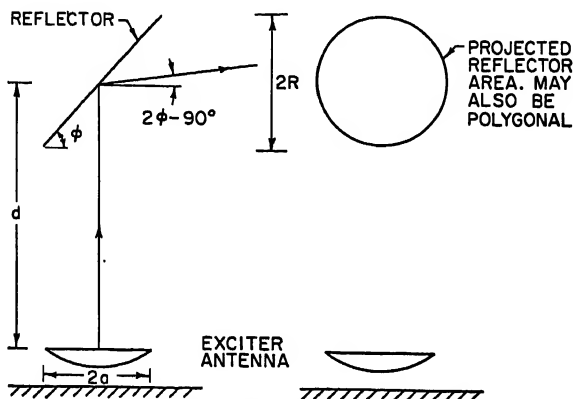
FIG. 13-5. Periscope antenna system.

which usually means that adjacent systems must use different frequencies. The coupling arises from three different sources: direct coupling between the exciter antennas, scattering from the structural members of the supporting towers and other nearby objects, and scattering from the elevated reflectors themselves. Of these only the first can be effectively controlled by any practical means, such as erecting conducting or absorbing screens between antennas.

Periscope antennas may be arranged in a variety of ways with different kinds of exciter antennas and elevated reflectors. Paraboloids are generally used as the exciting antenna with either rectangular or elliptical reflectors above. The reflector may be flat, or it may be parabolically curved to achieve somewhat greater gain. The antenna is usually placed so that the line joining the centers of the antenna and reflector is nearly vertical; however, this is not essential. The reflector is tilted to send the exit ray out at the proper angle of elevation and is usually so proportioned that its projected area is either circular or square. The vertical angle of tilt of the reflector must be carefully controlled since the elevation angle of the exit beam varies as twice this angle.

The gain of two commonly used types of periscopes has been calculated and verified experimentally.[8–9] In each case the exciter antenna is a paraboloid with 10 db square-law amplitude taper.* The reflector is assumed to be elliptical with circular projected area and may either be flat, as in Fig. 13-6, or curved to a section of a paraboloid with focus at the center of the exciter antenna, as in Fig. 13-7. The universal gain curves of Figs. 13-6 and 13-7 give the variation of the quantity η, in decibels, as a function of the dimensionless variable $\lambda d/4R^2$. Here η is defined as the over-all decibel gain of the periscope system minus the decibel gain of the exciter

---

* That is, the feed horn produces a field distribution in the paraboloid aperture which varies as the square of the radius from unity at the center to 0.316 at the edge.
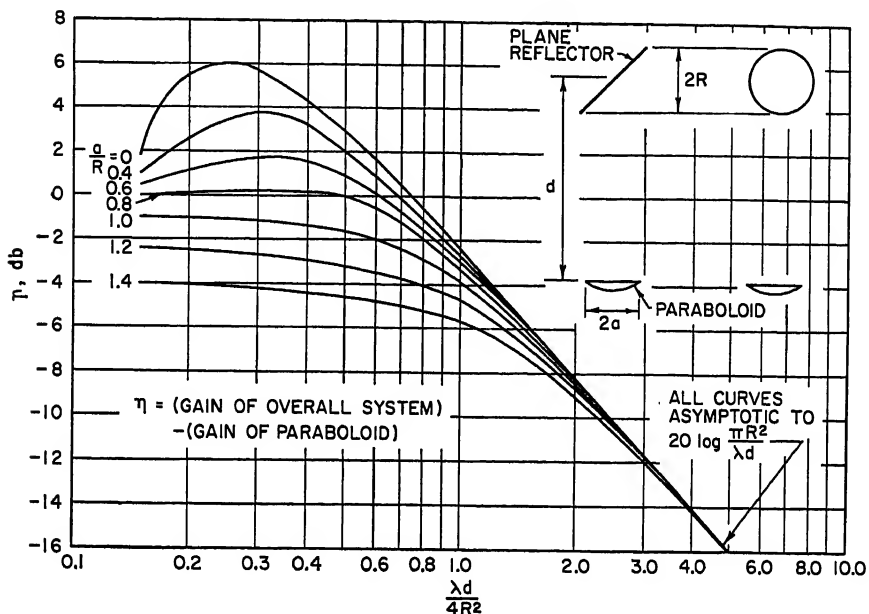
Fig. 13-6. Relative gain of periscope antenna system employing plane elevated reflector.
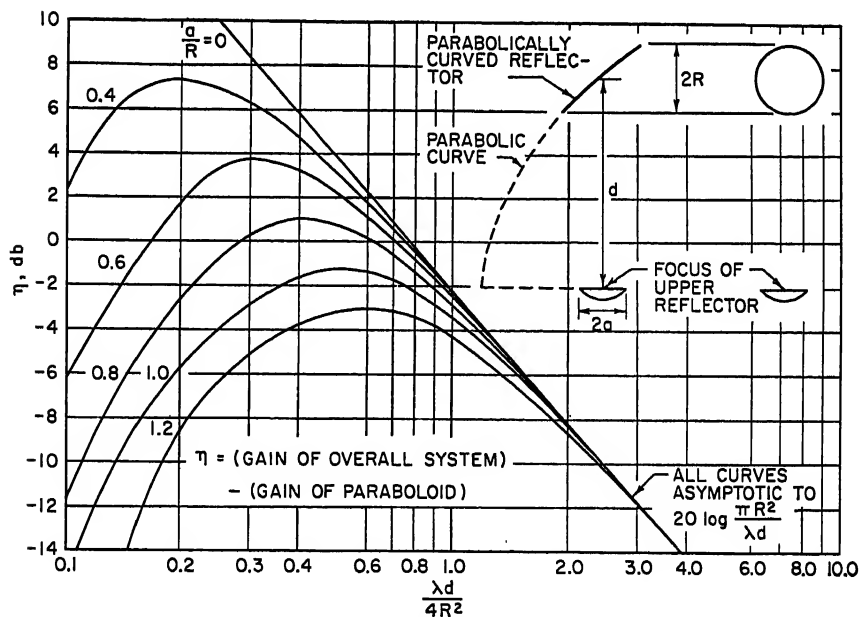
Fig. 13-7. Relative gain of periscope antenna system employing curved elevated reflector.

paraboloid. If the projected area of the elevated reflector is not circular but a regular polygon of four or more sides, η may be approximately obtained by using an effective reflector radius calculated from

$$R_{\text{eff}}{}^2 = \frac{A}{\pi} \tag{13-7}$$

where A is the area of the polygon.

The curves of Figs. 13-6 and 13-7 show that in general the periscope with a flat reflector is less sensitive to changes in frequency or separation than the periscope with a curved reflector. If the reflector has a larger diameter than the antenna ($a/R < 1$), the quantity η for either periscope is positive for certain values of $\lambda d/4R^2$, the larger values being obtained with the periscope with curved reflector.

The radiation patterns of periscope antenna systems depend in a rather complicated way on the many system variables. However, for most systems encountered in practice, experience has shown that the patterns out to the first two minor lobes may be obtained to a fair approximation by use of Table 13-1. In this table the elliptical reflector is assumed to have a circular projected area of radius R; the projected area of the rectangular reflector is assumed to be a square with sides equal to b. The first and second minor lobes of the periscope with an elliptical reflector are about 18 and 25 db, respectively, below the peak of the main lobe. Corresponding numbers for the rectangular reflector are about 14 and 18 db. Periscopes with polygonal reflectors fall in between the square and circular periscopes in their radiation properties, approaching the latter as the number of sides increases.

Table 13-1. Radiation Patterns of Periscope Antenna Systems

	Elliptical reflector	Rectangular reflector
3-db beamwidth, deg....................	$60\dfrac{\lambda}{2R}$	$52\dfrac{\lambda}{b}$
6-db beamwidth, deg....................	$82\dfrac{\lambda}{2R}$	$68\dfrac{\lambda}{b}$
First minimum, deg from axis...........	$73\dfrac{\lambda}{2R}$	$58\dfrac{\lambda}{b}$
First maximum, deg from axis...........	$95\dfrac{\lambda}{2R}$	$84\dfrac{\lambda}{b}$
Second minimum, deg from axis..........	$130\dfrac{\lambda}{2R}$	$116\dfrac{\lambda}{b}$
Second maximum, deg from axis..........	$156\dfrac{\lambda}{2R}$	$142\dfrac{\lambda}{b}$
Third minimum, deg from axis..........	$185\dfrac{\lambda}{2R}$	$174\dfrac{\lambda}{b}$

13.2. REFLECTORS FOR MICROWAVE TARGETS

Objects which scatter incident radiation so that at least a portion of it is reflected along the incident path to the radar antenna which launched it are known as targets. From the direction and the time of travel of the signal to the target and back again to the radar set, it is possible to locate the position of the target with considerable accuracy.

Many objects, both man-made and natural, act as radar targets. Objects such as trees, buildings, rain clouds, airplanes, ships, birds, and insects, all have been observed

as radar targets. Many of these incidental targets are not particularly efficient in reflecting echoes to the radar receiver.

It is possible, however, to design targets which will give much stronger echoes in proportion to their sizes than the incidental targets. These highly efficient targets may be placed at appropriate points along airport runways or shipping channels to serve as "buoys" for guiding radar-equipped aircraft or ships. Alternatively, they may be carried by aircraft or life rafts in order that these objects may be more readily located by ground control crews or rescue parties. Targets are sometimes used to produce standard echoes as a means of measuring radar performance.

Simple Geometrical Surfaces. Many radar targets are composed of simple geometrical surfaces. The surface of a building is much like a flat plate; a water tower is frequently a cylinder, and ships and aircraft may have surfaces which are spheroidal in geometry. A brief consideration of the reflecting properties of simple surfaces can give some insight into the echoing effectiveness of more complicated structures.

The effectiveness of a target is usually rated in terms of two quantities, one having to do with the echo strength, and the other relating to the solid angle over which the target is capable of responding. A sphere, for example, returns a rather weak signal but is operable at all angles of incident radiation. A flat plate, on the other hand, is an extremely efficient reflector but has a very sharp angle of response. The echoing strength is usually expressed by a quantity known as "scattering cross section," which for practical purposes may be defined as *the cross-section area of a conducting sphere of such a size that it would return an echo equal in strength to that from the target in question.* Scattering cross section is usually represented by the Greek letter σ. Sometimes the quantity "effective area" A_T is used. It is defined as *the area of an equivalent flat plate oriented so as to be perpendicular to the direction of the incident radiation.* For these definitions to be valid, the sphere and the flat plate are assumed to have dimensions which are large in comparison with the wavelength of the incident radiation. A_T and σ are related by a simple equation as given in the note below Fig. 13–8.

The angular response of a reflector is described in much the same way as that of an antenna. Response patterns may be plotted in terms of the angles of azimuth θ and elevation ϕ measured from the axis of maximum response of the target. Alternatively, the angle between the direction of maximum echo and that along which the echo is reduced by a specified amount, such as 3 or 10 db, may be used to describe the response.

The echoing properties of simple geometrical surfaces and several other targets are given in Fig. 13–8. The basic mathematical relations are given in the notes below the figure.

Dihedral Corner Reflectors. A dihedral corner reflector consists of two perpendicularly intersecting, flat conducting surfaces as shown in Fig. 13–8. A ray entering the corner in a plane perpendicular to the line of intersection of the reflecting planes will undergo a reflection from each surface and will return in the direction from which it came. The scattering cross section of a dihedral depends upon the wavelength, the size of the reflector, and the orientation of the reflector with respect to the direction to the radar antenna. In a plane perpendicular to the two corner surfaces the response pattern is quite broad. The scattering cross section σ varies in proportion to $[\sin (45° - \theta)]^2$ where θ is the absolute value of the angle between the direction to the radar antenna and the bisector of the corner angle. The maximum cross section occurs when the incident radiation enters the corner parallel to the bisector, that is, $\theta = 0°$. The response of the reflector in planes perpendicular to that of θ is a function of the wavelength and is usually very sharp. For this reason dihedrals are not often built for target use.

If the incident rays are polarized in a plane either parallel or perpendicular to the line of intersection of the corner planes, the reflected rays will be polarized in the same plane as the incident rays. If, however, incident rays are polarized in planes at 45°

TYPE	DIMENSIONS	MAXIMUM		ANGULAR RESPONSE	
		A_T	σ	θ	ϕ
SPHERE		$\dfrac{a\lambda}{2}$	πa^2	360°	360°
CYLINDER		$b\sqrt{\dfrac{a\lambda}{2}}$	$\dfrac{2\pi ab^2}{\lambda}$	360°	SHARP
FLAT PLATE		ab	$\dfrac{4\pi a^2 b^2}{\lambda^2}$	SHARP	SHARP
DIHEDRAL CORNER		$\sqrt{2}\,ab$	$\dfrac{8\pi a^2 b^2}{\lambda^2}$	± 30° (TO −10 DB ECHO LEVELS)	SHARP
TRIANGULAR TRIHEDRAL		$\dfrac{a^2}{\sqrt{3}}$	$\dfrac{4\pi a^4}{3\lambda^2}$	$\phi = 0$ graph (RELATIVE ECHO IN DB, θ from −50° to 50°)	$\theta = 0$ graph (RELATIVE ECHO IN DB, φ from −50° to 50°)
SQUARE TRIHEDRAL		$\sqrt{3}\,a^2$	$\dfrac{12\pi a^4}{\lambda^2}$	$\phi = 0$ graph (RELATIVE ECHO IN DB, θ from −50° to 50°)	$\theta = 0$ graph (RELATIVE ECHO IN DB, φ from −50° to 50°)

NOTES

A_T = EQUIVALENT FLAT-PLATE AREA OF TARGET

σ = SCATTERING CROSS SECTION OF TARGET

$\sigma = 4\pi \dfrac{A_T^2}{\lambda^2}$

$P_R = P_T \dfrac{A_R^2 A_T^2}{\lambda^4 d^4} = P_T \dfrac{A_R^2 \sigma}{4\pi \lambda^4 d^4}$ (FREE-SPACE TRANSMISSION)

P_T = POWER EMITTED BY RADAR

P_R = ECHO POWER COLLECTED BY RADAR

d = DISTANCE FROM RADAR TO TARGET

A_R = EFFECTIVE AREA OF RADAR ANTENNA = $\dfrac{G\lambda^2}{4\pi}$, WHERE G = GAIN

λ = WAVELENGTH IN SAME UNITS AS d, $\sqrt{A_R}$ AND $\sqrt{A_T}$

ALL DIMENSIONS ARE ASSUMED LARGE IN WAVELENGTHS

θ AND ϕ ARE ANGLES BETWEEN THE DIRECTION TO THE RADAR ANTENNA AND THE MAXIMUM RESPONSE AXIS OF THE TARGET

Fig. 13-8. Characteristics of various types of radar targets. The columns labeled A_T and σ give the maximum values of these quantities for optimum orientation of the target. G is the gain of an antenna over an isotropic radiator.

to the line of intersection, the reflected rays will be polarized perpendicularly to the incident rays.

Trihedral Corner Reflectors. A trihedral corner reflector consists of three reflecting planes assembled so as to form a right-angle corner. In general, a ray incident upon an interior surface of the corner will undergo a reflection from each of the three surfaces in turn and will return in a direction parallel to and with the same polarization

as the incident ray.   The path of such a ray is shown as 1-1' in Fig. 13-9a.   Some rays upon entering the corner will undergo two reflections but will escape the third and go off at an angle oblique to the incident ray.   Such rays are lost as radar echoes. The path of a typical ray of this type is shown as 2-2' in Fig. 13-9a.

In Fig. 13-9b it is assumed that the incident radiation is entering the reflector along an axis perpendicular to the plane of the figure.   Rays entering the shaded region will be triply reflected and returned to the radar.   Rays entering the un-shaded regions will be doubly reflected and lost, as in the case of ray 2-2' of Fig. 13-9a.   In Fig. 13-9c the reflector is rotated 30° and again the shaded area represents the region of triple reflection. The shaded area, equal to A_T, is evidently a function of the aspect angle.   Curves showing the variation of the response (proportional to A_T^2 or σ) of corner reflec-tors having both triangular and square sides are shown in Fig. 13-8.   The maxi-mum effective area for a corner reflector generally occurs for radiation entering parallel to the symmetric axis.   The latter makes equal angles with the three corner planes.

The corner-reflector response curves of Fig. 13-8 also exhibit sharp peaks at $\theta = \pm 40°$ and at $\phi = -35°$.   These occur when the reflector is oriented so that two of the planes produce a dihedral reflection in the manner described previ-ously.   There will be additional peaks at orientations which cause any one of the corner planes to be perpendicular to the incident radiation.   These peaks are not within the range of the curves in the fig-ure.   More extensive trihedral response curves will be found in Refs. 13 to 15.

Effect of Shape of a Trihedral.   A com-parison of the maximum values of σ (or A_T) shows that a corner reflector having square sides reflects a stronger signal along the symmetric axis than does a reflector having triangular sides, the lines of intersection of the corner planes being of equal length in either case.   On the

(a) CORNER REFLECTOR SHOWING RAY PATHS
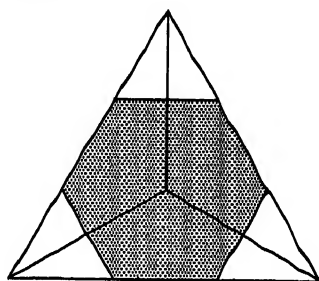
(b) EFFECTIVE AREA ON SYMMETRIC AXIS
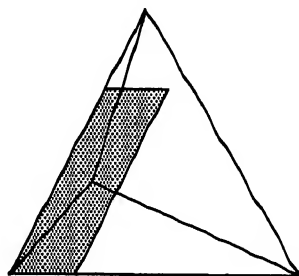
(c) EFFECTIVE AREA AT 30° ANGLE

FIG. 13-9. Trihedral corner reflectors: (a) Paths of rays. 1-1' represents a ray ex-periencing a triple reflection. 2-2' repre-sents a double reflection. (b) and (c) Variation of A_T (shaded) as reflector is rotated 30°.

other hand, the response patterns of the square corner are sharper than those of the triangular corner.

In general, broader response patterns can be obtained with a sacrifice in the ratio of the scattering cross section σ to the physical size of the reflector.   An example of this is shown in Fig. 13-10.   The figure shows two views of a modified corner reflector

designed to have a relatively flat response characteristic out to angles of 30° from the symmetric axis.   The reflector is evolved from a triangular corner reflector *ABC* by extending the three planes to form the notched contour *DEF*.   The original triangular reflector had an effective area defined by the shaded hexagon in Fig. 13-10*a*. The extension of the faces adds nothing to the axial effective area of the modified corner reflector.   However, at the 30° aspect angle shown in Fig. 13-10*b*, the effective
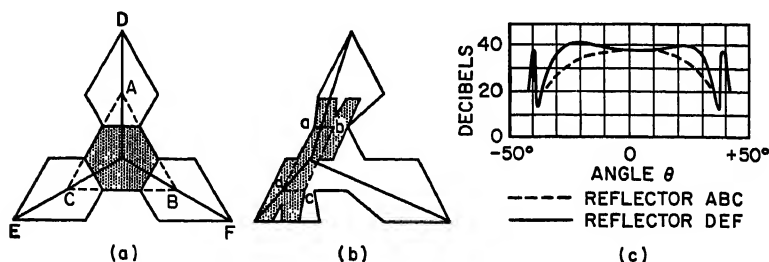
FIG. 13-10. Effect of shape of trihedral upon response pattern.

area of the original triangular corner is defined by the parallelogram *abcd*, and the effective area of the modified reflector is equal to the total shaded area.   The latter is approximately equal in value to the shaded hexagon in Fig. 13-10*a*.   The curve of Fig. 13-10*c* shows response patterns of the triangular reflector and the modified reflector.

By appropriate shaping of the contours of the corner-reflector surfaces, a wide variety of response characteristics can be obtained.

Effect of Errors in Construction upon Reflector Performance.   For optimum performance, the three planes of a corner reflector must be perfectly flat and the corner angles must be exactly 90°.   Results obtained with poorly constructed reflectors or
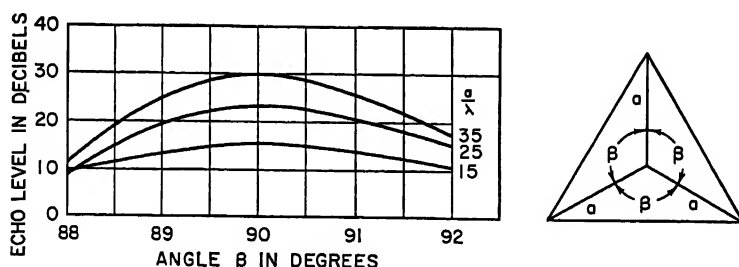
FIG. 13-11. Effect of error in all three corner angles upon trihedral echo response.   Incident radiation parallel to symmetric axis.

with reflectors using wire mesh for the surfaces may be disappointing, particularly if the dimensions of the reflector are larger than 20 wavelengths or so.   Wire mesh tends to give a warped surface, which results in part of the reflector returning radiation out of phase with that from another part.

Angular errors leading to a deviation of one-third wavelength at the outer edges of all three planes of a reflector will reduce the echo by about 3 db.   The angular tolerance, therefore, becomes smaller as the size of the reflector is increased.   Figure 13-11 shows some experimental curves of the variation of the echoes from various sizes of corner reflectors as the corner angles are changed.

Clusters of Corner Reflectors.   In order to extend the angular response of a target, clusters of corner reflectors are often used.   A simple cluster can be formed of three orthogonally intersecting planes.   Each octant of such an arrangement will be a corner reflector, and the cluster will give strong echoes over a wide range of aspects in both horizontal and vertical planes.   If a full 360° response is desired in the horizontal plane with only a ±30° response in the vertical, a group of five corner reflectors symmetrically arranged about a vertical axis will usually suffice.

Luneberg-lens Reflector.   An ingenious reflector, which exhibits a large scattering cross section over extremely wide response angles, has been developed.[16]   This reflector makes use of a Luneberg lens in the form of a dielectric sphere whose index of refraction varies with the distance r from the center in accordance with the relation

$$n = \left[2 - \left(\frac{r}{R}\right)^2 \right]^{\frac{1}{2}}$$

where R is the radius of the sphere.   This lens has the property of collecting the energy which falls upon the surface of one hemisphere, refracting it through the
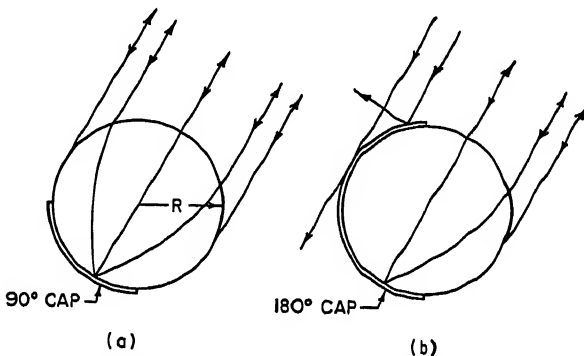
Fig. 13-12. Luneberg-lens reflectors: (a) 90° cap.   (b) 180° cap.

sphere, and bringing to a focus at the center of the surface of the opposite hemisphere.

If the energy is reflected at this focal point, it will be reradiated in the direction from which it originated.   As the direction of the incident radiation is changed, the focal point will shift its position accordingly.   Hence, if a portion of the opposite hemisphere is covered by a reflecting metallic cap, as shown in Fig. 13-12, the target will respond over a large range of angles of incidence.

If the reflecting cap is circular and subtends a conical angle of 90° at the center of the sphere, as shown in Fig. 13-12a, the reflector will have a uniform response over a conical angle of 90°.   With a 180° cap, the conical response angle will be increased beyond 90° but the response pattern will not be uniform because, as the incident angle changes, a variable portion of the incident radiation will be diverted by the outside surface of the cap.   This effect is shown in Fig. 13-12b.   Typical response patterns for the 90 and 180° caps are given in Fig. 13-13.

The theoretical scattering cross section of the Luneberg-lens reflector at the angle of maximum response is equal to the scattering cross section of a circular flat plate whose radius is equal to that of the sphere.

$$\sigma = \frac{4\pi^3 R^4}{\lambda^2}$$

where $R \gg \lambda$.   In practice, however, σ may be as much as 1.5 db below the theoretical value, due to losses and imperfections in the lens.

A corner reflector whose projected aperture along the symmetric axis is a circle equal in diameter to the Luneberg lens will have the same theoretical scattering cross section and will occupy a somewhat smaller volume than the lens. The lens, however, will operate over a much broader response angle. This is illustrated in Fig. 13-13, where the pattern of the corner reflector has been included for purposes of comparison.
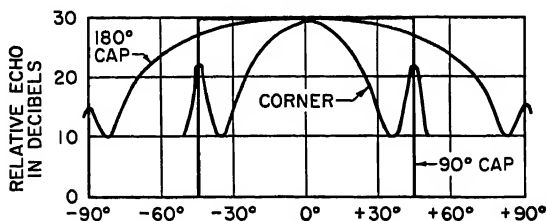
FIG. 13-13. Response patterns of Luneberg-lens reflectors with 90° and 180° caps compared with that of a corner reflector having the same maximum σ.

REFERENCES

1. H. Magnuski and T. F. Koch: "Passive Repeater Bends Microwave Beam," *Electronics*, vol. 26, pp. 134–137, February, 1953. Description of an installation of a single-mirror-type passive repeater at 6,000 Mc.
2. H. T. Friis: "A Note on a Simple Transmission Formula," *Proc. IRE*, vol. 34, pp. 254–256, May, 1946. Derivation of the transmission formula and discussion of its limitations.
3. H. L. Knudsen and M. Andreasen: "A Theory of Plane Reflectors in Microwave Antenna Systems," *Trans. Danish Acad. Tech. Sci.*, no. 3, 1952. Theoretical study of circular reflector and antenna.
4. H. G. Unger: "Ebene Spiegel zur Strahlumlenkung bei Richtantennen," *Frequenz*, vol. 6, no. 9, pp. 272–278, 1952. Theoretical study of a circular reflector and antenna.
5. W. C. Jakes, Jr.: "A Theoretical Study of an Antenna-reflector Problem," *Proc. IRE*, vol. 41, pp. 272–274, February, 1953. Circular reflector and paraboloid.
6. D. R. Crosby: "Theoretical Gain of Flat Microwave Reflectors," *IRE Convention Record*, pp. 71–75, 1954. Circular reflector and paraboloid.
7. J. Drexler: "An Experimental Study of a Microwave Periscope," *Proc. IRE*, vol. 42, p. 1022, June, 1954. Measurement of gain of circular reflector with paraboloid for three reflector sizes.
8. R. E. Greenquist and A. J. Orlando: "An Analysis of Passive Reflector Antenna Systems," *Proc. IRE*, vol. 42, pp. 1173–1178, July, 1954. Theoretical and experimental study of gain of circular reflector and paraboloid. Some pattern measurements reported.
9. E. Bedrosian: "The Curved Passive Reflector," *IRE Trans.*, AP-3, no. 4, pp. 168–173, October, 1955. Theoretical study of gain and radiation pattern for a curved circular reflector with paraboloid.
10. "Historical and Technical Survey," Summary Technical Report of the Committee on Propagation, National Defense Research Committee, vol. 1, pp. 82–85, 302–305, 1946. Cross sections of various targets and an excellent bibliography.
11. J. P. Nash and E. L. Hudspeth: "Corner Reflectors for Life Rafts," *MIT Rad. Lab. Rept.* 608, Aug. 1, 1944.
12. J. S. Hall: "Radar Aids to Navigation," MIT Radiation Laboratory Series, vol. 2, pp. 15–18, 324–331, McGraw-Hill Book Company, Inc., New York, 1947. Corner reflectors, properties and uses.
13. S. D. Robertson: "Targets for Microwave Radar Navigation," *Bell System Tech. J.*, vol. 26, pp. 852–869, October, 1947. Geometrical optics of corner reflectors and biconical reflectors.
14. R. C. Spencer: "Optical Theory of the Corner Reflector," *MIT Rad. Lab. Rept.* 433, Mar. 2, 1944.
15. G. C. Southworth: "Principles and Applications of Waveguide Transmission," pp. 475–481, D. Van Nostrand Company, Inc., Princeton, N.J., 1950.
16. Technical Bulletin 0-2-3, Emerson and Cuming, Inc., Boston, 1957, Luneberg-lens reflector.

Chapter 14

LENS-TYPE RADIATORS

Seymour B. Cohn

Rantec Corp.
Calabasas, California

14.1. BASIC LENS OPERATION

Curved reflectors (Chap. 12) and lenses are both commonly used as collimating elements in high-gain, narrow-beam microwave antennas. The choice between a reflector or lens for a given application depends upon many factors, such as the following. (1) The reflector is simpler to design, since it has but one surface, which obeys a more elementary law of geometric optics than the surfaces of the lens. (2) On the other hand, the more complex behavior of the lens is an advantage when additional parameters are required to achieve a special characteristic, such as the ability to scan
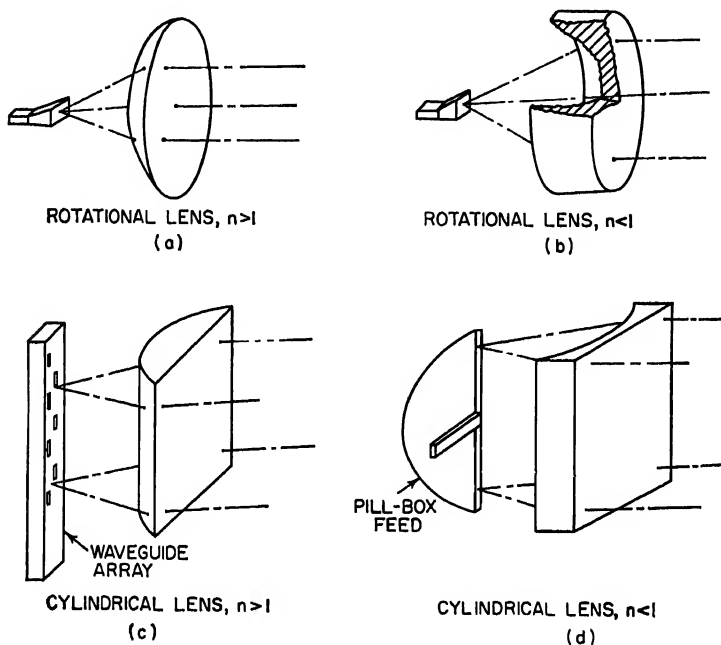
FIG. 14-1. Basic lens configurations useful at microwave frequencies.

over an angle wide compared with the beamwidth. (3) Although the lens is a more complicated structure than the reflector, its tolerances on surface shape are more lenient, and consequently its construction cost may frequently be little more or even less than that of the reflector. (4) The gain of a lens antenna is usually of the order of one or two decibels less than that of a reflector antenna, but with surface matching and extension of the feed horn to the rim of the lens, this discrepancy can actually be reversed. (5) The lens antenna usually has considerably less rearward radiation than the reflector antenna.

The patterns most commonly required of a lens antenna are highly directive beams of circular or oval cross sections (i.e., pencil or fan beams), with radiation in all other directions greatly suppressed. Figure 14-1 shows two methods of achieving such patterns; in methods *a* and *b* rotational lenses are used in conjunction with a point-source type of feed (the term rotational denotes that the surfaces of the lens are obtained by revolution of a curved line about the axis of the lens), while in methods *c* and *d* cylindrical lenses (i.e., lenses whose surfaces are generated by a straight line moving parallel to itself) are used in conjunction with a line-source feed. The cross-

section shape of the beam may be varied through choice of the feed pattern and of the width and height of the lens aperture.

At microwave frequencies, natural homogeneous dielectric media always have an index of refraction (or refractive index) greater than unity (i.e., a phase velocity less than that of light), which leads to the convex lens shapes of Fig. 14-1a and c. However, artificial (or fabricated) wave-propagating media may be constructed with any desired index of refraction ranging from considerably less than unity to considerably greater than unity. Examples of lenses constructed with an index of refraction less than unity are shown in Fig. 14-1b and d, where it is seen that a concave shape is required to focus a beam. Design data on the useful types of natural and artificial media are given in later paragraphs of this chapter. In general, the types having $n < 1$ are highly dispersive (that is, n varies sharply with frequency), while those having $n > 1$ are nondispersive, or relatively so. Thus lenses having n less than unity are usually limited to frequency bandwidths of perhaps 2 to 10 per cent, while lenses having n greater than unity may be designed to be operable over an octave or more.

Considerable information on microwave lens media and on lens surface design has been published, and are listed in the References at the end of the chapter (see especially Refs. 1 and 2). An extensive bibliography is given by Harvey.[2a]

14.2. LENS-SURFACE FORMULAS FOR $n > 1$

The more common lens shapes for an index of refraction greater than unity are shown in Fig. 14-2. The formulas given in the figure apply to both rotational and cylindrical surfaces. Design data for natural and artificial media having $n > 1$ are given in a later discussion.

Single Refracting Surface $n > 1$. The first four lenses of Fig. 14-2 achieve their focusing effect by refraction at only one of the two surfaces. In lenses a to c this occurs at the surface adjacent to the focal point, while in lense d the refraction occurs at the opposite surface. In each case, a lens surface is everywhere perpendicular to the incident rays, and hence the rays pass through this surface without being refracted. A disadvantage of these single-refracting-surface types when used in a transmitting antenna is that the nonrefracting surface lies in a constant-phase wavefront, and consequently a reflected wave from this surface will converge at the focal point and give rise to a reflection coefficient in the feed line approximately equal to the reflection coefficient of the surface. Since even a moderate VSWR will often adversely affect the stability of the transmitter tube, it is desirable that this surface reflection either be eliminated or prevented from entering the feed line. Several methods of matching lens surfaces to avoid reflection are given in the paragraphs on specific lens media. However, even in the presence of surface reflection, a high feed-line VSWR may be avoided by tilting the lens slightly (as in Fig. 14-3a), so that the refocused reflected energy will not enter the feeding antenna, or by displacing half of the lens a quarter wavelength along the axis with respect to the other half (as in Fig. 14-3b). In the latter case, the refocused reflected waves from the two halves of the lens arrive at the feed 180° out of phase and no energy enters the feed. Both the methods shown in Fig. 14-3 have been found effective in reducing the VSWR in the feed line and have not caused appreciable deterioration of the secondary antenna pattern. However, they do not eliminate the other effects of surface reflection, such as loss of gain and increase in side-lobe level due to scattering of the reflected energy. Wherever these factors are important, the surface-matching techniques to be described later are recommended.

Two Refracting Surfaces $n > 1$. Microwave lenses in which the rays are refracted at both surfaces have not been used as frequently as the single-refracting-surface

(a)

$$r = \frac{(n-1)f}{n\cos\theta - 1}$$

$$y = \sqrt{(n^2-1)x^2 + 2(n-1)fx}$$

(b)

$$r = \frac{(n-1)f_1 - (K-1)\lambda_0}{n\cos\theta - 1}$$

$$y = \left\{(n^2-1)x^2 + 2(n-1)f_1 x + 2(K-1)\lambda n x + 2f_1(K-1)\lambda + (K-1)^2 \lambda^2\right\}^{1/2}$$

$$K = 1, 2, 3, 4, ---$$

(c)

$$\Delta = \frac{\lambda}{n-1}$$

CURVED
SURFACE
SAME AS IN (a)

(d)

$$r_1 = f - d = \text{CONSTANT}$$

$$r_2 = \frac{(n-1)f}{n - \cos\theta_2}$$

$$y_1 = \sqrt{(f-d)^2 - (x_1+f)^2}$$

$$y_2 = \left\{-2\left(\frac{n-1}{n}\right)fx_2 - \left(\frac{n^2-1}{n^2}\right)x_2^2\right\}^{1/2}$$

(e)

SAME AS (f), WITH K=1

(f)

$$x_2 = \left\{\frac{(K-1)\lambda + (n-1)d + f - \sqrt{f^2 + y_1^2}}{n - \left(1 - \frac{y_1^2}{n^2(f^2+y_1^2)}\right)^{1/2}}\right\} \cdot \left[1 - \frac{y_1^2}{n^2(f^2+y_1^2)}\right]^{1/2}$$

$$y_2 = y_1\left[1 + \frac{x_2}{\left[n^2(f^2+y_1^2) - y_1^2\right]^{1/2}}\right], \quad K = 1, 2, 3, 4, ---$$
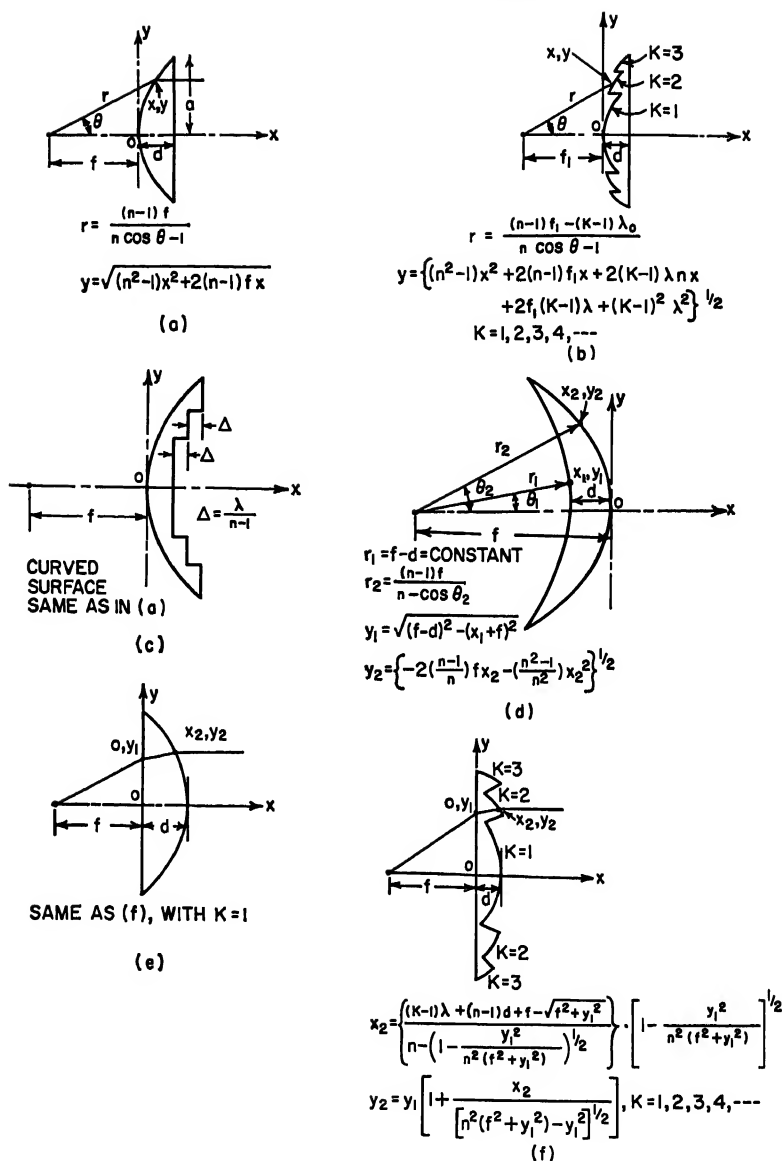
FIG. 14-2. Lens-shape design for media having $n > 1$.

types, but the greater difficulty in their design is frequently justified by advantages in performance. For example, a two-refracting-surface lens will not refocus surface reflections back into the feed line, and the additional design parameters permit the achievement of special properties, such as wide-angle scanning ability.

A two-refracting-surface lens that has had practical application is shown in Fig. 14-2e and f. This plano-convex design has good wide-angle scan properties when used with dielectric constants of the order of 2.5.[2,3] The general method of surface-shape

computation for other two-refracting-surface lenses having $n > 1$ is given in several references[1–5] and should be employed when a particular kind of performance is required that cannot be met by the designs of Fig. 14-2.

Zoning Formulas $n > 1$. In the case of physically large lenses, the use of continuous surfaces (as in Fig. 14-2a, d, and e) results in a massive structure that is heavy and difficult to produce without imperfections. Also, the long path lengths through the medium make its index of refraction highly critical. In order to alleviate these disadvantages, use is commonly made of discontinuous, or zoned, surfaces as in Fig. 14-2b, c, and f. Ray path lengths through any two adjacent zones are designed to differ from each other by exactly 360 electrical degrees (or a whole multiple thereof) so that a plane constant-phase front results on the collimated side of the lens.
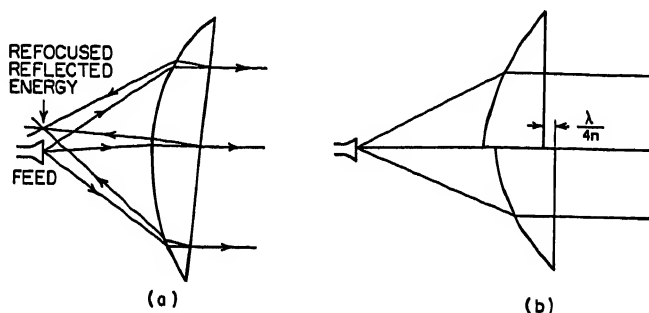
FIG. 14-3. Reduction of feed VSWR by means of (a) lens tilt, (b) quarter-wave displacement of half of the nonrefracting surface.

Figure 14-2b and c gives the surface-shape formulas for zoned versions of the lens of Fig. 14-2a, while Fig. 14-2f shows the zoned counterpart of Fig. 14-2e. In the formulas for b and f, the use of integers $K = 1, 2, 3, 4$, etc., gives a family of lens surfaces all of which provide the same focal point at $x = -f$ and produce plane wavefronts differing from each other in phase by $360K°$. In the use of these formulas, a thickness d on the axis is chosen and the central zone of the surface is computed for $K = 1$. At the radius for which the lens thickness is equal to the minimum allowed by mechanical considerations, the second zone is computed for $K = 2$. In a similar manner additional zones are computed with $K = 3, 4$, etc., until the desired lens diameter is attained. If the minimum allowable thickness is d_{min}, the maximum thickness is approximately $d_{min} + \lambda/(n - 1)$.

Effects of Zoning on Aperture Illumination, $n > 1$. Certain defects in the aperture illumination usually occur with zoned lenses and should be considered carefully in the lens design. For example, Fig. 14-4a shows how energyless (shadowed) bands occur in the aperture field in front of a refracting second surface of a lens. Inspection of the figure reveals that there is no way in which the zonal boundary can be shaped to eliminate the shadow. In fact, shadowing occurs in any lens for which $n > 1$, if the zone steps occur in a refracting surface on the side of the lens away from the focal point. The presence of these nonilluminated bands in the aperture results in an increased side-lobe level and decreased gain of the secondary pattern.

A second type of defect occurs when a first refracting surface is zoned, as in Fig. 14-4b. In this case, the rays between ray a and ray b are not properly refracted by the lens and are scattered in undesired directions. As a consequence the gain and side-lobe level are inferior to an unzoned lens. Although there is no shadowing in this case, discontinuities in aperture amplitude exist at the boundaries of the zones, deteriorating the secondary pattern still further.

However, zoning without shadowing or energy loss is possible if carried out on a nonrefracting surface of the lens. Figure 14-4c shows an example in the case of a plane second surface. It is necessary that the surface of the step between zones be perpendicular to the zoned surfaces. This type of zoning should provide the most satisfactory aperture illumination of the various types, but there still exist disturbances along the boundaries of the zones because of phase differences between the rays just inside and just outside the dielectric surface. Some decrease in efficiency of the zoned lens may therefore be expected compared with an unzoned lens, although the performance should be superior to that obtained with zoned refracting surfaces. In the special instance of a cylindrical lens in which the E vector is everywhere perpendicular to the step surfaces, this disturbance may be avoided by covering these surfaces with thin conducting sheets.

SHADOWING WITH NO LOSS OF ENERGY

(a)

NO SHADOWING, BUT LOSS OF ENERGY

(b)

NO SHADOWING OR LOSS OF ENERGY

(c)
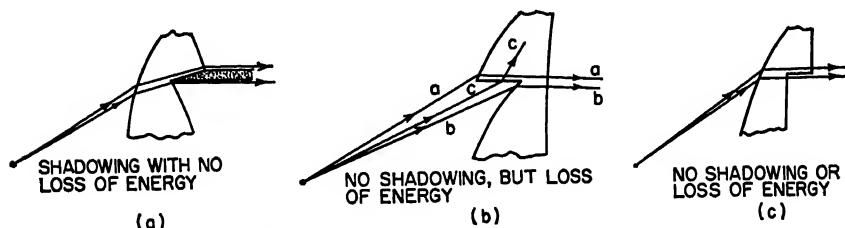
FIG. 14-4. Effect of zoning on aperture illumination, $n > 1$.

Bandwidth of Zoned Lenses, $n > 1$. The surface-shape design of an unzoned lens is independent of frequency, if n is constant. However, as may be seen from the formulas in Fig. 14-2, zoning introduces a dependence on frequency, and consequently a zoned lens has a limited bandwidth of satisfactory operation. Although each zone of the lens provides the same electrical path length from the focal point to the aperture plane on the opposite side of the lens, rays through adjacent zones will differ by exactly 360° only at the design frequency. If the lens has a total of N wavelength steps between the central and outer zones, the effective path-length difference between a ray through the outer zone and a ray through the central zone is $N\lambda_0$ at the design wavelength λ_0 and $N\lambda$ at any other wavelength λ. (If each zone steps by one wavelength, then N is one less than K of the outermost zone.) The phase error in wavelengths of the outer zone compared with the central zone is therefore

$$\delta = -N\Delta\lambda \tag{14-1}$$

A maximum phase variation of one-eighth wavelength is usually considered permissible in the aperture of a microwave antenna. The total bandwidth of the zoned lens is approximately $100(2\Delta\lambda/\lambda)$ per cent, and hence the bandwidth of a lens having N wavelength steps is

$$\text{Bandwidth} \approx \frac{25}{N} \quad \text{per cent} \tag{14-2}$$

Thus a zoned lens has an approximate bandwidth of 25 per cent for $N = 1$ but only 5 per cent for $N = 5$. If other sources of aperture phase error are present, it might be desirable to reduce the allowable tolerance on δ, thereby reducing the bandwidth below the figure permitted by Eq. (14-2).

14.3. LENS-SURFACE FORMULAS FOR $n < 1$

The lens formulas given in Fig. 14-2 apply for $n < 1$ as well as for $n > 1$. However, for convenience, the more important lens-surface design formulas for an index of

refraction less than unity are shown in Fig. 14-5 and apply to both rotational and cylindrical surfaces. Design data for media having $n < 1$ are given in a later discussion.

The lenses of Fig. 14-5a and b are single-refracting-surface types, since the plane surface lies in a constant-phase front. Consequently, the reflection from this surface converges into the focal point and will produce a high feed-line VSWR unless this
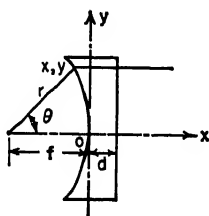
$$r = \frac{(1-n)f}{1 - n \cos \theta}$$

$$y = \sqrt{2(1-n)(-x)f - (1-n^2)x^2}$$

(a)
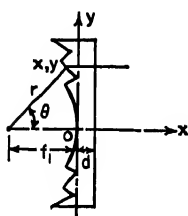
$$r = \frac{(1-n)f_1 + (K-1)\lambda_0}{1 - n \cos \theta}$$

$$y = \left[2(1-n)(-x)f_1 - (1-n^2)x^2 - 2(K-1)(-x)n\lambda \right.$$
$$\left. + 2(K-1)f_1 \lambda + (K-1)^2 \lambda^2 \right]^{1/2}$$

$$K = 1, 2, 3, 4,$$

(b)

RAY CONSTRAINED
TO PATH PARALLEL
TO x AXIS
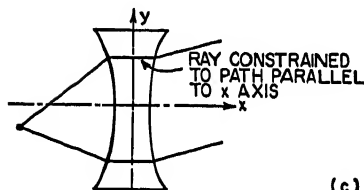
WIDE-ANGLE-SCAN TYPE
(SEE RUZE[6], BROWN[2])

(c)

CONSTRAINED
RAY
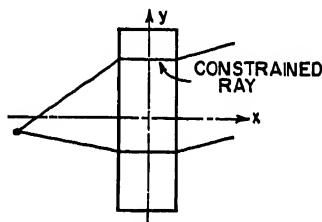
WIDE-ANGLE-SCAN TYPE
n VARIES WITH y.
(SEE RUZE[6])

(d)

Fig. 14-5. Lens-shape design for media having $n < 1$.

surface is matched to free space or unless the reflected energy is deflected away from the feed point by one of the methods shown in Fig. 14-3.

Single Refracting Surface, $n < 1$. The single-refracting-surface stepped design of Fig. 14-5b has been by far the most used of all microwave lenses. Its design is simple, since only one curved surface is involved, and the steps lead to a thin, light-weight, relatively noncritical structure. However, shadow bands at the steps cannot be avoided, as may be seen in Fig. 14-6. Although all the rays emanating from the focal point are collimated by the lens into a bundle of parallel rays, the shadow bands cause an increase in side-lobe energy and a decrease of gain, because of the discontinuities they introduce in the aperture illumination function. As in the case of

$n > 1$, zoning can be accomplished without shadowing or energy loss only if the steps are taken in an equiphase surface. Thus the plane surface in Fig. 14–5a could be successfully stepped, although the resulting meniscus-type lens shape would be more difficult to manufacture and to support than the flat shape of Fig. 14–5b.

The maximum thickness of the stepped lens for $n < 1$ is equal to $d_{min} + (1 - n)\lambda$, where d_{min} is the minimum thickness permitted in the mechanical design. The bandwidth limitation due to zoning is the same as for $n > 1$, and the bandwidth for a maximum phase variation of one-eighth wavelength is given by Eq. (14–2). However, the bandwidth of the actual lens is considerably less than this when the frequency
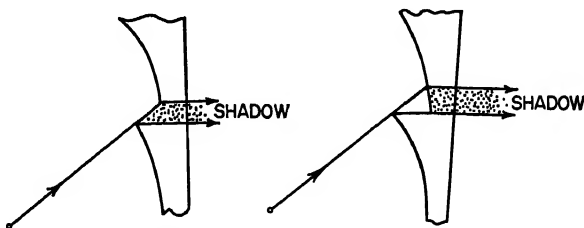
FIG. 14-6. Shadow introduced by zoned lens of Fig. 14-5b.

sensitivity of the refractive index is taken into account, since all known media having $n < 1$ exhibit a large rate of change of refractive index with frequency. Thus, in the common case of a metal-plate zoned lens having the shape shown in Fig. 14-5b, the bandwidth for an eighth-wavelength over-all phase variation is approximately

$$\text{Bandwidth} \approx \frac{25 n_0}{1 + (N + 1)/n_0} \qquad \text{per cent} \qquad (14\text{-}3)$$

where n_0 is the index of refraction at the center of the band, and N is the number of one-wavelength steps between the central and outer zones. In the case of frequency-sensitive media, zoning increases the bandwidth of a lens over that of an equivalent unzoned lens by two or three times. This is true, although zoning is itself frequency-sensitive, because the ray path lengths in the dispersive medium are greatly reduced by zoning. The bandwidth of a given lens antenna may be extended considerably beyond that given by Eq. (14-3) if the antenna is constructed to permit moving the feed horn along the lens axis, since the effect of a change in frequency is principally to change the focal length. Also, the use of a more complex medium makes a design for greater bandwidth feasible.[5a]

Wide-angle-scan Types, $n < 1$. Lenses with an index of refraction less than 1, other than those shown in Fig. 14-5a and b, have thus far had little use but have sufficient advantages to warrant future applications. The principal advantage to be gained is that of a considerably wider scan angle. A number of different wide-angle-scan lenses have been analyzed by Ruze, and for details on their design his article should be consulted.[6] A discussion of Ruze's work is also given by Brown.[2] Two of Ruze's most promising lens shapes are shown in Fig. 14-5c and d. In both cases, a metal-plate medium is assumed, with the plates oriented so as to constrain the rays into paths parallel to the lens axis. The configuration of Fig. 14-5d is particularly interesting because of the mechanical advantages of uniform thickness and plane surfaces and the electrical advantage gained through the avoidance of stepping. In this uniform-thickness lens, the index of refraction is varied with distance from the center in order to make the plane exit surface a constant-phase surface. In a lens of aperture large compared with the wavelength, the index of refraction must be stepped at frequent intervals, in order to maintain n in the practical range of about

0.5 to 0.9. Since this stepping does not affect the surface shape, it has no appreciable effect on the secondary pattern but does introduce a frequency sensitivity. Additional analysis of the lens shown in Fig. 14-5c is given by Proctor and Rees.[6a]

14.4. FACTORS AFFECTING GAIN OF LENS ANTENNAS

The gain of a lens antenna is dependent upon the following factors: (1) attenuation in the lens medium, (2) reflection from the surfaces, (3) amount of feed energy not incident upon the lens (spillover loss), and (4) the amplitude distribution in the aperture of the lens. The attenuation and reflection loss will be considered later in the paragraphs on specific lens media. However, at this point it may be noted that in the case of a lossy medium, stepping the lens reduces the attenuation loss, since it reduces the path lengths inside the lens.

Spillover Loss. Spillover loss may be avoided if the sides of the feed horn are extended to the edges of the lens. However, this is usually not done, since reflections from the lens surfaces are rereflected by the walls of the horn, and much of this reflected energy eventually emerges from the lens in undesired directions, thus increasing the side lobes by serious amounts. For this reason, a small feed horn has been used in most applications, with considerable spillover loss permitted. Surface matching is recommended for future lens antennas, since it increases the efficiency both by eliminating surface reflections and by permitting the use of a feed horn extended to the edges of the lens. The increase of gain that may be expected from the first factor is about $\frac{1}{2}$ db and from the second about 1 to 2 db. This total increase of gain of 1.5 to 2.5 db makes surface matching highly worthwhile.

For a given aperture-illumination taper, the proportion of feed power lost through spillover in a practical lens antenna design depends upon the shape of the lens. This is discussed in detail below, where it is shown that spillover loss is less for a concave surface adjacent to the feed horn than for a convex surface.

Effect of Lens Shape on Aperture Illumination. The purpose of most lenses is to focus the diverging radiation from a point or line source into a plane wavefront on the opposite side of the lens. The amplitude distribution of this plane wavefront is a function of the primary radiation pattern of the source and of the shape of the lens. The following formula[1] expresses this relationship for the single-refracting-surface lenses of Figs. 14-2a and b and 14-5a and b, when the curved surface is a *figure of rotation* and the feed is a point source.

$$A(\rho,\phi) = F(\theta,\phi) \sqrt{\frac{(n \cos \theta - 1)^3}{(n-1)^2(n - \cos \theta)} \left(\frac{f_1}{f_K}\right)^2} \tag{14-4}$$

In the case of a *cylindrical* surface[1]

$$A(y,z) = F(\theta,z) \sqrt{\frac{(n \cos \theta - 1)^2}{(n-1)(n - \cos \theta)} \frac{f_1}{f_K}} \tag{14-5}$$

These formulas apply to n either less than or greater than unity. The symbols ρ, θ, and y are coordinates indicated in Fig. 14-7a while ϕ and z are additional coordinates in a plane parallel to the aperture. $F(\theta,\phi)$ and $F(\theta,z)$ are the amplitude radiation patterns of the point- and line-source feeds measured at a constant radius equal to f_1, where f_1 is the focal length of the central zone of the lens. The dimension f_K is the focal length of the Kth zone of the lens and is related to f_1 by

$$f_K = f_1 - \frac{(K-1)\lambda}{n-1} \tag{14-6}$$

The amplitude functions $A(\rho,\phi)$ and $A(y,z)$ are measured in the plane of the lens

ROTATIONAL LENS, $A(\rho,\phi)/F(\theta,\phi)$
CYLINDRICAL LENS, $A(y,z)/F(\theta,z)$
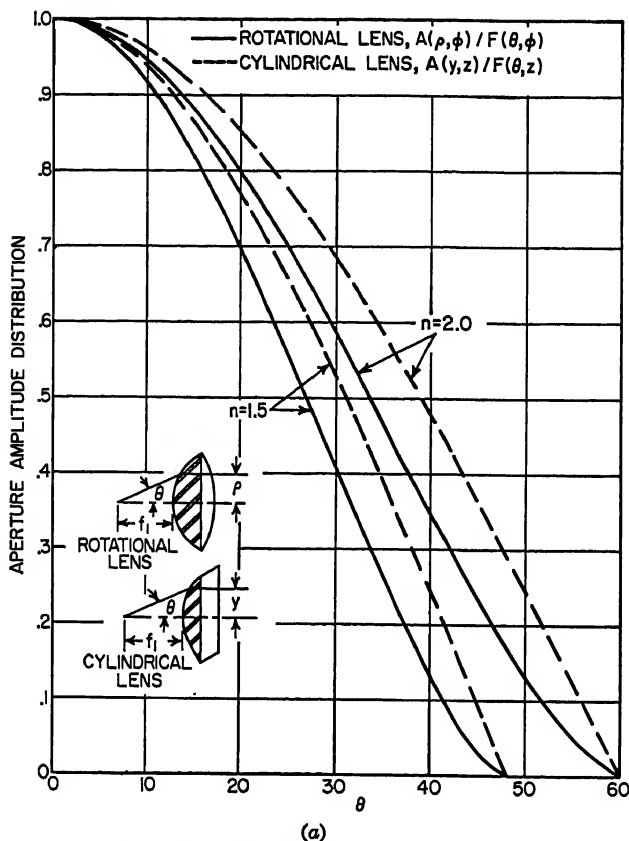
FIG. 14-7. Aperture-illumination ratios for the simple cylindrical

aperture and may be used to compute the secondary radiation pattern and gain of the lens antenna by means of formulas given in Chaps. 2 and 12.

Representative curves of $A(\rho,\phi)/F(\theta,\phi)$ and $A(y,z)/F(\theta,z)$ versus θ are shown in Fig. 14-7 for values of n ranging from 0.5 to 2.0. The behavior for rotational and cylindrical lenses is similar—for $n > 1$, the ratio decreases with θ, while for $n < 1$ the ratio increases. Thus an index of refraction greater than unity yields a decrease in aperture field strength at the edges of the lens compared with the primary feed pattern, while an index of refraction less than unity yields a gain. This fact is highly significant as it relates to spillover loss, since for a given edge taper of the aperture illumination the primary pattern must be more nearly uniform for $n > 1$ than for $n < 1$. Thus a greater primary beamwidth is necessary for $n > 1$, and the spillover loss is greater than for $n < 1$ (unless the feed horn extends to the edges of the lens). Zoning of a lens introduces discontinuities in the aperture distribution, as shown in Fig. 14-8, but reduces the total variation over the aperture.

The maximum power gain G in decibels of a lossless single-refracting-surface rotational lens fed at its focus may be computed from the following formula:

$$G = 20 \log_{10} \left[\frac{1}{\lambda f_1} \int_{\text{aperture}} \rho A(\rho,\phi) \, d\rho \, d\phi \right] + G_f \tag{14-7}$$

where G_f is the on-axis power gain of the feed in decibels, λ is free-space wavelength,

ROTATIONAL LENS
$A(\rho,\phi)/F(\theta,\phi)$

CYLINDRICAL LENS
$A(y,z)/F(\theta,z)$

$n=0.7$ 0.6 0.5
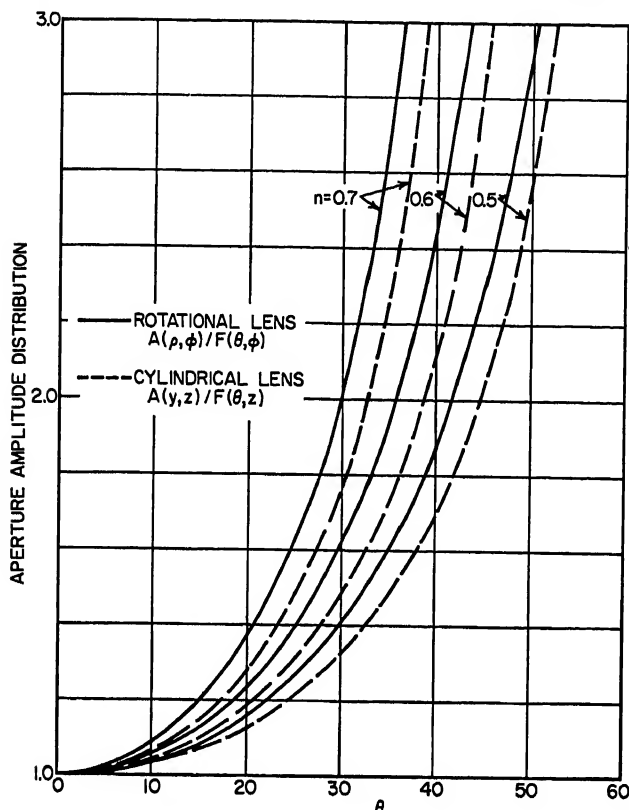
(b)

and rotational lenses of Figs. 14-2a and 14-5a: (a) $n > 1$, (b) $n < 1$.

f_1 is the focal length of the central zone, ρ is radius in the aperture plane, and $A(\rho,\phi)$ is found from Eq. (14-4), with $F(\theta,\phi)$ normalized to unity in the direction of the axis.

In a practical problem, G_f and the primary feed pattern may be computed or measured, $A(\rho,\phi)$ should then be calculated point by point, and then Eq. (14-7) may be evaluated by a numerical-integration procedure. Equation (14-7) takes account of spillover loss and aperture distribution. If reflection loss and dissipation loss occur, the true gain will be obtained by reducing the value computed from Eq. (14-7) by loss values in decibels to be given in later paragraphs on lens media.

For ordinary applications, Eqs. (14-4),
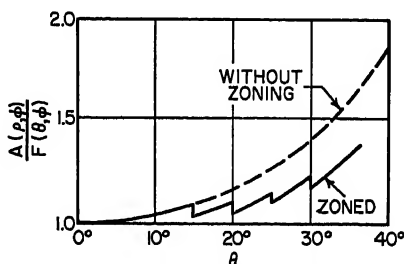
Fig. 14-8. Aperture-illumination ratio for a zoned rotational lens of type shown in Fig. 14-5b: $n = 0.5$, $f_1 = 40\lambda$.

(14-5), and (14-7) will be adequate. However, if the cross-polarized component of the aperture or the radiation field is an important consideration, a more precise formulation by E. M. T. Jones, taking this into account, should be consulted.[7]

14.5. NATURAL-DIELECTRIC LENSES

The term natural dielectric is intended here to cover both uniform and heterogeneous mixtures of dielectric materials as well as single pure compounds. In the case of heterogeneous mixtures (e.g., polyfoam and resin-impregnated Fiberglas), the variations in dielectric constant are assumed to be random and with spacing very small compared with wavelength, so that the electrical behavior is indistinguishable from that of a uniform material. The index of refraction n of a solid dielectric is related to the relative dielectric constant ϵ_r by

$$n = \sqrt{\epsilon_r} \qquad (14\text{-}8)$$

Usually only small microwave lenses are made of solid-dielectric media. In large lenses the weight of a natural lens and the difficulty of mounting it safely appear to make the various types of artificial dielectric media more desirable. However, recent advances in the manufacture of mixtures of titanium dioxide powder in a foamed dielectric may make large lenses of this medium practical to construct and utilize. In the case of circular lenses less than about 12 in. in diameter, and of thin cylindrical lenses (as in the mouth of a sectoral-horn line source), a solid dielectric is frequently the most satisfactory. This is particularly true at wavelengths under 1 cm, where artificial dielectrics are difficult to manufacture to sufficiently close tolerances.

A number of dielectrics suitable for use in microwave lenses are listed in the tables by Von Hippel.[8] For any particular application, the choice of the most suitable material will depend upon the refractive index, the maximum allowable loss in gain due to power dissipation in the material, and the requirements on physical strength and stability over the specified environmental conditions. Too low an index of refraction will result in excessive lens thickness, while too high a value will result in excessive reflection loss (unless surface-matching structures are used). The loss tangent (tan δ) of the dielectric should be as small as possible to minimize dissipation loss, but frequently a material must be selected on the basis of its physical characteristics even though its loss tangent is much larger than that of certain other materials.

In cases where its moderate strength and heat resistance are sufficient, polystyrene is to be recommended because of its exceptional electrical qualities, its ease of machining and molding, and its relative economy. Where greater strength and heat resistance are required and a higher index of refraction can be tolerated, several glasses and ceramics are available with low loss tangents. If more than a few tenths of a decibel of dissipation loss is permissible the great shock resistance and impact strength of various types of impregnated Fiberglas can be utilized. The mixtures of titanium dioxide powder in a dielectric foam appear to have particular advantages of lightness, low loss, and availability of a wide range of refractive-index values.

Dissipation Loss in Dielectric Lenses. The dissipative attenuation constant α, for a wave propagating in a solid-dielectric medium, is given by

$$\alpha = \frac{27.3n \tan \delta}{\lambda} \qquad \text{db/cm} \qquad (14\text{-}9)$$

where n is the index of refraction, tan δ the loss tangent of the medium at the operating frequency, and λ is the free-space wavelength in centimeters. In a zoned lens $d_{max} \approx \lambda/(n-1)$; therefore

$$\text{Dissipative attenuation of lens} \approx 27.3 \frac{n}{n-1} \tan \delta \qquad \text{db} \qquad (14\text{-}10)$$

A family of curves computed from Eq. (14-10) is plotted in Fig. 14-9. A comparison

of this graph and Ref. 8 shows that a number of materials are available that will
result in a lens attenuation of only a few tenths of a decibel.

Reflection Loss in Dielectric Lenses. The power-reflection coefficient of a single
interface between air and dielectric is given by

$$r_{\perp}^2 = \frac{\sin^2\left(\theta_1 - \sin^{-1}\dfrac{\sin\theta_1}{n}\right)}{\sin^2\left(\theta_1 + \sin^{-1}\dfrac{\sin\theta_1}{n}\right)} \qquad (14\text{-}11)$$

for perpendicular polarization (i.e., for the field vector E perpendicular to the plane
of incidence), where θ_1 is the angle between the ray direction in air and the normal
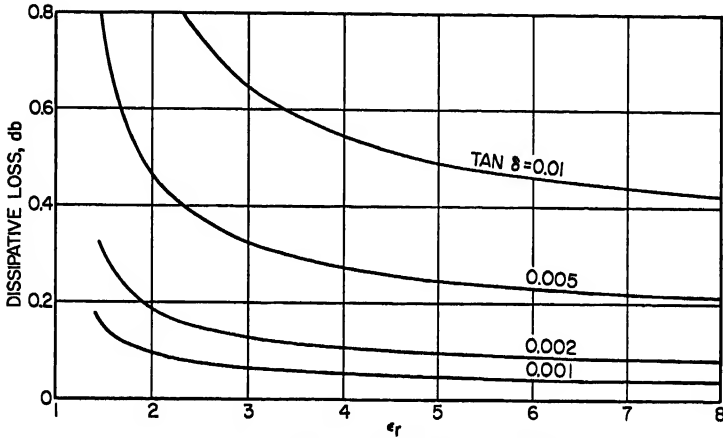
Fig. 14-9. Approximate dissipation loss in a zoned-dielectric lens.

to the surface, and n is the index of refraction of the dielectric. For parallel polariza-
tion (E in the plane of incidence) the power-reflection coefficient is

$$r_{\parallel}^2 = \frac{\tan^2\left(\theta_1 - \sin^{-1}\dfrac{\sin\theta_1}{n}\right)}{\tan^2\left(\theta_1 + \sin^{-1}\dfrac{\sin\theta_1}{n}\right)} \qquad (14\text{-}12)$$

For normal incidence ($\theta_1 = 0$), both Eqs. (14-11) and (14-12) reduce to

$$r^2 = \left(\frac{n-1}{n+1}\right)^2 \qquad (14\text{-}13)$$

The power-reflection coefficient is the same whether the incident wave is in air or in
the dielectric medium, as long as θ_1 specifies the ray direction in the air region. A
graph of Eqs. (14-11) and (14-12) appears in Fig. 14-10 for dielectric constants of 2.5
and 4.0. It is seen that for perpendicular polarization $r_{\perp}^2$ rises as θ_1 increases from
zero and equals unity at $\theta_1 = 90°$. For parallel polarization, $r_{\parallel}^2$ decreases with
increasing angle until it reaches zero at $\theta_1 = \tan^{-1} n$ (known as Brewster's angle), and
then increases to unity at $\theta_1 = 90°$.

In the case of the usual two surfaces of a lens, internal multiple reflections between
the surfaces have a pronounced effect. The total power-transmission coefficient of
the lens depends upon the phase length of the ray path in the dielectric and may lie
anywhere between a minimum of $T_{min}^2 = [(1 - r^2)/(1 + r^2)]^2$ and unity. For

polystyrene and normal incidence, this minimum is 0.82, which represents a 0.9-db loss. However, the usual lens varies widely in thickness over the aperture, and therefore numerous approximately sinusoidal fluctuations occur in the transmitted energy over the aperture. The average total-power-transmission coefficient of the lens is
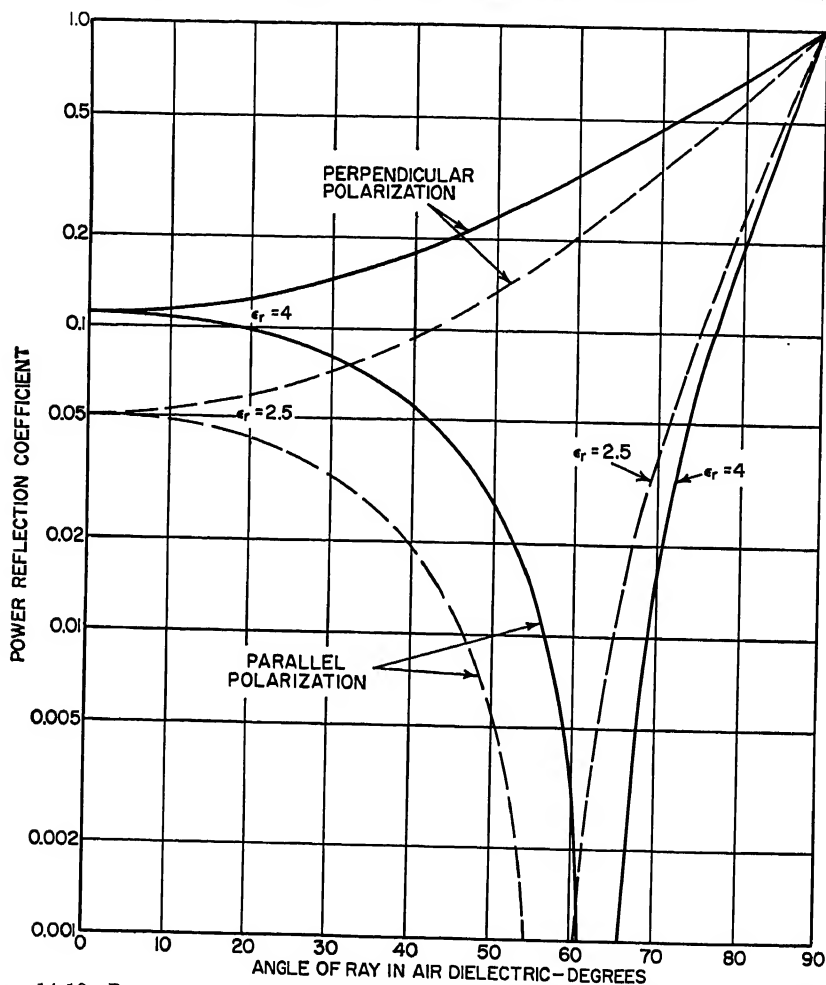
FIG. 14–10. Power-reflection coefficient at one boundary between air and a dielectric medium.

therefore approximately $T_{avg}^2 = \frac{1}{2}(1 + T_{min}^2) = (1 + r^4)/(1 + r^2)^2$. The major amount of energy passes through the lens at near-normal incidence, and hence a good average value to choose for r^2 is the normal-incidence value. Figure 14–10 shows this to be particularly true if waves of both polarizations are incident upon different portions of the lens. Thus the total average reflection loss of a dielectric lens is approximately

$$\text{Lens reflection loss} \approx 10 \log_{10}\left(1 + \frac{2r^2}{1 + r^4}\right) \approx 8.69\left(\frac{n - 1}{n + 1}\right)^2 \quad \text{db} \qquad (14\text{-}14)$$

For a polystyrene lens the average reflection loss is approximately 0.5 db.

Another serious effect of surface reflection is an increased side-lobe level due to the amplitude and phase variations over the aperture resulting from the reflection interaction. Also, with certain lens designs, the reflection from one of the surfaces is normally focused back into the feed, and special means, such as a ferrite isolator or the techniques of Fig. 14-3, are required to reduce the VSWR of the feed.

Methods of Matching Surfaces of Dielectric Lenses. The reflection loss and other deleterious effects of surfaces discussed above may be greatly reduced by surface-matching techniques.[9,10] One method of matching a lens of refractive index n is the
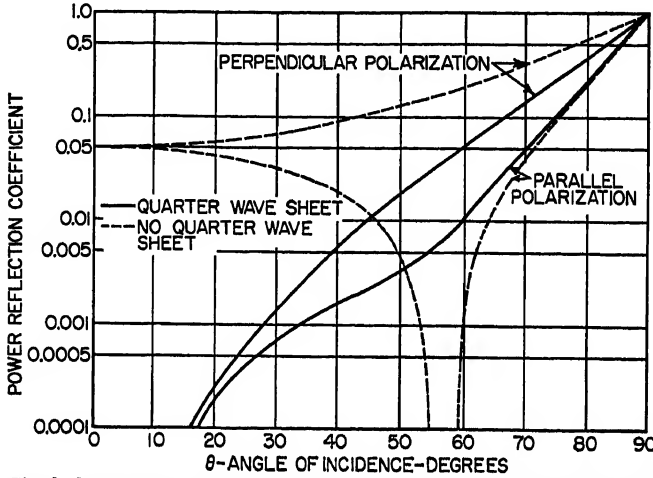
FIG. 14-11. Single-boundary power-reflection coefficient for a dielectric lens of refractive index 1.57 with and without a quarter-wave matching sheet.

same as that used in the optical-wavelength range. This involves the use of a quarter-wave surface layer of dielectric material having a refractive index approximately equal to $\sqrt{n}$.

The reduction in reflection loss obtained by quarter-wave-layer matching at normal incidence is shown as a function of angle in Fig. 14-11 for $n = 1.57$ ($\epsilon_r = 2.47$). A vast improvement is seen to occur at all angles up to at least 50° in both polarizations. If desired, the layer may be designed to favor larger angles, through the use of the following exact formulas for the dielectric constant and thickness of the matching layer as functions of the angle of incidence:

$$ t = \frac{\lambda}{4(\cos \theta_1)^{1/2}(\epsilon_{r_2} - \sin^2 \theta_1)^{1/4}} \tag{14-15} $$

For perpendicular polarization of incidence:

$$ \epsilon_{r_2} = \sin^2 \theta_1 + \cos \theta_1 (\epsilon_{r_2} - \sin^2 \theta_1)^{1/2} \tag{14-16} $$

For parallel polarization of incidence:

$$ \frac{\epsilon_{r_2} - \sin^2 \theta_1}{\epsilon_{r_2}^2} = \frac{\cos \theta_1(\epsilon_{r_2} - \sin^2 \theta_1)^{1/2}}{\epsilon_{r_2}} \tag{14-17} $$

where t is thickness of the layer measured perpendicular to the surface (plotted in Fig. 14-12 for $\epsilon_{r_2} = 2.55$), λ is free-space wavelength, θ_1 is angle between the ray in air and the surface normal, ϵ_{r_2} is relative dielectric constant of lens interior, and ϵ_{r_2} is

relative dielectric constant of surface layer. For incidence nearly normal, Eqs. (14-15) to (14-17) reduce to the well-known formulas $\epsilon_{r_2} = \sqrt{\epsilon_{r_3}}$ and $t = \lambda/(4\sqrt{\epsilon_{r_2}}.)$

Dielectric mixtures, which may also contain air as in foams, can be manufactured to have any desired dielectric constant and may therefore prove suitable for this
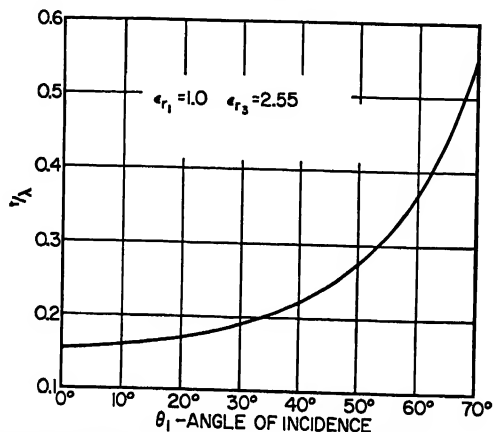
Fig. 14-12. Thickness of quarter-wave matching layer as function of incidence angle for dielectric lens of dielectric constant 2.55.

matching technique. However, the dielectric medium of the lens itself may be used in a *simulated* matching layer. In this case the effect of a quarter-wavelength matching layer is obtained by perturbing the shape of the air-dielectric boundary. Figure 14-13 shows some of the matching configurations that may be used. In each

Fig. 14-13. Simulated quarter-wave matching transformers for lens surface.

case a match may be obtained at a given frequency and angle of incidence by the proper adjustment of the depth of the perturbation and of one other parameter, such as the width of a groove.

Formulas have been obtained for corrugated-surface matching that have proved experimentally to be extremely accurate.[10] Figures 14-14 and 14-15 give design curves for the two orientations of the corrugations with respect to the E-field vector. In both cases perpendicular polarization of incidence is assumed. Although the calculations were made for a lens dielectric constant of 2.55, the curves are relatively insensitive to this quantity and should be quite accurate for dielectric constants from about 2.3 to 2.8. The depth of the corrugations, that is, the thickness of the matching layer, is given by Eq. (14-15), and by Fig. 14-12 for $\epsilon_{r_3} = 2.55$.

The design data in Figs. 14-14 and 14-15 should cover most practical needs. However, if ϵ_{r_3} differs widely from 2.55, accurate values may be solved from the transcendental equations given by Morita and Cohn,[10] or if l/λ is sufficiently small, the following exact formulas for $l/\lambda = 0$ may be used.

Corrugations parallel to E—perpendicular polarization:

$$\frac{d}{l} = \frac{\cos\theta_1\sqrt{\epsilon_{r_2} - \sin^2\theta_1} - \cos^2\theta_1}{\epsilon_{r_2} - 1}$$ (14-18)

Corrugations perpendicular to E—perpendicular polarization:

$$\frac{d}{l} = \frac{\epsilon_{r_2}}{\epsilon_{r_1} - 1}\left[1 - \frac{1}{\sin^2\theta_1 + \cos\theta_1\sqrt{\epsilon_{r_2} - \sin^2\theta_1}}\right]$$ (14-19)

Equation (14-18) is about 3 per cent high and Eq. (14-19) 2.5 per cent high for $2l/\lambda = 0.2$.
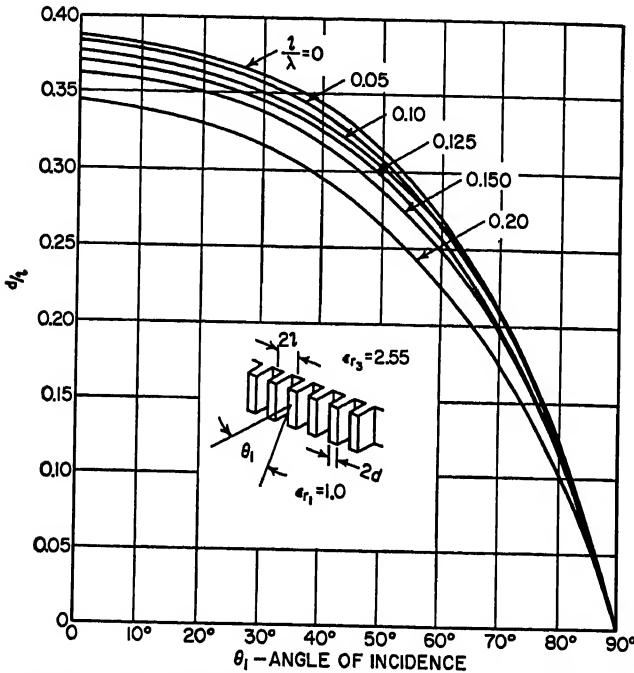
Fig. 14-14. Dielectric-lens matching with corrugations parallel to E field—perpendicular polarization, $\epsilon_{r_3} = 2.55$.

An approximate formula is also given by Morita and Cohn for lens matching by means of an array of cylindrical holes. For perpendicular polarization, and for center-to-center spacing s small

$$\frac{\text{Area of holes}}{\text{Total area}} = \frac{A(\epsilon_{r_2} + 1)(\epsilon_{r_2} - \sin^2\theta_1 - \cos\theta_1\sqrt{\epsilon_{r_2} - \sin^2\theta_1})}{2\epsilon_{r_2}(\epsilon_{r_2} - 1)}$$ (14-20)

where A is a correction factor determined experimentally. For the case of $s/\lambda \approx 0.16$, $\epsilon_{r_2} \approx 2.5$, and $\theta_1 \approx 45°$, A was found to be about 1.15. Similarly, a study of the waffle-iron configuration of Fig. 14-13 indicates that the ratio of dielectric area to total area on the surface is approximately equal to a correction factor B times d/l from Fig. 14-15. For the case of $2l/\lambda \approx 0.35$, $\epsilon_{r_1} \approx 2.5$, and $\theta_1 \approx 45°$, B was found experimentally to equal 0.88.
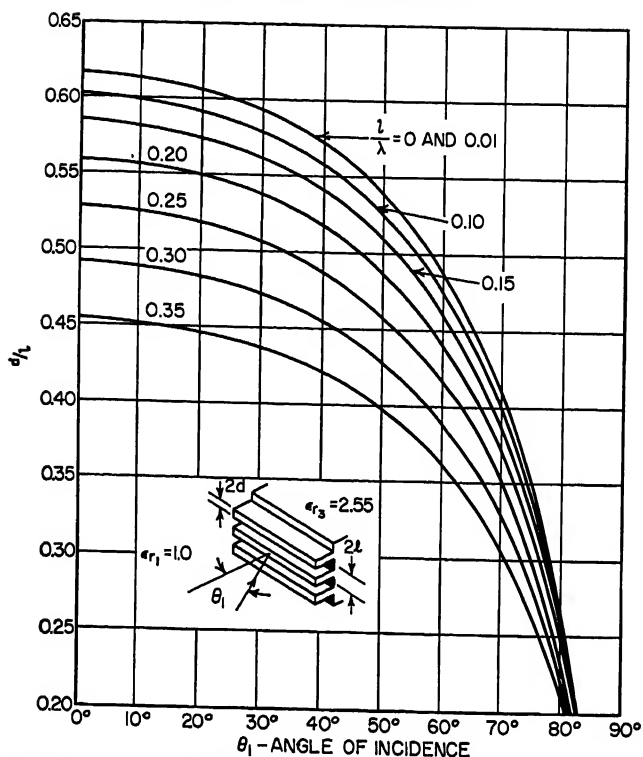
FIG. 14-15. Dielectric-lens matching with corrugations perpendicular to E field — perpendicular polarization, $\epsilon_{r3} = 2.55$.

Numerical lens-matching data for polarization parallel to the plane of incidence are not yet available, although the transcendental equations for corrugated surfaces are given by Morita and Cohn[10] for this case as well as for the perpendicular-incidence
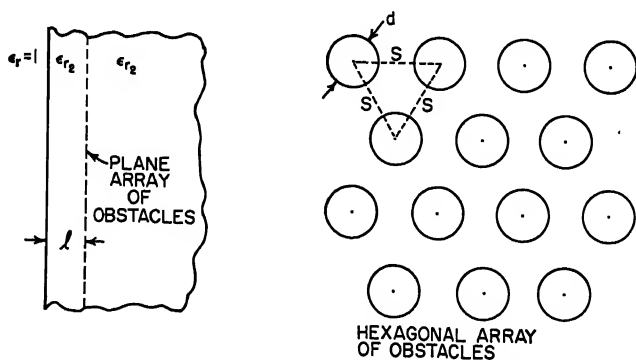
FIG. 14-16. Dielectric-lens matching by means of a plane array of obstacles.

case. However, Fig. 14-11 shows that a design for normal incidence ($\theta_1 = 0$) gives a very good match for parallel polarization out to at least 60°, and therefore such a design should be satisfactory for most purposes.

Another method of matching shown in Fig. 14-16 utilizes discrete conducting obstacles embedded in the dielectric at a prescribed distance from the surface.[9] The reduction of reflection loss that may be obtained with this type of matching is shown in Fig. 14-17 for a polystyrene surface designed for a match at normal incidence. The design formulas for a match at any angle of incidence are as follows:

$$\frac{\ell}{\lambda} = \frac{\phi/360°}{(\epsilon_{r_2} - \sin^2 \theta_1)^{1\!/\!2}} \qquad (14\text{-}21)$$

$$\frac{B}{Y_2} = \cot 2\phi \qquad (14\text{-}22)$$

where ℓ is the spacing of the obstacles from the surface, λ is free-space wavelength, ϵ_{r_2} is the dielectric constant of the lens, B/Y_2 is the normalized shunt susceptance of the
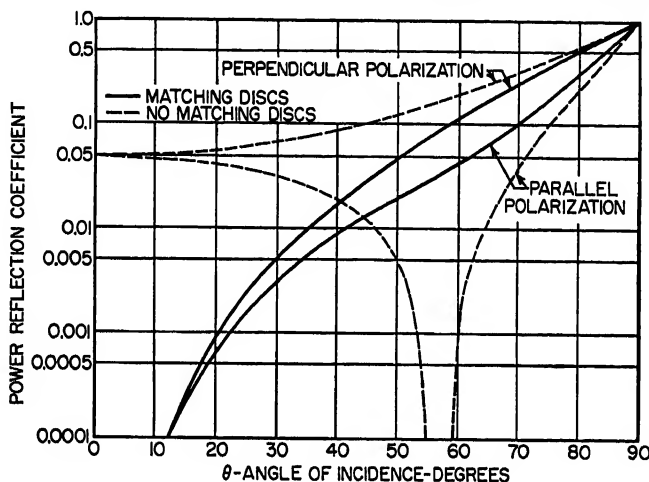
Fig. 14-17. Power-reflection coefficient of a single dielectric boundary with and without matching by a plane array of discrete obstacles—$\epsilon_r = 2.47$.

array of obstacles in the lens dielectric, and ϕ is the electrical distance between the obstacles and the surface (measured in the dielectric). The condition for perfect match gives ϕ as follows for perpendicular polarization:

$$\phi = -\tan^{-1}\left[\frac{(\epsilon_{r_2} - \sin^2 \theta_1)^{1\!/\!4}}{(\cos \theta_1)^{1\!/\!2}}\right] \qquad 90° < \phi < 135° \qquad (14\text{-}23a)$$

and for parallel polarization:

$$\tan^2 \phi = \frac{\epsilon_{r_2} \cos \theta_1}{\sqrt{\epsilon_{r_2} - \sin^2 \theta_1}} \qquad \begin{cases} 90° < \phi < 135° \text{ for } \theta_1 < \tan^{-1}\sqrt{\epsilon_{r_2}} \\ 0 < \phi < 45° \text{ for } \theta_1 > \tan^{-1}\sqrt{\epsilon_{r_2}} \end{cases} \qquad (14\text{-}23b)$$

In computing the matching parameters, ϕ should first be determined from Eq. (14-23a) or (14-23b), and then ℓ/λ and B/Y_2 from Eqs. (14-21) and (14-22). Finally, the dimensions and spacings of the obstacle array must be determined to give the desired value of B/Y_2. Theoretical relationships have been obtained by Jones and Cohn[9] for a hexagonal array of thin circular disks. For the general formulas that apply to the various cases involving discrete obstacles and wire grids, reference should be made to that article. Figure 14-18 shows the dependence of ℓ/λ and d/λ on polarization and angle of incidence for a hexagonal array of disks in a medium of $n = 1.57$, or $\epsilon_r = 2.47$.
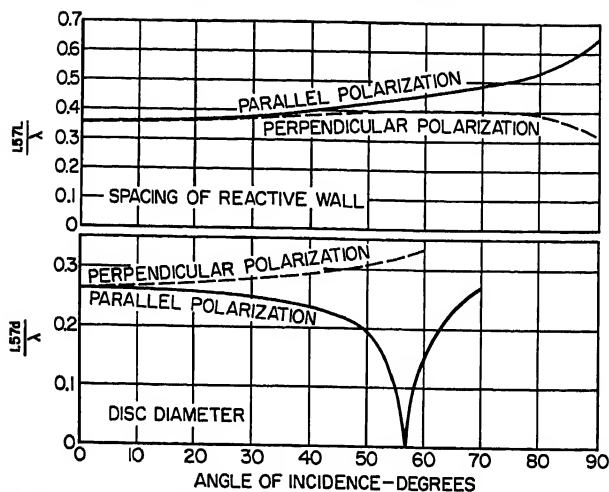
FIG. 14-18. Disk diameter and spacing from surface for a hexagonal array of disks matching a dielectric-lens surface at normal incidence—$\epsilon_r = 2.47$, $s = \lambda/3.14$.
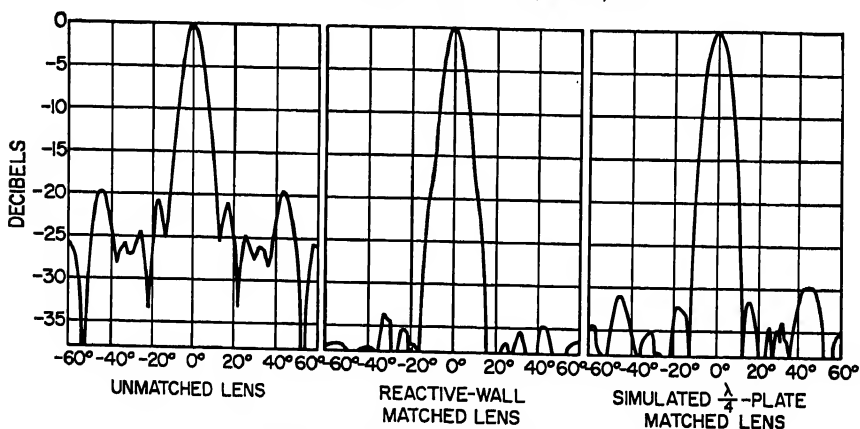
FIG. 14-19. Radiation patterns of unmatched and matched lenses.

Example of Lens Matching. The great improvement in performance that may be obtained when the surfaces of a dielectric lens are matched was demonstrated by measurements on three cylindrical lenses.[11] One of these lenses was unmatched, a second was matched by embedded conducting disks, and the third by corrugations perpendicular to the E-field vector. The radiation pattern of each lens mounted in an H-plane flared horn is shown in Fig. 14-19. The measured side-lobe level, relative gain, and input VSWR of the horn are tabulated for the three lenses:

Lens	Side-lobe level, db	Relative gain, db	VSWR
Unmatched......................	−19.5	0	1.01
Disk-matched....................	−34	+0.4	1.02
Corrugation-matched.............	−30	+0.1	1.055
(Horn alone)....................	......	.....	1.03

The high input VSWR of the unmatched lens is due to reflection from the plane second surface. The high side-lobe level is due to forward scattering of the reflected components by the walls of the horn. The side-lobe energy may be reduced considerably (and the gain somewhat) by providing absorbing material along the narrow walls of the horn or by eliminating these walls entirely so that the reflected energy may scatter in the rearward direction. However, the results with the two matched lenses show that a large reduction in VSWR and side-lobe level may be obtained by matching the surfaces while at the same time a small improvement in gain is achieved.

14.6. ARTIFICIAL DELAY LENSES

A wave-propagating lens medium with velocity less than that of light may be fabricated from metallic or dielectric obstacles arranged in a three-dimensional array.
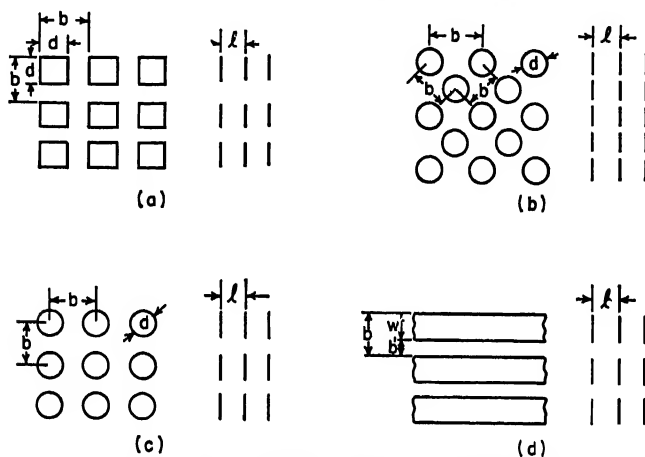
FIG. 14-20. Artificial delay media consisting of arrays of thin square, circular, and long-strip metallic obstacles.

Usually the obstacles are supported by a low-density dielectric foam. In a lens such a medium is capable of behavior identical with that of a natural dielectric, but with the advantage of greatly reduced weight. This advantage makes artificial delay media well suited for use in large lenses. A further advantage of artificial media is that the refractive index may be made to have any desired value over a wide range and may be varied easily throughout the lens. Furthermore, surface matching may be readily incorporated into the design.

The artificial delay lens was first introduced in an article by Kock.[12] A general discussion of the subject is given in the monograph by Brown[2] and in an article by Susskind.[13] Further discussion and a bibliography through 1953 are given by Swift and Higgins.[14] A still more recent bibliography is given by Harvey.[2a]

A number of different types of artificial delay media are available for lens design. Arrays of spheres can be made to behave like an isotropic natural dielectric. Figure 14-20 shows arrays of thin metallic obstacles which are not isotropic but are much lighter and more easily constructed than the sphere arrays. The arrays of square and circular obstacles can be used whenever the field-component vectors E and H are maintained approximately parallel to the plane of the obstacles, while in the case of the metal-strip arrays a further restriction is that H must be parallel to the length of the strips. Thus the thin-obstacle structures are useful only when the direction of wave propagation is closely perpendicular to the obstacle planes. This condition is

met in some of the more important lens-surface designs (for example, those of Fig. 14-2a–c), while in other cases the deviation from perpendicularity may not be serious.

Isotropic Arrays of Metal Spheres. Spherical-obstacle arrays have been treated theoretically by methods analogous to those used for molecular media.[12,15,16] Thus the equivalent dielectric constant ϵ_r is computed in terms of the electric polarization per unit volume induced by the incident electric field, and the equivalent permeability μ_r in terms of the magnetic polarization per unit volume induced by the incident magnetic field. The index of refraction is given in terms of ϵ_r and μ_r by $n = \sqrt{\epsilon_r \mu_r}$.

For a symmetrical three-dimensional array of metal spheres in a supporting medium of $\epsilon_{r_1} > 1$, $\mu_{r_1} = 1$ (e.g., foamed dielectric), the dielectric constant, permeability, and index of refraction are given by

$$\epsilon_r = \epsilon_{r_1} \frac{1 + 2g}{1 - g} \tag{14-24}$$

$$\mu_r = \frac{1 - g}{1 + g/2} \tag{14-25}$$

$$n = \sqrt{\epsilon_{r_1} \frac{1 + 2g}{1 + g/2}} \tag{14-26}$$

where
$$g = \frac{\pi D^3 N}{6} \left[\frac{1}{1 - (3.6 D/\lambda_1)^2} \right] \tag{14-27}$$

D is the diameter of each sphere, N is the number of spheres per unit volume, and $\lambda_1 = \lambda/\sqrt{\epsilon_{r_1}}$ is wavelength in the supporting medium. It will be noted that μ_r is less than unity. This results from the fact that the high-frequency magnetic field cannot penetrate the spheres. When D/λ_1 is less than 0.1, g is almost independent of frequency and n is almost constant. In this case $g = \pi D^3 N/6$ is the fraction of the medium occupied by the spheres, and this quantity is therefore called the *fractional volume*. For D/λ_1, greater than 0.1, these formulas predict a rise in refractive index with increasing frequency. The frequency-dependent factor in Eq. (14-27) takes into account the resonance of each sphere, which is assumed to occur at $D = \lambda_1/3.6$. Although there is theoretical justification for this factor, it is not rigorous, and therefore it is advisable to use Eq. (14-27) with caution above $D/\lambda_1 = 0.2$.

Static measurements made by Kharadly and Jackson[16a] have shown that Eqs. (14-24) and (14-27) (with $\lambda_1 = \infty$) are extremely accurate for a cubical array of spheres for D/b up to 0.80, where b is the center-to-center spacing. At $D/b = 0.85$, the formulas are still only about 2 per cent low. Kharadly and Jackson also give an improved formula, for $b/\lambda_1 \ll 1$, that agrees with their experimental data for D/b up to 0.98.

Isotropic Arrays of Dielectric Spheres. The use of dielectric spheres in an array has advantages over the use of metal spheres.[15,16] The principal advantage is that the magnetic field penetrates the dielectric sphere freely, and hence $\mu_r = 1$ and $n = \sqrt{\epsilon_r}$. Thus a net increase in n usually occurs when dielectric material is substituted for metal, even though ϵ_r is somewhat less with dielectric spheres of the same diameter and spacing. The refractive index for dielectric spheres is

$$n = \sqrt{\epsilon_{r_1} \frac{1 + 2h}{1 - h}} \tag{14-28}$$

where
$$h = \frac{\pi D^3 N}{6} \frac{\epsilon_{r_2} - \epsilon_{r_1}}{\epsilon_{r_2} + 2\epsilon_{r_1}}, \qquad \frac{D}{\lambda_2} < 0.25 \tag{14-29}$$

ϵ_{r_1} is the dielectric constant of the supporting medium and ϵ_{r_2} that of the spheres, D is the diameter of each sphere, N the number of spheres per unit volume, and $\lambda_2 = \lambda/\sqrt{\epsilon_{r_2}}$. For $D/\lambda_2 > 0.25$, Lewin has found theoretically that ϵ_{r_2} in Eq. (14-29) should be replaced in both numerator and denominator by $\epsilon_{r_2}(1 + \theta^2/10) +$

$9\theta^4/700 + \cdots$), where $\theta = \pi D/\lambda_2$ (Refs. 13 and 15). When thus modified, Eqs. (14–28) and (14–29) are believed to be accurate for D/λ_2 up to 0.5. A close experimental check has been made for $D/\lambda_2 = 0.16$ (Ref. 16), and above that figure it is advisable to use the formulas with caution.

Voids in a Solid Dielectric. Equations (14–28) and (14–29) also apply to the case of an array of spherical voids in a solid-dielectric medium. In this case, ϵ_{r_2} is set equal to unity while ϵ_{r_1} is the dielectric constant of the solid medium surrounding the voids.

The same equations have also been used with good engineering accuracy for voids of cylindrical shape.[17,17a] In this case, holes were drilled in dielectric plates that were then stacked to form the lens. The holes in adjacent plates were nonaxial, and therefore the cylinders had a length equal to the thickness of the plate and approximately equal to their diameters. In using Eqs. (14–28) and (14–29), the quantity $\pi D^3 N/6$ was replaced by the actual fractional volume of the voids with respect to the total volume.

Equivalent-molecular-medium Analysis for Arrays of Thin Obstacles. The original method used for computing the refractive index of arrays of thin obstacles utilizes the analogy to a molecular medium.[12] For obstacles much smaller than their spacings, and for spacings much smaller than the wavelength, the following formulas hold for the equivalent dielectric constant, permeability, and refractive index of a three-dimensional array of parallel thin obstacles:

$$\epsilon_r = \epsilon_{r1}\left(1 + \frac{\alpha_e N}{\epsilon_1}\right) \tag{14-29a}$$

$$\mu_r = \mu_{r1}\left(1 + \frac{\alpha_m N}{\mu_1}\right) \tag{14-29b}$$

$$n = \sqrt{\epsilon_r \mu_r} \tag{14-29c}$$

where ϵ_{r_1} and μ_{r_1} are relative constants of the medium embedding the obstacles (μ_{r_1} usually $= 1$), α_e and α_m are, respectively, the electric and magnetic polarizabilities of an isolated obstacle for the particular orientation of the impressed electric or magnetic field (assumed to be parallel to an axis of symmetry of the obstacle), N is the number of obstacles per unit volume, and ϵ_1 and μ_1 are the absolute constants of the embedding medium. Note that if the magnetic field is parallel to the obstacles, this field is undisturbed, and $\mu_r = \mu_{r_1}$ (usually $= 1$). In this case

$$n = \sqrt{\epsilon_r} \tag{14-29d}$$

A chart giving α_e/ϵ_1 and α_m/μ_1 for many obstacle shapes with various field orientations appears in Fig. 14–21.[18,18a] Note that in two-dimensional arrays of strips, rods, etc., N in Eqs. (14–29a) and (14–29b) represents the number of obstacles per unit area in a cross section perpendicular to the long axes of the obstacles.

It is seen from the above equations and Fig. 14-21 that ϵ_r and μ_r depend upon the E- and H-field directions. If these directions are not parallel to axes of symmetry of the medium, tensor expressions for ϵ_r and μ_r are required in analysis, and birefringent (double-refractive) effects will occur.[18b]

Equation (14–29a) has been found to hold quite accurately for obstacle dimensions up to about six-tenths of the center-to-center spacings. For symmetrical arrays of metal spheres, the Clausius-Mosotti modification [Eqs. (14–24) and (14–25)] gives good results for much closer spacing. In the case of a tetragonal array of very thin obstacles, with E in the plane of the obstacles, the following formula due to Brown and Jackson[18c] gives excellent results for the dielectric constant for $\ell/b \geq 0.6$ and $b/\lambda_1 \leq 0.1$.

$$\epsilon_r = \epsilon_{r1}\left(1 + \frac{\alpha_e N/\epsilon_1}{1 - 0.360\alpha_e/b^3\epsilon_1}\right) \tag{14-29e}$$

OBSTACLE SHAPE	ELECTRIC POLARIZABILITY	MAGNETIC POLARIZABILITY
THIN CIRCULAR DISKS	$\dfrac{a_e}{\epsilon_1} = \dfrac{2d^3}{3}$	$\dfrac{a_m}{\mu_1} = \dfrac{d^3}{3}$
THIN ELLIPSES	$\dfrac{a_e}{\epsilon_1} = \dfrac{4\pi ab^2 k^2}{3(1-k^2)[F(k)-E(k)]}$ $\dfrac{a_e}{\epsilon_1} = \dfrac{4\pi ab^2 k^2}{3[E(k)-(1-k^2)F(k)]}$	$\dfrac{a_m}{\mu_1} = \dfrac{4\pi ab^2}{3E(k)}$
THIN SQUARES	$\dfrac{a_e}{\epsilon_1} = 1.032 d^3$	$\dfrac{a_m}{\mu_1} = 0.455 d^3$
THIN RECTANGLES	$\dfrac{a_e}{\epsilon_1} = \dfrac{\pi w^2 \ell}{4}$	$\dfrac{a_m}{\mu_1} = \dfrac{\pi w^2 \ell}{4}$
THIN INFINITE STRIPS	$\dfrac{a_e}{\epsilon_1} = \dfrac{\pi w^2}{4}$ SEE TEXT	$\dfrac{a_m}{\mu_1} = \dfrac{\pi w^2}{4}$
CIRCULAR CYLINDERS	$\dfrac{a_e}{\epsilon_1} = 2\pi a^2$ SEE TEXT	$\dfrac{a_m}{\mu_1} = 2\pi a^2$ $\dfrac{a_m}{\mu_1} = \pi a^2$ SEE TEXT
SPHERES	$\dfrac{a_e}{\epsilon_1} = 4\pi a^3$	$\dfrac{a_m}{\mu_1} = 2\pi a^3$
MODERATELY THICK OBSTACLES		$\dfrac{a_m}{\mu_1} = \tau$

FIG. 14-21. Electric and magnetic polarizabilities for obstacles of various shapes and for various field orientations. $F(k)$ and $E(k)$ are complete elliptic integrals, $k = \sqrt{1 - (b/a)^2}$, τ is the volume occupied by an obstacle.

Comparisons with experimental data show the formula to be about $1\frac{1}{2}$ per cent low for $d/b = 0.833$ in the case of disks and about $2\frac{1}{2}$ per cent low for $d/b = 0.85$ in the case of squares. The formula presumably holds for thin obstacles of other shapes (e.g., elliptical) in tetragonal arrays, but this fact has not been tested experimentally.

Other formulas for the equivalent dielectric constant of obstacle arrays are available. Brown and Jackson[18c] give a formula that compares very well with experiment in the case of tetragonal arrays of thin disks for $\ell/b \leq 0.6$. Kharadly and Jackson[16a] give modifications of Eq. (14-29a) that give excellent results compared with their experimental data for square arrays of cylinders of diameter up to 0.98 times the center-to-center spacings and for square arrays ($\ell/b = 1$) of strips for w/b up to 0.7.

Equivalent-transmission-line Method. Although the molecular-medium method can be extended into the range $b/\lambda_1 > 0.1$ through the use of correction terms,[12] generally better results may be obtained by the equivalent-transmission-line method.[19-21] The way this method is applied is illustrated by Fig. 14-22, which shows a number of
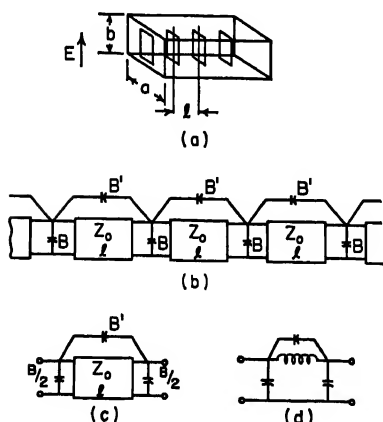
FIG. 14-22. Equivalent circuit of obstacles in a parallel-plane line.

conducting obstacles in a parallel-plane transmission line. That each obstacle represents an infinite planar array of obstacles is easily seen by considering the images of the obstacle in the horizontal electric walls and vertical magnetic walls of the parallel-plane line. Hence the phase velocity and refractive index of a TEM wave traveling in the transmission line are identical with the same quantities in the equivalent infinite array of obstacles. A circuit representing the transmission line loaded with obstacles is given in Fig. 14-22b. The susceptance B represents the shunt susceptance of a single obstacle in the transmission line, while the bridging susceptance B' represents an effect of close proximity of successive obstacles in the line. A single section of the periodic circuit is shown in Fig. 14-22c, and its lumped-constant equivalent in d.

The normalized shunt susceptance B/Y_0 (where Y_0 is the characteristic admittance of the parallel-plane line) is the most important quantity in the equivalent circuit of Fig. 14-22. The bridging normalized susceptance B'/Y_0 vanishes for all practical purposes when ℓ/b is greater than 0.75. Even for smaller ℓ/b, B'/Y_0 has negligible effect for $b/\lambda_1 < 0.2$ (λ_1 is wavelength in the supporting medium). Values of B'/Y_0 have been computed only in the case of the metal-strip medium, which will be considered separately. Formulas for refractive index and image admittance (effective characteristic admittance) of the medium are as follows, with B' omitted from the circuit:

$$n = \frac{\sqrt{\epsilon_{r1}}}{\phi} \cos^{-1} \left(\cos \phi - \frac{B}{2Y_0} \sin \phi \right) \tag{14-30}$$

$$y_I = \sqrt{\epsilon_{r1}} \left[1 + \frac{B}{Y_0} \cot \phi - \left(\frac{B}{2Y_0} \right)^2 \right]^{1/2} \tag{14-31}$$

where λ is free-space wavelength, $\lambda_1 = \lambda/\sqrt{\epsilon_{r1}}$ is wavelength in the embedding dielectric (such as dielectric foam), ϵ_{r1} is the dielectric constant of the embedding dielectric, ℓ is spacing of the obstacles in the line, $\phi = 360°\ell/\lambda_1$ is electrical line length between obstacles, and y_I is the image admittance of the medium normalized with respect to the characteristic admittance of free space. The image admittance is evaluated in the plane of the obstacles at the surface of the medium. The following low-frequency forms of Eqs. (14-30) and (14-31) are accurate up to about $b/\lambda_1 = 0.1$.

$$n = \sqrt{\epsilon_{r1}} \left(1 + \frac{B}{Y_0} \frac{\lambda_1}{2\pi\ell} \right)^{1/2} \tag{14-32}$$

$$y_I = n \tag{14-33}$$

Metal-strip Medium. In the case of the medium of Fig. 14-20d composed of very thin metal strips, the following formula gives B/Y_0 for use in Eqs. (14-30) to (14-32):

$$\frac{B}{Y_0} = \frac{4b}{\lambda_1} \log_e \csc \frac{\pi b'}{2b} \qquad \frac{b}{\lambda_1} < 0.2, \frac{\ell}{b} > 0.75 \tag{14-34}$$

If $b/\lambda_1 > 0.2$, with $\ell/b > 0.75$, a graph of B/Y_0 given by Marcuvitz[22] may be used.

However, in a practical metal-strip medium it is usually desirable to violate both of the conditions specified for Eq. (14-34). The formulas given by Cohn[19] cover all values of b/λ_1 and ℓ/b and include the full effect of both B and B' in the equivalent circuit of Fig. 14-22. Because the formulas do not lend themselves to ready computation, they are not included here, but a set of values of n and y_1 computed from these formulas are given in Table 14-1. Experimental measurements of refractive index have been made on five different test samples for ℓ/b ranging from $3/4\pi$ to $3/2\pi$, w/b from 0.5 to 0.7, and b/λ_1 from 0.1 to 0.5 (Ref. 23). The maximum discrepancy between the theoretical and experimental values in the complete set of measured refractive-index points was only 2.2 per cent, and in most cases the agreement was much better.

Other formulas for the metal-strip medium have been derived by Kock,[12] Kharadly and Jackson,[16a] Sharpless,[24] and Howes and Whitehead.[25]

Medium Containing Thin Metallic Square and Circular Obstacles. The arrays of Fig. 14-20a–c are the most suitable for cases in which the field vectors E and H are confined to a plane parallel to the obstacles but whose orientations are not fixed in that plane. Precise static values of the quantity $B\lambda_1/Y_0b$ have been measured by an electrolytic-tank technique as a function of d/b and ℓ/b This experimental method takes exact account of all proximity effects.[21] The data are listed in Table 14-2 for the cases of Fig. 14-20a–c.

Table 14-1. Refractive-index and Image-admittance Values for the Metal-strip Delay Medium

ℓ/b	b/λ	$\frac{w}{b} = 0.5$		$\frac{w}{b} = 0.6$		$\frac{w}{b} = 0.7$	
		n	y_I	n	y_I	n	y_I
$3/4\pi$	0	1.237	1.237	1.361	1.361	1.536	1.536
	0.3	1.280	1.182	1.432	1.270	1.646	1.388
	0.4	1.322	1.125	1.505	1.175	1.770	1.233
	0.5	1.405	1.036	1.657	1.017	2.055	0.9518
$1/\pi$	0	1.225	1.225	1.337	1.337	1.490	1.490
	0.3	1.263	1.164	1.399	1.236	1.583	1.325
	0.4	1.301	1.103	1.465	1.133	1.697	1.152
	0.5	1.370	0.9971	1.603	0.9454	1.947	0.8115
$3/2\pi$	0	1.188	1.188	1.279	1.279	1.400	1.400
	0.3	1.216	1.108	1.325	1.148	1.475	1.187
	0.4	1.243	1.028	1.376	1.003	1.567	0.9402
	0.5	1.299	0.8669	1.488	0.7109	1.924	0.2195
$2/\pi$	0	1.154	1.154	1.229	1.229	1.328	1.328
	0.3	1.176	1.048	1.267	1.056	1.394	1.047
	0.4	1.200	0.9229	1.316	0.8385	1.504	0.0490
	0.5	1.253	0.6155	*	*	*	*

* Imaginary values.

These values may be used for b/λ_1 up to about 0.25, where resonance effect begins to make $B\lambda_1/Y_0b$ increase above its static value. With the aid of these values and Eq. (14-30) or (14-32), accurate values of refractive index may be computed (subject to the restrictions of the equations) for the arrays of thin obstacles to which the $B\lambda_1/Y_0b$ values apply. Graphs of refractive index versus d/b and ℓ/b for the three cases were computed from Eq. (14-32) and are given by Cohn.[21] Static values of $\epsilon_r (= n^2)$ have been obtained by another experimental method by Kharadly and Jackson for arrays of strips, cylinders, and disks.[16a] The agreement with Cohn's theoretical results for strips and experimental results for disks is generally very good.

In practical lens media it is frequently desirable to make $b/\lambda_1 > 0.2$ and $\ell/b < 0.75$, which exceeds the range of validity of Eq. (14-30). Measured high-frequency refractive-index data have been presented by Cohn to cover these ranges.[26] He gives separate graphs of refractive index versus b/λ_1 and d/b for ℓ/b spacings of 0.25, 0.35, and 0.5, for both square obstacles (Fig. 14-20a) and circular obstacles with hexagonal distribution (Fig. 14-20b). One of these graphs is reproduced in Fig. 14-23. When using these data, it is important to note that the obstacles in the test samples con-

sisted of 0.001-in.-thick silver which had been silk-screened on 0.005-in.-thick polystyrene sheets, these sheets being separated by polystyrene-foam spacers. The dielectric constant of the foam was 1.03. The center-to-center spacing b was 0.950 in. Appreciable differences in refractive index will occur for different constructions. A simple procedure is given by Cohn which takes account of changes in dielectric constant, changes of sheet thickness, etc.[26] Although this correction technique is an approximate one, it has given excellent results in several applications where the

Table 14-2. Values of $B\lambda_1/Y_0 b$ for Thin Square and Circular Obstacles

d/b	$\ell/b = 0.25$	$\ell/b = 0.35$	$\ell/b = 0.50$	$\ell/b = 0.65$	$\ell/b \geq 0.75$
		(a) Square obstacles			
0.50	0.648	0.768	0.830	0.855	0.859
0.60	1.16	1.35	1.475	1.54	1.56
0.70	1.95	2.25	2.45	2.53	2.57
0.75	2.48	2.87	3.11	3.21	3.25
0.80	3.18	3.62	3.97	4.13	4.18
0.85	4.25	4.78	5.15	5.32	5.37
		(b) Circular obstacles, square distribution			
					$\ell/b > 0.8$
0.60	0.68	0.81	0.93	0.97	0.98
0.70	1.13	1.34	1.51	1.58	1.60
0.75	1.45	1.71	1.91	1.98	2.01
0.80	1.85	2.17	2.40	2.50	2.54
0.85	2.35	2.72	3.00	3.11	3.17
		(c) Circular obstacles, hexagonal distribution			
				$\ell/b \geq 0.65$	
0.50	0.525	0.595	0.630	0.635	
0.60	0.915	1.025	1.095	1.100	
0.70	1.48	1.69	1.82	1.86	
0.75	1.89	2.13	2.31	2.38	
0.80	2.39	2.71	2.96	3.03	
0.85	3.09	3.50	3.78	3.87	

obstacles were applied directly to the dielectric-foam separators and where the dielectric constant of the foam ranged from 1.06 to 1.19.

Methods of Matching Artificial Delay Lenses. In the case of thin-obstacle arrays where H is parallel to the plane of the obstacles, and also in the case of thick dielectric obstacles such as dielectric spheres, the low-frequency image admittance (or characteristic admittance) of the medium is equal to the refractive index. This is typified by the data of Table 14-1 for the metal-strip medium. Thus Eq. (14-13) applies to these types of media. In the case of a metal-sphere array, the low-frequency image admittance is equal to $\sqrt{\epsilon_r/\mu_r}$, which is always greater than n, and hence results in an even larger surface reflection.

At $b/\lambda_1 > 0.1$, the problem of surface reflection is more complex. With reference to Fig. 14-22, the image admittance is best defined in the plane of the obstacles. It is seen from the figure that the surface obstacles should have one-half the shunt susceptance of the internal obstacles if a discontinuity susceptance at the surface plane is to be avoided. Thus the surface obstacles must be of smaller size than the internal

obstacles. If the surface obstacles are made the same size as the internal obstacles, the discontinuity susceptance included at the junction of air and the delay medium invariably increases the reflection.

Equation (14-31) and Table 14-1 both show that y_I decreases more and more rapidly with increasing frequency until it reaches zero at the cutoff frequency of the medium. Since y_I is in all cases greater than unity at $b/\lambda_1 = 0$, it is necessarily
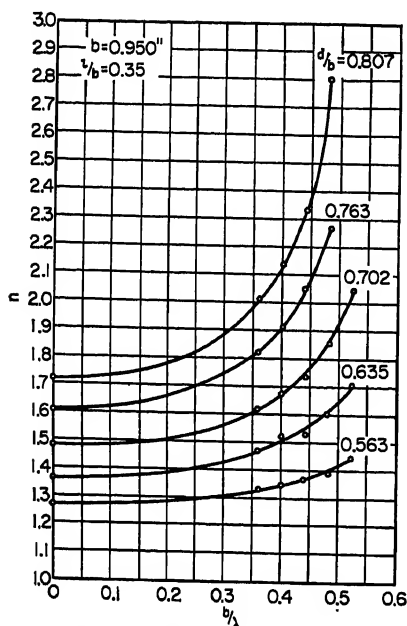
FIG. 14-23. Index of refraction of thin square obstacles on 0.005-in. polystyrene sheets spaced by polyfoam, $l/b = 0.35$
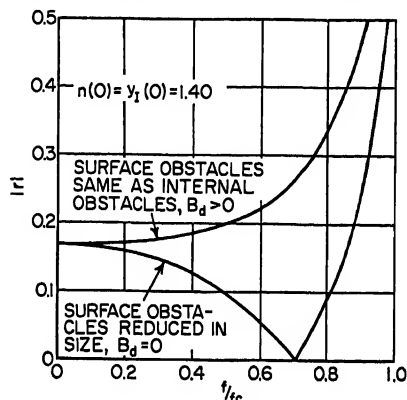
FIG. 14-24. Voltage-reflection coefficient at a single boundary of an artificial delay medium with and without a discontinuity susceptance. f_c is the cutoff frequency of the medium.

equal to unity at some particular value of b/λ_1, generally between 0.3 and 0.5. At this value of b/λ_1, a perfect surface match may therefore be obtained.[19] This is indicated by Fig. 14-24, which shows the voltage reflection coefficient vs. frequency for two cases: one where the surface discontinuity susceptance is reduced to zero through modification of the surface obstacles; the other for surface obstacles equal to the internal obstacles. The improvement due to the surface modification is clearly apparent, even when the lens medium is not used near the frequency of perfect match.

A close approximation to the ideal case of zero discontinuity susceptance may be achieved by choosing the size of the surface obstacles to conform to the following relationship:

$$[B(\ell/b) + B(\infty)]_{\text{surface obstacle}} = [B(\ell/b)]_{\text{internal obstacle}}$$

(14-35)

$$\frac{B_m}{Y_0} = \cot 2\phi_m, \quad \ell_m = \frac{\phi_m \lambda}{360°}$$

$$\phi_m = \tan^{-1}\left(\frac{1}{y_I}\right)^{1/2}$$
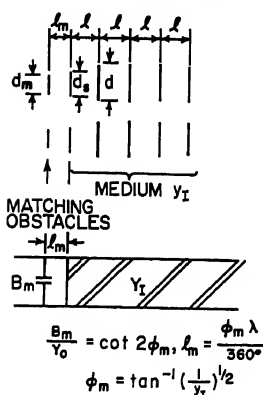
FIG. 14-25. The use of additional obstacles to match the surface of an array of obstacles.

The susceptance $B(\ell/b)$ applies to the ℓ/b of the lens, while $B(\infty)$ is the limiting value for ℓ/b large. These susceptances may be obtained from Table 14-2, for a number of different cases. It has been found in all cases, including the metal-strip case, that a

reduction in dimension (d or w) of the surface obstacles to 0.75 times the dimension of the internal obstacles yields a good match.

Although the above method of matching is simple, it limits the choice of b/λ_1 for the medium. Another method that would be applicable for any value of b/λ_1 is shown in Fig. 14-25. A plane array of obstacles of dimension d_m is placed at distance ℓ_m from the surface of the lens medium. The equivalent circuit of the figure applies if the obstacle dimension d_s is made less than d as described above to eliminate the discontinuity shunt susceptance at that point. Formulas in the figure give the spacing ℓ_m and the normalized suscep-tance B_m/Y_0. The latter may be ob-tained from Eq. (14-34) for metal strips and from Table 14-2 for thin square or circular obstacles.

Construction Methods for Artificial Delay Lenses. The most practical methods of construction have utilized low-dielectric-constant foam support for the obstacles. For example, Fig. 14-26

FIG. 14-26. Method of supporting an array of spherical obstacles in a dielectric-foam medium.

shows how spherical obstacles may be supported by layers of dielectric foam. Alter-nate layers contain cylindrical holes in the desired array pattern, and the obstacles are set into these holes. Other layers without holes hold the spheres in place and maintain the proper vertical spacing.

A method of construction suitable for metal-strip lenses is shown in Fig. 14-27. A lens of this type was designed by Kock for use in microwave relay systems.[12] As shown in the figure, the individual strips are cut to lengths that provide the correct
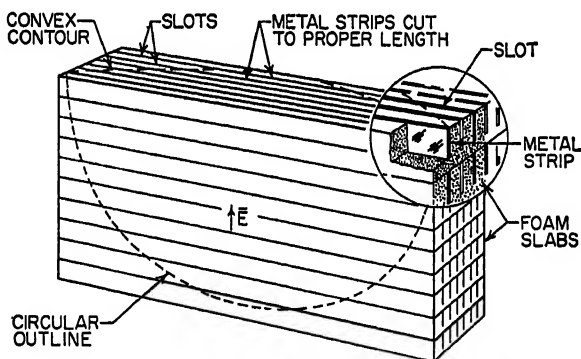
FIG. 14-27. Construction of a metal-strip delay lens.

convex contour for focusing the wave. The strips are inserted into slots cut in dielectric-foam slabs, and the slabs are then stacked within a supporting frame to form the complete lens.

Another construction technique that is suitable for any type of thin obstacle utilizes obstacles that consist of conducting paint that is silk-screened, or sprayed through a stencil, onto the surface of dielectric-foam spacers. Particularly good results have been obtained with the silk-screening technique using Dupont No. 4929 high-con-ductivity silver paint. The foam should be made with either a very fine grain or with a smooth skin on the surface. The latter is easily obtained by foaming the spacers between flat plates. An alternative method is to silk-screen the obstacles on thin dielectric sheets, such as 0.005-in. polystyrene, and to space these by dielectric-

foam layers. The lens assembly may be cemented together to form a light, strong mass containing the lens.

14.7. PATH-LENGTH LENS MEDIUM

Another type of artificial delay medium, which is also due to Kock, is called the path-length medium.[27] As illustrated by Fig. 14-28, an effective retardation of phase velocity in the lens medium is obtained by constraining the wave to follow a serpentine
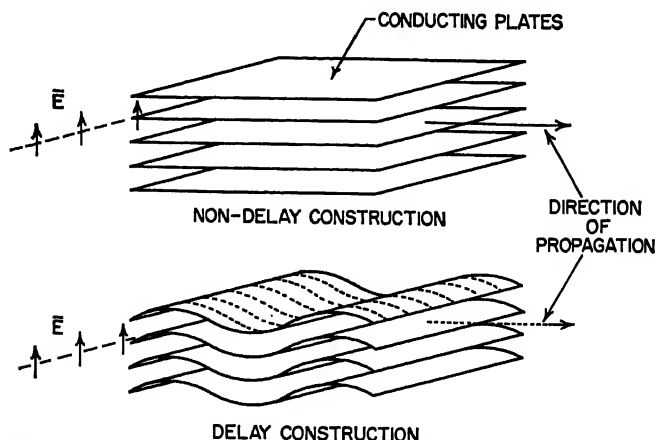
FIG. 14-28. Use of conducting plates or grids (shown dotted) to effect a wave delay.

path. This is shown clearly in the example of Fig. 14-29, where a hyperboloidal lens is formed of flat plates slanted with respect to the lens axis. Examination shows that the effective refractive index of the lens is related to the slant angle θ by

$$n = \frac{1}{\cos \theta} \qquad (14\text{-}30)$$

Closely spaced wire grids may also be used to force the wave in the medium to follow an elongated path.

Path-length lenses have the advantage over other artificial lens media that the refractive index is independent of frequency and may therefore be used over very broad bandwidths, subject only to the condition that the plate or wire spacing be less than a half wavelength. They also have the advantages of much wider tolerances and fewer parts. However, they possess a number of disadvantages which must be evaluated carefully in any application. For example, the electric field must be polarized parallel to the plane of constraint. Also, in the case of slant-plate construction, the aperture illumination is distorted in the plane of constraint and scanning in this plane affects the focusing of the beam.

Another example of the path-length principal is in the design of line sources. Here a parallel-conducting-sheet region is shaped so that a cylindrical TEM wave emerging radially from a source is changed into a plane wave at the linear aperture. By Fermat's principle the ray paths are geodesics of the mean surface between the conducting sheets. One example of this type of construction is the double-layer pillbox. Another is a geodesic analogue of the Luneberg Lens. These are described in more detail in Chap. 15.
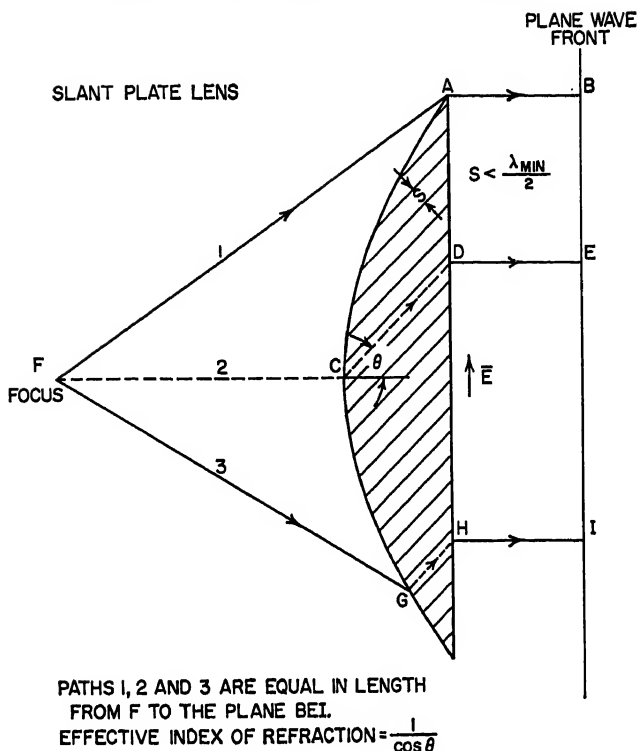
FIG. 14-29. Slant-plate path-length lens.

Figure labels:

PLANE WAVE FRONT

SLANT PLATE LENS

$S < \dfrac{\lambda_{MIN}}{2}$

A B

D E

θ

F
FOCUS

C

$\bar{E}$

H I

G

PATHS 1, 2 AND 3 ARE EQUAL IN LENGTH
FROM F TO THE PLANE BEI.
EFFECTIVE INDEX OF REFRACTION $= \dfrac{1}{\cos\theta}$

14.8. METAL-PLATE WAVEGUIDE LENSES

In the metal-plate waveguide medium, the phase velocity exceeds that of free space, and hence the index of refraction is less than 1 (Ref. 28). Thus if the plate surfaces are spaced a apart (Fig. 14-30), the refractive index is given by

$$n = \sqrt{1 - \left(\frac{\lambda}{2a}\right)^2} \qquad (14\text{-}37)$$

The metal-plate waveguide medium operates in the fundamental TE mode of wave propagation, which requires the electric-field vector to be parallel to the plates, as shown in Fig. 14-30. When a single set of parallel plates is used as in this figure, it is necessary to avoid a wave with an electric-field component perpendicular to the plates, since this would excite a TEM mode propagating between the plates with the velocity of light. The energy in the TEM mode would not be focused, and the over-all result would be a loss of gain and increased minor lobes. However, if two mutually perpendicular sets of parallel plates are used so as to form channels of square cross section in the direction of desired propagation (egg-crate construction), the phase velocity and index of refraction will be the same for any incident polarization.

Constrained Refraction. An important difference between metal-plate and ordinary dielectric media is the constraint in wave direction caused by the plates. This is illustrated by Fig. 14-30, where it is seen that in the H plane the rays in the medium must always be parallel to the plates, irrespective of the angle of incidence; that is,
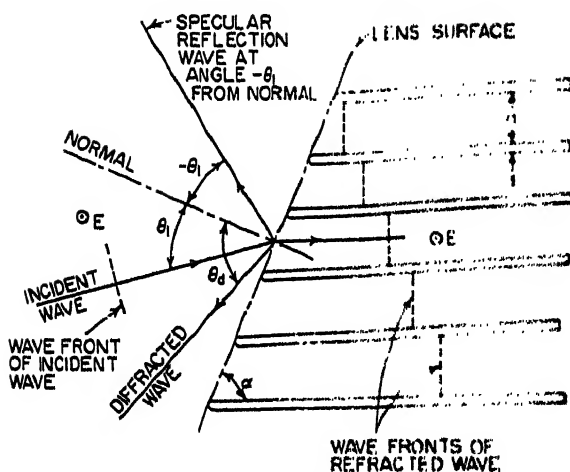
Fig. 14-30. Constrained refraction in H plane.

UNCONSTRAINED REFRACTION
(a)

CONSTRAINED REFRACTION
(b)
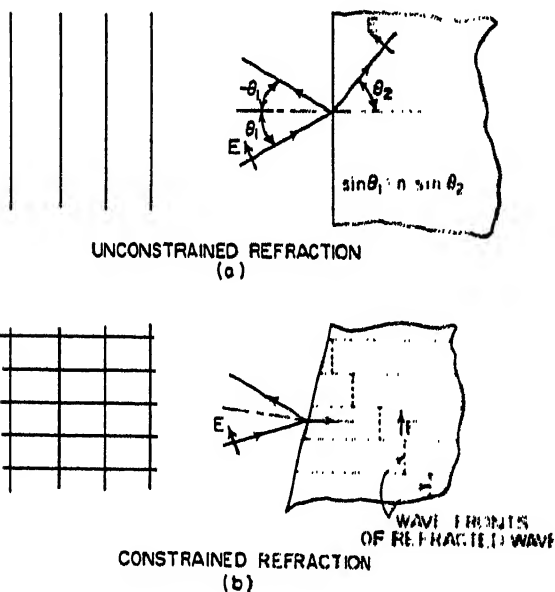
Fig. 14-31. Unconstrained and constrained refraction in E plane.

Snell's law of refraction does not hold. However, Fig. 14-31a shows that in the E plane, a single set of plates offers no constraint, and hence the ray angles obey Snell's law. If egg-crate construction is used, as in Fig. 14-31b, constraint occurs in the E plane as well as in the H plane, and rays are necessarily directed parallel to the channels.

Whether or not constraint is an important consideration depends upon the shape of the lens. The shape designs given in Fig. 14-5a and b are such that Snell's-law refraction will direct the rays in the medium parallel to the lens axis. Therefore, if the plates are parallel to the axis, as will usually be the case, constraint will have no

effect. In the shape designs sketched in Fig. 14-5c and d, constraint is purposely used to achieve wide-angle-scan performance unattainable with nonconstrained media.[6] One important point to notice is that in rotational lenses other than those of Fig. 14-5a and b, constraint must be provided in both the E and H plane (by egg-crate construction). If constraint were offered only in the H plane, the lens cross section would have to be different in the two planes to obtain focusing.

Limitations on Plate Spacing. A basic limitation on the choice of plate separation a results from the fact that the medium must operate between the cutoff frequencies of the fundamental and next higher TE modes. This requires that

$$0.5 < \frac{a\sqrt{\epsilon_r}}{\lambda} < 1.0 \qquad (14\text{-}38)$$

where ϵ_r is the relative dielectric constant of the material between the plates. This is usually air, and hence ϵ_r is usually equal to unity. For air dielectric, this range of a/λ corresponds to a range in refractive index of

$$0 < n < 0.866 \qquad (14\text{-}39)$$

However, a further restriction on plate spacing must be imposed if the existence of diffracted waves due to grating effect is to be avoided. It will be shown later how such diffracted waves cause considerable loss of transmitted power, distortion of the aperture illumination function, and consequent loss of gain and increase of minor lobes. The presence of one diffracted wave is shown in Fig. 14-30. This occurs in the direction in which the diffracted waves from the individual plate edges combine in phase. It can only occur when the plate spacing exceeds a particular value and will be avoided if the following condition is met:

FIG. 14-32. Limiting angle of incidence for pure specular reflection vs. plate spacing.

$$\frac{\lambda \sin \alpha}{a + t} - 1 > |\sin \theta_1| \qquad (14\text{-}40)$$

where the various symbols are as defined in Fig. 14-30. The limiting value of this formula is shown graphically in Fig. 14-32, where the angle θ_1 of the ray in free space is plotted versus $(a + t)/\lambda$ for different values of α from 30 to 90°. For each particular value of α the region to the lower left of the curve gives the ranges of θ_1 and $(a + t)/\lambda$ in which diffracted waves are avoided. Equation (14-40) is also the condition for avoiding a diffracted wave when the incident wave is in the metal-plate region, and the transmitted ray emerges at angle θ_1.

Reflection and Transmission at an Interface. For the case of E parallel to the plane of incidence and parallel to the plates (Fig. 14-31a) the power-reflection coefficient is (Ref. 2, p. 58)

$$|r|^2 = \frac{\sin^2(\theta_1 - \theta_2)}{\sin^2(\theta_1 + \theta_2)} \qquad (14\text{-}41)$$

where θ_1 is the ray angle in free space and θ_2 the ray angle in the parallel-plate medium, both angles measured from the normal to the surface. The plates are assumed to be very thin*. Figure 14-31a shows the case of a wave incident from free space, but Eq. (14-41) also holds for a wave incident from the metal-plate region. The reflected
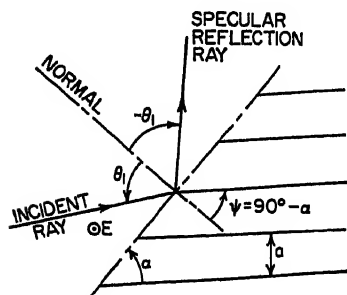
FIG. 14-33. Boundary of H-plane array of very thin metal plates.

ray is then within the metal-plate region at angle $-\theta_2$. It is of interest to note that Eq. (14-41) is the same formula as in the case of a solid dielectric with E perpendicular to the plane of incidence (Eq. 14-11). Equation (14-41) and Snell's law of refraction hold for all angles of incidence [if $0.5 < (a + t)/\lambda < 1.0$], and diffracted waves do not occur. However, this is not true of parallel polarization of incidence on a constrained medium (Fig. 14-31b), and a solution for that case is not available.

Considerable published information is available for the case of E perpendicular to the plane of incidence and parallel to the edges of a set of very thin plates (Fig. 14-33).* The basic analysis is due to Carlson and Heins,[30] while further theoretical work was done by Lengyel,[31] Berz,[32] and Whitehead.[33] In the range of θ_1 free of diffracted waves, as given by Eq. (14-40) and Fig. 14-32, the
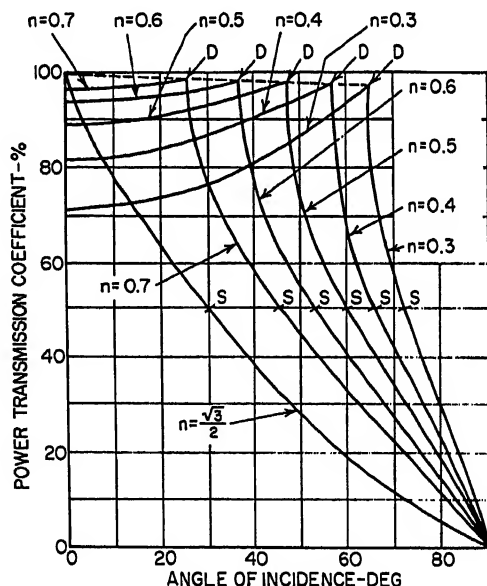
FIG. 14-34. Relative power transmitted into metal-plate medium, $\psi = 0$.

power-reflection coefficient for a wave incident on an array of plates is

$$|r|^2 = \left[\frac{\cos (\theta_1 + \psi) - n}{\cos (\theta_1 + \psi) + n} \right] \left| \frac{\cos (\theta_1 - \psi) - n}{\cos (\theta_1 - \psi) + n} \right| \tag{14-42}$$

where θ_1 is the ray angle in free space, ψ is the angle between the normal to the boundary and the plates, and n is the refractive index given by Eq. (14-37). The specularly

* Arrays of thick plates have been treated by Primich[20] for $\theta_1 = 0$ and $\psi = 0$.

reflected wave propagates at angle $-\theta_1$. Because of reciprocity, this formula also applies to waves in the plate region incident upon the free-space boundary, where the waves between the plates are phased to produce a transmitted wave propagating at angle θ_1 to the normal. For normal incidence and $\psi = 0$, Eq. (14-42) reduces to $|r|^2 = (1 - n)^2/(1 + n)^2$, which is identical with the corresponding formula for a solid-dielectric boundary [Eq. (14-13)]. In the range of θ_1 where diffracted waves may
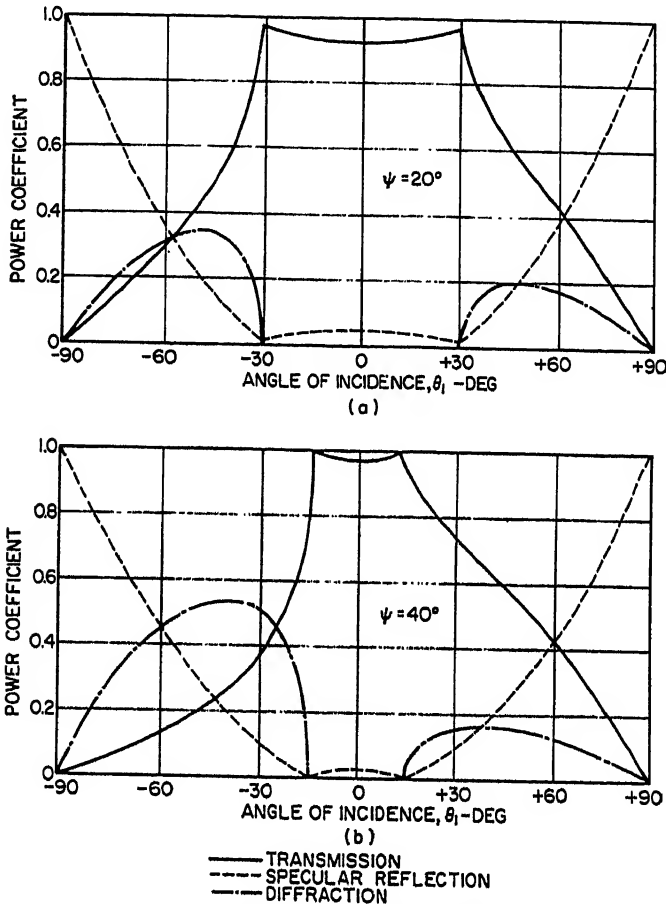
FIG. 14-35. Relative-power transmission and reflection for staggered boundary of metal-plate medium, $n = 0.6$.

exist, Eq. (14-42) is no longer valid. Formulas for this range have been derived by Lengyel,[31] Berz,[32] and Whitehead[33] and are much more complicated than Eq. (14-42).

Figure 14-34 shows the percentage of power transmitted into a metal-plate medium, for the conditions of Fig. 14-33 and $\psi = 0$. To the left of the break in each curve, the nontransmitted power is reflected in the specular reflected wave, while to the right of the break, the nontransmitted power is divided between the specular reflected wave and a diffracted wave. The power loss in the latter region is seen to be very great, and if at all possible, it is advisable to avoid this region in a lens design. At the points S, the angle θ_d of the diffracted wave is equal to θ_1 of the incident wave (Fig. 14-30).

When $\psi \neq 0$, the reflection and transmission quantities are not symmetrical about $\theta_1 = 0$. This is illustrated by the graphs of Fig. 14-35 for $\psi = 20°$ and 40°. These graphs show the portions of the power in an incident wave that are transmitted, reflected in a specular manner, and diffracted.

Examples of the effect of transmission loss have been computed by Whitehead for various lens shapes.[33] The results are shown in Fig. 14-36 for the principal H plane of a nonstepped plano-ellipsoidal lens. The solid curve is the proportion of power transmitted through the lens (ignoring multiple internal reflections) as a function of the aperture coordinate y, while the dotted curve is proportional to the amplitude distribution on the plane surface of the lens. The loss in energy is seen to be consider-
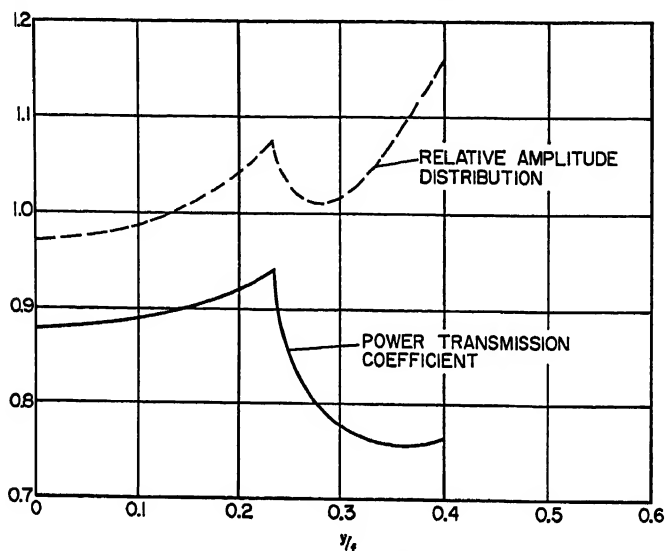
Fig. 14-36. Proportion of power transmitted through lens and amplitude distribution to be expected across aperture for plano-ellipsoidal lens of Fig. 14-5a, $n = 0.6$.

able, and the irregular aperture illumination is certain to increase substantially the minor-lobe level.

The discontinuity effect at the boundary of the metal-plate waveguide medium also results in a phase change. Formulas giving this phase change have been derived by Lengyel,[31] Berz,[32] and Whitehead.[33] Graphical plots of this phase change vs. angle of incidence are given by Berz and Whitehead and show a moderate variation with angle of incidence. Calculations by Whitehead for a typical plano-ellipsoidal lens show that substantial curvature of the wavefront occurs at the aperture when the feed element is at the focal point but that the wavefront may be made almost plane by moving the element slightly away from the focal point.

The above-described data for perpendicular polarization of incidence on a set of parallel plates apply equally well to an array of thin-walled square or rectangular tubes (Fig. 14-31b). However, for parallel polarization, the constraint offered by the array of tubes has a large effect on its reflection characteristics. This has been investigated by Wells,[33a] who has found that at the angle of incidence for which the diffracted wave first appears, a strong, sharp peak of specular reflection also occurs.

Methods of Reducing Reflection Losses. Within the angle-of-incidence range given by Eq. (14-40) and Fig. 14-32, the reflection from the surface of a metal-plate waveguide lens may be canceled through the introduction of an additional reflecting

discontinuity. Possible structures are shown in Fig. 14-37, where in case *a* a dielectric sheet is placed outside the lens, and in case *b* obstacles are placed inside the lens. In both cases the magnitude and phase of the additional reflection are adjusted to cancel the reflection of the metal-plate array. The magnitude depends upon the dielectric constant and thickness of the dielectric sheet, or the shape and size of the obstacles, while the proper phase relationship is obtained through choice of the spacing of the dielectric sheet or obstacles from the edges of the plates. The correct design for a given lens may be obtained experimentally. However, a theoretical design may also be computed through the use of graphical and tabulated data given by Lengyel for the magnitude and phase of the reflection coefficient of the boundary.[31]

Fig. 14-37. Techniques for reducing surface reflections in metal-plate lenses.

In a practical lens design, it is difficult to avoid the ranges of θ_1 in which diffracted waves occur. Many early designs of metal-plate waveguide lenses did not do this,
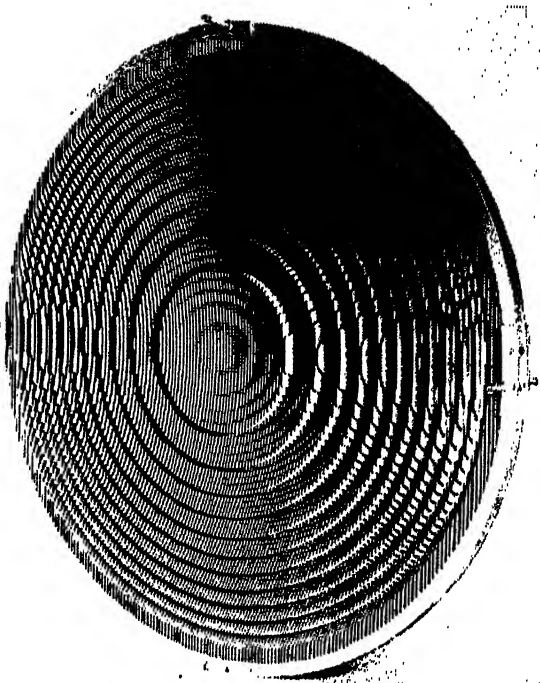
Fig. 14-38. An $F/0.95$ lens of stepped construction.

and as a result considerable loss of gain resulted. One method of avoiding this condition, as may be seen from Fig. 14-32, is to reduce the plate spacing compared with wavelength. However, when this is done, the index of refraction is also reduced.

which increases the reflection loss at angles near normal incidence and reduces the bandwidth. A further possibility is to fill the regions between the plates with dielectric material or to introduce ridges parallel to the axis of the lens in a manner analogous to ridge waveguide.[5a,34] In this way the plate spacing may be reduced to the point where diffraction is no longer a problem, while the index of refraction remains at a reasonable value.

Another method of avoiding diffracted waves is to use a staggered arrangement of waveguide channels, as in Fig. 14-37c.[33a] For waves of either polarization lying in the indicated plane of incidence, the spacing between scattering edges is effectively cut in half, thus doubling the frequency at which a diffracted wave would first appear. This staggered arrangement also eliminates the sharp peak of specular reflection that occurs with the nonstaggered array of tubes for parallel polarization.

Examples of Construction of Metal-plate Waveguide Lenses. Figure 14-38 is a photograph of a stepped metal-plate plano-ellipsoidal lens of the type given in Fig. 14-5b. This lens has an aperture of 40 wavelengths. The sheet-metal plates were cut to their individual shapes and then assembled inside a frame with metal spacers. This type of lens is limited to a polarization parallel to the plates. Another method of construction that is useful for very short wavelengths is to assemble alternate layers of foamed dielectric and metallic foil and then to machine the lens contour on this laminated block.

A particularly rigid lens structure may be obtained through the use of egg-crate construction. Furthermore, if the channels in the lens are made square, the lens may be used with any polarization. Figure 14-39 shows a technique of manufacture that has been found highly satisfactory. Slots are punched in the

FRONT VIEW OF PORTION OF LENS
(a)
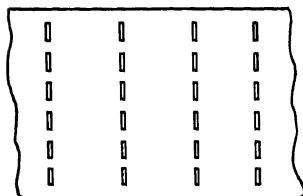
TYPICAL HORIZONTAL PLATE
(b)
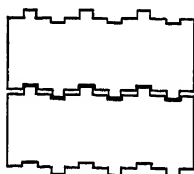
TYPICAL VERTICAL PLATES
(c)

Fig. 14-39. Method of construction of egg-crate-type medium.
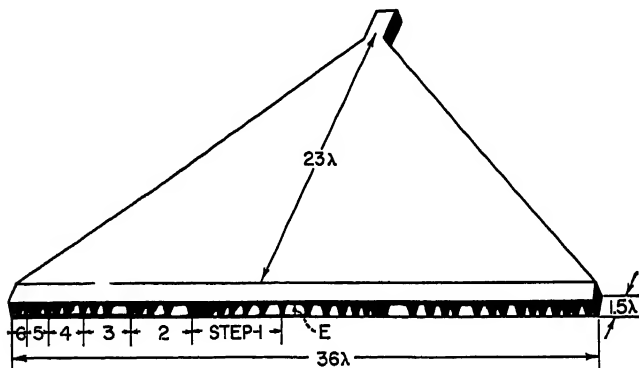
Fig. 14-40. An *H*-plane sectoral horn equipped with a constant-thickness waveguide lens.

horizontal plate to accommodate the tabs in the vertical plates. The tabs must be spaced along the joint by no more than a quarter wavelength if sufficiently good electrical conductivity is to be obtained. The various sheet-metal plates are precut to proper shape, and as each layer is added in assembly, the tabs are staked in place. The resulting structure is very rigid, particularly when held by a surrounding frame.

A line-source type of waveguide lens is shown in Fig. 14-40.[28] The lens is located in the mouth of an H-plane sectoral horn whose height is made less than $\lambda/2$ in order to prevent a horizontally polarized field component. In this case the lens is of uniform thickness, and focusing is obtained by varying the plate spacing along the aperture. The minor-lobe level and input VSWR of this type of lens can frequently be improved by placing absorbing material along the sides of the horn to absorb the reflected energy scattered back from the surfaces of the lens.

14.9. ADDITIONAL LENS MEDIA HAVING $n < 1$

In addition to the metal-plate waveguide medium two other types of lens media having $n < 1$ have received attention. Their performance resembles that of the metal-plate waveguide medium in that they are highly dispersive and possess a highpass (or bandpass) filter characteristic. Also, they are completely metallic.
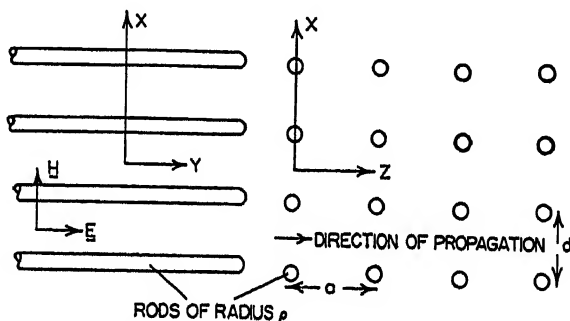
FIG. 14-41. The metal-rod medium

One of these media is the metal-rod structure of Fig. 14-41, which has been analyzed in detail by J. Brown.[2] The performance of this medium may be understood most simply by considering it to be a generalization of the metal-plate waveguide medium. Thus if the spacing d is made greater than $\lambda/2$ and a is made very small compared with d, the horizontal rows of rods will behave like metal plates and the spaces between these rows will behave like waveguide channels.[28] Brown has shown that wave propagation with $n < 1$ is still obtained when the spacing a is made an appreciable part of a wavelength, while at the same time the spacing d may be decreased to less than a half wavelength, thus eliminating the possibility of diffracted waves due to grating effect. In addition, if $a = d$, the index of refraction will be virtually independent of direction in the plane perpendicular to the rods. This may or may not be an advantage, depending upon whether nonconstrained or constrained refraction is desired in that plane. A family of theoretical curves of refractive index as a function of rod radius, spacing, and wavelength is given in Fig. 14-42 for the case of $a = d$. Examination of the figure shows that practical rod diameters may be obtained at wavelengths of about 10 cm or greater. Thus this method of construction is applicable in the range where very large lenses are needed and where the lightweight metal-rod construction is particularly advantageous. However, at this date only small experimental lenses of this type are known to have been made.

Another lens medium having $n < 1$ is an array of thin metal sheets perpendicular to the direction of propagation, with each sheet perforated by an array of apertures. The spacing and diameter of the apertures and the spacing of the sheets are designed so that free propagation of the electromagnetic wave occurs. It is most convenient to use a constant-thickness lens and to obtain focusing by varying the refractive index as a function of radius. Extensive theoretical and experimental data have been
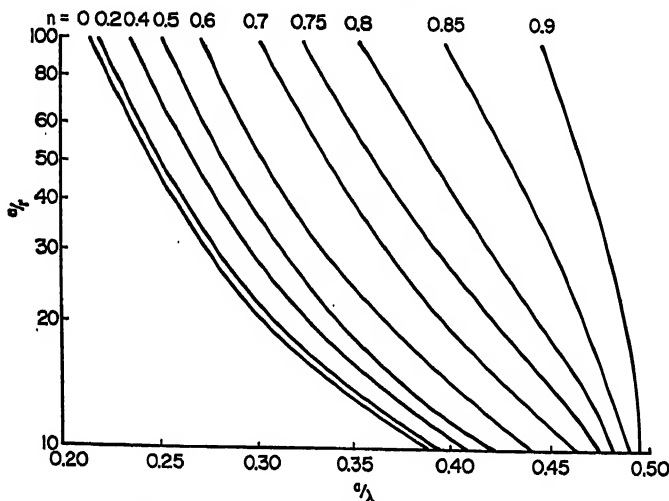
FIG. 14–42. Refractive index of metal-rod medium, $a = d$.

presented on this lens medium by Simon[35a] and Broussaud,[36] and the reader should refer to their papers for details.

14.10. VARIABLE-REFRACTIVE-INDEX LENS DESIGNS

The case of varying the refractive index in artificial delay media and in mixtures of natural dielectrics makes possible the design of lenses having properties unattainable with uniform media. A good discussion of this subject is given in the monograph by J. Brown.[2] Several examples of variable refractive index in metal-plate waveguide media are mentioned in Sec. 14.8. The Luneberg lens[37] is another design that has found many recent applications.

In its basic form, the Luneberg lens is a dielectric sphere in free space whose index of refraction is varied radially according to the following formula:

$$n(r) = \left[2 - \left(\frac{r}{R} \right)^2 \right]^{1/2} \qquad (14\text{-}43)$$

where $n(r)$ is refractive index at radius r, and R is the outer radius of the sphere. Rays emanating from a point source situated on the surface of the sphere are focused into a bundle of parallel rays emerging from the opposite side of the sphere. Lenses of this type have been constructed of foamed dielectric containing many small glass spheres whose spacings were varied to yield the desired refractive-index relationship. They have also been made of spherical shells of graded-dielectric constant fitted one within the other to form the complete lens.

The Luneberg principle has been incorporated into two-dimensional lens designs. Various types of refracting media have been used, such as parallel metal plates

REFERENCES

14-41

propagating the TEM mode with a graded-dielectric disk insert, metal plates propagating a TE_1 waveguide mode with a radial variation in plate spacing, and parallel nonplanar plates propagating the TEM mode, with focusing provided through the nonuniform geodesic path length. In addition, many other types of designs related to the Luneberg design have been introduced, some of which offer advantages for scanning antennas. A comprehensive treatment of these is given by Kunz[38] and in Chap. 15.

REFERENCES

1. S. Silver: "Microwave Antenna Theory and Design," MIT Radiation Laboratory Series, vol. 12, chap. 11, McGraw-Hill Book Company, Inc., New York, 1949. Chapter 11, by J. R. Risser, contains considerable basic information on dielectric and metal-plate waveguide lenses.
2. J. Brown: "Microwave Lenses," Methuen & Co., Ltd, London, 1953. This very worthwhile reference book covers concisely (in its 125 pages) virtually every aspect of microwave lenses. It also contains an extensive bibliography through 1951.
2a. A. F. Harvey: "Optical Techniques at Microwave Frequencies," *Proc. IEE (London)*, pt. B, vol. 106, pp. 141-157, March, 1959. Reviews lens and other microwave-optical techniques. Contains a bibliography of 162 references.
3. F. G. Friedlander: "A Dielectric-lens Aerial for Wide-angle Beam Scanning," *J. IEE (London)*, pt. IIIA, vol. 93, p. 658, 1946. Design of dielectric lenses for wide-angle scan.
4. R. L. Sternberg: "Successive Approximation and Expansion Methods in the Numerical Design of Microwave Dielectric Lenses," *J. Math. and Phys.*, vol. 34, pp. 209-235, January, 1956. Gives design method for wide-angle-scanning binormal dielectric lenses.
5. F. S. Holt and A. Mayer: "A Design Procedure for Dielectric Microwave Lenses of Large Aperture Ratio and Large Scanning Angle," *IRE Trans.*, vol. AP-5, pp. 25-30, January, 1957. Gives results similar to that of Ref. 4 but using a desk calculator.
5a. E. K. Proctor: "Methods of Reducing Chromatic Aberration in Metal-Plate Microwave Lenses," *IRE Trans.*, vol. AP-6, pp. 231-239, July, 1958. Slot-loaded ridge waveguides make possible greater bandwidth, improved scanning, and elimination of stepping.
6. J. Ruze: "Wide-angle Metal-plate Optics," *Proc. IRE*, vol. 38, pp. 53-59, January, 1950. Gives design equations and experimental data for constrained metal-plate lenses designed for wide-angle-scan performance.
6a. E. K. Proctor and M. H. Rees: "Scanning Lens Design for Minimum Mean-square Phase Error," *IRE Trans.*, vol. AP-5, pp. 348-355, October, 1957. A calculus-of-variations analysis leads to design parameters close to those of Ruze.[6]
7. E. M. T. Jones: "Paraboloid Reflector and Hyperboloid Lens Antennas," *IRE Trans.*, vol. AP-2, pp. 119-127, July, 1954. Theoretical analysis with particular attention to the cross-polarized side lobes obtained with different types of feeds.
8. A. R. Von Hippel: "Dielectric Materials and Applications," John Wiley & Sons, Inc., New York, 1954. Contains extensive data on the electrical properties of dielectric materials over the complete range of useful frequencies.
9. E. M. T. Jones and S. B. Cohn: "Surface matching of Dielectric Lenses," *J. Appl. Phys.*, vol. 26, pp. 452-457, April, 1955. Describes lens matching by quarter-wave layers and reactive walls, with design formulas for the latter.
10. T. Morita and S. B. Cohn: "Microwave Lens Matching by Simulated Quarter-wave Transformers," *IRE Trans.*, vol. AP-4, pp. 33-39, January, 1956. Design formulas and graphs for matching dielectric lenses by grooving or otherwise perturbing the surfaces.
11. E. M. T. Jones, T. Morita, and S. B. Cohn: "Measured Performance of Matched Dielectric Lenses," *IRE Trans.*, vol. AP-4, pp. 31-33, January, 1956. An experimental study shows a vast improvement in lens performance by means of the matching techniques of Refs. 9 and 10.
12. W. E. Kock: "Metallic Delay Lenses," *Bell System Tech. J.*, vol. 27, pp. 58-82, January, 1948. This is the basic reference on artificial delay media.
13. C. Susskind: "Obstacle Type Artificial Dielectrics for Microwaves," *J. Brit. IRE*, vol. 12, pp. 49-62 January, 1952. A review article on artificial delay media.
14. W. B. Swift and T. J. Higgins: "Determination of the Design Constants of Artificial-dielectric UHF Lenses by Use of Physical Analogy," *Proc. Nat. Electronic Conf.*,

vol. 9, pp. 825–832, February, 1954. Discussion of analysis and measurement methods. Contains extensive list of references through September, 1953.

15. L. Lewin: "The Electrical Constants of a Material Loaded with Spherical Particles," *J. IEE (London)*, pt. III, vol. 94, p. 65, 1947. Contains formulas applicable to the design of spherical-obstacle lens media.

16. R. W. Corkum: "Isotropic Artificial Dielectric," *Proc. IRE*, vol. 40, pp. 574–587, May, 1952. Experimental study of cubic arrays of metal and dielectric spheres.

16a. M. M. Z. Kharadly and W. Jackson: "The Properties of Artificial Dielectrics Comprising Arrays of Conducting Elements," *Proc. IEE (London)*, pt. III, vol. 100, pp. 199–212, July, 1953. Experimental static values of equivalent-dielectric constant for arrays of strips, rods, spheres, and disks. Theoretical formulas are given that agree in the case of moderate proximity.

17. C. Goatley and C. F. Parker: "Symmetrical Microwave Lenses," IRE Convention Record, pt. I, pp. 13–19, 1955. Describes several types of lens shapes and gives a method of constructing a variable-n dielectric-lens medium containing cylindrical voids.

17a. K. S. Kelleher and C. Goatley: "Dielectric Lens for Microwaves," *Electronics*, vol. 28, pp. 142–145, August, 1955. Describes the constant-thickness variable-n lens of Ref. 17.

18. S. B. Cohn: "The Electric and Magnetic Constants of Metallic Delay Media Containing Obstacles of Arbitrary Shape and Thickness," *J. Appl. Phys.*, vol. 22, pp. 628–634, May, 1951. Electric and magnetic polarizabilities are given for many shapes of obstacles.

18a. S. B. Cohn: "Artificial Dielectrics for Microwaves," pp. 465–480, Proceedings of the Symposium on Modern Advances in Microwave Techniques, Polytechnic Institute of Brooklyn, 1955.

18b. G. Estrin: "The Effects of Anisotropy in a Three-dimensional Array of Conducting Disks," *Proc. IRE*, vol. 39, pp. 821–826, July, 1951. Analysis of double-refraction effects analogous to that of optical crystals.

18c. J. Brown and W. Jackson: "The Relative Permittivity of Tetragonal Arrays of Perfectly Conducting Thin Discs," *Proc. IEE (London)*, pt. B, vol. 102, pp. 37–42, January, 1955. Gives two static formulas for equivalent-dielectric constant, one highly accurate for $l/b \geq 0.6$, the other for $l/b \leq 0.6$.

19. S. B. Cohn: "Analysis of the Metal-strip Delay Structure for Microwave Lenses," *J. Appl. Phys.*, vol. 20, pp. 251–262, March, 1949; also "Addendum," *ibid.*, p. 1011, October, 1949. Gives formulas derived by equivalent-transmission-line method. One set of formulas and a table of computed values (in the Addendum) take full account of proximity and frequency.

20. J. Brown: "The design of metallic delay dielectrics," *Proc. IEE (London)*, pt. III, vol. 97, pp. 45–48, January, 1950. Gives formulas for metal-strip medium derived by equivalent-transmission-line method. Takes partial effect of proximity and frequency.

21. S. B. Cohn: "Electrolytic-tank Measurements for Microwave Metallic Delay-lens Media," *J. Appl. Phys.*, vol. 21, pp. 674–680, July, 1950. Equivalent-transmission-line method, with experimental susceptance data given for arrays of circular and square metallic obstacles.

22. N. Marcuvitz: "Waveguide Handbook," M.I.T. Radiation Laboratory Series, vol. 10, p. 220, fig. 5.1-4, McGraw-Hill Book Company, Inc., New York, 1951. Graph of the normalized susceptance of a metal-strip obstacle in the equivalent transmission line.

23. S. B. Cohn: "Experimental Verification of the Metal-strip Delay-lens Theory," *J. Appl. Phys.*, vol. 24, pp. 839–841, July, 1953. Measurements of refractive index verify the analysis of Ref. 19.

24. W. M. Sharpless: "Artificial Dielectrics for Microwaves," *Proc. IRE*, vol. 39, pp. 1389–1393, November, 1951. Gives a closed-form expression for refractive index of metal-strip medium.

25. K. J. Howes and E. A. N. Whitehead: To be published in *Proc IEE (London)*. Exact solution of metal-strip medium in limit $b/\lambda = 0$.

26. S. B. Cohn: "Microwave Measurements on Metallic Delay Media," *Proc. IRE*, vol. 41, pp. 1177–1183, September, 1953. Presents graphs of directly measured values of refractive index at microwave frequencies for arrays of thin circular and square disks.

27. W. E. Kock: "Path-length Microwave Lenses," *Proc. IRE*, vol. 37, pp. 852–855, August, 1949. Introduces the path-length lens with examples of construction techniques.

28. W. E. Kock: "Metal Lens Antennas," *Proc. IRE*, vol. 34, pp. 828–836, November, 1946. This is the basic reference on metal-plate waveguide lenses. Gives design formulas, examples of construction, and measured patterns.

29. R. I. Primich: "A Semi-infinite Array of Parallel Metallic Plates of Finite Thickness for Microwave Systems," *IRE Trans.*, vol. MTT-4, pp. 156–166, July, 1956. It is shown for normal incidence and given n that finite plate thickness can reduce reflections.

30. J. F. Carlson and A. E. Heins: "The Reflection of an Electromagnetic Plane Wave by an Infinite Set of Plates," *Quart. Appl. Math.*, vol, 4, pp. 313–329, 1947. Mathematical solution for polarization perpendicular to the plane of incidence.

31. B. A. Lengyel: "Reflection and Transmission at the Surface of Metal-plate Media," *J. Appl. Phys.*, vol. 22, pp. 265–276, March, 1951. Extension of Carlson and Heins theory to take account of diffracted beams. Theoretical formulas and experimental verification.

32. F. Berz: "Reflection and Refraction of Microwaves at a Set of Parallel Metallic Plates," *Proc. IEE (London)*, pt. III, vol. 98, pp. 47–55, January, 1951. Analysis similar to that of Ref. 31, but with restriction that the boundary surface is perpendicular to plates.

33. E. A. N. Whitehead: "The Theory of Parallel-plate Media for Microwave Lenses," *Proc. IEE (London)*, pt. III, vol, 98, pp. 133–140, March, 1951. Similar to Ref. 31 and contains many theoretical graphs for different angles of plate stagger and for typical lens shapes.

33a. E. M. Wells: "Some Experiments on the Reflecting Properties of Metal-tube Lens Medium," *Marconi Rev.*, vol. 17, pp. 74–85, 1954. Experimental data for both polarizations are given for arrays of square tubes.

34. R. L. Smedes: "High-efficiency Metallized-Fiberglas Microwave Lens," presented at IRE National Convention, New York, Mar. 19–22, 1956. A waveguide-type lens is described that utilizes dielectric and ridge loading, surface matching, and variable refractive index, in order to achieve improved performance compared with the usual metal-plate waveguide lens.

35. J. Brown and S. S. D. Jones: "Microwave Lenses," *Electronic Eng.*, vol. 22, pp. 127, 183, 227, 264, 368, and 429, 1950. Design information for the rodded medium.

35a. J. C. Simon: "Étude de la diffraction des écrans plans et application aux lentilles hertziennes," *Ann. Radioélectricité*, vol. 6, pp. 205–243, July, 1951. Design data for lenses consisting of a set of perforated metal sheets.

36. G. Broussaud: "Étude de la diffraction des ondes électromagnétiques par un réseau de plaques percées de trous," *Ann. Radioélectricité*, vol. 10, pp. 42–63, January, 1955. Further analysis and design information for the perforated-metal-sheet lens.

37. R. K. Luneberg: "The Mathematical Theory of Optics," Brown University Press, Providence, R. I., 1944. The basic reference on the Luneberg lens.

38. K. S. Kunz: "Propagation of Microwaves between a Parallel Pair of Doubly Curved Conducting Surfaces," *J. Appl. Phys.*, vol. 25, pp. 642–653, May, 1954. Gives generalized treatment and tabulates six types of geodesic path-length lenses equivalent to Luneberg lens.

Chapter 15

SCANNING ANTENNAS

Kenneth S. Kelleher

Aero Geo Astro Corp.
Alexandria, Virginia

15.1. BASIC SCANNING PRINCIPLES

The material covered in this chapter does not include all scanning antennas, but is limited to those systems capable of producing a scanning beam without motion of either the focusing objective or the external portion of the radiating structure. It therefore excludes the simple scanning obtained from mount rotation or the conical scanning from feed rotation. These scanner types have been adequately treated elsewhere.[1]

In the selection of scanning types to be included, an attempt has been made to discuss all known scanning ideas. For security reasons, this attempt has not met with complete success, first, because some classified ideas have not been described in available literature and, second, because some ideas which have been described are still classified and so cannot serve as subject matter for this book. However, the scanners which are considered represent all but a very small percentage of the known designs.

General Types of Scanners. One of the simplest types of scanners consists of a focusing objective and a point-source feed. The objective can be a paraboloidal

Fig. 15-1. Scanning with focusing objectives.
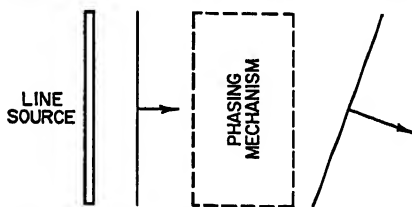
Fig. 15-2. Scanning of beam from line source.

reflector or a simple lens with a hyperboloid for one face and a plane surface for the other face. The scanning action of these objectives can be understood by considering Fig. 15-1. When the point source is at the focal point of either objective, a plane wave is produced which propagates along the direction of the system axis. When the point source is moved away from the axis, the plane wave propagates in a direction at some angle to the axis. It is evident, then, that as the source is moved, the antenna beam formed by the plane wave is scanned through space.

Another entirely different method of scanning is indicated in Fig. 15-2. Here the line-source radiator with all points in phase introduces a wave into a phasing mechanism which produces a uniform phase variation so that the final wave is tilted with respect to its original direction. A change in the phasing mechanism can be used to produce a variation in the tilt of the emerging beam. Scanning can then be achieved

with a fixed line source and an element capable of varying the phase uniformly along the length of the line source.

Limitations of Scanners. If the scanning system were as simple as that indicated above, there would be no scanning problems and no need for inclusion of this chapter in the Handbook. Actually, none of the components described is perfect, so the scanning problem has become that of perfecting the basic elements. The limitations on these elements are: first, the focusing objective is satisfactory for only a limited set of feed-horn positions; second, the feed source used with the focusing objective cannot always be rapidly moved from place to place so as to produce the desired scanning; finally, the phasing mechanism used with a line source possesses mechanical or electrical problems which limit its utility. Since methods of avoiding these limitations form the basis of the various scanning designs, the investigations have fallen into three corresponding classes. These involve work directed toward obtaining (1) a wide-angle focusing objective, (2) a motion of the feed source, and (3) a phase variation along a line source. The greatest amount of work has been done on the wide-angle objectives; these form the bulk of the available material, and so they will be discussed in four of the six following sections. The feed-motion systems will be the subject of the fifth section, and the line-source scanners will be considered in the last section.

15.2. SYMMETRICAL SCANNING SYSTEMS

The systems listed under this heading have the property that a simple analysis indicates a constant radiation pattern over the angle of scan. This property follows from the fact that all components in the system are formed from surfaces of revolution having the same axis of rotation. In such a system, the relative orientation of the final rays are unchanged as the feed source is moved on an arc of a circle with center on the axis of revolution. It is sometimes said that this system has no preferred microwave-optical axis, that is, no one direction in which the radiation beam characteristics are superior to all other directions.

Luneberg Lens. The best-known symmetrical scanning system is a lens described by Luneberg[2] and investigated further by Eaton[3] and others. In its complete form, the lens is a sphere with the property that energy from a feed source at any point on the spherical surface which is propagated through the sphere is focused into parallel rays emerging from the other side of the sphere. Perfect focusing is obtained for all feed positions on the surface.

Fig. 15-3. Geometry of Luneberg-lens cross section.

This lens is formed as a nonhomogeneous medium in which the index of refraction n varies with lens radius r according to the expression $n^2 = 2 - r^2$ for a unit radius sphere. A central cross section of the sphere is shown in Fig. 15-3, together with typical ray paths through the lens. The ray paths are sections of ellipses which are given in polar coordinates by the expression $r^2 = \sin^2 \alpha /[1 - \cos \alpha \cos (2\theta - \alpha)]$, where α is the feed angle defining a particular ray. Because the lens is a symmetrical structure, certain relationships between angles in the system are evident from Fig. 15-3. The most important is the equiangular relationship between the following: the angle formed between ray and the radius vector at the point where the ray leaves the lens; the polar angle defined by the radius vector to the point at which the ray leaves the lens; and the feed angle, i.e., the angle measured at the source point between the

central ray and the general ray. Another point of interest is the fact that the radius vector normal to the ray path bisects the ray path within the lens. Further geometrical information obtained from Fig. 15-3 shows that the path length of a ray within the lens can be obtained as a function of the feed angle. For maximum feed angle of 90°, the ray travels along the lens periphery for a distance of $\pi/2$. Other path lengths within the lens can be determined from the fact that this optical path length equals $\pi/2 + \cos \alpha$. From the path-length variation, it is possible to give an expression for the variation in phase across the semicircular output arc of the lens cross section as $1 - \cos \alpha$, where α is the polar angle.

Another significant property of the Luneberg lens is the fact that the rays emerging from the feed horn do not appear in a uniform manner across the aperture, but instead tend to spread out in the center and approach a theoretically infinite concentration at the edges. Because of this fact, the analytical aperture illumination is obtained from the original feed pattern multiplied by the factor sec α.

Two-dimensional Luneberg Lens. Many interesting variations of the Luneberg lens have been analyzed. The simplest to consider is one in which only a plane section of the lens is utilized.[4] The ray paths through this section are, of course, identical with those of Fig. 15-3. However, the emerging wavefront is not a plane but is a saddle-shaped surface. This surface is the envelope of the Huygens wavelets, with centers on the semicircular aperture. In rectangular coordinates, this surface is given by the parametric expression

$$x = \beta$$

$$y = \frac{\sqrt{1 - \alpha^2}}{\alpha} (1 - \beta - \alpha)$$

$$z = \left[(1 - \alpha^2)^2 - (\beta - \alpha)^2 - \frac{1 - \alpha^2}{\alpha^2} (1 - \beta - 2\alpha)^2 \right]^{\frac{1}{2}}$$
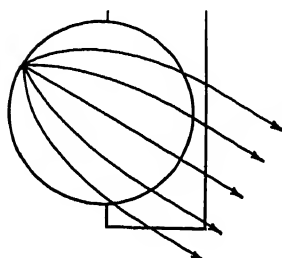
FIG. 15-4. Luneberg lens with linear aperture.

Because of this distorted wavefront, certain limitations exist in the radiation pattern. This pattern has been carefully analyzed in Ref. 4, where it is shown that a side-lobe level of 17 to 18 db exists for all normal feed-horn illuminations. This problem can be circumvented by introducing a linear aperture, as shown in Fig. 15-4. A cylindrical wavefront is produced by this system, so the pattern expected is similar to that obtained from an ordinary line source. It should be pointed out that the introduction of the linear aperture destroys the symmetry of the lens and so limits the system to narrower angles of scan. Experimental models using the linear aperture have been shown to have side lobes of 25 db.[5] It should be remembered that experimental data depend on many different design parameters, so that no direct comparison can be made.

Virtual-source Luneberg Lens. Another variation of the Luneberg lens involves the addition of plane metallic reflectors passing through the center of the lens.[6] The addition of such reflectors produces virtual sources whose positions depend on the orientation of the real feed

FIG. 15-5. Ray paths in virtual-source Luneberg lens.

source and the metallic reflector. Figure 15-5 shows a lens cross section with a single reflector in place. From a consideration of the ray paths, it is evident that a perfect virtual image of the real source is formed. It should be noted from the figure that

not all the energy from the real source which passes through the lens strikes the reflector. Therefore this antenna will produce two focused beams, one from the real source and one from the virtual source.

It is possible to add more plane reflectors and create a complexity of virtual sources. The analysis of the problem of multiple reflectors is too detailed to be included in this Handbook, but can be obtained in Ref. 6. Experimental information on a virtual-source Luneberg is given in Fig. 15-6. This lens was a two-dimensional model with a single plane reflector. The curves indicate that the lens is usable over a scan angle of 120°.
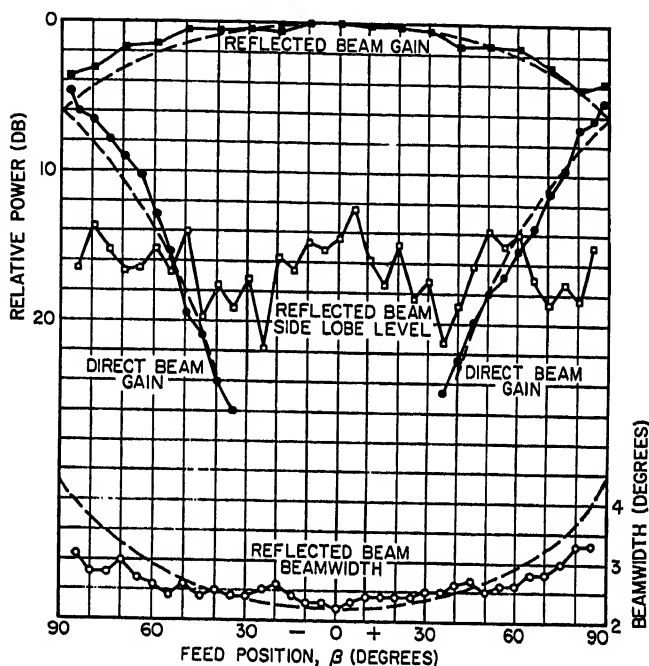
FIG. 15-6. Experimental and calculated data for virtual-source Luneberg lens.

Small-feed-circle Luneberg Lens. Another variation of the spherical Luneberg lens has produced a system with smaller radius of the feed circle and with limited angle of scan. It is interesting to see that the requirement for a smaller feed circle and perfect focusing does not produce a unique expression for the variation in the index of refraction; at present, three general expressions are available.

The first expression was obtained by Eaton in Ref. 3. He considered a sphere of unit radius, with refractive index equal to unity on the surface and with a feed position at any distance, less than or equal to unity, from the center of the sphere. If the radius of the feed circle is denoted by a, then the variation in index is given by the following expression:

$$n^2 = \frac{2a - r^2}{a^2} \qquad \text{for } 0 \leq r \leq a$$

$$n^2 = \frac{2 - r}{r} \qquad \text{for } a \leq r \leq 1$$

From the expression it can be seen that if the feed-circle radius is one-half the radius of the sphere, the index at the center is 2, the index at the feed circle is 1.7, and at the

edge of the lens the index is unity. The variation in index can be shown to be continuous with discontinuous slope at the point a.

The second expression for a small-feed-circle Luneberg lens was derived by J. Brown.[7] He indicated that the problem could be attacked by assuming a certain variation in index between the feed circle and the outer surface and then computing the variation within the feed circle which would yield the desired focusing properties. He considered the problem of bringing all rays incident upon the lens surface into the feed point and displayed two solutions to this problem. The first solution involves choosing a refractive index which is constant in the outer region. In terms of the variables used above, the refractive index was chosen as $1/a$. With this constant value of refractive index, the index variation in the inner region was found by a numerical-integration process. For a feed-circle radius of one-half the lens radius, the results showed that the index had a maximum value of 2.34 at the lens center and decreased monotonically to the value 2 at the feed circle. The index in the outer region had the constant value of 2. The variation in index is then continuous, but the slope of the variation is discontinuous at the feed circle.

Since there is an abrupt discontinuity in the index of refraction at the lens surface, a ray passing from the region in which the index is 2 into free space where the index is 1 suffers reflection and refraction. In order to avoid this problem, Brown considered a lens with index of unity at the surface. He showed that it was impossible under this condition to select a constant index in the outer region. He found one permissible index variation to be

$$r^2 n^2 = 1 + \gamma(1 - r)(r - a)$$

where γ is a positive constant. Using this value of index of refraction for the outer region, it was possible to evaluate the index in the inner region from the following expression:

$$4an^2 = (1 + P) \frac{\{\sqrt{\gamma}\,(1 + a) + [4P^2 + \gamma(1 - a)^2]^{1/2}\}^2}{(P + \sqrt{\gamma a})^2}$$

where $P^2 = 1 - r^2 n^2$.

Brown selected a value of γ equal to $4/a$, since such a value minimized the refractive index required at the lens center. The refractive index varied continuously from 2.2 at the center to 2.0 at the feed circle, and thence to unity at the surface. The slope of the refractive index vs. radius curve was discontinuous at the feed circle.

A third small-feed-circle Luneberg was obtained by Gutman.[8] He selected an index variation given by the expression $n^2 = (1 + a^2 - r^2)/a^2$, and then showed that with the feed at a distance a from the lens center, the outgoing rays would be parallel. It is obvious from this expression that the index and its slope are continuous functions of the radius. For a feed-circle radius equal to one-half the lens radius, the index varies from 2.24 at the lens center to 2 at the feed-circle radius and to unity at the surface.

It is evident, then, that many expressions are available for the design of a small-feed-circle Luneberg. A comparison of the various designs can be made for feed-circle radius one-half the lens radius on the basis of the maximum refractive index required and the maximum effective aperture obtained. This is done in Table 15-1, where it can be seen that Eaton's design provides a minimum in the required index but Brown's design provides a maximum effective aperture with only a small increase in refractive index.

Geodesic Analogue of Luneberg Lens. Another variation of the Luneberg lens is obtained using the relationship between geodesics on a surface and ray propagation in a plane, variable-index medium. The relationship can be understood by considering Fig. 15-7, which shows geodesics on a surface and the corresponding rays in a plane. A given element of geodesic-arc length on the surface corresponds to an element of

Table 15-1. Comparison of Small-feed-circle Luneberg Lenses

	Maximum refractive index	Effective aperture, %
Eaton............	2.0	86.6
Brown...........	2.2	100
Gutman..........	2.24	100

optical-path length in the plane. Since the required index variation in the plane is known, it is possible, by relating arc-length elements, to determine the required surface containing the geodesics.[9] It can be shown that this surface is a surface of revolution whose generating curve is given in rectangular coordinates by the expression

$$Z = \sqrt{P^2 + \frac{R^2}{4} + P} - \frac{1}{3}\ln\left(\frac{\sqrt{3}}{2}\sqrt{1+P} + \frac{\sqrt{1+3P}}{2}\right)$$

where Z = coordinate along axis of revolution
$P^2 = 1 - R^2$
$R^2 = X^2 + Y^2$

A major problem arises in constructing the geodesic analogue of the Luneberg lens. From a consideration of Fig. 15-7, it can be seen that the rays leave the dome-shaped
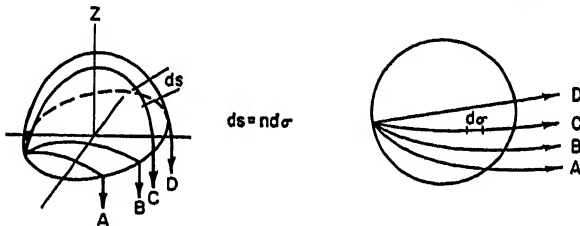
Fig. 15-7. Rays on a surface and in the corresponding variable-index region.

surface along a cylindrical surface and are not focused in a plane as required in the original lens. In order to correct for this fact, that the analogue surface has vertical tangents at its periphery, a toroidal bend is introduced. This bend produces some defocusing of the family of rays.

In order to avoid the defocusing introduced by the toroidal bend, Warren[11] developed an analogue of the Luneberg lens whose surface had horizontal tangents at the periphery. The surface is obtained by a method of approximation, which amounts to a construction as a series of conical sections, the slope of each cone being chosen to focus the ray at a particular feed angle. Warren developed another analogue in which a toroidal bend was introduced in the feed region so that the feed horn could be mounted and rotated under the dome of the lens.

An extension of the techniques employing parallel surfaces to achieve lens effects has been described in an article by Kunz.[11a] A great amount of work in the same field has been carried out under the direction of G. Toraldo di Francia in Italy. This material has been published in reports from the University of Florence and in Refs. 11b and 11c. The general lens type has been named by Toraldo "conflection lenses" to symbolize the fact that the ray is bent with the surface.

Another variation of the Luneberg lens has been proposed by Berkowitz in unpublished material. He suggests a combination of the two-dimensional Luneberg lens and a small-feed-circle lens. In this unit, the lens would be constructed with the required index variation in the outer region. This variation could be that given by

the design of Eaton, Brown, or Gutman. He proposes a replacement of the inner region by a circular waveguide array whose elements are phased so as to yield the phase front originally produced by an index variation in the inner region.

Methods of Constructing Luneberg Lenses. Many different methods have been proposed for constructing the Luneberg lens. A straightforward approach would involve an approximation to the sphere by a center sphere and several spherical shells.[12] The center would have a dielectric constant of about 2, while the shells would have decreasing values of dielectric constant with increasing radius. Through use of a sufficient number of dielectric constants, a sufficiently close approximation to the required lens can be obtained.

Another method of obtaining the Luneberg sphere consists of the use of artificial dielectrics. In its most practical form, the elements forming the dielectric would be spheres. These could be either high-dielectric spheres in a low-dielectric base[13] or spherical voids (dielectric constant of unity) in a high-dielectric base.[14] It has been shown that the dielectric constant for either type of medium is dependent upon the fractional volume occupied by the obstacles.

The expressions for the dielectric constant K as a function of fractional volume are given below for the two cases considered:

Spherical voids: $K = \dfrac{K_1(1 + 2FC)}{1 - FC}, \qquad C = \dfrac{K_1 - 1}{2K_1 + 1}$

Dielectric spheres: $K = \dfrac{K_1(1 + 2FC)}{1 - FC}, \qquad C = \dfrac{K_1 - K_2}{2K_1 + K_2}$

where F = fractional volume

K_1 and K_2 = lower-dielectric constant and higher-dielectric constant, respectively

The spherical obstacles of the artificial dielectric could be replaced with cylinders without introducing major errors in the final lens; however, most other methods of constructing the spherical Luneberg lens suffer from lack of isotropy. Thin metallic cylinders parallel to a given axis in the Luneberg sphere could be used if the feed source were maintained in the equatorial plane of the sphere. Other artificial dielectrics would require similar restrictions on the feed source in order to maintain satisfactory pattern characteristics.

If a two-dimensional model of the lens is considered, all the previous methods of construction are applicable and, in addition, the geodesic analogue in parallel plates can be used. Another construction method involves obtaining the required refractive index by using the concept that the phase velocity of a wave can be varied by varying the spacing between parallel plates.[4,15] If the electric-field vector is parallel to the plates, the required refractive index is obtained by varying plate spacing a, according to the following formula:

$$a = \frac{\lambda}{2\sqrt{K_e - 2 + r^2}}$$

where K_e = dielectric constant for medium between parallel plates

r = radial coordinate, $0 \leq r \leq 1$

Thin metallic cylinders can be used between parallel plates to produce the variation in refractive index required in the Luneberg lens. If the pins are mounted between the plates so that they are perpendicular to but do not contact either plate, the desired variation can be obtained by varying the length and spacing of the pins.

Surface-of-revolution Scanner. Scanners in this category are constructed from a parallel-plate region. They are analyzed by considering that the wave traveling between the parallel plates can be confined to a surface midway between the plates. This "mean" surface can then be considered from a geometrical standpoint and the ray paths taken as geodesics.

The scanner considered here is a parallel-plate region whose mean surface is a surface of revolution. This surface is intended to satisfy the following conditions.[9]

1. Contains a circle (the feed circle).
2. Contains a straight-line segment (the aperture).
3. All geodesics joining a fixed point of the feed circle to points of the aperture meet the aperture at constant angle (optical requirement).
4. All geodesics normal to the feed circle pass through a fixed point (the center of illumination) of the aperture (illumination requirement).

At the present time, no such surface has been found. If requirement 4 is eliminated, a solution is possible which is known as the R-and-$2R$ scanner.[10] The action of this scanner can be understood by considering the mean surface laid out in Fig. 15-8. Here the source is placed on the feed circle of radius R. Energy passes across this mean surface to the opposite side of the circle, where it encounters the output region with boundaries which include a circle of radius $2R$ and the linear aperture. From simple geometry, the path length of a ray in the initial region is given by $2R \cos \alpha$, where α is the feed angle. The ray path in the output region is given by $2R(1 - \cos \alpha)$, so it is evident that all

FIG. 15-8. Geometry of general ray in R-and-$2R$ scanner.

path lengths from the source to the aperture are equal. For another position on the feed circle, because of the symmetry in the final structure, all rays meet the aperture at a constant angle so that perfect focusing is available. This could be proved in a straightforward manner for the developed surfaces. For feed positions other than that of Fig. 15-8, the central ray does not pass through the center of the aperture, so that the utility of the scanner is limited. As the feed horn scans, the maximum intensity appears at various positions in the aperture, and during the greater part of the scan, the energy lies at either end of the aperture.

A lens of the type described above was constructed by introducing an imaging reflector in the initial parallel-plate region and rolling this region into a cone with the feed arc formed into a complete circle on the base of the cone. The on-center radiation pattern had a beamwidth of 0.6° and a side-lobe level of 16 db.

The majority of the other surface-of-revolution scanners are an outgrowth of the work of Myers.[17] The surface considered has been either a cone or a cylinder. Since both of these are developable surfaces, it is possible to analyze the ray paths with simple geometry. The general problem is indicated in Fig. 15-9, which shows a developed cone having a sectoral angle designated as θ. From a consideration of arc lengths on the cone and on the circular top and bottom planes, one has that

$$2\theta R_2 = 2\pi r_2 \qquad 2\theta R_1 = 2\pi r_1$$

and, therefore,

$$\frac{r_2}{R_2} = \frac{r_1}{R_1}$$

Further investigation of the arc lengths along the discontinuities in the conical surface shows that $R_1 \theta_1 = r_1 \varphi_1$ and $R_2 \theta_2 = r_2 \varphi_2$. It can, therefore, be seen that $\theta_2/\varphi_2 = \theta_1/\varphi_1$. Because geodesics on the surface form equal angles with the normal to a surface discontinuity, one can write that $\alpha = \gamma$ and $\beta = \varphi_2$.

For a cone in which r_1 and r_2 are nearly equal, $\alpha \approx \beta$ and some consideration can be given to the maximum distance b at which a ray can be normal to the aperture. It can be shown that $b = r_2 \sin \alpha$. Since r_2 is a constant, the maximum value of b occurs

by large sin α or large values of the feed-circle radius a. If a is set at its maximum value of r_1, a simple lens design can be evolved: For a length L of the cone, if a ray crossing the aperture at b is in phase with the central ray, then the length L must be $r_2 \cos \varphi_2$. This design is exact only when the disk radii r_1 and r_2 are equal, i.e., when the cone becomes a cylinder. It should be noted that the ray tracing was limited to a single point on the aperture. The phase of the field between this point and the center will vary with maximum deviation for large values of b.

Rotman[18] has investigated several experimental models of the cylindrical scanners indicated in Fig. 15-10. The half-cylinder unit shown on the left possesses the general characteristics required in the surface-of-revolution scanner. The model on the right represents an improvement in symmetry obtained by eliminating the requirement for a linear aperture and permitting the energy to radiate from the circular aperture.
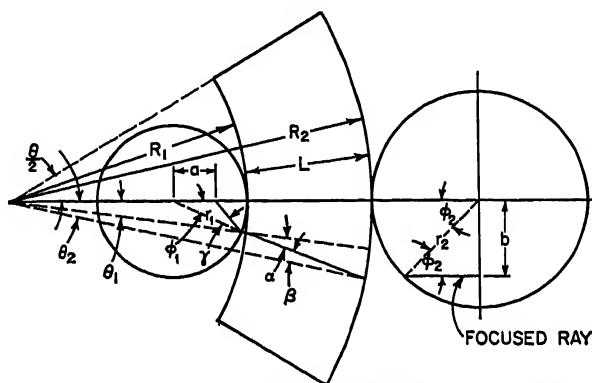
FIG. 15-9. Geometry of the conical surface-of-revolution scanner.
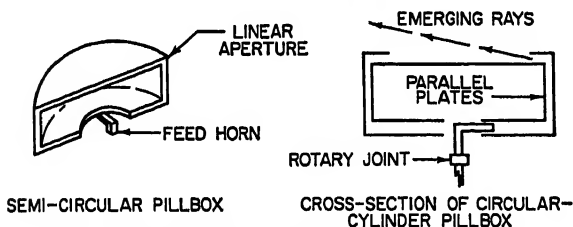
FIG. 15-10. Cylindrical surface-of-revolution scanner.

Both types of scanners have been designed to provide beamwidths less than 30 per cent broader than could be obtained from an aperture of length equal to the scanner diameter.

Concentric-lens Scanner. The concentric-lens scanner is related to the scanners described immediately above. It is made up of a cylinder, or one-half cylinder, whose height is very small compared with its diameter. This scanner contains a lens whose surfaces are concentric with the cylinder surface; this lens can be mounted in either the upper or lower pillbox region.

Rotman studied concentric-lens systems in which the lens was mounted in the lower (feed-horn) region, as shown in Fig. 15-11. Kales and Chait studied a scanner in which the lens was mounted in the upper (output) region. They found that if the radius of the cylinder was R and the lens radii were R_1 and R_2, then a useful lens is obtained using the relation $1/R = 1/R_1 - 1/R_2$.

Another type of concentric-lens system is obtained by using a section of a sphere as

a reflector and employing a lens which is a spherical shell. The lens design could be obtained from the formula of the last paragraph, where the radii are related to spherical surfaces rather than cylindrical surfaces. More detailed analysis of a lens of this type can be obtained from Ref. 19. In general, the concentric-lens type of scanner has not proved satisfactory.

Corrected-feed Systems. One possibility for obtaining parallel rays in a symmetrical system involves choosing symmetrical focusing elements and then adapting the feed system to produce something other than a spherical wave. This technique, in which the point-source feed is replaced by a more complex feed, is called a corrected-feed scanner. In its simplest form, a spherical reflector is used with a feed system consisting of three waveguides,[18] as shown in Fig. 15-12. This feed system is arranged so that the relative amplitude and phase of the energy in the outside waveguides can be varied with respect to that in the

FIG. 15-11. Pillbox-concentric-lens system.

center waveguide to produce good radiation patterns in the plane of the three waveguides. In order to obtain good patterns in any plane, a more complex feed structure must be introduced. An experimental investigation showed that it was difficult to reduce the lobes in more than one plane; successful results were obtained when the feed was used with a pillbox which had a circular reflector. Once satisfactory patterns have been obtained, it is possible to move the feed structure on an arc with center at the center of the sphere and obtain a relatively constant pattern over the angle of scan.

Other feed-correction systems have been used in parallel-plate regions. One of these employed a feed system similar to that used with the sphere. Another one obtained correction by use of a lens mounted between the feed and the cir-

FIG. 15-13. Rotating feed system using correcting lenses in a parallel-plate system.

FIG. 15-12. Three-waveguide coupling system for feed correction.

cular-pillbox reflector. This lens was arranged to rotate with the feed so as to provide a corrected source. Figure 15-13 shows the details of this system, which is described in Ref. 16.

15.3. OPTICAL ANALOGUES

This section deals with scanners which have a microwave-optical axis. In an effort to preserve radiation characteristics as the beam is scanned away from this axis, these systems are designed to satisfy a certain optical condition credited to Abbe. The Abbe sine condition has the interpretation that, in a plane cross section of the optical system, the corresponding initial and final rays, when extended, intersect on a circle of radius equal to the focal length of the system. In optics, it is shown that systems satisfying this condition have no "coma" for source positions near the focus. As applied to scanners, it is interpreted to mean that for small displacements of the feed from the axis, there are no odd-order phase errors present in the radiated beam. Since

these phase errors are the primary cause of pattern deterioration at off-axis positions, there is some merit in the use of this condition.

Schmidt Lens. This system consists of a spherical reflector, together with a nearly plane correcting lens which passes through the center of the sphere. A derivation of the design of this system is contained in Ref. 20. The result is that the lens cross section in Fig. 15-14 can be defined in parametric form by the following expression:

$$x = \frac{2\cos\theta - f\cos 2\theta - c\cos\psi}{\Delta}$$

$$y = \frac{(2\sin\theta - f\sin 2\theta)(1 - n\cos\psi) - c\sin\psi + n\sin\psi(2\cos\theta - f\cos 2\theta)}{\Delta}$$

where $\Delta = 1 - n\cos\psi$
$\psi = \theta - \varphi$
$\sin\varphi = (f\sin\theta)/\rho$
$\rho = (1 + f^2 - 2f\cos\theta)^{1/2}$
$c = 2 - f$

The same reference describes an improvement over the original design in which the outer edges of the lens are modified to provide correction at a feed position other than the axial position. This position is given by a point on an arc of radius f with center at the origin; the point is at an angular position β from the axis. The coordinates for the edges of the lens are obtained from the expression

$$x = u\cos\beta - v\sin\beta \qquad y = u\sin\beta + v\cos\beta$$

where $u = \{2\cos\theta - f\cos 2\theta - c\cos\psi + n\sin\alpha\,[f\sin(\theta + \varphi) - 2\sin\varphi]\}/\Delta$
$v = \{2\sin\theta - f\sin 2\theta - c\sin\psi + n\cos\alpha\,[f\sin(\theta + \varphi) - 2\sin\varphi]\}/\Delta$

Here $\quad\quad \Delta = 1 - n\cos(\psi + \alpha) \quad\quad \psi = \theta - \varphi \quad\quad \sin\varphi = \dfrac{f\sin\theta}{\rho}$

$$\rho = (1 + f^2 - 2f\cos\theta)^{1/2} \quad\quad c = 2 - f \quad\quad \alpha = \beta - i$$

where $n\sin i = \sin\beta$

Several experimental models of the Schmidt system have been built in parallel-plate media. Some of these have involved a single layer of parallel plates with a circular reflector, while others employ a double layer and a toroidal-bend reflector. Excellent scanning performance has been obtained on all models which utilized a dielectric lens. Metal-plate lenses have been less satisfactory.

The Mangin Mirror. The Mangin mirror consists of a spherical reflector with correcting lens in contact with the reflector. The outer lens surface is spherical with a radius and center different from that of the reflector. This system, when used in the field of optics, was found to have little coma; for this reason, it was thought that it might provide focusing not only for a feed on the axis but also for feed positions off axis.
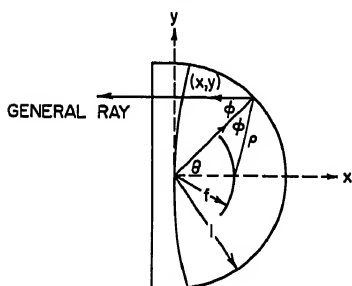
Fig. 15-14. Geometry of Schmidt lens.

The design of the element is based on a feed position along the system axis. By proper choice of feed position, as well as the radii and centers of the spherical surface, it is possible to obtain a design which yields a focused beam. The design is, of course, not unique; a different combination of the available parameters will also yield a system with the desired focusing properties.

None of the antenna designs is concerned with feed positions off axis, so in order to evaluate the Mangin mirror as a scanner, it is necessary to perform detailed ray tracing

for off-axis positions or to build and test a number of experimental models. The models constructed to date have been in the form of complete spherical surfaces or of sections of these surfaces mounted in a double-layer parallel-plate region. None of the designs studied to date has yielded off-axis patterns which are superior to those obtained from the simple paraboloid.[21]

Berti System. An optical analogue similar to that of the Mangin mirror involves a correcting lens in contact with the reflector, arranged so that the incident rays pass through a lens surface of different radius from that of the reflected rays. Such a system can be conveniently constructed in a double-layer parallel-plate region, since the lens structure in one layer has a different radius from that in the other layer. It is evident that additional parameters over and above those of the Mangin mirror are available in this instance. However, the availability of the parameters does not ensure better scanning properties until they are used in a design adapted to an off-axis feed position.

Schwarzschild System.[22] This system employs multiple mirrors rather than a lens and mirror. It is a two-mirror device based on a general optical method developed by Schwarzschild.[22] Such a system, in optical terminology, has no spherical aberration or coma. The only experimental system using this principle was built in the form of triple-layer parallel-plate region.[23] The feed horn moved on a 90° arc of a circle in the first layer. Energy from the feed was reflected at the first toroidal-bend reflector, passed through the middle layer, was reflected from the second bend, and left the parallel plates through a linear aperture in the third layer.

The surfaces of the first and second reflector were calculated, respectively, from the equations

$$x_1 = 0.5y^2 - 0.03125y^4 - 0.22y^6$$

and

$$x_2 = 0.75y^2 - 5.96025y^4 + 40.53y^6$$

where the coordinate x is parallel to the direction of the optical axis. Little experimental data are available on this system.

Zeiss-Cardioid. This system is similar to the Schwarzschild in that it employs two reflectors. The major difference is

Fig. 15-15. Geometry of Zeiss-Cardioid reflector system.

that it uses simple reflecting surfaces and yields perfect focusing for the feed on the axis. The mirrors used are a circle and a cardioid. The design of this system can be understood by considering Fig. 15-15. If the position of the feed horn is taken as the origin, then the reflecting surfaces have the following equations:

Reflector 1: $$\rho = 1 + \cos\theta$$
Reflector 2: $$(x - \tfrac{1}{2})^2 + y^2 = 1$$

An X-band model of this reflector system with an aperture of 36 in. had a half-power beamwidth of 3.3°, using a wavelength of 3.2 cm. This antenna, investigated by W. Rotman at the Air Force Cambridge Research Center, proved capable of scanning through a total angle greater than 15 beamwidths with a loss in gain of less than 1 db.

Coma-corrected Reflector. One scanner which satisfies the Abbe sine condition employs a reflector which is adjusted so that the incident ray and reflected ray meet on a circle whose center is at the source position. One possibility for forming this reflector employs sections of parabolic cylinders in a parallel-plate region. These

cylinders are arranged so that the reflected bundle of rays from each cylinder is one wavelength out of phase with adjacent bundles. All rays are parallel to the system axis, and by placing the parabolic cylinders along a circular arc with center at the source point, the Abbe sine condition is satisfied. The reflected wavefront from this system is a stepped surface with one wavelength difference between each step. The radiation pattern from such a wavefront is satisfactory over a narrow frequency band. For single frequency operation, the pattern deteriorates at positions of the feed away from the axis; it has not definitely been established that the off-axis performance is superior to a paraboloid. Another similar method of forming the coma-corrected reflector replaces the parallel-plate region and point source by parabolic cylinders and a line source.

A third method utilizes a reflector surface made up of square waveguides. The front face of the waveguides is tangent to a spherical surface with center at the feed point. The back of the waveguides is tangent to an ellipsoidal surface. The equation of the ellipse cross section is given by

$$\frac{(2nx - 1)^2}{(2n - 1)^2} + y^2 = 1$$

where n is the refractive index of the waveguide.

Focusing is obtained from the waveguide coma-corrected reflector because of the fact that incident energy from the feed is carried through each of the waveguides, reflected from the ellipsoidal surface, and reradiated to form a plane wave. Since the incident ray and reflected ray in any plane lie on a circle with center at the feed point, the Abbe sine condition is satisfied. A parallel-plate version of this waveguide system was studied experimentally without discovering any desirable scanning features.

15.4. LENSES WITH OPTICAL AXIS

Many existing scanning systems use relatively simple lens structures as the focusing objective. The parameters considered to optimize the scanning properties have been the index of refraction and the shapes of the two lens surfaces.

Two methods of determining the lens surfaces have been proposed for obtaining good scanning properties from a constant index-of-refraction lens. The first, which has general application, is based on the Abbe sine condition. The basis for this criterion was discussed in the section on optical analogues. The second, a much more useful method, is the two-point correction method; the lens is designed to focus incoming plane waves from two directions into two points, symmetrically located with respect to the optical axis. This method is most conveniently applied to the constrained type of lens employing waveguide construction. It has been applied to a dielectric-type lens, but no exact mathematical expression is available for the lens surfaces.

The application of a variable-index-of-refraction medium has been considered in the design of lenses with optical axis. This variation has been obtained by varying the plate spacing in a metal-plate lens, by varying waveguide loading in a constrained lens, by using a number of different dielectric materials to approximate the desired variation, and by using a void-dielectric medium.

Dielectric Lens. The simplest type of scanning lens is that which uses a constant index of refraction, a hyperboloid as the initial surface, and a plane as the secondary surface. The design of this lens is based on a feed at one focal point of the hyperboloid. Rays from the feed are focused by the lens into a plane wave whose direction of propagation coincides with the lens axis. The lens cross section, shown in Fig. 15-16, is a hyperbola whose eccentricity is equal to the index of refraction of the dielectric material. In the notation of the figure, the focal length of the system is $f = c + a$ and the index is $n = c/a$. For a given focal length f and index n, one can solve for c

and a so that the hyperbola in rectangular coordinates is

$$x^2 - y^2 (n^2 - 1) = \frac{f^2}{(n+1)^2}$$

Since the lens is designed only for on-axis focusing, exceptional scanning qualities are not expected. One experimental lens investigated in the millimeter waveband scans a beam of 2° over a total angle of 20°, with side lobes always less than 20 db. The gain of this lens was about 2.5 db less than could be obtained from a paraboloid
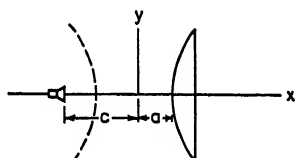
FIG. 15-16. Geometry of dielectric lens.
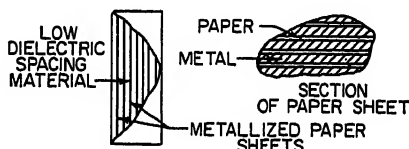
FIG. 15-17. Artificial-dielectric lens for scanning.

of equal aperture. This loss in gain could be traced to reflections at the lens surfaces and to high loss tangent for the Lucite dielectric in the millimeter waveband.

In an effort to reduce the weight and the dielectric loss of the previous lens, a second lens was considered. This model employed wavelength steps (as described in Chap. 14) in the hyperboloid surface. Three steps were used, so that the lens face was made up of three sections, each of which was formed as a hyperboloid surface. The scanning properties were similar to those of the unstepped lens; however, a loss in gain of 3 db was reported. It is interesting to note that the use of steps, although reducing the amount of dielectric material, produced an increase in the antenna loss.

Another type of dielectric lens employs an artificial-dielectric medium.[24] The lens construction can be understood from Fig. 15-17. Since the metallic obstacles employed were obtained from a metal-spray process, a lightweight, compact construction was achieved at the expense of some loss in the conductors. A comparison was made between this lens and a metal-plate lens of similar design. It was found that the gain was 2.8 db below that of the metal-plate lens but that 4 db of the over-all loss (compared with a

FIG. 15-18. Symmetrical-dielectric lens.

paraboloid) could be attributed to the construction materials. With better construction, the lens might have less loss than a metal-plate lens; the scanning properties were slightly superior to those of the metal-plate lens.

Another dielectric lens which has been used for scanning involves a symmetrical element with identical initial and secondary surfaces. A feature of this lens is that two scanning feeds can be used simultaneously, one on either side of the lens. The two beams can cover sectors 180° apart in space.

The design of this lens is based on the assumption that the lens can be closely approximated by a prism between the points where a ray enters and leaves the surface. The coordinates of the lens surface can be found from the following expression, where all the parameters are given in Fig. 15-18:

$$x = \frac{[f(1 - \sec \varphi) + 2a(n - 1)](2 \cos^2 \alpha \sin \omega - \sin \beta)}{(n - \cos \alpha) \sin \beta + (n \sec \alpha - \sec \varphi)(2 \cos^2 \alpha \sin \omega - \sin \beta)}$$
$$y = (f - x) \tan \varphi$$

The three angles β, φ, and α are known in terms of the parameter ω:

$$\beta = 2\omega - \cos^{-1}\left(\frac{\cos \omega}{n}\right)$$

$$\varphi = \omega - \cos^{-1}(n \cos r_1)$$

$$\alpha = \cos^{-1}\left(\frac{\cos \omega}{n}\right) - \omega$$

The surface is found by selecting values of the parameter ω, computing the three angles, and substituting their values into the expressions for x and y.

Because the lens design is based on focusing at an axial point, there is no reason to expect superior off-axis performance. One experimental model showed that the 12° beam could be scanned over a total angle of 40°. Best scanning can be obtained with long focal-length lenses.

Wide-angle Dielectric Lenses. The Abbe sine condition, which was described in the section on optical analogues, has been used in the design of a dielectric lens. The greatest amount of work using this condition was done by Friedlander.[25] He found that he could closely approximate the circle of intersection between initial rays and final rays by use of a relatively simple lens. Instead of using two curved surfaces, his lens had a plane face for the initial surface and a curved face for the final surface. With a refractive index of 1.6 and $f/D = 1$, he found a deviation from the sine condition of the order of $\frac{1}{8}$ of 1 per cent of the focal length. An experimental lens of 50λ aperture gave satisfactory patterns over a 20° total scan angle.

A careful study of dielectric lenses has been made by the group under Professor Woonton at McGill University. They have investigated the aberrations produced in scanning and have shown that the effects of these aberrations in the presence of diffraction can be related to the theoretical optical work of Nijboer.[19]

A lens system which gives promise of wide-angle focusing is one which uses two curved surfaces to obtain perfect focusing of waves from two different directions. Some work has been done on this type of lens in this country and in England. Because of the complexity of the problem, an exact solution of the three-dimensional lens has not been achieved; however, there are several different methods for determining the required surfaces in a two-dimensional-lens structure. The two most useful methods are the "algebraic curve" and the "lattice." The first assumes that the two-dimensional-lens faces are algebraic curves and then determines the coefficients of the algebraic expressions by selected ray tracing. The second is a step-by-step procedure, adapted to computer use, in which points on the two lens surfaces are found by considering alternately the two focal points. Some effort has been made toward designing a three-dimensional lens by using a two-dimensional design to form the lens faces as surfaces of revolution; however, the resulting lens has serious astigmatism.

Metal-plate Lenses. The simple metal-plate lens described in Chap. 14 has been used successfully as a scanning antenna. This lens design provides perfect focusing for a single position of the feed; wide-angle performance is obtained by choosing a long focal length. Some problems which arise at off-axis feed positions are related to the basic nature of the metal-plate lens. Since the lens is a periodic structure, diffraction lobes[26] appear which increase with increase in scan angle; these lobes are in addition to the normal "coma" lobes. In order to prevent them from becoming objectionable, it is necessary to limit the angle which the incident rays make with the lens surface; this limitation in turn limits the feed displacement and the angle of scan.

Metal-plate lenses can be designed for improved performance by using the Abbe sine condition. One such lens design uses square-waveguide elements which constrain the incident energy to travel through the lens in a direction parallel to the lens axis. Such a design simplifies considerably the analysis of the system, since the refraction follows a much simpler expression than that given by Snell's law. One lens design offered[27]

not only satisfied the Abbe sine condition but also, by proper choice of the waveguide medium, yielded a system which would operate over a broader band than that possible with the normal metal-plate lens.

One of the earlier metal-plate scanning lenses was constructed between parallel plates with the general form shown in Fig. 15-19.[16] In this lens, the initial surface was curved and the index of refraction was varied in the y dimension. The design of the system then employed three basic variables: (1) the lens surface, (2) phase delay between input and output of a given lens channel, and (3) constraint of energy entering at a given point to leave at a desired point.

The lens surface is given by the circle $(x - \frac{1}{2})^2 + y^2 = (\frac{1}{2})^2$ where the coordinates are shown in Fig. 15-19. The phase delay for a particular channel is found in terms of the delay in the central channel and the coordinate x. The required expression is $s_1 - s_0 = 1 - \sqrt{1 - x}$. The final variable, the distance from the axis to a general emerging ray, is given by the expression $y_1 = \sqrt{x}$.

Experimental results on this lens showed that it maintained a constant beamwidth of 2.2° over a scan angle of 40°; no information is available on the side-lobe level. In taking these data, the feed horn was confined to a circle of unit radius.
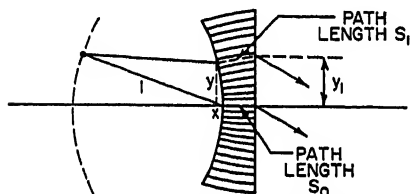
FIG. 15-19. Lens using path-length correction.
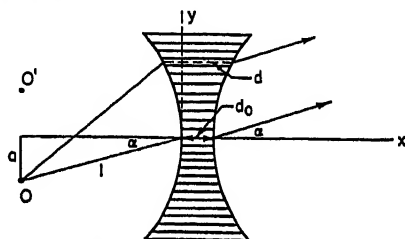
FIG. 15-20. Two-point-correction lens.

Metal-plate Lenses with Two-point Correction. A decided improvement in scanning has been achieved when the Abbe sine condition of optics is ignored and, instead, the lens is designed to provide perfect focusing at two points.[28] Figure 15-20 indicates the geometry of such a design in a two-dimensional lens. This design employs a constrained lens of constant refractive index. The lens surfaces are chosen so that plane waves arriving from the directions $+\alpha$ and $-\alpha$ are exactly focused at the points 0 and 0', respectively. Using the design geometry of the figure, it can be shown that the first lens surface is an ellipse given by $(x/a + 1)^2 + y^2 = 1$. The second lens surface is obtained by determining the lens thickness at any point. An expression involving the lens thickness as a function of the lens constants and the coordinate x is given as $ax = (n - a)(d - d_0)$, where n is the refractive index and the other parameters are given in the figure.

A second two-dimensional lens utilized a variable index but a plane outer surface. In this case, the inner surface was identical with that of the lens in the previous paragraph and the variation in the refractive index was given by the expression $(n - n_0)d_0 = nx - m\lambda$. The term $m\lambda$ has been introduced into this expression to obtain wavelength steps in the lens. This is necessary in order to minimize the range over which the refractive index must vary. Since waveguide techniques are utilized, the refractive index is limited to values between 0.5 and 0.9.

A three-dimensional lens can be obtained which produces perfect focusing at two points. The inner lens surface is an ellipsoid, given by the expression

$$\left(\frac{x}{a_0} + 1\right)^2 + y^2 + \left(\frac{z}{a_0}\right)^2 = 1$$

Here the symbols are those of Fig. 15-20, and the coordinate z is measured normal to the xy plane. Once the inner surface is found, the outer surface is obtained from an expression involving the lens thickness: $ax = (n - a)(d - d_0)$.

An important improvement in the performance of a constrained lens with two-point correction has been obtained by Peeler.[29] His design utilized the basic lens, together with steps which were arranged to minimize the phase errors in the "on-axis" position. He thus had corrections at three points and an over-all reduction in phase errors at all scan positions. Computations on the final design showed phase errors of less than one-tenth wavelength over the aperture throughout the scanning of a $\frac{1}{2}°$ beam through 20°.

Another use of the constrained lens involves a symmetrical structure having two axial focal points, one on either side of the lens. The two scanned beams cover sectors 180° apart in space. Because constraining elements are used, Snell's law does not apply and the lens derivation is obtained without recourse to any assumptions. Each face of the lens has a cross section, given in polar coordinates by

$$\rho = 2(1 - n)/[1 - (2n - 1) \cos \theta]$$

for a lens of unit focal length; the origins for the polar coordinates coincide with the feed positions on either side of the lens, which has an arbitrary thickness.

Variable-index Lenses. One variable-index lens, the Luneberg lens, has already been considered in the section on symmetrical scanning systems. There are other lenses with optical axes and employing a variation in the refractive index. One of these is the modification of the Maxwell-Fish-Eye lens, in which the complete sphere is replaced by a hemisphere. The optical axis is the line perpendicular to the plane surface and passing through the center of the sphere. The lens is designed to give perfect focusing for a source at the point where this axis touches the sphere surface; little is known of the off-axis performance. The lens is designed through use of the formula $n = 2/(1 + r^2)$, where r is the radial coordinate whose maximum value is unity.

A second variable-index lens is the constant-thickness lens of Luneberg. A cross section of this lens, together with ray paths from a feed source, is given in Fig. 15-21. This system has an optical axis, namely, the x axis in the figure. The refractive index varies only with the y coordinate according to the expression $n = n_0 \operatorname{sech} (y\pi/2T)$, where n_0 is the index at $y = 0$ and T is the lens thickness. No information is available on the off-axis performance of this lens.

FIG. 15-21. Luneberg constant-thickness lens.

A final variable-index lens is the Kelleher lens,[30] with geometry similar to that of the constant-thickness Luneberg lens. In this lens, the feed horn is placed on the optical axis some distance from the lens surface. The lens design is based on a focusing of rays from this feed horn. An assumption is made that the index variation between the point where a ray enters and leaves the lens is square-law in nature. The lens equation is given by

$$T \left(n^2 - \frac{2 \sin^2 \theta}{3} \right) = \sqrt{n^2 - \sin^2 \theta} \, [n_0 T - (\sec \theta - 1)]$$

where T = lens thickness
n_0 = index at axis
θ = angle between an arbitrary incident ray and axis

An analysis of the scanning performance of this lens indicates that although the lens is designed for a single axial point, it should be effective over a wide angle. Experimental data indicate that an 8° beam could be scanned over a total angle of 60°.

15.5. SCANNING WITH REFLECTORS

The simplest type of focusing objective is the reflector. This is a lightweight component, relatively easy to construct, and so has found wide application in the scanning field. The majority of the reflectors have been paraboloids; others of interest are a section of spherical surface, a torus, or a parabolic torus. These will be considered in turn in the discussion which follows.

Paraboloidal Reflector. The paraboloidal reflector has been used as a scanner in many forms, of which the simplest is the symmetrical one with the vertex of the paraboloid at the center of the reflecting surface (circular aperture). Other reflectors were formed of sections of the paraboloid surface which did not include the vertex point or which included this point at some off-center position. The aperture of these reflector types does not fit any simple plane curve, although they could be normally approximated by an ellipse. Since there are so many different reflectors, it is impossible to describe the scanning performance of each. However, information is available on the circular-aperture reflector, and some idea of the scanning properties of the remaining reflectors can be obtained from this information.

The parameters available in the circular-aperture reflector are the aperture width, aperture illumination, and the focal length. An analysis of the pattern of the circular aperture with feed displaced from the focal point showed minimum variation of pattern shape with moderate changes of the aperture width in wavelength.[21] For the aperture widths of interest, it is only necessary to consider the illumination and the focal length; Ref. 21 shows data for two illuminations and four focal lengths.

Since it is impossible to give all the results of this reference, a general discussion will suffice. Most of the data was taken with the feed horn moved off axis in the H plane; a check of the characteristics of the feed horn moved off in the E plane showed agreement within experimental error. The implication is that the variation in scanning characteristics is a scalar problem, independent of polarization. A check on the variation in the cross-polarized component over the angle of scan showed that it was relatively constant over the angle of scan and dropped in intensity at the edges of the scan sector.

The data for all four reflectors showed a decrease in gain and an increase in side-lobe level as the beam was scanned away from the axis. The side lobe on the axial side of the pattern increased rapidly, while that on the other side of the pattern was merged into a main beam. Figure 15-22 shows a typical pattern variation over the angle of scan. Some difference was noted in the pattern characteristics with change in aperture illumination. With 10-db illumination, the side-lobe level increased more rapidly than with the 20-db illumination. The 10-db illumination showed better gain characteristics for long focal length, while the 20-db illumination was better for short-focal-length reflectors. The scanning characteristics improved with an increase in focal length; best results were obtained with the longest focal length, which corresponded to an f/D ratio of 0.75.

A study was made of the orientation of the feed during scanning. The two possibilities considered involved pointing the feed toward the vertex of the reflector or pointing it so that its axis was parallel to the axis of the reflector. Only minor differences in the patterns were found with changes in feed orientation, so that it was impossible to say that one or the other orientation was superior. It was found that best scanning results were obtained when the feed was moved along a line perpendicular to the reflector axis. For feed positions at which a side-lobe level greater than 15 db

can be tolerated, the best location of the feed is on a path which at large angles bends away from the reflector.

Most deductions concerning scanning performance are based on radiation patterns taken in the plane of scan. Patterns taken in the other principal plane showed that the beam varied only slightly with feed positions and that for the larger scan angles the first side lobe was merged into the main beam.

One very interesting effect arises from the study of the scanning performance of the paraboloid. It is found that if the feed horn is moved through a certain angle away from the axis, then the radiated beam is displaced through a smaller angle from the axis. The ratio between the angle which a radiated beam makes with the axis and the angle which the feed displacement from the axis subtends at the vertex is called
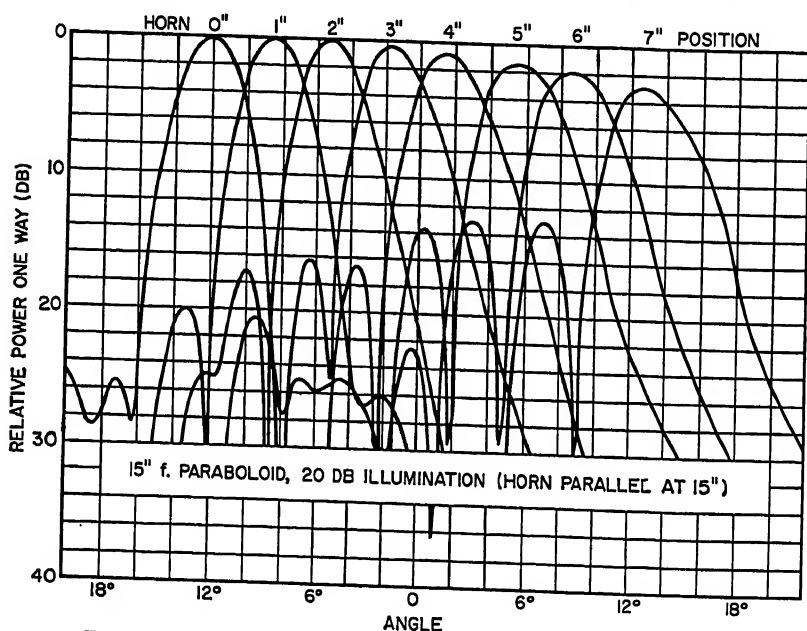
FIG. 15-22. Patterns from paraboloid with feed displaced from axis.

the beam factor. It was found that the beam factor was dependent upon the focal length, the aperture distribution, and the position off axis. Of these three parameters, the focal length was the most significant. For moderate displacements from the axis, the beam factor showed only slight variation with feed position. An expression for the beam factor for small displacements is

$$ \text{BF} = 1 - \frac{\int_0^{x_0} \dfrac{B_1(x)x^2\, dx}{x+4}}{\int_0^{x_0} B_1(x)x^2\, dx} $$

where $x_0 = D_x/2f$

D_x = aperture dimension along X axis

$B_1(x)$ = illumination function

It is evident that this expression includes the effect of aperture illumination and focal length. Figure 15-23 shows a plot of the beam factor obtained from experimental data, together with points on the axis obtained from the expression above. It is

evident that the expression matches closely the measured data in the neighborhood of the axis.

Spherical Reflector. Because of their inherent symmetry, the spherical reflectors have been felt to be useful in scanning applications. If the feed radiator is arranged to illuminate only a sector of the sphere, little change in pattern will be obtained as the feed horn is scanned to illuminate other identical sectors. However, if a direct comparison is made of a spherical reflector with a paraboloidal reflector of the same aperture dimensions,[21] then the sphere yields patterns which vary with scan angle in a manner similar to that produced by the paraboloid (Fig. 15-22), except that the side-lobe level is everywhere higher than that of the paraboloid.
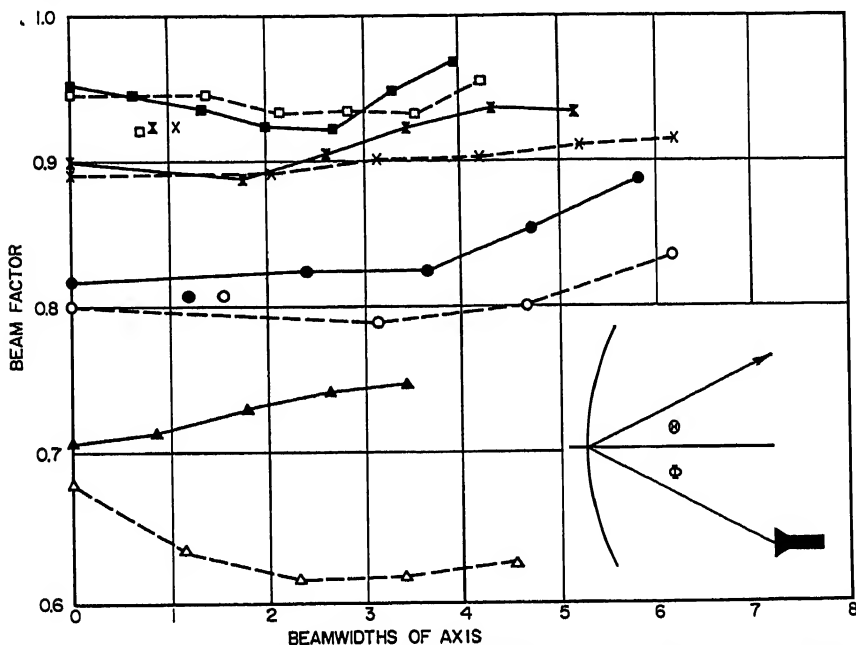
FIG. 15-23. Beam factor as a function of focal length and edge illumination in a 30-in. paraboloid: — ·· ·· 20-db illumination. — · — · · 10-db illumination. △ = 7.5-in. focal length, ○ = 10.6-in. focal length, × = 15-in. focal length, □ = 22.5-in. focal length.

Other data taken on the sphere showed little variation in the cross-polarized intensity throughout the angle of scan. Improved performance was noted when the sphere radius was increased and when the aperture illumination was decreased from 10 to 20 db at the edges of the reflector.

Work on spherical reflectors in England[21] is consistent with that of Ref. 21 since it shows that narrow beams can be obtained over a relatively wide angle of scan but that the side lobes remain at a high level throughout the scan.

Torus Reflector. Another reflector which has been suggested for scanning applications is the torus, obtained by rotating an arc of a circle completely about an axis which lies in the plane of the circle. In order that it be useful, it is necessary that the reflecting surface be made up of rods at 45° to the axis of revolution. A feed horn which yields polarization parallel to the reflecting elements is placed within the torus surface. The energy focused by the reflector appears at the opposite surface of the torus with a polarization normal to the reflecting elements so that it passes through the torus surface and forms a radiated pattern in space. Because of the symmetry of this

reflector, the feed horn can be moved on a circle of constant radius to yield a scanning of the focused beam.

The parameters available in the design of this reflector are the radius of the feed circle, the distance from the axis of revolution to the vertex of the circular arc, and the axial extent of the surface. With one choice of parameters, the torus degenerates into a section of a spherical surface. Other variations upon the basic design would include the substitution of any plane curve for the circular arc. In this way, the beam shaping in the plane normal to the plane of scan can be achieved.

The basic limitation on the torus scanner is similar to that of the spherical reflector; perfect focusing cannot be achieved. However, if the radiation characteristics obtained are satisfactory, then this scanner offers a lightweight, compact structure capable of sweeping a beam through 360° in azimuth.

Parabolic-torus Reflector. One variation of the torus scanner, which has been investigated in some detail,[32] is that obtained by replacing the circular arc with a parabolic arc and by limiting the rotation of the parabolic arc about the axis of revolution to an angle of less than 180° so that the reflector does not require the polarization properties of the previous torus. The parameters available in the design of this system are the focal length of the parabola, the distance of the axis of revolution to the vertex of the parabola (torus radius), the angle of revolution, and the axial length.

A study was made of the wavefront produced by the parabolic torus when illuminated by a point-source feed. A satisfactory reflector was the half torus, which used a parabolic arc, one of whose end points was the parabola vertex.

——— PATTERN IN PLANE OF CIRCULAR ARC
– – –PATTERN IN PLANE OF PARABOLIC ARC

Fɪɢ. 15-24. Patterns from parabolic torus:
——— Pattern in plane of circular arc.
– – – – – Pattern in plane of parabolic arc.

With a ratio of focal length to radius of about 0.45, a minimum deviation from a plane wave was obtained. The patterns measured with this reflector are shown in Fig. 15-24. It is evident that reasonable side-lobe levels can be obtained in the plane of scan and good side-lobe levels can be obtained in the other plane. However, one important characteristic of this type of reflector is the higher side lobes which appear in the planes at 45° to the principal planes. Data obtained on this reflector show the lobes as high as 13 db in these planes. For applications where these lobes are not objectionable, this reflector is superior to the paraboloid and sphere.

Another parabolic-torus reflector was the full torus, which had a circular aperture similar to the paraboloids previously described. This reflector showed radiation characteristics unlike that of the half torus; the side lobes were merged into the main beam to produce a tent-shaped structure. The maximum side lobes were in principal planes.

Frequency-scanning Reflector. It is possible to obtain scanning from a fixed reflector and a fixed feed if the reflector is arranged so that its effective surface varies with frequency. This variation in surface with frequency can be obtained by using a

reflector surface of many pyramids which are joined at their base.   The space between pyramids forms waveguides of varying cross sections so that the effective reflector depends on the incident wavelength.   The design details have not yet appeared in the literature.

15.6. FEED-MOTION SYSTEMS

The scanning systems described in this section are used together with one of the focusing objectives of the earlier sections.   These scanners satisfy the general requirement of moving a point source rapidly over a curve or a surface in space.   The great majority of the feed-motion systems produce a beam moving through a plane in space so that the feed path is a plane curve.   If a scan over a volumetric region is desired, it can be obtained by a combination of several scans, each confined to a different plane.

There are two general methods of scanning over a plane, namely, "oscillating" scan and "saw-tooth" scan.   In the first, the beam sweeps across a plane and then returns by the same route; this can be accomplished simply by mechanical oscillation of the feed horn.   The saw-tooth scan is one in which the beam sweeps across the plane of scan and then steps back instantaneously to its initial point.   This normally requires a more complex feed system, but it is more efficient since the beam equally covers all positions in the plane of scan.

If we ignore the simple feed-horn oscillation, all existing feed-motion systems can be placed in three categories, namely, the virtual-source scanner, the organ-pipe scanner, and the moving-slot scanner.   In a practical application, the virtual-source scanner utilizes a source produced by a reflection, or a refraction, at some optical component between a real source and the focusing objective.   In most of these scanners, the feed horn, a real source, is rotated continuously in front of an imaging reflector, which forms the virtual source.   However, it is possible to obtain the same effect by holding the feed horn fixed and rotating a refractive prism.   In either case, the apparent feed-source motion is approximately saw-tooth in nature.

The organ-pipe scanner is a system in which rapid, rotary motion of a small feed horn is converted into motion along the desired feed path through the simple process of connecting, with waveguide channels, points on the feed circle to points on the desired feed path.   A variation in this system occurs when the feed horn is held fixed and a section of the waveguide channel is rotated to accomplish the same purpose.   The remaining type of feed-motion system employs a moving slot in a waveguide wall. These scanners yield motion along a straight line from some rotary motion in the feed system.

Lewis Scanner.   One of the earliest virtual-source scanners was the Lewis scanner, which employed a parallel-plate region. The action of this scanner is evident from Fig. 15-25, where rays from the real source strike a reflector strip at 45° to the antenna aperture and so produce a virtual source which feeds the lens.   The straight-line feed path is formed into a circle by rolling the parallel-plate region into a cylinder.

Fig. 15-25. Lewis scanner.

A rotation of the feed about the base of the cylinder produces a virtual source which appears to be moving along a straight line.   Some dead time occurs when the feed horn is opposite the position on the cylinder where the two ends of the feed path are joined.   The amount of dead time depends on the length of the feed path and the size of the feed horn; normally, it represents about 20 per cent of the scanning time.

Robinson Scanner.   The Robinson scanner[33] is a virtual-source system, made up in parallel plates in a manner similar to that of the Lewis scanner.   The major differences

are the absence of the focusing lens and the use of a more complex imaging reflector. This scanner uses a developable surface which, in planar form, is an isosceles trapezoid. When the surface is developed, the smaller base is bent to lie above the larger base and then the two ends of the base are brought together to form a circle (Fig. 15-26). Since the surface was developed from a plane, ray paths can be found from a consideration of the rays in a plane. Rays emanating from a horn moving on the feed circle leave the aperture in the same manner as those rays which might come from a feed
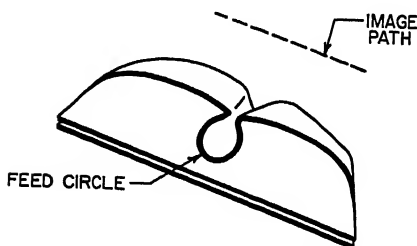
FIG. 15-26. Robinson scanner.

moving along the smaller base of the trapezoid. The rotary horn motion then produces an apparent linear motion of a virtual source.

The dead time found in this feed-motion system occurs when the feed is opposite the end points of the smaller trapezoid base; its value depends on the feed-horn size and the circumference of the feed circle and so is similar to that of the Lewis scanner.

Virtual-source Scanner. In this system, the feed horn rotates in the lower level of a two layer parallel-plate region.[34] Energy from the feed is reflected into the upper layer by a parabolic cylinder placed at the junction between the upper and lower layers (Fig. 15-27). The reflected rays appear to come from a virtual source which moves along an approximately linear path while the feed horn moves through an arc of 120°.

The center of the feed-horn circle corresponds to the focal point of the parabolic cylinder; its radius is about 80 per cent of the focal length. Since this feed is used for only 120° of rotation, a complete system would require three feed horns and a suitable switching mechanism. The dead time for this system will then depend on the amount of the rotation cycle required to switch from one feed to the next.
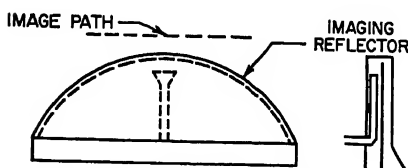
FIG. 15-27. Virtual-source scanner.
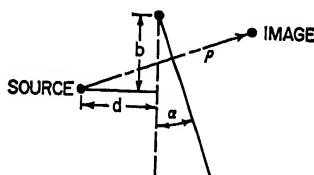
FIG. 15-28. Tilting-plane scanner.

Tilting-plane Scanner. A variation of the virtual-source scanner is obtained when the feed horn is held fixed as it directs the energy into a plane reflector. The reflected rays appear to come from a virtual source behind the reflector. The position of this virtual source depends on the orientation of the plane. Consider an initial position with the plane vertical and the source in a horizontal plane a distance d from the reflector. If the plane is tilted about a horizontal line at a distance b from the horizontal plane (Fig. 15-28), then the equation of the virtual-source path is given by $\rho = 2(d \cos \alpha + b \sin \alpha)$.

Prism Scanner. It was shown that virtual sources could be obtained using various types of reflectors. Similar sources can be obtained using refracting elements such as prisms. In its simplest form, the prism scanner would employ an element placed between the feed and the objective and positioned near the feed. Figure 15-29 shows two possible prisms—the circular element in which scanning is obtained by simple rotation and the triangular element in which scanning is achieved by an oscillation of the triangle.

The design problems associated with this type of scanner are concentrated on obtaining a good virtual source and minimizing the curvature of the path, followed by the virtual source during the scan cycle. From the nature of the problem, most of the design work is experimental in nature.
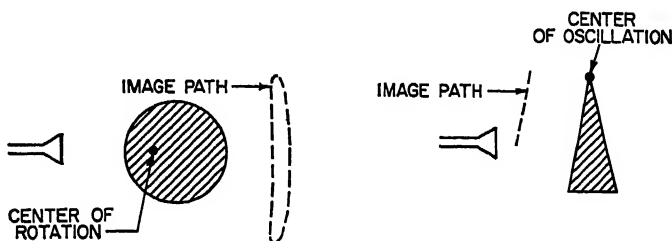
FIG. 15-29. Prism scanners.

NRL Organ-pipe Scanner.[35] The action of this scanner can best be understood by considering Fig. 15-30. It can be seen that energy is introduced into certain wave-guide channels at the feed circle. It propagates through these waveguides, which are all of equal length to the aperture of the system. A rotation of the feed horn produces a change in the channels which are fed and so produces a motion of the radiated energy across the scanner aperture.

The problems associated with this scanner are centered in the transition region between the feed horn and the waveguide channels. By proper choice of dimensions here, the transition loss can be held to less than 0.25 db. The standing-wave ratio is minimized by maintaining the intersection between channels to a value less than
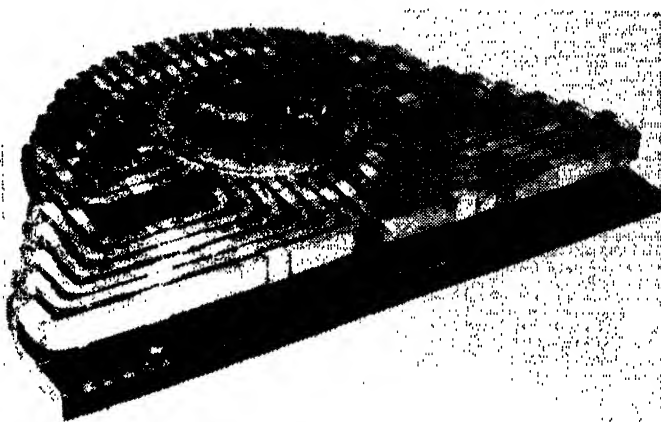
FIG. 15-30. NRL organ-pipe scanner.

$\frac{1}{64}$ in. It was found that the VSWR varied with feed rotation, depending on the number of channels which were fed at any one time; best results were obtained using a horn which energized $2\frac{1}{2}$ waveguide channels.

A variation in this basic structure would permit the scanner aperture which did not lie along a straight line but fitted any design curve. Another variation would involve a change in the spacing between the channel outputs; such a change would produce a nonuniform scanning with a constant rotation of the feed horn.

Sectoral Organ Pipe. If a circular feed path is desired, the radius of the feed circle can be minimized by introducing a sector of an organ pipe. In this system, channels

on the feed circle follow radial lines to the desired scan circle. For constant feed rotation, several horns and a waveguide switch are required.

RCA Organ Pipe.[16] A variation of the organ-pipe principle is obtained when the feed horn is held fixed and a section of the waveguide channels is rotated. One of the possible channel-rotation systems is shown in Fig. 15-31. From a consideration of the figure, it is seen that with rotation of the cylindrical-channel region the radiated energy is moved along the scanner aperture.

Tape Scanner. The simplest type of moving-slot scanner involves the physical motion of slots in one face of a waveguide.[16] One system considered is shown in Fig. 15-32. Here energy in a linear length of waveguide is radiated through two slots which move along the waveguide length. To couple out all energy within the guide, it is necessary to move an effective waveguide short circuit in synchronism with the slots. This is done by gearing to the tape drive a rotary phase shifter which is terminated in a short circuit.

The major problem associated with this system is that of obtaining a tape which will fit tightly against the fixed waveguide section and yet will be flexible enough to pass

FIG. 15-31. RCA organ-pipe scanner.
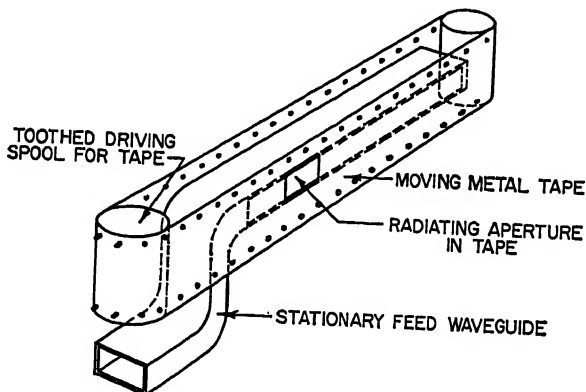
FIG. 15-32. Tape scanner.

around the rotor. One additional problem relates to the means of providing r-f chokes around the periphery of the open-sided waveguide. Successful choke designs were obtained and good results were found using metal plate in place of the tape.

Helical-slot Scanner. Another type of moving-slot scanner utilizes the similar waveguide system with one waveguide wall removed. The slot radiator is formed between the waveguide opening and a helical opening on a circular cylinder (Fig. 15-33).

FIG. 15-33. Helical-slot scanner.

As the cylinder is rotated, the effective radiating aperture moves along the straight line corresponding to the position of the opening in the waveguide.[37]

The major difficulty encountered in the design of this scanner was traced to the r-f choke problem. Any chokes parallel to the waveguide opening were inefficient at the

position of the radiating slot because of the lack of necessary "cover plate." Various remedies were attempted in order to improve this situation, including the use of both rectangular and circular waveguide. It was found impossible to obtain satisfactory radiation patterns because of the choke problem. It appeared that the rectangular waveguide was superior to the circular one, since the field within this guide held the same polarization whereas the polarization varied in the circular waveguide with motion of the slot.

15.7. LINE-SOURCE SCANNING SYSTEMS

The systems considered under this heading are formed from a line source, together with some means of varying the phase along the line source. In each case a fan beam is scanned which can be focused into a pencil beam by means of an additional focusing element.

Prism Scanners. One means of scanning with a line source employs an adaptation of the optical prism. The beam from the line source passes through the prism and is deflected at an angle which depends on the prism construction and its orientation with respect to the line source. A motion of the prism can be arranged to produce a scan of the beam. The simplest prism would employ an oscillating motion; however, the prism could be formed as a cone which could be rotated about a line other than the cone axis to produce a scanning of the beam.

Another possibility would involve a prism composed of a metal-plate medium. If the line source were varied in frequency, then the effective index of the prism would vary for the different frequencies. The result would be a scanning of the beam which passes through the prism.

Foster Scanner. An ingenious method of introducing phase shift in the beam from a line source employs a parallel-plate region formed between two cones.[38] In its
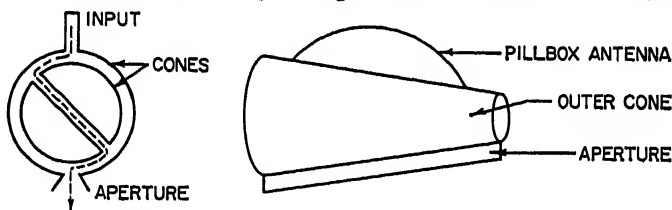
FIG. 15-34. Foster scanner.

simplest form, the line source is mounted along an element of the outer cone. Energy from the line source is introduced into the parallel-plate region so that it propagates through the region between the cones. This energy then leaves the parallel-plate region through a radiating aperture which lies along an element of the outer cone.

The scanning action of this antenna can be understood by considering Fig. 15-34. The energy in the parallel-plate region is carried between the surfaces of the cones, passes through a planar region within the inner cone, and then propagates again through a section of the curved region to the output aperture. When the plane section coincides with the input and output apertures, a fixed reference phase appears across the output. As the cone is rotated so that energy passes through the curved regions and the plane region, additional phase delay is introduced in the rays at the base compared with those at the top, since the arc length at the base is greater than that at the top. It is possible then, with a rotation of the cone, to achieve a variation in phase across the aperture, and hence obtain the scanning of the radiated beam.

The modification in the basic design involves placing the line source on the inner cone. In this system, the plane parallel-plate region is eliminated and scanning is obtained by varying the position of the line source with respect to the aperture. When

the line source coincides with the aperture, a certain reference phase is obtained across the aperture. As the inner cone is rotated so that the line source leaves the aperture, the path length across the base of the cone is greater than that across the top so that the phase at the base of the aperture is delayed with respect to that at the other end, and hence scanning is obtained.
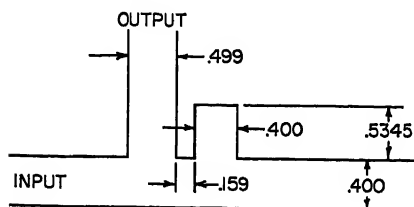
FIG. 15-35. Choke barrier for Foster scanner.

For narrow-band operation, the best arrangement for a Foster scanner involves using the line source on the inner cone, together with an r-f choke arrangement for directing the wave toward the output aperture.[38] At the output aperture, another choke arrangement is used to deflect the beam into free space. The details of this choke are shown in Fig. 15-35.

Scanning Arrays. A scanning system can be obtained by using a waveguide slot array and varying the phasing between the individual slots. One widely used system is known as the Eagle scanner.[39] This employs a variation in the wide dimension of waveguide to produce a variation in the phasing velocity of the wave within the guide, and hence a variation in the element phasing. The most effective scanner has employed a feed at either end of the waveguide and a switching mechanism between the two feed points. The difficulties encountered on this scanner are largely mechanical, since a reciprocating motion of the waveguide walls is necessary in order to achieve scanning. A further problem is the high mismatch and loss in gain when the beam is scanned to a position normal to the waveguide array.

Another slot array was built into coaxial line in which the inner conductor was rotated so that the disks moved in an eccentric manner to vary the phasing velocity of
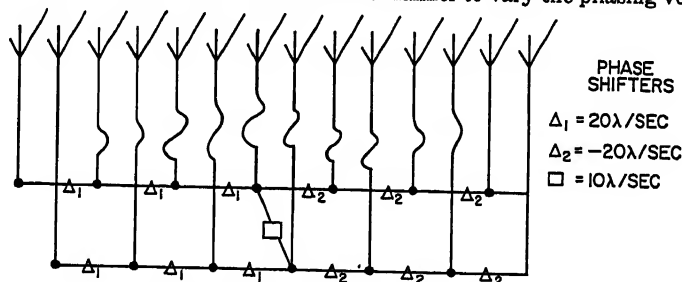
FIG. 15-36. Schematic of FH-MUSA scanner.

the wave in the coaxial line. The simple rotation to obtain scanning made this system attractive, but there was a limit to the amount of phase variation which could be achieved, and hence a limit to the possible scan angle.

A third system replaced the simple array elements with a continuous slot at the upper and lower corner of the narrow waveguide wall. This system used a motion of the narrow waveguide wall, which produced a variation in the phase velocity, and hence a scan of the radiated beam.

Another method of scanning using an array involves varying the phase velocity in the waveguide by varying the frequency of the transmitting source. Since no r-f chokes and no mechanical motion are required, this type of scan yields a simple antenna system. A final method of scanning using an array involves feeding the array elements individually and introducing a phase shift in the transmission lines leading to each element. A very successful scanner of this type employed a 14-element system with 13 phasing elements.[40] A schematic of the transmission lines in this system is given in Fig. 15-36. The only apparent disadvantages of the system lie in the com-

plexity of the transmission lines and the fact that some $2\frac{1}{2}$ db loss occurs in the transmission-line network.

Scanning with Circular Array. A relatively simple type of scanner can be obtained using an array of dipole or slot elements mounted on a circular cylinder. Each array element is connected through transmission line to an r-f commutator assembly mounted in the center of the array. The amplitude of the phase of the individual elements will depend on the transmission line used and on the feed system associated with the commutator. Many different types of excitation are possible[41]; the most widely used has been that in which all elements are in phase on the cylinder or in which the phasing is arranged so that all elements are in phase along a line tangent to the circle.

One system, which has been constructed, has proved to be rather successful in the UHF frequency band.[42] One hundred broadband dipoles were mounted on a cylindrical reflector whose diameter was 30 ft and whose height was 6 ft. The commutator and feed system were arranged so that 36 of the dipole elements were energized at any one time. Scanning was obtained by simple switching in the commutator.

REFERENCES

1. W. M. Cady, M. B. Karelitz, and L. A. Turner: "Radar Scanners and Radomes," McGraw-Hill Book Company, Inc., New York, 1948. A discussion of scanning systems from a practical standpoint.
2. R. K. Luneberg: "Mathematical Theory of Optics," Brown University Press, Providence, R.I., 1944. A theoretical discussion and application of mathematics to optics.
3. J. E. Eaton: "An Extension of the Luneberg-type Lenses," *Naval Research Lab. Rept.* 4110, 1953. A variation of the Luneberg-lens problem in which the source is permitted to lie within the unit sphere and lenses produce other wavefronts as well as the plane wave.
4. G. D. M. Peeler and D. H. Archer: "A Two-dimensional Microwave Luneberg Lens," *Naval Research Lab. Rept.* 4115, 1953. A description of a two-dimensional Luneberg lens constructed between almost-parallel plates. It includes mathematical and experimental considerations of the lens characteristics.
5. A. H. Schaufelberger and L. F. Culbreth: "A Geodesic Analogue of the Luneberg Lens," paper presented at 1955 URSI meeting in Washington, D.C. A lens composed of a parallel-plate region; experimental data showed low side lobes. The lens is basically that of Ref. 10.
6. G. D. M. Peeler, K. S. Kelleher, and H. P. Coleman: "Virtual Source Luneberg Lenses," *Naval Research Lab. Rept.* 4194, 1953. An analytical discussion, with experimental data, of the characteristics of a Luneberg sphere with metallic planes passing through the center.
7. J. Brown: "Microwave Wide Angle Scanner," *Wireless Eng.*, vol. 30, no. 10, p. 250, 1953. A study of the Luneberg lens with feed within the unit sphere.
8. A. S. Gutman: "Modified Luneberg Lens," *J. Appl. Phys.*, vol. 25, 1954. A description of a lens in which the feed can be mounted within the unit sphere.
9. R. F. Rinehart: "A Solution of the Rapid Scanning Problem for Radar Antennae," *J. Appl. Phys.*, vol. 19, p. 860, 1948. A derivation of a mean surface in a parallel-plate region, which surface serves as an analogue to a two-dimensional Luneberg lens.
10. R. F. Rinehart: "A Family of Designs for Rapid Scanning Radar Antennas," *Proc. IRE*, vol. 40, no. 6, p. 687, 1952. A derivation of lenses similar to that of Ref. 9, except that a plane dielectric region permits the use of a smaller feed circle.
11. F. G. R. Warren and S. E. A. Pinnell: "Tin Hat, Scanning Antennas," RCA Victor Co., Montreal, Canada. An analogue of the Luneberg lens which has tangents at its periphery, whose directions are in the plane of propagation.
11a. K. S. Kunz: "Generalization of the Rinehart-Luneberg Lens," *J. Appl. Phys.*, vol. 25, p. 642, 1954.
11b. G. Toraldo: "Conflection Doublets," *J. Opt. Soc. Am.*, vol. 45, p. 621, 1955. Application of optical techniques to the Surface of Revolution scanner.
11c. G. Toraldo: "A Family of Perfect Configuration Lenses of Revolution," *Optica Acta (Paris)*, vol. 1, no. 4, p. 157, 1955. Generalization of Myers and Rinehart's work.
12. M. C. Volk and G. D. M. Peeler: "A Three-dimensional Microwave Luneberg Lens," paper presented at 1955 URSI meeting in Washington, D.C. A description of a lens constructed of a center spherical core and spherical shells of increasing radius.

13. R. W. Corkum: "Isotropic Artificial Dielectric," *Proc. IRE*, vol. 40, no. 5, p. 574, May, 1952. A theoretical and experimental analysis of dielectric spheres in a low-dielectric base medium.

14. W. O. Puro and K. S. Kelleher: "Isotropic Variable Index Media," IRE Convention Record, pt. 1, Antennas and Propagation, 1954. A theoretical and experimental investigation of spherical voids in a dielectric.

15. S. S. D. Jones: "A Wide Angle Microwave Radiator," *Proc. IEE (London)*, pt. III, vol. 97, p. 225, July, 1950.

16. H. B. Devore and H. Iams: "Microwave Optics between Parallel Conducting Sheets," *RCA Rev.*, vol. 9, December, 1948. A discussion of several microwave optics devices studied at RCA during and immediately after World War II.

17. S. B. Myers: "Parallel Plates Optics for Rapid Scanning," *J. Appl. Phys.*, vol. 18, no. 2, p. 211, February, 1947. A discussion of the general figure-of-revolution scanner formed as the mean surface of a parallel-plate region. This article discussed the scanner of Ref. 16 and considered other scanners in which the mean surface was a cone.

18. W. Rotman: "A Study of Microwave Double Layer Pillboxes. Part I, Line Source Radiators," Air Force Cambridge Research Center Rept. AF CRC-TR-54-102, July, 1954. Discussion of several types of antennas related to those of Ref. 17.

19. A. Bouwers: "Achievements in Optics," Elsevier Press, Inc., Houston, Tex., 1950. A discussion of the work on optics in The Netherlands during and immediately previous to World War II.

20. H. N. Chait: "A Microwave Schmidt System," *Naval Research Lab. Rept.* 3989, 1952. An analytical and experimental investigation of the Schmidt lens system in a microwave parallel-plate structure.

21. K. S. Kelleher and H. P. Coleman: "Off-axis Characteristics of the Paraboloidal Reflector," *Naval Research Lab. Rept.* 4088, 1952. A study of radiation patterns from paraboloids and spheres.

22. K. Schwarzchild: "Untersuchungen zur geometrischen Optik," pt. II, *Ges. Wiss. Gottingen Math. Phys.*, Klasse IV, 1905; and H. Chrétien: "Cours de calcul des combinaisons optiques," *Rev. Opt.*, 1938, pp. 572–586. A mathematical discussion of multiple reflector telescope systems.

23. Reference 1, p. 55. A discussion of a Schwarzchild scanner used in the microwave region.

24. J. P. A. Martindale: "Lens Aerials," *J. Brit. IRE*, May, 1953. A discussion of lenses used in scanning applications.

25. F. C. Friedlander: "A Dielectric-lens Aerial for Wide-angle Beam Scanning," *J. IEE (London)*, pt IIIa, vol. 93, no. 4, p. 658, 1946. A description of a dielectric lens which satisfies the Abbe sine condition.

26. B. A. Lengyel: "Physical Optics of Metal Plate Media, Part 1. Theoretical Considerations," *Naval Research Lab. Rept.* 3534, 1949. A discussion, including graphs of the performance expected, of metal-plate media.

27. N. I. Korman and J. R. Ford: "An Achromatic Microwave Antenna," *Proc. IRE*, vol. 38, no. 12, p. 1445, December, 1950. A brief mathematical discussion of a broadband lens using metal-plate media.

28. J. Ruze: "Wide Angle Metal Plate Optics," *Proc. IRE*, vol. 38, p. 53, January, 1950. Design equations with experimental data for constrained metal-plate lenses.

29. G. D. M. Peeler and W. F. Gabriel: "Volumetric Scanning Antenna," Convention Record of IRE, 1955. This describes the feed-and-lens system of a scanning antenna. The lens has two-point correction, together with on-axis correction obtained by a stepping technique.

30. C. Goatley and C. F. Parker: "Symmetrical Microwave Lenses," Convention Record of IRE, 1955. A discussion of three microwave lenses, together with experimental data.

31. J. Ashmead and A. B. Pippard: "The Use of Spherical Reflectors as Microwave Scanning Aerials," *J. IEE (London)*, pt. IIIa, March, 1946. Analysis and experimental data on several spherical-reflector systems.

32. K. S. Kelleher and H. H. Hibbs: "A New Microwave Reflector," *Naval Research Lab. Rept.* 4141, 1953. An analysis, together with experimental data, on two types of parabolic-torus reflectors.

33. Reference 1, p. 45. A description of the Robinson scanner.

34. K. S. Kelleher: "A Virtual Source Scanner," *Naval Research Lab. Rept.* 3957, 1952. An analysis, together with experimental data, of a virtual-source system formed in a two-layer-pillbox region.

35. K. S. Kelleher and H. H Hibbs: "An Organ Pipe Scanner," *Naval Research Lab. Rept.* 3842, 1951. A discussion of the design, together with experimental data, of an organ-pipe scanner.

36. W. F. Gabriel: Unclassified paper presented at Third Scanning Symposium, Naval Research Laboratory, 1953. A description of an experimental model of the tape scanner.
37. W. F. Gabriel: Unclassified paper presented at Third Scanning Symposium, Naval Research Laboratory, 1953. A discussion of the basic problems associated with chokes in the helical-slot scanner.
38. R. C. Honey and E. M. T. Jones: "A Mechanically Simple Foster Scanner," paper presented at 1955 URSI meeting in Washington, D. C. Discussion of the improvement obtained in the Foster scanner when the toothed barriers are replaced by choke barriers.
39. Reference 1, p. 185. Discussion of Eagle scanner.
40. M. J. Kelly: "Radar Systems and Components," p. 845, D. Van Nostrand Company, Inc., Princeton, N.J., 1949. A discussion of a polyrod array used in a fire-control radar.
41. R. H. Duhamel: "Pattern Synthesis for Antenna Arrays on Circular, Elliptical, and Spherical Surfaces," University of Illinois, Electrical Engineering Research Laboratory, Urbana, Ill., 1952. Mathematical discussion of radiation patterns from arrays.
42. R. C. Benoit and W. M. Furlow: "Wullenweber-type Ultra-high-frequency Radio Direction Finder," paper presented at 1955 IRE meeting in New York. Discussion of a 100-element circular array operating from 100 to 1,000 Mc.

Chapter 16

SURFACE- AND LEAKY-WAVE ANTENNAS

Francis J. Zucker

Air Force Cambridge Research Laboratories
Bedford, Massachusetts

16.1. INTRODUCTION

The terms *surface-* and *leaky-wave antennas* cover a large variety of structures. What ties these together is a common point of view in their design, which is based on the characteristics of the traveling wave that propagates along the antenna aperture. Because the aperture is generally several wavelengths long, surface- and leaky-wave antennas become physically large at low frequencies. They find some use as ground structures in the h-f band, but their principal applications lie slightly below and in the microwave region.

Surface- and leaky-wave antennas are part of the larger class of traveling-wave antennas. Other traveling-wave antennas include long wires and rhombics (Chap. 4), helical antennas (Chap. 7), and slot arrays (Chap. 9).

The three basic types of traveling-wave antennas treated in this chapter are shown in Fig. 16-1. The dielectric-rod antenna (Fig. 16-1a) supports a *surface wave*, or *trapped wave,* so called because it carries its energy within a small distance from the interface. This wave does not radiate except at a discontinuity, such as the termination of the structure. The radiation pattern, usually end-fire, can be viewed as a combination of direct radiation from the feed F and surface-wave radiation from the transverse plane T passing through the terminal discontinuity. Such *end-fire surface-wave antennas* (Secs. 16.3 and 16.4) can be constructed of dielectric material, as

in Fig. 16-1a, or of artificial dielectric such as a corrugated-metal surface. Their principal use is in low-silhouette or flush-mounting applications.

The traveling wave carried by a two-wire line (Fig. 16-1b) is still a surface, or trapped, wave, but discontinuities placed at intervals along the line—in this instance, proximity-coupled dipoles—make the antenna radiate like an array of slots cut into waveguide. The pattern characteristics of such *surface-wave-excited arrays of discrete elements* (Secs. 16.5 and 16.6) are analogous to those of the nonresonant slot array (Chaps. 5 and 9), but design information, by comparison with that on slot arrays, is rather meager. As with slots, beams can be shaped and they can be produced at any angle with the array axis (other than broadside, which is difficult to achieve).
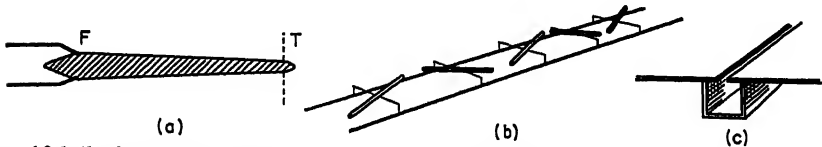
FIG. 16-1. Surface- and leaky-wave antenna types: (a) Dielectric rod. (b) Array of proximity- coupled dipoles (thin lines are dielectric supports). (c) Long slot in waveguide.

The traveling wave that results when discontinuities are so densely spaced along the line that there are many per wavelength, or they in fact merge into a continuous perturbing structure, is illustrated by the long slot in waveguide (Fig. 16-1c). Because the wave radiates continuously as it travels along the aperture, this type is called a *leaky wave* (Secs. 16.7 and 16.8). Although they closely resemble surface-wave-excited arrays of discrete elements in techniques and varieties of pattern control, leaky-wave antennas have the disadvantage that the main beam cannot be placed in the back quadrant ($90° < \theta < 180°$, where θ is the angle off end fire). They have, on the other hand, several advantages: most leaky-wave antennas can be mounted on curved surfaces, many can be frequency-scanned from near broadside to near end fire without beam broadening, and design information available on some of them is so precise that pattern specifications can be met with the highest accuracy.

Two antenna structures treated in this chapter are also discussed in other chapters. Information on the ordinary Yagi-Uda array in Chap. 5 is supplemented here with data especially applicable to long Yagis, for which the surface-wave aspect is the dominant design principle. Slot arrays are fully treated in Chap. 9 from the point of view of discrete elements fed from a common waveguide. When dealing with very closely spaced nonresonant slots, or a continuous slot along the entire length of the antenna, it is best to base the design on the leaky-wave concept. These types of slot arrays are therefore covered here rather than in Chap. 9.

Surface- and leaky-wave antennas can be designed for omnidirectional coverage, shaped beams, fixed pencil beams, scanning in elevation or azimuth, and for any kind of polarization. Because of their large diversity, they have few features in common. Most of them lend themselves to flush, or at least low-silhouette, installation. A few of them attain pattern bandwidths of 2:1, the more usual being around ±10 or ±15 per cent. Most of them are easily impedance-matched. Their many airborne and missile applications include antennas for communications, search radar, command guidance, ground mapping, and homing. When high power is not a requirement, they lend themselves well to printed-circuit techniques. With the exception of several television and ionospheric scatter antennas in France and satellite-tracking antennas in the United States, no ground applications have been reported, though the field looks promising.

16.2. PROPERTIES AND MEASUREMENT OF SURFACE AND LEAKY WAVES

For design purposes, a surface wave is sufficiently characterized by a single parameter, for example, the wavelength in the direction of propagation along the interface, and a leaky wave by two parameters, usually the wavelength and the leakage attenuation along the interface. The various surface- and leaky-wave parameters will now be defined and formulas given for their interrelationship; it will then be shown how the parameters can be calculated if the surface impedance is known, or how they can be determined by measurements.
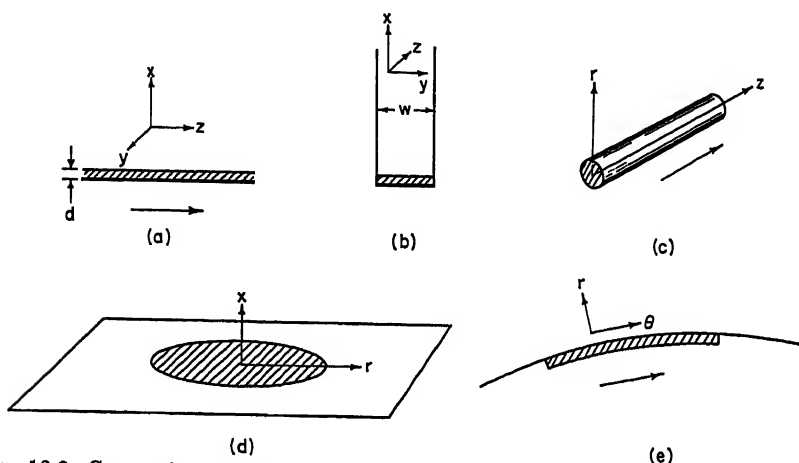
Fig. 16-2. Geometries for surface-wave propagation over dielectric sheets: (a) Infinite plane sheet-on-metal. (b) Rectangular duct. (c) Axial-cylindrical rod. (d) Radial-cylindrical sheet-on-metal. (e) Azimuthal-cylindrical or spherical cap. Heavy lines indicate metal surfaces. Arrows point in direction of propagation.

Interrelationship of Parameters. The governing relation is the separability condition for the wave equation. In rectangular coordinates (Fig. 16-2a),

$$k_x{}^2 + k_y{}^2 + k_z{}^2 = k^2 \qquad (16\text{-}1)$$

where the k's, called wave numbers, are in general complex, for example, $k_x = \beta_x - j\alpha_x$, with β_x the phase constant in radians per unit length (inches, centimeters, or meters), and α_x the attenuation in nepers per unit length. The wave number k is that of the medium in which the wave travels, $k = \omega \sqrt{\epsilon_0\mu_0}$, with ω the angular frequency, ϵ_0 the dielectric constant, and μ_0 the permeability. In air, k is pure real; it is related to the wavelength λ by $k = \beta = 2\pi/\lambda$ and to the phase velocity of light c by $k = \omega/c$. Similarly, the phase constant β_z along the surface is related to the surface wavelength λ_z by $\beta_z = 2\pi/\lambda_z$ and to the surface phase velocity v_z by $\beta = \omega/v_z$. The following ratios are therefore equivalent:

$$\frac{\beta_z}{k} = \frac{\lambda}{\lambda_z} = \frac{c}{v_z} \qquad (16\text{-}2)$$

When this ratio is greater than 1, we speak of a "slow" wave (i.e., slower than light, because $v_z < c$); when less than 1, of a "fast" wave ($v_z > c$). The surface wavelength λ_z of slow waves is shorter than λ; of fast waves, longer than λ (as in shielded waveguide).

A *surface* wave is one that propagates parallel to the interface and decays vertically to it; that is, the phase constant β_z is zero, and $k_x = -j\alpha_x$ (pure attenuation), with α_x positive. Assume first that the wave extends indefinitely in the transverse direction, so $k_y = 0$ (Fig. 16-2a). Equation (16-1) requires that k_z be pure real, that is, there can be no attenuation in the direction of propagation, and we obtain the simple but basic relation

$$\beta_z{}^2 = k^2 + \alpha_x{}^2 \qquad (16\text{-}3a)$$

or equivalently, using Eq. (16-2),

$$\frac{\lambda}{\lambda_z} = \frac{c}{v_z} = \sqrt{1 + \left(\frac{\alpha_x\lambda}{2\pi}\right)^2} \qquad (16\text{-}3b)$$

from which it follows that this is a slow wave. Equation (16-3b) is plotted as the dashed line in Fig. 16-3b. Slower-than-light surface waves are used chiefly in end-fire antenna design (Secs. 16.3 and 16.4). Figure 16-3a illustrates constant-phase and constant-amplitude fronts, which are at right angles to each other provided only that the medium above the interface is lossless. (Ohmic losses in the surface produce a slight forward tilt in the phase front and a small α_z.) The more closely the surface phase velocity approaches that of light, the smaller is α_x [Eq. (16-3b)], and the larger, therefore, the vertical extent of the surface wave in Fig. 16-3a.

All components of the total electromagnetic field of the surface wave, for example, E_z, are of the form

$$E_z(x,z,t) = E_x e^{-\alpha_x x} \cdot e^{-j\beta_z z} \cdot e^{j\omega t} \qquad (16\text{-}4)$$

FIG. 16-3. Phase and amplitude contours of a plane surface wave: (a) Solid lines, constant-phase fronts; dashed lines, constant-amplitude fronts; shaded region shows amplitude decay. (b) Solid lines, height x/λ above surface of 3-db, 10-db, and 25-db constant amplitude or power contours as function of relative surface wavelength λ/λ_z, (use left-hand ordinate); numbers in parentheses refer to percentage of total energy carried by surface wave between interface and each contour. Dashed line, relation between relative surface wavelength and vertical attenuation $\alpha_x\lambda$ according to Eq. (16-3b) (use right-hand ordinate).

The vertical decay of the E_z, E_x, and H_y components of a TM surface wave ($H_z = 0$) is shown in Fig. 16-4a, and the composite electric-field lines over a full wavelength interval (longitudinal section) in Fig. 16-4b. It can be shown that E_z is in phase with H_y, E_x in phase quadrature. The first two components therefore carry all the power along the interface, while E_x and H_y form a vertically pulsating storage field. The dielectric slab-on-metal below the interface in Fig. 16-4 is used as an example. Since the form of Eq. (16-4), and thus of the surface-wave field lines, does not depend on the detailed structure of the medium below the interface, a multilayer dielectric or a corrugated sheet, etc., could have been shown equally well.

The field (or power) decay in decibels is plotted as a function of height x/λ above surface in Fig. 16-3b [based on Eq. (16-3a)]. Assuming a relative surface wavelength λ/λ_z (or relative phase velocity c/v_z) equal to 1.1, for example, the field at height $x = \lambda$ has decayed 25 db below its value at the interface.

Assume next that two parallel walls are erected normal to the surface, forming a duct in the z direction (Fig. 16-2b). [Examples other than the dielectric-loaded channel in this figure are the channel with corrugated bottom and the trough guide (Sec. 16.6).] The transverse wave number is fixed by the duct width w as in conven-

tional waveguide theory; from Eq. (16-1), we now have, instead of Eq. (16-3a),

$$\beta_z{}^2 = k^2 + \alpha_x{}^2 - \left(\frac{n\pi}{w}\right)^2 \qquad n = 0, 1, 2, \cdots \qquad (16\text{-}5a)$$

If $n = 0$ (no variation in y direction), Eqs. (16-3), and therefore also Fig. 16-3b, still apply. If $n = 1$ (half a sinusoid in y direction),

$$\frac{\lambda}{\lambda_z} = \frac{c}{v_z} = \sqrt{1 + \left(\frac{\alpha_x \lambda}{2\pi}\right)^2 - \left(\frac{\lambda}{2w}\right)^2} \qquad (16\text{-}5b)$$

Since the second term is usually smaller than the third, it follows that the wave is usually, though not necessarily, faster than light. Fast surface waves are used to
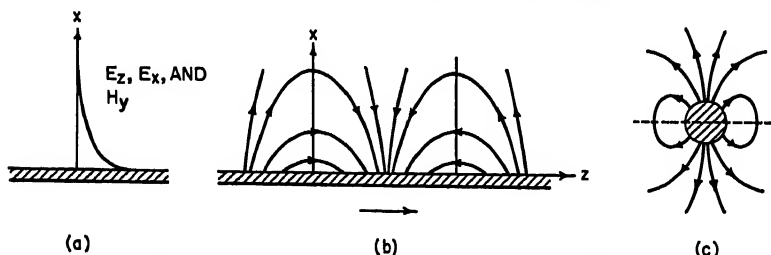
Fig. 16-4. Surface-wave field structure above interface: (a) TM-wave components on plane surface. (b) Composite electric-field lines over one-wavelength interval (arrow in direction of propagation). (c) Composite electric-field lines of HE_{11} wave on axial-cylindrical surface (cross section). Dashed line shows electric-image plane (Sec. 16.4).

excite arrays of discrete elements (Secs. 16.5 and 16.6). The field and power decay still follows Fig. 16-3a and b, provided that the abscissa in Fig. 16-3b is relabeled $\sqrt{(\lambda/\lambda_z)^2 + (\lambda/2w)^2}$ to account for the difference between Eqs. (16-3b) and (16-5b). The heights x/λ corresponding to the 25-db contour in Fig. 16-3b are useful for estimating the extent to which the duct walls, which theoretically must be infinite in height, may be lowered without perturbing the surface wave.

Surface-wave geometries other than rectangular are shown in Fig. 16-2c–e. The separability condition for the wave equation in axial- and radial-cylindrical coordinates (Fig. 16-2c and d) reads

$$k_r{}^2 + k_z{}^2 = k^2 \qquad (16\text{-}6)$$

(note that k_θ does not appear), which is formally identical with Eq. (16-1) for the case $k_y = 0$. The interrelationships of the surface-wave parameters given in Eqs. (16-3) still hold if k_r is substituted for k_z. Above the surface, the field components decay like Hankel functions; in the axial-cylindrical case, for example,

$$E_z(r,z,t) = E_z \cdot H_0{}^{(2)}(\alpha_r r) \cdot e^{-j\beta_z z} \cdot e^{j\omega t} \qquad (16\text{-}7)$$

The circumferential field dependence in the case of the HE_{11} mode—the one of principal interest in this geometry—is one full sinusoid. Composite E lines for this *hybrid* wave (so called because of the presence of both E_z and H_z) are shown in Fig. 16-4c. [The structure inside the circular interface could equally well be a metal rod with dielectric mantle, an array of circular disks (cigar antenna), or even an array of dipoles (Yagi).] For large radii, the Hankel function is asymptotic to the exponential, and Eq. (16-7) differs negligibly from Eq. (16-4). As a consequence, the 25–db contours in Fig. 16-3b still hold and the 10-db contours nearly so; these curves are useful in estimating the degree of coupling between adjacent end-fire line sources.

In the radial-cylindrical case, the field components decay exponentially away from the surface, so that Fig. 16-3b applies exactly. But the constant-amplitude fronts will now no longer be parallel to the surface because the field components decay radially like Hankel functions (asymptotically like $1/\sqrt{r}$), bringing the fronts closer to the surface with increasing r.

In the azimuthal-cylindrical or spherical case it can be shown that the wave numbers are always complex, so that these surface waves are no longer completely trapped. Because the radius of curvature is usually large, it is convenient to treat azimuthal waves as a perturbation of Eqs. (16-3) for flat surfaces.

A *leaky* wave is one that radiates continuously as it propagates along a plane interface. Assuming $k_y = 0$, which is usually the case, Eq. (16-1) reads

$$(\beta_x - j\alpha_x)^2 + (\beta_z - j\alpha_z)^2 = k^2 \tag{16-8a}$$

[Upon substitution of β_r and α_r for β_x and α_x, Eq. (16-8a) also holds in axial- and radial-cylindrical coordinates.] Equating imaginary parts,

$$\alpha_x\beta_x + \alpha_z\beta_z = 0 \tag{16-8b}$$

where α_z and β_z are of equal sign (attenuation in direction of propagation along surface), β_x is positive (leakage away from surface), and α_x is therefore negative; that is, the leaky-wave field *increases* away from the interface. The phase and amplitude fronts can now be sketched (Fig. 16-5); they are at right angles to each other, as in the surface-wave case;

Fig. 16-5. Phase and amplitude fronts of a plane leaky wave. Solid lines, constant-phase fronts; dashed lines, constant-amplitude fronts; shaded region shows amplitude decay.

in fact, the leaky wave looks like an upside-down, tilted surface wave. It is convenient to introduce a *net* phase constant $\beta = \sqrt{\beta_x{}^2 + \beta_y{}^2}$ and a *net* attenuation constant $\alpha = \sqrt{\alpha_x{}^2 + \alpha_y{}^2}$, as indicated in Fig. 16-5. Equating the real parts of Eq. (16-8a), one finds

$$\beta^2 - \alpha^2 = k^2 \tag{16-8c}$$

which means that in the direction of emergence the leaky-wave phase velocity is slower than that of light [cf. Eq. (16-3a)]. The phase constant along the interface is (Fig. 16-5)

$$\beta_z = \beta \cos\theta = k\sqrt{1 + \left(\frac{\alpha}{k}\right)^2} \cos\theta \tag{16-9}$$

which may be larger or smaller than k, depending on the amount of *net* attenuation in the leaky wave and on its angle of emergence; it is usually smaller, and along the interface, leaky waves are therefore usually, though not necessarily, faster than light. The angle of emergence, using Eqs. (16-9) and (16-2), is

$$\cos\theta = \frac{\beta_z}{\beta}$$

$$= \frac{\lambda}{\lambda_z} \frac{1}{\sqrt{1 + (\alpha\lambda/2\pi)^2}} \tag{16-10a}$$

If $\alpha\lambda$ is much smaller than 2π, as is usually the case, we may write

$$\cos\theta = \frac{\lambda}{\lambda_z} \tag{16-10b}$$

Antenna designs based on leaky waves are described in Secs. 16.7 and 16.8.

Calculation of Surface- and Leaky-wave Parameters. Surface waves are modes on unshielded waveguides; leaky waves are "improper" modes, so called because they violate the radiation condition [negative α_x, Eq. (16-8a)]. Both are solutions of the homogeneous (source-free) wave equation subject to the boundary conditions at the interface. As in the case of shielded waveguides, the boundary-value problem is often conveniently stated in terms of the "transverse resonance condition," which requires that the equivalent network of a transverse section through the waveguide be resonant.[1] With Z_x the impedance looking straight up from the interface, and Z_s the surface impedance looking straight down, the resonance condition reads

$$Z_x + Z_s = 0 \qquad (16\text{-}11)$$

Z_x depends on the geometry and the mode; in rectangular coordinates,

$$Z_x = \frac{k_x}{\omega\epsilon_0} \qquad \text{for TM waves} \qquad (16\text{-}12a)$$

$$Z_x = \frac{\omega\mu_0}{k_x} \qquad \text{for TE waves} \qquad (16\text{-}12b)$$

In the case of a surface wave, $k_x = -j\alpha_x$; Z_x is therefore capacitive in Eq. (16-12a) and inductive in Eq. (16-12b). It follows from Eq. (16-11) that the TM surface wave requires an inductive surface, $Z_s = jX_s$, and the TE surface wave a capacitive surface, $Z_s = -jX_s$ (X_s positive). Equation (16-11) now reads

$$\frac{\alpha_x}{k} = \frac{X_s}{R_e} \qquad \text{for TM waves} \qquad (16\text{-}13a)$$

$$\frac{\alpha_x}{k} = \frac{R_e}{X_s} \qquad \text{for TE waves} \qquad (16\text{-}13b)$$

where $R_e = \sqrt{\mu_0/\epsilon_0} = 377$ ohms. β_s or λ/λ_s follow immediately from Eqs. (16-3). Leaky waves, for which k_x is complex, require a complex surface impedance to satisfy Eq. (16-11). Instead of a single equation for α_x [Eq. (16-13a) or (16-13b)], one then obtains two equations, yielding α_x and β_x, and therefore β_s and α_s [Eqs. (16-8)].

Knowledge of the surface impedance thus solves the boundary-value problem. It is instructive to calculate this impedance for two simple cases: surface waves on a dielectric slab-on-metal and on a corrugated-metal sheet. Looking down from the air-dielectric interface in Fig. 16-2a, one sees a dielectric-loaded region short-circuited at the end. Using transmission-line theory, assuming that the wave is TM, and noting that a wave that is TM in the direction of propagation is also TM transverse to it,

$$X_s = \frac{k_x}{\omega\epsilon_1} \tan k_x d \qquad (16\text{-}14)$$

where k_x is the vertical wave number in the slab of dielectric constant ϵ_1. Since X_s must be positive real, $k_x = \beta_x$. [One could now write the field components below the interface in the form of Eq. (16-4), with a sinusoidal variation in x replacing the exponential decay; the field configuration below the interface, however, is rarely of interest to the engineer.] Substitution of Eq. (16-14) in Eq. (16-13a) gives one equation in two unknowns, α_x and β_x. α_x is a function of β_s through Eq. (16-3a); β_x can also be expressed as a function of β_s, since Eq. (16-1) reads

$$\beta_x^2 + \beta_s^2 = k_1^2$$

in the dielectric medium ($k_1 = \omega\sqrt{\mu_1\epsilon_1}$). The solution[2] shows that the lowest TM mode has no cutoff and that the phase velocity of the surface wave lies between c and $c\sqrt{\epsilon_1/\epsilon_0}$, approaching the free-space velocity in air for very thin sheets and

the free-space velocity in the dielectric for thick sheets (numerical results in Sec. 16.4). The analysis for a TE wave uses Eq. (16-13b) and results in a lowest mode that does have a cutoff. It is worth pointing out that below cutoff a surface wave does not become evanescent but ceases to exist altogether.

The interface of the corrugated-metal sheet (Fig. 16-6) is an imaginary plane through the top of the teeth. X_s is zero over the teeth and equals $R_c \tan kd$ over the grooves, which are short-circuited parallel-plane transmission lines (inductive in the range $0 < kd < \pi/2$). If there are many grooves per wavelength, the surface impedance over the teeth and grooves may be averaged; that is, $X_s \cong [g/(g + t)]R_c \tan kd$. Substitution in Eq. (16-13a) gives one equation in one unknown. The results of this approximation turn out to be good provided there are at least five grooves per wavelength. A more exact calculation takes into account the higher-order (below-cutoff) modes at the mouth of the grooves, which produce higher-order waves along the interface that modify the field lines sketched in Fig.

FIG. 16–6. Corrugated-metal surface. Arrow points in direction of propagation.

16-4a and b only in the close vicinity of the teeth (see Sec. 16.4 for numerical results). No TE wave exists because the E_y component is shorted out by the teeth.

The surface impedance of many structures can be found in the "Waveguide Handbook,"[1] but the subsequent calculations are not always simple. This is especially true of the complex transcendental equations that arise in the case of leaky waves, for which a special perturbation method has been developed.[3] If a structure is required whose surface- or leaky-wave parameters are not found in Sec. 16.4, 16.6, or 16.8 nor in the referenced literature, it is best to determine them by measurement.

Measurement of Surface- and Leaky-wave Parameters. In the case of surface waves, a vertical metal plate large enough to reflect at least 90 per cent of the incident energy (use Fig. 16-3b to determine minimum size) produces deep nulls at half-wavelength intervals along the surface. Because of turbulence in the aperture field near the feed, measurements should be made at a minimum distance from the feed given by

$$d_{\text{min}} \cong \frac{0.17\lambda}{(\lambda/\lambda_z) - 1} \qquad (16\text{-}15)$$

[see Eq. (16-19)]. If the frequency is so low that reflector size becomes a problem, the distance between nulls is found by feeding the probe signal into a phase-comparison circuit (using magic T and attenuator) that measures the traveling-wave phase with respect to a reference signal.

The probe used in these measurements should have a small cross section so as not to perturb the field. It needs chokes to suppress antenna currents on its outer conductor, and it must couple only into the E or the H field, with good discrimination against the unwanted one. A coaxially-fed monopole or a waveguide horn pinched at the mouth (with dielectric loading to keep it above cutoff)[4] is very satisfactory; loops and horizontal dipoles less so. The distance between probe and aperture should be as small as possible without perturbing the aperture field, and it should be held constant by providing a rigid probe carriage.

Using Eq. (16-10b), λ_z of a leaky wave can be determined from the direction of the main beam in the radiation pattern. Alternatively, to measure λ_z and at the same time α_z, one can use the same probe-and-comparison-circuit method as with surface waves, but it is usually simpler and more accurate to compare the phase and power level at the termination of a section of leaky waveguide with the phase and power level at the end of an equal-length unperturbed waveguide. Let ϕ be the phase at the termination of, say, the long slot in Fig. 16-1c as measured by a probe inserted into the guide, and ϕ' the phase in the same location when the slot has been filled or covered

with metal.   The unknown leaky wavelength is given by

$$\frac{1}{\lambda_s} = \frac{1}{\lambda_s'} + \frac{\phi - \phi'}{2\pi} \tag{16-16}$$

where the wavelength λ_s' in the shielded waveguide must also be measured.   Similarly, let P be the power level in decibels at the end of the long slot and P' the power level in decibels in the shielded guide; then

$$\alpha_s = \frac{P' - P}{\ell} \quad \text{db/unit length}$$

$$= 0.115\,\frac{P' - P}{\ell} \quad \text{nepers/unit length} \tag{16-17}$$

where ℓ is the length of the slot in arbitrary units.   If high accuracy is required, wall losses in the test section must be taken into account.

The measurement of *discontinuities* on surface waveguides is discussed in Sec. 16.5.

16.3. SURFACE-WAVE ANTENNAS: DESIGN PRINCIPLES

The design philosophy is developed first for line sources, then for arrays of line sources and area sources.   Special beam-shaping techniques, circular polarization, and scanning are treated at the end of this section.
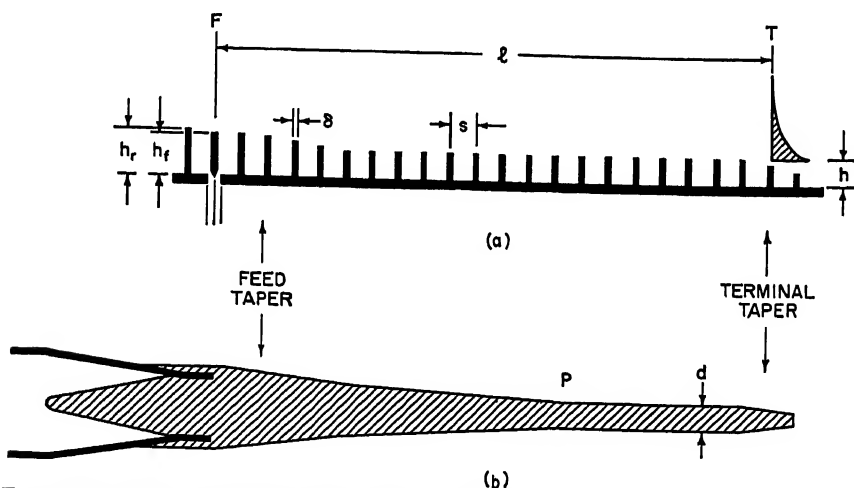
FIG. 16-7. Surface-wave antenna structures: (a) Yagi (row of monopoles) on ground plane, excited by dipole-reflector combination. (b) Dielectric rod, excited by circular or rectangular waveguide (broad wall in plane of paper).   Structure (a) is shown optimized for maximum gain or minimum beamwidth, (b) for low sidelobes.

Radiation of Surface-wave Antennas.   Before presenting design principles (for optimum gain, beamwidth, sidelobe level, and bandwidth), it is useful to examine how surface-wave antennas radiate.   Two typical structures are shown in Fig. 16-7. The feed F (consisting of a monopole and reflector in Fig. 16-7a and of a circular or rectangular waveguide in Fig. 16-7b) couples a portion of the input power into a surface wave, which travels along the antenna structure to the termination T, where it radiates into space.   The ratio of power in the surface wave to total input power (efficiency of excitation) is usually between 65 and 75 per cent.   Power not coupled

into the surface wave is directly radiated by the feed in a pattern resembling that radiated by the feed when no antenna structure is in front of it.

The tapered regions in Fig. 16-7 serve diverse purposes. The *feed taper* increases the efficiency of excitation and also affects the shape of the feed pattern. The *body taper* (extending to point P in Fig. 16-7b) suppresses sidelobes and increases bandwidth. At the termination T, some of the surface wave is reflected, the magnitude of the reflection coefficient R being small if the phase velocity is close to that of light:[5]

$$|R| \cong 1 - \frac{\lambda_s}{\lambda}$$

Because the reflected surface wave spoils the pattern and bandwidth of the antenna, a *terminal taper* is used to reduce it to a negligible value.

The surface wave illuminates the terminal aperture (plane perpendicular to the antenna axis through T) in a circular region whose radius increases as the transverse attenuation of the surface wave diminishes, or equivalently, as the surface phase velocity approaches that of light [Eq. (16-3b)]. The larger the illuminated region, the higher the gain produced in the radiation pattern. Since the surface-wave phase front lies in the aperture plane, the pattern peaks in the end-fire direction. A simple but only approximate expression[6] for the terminal radiation pattern $T'(\theta)$ is

$$T'(\theta) \cong \frac{1}{(\lambda/\lambda_s) - \cos \theta} \quad (16\text{-}18)$$

FIG. 16-8. Radiation pattern of 4λ-long surface-wave antenna adjusted for maximum gain in accordance with Eq. (16-20b) ($\lambda/\lambda_s = 1.08$). $T(\theta)$ is the H-plane pattern of the surface-wave distribution in the terminal plane. For comparison, $\sin \xi/\xi$ is also shown (shaded region).

where θ is the angle off end fire, and λ_s is the surface wavelength at T (just to the left of the terminal taper, to be precise). This pattern has neither nulls nor sidelobes and, as expected, falls off more rapidly the closer λ/λ_s is to 1. More accurate expressions[7,8] and an experimental determination[9] indicate that the pattern is actually about 20 per cent narrower than in Eq. (16-18). The dashed line in Fig. 16-8 shows this corrected terminal radiation pattern for $\lambda/\lambda_s = 1.08$, which is the optimum relative phase velocity for a maximum-gain antenna 4λ long [Eq. (16-20b)].

The radiation pattern of the feed shown in Fig. 16-7a is quite broad (approximately a cardioid in polar coordinates). In combination with the terminal radiation $T(\theta)$, it produces the total surface-wave antenna pattern, shown by the solid line in Fig. 16-8 (experimental data for antenna length $\ell = 4\lambda$, $\lambda/\lambda_s = 1.08$). In the vicinity of end fire, the terminal pattern predominates; as θ increases, interference with the feed pattern first narrows the beam and then produces a sidelobe at 35°; beyond 45° the feed pattern predominates. Patterns of all surface-wave antennas adjusted for maximum gain look like those in Fig. 16-8, except that for antennas longer than 4λ the pattern spreads less in θ (first sidelobe closer to end fire than 35°), and for shorter structures it spreads more. The field beyond the first sidelobe falls off more rapidly the larger the end-fire gain of the feed radiation.

The curves in Fig. 16-8 are for the H plane, in which the element pattern of the

Yagi monopoles (Fig. 16-7a) is omnidirectional. In the E plane, $T(\phi)$ (ϕ is the angle off end fire) is narrowed by multiplication with the E-plane element factor (a dipole pattern modified by the effects of mutual impedance), which for $\phi < 60°$ approximates $\cos \phi$ and then decays more gradually (no null at $\phi = 90°$). The total pattern in the E plane is therefore also narrower than in the H plane, and sidelobes are lower by 2 to 3 db.

In the case of the HE_{11} mode on a dielectric rod (Fig. 16-7b), the E- and H-plane element factors, and consequently the beamwidths and sidelobe levels, are more nearly the same. The sidelobe level is now usually *higher* by 0.5 to 1.5 db in the E plane than in the H plane, the precise amount depending on the relative shape of the E- and H-plane feed patterns.

Instead of being regarded as a combination of feed and terminal radiation, the surface-wave antenna pattern can be viewed as an integral over the field distribution along the antenna structure. What this distribution looks like can be seen in Fig. 16-9: the amplitude $A(z)$ along the row of monopoles (Fig. 16-7a) starts with a hump near the feed and flattens out as the surface wave peels itself out of the near field of feed and feed taper.

FIG. 16-9. Amplitude $A(z)$ of field along surface-wave antenna structure. At ℓ_{min} surface wave is well established over its entire cross section.

The surface wave is well established at a distance ℓ_{min} from the feed where the radiated wave from the feed, propagating at the velocity of light, leads the surface wave by about 60°:

$$\ell_{min}k_s - \ell_{min}k = \frac{\pi}{3} \qquad (16\text{-}19)$$

[whence Eq. (16-15)]. The location of ℓ_{min} on an antenna designed for maximum gain is seen in Fig. 16-9 to be about halfway between feed and termination. Since the surface wave is fully developed from this point on, the remainder of the antenna length is used solely to bring feed and terminal radiation into the proper phase relation for maximum gain. (In the absence of a feed taper, ℓ_{min} occurs closer to F and the hump is higher.)

Were there no hump at all, the surface-wave antenna would radiate the familiar $\sin \xi/\xi$ pattern [$\xi = (\pi\ell/\lambda)(\lambda/\lambda_s - \cos \theta)$] produced by constant-amplitude illumination. This pattern is shown for comparison in Fig. 16-8 (shaded region); it is an unnatural pattern for parasitically excited antennas, which necessarily have feed turbulence.

Low sidelobe and broadband designs require tapers that extend over a substantial part of the antenna (Fig. 16-7b). Although the field along one particular taper has been examined in detail,[10,11] the effect of tapers on the total radiation pattern is not well understood. When the taper is very gradual, the phase velocity at each point has the value one would expect from the local surface impedance; when it is sharp, a leaky wave is produced, which fills in the minima of the pattern, widens the beam, and reduces sidelobes.

Design for Maximum Gain. The phase velocity along the antenna and the dimensions of the feed and terminal tapers in the maximum-gain design of Fig. 16-7a must now be specified.

If the amplitude distribution in Fig. 16-9 were flat, maximum gain would be obtained by meeting the Hansen-Woodyard condition (strictly valid only for antenna lengths $\ell \gg \lambda$; see Chap. 5), which requires the phase difference at T between the

surface wave and the free-space wave from the feed to be approximately $180°$:

$$\ell k_z - \ell k = \pi,$$

or, equivalently,

$$\frac{\lambda}{\lambda_z} = 1 + \frac{\lambda}{2\ell} \qquad (16\text{-}20a)$$

which is plotted as the upper dashed line in Fig. 16-10.

Since the size and extent of the hump are a function of feed and feed-taper construction, the optimum terminal phase difference for a prescribed antenna length cannot easily be calculated. Experimental work on Yagis (but without feed taper) by
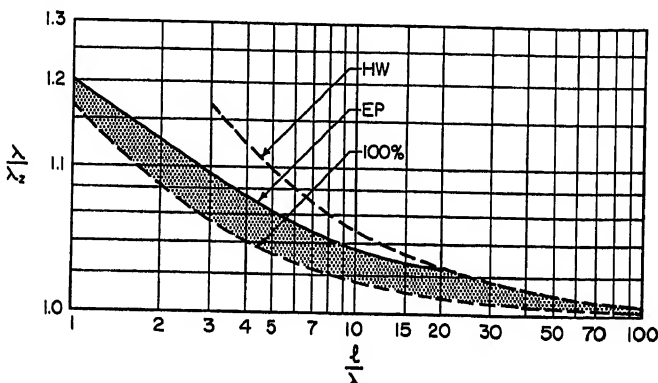
Fig. 16-10. Relative-phase velocity $c/v = \lambda/\lambda_z$ for maximum-gain surface-wave antennas, as a function of relative antenna length ℓ/λ. *HW*: Hansen-Woodyard condition, Eq. (16-20b); *EP*: Ehrenspeck and Poehler experimental values, Eq. (16-20b); 100 per cent: idealized perfect excitation, Eq. (16-20c).

Ehrenspeck and Poehler[12] and Ehrenspeck[13] has shown that the optimum terminal phase difference lies near $60°$ for very short antennas, rises to about $120°$ for ℓ between 4λ and 8λ, then gradually approaches $180°$ for the longest antenna measured (20λ). Therefore

$$\frac{\lambda}{\lambda_z} = 1 + \frac{\lambda}{p\ell} \qquad (16\text{-}20b)$$

with p starting near 6 for $\ell = \lambda$, diminishing to approximately 3 for ℓ between 3λ and 8λ and to 2 at 20λ. This relation is plotted as the solid curve in Fig. 16-10. In the presence of a feed taper, the optimum λ/λ_z values lie slightly *below* this curve.

If the efficiency of excitation is very high, interference between feed and terminal radiation is of minor importance, and the antenna need just be long enough so that the surface wave is fully established, that is, $\ell = \ell_{min}$ in Fig. 16-9. From Eq. (16-19),

$$\frac{\lambda}{\lambda_z} = 1 + \frac{\lambda}{6\ell} \qquad (16\text{-}20c)$$

which is plotted as the lower bound of the shaded region in Fig. 16-10.

Because feeds are more efficient when exciting slow surface waves than when the phase velocity is close to that of light, the solid line starts near the lower bound and ends at the upper. So long as λ/λ_z falls within the shaded region, its precise adjustment is not too critical; with $\ell = 4\lambda$, and in the presence of a feed taper, the gain drops only 1 db if λ/λ_z lies on the dashed lower instead of just below the solid upper bound.

Although this technique for maximizing the gain has been strictly verified only for

Yagi antennas, data available in the literature on other structures suggest that optimum λ/λ_s values lie on or just below the solid curve in all instances. To produce these optimum values, the dependence of λ/λ_s on the structural parameters of the antenna must be calculated or measured (as described in Sec. 16.2) or looked up in the literature; the more important cases are plotted in Sec. 16.4.

The feed taper should begin at F with λ/λ_s between 1.2 and 1.3 and extend over approximately 20 per cent of the full antenna length. Its exact shape is not important
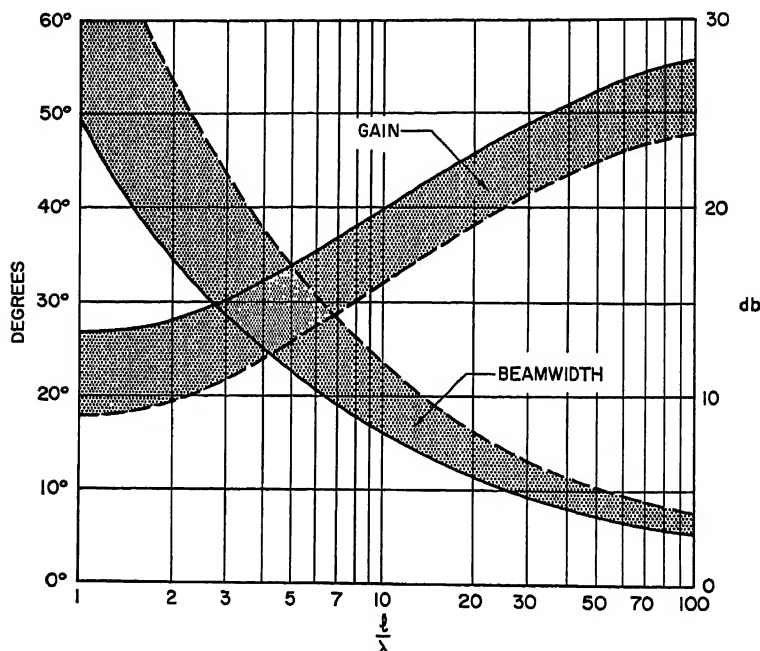
Fig. 16-11. Gain and beamwidth of surface-wave antenna, as a function of relative antenna length l/λ. For gain (in decibels above an isotropic source), use right-hand ordinate, for beamwidth, left-hand ordinate. Solid lines are optimum values; dashed lines are for low-sidelobe and broadband design.

so long as a smooth transition is made to the main body of the antenna. The terminal taper should be approximately 0.5λ long, and to match the surface wave to space, λ_s at the end of the taper should be as close as possible to λ. In the case of a polyrod ($\epsilon = 2.56$), for example, Fig. 16-18 shows that λ_s is reasonably close to λ when

$$d/\lambda = 0.23$$

and the end of the rod is therefore blunt rather than pointed.

The *gain* above an isotropic radiator of a long ($l \gg \lambda$) uniformly illuminated end-fire antenna whose phase velocity satisfies Eq. (16-20a) was shown by Hansen and Woodyard to be approximately

$$G \cong \frac{7l}{\lambda}$$

If the design is based on the optimal phase velocities and taper dimensions just described, the gain for l between 3λ and 8λ is

$$G \cong \frac{10l}{\lambda} \tag{16-21}$$

which is 1.5 db above the Hansen-Woodyard gain. For shorter lengths the gain may be 30 per cent higher; for longer lengths, the proportionality factor slowly decreases because of ohmic loss and the difficulty of designing an efficient feed. Maximum gains reported in the literature are plotted in decibels as a function of ℓ/λ in Fig. 16-11 (solid-line margin of shaded region marked "gain"). These gains involve a slight degree of "supergaining," but not enough to produce excessively narrow bandwidths or high ohmic loss.

The half-power *beamwidth BW* of a maximum-gain design is approximately

$$BW = 55 \sqrt{\frac{\lambda}{\ell}} \quad \text{degrees} \qquad (16\text{-}22)$$

which lies just above the lower (solid-line) margin of the shaded region marked "beamwidth" in Fig. 16-11. Equation (16-22) gives an average figure, the beamwidth, usually, being slightly narrower in the E plane and slightly wider in the H plane.

The *sidelobe* level, for ℓ between 3λ and 8λ, is about 11 db in the H plane and 10 or 14 db in the E plane of a dielectric rod or Yagi, respectively (cf. above). For shorter antennas the sidelobes are somewhat higher, for longer antennas lower.

The *bandwidth* within which the gain drops at most 3 db is between ± 10 per cent and ± 15 per cent; below the design frequency, gain slowly decreases as beamwidth widens; above it, the pattern deteriorates rapidly as the main beam splits and sidelobes rise.

By comparing Eq. (16-21) with the gain of a parabolic dish (assuming equal sidelobe level), the surface-wave antenna length is found to be related to the diameter d of an equal-gain dish by

$$\frac{\ell}{\lambda} \cong \left(\frac{d}{\lambda}\right)^2 \qquad (16\text{-}23)$$

This "trade-off" between a broadside and an end-fire structure becomes very disadvantageous to the latter as ℓ/λ increases, and surface-wave antennas longer than 10λ are rarely used. This limits the gain of surface-wave line sources in practice to 20 db. (Arrays of line sources and end-fire area sources are practical for much higher gains.)

The gain predicted by Eq. (16-21) is for feeds of the type shown in Fig. 16-7, with radiation patterns that are not very directive. Increasing the feed directivity increases the total antenna gain. For feeds whose radial extent is not much larger than the antenna cross section, it has been found experimentally[14] that a 1- or 2-db increase in the end-fire gain of the feed produces an approximately equal increase in the total antenna gain. If the feed is much larger than the antenna cross section, the gain continues to rise, though at a slower rate. A large horn aperture, corner reflector, or dish can add as much as 3 or 4 db. Structures of this sort are part surface-wave, part aperture antenna.
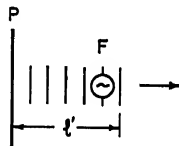
FIG. 16-12. Back-fire antenna. (Reference 15.)

The *back-fire* antenna, which also combines these two features, produces a gain about 4 db above that of Eq. (16-21).[15] It consists of a surface-wave line source (for example, a Yagi, Fig. 16-12) terminated by a flat circular plate P, which reflects the surface wave launched by the feed back toward F, where it radiates into space. Its radiation mechanism is not completely understood. The optimum phase velocity is chosen with the aid of the solid curve in Fig. 16-10, but ℓ in this context must be reinterpreted as twice the physical antenna length ℓ' of the backfire antenna, since the surface wave traverses the antenna twice. Using Eq. (16-20b), the relation between surface phase velocity and ℓ' (for ℓ' between 1.5λ and 4λ) is $\lambda/\lambda_z = 1 + \lambda/6\ell'$. The feed taper should be much reduced in size or omitted. The plate diameter d is

related to ℓ' by

$$\frac{d}{\lambda} \cong 1.5 \sqrt{\frac{\ell'}{\lambda}}$$

which implies that the plate is approximately as large as a parabolic dish whose gain equals that of the backfire antenna. For $\ell' = 2\lambda$, the gain is 19 db, sidelobes are 12 db down, bandwidth is at least 20 per cent. Easier and cheaper to build than a parabolic dish, the backfire antenna might be competitive for gains up to 25 db (provided sidelobes do not have to be very low); it is superior to ordinary end-fire antennas so long as low silhouette is not a requirement.

Design for Minimum Beamwidth. The approximate relation between E-plane beamwidth BW_E, H-plane beamwidth BW_H, and gain of a surface-wave antenna is

$$G \cong \frac{30,000}{BW_E BW_H}$$

The half-power beamwidth of a maximum-gain design [Eq. (16-22)] can be made 10 per cent narrower by increasing the direct feed radiation, which causes it to interfere destructively with $T(\theta)$ at a smaller angle θ than in Fig. 16-8. This is done by starting the feed taper with λ/λ_s less than 1.25. Narrowest beamwidths reported in the literature are plotted in Fig. 16-11 as the solid-line margin of the shaded region marked "beamwidth." (Usually E-plane patterns are slightly narrower, H-plane patterns slightly wider.) Sidelobes are about 1 db higher than in the maximum-gain case.

Design for Minimum Sidelobe Level. The fairly high sidelobes of the maximum-gain design can be reduced by increasing λ/λ_s to 1.35 at the start of the feed taper, letting $\lambda/\lambda_s \cong 1.2$ at the end of the feed taper and continuing to taper over a large fraction of the total antenna length (to P in Fig. 16-7b). In the constant cross-section region between P and T, λ/λ_s is chosen to lie on the lower margin of the shaded region in Fig. 16-10. If P is two-thirds of the distance from F to T, the sidelobes of a 6λ-long antenna are down at least 18 db in the H plane and 17 or 21 db in the E plane of a dielectric rod or yagi, respectively, at the cost of a 1.5-db drop in gain and a 10 per cent rise in beamwidth.[16,17] As in the case of the optimum-gain design, the sidelobe level decreases monotonically with increasing antenna length.

The backlobe is suppressed by increasing the end-fire directivity of the feed pattern. A 25- to 30-db level can be achieved without resorting to feeds that are much larger than the antenna cross section.

By tapering more sharply near F, then flattening out gradually to a value of λ/λ_s close to 1 at T, the H-plane sidelobe level can be reduced to 20 db.[17] Gain and beamwidth then lie on the dashed margins of the shaded bands in Fig. 16-11. (No precise design information is available on this technique.) A further reduction to 30 db in the H-plane sidelobe level is achieved by

FIG. 16-13. Parasitic side rows for sidelobe suppression in one plane (top view; dots indicate dipoles, or monopoles above a ground plane).

placing parasitic side rows on either side of the center array[18] (Fig. 16-13). The side-row length ℓ' is slightly longer than 0.5ℓ. λ/λ_s is the same as on the center array [use Eq. (16-20b)], and the spacing d is optimum when the side rows lie just beyond the 11-db contour of the surface wave on the center array; or, using Fig. 16-3b and Eq. (16-20b),

$$\frac{d}{\lambda} \cong 0.25 \sqrt{\frac{\ell}{\lambda}}$$

The gain is the same as for a maximum-gain design [Eq. (16-21)].   To reduce side-lobes in all planes, parasitic side rows would have to be placed all around the center array.

Design for Broad Pattern Bandwidth.[19]   The ±15 per cent bandwidth of most surface-wave antennas can be extended to as much as ±33 per cent (2:1) at the cost of a 2-db gain decrease from optimum at mid-frequency.   At the feed, the mid-frequency value of λ/λ_s should be 1.4.   A uniform taper extends from the feed to the termination, as shown in Fig. 16-1a.   At the low-frequency end of the band, gain and beamwidth lie close to the solid margins of the shaded strips in Fig. 16-11; at the high-frequency end, close to the dashed margins.   Thus gain is constant within ±1.5 db and beamwidth within ±15 per cent.   On a structure 13.5λ long at mid-frequency, sidelobes were down at least 11 db throughout the band.[19]

The bandwidth figures just quoted apply to the polyrod ($\epsilon = 2.56$) and to all surface-wave antennas whose dispersion curve (variation of λ/λ_s with frequency) resembles that of the polyrod.   The data presented in Sec. 16.4 show that dispersion increases with increasing dielectric constant; dielectric rods with $\epsilon < 2.56$ are therefore more broadband and rods with $\epsilon > 2.56$ less broadband than polyrods.   The dispersion of artificial dielectrics varies; corrugated surfaces are comparable with polyrods, Yagis are considerably more dispersive (precise bandwidth figures not known).

The input impedance of most surface-wave antennas is slightly capacitive and changes slowly with frequency.   A tapered dielectric section in waveguide (Figs. 16-1a and 16-7b) provides good matching over a 2:1 bandwidth if 1.5λ long at mid-frequency, and over a smaller bandwidth if shorter.   To minimize the VSWR, an inductive iris is placed close to the insertion point of the rod.   Equivalent techniques apply in the case of antennas other than dielectric rods, and input transmission lines other than waveguide.

Feeds.   Design principles of feeds and feed tapers for optimum gain, sidelobes, and bandwidth have already been stated.   Specific structures will now be described.

In Fig. 16-7a, the feeder and reflector monopoles are spaced 0.2λ apart, $h_r = 0.23\lambda$, and $h_f = 0.21\lambda$.[12]   These figures apply to $\delta = 0.048\lambda$; if the elements are thicker, they must be made slightly shorter.   The backlobe is between 12 and 15 db down.   By replacing the reflector monopole with a semicircular plate (radius = h_r) or a small corner or parabolic reflector (height = h_r), one increases the gain of the feed by at least 1.5 db, and therefore (see above) the total antenna gain by approximately the same amount.   The sidelobes are decreased by at least 2 db; the backlobe is 25 to 30 db down.

To couple from the dominant mode in rectangular waveguide, one replaces the feeder monopole by a metal half ring[20] (Fig. 16-14a); the excitation efficiency of this feed, with semicircular reflector plate, is around 80 per cent.   Another, slightly less efficient but simpler, waveguide feed uses two or more slots to couple into the surface-wave structure.   The waveguide should be dielectric-loaded so that its phase velocity approximates that in the surface-wave structure, and the slots are spaced about a quarter wavelength apart in the dielectric.   Instead of cutting slots, the entire broad face of a dielectric-filled waveguide can be opened (Fig. 16-14b); by tapering the height of the waveguide over the appropriate length, feed and feed taper can be combined in a single design.   In low-power applications, strip lines can be slot- or dipole-coupled to the antenna.[21]   In the absence of the ground plane one uses a center-fed dipole (coaxial input with built-in balun, Fig. 16-14c) or a folded dipole (usually preferred with two-wire input).

The coaxially fed metal cap (Fig. 16-14d), popular as a dielectric-rod feed or "cigar"-antenna feed at UHF because of good efficiency combined with mechanical strength, forms the transition between feed types a and b of Fig. 16-7.   Type b can handle much higher power than type a.   In Fig. 16-7b the waveguide can be rectangu-

lar (with TE_{10} mode) or circular (TE_{11} mode). A variant of this form, suitable for Yagi or cigar-antenna excitation, is shown in Fig. 16-14e. If the horn aperture is considerably larger than the antenna cross section (Fig. 16-14f), the surface-wave structure should start well inside, and it is in fact desirable to have the horn extend just beyond the end of the feed taper, as indicated. (Theoretical work shows that, for their size, horn apertures are not very efficient surface-wave exciters,[22] but if the direct-feed radiation of the horn is well collimated—the design can be based on Chap. 10—a large total antenna gain will be produced.)

Patterns that closely approximate the sin ξ/ξ shape have been obtained by flaring a parallel wire into a 60° V (Fig. 16-14g),[23] or by running an unflared parallel wire (loaded with transverse wire stubs to reduce phase velocity) alongside the antenna;[24] both
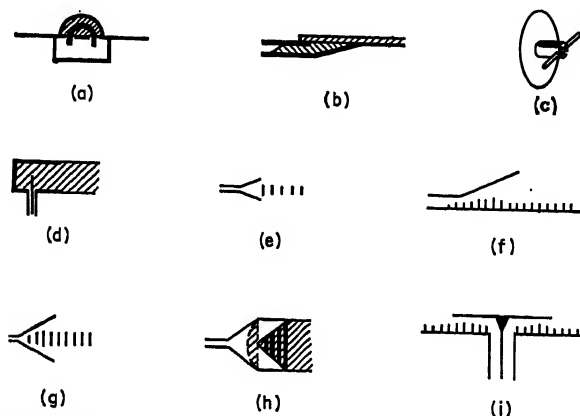
FIG. 16-14. Surface-wave antenna feeds: (a) Semicircular wire coupled to waveguide. (Reference 20.) (b) Dielectric-filled waveguide with open broad wall. (Reference 38.) (c) Dipole and reflector feed. (d) Circular waveguide cap. (e) and (f) Horn exciters. (g) Parallel-wire (distributed) feed. (Reference 23.) (h) Flared transition with lossy strips (with collimating lens shown in horn aperture). (Reference 27.) (i) Coaxial excitation of disk.

structures extend over a third of the antenna length. Feeds of this type are called *distributed*. In the hope of obtaining good phase and amplitude control over the entire antenna aperture, feeds have been studied that couple continuously from one end of the antenna to the other, for example, a waveguide slot-coupled to a dielectric slab.[25,26] These designs have not been very successful to date, principally because energy flow along two such closely coupled waveguides is difficult to control. If precise aperture illumination is desired, one must abandon surface-wave antennas and turn to the end-fire structures among the surface-wave-excited arrays of discrete elements (Secs. 16.5 and 16.6).

Variants of Fig. 16-7a and b are also used to excite surface-wave area sources. Rectangular dielectric or corrugated surfaces are fed by placing a slotted waveguide alongside, or a hoghorn, or a horn with correcting lens (Chap. 14). The last is frequently plagued by transverse standing waves, which produce sidelobes in azimuth (yz plane). To suppress these, a flared transition (1λ long at mid-frequency) with transverse conducting ("aquadag") strips can be used (Fig. 16-14h).[27] It keeps sidelobes below 20 db over a frequency range of at least 2:1, at a cost of 1 or 2 db due to the lossy strips.

Radial-cylindrical area sources (disks, Fig. 16-2d) can be center-fed with a simple monopole feeder; its efficiency of excitation turns out to be higher than with line

sources. A higher-gain feed is shown in Fig. 16-14i, where the coaxial input is excited in the TEM mode for vertical polarization on the disk and in the TE_{01} mode for horizontal polarization. A completely flush installation could be achieved by coupling through two or more annular slots. All the arrangements previously described for line sources can be carried over, and the optimum design principles for feed and feed taper still apply.

Special feeds for circular polarization and scanning are mentioned at the end of this section.

Arrays of Line Sources. Yagis, dielectric rods, and other surface-wave line sources can be arranged in a plane or volume array. The surface-wave illumination in the terminal plane of a plane array is scalloped (Fig. 16-15a), the overlapping dotted
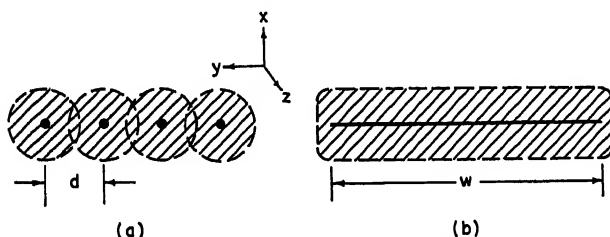
Fig. 16-15. Two-dimensional surface-wave antennas: (a) Array of line sources. (b) Area source. (Transverse cross sections.)

circles representing the 25-db contours of the transverse field decay. Assuming identical end-fire elements and negligible interaction between them, the array gain G_a is the sum of the individual gains G. Letting n be the number of elements and using Eq. (16-21),

$$G_a = nG \cong 10n \frac{\ell}{\lambda} \qquad (16\text{-}24)$$

Interaction between adjacent elements is found to be negligible if the crossover is at about the 12-db contour; the minimum separation d is therefore [Fig. 16-3b and Eq. (16-20b)]

$$\frac{d}{\lambda} \cong 0.5 \sqrt{\frac{\ell}{\lambda}} \qquad (16\text{-}25a)$$

The exact value depends on the polarization (coupling is less in the E than the H plane) and on the direct coupling between feeds. Too close a spacing produces a loss in gain. An upper limit on the spacing is obtained by requiring that the first principal sidelobe of the array pattern be strongly attenuated through multiplication with the element pattern. The angle with end fire of the array sidelobe must therefore be at least that of the first minimum in the element pattern, a criterion that corresponds to a crossover of about 22 db, or a maximum separation

$$\frac{d}{\lambda} \cong \sqrt{\frac{\ell}{\lambda}} \qquad (16\text{-}25b)$$

The principle of pattern multiplication, which has just been invoked, is useful only for a first design, since the element patterns are somewhat distorted by the presence of the other elements. The optimum spacing, which lies somewhere between the d/λ values given by Eqs. (16-25), must therefore be found empirically.

The beamwidth BW_a in the plane of the array (azimuth) is approximately

$$BW_a \cong \frac{65\lambda}{nd} \quad \text{degrees} \qquad (16\text{-}26)$$

Sidelobes can be reduced by tapering the amplitude at the feeds. In the elevation plane, beamwidth and sidelobes are controlled by the element pattern. The bandwidth is less than for individual elements, probably about ±5 per cent.

Low-silhouette requirements often force the choice of a horizontal plane array of end-fire elements in place of a vertical cylindrical reflector (or rectangular mattress array). The trade-off between them, assuming equal gain and sidelobes and equal width in the y direction (Fig. 16-15a), is

$$\frac{\ell}{\lambda} \cong \left(\frac{h}{\lambda}\right)^2 \qquad (16\text{-}27)$$

[cf. Eq. (16-23)], where ℓ is the length of the end-fire elements and h the height (in the x direction) of the equivalent reflector or broadside array. Because of space limitations, the line sources cannot always be equal in length. Equation (16-24) is then inapplicable, but the spacing between elements is still controlled by Eqs. (16-25).

A volume array of end-fire elements occupies almost as large an area in the transverse (xy) plane as the dish it replaces and has advantages in terms of transportability, ease of erection, and minimum weight needed for mechanical strength against certain kinds of stresses. Spillover is more easily controlled than with a conventional dish, but sidelobe control becomes more difficult and the bandwidth is much narrower. In the design of these arrays, the number of end-fire elements can be reduced by increasing their length; according to Eq. (16-24), $n = G\lambda/10\ell$. This relation clarifies the trade-off between an end-fire volume array and a broadside mattress array of dipoles: though one cannot increase the total gain by replacing the dipoles with higher-gain end-fire elements, one can reduce the number of elements (and thus of separate feeds) while keeping the gain constant.

Arrays of end-fire elements can be fed in cascade from a common transmission line (like slots in waveguide), but a corporate feed structure (branching transmission lines) produces better bandwidth.

Area sources are usually rectangular or circular (Fig. 16-2d). The terminal-plane illumination, sketched in Fig. 16-15b for the rectangular case, is smooth. With w the width and ℓ the length of a rectangular area, the gain G_a is

$$G_a \cong 12\frac{w}{\lambda}\sqrt{\frac{\ell}{\lambda}}$$

(assuming 11-db sidelobes). Beamwidths are given by Eqs. (16-22) and (16-26). Sidelobes in azimuth are those of the feed. Bandwidth is better than for arrays of line sources. Equation (16-27) still describes the trade-off with a cylindrical reflector of the same width and gain.

The gain of a circular disk (diameter $2r$) is approximately $4.5\sqrt{r/\lambda}$. Beamwidth in elevation is $50\sqrt{\lambda/r}$ degrees; in azimuth the pattern is omnidirectional. Sidelobe level in elevation is controlled as in the case of a line source. Bandwidth is at least 20 per cent. The trade-off between disk diameter and height h of an equivalent axial line source is $2r/\lambda \cong (h/\lambda)^2$, which is of the same form as Eqs. (16-23) and (16-27).

In a compromise between a plane array of end-fire elements and a continuous area source, the end-fire elements are sometimes spaced much closer than prescribed by Eq. (16-25a). The element pattern is then appreciably distorted by scattering from the neighboring elements, and the amplitude and phase distribution at the feeds, calculated to produce a prescribed pattern, must be modified by trial and error to produce this pattern in fact.[29]

The elevation pattern of area sources can be controlled to some extent by placing them on a finite and curved ground plane (see below).

Effect of Finite Ground Plane on the Radiation Pattern. Vertically polarized surface-wave line or area sources are often mounted on a ground plane whose finite length g (Fig. 16-16a) distorts the antenna pattern in two ways: by tilting the beam through an angle ψ away from end fire and by broadening it to a half-power beamwidth BW'. The tilt is maximum when $g = 0$ (no ground plane in front of antenna):[30,31]

$$\psi_{max} \cong 60 \sqrt{\frac{\lambda}{\ell}} \quad \text{degrees}$$

(which is a full half-power beamwidth BW of the unperturbed pattern); the beam then broadens so that the 3-db level lies in the end-fire direction, and BW' is slightly over twice as wide as the unperturbed BW (Fig. 16-16b and c). The tilt can be reduced by slowing the surface wave down from its infinite-ground-plane optimum, but this increases sidelobes and decreases gain. The gain, on the other hand, is optimized by speeding the wave up, at the expense of increased tilt.[31]

As g increases, the beam tilt decreases: when $g = \ell$, $\psi \cong 0.7\psi_{max}$; $g = 3\ell$, $\psi \cong 0.5\psi_{max}$; $g = 20\ell$, $\psi \cong 0.2\psi_{max}$—a very gradual approach to the infinite-ground-plane condition. The beamwidth approaches the unperturbed value more rapidly: when $g = \ell$, $BW' \cong 1.25 BW$.[30] Modifying the surface-wave velocity again has an opposite effect on beam tilt and gain.

If no beam tilting or loss in gain can be tolerated, flush mounting must be abandoned

(a)

(b)   (c)

(d)

FIG. 16-16. Effect of finite ground plane on the radiation pattern of an end-fire antenna: (*a*) Finite ground plane. (*b*) Pattern on infinite ground plane. (*c*) Pattern in absence of ground plane. (*d*) Antenna on curved ground plane.

in favor of a full-size structure (pod-mounted to reduce drag, if necessary). A less drastic remedy is to reduce the tilt angle, at a small cost in gain, by bending the antenna and ground plane into a cylindrical or spherical "cap."[32–34] The curvature produces an attenuation in the surface wave, which can be enhanced by tapering the antenna along its entire length (Fig. 16-16d). If the total attenuation is such that about 50 per cent of the power has leaked off before the surface wave reaches the termination, the tilt angle will be reduced to near zero no matter how short the ground plane.[31]

Beam-shaping Techniques. A finite, flat ground plane can be used to advantage when a tilted beam is desired. With $g = \ell$, for example, the tilt angle ψ is somewhat smaller than ψ_{max}, the sidelobe level is low, and the gain only slightly less than optimum for that antenna length.

The leakage attenuation caused by bending the antenna not only brings the beam down closer to end fire but also fills in the nulls of the elevation pattern. By also tapering the antenna and by varying g and bending the ground plane (Fig. 16-16d), cosecant-squared or other shaped patterns in elevation can be closely approximated.

Beam-shaping methods are seen to be rather limited and largely based on cut-and-try procedure. Attempts to synthesize a prescribed pattern by varying the surface impedance along the antenna, and thus generating an entire spectrum of surface and leaky waves ("modulated" surface waves), have not yet borne fruit for the engineer.

Linear and Circular Polarization. The HE_{11} mode on a dielectric rod or other rotationally symmetric structure is linearly polarized in a plane fixed by the orientation of the feed (vertical in Fig. 16-4c). The plane can be rotated by turning the feed mechanically or by using a ferrite rotator.[35]

Circular polarization is obtained by exciting any structure that is symmetric in at least two orthogonal planes—dielectric rod, cigar antenna, array of crossed dipoles—with a circularly polarized feed. By changing feeds, left- and right-hand circular polarization and cross polarization can be obtained from a single structure.

The helix (Chap. 7), which is a surface-wave antenna when operated in its axial mode, produces a circularly polarized pattern whose handedness depends on the sense in which the helix turns. Twisting a Yagi[24] or any other line source through 180° along its length and letting the surface phase velocity satisfy the Hansen-Woodyard condition also produces a circularly polarized pattern, but sidelobes are high.

The TM mode on a flat surface is vertically polarized (Fig. 16-4b), the TE mode horizontally. In Sec. 16.4 two area sources are described whose parameters can be chosen so that the surface will support a TM and a TE mode with identical phase velocities. By exciting these with equal amplitude and a phase difference of 90°—the feed design is rather involved[34]—a circularly polarized end-fire pattern is produced.[6]
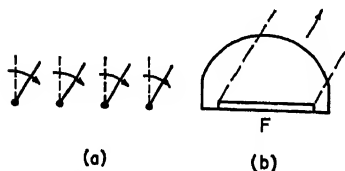
FIG. 16-17. Scanning of surface-wave antennas: (a) Mechanical rotation of individual line-source elements. (b) Electronically scanned area source (F is the linear feed array).

Scanning. Arrays of line sources can be scanned mechanically by rotating the array as a whole. Because of the directivity of the element patterns, electronic scanning by phase shifting between feeds in an array is necessarily confined to small angles.[35] [If each element could be tilted about its feed point (Fig. 16-17a),[36] the combined electromechanical scan angle would be larger, though still limited by the requirements of Eqs. (16-25).] With suitable ferrite components in the feed lines, beam switching or lobing and circular or spiral scan can all be accomplished.[35]

Area sources are scanned in azimuth by scanning the line-source feed; to keep the antenna length independent of scan angle, the area can be shaped as in Fig. 16-17b. A corrugated surface of this shape has been frequency-scanned over ±30° with no deterioration in its low-sidelobe azimuth and shaped elevation pattern.[37]

The Luneberg lens and its variants (Chap. 15) can be constructed in the form of a dielectric disk that supports a TM surface wave.[38] Excited near its rim by a rotating feed of the type shown in Fig. 16-14b, this lens can be scanned 360° in azimuth, with modest control over the beam shape in elevation.

16.4. SURFACE-WAVE ANTENNAS: SPECIFIC STRUCTURES

Numerical values of λ/λ_s and design details for specific structures are presented in this section. None of the general design information in Sec. 16.3, which is applicable to all surface-wave antennas, will be repeated here. Line sources are listed before area sources; in both instances, dielectric structures precede their artificial dielectric counterparts.

The λ/λ_s curves are displayed for several values of relative dielectric constant ϵ, ranging from 2.56 (polystyrene) to 165 (a calcium titanate ceramic). Hard, low-loss, high-temperature materials are of special interest, for example, fused quartz ($\epsilon \cong 3.7$), pyroceram ($\epsilon \cong 5.6$), and alite (an aluminum oxide, very durable, $\epsilon \cong 8.25$).

The dielectric-loss tangent δ, which is temperature-dependent, produces a plane-

wave attenuation

$$\alpha\lambda = \sqrt{\epsilon}\ \tan\ \delta$$

in an infinite medium, but since a large fraction of the surface wave propagates outside the medium, the surface-wave attenuation $\alpha_s\lambda$ is smaller. For $\lambda/\lambda_s = 1.2$, $\alpha_s \cong 0.7\alpha$; for $\lambda/\lambda_s = 1.03$, $\alpha_s \cong 0.1\alpha$.[39] So long as δ is smaller than 10^{-2}, the loss will therefore be less than 0.1 db per wavelength. Recent data on long Yagis[40] indicate that for λ/λ_s near 1, loss in artificial dielectrics is likewise negligible, provided all joints are firmly press-fit or soldered and the metal is of high conductivity. As the corrugations or dipole elements approach resonance, λ/λ_s increases and ohmic losses rise sharply. A typical figure for loss in a 6λ-long dielectric rod or Yagi is 0.5 db. (Since the maximum-gain curve in Fig. 16-11 is based on experiment, the effect of ohmic loss is included.) Surface-wave losses can be measured by the resonator method.[41]

Because at low frequencies the metal elements of artificial dielectrics can be constructed of slender poles and chicken wire, they weigh far less than solid dielectrics. Large ground structures at UHF or below are therefore invariably artificial dielectrics. In the microwave range, the choice of medium depends on mechanical strength, temperature behavior, erosion resistance, and cost; ordinary dielectrics—some of which can be cheaply molded into cavities recessed in the skin—are usually preferred for flush airplane or missile installation.

Dielectric Rod[7,16,19,20,35,39,42–47] (termed "polyrod" and "ferrod" when made of polystyrene and ferrite material, respectively). See Fig. 16-18a for phase velocity as a function of rod diameter. The

FIG. 16-18. Dielectric rod: (a) Relative phase velocity[29,42–44] (in case of noncircular cross section, replace d/λ by $1.13\ \sqrt{A}/\lambda$). (b) Conventional feed. (*Courtesy of G. C. Southworth and D. Van Nostrand Company, Inc.*[48])

higher the dielectric constant, the thinner the rod (for a given gain) and the lighter therefore the weight; also, however, the larger the dispersion and therefore narrower the bandwidth.

Modes higher than the fundamental HE_{11} cannot propagate provided $d/\lambda < 0.626/\sqrt{\epsilon}$. The first two higher modes, TE_{01} and TM_{01}, produce a null in the end-fire direction.

Cross sections other than circular are often useful. To a good approximation,[39] the phase velocity depends only on the cross-section area A, and Fig. 16-18a therefore remains valid if d is replaced by $1.13\ \sqrt{A}$. Sliced in half along the plane of electric symmetry (Fig. 16-4c)—which does not affect the phase velocity—a circular or rectangular rod can be placed on a ground plane ("dielectric-image line," Fig. 16-19a and b); when recessed for flush mounting, this structure is called the "dielectric channel guide" (Fig. 16-19c). Another variant, the dielectric tube,[47] has also been studied, but appears to have no advantages over ordinary rods.

Mallach[43] found that for optimum design, the rod diameter at the feed end of a linearly tapered dielectric rod should be $d_{max}/\lambda \cong [\pi(\epsilon - 1)]^{-\frac{1}{2}}$, and at the termina-

tion, $d_{min}/\lambda \cong [2.5\pi(\epsilon - 1)]^{-\frac{1}{2}}$. In the range $2.5 < \epsilon < 20$, this rule corresponds to letting λ/λ_s at the feed be roughly equal to 1.1 and at the termination to 1.0. The resulting patterns are often adequate but can be improved by using the methods described in Sec. 16.3.

A rough approximation to the rod pattern, due to Zinke,[43] consists in multiplying the $\sin \xi/\xi$ pattern shown in Fig. 16-8 by the factor $\cos [(\pi d/\lambda) \sin \theta]$ (but the predicted sharp nulls do not in fact exist).

Figure 16-18b shows details of a conventional feed that has proved itself in practice. Other feeds are illustrated in Figs. 16-7 and 16-14. In the case of waveguide feeds, it has been found desirable,[16] both for snug fitting and sidelobe suppression, to wrap dielectric tape around the feed point or, equivalently, to let the diameter of the waveguide feed be slightly smaller than that of the dielectric rod at the feed point, as shown in Fig. 16-7b. If $\epsilon > 8$, the rod can be fed over a narrow band by direct insertion in the narrow side of a waveguide, or in a cavity.[35]

FIG. 16-19. Dielectric image lines and channel guide: (a) and (b) Image lines (identical λ/λ_s if cross section, areas are the same). (c) Channel guide.

Dielectric Channel Guide[27,49,50] (Fig. 16-19c). Two modes are of interest, a vertically polarized one that is a deformation of the HE_{11} rod mode, and a horizontally polarized one. The phase velocity of the vertically polarized mode is very slightly faster in Fig. 16-19c than in Fig. 16-19a or b. The mode may be slightly leaky (small attenuation in axial direction), but this is not known with certainty. The structure
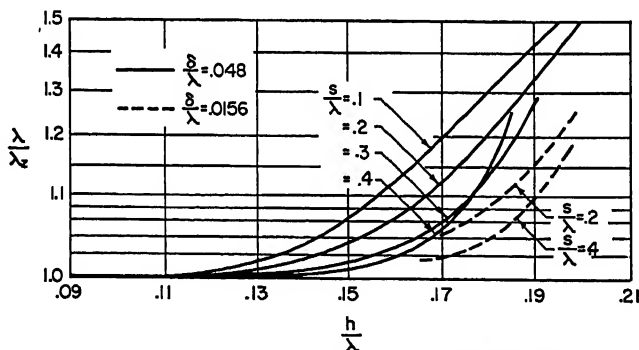
FIG. 16-20. Relative phase velocity on Yagi antenna. (*After Ehrenspeck and Poehler*[12] *and Frost.*[51]) For meaning of parameters, see Fig. 16-7a.

can be viewed as a channel of the type shown in Fig. 16-2b, but with most of the sidewalls removed. The phase velocity is then determined as follows: we rewrite Eq. (16-5b) in the form

$$\frac{\lambda}{\lambda_s} = \sqrt{\left(\frac{\lambda}{\lambda_s'}\right)^2 - \left(\frac{\lambda}{2w}\right)^2}$$

where λ/λ_s' is the relative phase velocity on an infinitely wide slab-on-metal, as given in Fig. 16-24c. Removal of the sidewalls above the dielectric-air interface appears to have negligible effect on the phase velocity[27] and, at least so long as $\lambda/\lambda_s > 1$ (w not too narrow), introduces little if any leakage attenuation.

The horizontally polarized mode is the lowest-order TE mode in the channel of Fig. 16-2b (slightly perturbed by the removal of most of the sidewalls), which in turn

is identical with the lowest-order TE mode on a dielectric slab-on-metal (solid curves, Fig. 16-24*d*).

The dielectric-filled channel also supports leaky waves, and care must be taken not to choose parameters that allow these to be excited (Sec. 16.8).

Yagis[12,13,51-55] (sometimes referred to as "ladder" arrays). Figure 16-20 shows that the phase velocity is controlled by adjusting spacing, height, and diameter of the monopole elements. The dispersion is more pronounced than on a dielectric rod, and the best-reported bandwidth (within which the gain drops no more than 3 db) is only ±10 per cent; this can perhaps be improved by application of the broadband design method described in Sec. 16.3. The bandwidth of an array of Yagis is at best ±5 per cent.

The curves in Fig. 16-20 apply to the row of monopoles shown in Fig. 16-7*a* and equally to a row of dipoles (element height 2*h*). A center boom for mounting the dipole elements has negligible effect on the phase velocity provided the total dipole span 2*h* includes the boom diameter. Yagis can be photo-etched on a copper-clad dielectric sheet;[54,55] since the dielectric slows down the wave, the element height needed to produce

FIG. 16-21. Relative phase velocity on cigar antenna. (*After Simon and Weill.*[14])
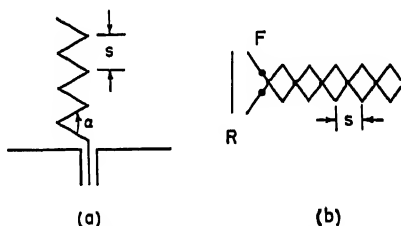
FIG. 16-22. Zigzag antennas: (*a*) Unbalanced (above ground plane).[58] (*b*) Balanced (*R* reflector, two-wire line feed connects at *F*). (Reference 57.)

a given phase velocity is less than indicated in Fig. 16-20.

See Sec. 16.3 for variants of the Yagi that produce very high gain (the "back-fire" antenna, Fig. 16-12) or very low sidelobes (Yagi with parasitic side rows, Fig. 16-13). For circular polarization, Yagi elements can be shaped in the form of a cross.

Cigar Antenna[14,56] (Fig. 16-21). Metal disks mounted on a central metal boom support an HE_{11} mode that closely resembles the Yagi mode. An 80λ-long cigar produced a gain of 28 db. Just as in the case of the dielectric rod, the polarization may be linear or circular.

Zigzag Antenna[57,58] (Fig. 16-22). This antenna is a projection of the helix on a plane. No curves are available that relate the parameters to the relative phase velocity. An analysis based on regarding the antenna as an array of V elements results in the requirement

$$\sin \frac{\alpha}{2} = \frac{s/\lambda}{1 + s/\lambda}$$
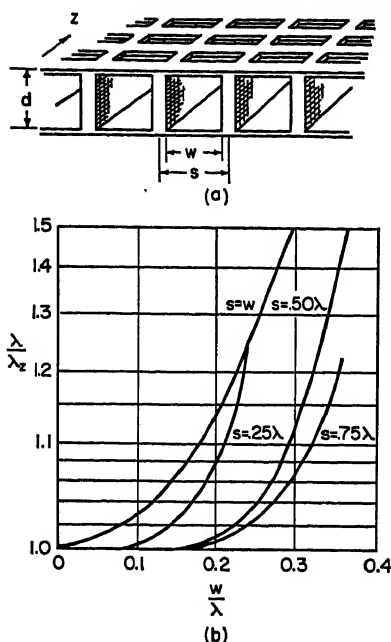
FIG. 16-23. Waveguide-loaded slot array: (a) Antenna structure (bottom plate not needed if $d > w$). (b) Relative phase velocity, assuming six or more slots per wavelength in z-direction, and zero top-plate thickness. (*From Hyneman and Hougardy.*[59])

The bandwidth of the unbalanced zigzag[58] is reported to be ±5 per cent; of the balanced zigzag,[57] ±25 per cent.

Waveguide-loaded Slot Array[59] (Fig. 16-23). A vertically polarized wave propagates along nonresonant slots that are loaded by below-cutoff waveguide ($w < \lambda/2$; height of waveguide not critical but should be $>w$). This antenna is easily arrayed into an area source, as shown, and in this form closely resembles a corrugated surface. It could be fabricated by stretching transverse wires across longitudinal metal vanes.

Dielectric Sheets and Panels.[2,6,32–34,60–65] Because of the imaging properties of vertically polarized waves, the lowest-order TM mode on a dielectric sheet-on-metal is identical with that on a panel of twice the sheet thickness (Fig. 16-24a–c). This wave has no cutoff frequency; its properties are discussed in Sec. 16.2, and Fig. 16-4 shows the field configuration.

The lowest-order horizontally polarized wave on a dielectric sheet–on-metal produces a null in the end-fire direction and has a cutoff (solid curves, Fig. 16-24d). On a panel, on the other hand, the lowest-order horizontally polarized wave produces a maximum in the end-fire direction and has no cutoff (dashed curves, Fig. 16-24d).
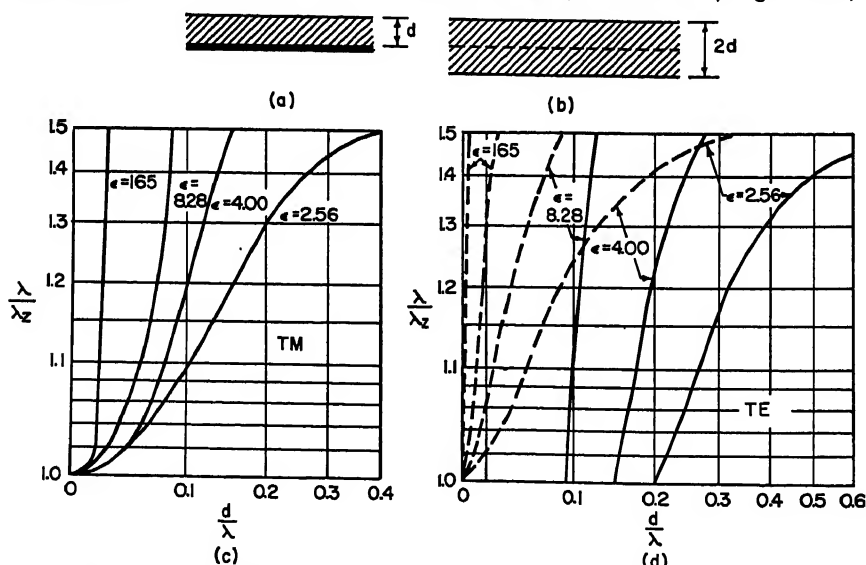
FIG. 16-24. Dielectric sheets and panels: (a) Sheet-on-metal. (b) Panel. (c) Lowest-order TM mode on sheet or panel. (d) Lowest-order TE mode on sheet (solid curves) and panel (dashed curves).

(The next higher TE mode on the panel is identical with the lowest TE mode on the sheet, but because of the end-fire null it is not a useful mode.)

In designing tapered sheets on metal, a flush air-dielectric interface can be maintained by contouring the depth of ground plane. Good contact between dielectric and ground plane is needed, since air spaces affect the phase velocity.[6]

Circular dielectric disks[63] and spherical caps[33,34] are useful as omnidirectional beacon antennas. For design principles, see Sec. 16.3 (paragraphs on effect of finite ground plane on the radiation pattern and on beam-shaping techniques). Figure 16-24c and d is still applicable, since λ/λ_s is only slightly affected by a decreasing radius of curvature. The leakage attenuation has been calculated by Elliott.[33] Patterns provide good null filling to 45° off end fire and have a bandwidth of ±8 per cent.[34]

Circular (or cross) polarization, as mentioned in Sec. 16.3, can be produced if the surface-wave structure supports a TM and a TE wave with identical phase velocities. One example is the two-layer dielectric sheet,[6,64] illustrated in Fig. 16-25a for the case in which the lower layer is air. Given λ/λ_s, Fig. 16-25b prescribes the layer thickness (with $\epsilon = \epsilon_1/\epsilon_0$ as a parameter). Another, structurally superior example is the simple-layer dielectric in which longitudinal metal vanes are embedded that short out the vertically polarized mode while leaving the horizontally polarized one unperturbed (Fig. 16-25c). The TM wave therefore "sees" a thinner sheet than the TE wave, and for a prescribed λ/λ_s, Fig. 16-24c and d gives the values (in first approximation) of the vane height and total layer thickness. For details, see Hansen.[65]

Corrugated Surface.[30,32-34,37,50,66-69] The grooves in Fig. 16-6 can be filled with a medium of dielectric constant ϵ, but to keep λ/λ_s unchanged, they must in that case be made shallower, in the approximate ratio $1:\sqrt{\epsilon}$, than in Fig. 16-26. The fabrication of a corrugated surface is expensive at microwave frequencies, and a waveguide-loaded slot array (see above) may be a more economical choice; at lower frequencies, the corrugated surface is relatively cheaper since it can consist, for example, of a row of chicken-wire fences.

This structure is less dispersive, and therefore more broadband, than a Yagi. As described in Sec. 16.3 (Fig. 16-17b), it can be frequency-scanned in azimuth.

Combined with its mirror image, the corrugated surface becomes a series of teeth of height 2h ("sole" antenna[56]); Fig. 16-26 is still applicable.
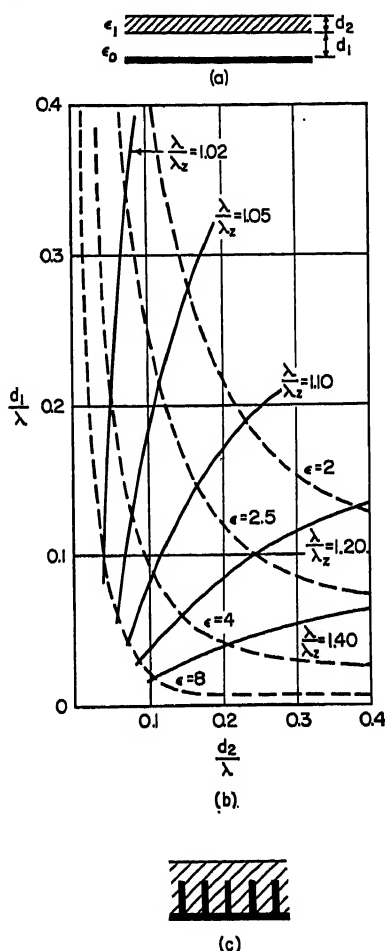
FIG. 16-25. Circular (or cross) polarization on dielectric sheets: (a) A simple double-layer structure. (b) Parameter combinations (with $\epsilon = \epsilon_1/\epsilon_0$) that allow (a) to support a circularly polarized surface wave with λ/λ_s between 1.02 and 1.40. (*From Plummer and Hansen.*[64]) (c) Longitudinal metal vanes embedded in dielectric. (Reference 65.)

Pin-bed Antenna ("Fakir's Bed").[70]   The curves in Fig. 16-27 assume that the pin spacing s is the same in the z and y directions and that there are several pins per wavelength; the surface is in that case isotropic.   If embedded in dielectric, the pins must be made shorter than in Fig. 16-27.
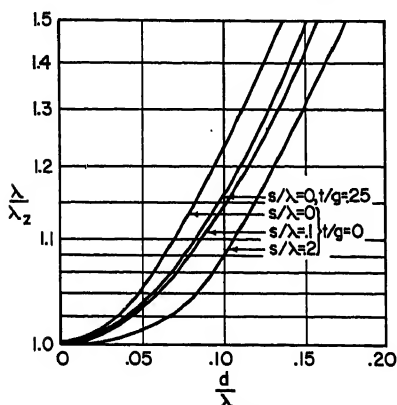
FIG. 16-26. Relative phase velocity on corrugated-metal surface; for meaning of parameters, see Fig. 16-6, with $s = t + g$. (*After Reynolds and Lucke*[50] *and Hurd.*[68])
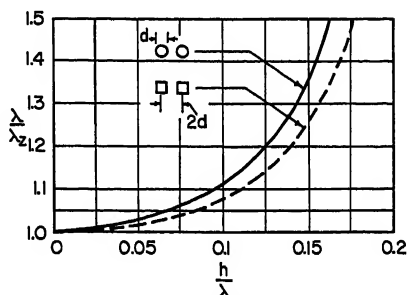
FIG. 16-27. Relative phase velocity on pin-bed antenna. (*After Querido.*[70])

16.5. SURFACE-WAVE-EXCITED ARRAYS OF DISCRETE ELEMENTS: DESIGN PRINCIPLES

The array of dipoles proximity-coupled to a two-wire line (Fig. 16-1b) has much in common with a nonresonant slotted waveguide.   Both antennas are arrays of discrete elements excited by a traveling wave, one in shielded, the other on open waveguide. Both produce shaped patterns or narrow beams directed at any angle (other than broadside, where the cumulative impedance mismatch of the slots or dipoles is prohibitively high).   Design techniques therefore closely follow those in Chap. 9. Rarely competitive with waveguide slots in the microwave range (because less suitable for high-precision design), surface-wave-excited arrays of discrete elements are most useful at lower frequencies, where waveguides are too bulky; they may also find application in the submillimeter range, where waveguides are too small.

Direction of Main Beam.   As with slot arrays, successive radiating elements can be placed so that they are excited with the phase of the traveling wave, or with an additional phase difference of 180° ("phase reversal," Fig. 16-1b).   Assuming constant phase progression along the array and constant (or moderately tapered) amplitude and using simple array theory (Chap. 2), we obtain for the direction of the main beam, without phase reversal,

$$\cos \theta_m = \frac{\lambda}{\lambda_s} - \frac{\lambda}{s} m \qquad (16\text{-}28a)$$

and with phase reversal,

$$\cos \theta_n = \frac{\lambda}{\lambda_s} - \frac{\lambda}{s} \left(n + \tfrac{1}{2} \right) \qquad (16\text{-}28b)$$

where θ is the angle off end fire, s the spacing between elements, and m or $n = 0$, 1, 2, . . . the order of the beam. The spacing must be small enough so that no

secondary principal lobes appear at real angles. The position of the principal lobes nearest the main lobe is found by replacing m by $m + 1$ and $m - 1$ in Eq. (16-28a) [and likewise for n in Eq. (16-28b)]. As s increases, principal lobes appear first in the end-fire or back-fire ($\theta = 180°$) direction; they will not appear provided their angle is imaginary, or[71]

$$\frac{s}{\lambda} \leq \frac{1}{1 + |\cos \theta_m|} \tag{16-29}$$

(and likewise for n), where the equality sign holds only if the element pattern has nulls along the array axis. According to Eq. (16-29), the maximum permissible spacing increases from $\lambda/2$ at end fire and back fire to λ at broadside.
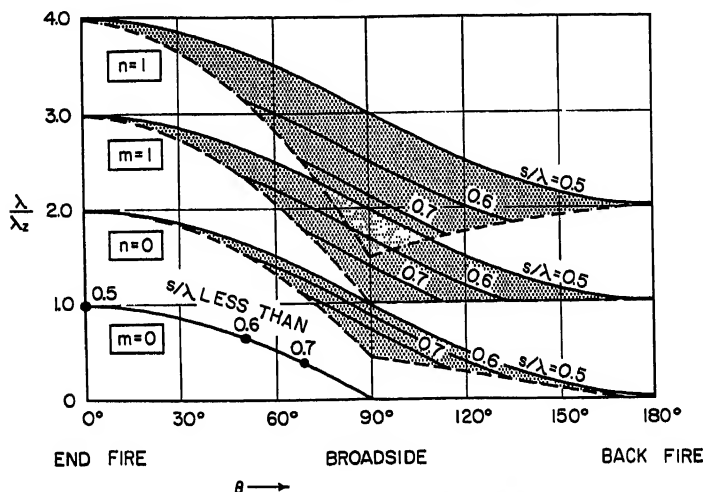
FIG. 16-28. Angle θ between main lobe and array axis of an array of discrete elements spaced s/λ apart and excited by a traveling wave with relative phase velocity λ/λ_z. Curves marked m are for identical consecutive elements, n for alternately phase-reversed elements [Eqs. (16-28)]. Range of curves satisfies Eq. (16-29) (no other principal lobes). The curves $m = 0$ and $n = 0$ apply also to leaky waves (Secs. 16.7 and 16.8).

Because of mutual coupling between elements and to save on the total number in the array, we usually impose $s \geq \lambda/2$ as a lower bound.

Figure 16-28, which combines Eqs. (16-28) and (16-29), shows the dependence of main-beam angle on λ/λ_z and on the *permissible* spacings. [If $m = 0$ in Eq. (16-28a), s is arbitrary except for its upper bound, which is explicitly indicated in Fig. 16-28.] It is seen that, provided λ/λ_z and s/λ values can be freely assigned, the $m = 0$ mode of operation allows the main beam to be positioned anywhere between end fire and broadside and all other modes anywhere between end fire and back fire. Very slow and very fast traveling waves, however, are not easily realized, so that usually λ/λ_z lies in the vicinity of 1. In that case, the $m = 0$ mode is useful only for near-end-fire radiation (e.g., trough guide with periodic discontinuities that are not phase-reversed, Sec. 16.6); the $n = 0$ mode, only for near-broadside radiation (e.g., phase-reversed dipoles, Fig. 16-1b); and the $m = 1$ mode, for radiation from near broadside all the way to back fire (e.g., proximity-coupled dipoles that are not phase-reversed). Higher modes of operation require λ/λ_z to be well above 1 (very slow waves), and no practical applications are in fact known for $m \geq 2$ and $n \geq 1$.

If $\lambda/\lambda_z = 1$ and $s = \lambda/2$ (no phase reversal), Fig. 16-28 shows that two main beams arise, one end-fire ($m = 0$), the other back-fire ($m = 1$). To suppress one of these,

the element pattern must have a null in the unwanted direction. A suitable element for end-fire radiation consists of two identical sources spaced $\lambda/4$ apart on the surface-wave transmission line; these radiate a cardioid pattern with a null at $\theta = 180°$. An end-fire array of such elements is therefore simply an array of identical sources spaced $\lambda/4$ apart.

As in the case of slot arrays, the surface-wave-excited array can be made resonant by terminating it with a short. To hold the variation of input impedance with frequency to a minimum, such an array is usually center-fed. Figure 16-28 is still applicable, but two beams are now produced, one at θ and the other at $180° - \theta$; at broadside these merge into a single beam.

Control of Aperture Distribution. Although in general a four-terminal network is needed to represent a transmission-line discontinuity, a shunt conductance usually suffices, especially if the axial dimension of the element is much smaller than λ or if the element is resonant. The conductances must be so chosen as to produce the amplitude distribution prescribed over the array. The normalized element conductance $g_i = G_i/Y_c$ (Y_c is the characteristic admittance of the matched transmission line, Fig. 16-29) is much smaller than 1 if there are many elements in the array (array length $\ell \gg \lambda$). We can then approximate the normalized conductance per unit length, g_i/s, by the smoothed continuous function $g(z)$ [with $g(z_i) = g_i/s$]. In Fig. 16-29, the power loss due to radiation by element i is g_i times the power incident at i; in the continuous case, therefore,

FIG. 16-29. Transmission line loaded with elements that can be represented as shunt conductances.

$$-\frac{dP(z)}{dz} = g(z)P(z) \tag{16-30}$$

The rate of power loss is also related to the smoothed amplitude distribution $A(z)$:

$$-\frac{dP(z)}{dz} = aA^2(z) \tag{16-31}$$

where a is a proportionality constant. Therefore

$$g(z) = \frac{aA^2(z)}{P(z)} \tag{16-32}$$

Integrating Eq. (16-31), we obtain

$$-P(z) + P_{\text{in}} = a \int_0^z A^2(z)\, dz$$

$$-P_l + P_{\text{in}} = a \int_0^l A^2(z)\, dz$$

(with P_{in} the input power, P_l the power dissipated in the load), which on substitution in Eq. (16-32) gives the result

$g(z_i)$ (in normalized conductance per unit length) $= \dfrac{g_i}{s}$

$$= \frac{A^2(z_i)}{\dfrac{1}{1 - P_l/P_{\text{in}}} \int_0^l A^2(z)\, dz - \int_0^{z_i} A^2(z)\, dz} \tag{16-33}$$

(We can also write $g_i N/l$ for g_i/s, where N is the total number of elements.) Using Eq. (16-33), one plots $g(z)$ (see, for example, Fig. 16-30) and marks the ordinates at

the element positions z_i. The method gives good results with as few as 20 radiators, fair results with 10.

Measurement of Element Conductances. With Fig. 16-28 and Eq. (16-33) the basic design is complete. In constructing the array, one needs to know λ/λ_s on the transmission line and also the dependence of conductance on the element parameters, for example, on angular orientation of the dipole in Fig. 16-1b and on its distance from the two-wire line. λ/λ_s is measured as described in Sec. 16.2, but in the presence of the elements, since these load the line (usually so as to slow down the wave).

To measure the characteristics of the element, one places it $\lambda/4$ (or $3\lambda/4$) in front of a short and plots the input admittance on the Smith chart as a function of the element parameters, for example, of length of dipole when the dipole is set at a particular angle with respect to the array axis. Where the curve crosses the real axis, the admittance is pure shunt and, since $G < Y_c$, the normalized conductance equals the inverse of the voltage standing wave ratio, $g = (VSWR)^{-1}$. If the elements are to be strongly coupled, it is desirable to make them purely shunt; otherwise, small susceptance values are permissible, and often unavoidable.

The procedure just described does not take into account the mutual impedances between elements in the array, and their effect is usually not negligible. By arranging N (at least 20) *identical* elements on a line (chosen on the basis of the Smith-chart curves to be reasonably near resonance) and measuring the total insertion loss, the conductance can be determined in the presence of mutual-impedance effects. Consider a single element placed on a line terminated by Y_c: the ratio of power radiated to power transmitted by this element is

$$\frac{P_{rad}}{P_{tr}} = \frac{G}{Y_c} = g$$

Therefore

$$P_{tr} = P_{in} - P_{rad} = P_{in} - gP_{tr}$$

so that the insertion loss is

$$\frac{P_{in}}{P_{tr}} = 1 + g$$

For N elements,

$$10 \log (1 + g) = \frac{\text{insertion loss in db}}{N} \tag{16-34}$$

from which g, called the "incremental" conductance, can be computed.

Details of a test setup for the shorted-line and insertion-loss methods are given by Montgomery.[72]

Some elements can be coupled very strongly to the surface wave, more so than ordinary slots to a waveguide mode; short arrays of these therefore waste less power in the load than slot arrays of the same length.

For broadside radiation, elements are needed whose equivalent circuit, like that of an inclined displaced slot in waveguide, is a pi network, rather than a shunt conductance; in cascade, these networks approximate a lossy transmission line, which does not allow a large reflected wave to build up even though $s = \lambda/2$. Only two such surface-wave-excited elements have been studied, the "notch" in trough guide and the "sandwich-wire" antenna with sinusoidal inner conductor. (Sec. 16.6. See also Fig. 16-45b and text in Sec. 16.8.)

Array Synthesis and Beam Shaping. All the general synthesis techniques described in Chap. 2 are applicable to surface-wave-excited arrays. For low-sidelobe design, the method due to Taylor[73] is the most useful; it allows far-out sidelobes to decrease more rapidly than near-in ones and requires less coupling near the load end than

other low-sidelobe designs. Worked-out conductance values corresponding to 25- and 30-db sidelobe level, and different powers in the load, are shown in Fig. 16-30.[71] Arrays should be overdesigned, e.g., for a 30-db sidelobe level when 26 or 27 db is required.
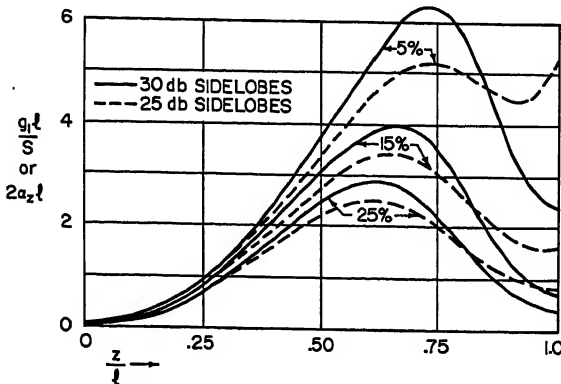
Fig. 16-30. Normalized element conductance g_i (or leaky-wave attenuation α_z) for Taylor distribution, as a function of normalized length z/l along array, sidelobe level, and percentage of power dissipated in load. (*Adapted from Dion.*[71])

For beam shaping, techniques by Woodward, Schelkunoff, Chu, Dunbar, and Sletten are available; see Chap. 2, also Silver,[74] Fry and Goward,[75] Dunbar,[76] and Sletten et al.[77]

Gain, Beamwidth, and Sidelobe Level of Linear Arrays. General array theory, as described in Chaps. 2 and 5, is fully applicable. If we assume dipole elements that are transverse to the array axis, and constant amplitude illumination, the gain of a line source of length l (with $N > 20$) is

$$G \cong \frac{4l}{\lambda} \tag{16-35}$$

above an isotropic source. Equation (16-35) is *independent* of angle of radiation. At end fire, the gain can be increased by 2 db above that of Eq. (16-35) ($G \cong 7l/\lambda$) by satisfying the Hansen-Woodyard condition (Eq. 16-20a). If we assume dipole elements that are parallel to the array axis, the gain is $G \cong 2l/\lambda$ at broadside and decreases monotonically to zero at end fire.

The half-power beamwidth at broadside, assuming constant illumination, is 51 λ/l degrees; at angles other than broadside, but not too near end fire, l must be replaced by $l_p = l \sin \theta$, the geometric projection of l in the plane perpendicular to θ (Fig. 16-31). Near end fire, where this relation no longer holds, a smooth transition is made to the end-fire half-power beamwidth, which is 105 $\sqrt{\lambda/l}$ degrees if $\lambda/\lambda_z = 1$ and 73 $\sqrt{\lambda/l}$ degrees if λ/λ_z is increased to its Hansen-Woodyard value. Details of the transition region are given by Bickmore.[78]

Fig. 16-31. Aperture length l and its projection l_p normal to beam direction.

The sidelobe level is 13 db with constant aperture illumination but can be lowered drastically (Fig. 16-30). As with slot arrays, secondary lobes are produced by variations in the element pattern; these are significant only with phase-reversed elements, which are alternately oriented at opposite angles or displaced on opposite sides of the array axis.[70]

Arrays of Line Sources; Area Sources. Two useful V arrangements of line sources are shown in Fig. 16-32; the line sources in (a) produce a beam between end fire and broadside, in (b) between broadside and backfire. The arms of the V could also be an array of line sources or an area source. To suppress the undesirable (dashed) lobe, a reflector plate can be mounted a quarter wavelength behind each arm, or if that is not feasible, the two kinds of V can be combined into a rhombic arrangement.

Surface-wave-excited linear arrays placed side by side—at a distance sufficient to prevent interaction of the surface waves (use 25-db contours in Fig. 16-3b)—have characteristics similar to two-dimensional slot arrays. Mutual coupling between elements is serious or not, depending on whether adjacent elements are oriented broadside to each other or end to end.
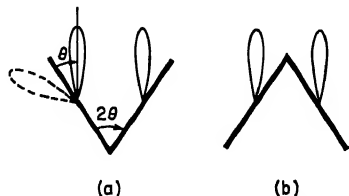
FIG. 16-32. V arrangements of line sources (fed from apex).

A single surface wave can be made to excite a two-dimensional array of discrete elements. Although it has been tried to date with only one structure—the dielectric-image line-excited two-dimensional slot array[80] (Fig. 16-33)—the method applies to any open waveguide and to radiating elements other than slots. The (loosely bound) surface wave excites each row in phase with an illumination corresponding to its radial
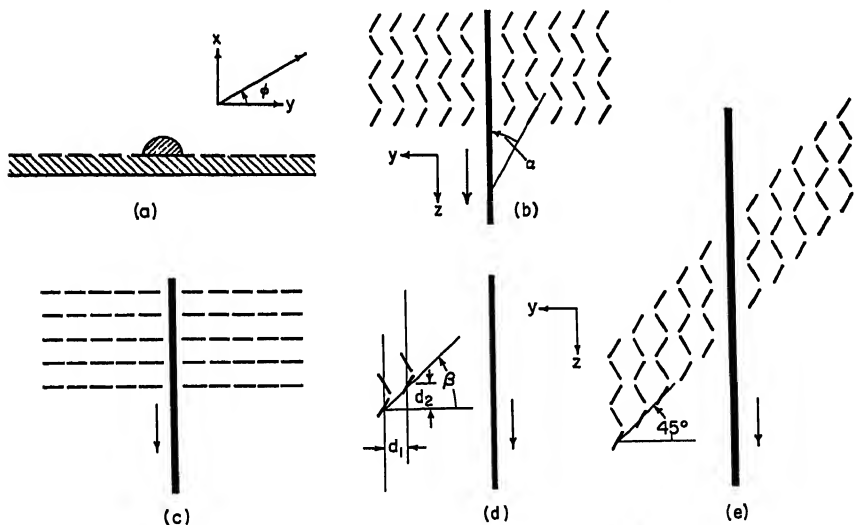
FIG. 16-33. Parasitic excitation of two-dimensional slot array.[80,99] (a) Transverse cross section. (b) Arrangement for broadside radiation. (c) Arrangement for end-fire radiation. (d) Pair of corresponding slots in adjacent "slipped" columns. (e) Arrangement for "side-fire" radiation.

decay [Eq. (16-7)] and each column with a λ/λ_s slightly larger than 1. Thus each row radiates broadside to itself, and each column at an angle that depends on the spacing of the elements and on whether they are phase-reversed or not; it is seen from Fig. 16-28 that this angle can be end-fire ($m = 0$), between 70° and broadside ($n = 0$), or between broadside and back fire ($m = 1$). In combination, the rows and columns can therefore produce a large variety of pencil beams (Fig. 16-33b and c) or fan beams that are shaped in the xz plane. By "slipping" adjacent columns with respect to each other,

the beam can also be swung in the transverse (xy) plane. In Fig. 16-33d, which shows a pair of corresponding slots in two adjacent columns, radiation from a slot on the left leads radiation from its mate on the right by $d_1 \cos \phi$ (ϕ is the angle off the y direction in the xy plane, Fig. 16-33a) and lags by $d_2 \lambda / \lambda_s$; the beam direction is then given by

$$\cos \phi = \frac{\lambda}{\lambda_s} \cdot \tan \beta \qquad (16\text{-}36)$$

Figure 16-33e illustrates the case $\phi = 0$ ("side fire," $\beta = 45°$). Strictly speaking, arrays of slipped columns should be rhomboid in shape, as shown, but if the columns are very much longer than the rows, substitution of the more convenient rectangular shape can be expected to have negligible effect on the pattern.

Circular Polarization. With one exception, suitable for end-fire radiation only (Fig. 16-34c), no circularly polarized elements have been studied. A parallel-plate technique that produces circular polarization from an array of 45° inclined edge slots[81] might, under special circumstances, be made applicable to surface-wave-excited elements.

Scanning. A mechanical change in phase velocity swings the beam through angles that can be read off directly by following the solid lines in Fig. 16-28. Frequency scanning cuts across the solid lines; Fig. 16-28 shows that, since s/λ increases with frequency, a given variation in λ / λ_s produces a larger scan angle in the case of frequency than in the case of mechanical scanning.

A third method of scanning consists in varying s/λ (with a scissors-type arrangement) while keeping λ / λ_s constant ("stretch" array[82]). If, for example, $\lambda / \lambda_s \cong 1$, the beam swings from about 75° to broadside in the $n = 0$ mode and from broadside to backfire in the $m = 1$ mode. In practice, λ / λ_s may be expected to increase as s/λ decreases (elements load line more strongly), which reduces the scan angle (Fig. 16-28). Since the number of elements in a "stretch" array is constant, the array length, and thus the gain [Eq. (16-35)] and beamwidth, become functions of scan angle.

In the fourth method, "amplitude" scanning[83] (which has not to date been applied to surface-wave-excited elements), the beam is moved by changing the degree of coupling of each element while leaving both λ / λ_s and s/λ constant.

16.6. SURFACE-WAVE-EXCITED ARRAYS OF DISCRETE ELEMENTS: SPECIFIC STRUCTURES

Numerical values of element conductances and design details for specific surface-wave-excited antennas are presented in this section. None of the general design information in Sec. 16.5 will be repeated here. The term "surface-wave-excited" is taken in a wide sense to include any open transmission lines or waveguide. The structures are grouped as follows: two-wire line arrays (proximity-coupled dipoles), strip-line-derived arrays (sandwich wire, trough guide), dielectric-waveguide-derived arrays (spiked rod, stepped strip, dielectric-image-line-excited slot array, dielectric wafer), and two arrays excited by a beam launched from the termination of a surface-wave line ("surface-wave-turnstile" and "pinecone" antennas). Though they have not been explored in this connection, other known waveguides could equally well be used—any of the structures in Sec. 16.4, for example, or the dielectric channel (Fig. 16-2b), or the H guide[84] (Fig. 16-24b, with vertical sidewalls erected as in Fig. 16-2b but reaching from $x = -\infty$ to $x = +\infty$).

Direct feed radiation, which is negligible in the case of parallel-wire and trough-guide-excited arrays, can never be completely suppressed in the case of dielectric-waveguide-excited arrays; in the context of the present section this is spurious radiation.

Two-wire Line with Proximity-coupled Dipoles[85-89] ("Sletten" array, Figs. 16-1b and 16-34). Similar to the low-frequency "fishbone" antenna (Chap. 5) but with
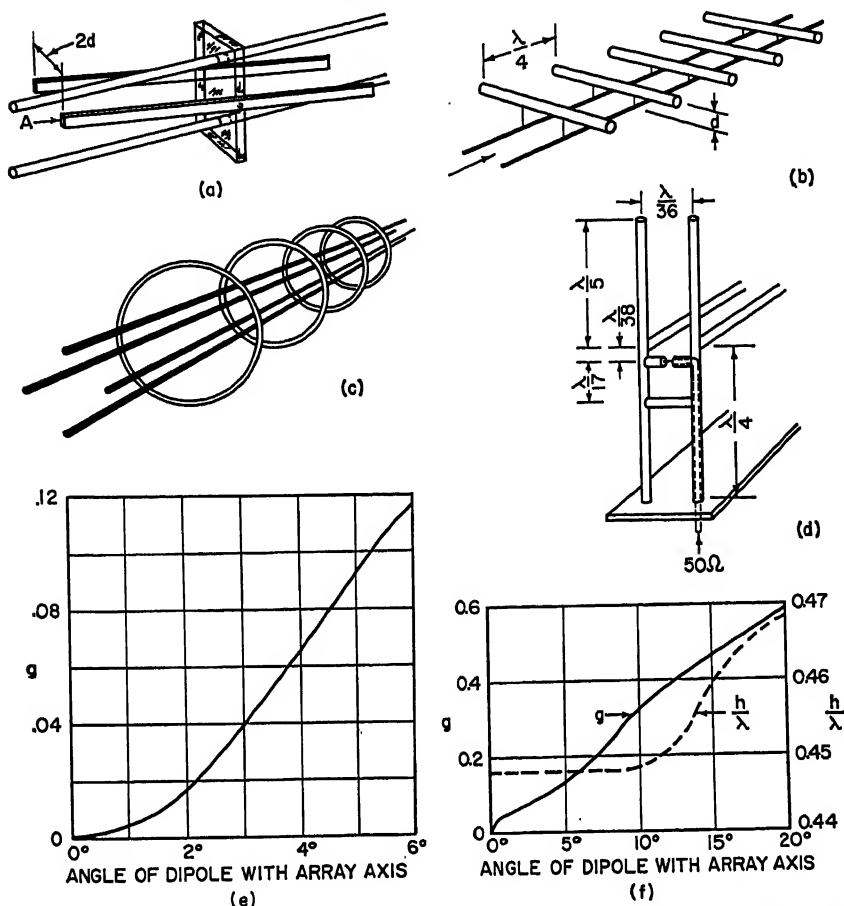
FIG. 16-34. Proximity-coupled dipoles: (a) Pairs of dipoles mounted on both sides of two-wire line for good omnidirectional coverage in plane transverse to array. (*After Sletten and Forbes.*[85]) (b) End-fire array (spacing between dipoles and line shown variable). (c) Array of rings excited by orthogonal pair of two-wire lines for end-fire circular (or cross) polarization. [(b) *and* (c) *after Forbes.*[89]] (d) Balun construction for transition from coaxial to two-wire line. (*After Sletten et al.*[87]) (e) Normalized element conductance g as a function of dipole angle of rotation for antenna in Fig. 16-1b, with element spacing above wires $d = 0.03\lambda$, dipole length $= 0.446\lambda$, center-to-center wire separation $= \lambda/36$. (*After Sletten et al.*[87]) (f) Normalized element conductance g and dipole resonant length h as a function of dipole angle of rotation for antenna in Fig. 16-34a, with $A = 8.5 \times 10^{-5}\lambda^2$, transverse element spacing $2d = 0.118\lambda$, center-to-center wire separation $= \lambda/36$. (*Based on data in Sletten and Forbes.*[85])

elements that are proximity-coupled rather than being tied to the line directly or through a capacitor, the array of dipoles excited by a two-wire line is most useful in the VHF and UHF ranges and is well suited for high-power application. With the dipoles as shown in Figs. 16-1b and 16-34a, either m- or n-type radiation patterns can be produced (Fig. 16-28), except near end fire, where the element pattern has a null. Arranged as in Fig. 16-34b, the dipoles cannot be phase-reversed and the radiation is confined to near end fire (interdipole spacing $= \lambda/4$; see Sec. 16.5, paragraph on

direction of main beam). The two orthogonal pairs of wires in Fig. 16-34c can be fed 90° out of phase to produce circularly polarized end-fire radiation.[89]

Because of loading by the elements, λ/λ_s on the two-wire line is slightly larger than 1. The degree of coupling depends primarily on the distance d between dipole and line (Fig. 16-34a and b) and on the angle between dipole and array axis; secondarily on dipole length and on spacing between wires. For equal coupling, d is an order of magnitude greater in Figs. 16-1b and 16-34a than in Fig. 16-34b (0.05λ versus 0.005λ for $g = 0.25$). Although there are exceptions,[88] the coupling generally decreases monotonically with increasing d. It rises to a maximum between 20° and 40° and then decreases again as the angle between dipole and array axis increases.

The measurement of dipole coupling and resonant length is described in Sec. 16.5 [see Eq. (16-34) and text]. Figure 16-34e and f shows results for the structures in Figs. 16-1b and 16-34a, respectively. Sufficiently large coupling is achieved with small dipole angles; the element patterns are therefore fairly uniform. The dipole resonant length is near 0.45λ. If $d \ll 0.05\lambda$, it becomes very difficult to find the dipole resonant length, and for transverse dipoles (Fig. 16-34b), resonance does not in fact exist.[89]

A vertically erected, center-fed, resonant VHF-UHF communications array with elements of the type shown in Fig. 16-34a gave good performance over a ±10 per cent band with a pattern omnidirectional in azimuth and shaped in elevation (VSWR = 1.2:1 at the design frequency).[85] In another interesting application of the two-wire line, a satellite-tracking antenna with elements of the type shown in Fig. 16-1b was fed from both ends; with the aid of a suitable comparison circuit, this allowed reception on both sum and difference patterns.[86,87] The type of balun used in this design is illustrated in Fig. 16-34d; note that balance does not depend on the height of the coaxial feed from the ground plane, or on the tuning parameters.

Sandwich-wire Antenna.[90,91] If the top and bottom plates and the center conductor of a strip line (Fig. 16-35a) coalesce into wires (Fig. 16-35b) and the center wire is snaked along its length (Fig. 16-35c), those portions of it that are not parallel to the outer wires (which are at ground potential) will radiate, producing n-type patterns (Fig. 16-28). The outer-wire spacing must be less than λ, and the feed can be coaxial or strip-line.

Flush-mounted and backed by a cavity (Fig. 16-35d and e), the antenna radiates an omnidirectional beam polarized transversely to the array axis. Detailed information is available for the case where the center strip is sinusoidal.[91] The relative phase velocity is calculated on the assumption that the wave velocity along the undulating strip is that of light. This makes λ/λ_s a function of a/s, where a is the amplitude of the sinusoid (Fig. 16-35e). The result for a strip surrounded by air is shown in Fig. 16-35f (dashed curve); for a strip printed on a Teflon-Fiberglas sheet, the phase velocity is 5 per cent less (solid curve). Experimental results are in close agreement with this theory.[91]

Although most of the radiation comes from the region where the strip crosses the center line (marked A in Fig. 16-35e), some of it is distributed along the entire length of the sinusoid; the radiation mechanism therefore approaches that of a leaky wave, and the equivalent circuit of a section of sandwich wire is a pi network. The element conductance (elements in this context are considered localized at points A) is a function of a/s and a/λ. Because both λ/λ_s and g are functions of a/s and thus cannot be chosen independently of each other—a situation typical of most leaky-wave antennas (Sec. 16.8)—the design procedure is slightly more complicated than described in Sec. 16.5. Rewrite Eq. (16-28b) in the form

$$\cos \theta = \frac{\lambda}{\lambda_s} - \frac{\lambda}{2a}\frac{a}{s} \qquad (16\text{-}28b')$$
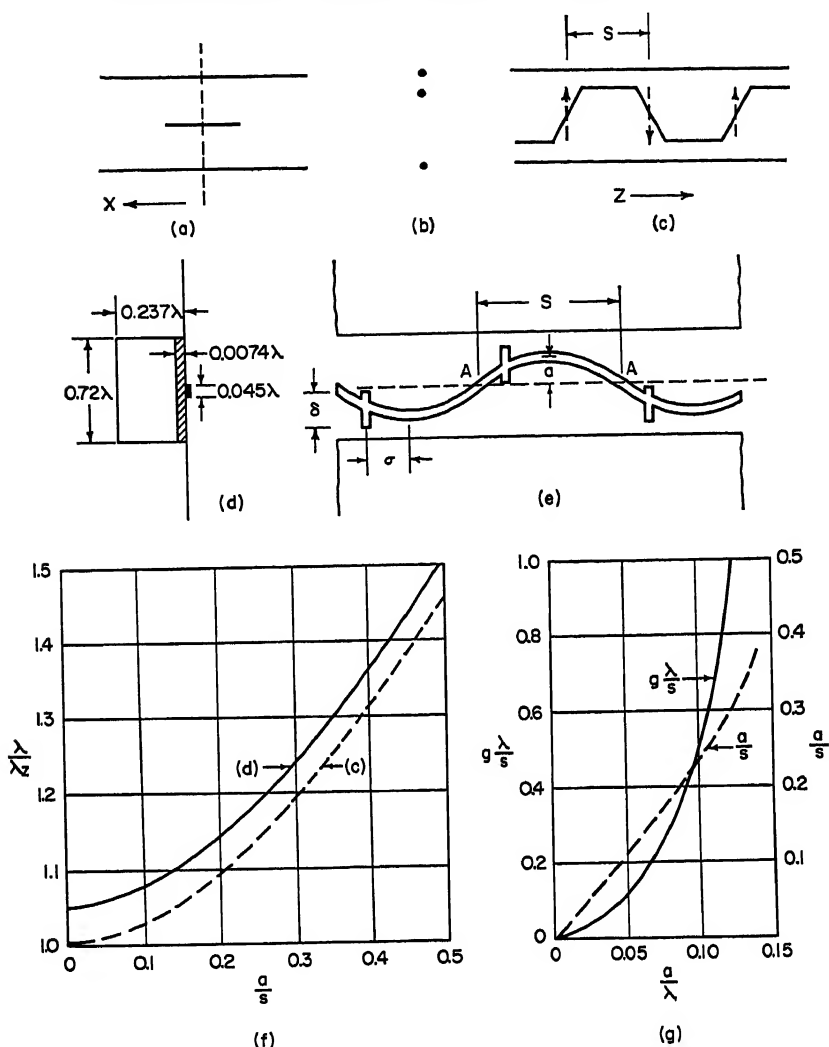
FIG. 16-35. Sandwich-wire antenna: (a) Strip-line (transverse cross section). (b) and (c) Transverse and longitudinal cross section of sandwich wire with trapezoidal center conductor (dotted arrows indicate location and direction of radiating currents). (d) and (e) Transverse and longitudinal cross section of cavity-backed sandwich wire with sinusoidal center conductor. (f) Relative phase velocity on sandwich-wire line shown in (d) and (e) (solid curve: center strip supported by Teflon-Fiberglas sheet; dashed curve: center strip in air). (g) Normalized element conductance and relative amplitude a/s as a function of a/λ, for broadside radiation from (d) and (e). [(a)–(e) and (g) after Rotman and Karas.[91]]

Pick a series of values of a/s (it is usually sufficient to cover the range $0 < a/s \leq 0.5$). Figure 16-35f then fixes the corresponding λ/λ_z values. Substituting each pair of a/s and λ/λ_z values in turn in Eq. (16-28b') forces the choice of the corresponding a/λ values. The conductance is then determined experimentally for each allowed combination of a/s and a/λ, and these measurements will not be valid for any other com-

bination. Example: let the prescribed radiation be broadside ($\theta = 90°$), and the structure be that of Fig. 16-35d and e. For $a/s = 0.1$, the solid curve in Fig. 16-35f gives $\lambda/\lambda_s = 1.078$. Using Eq. (16-28$b'$), $a/\lambda = 0.046$, and similarly for other values of a/s. It is convenient to plot the resulting curve of a/s versus a/λ (dashed curve in Fig. 16-35g). We must now measure g as a function of these paired-off a/s and a/λ values; for $a/s = 0.1$ and $a/\lambda = 0.046$ (which, incidentally, implies $s/\lambda = 0.46$), g turns out to be 0.047, and so on for other pairs. Since each of the resulting g values holds for a different s, it is best to plot not g but $g(\lambda/s)$ ($= 0.1$ in our example) as a function of a/λ, as shown by the solid curve in Fig. 16-35g. Beam shaping is achieved by using these conductance values in conjunction with Eq. (16-33). Note that our curve holds *only* for broadside radiation; for any other angle, g would have to be measured as a function of an entirely different set of parameter pairs.

Small though the impedance mismatch at broadside is for these elements, stubs are needed to make it negligible. The dimensions are (Fig. 16-35e)[91] $\sigma = 0.09\lambda$, $\delta/\lambda \cong a/\lambda + 0.043$, stub width = 0.024λ. The VSWR is less than 1.4:1 over a ±15 per cent band. A flat array of such side-by-side line sources, end-fed with a corporate structure, had a pattern bandwidth of ±15 per cent within which beamwidth and sidelobes stayed fairly constant; the squint angle was ±8 per cent. This array has also been mounted on a surface curved transversely to the line sources.[91]

Variants of Fig. 16-35c can be used as omnidirectional communication antennas when horizontal polarization is required in azimuth[90] (for vertical polarization, use two-wire line with proximity-coupled axial dipoles).

The Babinet equivalent of Fig. 16-35e, which has not been explored, might be useful at microwave frequencies if the polarization is to be orthogonal to that of the sandwich wire.

Trough-guide Antennas[92–94] (Fig. 16-36)   Characterized by mechanical simplicity and greater (by 50 per cent) bandwidth for single-mode propagation than rectangular waveguide, the trough guide is well suited for exciting radiating discontinuities and has also found application as a leaky-wave antenna (Fig. 16-45 in Sec. 16.8). It can be viewed as a strip transmission line operated in its first higher (a TE) mode; the plane bisecting the strip line (dashed line, Fig. 16-35a) is an electric null plane of this mode and can therefore be short-circuited (see inset in Fig. 16-36a). The mode obeys the familiar dispersion relation

$$\frac{\lambda}{\lambda_s} = \sqrt{1 - \left(\frac{\lambda}{\lambda_c}\right)^2}$$

with $\lambda_c = 2w$. It cannot propagate if $w/d > 9.6$, and the curves shown are in fact not quite reliable for $w/d > 4$.[92] Zero fin thickness is assumed, the effect of finite thickness being negligible for antenna design purposes. Figure 16-3b [with relabeled abscissa—see discussion in connection with Eq. (16-5b)] helps in estimating the extent to which the (theoretically infinite) sidewalls can be reduced in height without perturbing the mode. If the center fin is serrated (Fig. 16-36b),[93] one obtains a very large range of phase velocities, including slower-than-light velocities, and of dispersion characteristics (for which the above equation does not hold; see Fig. 16-36c). In this form, the trough guide is well suited for mechanical and frequency scanning. One method, due to W. Rotman, would consist in arranging three serrated center fins side by side (with negligible spacing in between); as the center fin is moved through the short distance of one serration period p (the outer fins remaining static), the phase velocity is swept through its entire range.

Successive discontinuities can be placed on the same side of the center fin (m modes, Fig. 16-28) or on alternately opposite sides (n modes). The "L rod" (Fig. 16-36d)[94] consists of a horizontal radiating and a vertical tuning element; it is a resonant radiator
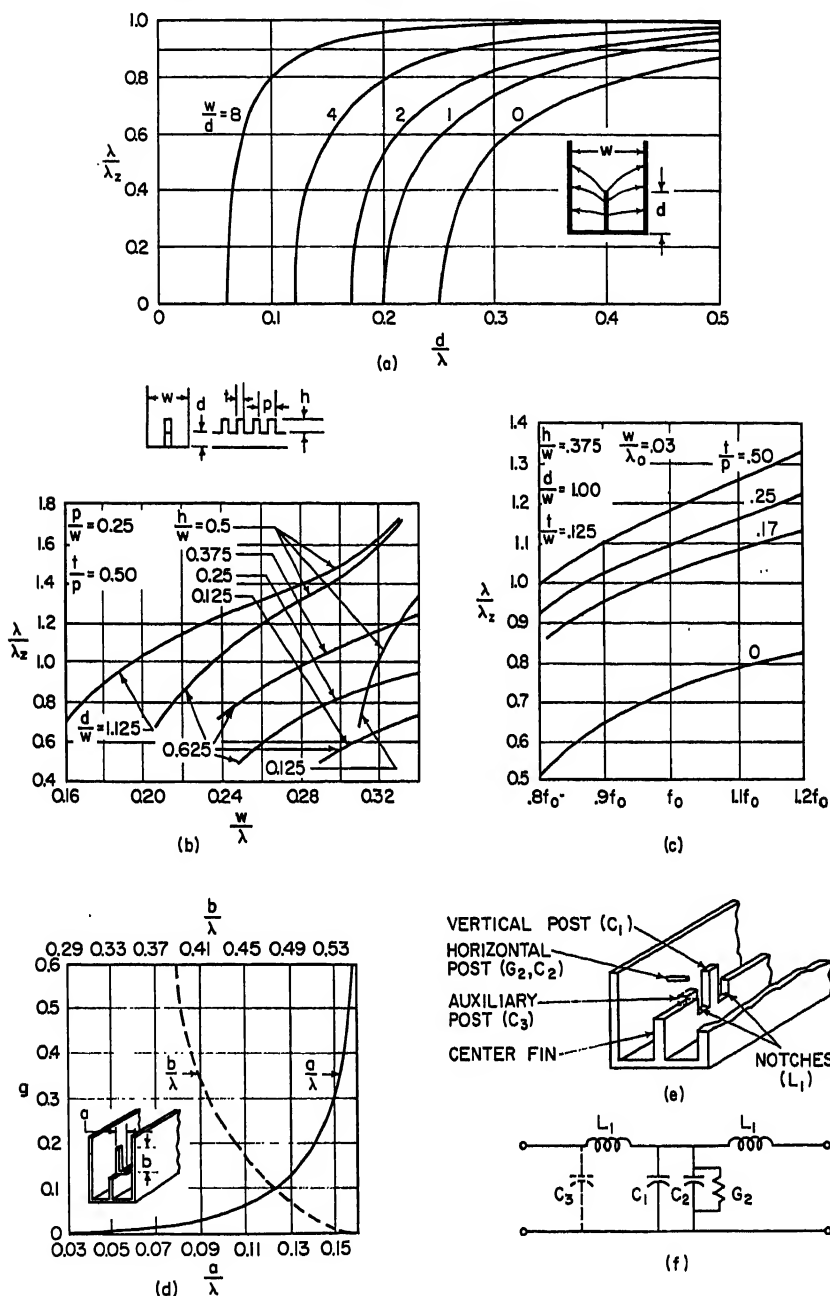
FIG. 16-36.   Trough-guide antenna: (a) Relative phase velocity on trough guide.   (*Based on data in Oliner*[92] *and Oliner and Rotman.*[93]   See text for restrictions on parameter ranges.) (b) Relative phase velocity on trough guide with serrated center fin.   (*After Oliner and Rotman.*[93])   (c) Dispersion around center frequency $f_0 = 2\pi/\lambda_0$ in trough guide with serrated center fin.   (*After Oliner and Rotman.*[93])   (d) "L-rod" radiating element.   (*After Rotman and Naumann.*[94])   (e) and (f) Notch element and its equivalent circuit.   (*From Rotman and Naumann.*[94])

(therefore bandwidth-limited) and produces a good range of normalized conductance values. Except for a useful equivalent circuit, no data are available on the notch (with compensating posts) element (Fig. 16-36e),[94] which is also horizontally polarized. Because its equivalent circuit is a pi network (Fig. 16-36f), this element is nonresonant and could be used for broadside radiation (Sec. 16.5).

A vertical post located on the center fin and extending above the level of the sidewalls would produce vertical polarization; arrays consisting of several such posts per wavelength are described in Sec. 16.8 (Fig. 16-45c).

Dielectric Rod or Image Line with Discontinuities. For λ/λ_z, see Fig. 16-18a. Short pieces of wire can be radially inserted in the dielectric, extending partially into air. Conductance values and resonant lengths of spike are given[95] as a function of its

(a)   (b)

(c)
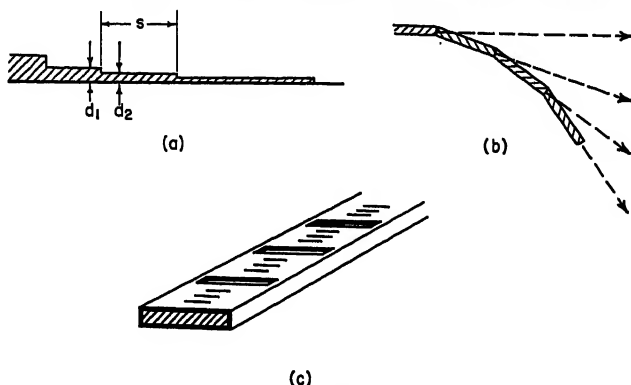
FIG. 16-37.   Dielectric-strip antennas: (a) Longitudinal cross section of stepped dielectric strip.[97] (b) Top view of strip with successive segments bent in ground plane, so that radiation from individual steps (arrows) produces a prescribed pattern.[98] (c) Wafer antenna.[100]

circumferential location and depth of insertion. Some spurious radiation is produced by the surface-wave launcher and by variations in the orientation of the spikes which control the amplitude distribution along the array. Either m or n modes can be realized (Fig. 16-28).

Beads of higher dielectric constant and larger diameter than the dielectric rod along which they are inserted at constant intervals produce m-mode radiation, but the patterns are not very clean.[99]

Stepped Dielectric Strips. See Fig. 16-19 and accompanying text in Sec. 16.4; the polarization is vertical. The steps may be changes in thickness (Fig. 16-37a) or in dielectric constant. The normalized step conductances can be calculated from formulas given by Robieux[97] for the surface-wave transmission coefficients of the discontinuities:

$$g = \frac{(d_1 - d_2)^2}{4d_1 d_2} \qquad \text{(for steps as in Fig. 16-37a)}$$

$$g = \frac{\epsilon_1 + \epsilon_2 - 2\epsilon_0}{4(\epsilon_1 - \epsilon_0)(\epsilon_2 - \epsilon_0)} \qquad \text{(for discontinuities in } \epsilon\text{)}$$

where the subscripts 1 and 2 refer to the structure before and after the step, respectively. These expressions show that if the surface wave is loosely bound (small d_1 and d_2, or ϵ_1 and ϵ_2 not much larger than ϵ_0), a small step produces a large g.

The element pattern peaks near end fire; if the strip is wide, the peak is very close to 0°, if narrow, close to $\alpha_{z1}\lambda/2\pi$ radians, where α_{z1} is the vertical decay constant just before the step, and the step is assumed to be small. The element-pattern beamwidth

for wide or narrow strips is about $1.2\alpha_{z1}\lambda/2\pi$ radians, which is quite narrow if the wave is loosely bound. The array as a whole is therefore not useful in directions other than near end fire.

The interelement spacing is not uniform, but fixed by the requirement that a step must be located so as to be in the far field of the radiation from the preceding step: $s/\lambda \cong 10/(\alpha\lambda)^2$ [which is a slightly shorter distance than that prescribed by Eqs. (16-15) and (16-19)]. If the steps are small, the array acts like a continuously tapered surface-wave antenna, with gain and other pattern characteristics as described in Sec. 16.3.

The array can also be bent in the ground plane in such a way that the step radiations form a cosecant-squared pattern in azimuth (Fig. 16-37b).[98]

Dielectric-image-line-excited Two-dimensional Slot Array[80,99] ("Cooper" array, Fig. 16-33). Design principles for an array of this type are given in Sec. 16.5 [see Eq. (16-36) and text]. To produce radiation in a half space only, the plane containing the slots can be backed, at a distance of 0.25λ in the dielectric filler, by a reflecting sheet (Fig. 16-33a), or else the slots can be deep-etched in a single thick metal sheet. Because of spurious radiation from the surface-wave feed and losses in the parallel-plate dielectric, the efficiency of models constructed so far has not been high.

Slots are of resonant length. Their amplitude of excitation depends on relative location in the exciting field (i.e., on distance from image line and on surface-wave parameter α_r) and on the angle α (Fig. 16-33b). The largely longitudinal ground-plane current excites two slot field components:

$$E_y = p \sin \alpha \cos \alpha$$
$$E_z = p \sin^2 \alpha$$

(p is a proportionality constant). E_y is zero in Fig. 16-33c (end-fire radiation), but when α is small, as is usually the case (Fig. 16-33b), broadside radiation, E_y is the dominant component. Conversely, E_z, which is dominant in the end-fire case, is zero at broadside, because phase reversal cancels contributions from successive slots.

FIG. 16-38.   (a) Surface-wave turnstile. (Reference 101.) (b) Pinecone antenna. (Reference 102.)

Dielectric Wafer[100] (Fig. 16-37c). A TM surface wave travels along the closely spaced nonresonant slots cut into a flat, metal-clad dielectric waveguide and excites the larger, resonant slots. Center-fed and operated as a resonant array, the antenna radiates a broadside beam.

Surface-wave Turnstile[101] (Fig. 16-38a). A dielectric rod with metal core supports two modes without cutoff: one closely resembles that in Fig. 16-4c, the other, called a Goubau mode, is radially symmetrical. Launched from below, the latter mode excites spikes arranged helically on a metal pole (pitch = λ). Successive spikes in each of the two orthogonal planes containing the pole are phase-reversed and spaced $\lambda/2$; hence the radiation is broadside, omnidirectional, and horizontally polarized. The spike-on-pole structure acts like an artificial dielectric that slightly binds and slows up the illuminating beam.

Pinecone Antenna[102] (Fig. 16-38b). Similar in principle to the surface-wave turnstile, this antenna consists of a helix that launches a circularly polarized beam to

illuminate a stack of metal rings above it. Spaced approximately 1λ apart, these radiate broadside. Sharp elevation patterns were obtained by adjusting the diameter and exact spacing of individual rings.

16.7. LEAKY-WAVE ANTENNAS: DESIGN PRINCIPLES

Leaky waves arise when a shielded waveguide is perturbed continuously (Fig. 16-1c), or at intervals that are short compared with wavelength (Fig. 16-40 in Sec. 16.8), or when an open waveguide is perturbed in either manner (Fig. 16-45a and c). The interrelationships of leaky-wave parameters are described by Eqs. (16-8) to (16-10); β_s and α_s are both related to the geometry of the structure and can be rigorously calculated in some instances (Sec. 16.2). Design principles follow closely those for waveguide slot arrays and arrays of surface-wave-excited elements; the discussion in this section therefore parallels that in Sec. 16.5.

Direction of Main Beam. Equation (16-10b) for the angle of emergence of a leaky wave is identical with Eqs. (16-28) provided $s = 0$. This would mean that all modes in Eqs. (16-28) degenerate into the case $m = 0$ and that the leaky-wave beam is therefore restricted to the forward quadrant, excluding broadside (Fig. 16-28). It is possible, however, to make use of the $n = 0$ mode as well by alternately phase-reversing successive sections of leaky waveguide, as shown in Fig. 16-45b. Since the equivalent circuit of a section of leaky guide is a lossy transmission line, this arrangement allows the beam to be placed in the broadside position without giving rise to a large impedance mismatch. Radiation in the back quadrant, though possible in the $n = 0$ mode, has not so far been achieved, perhaps because the element pattern of the individual leaky-wave section is too directional along end fire to allow good array patterns to be produced for $\theta > 90°$.

Since leaky waveguides are dispersive, λ/λ_s usually being a monotonically increasing function of frequency, the beam moves [Eq. (16-10b)] in the direction of decreasing θ (from broadside toward end fire) with increasing frequency. Solutions of Eq. (16-11) show that the dispersion of most leaky waveguides is of the familiar form

$$\frac{\lambda}{\lambda_s} = \sqrt{1 - \left(\frac{\lambda}{\lambda_c}\right)^2} \tag{16-37}$$

where λ_c is a function of geometry only. Equations (16-10b) and (16-37) can be combined in that case to show explicitly the dependence of main lobe direction on frequency.

Control of Aperture Distribution. The power distribution along the aperture is controlled by varying the leakage along it, as illustrated in Fig. 16-41a (Sec. 16.8). With a variable α_s, the power distribution is given by

$$P(z) = P_{\text{in}} \exp\left[-2\int_0^z \alpha_s(z)\,dz\right]$$

(which takes on a more familiar form if α_s is constant). Differentiating,

$$-\frac{dP(z)}{dz} = 2\alpha_s(z)P(z)$$

which is the same as Eq. (16-30) if $2\alpha_s(z)$ is substituted for $g(z_i) = g_i/s$. Equation (16-33), the basic design equation, therefore still holds provided we write $2\alpha_s(z)$ instead of g_i/s on the left-hand side and drop the subscripts i on the right, since α_s is a continuous function of z. The units of $\alpha_s(z)$ in this equation are *nepers per unit length* (multiply by 8.68 to obtain decibels per unit length).

The large values of α_s required to keep P_l in Eq. (16-33) small in short arrays are realizable with many of the structures described in Sec. 16.8.

See end of Sec. 16.2 for the *measurement* of leaky-wave parameters.

Array Synthesis and Beam Shaping. The techniques mentioned in Sec. 16.5 are applicable; see especially Taylor[73] (Fig. 16-30) and Dunbar.[76] Kelly[103] has shown that an amplitude distribution in Eq. (16-33) of the simple form $A(z) = 1 - \pi z/l$ (l is the antenna length), with linear phase progression, results in a good approximation (within ± 1.5 db) to the often needed $\csc^2 \theta \cos^{1/2} \theta$ pattern. Some synthesis problems require θ, and thus λ/λ_s [Eq. (16-10b)] to be variable along the aperture (functions of z).

Leaky-wave antennas can be designed for installation on a curved surface, a feature
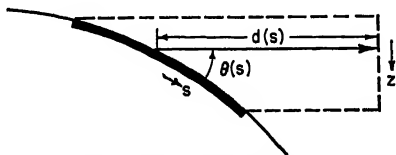
FIG. 16-39. Curved leaky-wave antenna.

not possessed by surface-wave-excited arrays (since it is too complicated to control the pattern in the presence of both element radiation and curvature-induced leakage radiation); the change in β_s and α_s has been found negligible in the case of leaky-wave structures that are perturbations of shielded guides (e.g., a long slot) provided that the radius of curvature is larger than 20λ. It is clear from Fig. 16-39 that the relative phase velocity must vary along s in order to produce a beam that keeps pointing in the same direction in space (at right angles to the projected aperture z):

$$\frac{\lambda}{\lambda_s(s)} = \cos [\theta(s)]$$

where $\theta(s)$ is prescribed by the geometry. The required aperture distribution $A(s)$ in the curved aperture is obtained from the prescribed distribution $A(z)$ in the projected aperture by conservation of power. If the curved antenna is an area source (width transverse to the page), then

$$A^2(s) = A^2(z) \sin [\theta(s)]$$

where $A^2(s)$ and $A^2(z)$ have dimensions of power per unit area. If the curved antenna is a line source (not confined between parallel plates), energy spreads at all angles with the page and[104]

$$A^2(s) = A^2(z)\, d(s) \sin [\theta(s)]$$

where $A^2(z)$ has dimensions of power per unit area but $A^2(s)$ power per unit length (along s); $d(s)$ is prescribed by the geometry.

Beam shaping can also be accomplished if the antenna is placed on a surface bent in the shape of a polygon.[104]

Gain, Beamwidth, and Sidelobe Level. See Sec. 16.5 for characteristics at a single frequency. For behavior as a function of frequency, see paragraph on scanning at the end of this section.

Arrays of Line Sources; Area Sources. To obtain directivity in both planes, a flared horn can be attached to the leaky guide or several guides can be placed parallel to each other. The mutual interaction of parallel leaky-wave antennas depends on whether the elemental radiators are end-to-end or broadside. With transverse slots (Figs. 16-40, 16-43, etc.), the magnetic dipoles are end-to-end and the coupling is slight; with TE-excited longitudinal slots (Figs. 16-41a and b, 16-42a, etc.), the magnetic dipoles are broadside, and although β_s is affected only negligibly, α_s is much perturbed. Detailed analysis in the case of two long slots excited in phase shows[106] that for very small spacings between line sources, α_s is almost twice its unperturbed value. As the spacing increases, α_s decreases and then oscillates about its unper-

turbed value, the amplitude of oscillation remaining quite large even when the spacing is several wavelengths. If arrays of such slots are to be designed (although it would be far simpler to use an area source instead), the drastic change in the element pattern due to the presence of all other slots must be taken into account.[29]

Several area sources are described in Sec. 16.8. With two of these, one vertically and the other horizontally polarized (Figs. 16-44 and 16-46), extremely precise pattern control has been achieved, both in the elevation plane and in the plane perpendicular to it (in which the beam shape is controlled by the phase and amplitude distribution in the feed).

The V arrangement shown in Fig. 16-32a is useful for leaky line or area sources; Fig. 16-32b is inapplicable since the beam cannot be placed in the back quadrant.

Feeds. If the transition from unperturbed to leaky guide is not too abrupt—and it need not be, since the α_s required near the feed is invariably small—there will be no detectable spurious feed radiation (a situation very unlike that with surface waves). There will also be no appreciable impedance mismatch, and the input impedance of a leaky-wave antenna is therefore largely that of the feed itself.

To decrease the power carried in the initial section of the leaky guide, and thus lessen the danger of voltage breakdown in high-power application, a feeding guide can be coupled (through slots in a common wall) to the leaky guide along its entire length.[107] Distributed feeds of this type have also been explored, though not perfected, for pattern control and scanning.[25,108]

Suitable feeds for area arrays are either a (narrow-band) broadside slot array or a (much wider-band) pillbox arrangement such as a hoghorn. Details on the latter are given by Honey;[109] see also Chaps. 10 and 12.

Termination. Resistance cards, e.g., three tapered 200-ohm cards arranged parallel to each other and to the waveguide sidewalls, make satisfactory loads in waveguide or parallel-plate systems. To test whether a design has been successful with respect to dissipating negligible power in the load, one can check the effect on the radiation pattern by short-circuiting the termination; the change should be insignificant.

Effect of Radome. Nishida[110] has shown that a thin dielectric cover placed over a long slot increases β_s very slightly and considerably reduces α_s. This means that the direction of the main beam shifts very little, but the beam shape is impaired, and attenuation measurements should, therefore, be performed in the presence of the radome in an early design stage.

Circular Polarization. Two circularly polarized leaky-wave antennas have been proposed; they are described in Sec. 16.8, in connection with the structures illustrated in Figs. 16-43 and 16-45. See also the remark on circular polarization in Sec. 16.5.

Scanning. Mechanical scanning, as with slot arrays, can be accomplished by moving a sidewall or by inserting a variable amount of dielectric loading in the guide.[74]

When frequency-scanned, the main beam moves as described in the discussion preceding Eq. (16-37). The scan angle is limited by mode cutoff at the low-frequency end, and by the excitation of higher modes at the high-frequency end. If Eq. (16-37) applies—and it usually does—leaky-wave antennas exhibit the attractive property of constant beamwidth over the entire scanning range. The beamwidth depends on the antenna length ℓ_p/λ projected normally to the beam direction (half-power beamwidth = $55\lambda/\ell_p$ degrees for constant aperture illumination; Sec. 16.5). From Fig. 16-31,

$$\ell_p = \ell \sin \theta = \ell \sqrt{1 - \cos^2 \theta}$$

Using Eqs. (16-10b) and (16-37),

$$\frac{\ell_p}{\lambda} = \frac{\ell}{\lambda} \sqrt{1 - \left(\frac{\lambda}{\lambda_s}\right)^2} = \frac{\ell}{\lambda_c} \qquad (16\text{-}38)$$

a ratio that depends only on the antenna geometry and is thus independent of frequency.[109] If in addition α_z, and hence the aperture illumination, do not change materially over the frequency range, the beamwidth and sidelobe level will remain constant. In the case of the inductive-grid antenna (Fig. 16-46) the beam scans from 30 to 70° over almost a frequency octave; the elevation beamwidth remains constant over the upper two-thirds of this band, increasing very slowly at lower frequencies because of a gradual change in α_z, and the sidelobe level remains below its preassigned value (23 db) over the entire band.

Since the beamwidth in the plane perpendicular to the elevation pattern depends on the feed, and thus necessarily broadens with decreasing frequency, the gain of the antenna must also drop with frequency, but it will do so at a *slower* rate than the gain of a dish (about 4 db over almost a frequency octave in the case of the inductive-grid antenna).

Mechanical and frequency scanning have also been explored in connection with curved leaky antennas.[104]

16.8. LEAKY-WAVE ANTENNAS: SPECIFIC STRUCTURES

Leaky-wave structures are listed in accordance with the unperturbed waveguide from which they derive: first strip-line, then ordinary waveguide (long slots in rectangular and circular, nonresonant slots in rectangular guide), then trough guide, and last, parallel-plate guide (transverse and longitudinal strips, holes, and disks).

The first leaky-wave antenna was a long slot in waveguide, invented by Hansen[111] (a useful reference for early leaky-wave antenna work is Southworth[48]). Almost all the structures listed here are, like the long slot, perturbations of shielded guides; the one exception (leaky trough guide, Fig. 16-45) can serve as a model for methods of introducing leakage in other open guides, for example, in channels of the type shown in Fig. 16-2b or in H guide.[84]

In choosing an antenna for design, one should first examine the data presented here to see whether the range of α_z values required by Eq. (16-33), as modified in Sec. 16.7, is obtainable from the proposed structure, then whether these α_z values are compatible with the requirements imposed by Eq. (16-10b) on λ/λ_z. In many instances, α_z and λ/λ_z are so coupled by the *same* geometric parameters as to preclude accurate beam shaping (except for special cases). True freedom in design is achieved only when the parameters that control α_z are entirely separate from those that control λ/λ_z (see the inductive-grid antenna, Fig. 16-46).

Some of the data shown are experimental, some theoretical; whenever both were available, those that seemed more reliable were plotted. With very accurate data, extremely precise pattern control can be achieved. The display is usually in terms of λ/λ_z and $\alpha_z\lambda$ as a function of the geometric parameters (z as always is in the direction of propagation along the guide), but because of the various ways in which parameters can be related to λ_z and α_z, it is sometimes advantageous to arrange the data differently. The dimensionless constant $\alpha_z\lambda$ is in nepers per wavelength; multiply by 8.68 to convert into decibels per wavelength [but note that nepers are needed in connection with the basic Eq. (16-33), as modified in Sec. 16.7].

Fig. 16-40. Coaxially-fed nonresonant slots. (Reference 112.)

Leaky Coaxial Lines (Fig. 16-40). Less dispersive than waveguide structures that satisfy Eq. (16-37), a leaky TEM-mode line is called for whenever one tries to hold the beam position reasonably constant over a frequency band. Leakage is controlled by varying the slot length and/or displacing the inner conductor from the center.[112]
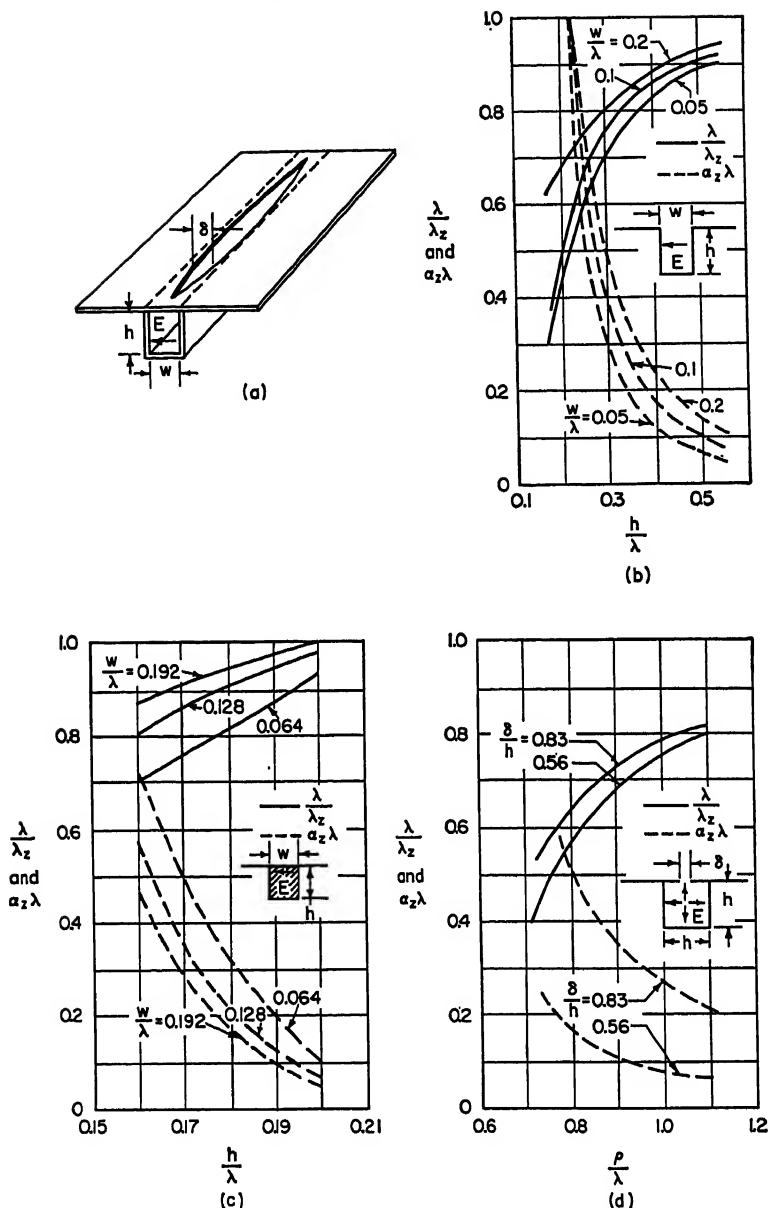
FIG. 16-41. Long slots in rectangular waveguide: (a) Narrow TE slot shown with lip of variable width. (b)–(d) Relative phase velocity λ/λ_s and leakage attenuation $\alpha_z\lambda$ on (b) TE channel, (c) Dielectric-filled channel ($\epsilon = 2.56$) with hybrid (quasi-TE) excitation, (d) Narrow TM slot. (After Hines, Rumsey, and Walter[115] and Goldstone and Oliner.[3])

Good shaped patterns have been produced with this antenna, but no data are available on λ/λ_z and $\alpha_z\lambda$ as a function of the parameters.

Long Slots in Rectangular Waveguide.[3,104,113-115] By proper positioning of a longitudinal slot in the walls of rectangular waveguides, any one of the following field configurations can be excited:[115]

1. TE (no E_z in slot): slot must be narrow and placed where wall currents are perpendicular to it, e.g., Fig. 16-41a and b. The elemental radiation pattern is that of a z-directed magnetic dipole; hence end-fire radiation is zero.

2. TM (no H_z): slot must be placed where currents are parallel to it, e.g., Fig. 16-41d. Elemental pattern is that of an x-directed electric dipole.

3. Hybrid with negligible E_y: guide must be filled with dielectric ($\epsilon \geq 2.0$), e.g., Fig. 16-41c.

4. Hybrid with negligible H_y: guide must be *partially* filled with dielectric and excited in lowest-order hybrid mode (not illustrated).

Configurations 2 to 4 are sometimes termed "channel-guide" antennas; configuration 3 is known to support also waves with negligible leakage (Fig. 16-19c and accompanying text, Sec. 16.4).   Because of the presence of several field components in the channel-guide slots, the far-field patterns are linearly polarized only provided[115] $0.4 \leq w/\lambda \leq 0.9$, $1 \leq \epsilon \leq 2.5$, and $0.4 \leq \lambda/\lambda_z \leq 1.0$.

All the structures in Fig. 16-41 have been treated theoretically.[3,113,114]   In the case of Fig. 16-41a, for example, λ/λ_z and $\alpha_z\lambda$ are explicitly related to the geometric parameters by[3]

$$\frac{\lambda}{\lambda_z} = \frac{\lambda}{\lambda_{z0}}\left(1 - \frac{\lambda_{z0}^2}{2\pi^2 hw}\frac{p}{1+p^2}\right)$$

$$\alpha_z\lambda = \frac{\lambda\lambda_{z0}}{\pi hw}\frac{1}{1+p^2}$$

where

$$p = \frac{2}{\pi}\left[\ln\left(\csc\frac{\pi\delta}{2w}\right) + \ln\left(1.526\frac{h}{\delta}\right)\right]$$

and λ_{z0} is the guide wavelength ($= \lambda/\sqrt{1-(\lambda/2h)^2}$) in the unperturbed waveguide ($\delta = 0$). These explicit expressions are based on a perturbation calculation that is valid only provided $\delta \ll w$. Zero ground-plane thickness is assumed. Though not strictly separable, λ/λ_z is primarily controlled by variations in h (through λ_{z0}) and $\alpha_z\lambda$ by variations in δ. Dielectric or other loading of the guide[104] will primarily affect λ/λ_z.

Results for the other structures in Fig. 16-41 are displayed graphically.

Because they require a smaller variation in guide parameters to cover a prescribed range in $\alpha_z\lambda$, TM- and hybrid-excited slots lend themselves somewhat more easily to pattern control than TE-excited slots. Even so, good control has been achieved with the slot in Fig. 16-41a,[104,115] a typical result being that a Gaussian amplitude distribution produces low sidelobes over a 2:1 frequency range in which the beam swings from 38° to 18° off end fire.

Long Slots in Circular Waveguide[115-117] (Fig. 16-42). Perturbation formulas are available that relate the relative phase velocity and leakage explicitly to the geometric parameters.[117]

Closely Spaced Slots and Holes in Rectangular Waveguide. Like the long slot in Fig. 16-41a, the closely spaced slots in Fig. 16-43a are excited by the dominant TE waveguide mode. The element pattern in this instance is that of a transverse magnetic dipole (vertical polarization). Also as in the case of the long slot, λ/λ_z is primarily controlled by varying the width of the broad waveguide wall (h in Fig. 16-41a, w in Fig. 16-43a). $\alpha_z\lambda$ depends primarily on slot spacing and width (Fig. 16-43b and c)[118] and on the width of the narrow waveguide wall (no curves available).

Though not strictly separable, both λ/λ_z and $\alpha_z\lambda$ can be accurately controlled over a wide range of values by appropriate variations in the large number of available parameters.

Hyneman[118] points out that over a certain range of the parameters a surface wave exists together with the leaky wave, but recent experimental work suggests that over
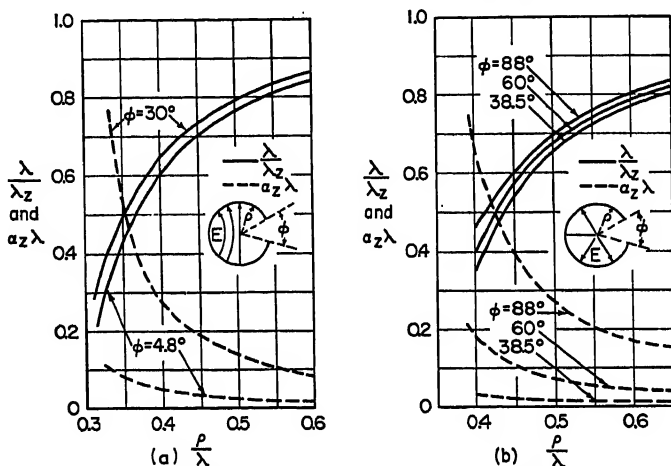
FIG. 16–42. Long slots in circular waveguide: (a) TE. (b) TM. (*After Harrington*[116] *and Goldstone and Oliner.*[117])
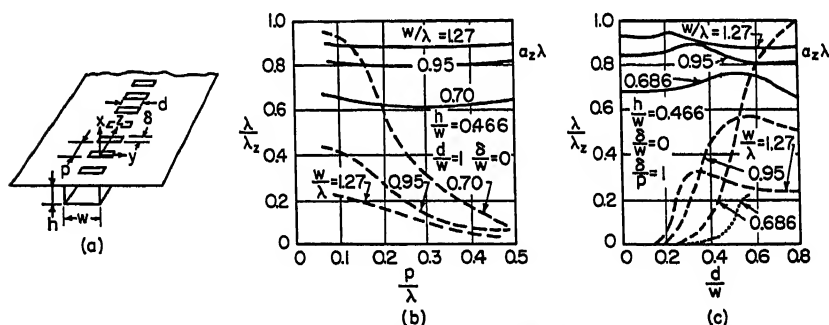
FIG. 16–43. Closely spaced slots in rectangular waveguide. (*After Hyneman.*[118]) (a) Structure. (b) and (c) Relative phase velocity and leakage attenuation as a function of parameters (curves are based on theoretical values for infinitely many slots per wavelength, also valid experimentally for $\delta/w = 0.033$, $\delta/p = 0.4$). Discrepancy in (c) between dotted curve (*after Kelly and Elliott*[103]) and corresponding dashed line may be due to fact that Kelly's and Elliott's slots were milled to their required length while Hyneman's slots were milled across entire width of guide and then partially covered by metal foil.

much of this range the effects of the spurious mode—if it is excited at all—cannot be detected in the radiation pattern.[40]

A circularly polarized line source can be obtained by milling closely spaced transverse slots in all four sides of a square waveguide and exciting it with two orthogonal TE modes 90° out of phase.[119]

The "serrated" waveguide analyzed by Elliott[103,120] looks like Fig. 16–43a but has a top wall of considerable thickness, variations in which control $\alpha_z\lambda$. Since closely spaced thick slots are difficult to manufacture, this guide has not found application.

(See, however, the related plane array of thick transverse slots, Fig. 16–44 and text.)

Theoretical results are available for closely spaced round holes in rectangular waveguide.[3]

Plane Array of Thick Transverse Slots.[121] The array of waveguides in Fig. 16–44 is TE-excited by means of a hoghorn or other arrangement. Each guide in turn excites an array of slots approximately one-quarter wavelength thick, which couple only a small amount of power from the guide and do not appreciably perturb the guide phase velocity. Since the interslot spacings s lie between 0.25λ and λ, this antenna is not really a leaky guide but a shielded-waveguide-excited array of discrete elements and could have been included in Chap. 9. It is presented here for the sake of completeness and because of its close relationship to the serrated waveguide (see above).
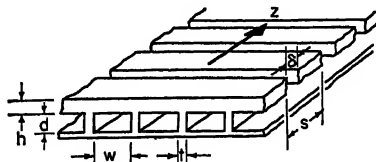
FIG. 16–44. Plane array of thick transverse slots. (Reference 121.)

The main-beam direction is given by the $m = 0$ curve in Fig. 16–28. The pattern bandwidth is approximately 1.6:1, limited by mode cutoff at the low- and by Eq. (16–29) at the high-frequency end. In one particular application, the beam swings from 71° to 34° off end fire, and since Eq. (16–38) applies (Sec. 16.7), the elevation-pattern (E-plane) beamwidth stays constant over the entire frequency range.

At the frequency for which the equivalent electric thickness of the top wall is 0.25λ, the relative phase velocity is that of the waveguide ($\lambda/\lambda_z = \sqrt{1 - (\lambda/2w)^2}$). At lower frequencies, the slots load the guide capacitively, slightly decreasing λ/λ_z; at higher frequencies, λ/λ_z slightly increases. The electric thickness is 0.25λ provided

$$h = \frac{\lambda}{4} - \frac{\delta}{\pi}\left(1 + \ln\frac{2s}{\pi\delta} + \ln\frac{d}{2\delta}\right)$$

(see Fig. 16–44 for meaning of symbols).

The element normalized conductance is

$$g = 1.54 \frac{w^2\delta^2}{\lambda_z s\, d(w + t)}$$

(s appears in this expression because the underlying analysis[121] takes into account the mutual impedance between slots.) g is controlled by varying δ, and to satisfy the first equation, h must be variable along the array; flexing of the bottom surface in the z direction is avoided by holding $h + d$ constant.

Leaky Trough-guide Antennas[94,122,123] (see also Fig. 16–36 and Sec. 16.6). The design parameters of the asymmetric trough guide (Fig. 16–45a) are chosen as follows:

1. From Eqs. (16–10b) and (16–37) determine λ/λ_z and $\alpha_z\lambda$, respectively.

2. Calculate

$$n = \frac{\alpha_z\lambda}{\lambda_z/\lambda - \lambda/\lambda_z}$$

3. Use the table to find values of p and q corresponding to n:

n	0.000	0.025	0.126	0.320	0.465	0.672	0.886	1.118
p	0.250	0.263	0.277	0.293	0.299	0.305	0.309	0.307
q	0.250	0.237	0.221	0.205	0.194	0.183	0.170	0.153

4. Then

$$\frac{d_1}{\lambda} = \frac{p}{\sqrt{1 - (\lambda/\lambda_z)^2}} - \frac{\delta}{\lambda}$$

$$\frac{d_2}{\lambda} = \frac{q}{\sqrt{1 - (\lambda/\lambda_z)^2}} - \frac{\delta}{\lambda}$$

where $\delta \cong (w/\pi) \ln 2$ (assuming d_1 and $d_2 > w$; otherwise see Oliner[92,122]). This procedure, which automatically "uncouples" the parameters controlling λ/λ_z and
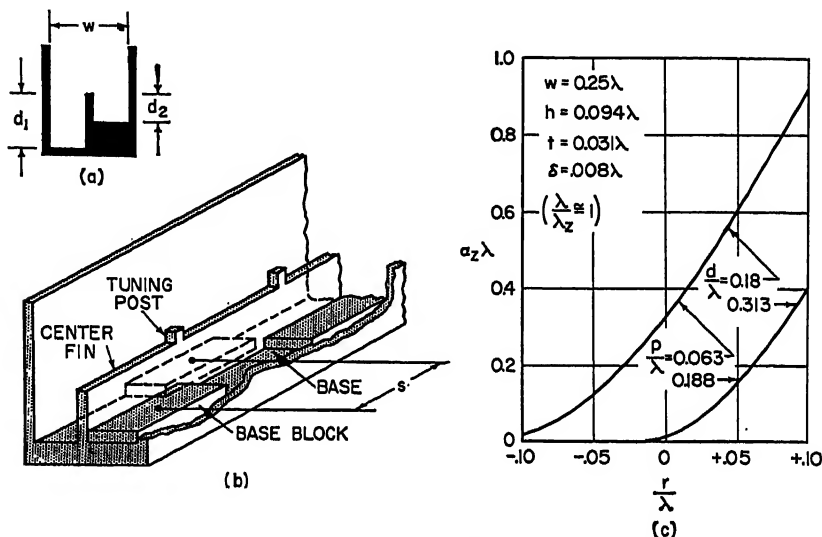
Fig. 16-45. Leaky trough-guide antennas. (a) Continuously asymmetric trough guide. (Reference 122.) (b) Periodically asymmetric trough guide. (*From Rotman and Oliner.*[122]) (c) Leakage attenuation of trough guide with serrated center fin protruding a distance r/λ above level of sidewalls (negative values of r/λ correspond to center fin below sidewall level; δ = fin thickness; other symbols as in Fig. 16-36b). (*After Rotman and Karas.*[123])

$\alpha_z\lambda$, is adapted from Rotman and Naumann[94]; formulas that give λ/λ_z and $\alpha_z\lambda$ explicitly (but coupled) in terms of the geometric parameters have been derived by Oliner.[122] Our expressions assume that the frequency is not too near cutoff ($\lambda/\lambda_z > 0.5$) and that $\alpha_z\lambda$ is small; they also neglect the finite thickness of the center fin, which if taken into account is found to slightly increase λ/λ_z and decrease $\alpha_z\lambda$.[122]

By alternately reversing successive asymmetric sections (Fig. 16-45b)[94,122] and by serrating the center fin as in Fig. 16-36b to obtain a wide range of λ/λ_z values, the main beam can be placed anywhere between end fire and just beyond broadside on the $n = 0$ curve in Fig. 16-28 (see Sec. 16.7 on possible reason for observed pattern deterioration in back quadrant). The relative phase velocity of the periodically asymmetric trough guide is approximately the same as that of the corresponding continuously asymmetric one, but α_z is somewhat less, because in the immediate vicinity of the interface between successive base blocks (Fig. 16-45b) the periodic structure resembles a symmetric trough guide and radiates less; α_z must therefore be measured.[94,122] [The radiation mechanism of the periodically asymmetric trough guide closely resembles that of the sandwich wire (Sec. 16.6) except that the radiation is distributed slightly more evenly along its length.] As in the case of the sandwich-wire antenna, small tuning posts (Fig. 16-45b) are needed to suppress the reflected

wave when the radiation is broadside. The optimum dimensions are found experimentally by minimizing the input VSWR to a line with, say, 10 identical blocks, terminated in a matched load. It is found that the higher the block, the higher the tuning post and the larger the distance from the block interface at which it must be placed.[122]
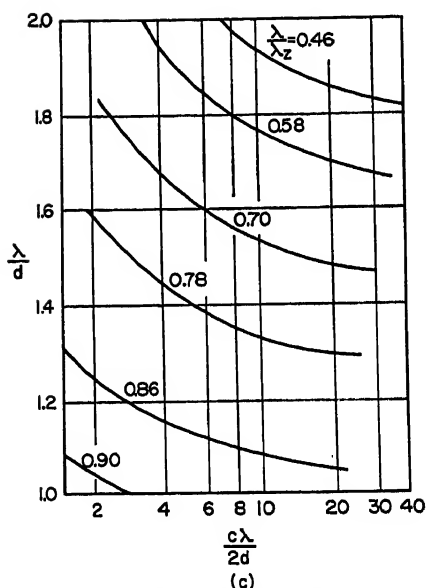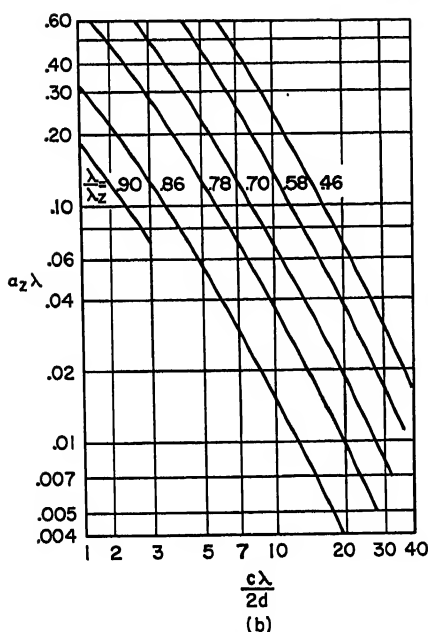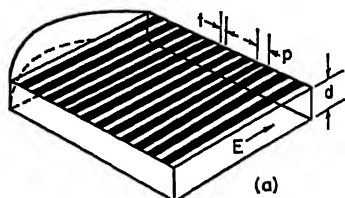
Fig. 16-46.   Inductive grid antenna: (a) Structure.   (b) and (c) Relative phase velocity and leakage attenuation as a function of the parameters, with $c = 2\pi d/p \ln [\csc (\pi t/2p)]$. (After Honey.[109])

The symmetric trough guide with serrated fin (Fig. 16-36b) produces a leaky wave if the sidewalls are lowered appreciably.[123] From Fig. 16-45c, which shows $\alpha_z\lambda$ values measured in one particular instance, it appears that leakage begins as the sidewalls approach the level of the teeth and increases monotonically as they are lowered still further, and also that $\alpha_z\lambda$ increases with the number of teeth per wavelength. λ/λ_z is only negligibly affected by the reduction in sidewall height.

Circular polarization could be obtained by combining the horizontally polarized asymmetric trough with the vertically polarized protruding-teeth structure.[123] Scanning methods are mentioned in Sec. 16.6, under trough-guide antenna.   Note that Eqs. (16-37) and (16-38) apply neither to the asymmetric nor to the serrated-fin leaky trough guide.

Inductive-grid Antenna (Transverse Strips)[109] (also called "Honey" array, Fig. 16-46).   Unlike the plane array of thick transverse slots (see above), this antenna is horizontally polarized, and it is a true leaky-wave structure (many strips per wavelength).   Because λ/λ_z and $\alpha_z\lambda$ can be independently controlled and are known very accurately, radiation patterns have been produced that differ by only 0.5 db from the design value, even in regions 40 db below the peak.   The full pattern bandwidth,
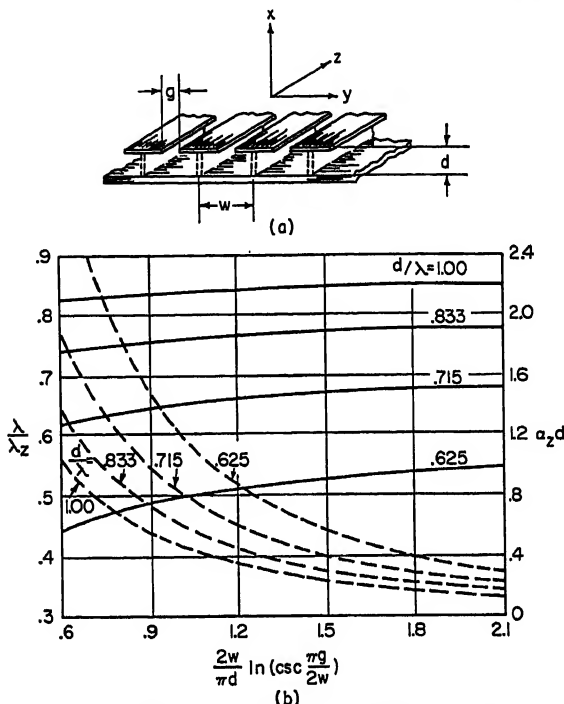
Fig. 16-47. Longitudinal strips: (a) Structure (E field in y direction). (b) Relative phase velocity (solid curves) and leakage attenuation (dashed curves) as a function of the parameters. (*After Honey.*[125])

within which the beam scans from 70° to 30° off end fire, is 1.8:1.   The elevation-pattern (H-plane) beamwidth remains constant over a 1.5:1 range, then increases at the low-frequency end of the band (by 35 per cent at 70°).

λ/λ_z depends primarily on the grid-to-bottom-plate spacing d, $\alpha_z\lambda$ primarily on the grid parameters.   The design procedure is to read the abscissa value in Fig. 16-46b corresponding to the desired λ/λ_z and $\alpha_z\lambda$ and then to use Fig. 16-46c for determining d. (The bottom plate is therefore necessarily flexed in the z direction.)   Figure 16-46a shows flat strips that can be photo-etched on Teflon-Fiberglas laminate and supported by polyfoam.   The curves in Fig. 16-46b and c, however, also apply to a grid of transverse round wires with diameter $t/2$, except that a correction term is needed if the wire-to-wire spacing p is an appreciable fraction of a wavelength.[109]

An omnidirectional radial-cylindrical variant of the inductive-grid antenna produced good patterns over a 1.5:1 frequency range.[124]

Longitudinal Strips[125] (Fig. 16-47).   Because it is difficult to achieve tight control over $\alpha_z\lambda$ when the leakage is small (as it must be in long arrays), this antenna is less satisfactory than the inductive grid.   Formulas are available that give the explicit dependence of phase velocity and leakage on the parameters.[3]

Holey-plate and Mushroom Antennas.[126] Since the center-to-center spacings between holes in Fig. 16-48a and b and between disks in Fig. 16-48c lie between 0.25λ and λ, these antennas are not really leaky waveguides but, like the plane array of thick transverse slots (see above), belong to the group of shielded-waveguide-excited discrete elements. We include them here for the sake of completeness and because they are, like the transverse and longitudinal strips, perturbations of parallel-plate structures.

If the holes in Fig. 16-48a and b are small ($\delta/\lambda < 0.3$), the normalized element conductance $g \cong 10(\delta/\lambda)^6$. The plate spacing is close to a quarter wavelength: $d/\lambda \cong 0.25 + \sqrt{g}/4\pi$. The relative phase velocity is so close to 1 that end-fire
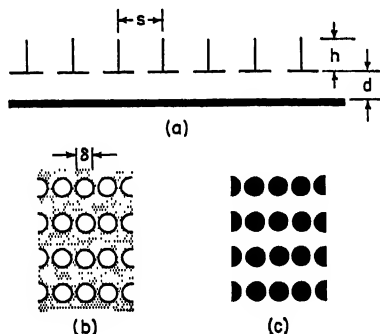
FIG. 16-48. Holey-plate and mushroom antennas: (a) Top view. (b) Longitudinal cross section of holey-plate (with $h \cong \lambda/3$). (c) Top view of mushroom antenna. (*After Broussaud.*[126])

radiation ($m = 0$ in Fig. 16-28) as well as radiation in the back quadrant ($m = 1$) is produced. Broussaud erects transverse vanes between rows of holes (Fig. 16-48a) and finds that this suppresses the end-fire radiation. The vanes presumably load the parallel-plate structure inductively, thus increasing λ/λ_z slightly above 1 (Fig. 16-28); any other type of inductive loading would do as well.

The holey plate is excited by a TEM wave and produces an E-plane elevation pattern. Its Babinet equivalent, the array of disks (Fig. 16-48c), is TE-excited and produces an H-plane elevation pattern; because its E field is y-directed, the disks can be supported on metal stems (hence "mushroom" antenna).

REFERENCES

1. N. Marcuvitz (ed.): "Waveguide Handbook," MIT Radiation Laboratory Series, vol. 10, McGraw-Hill Book Company, Inc., New York, 1951.
2. S. S. Attwood: "Surface Wave Propagation over a Coated Plane Conductor," *J. Appl. Phys.*, vol. 22, p. 504, 1951.
3. L. O. Goldstone and A. A. Oliner: "Leaky Wave Antennas I: Rectangular Wave-guides," *IRE Trans. on Antennas Propagation*, AP-7, p. 307, 1959.
4. J. H. Richmond and T. E. Tice: "Probes for Microwave Near-field Measurements," *IRE Trans. on Microwave Theory Tech.*, MTT-3, p. 32, 1955.
5. W. S. Lucke: "On the Terminated Corrugated Surface," Third Quarterly Progress Report, Contract W 36-039-sc-44524, Stanford Research Institute, Menlo Park, Calif., 1950.
6. H. Ehrenspeck, W. Gerbes, and F. J. Zucker: "Trapped Wave Antennas," *1954 IRE Natl. Conv. Record*, pt. 1, p. 25, 1954.
7. J. Brown and J. O. Spector: "The Radiating Properties of End-fire Aerials," *Proc. IEE*, pt. B, vol. 104, p. 27, 1957.
8. A. F. Kay, "Scattering of a Surface Wave by a Discontinuity in Reactance," *IRE Trans. on Antennas Propagation*, AP-7, p. 22. 1959.

9. F. J. Zucker: "A Surface Wave Antenna Paradox," paper presented at URSI Fall Meeting, Pennsylvania State University, University Park, Pa., 1958.

10. L. Felsen: "Field Solutions for a Class of Corrugated Wedge and Cone Surfaces," MRI Electrophys. Group Memo. 32, Polytechnic Institute of Brooklyn, Brooklyn, N.Y., 1957.

11. V. I. Talanov: "On Surface Electromagnetic Waves in Systems with Nonuniform Impedance," *Izvest. VUZ MVO (Radiofizika)*, vol. 2, p. 32, 1959. (Translated from the Russian by Morris P. Friedman, Inc., Air Force Cambridge Research Center Report TN-59-768.)

12. H. W. Ehrenspeck and H. Poehler: "A New Method for Obtaining Maximum Gain from Yagi Antennas," *IRE Trans. on Antennas Propagation*, AP-7, p. 379, 1959.

13. H. W. Ehrenspeck and W. Kearns: Unpublished experimental data, Air Force Cambridge Research Center, Bedford, Mass., 1959.

14. J.-C. Simon and G. Weill: "A New Type of Endfire Antenna" (in French), *Ann. Radioélectricité*, vol. 8, p. 183, 1953.

15. H. W. Ehrenspeck: U.S. Patent applied for, Air Force Cambridge Research Center, Bedford, Mass. (1959).

16. F. E. Boyd and D. H. Russell: "Dielectric-guide Antennas for Aircraft," Naval Research Lab. Rept. 3814, 1951.

17. F. J. Zucker and W. Kearns: Unpublished experimental data, Air Force Cambridge Research Center, Bedford, Mass., 1959.

18. H. W. Ehrenspeck and W. Kearns: "Two-dimensional End-fire Array with Increased Gain and Side Lobe Reduction," *1957 IRE WESCON Conv. Record*, pt. 1, p. 217, 1957.

19. C. F. Parker and R. J. Anderson: "Constant Beamwidth Antennas," *1957 IRE Natl. Conv. Record*, pt. 1, p. 87, 1957.

20. R. H. DuHamel and J. W. Duncan: "Launching Efficiency of Wires and Slots for a Dielectric Rod Waveguide," *IRE Trans. on Microwave Theory Tech.*, MTT-6, p. 277, 1958.

21. A. D. Frost, C. R. McGeogh, and C. R. Mingins: "The Excitation of Surface Waveguides and Radiating Slots by Strip-circuit Transmission Lines," *IRE Trans. on Microwave Theory Techniques*, MTT-4, p. 218, 1956.

22. A. L. Cullen: "The Excitation of Plane Surface Waves," *Proc. IEE*, pt. IV, monograph 93R, vol. 101, p. 225, 1954.

23. D. K. Reynolds: "Broadband Traveling Wave Antennas," *1957 IRE Natl. Conv. Record*, pt. 1, p. 99, 1957.

24. D. K. Reynolds and R. A. Sigelmann: "Research on Traveling Wave Antennas," AFCRC-TR-59-160 [Final Report, Contract AF19(604)-4052], Seattle University, Seattle, Wash., 1959.

25. W. L. Weeks: "Coupled Waveguide Excitation of Traveling Wave Antennas," *1957 IRE WESCON Conv. Record*, pt. 1, p. 236, 1957.

26. R. R. Hodges, Jr.: "Distributed Coupling to Surface Wave Antennas," Contract AF33(616)-3220, University of Illinois, Urbana, Ill., 1957.

27. B. T. Stephenson and C. H. Walter: "Endfire Slot Antennas," *IRE Trans. on Antennas Propagation*, AP-3, p. 81, 1955.

28. Unreported work at GB Electronics Corp., Valley Stream, N.Y., Technical Research Group, Inc., Somerville, Mass., and Air Force Cambridge Research Center, Bedford, Mass., 1958.

29. J. N. Hines, V. H. Rumsey, and T. E. Tice: "On the Design of Arrays," *Proc. IRE*, vol. 42, p. 1262, 1954.

30. R. S. Elliott: "On the Theory of Corrugated Plane Surfaces," *IRE Trans. on Antennas Propagation*, AP-2, p. 71, 1954.

31. R. A. Hurd: "End-fire Arrays of Magnetic Line Sources Mounted on a Conducting Half-plane," *Can. J. Phys.*, vol. 34, p. 370, 1956.

32. R. S. Elliott: "Azimuthal Surface Waves on Circular Cylinders," *J. Appl. Phys.*, vol. 26, p. 368, 1955.

33. R. S. Elliott: "Spherical Surface-wave Antennas," *IRE Trans. on Antennas Propagation*, AP-4, p. 422, 1956.

34. R. E. Plummer: "Surface-wave Beacon Antennas," *IRE Trans. on Antennas Propagation*, AP-6, p. 105, 1958.

35. F. Reggia, E. G. Spencer, R. D. Hatcher, and J. E. Tompkins: "Ferrod Radiator System," *Proc. IRE*, vol. 45, p. 344, 1957.

36. This idea is due to personnel at GB Electronics Corp., Valley Stream, N.Y.

37. R. W. Hougardy and R. C. Hansen: "Scanning Surface Wave Antennas," *IRE Trans. on Antennas Propagation*, AP-6, p. 370, 1958.

38. C. H. Walter: "Surface Wave Luneberg Lens Antenna," Report 667-32, Ohio State University Research Foundation, Columbus, Ohio, 1957.

39. S. P. Schlesinger and D. D. King: "Dielectric Image Lines," *IRE Trans. on Microwave Theory Tech.*, MTT-6, p. 291, 1958.
40. A. F. Kay: Unpublished work under AFCRC Contract AF19(604)-3476, Technical Research Group, Inc., Somerville, Mass., 1959.
41. E. H. Scheibe, B. G. King, and D. L. Van Zeeland: "Loss Measurements of Surface Wave Transmission Lines," *J. Appl. Phys.*, vol. 25, p. 790, 1954.
42. G. E. Mueller and W. A. Tyrrell: "Polyrod Antennas," *Bell System Tech. J.*, vol. 26, p. 837, 1947.
43. D. G. Kiely: "Dielectric Aerials," Methuen & Co., Ltd., London, 1953.
44. L. W. Mickey and G. G. Chadwick: "Closely Spaced High Dielectric Constant Polyrod Arrays," *1958 IRE Natl. Conv. Record*, pt. 1, p. 213, 1958.
45. R. W. Watson and C. W. Horton: "The Radiation Patterns of Dielectric Rods—Experiment and Theory," *J. Appl. Phys.*, vol. 19, p. 661, 1948; "On the Calculation of Radiation Patterns of Dielectric Rods," *J. Appl. Phys.*, vol. 19, p. 836, 1948.
46. R. Chatterjee and S. K. Chatterjee: "Some Investigations on Dielectric Aerials," pt. I, *J. Indian Inst. Sci.*, vol. 38, p. 93, 1956; pt. II, *J. Indian Inst. Sci.*, vol. 39, p. 134, 1957.
47. R. E. Beam: "Wave Propagation in Dielectric Tubes," Final Report, Contract DA36-039-sc-5397, Northwestern University, Evanston, Ill., 1952.
48. G. C. Southworth: "Principles and Applications of Wave-guide Transmission," D. Van Nostrand Company, Inc., Princeton, N.J., 1950.
49. W. Rotman: "The Channel Guide Antenna," *Proc. Natl. Electronics Conf.*, vol. 5, p. 190, 1949.
50. D. K. Reynolds and W. S. Lucke: "Corrugated End-fire Antennas," *Proc. Natl. Electronics Conf.*, vol. 6, p. 16, 1950.
51. J. O. Spector: "An Investigation of Periodic Rod Structures for Yagi Aerials," *Proc. IEE*, pt. B, vol. 105, p. 38, 1958.
52. A. D. Frost: "Surface Waves in Yagi Antennas and Dielectric Waveguides," Final Report, Contract AF19(604)-2154, AFCRC-TR-57-368, Tufts University, Medford, Mass., 1957.
53. D. L. Sengupta: "On the Phase Velocity of Wave Propagation along an Infinite Yagi Structure," *IRE Trans. on Antennas Propagation*, AP-7, p. 234, 1959.
54. J. A. McDonough and R. G. Malech: "Recent Developments in the Study of Printed Antennas," *1957 IRE Natl. Conv. Record*, pt. 1, p. 173, 1957.
55. R. G. Malech: "Lightweight High-gain Antenna," *1958 IRE Natl. Conv. Record*, pt. 1, p. 193, 1958.
56. J.-C. Simon and V. Biggi: "A New Type of Antenna and its Application to Long Distance Television Transmission" (in French), *L'Onde électrique*, vol. 34, p. 883, 1954.
57. W. A. Cumming: "A Nonresonant Endfire Array for VHF and UHF," *IRE Trans. on Antennas Propagation*, AP-3, p. 52, 1955.
58. D. L. Sengupta: "The Radiation Characteristics of a Zig-zag Antenna," *IRE Trans. on Antennas Propagation*, AP-6, p. 191, 1958.
59. R. F. Hyneman and R. W. Hougardy: "Waveguide Loaded Surface Wave Antenna," *1958 IRE Natl. Conv. Record*, pt. 1, p. 225, 1958.
60. L. Hatkin: "Analysis of Propagating Modes in Dielectric Sheets," *Proc. IRE*, vol. 42, p. 1565, 1954.
61. F. E. Butterfield: "Dielectric Sheet Radiators," *IRE Trans. on Antennas Propagation*, AP-3, p. 152, 1954.
62. R. L. Pease: "On the Propagation of Surface Waves Over an Infinite Grounded Ferrite Slab," *IRE Trans. on Antennas Propagation*, AP-6, p. 13, 1958.
63. E. M. T. Jones and R. A. Folsom, Jr.: "A Note on the Circular Dielectric Disk Antenna," *Proc. IRE*, vol. 41, p. 798, 1953.
64. R. E. Plummer and R. C. Hansen: "Double-slab Arbitrary-polarization Surface-wave Structure," *Proc. IEE*, pt. C, monograph 238R, 1957.
65. R. C. Hansen: "Single Slab Arbitrary Polarization Surface Wave Structure," *IRE Trans. on Microwave Theory Tech.*, MTT-5, p. 115, 1957.
66. W. Rotman: "A Study of Single-surface Corrugated Guides," *Proc. IRE*, vol. 39, p. 952, 1951.
67. M. Ehrlich and L. Newkirk: "Corrugated Surface Antennas," *1953 IRE Natl. Conv. Record*, pt. 2, p. 18, 1953.
68. R. A. Hurd: "The Propagation of an Electromagnetic Wave along an Infinite Corrugated Surface," *Can. J. Phys.*, vol. 32, p. 724, 1954.
69. E. M. T. Jones: "An Annular Corrugated-surface Antenna," *Proc. IRE*, vol. 40, p. 721, 1952.
70. H. B. Querido: "Surface Wave Fields and Phase Velocity Variations of Grounded Dielectric Sheets and of Periodic Structures of Metal Posts on a Ground Plane," Rept. 667-46, Ohio State Univ. Research Foundation, Columbus, Ohio, 1958.

71. A. Dion: "Nonresonant Slotted Arrays," *IRE Trans. on Antennas Propagation*, AP-6, p. 360, 1958.

72. C. G. Montgomery: "Technique of Microwave Measurements," MIT Radiation Laboratory Series, vol. 11, McGraw-Hill Book Company, Inc., New York, 1948.

73. T. T. Taylor: "Design of Line-source Antennas for Narrow Beamwidths and Low Sidelobes," *IRE Trans. on Antennas Propagation*, AP-3, p. 16, 1955.

74. S. Silver: "Microwave Antenna Theory and Design," MIT Radiation Laboratory Series, vol. 12, McGraw-Hill Book Company, Inc., New York, 1949.

75. D. W. Fry and F. K. Goward: "Aerials for Centimetre Wave-lengths," Cambridge University Press, New York, 1950.

76. A. Dunbar: "On the Theory of Antenna Beam Shaping," *J. Appl. Phys.*, vol. 23, p. 847, 1952.

77. C. J. Sletten, P. Blacksmith, and G. R. Forbes: "New Method of Antenna Array Synthesis Applied to Generation of Double-step Patterns," *IRE Trans. on Antennas Propagation*, AP-5, p. 369, 1957.

78. R. W. Bickmore: "A Note on the Effective Aperture of Electrically Scanned Arrays," *IRE Trans. on Antennas Propagation*, AP-6, p. 194, 1958.

79. H. Gruenberg: "Second-order Beams of Slotted Waveguide Arrays," *Can. J. Phys.*, vol. 31, p. 55, 1953.

80. H. W. Cooper, M. Hoffman, and S. Isaacson: "Image Line Surface Wave Antenna," *1958 IRE Natl. Conv. Record*, pt. 1, p. 230, 1958.

81. J. N Hines and J. Upson: "A Line Source with Variable Polarization," *IRE Trans. on Antennas Propagation*, AP-6, p. 152, 1958.

82. C. J. Sletten and F. S. Holt: Internal Memoranda on "Stretch" Array, Air Force Cambridge Research Center, Bedford, Mass., 1958.

83. C. J. Sletten, P. Blacksmith, Jr., and L. F. Shodin: "Amplitude Scanning of Antenna Arrays," AFCRC-TR-58-124, Air Force Cambridge Research Center, Bedford, Mass., 1958.

84. F. J. Tischer: "The H-guide, a Waveguide for Microwaves," *1956 IRE Natl. Conv. Record*, pt. 5, p. 44, 1956.

85. C. J. Sletten and G. R. Forbes: "A New Antenna Radiator for VHF-UHF Communications," AFCRC-TR-57-114, Air Force Cambridge Research Center, Bedford, Mass., 1957.

86. C. J. Sletten, F. S. Holt, P. Blacksmith, Jr., G. R. Forbes, L. F. Shodin, and H. J. Henkel: "A New Satellite Tracking Antenna," *1957 IRE WESCON Conv. Record*, pt. 1, p. 244, 1957.

87. C. J. Sletten, F. S. Holt, P. Blacksmith, Jr., G. R. Forbes, L. F. Shodin, and H. J. Henkel: "A New Single Antenna Interferometer System Using Proximity-coupled Radiators," AFCRC-TR-58-115, Air Force Cambridge Research Center, Bedford, Mass., 1958.

88. S. R. Seshadri and K. Iizuka: "A Dipole Antenna Coupled Electromagnetically to a Two-wire Transmission Line," *IRE Trans. on Antennas Propagation*, AP-7, p. 386, 1959.

89. G. R. Forbes: "An Endfire Array Continuously Proximity-coupled," AFCRC-TR-59-368, Air Force Cambridge Research Center, Bedford, Mass., 1959.

90. W. Rotman and N. Karas: "The Sandwich Wire Antenna: A New Type of Microwave Line Source Radiator," *1957 IRE Natl. Conv. Record*, pt. 1, p. 166, 1957.

91. W. Rotman and N. Karas: "Printed Circuit Radiators: The Sandwich Wire Antenna," *Microwave J.*, vol. 2, no. 8, p. 29, 1959.

92. A. A. Oliner: "Theoretical Developments in Strip Transmission Line," *Proc. Symposium on Modern Advances in Microwave Tech.*, p. 379, Polytechnic Institute of Brooklyn, Brooklyn, N.Y., 1954.

93. A. A. Oliner and W. Rotman: "Periodic Structures in Trough Waveguides," *IRE Trans. on Microwave Theory Tech.*, MTT-7, p. 134, 1959.

94. W. Rotman and S. J. Naumann: "The Design of Trough Waveguide Antenna Arrays," AFCRC-TR-58-154, Air Force Cambridge Research Center, Bedford, Mass., 1958.

95. J. W. Duncan and R. H. DuHamel: "A Technique for Controlling the Radiation from Dielectric Rod Waveguides," *IRE Trans. on Antennas Propagation*, AP-5, p. 284, 1957.

96. G. E. Mueller: "A Broadside Dielectric Antenna," *Proc. IRE*, vol. 40, p. 71, 1952.

97. J. Robieux: Final Report, Contract AF61(514)-933, Compagnie Générale de T.S.F., Paris, 1956.

98. J. Robieux: Section III of Final Report, Contract AF61(514)-1149, Compagnie Générale de T.S.F., Paris, 1957.

99. M. Hoffman: "Dielectric Image Line Surface Wave Antenna," AFCRC-TR-57-188 [Final Report, Contract AF19(604)-1551], Litton Industries, College Park, Md., 1957.

100. E. Sion: Final Report, AFCRC-TR-55-101, Contract AF19(604)-780, Airborne Instruments Laboratory, Mineola, N.Y., 1955.
101. E. H. Scheibe: Final Report, Contract DA36-039-sc-71158, University of Wisconsin, Madison, Wis., 1958.
102. J.-C. Simon: "Antenne omnidirectionelle type 'pomme de pin,'" Internal Report, Compagnie Générale de T.S.F., Paris, 1955.
103. K. C. Kelly and R. S. Elliott: "Serrated Waveguide—Part II: Experiment," *IRE Trans. on Antennas Propagation*, AP-5, p. 276, 1957.
104. C. H. Walter: "Curved Slot Antennas," Report 667-1, Contract AF33(616)-3353, Ohio State University Research Foundation, Columbus, Ohio, 1956.
105. P. Foldes: "Traveling-wave Cylindrical Antenna Design—A Graphical Synthesis Method," *IRE Trans. on Antennas Propagation*, AP-7, p. 74, 1959.
106. S. Nishida: "Coupled Leaky Waveguides I: Two Parallel Slits in a Plane," MRI Report R-732-59, PIB-660; "II: Two Parallel Slits in a Cylinder," MRI Report R-746-59, PIB-674, Polytechnic Institute of Brooklyn, Brooklyn, N.Y., 1959.
107. J. A. Barkson: "Coupling of Rectangular Wave Guides Having a Common Broad Wall Which Contains Uniform Transverse Slits," *1957 IRE WESCON. Conv. Record*, pt. 1, p. 30, 1957.
108. R. H. MacPhie: "Use of Coupled Waveguides in a Traveling Wave Scanning Antenna," Antenna Lab. Rept. 36, Univ. Ill., Urbana, Ill., 1959.
109. R. C. Honey: "A Flush-mounted Leaky-wave Antenna with Predictable Patterns," *IRE Trans. on Antennas Propagation*, AP-7, p. 320, 1959.
110. S. Nishida: "Theory of Thin Dielectric Cover on Slitted Rectangular Waveguide Antenna," MRI Report R-754-59, PIB-682, Polytechnic Institute of Brooklyn, Brooklyn, N.Y., 1959.
111. W. W. Hansen: U.S. Patent 2402622 (1940).
112. R. J. Stegen and R. H. Reed: "Arrays of Closely Spaced Non-resonant Slots," *IRE Trans. on Antennas Propagation*, AP-2, p. 109, 1954.
113. A. L. Cullen: "Channel Section Waveguide Radiator," *Phil. Mag.*, 7th ser., vol. 40, p. 417, 1959.
114. V. H. Rumsey: "Traveling-wave Slot Antennas," *J. Appl. Phys.*, vol. 24, p. 1358, 1953.
115. J. N. Hines, V. H. Rumsey, and C. H. Walter: "Traveling-wave Slot Antennas," *Proc. IRE*, vol. 41, p. 1024, 1953.
116. R. F. Harrington: "Propagation along a Slotted Cylinder," *J. Appl. Phys.*, vol. 24, p. 1366, 1953.
117. L. O. Goldstone and A. A. Oliner: "Leaky Wave Antennas II: Circular Waveguides," AFCRC-TN-58-141, Contract AF19(604)-2031, Polytechnic Institute of Brooklyn, Brooklyn, N.Y., 1958.
118. R. F. Hyneman: "Closely-spaced Transverse Slots in Waveguide," *IRE Trans. on Antennas Propagation*, AP-7, p. 335, 1959.
119. This suggestion is due to A. F. Kay, Technical Research Group, Inc., Somerville, Mass.
120. R. S. Elliott: "Serrated Waveguide—Part I: Theory," *IRE Trans. on Antennas Propagation*, AP-5, p. 270, 1957.
121. E. M. T. Jones and J. K. Shimizu: "A Wide-band Transverse-slot Flush-mounted Array," AFCRC-TN-975, Contract AF19(604)-3502, Stanford Research Institute, Menlo Park, Calif., 1959.
122. W. Rotman and A. A. Oliner: "Asymmetrical Trough Waveguide Antennas," *IRE Trans. on Antennas Propagation*, AP-7, p. 153, 1959.
123. W. Rotman and N. Karas: "Trough Waveguide Radiators with Periodic Posts," AFCRC-TR-58-356, Air Force Cambridge Research Center, Bedford, Mass., 1958.
124. R. V. Hill and G. Held: "A Radial Surface Wave Antenna," Tech. Rept. 27, Univ. Washington, Seattle, Wash., 1958.
125. R. C. Honey: "Horizontally-polarized Long-slot Array," Technical Report 47, Contract AF19(604)-266, Stanford Research Institute, Menlo Park, Calif., 1954.
126. G. Broussaud: "A New Antenna Type of Plane Structure" (in French), *Ann. Radioélectricité*, vol. 11, p. 70, 1956.

Chapter 17

METHODS OF OBTAINING CIRCULAR POLARIZATION

Warren B. Offutt

Lorne K. DeSize

and

William H. Yale

All of Airborne Instruments Laboratory
Melville, Long Island, New York

17.1. GENERAL DISCUSSION*

The plane of polarization, or simply the polarization of a radio wave, is defined by the direction in which the electric vector is aligned during the passage of at least one

* This section contributed by W. B. Offutt.

full cycle. In the general case, both the magnitude and the pointing of the electric vector will vary during each cycle and the electric vector will map out an ellipse in the plane normal to the direction of propagation at the point of observation. In this general case (shown in Fig. 17-1a) the polarization of the wave is said to be elliptical. The minor-to-major axis ratio of the ellipse is called the ellipticity and will be expressed
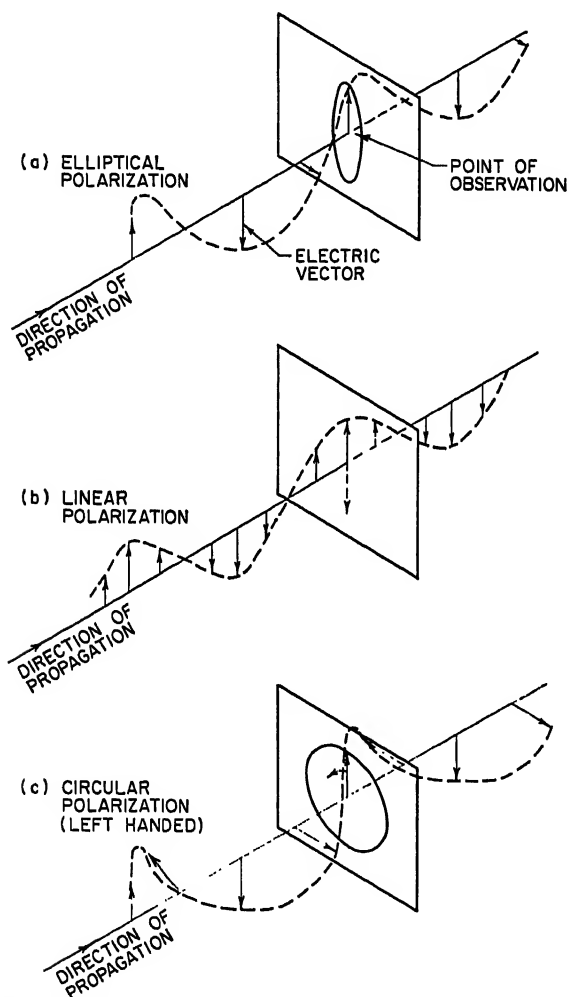
FIG. 17-1. Diagrammatic illustration of waves of various polarization: (a) Elliptical polarization. (b) Linear polarization. (c) Circular polarization (left-hand).

in this chapter in decibels. (Although the axis ratio is less than unity, when expressing ellipticity in decibels, the minus sign is frequently omitted for convenience.) The direction in which the major axis lies is called the polarization orientation and in this chapter will be measured from the vertical (Fig. 17-2).

The two special cases of ellipticity of particular interest are (1) an ellipticity of ∞ db (minor-to-major axis ratio zero), which is linear polarization, and (2) an ellipticity of 0 db (minor-to-major axis ratio unity), which is circular polarization.

A linearly polarized wave is therefore defined as a transverse electromagnetic wave whose electric-field vector (at a point in a homogeneous isotropic medium) at all times lies along a fixed line.

A circularly polarized wave is similarly defined as a transverse electromagnetic wave for which the electric- and/or magnetic-field vector at a point describes a circle.

In attempting to produce a linearly polarized wave, elliptical polarization is thought of as imperfect linear polarization, while in attempting to produce a circularly polarized wave, elliptical polarization is thought of as imperfect circular polarization.

Confusion occasionally results in the use of mental pictures similar to Figs. 17-1 and 17-2 when one overlooks the fact that although the electric vector makes one complete revolution (Fig. 17-2) per cycle, it does not rotate at a uniform rate, *except* in the special case of a circularly polarized wave. In this special case, rotation occurs at the rate of ω radians/sec.
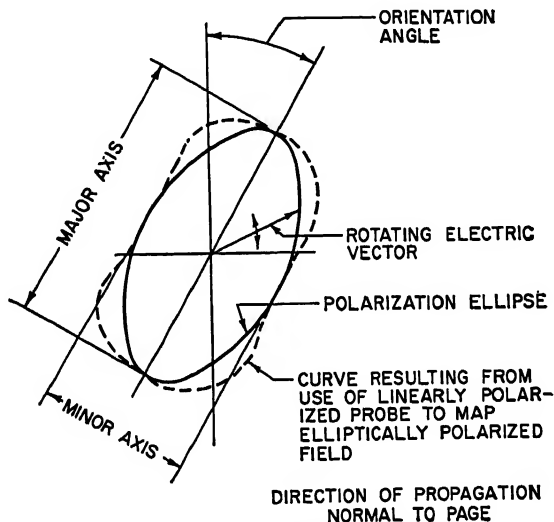
FIG. 17-2. Polarization ellipse.

Figure 17-1c shows a circularly polarized wave having a left-hand sense. It is also possible, of course, to have right-hand circularly polarized waves. The definition of right-hand circular polarization as standardized by the IRE and as used in this chapter is as follows: For an observer looking in the direction of propagation, the rotation of the electric-field vector in a transverse plane is clockwise for right-hand polarization. Similarly, the rotation is counter-clockwise for left-hand polarization.

One simple way of experimentally determining the sense of rotation of a circularly polarized wave is to make use of two helical beam antennas of opposite sense. A right-hand helical antenna transmits or receives right-hand polarization while a left-hand helical antenna will transmit or receive left-hand polarization. If a circularly polarized wave is received first on a right-hand helical antenna and then on a left-hand helical antenna, the antenna which receives the greater amount of signal will have a sense which corresponds to the sense of the received wave.

In the case of an elliptically polarized wave, the sense will be taken to be the same as that of the predominant circular component.

The same definition of sense is not used by all workers in the field. The work of different authors should be compared with this precaution in mind.

Typical Applications. Although there is reasonably general agreement on the above definitions, the use of the words "circular polarization" does not always have quite the same meaning to different workers in the field. The difference lies in the permissible departure (for the application at hand) from precise polarization circularity before the circularly polarized antenna becomes unsatisfactory. The application of a circularly polarized antenna usually falls in one of two categories. The first category is
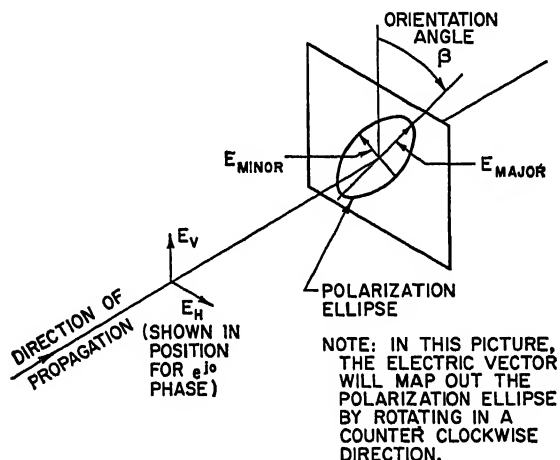
$$E_V = \frac{1}{2}\left[E_{MAJOR}\left(1 + e^{j2\beta}\right) + E_{MINOR}\left(1 - e^{j2\beta}\right)\right]$$

$$E_H = \frac{e^{j\frac{\pi}{2}}}{2}\left[E_{MAJOR}\left(1 - e^{j2\beta}\right) + E_{MINOR}\left(1 + e^{j2\beta}\right)\right]$$

Fig. 17-3. Linear-component synthesis of an elliptically polarized wave having predominantly left-hand sense.

the use of a circularly polarized antenna to provide response to a linearly polarized wave of arbitrary orientation. The second category is the use of a circularly polarized antenna for suppression of precipitation clutter in radar service.[31] Table 17-1 shows typical characteristics for each of these applications.

Table 17-1. Two Typical Applications of Circularly Polarized Antennas and Their Characteristics

	Response to linear polarization of arbitrary orientation	Precipitation-clutter suppression in radar service (values based on search radar)
Ideal ellipticity*..............	0 db	0 db
Satisfactory ellipticity*........	−3 db	−0.5 db
Unsatisfactory ellipticity*.....	−10 db	−1.5 db
Azimuth beamwidth	Omnidirectional	1–5°
Elevation beamwidth	20°	20°
Bandwidth...................	Greater than 50 %	5–15 %
SWR.......................	5	1.15
Power rating................	Milliwatt Level	>100 kw, <10 megawatts

* Over all or almost all of the radiation pattern.

Polarization Synthesis. Any elliptically polarized wave can be synthesized from two waves linearly polarized at right angles to each other. For example, a circularly polarized wave will be produced by the coexistence of a vertically and a horizontally polarized wave, each having the same strength, and with a 90° phase difference between them. If they have other than the same strength and/or other than a 90° relationship, the resulting wave will be elliptically polarized. If, for example, the magnitude of the vertically polarized wave is zero, the resulting wave is linearly polarized and has a horizontal orientation. Further, if the two waves have equal magnitude but 0° phase difference, the resulting wave is linearly polarized with 45° orientation. There are two possible combinations of vertically and horizontally polarized waves that can produce a wave of some specific ellipticity. One of the combinations will produce a predominantly left-hand wave, and the other combination will produce a predominantly right-hand wave. Figures 17-3 and 17-4 show the two cases. Separate
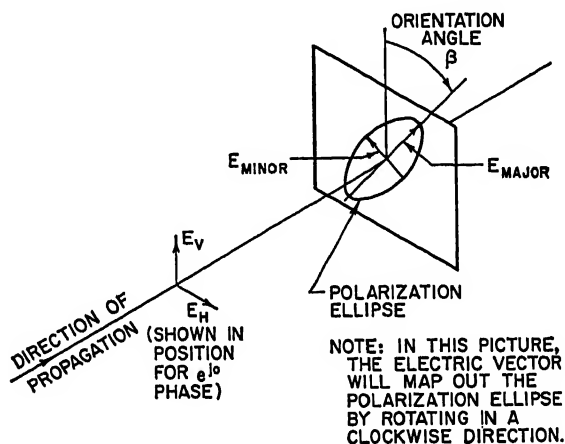
$$E_V = \frac{1}{2}\left[E_{MAJOR}\left(1 + e^{j2\beta}\right) - E_{MINOR}\left(1 - e^{j2\beta}\right)\right]$$

$$E_H = \frac{e^{j\frac{\pi}{2}}}{2}\left[E_{MAJOR}\left(1 - e^{j2\beta}\right) - E_{MINOR}\left(1 + e^{j2\beta}\right)\right]$$

FIG. 17-4. Linear-component synthesis of an elliptically polarized wave having predominantly right-hand sense.

illustrations are provided to emphasize the need for care in specifying the coordinate system in this work and the need for consistency in adhering to the selected coordinate system while performing and interpreting any theoretical or experimental work.

It is often of interest to know only the ratio of the magnitudes of the vertically and horizontally polarized waves forming an elliptically polarized wave and the phase angle between them. Such information can be obtained graphically with the aid of Fig. 17-5. In this chart, the phase angle shown is the relative phase of the vertical element when the relative phase of the horizontal element is zero.

Example: Given an ellipticity of 3.0 db and an orientation of $\beta = 37°$.

Find the ratio of the magnitudes of the vertically and horizontally polarized waves and the phase angle between them. Draw a line from the center of the chart to the periphery at the 37° point. Lay off a distance from the chart center to the $V/H = 3.0$ db line measured on the horizontal diameter. Read $V/H = 0.8$ db and

a phase angle of 71° for predominantly right-hand sense or 289° for predominantly left-hand sense.

It is also possible to synthesize any elliptically polarized wave from two circularly polarized waves having opposite senses. For example, a linearly polarized wave will be produced by the coexistence of a right-hand and a left-hand circularly polarized wave of the same strength. The orientation of the resulting linearly polarized wave will be determined by the phase difference between the two circularly polarized waves. Figure 17-6 provides the formulas for calculating the values.
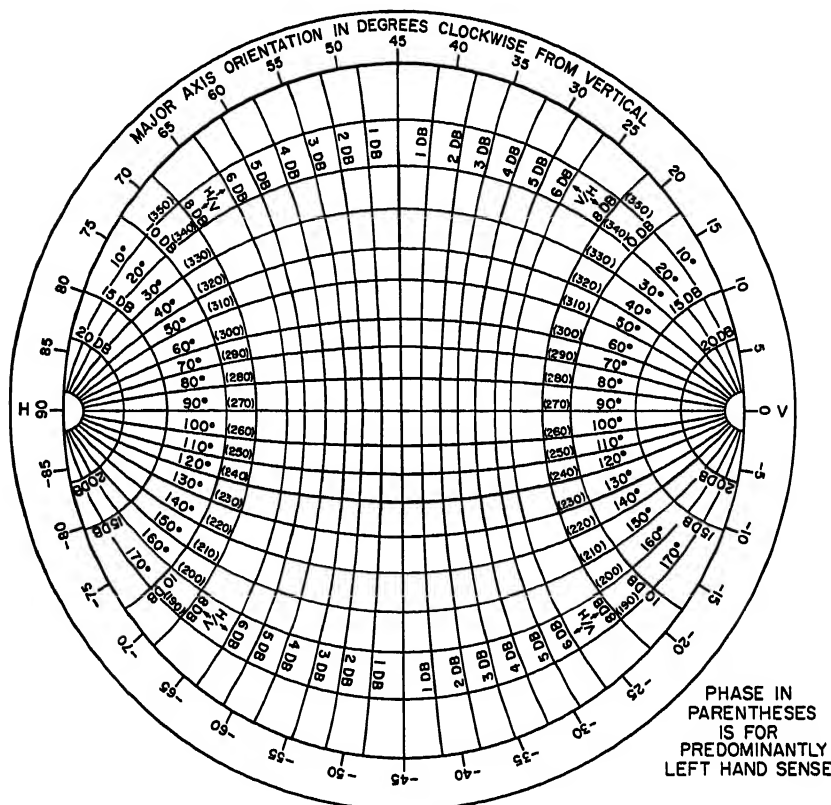
FIG. 17-5. Polarization chart.

Transmission between Two Elliptically Polarized Antennas. In order that a receiving antenna may extract the maximum amount of energy from a passing radio wave, it is necessary for it to have a polarization identical with that of the passing wave. For example, a vertically polarized receiving antenna should normally be used to receive a signal from a vertically polarized transmitting antenna. (The discussion assumes no polarization distortion in the transmission path.) Similarly, a right-hand circularly polarized antenna should be used for reception of waves from a right-hand circularly polarized transmitting antenna. In general, maximum transmission will result between two elliptically polarized antennas when:

1. Their axis ratios E_{minor}/E_{major} are the same.
2. Their predominant senses are the same.
3. Their ellipse orientations are related by a minus sign, that is, $\beta_{trans} = -\beta_{rec}$.

Note that condition 3 will result in parallel-ellipse major axes in space and implies that only in three special cases will identical antennas at each end of the circuit with the same orientation yield maximum transmission. These three cases are:

1. $\beta = 0$.
2. $\beta = \pm 90°$.
3. $E_{minor}/E_{major} = 1$, so that β has no significance.

Identical antennas can always be made to yield maximum transmission, however, if they are rotated so as to cause the major axes of their waves to be parallel in space.

FOR A PREDOMINANTLY
LEFT HANDED WAVE

$$E_L = \frac{E_{MAJOR} + E_{MINOR}}{2}$$

$$E_R = \left(\frac{E_{MAJOR} - E_{MINOR}}{2}\right) e^{j2\beta}$$

FOR A PREDOMINANTLY
RIGHT HANDED WAVE

$$E_L = \frac{E_{MAJOR} - E_{MINOR}}{2}$$

$$E_R = \left(\frac{E_{MAJOR} + E_{MINOR}}{2}\right) e^{j2\beta}$$

NOTE: THE REFERENCE SYSTEM IS SUCH THAT ZERO PHASE DIFFERENCE BETWEEN E_R AND E_L WILL CAUSE E_{MAJOR} TO BE VERTICAL.
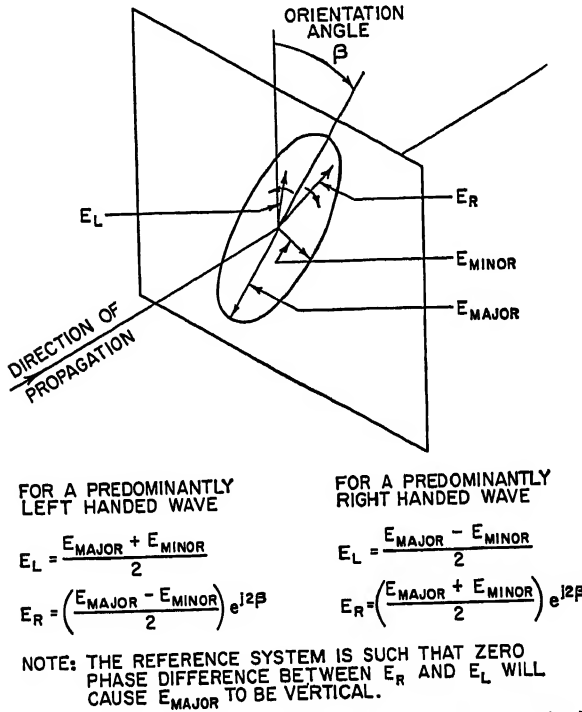
FIG. 17-6. Circular component synthesis of an elliptically polarized wave.

When two arbitrarily polarized antennas are used, the normalized output power from the receiving-antenna terminals will be

$$\frac{P}{P_{max}} = \frac{|(E_{R_1}E_{R_2} + E_{L_1}E_{L_2})|^2}{(E_{R_1}{}^2 + E_{L_1}{}^2)(E_{R_2}{}^2 + E_{L_2}{}^2)} \qquad (17-1)$$

Similar expressions in terms of linear components, or axial ratios, may be found in Refs. 2 and 3.

The values of E_R and E_L may be obtained with the aid of Fig. 17-6. Table 17-2 shows some typical combinations of interest.

Orthogonality. For any arbitrarily polarized antenna, there can be another antenna polarized such that it will not respond to the wave emanating from the first

antenna.   The polarizations of the two are said to be orthogonal.   Using the convention of Fig. 17-6 two polarization ellipses will be orthogonal if they satisfy the relation

$$-E_{R_1}E_{R_2} = E_{L_1}E_{L_2} \qquad (17\text{-}2)$$

Figure 17-5 can be used to determine the orthogonal-polarization ellipse to a given ellipse by performing an inversion through the center of the chart and reading the phase-shift scale associated with the opposite predominant sense.

Table 17-2. Transmission Efficiency with Various Polarizations at the Transmitting and Receiving Antennas

Antenna 1		Antenna 2		P/P_{max}
Vertical, e.g.: $E_R = 1$ $E_L = 1e^{j0}$	$\beta = 0$	Vertical, e.g.: $E_R = 1$ $E_L = 1e^{j0}$	$\beta = 0$	1
Vertical, e.g.: $E_R = 1$ $E_L = 1e^{j0}$	$\beta = 0$	Horizontal, e.g.: $E_R = 1$ $E_L = 1e^{j\pi}$	$\beta = 90°$	0
Vertical, e.g.: $E_R = 1$ $E_L = 1e^{j0}$	$\beta = 0$	Circular (right), e.g.: $E_R = 1$ $E_L = 0$		½
Circular (right), e.g.: $E_R = 1$ $E_L = 0$		Circular (left), e.g.: $E_R = 0$ $E_L = 1$		0
Circular (left), e.g.: $E_R = 0$ $E_L = 1$		Circular (left), e.g.: $E_R = 0$ $E_L = 1$		1

Reflection.   When a vertically polarized wave is reflected from a smooth surface, there is no change in its character.*   When a horizontally polarized wave is reflected from a smooth surface, because of the coordinate-system reversal in space when one looks in the reversed direction of propagation, there is a 180° phase change.   When a circularly polarized wave is reflected from a smooth surface, its horizontal component is altered by 180°; hence the sense of the wave is reversed.   For an elliptically polarized wave, reflection is equivalent to altering the differential phase shift (e.g., the phase difference between the horizontally and vertically polarized linear components) by 180°.   The new polarization ellipse may be determined with the aid of Fig. 17-5 by inverting the original (before reflection) ellipticity across the horizontal diameter and reading the phase-shift scale corresponding to the opposite predominant sense.

Circularly polarized antennas are unique in being entirely unable to "see" their own images in any symmetrical reflecting surface, since the reflected wave has its sense reversed and is therefore orthogonal to the polarization of the antenna from which it originated.

Measurement Problems.   The measurement of circularly polarized antennas is discussed in Chap. 34.   It will be sufficient to call attention here to the unusual degree of sensitivity of polarization measurement to small distorting influences of secondary paths in a measuring setup.   Figure 17-7 illustrates the conditions.

* Strictly speaking, this statement is correct only if the smooth surface is the interface between a normal propagation medium and one having an impedance of infinity.   However, we are here interested only in the relative difference between the vertical and horizontal cases, so this detail will be overlooked.
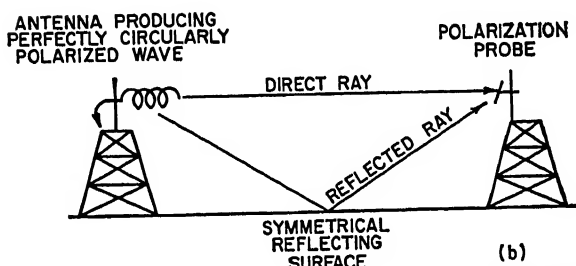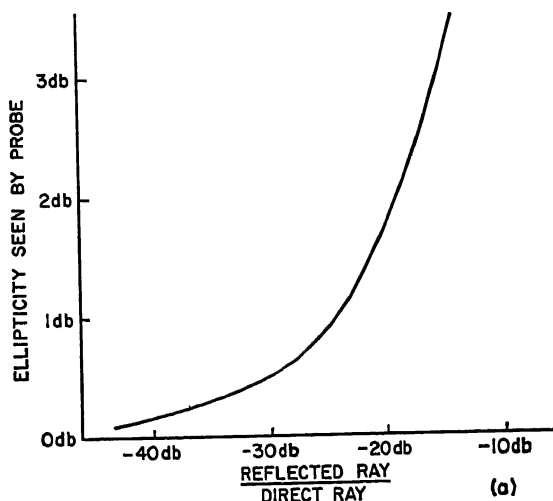
Fig. 17-7. Influence of the reflected wave on the measurement of a circularly polarized wave.

17.2. COMBINATIONS OF ELECTRIC AND MAGNETIC ANTENNAS*

Circular polarization can be achieved by a combination of electric and magnetic antennas provided that the fields produced by these antennas are equal in magnitude and in time-phase quadrature. A simple case of this combination is a horizontal loop and a vertical dipole.[14] The time-phase-quadrature relationship is a fundamental relationship between the fields of a loop and a dipole when their currents are in phase. If the loop and dipole are oriented as in Fig. 17-8, the fields in the plane of the loop are given by

$$E_L = jCJ_1(ka)e^{j(\omega t - kr)} \qquad (17\text{-}3)$$
$$E_D = C_1 e^{j(\omega t - kr)} \qquad (17\text{-}4)$$

where C and C_1 = constants
$k = 2\pi/\lambda$
λ = free-space wavelength
a = radius of loop
r = distance from center of loop
J_1 = Bessel function of the first order
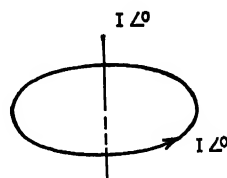
Fig. 17-8. Horizontal loop and vertical dipole.

* This section contributed by L. K. DeSize.

provided that the currents in the loop and dipole are in phase.   Thus, if

$$CJ_1(ka) = C_1 \qquad\qquad (17\text{-}5)$$

the resulting field of the combination will be circularly polarized.   Equation (17-5) will be true if the loop diameter is less than about 0.6 wavelength and the dipole length is less than a half wavelength.   In this particular combination it should be noted that the resulting radiation pattern is circularly polarized at all points since the individual pattern of the loop and dipole are essentially the same.   However, in practice this is difficult to obtain, except over narrow bandwidths, because of the different impedance characteristics of the loop and dipole.

SLOT FEED LINE — CYLINDER FEED LINE
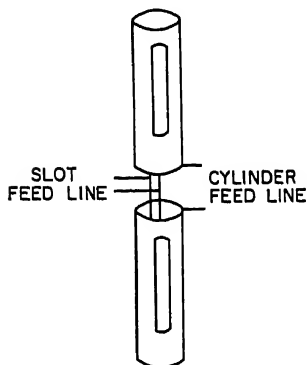
FIG. 17-9. Slotted-cylinder circularly polarized antenna.

A second combination is that shown in Fig. 17-9, consisting of two vertical one-half-wavelength-long cylinders in which vertical slots are cut.[14]   Feeding the two vertical cylinders will give a vertically polarized omnidirectional pattern in the plane normal to the axis of the cylinders, while feeding the two slots will give a horizontally polarized pattern in the same plane.   If the power to both feeding arrangements is adjusted to be equal and the phase adjusted by controlling the length of the feed lines such that the two are in time-phase quadrature, the resulting pattern will be circularly polarized.

The normal radiation (broadside) mode of a helix can also be considered as a combination of electric and magnetic antennas (dipoles and loops) producing circular polarization.   This type of antenna has previously been discussed in Chap. 7.

A pair of crossed slots in the broad wall of a rectangular waveguide in which the field configurations in the waveguide are such that one slot is in time-phase quadrature with the other can also be considered as a combination of electric and magnetic antennas producing circular polarization.   This combination will be discussed in more detail in the following section.

17.3. COMBINATIONS OF SIMILAR ANTENNAS*

Two or more similar antennas when properly oriented in either time phase or space phase or a combination of both may be used to give a circularly polarized radiation
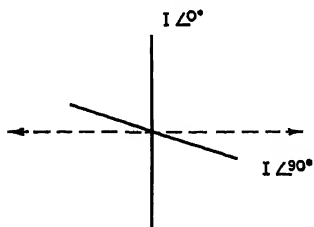
FIG. 17-10. Crossed dipoles—current in phase quadrature.
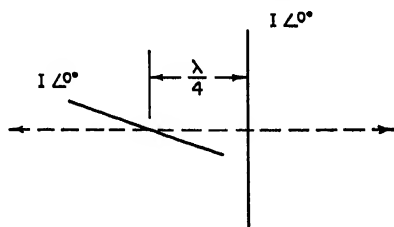
FIG. 17-11. Crossed dipoles current in phase—λ/4 separation.

field.   A simple case is a pair of crossed half-wavelength dipoles.   In Fig. 17-10, circular polarization is obtained by having the equal currents in the dipoles in phase

* This section contributed by L. K. DeSize.

quadrature. Radiation in one direction is right circularly polarized and left circularly polarized in the opposite direction. If the pair of crossed dipoles are fed in phase and separated in space by a quarter wavelength as shown in Fig. 17-11, circular polarization is again produced: however, the sense is the same in both directions. In both of these combinations the resulting field is circularly polarized only on axis. The deviation in circularity as a function of the off-axis angle is plotted in Fig. 17-12.

Another case of a simple combination of similar antennas to produce circular polarization is a pair of narrow slots at right angles and located at the proper point in the broad wall of a rectangular waveguide.[15] This may be explained by noting that the equations for the transverse and
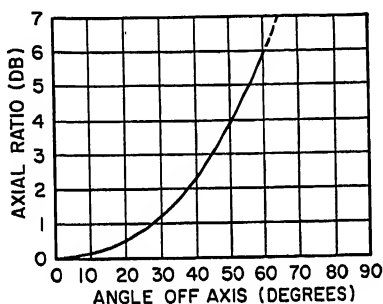
Fig. 17-12. Deviation of circularity as a function of off-axis angle for a pair of crossed dipoles.
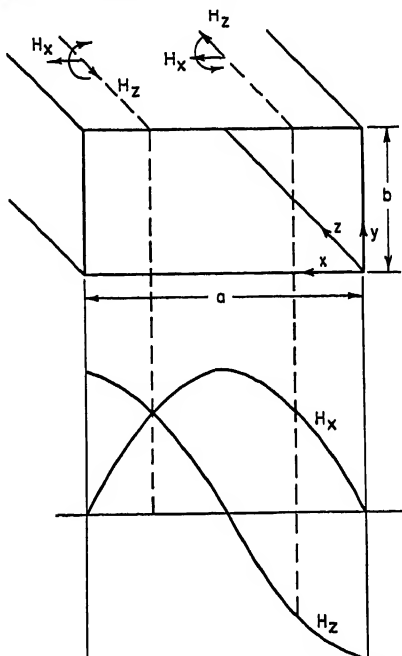
Fig. 17-13. Field configuration, TE_{10} mode.

longitudinal magnetic fields of the dominant (TE_{10}) mode in rectangular waveguide (Fig. 17-13) are

$$H_x = H_0 \sqrt{1 - \left(\frac{\lambda}{2a}\right)^2} \sin \frac{\pi x}{a} \qquad (17\text{-}6)$$

$$H_s = -jH_0 \frac{\lambda}{2a} \cos \frac{\pi x}{a} \qquad (17\text{-}7)$$

From these two equations it may be seen that the fields are in phase quadrature and there are two values of x at which $|H_x| = |H_s|$. These values of x are given by

$$x = \frac{a}{\pi} \text{ctn}^{-1} \left[\pm \sqrt{\left(\frac{2a}{\lambda}\right)^2 - 1} \right] \qquad (17\text{-}8)$$

Two crossed slots at either of these points will then radiate circularly polarized energy. Figure 17-14 is a plot of x versus λ over the wavelength range between the cutoff of the TE_{10} and TE_{20} modes. The orientation of the slots is arbitrary, and they may be made resonant and thus radiate a large amount of power (Chap. 9). The theoretical axial ratio for $x = a/4$ is shown in Fig. 17-15, which gives circular polarization at a frequency for which $\lambda = 2a/\sqrt{2}$.

The equiangular spiral,[16] which is one of a class of frequency-independent antennas,[17] where the antenna is completely defined by angles, is another case of a combination of
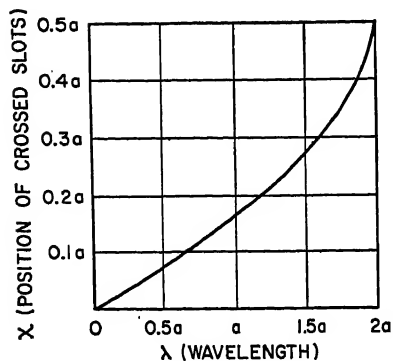
FIG. 17-14. Position of crossed slots for circular polarization vs. wavelength.
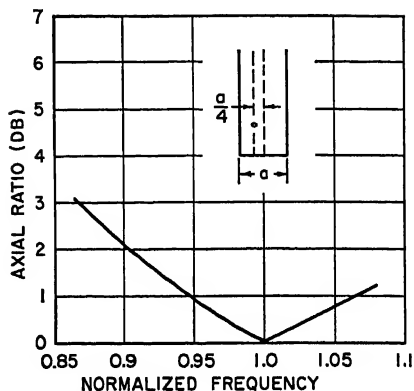
FIG. 17-15. Theoretical axial ratio for $x = a/4$.

similar antennas which produce circular polarization (Chap. 18). If a conductor with edges defined by the two curves

$$\rho_1 = ke^{a\theta} \qquad (17\text{-}9)$$

and

$$\rho_2 = ke^{a(\theta-\delta)} \qquad (17\text{-}10)$$

is combined with a second conductor defined by the two curves

$$\rho_3 = ke^{a(\theta-\pi)} \qquad (17\text{-}11)$$

and

$$\rho_4 = ke^{a(\theta-\pi-\delta)} \qquad (17\text{-}12)$$

(which simply is the first conductor with a 180° rotation), the result is a balanced antenna of infinite length. In practice, the antenna will be finite in size and therefore limited in operation as a function of frequency. Figure 17-16 shows a practical antenna.

If the arm length is longer than approximately one wavelength, the field on the axis perpendicular to the plane of the antenna will be circularly polarized. Pattern bandwidths of better than 20:1 have been measured with this type of antenna with correspondingly good impedance bandwidths. The axial ratio for a typical antenna which consists of a spiral slot cut in a large ground plane is shown in Fig. 17-17, and a SWR plot is shown in Fig. 17-18.

An omnidirectional circularly polarized antenna[18] can be obtained by four in-phase half-wavelength dipoles arrayed in a circle of about one-third wavelength in diameter and inclined to the horizontal as shown in Fig. 17-19. The axial ratio in the horizontal plane for this configuration is less than 1 db.

FIG. 17-16. Equiangular spiral.

The same general type of pattern can also be obtained by using an array of inclined slots on a cylinder feeding a biconical horn (Fig. 17-20). In this case the slant length of the biconical horn is adjusted to give a time-phase-quadrature relationship between the two modes of propagation for horizontal and vertical polarization. There is no
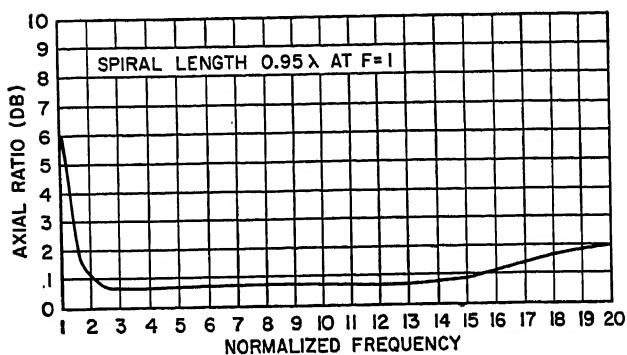
FIG. 17-17. Measured axial ratio of typical equiangular spiral.
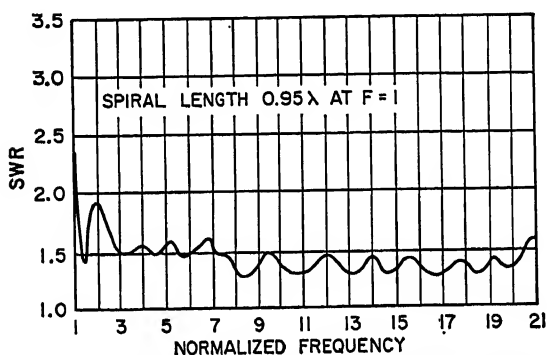
FIG. 17-18. Measured SWR of typical equiangular spiral.
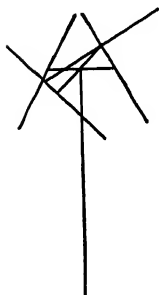
FIG. 17-19. Four-dipole omnidirectional circularly polarized antenna.
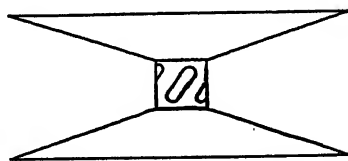
FIG. 17-20. Circularly polarized biconical horn.
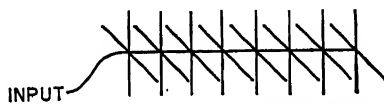
FIG. 17-21. Circularly polarized Yagi.

simple theoretical relationship that enables one to specify the slant length to give circular polarization, and it is best done on an experimental basis.

The combination of crossed half-wavelength dipoles can be used to feed a crossed Yagi structure to give a directional circularly polarized beam as suggested in Fig. 17-21.

Directional beams can, in general, be produced by using any of the basic combinations in arrays.

17.4. HELICAL ANTENNAS

Circularly polarized helical antennas are included in the general discussion of helical antennas presented in Chap. 7.

17.5. DUAL-MODE HORN RADIATORS*

A conventional waveguide horn may be used for the radiation and beaming of circularly polarized waves, provided that it is fed with waveguide capable of propagating vertically and horizontally polarized waves simultaneously. The horn may be either symmetrical or asymmetrical, that is, square (round) or rectangular (elliptical). Figure 17-22 illustrates the two types.
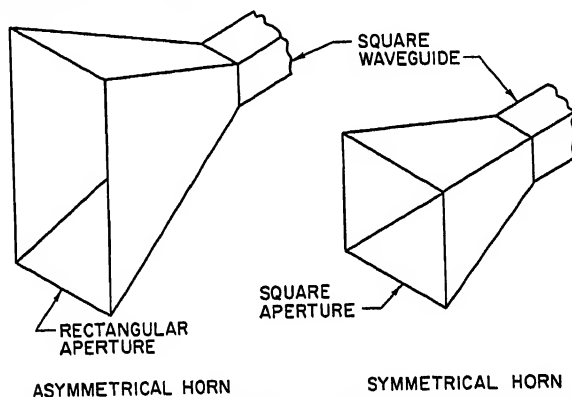
FIG. 17-22. Examples of symmetrical and asymmetrical dual-mode horns.

Symmetrical Case. A circularly polarized field will be obtained on the peak of the radiation pattern when the horn is fed through the square waveguide with equal-amplitude vertically and horizontally polarized modes arranged to be in quadrature. The radiated field will not, in general, be circularly polarized at other points on the radiation pattern because the vertically and horizontally polarized radiation patterns will have different beamwidths in almost any particular plane of interest. Such is the case because the horizontal dimension (for example) of the aperture is an E-plane dimension for the horizontally polarized field and an H-plane dimension for the vertically polarized field. Figure 17-23 illustrates a typical variation in ellipticity as a function of position on the radiation pattern.

There are two practical methods useful in compensating for the two different beamwidths. Figure 17-24 shows the methods applied to the *azimuth plane* only of the horn of Fig. 17-23. In actual practice, it is necessary to apply one of these methods (usually method B) to the elevation plane as well as to the azimuth plane.

Although the above two paragraphs have used the azimuth plane as an example, the discussion is of course equally applicable to the elevation plane.

* This section contributed by W. B. Offutt.
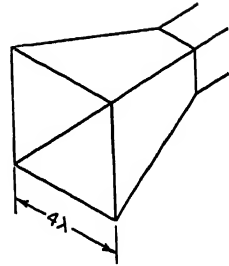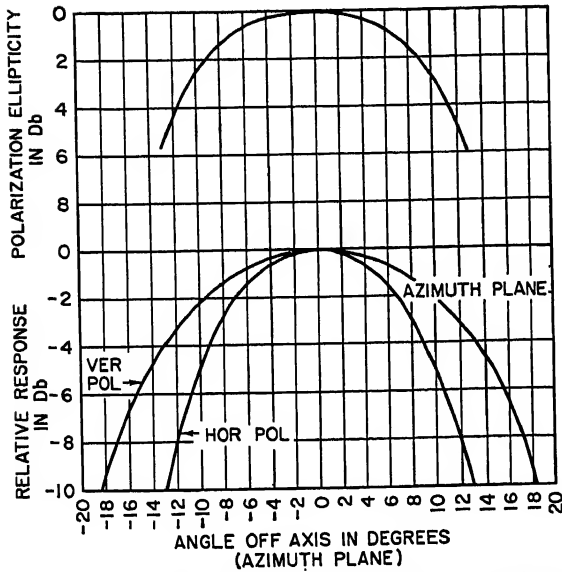
FIG. 17-23. Typical variation in polarization ellipticity.
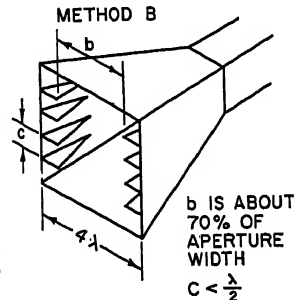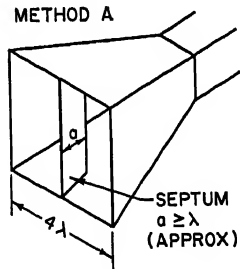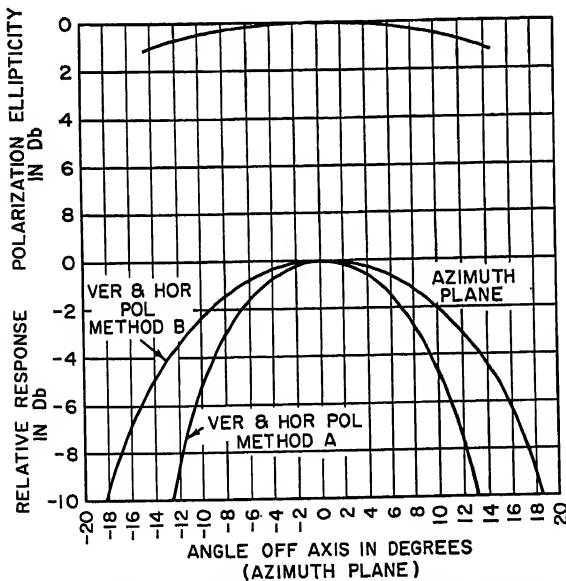
FIG. 17-24. Two methods of compensating dual-mode horns for improved circularity.

When designing a circularly polarized horn for some specific radiation-pattern width, the standard design methods (such as in Chap. 10 and Ref. 19) are applicable, bearing in mind of course that an *E*-plane dimension for one polarization is an *H*-plane dimension for the other and also bearing in mind the effects of any compensating scheme such as shown in Fig. 17-24.

When the horn is designed for very broad beamwidths so that its aperture dimension is between λ and $\lambda/2$, it is usually not necessary to employ pattern compensation.

When the horn is designed along conventional pyramidal or sectoral lines, phase tracking for the vertically and horizontally polarized fields is usually not a problem; that is, the radiation centers of phase for the two polarizations are sufficiently close so that differential phase-shift variations over the radiation pattern usually do not exceed about 10 to 15° within the tenth-power points on the beam.

Horns are sometimes constructed with a wide flange around the aperture for mechanical reasons. Although control of the flange width may be used as a third method for pattern compensation, its use is not recommended because it will be ineffective on large horns and will have a degrading influence on phase tracking on small horns. On small horns especially, the flange width should be no larger than necessary.

λ IS OPERATING WAVELENGTH IN SAME UNITS AS A, B AND L

$$\Delta = \frac{2\pi}{\lambda} \int_0^L \left\{ \sqrt{1 - \frac{\frac{1}{2}\lambda}{A_2 + \frac{A_1 - A_2}{L}\ell}} - \sqrt{1 - \frac{\frac{1}{2}\lambda}{B_2 + \frac{B_1 - B_2}{L}\ell}} \right\} d\ell$$
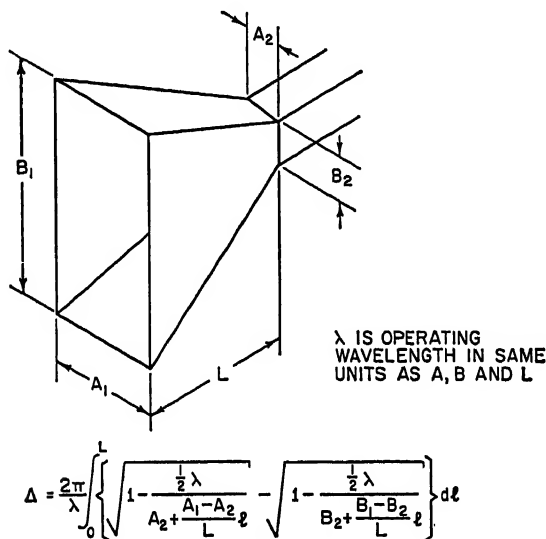
Δ IS DIFFERENTIAL PHASE SHIFT IN RADIANS

FIG. 17-25. Method of determining differential phase shift in a horn.

Asymmetrical Case. The previous discussion is also applicable to asymmetrical horns, except that circularly polarized fields on the peak of the radiation pattern will not be obtained unless allowance is made for the difference in phase velocity of the vertically and horizontally polarized waves within the asymmetrical horn flare. This differential phase shift may attain quite large values in some horns. For example, a measured differential phase shift of about 220° has been observed at 2,800 Mc in a horn having a flare length of about 14 in., a width of 2.84 in., and a height of 7.8 in.

The magnitude of differential phase shift can be computed to an accuracy of perhaps 10 per cent by evaluating the integral

$$\text{Differential phase shift} = \int_0^L [\beta(\ell) - \beta(\ell)] \, d\ell$$
$$\qquad\qquad\qquad\qquad\quad \text{Vpol} \quad \text{Hpol}$$

in which L is the flared length of the horn, and $\beta(l)$ is based simply on the appropriate width of the flare and the operating wavelength. Figure 17-25 shows the information in detail. Note that the differential phase shift may vary fairly rapidly with fre-

quency. In the example mentioned above, the differential phase shift increased about 15° for every 100-Mc decrease in frequency between 2,900 and 2,700 Mc.

Methods of Obtaining Quadrature. Quadrature phase relationship between two orthogonally polarized modes in round or square waveguide may be achieved by any of the following techniques:

1. Rectangular or elliptical cross section
2. Ridge guide
3. Dielectric slab
4. Multiple-lumped-element loading
5. Turnstile junction

The choice of method must be based on the application, keeping such things in mind as ease of design, bandwidth, power-handling capacity, ease of adjustment, and ease of fabrication. Table 17-3 shows the trend of these characteristics in order.

Table 17-3. Order of Preference of Methods for Obtaining Phase Quadrature

Method	Ease of design	Bandwidth	Power-handling capacity	Ease of adjustment	Ease of fabrication (small quantity)
Rectangular or elliptical cross-section guide....	1	5	1	5	4
Ridge guide............	4	3	2	2	3
Dielectric slab..........	5	2	5	3	1
Multiple-lumped-element loading.......	2	1	3	1	2
Turnstile junction.......	3	4	4	4	5

NOTE: This table is based on somewhat limited information and therefore indicates trends only. There is no assurance that the orders shown will be precisely maintained for all circumstances.

The first three methods above are based on causing the phase velocity of the vertically and horizontally polarized modes to be different within the same section of guide. This section of guide will then be of different phase length for the two polarizations. Selection of the appropriate length to furnish the requisite differential phase shift is the last step in the design process.

For example, a rectangular section of waveguide, carrying TE_{01} and TE_{10} modes and having internal dimensions a and b, will produce differential phase shift at the rate of

$$\frac{2\pi}{\lambda}\left[\sqrt{1-\left(\frac{\lambda}{2a}\right)^2}-\sqrt{1-\left(\frac{\lambda}{2b}\right)^2}\right] \quad \text{radians/unit length}$$

The values for a, b, and λ must be in the same units, of course. If such a section is to be connected to a square waveguide, it will be necessary to employ a suitable intermediate transformer section. Quarter-wavelength sections having an impedance equal to the geometric mean of the input and output impedances are satisfactory. Note that the differential phase shift (which can be computed with the aid of the above formula) of the transformer will contribute to the total.

Ridge guide can be handled in the same manner as the above rectangular guide. In the ridge case, however, the quantities $2a$ and $2b$ in the above expression should be replaced with λ_{cutoff} for TE_{01} and λ_{cutoff} for TE_{10}, respectively.

Dielectric-slab loading in a square guide will also produce a difference in phase
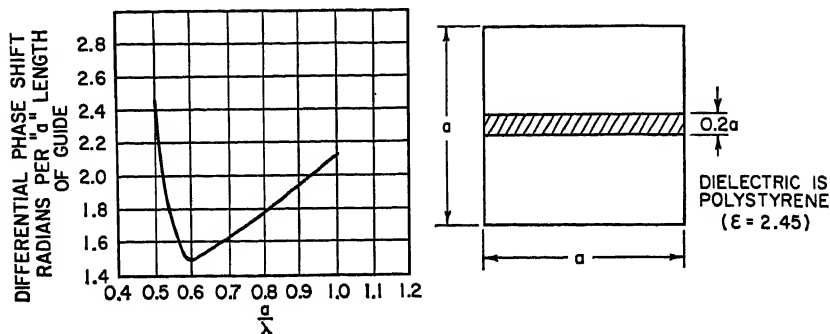
Fig. 17-26. Differential phase shift in a partially loaded square waveguide.
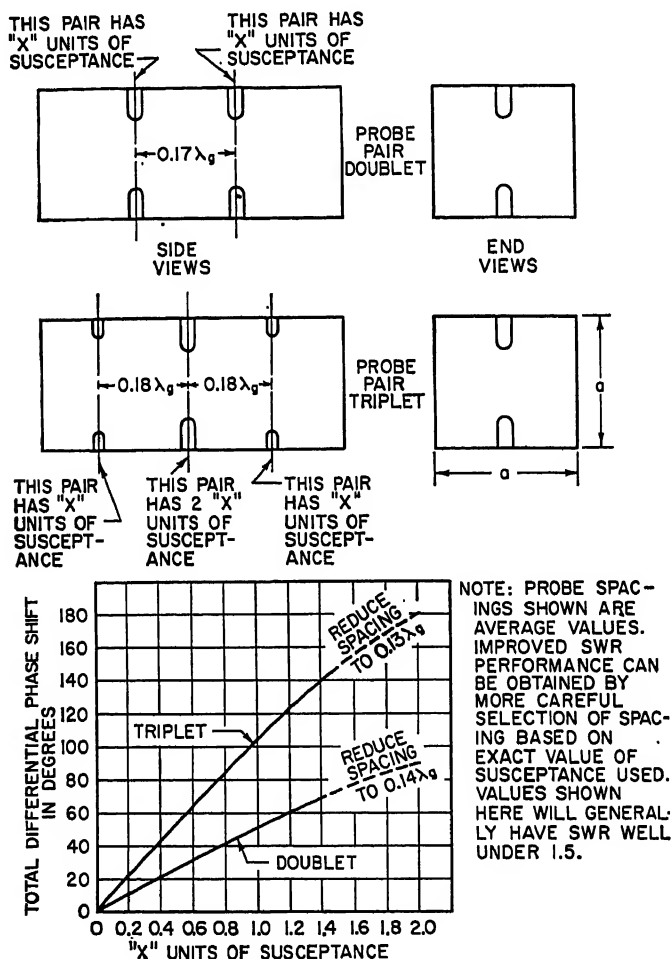
Fig. 17-27. Probe phase-shifter design.

velocity for the two modes of interest. Figure 17-26 provides the pertinent information for a typical case. Just as above, it is necessary to provide means for obtaining an impedance match at each end of the phasing section. It is not sufficient as a rule to have the phasing section as a whole appear matched; it is important to have each
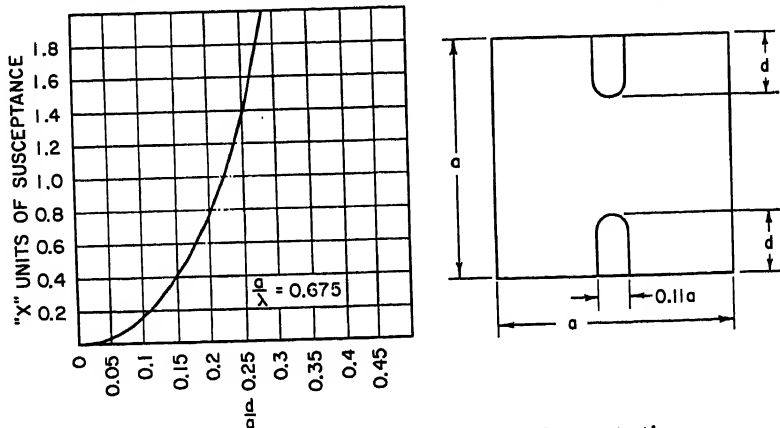
Fig. 17-28. Susceptance as a function of probe penetration.
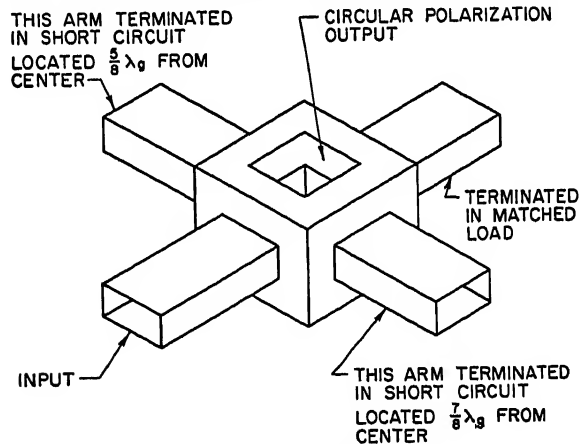
Fig. 17-29. Turnstile junction.

end matched by itself. If this precaution is not observed, it will be found very difficult to predict total phase shift, as well as the change in phase shift with a change in geometry. In short, adjustment, or tailoring, is difficult. The power-handling capacity will be somewhat lower also.

Lumped-element loading in a square guide has also been used successfully. The use of probe pairs is particularly convenient. Pair doublets and pair triplets are the most convenient, with the latter providing greater bandwidth and greater power-handling capacity for a given differential phase shift. Figure 17-27 shows the design data for the doublet and triplet cases. The length of the probe necessary for a given value of susceptance is shown in Fig. 17-28.

Circularly polarized waves can be generated directly in a waveguide junction known as a turnstile junction (not to be confused with turnstile antenna). The general geometry is illustrated in Fig. 17-29.

Dual-mode Generation.   This section has thus far concerned itself with the radiation and phasing of dual modes forming a circularly polarized wave.   The generation of these two modes in a section of square (or round) guide can be accomplished in several ways, of which the two most common are:

1. Coaxial cable probes at right angles
2. Conventional rectangular waveguide inclined at 45°

The second case is especially convenient because the ratio of magnitudes of the vertically and horizontally polarized waves can be altered merely by altering the inclination of the rectangular guide.

In generating and guiding dual modes in square or round guide, care should be employed to keep the geometry symmetrical about each of the two principal longitudinal planes.   Any asymmetry will tend to excite the TM_{11} or TE_{11} modes.   For square or round guide, these two modes will usually not be very far from cutoff.   For example, in square guide, with dimensions a high and a wide, cutoff for the TE_{01} and TE_{10} modes occurs at $\lambda = 2a$.   The cutoff for TM_{11} and TE_{11} occurs at $\lambda = 2\sqrt{2}\,a$, or only about 41 per cent above cutoff for the dominant modes.
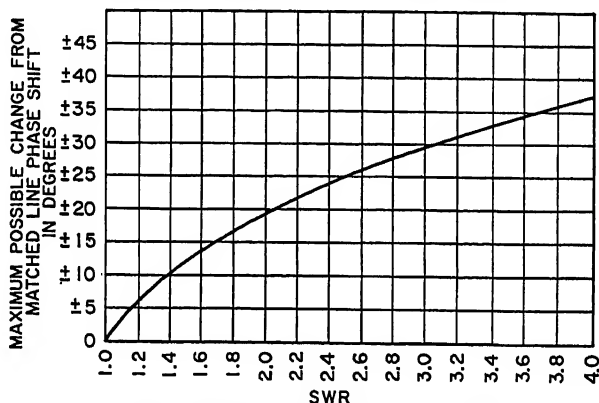
FIG. 17-30. Possible phase variation with SWR.

In all the discussion above concerning phase shift, it has been assumed that there is an impedance match for both of the generated dual modes.   The existence of mismatch may produce an unexpected alteration in the phase shift.   For example, if there is a perfect match for both the vertically and horizontally polarized modes, and the differential phase shift noted, the appearance of a mismatch in one of the modes may produce a change in differential phase shift as shown in Fig. 17-30.   If the same magnitude mismatch appears in both modes, the change may be as large as twice that of Fig. 17-30.

At the time of this writing, it appears that significant contributions to the circular-polarization art may come about through the use of ferrites.   So far, ferrite phase shifters similar in general appearance to the dielectric-slab configuration above have been the most common application of ferrites to this field.   Difficulties include power limitation and temperature instability.   It is probable that more extensive and interesting application of ferrites will be made to the circular-polarization art within the next five years.

17.6. TRANSMISSION-TYPE POLARIZERS*

Transmission-type polarizers are designed to take existing linearly polarized energy and transform it into circularly polarized energy.   The advantage of such polarizers

* This section contributed by W. H. Yale.

is that their design is relatively independent of the characteristics of the source of the wave on which they operate. The disadvantage is that this type of polarizer tends to be quite large physically and difficult to modify or adjust.

A transmission-type polarizer is a structure that exhibits a differential phase shift to two mutually perpendicular electric vectors. This differential phase shift is then adjusted to be 90°, and assuming the two perpendicular vectors are equal in magnitude, circular polarization results.

The simplest type of polarizer is a parallel-metal-plate structure (Fig. 17-31). In this structure, the incident linearly polarized energy is inclined at an angle of 45° to the plane of the metal plates, so that there are two equal field components, one parallel

LINEAR POLARIZATION

PARALLEL
COMPONENT

INCIDENT FIELD

45°

PERPENDICULAR
COMPONENT

DIRECTION OF
PROPAGATION

$\ell = \dfrac{3\lambda_0}{4}$

$\ell = \dfrac{\lambda_0}{2}$

$a = 0.671\lambda_0$

$\lambda_g = \dfrac{\lambda_0}{\sqrt{1 - \dfrac{\lambda_0}{2a}}}$

$\lambda_0 =$ FREE SPACE
WAVELENGTH

CIRCULAR POLARIZATION

PERPENDICULAR
COMPONENT

PARALLEL
COMPONENT

90°

DIRECTION OF
PROPAGATION
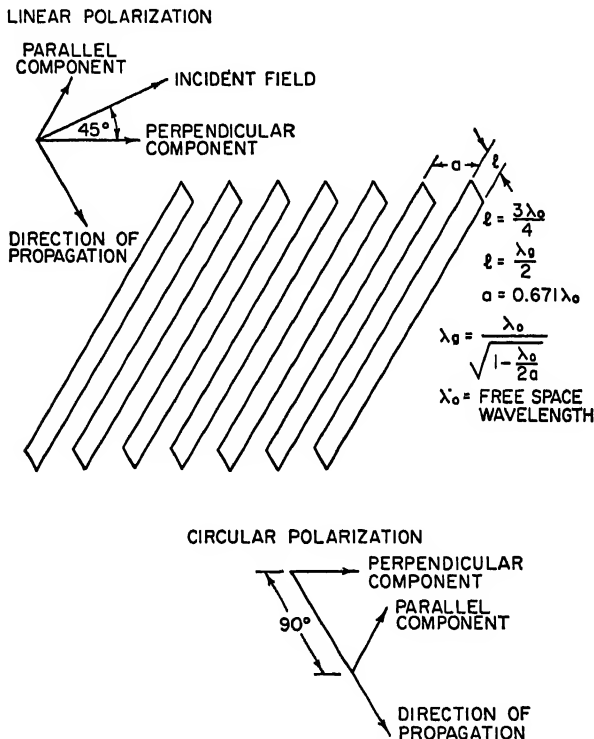
FIG. 17-31. Parallel-plate polarizer.

to the plates and one perpendicular to the plates. The component perpendicular to the plates will pass through the structure undisturbed, while the component parallel to the plates will see a parallel-plate waveguide structure, and hence a phase shift relative to free-space propagation. If the spacing and length of the plates are adjusted so that the field parallel to the plates is advanced $\lambda/4$ (90°) in phase with respect to the field perpendicular to the plates, the two fields at the exit of the plates are now in space-and-time quadrature, and hence result in a circularly polarized wave. This structure is commonly referred to as a "quarter-wave plate."

The parallel plate structure is an anisotropic dielectric, with a dielectric constant less than unity. Any anisotropic dielectric, regardless of dielectric constant, will act as a transmission-type polarizer, provided that the amplitude and phase requirements are met.

There are several ways to produce an anisotropic dielectric: (1) parallel metal plates,[26,30] (2) parallel dielectric plates[27] (Fig. 17-32), and (3) a lattice structure composed of strips or rods.[28,29] The differences between the three methods are frequency sensitivity, weight, and ease of design, since the size remains relatively constant for a given application. The first two methods are the heaviest, while the last two are the least frequency-sensitive. The three methods are listed in order of the complexity of their design.
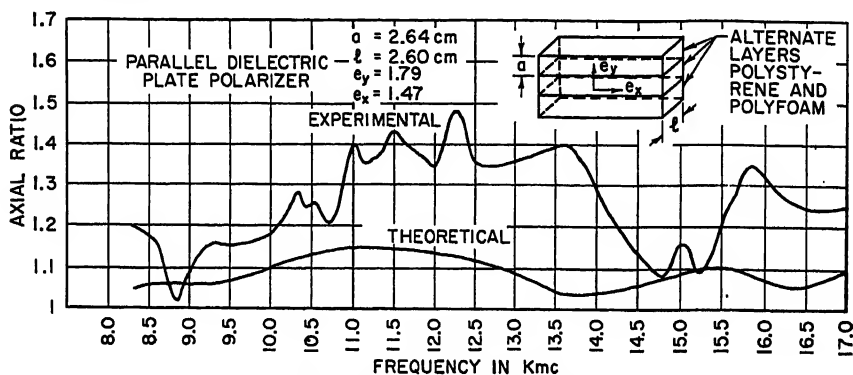
FIG. 17-32. Parallel-dielectric-plate polarizer.

The transmission-type polarizers are applicable to radars employing line sources, in which the individual elements cannot be readily circularly polarized.

17.7. REFLECTION-TYPE POLARIZERS*

Reflection-type polarizers are essentially transmission-type polarizers cut in half and placed on a conducting sheet.

The simplest type of reflection-type polarizer is a series of metal vanes on a conducting sheet.[30] These vanes are one-eighth-wavelength high. The incident energy is polarized at 45° to the vanes, so that the component parallel to the vanes is reflected by edges of the vanes and the component perpendicular to the vanes is reflected by the conducting sheet, thus delaying it 90° with respect to the parallel component and producing circular polarization.

Another method of obtaining circular polarization utilizes the difference in phase between the perpendicular and parallel components, when totally reflected from the surface of a lossless dielectric.[11] This occurs if the dielectric constant e is greater than 5.8. The angle θ_0 at which this occurs is given by $\sin^2 \theta_0 = 2/(e + 1)$.

17.8. RADAR PRECIPITATION-CLUTTER SUPPRESSION†

Precipitation clutter is the name given to the radar echo from such targets as rain, snow, etc. It is not unusual for a radar to be rendered useless because precipitation clutter is sufficiently strong and extensive to hide the presence of a desired target (such as an aircraft). Because raindrops are substantially spherical (or at least much more so than an aircraft), they qualify as symmetrical reflectors. As mentioned in Sec. 17.1, a circularly polarized antenna is unable to see its own image in a symmetrical reflector. Therefore, if the radar antenna is circularly polarized, the echo from a symmetrical target such as a spherical raindrop will be circularly polarized with the wrong

* This section contributed by W. H. Yale.
† This section contributed by W. B. Offutt.

sense to be accepted by the antenna and will not be received.   The echo from a composite target such as an aircraft will have scrambled polarization and will usually contain a polarization component to which the circularly polarized radar antenna can respond.

In other words, then, if the radar antenna is perfectly circularly polarized and the clutter is caused by spherical raindrops, the clutter cancellation will be perfect, enabling the presence of an otherwise hidden composite target to be detected.   When the radar antenna is elliptically polarized, the cancellation of an echo from symmetrical targets will not be complete; also, if the antenna is circularly polarized and the target is not symmetrical, cancellation will not be complete.

Cancellation Ratio.   Cancellation ratio is defined as the ratio of radar power received from a symmetrical target when using a precipitation-clutter-suppression technique to the power received from the same target when not using the suppression technique.   Figure 17-33 shows cancellation ratio as a function of the polarization ellipticity of the antenna illuminating the symmetrical target.
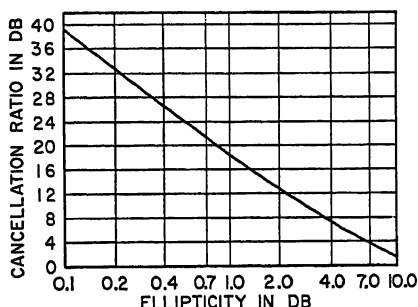
Fig. 17-33. Cancellation ratio as a function of polarization ellipticity.

Cancellation of Various Targets.   Table 17-4 shows the extent of cancellation of various targets when the antenna is perfectly circularly polarized.

Table 17-4. Cancellation of Various Targets for Circular Polarization

Target	Return using circular polarization relative to return using linear polarization
Sphere	Complete cancellation
Disk facing radar	Complete cancellation
Large sheet facing radar	Complete cancellation
Wire grating facing radar (wires parallel to linear polarization for that case)	6-db cancellation
Double-bounce corner reflector	Zero cancellation
Triple-bounce corner reflector	Complete cancellation

Integrated Cancellation Ratio.   A suitable figure of merit for circularly polarized radar antennas is the integrated cancellation ratio.   The integrated cancellation ratio is defined as ratio of radar power received with circular polarization to the radar power received with linear polarization when the antenna, in both instances, is completely surrounded by an infinite number of randomly distributed small symmetrical targets. The integrated cancellation ratio places proper emphasis on the necessity for having the radar beam circularly polarized all over, and not just on its peak.   The rain cloud causing the clutter does not exist only on the beam peak; therefore it is necessary to have the complete beam circularly polarized if the most effective cancellation is to be obtained.

Table 17-5 shows a chart form useful in computing the integrated cancellation ratio from a set of point-by-point measurements on the radiation pattern.

With careful design, integrated cancellation ratios of 30 or 35 db can be obtained with large reflector-type antennas.   For operation over a 5 or 10 per cent band, and because of the nonideal shape of normal raindrops, an integrated cancellation ratio of 20 db is usually considered to be adequate.   It is fairly safe to assume that the integrated cancellation ratio is the limit of performance that can be expected with a given antenna; usually the actual performance will be somewhat poorer because of nonideal shape of the water particles.

Table 17-5. Chart Form for Integrated-cancellation-ratio Computation

Azimuth angle, ϕ	Eleva-tion angle, θ	Sin θ	One-way response		One-way response		Total power returned, $(P_{max} + P_{min})^2 \sin \theta$	Total power received, $(P_{max} - P_{min})^2 \sin \theta$
			P_{max}, db	P_{min}, db	P_{max}	P_{min}		
						Σ		

$$\text{Integrated cancellation ratio} = \frac{\Sigma \text{ total power received}}{\Sigma \text{ total power returned}}$$

NOTES:

1. ϕ is the azimuth angle of the point on the beam being measured.

2. θ is the elevation angle of the point on the beam being measured. It is measured from the vertical; that is, straight up is zero.

3. One-way response in decibels is the signal (usually referred to the peak of the beam) measured by a linearly polarized rotatable antenna placed at a suitable distance from the circularly polarized antenna being measured. P_{max} is the maximum response obtained as the linearly polarized antenna is rotated to investigate the polarization ellipticity. P_{min} is the minimum response obtained as the linearly polarized antenna is rotated.

4. The second "one-way-response" pair of columns is for the power ratio associated with the decibel values in the preceding columns. If the data are taken directly in power, the decibel columns need not be used.

REFERENCES

1. G. A. Deschamps: "A New Chart for the Solution of Transmission-line and Polarization Problems," *Elec. Commun.*, September, 1953, pp. 247-254. Discussion of the properties of a chart formed by the orthographic projection of the Poincaré sphere.
2. W. Sichak and S. Milazzo; "Antennas for Circular Polarization," *Proc. IRE*, August, 1948, pp. 997-1001. Derivation of expression for voltage induced in an arbitrarily polarized antenna by an arbitrarily polarized wave, plus typical applications.
3. L. Hatkin; "Elliptically Polarized Waves," *Proc. IRE*, December, 1950, p. 1455. Simplified derivation of expression for voltage induced in an arbitrarily polarized antenna by an arbitrarily polarized wave.
4. G. Sinclair: "The Transmission and Reception of Elliptically Polarized Waves," *Proc. IRE*, February, 1950, pp. 148-151. Definition and development of a complex effective height which describes antenna performance for arbitrary polarization characteristics.
5. J. I. Bohnert: "Measurements on Elliptically Polarized Antennas," *Proc. IRE* May, 1951, pp. 549-552. Description of measurement techniques for elliptically polarized antennas using both circular and linear components. Definition of gain and beamwidth.
6. M. G. Morgan and W. R. Evans: "Synthesis and Analysis of Elliptic Polarization Loci in Terms of Space-Quadrature Sinusoidal Components," *Proc. IRE*, May, 1951, pp. 552-556. Development of the polarization ellipse from two and three orthogonal components. A rectangular-polarization chart is also shown.
7. S. A. Schelkunoff and H. T. Friis: "Antennas: Theory and Practice," pp. 390-393, John Wiley & Sons, Inc., New York, 1952. Calculation of transmission between two elliptically polarized antennas. Definition of a complex radiation vector to facilitate above calculation.

8. V. H. Rumsey: "Transmission between Elliptically Polarized Antennas," *Proc. IRE*, May, 1951, pp. 535–540. Development of the analogy between impedance and polarization concepts and application of the analogy to transmission and reception between two elliptically polarized antennas.

9. G. A. Deschamps: "Geometrical Representation of the Plane Electromagnetic Wave," *Proc. IRE*, May, 1951, pp. 540–544. Description of the use of the Poincaré sphere for polarization manipulations and illustration of both orthographic and stereographic projections of this sphere on a plane.

10. M. L. Kales: "Elliptically Polarized Waves and Antennas," *Proc. IRE*, May, 1951, pp. 544–549. Development and application of a complex-vector algebra particularly suited for circular-polarization problems.

11. J. A. Stratton: "Electromagnetic Theory," pp. 279–280, 499–500, McGraw-Hill Book Company, Inc., New York, 1941. Mathematical definition of an elliptically polarized wave and discussion of formation of a circularly polarized wave by total reflection from a dielectric interface.

12. S. A. Schelkunoff: "Electromagnetic Waves," pp. 248–249, C. Van Nostrand Company, Inc., Princeton, N.J., 1951. Mathematical definition of an elliptically polarized wave.

13. Y. C. Yeh: "The Received Power of a Receiving Antenna and the Criteria for its Design," *Proc. IRE*, February, 1949, pp. 155–158. Development of formulas for transmission and reception between two antennas of arbitrary polarization and application to practical problems.

14. C. E. Smith and R. A. Fouty: "Circular Polarization in F-M Broadcasting," *Electronics*, vol. 21, pp. 103–107, September, 1948. An application of the slotted cylinder for a circularly polarized omnidirectional antenna.

15. A. J. Simmons: "Circularly Polarized Slot Radiators," *IRE Trans.*, vol. AP-5, no. 1, pp. 31–36, January, 1957. A theoretical and experimental investigation of producing circular polarization by using two crossed slots in the broad wall of a rectangular waveguide.

16. J. D. Dyson: "The Equiangular Spiral Antenna," *Univ. Illinois, Antenna Lab.*, TR 21, September 15, 1957. A comprehensive experimental investigation of the pattern and impedance properties of equiangular spirals.

17. V. H. Rumsey: "Frequency Independent Antennas," IRE National Convention Record, pt. I, pp. 114–118, 1957. An excellent theoretical treatment of antennas whose pattern and impedance characteristics are independent of frequency.

18. G. H. Brown and O. M. Woodward, Jr.: "Circularly-polarized Omnidirectional Antenna," *RCA Rev.*, vol. 8, pp. 259–269, June, 1947. A theoretical and experimental investigation of a circularly polarized antenna system consisting of four inclined dipoles arrayed around a mast.

19. D. R. Rhodes: "An Experimental Investigation of the Radiation Patterns of Electromagnetic Horn Antennas," *Proc. IRE*, September, 1948, p. 1103. Design data for horns.

20. W. P. Ayres: "Broadband Quarter Wave Plates," *IRE Trans. on Microwave Theory Techn.*, October, 1957, pp. 258–261. Design data on dielectric-slab quarter-wave plates for use in dual-mode waveguide.

21. H. S. Kirschbaum and L. Chen: "A Method of Producing Broad-band Circular Polarization Employing an Anisotropic Dielectric," *IRE Trans. on Microwave Theory Tech.*, July, 1957, pp. 199–203. Design data on dielectric quarter-wave plates for use in dual-mode waveguides and windows.

22. O. M. Woodward: "A Circularly Polarized Corner Reflector Antenna," *IRE Trans. on Antennas and Propagation*, July, 1957, pp. 290–297.

23. H. N. Chait: "An Arbitrarily Polarized Antenna for Use at X-Band," *Naval Research Lab. Rept.* 3416, Mar. 15, 1949. Use of hybrid and phase shifter to provide excitation for dual-mode horn.

24. P. A. Crandell: "A Turnstile Polarizer for Rain Cancellation," *IRE Trans. on Microwave Theory Tech.*, January, 1955, p. 10. Description of turnstile polarizer in X-band radar antenna.

25. D. L. Margerum: "Broadbanding Circular Polarization Transducers," *IRE Trans. on Microwave Theory Tech.*, November, 1953. Discussion of tapered-elliptical and dielectric-slab phase-shifting sections.

26. J. Ruze: "Metal Plate Optics," *Proc. IRE*, January, 1950, p 53. The design equations for constrained metal-plate lenses are derived.

27. H. S. Kirschbaum and L. Chen: "A Method of Producing Broad-band Circular Polarization Employing an Anisotropic Dielectric," *IRE Trans. on Microwave Theory Tech.*, July, 1957, pp. 199–203. A procedure is described whereby it is possible to

design circular polarizers for both waveguide and window form to be used over a broadband of frequencies.

28. J. A. Brown: "The Design of Metallic Delay Dielectrics," *Proc. IEE (London)*, pt. III, vol. 97, no. 45, p. 45, January, 1950. A theory of metallic delay dielectrics, which is more accurate than existing theories and is based on an analogy with shunt-loaded transmission lines, has been developed for the simplest case, when the delay medium consists of an array of infinitely long conducting strips. (See also Chap. 14).

29. H. S. Bennett: "The Electromagnetic Transmission Characteristics of the Two-dimensional Lattice Medium," *J. Appl. Phys.*, vol. 24, no. 6, p. 785, June, 1953. The behavior of the two-dimensional lattice medium is investigated in the presence of electromagnetic energy.

30. J. F. Ramsay: "Circular Polarization for C. W. Radar," Marconi's Wireless Telegraph Co., Ltd., 1952. Proceedings of a conference on centimetric aerials for marine navigational radar, held June 15–16, 1950, in London.

31. W. B. Offutt: "A Review of Circular Polarization as a Means of Precipitation-clutter Suppression and Examples," *Proc. Natl. Electronics Conf.*, vol. 11, 1955.

Chapter 18

FREQUENCY-INDEPENDENT ANTENNAS

GEORGES A. DESCHAMPS

University of Illinois
Electrical Engineering Research Laboratory
Urbana, Illinois

and

RAYMOND H. DuHAMEL

Collins Radio Company
Cedar Rapids, Iowa

18.1. BASIC PRINCIPLES

The two types of antennas described in this chapter are capable of bandwidths of operation that were believed impossible a few years ago. Both represent the development of relatively simple yet powerful ideas.

The first idea[1] evolves from the observation that the properties of an antenna, impedance and pattern, are determined by its shape and by its dimensions evaluated in wavelength. If by an arbitrary scaling the antenna is transformed into a structure equal to the original one, its properties will be independent of the frequency of operation. The antenna then satisfies the *angle condition*, which means that its form can be specified entirely by angles only and not by any particular dimension. There are two classes of antennas satisfying this condition. *Conical antennas* made up of infinite cones of arbitrary cross section having a common apex and *equiangular antennas* having their surfaces generated by equiangular spirals having a common axis and the same defining parameter.

The second idea[2] is that if a structure becomes equal to itself by a particular scaling of its dimensions, by some ratio τ, it will have the same properties at a frequency f and at the frequency τf. It results from this that the impedance, or any other characteristic, is a periodic function, with the period log τ, of the logarithm of frequency. The antennas obtained from this principle are called *log-periodic*. By making τ close enough to 1, the variation of the properties over the frequency band $(f, \tau f)$, and therefore everywhere, can be expected to be small. In practice, even with τ not very close to 1, good frequency-independent behaviors are observed.

To conform to the conditions stated above, equiangular as well as log-periodic structures should extend from the center of expansion 0, which is also the feed point, up to infinity. A practical antenna is obtained by taking a section of the ideal infinite structure contained between two spheres of center 0 and of radii r_1 and r_2, respectively.

Inside the smaller sphere is the feed region where the infinite structure, which ideally should converge to the point 0, is replaced by some coupling mechanism to the feed transmission line or waveguide. The length r_1 determines the highest frequency of operation f_1 of the antenna by the condition that r_1 must be small enough, compared with the wavelength λ_1, to make the exact shape of the coupling mechanism have little influence on the impedance or on the resulting current distribution over the antenna. Ultimately the dimension r_1 is fixed by the size of the waveguide or transmission line connected to the structure.

The outside dimension of the antenna, specified by the radius r_2, determines the lowest frequency of operation by the following considerations. It is observed, for some structures, that the currents (or the field components near to the material boundaries of the structure) decrease rapidly with the distance to the center. Thus it becomes possible to cut off the structure at the distance where these currents are so small with respect to the current I_0 at the feed point that they can be suppressed without changing appreciably the radiation pattern or the impedance seen at the feed point. For a given frequency the distance at which this happens is proportional to the corresponding wavelength. Thus the lower cutoff frequency may be decreased at will by increasing the size of the antenna.

The rapidity of decrease of the currents with distance depends on the particular structure considered. For conical antennas excited at the center point, the field is transverse to the radial direction and decreases only as the inverse of the distance r to the center. When taking a finite portion of such an antenna, however large, the end effect will produce variations of the radiation pattern. Equiangular and some log-periodic antennas, on the other hand, exhibit a decrease of current with distance faster than $1/r$. The end effect becomes negligible at a distance, in wavelength,

depending on the exact shape of the structure. Thus some antennas will be more compact than others for a given frequency λ_2 and a given relative importance of end effect.

A property common to both types of antennas and related to the absence of end effect is that the radiation field must be substantially zero in the direction of the conductors forming the structure, seen from the center point.

For log-periodic structures another concern of importance is the variation of impedance or pattern over a period. Not all log-periodic structures are equally good from this point of view, but it is remarkable that, for some of them, very uniform performances are obtained even when the ratio τ is not close to 1.

Some relations between the two types of antennas should be noted. Equiangular antennas are special cases of log-periodic antennas with a period $\log \tau = 2\pi a$ (a defined below). This property is not destroyed if the cones of revolution on which the spirals lie are distorted or given different axes. For example, one cone may be flattened, or several equiangular spiral arms with the same apex but different axes may form an array having the log-periodic property.

A class of log-periodic elements is obtained by taking a section of a solid equiangular structure by a plane passing through its axis. The structures in Figs. 18–10c and 18–10d have this property. Besides reproducing themselves by expansion in the ratio τ, these structures will also reproduce by a reflection through the axis followed by an expansion in the ratio $\tau^{\frac{1}{2}}$. Antennas made of such elements usually exhibit smoother impedance characteristics than those that are simply log-periodic.

Although, strictly speaking, none of the finite-size antennas considered is truly frequency-independent over the range 0 to ∞, the name is justified because the possibilities for increasing the bandwidth are almost unlimited. Without changing the design, but simply by adding some turns to the spirals or some sections to the log-periodic antenna, any desired bandwidth can be achieved.

18.2. EQUIANGULAR ANTENNAS

General Characteristics. The structure of an antenna satisfying the angle condition must be such that if it is expanded in an arbitrary ratio τ about the feed point 0, the configuration obtained becomes congruent to the original one. Either it will coincide with the original structure, or it will coincide with a structure deduced from the original one by a rotation about some axis D passing through the point 0.

The first condition is satisfied by conical structures having a common apex. Antennas obtained by taking finite sections of such structures, the discone antenna, for example, have indeed broadband properties.[3] However, they are not frequency-independent in the sense discussed in the preceding section since any finite portion, however large, will show end effects. The bandwidth therefore cannot be increased at will by increasing the size.

The other type of structure (equiangular) has been characterized by Rumsey.[1] He has shown that the following conditions must be satisfied:

1. The axis of rotation D must be independent of τ.
2. The angle of rotation about D must be proportional to the logarithm of τ.

$$\tau = e^{a\phi} \tag{18-1}$$

These equiangular structures, in contrast to the conical ones, show proper attenuation of the current with distance (with varying degree, according to the parameters of the structure) and lead to frequency-independent antennas.

Geometry. Using D as the z axis in a conventional system of spherical coordinates, the property may also be expressed by stating that the surfaces bounding the antenna

must have equations of the form

$$F(\theta, re^{-a\phi}) = 0 \qquad (18\text{-}2)$$

where F is an arbitrary function and a is a constant.

The rotation expansion T^ϕ resulting from a rotation about D through the angle ϕ, followed (or preceded) by an expansion about 0, in the ratio $\tau = e^{a\phi}$, will carry the structure onto itself. (The exponential notation T^ϕ is justified by the obvious property
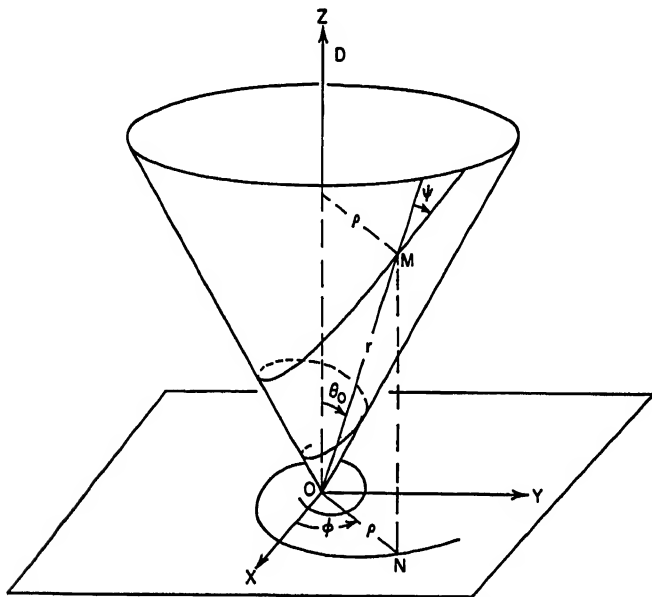
FIG. 18-1. Geometry of the equiangular spiral.

$T^\phi T^\psi = T^{\phi+\psi}$.) Starting from an arbitrary point M, the point $T^\phi(M)$, as ϕ is varied, will describe an equiangular spiral, either in the plane $z = 0$ or on a cone of revolution having D as axis. All surfaces of an antenna satisfying Rumsey's condition will be generated by such spirals having a common axis and the same parameter a.

Figure 18-1 shows an equiangular spiral. It is drawn on a cone of revolution about D,

$$\theta = \theta_0 \qquad (18\text{-}3)$$

and its equation is

$$r = r_0 e^{a\phi} \qquad (18\text{-}4)$$

or

$$\rho = \rho_0 e^{a\phi} \qquad (18\text{-}5)$$

The spiral is called equiangular because it makes a constant angle ψ with the radius vector.

$$\tan \psi = \frac{\sin \theta_0}{a} \qquad (18\text{-}6)$$

The arc length s from the origin 0 is finite and proportional to the distance r.

$$s = \frac{r}{\cos \psi} \qquad (18\text{-}7)$$

The projection of the spiral on the xy plane is also equiangular with the same parameter a. In the plane $z = 0$ the equiangular spirals with the paramenter

$$a' = -\frac{1}{a} \tag{18-8}$$

are orthogonal to those with parameter a. On the cone $\theta = \theta_0$ the spirals of the orthogonal set have the parameter

$$a' = -\frac{\sin^2 \theta_0}{a} \tag{18-9}$$

Pattern Rotation. When the infinite structure is fed at the center by a constant current source of unit intensity, the electric field at frequency f, at some point M, is $\mathbf{E}(M,f)$. If the frequency is changed to $f' = f/\tau$, which amounts to a scaling τ of the dimensions, the field becomes

$$\mathbf{E}\left(M, \frac{f}{\tau}\right) = \frac{1}{\tau^2}\, T^\phi\, \mathbf{E}(T^{-\phi}M, f) \tag{18-10}$$

where the rotation expansion T^ϕ corresponds to $\phi = (1/a) \ln \tau$.

The radiation pattern is defined by the field on a large sphere of radius R.

$$\mathbf{E}(\theta,\varphi,R) = \frac{e^{-jkR}}{R}[\hat{\theta}P_\theta(\theta,\varphi) + \hat{\varphi}P_\varphi(\theta,\varphi)] \tag{18-11}$$

($\hat{\theta}$ and $\hat{\varphi}$ are unit vectors in direction of coordinates.) The relation (18-10) implies that both function P_θ and P_φ satisfy the relation

$$P\left(\theta, \varphi, \frac{f}{\tau}\right) = P\left(\theta, \varphi - \frac{1}{a} \ln \tau, f\right) \tag{18-12}$$

When the frequency is changed from f to f/τ, the pattern is rotated about D through the angle $(1/a) \ln \tau$. For finite structures this has been verified experimentally over the bandwidth of operation of the antenna.

Practical Structures. Simple practical structures are made of conducting wires or of metallic sheets. Although ideally the wires or the sheets should be tapered according to distance to satisfy the equiangular condition, in practice a wire of constant radius or a sheet of constant thickness may be used over moderately wide frequency bands 5:1 or 10:1).

The structures on which most data have been collected[4,5] are variants of the dipole (where the two halves have been twisted into a pair of equiangular arms) or of the slot antenna (where the edges of the slot are equiangular spirals extending from the feed point). Some multiarm structures have also been considered.

Planar Structures. The planar structures are made of two symmetrical equiangular arms as shown in Figs. 18-2 and 18-3.

Parameters defining the infinite structure are:

1. The rate of spiral $1/a$ which defines the expansion ratio $e^{a\phi}$ corresponding to the rotation ϕ. It also determines the angle $\psi = \tan^{-1}(1/a)$ at which radial lines cut the spirals.

2. The arm width specified either by the angle δ or by the ratio $K = e^{-a\delta}$. When $\delta < 90°$, the structure may be considered as a slot of angular width $180° - \delta$ rather than as a dipole. Figure 18-6 gives a conversion from a and δ to K and to ψ.

The finite antenna is described by the cutoff radii r_1 and r_2 and the exact manner in which it is terminated outside of this section. If the structure is large enough to

accommodate the given frequency band, the exact shape of the termination does not matter.

The antenna may be fed by a balanced line brought into the center point along the axis. A method to be preferred, which does not disturb the field as much, consists of using a coaxial cable embedded into one arm of the spiral. Because of the rapid attenuation of the fields with distance along the spiral, no appreciable current flows in the free parts of the cable. For symmetry a dummy cable is sometimes soldered to
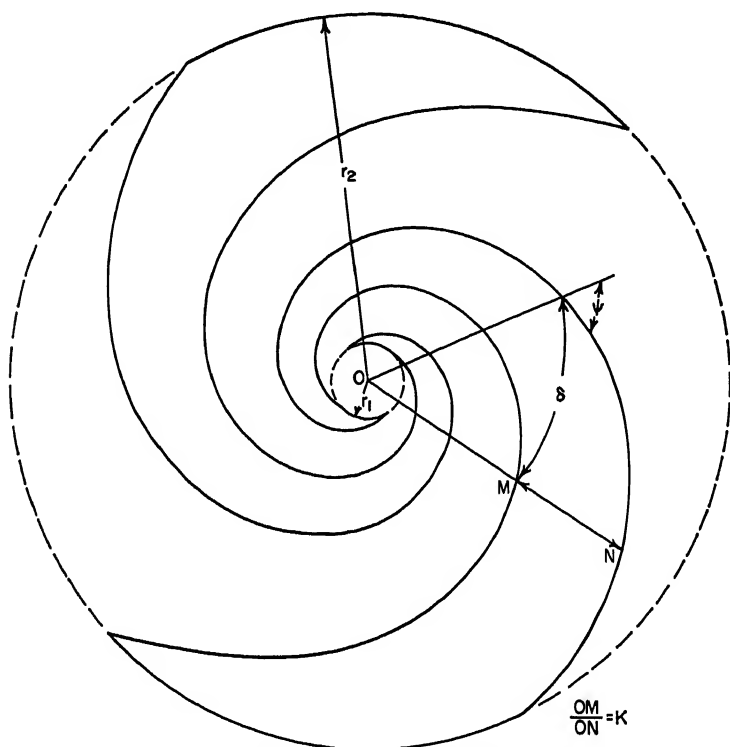
FIG. 18-2. Two-arms equiangular antenna: outline and parameters.

the other arm of the spiral in a similar configuration. Figure 18-4 shows the feed region of the antenna shown in Fig. 18-3.

The decrease of currents on the antenna, with distance to the center, appears to be approximately exponential. It is less rapid for narrow-arm or narrow-slot structures and increases with the rate of spiral $1/a$. On a wide arm the decrease is faster on the inner edge than on the outer one. The phase velocity for the currents along the antenna is close to free-space velocity at the center and increases with distance.

Impedance. The impedance for the infinite equiangular structure is real and independent of frequency. (If the structure has more than two terminals, this is true of the impedance matrix.)

Practical antennas differ from this ideal because they are finite and because the sheets or the wires are not tapered. In spite of this difference, standing-wave ratios close to unity may be obtained over the band of operation.

The thin two-armed symmetrical planar antennas with $\delta = 90°$ being self-complementary should have an impedance of 60π ohms. Values observed experimentally

FIG. 18-3. Two-arms equiangular antenna cut in a metal plate.

FIG. 18-4. The feed region of antenna in Fig. 18-3.
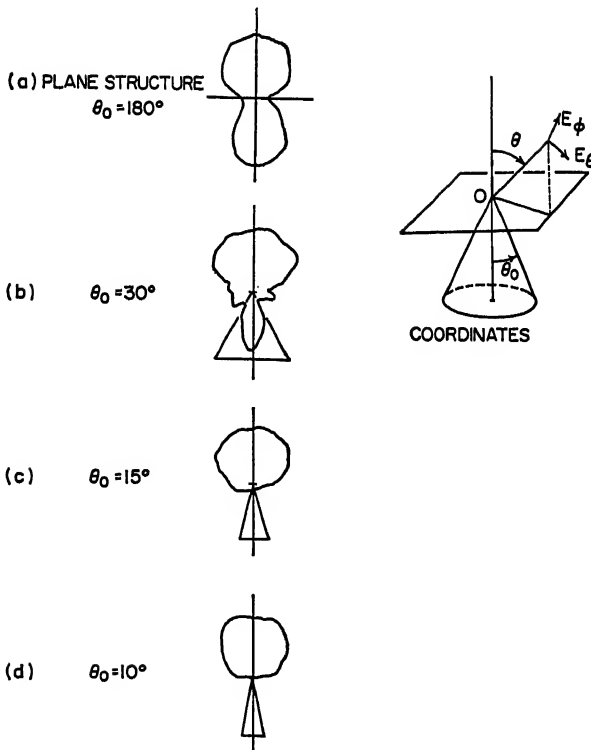
FIG. 18-5. Typical radiation patterns as a function of the cone half angle. The patterns shown are those of the E_ϕ field versus θ. The E_θ patterns are very similar. Both are essentially independent of ϕ. The spiral arm had a ratio $K = 0.925$ and made the angle $\psi = 73°$ with the radius vector.
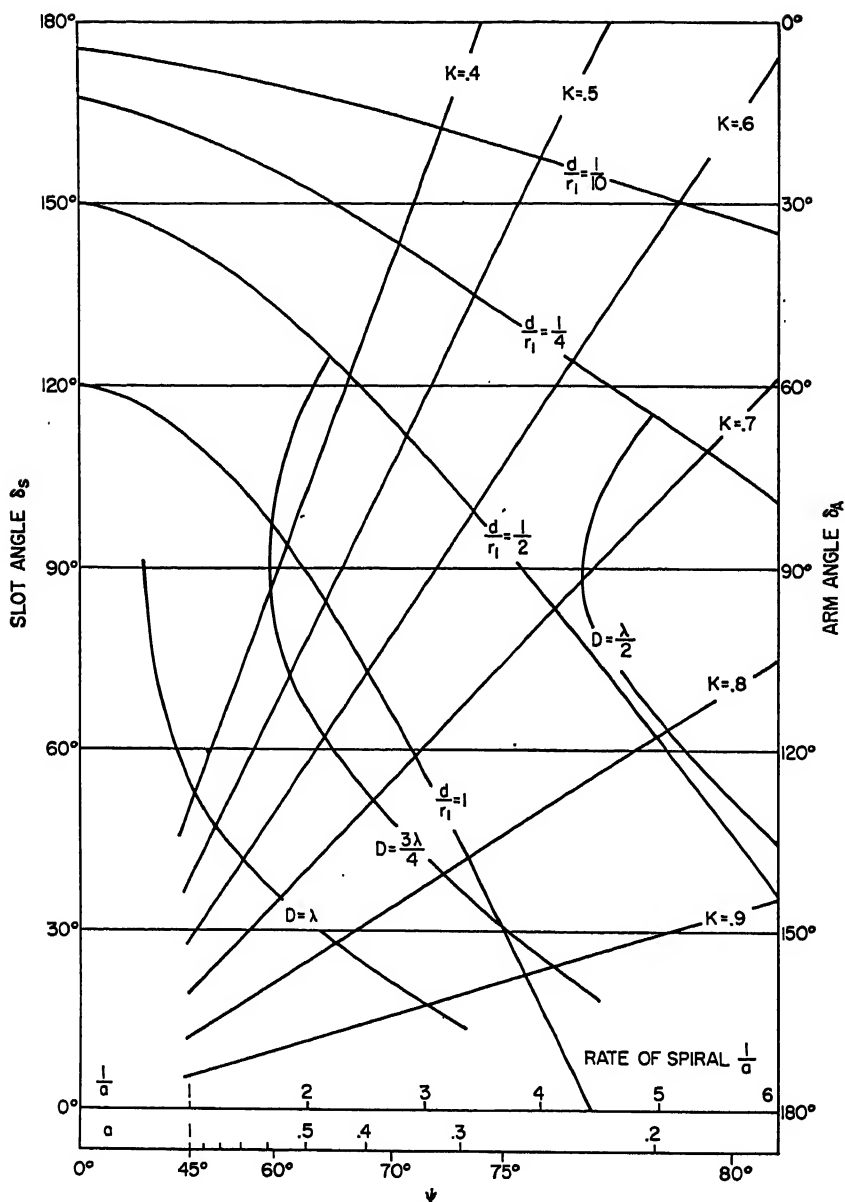
FIG. 18-6. Design chart for two-arms antenna:

D	Outer diameter of structure.
d	Cable diameter of minimum arm width.
K	Ratio of distances from the center to the edges of the slot. (To find this ratio for an arm read the arm angle δ_A on δ_S scale.)
r_1	Radius of feed region.
ψ	Constant angle between an equiangular spiral and the radius vector.

(about 120 ohms) are lower because of the presence of the cable feeding the structure. Narrow-arm structures have higher impedances.

Radiation Pattern. A typical radiation pattern for the planar structure is shown in Fig. 18-5a. The field is practically circularly polarized over the frequency band of operation. (The axial ratio of the field on the axis is a convenient criterion for defining the edges of the band.)

The pattern does not change much with the parameters a and δ of the structure. It is more closely circular for high rate of spiral. For low rates of spiral the pattern shows asymmetry and its rotation with frequency may be observed.
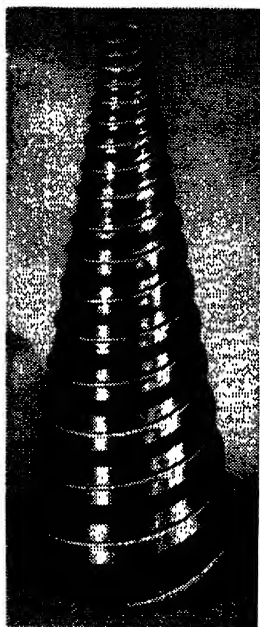
FIG. 18-7. Equiangular spiral on a cone.
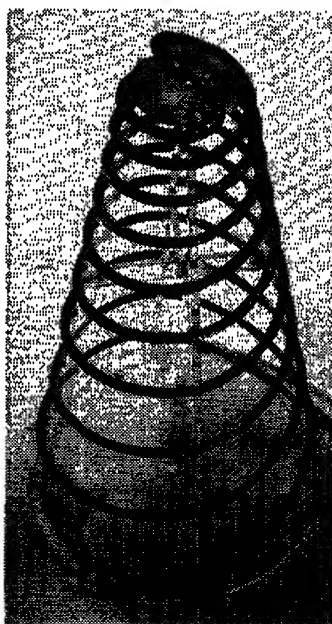
FIG. 18-8. Conical equiangular antenna made of coaxial cables.

The currents on the antenna have odd symmetry with respect to the axis D; the field everywhere has the same symmetry and therefore does not contain any multipole components with $e^{jm\phi}$ variation, where m is even. In particular, there is no dipole moment along D either electric or magnetic. The patterns obtained experimentally are fairly well represented by electric and magnetic dipoles perpendicular to D.

Design Considerations. The problem is to design an antenna of the type described above with frequency-independent behavior over a band f_2 to f_1.

The high-frequency cutoff f_1 being given, the radius of the feed region must be small compared with the wavelength ($r_1 \simeq \lambda_1/8$, for example). If the feed line is a coaxial cable embedded in one of the arms, the arm width at the radius r_1 must be at least equal to the coaxial-cable diameter d. Lines of constant d/r_1 are shown in Fig. 18-6. For a given diameter d of cable and a given r_1, determined by λ_1, the acceptable pairs (a,δ) lie below the corresponding d/r_1 curve.

The low-frequency cutoff f_2 is linked to the attenuation along the spiral, which in turn depends on a and δ. The diameter of the antenna in wavelength, $2r_2/\lambda_2$, at the lower edge of the band becomes a function of a and δ once the performance of the antenna at frequency f_2 has been specified. The curves $2r_2/\lambda_2$, labeled D/λ on Fig. 18-6,

have been constructed using as a criterion of performance the condition that the axial ratio should be less than 2 in the direction of the axis. For other performance requirements these curves indicate only the order of magnitude of the diameter D.

The ratio $(r_2/r_1)/(f_1/f_2)$ = dimension ratio/frequency ratio may be taken as a figure of merit of a particular structure, indicating how compact the antenna can be made for a given bandwidth. This ratio is normally close to 1 and larger.

Nonplanar Structures. The balanced two-arms equiangular antenna may be wrapped on the surface of a cone of revolution as shown in Fig. 18-7. The resulting pattern becomes unidirectional, with the major lobe in the direction of the apex. It is still substantially circularly polarized over a wide portion of the pattern. The pattern is usually smoother than for the bidirectional or planar antenna. Successful antennas have been made replacing the tapered arm by a pair of spiral coaxial cables, one of them being used as the feed line as shown in Fig. 18-8. Variations of the pattern with cone angle are shown in Fig. 18-5. The design considerations discussed above apply to these structures if a is replaced by $a/\sin \theta_0$.

For a sufficient rate of spiral the pattern remains circularly polarized a long way off the axis, and because of the odd symmetry of the currents, there is no dipole moment along the axis. When the antenna is rotated about the axis through some angle α, the phase of the field in the main lobe changes also by α. This property may be used for phasing the elements of an array.

18.3. LOG-PERIODIC ANTENNAS

General Characteristics. The geometry of log-periodic antenna structures is chosen so that the electrical properties must repeat periodically with the logarithm of the frequency. Although this appears to be a backward approach to the broadband-antenna problem, nevertheless frequency independence can be obtained when the variation of the properties over one period, and therefore all periods, is small. The log-periodic design principles are illustrated in Fig. 18-9. A metal-sheet log-periodic structure with trapezoidal teeth is shown in Fig. 18-9a. The two half structures are fed against each other by a generator placed between their vertices. The four sets of teeth are defined by similar curves, the equations for which may be written in polar coordinates as $\theta = g(r)$, where $g(r)$ is some function of r. If θ is plotted vs. the $\ln r$ in rectangular coordinates, that is, $\theta = f(\ln r)$, then the log-periodic principles demand that f be a periodic function. This is illustrated in Fig. 18-9b where the two curves which define the upper half structure of Fig. 18-9a are plotted vs. the $\ln r$. Letting $\tau = R_{n+1}/R_n$, where R_n is the distance from the vertex to the outer edge of the tooth, it is seen that the period of the curve is $\ln (1/\tau)$. Other shapes of teeth, such as triangular or curved teeth, lead to other types of periodic curves when θ is plotted vs. logarithm of r. It may be seen that the logarithmic principle implies two conditions. The first is that all similar sets of dimensions, such as R_1, R_2, R_3, etc., must form a geometric sequence with the same geometric ratio τ. The second is that angles are used to a considerable extent in defining the antenna. For example, the extremities of the teeth and the triangular supporting section of the teeth are defined by angles.

Now if the antenna structure of Fig. 18-9a were infinitely large and infinitely precise near the feed point, it is easily reasoned that the structure must look exactly the same to the generator every time the frequency is changed by the factor τ. The current distribution on the structure at τf_0 is identical with that at f_0 except that everything is moved out one step. Thus, since the wavelength has changed by a proportionate amount, the radiation pattern and the input impedance must be the same at τf_0 and f_0. This is illustrated in Fig. 18-9c where the magnitude of the input impedance varies periodically with the logarithm of frequency. Because of the special left-right asymmetry of the structure of Fig. 18-9a (with $r_n = \sqrt{\tau}\, R_n$), the period of the imped-

ance curve is $\frac{1}{2} \ln (1/\tau)$ rather than $\ln (1/\tau)$. The radiation pattern also exhibits a similar periodicity with frequency, but with a period equal to $\ln (1/\tau)$.

If the variation of the impedance and pattern is small over a period, and therefore all periods because of the repetitive characteristics, it is seen that the result is essentially a frequency-independent antenna. Fortunately, some *finite* log-periodic structures provide frequency-independent operation above a certain low-frequency cutoff, which occurs when the longest tooth is approximately one-quarter wavelength long. Frequency-independent operation above the cutoff frequency is possible because log-periodic antennas display little end effect. It is found that the currents on the structure die off quite rapidly past the region where a quarter-wave tooth exists. This

(a)
TRAPEZOIDAL TOOTH LOG PERIODIC
STRUCTURE

(b)
PLOT OF θ VS. $\ln r$ FOR STRUCTURE
OF (a)

(c)
PLOT OF $|Z_{IN}|$ VS. $\ln f$
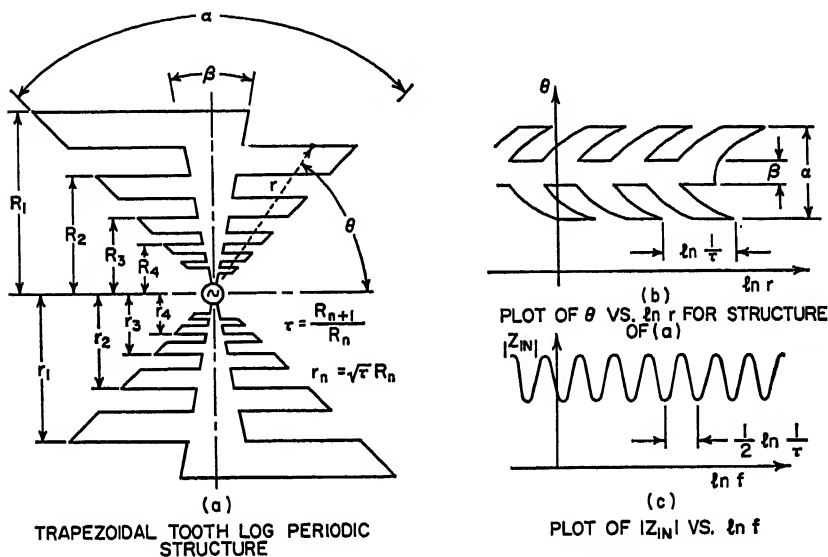
FIG. 18-9. Log-periodic antenna characteristics.

means that a smaller and smaller portion of the antenna is used as the frequency is increased, which is another way of saying that the effective electrical aperture (the aperture measured in wavelengths) is essentially independent of frequency. Since it is not possible to extend the antenna to the origin because of the presence of the feed transmission line, a high-frequency cutoff occurs when the shortest tooth is about one-quarter wavelength long.

The structure of Fig. 18-9a is horizontally polarized and has a bidirectional beam, with the beams pointing into and out of the paper. If the input impedance is plotted on a Smith chart over a frequency range of several periods, it will be found that the locus forms an approximate circle with the center lying on the zero reactance line. The characteristic impedance of the log-periodic structure is defined as the geometric mean of the maximum and minimum real values on the locus. The VSWR referred to this characteristic impedance is then simply equal to the ratio of the maximum impedance to the characteristic impedance.

Practical Structures. There is an infinite variety of log-periodic structures. A few of the successful and most practical structures[2,6,7,8] are illustrated in Fig. 18-10. Figure 18-10a and b shows wire versions of log-periodic structures with trapezoidal and triangular teeth, respectively. Figure 18-10c and d shows sheet structures with circular and triangular teeth. For all the structures shown, the angle α defines the

extremities of the teeth and the angle β defines the central supporting structure. All the various structures illustrated have similar radiation pattern and impedance characteristics. The radiation is due mostly to currents flowing in the teeth, and hence the polarization is transverse to the center line of the half structure.

By orienting the two half structures at an angle ψ with respect to each other, as shown in the nonplanar arrangement of Fig. 18-10a, a unidirectional beam pointing

(a)
WIRE TRAPEZOIDAL TOOTH

(b)
WIRE TRIANGULAR TOOTH

(c)
SHEET CIRCULAR TOOTH

(d)
SHEET TRIANGULAR TOOTH
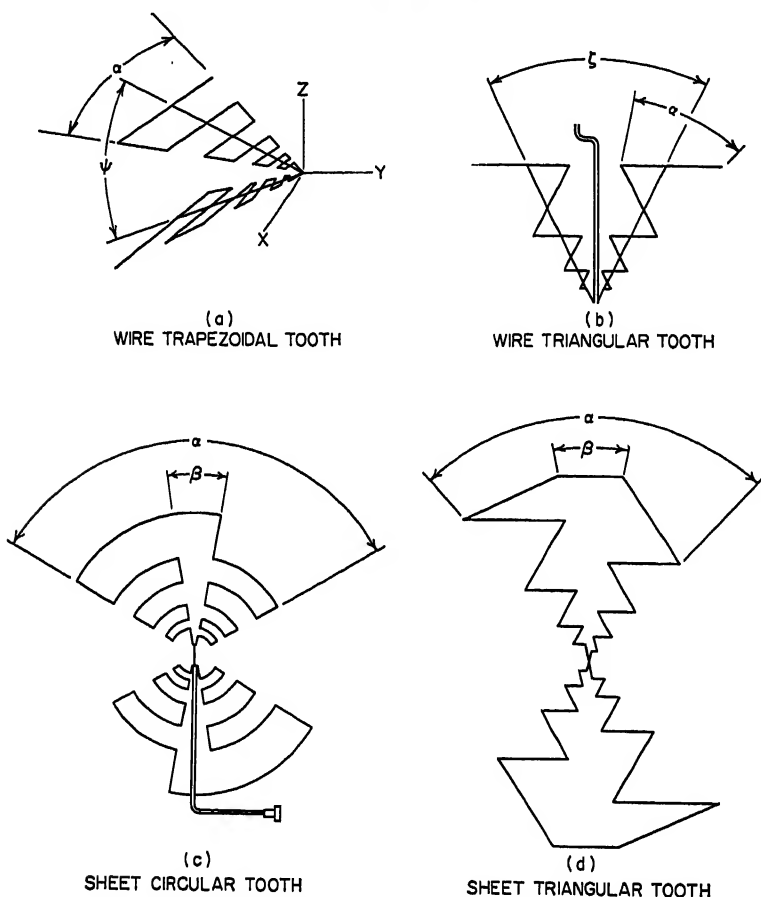
FIG. 18-10. Several types of log-periodic antennas.

along the positive Y axis is formed.[6] A unidirectional beam may also be formed with the coplanar arrangement[8] shown in Fig. 18-10b where the center lines of the two half structures are separated by an angle ζ. For this case the beam would point down.

Theoretically, the thickness of the sheets and the diameter of the wires should increase linearly with distance from the vertex of the half structures. Practically, this is not necessary for bandwidths less than 5:1. The greater the bandwidth, the more tapering is required. Bandwidths of 20:1 are easily achieved, and bandwidths of 100:1 are feasible if the theoretical design is closely approximated.

The two half structures form a balanced antenna. It may be fed with a balanced two-wire line with wires attached to the vertices of the half structures and placed to minimize distortion of the radiation pattern. For unidirectional structures the trans-

mission line is usually brought in along the line bisecting the center lines of the two half structures as shown in Fig. 18-10b. The antennas may also be fed with a coaxial line which is brought in along the center line of and bonded to one half structure. A dummy cable is usually added to the other half structure to keep the antenna balanced. This type of feed forms in effect a frequency-independent balun.

A recent[9] and rather simple type of log-periodic antenna is illustrated in Fig. 18-11. It consists of an array of dipoles with lengths and spacings arranged in a log-periodic manner. The dipoles are excited by a uniform two-wire line with the line transposed between adjacent dipoles. The antenna may be fed with a balanced line connected to the feed point or a coaxial line entering from the right and passing through and inside
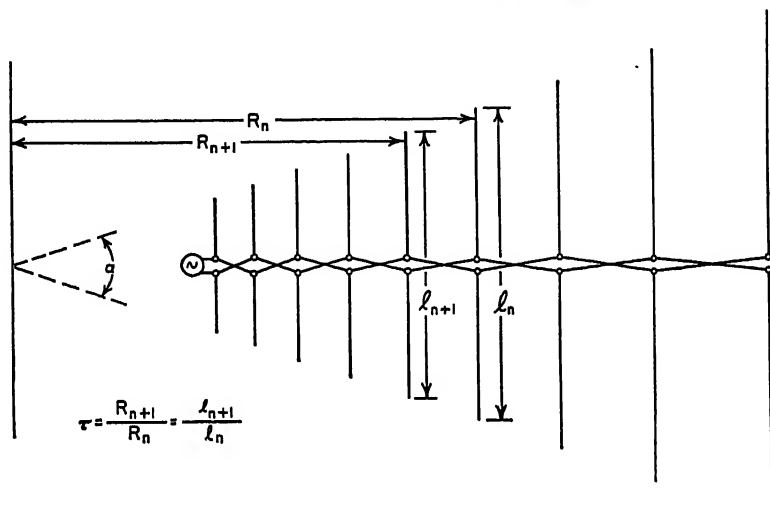
Fig. 18-11. A log-periodic dipole array.

one of the balanced lines to the feed point. It may be noticed that this antenna may be derived from that of Fig. 18-9 by letting the tooth width and the angle β approach zero and then folding the two half structures about the horizontal axis so that the angle ψ approaches zero.

All the various types of half structures described above are planar in form. The log-periodic principles can easily be generalized to include nonplanar half structures or three-dimensional structures. An example of the former is a wire trapezoidal tooth structure with the transverse wires curved so as to lie on the surface of a cone and the vertex coinciding with the vertex of the half structure. A solid biconical antenna with transverse troughs cut in the cones in a log-periodic manner is an example of a three-dimensional structure. Since these more complex structures have not proved too feasible as yet, they do not warrant further discussion.

It should be pointed out that many types of log-periodic structures are not broad-band because of either extreme variation over a period or severe end effect which destroys the periodicity of the electrical characteristics. Only the successful structures are described herein. Unfortunately, it is not possible to determine a priori the frequency-independent types of log-periodic antennas.

Since log-periodic antennas are too complex to analyze by present-day theoretical methods, they must be investigated by logical experimental methods. However, their repetitive nature greatly simplifies the initial experimental investigation because the characteristics need only be measured over one or two periods of frequency. The

operation over other periods may be readily predicted. Although a large amount of experimental data has been obtained, much remains to be done.

Self-complementary Structures. A means for obtaining an antenna with a constant input impedance is to take a self-complementary structure, i.e., a planar structure, in which the metal area is congruent to the open area. Booker[10] has shown, using an extension of Babinet's principle, that the product of the impedances of two complementary structures equals the square of $60\pi = 189$ ohms. Therefore a self-complementary structure has an impedance of 60π ohms, independently of frequency. This does not ensure constancy of the radiation pattern, but log-periodic structures, for

(a)   (b)
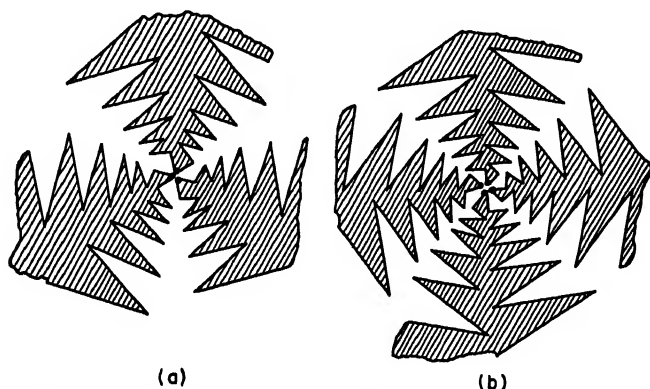
Fig. 18-12. Self-complementary structures with three- and fourfold symmetry. For (a) a rotation of $2\pi/3$ brings the structure onto itself while a rotation of $\pi/3$ brings it onto the complementary structure. For (b) rotation of $\pi/2$ and $\pi/4$, respectively, produces these results.

instance, that are also self-complementary will have a constant input impedance even over the period f to τf.

Self-complementarity implies an infinite structure. However, in cases, where the end effects can be neglected, a finite portion of the ideal structure behaves almost as if it were infinite over a frequency range that may be increased at will by extending the structure.

Booker's relation applies only to two-terminal structures such as a narrow strip and the complementary slot fed at the center point. The relation has been extended[11] to the impedance matrices Z_1 and Z_2 of two complementary structures, as follows. Introducing the matrix

$$\Delta = \begin{vmatrix} 1 & -1 & 0 & 0 & \cdots & 0 \\ 0 & 1 & -1 & 0 & \cdots & 0 \\ 0 & 0 & 1 & -1 & \cdots & 0 \\ \cdot & \cdot & \cdot & \cdot & & \cdot \\ \cdot & \cdot & \cdot & \cdot & & \cdot \\ \cdot & \cdot & \cdot & \cdot & & \cdot \\ -1 & 0 & 0 & 0 & \cdots & 1 \end{vmatrix} \qquad (18\text{-}13)$$

of order n and its transpose Δ', the relation is

$$\Delta' Z_1 \, \Delta Z_2 = \eta^2/4 \qquad (18\text{-}14)$$

where η is the intrinsic impedance of the surrounding medium ($\eta \simeq 120\pi$ in air).

When an n-terminal antenna is self-complementary and has also n-fold symmetry (Fig. 18-12), it is possible, by using this relation, to compute its impedance matrix.

Introducing $\epsilon = \exp\,(2\pi j/n)$, the eigenvectors of the matrix Z are

$$I_m = [1,\ \epsilon^m,\ \epsilon^{2m},\ \ldots\ ,\ \epsilon^{(n-1)m}] \qquad (18\text{-}15)$$

and the corresponding eigenvalues are

$$Z_m = \frac{\eta/4}{\sin\left(\pi\dfrac{m}{n}\right)} \qquad (18\text{-}16)$$

From this, the coefficients of the matrix Z for any value of n may be computed, and by straightforward circuit analysis, the impedances obtained by connecting the terminals in groups may also be deduced. A wide range of frequency-independent impedances may thus be realized.
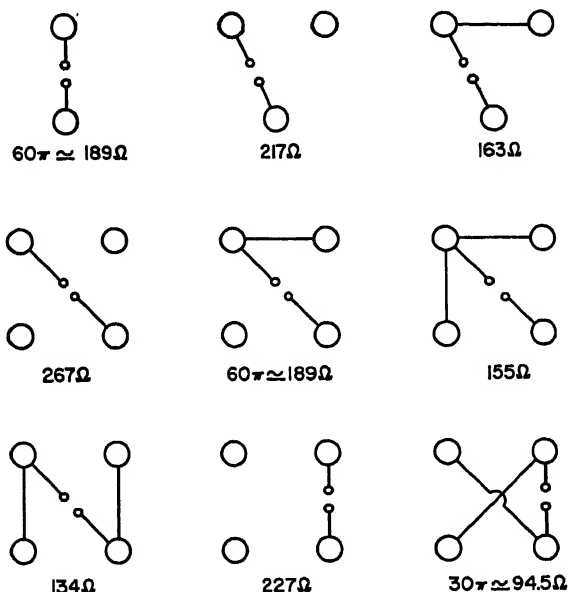
Fig. 18-13. Constant impedances obtainable with self-complementary symmetrical structures having two, three, and four terminals. The terminals of the structures are represented by the circles. After connecting them as shown in each figure, the impedance between the two dots has the value indicated under it.

Figure 18-13 gives impedances computed by this method for the symmetrical self-complementary structures with two, three, and four terminals.

Element Characteristics. Radiation properties of log-periodic structures may be better understood when it is realized that each of the half structures produces a unidirectional beam by itself. As mentioned earlier, the absence of end effect implies a unidirectional pattern. Although it is necessary to feed two half structures against each other or one against the ground in order to obtain wideband operation, it has been demonstrated[8] by special measurement techniques that the half structure does produce a unidirectional beam pointing in the direction of its center line. Figure 18-14 demonstrates the variation of the E- and H-plane beamwidths of a single half structure with wire trapezoidal teeth as a function of the design parameter α. The E plane is defined as the plane which includes the half structure, and the H plane is the normal plane, which includes the center line of the half structure.

For a given α angle, there is a minimum value of the design ratio τ which can be used. For values of τ smaller than this minimum, the pattern breaks up considerably, and for larger values the beamwidths will decrease. The approximate minimum value of τ which can be used is plotted in Fig. 18-14 (solid curve) as a function of the parameter α. The E- and H-plane beamwidths for this minimum value of τ are also shown as solid lines. The dashed curves for the E- and H-plane beamwidths correspond to the dashed curve for τ, which is somewhat larger than the minimum value. It is noticed that the E-plane and especially the H-plane beamwidths decrease as α is decreased and
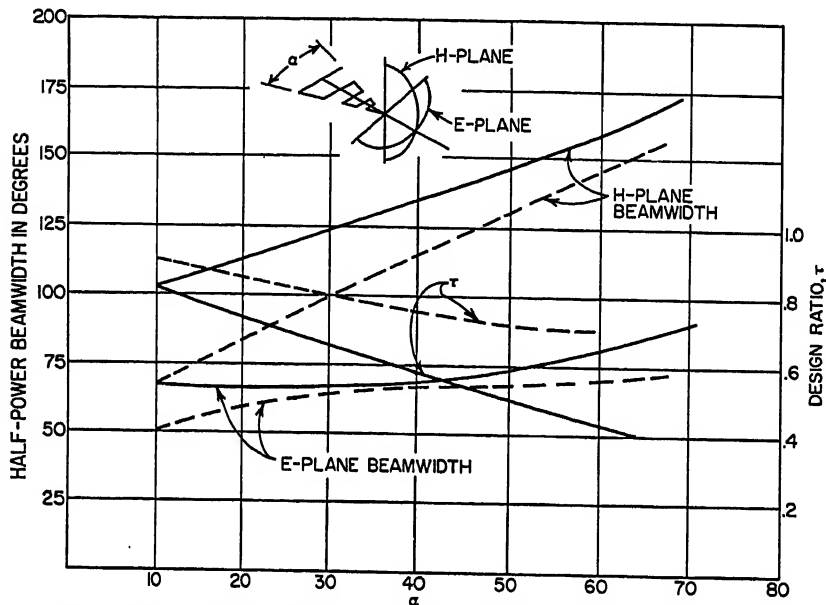
FIG. 18-14. Pattern characteristics of wire trapezoidal tooth element for: —·—·— Approximate minimum value of τ. – – – A larger value of τ.

τ is increased. For a given lower-frequency limit, which implies that the last transverse-element length remains fixed, then decreasing α and increasing τ means that the length of the structure and the number of transverse elements, respectively, is increased. The pattern behavior for the other types of half structures is very similar to that shown in Fig. 18-14.

An insight into the unidirectional behavior of log-periodic antennas may be gained from the dipole structure of Fig. 18-11. First, consider two parallel dipoles placed side by side with a spacing l. If the current in the dipole on the right leads the current in the dipole on the left by $\pi - \beta l$ (where $\beta = 2\pi/\lambda$), then the array will produce a beam to the left and a null to the right. Now, assuming for the array of Fig. 18-11 no mutual impedance between dipoles and only an incident transmission-line wave traveling to the right, it is seen that the voltage applied to a dipole leads the voltage applied to the first dipole to the left by $\pi - \beta l$. This suggests then that the array should produce a unidirectional pattern to the left. The same argument applies to the other types of half structures wherein the phase reversal π is accomplished by the fact that adjacent teeth point in opposite directions from the central section which distributes current to the teeth. This phase reversal appears to be a basic requirement for frequency-independent operation of log-periodic antennas.

The pattern characteristics for the dipole structure of Fig. 18-11 with design parameters α_0 and τ_0 are nearly the same as those for a wire trapezoidal tooth structure (Fig. 18-14) with parameters α_0 and τ_0.[2]

The phase center of a log-periodic half structure does not lie at the vertex; rather it lies some distance d behind the vertex. Figure 18-15 shows the distance of the phase center from the vertices as a function of α for wire trapezoidal tooth structures. For a fixed structure the distance as measured in wavelengths is essentially independent of frequency. For values of α less than 60° and for values of τ above the minimum value of τ given in Fig. 18-14, the position of the phase center is essentially independent of τ. Measurements[12] indicate that d depends upon τ in a complex manner for α greater than

FIG. 18-15. Distance from vertex to phase center as a function of α.

60°. The phase center lies on the center line of the half structure at a point near where a half-wave transverse element exists.

18.4. ARRAYS OF LOG-PERIODIC ELEMENTS

The pattern of an array of periodic elements may be considered as the simple superposition of the patterns of the individual elements if it is assumed that the presence of other elements does not affect the pattern of an element. In order to obtain frequency-independent operation with an array, it is necessary that the locations of the elements with respect to each other be defined by angles rather than distances. This implies that all the elements have their vertices or feed points at a common point.

Log-periodic arrays are unique in two respects. First, although the element patterns are identical in shape (assuming design parameters are identical), they point in different directions. Second, since the radiation from an element may be considered to emanate from the phase center, the array sources lie on the surface of a sphere for a two-dimensional array and on a circle for a one-dimensional array. Thus the array theory is more complex and much less amenable to synthesis procedures than that for linear arrays of isotropic elements.

Two-element-array Pattern Characteristics. The log-periodic antennas consisting of two half structures discussed in Sec. 18.3 may be considered as an array of two elements. The pattern can easily be calculated once the element pattern and distance from the vertex to the phase center are known. A schematic representation of a two-element array is given in Fig. 18-16. The radial lines separated by the angle ψ represent the two elements, and d is the distance to the phase center. The direction to a distant field point is given by φ. Typical element patterns are shown in the schematic. The pattern of the array is given by

FIG. 18-16. Schematic representation of two-element array.

$$E = \cos^n\left(\frac{\varphi + \psi}{2}\right) \exp\left(\beta d \sin\frac{\psi}{2}\sin\varphi\right) + \cos^n\left(\frac{\varphi - \psi}{2}\right) \exp\left(-\beta d \sin\frac{\psi}{2}\sin\varphi\right)$$

$$(18\text{-}17)$$

where $\cos^n(\varphi/2)$ is an assumed functional form for the element pattern. Given the half-power beamwidth of an element (which may be measured or read from curves), the approximate value of the exponent n may be determined from Fig. 18-17. For an H-plane array (like Fig. 18-10a) the H-plane beamwidth is used and for an E-plane array (like Fig. 18-10b) the E-plane beamwidth is used to determine n. The beamwidths may be obtained from Fig. 18-14. Although this procedure neglects the effect of the presence of one half structure on the pattern of the other, it will give fairly accurate results, especially for values of α smaller than 60°.

Figure 18-18 shows the variation of the H-plane beamwidth, gain, and front-to-back ratio with the angle ψ for a wire-trapezoidal-tooth H-plane array with $\alpha = 60°$ and $\tau = 0.6$. The E-plane beam-width is nearly independent of the angle ψ, and its value is approximately 63°. Of course, for $\psi = 180°$, a bidirectional beam is produced. Notice that if both high gain and front-to-back ratio are desired, a compromise value of ψ must be chosen. As to be expected, the H-plane beamwidth decreases rapidly with increasing ψ since

FIG. 18-17. Relation between element beamwidth and n.
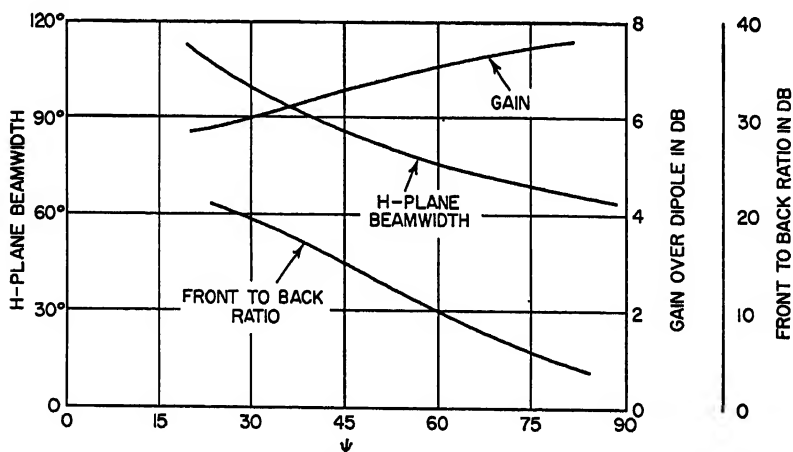
FIG. 18-18. Effect of angle ψ on pattern characteristics for antenna with $\alpha = 60°$ and $\tau = 0.6$.

this effectively increases the H-plane aperture of the antenna. E-plane patterns for a structure with $\alpha = 60°$, $\tau = 0.6$, and $\psi = 35°$ are given in Fig. 18-19 over a bandwidth of 10:1. Except for $f = 60$ Mc, which is very close to the lower cutoff frequency, the beamwidth does not vary more than ±7 per cent. The H-plane patterns are of a similar shape but have wider beamwidths.

A split beam with a null in the direction in which the structure points can be obtained by rotating one of the half structures 180° about its center line.   This effects a reversal of the phase of the half structure and may be accounted for in Eq. (18-17) by changing the sign of the second term.
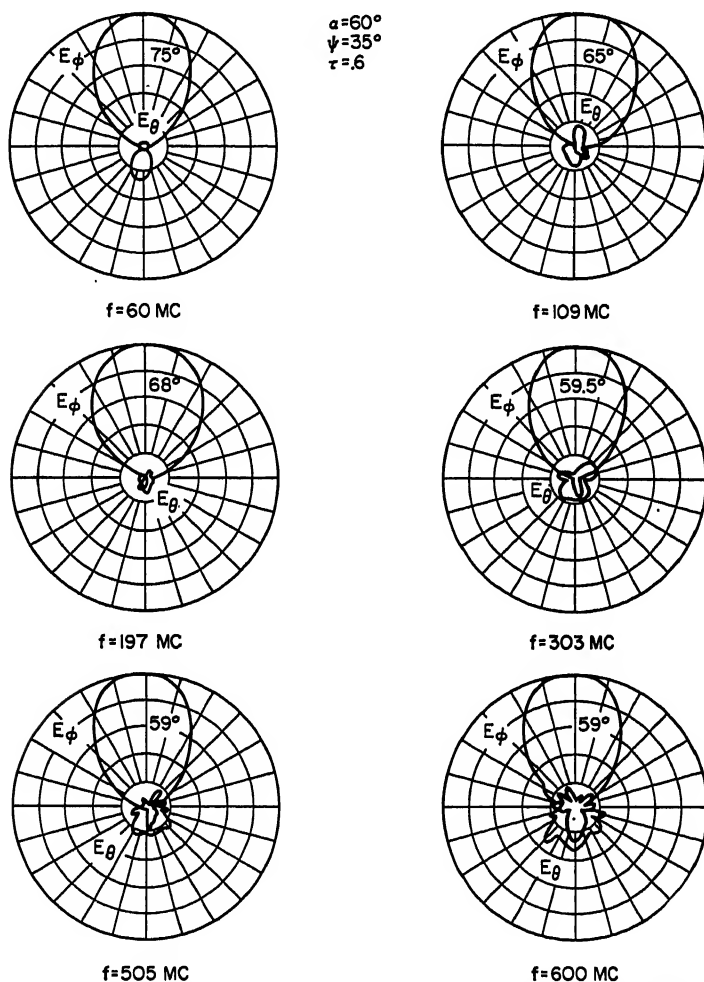
FIG. 18-19. E-plane patterns for a wire trapezoidal tooth structure with $\alpha = 60°$, $\tau = 0.6$, and $\psi = 35°$.

Two-element-array Impedance Characteristics.   Unfortunately, insufficient information on the variation of the input impedance of log-periodic structures as a function of the defining parameters has been obtained to allow the design of antennas without resorting to considerable experimental investigation.   Figure 18-20 gives some information on the variation of the characteristic impedance versus ψ for various types of H-plane arrays.   It will be noticed that in all cases the characteristic impedance decreases as the angle ψ is decreased.   Also, it is apparent that the characteristic impedance decreases as the angle α is increased.   It appears, in general, that a wire

structure has a characteristic impedance somewhat higher than that for a sheet structure, with the same values of α and τ.   There does not appear to be a definite trend in variation of impedance with the τ ratio.   For example, increasing τ for the wire structure increases the characteristic impedance, whereas it decreases the characteristic impedance for the circular tooth sheet structure.
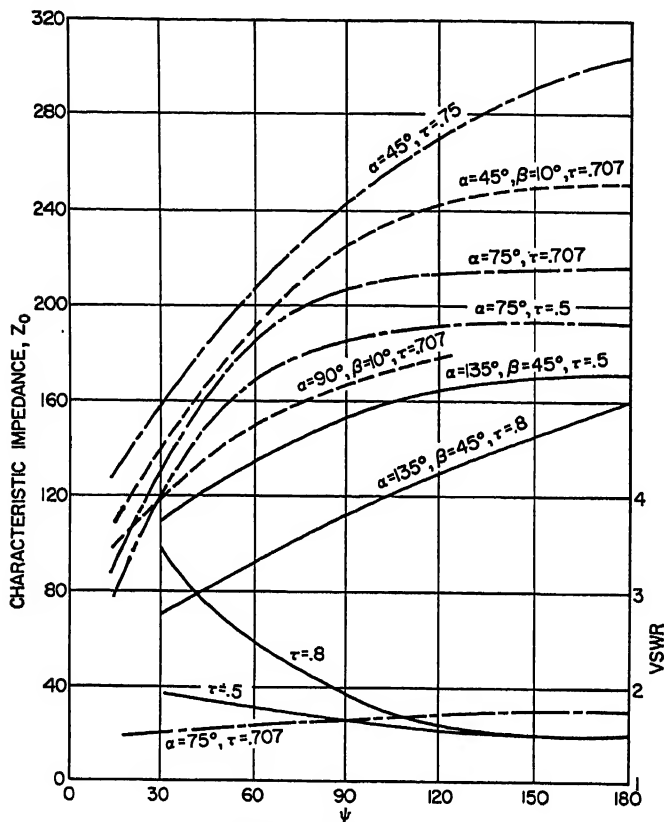
FIG. 18-20. Variation of Z_0 and VSWR with ψ for sheet structures with: Circular teeth (— — —).   Trapezoidal teeth (– – – –).   Wire structure with trapezoidal teeth (· · ·).

A few curves of the VSWR referred to the characteristic impedance are also given on the plot.   It will be noticed that the VSWR increases, especially for the circular tooth sheet structure, with $\tau = 0.8$, as ψ is decreased.   For all the other structures, the VSWR remains less than 2:1 over the range of ψ values considered.   In some, but not all, cases it has been found that the VSWR rises rapidly as ψ approaches zero for the wire structures.

The impedance variation for E-plane arrays is similar to that for H-plane arrays except that the angular spacing must be greater than $\frac{3}{2}\alpha$ in order to avoid excessive VSWR's.

For the ψ values of most interest, that is, from 15 to about 90°, it is noticed that the characteristic impedance ranges from approximately 70 to 240 ohms.   Thus it is necessary to use a wideband technique to match this impedance to a coaxial or a

balanced line.   The tapered-line transformers described in Refs. 13 and 14 are ideally suited for matching this impedance over theoretically unlimited bandwidths.   These transformers usually require a length on the order of 0.4 to 0.5 wavelength at their lowest frequency of operation.

The impedance behavior of the dipole structure of Fig. 18-11 is illustrated in Fig. 18-21.   These results were obtained with a balanced-line characteristic impedance of 105 ohms.
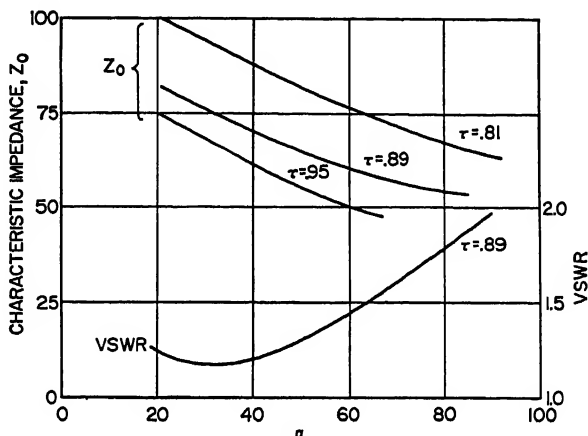
FIG. 18-21. Variation of Z_0 and VSWR with α for log-periodic dipole array.

In designing log-periodic antennas for bandwidths of 10:1 or greater, it is usually found that the characteristic impedance decreases gradually as the frequency is increased over this range.   This variation is due to improper construction of the antenna; that is, it is usually not practical to taper the diameter of wires or thickness of the sheets according to theory because of mechanical limitations.   However, this variation is not serious since many types of log-periodic antennas have been built with a tapered-line input transformer such that the complete system covers a 10:1 frequency range with a VSWR less than 2:1.

Several wire-trapezoidal-tooth unidirectional structures were built with $\alpha = 67\frac{1}{2}°$, $\tau = 0.6$, and $\psi = 37°$, but with the wire sizes varying over a 10:1 range.   It was found that the wire size had a negligible effect on the patterns but that the characteristic impedance decreased about 30 per cent as the wire sizes increased by a factor of 10:1.

Multielement Arrays.   A schematic representation of an array of N elements as viewed from the top is illustrated in Fig. 18-22.   The radial lines defined by δ_n represent the elements of the array.   The α and τ parameters for the N elements are made identical so as to assure identical element patterns.   The xy-plane radiation pattern of the array is given by
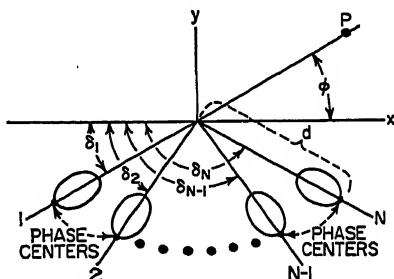
FIG. 18-22. Geometry for array of end-fire elements.

$$E(\phi) = \sum_{n=1}^{N} A_n f(\phi - \delta_n) e^{-j[\beta d \cos(\phi - \delta_n) - \gamma_n]} \qquad (18\text{-}18)$$

where $f(\phi)$ is the element pattern and $\beta d \cos(\phi - \delta_n)$ represents the phase advance of the phase center relative to the origin. The function f may take the same form as that used previously, that is, $f(\phi) = \cos^n(\phi/2)$. The value of the feed-point current for the nth element is given by A_n. In nearly all practical cases, $A_n = 1$ for all n. This is accomplished in practice by connecting half of the elements together and feeding them against the other half. The parameter γ_n is the relative phase of the field radiated from the nth element. It may be controlled by expanding or contracting the element according to the phase-rotation principle to be described later.

The assumptions made in Eq. (18-18) are that the element patterns and input impedances are identical. Although mutual effects can make these assumptions invalid, good correlation between theory and experiment has been obtained. Cut-and-try synthesis procedures may be used with Eq. (18-18).

A basic characteristic of logarithmically periodic antennas is the phase-rotation phenomenon. It has been verified experimentally that if the phase of the electric field received at a distant dipole (Fig. 18-23) is measured relative to the phase of the current at the feed point of the structure, the phase of the received signal will be delayed 360° as the structure is expanded through a period. In Fig. 18-23 the distance to an arbitrary transverse element is given by KR_n. The expansion of the structure through a period is accomplished by letting K increase from 1 to $1/\tau$. During this expansion all lengths involved in the structure are multiplied by K. In Fig. 18-23 the phase delay in radians is plotted vs. the logarithm of K. The ideal phase variation is given by the solid straight line. Measurements have indicated that the actual phase variation is somewhat like the dashed line. The approximate measurements made to date indicate that the deviation of the dashed line from the straight line is not more than 15°. The relation between γ_n and K_n is given by

FIG. 18-23. Illustration of phase-rotation phenomena for log-periodic antennas.

$$K_n = \exp\left[\frac{\gamma_n}{2\pi}\ln\tau\right] \qquad (18\text{-}19)$$

Fortunately, the phase center and the element patterns are independent of the expansion or contraction of a logarithmically periodic element.

The information given above in Figs. 18-14, 18-15, and 18-23 is sufficient for predicting the pattern of an array of similar end-fire elements. The method can be extended to cover a combination of E- and H-plane arrays. The phase-rotation phenomenon is extremely important since it allows a frequency-independent method of phasing the elements of the array.

Experimental and theoretical patterns for a six-element phased-H-plane array of wire trapezoidal tooth elements are given in Fig. 18-24. The values of the design parameters for this array were $\alpha = 9.5°$, $\tau = 0.88$, $N = 6$, $\delta_n - \delta_{n-1} \approx 17°$ for all n, and $d/\lambda = 1.95$. The elements were phased to produce a beam-cophasal condition. The gain of the array was 14 db over a dipole.

Although gains up to 18 db are feasible by using a combined E- and H-plane array, the size and complexity of the antenna become great since it is necessary to use very small α angles and τ values near unity.

Design Procedure. In designing an array, a judicious choice of the parameters N, α, τ, and δ_n should be made so as to achieve a minimum amount of space and material and number of elements. Although the design method is cut and try, a rough approximation to an optimum design may be obtained by the following procedure. The procedure is the same for arrays in the E plane and H plane. Given a desired beamwidth, the equivalent broadside aperture D may be calculated from

$$\frac{D}{\lambda} = \frac{40}{\bar{\varphi}} \qquad (18\text{-}20)$$

where $\bar{\varphi}$ is the half-power beamwidth in degrees. The number 40 instead of 50 (which
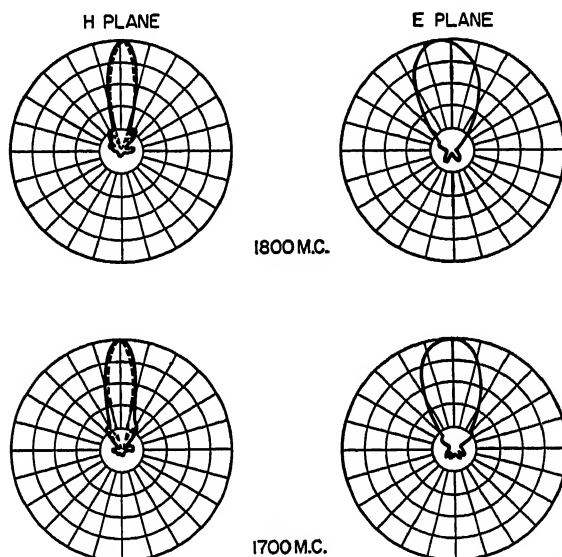
FIG. 18-24. Predicted (– – – –) and measured (———) patterns of six-element phased array.

is for a uniform aperture) is used because the end-fire directivity of the elements tends to enhance the effective aperture. The distance between the phase centers of the two outer elements must be approximately D. Results indicate that a reasonable maximum spacing between the phase centers of adjacent elements is 0.7 wavelength. Thus the number of elements may be determined approximately from

$$N - 1 \approx \frac{D}{0.7\lambda} = \frac{57.1}{\bar{\varphi}} \qquad (18\text{-}21)$$

For a one–dimensional array N must be even in order to present a balanced load to the feed line. The maximum value of the angle $\delta_N - \delta_1$, which defines the sector occupied by the array, depends on the beamwidth of the element pattern. If $\delta_N - \delta_1$ is greater than the element beamwidth, then elements 1 and N will contribute little to the formation of the main beam. An examination of Fig. 18-14 indicates that reasonable maximum values of $\delta_N - \delta_1$ are 60° for an E-plane array and 70 to 130° for an H-plane array. If low first side lobes are desired, values somewhat smaller than the maximum should be chosen.

The distance d to the phase center is equal to

$$\frac{d}{\lambda} = \frac{D}{2\lambda \sin\left(\frac{\delta_N - \delta_1}{2}\right)} = \frac{20}{\bar{\varphi} \sin\left(\frac{\delta_N - \delta_1}{2}\right)} \tag{18-22}$$

The angle α is then determined from Fig. 18-15 since d/λ is known. The minimum value of τ is then determined from Fig. 18-14. It is usually desirable to use the minimum value of τ since the element beamwidth has little influence on the array pattern for $N \geq 4$.

Since A_n and $(\delta_n - \delta_{n-1})$ are usually made independent of n, the remaining parameter to determine is K_n. If high gain and a beam direction of ϕ_0 are desired, then K_n is chosen so that $[\beta d \cos(\phi_0 - \delta_n) - \gamma_n]$ has the same value for all n. Equation (18-19) gives the relation between K_n and γ_n.

For shaped beams γ_n, and hence K_n, would be determined on a cut-and-try basis.

After the approximate synthesis given above, the array pattern may be calculated by the method of the preceding section.

The above procedure determines the parameters α, τ, δ_n, K_n, and N. It remains to determine the type and size of the elements. For frequencies above about 500 Mc, a sheet structure should be used, and for ranges below that, wire structures should be used. If it is desired to cover a frequency range which overlaps 500 Mc, it may be necessary, because of mechanical considerations, to use wire construction for the back of the structure and a sheet or printed-circuit construction for the front of the structure. A gradual transition between the two types of structures may be made with only a small effect upon the electrical characteristics.

If minimum antenna size is important, rectangular or trapezoidal teeth should be used. If not, triangular teeth may be used or other similar versions. Curved teeth may also be used if the α angle is not too large.

The size of the element is determined from the lowest frequency required. Approximately, the largest tooth for a sheet structure should be about a quarter wavelength long at the lowest frequency and the longest transverse wire for the wire structure should be approximately a half wavelength long. The highest frequency determines the length of the shortest teeth and wires in a similar manner. For high-power or microwave applications, the size of the input cable or transmission line may limit the upper frequency.

The preceding theory and curves may be used to predict the performance of the initial design. If it is close, then the antenna model should be constructed and a pattern and impedance investigation should be performed over a period so as to determine the exact parameters. Once this is done, then the antenna should be checked over the complete frequency range, including measurement of the input impedance. It is then possible to design the tapered-line transformer for feeding the antenna.

For applications which demand minimum antenna size, it is possible to use end loading on the tips of a few of the largest teeth. The lower-frequency cutoff may be lowered 15 or 20 per cent by this means.

18.5. SPECIAL APPLICATIONS

Arrays over Ground. Although the above antennas have radiation patterns which are essentially independent of frequency, many applications demand that the antenna be placed near ground. If one of these antennas is placed with its feed point above ground, then it is apparent that the resultant pattern will be frequency-dependent since its electrical height above ground changes with frequency. However, the above array theory suggests that if log-periodic elements are inclined with respect to ground and

with their feed points at ground level, then the resultant radiation pattern will be frequency-independent. The elements can be placed so that with their images they form either H-plane or E-plane arrays or a combined E- and H-plane array. For an equivalent H-plane array there will, of course, be a null in the resultant pattern on the horizon. The array theory above may be used to calculate the resultant pattern by adjusting the phase of the image elements. For an H-plane array, the phase of the image element will be 180° different from that of the element above ground, whereas for an E-plane array, the phase of the image element would be the same as that of the element.

A very important application for this type of an antenna is for point-to-point communication circuits.[15] Figure 18-25 shows a two-element array above ground

$$\tau = \frac{R_{N+1}}{R_N}$$
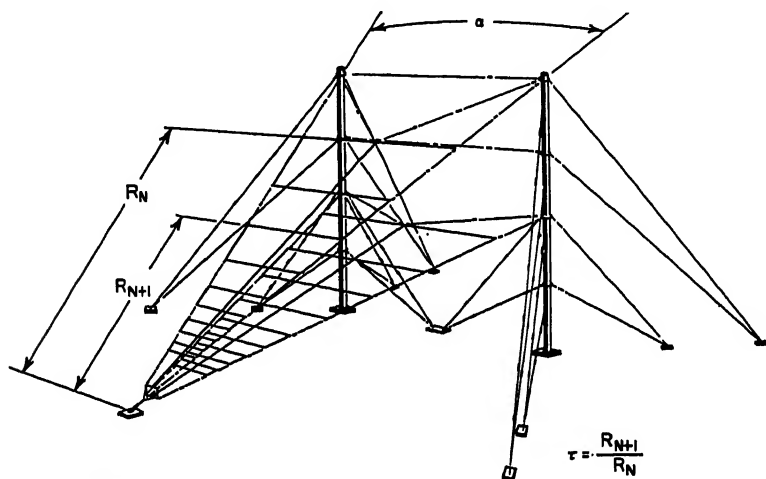
Fig. 18-25. Log-periodic H-F antenna with frequency-independent elevation pattern.

oriented so that they and their image elements form an H-plane array. Theoretically, the feed point of the antenna should be at ground level, but in practice the feed point is placed a small height above ground to protect personnel from high r-f voltages. Except for very short distances, high-frequency point-to-point communication is accomplished by reflection of the radio waves from the ionosphere. The vertical angle of arrival or departure (from the ground) depends upon the distance between the points and the height of the reflecting layer. Although its value ranges from 70° down to a few degrees for various circuits, its value for a particular circuit is relatively constant since the height of the reflecting layer does not change by a great amount. However, because of changing ionospheric conditions during the sunspot cycle and from night to day, it is necessary to change the operating frequency over bandwidths of 4 or 6:1. Thus it is most desirable to have an antenna for which the vertical angle of the main lobe is independent of frequency. Present-day antennas, such as the dipole, rhombic, billboard, discone, etc., do not satisfy this requirement.

The direction of the main lobe for the structure of Fig. 18-25 may be controlled by the α angle of the individual element and the angles of the elements with respect to ground. The size of the structure is determined by the lower-frequency limit. Figure 18-26 shows the vertical-plane pattern for a structure with $\alpha = 14°$ and $\tau = 0.75$. The two half structures are oriented at angles of 32 and 48° with respect to ground. The dimensions of the antenna at the lowest frequency are given in wavelengths in the figure. The lower half structure is scaled so that its radiation leads that of the upper

by 130°. This particular phasing increases the gain 5 db over that obtained with no difference in phasing. Although the gain for this type of antenna is only moderate (13.4 db over a dipole), maximum use of this gain is made over the complete frequency range. The gain for this structure can be increased 3 db by adding two additional elements to the side to form a combined E- and H-plane array.

$$a = 14°$$
$$\tau = .75$$
GAIN = 13.4 DB OVER DIPOLE
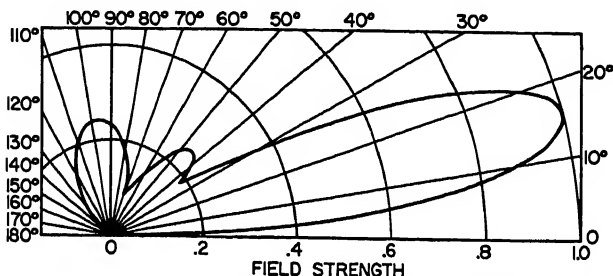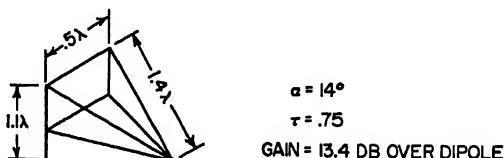
Fig. 18-26. Elevation pattern and design parameters for typical antenna of Fig. 18-25.

If vertical polarization is required rather than horizontal polarization (which is obtained for the structure above), then the two-element array can be rotated 90° about its center line so that the plane of each of the half structures would be normal to the ground plane.

Feeds for Reflectors and Lens. Many applications call for the use of high-gain antennas which will work over extremely wide frequency ranges. Although lens- or reflector-type antennas are ideally suited, their bandwidths have been limited in the past by that of the primary feed. Ideally, the radiation pattern and input impedance of the primary radiator should be independent of frequency; thus unidirectional log-periodic or equiangular antennas are well suited for this application. The required design information for log-periodic feeds is the primary pattern, phase-center and input-impedance.

Figure 18-27 shows the angle subtended by a circular-parabolic reflector as observed from the focal point as a function of the f/d ratio. Figure 18-28 shows the variation of the E-plane and H-plane 10-db beamwidths and the side-lobe level as a function of ψ for several different values of α for two-element sheet trapezoidal
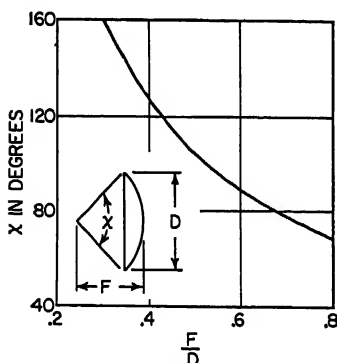
Fig. 18-27. Angle subtended by parabolic reflector as a function of F/D.

tooth structures. The largest side lobe nearly always occurs in the opposite direction of the beam. If a 10-db taper is desired, it is seen that a two-element structure can be designed so as to give fairly good illumination tapers for f/d ratios from about 0.35 to 0.6.

Another type of structure which is well suited for feeds is the triangular tooth sheet structure[16] illustrated in Fig. 18-10.   Figure 18-29 shows the variation of the 10-db beamwidths for a two-element H-plane array of triangular tooth sheet structures as a
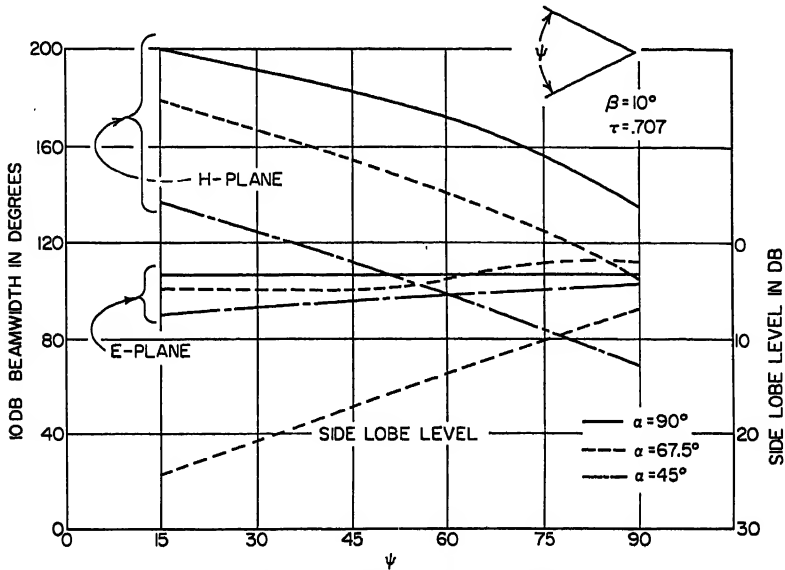
FIG. 18-28.   Pattern characteristics of sheet trapezoidal tooth structure.
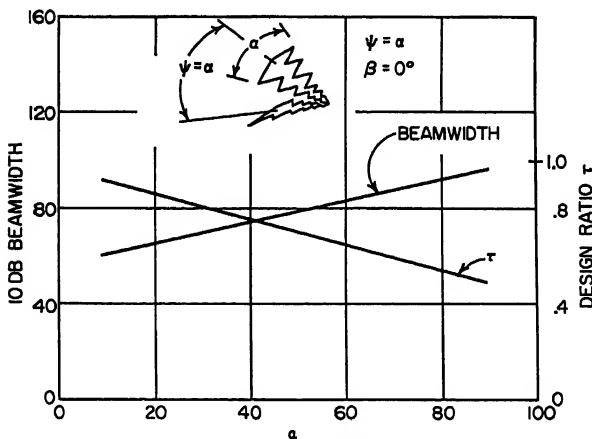
FIG. 18-29.   Pattern characteristics of sheet triangular tooth structure.

function of α and with $\psi = \alpha$.   The E-plane and H-plane beamwidths are approximately equal, so that one curve applies to both.   Assuming a 10-db taper, this type of feed would be suitable for f/d ratios ranging from 0.55 to 0.9.

In general, and especially for α angles greater than 45°, the E- and H-plane phase centers of a single element do not coincide.   Except for the special case of $\psi = 0$, the E- and H-plane phase centers for a two-element H-plane array will not coincide even if the element phase centers do.   The array phase centers will lie on a line bisecting the

center lines of the two half structures. Letting d and ℓ represent the distances from the vertex to the element and array phase centers, respectively, it is easy to show that ℓ/λ equals $d/\lambda \cos \psi/2$ for the E-plane phase center provided that the element phase centers coincide and that the mutual effects between the two half structures are negligible. The positive direction of ℓ is toward the back end of the array. If these assumptions are not valid, then the variation of the E-plane phase center with ψ is more complex.
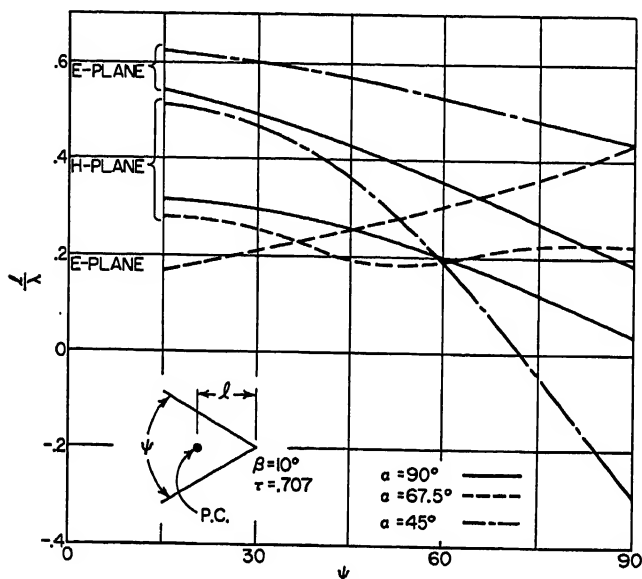
Fɪɢ. 18-30. Dependence of phase center on ψ for sheet trapezoidal tooth structure.

Assuming negligible mutual effects, a simple calculation[12] leads to the following formula for the array H-plane phase center:

$$\frac{\ell}{\lambda} = \frac{d}{\lambda} \left(\cos \frac{\psi}{2} - \frac{\pi}{\bar{\phi}} \sin \frac{\psi}{2} \tan \frac{\psi\pi}{4\bar{\phi}} \right) \qquad (18\text{-}23)$$

where $\bar{\phi}$ is the element H-plane half-power beamwidth. The reason for the movement of the phase center toward the vertex is that the two H-plane element patterns point in different directions.

Figure 18-30 shows the measured variation of E- and H-plane phase centers with ψ for three values of α for a two-element H-plane array with sheet trapezoidal tooth elements. The results for $\alpha = 45°$ and $90°$ follow the theory fairly close, but the behavior for $\alpha = 67.5°$ is peculiar.

The variation of the phase centers with α for a sheet trapezoidal tooth structure with $\psi = 45°$ is illustrated in Fig. 18-31. Again peculiar results are obtained, since it would be expected that the phase center would monotonically approach the vertex as α is increased.

Since the phase centers will move toward the vertex as the frequency is increased (ℓ/λ is independent of frequency), it is apparent that ℓ/λ should be as small as possible. From Eq. (18-7) it is seen that the H-plane phase center may be made arbitrarily close to the vertex by the proper choice of $\bar{\phi}$ and ψ. However, a $180°$ ψ angle is required to make the E-plane phase center lie at the vertex. This is undesirable because the feed

$\psi = 45°$
$\beta = 10°$
$\tau = .707$
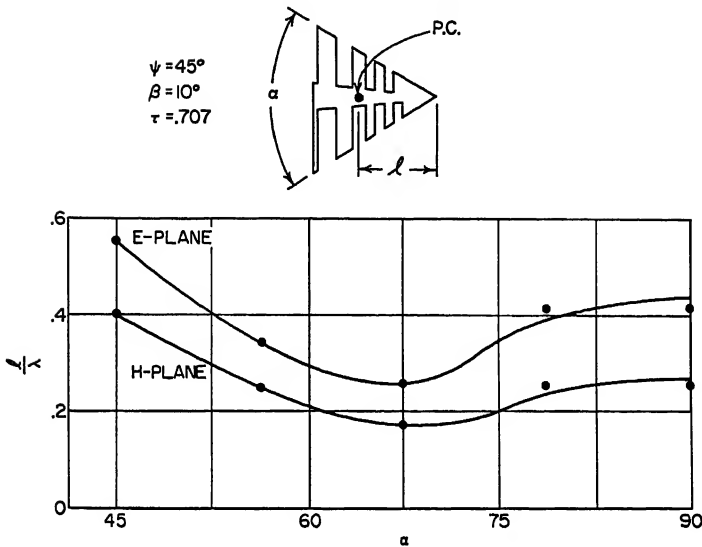
FIG. 18-31. Dependence of phase center on α for sheet trapezoidal tooth structure.
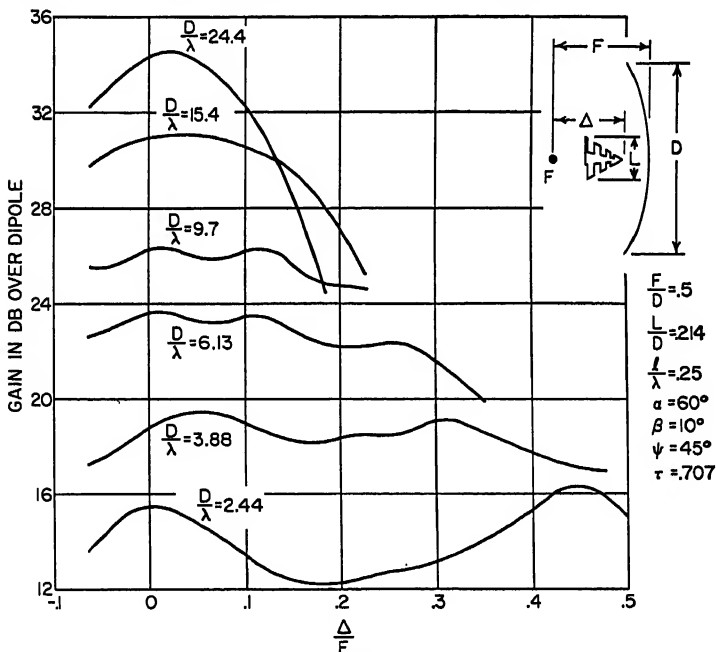
FIG. 18-32. Reflector gain as a function of feed placement over a 10:1 frequency range.

is then bidirectional and the H-plane phase center will lie in front of the feed. Thus it is necessary to choose a compromise value of the design parameters and allow the phase center to move with frequency.

The movement of the phase center with frequency makes it necessary to determine an optimum location of the feed for a given frequency range. This may be done by

performing the gain measurements reported in Fig. 18-32. It shows the variation of gain of a 4-ft dish at six frequencies over the frequency range of 600 to 6,000 Mc as a function of the displacement of the feed vertex from the focal point. It will be noticed that a relative displacement of 0.025 results in a maximum loss in gain less than $\frac{1}{2}$ db due to movement of the phase center with frequency. In general, the feed should be located so that the phase center of the feed at the highest frequency is slightly on the dish side of the focal point. For dishes considerably larger than 4 ft over the same frequency range, the loss in gain over the band would be somewhat greater. It is possible to
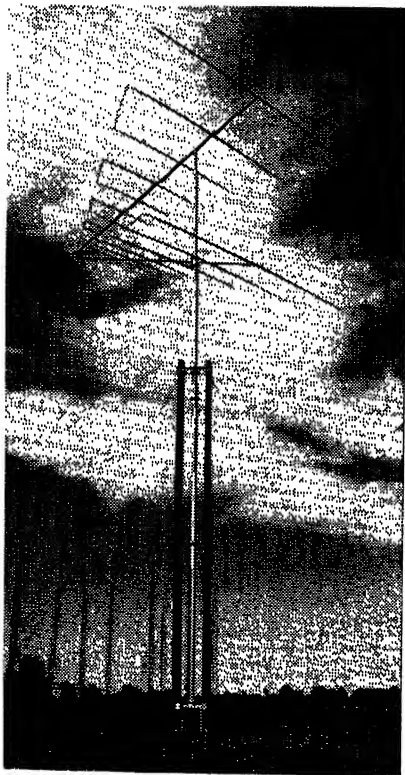
Fig. 18-33. Log-periodic H-F antenna for 11.1- to 60-Mc range (Collins Radio Co. Type 237A-2).
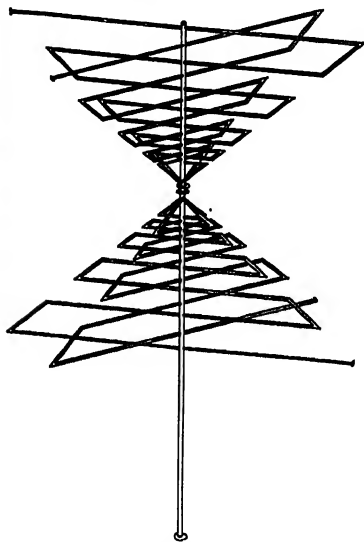
Fig. 18-34. Omnidirectional antenna with horizontal polarization.

design a feed for use with a dish with a VSWR less than 3 and, with extreme care, less than 2 over at least a 10:1 frequency range.[12]

H-F Communications Antenna. Figure 18-33 is a picture of a wire trapezoidal tooth structure with self-supporting elements for the frequency range of 11 to 60 Mc. The azimuthal beamwidth is about 60°, and the free-space vertical beamwidth is about 90°. The free-space gain is 8 db over an isotropic antenna, and the side lobes are more than 16 db down. The VSWR is less than 2:1. The power-handling capacity is 50 kw. The values of the design parameters for the structure are $\alpha = 60$, $\psi = 37$, and $\tau = 0.6$.

Omnidirectional Antenna. An omnidirectional horizontally polarized antenna is illustrated in Fig. 18-34. This consists of two planar log-periodic structures placed at right angles to each other, with one structure scaled by the factor $\tau^{1/4}$ so as to give an omnidirectional radiation pattern in the plane transverse to the axis of the antenna. This is accomplished since each planar structure produces approximately a figure-of-eight pattern and the scaling of one structure provides the 90° phase shift to give an

omnidirectional pattern similar to that obtained with a turnstile antenna. Experiments show that omnidirectional patterns within ±2 db are easily achieved over extreme bandwidths and that H-plane beamwidths of about 60° are easily obtained. Typical design parameters are $\alpha = 90°$ and $\tau = 0.707$ for a wire trapezoidal tooth structure.

Circularly Polarized Antenna. Figure 18-35 is a picture of a circularly polarized unidirectional log-periodic antenna. Two opposite half structures are fed against each
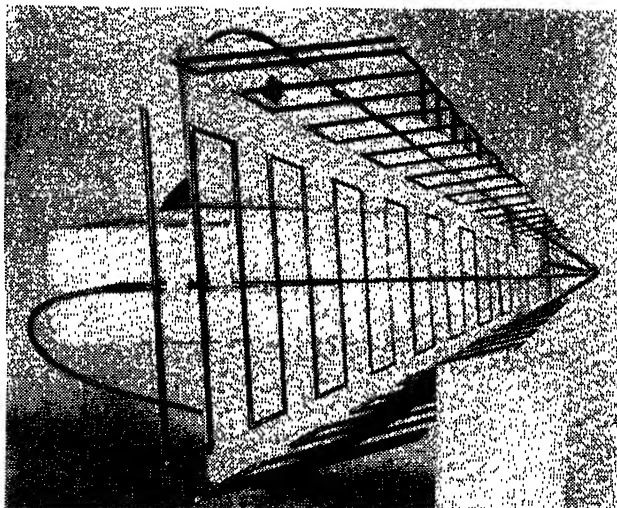
FIG. 18-35. Circularly polarized log-periodic antenna.

other to provide a linearly polarized unidirectional beam, and the other two structures are fed against each other to provide a linearly polarized unidirectional beam with orthogonal polarization. The 90° phasing between the two polarizations is obtained by scaling one pair of structures by the factor $\tau^{1/4}$. The sense of circular polarization can easily be changed by reversing the feed lines to one pair of structures. Axial ratios less than 2:1 can be obtained over extreme bandwidths, and the E- and H-plane beamwidths can be made approximately equal by proper adjustment of the design parameters α, ψ, and τ.

REFERENCES

1. V. H. Rumsey: "Frequency Independent Antennas," IRE National Convention Record, pt. I, pp. 114–118, 1957.
2. R. H. DuHamel and D. E. Isbell: "Broadband Logarithmically Periodic Antenna Structures," IRE National Convention Record, pt. I, pp. 119–128, 1957.
3. A. G. Kandoian: "Three New Antenna Types and Their Applications," *Proc. IRE*, vol. 34, pp. 70w–75w, February, 1946.
4. J. D. Dyson: "The Equiangular Spiral," *IRE Trans.*, vol. AP-7, no. 2, April, 1959.
5. J. D. Dyson: "The Unidirectional Equiangular Antenna," *IRE Trans.*, vol. AP-7, no. 4, pp. 329–334, October, 1959.
6. D. E. Isbell: "Nonplanar Logarithmically Periodic Antenna Structures," University of Illinois, Antenna Laboratory TR 30, Feb. 20, 1958, Contract AF 33(616)-3220.
7. R. H. DuHamel and F. R. Ore: "Logarithmically Periodic Antenna Designs," IRE National Convention Record, pt. I, pp. 139–151, 1958.
8. R. H. DuHamel and D. G. Berry: "Logarithmically Periodic Antenna Arrays," Wescon Convention Record, pt. I, pp. 161–174, 1958.
9. D. E. Isbell: "Log Periodic Dipole Arrays," *IRE Trans.*, vol. AP-8, no. 3, pp. 260–267, May, 1960.

10. H. G. Booker: "Slot Aerials and Their Relation to Complementary Wire Aerials (Babinet's Principle)," *J. IEE (London)*, pt. IIIA, pp. 620–627, 1946.
11. G. A. Deschamps: "Impedance Properties of Complementary Multiterminal Planar Structures," *Proc. Toronto Symposium on Electromagnetic Theory*, special supplement to *IRE Trans.*, vol. AP-7, p. S371, 1959.
12. R. H. DuHamel and F. R. Ore: "Log Periodic Feeds for Lens and Reflectors," IRE National Convention Record, pt. I, p. 128, 1959.
13. S. B. Cohn: "Optimum Design of Stepped Transmission-line Transformers," *IRE, Trans.*, vol. MTT-3, p. 16, April, 1955.
14. R. W. Klopfenstein: "A Transmission Line Taper of Improved Design," *Proc. IRE*, vol. 44, p. 31, January, 1956.
15. R. H. DuHamel and D. G. Berry: "A New Concept in High Frequency Antenna Design," IRE National Convention Record, pt. I, p. 42, 1959.
16. D. E. Isbell: "A Log-periodic Reflector Feed," *Proc. IRE*, vol. 47, p. 1152, June, 1959.

Chapter 19

LOW-FREQUENCY ANTENNAS*

C. A. MARTIN
and
P. S. CARTER

RCA Laboratories
Rocky Point, New York

19.1. GENERAL DISCUSSION

Although radio development in the last thirty years has occurred mainly at medium and higher frequencies, the propagation characteristics of low-frequency (LF) waves still tend to recommend that region for certain special services. At low frequencies, ground waves are subject to less attenuation and sky waves are less affected by ionospheric conditions and disturbances. These characteristics make the region especially favorable for communications and for navigational aids to widely dispersed ships and aircraft. Another characteristic, applying especially to *very* low frequencies (VLF), is the ability of the waves to penetrate into salt water, making communications with submerged submarines possible.

The advantage of low frequencies would increase continually with decreasing frequency except for the tendency of the prevailing atmospheric noise (static) level to increase at the same time. The result is the existence of an optimum frequency with respect to signal-to-noise ratio at the receiving location for a given transmitting antenna. For example, the optimum frequency for the New York–London low-frequency circuit has been found to be about 40 kilocycles per second (kc).[1]

Low frequencies are of special utility in polar regions. This is because ionospheric disturbances are extra severe and atmospheric noise levels are relatively low in these areas.

* 15 to 500 kilocycles per second.

The main disadvantages of low frequencies are the high cost and practical difficulties associated with the construction of radiators having dimensions appreciable with respect to the wavelength. For this reason it is generally not feasible to obtain directive gain by the use of either a high antenna or an array. In a few cases having especially severe performance requirements, antennas with effective lengths near a quarter wavelength are used. Usually, however, cost and practical considerations result in the radiators being electrically in the "small" category. (A definition for a small antenna which is adopted here is stated in chap. 10 of Ref. 2 as follows: " . . . *an antenna is said to be small if its largest dimension, measured from its input terminals, does not exceed one-eighth of the wavelength*.") Small antennas have special problems in connection with efficiency, power capacity, and bandwidth. The requirements in regard to these characteristics are so varied and the economic factor is so important that little standardization has been obtained in low-frequency transmitting-antenna systems. Existing radiators are in the form of vertical radiators, umbrella-loaded vertical radiators, and flat-tops (of a large variety of sizes and shapes) fed by downleads.

Receiving-antenna problems are generally less severe than those of transmitting antennas at low frequencies. Since atmospheric noise rather than receiver noise is the controlling factor in regard to signal-to-noise ratio, the efficiency of the receiving antenna is of very minor importance. For the same reason, directive gain[28] is of great importance, and therefore loops and wave antennas have found favor for this application.[1,3,4,6]

19.2. LOW-FREQUENCY-ANTENNA CHARACTERISTICS

The antenna input resistance R_a may be considered as being composed of two main parts: R_{ar} associated with radiated power and R_{al} associated with power lost in heat. Loss of power occurs in the ground, in conductors and insulators, and in some cases in corona discharge. Figures 19-1 and 19-2 show plots of theoretical radiation resistance R_{ar} for the two assumed current distributions depicted in the figures. Figure 19-1, which pertains to a sine-wave current distribution, is more generally applicable to the largest antennas under consideration here. Figure 19-2, which ranges down to very low values of radiation resistance, is more useful in connection with the smallest. In practice, the antenna is energized by a transmitter through an electrical network which may consist of either a tuning element alone or, effectively, a tuning element and an L, T, or π network. In the present discussion the antenna circuit is considered to be composed of the antenna, a tuning element of resistance R_t, and a zero-loss generator. The antenna efficiency is defined by the equation

$$\text{Eff} = \frac{R_{ar}}{R} \tag{19-1}$$

where $R = R_a + R_t = R_{ar} + R_{al} + R_t$.

A few unusually large low-frequency antennas have equivalent lengths somewhat greater than a quarter wavelength and therefore inductive input reactances; however, most are in the small category and have high capacitive reactance. In any case, the input reactance X_a can be represented with good accuracy throughout the frequency range under consideration by the equation

$$X_a = -Z_0 \cot \frac{2\pi\ell}{\lambda} \qquad \text{ohms} \tag{19-2}$$

where Z_0 is the characteristic impedance, ℓ is the length of an *equivalent uniform* transmission line, and λ is the wavelength, ℓ and λ being expressed in the same units. For the special case of a vertical cylindrical radiator of height h and radius a ($a \ll h$), Eq. (19-2)

is commonly evaluated by letting $\ell = h$ and

$$Z_0 = 60 \left[\ln \left(\frac{2h}{a} \right) - 1 \right] \quad \text{ohms} \tag{19-3}$$

where h and a are expressed in the same units. Equation (19-3) is the *average* value of the characteristic impedance of the cylinder as derived in Chap. 13 of Ref. 2.
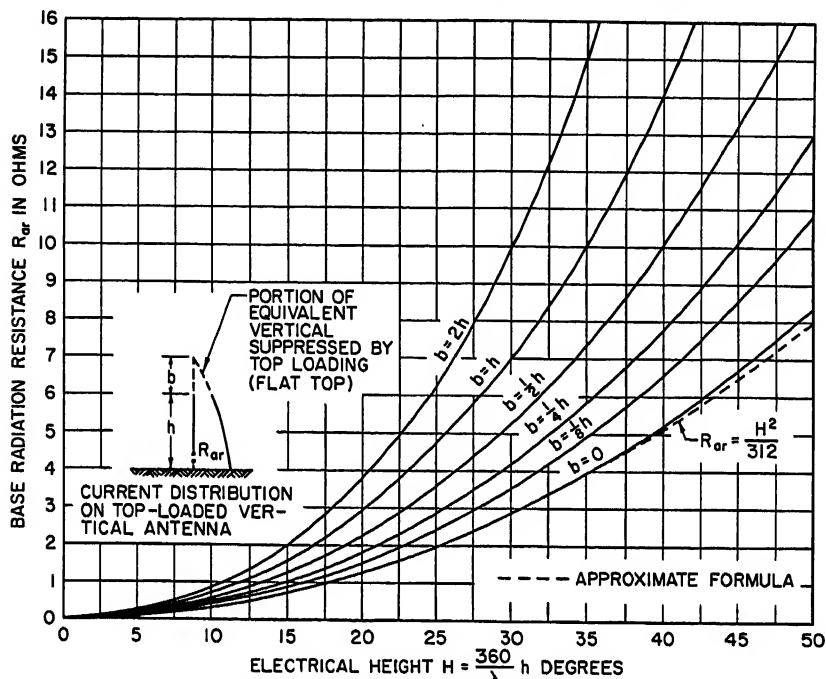
FIG. 19-1. Theoretical radiation resistance of vertical antenna for assumed sine-wave current distribution. (*Reference 5.*)

Another expression for Z_0, which fits experimentally measured values for short vertical radiators more closely than does Eq. (19-3),[3] is

$$Z_0 = 60 \left[\ln \left(\frac{h}{a} \right) - 1 \right] \quad \text{ohms} \tag{19-4}$$

The Q of the antenna circuit with zero-loss generator is conventionally given by the equation

$$Q = \frac{f_0 \left(\dfrac{dX}{df} \right)_{f_0}}{2R} = \frac{|X_a| + f_0 \left(\dfrac{dX_a}{df} \right)_{f_0}}{2R} \tag{19-5}$$

where X is the total circuit reactance ($X = X_a + X_l$) and $|X_a|$ is the magnitude of the antenna reactance at the operating frequency f_0. Equation (19-5) holds for the total range of antenna sizes under consideration, from very small to somewhat larger than a quarter wavelength. The bandwidth of the circuit is determined by the equation

$$\text{BW} = \frac{f_0}{Q} \tag{19-6}$$
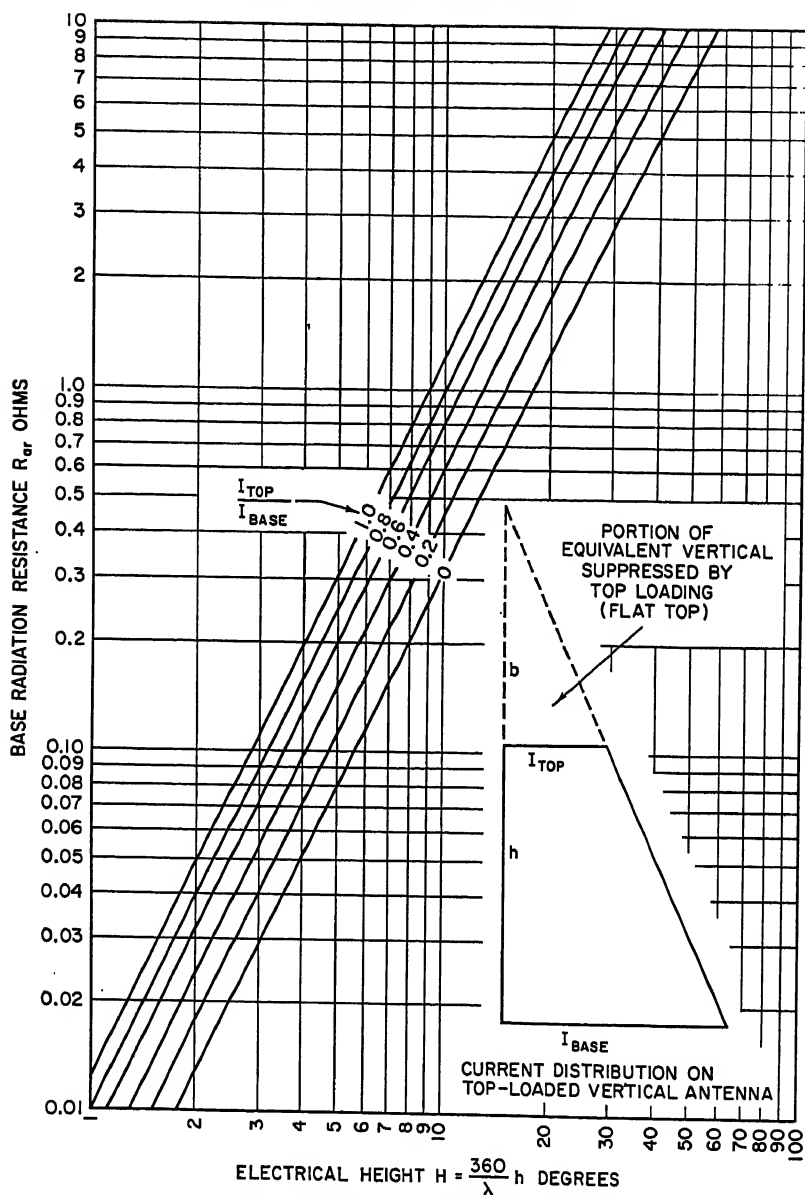
FIG. 19-2. Theoretical radiation resistance of vertical antenna for assumed linear current distribution. (*Reference 6.*)

Since no prescribed method of determining the Q factor or bandwidth of an antenna has become standard, these quantities are not always defined in the literature as they are defined here. Sometimes the transmitter internal impedance is assumed to double the bandwidth of the antenna alone, and sometimes the effect of the tuning element is neglected. Actually, the effect of the transmitter impedance is not zero, as Eqs. (19-5) and (19-6) imply, but it is not possible to specify the effect in general. In many cases

the exact matching of the transmitter impedance by the antenna load would seriously overload the transmitter. References 9, 10, 11, and 24 contain interesting information in regard to the over-all bandwidth question, including the effect of coupling networks between the transmitter and antenna.

The main consideration in low-frequency-antenna design is often the amount of power to be radiated in order to obtain a required range of communication. In other cases the determining factor is that of obtaining a low value of antenna Q, in order to satisfy a bandwidth requirement in regard to the transmission of a short-pulse, high-speed radiotelegraphy or high-fidelity radiotelephone. In many ways these two performance requirements are similar; for example, the size of the antenna needed increases as either requirement becomes more severe. The quality of a small antenna, in regard to efficiency, power capacity, and bandwidth, increases with antenna height. However, at low frequencies the height needed in a simple vertical radiator is often greater than is practical to construct. It is then necessary to use some form of top loading in order to obtain the required performance.

The characteristics of short vertical radiators may be improved by adding a top-loading umbrella. As the length of the umbrella wires increases, the antenna effective height increases to a maximum, because of the increase in height of the center of charge, after which it decreases, because of the umbrella's shielding effect on the vertical radiator. The umbrella also tends to increase the bandwidth to a certain extent by decreasing both the reactance and the slope of the reactance vs. frequency curve of the antenna [Eqs. (19-5) and (19-6)]. A further effect of the umbrella, which is important in some cases, is to decrease the voltage, and hence the power loss, associated with the base insulator. On the disadvantage side, the umbrella cables place an additional mechanical load on the tower, tending to increase its cost. For the last reason, the simple vertical radiator is preferred to the umbrella in some low-frequency applications. Examples of umbrella-loaded vertical radiators are described in Refs. 5 and 14.

At VLF, practical towers are electrically so short that a large amount of top loading is generally required. Although the top loading is beneficial to a certain extent in increasing the effective height, the required amount of top loading is usually determined by the maximum antenna voltage that can be tolerated—up to about 250,000 volts at the present stage of insulation development. For a given effective height the power radiated determines the antenna current. Since the antenna voltage is equal to the product of the current and the capacitive reactance, the maximum allowable voltage specifies the minimum antenna capacitance, and thereby the size flat-top required. Tower-base insulators are not satisfactory at high voltages, and it is necessary to support the flat-top from masts or towers by long tubular insulators and to feed the flat-top by downleads similarly insulated at the ground. As a result of these considerations a typical VLF antenna consists of an extremely large flat-top supported by towers and fed by one or more cage downleads.

In the design stage, the characteristics of radiation resistance and reactance occurring in Eqs. (19-1) and (19-5) are generally determined under the assumptions that the antenna is lossless and its ground plane is infinite. Because of the effect of towers and guys, edge and end effects of flat-tops, and the general complexity of low-frequency antennas, these characteristics cannot be rigorously calculated and it is necessary to determine them by either approximate calculations or by experiment.

In some situations, mainly those in which the antenna is electrically quite large, the characteristics can be determined by impedance measurements, using a small-scale model mounted on a large ground plane.[6,7,12,13] Such measurements yield useful information in regard to those antenna characteristics which are not greatly affected by losses. When a large-scale factor is used, it is usually necessary to idealize various sections of antenna, such as lattice towers by cylinders, the configurations of the wires in the flat-top by a metal sheet, and cages by wires. In this case, some judgment or

theoretical calculation is necessary to correct the measured results to apply to the actual conditions.

In one instance reported in the literature,[14] several design problems connected with an 820-ft umbrella-loaded vertical antenna were investigated, using an existing 240-ft broadcast tower as a support for the experimental umbrella. According to the theory of models,[13] the model measurements at 610 kc correctly represented the full-scale antenna as if it were located on a site having a value of ground conductivity equal to that of the experimental site divided by the scale factor, or approximately by 3. However, much experience with broadcast antennas has shown that, for the electrical height involved and for the ground systems of both the model and the proposed antenna, the effect of substantially perfect ground is obtained regardless of the ground conductivity (for example, see Ref. 6, sec. 2.1.2). The experiment was successful in predicting with good accuracy the final performance of the full-scale antenna with respect to both impedance and field-strength characteristics.

When the proposed antenna is in the small category, many problems associated with the design can be attacked from an electrostatic rather than an electromagnetic viewpoint. The reactance of a small antenna can be represented by the combination of a lumped capacitance C_a and a lumped inductance L_a in series (Ref. 2, sec. 10.2). The capacitance is of chief importance since it determines the antenna voltage [given by $I/(\omega C_a)$] and the Q factor [given by $1/(R\omega C_a)$]. Usually, in connection with antennas of this class, it is necessary to consider the antenna inductance only in so far as it affects the value of tuning inductance required. For example, the static capacitance assignable to each downlead of the antenna shown in Fig. 19-8 is about 1,000 ohms, whereas the corresponding antenna inductive reactance is only 18 ohms.

For any grounded antenna, there exists a length of vertical wire which, if caused to carry a uniformly distributed current equal to the input current of the antenna, would produce a distance field strength on the horizon equal to that of the antenna, assuming infinite ground conductivity in both cases. The length of the hypothetical wire is commonly called the "effective height" (h_e) of the antenna. A quarter-wave grounded vertical wire has an effective height equal to $2/\pi$ times the actual height. In the case of a small antenna, a definition which is equivalent to that just stated but which is of more general utility is: *the effective height is the height of the center of charge in the antenna, its supports, and other nearby elevated structures, assuming the antenna to be raised to a d-c potential above ground.* It should be noted that the charges induced in the supports and other nearby objects oppose the charges in the antenna, thereby reducing the effective height. The effective height of a short vertical radiator, unloaded and standing alone, is approximately equal to one-half the actual height. This is equivalent to assuming a linear distribution of current in the first definition and, equivalently, a uniform distribution of charge in the second definition. That curve of Fig. 19-2 which is labeled $I_{top}/I_{base} = 0$ pertains to this particular condition. In general, the radiation resistance of any small grounded antenna is related to the effective height h_e by the equation

$$R_{ar} = 160\pi^2 \left(\frac{h_e}{\lambda}\right)^2 \quad \text{ohms} \tag{19-7}$$

where h_e and λ are expressed in the same units. Equation (19-7) applies to that curve of Fig. 19-2 which is labeled $I_{top}/I_{base} = 1.0$ with $h = h_e$.

Figure 19-3 shows a typical low-frequency antenna. A large capacitance C_1 between the flat-top and ground, besides establishing the effective height near that of the flat-top, is beneficial in reducing the voltage and the Q factor of the antenna. The downlead and the towers increase the antenna capacitance; on the other hand, however, they detract from the effective height established by the flat-top—a very considerable amount in typical VLF antennas. Consequently, mainly the flat-top

is depended upon to obtain the desired minimum capacitance. The downlead capacitance C_2 is made as small as possible (consistent with the voltage-gradient limitation on the downlead), and the coupling between the flat-top and the tower, represented in Fig. 19-3 by C_3, is made as small as is practical.

The electrostatic nature of the design problems of small antennas justifies a unique experimental procedure called the "tank method."* The antenna (including supports) is modeled on a copper sheet, and the whole is placed in tap water contained in a tank which is constructed of insulating material. The model is sectionalized into n sections, each section being isolated electrically and furnished with an insulated lead running out of the tank. Provision is made to measure the current in each
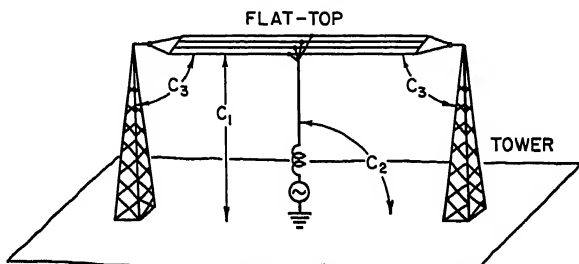
FIG. 19-3. Typical low-frequency antenna.

section, with the sections composing the antenna being maintained at the same potential and the tower sections at ground (copper-sheet) potential. Alternating current is used in order to avoid polarization. The lines of current flow in the tank correspond exactly to electrostatic flux in the air, and the current values in the antenna sections correspond to electrostatic charges in the full-scale antenna. The antenna effective height is determined from the equation

$$h_e = \frac{\sum_{i=1}^{n} I_i h_i}{I} \times \text{scale of model} \qquad (19\text{-}8)$$

where I_i = current in ith section taken positive for antenna sections and negative for tower sections

h_i = average height of ith section

I = total current in antenna

The antenna capacitance C_a is obtained from the measured resistance values of the antenna model R_m and that of a standard R_s, immersed in the same tank. The standard is of such a form that its capacitance in air may be readily calculated, such as a horizontal disk provided with a guard ring. Then

$$C_a = \frac{R_s C_s}{R_m} \times \text{scale of model} \qquad (19\text{-}9)$$

An alternative means of determining h_e may be provided in the tank experiments. For this purpose a probe is placed at a position remote from the model on a wall of the tank. Two experimental set-ups are used: (1) the flat-top only in place and (2) the entire model, including supports in place. The probe potentials V_1 and V_2 are measured with the model at the same potential for the two conditions. The ratio

---

* Early literature contains numerous references to the tank method of measuring antenna capacitance. The material contained here was obtained from a 1920 unpublished General Electric Company report concerned with tank experiments to solve various design problems connected with the Rocky Point antenna of Fig. 19-8.

V_2/V_1 is called the "shielding factor" (SF). The values of capacitance C_1 and C_2 ($= C_a$) are also measured for the two conditions.   Then

$$h_e = \frac{C_1}{C_2} \, (\text{SF}) \, (\text{average height of flat-top}) \qquad (19\text{-}10)$$

As examples of the application of the tank experimental methods, the following design problems in connection with the Rocky Point antenna (Fig. 19-8) were investigated.

1. The effect of the steel tower bridge on the antenna wire capacitance and the determination of the optimum distance between the wire and the bridge
2. The effect of the steel tower on the antenna wire capacitance and the determination of the optimum distance between the tower and the wire nearest to it
3. The effect of the tower on the downlead and the optimum location of this lead
4. The effective height of the antenna
5. The capacitance of the antenna

For application to the design of *very* small antennas (including virtually all VLF antennas), the tank-model method has two definite advantages over the model-in-air method mentioned above.   First, the radiation resistance, because it is extremely small, is difficult to measure directly as in the model-in-air method.   Second, the data provided by the sectional currents in the model-in-tank method allow the evaluation of effects of the individual sections, as in the Rocky Point antenna experiment.   The same difficulties in accurately modeling the various components of the antenna when very large scale factors are used are encountered in both experimental procedures.

Other experimental methods for determining the characteristics of small antennas have been used in the investigation of low-frequency antennas on aircraft.[15]

An approximate method of calculating antenna capacitance which is sufficiently accurate for many low-frequency antenna applications was suggested by G. W. O. Howe in 1914.   The method is discussed in detail in Refs. 16 and 17 and in Ref. 2, chap. 10.   The antenna and its supports are considered to be divided into parts, and the charge carried by each part is determined by means of mutual (and self-) potential coefficients.   The approximate values of the potential coefficients are calculated by averaging over each part the potential due to an assumed uniformly distributed unit charge on each of the other parts (and itself).   The method can be readily extended to obtain the effective height as well as the capacitance of the antenna.   If a uniformly distributed charge is assumed for a downlead which is top-loaded by a nonradiating flat-top having nonradiating supports, the radiation is given precisely by the curves of Fig. 19-2.   It is interesting to note that Howe's method obtains for the capacitance to ground of an *unloaded* vertical radiator the equation

$$C_a = \frac{2\pi\epsilon_v h}{[\ln (h/a) - 1]} \qquad \text{farads} \qquad (19\text{-}11)$$

where ϵ_v = absolute dielectric constant of free space $\simeq (1/36\pi) \, 10^{-9}$ farad/meter
$\quad h$ = height, meters
$\quad a$ = radius, meters
which is consistent with Eq. (19-4), an experimentally verified equation for the characteristic impedance of a short vertical radiator.

19.3. MULTIPLE-TUNED ANTENNA

Multiple tuning was originally devised by E. F. W. Alexanderson for the purpose of reducing the ground loss of VLF antennas of the long inverted-L type.[18]   Essen-

tially, a multiple-tuned antenna consists of a number of antennas having closely coupled radiation characteristics but with substantially independent ground systems.

Consider first (Fig. 19-4a) a long narrow flat-top of capacitance C_a fed by a single downlead of negligible capacitance and tuned by a coil of inductance $L_{tc} = 1/\omega^2 C_a$. Neglecting the antenna inductance and all losses except those in the tuning coil and ground, the equivalent circuit is as shown in Fig. 19-4b. For a given antenna current

a. SINGLE-TUNED ANTENNA

b. SINGLE-TUNED EQUIVALENT CIRCUIT

c. MULTIPLE-TUNED ANTENNA

d. MULTIPLE-TUNED EQUIVALENT CIRCUIT
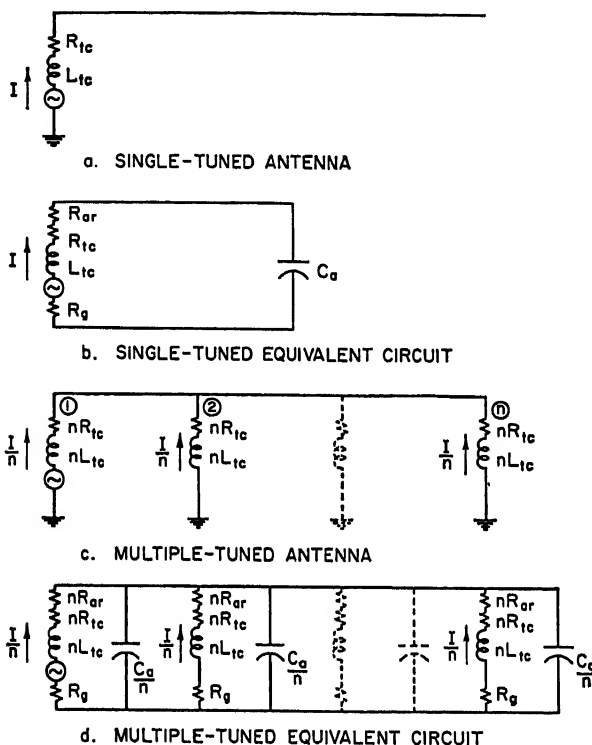
FIG. 19-4. Single-tuned and multiple-tuned flat-top antenna.

I, the power radiated is $I^2 R_{ar}$ and the powers lost in the tuning coil and ground are $I^2 R_{tc}$ and $I^2 R_g$, respectively. For the usual condition that the feed resistance $R_{ar} + R_{al} + R_g$ is small compared with the capacitive reactance $1/\omega C_a$, the antenna voltage is very nearly $I/\omega C_a$.

Next consider the same flat-top fed by a number (n) of spaced downleads (Fig. 19-4c and d) with the same *total* antenna current (the sum of the downlead currents). With a tuning inductance of nL_{tc} in each downlead, the circuit is again resonant and the current in each downlead is equal to I/n. If the individual antenna sections are small, all currents are substantially in phase. Assuming equal values of coil Q in both single- and multiple-tuned cases, the resistance of each coil is nR_{tc}. The total radiated power for a given total current I is the same as for the previous case; therefore, the radiation resistance assignable to each downlead is nR_{ar}. The total power lost in the tuning coils is the same as before, being equal to $(I/n)^2(nR_{tc})n$, or $I^2 R_{tc}$, but that in the ground, under the assumption of an equal value of ground resistance for each downlead in both single- and multiple-feed cases, is reduced to $(I/n)^2 R_g n$, or

$I^2(R_g/n)$. The total power into the antenna is therefore equal to

$$I^2\left(R_{ar} + R_{tc} + \frac{R_g}{n}\right)$$

If the individual ground resistance R_g is much larger than $R_{ar} + R_{tc}$, this input power is much less than for the single-tuned case, $I^2(R_{ar} + R_{tc} + R_g)$. Since the current supplied by the generator is I/n, the input resistance of the antenna is equal to $n^2(R_{ar} + R_{tc} + R_g/n)$. The antenna voltage is the same as for the single-tuned condition.

In application to multiple-tuned antennas, in general, the ratio of total current to the generator current is defined as the "feed ratio" (n in the case of the example). The antenna input resistance is called the "feed resistance." The total antenna power for unit *total* current is defined as the "multiple" resistance and is equal to the feed resistance divided by the square of the feed ratio.

Four factors tend to limit the extent to which multiple tuning should be carried for a given flat-top. First, the several downleads subtract somewhat from the effective height established by the flat-top. Second, as the number of downleads increases, their ground currents tend to overlap to a greater degree, resulting in the multiple tuning being less effective in improving the efficiency. Third, each additional downlead represents added costs in respect to itself, its tuning coils, and the mechanical loads it places on the towers, halyards, and insulators. Fourth, the antenna adjustments, when a substantial change in operating frequency is made, become more difficult as the number of tuning coils increases.

For the case of a vertical radiator having a relatively small amount of top loading, it is not feasible to supply independent and uncoupled ground systems for several downleads. Then the full advantage with regard to reduction of ground loss is not realized by multiple tuning. However, the general principle may be employed in order to simulate a vertical radiator of large radius and to increase the input resistance of the antenna. In this case the input resistance is equal to the single-tuned input resistance multiplied by the square of the feed ratio. Some such applications of multiple tuning are discussed in Ref. 6.

19.4. LOW-FREQUENCY GROUND SYSTEMS

A large variety of ground-system types have been used with low-frequency antennas. In contrast with the situation at broadcast frequencies where the radial-wire ground system has been generally adopted, no one type has become universally standard for low-frequency application. There are little quantitative data available by which the performance of the various types can be compared directly. This situation requires that the subject be presented mainly on the bases of history and practice.

Most low-frequency installations of recent years have included a radial-wire ground system. This type consists of a large number of generally radial wires, laid on or buried in the ground, extending out from the points of feed. Copper mesh is commonly included near the feed points to shield the ground from the high field existing there and to serve as a convenient termination for the inner ends of the radials. The outer ends are ordinarily terminated on ground stakes. As pertains to the design of all other parts of a low-frequency antenna, cost balanced against performance is the major consideration in determining the amount of labor and material to put into the ground system. The ground loss decreases as both the number and the length of the radials are increased. Up to 360 wires and lengths up to one-half wavelength have been used, although ordinarily that length is impractical at low frequencies. A design method applying to this type of ground system is given in Ref. 19. Installations of radial-wire ground systems are described in Refs. 10, 14, 20, and 22 to 25.

"Multiple-star" ground systems have been used in several VLF installations. In this type a number of relatively small radial-wire systems are scattered over that ground area in which all significant ground currents occur. The ground current collected by each star is returned to the downlead by way of an overhead bus. For design purposes, the resistance R_s of each star is calculated from a d-c equation such as[39]

$$R_s = \frac{\rho}{n\pi\ell}\left[\ln\left(\frac{2\ell}{an}\right) + 1.23n - 2.23\right] \quad \text{ohms} \quad \text{for } n > 6 \quad (19\text{-}12)$$

where ρ = ground resistivity, ohms/meter cube
  n = number of wires in star
  ℓ = length of each wire, meters
  a = radius of wire, meters

The ground current collected by each star I_s is determined according to the portion of the antenna flux assignable to the star. The total ground loss, $\Sigma I_s^2 R_s$ watts, is then calculated. By dividing this loss value by the square of the antenna current, the equivalent ground resistance R_g is calculated.
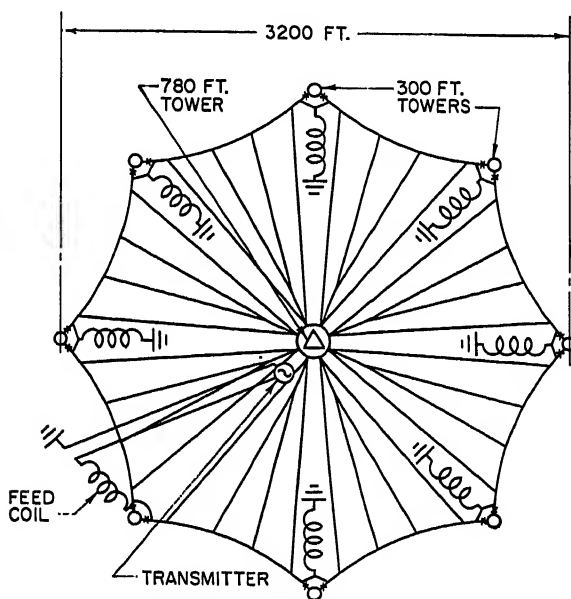
FIG. 19-5. Tuckerton, N.J., VLF umbrella antenna. Effective height, 315 ft; capacitance, 0.050 μf; allowable voltage, 160 kv; efficiency at 18.000 kc, 22 per cent. (*Courtesy of RCA Communications, Inc.*)

An example of a multiple-star system is that, shown in Fig. 19-6, of the multiple-tuned Tuckerton umbrella antenna (Fig. 19-5). The "equalizer" coil 1, shown in the figure at the center star of the system for each downlead, is of such inductance that the same current is drawn from the subsoil star to which it is connected as from other stars of the division. A bridge circuit is effectively formed by coil 2 combined with the capacitance from antenna to mast and the effective inductance of the star distribution system combined with the capacitance from antenna to ground. The inductance of coil 2 is adjusted so that no current flows in the direct ground connection at the base of the mast. Coils 2 and 3 combined perform a similar function in regard to the current induced in the copper tuning house. The antenna efficiency of 22 per

cent reported for Tuckerton is high considering the small amount of wire employed by the multiple-star ground system; however, the ground problem there is relatively easy because the site is a salt marsh of extremely high conductivity.

Multiple tuning was first employed in 1917 with the very-low-frequency New Brunswick antenna then under the control of the U.S. Navy. That antenna was
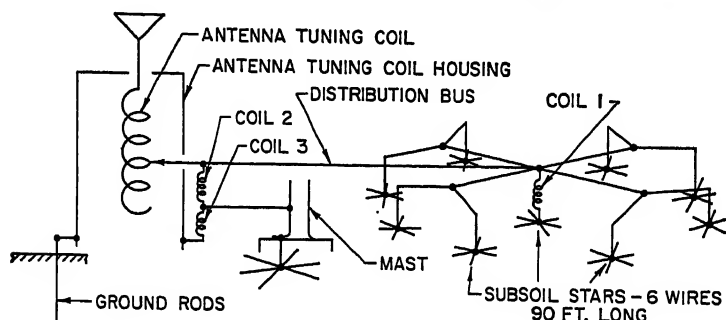
Fig. 19-6. Multiple-star ground system of Tuckerton antenna (Fig. 19-5). Typical for each tuning coil. (*Courtesy of RCA Communications, Inc.*)
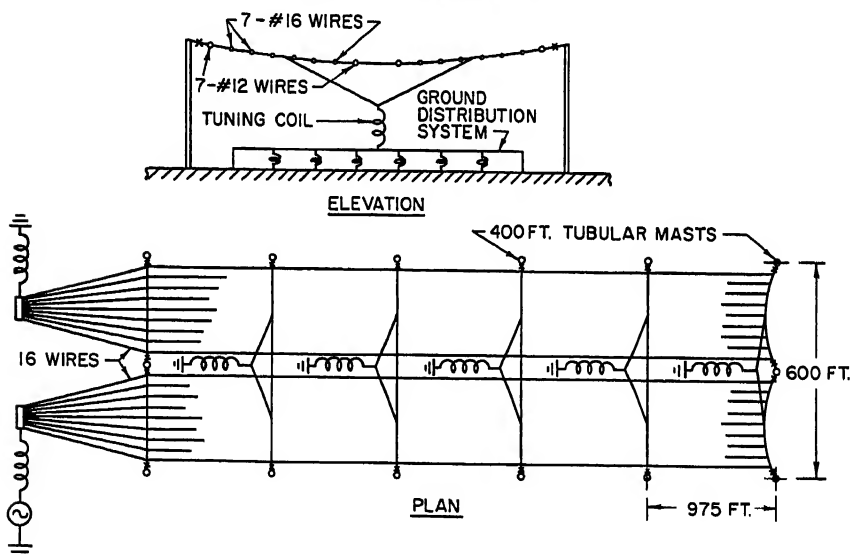
Fig. 19-7. New Brunswick, N.J., VLF antenna and ground-distribution system. Effective height, 223 ft; capacitance, 0.068 μf; allowable voltage, 125 kv; efficiency at 22.140 kc, 11 per cent. (*Courtesy of RCA Communications, Inc.*)

originally installed by the American Marconi Company as an inverted-L type (in accordance with Fig. 19-7 but without the unfed downleads). It had a ground system consisting of a number of plates buried in a 300-ft-radius circle with center at the feed point, plus 16 buried wires, spaced over the width and extending over the length of the flat-top. At 35 kc the input resistance of the inverted-L was 3.8 ohms and the radiation resistance was estimated to be 0.07 ohm. During the changeover to multiple tuning, experiments were made which confirmed that the field strength at a distant receiving position was dependent only on the total antenna current. The multiple

resistance obtained, with the tuning coil of each unfed downlead directly connected to all the buried ground wires by means of a transverse tie wire, was 0.9 ohm. With this arrangement, however, it was discovered that the most central buried wires carried almost all the ground current. To correct this condition "equalizing" coils were inserted between the tuning coil and the individual ground wires, as shown in Fig. 19-7. These were adjusted to force an equal distribution of the current among the ground wires. The equalizing coils further reduced the multiple resistance from 0.9 to 0.7 ohm.

An overhead ground system called a "capacitance" ground has been used in conjunction with a buried system in some VLF installations. The function of the overhead system was to reduce the ground currents directly beneath the antenna, where otherwise they tend to be highly concentrated. Such a system was used for a time with the New Brunswick antenna of Fig. 19-7 after the changeover to multiple tuning,
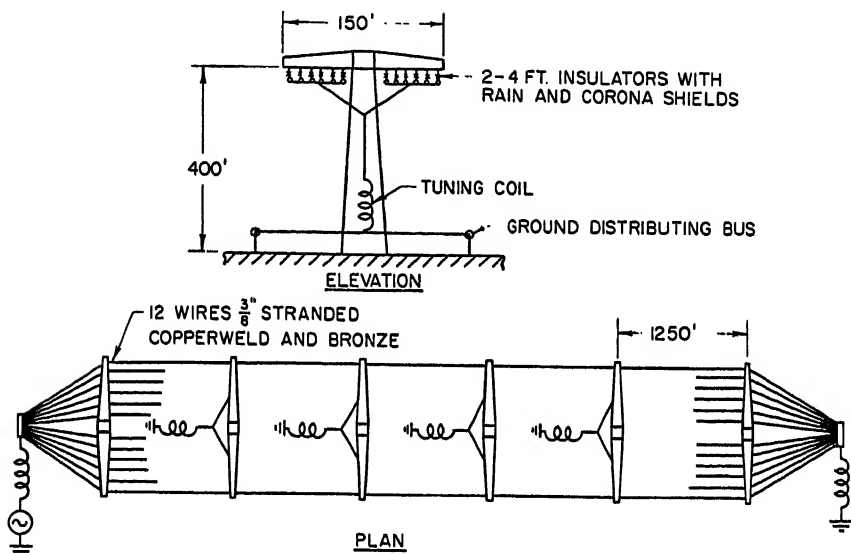
FIG. 19-8. Rocky Point, N.Y., VLF antenna. Effective height, 272 ft; capacitance 0.050 μf; allowable voltage, 150 kv; efficiency at 18.220 kc, 10 per cent. (*Courtesy of RCA Communications, Inc.*)

described above. In that case the capacitance ground consisted of a grid of wires about 10 ft above ground and covering most of the area directly under the antenna. The connections of the buried system and the capacitance ground to the tuning coils were such that the latter operated at a potential opposite to that of the antenna with respect to ground. The relative potentials were so adjusted that the ground current divided equally between the two systems. This capacitance ground was effective in reducing the multiple resistance from 0.7 to 0.5 ohm. On the other hand, it required much maintenance because of damage by ice storms, and it hindered maintenance aloft to such an extent that it was finally discarded. At the time of removal, the buried-wire ground system was overhauled and improved so that a still lower value of multiple resistance (0.35 ohm at 22 kc) was obtained.

Another example of a ground system for a multiple-tuned antenna is that of the Rocky Point antenna (Fig. 19-8). Sixty buried "stars," half on each side of the antenna, are located with their centers spaced 250 ft on lines 150 ft from the line of towers. Each star consists of 40 wires, each 125 ft long. From the stars, buried

wires spaced 10 ft extend out alternately to distances of 500 and 1,000 ft from the line of towers. Figure 19-9 shows the ground distribution and equalizing system for each tower and downlead. The ground connections shown in the figure are to the buried stars. The distribution buses run the entire length of the antenna and are supported on telephone poles. The equalizing coils are wound on those poles and are adjusted to give equal current at each grounding point. The tower coil, which is connected between the distribution bus and a lead sloping up to the tower's 60-ft level, is adjusted to divert the tower current from its normal path through the earth into the overhead distribution system.
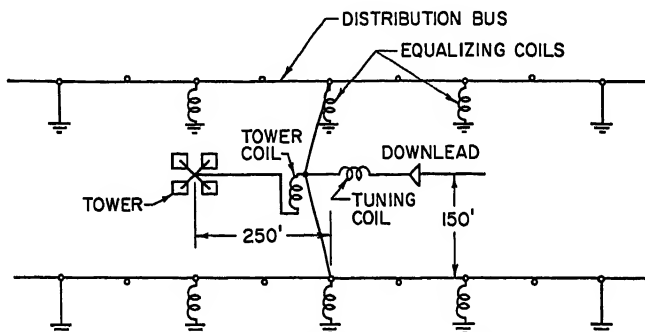
FIG. 19-9. Ground-distribution and equalizing system for Rocky Point antenna (Fig. 19-8). Typical for each downlead. (*Courtesy of RCA Communications, Inc.*)

An example of a recently designed ground system for a VLF multiple-tuned antenna is that of the Air Force antenna at Marion, Mass.* This antenna, which is practically the same as the New Brunswick antenna of Fig. 19-7, was used in the past by RCA Communications, Inc., with a ground system similar to that described above for New Brunswick, excepting that, at Marion, a number of stars covered an additional area nominally 250 ft beyond the periphery of the antenna. An overhead distribution system, with equalizing coils to distribute the ground current both longitudinally and laterally from each downlead position, was employed. Under more recent operation by the U.S. Air Force at a frequency about 26 kc, an average value of multiple resistance of 0.32 ohm, with variations up to 0.615 ohm when the ground was very dry, was obtained. The multiple resistance was estimated to be made up of radiation resistance 0.050 ohm, resistance of tuning coils and antenna wires 0.140 ohm, and the remainder ground-loss resistance. Thus the estimated average ground-loss resistance was 0.130 ohm, and the average efficiency was 0.05/0.32, or 15.6 per cent.

Besides being very inefficient under prolonged dry-weather conditions, the ground system at Marion developed several minor faults in its overhead portion, causing interference to local broadcast and television reception and also starting several field fires. Consequently, the Air Force sponsored a rehabilitation under which the overhead ground distribution was removed and a buried radial-wire system, sketched in Fig. 19-10, was installed over the original buried portion. The only overhead members included in the revised installation were two cages running from a copper square between the two end downleads to the transmitter and to tuning coil 1B, respectively. The value of multiple resistance obtained after the rehabilitation was 0.219 ohm, which figure represents an estimated ground-loss resistance of 0.029 ohm (22 per cent of the previous average value) and an efficiency of 23 per cent.

* Descriptive details and performance characteristics of both original and rehabilitated ground systems were furnished by J. L. Finch of RCA Communications, Inc., with permission of the U.S. Air Force.
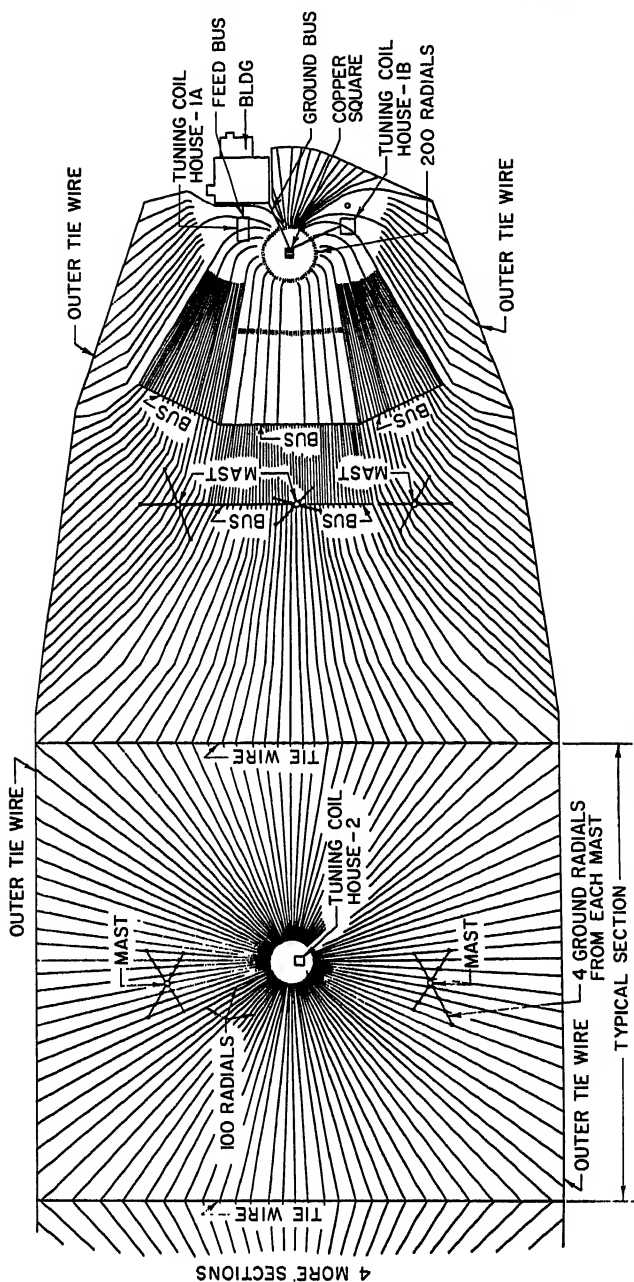
Fig. 19-10. Rehabilitated ground system of Air Force VLF antenna at Marion, Mass. The antenna is practically the same as the New Brunswick antenna (Fig. 19-7). (*Courtesy of U.S. Air Force and RCA Communications, Inc.*).

The extensive usage at VLF of the multiple star and other special types has tended to complicate the standardization of low-frequency ground-system design. It has been argued that the special types and the overhead distribution and equalizing systems, although not necessary at higher frequencies, are required at VLF because of the extra difficulties of the grounding there. The question has remained open because of the general lack of quantitative experimental VLF data available by which the performance of the various types could be compared under equal circumstances. The recent Air Force results at Marion are especially important in that they tend to oppose the arguments favoring the special types of systems. With the same antenna, site, and expanse of ground system and at the same very low frequency, a generally radial ground system resulted in considerably less ground loss than had previously been obtained with a combination of multiple stars, parallel-wire grid, and a complex overhead distribution and equalizing system.

Even though, on the basis of evidence now available, the radial-wire system were to be accepted as preferable to any of the special types, the design of low-frequency ground systems would necessarily remain relatively unstandardized, as compared with ground systems for broadcast radiators. This is because of the extra importance and variety of the economic factor, the requirement of lower values of ground loss due to the electrically small size of the antennas, and the variety of antenna types used at low frequencies.

19.5. MISCELLANEOUS PROBLEMS OF LOW-FREQUENCY ANTENNAS

The large physical size and the electrical smallness of low-frequency antennas cause several miscellaneous problems. These are especially evident in VLF antennas but may also be present in the larger or higher-power LF antennas.

A low-frequency installation involves a considerable amount of structual design. The wires in the antenna are subject to loads because of their own weight, the weight of ice (in most locations), and windage. Ice loading and windage are especially severe in the far north, and windage is high in hurricane belts. Stresses in the antenna wires and halyards are dependent on allowable antenna sag and shift, which may be limited by electrical considerations. In order to limit stresses in the antenna and loads on the towers, halyards are sometimes provided with counterweight assemblies or friction drums. Provisions are often made to melt sleet on the flat-top by means of 60-cycle power. Protective devices may be added to release the flat-top when failure of the 60-cycle power supply causes the ice formation to be especially heavy. These subjects are treated in more detail in Refs. 26 to 28. The structural design of low-frequency antennas is a specialized field, the details of which are usually accomplished by the companies furnishing the towers or the antenna wire. However, because of practical and economical considerations and the interrelation of design problems, the antenna design is generally the result of a considerable amount of mutual effort by structural and radio engineers. Interesting antenna structural information is contained in Refs. 6, 10, 11, 20 to 23, and 29 to 34.

VLF antenna insulators are generally of tubular porcelain. To withstand the large mechanical loads provided by large flat-tops, tubes up to 6 in. in diameter and rated at working loads of about 12,000 lb are used; often two, three, and four of these are connected in parallel by means of load-equalizing yokes. Insulators up to 6 ft in length and rated as high as 150 kv are employed. In a few cases two are connected in tandem to withstand still higher antenna voltage. Individual porcelain insulators have very small losses, but a typical VLF antenna may use enough of them so that they dissipate an appreciable amount of power. Losses in such insulators are discussed in Refs. 29 and 35. Another type of insulator having higher mechanical load ratings than the conventional porcelain type has been incorporated in several LF

antennas in recent years. This type consists of an oil-filled porcelain tube containing a "safety core" (a phenolic-resin impregnated link between end caps).[6,7]

The question of whether or not to insulate the guys and masts supporting flat-tops is mainly an economic one. These insulators tend to reduce the charges induced in the guys and masts and thereby to increase the antenna's effective height. If the insulators are used, it is extremely important, because of the high voltages to which they are subjected, that the insulation material be of high quality. Base insulators are employed to advantage in the masts of the Rugby antenna.[30] On the other hand, in the case of the Tuckerton umbrella of Fig. 19-5, a considerable increase in antenna efficiency was obtained by replacing weathered insulators in the central mast with metal blocks. The insulation of guys and masts is discussed in more detail in Refs. 5, 14, 29, 30, and 37.

Corona is an important design consideration of VLF antennas because of the extremely high voltages to which they are subjected. As the power into the antenna is increased above the point at which corona discharge starts, the antenna input resistance increases rapidly, representing a corresponding decrease in efficiency. Ordinarily, precautions are taken in the antenna design to prevent the occurrence of corona. Consideration is given to voltage gradients in the selection of wire size (hollow and jute core conductors have been used on this account), and attention is given the elimination of sharp corners on antenna fittings and to maintaining large separations between high-potential components and grounded objects. These represent electrostatic problems the solution of which can be facilitated by calculations according to Howe's method or by use of the water-tank experimental method.

The losses in the tuning coil and variometer of a VLF antenna are usually appreciable. These losses occur in the coil conductors, in the coil frame, and in the surroundings. The loss in the conductors can be made small by using Litzendraht wire having thousands of insulated strands, each 0.005 to 0.010 in. in diameter, and by making the coil physically large. The loss in the frame is made low by the use of low-loss insulating material, such as porcelain, and the absolute minimum of metal fittings. In order to make the loss in the surroundings as low as possible, the room containing the tuning coil is often lined with copper sheet. References 20, 22, 29, 30, and 36 contain interesting information in regard to existing tuning coils and variometers for VLF antennas.

REFERENCES

1. A. Bailey, S. W. Dean, and W. T. Wintringham: "The Receiving System for Long-wave Transatlantic Radio Telephony," *Proc. IRE*, vol. 16, pp. 1645–1705, December, 1928. Derives the optimum low frequency for the New York–to–London circuit. Shows performance characteristics of Rocky Point antenna (Fig. 19-8) at 18 and 60 kc. Describes a wave antenna array used for reception.
2. S. A. Schelkunoff and H. T. Friis: "Antennas: Theory and Practice," John Wiley & Sons, Inc., New York, 1952. Contains theoretical justification for the electrostatic treatment of small antennas. Discusses methods for the calculation of antenna capacitance and inductance. Explains reduction in ground loss obtained by multiple tuning.
3. H. H. Beverage, C. W. Rice, and E. W. Kellogg: "The Wave Antenna," *Trans. AIEE,* vol. 42, pp. 215–266. Presents the results of experiments with first wave antenna. Discusses the theory of wave antennas.
4. A. G. Lee: "The Radio Communication Service of the British Post Office," *Proc. IRE*, vol. 18, pp. 1690–1729, October, 1930. Describes several low-frequency transmitting stations. Describes array of loop antennas used for VLF reception.
5. C. E. Smith and E. M. Johnson: "Performance of Short Antennas," *Proc. IRE*, vol. 35, pp. 1026–1038, October, 1947. Discusses characteristics of short vertical radiators. Presents low-frequency measurements of antenna impedance and field strength using an existing broadcast tower with various amounts of top-loading umbrella added.
6. E. A. Laport: "Radio Antenna Engineering," chap. 1, McGraw-Hill Book Company, Inc., New York, 1952. Explains characteristics of small antennas. Describes low-

frequency application of Beverage (wave) and Adcock antennas. Describes scale-model measurement of impedance characteristics. Presents measured impedance characteristics of several representative low-frequency configurations, some obtained from existing antennas and others from scale models.

7. Keith Henney (ed.): "Radio Engineering Handbook," McGraw-Hill Book Company, New York, 1950. Section entitled "Low-frequency Transmitting Antennas (below 300 Kc)," by E. A. Laport, pp. 609–623, explains characteristics of small antennas. Describes low-frequency application of Beverage (wave), Adcock, and whip antennas. Describes scale-model measurement of impedance characteristics.

8. E. C. Jordan: "Electromagnetic Waves and Radiating Systems," chap. 14, Prentice-Hall, Inc., Englewood Cliffs, N.J., 1950. Discusses characteristics of short antennas.

9. W. H. Doherty: "Operation of AM Broadcast Transmitter into Sharply Tuned Antenna Systems," *Proc. IRE*, vol. 37, pp. 729–734, July, 1949. Shows the impairment of bandwidth of a broadcast transmitter caused by a high-Q antenna.

10. N. Ashbridge, H. Bishop, and B. N. MacLarty: "Droitwich Broadcasting Stations," *J. IEE (London)*, vol. 77, pp. 447–474, October, 1935. Contains a description in some detail and measured performance characteristics pertaining to a 1935, 150 kw, l-f, BBC broadcast antenna of the T type. Explains the procedure used in the design of a broadbanding network and shows the performance of the network.

11. E. K. Sandeman: "Radio Engineering," vol. I, chap. 16, John Wiley & Sons, Inc., New York, 1948. Treats antenna coupling networks in general. Explains the procedure used in the design of the 1935 Droitwich broadbanding network. Describes mechanical design methods for flat-tops.

12. G. H. Brown and R. King: "High Frequency Models in Antenna Investigations," *Proc. IRE*, vol. 22, pp. 457–480, April, 1934. Describes and justifies the use of small-scale models to investigate problems of vertical radiators.

13. J. A. Stratton: "Electromagnetic Theory," sec. 9.3, McGraw-Hill Book Company, Inc., New York, 1941. Treats electrodynamic similitude and the theory of models.

14. C. E. Smith, J. P. Hall, and J. O. Weldon: "Very High-power Long Wave Broadcasting Station," *Proc. IRE*, vol. 42, pp. 1222–1235, August, 1954. Contains a description and measured performance characteristics of a low-frequency umbrella-loaded vertical radiator. Presents measurements using a 1/3.5 scale model to settle various design problems.

15. J. T. Bolljahn and R. F. Reese: "Electrically Small Antennas and the Low-frequency Aircraft Antenna Problem," *Trans. IRE*, vol. AP-1, no. 2, pp. 46–54, October, 1953. Describes methods of measuring patterns and effective height of small antennas on aircraft by means of models immersed in a uniform field.

16. G. W. O. Howe: "The Capacity of Radio Telegraphic Antennae," *Electrician*, vol. 73, pp. 829–832, 859–864, 906–909, August and September, 1914; "The Capacity of Aerials of the Umbrella Type," *Electrician*, vol. 75, pp. 870–872, September, 1915; "The Calculation of Capacity of Radio Telegraph Antennae, Including the Effects of Masts and Buildings," *Wireless World*, vol. 4, pp. 549–556, 633–638, October and November, 1916; "The Calculation of Aerial Capacitance," *Wireless Engineer*, vol. 20, pp. 157–158, April, 1943. Discuss application of Howe's average potential method for situations stated in the titles.

17. F. W. Grover: "Methods, Formulas, and Tables for Calculation of Antenna Capacity," *Natl. Bur. Standards (U.S.) Sci. Papers*, no. 568. Discusses and employs Howe's average potential method. Out of print, but available in libraries.

18. E. F. W. Alexanderson: "Trans-oceanic Radio Communications," *Proc. IRE*, vol. 8, pp. 263–286, August, 1920. Explains the theory of multiple tuning and states the results obtained when applied to the New Brunswick, N.J., VLF antenna.

19. F. R. Abbott: "Design of Optimum Buried-conductor RF Ground System," *Proc. IRE*, vol. 40, pp. 846–852, July, 1952. Derives a design procedure for a radial wire ground system to obtain maximum power radiated per unit over-all cost.

20. J. R. Redman: "The Giant Station at Jim Creek," *Signal*, January–February, 1951, pp. 15. Describes U.S. Navy 1,200 kw VLF installation.

21. T. D. Hobart: "Navy VLF Transmitter Will Radiate 1,000 KW," *Electronics*, vol. 25, pp. 98–101, December, 1952. Describes U.S. Navy VLF installation of Ref. 20.

22. W. West, A. Cook, L. L. Hall, and H. E. Sturgess: "The Radio Transmitting Station at Criggion," *J. IEE (London)*, pt. IIIA, vol. 94, pp. 269–282, 1947. Contains description and measured performance characteristics of a VLF antenna.

23. S. D. Sturgis: "World's Third Tallest Structure Erected in Greenland," *Civil Eng.*, pp. 381–385, June, 1954. Describes structural details and installation procedures for a U.S. Air Force 1,205-ft low-frequency vertical radiator.

24. J. A. Pierce, A. A. McKenzie, and R. H. Woodward: "Loran," chap. 10, MIT Radiation Laboratory Series, McGraw-Hill Book Company, Inc., New York, 1948. Con-

tains a description and performance characteristics of temporary 1,290-ft balloon-supported antenna used by the U.S. Air Force at 180 kc.

25. N. Wells: "Aerial Characteristics," *J. IEE (London)*, pt. III, vol. 89, pp. 76–99, June, 1942. Contains a description and performance characteristics of a low-frequency antenna employing a variation of the multiple-tuning principle.

26. J. H. Shannon: "Sleet Removal from Antennas," *Proc. IRE*, vol. 14, pp. 181–195, April, 1926. Describes the sleet-melting and weak-link provisions for the Rocky Point VLF antenna of Fig. 19-8.

27. H. Pender and K. Knox (eds.): "Electrical Engineers' Handbook," 3d ed., vol. 5, "Electric Communications and Electronics," sec. 13, p. 67, John Wiley & Sons, Inc., New York, 1936. Refers to sleet-melting facilities for antennas.

28. A. E. Knowlton (ed.): "Standard Handbook for Electrical Engineers," 7th ed., sec. 13, p. 261, McGraw-Hill Book Company, Inc., New York, 1941. Gives design equation for sleet-melting current required on power-transmission lines.

29. N. Lindenblad and W. W. Brown: "Main Considerations in Antenna Design," *Proc. IRE*, vol. 14, pp. 291–323, June, 1926. Discusses VLF antenna features and design problems and methods.

30. E. H. Shaughnessy: "The Rugby Radio Station of the British Post Office," *J. IEE (London)*, vol. 64, pp. 683–713, June, 1926. Contains a detailed description and measured performance characteristics of a VLF antenna.

31. F. Hollinghurst and H. F. Mann: "Replacement of the Main Aerial System at Rugby Radio Station," *P.O. Elec. Eng. J.*, pp. 22–27, April, 1940. Describes changes made to Rugby VLF antenna in 1927 and in 1937.

32. R. A. Weagand: "Design of Guy-supported Towers for Radio Telegraphy," *Proc. IRE*, vol. 3, pp. 135–159, June, 1915.

33. A. W. Buel: "The Development of the Standard Design for Self-supporting Radio Towers for the United Fruit and Tropical Radio Telegraph Companies," *Proc. IRE*, vol. 12, pp. 29–82, February, 1924.

34. Jacob Feld: "Radio Antennas Suspended from 1000 Foot Towers," *J. Franklin Inst.*, vol. 239, pp. 363–390, May, 1945. Describes the mechanical design of a flat-top antenna on guyed masts.

35. W. W. Brown: "Radio Frequency Tests on Antenna Insulators," *Proc. IRE*, vol. 11, pp. 495–522, October, 1923. Discusses design and electrical tests of porcelain insulators for VLF antennas.

36. W. W. Brown and J. E. Love: "Design and Efficiencies of Large Air Core Inductances," *Proc. IRE*, vol. 13, pp. 755–766, December, 1925. Describes several designs and characteristics of VLF antenna tuning coils.

37. H. P. Miller, Jr.: "The Insulation of a Guyed Mast," *Proc. IRE*, vol. 15, pp. 225–243, March, 1927. Discusses the value of mast and guy insulation in VLF antennas and describes procedures to determine their voltage duties and best placement.

38. IRE Standards on Antennas, Modulation Systems, and Transmitters, Definition of Terms, 1948, and Standards on Antennas, Methods of Testing, 1948.

39. E. D. Sunde: "Earth Conduction Effects in Transmission Systems," D. Van Nostrand Company, Inc., Princeton, N.J., 1949. Contains formulas useful in the design of multiple-star ground systems.

Chapter 20

MEDIUM-FREQUENCY BROADCAST ANTENNAS

Howard T. Head

A. D. Ring & Associates
Washington, D.C.

20.1. INTRODUCTION

General. Medium-frequency broadcast transmitting antennas are generally vertical radiators ranging in height from one-sixth to five-eighths wavelength or higher, depending upon the operating characteristics desired and economic considerations. The physical heights vary from about 150 to 800 or 900 ft above ground, making the use of towers as radiators practical. The towers may be guyed or self-supporting; they are usually insulated from ground at the base, although grounded, shunt-excited radiators are occasionally employed.

Scope of Design Data. The design formulas and data in this chapter are primarily applicable to broadcast service (535 to 1,605-kc band). However, the basic design principles are valid for transmitting antennas for other services in the medium-frequency band (300 to 3,000 kc).

Characteristics of Radiators. Maximum radiation is produced in the horizontal plane, increasing with radiator height up to a height of about five-eighths wavelength. The radiated field from a single tower is uniform in the horizontal plane, but decreases with angle above the horizon and is zero toward the zenith. Radiators taller than one-half wavelength have a minor lobe of radiation at high vertical angles; for a height of one wavelength, the energy in this lobe is maximum and negligible energy is radiated in the horizontal plane. Radiators taller than five-eighths wavelength may be utilized by sectionalizing the tower approximately each half wavelength (Franklin type) and supplying the current to each section in the same relative phase. Figure 20-1 shows vertical radiation patterns for several commonly employed antenna heights, both for constant power and for constant radiated field in the horizontal plane.

Ground Currents. Current return takes place through the ground plane surrounding the antenna. High earth current densities are encountered and require metallic ground systems to minimize losses.

Choice of Plane of Polarization. Vertical polarization is almost universally employed because of superior ground-wave and sky-wave propagation characteristics. Ground-wave attenuation is much greater for horizontal than for vertical polarization, and

ionospheric propagation of horizontally polarized signals is more seriously influenced by geomagnetic latitude and direction of transmission. Horizontal antennas immediately above ground produce negligible fields in the horizontal plane, but radiate relatively large fields at high vertical angles for low antenna heights. This high-angle radiation is desirable only under special circumstances.
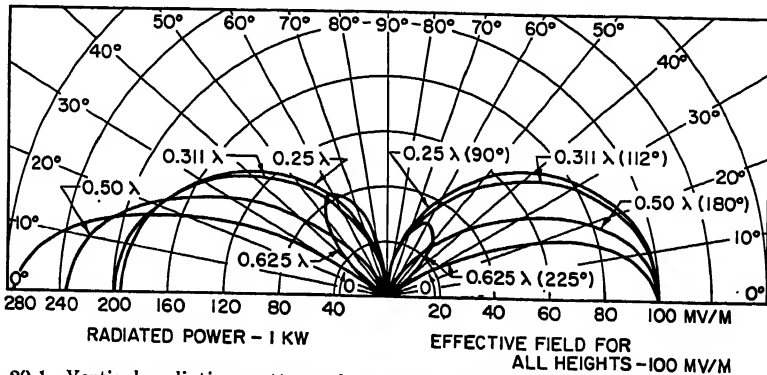
FIG. 20-1. Vertical radiation patterns for different heights of vertical antennas. (*FCC Broadcast Technical Standards.*)

Performance Required of Medium-frequency Broadcast Antennas. The performance required is determined by the class of station and channel assignment. In North America, three classes of broadcast channel are established: clear, regional, and local. Class I stations, operating on clear channels, are assigned to provide ground-wave service during daytime and both ground-wave and sky-wave service at night. All other classes of station are assigned to render ground-wave service only. Class II stations are secondary stations operating on clear channels, employing directional antennas to protect the service areas of Class I stations. Class III stations are assigned to regional channels and employ directional antennas where required for mutual protection. Class IV stations are assigned to local channels; both directional and nondirectional antennas are authorized.

Minimum required antenna performance and power limitations for each class of broadcast station in North America are established by treaty as shown in Table 20-1.

Table 20-1. Antenna Performance and Power Limitations

Class of station	Required minimum effective field for 1-kw power (unattenuated field at 1 mile), mv/meter	Minimum and maximum power, kw*
I	225	10 –50
II	175	0.25–50
III	175	0.5 –5
IV	150	0.1 –1

* Higher powers may be employed on certain channels.

Class I stations, which render both ground-wave and sky-wave service at night, require radiation patterns in the vertical planes to provide maximum sky-wave signal

beyond the primary (ground-wave) service area and minimum sky-wave signal within the primary area (antifading antennas)[1].

20.2. CHARACTERISTICS OF VERTICAL RADIATORS

Assumptions Employed in Calculating Radiator Characteristics. Characteristics of tower antennas are ordinarily computed assuming sinusoidal current distribution in a thin conductor over a perfectly conducting plane earth, with wavelength along the radiator equal to the wavelength in free space. The effect of the earth plane is represented by an *image* of the antenna as shown in Fig. 20-2. These assumptions provide sufficiently accurate results for most purposes, but in the determination of base operating resistance and reactance the finite cross section of the tower must be taken into account. Also, the finite cross section modifies the vertical radiation patterns slightly. This effect is of significance only in antifading antennas for clear channel stations and in certain directional antenna systems (discussed in Sec. 20.4, Directional Antennas). Except as noted, all formulas and data in this chapter are based on the assumptions stated above.

Field Produced by Vertical Radiator. The field in the horizontal plane is a function of the current flowing and the electrical height. For *uniform* current in a vertical radiator over a perfectly conducting plane earth, the radiated field is 0.651 mv/meter (unattenuated field at 1 mile) per degree-ampere. For other current distributions, the radiation is proportional to the maximum current and the *form factor K* of the antenna. For sinusoidal current distribution, the radiated field is

FIG. 20-2. Current distribution on vertical antenna and image of vertical antenna over perfectly conducting plane.

$$E_r = 37.25 I_0 (1 - \cos G) \qquad \text{unattenuated field, mv/meter at 1 mile} \qquad (20\text{-}1)$$

where I_0 = loop current, amp
$1 - \cos G = K$, form factor for sinusoidal current distribution
G = electrical height of radiator above ground

Radiation Resistance. The loop current I_0 is related to the radiated power P_r by the *loop radiation resistance* $R_r = P_r / I_0^2$. Figure 20-3 shows the radiated field for a power of 1 kw and the radiation resistance as a function of antenna height G. The radiation resistance may be calculated from

$$R_r = 15\{4 \cos^2 G \, \text{Cin} \, (2G) - \cos 2G \, \text{Cin} \, (4G) - \sin 2G[2\text{Si} \, (2G) - \text{Si} \, (4G)]\} \qquad (20\text{-}2)$$

where
$$\text{Cin} \, (x) = \int_0^x \frac{1 - \cos x}{x} \, dx \qquad \text{(cosine integral)}$$
$$= \ln x + C - \text{Ci} \, (x)$$
$$\text{Ci} \, (x) = -\int_x^\infty \frac{\cos x}{x} \, dx \qquad \text{(cosine integral)}$$
$$C = 0.5772 \cdot \cdot \cdot \cdot \text{(Euler's constant)}$$
$$\text{Si} \, (x) = \int_0^x \frac{\sin x}{x} \, dx \qquad \text{(sine integral)}$$

Operating Base Resistance. For sinusoidal current distribution, the *base radiation resistance* is related to the loop radiation resistance by R_r(base) $= R_{r(\text{loop})}/\sin^2 G$. However, the actual base resistance of a practical tower radiator may vary widely from this value because of the finite cross section of the tower and other effects. The operating base resistance and reactance may be estimated from Fig. 20-4a and b,[2] which shows the base resistance and reactance as a function of the *characteristic impedance* Z_0 of the radiator, given approximately by

$$Z_0 = 60 \left(\ln \frac{2G}{a} - 1 \right) \quad \text{ohms} \tag{20-3}$$

where a = equivalent radius of antenna [Chap. 3 and Eq. (21-40)]. Resistance and reactance measurements by Brown and Woodward[3] on cylindrical scale models of a tower antenna over a reflecting plane are given in Figs. 3-3 and 3-4 where the notation for the height A corresponds to the notation G of this chapter.
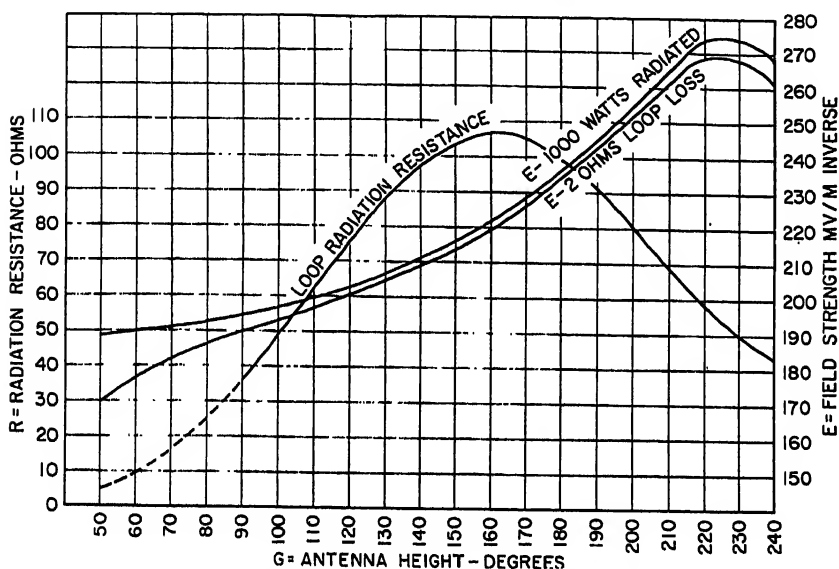
FIG. 20-3. Radiated field and radiation resistance as a function of antenna height G.

Vertical-radiation Characteristic. The relative field pattern in a vertical plane through the radiator is known as the *vertical-radiation characteristic*. It is defined as having unit value in the horizontal plane ($\psi = 0°$).* Based on the assumptions stated above, the vertical-radiation characteristic is

$$f(\psi) = \frac{\cos (G \sin \psi) - \cos G}{(1 - \cos G) \cos \psi} \tag{20-4}$$

Values of the vertical-radiation characteristics for a number of antenna heights are given in Fig. 20-5.

---

* The symbol ψ is used in this Handbook to denote elevation angle above the horizontal plane, in accordance with IRE recommended standard notation. The symbol θ has been commonly used in medium-frequency antenna design to denote this angle, and this usage will be found in various references. However, the IRE recommendation is followed in this chapter to provide a notation consistent with that employed in the remainder of the book.
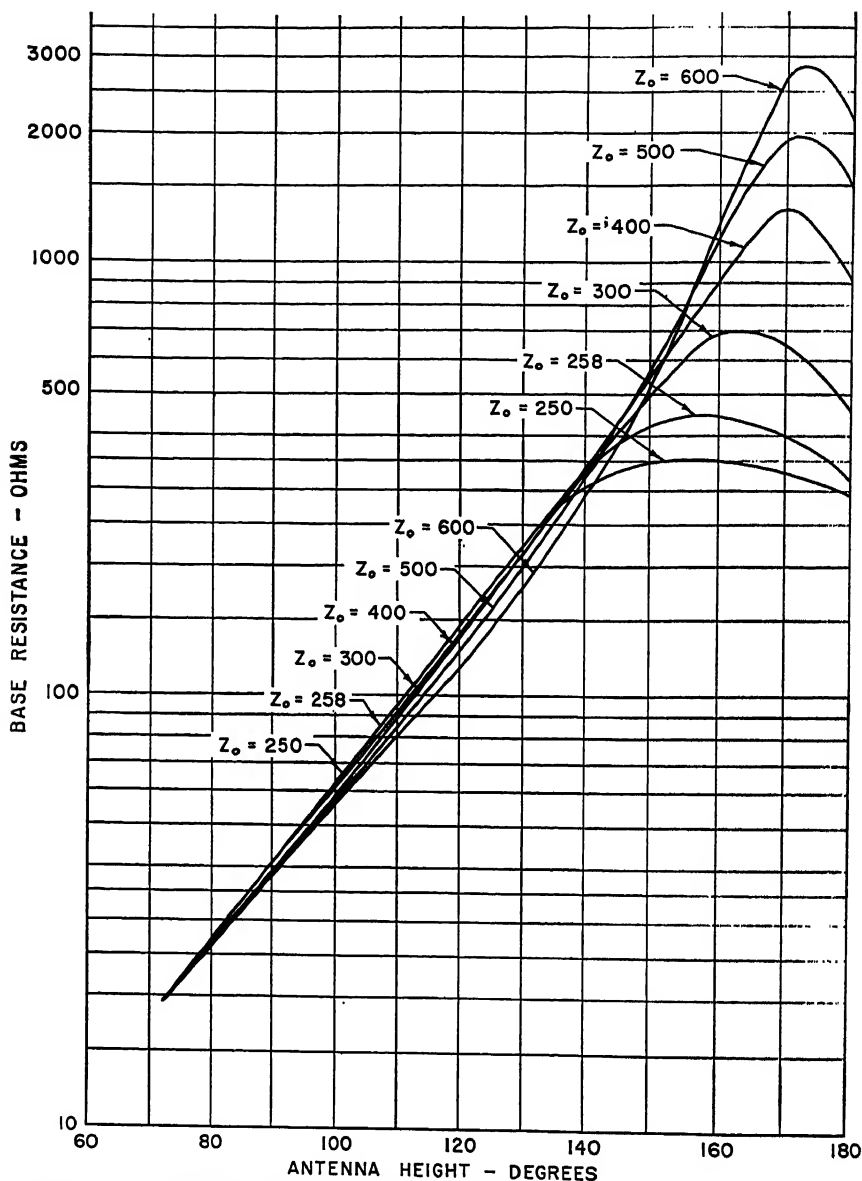
FIG. 20-4a. Base resistance of cylindrical antennas as a function of characteristic impedance Z_0. (*Reference 2.*)

General Formulas for Calculating Radiating Characteristics. The form factor and vertical-radiation characteristic establish the radiated field in the horizontal and vertical planes. For any current distribution, they may be determined from

$$Kf(\psi) = \int_0^G \frac{I(z)}{I_0} \cos \psi \cos (z \sin \psi) \, dz \qquad (20\text{-}5)$$
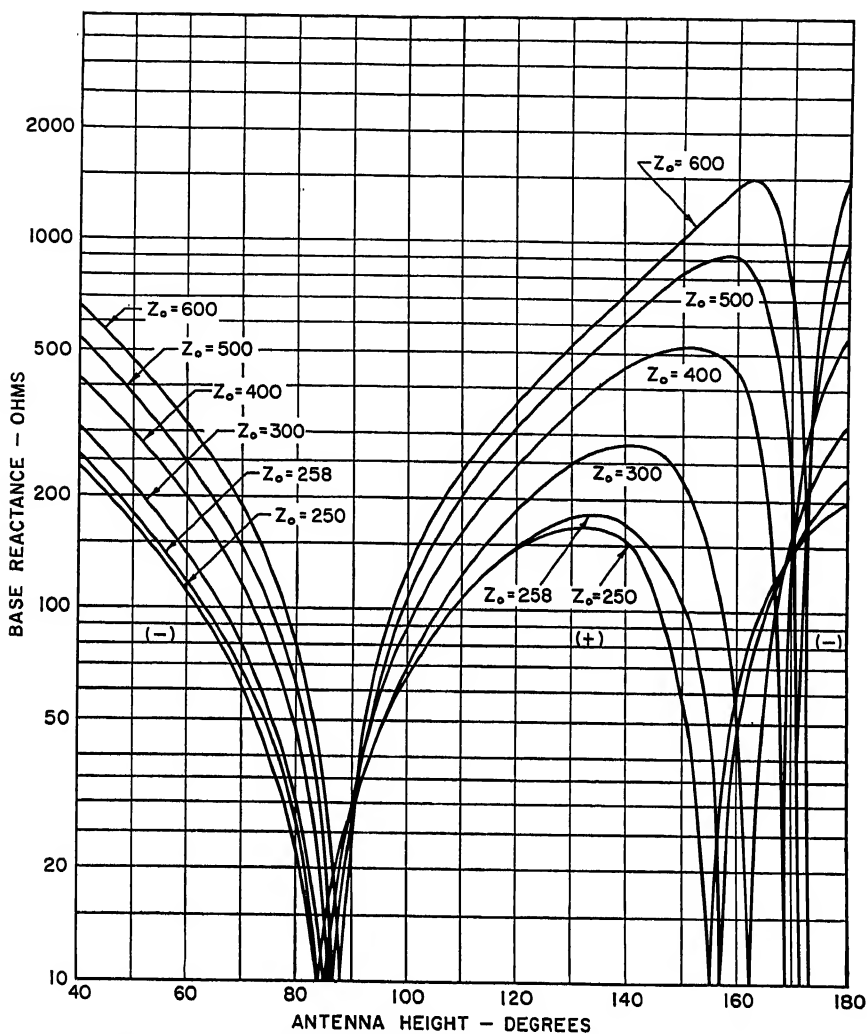
FIG. 20-4b. Base reactance of cylindrical antennas as a function of characteristic impedance Z_0. (*Reference 2*.)

where z = height of current element dz

$I(z)$ = current at z

I_0 = maximum current in radiator

ψ = elevation angle

The radiation resistance is*

$$R_r = 60 \int_0^{\pi/2} |Kf(\psi)|^2 \cos \psi \, d\psi \qquad (20\text{-}6)$$

These integrations may be performed graphically. It is convenient to integrate

* An alternative method of calculation is given by Carter.[4]
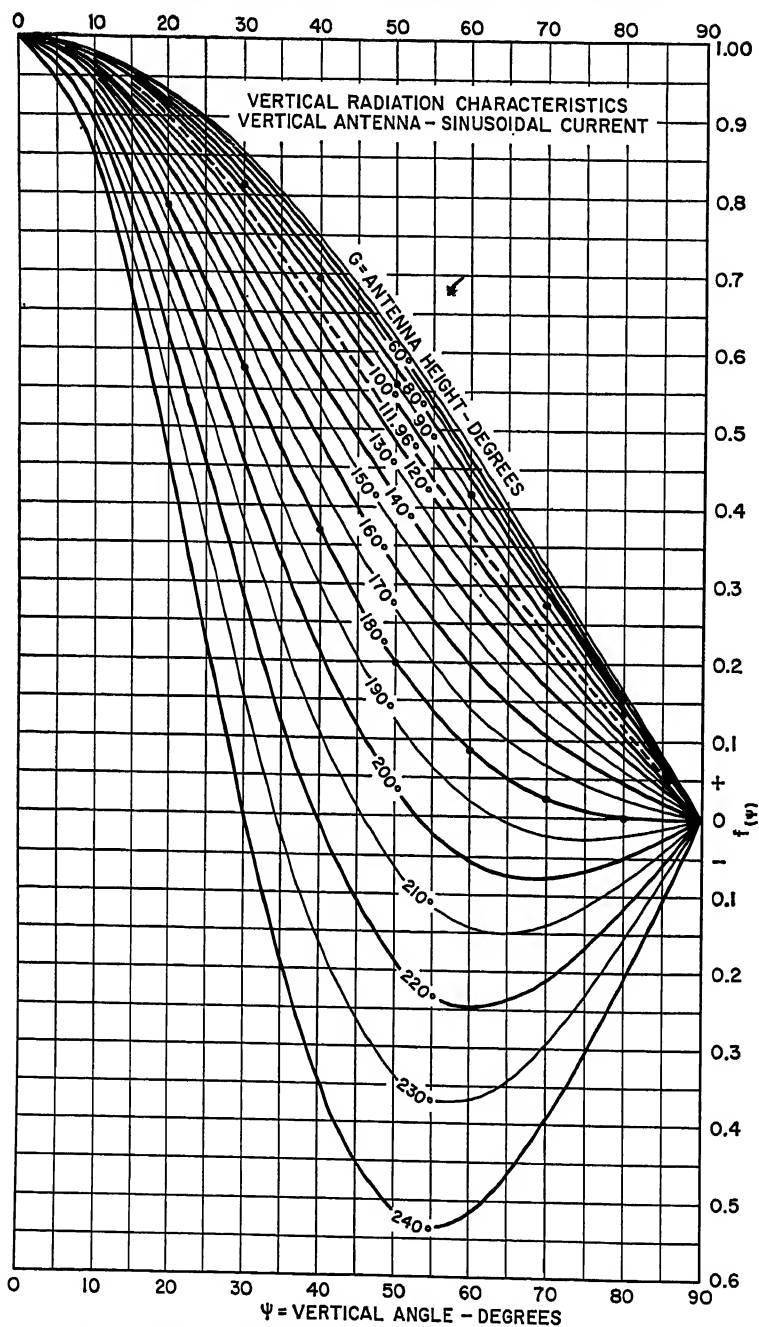
FIG. 20-5. Vertical-radiation characteristic as a function of antenna height G. The negative values correspond to minor lobes at the higher vertical angles.

Eq. (20-6) in polar coordinates by plotting $Kf(\psi) \sqrt{\cos \psi}$. The area of a quadrant in polar coordinates is $A = \int_0^{\pi/2} \frac{\rho^2}{2} d\theta$.

Effects of Finite Cross Section. *Current Distribution.* The effect of finite tower cross section on the current distribution and vertical-radiation characteristic may be taken into account by assuming a current distribution of the following form, suggested by Schelkunoff[2]:

$$I(z) = I_0 \sin [\gamma(G - z)] + jkI_0(\cos \gamma z - \cos \gamma G) \qquad (20\text{-}7)$$

where I_0 = maximum in-phase current

$\gamma = \lambda_0/\lambda$ ratio of wavelength in free space to wavelength along tower

G = height of tower, electrical degrees

$k \approx 50/(Z_0 - 45)$ for antenna heights near $\lambda/2$

$Z_0 = 60[\ln (2G/a) - 1]$, characteristic impedance of tower

a = equivalent tower radius [Eq. (21-40), p. 21-16]

When the cross section is vanishingly small, Z_0 is very large, $k \to 0$, and the current distribution approaches the simple sinusoidal.

For short towers, this current distribution is very nearly the simple sinusoidal; for a quarter-wave tower, the two are identical, except for the reduced wavelength. For
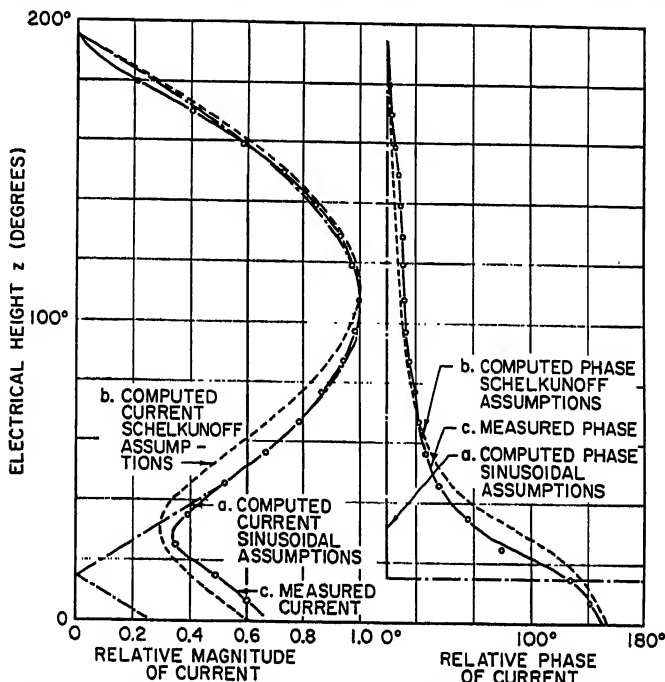
FIG. 20-6. Effect of finite cross section on current and phase distribution along a 190° tower. Curves *b* were computed from Eq. (20-7).

towers higher than a quarter wavelength, the departure becomes significant. Figure 20-6 shows the calculated relative amplitude and phase of the current for a height of 190°, based on both assumptions and the results of actual measurements. The measurements were taken at 1,420 kc on a guyed tower of uniform triangular cross section 360 ft high and 2 ft on a side. A value of $k = 0.132$ was established for these

dimensions. The value of γ, estimated by establishing the resonant length $\lambda/2$ for a tower of this cross section from Fig. 20-4b, was 1.094.

Vertical-radiation Characteristic and Form Factor. Applying Eq. (20-5) to the Schelkunoff current distribution, the form factor K_2 and vertical-radiation characteristic $f_2(\psi)$ become

$$K_2 f_2(\psi) = \frac{\gamma \cos \psi}{\gamma^2 - \sin^2 \psi} \left[\cos (G \sin \psi) - \cos \gamma G \right] + jk \cos \psi \left[\frac{\gamma \sin \gamma G \cos (G \sin \psi)}{\gamma^2 - \sin^2 \psi} \right.$$
$$\left. - \frac{\sin \psi \cos \gamma G \sin (G \sin \psi)}{\gamma^2 - \sin^2 \psi} - \frac{\cos \gamma G \sin (G \sin \psi)}{\sin \psi} \right] \quad (20\text{-}8)$$

Figure 20-7 shows vertical-radiation characteristics for a 190° radiator for the three current distributions of Fig. 20-6. The variations are relatively small and would
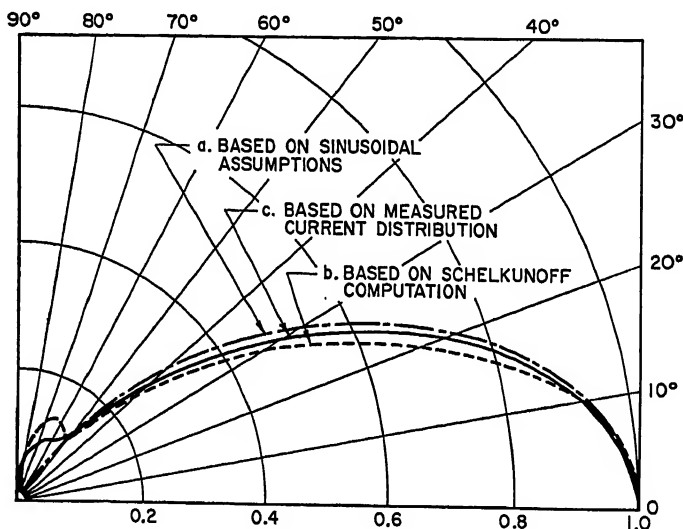
FIG. 20-7. Computed vertical-radiation characteristics for the current distributions of Fig. 20-6.

have only minor practical effects in nondirectional radiators or in directional-antenna systems employing identical towers. However, for directional-antenna systems employing tall towers of different heights, the variations in amplitude and phase of the vertical-radiation characteristics must be taken into account (see Sec. 20.4, Directional Antennas).

Shunt-fed Radiators. Energy may be supplied to a grounded tower by shunt excitation, using a slant-wire feed as shown in Fig. 20-8a. The dimensions h/λ and d/λ shown in the figure determine the impedance at the end of the slant wire. Figure 20-8a shows the impedance of a quarter-wave shunt-fed tower as a function of those dimensions, as measured by Morrison and Smith.[5] Figure 20-8b shows the variation of impedance with frequency for a tower of fixed dimensions.

The currents in the slant wires and between the tap point and ground modify the vertical radiation pattern of the shunt-fed tower and result in a slight nonuniformity in radiation in the horizontal plane. Figure 20-9 shows typical variations in vertical pattern resulting from shunt feed. The radiated field from a shunt-fed tower is essentially the same as that from a series-fed tower of the same height.
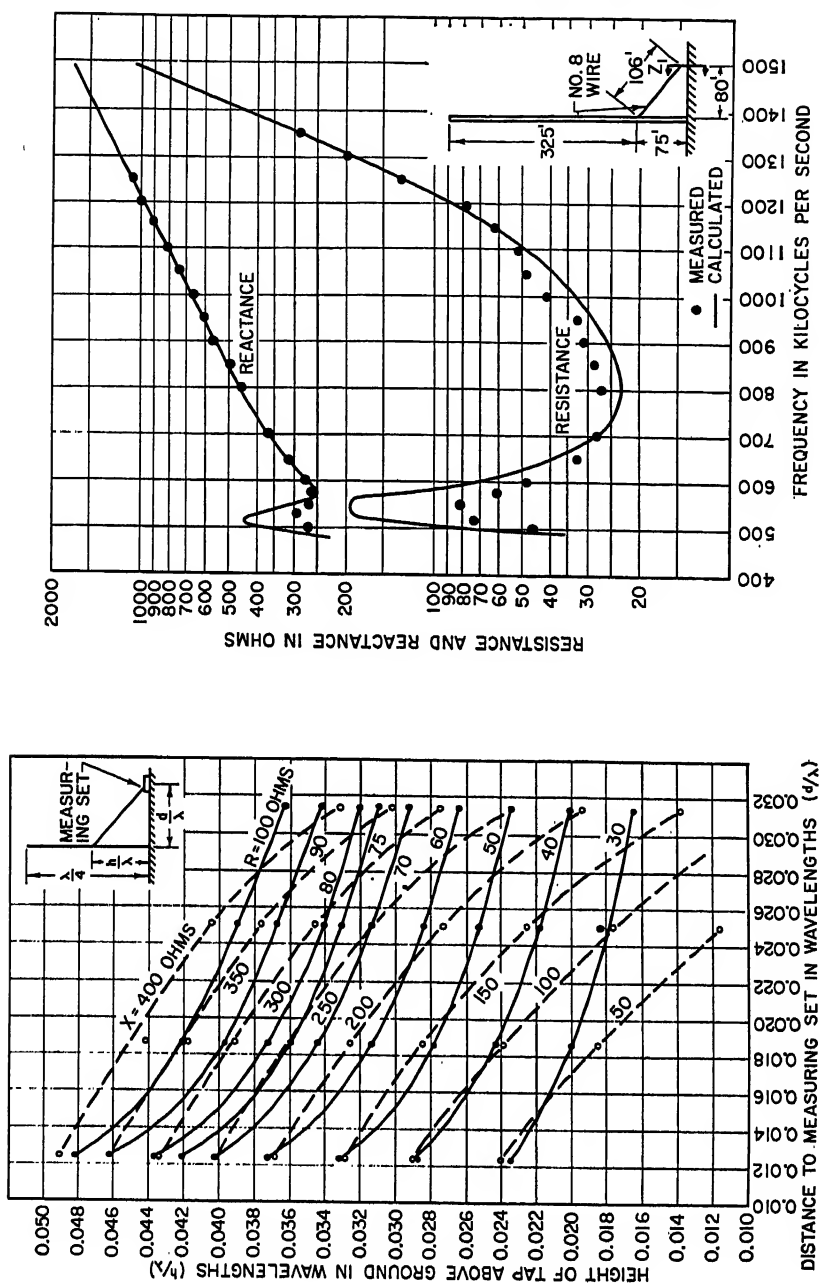
FIG. 20-8a. Measured impedance of quarter-wave shunt-fed tower as a function of feed-system dimensions.
FIG. 20-8b. Measured impedance of shunt-fed tower of fixed dimensions as a function of frequency.
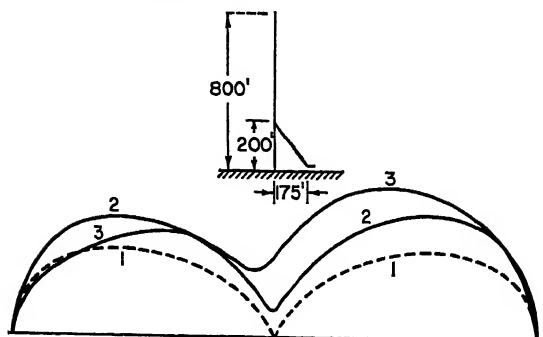
1. IDEAL VERTICAL PATTERN FROM SINUSOIDAL THEORY
2. MEASURED PATTERN NORMAL TO FEED-WIRE PLANE
3. MEASURED PATTERN IN PLANE OF FEED-WIRE

FIG. 20-9. Effect of shunt feed on vertical-radiation characteristic.   (*Reference 27.*)
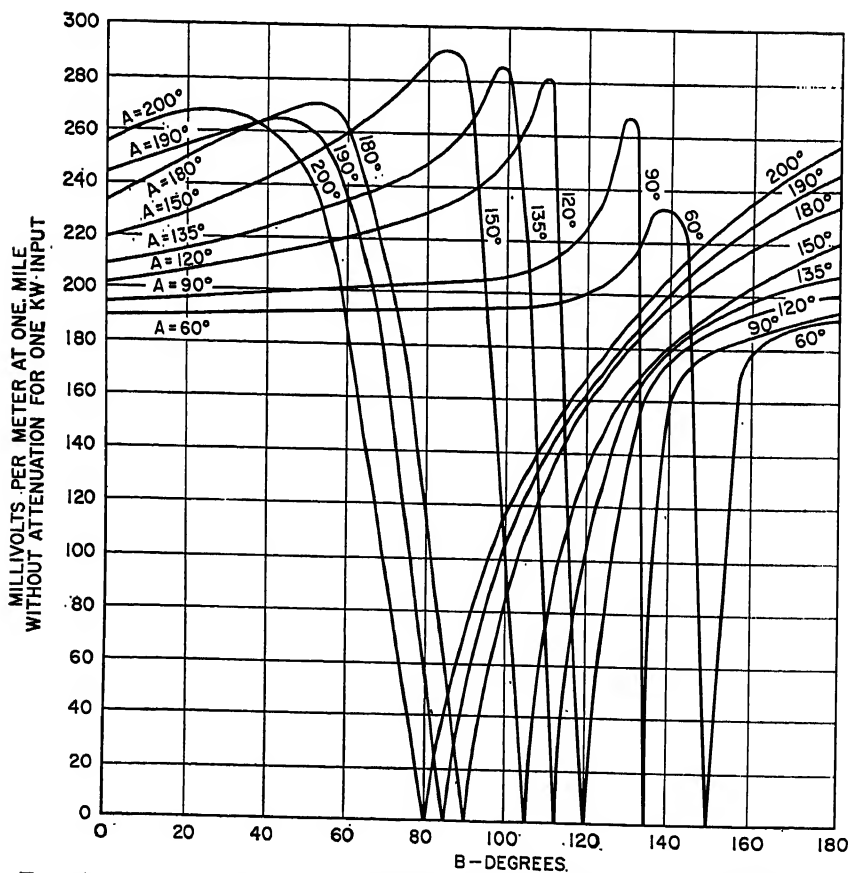
FIG. 20-10. Effect of top loading on effective field of vertical radiator.   (*Reference 6.*)

Top-loaded Radiators.   The radiating characteristics may be modified by altering the current distribution.   Top loading is sometimes employed, with a capacity "hat" mounted on the tower top.   This capacity has essentially the same effect (within
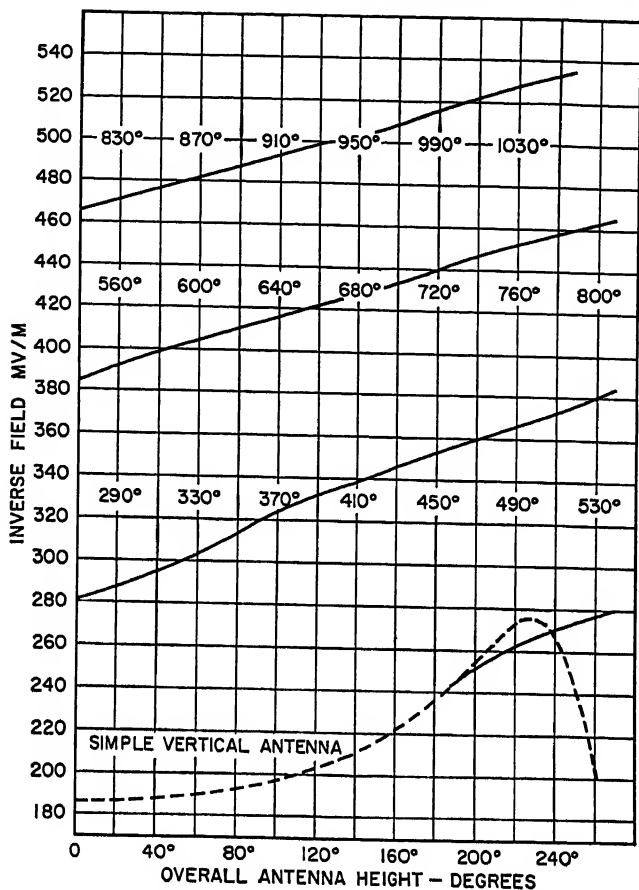
Fig. 20-11a. Radiating efficiency of sectionalized vertical radiator as a function of over-all height *G*.

limits) as increasing the tower height.   A capacity disk of radius *r* at the tower top is equivalent to an electrical length of

$$B = \frac{rZ_0}{15\pi} \qquad (20\text{-}9)$$

Z_0 is defined in Eq. (20-3).

The vertical-radiation characteristic and form factor of the top-loaded antenna are given by[6]

$$Kf(\psi) = \frac{\cos B \cos (A \sin \psi) - \sin \psi \sin B \sin (A \sin \psi) - \cos G}{\cos \psi} \qquad (20\text{-}10)$$

where *A* = electrical height of vertical portion of antenna
    B = equivalent electrical height of top load [Eq. (20-9)]
    G = *A* + *B*

Figure 20-10 shows computed effective fields for top-loaded antennas of various heights.

Sectionalized Radiators. *Effects of Sectionalization.* Antenna heights above five-eighths wavelength may be employed to obtain increased effective field by dividing the tower with insulators into sections of approximately one-half wavelength. The currents in each section are maintained in phase. Figure 20-11a shows the computed increase in effective field using such sectionalization.

Fig. 20-11b. Two methods of sectionalizing vertical radiators.

For heights less than one wavelength, the tower may be sectionalized in either of the arrangements shown in Fig. 20-11b. The vertical-radiation characteristic for the two arrangements, based on simple sinusoidal current distribution, is

Case I:
$$Kf(\psi) = \frac{2 \cos (90 \sin \psi) \cos (H \sin \psi) + \cos (G_1 \sin \psi) - \cos G_1}{\cos \psi} \tag{20-11}$$

Case II:
$$Kf(\psi) = \frac{2 \cos (G_1 \sin \psi)[\cos (G_1 \sin \psi) - \cos G_1]}{\cos \psi} \tag{20-12}$$

Effects of Finite Cross Section of Sectionalized Radiators. The actual current distribution on sectionalized towers varies from simple sinusoidal in the manner dis-
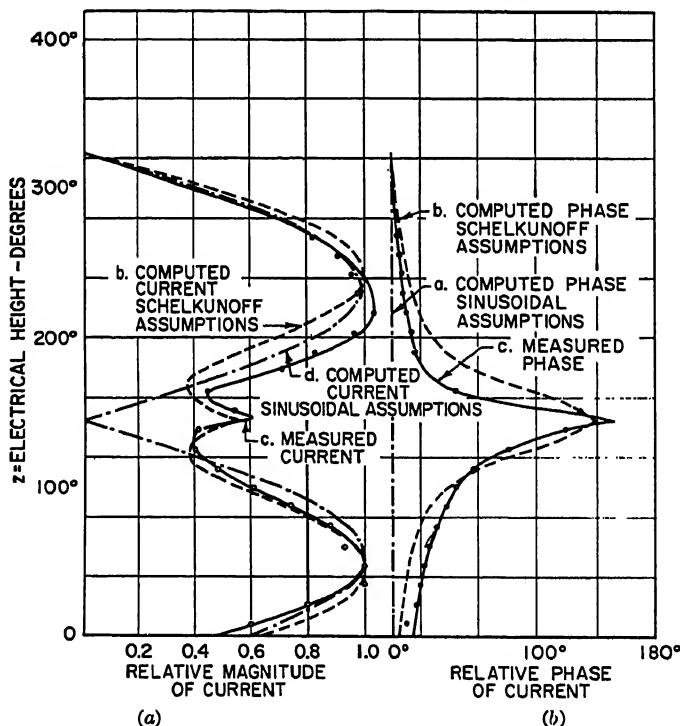
Fig. 20-12. Effect of finite cross section on current and phase distribution along a sectionalized tower having an over-all height of 322°. Curves *b* were computed from Eq. (20-13a) and (20-13b).

cussed above. In this case, the upper section of the tower is a half wavelength (or very nearly so) and the base termination is adjusted to provide the same current
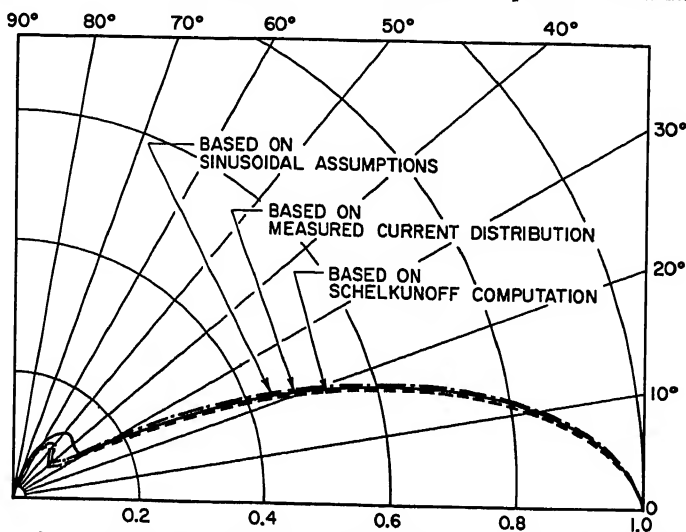
FIG. 20-13. Computed vertical-radiation characteristics for the current distributions of Fig. 20-12.
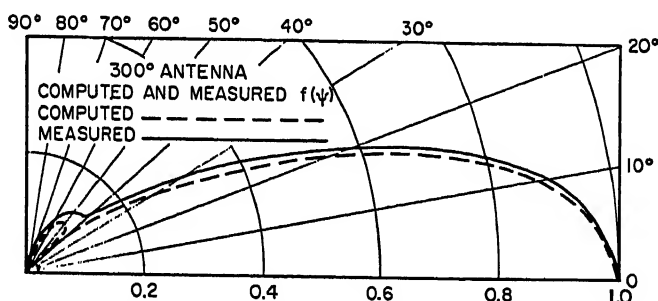
FIG. 20-14. Computed and measured vertical radiation patterns for the 300° sectionalized radiator in use at WHO, Des Moines, Iowa. The measurements were made through the use of a helicopter. (*Courtesy of Central Broadcasting Co.*)

distribution on the lower section as on the upper section. For these conditions, the currents are (Fig. 20-11b, Case I):

$$I_1(z)$$
$$\text{top section} = I_0 \sin \left[\gamma(G_0 - z)\right] + jkI_0\{1 + \cos \left[\gamma(G_1 - z)\right]\} \quad (20\text{-}13a)$$
$$I_2(z)$$
$$\text{bottom section} = I_0 \sin \left[\gamma(G_1 - z)\right] + jkI_0\{1 + \cos \left[\gamma(G_1 - z)\right]\} \quad (20\text{-}13b)$$

where $\gamma = \lambda_0/\lambda$, ratio of wavelength in free space to wavelength along tower.

The form factor and the vertical-radiation characteristic are given by

$$K_0 f_0(\psi) = \frac{\gamma \cos \psi}{\gamma^2 - \sin^2 \psi} \left[\cos \left(G_0 \sin \psi\right) - \cos \gamma G_1 - 2 \cos \gamma\pi \cos \left(G_1 \sin \psi\right)\right]$$
$$+ jk \cos \psi \left\{ \frac{\sin \left(G_0 \sin \psi\right)}{\sin \psi} + \frac{\gamma}{\gamma^2 - \sin^2 \psi} \left[\sin \gamma G_1 - 2 \sin \gamma\pi \cos \left(G_1 \sin \psi\right) \right. \right.$$
$$\left. \left. + \frac{\sin \psi \sin \left(G_0 \sin \psi\right)}{\gamma} \right] \right\} \quad (20\text{-}14)$$

Figure 20-12 shows the measured current distribution on a sectionalized tower compared with that for the two assumptions.   Figure 20-13 shows the vertical-radiation characteristics; curve C was determined from Eq. (20-5) by mechanical integration. Figure 20-14 is a measured vertical radiation pattern for a sectionalized tower having similar electrical dimensions.

20.3. GROUND SYSTEMS

General Requirements.   The ground system for a medium-frequency antenna usually consists of 120 buried copper wires, equally spaced, extending radially outward from the tower base to a minimum distance of one-quarter wavelength.   In addition, an exposed copper-mesh ground screen may be used around the base of the tower when high base voltages are encountered.
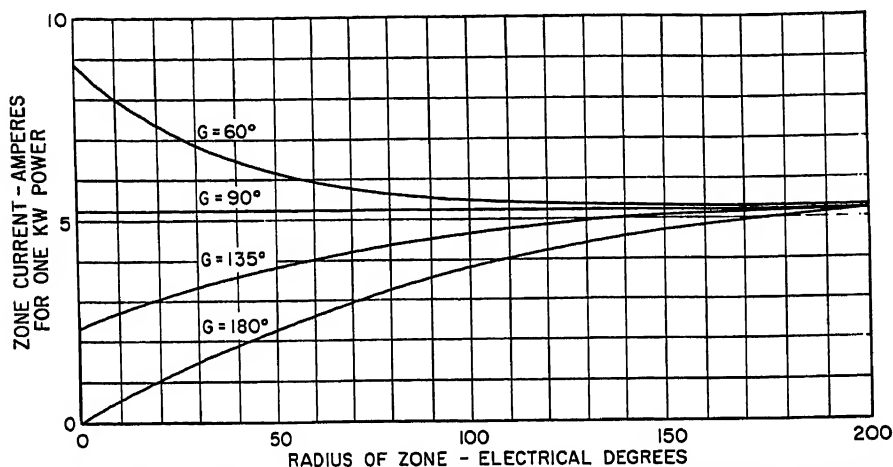
Fɪɢ. 20-15. Zone currents returning to the antenna as a function of antenna height G.

Wire size has a negligible effect on the effectiveness of the ground system and is chosen for mechanical strength; AWG No. 10 or larger is adequate.   The wires are buried for mechanical protection.   A depth of 4 to 6 in. is generally adequate, although the wires may be buried to a depth of several feet if desired in order to permit cultivation of the soil.   When such deep burial is required, the wires should descend to the required depth on a smooth, gentle incline from the tower base, reaching the ultimate depth some distance from the tower.   If this precaution is observed, the deep burial will have relatively little effect on the effectiveness of the ground system for typical soil conditions.

Nature of Ground Currents.   Ground currents are conduction currents returning directly to the base of the antenna.   The total earth current flowing through a cylinder of radius x concentric with the antenna is known as the *zone current*.   It is a function of tower height and is given by

$$I_{zone} = I_0[\sin r_2 - \cos G \sin x + j(\cos r_2 - \cos G \cos x)] \qquad (20\text{-}15)$$

where I_0 = loop antenna current

G = electrical height of antenna

$r_2 = \sqrt{x^2 + G^2}$

Figure 20-15 shows the variation of zone current with antenna height and zone radius.

Effect of Ground-system Losses on Antenna Performance. Ground-system losses dissipate a portion of the input power and reduce the field radiated from the antenna. These losses are equivalent to the power dissipated in a resistor in series with the antenna impedance.[7] Computed values of radiated field based on an assumed series loss resistance of 2 ohms give results for typical installations in good agreement with actual measured effective field strengths. The curves of Fig. 20-3, showing radiated field "with 2-ohm loss," are computed on the basis of this assumed power dissipation. For directional-antenna systems (Sec. 20.4), a series loss of 2 ohms is assumed for each radiator.

Effect of Local Soil Conductivity on Ground-system Requirements. A less elaborate ground system may be effective in soil of high local conductivity,[8,9] although adequate local-conductivity data are rarely available.

For a sea-water site (conductivity, approximately 4.6 mhos/meter), the salt water provides an adequate ground system; a submerged copper ground screen is employed to make "contact" with the salt water.

Ground Systems for Multielement Arrays. Individual ground systems are required for each tower of a multielement array. If the individual systems would overlap,

120 RADIALS SPACED EVENLY
AROUND EACH TOWER

COPPER BUS
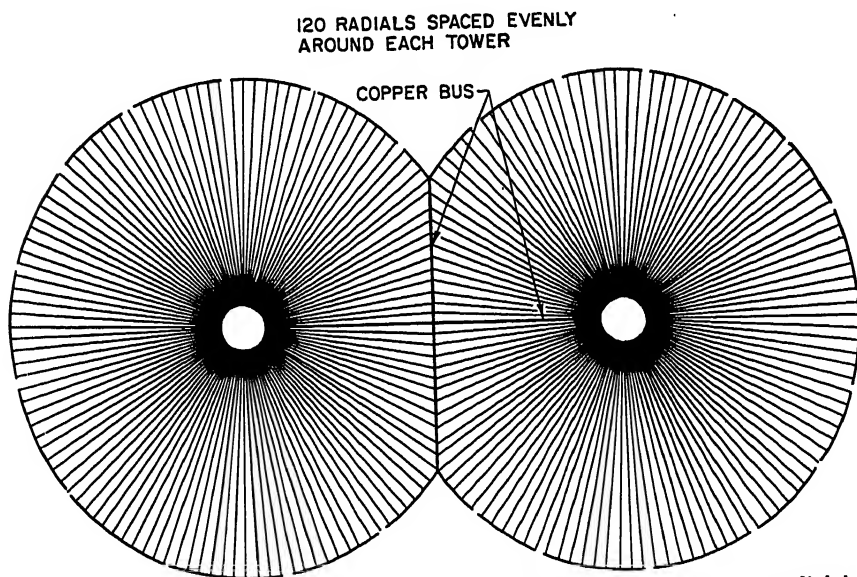
FIG. 20-16. A typical ground system for a two-element directional antenna. The adjoining systems do not overlap but are terminated in a common bus.

the adjoining systems are usually terminated in a common bus. Complete systems may be installed around each tower when high ground currents are expected. Figure 20-16 shows a typical multielement ground system.

20.4. DIRECTIONAL ANTENNAS

Purpose of Directional-antenna Systems. A directional antenna employs two or more radiators to produce radiation patterns in the horizontal and vertical planes different from those produced by a single radiator. Directional antennas are principally used to reduce the radiated signal toward other stations on the same or adjacent

channels to avoid interference, although the resulting concentration of radiated signal in other directions may be utilized to improve service to specific areas.

Permissible Values of Radiation. Methods of computing interference and establishing maximum permissible values of radiation to avoid interference are described in detail in the Federal Communications Commission (*FCC*) Broadcast Technical Standards.[25] For interference from ground-wave signals, radiation in the horizontal plane only is considered; from sky-wave signals, throughout a specified range of vertical angles. Suppression of radiation is required over sufficient arc to subtend the protected station's service area.

Computation of Pattern Shape. *Fundamental Considerations: Two-element Systems.* The principles underlying the computation of shape of radiation patterns from two-element arrays are fundamental and may be extended to the computation of shape of patterns from multielement arrays.
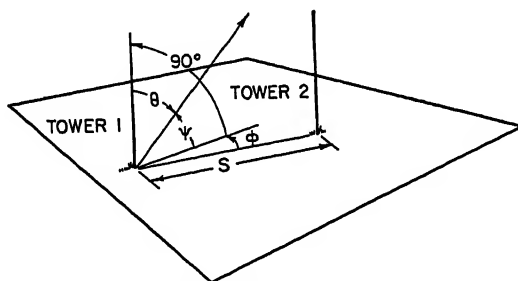
FIG. 20-17. Notation used in Eq. (20-16).

The field strength at any point from two radiators receiving r-f energy from a common source is the vector sum of the fields from each of the two radiators. At large distances the antenna system may be considered to be a point source of radiation. Referring to Fig. 20-17, and considering tower 1 to be reference, or zero, phase, the radiated field from the array at the angle φ, ψ is

$$E_r = E_1 f_1(\psi) \underline{/0} + E_2 f_2(\psi) \underline{/\alpha_2} \qquad (20\text{-}16)$$

where α_2, the difference in phase angle between the two fields, is the sum of the *time-phase-angle* difference A_2 and the *apparent space–phase-angle* difference:

$$\alpha_2 = s \cos \varphi_2 \cos \psi + A_2 \qquad (20\text{-}17)$$

where E_1 = field radiated by element 1

    E_2 = field radiated by element 2

    $f_1(\psi)$ = vertical-radiation characteristic of element 1

    $f_2(\psi)$ = vertical-radiation characteristic of element 2

For towers of equal height,

$$E_r = f(\psi)[E_1{}^2 + E_2{}^2 + 2E_1 E_2 \cos (s \cos \varphi \cos \psi + A_2)]^{\frac{1}{2}} \qquad (20\text{-}18)$$

Letting $F_2 = E_2/E_1$ and rearranging,

$$E_r = E_1 f(\psi) \sqrt{2F_2} \left[\frac{1 + F_2{}^2}{2F_2} + \cos (s \cos \varphi \cos \psi + A_2) \right]^{\frac{1}{2}} \qquad (20\text{-}19)$$

The second term under the last radical in Eq. (20-19) varies with φ and ψ from -1 to $+1$; the first term is always equal to or greater than $+1$ for real, positive values of F_2 and is unity when $F_2 = 1$.

The magnitude of E_r is a minimum when

$$\cos\,(s \cos \varphi \cos \psi + A_2) = -1 \tag{20-20}$$

which occurs when $s \cos \varphi \cos \psi + A_2 = 180 \pm 360n$ degrees; if $F_2 = 1$, E_r will be zero.

For $F_2 = 1$, Eq. (20-19) simplifies to

$$E_r = 2E_1 \cos \left(\frac{s}{2} \cos \varphi \cos \psi + \frac{A_2}{2} \right) \tag{20-21}$$

Combinations of equations of the two-element form are widely used in establishing and computing patterns for multielement arrays. Horizontal-plane patterns for two-element arrays for a variety of spacings and phasings are shown in Fig. 5-2. The patterns shown* are for equal fields in the two radiators ($F_2 = 1$); the effect of unequal fields is to "fill" the nulls of the pattern. For a given spacing the angular position of the minimum is changed only by changing the phase angle. The value of E_r is unchanged by substituting for F_2 its inverse $F'_2 = 1/F_2$.

Three or More Elements: General Equations. The pattern shape of directional arrays of three or more elements may be computed by an extension of Eq. (20-16). For three elements as shown in Fig. 20-18,
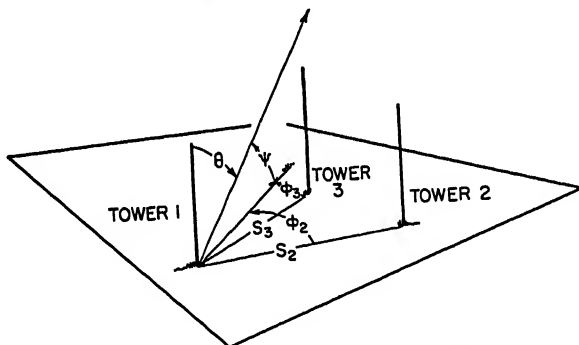
FIG. 20-18. Notation used in Eq. (20-22).

$$E_r = E_1 f_1(\psi)\underline{/0} + E_2 f_2(\psi)\underline{/\alpha_2} + E_3 f_3(\psi)\underline{/\alpha_3} \tag{20-22}$$

or in general for n elements,

$$E_r = E_1 f_1(\psi)\underline{/0} + E_2 f_2(\psi)\underline{/\alpha_2} + E_3 f_3(\psi)\underline{/\alpha_3} + \cdots + E_n f_n(\psi)\underline{/\alpha_n} \tag{20-23}$$

where $\alpha_n = s_n \cos \varphi_n \cos \psi + A_n$.

Three or More Elements: Simplified Formulas for Special Cases. The general formula is unwieldy for most design purposes and does not provide convenient means for establishing the angular position or depth of the minima. Many commonly used array configurations may be computed through the use of the following formulas:
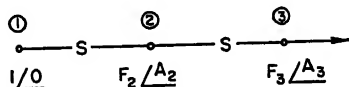
FIG. 20-19

* The phase angle A_2 is equal to $360°T$.

$$E_r = E_1 f(\psi)\ \sqrt{4 r_2 r_3}\ \left\{ \left[\frac{1 + r_2{}^2}{2 r_2} + \cos\ (s \cos \varphi \cos \psi + a_2) \right] \right.$$

$$\left. \left[\frac{1 + r_3{}^2}{2 r_3} + \cos\ (s \cos \varphi \cos \psi + a_3) \right] \right\}^{\frac{1}{2}} \quad (20\text{-}24)$$

$$F_2 \underline{/A_2} = r_2 \underline{/a_2} + r_3 \underline{/a_3}$$
$$F_3 \underline{/A_3} = r_2 r_3 \underline{/a_2 + a_3}$$
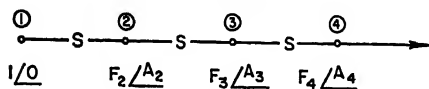
Fɪɢ. 20-20

$$E_r = E_1 f(\psi)\ \sqrt{8 r_2 r_3 r_4}\ \left\{ \left[\frac{1 + r_2{}^2}{2 r_2} + \cos\ (s \cos \varphi \cos \psi + a_2) \right] \right.$$

$$\left[\frac{1 + r_3{}^2}{2 r_3} + \cos\ (s \cos \varphi \cos \psi + a_3) \right]$$

$$\left. \left[\frac{1 + r_4{}^2}{2 r_4} + \cos\ (s \cos \varphi \cos \psi + a_4) \right] \right\}^{\frac{1}{2}} \quad (20\text{-}25)$$

$$F_2 \underline{/A_2} = r_2 \underline{/a_2} + r_3 \underline{/a_3} + r_4 \underline{/a_4}$$
$$F_3 \underline{/A_3} = r_2 r_3 \underline{/a_2 + a_3} + r_2 r_4 \underline{/a_2 + a_4} + r_3 r_4 \underline{/a_3 + a_4}$$
$$F_4 \underline{/A_4} = r_2 r_3 r_4 \underline{/a_2 + a_3 + a_4}$$
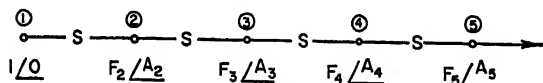
Fɪɢ. 20-21

$$E_r = E_1 f(\psi)\ \sqrt{16 r_2 r_3 r_4 r_5}\ \left\{ \left[\frac{1 + r_2{}^2}{2 r_2} + \cos\ (s \cos \varphi \cos \psi + a_2) \right] \right.$$

$$\left[\frac{1 + r_3{}^2}{2 r_3} + \cos\ (s \cos \varphi \cos \psi + a_3) \right] \left[\frac{1 + r_4{}^2}{2 r_4} + \cos\ (s \cos \varphi \cos \psi + a_4) \right]$$

$$\left. \left[\frac{1 + r_5{}^2}{2 r_5} + \cos\ (s \cos \varphi \cos \psi + a_5) \right] \right\}^{\frac{1}{2}} \quad (20\text{-}26)$$

$$F_2 \underline{/A_2} = r_2 \underline{/a_2} + r_3 \underline{/a_3} + r_4 \underline{/a_4} + r_5 \underline{/a_5}$$
$$F_3 \underline{/A_3} = r_2 r_3 \underline{/a_2 + a_3} + r_2 r_4 \underline{/a_2 + a_4} + r_2 r_5 \underline{/a_2 + a_5}$$
$$\qquad\qquad + r_3 r_4 \underline{/a_3 + a_4} + r_3 r_5 \underline{/a_3 + a_5} + r_4 r_5 \underline{/a_4 + a_5}$$
$$F_4 \underline{/A_4} = r_2 r_3 r_4 \underline{/a_2 + a_3 + a_4} + r_2 r_3 r_5 \underline{/a_2 + a_3 + a_5}$$
$$\qquad\qquad + r_2 r_4 r_5 \underline{/a_2 + a_4 + a_5} + r_3 r_4 r_5 \underline{/a_3 + a_4 + a_5}$$
$$F_5 \underline{/A_5} = r_2 r_3 r_4 r_5 \underline{/a_2 + a_3 + a_4 + a_5}$$
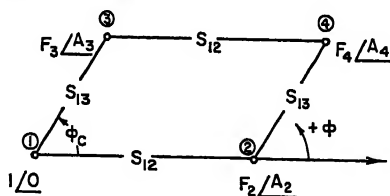
Fɪɢ. 20-22

$$E_r = E_1 f(\psi)\ \sqrt{4 F_2 F_3}\ \left\{ \left[\frac{1 + F_2{}^2}{2 F_2} + \cos\ (s_{12} \cos \varphi \cos \psi + A_2) \right] \right.$$

$$\left. \left[\frac{1 + F_3{}^2}{2 F_3} + \cos\ [s_{13} \cos\ (\varphi - \varphi_c) \cos \psi + A_3] \right] \right\}^{\frac{1}{2}} \quad (20\text{-}27)$$

provided $F_4 \underline{/A_4} = F_2 F_3 \underline{/A_2 + A_3}$.

In these formulas, the field is the product of several two-element-array expressions and will be zero whenever any of the component expressions are zero. For $r_n \neq 1$, the position of the minima may be shifted slightly; however, this shift is usually small. Formulas (20-24) to (20-27) are valid for computing patterns in the vertical planes only for towers of equal height.

Other frequently employed expressions for the radiated field from multielement arrays are as follows.
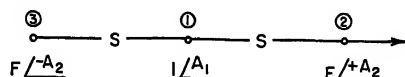
FIG. 20-23

$$E_r = E_1[f_1(\psi)\cos A_1 + 2Ff_{2,3}(\psi)\cos(s\cos\varphi\cos\psi + A_2) + jf_1(\psi)\sin A_1] \quad (20\text{-}28)$$

The imaginary term vanishes for $A_1 = 0$, and nulls will be produced in the horizontal plane where

$$s\cos\varphi + A_2 = \cos^{-1}\left(-\frac{1}{2F}\right) \quad (20\text{-}29)$$

Formula (20-28) may be employed for computing patterns in the vertical planes where the center tower is of a different height from the end towers; the latter, however, must be of the same height.
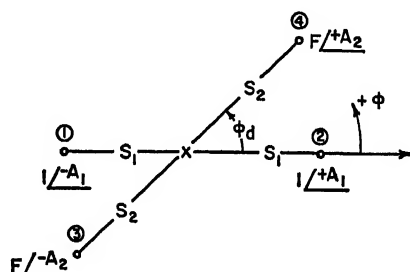
FIG. 20-24

$$E_r = 2E_1\{f_{1,2}(\psi)\cos(s_1\cos\varphi\cos\psi + A_1) + Ff_{3,4}(\psi)\cos[s_2\cos(\varphi - \varphi_d)\cos\psi + A_2]\} \quad (20\text{-}30)$$

Formula (20-30) may be employed for towers of unequal height if $f_1(\psi) = f_2(\psi)$ and $f_3(\psi) = f_4(\psi)$.

Computation of Pattern Size

1. *General.* Formulas (20-16) to (20-30) establish the shape of radiation patterns; to determine the magnitude of radiation, the *reference field* E_1 must be evaluated.

2. *Total resistance.* The current I_1 in the reference element is related to the total radiated power P_r by the *total resistance* R_t of the array:

$$R_{t1} = \frac{P_r}{I_1{}^2} \quad (20\text{-}31)$$

where the subscript 1 indicates that the total resistance is referred to the current in element 1. The radiated field is directly proportional to the current, and

$$E_1 = E_0\left(\frac{R_{r1}}{R_{t1}}\right)^{1/2} \quad (20\text{-}32)$$

where E_0 is the effective field of the reference element, operating independently and without loss, and R_{r1}, the radiation resistance, as shown in Fig. 20-3. The total resistance is calculated from the operating resistances of each element of the array, as discussed in the following section.

3. *Mutual impedance: definition for antenna case.* The mutual impedance between two antennas is defined in the usual manner:

$$Z_{12} = Z_{21} = \frac{V_1}{I_2} = \frac{V_2}{I_1} \tag{20-33}$$

The mutual impedance is a complex quantity:

$$Z_{12} \underline{/\sigma_{12}} = R_{12} + jX_{12} = (R_{12}{}^2 + X_{12}{}^2)^{\frac{1}{2}} \underline{/\tan^{-1}\frac{X_{12}}{R_{12}}} \tag{20-34}$$

The mutual impedance is a function of the spacing between the antennas and the height of the elements. Figure 20-25 shows the magnitude and phase angle of the mutual impedance for equal antenna heights over the commonly encountered range of antenna heights and spacings. Figure 20-26 shows values for antennas of unequal height.[*] The general equations for mutual resistance and reactance between two antennas of unequal height have been derived by Cox in Ref. 10.

4. *Operating resistance of radiators in a directional-antenna system.* The *operating resistance* of a radiator in a directional array is the sum of the radiation resistance R_r, an assumed loss resistance R_a (see Sec. 20.3, Ground Systems), and the *coupled resistance R_c*:

$$R_0 = R_r + R_a + R_c \tag{20-35}$$

The coupled resistance of element 1 is

$$R_{c1} = M_{12}Z_{12}\cos(\mu_{12} + \sigma_{12}) + M_{13}Z_{13}\cos(\mu_{13} + \sigma_{13})$$
$$+ \cdots + M_{1n}Z_{1n}\cos(\mu_{1n} + \sigma_{1n}) \tag{20-36}$$

and the coupled reactance is

$$X_{c1} = M_{12}Z_{12}\sin(\mu_{12} + \sigma_{12}) + M_{13}Z_{13}\sin(\mu_{13} + \sigma_{13})$$
$$+ \cdots + M_{1n}Z_{1n}\sin(\mu_{1n} + \sigma_{1n}) \tag{20-37}$$

where M_{1n} = current ratio between tower n and tower 1
Z_{1n} = mutual impedance between tower n and tower 1
μ_{1n} = phase angle of current between tower n and tower 1
σ_{1n} = phase angle of Z_{1n}

Note that M_{12} is the *current* ratio of tower 2 referred to tower 1. The loop-current ratio and the *field* ratio are related by the ratio of the form factors:

$$\frac{M_{12}}{F_{12}} = (1 - \cos G_1)/(1 - \cos G_2) \qquad \text{(loop-current reference)} \tag{20-38}$$

The base resistance of a radiator in a directional array will usually be different from the operating resistance computed from Eq. (20-35). The determination of base operating resistance is discussed below.

5. *Computation of total resistance: formulas.* The total resistance R_{t1} is

$$R_{t1} = R_{01} + M_{12}{}^2R_{02} + M_{13}{}^2R_{03} + \cdots + M_{1n}{}^2R_{0n} \tag{20-39}$$

To check the computation, and in preliminary work where individual operating resist-

---

[*] Graphs of mutual impedance between antennas of unequal height, for a wide range of different heights, are given by Carl E. Smith in Ref. 29.
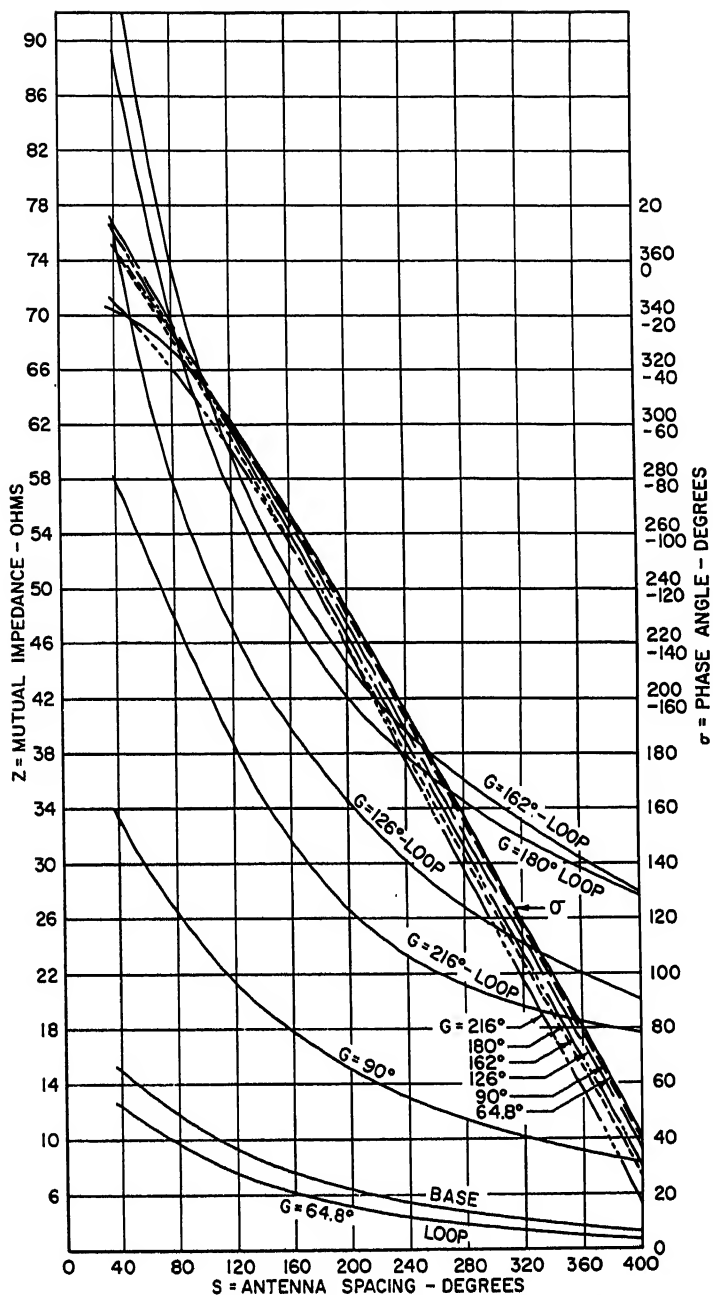
Fig. 20-25. Mutual impedance between vertical antennas of equal height as a function of antenna height G and spacing S, in electrical degrees.
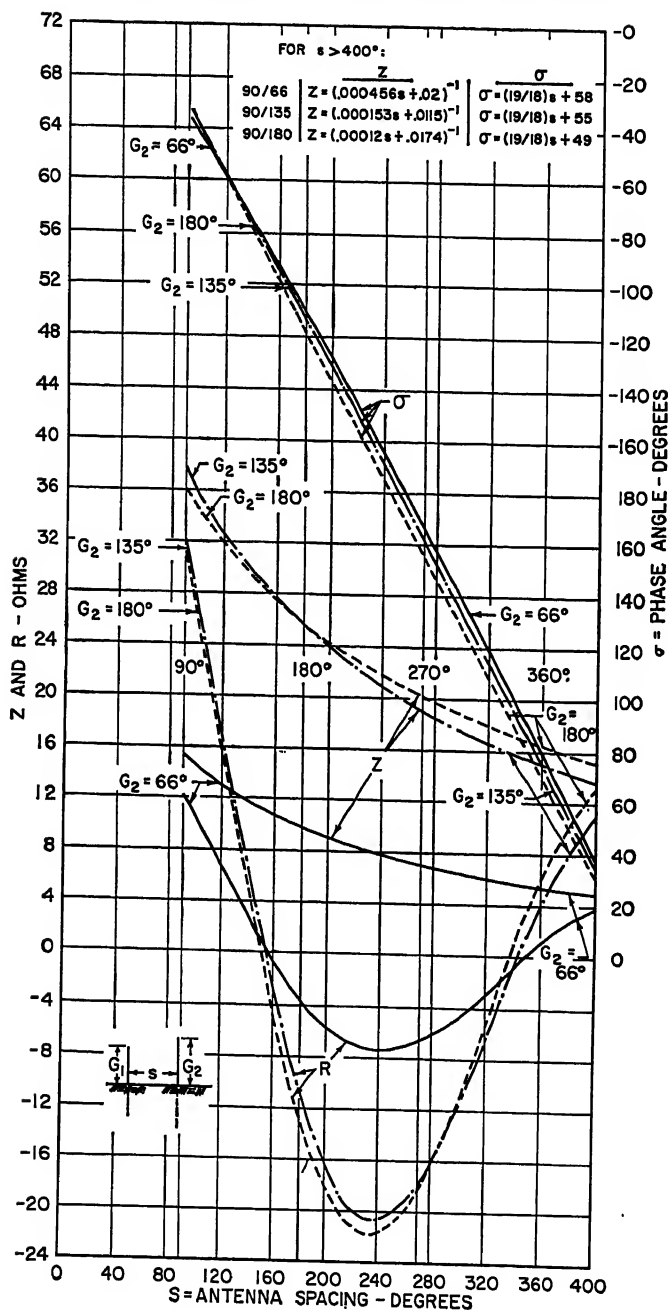
FIG. 20-26. Mutual impedance (loop current reference) between a quarter-wave vertical antenna and a second vertical antenna of the height indicated (G_2 in electrical degrees) as a function of spacing S in electrical degrees.

ances are not needed, the following formula may be used:

$$R_{t1} = (1 + M_{12}{}^2 + M_{13}{}^2 + \cdots + M_{1n}{}^2)\,(R_r + R_a)$$
$$+ 2R_{12}M_{12}\cos\mu_{12} + 2R_{13}M_{13}\cos\mu_{13} + \cdots$$
$$+ 2R_{1n}M_{1n}\cos\mu_{1n} + 2R_{23}M_{12}M_{13}\cos\mu_{23}$$
$$+ 2R_{24}M_{12}M_{14}\cos\mu_{24} + \cdots$$
$$+ 2R_{mn}M_{1m}M_{1n}\cos\mu_{mn} \qquad (20\text{-}40)$$

where M_{1n} = current ratio between tower n and tower 1

R_{mn} = mutual resistance between tower m and tower n

μ_{mn} = phase angle of current between tower m and tower n

6. *Mutual impedance: determination of mutual resistance by mechanical integration.* Where mutual resistance cannot be readily calculated, it may be determined by mechanical integration, using the following relationship:

$$R_m = 60 \int_0^{\pi/2} K_1 f_1(\psi) K_2 f_2(\psi) \cos\psi J_0(s\cos\psi)\,d\psi \qquad (20\text{-}41)$$

K_1, K_2, $f_1(\psi)$, and $f_2(\psi)$ are the form factors and vertical-radiation characteristics for the two radiators, as determined from Eq. (20-5). $J_0(s)$ is the zeroth-order Bessel function, and s is expressed in radians.

The self-resistance may be determined from Eq. (20-6) for use in Eq. (20-40).

7. *Determination of reference field by mechanical integration (hemispherical integration).* The value of E_1 may be established by mechanical integration. An assumed value E_{1a} is taken (unity or other convenient value), and azimuthal patterns are computed for fixed vertical angles (usually at 10° intervals). The rms values for each vertical angle are determined (see below under effective field), multiplied by $\sqrt{\cos\psi}$, and the products plotted versus ψ on polar-coordinate paper. The area A of this plot is measured with a planimeter. The true value of E_1 is related to the assumed value E_{1a} by

$$E_1 = E_{1a}\frac{107.6}{\sqrt{A}} \qquad \text{unattenuated field, mv/meter, at 1 mile} \qquad (20\text{-}42)$$

Base Operating Impedance of Radiators. *General.* The base operating resistance of a tower in a directional-antenna array is usually different from the computed operating resistance. The base operating resistance and reactance may be estimated as follows. Estimate the base resistance and reactance of the tower from Fig. 20-4 or Figs. 3-3 and 3-4. Compare the estimated base resistance R_{base} with the loop radiation resistance R_r. Then assume the base mutual impedance[11] to be

$$Z_{m(base)} = Z_m(R_{base}/R_r)$$

and substitute these values in Eqs. (20-36) and (20-37).

Parasitic (Zero-resistance) Elements. A radiating element operating at zero resistance and not supplied with power by connections from the distribution circuits is said to be parasitic. This condition obtains when the negative coupled resistance is equal to the sum of the radiation resistance and loss resistance. A parasitic element properly tuned will operate in phase-and-field-ratio relationships approximating those computed. In critical multielement arrays, independent control of phase and amplitude is required and parasitic radiators should be avoided. However, they may be employed in antennas designed primarily for power gain.

Negative-resistance Elements. A negative-resistance element receives more power by coupling to the other elements than is required to obtain the desired field from the element. The excess power is sometimes dissipated in a resistor but is usually

returned to the positive-resistance elements through the power-distributing circuits (see below).

Effective Field. *Definition.* The root-mean-square value of the radiation pattern in the horizontal plane (in unattenuated field at 1 mile) is referred to as the *effective field.* The effective field of a directional antenna is modified from that for a single radiator by directivity at vertical angles and higher ground losses.

Figure 20-27 shows the no-loss effective fields in the horizontal plane for two quarter-wave antennas for a wide range of phasing and spacing. These curves assume equal fields from the two radiators and ignore ground losses.
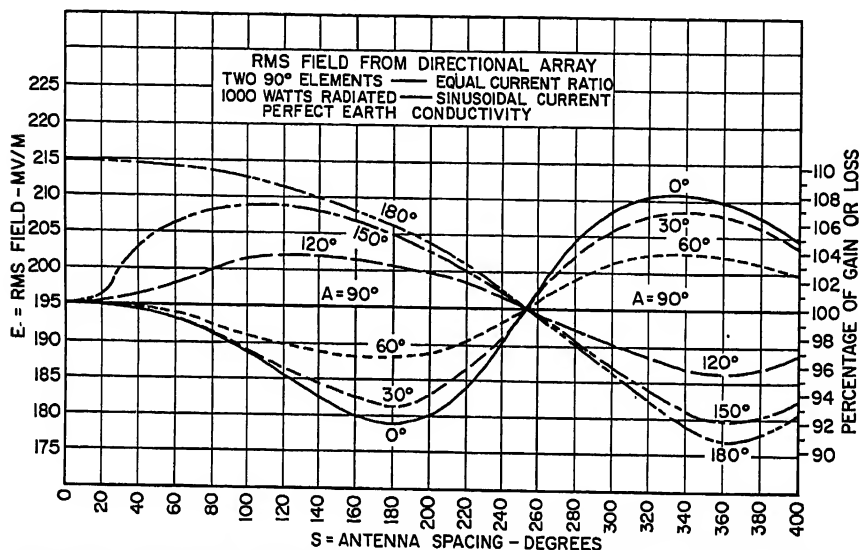
Fig. 20-27. Root-mean-square horizontal-plane values of two-element radiation patterns.

Calculation of Directional-antenna Effective Field. The rms field may be determined by plotting the horizontal-plane pattern on polar-coordinate paper and measuring the area with a planimeter, or it may be calculated from

$$E_{\text{rms}} = \left[\sum_{j=1, \, k=1}^{n} E_j E_k \cos \mu_{jk} J_0(s_{jk}) \right]^{\frac{1}{2}} \tag{20-43}$$

where E_j = field radiated in horizontal plane from element j
  E_k = field radiated in horizontal plane from element k
  n = number of elements in array
  μ_{jk} = phase angle between fields radiated from elements j and k
  s_{jk} = spacing between elements j and k, radians
$J_0(s)$ = Bessel function of order zero

Occasionally the rms value is desired at a vertical angle above the horizontal. For this case,

$$E_{\text{rms}(\psi)} = \left[\sum_{j=1, \, k=1}^{n} E_j f_j(\psi) E_k f_k(\psi) \cos \mu_{jk} J_0(s_{jk} \cos \psi) \right]^{\frac{1}{2}} \tag{20-44}$$

where $f(\psi)$ is the vertical-radiation characteristic.

Choice of Orientation and Spacing in Directional-antenna Design. The required placement of towers in a directional array is determined by the general shape of pattern desired. In-line arrays produce patterns having line symmetry; other configurations may or may not exhibit symmetry, depending upon the operating parameters. Closely spaced towers have mutual impedances which are relatively large compared with the self-resistances; this may result in low operating resistances and high circulating currents, which make for instability and high losses and should be avoided. In general, these effects may occur when spacings less than about one-quarter wavelength are introduced; they may be evaluated by computing the no-loss effective field of the array ($R_a = 0$) and comparing this value with that for an assumed 2-ohm series loss (see Sec. 20.3, Ground Systems). If the effective field with 2 ohms loss is substantially less than the no-loss effective field, or less than FCC minimums, the possibility of reducing losses through the use of wider spacings must be explored.

Choice of Tower Height. The choice of tower height is governed by the effective field required, the need for adequately high base resistances, and the desired vertical-radiation patterns. These requirements are usually met by heights on the order of one-quarter wavelength; shorter towers are sometimes employed on the lower frequencies, for practical reasons, so long as the required minimum effective field is obtained and adequately high base resistances are provided. Taller towers produce higher effective field strengths and may reduce radiation at high vertical angles.

Effect of Finite Radiator Cross Section on Directional Antennas. The modified current distribution due to the finite cross section of practical tower radiators (see above) results in a complex vertical-radiation characteristic different from that computed using the simplified assumptions. Where towers of unequal height are employed, the differences in amplitude (and sometimes phase) of vertical-radiation characteristics must be taken into account. The radiation from an array employing towers of unequal height may be computed using Eq. (20-16), (20-22), or (20-23). The difference in phase angle requires the substitution for α_n of the angle α'_n, which includes an additional term, δ_n:

$$\alpha'_n = s_n \cos \varphi_n \cos \psi + A_n + \delta_n \qquad (20\text{-}45)$$

where δ_n = phase-angle difference between $f_1(\psi)$ and $f_n(\psi)$ at angle ψ.

20.5. CIRCUITS FOR SUPPLYING POWER TO DIRECTIONAL AND NONDIRECTIONAL ANTENNAS

General. Radio-frequency power must be supplied to the individual radiators of the directional-antenna system in the proper proportions and phase-angle relationships to produce the desired radiation patterns. Means for controlling the current ratios and phase angles are required to permit adjustment and maintenance of the patterns. The circuits must provide a load into which the transmitter will operate properly.

The required functions are shown in block form in Fig. 20-28. The antenna tuning units transform the operating base impedances of the radiators to the characteristic impedance of the transmission lines and provide a portion of the required phase shift. Additional phase shift is introduced by the transmission lines. The phase-control networks contain variable components for phase control. The power-dividing network supplies variable voltages to each line for power control.

Types of Circuits Employed. Lumped-constant networks of the L, T, or π type are ordinarily employed for impedance transformation and phase-shift networks. Phase-delay networks are preferred to phase-advance networks, where feasible, because of their greater harmonic suppression.

Required reactance values for the L, T, and π networks shown in Fig. 20-29, as functions of phase shift and impedance transformation, can be computed using the follow-

ing formulas:

$$a = \frac{r \sin \beta}{\sqrt{r} - \cos \beta} \qquad b = \sqrt{r} \sin \beta \qquad c = \frac{\sqrt{r} \sin \beta}{1 - \sqrt{r} \cos \beta}$$

$$r = \frac{R_1}{R_2} > 1 \qquad \beta = \text{desired phase shift} \tag{20-46}$$

Design of Antenna Tuning Units.   The antenna tuning-unit design is based on the estimated base operating impedance of the radiators (Sec. 20.4).   The transformation
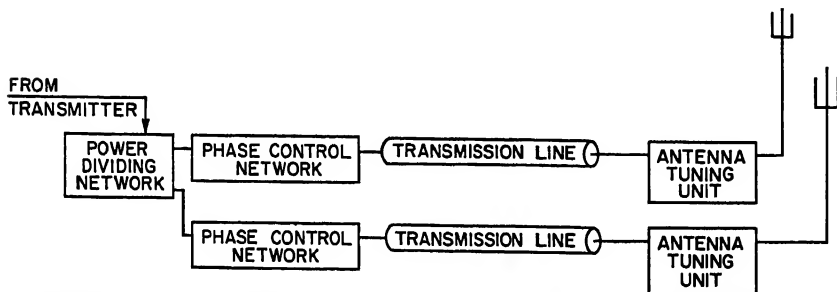
FIG. 20-28. Required functions in antenna tuning, phasing, and power-dividing gear, shown n block form.

ratio r is the ratio between the operating base resistance and the characteristic imped-ance of the transmission line, and β is the desired phase shift.   The antenna reactance constitutes an equivalent reactance in the antenna arm of the network; the T network is thus somewhat more convenient than the π network for the antenna tuning unit.
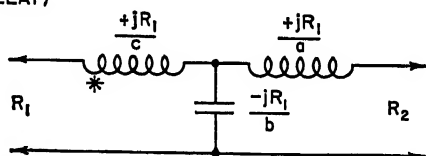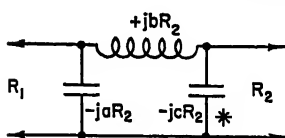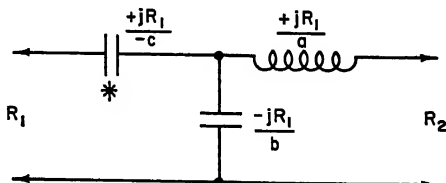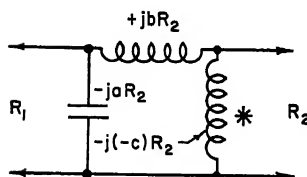
FIG. 20-29. T and π networks suitable for impedance transformation and phase control.

For a nondirectional radiator, the phase shift introduced is only incidental to the impedance transformation.   Since any value of phase shift may be employed, an L network may be used or a T network with phase shift near 90°.

Transmission-line Requirements.   Transmission lines may be either of the concentric or open-wire, unbalanced type.   Concentric lines have a lower characteristic impedance, usually requiring less transformation between tower and line; their complete shielding eliminates any radiation from the line.   The phase shift introduced by a transmission line terminated in its characteristic impedance is equal to the electrical length of the line.   The velocity of propagation is $v = c\sqrt{\epsilon}$, where c is the velocity of light and ϵ the dielectric constant of the line insulation material.

Phase-control Networks.   Phase-control networks usually employ unit transformation and values of phase shift near 0° or 90°.   For phase shift near 0°, a series-resonant circuit may be employed; the phase shift is $\beta = \tan^{-1}(X/Z_0)$, where Z_0 is the characteristic impedance of the transmission line.

Power-division Circuits.   A typical circuit for power division is shown in Fig. 20-30a. L_1 is a continuous voltage divider; vernier inductors $L_{2,3,4}$ are tapped across
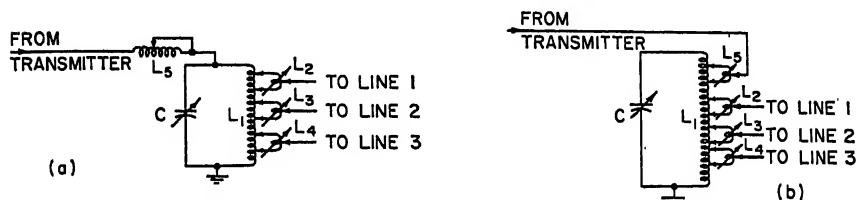
FIG. 20-30. Typical circuits for controlling the distribution of power among the elements of a directional-antenna system.
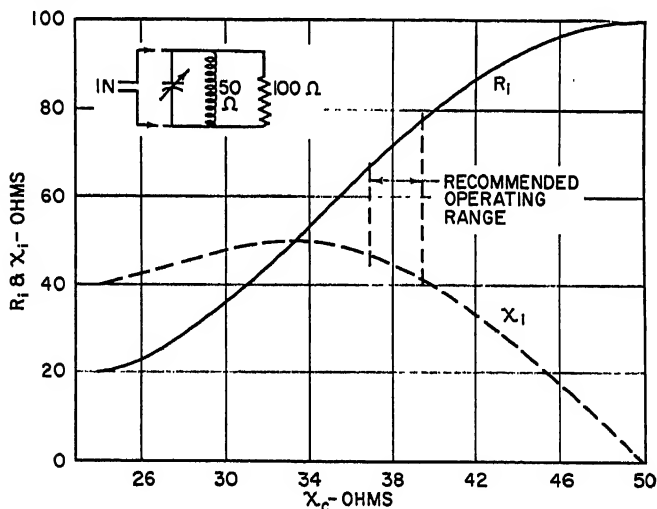
FIG. 20-31. Design chart for power-distribution circuit of Fig. 20-30.

one or two turns of L_1, and sliding contacts provide continuous variation.   The impedance of the combination is transformed by the L network, condenser C, and inductor L_5 to the desired impedance.

To design the power-division network, the desired input resistance (known as the *common-point resistance*) is first established.   This is usually chosen to be the same value as the characteristic impedance of the transmission lines, particularly if the transmitter must also supply power to a single tower for nondirectional operation.   The common-point current to deliver the required power to this load may then be

computed. (FCC Standards provide a slight additional power to compensate for circuit losses. For powers of 5 kw and less, the common-point resistance is multiplied by 0.925 and for higher powers by 0.95, in computing power.)

The required values of L_1 and C are determined from the equivalent circuit of Fig. 20-31, which shows the input resistance and reactance as a function of the reactance X_c of condenser C. Figure 20-31 is plotted for a maximum input resistance of 100 ohms and may be applied to other desired values by applying the required ratio to the components.

A variation in this type of power-dividing circuit is shown in Fig. 20-30b. In this circuit, the value of C is chosen to resonate the power-dividing tank at a value of input resistance somewhat greater than required, with the input-resistance control provided by inductor L_s. This circuit is resonant, and no input reactor is required.

Special Problems. *Very High or Very Low Operating Resistances.* Special problems are presented by radiators with very low or very high base operating resistances. L, T, or π networks cannot conveniently provide transformation ratios exceeding about 10:1; when higher transformation ratios are required, a tank circuit, as shown in Fig. 20-32, may be used. The reactance L_1 in series with the antenna is adjusted to resonate the operating base reactance and make the antenna a resistive load to the tank circuit.

(a) VERY LOW ANTENNA RESISTANCE

(b) VERY HIGH ANTENNA RESISTANCE

Fig. 20-32. Use of tank circuit for high-impedance transformation ratio.

Negative-resistance Elements. Power flows in the reverse direction from an element having a negative resistance. In computing phase shifts, this effect is taken into account by considering phase-delay networks and transmission lines as phase-advance circuits, and vice versa. In addition, the fact that the negative-resistance element is delivering rather than consuming power is equivalent to an additional 180° of phase shift at the point of power division.

20.6. ADJUSTING DIRECTIONAL-ANTENNA ARRAYS

General Requirements. A directional antenna must be adjusted to produce a radiation pattern substantially in accordance with its design. In the United States, the construction permit issued by the FCC specifies maximum permissible values of radiation in pertinent directions.

Sampling System. An indication of the field-ratio and phase-angle relationships among the radiators is needed to adjust a directional-antenna system. This is provided by permanently installed *sampling loops* mounted on the towers, connected by *sampling lines* to *sampling meters* and a *phase monitor*.

The sampling loop is mounted on one leg of the tower near the current antinode and develops an induced voltage proportional to the current in the tower leg. It

should be at least 30 ft above the ground, to avoid voltages induced by capacity and other nonradiating currents near the tower base. Shielded or unshielded loops of one or two turns are used; the use of a shielded loop minimizes voltages developed by the tower r-f potential. The outer conductor of the sampling line is usually bonded to the tower, and the sampling line is transferred across the base insulator by means of an isolation inductor wound of a suitable length of sampling line.

The individual sampling lines may be cut to the same length, making the phase delay on all lines equal. Excess line should be stored so as to be exposed to the same weather conditions as the longer portions of the other lines.

The sampling-current ratios may be measured by means of r-f or rectifier-type milliammeters connected to the terminating resistors at the ends of the sampling lines. The phase angles may be measured with any of several types of phase monitor manufactured for the purpose.

Initial Adjustment. The initial adjustment of a directional-antenna system is effected by setting the reactances of the antenna tuning and power-dividing components to their computed values and supplying power to the antenna system. Usually, the phase and field-ratio indications will be different from those desired. The adjustable tuning components are then varied until the phase and field-ratio indications correspond closely to the computed values.

Preliminary field-strength measurements must then be made to determine the approximate shape of the pattern and the changes which are required to bring this shape into agreement with the computed shape. Initial measurements are usually *cross-minima* measurements, made each few degrees of bearing along a measuring course passing through the region of the pattern which is of interest. Both the directional and nondirectional fields are measured, and the ratios of these two field strengths are determined along each bearing. These ratios are plotted and compared with the computed pattern ratios, and the plot is analyzed to determine what changes in phase and current relationships are necessary to bring the pattern into agreement with computations. This usually requires an analysis of the vector diagram (Fig. 20-33).

Use of Vector Diagrams. Figure 20-33*b* is a typical vector diagram of a three-element directional antenna, for the pattern shown in Fig. 20-33*a*. The lengths of the vectors are proportional to the magnitudes of the fields radiated from the towers, and the angles of the vectors are the phase angles α_n for the indicated bearings. A study of the diagram will indicate the changes required to change the location or depth of an individual minimum, leaving the other unchanged or modified as required.

The required changes are determined from this analysis and made, using the indications of the sampling meters and phase monitor. The cross-minima measurements are then repeated. When the cross-minima measurements indicate the pattern shape to be properly established, complete route measurements, field-strength measurements, common-point resistance measurements, and transmission-line standing-wave-ratio measurements must be made (see under proof of performance below).

Special Techniques. A frequently helpful technique in the initial adjustment of the pattern is that of stationing observers with field-strength meters in each of the minima of the pattern, maintaining communication over telephone lines or with high-frequency radio. The currents and phases are varied until minimum field strength is obtained along all desired bearings simultaneously; this establishes the required sampling-current and phase-monitor indications for a pattern with deep minima, from which the correct parameters for the desired pattern may be determined.

Proof of Performance. A *proof of performance* is required in the United States for all directional-antenna systems before regular operation is authorized. The following discussion summarizes the major requirements, full details of which may be found in the Radio Broadcast Standards and Rules and Regulations of the FCC.
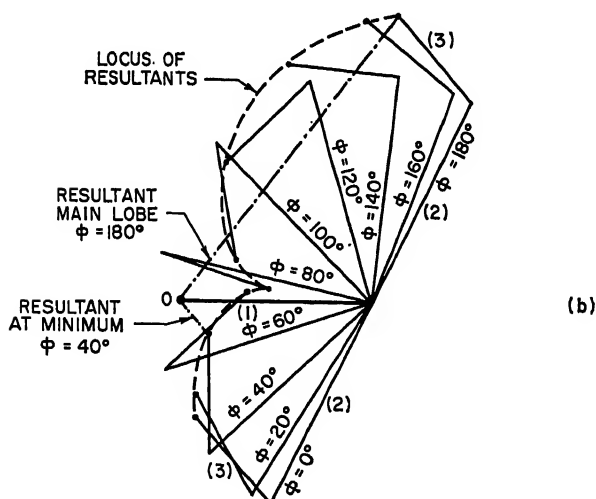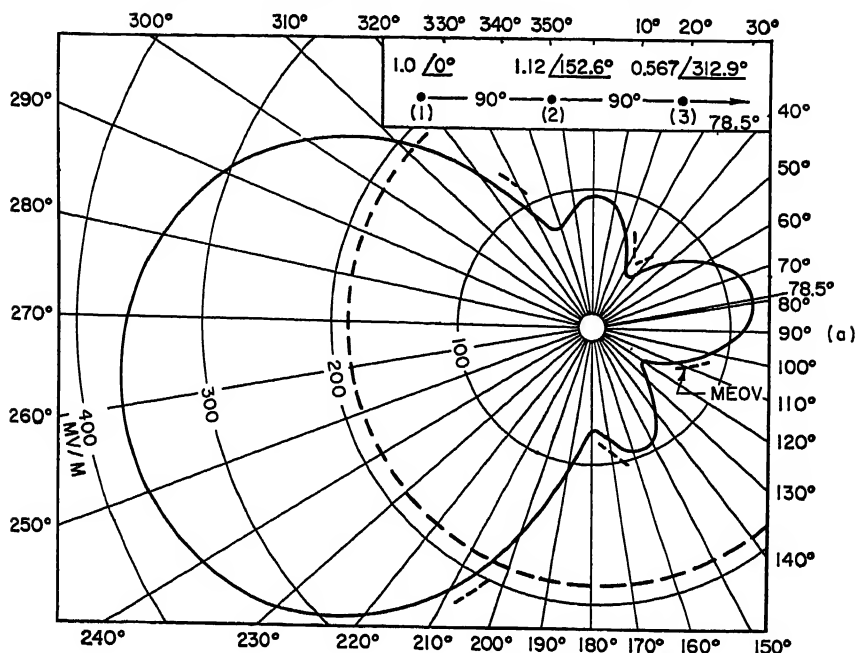
FIG. 20-33. Three-element directional-antenna pattern in the horizontal-plane and vector diagram.

After the final adjustment of the directional-antenna system, the common-point resistance must be measured and the antenna system operated at the required power. Field-strength measurements are required to be made along eight or more radial routes from the antenna, at specified distance intervals, out to a distance of 15 or more miles. Complete measurements must be made for both directional and nondirectional operation. Measurements must be made in at least eight directions; more if required to determine the shape of the pattern. These directions must include all directions in which a maximum permissible value of radiation is specified in the construction permit.

The measured field strengths will be the attenuated fields, and the soil conductivity must be established to determine the unattenuated field. This is done by plotting the measured fields vs. distance from the antenna on suitable graph paper (usually 7- × 2.2-cycle log-log, K & E No. 359-127G) and comparing the measured values with graphs of field strength vs. distance for the frequency involved and the expected range of conductivity values. Such graphs are contained in the sources listed in the bibliography.[12,25]

After the pattern is properly adjusted and the adjustment confirmed by the proof of performance, *monitor points* are established in each direction specified by the construction permit. The field strengths for directional operation are measured at each monitor point at regular intervals to provide an indication of any variation in radiated field.

20.7. MISCELLANEOUS PROBLEMS

Guy-wire Insulation. Guy wires supporting tower radiators must be insulated from the tower and from ground and must be broken up into sections sufficiently short so that the induced currents do not distort the radiation pattern. Strain insulators are installed at the guy anchor, the point of attachment to the tower, and at intervals along the guy wire. The maximum length of any individual guy-wire section should not exceed $\lambda/8$ to $\lambda/10$.

Voltages in High-power Arrays. The voltages commonly encountered in medium-frequency antennas and antenna arrays are rarely high enough to present corona or insulation problems. The voltage across the base insulator is

$$V_{base} = I_{base} \sqrt{R_{base}^2 + X_{base}^2}$$

The voltages on guy-wire insulators may be roughly estimated for a typical guy system as having a maximum value of 30 volts per wavelength for one watt of power in the antenna. An extensive discussion of antenna voltages is given by Brown.[13]

Circuits across Base Insulator. *A-C Power Supply.* It is often necessary to cross the base insulator of a tower antenna with a-c power circuits. Power for aeronautical obstruction lighting on the tower or other purposes may be supplied by means of chokes or transformers. Lighting chokes are wound of ordinary insulated copper wire on a suitable form, with a sufficient number of turns to provide a reactance at the operating frequency which is high compared with the tower base impedance. Radio-frequency bypass condensers are installed between individual windings.

Alternating current can be supplied by an Austin transformer, consisting of linked toroidal cores mounting the primary and secondary windings. There is an air gap of several inches between the two cores, and the only effect on the r-f characteristics of the tower is the shunting capacitance of the transformer.

FM and Television Transmission Lines. Tower antennas frequently support frequency-modulation and television transmitting antennas, as well as transmitting and receiving antennas for other radio services. FM power can be transferred across the

base insulator through the use of tightly coupled transformers designed for the purpose. The coupling elements are arranged to provide an adequate air gap for isolation at the medium frequency, and the only effect at the medium frequency is that due to the shunt capacity.

FM and television transmission lines (and other metallic circuits) may be isolated from the tower at the medium frequency by a quarter-wave isolation section of line. In Fig. 20-34a, the outer conductor of the television coaxial cable is grounded immediately before the rise up the tower and is supported on insulated hangers to a point
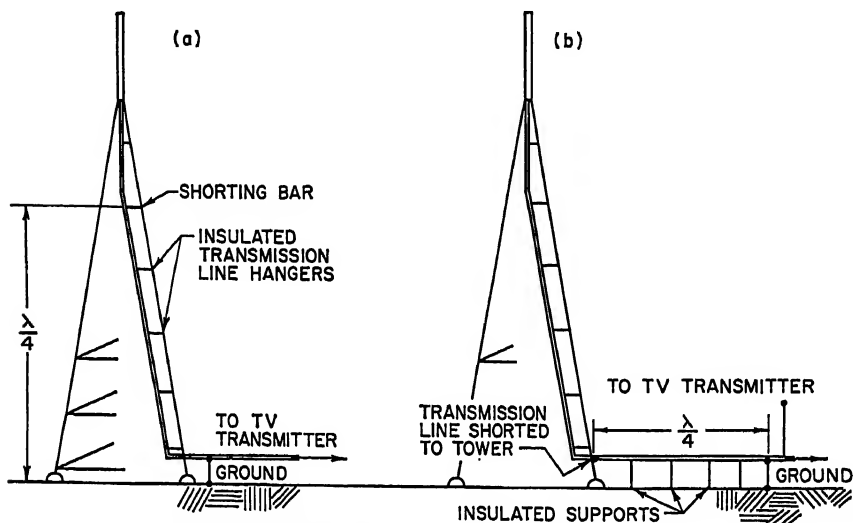
FIG. 20-34. Two methods of isolating television transmission line from medium-frequency radiators.

approximately one-quarter wavelength from ground, where it is connected to the tower. The outer conductor of the television line and the tower constitute a shorted quarter-wavelength transmission line at the medium frequency, resulting in a high impedance at the tower base. In Fig. 20-34b, the quarter-wavelength section is installed along the ground rather than up the tower. This method is useful or often necessary with towers shorter than one-quarter wavelength.

Simultaneous Use of Single Tower at Two Frequencies. It is occasionally desired to use a single tower radiator simultaneously at two different frequencies. This may be done by employing suitable filters to isolate the two transmitters from each other, as shown in Fig. 20-35. The isolation networks are *acceptor-rejector* filters, series-resonant at one frequency and parallel-resonant at the other. In filter 1, for example, L_1 and C_1 are tuned to series resonance at 600 kc. At 900 kc, the combination is inductive, and this inductive reactance is parallel-resonated with C_2. Filter 2 presents a low impedance at 900 kc and a high impedance at 600 kc. Filters 3 and 4 offer a low impedance to ground to the unwanted signals.

Selection of Transmitter Sites. *General.* Transmitter sites must be selected in an area providing sufficient ground which is reasonably flat and level, of high local conductivity, free of obstructions which might interfere with the proper functioning of the radiating system, and so located as to provide maximum signal to the principal city and the service area. This last requirement, applied to operation with a direc-

tional-antenna system, usually dictates a choice of site which will place the main radiation lobe in the direction of the city.

Site Surveys. The FCC Radio Broadcast Standards require a *minimum* signal of 25 mv/meter to the business and industrial areas of the principal city. Preferably, this minimum signal should be delivered to the entire city. The expected signal may best be determined by means of a *site survey.* A temporary antenna and low-power transmitter are installed at the proposed site, and field-strength measurements are made along one or more routes from the antenna through the city to be served. The actual effective conductivity may then be determined from the measurements (see above under proof of performance of directional antennas).
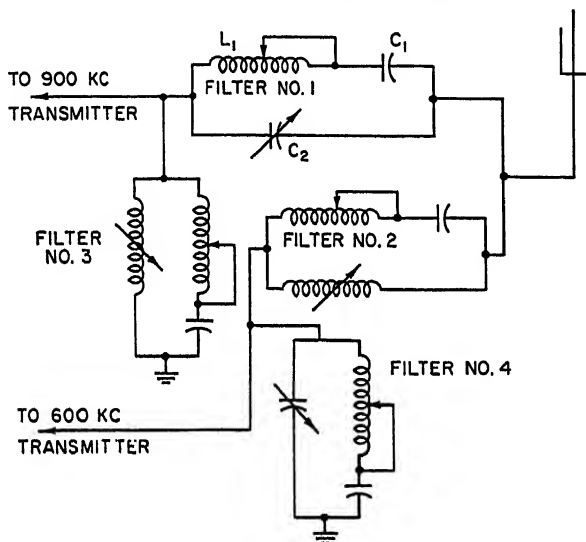
Fig. 20-35. Group of acceptor-rejector filters for supplying power at 600 and 900 kc simultaneously to a single radiator.

In the absence of site-survey test measurements, use may be made in the United States of a map of average soil conductivities given in the FCC Radio Broadcast Standards, which shows average soil conductivities for large general areas.[14,25,26] However, this map shows average conductivities only, and local conductivities may differ substantially. Consequently, a careful inspection of the path to the city must be made, and even then the map should be used conservatively.

Effect of Signal Scattering and Reradiation by Nearby Objects. *General.* Structures and terrain features near the transmitter site may reflect the signal from the antenna or may reradiate sufficient signal to affect the performance of the antenna. These effects will usually not be indicated by the conventional site survey.

Short Towers. The reradiation from a short tower in the field of the antenna may be estimated by two methods. In the first, the mutual impedance Z_m between the antenna and the short tower is determined and the base impedance Z_{base} of the short tower is estimated, using data such as the curves of Fig. 20-4. The current I_2 flowing in the second tower will be $I_2 = I_1(Z_m/Z_{base})$, where I_1 is the current in the reference tower. The field due to this current may be computed from Eq. (20-1). This method is applied to a directional antenna by computing the individual currents induced by each tower of the directional antenna and taking their vector sum.

The second method requires a knowledge of the effective height of the second tower,

which for a short tower ($\lambda/4$ or less) is

$$H_{\text{eff}} = \frac{\lambda}{\pi} \frac{\sin^2 (G/2)}{\sin G} \qquad (20\text{-}47)$$

The voltage V_i induced in the second tower in an incident field of E_i is $H_{\text{eff}} E_i$, and the current which will flow is V_i/Z_{base}, from which the reradiated field may be computed as above.

High-tension A-C Power Lines. Alternating-current power lines and their supporting towers near the antenna may produce objectionable reradiation. Negligible voltages are induced in the horizontal line by the vertically polarized signal, but voltages induced in the towers may cause current to flow in closed loops formed by the towers and the horizontal grounding wires connecting the tops of the towers. The r-f currents flowing in the towers may be estimated with limited accuracy by considering the towers to be top-loaded and applying the methods discussed above, under short towers. However, the typical case involves many variable factors, and the problem does not yield readily to a theoretical analysis.

Large Objects, Including Buildings and Hills. Large buildings near the transmitter site, mountains, or rugged terrain may distort the radiation pattern of directional or nondirectional antennas. The effects may be serious in the case of a directional-antenna system requiring a high degree of signal suppression, particularly if the buildings or hills are in the main radiation lobe of the antenna.

Such objects are usually too irregular to apply analytic methods to a determination of reradiation. Their effect may often be estimated on the basis of experience with similar objects. If the source of reradiation can be readily isolated, as for example a single large standpipe, field-strength measurements made as part of the site survey along a direct line between the test transmitter and the reradiating object will, when plotted versus distance from the reradiating object, exhibit a standing-wave pattern from which the magnitude of reradiation can be deduced with reasonable accuracy.

Another technique in estimating reradiation which has been applied with some success is that of making the site test using a simple two-element test antenna to produce a radiation pattern having deep minima. Site-test field-strength measurements in the minima will indicate reradiated and "scatter" signal. This technique is useful in situations such as rugged terrain, where reradiation cannot be ascribed to an individual source.

Tall Towers: General. It is frequently desired to erect tall towers to support FM and television transmitting antennas, or for other purposes, in the immediate vicinity of a medium-frequency antenna. These structures are usually of sufficient electrical height to be capable of substantial reradiation in high incident fields. The method of estimating reradiation for short towers discussed above loses its accuracy for towers taller than about one-quarter wavelength.

Tall Towers: Control of Reradiation. The tower location should be chosen to have minimum effect on the medium-frequency antenna. If the tower is to be installed in the immediate vicinity of a medium-frequency directional antenna, the field strength should be computed at a number of locations and a position chosen for the tower where the incident field is a minimum.

The reradiation from a tower of this height may be controlled by insulating the tower from ground and installing sectionalizing insulators at one or more levels. Guy wires must be insulated at suitable intervals, and transmission and a-c lines must be isolated as discussed above. When sectionalizing insulators are used, the reradiation from each section of the tower may be estimated as discussed under short towers above; the maximum reradiation will then be the scalar sum of the contributions from each section.

The reradiation from tall towers may be controlled to some extent without sectionalizing insulators by insulating the tower from ground and installing a suitable reactor between the tower and ground. Figure 20-36 shows measured variations in current distribution obtained by this method.
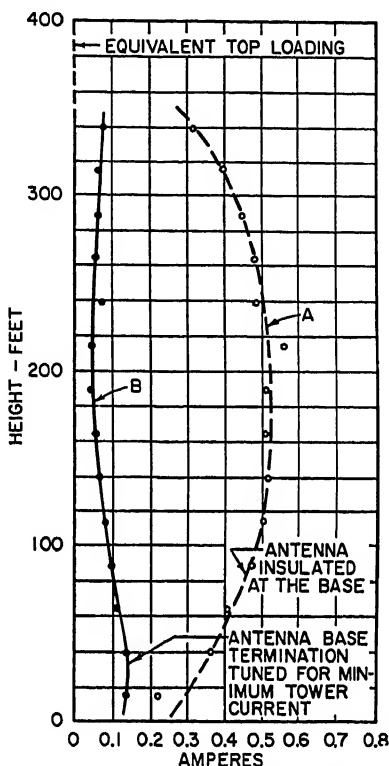
FIG. 20-36. Detuning of tall tower by choice of suitable base reactance. The reradiating tower is a top-loaded tower having a height equivalent to 400 ft. The incident field is 1 v/meter at 970 kc. Curve *A* shows the measured current, with the base of the tower insulated from ground, and curve *B* shows the current flowing with a reactance of +57 ohms between the tower and ground; this reactance produced minimum current at the antinode of curve *A*. Mechanical integration of the curves indicates a reradiated field of 57 mv/meter for curve *A* and a maximum reradiated field of 6 mv/meter for curve *B*. This is probably greater than that actually obtaining, because of phase differences in the current along the tower.

Protection against Static Discharges and Lightning. In the absence of suitable precautions, static charges accumulate on towers and guy wires and may discharge to ground. This discharge ionizes the path, and a sustained r-f arc may follow. Protection can be provided to minimize the accumulation or quench the arc, but relatively little protection can be provided against direct lightning hits. A lightning rod or rods extending above the beacon on the tower top will provide some protection to the beacon, and horn or ball gaps at the tower base provide protection to the base insulator. However, the magnitude of lightning currents usually results in damage to the meters and tuning components. This is true of both insulated series–excited towers and grounded shunt–excited towers.

A d-c path from the tower to ground will minimize static accumulation. A separate

radio-frequency choke, the tuning inductor, or the sampling-line inductor may be connected to maintain the tower at d-c ground potential. Difficulty may occasionally be experienced with charges accumulating on the individual guy wires and arcing across the guy insulators. This may be eliminated by installing static drain resistors across each guy insulator. These resistors may have a value of 50,000 to 100,000 ohms and should have an insulation path somewhat longer than provided by the guy insulator.

Transmitter protection may be provided by a circuit such as shown in Fig. 20-37. Radio-frequency power is supplied to the load R_{load} through inductance L, which has
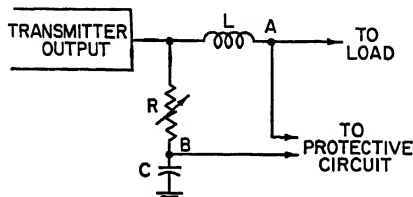
FIG. 20-37. Transmitter protective circuit. R, L, C, and the load form a Maxwell bridge.

a low reactance. Values for R and C are chosen to present a very high impedance compared with L and R_{load}. If the load is purely resistive and $R/X_C = X_L/R_{load}$, points A and B will be at the same r-f potential. Any change in the load, due to arcing or other causes, will produce a voltage between A and B, which may be used to actuate protective devices.

REFERENCES

Articles

1. Charles L. Jeffers: "An Antenna for Controlling the Nonfading Range of Broadcasting Stations," *Proc. IRE*, vol. 36, pp. 1426–1431, November, 1948.
2. S. A. Schelkunoff: "Theory of Antennas of Arbitrary Size and Shape," *Proc. IRE*, vol. 29, pp. 493–521, September, 1941.
3. George H. Brown and O. M. Woodward, Jr.: "Experimentally Determined Impedance Characteristics of Cylindrical Antennas," *Proc. IRE*, vol. 33, pp. 257–262, April, 1945.
4. P. S. Carter: "Circuit Relations in Radiating Systems and Applications to Antenna Problems," *Proc. IRE*, vol. 20, pp. 1004–1041, June, 1932.
5. J. F. Morrison and P. H. Smith: "The Shunt-excited Antenna," *Proc. IRE*, vol. 25, pp. 673–696, June, 1937.
6. G. H. Brown: "A Critical Study of the Characteristics of Broadcast Antennas as Affected by Antenna Current Distribution," *Proc. IRE*, vol. 24, pp. 48–81, January, 1936.
7. Carl E. Smith and Earl M. Johnson: "Performance of Short Antennas," *Proc. IRE*, vol. 35, pp. 1026–1038, October, 1947.
8. J. R. Wait and W. A. Pope: "The Characteristics of a Vertical Antenna with a Radial Conductor Ground System," IRE National Convention Record, pt. 1, Antennas and Propagation, p. 79, 1954.
9. Frank R. Abbott: "Design of Optimum Buried-conductor RF Ground System," *Proc. IRE*, vol. 40, pp. 846–852, July, 1952.
10. C. Russell Cox: "Mutual Impedance between Vertical Antennas of Unequal Heights," *Proc. IRE*, vol. 35, pp. 1367–1370, November, 1947.
11. G. H. Brown: "Directional Antennas," *Proc. IRE*, vol. 25, pp. 78–145, January, 1937.
12. K. A. Norton: "The Calculation of Ground-wave Field Intensity over a Finitely Conducting Spherical Earth," *Proc. IRE*, vol. 29, pp. 623–639, December, 1941.
13. George H. Brown: "A Consideration of the Radio-frequency Voltages Encountered by the Insulating Material of Broadcast Tower Antennas," *Proc. IRE*, vol. 27, pp. 566–578, September, 1939.
14. Harry Fine: "An Effective Ground Conductivity Map for Continental United States," *Proc. IRE*, vol. 42, pp. 1405–1408, September, 1954.

15. Pierre Baudoux: "Current Distribution and Radiation Properties of a Shunt-excited Antenna," *Proc. IRE*, vol. 28, pp. 271–275, June, 1940.
16. G. H. Brown, R. F. Lewis, and J. Epstein: "Ground Systems as a Factor in Antenna Efficiency," *Proc. IRE*, vol. 25, pp. 753–787, June, 1937.
17. George H. Brown: "The Phase and Magnitude of Earth Currents near Radio Transmitting Antennas," *Proc. IRE*, vol. 23, pp. 168–182, February, 1935.
18. A. B. Chamberlain and W. B. Lodge: "The Broadcast Antenna," *Proc. IRE*, vol. 24, pp. 11–35, January, 1936.
19. W. W. Hansen and J. G. Beckerley: "Concerning New Methods of Calculating Radiation Resistance, Either with or without Ground," *Proc. IRE*, vol. 24, pp. 1594–1621, December, 1936.
20. Ronold King: "Self- and Mutual Impedances of Parallel Identical Antennas," *Proc. IRE*, vol. 40, pp. 981–988, August, 1952.
21. Clifford H. Moulton: "Signal Distortion by Directional Broadcast Antennas," *Proc. IRE*, vol. 40, pp. 595–600, May, 1952.
22. C. A. Nickle, R. B. Dome, and W. W. Brown: "Control of Radiating Properties of Antennas," *Proc. IRE*, vol. 22, pp. 1362–1373, December, 1934.
23. Lynne C. Smeby: "Short Antenna Characteristics: Theoretical," *Proc. IRE*, vol. 37, pp. 1185–1194, October, 1949.
24. Karl Spangenberg: "Charts for the Determination of the Root-mean-square Value of the Horizontal Radiation Pattern of Two-element Broadcast Antenna Arrays," *Proc. IRE*, vol. 30, pp. 237–240, May, 1942.

Books

25. Rules and Regulations of the Radio Broadcast Series, Federal Communications Commission, pt. 3, U.S. Government Printing Office, 1959.
26. "Effective Radio Ground-conductivity Measurements in the United States," *Natl. Bur. Standards (U.S.) Circ.* 546, February, 1954.
27. Edmund A. Laport: "Radio Antenna Engineering," McGraw-Hill Book Company, Inc., New York, 1952.
28. S. A. Schelkunoff and Harald T. Friis: "Antennas: Theory and Practice," John Wiley & Sons, Inc., New York, 1952.
29. Carl E. Smith: "Theory and Design of Directional Antennas," Cleveland Institute of Radio Electronics, Cleveland, Ohio, 1949.
30. Frederick Emmons Terman: "Radio Engineers' Handbook," McGraw-Hill Book Company, Inc., New York, 1943.
31. H. Paul Williams: "Antenna Theory and Design," vol. 2, Sir Isaac Pitman & Sons, Ltd., London, 1950.

Chapter 21

HIGH-FREQUENCY ARRAYS

Stephen W. Kershner

A. D. Ring & Associates
Washington, D.C.

21.1. GENERAL DISCUSSION

High-frequency antenna arrays are utilized in the range of frequencies from 3 to 30 Mc for medium- and long-distance communications and broadcasting by means of ionospheric propagation. Ionospheric transmission over large distances usually involves high over-all transmission losses, especially under unfavorable propagation conditions. The relatively high initial and operating cost of high-power transmitters makes high-gain transmitting and receiving antennas desirable to provide a high degree of directivity in the directions of communications. High-gain antenna arrays are also in common use for international broadcasting stations where transmissions are desired to a specified political area or areas. In addition to providing an increase in signal in the target area, the use of high-gain directional arrays decreases radiation in undesired directions, thus reducing potential interference to other services.

The design requirements for a high-frequency transmitting or receiving array include the frequency range, vertical and horizontal angles at which maximum radiation is desired, the power input, and mechanical requirements.

The frequency range should be established by a propagation study to determine the optimum working frequency (OWF) for the path involved, which varies according to the distance and location, time of day, season of the year, and with sunspot activity. Details of such a study are beyond the scope of this Handbook, but may be found in the literature.[1-4] The final frequency or range of frequencies specified for antenna design purposes should be based on the propagation study and the availability of frequency assignments.

The range of vertical angles pertinent to ionospheric propagation depends on the distance, effective layer height, and mode of propagation (i.e., one-hop, two-hop, etc.). Figure 21-1 is a graph showing the elevation angles pertinent to one-hop transmission for various virtual layer heights. The height of the E layer may be considered constant at approximately 110 km, but the height of the $F2$ layer varies widely according to the time of day, season of the year, and location. A detailed propagation study is required to determine the range of vertical angles for antenna design purposes. As a rough estimate, however, a range of $F1$ and $F2$ virtual layer heights of approximately 250 to 400 km may be used in conjunction with Fig. 21-1 to determine the approximate vertical-angle range. In the case of transmission or reception over distances of more than 4,000 km, maximum signal results from low-angle transmission in the range from 2 to 15°, with the lower angles generally providing better results.

The horizontal range of angles or beamwidth required for point-to-point circuits depends on irregularities in the ionosphere and the effects of magnetic storms, which cause deviations from great-circle paths. It has been shown that directions of arrival of short-wave signals may vary as much as ±5° in the horizontal plane because of these effects.[5] This makes use of antennas with extremely narrow horizontal beamwidths undesirable, especially on circuits which skirt or traverse the auroral zone. International broadcasting requires that the horizontal angle subtend the target area with due allowance for path-deviation effects.

Mechanical requirements must also be determined in regard to wind and ice loading, antenna-size or tower-height limitations, or any other special restrictions imposed by the site or other considerations.

An important factor in establishing a new transmitter or receiver station is the selection of a suitable site. Where long-distance circuits are involved, it is essential that an area be selected with no obstructions projecting more than a few degrees in elevation angle in the directions of transmissions. A reasonably flat area of good ground conductivity is required to ensure good performance of the antennas. The flat area should extend from the antennas to beyond the distance where ground reflections of signals will occur in the directions of transmission. In selecting a receiving site, similar requirements are involved; however, in this case it is also important that

the site be removed from nearby transmitter stations which might cause interference to reception. Receiving sites should also be carefully chosen to avoid interference from other sources, such as power lines or other types of man-made interference.

In selecting a transmitter site, the effect of ground conductivity on performance of the antennas should be considered. For horizontal polarization (usually employed for land-based short-wave arrays), soil of moderate to good conductivity provides effective reflection for the range of angles usually employed for short-wave transmission. For vertically polarized antennas, high ground conductivity is required to prevent undue losses at the lower radiation angles. Graphs for determining reflection coefficients are given by Terman.[6]
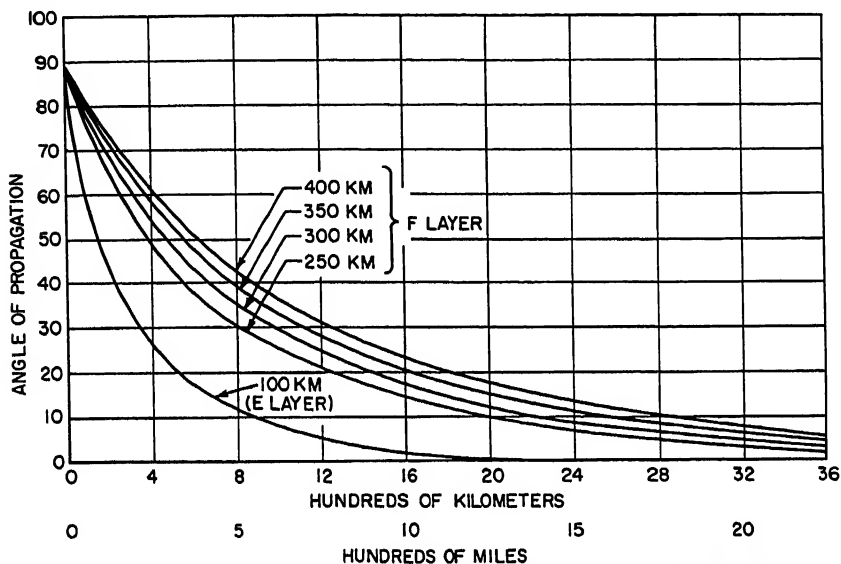
FIG. 21-1. Vertical-radiation angles for one-hop circuits. (*Reference 22.*)

Most short-wave antennas in use today are of the simple horizontal dipole, curtain or rhombic types. Simple horizontal dipoles are effective where low-cost antennas are required, space is at a premium, or a large beamwidth is required. Curtain arrays comprised of many dipole elements are capable of providing high directivity and gain with good performance over a fairly wide range of frequencies by utilizing recently developed techniques. Curtain antennas of good design are characterized by high efficiency and low power loss due to heat dissipation or radiation in undesired minor lobes. Rhombic antennas provide effective operation over fairly wide frequency ranges and excellent input-impedance characteristics over wide frequency ranges. The rhombic antenna is normally terminated in a resistor load with a resulting power loss of from 2 to 3 db. In addition, the power loss due to side-lobe radiation is generally somewhat greater than in well-designed curtain arrays.

The following paragraphs outline detailed design information on horizontal dipoles, curtain arrays, and rhombic antennas. A section is also included on more unusual types of high-frequency antennas.

21.2. SINGLE HORIZONTAL DIPOLE ABOVE GROUND

Perhaps the simplest type of antenna in general use for short-wave applications is a single horizontal-dipole radiator supported at a suitable height above ground

(Fig. 21-2). For sinusoidal current distribution and a perfectly conducting ground, the field intensity at unit distance (1 mile) and other pertinent parameters may be determined from

$$F = 2E_1 \sqrt{P} \, f(\varphi') \sin \, (h \sin \, \psi) \qquad (21\text{-}1)$$

$$E_1 = E_0 \sqrt{\frac{R_r}{R_1}} \qquad (21\text{-}2)$$

$$R_1 = R_r + R_a - R_m(2h) \qquad (21\text{-}3)$$

$$f(\varphi') = \frac{\cos \, (\ell \sin \, \varphi') - \cos \, \ell}{(1 - \cos \, \ell) \cos \, \varphi'} \qquad (21\text{-}4)$$

$$\sin \, \varphi' = \sin \, \varphi \cos \, \psi \qquad (21\text{-}5)$$

where F = field intensity at unit distance (1 mile) at horizontal angle φ from equatorial plane and vertical angle ψ above horizon, mv/meter

E_1 = field intensity at unit distance (1 mile) in the equatorial plane radiated by dipole element alone for 1-kw power, mv/meter

P = power input, kw

$f(\varphi')$ = directivity factor of dipole radiator element

φ' = angle between equatorial plane and line of propagation

h = height of radiator above ground, degrees

E_0 = field intensity at 1 mile in equatorial plane radiated by an isolated dipole for a power of 1 kw, mv/meter

R_r = radiation resistance of isolated dipole referred to current maximum, ohms

R_1 = operating resistance of dipole radiator at height h above ground referred to current maximum, ohms

R_a = assumed loss resistance referred to current maximum, ohms

$R_m(2h)$ = mutual resistance between dipole and its image (spacing = $2h$) referred to current maximum, ohms

ℓ = half length of dipole radiator

Values of $f(\varphi')$ may be obtained from Fig. 20-5 by placing $\psi = \varphi'$ and $G = \ell$. Values of E_0 may be obtained by multiplying values obtained from Fig. 20-3 by 0.707 to take account of the difference between a vertical radiator above ground and an isolated dipole in free space. Values of R_r and R_m may likewise be obtained from
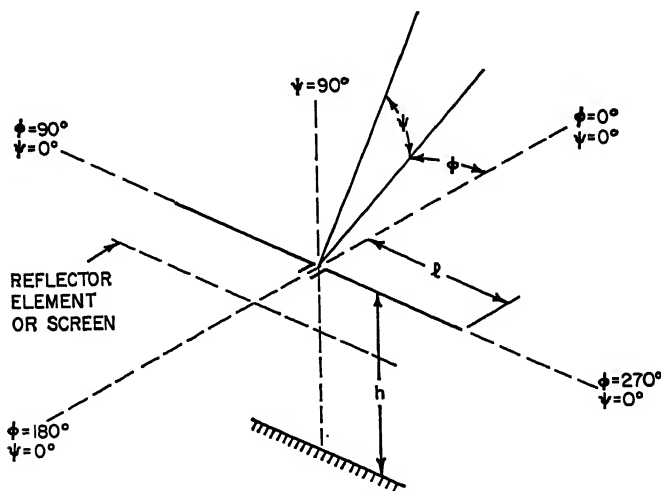
FIG. 21-2. Horizontal dipole above ground showing symbols used.
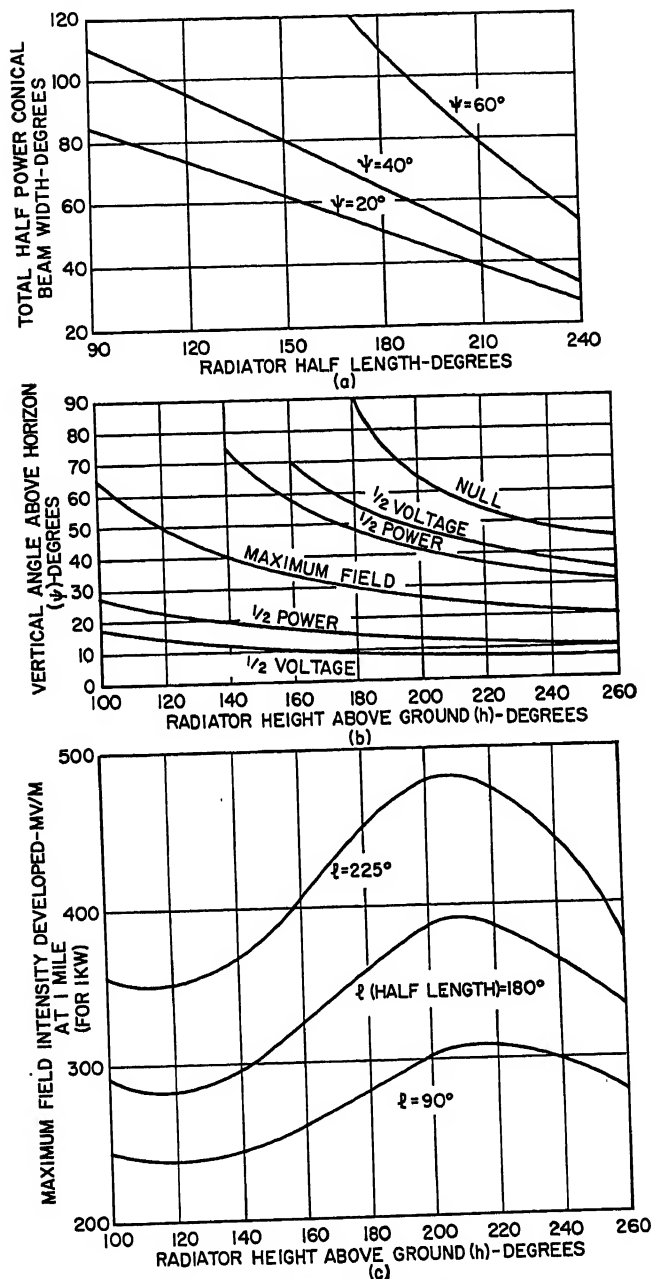
FIG. 21-3. Design curves for single horizontal radiator above ground showing: (a) Conical beamwidth. (b) Vertical-radiation characteristics in the equatorial plane. (c) Maximum field intensity developed for 1 kw power.

Figs. 20-3 and 20-25; however, the resistance values given for vertical radiators above ground must be multiplied by 2 to obtain values for dipoles in free space.

For any given height, the maximum field intensity F_{max} occurs in the equatorial plane ($\varphi = 0$ and $180°$) when $h \sin \psi = 90°$. Figure 21-3 shows the vertical angle at which maximum, half-power, and half-voltage field intensities occur for the range of heights used for most applications. Figure 21-3 also shows values of F_{max} versus height for several values of dipole half length. F_{max} increases as the length is increased up to the optimum half length of $225°$. F_{max} also increases as the height is increased up to approximately $210°$. Figure 21-3 also shows the conical beamwidth for half-power field intensities as a function of the half length and the vertical angle ψ. Figure 21-3 provides the important characteristics of the main lobe of the radiation patterns for dipole lengths and heights normally employed for short-wave applications.

21.3. MULTIELEMENT HORIZONTAL-DIPOLE ARRAYS (CURTAINS)

The directivity and gain of antennas using horizontal dipoles may be increased by adding additional elements. The vertical directivity is increased by stacking elements one above the other to form a bay of two or more radiators. Horizontal, or more correctly, conical directivity may be increased by adding additional bays with the elements of adjacent bays collinear. A group of two or more such bays is termed a curtain. Finally, the antenna may be made unidirectional by adding a reflector curtain behind the radiator curtain. This provides an increase in gain of about 3 db, with very little effect on the pattern shape in the forward direction. The reflector curtain may be formed of tuned elements operated as parasitic reflectors, or a vertical reflector screen composed of closely spaced horizontal wires may be employed to provide reflector action approaching that of a highly conductive vertical plane.

Single Bays. Assuming sinusoidal current distribution and a perfectly conducting flat earth, the radiation pattern of a single bay comprising two parallel dipole radiating elements excited with equal in-phase currents, centers spaced S_v degrees vertically and with a height of h degrees to the mid-point between the radiators (Fig. 21-4), is given by

$$F = 4E_1 \sqrt{P} f(\varphi') \sin (h \sin \psi) \cos \left(\frac{S_v}{2} \sin \psi\right) \tag{21-6}$$

$$E_1 = E_2 = E_0 \sqrt{\frac{R_r}{R_{tt}}} \tag{21-7}$$

$$R_t = 2R_r + 2R_a + 2R_m(S_v) - 2R_m(2h) - R_m(2h - S_v) - R_m(2h + S_v) \tag{21-8}$$

where R_t = total operating resistances of the two elements; otherwise the terminology of Sec. 21.2 is followed.

Figure 21-4 shows the maximum field intensity developed by a two-radiator bay for a power of 1 kw and radiator half lengths of $180°$ ($\lambda/2$). The maximum field intensity is shown for a vertical spacing S_v of $180°$ and for the vertical spacing which provides maximum field intensity for a given height. Analysis of Fig. 21-4 shows that spacings somewhat greater than $180°$ provide maximum field intensity. Approximate maximum field intensity values for other length radiators may be obtained by multiplying the values obtained from Fig. 21-4 by the ratio of E_0 for the pertinent length to 167 mv/meter, the E_0 for a radiator with a half length of $180°$ ($\lambda/2$). Analysis of Fig. 21-4 enables a determination of the optimum vertical spacing for any given height.

Figure 21-4 also shows pertinent characteristics of the main lobe of the vertical radiation pattern for spacing between radiators of 180 and $240°$. The angles of maximum, half power, half voltage, and zero field intensities are given.

For four elements stacked vertically with a spacing of S_v degrees between adjacent
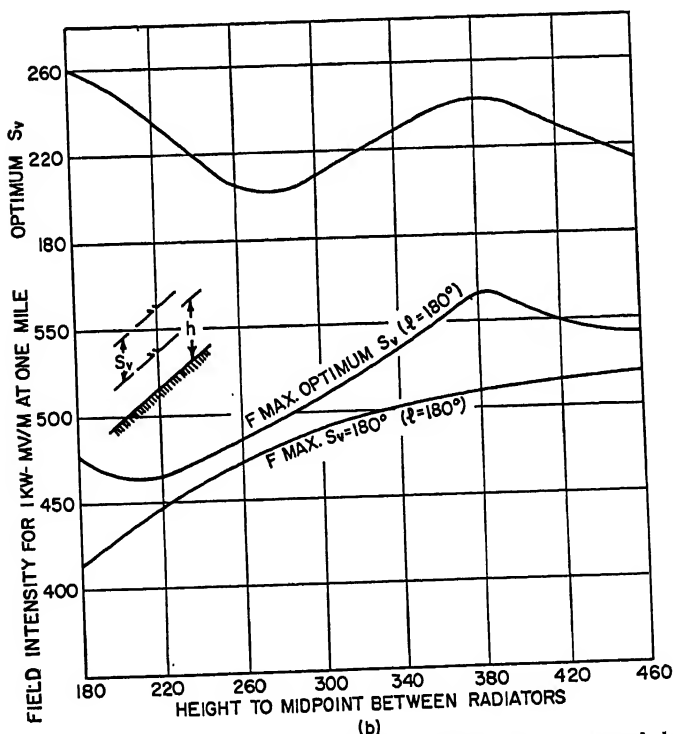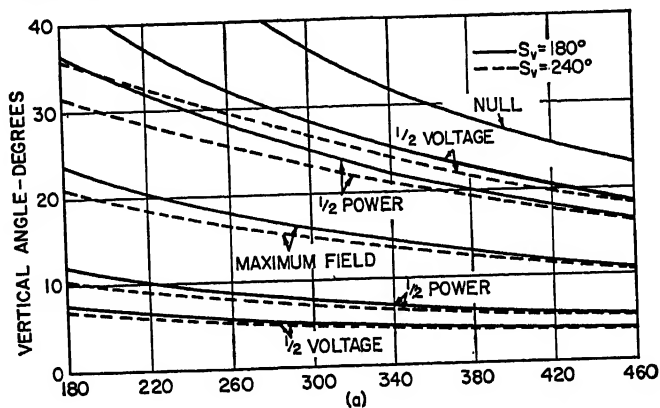
Fig. 21-4. Design curves for two stacked horizontal radiators above ground showing: (a) Vertical-radiation characteristics in equatorial plane. (b) Optimum vertical spacing for maximum field intensity, and F_{max} for 1 kw power ($l = 180°$).

radiators and height h to mid-point between lower radiator 1 and upper radiator 4 (Fig. 21-5), the radiation pattern is given by

$$F = 8E_1 \sqrt{P} f(\varphi') \sin (h \sin \psi) \cos \left(\frac{S_v}{2} \sin \psi\right) \cos (S_v \sin \psi) \qquad (21\text{-}9)$$

$$E_1 = E_0 \sqrt{\frac{R_r}{R_t}} \qquad (21\text{-}10)$$

$$R_t = 4(R_r + R_o) + 6R_m(S_v) + 4R_m(2S_v) + 2R_m(3S_v) - R_m(2h + 3S_v)$$
$$- 2R_m(2h + 2S_v) - 3R_m(2h + S_v) - 4R_m(2h) - 3R_m(2h - S_v)$$
$$- 2R_m(2h - 2S_v) - R_m(2h - 3S_v) \qquad (21\text{-}11)$$

R_t is the total operating resistance of the four elements which are assumed to be excited by equal in-phase currents.

Figure 21-5 shows values of maximum developed field intensity for 1-kw power vs. height for radiator spacings of 180 and 220° based on a radiator half length of 180°.

Figure 21-5 also shows the vertical radiation angles for maximum field intensity, half power, half voltage, and zero field intensity for different heights for radiator spacings of 180 and 220°.

Multibay Curtains. Assuming sinusoidal current distribution and a perfectly conducting flat earth, the pattern for a single curtain of two identical bays of horizontal-dipole elements, all with equal in-phase currents, is

$$F = 2E_1 f(\varphi') \sqrt{P} f(\psi) \cos \left(\frac{S_h}{2} \sin \varphi'\right) \qquad (21\text{-}12)$$

where, for a single horizontal radiator per bay,

$$f(\psi) = 2 \sin (h \sin \psi) \qquad (21\text{-}13)$$

for two stacked elements per bay,

$$f(\psi) = 4 \sin (h \sin \psi) \cos \left(\frac{S_v}{2} \sin \psi\right) \qquad (21\text{-}14)$$

and for four stacked elements per bay,

$$f(\psi) = 8 \sin (h \sin \psi) \cos \left(\frac{S_v}{2} \sin \psi\right) \cos (S_v \sin \psi) \qquad (21\text{-}15)$$

where $f(\psi)$ = vertical directivity of one bay
    S_h = horizontal spacing between centers of bays, degrees
    S_v = vertical spacing between radiators in one bay
    φ' = angle defined by Eq. (21-5).

The evaluation of E_1 for two-bay curtains by mutual-impedance method requires data for the mutual impedance between parallel staggered elements which are not available for the general case of odd-wavelength spacings and lengths. Values of mutual resistance for spacing intervals of 0.5λ for radiators of half length $\lambda/4$ are given by Kraus[7] and Pistolkors.[8] Equations for mutual impedance between parallel and staggered elements are given by Carter.[9] Because of the complexity of the mutual computations it is sometimes more convenient to evaluate E_1 by a graphical integration process. Conical radiation patterns are computed (for unit or assumed value of E_1) and the rms value determined by planimeter measurement of the polar conical patterns. These conical rms values are multiplied by $\sqrt{\cos \psi}$ and plotted on polar graph paper versus ψ (one quadrant). E_1 is then adjusted to make the enclosed area equal to 11,600 (mv/meter)², where the radiated power is 1 kw and field intensities are for the unit distance of 1 mile.
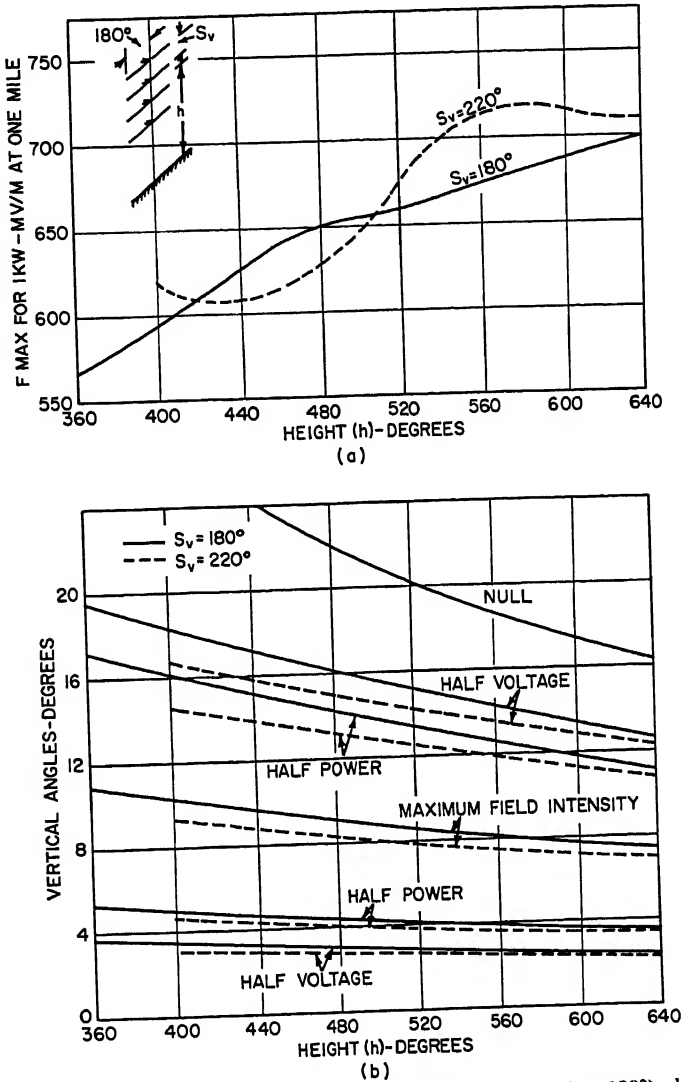
Fig. 21-5. Design curves for four stacked horizontal radiators ($l = 180°$) showing: (a) Maximum field intensity for vertical spacings (S_V) of 180 and 220°. (b) Vertical-radiation characteristics.

The pattern for three equal bays of radiators spaced S_h degrees between adjacent bay centers, all elements with equal in-phase currents, with other assumptions as outlined above, may be determined from

$$F = E_1 f(\varphi') \sqrt{P} f(\psi)[1 + 2 \cos (S_h \sin \varphi')] \tag{21-16}$$

where $f(\psi)$ depends on the number of radiating elements in each bay as given above in Eqs. (21-13) to (21-15).

Figure 21-6 shows the approximate gain of a two-bay antenna over a single bay with $l = 180°$ on the assumption that F_{max} in the equatorial plane falls at an angle ψ of approximately 15°. The relative gains were determined by assuming that the power gains were inversely proportional to the areas of the conical patterns for $\psi = 15°$. This method provides good accuracy for antennas with main lobes between $\psi = 10°$ and $\psi = 20°$ and with no large high-angle lobes.

Figure 21-6 also shows the conical beamwidth of two-bay curtains as functions of radiator length and bay spacing. The beamwidth is shown for an elevation angle of 15°; however, the data may be applied for vertical angles of 10 to 20° with good accuracy.
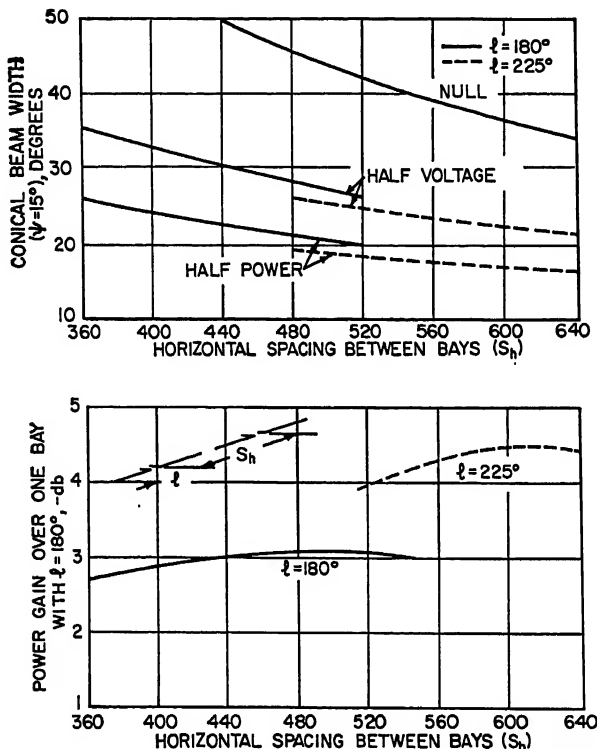
FIG. 21-6. Conical beamwidth of a two-bay antenna with horizontal radiators and approximate power gain compared with a single bay with $l = 180°$.

Curtain Arrays with Tuned Reflectors. Most applications require transmission (or reception) in only one general direction over a specified range of azimuth angles. To avoid unnecessary loss by radiation in the unused directions, tuned reflector elements may be erected behind the radiator elements. For the simple case of one horizontal radiating element and a parallel parasitic (zero-power) reflector element of the same length and height (Fig. 21-2), the radiation pattern is given by

$$F = 2E_1 \sqrt{P}\, f(\varphi')\, \sin\,(h \sin \psi)\, \sqrt{2M} \left[\frac{1 + M^2}{2M} + \cos\,(A - S_r \cos \varphi \cos \psi) \right]^{\frac{1}{2}}$$

(21-17)

$$E_1 = E_0 \sqrt{\frac{R_r}{R_1}}$$

(21-18)

$$R_1 = R_r + R_a - R_m(2h) + MZ_m(S_r) \cos [\sigma(S_r) + A] - MZ_m(S_d) \cos [\sigma(S_d) + A] \tag{21-19}$$

$$M = \frac{Z_m(S_d) \cos [\sigma(S_d) - A] - Z_m(S_r) \cos [\sigma(S_r) - A]}{R_r + R_a - R_m(2h)} \tag{21-20}$$

$$S_d = \sqrt{S_r^2 + (2h)^2} \tag{21-21}$$

where E_1 = field developed by radiator element for 1 kw at unit distance (1 mile), mv/meter

M = current or field ratio of reflector element referred to radiator element

A = relative phase angle of current in reflector element relative to current in radiator element, degrees

R_1 = operating resistance of radiator element referred to maximum current, ohms

S_r = spacing between radiator and reflecting elements, degrees

φ = horizontal angle measured from equatorial plane ($\varphi = 0$ for direction with radiator element forward of reflector element)

ψ = vertical angle above horizon

Z_m/σ = complex mutual impedance between elements for spacings indicated referred to maximum current, ohms

The optimum phase for the parasitic reflector element may be determined by solving Eq. (21-17) for several values of A and choosing the value which provides maximum field intensity at the required vertical angle. Figure 21-7 shows three vertical radiation patterns for practical values of heights, spacings, and radiator lengths.

For a complete antenna comprised of two bays and an identical curtain of tuned reflector elements, all radiator elements with equal in-phase currents and reflector elements with currents of ratio M at phase angle A relative to the radiator elements, the equation for determining the radiation pattern is

$$F = 2E_1 \sqrt{P} f(\varphi')f(\psi) \cos \left(\frac{S_h}{2} \sin \varphi'\right) \sqrt{2M} \left[\frac{1 + M^2}{2M} + \cos (A - S_r \cos \varphi \cos \psi)\right]^{1/2} \tag{21-22}$$

Similarly, for a three-bay curtain antenna with reflector elements, the radiation pattern is given by

$$F = E_1 \sqrt{P} f(\varphi') f(\psi)[1 + 2 \cos (S_h \sin \varphi')]$$
$$\sqrt{2M} \left[\frac{1 + M^2}{2M} + \cos (A - S_r \cos \varphi \cos \psi)\right]^{1/2} \tag{21-23}$$

where $f(\psi)$ is the bay vertical directivity given by Eqs. (21-13) to (21-15), with remaining terminology as given above. Exact evaluation of M and E_1 for such an array becomes a tedious process requiring staggered mutual-impedance data. A good approximate method is to evaluate M and E_1 for a single bay, neglecting the effect of the other bay, and then use these values in computing the patterns and gain. The E_1 thus determined should be divided by $\sqrt{2}$ for a two-bay antenna as the total power is equally divided between bays. This approximate method neglects the mutual impedance between elements in adjacent bays. A further refinement of this method is to determine the ratio M by single-bay computations and then complete the hemispherical-integration process. An alternative method is to compute the power gain of a single bay and then determine the power gain of the multibay antenna by comparison of the single and multibay conical radiation patterns computed for the vertical angle of maximum signal. The power gain of the three-bay antenna over the single-bay antenna will be very nearly equal to the ratios of the areas of the two conical patterns

adjusted for equal maximum radiation values. This method may also be applied to curtain arrays with screen-type reflector elements.

A reasonably good estimate of the gain of a two-bay curtain antenna with reflector elements may be obtained by determining E_{max} for a single radiator bay of the type
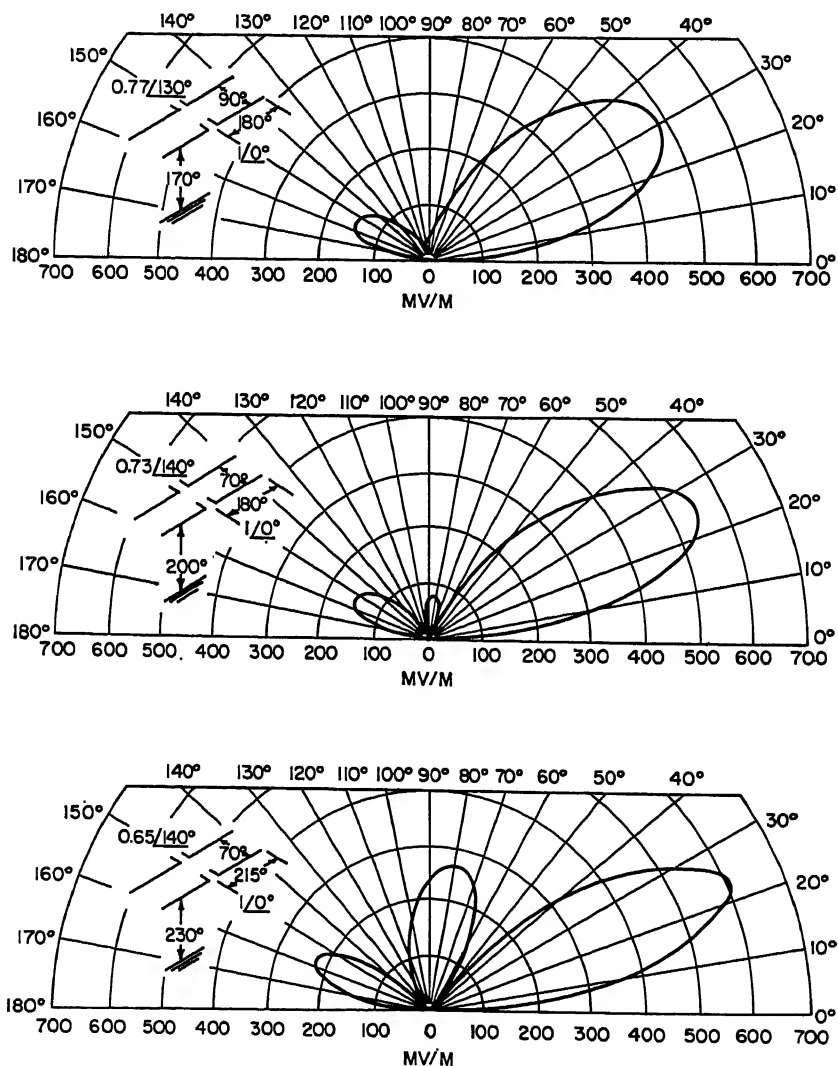
Fig. 21-7. Typical vertical radiation patterns for dipole radiator and tuned reflector element above ground (power = 1 kw).

used from Fig. 21-3, 21-4, or 21-5 and multiplying E_{max} by the appropriate factor, giving the effect of the additional bay as shown by Fig. 21-6. This adjusted E_{max} figure is then increased by 2.5 to 3.0 db to approximate the increase in gain due to the reflector elements. Typical gain values thus determined have been found to be in good agreement with gains computed by the more rigorous methods outlined above.

Curtain Arrays with Screen-type Reflectors. The radiation pattern for a multi-element curtain-antenna system with an infinite highly conducting vertical reflecting plane spaced S_r degrees behind the radiator curtain is given by:

For one bay,

$$F = 2E_1 f(\varphi') \sqrt{P} f(\psi) \sin (S_r \cos \varphi \cos \psi) \qquad (21\text{-}24)$$

For two identical bays,

$$F = 4E_1 f(\varphi') \sqrt{P} f(\psi) \cos \left(\frac{S_h}{2} \sin \varphi'\right) \sin(S_r \cos \varphi \cos \psi) \qquad (21\text{-}25)$$

For three identical bays,

$$F = 2E_1 f(\varphi') \sqrt{P} f(\psi) [1 + 2 \cos (S_h \sin \varphi')] \sin (S_r \cos \varphi \cos \psi) \quad (21\text{-}26)$$

where $f(\varphi')$ is given by Eq. (21-4), and $f(\psi)$ is given by Eqs. (21-13) to (21-15).

For the case of a single horizontal radiator of height h spaced S_r degrees in front of a vertical, parallel reflecting screen,

$$F = 4E_1 f(\varphi') \sqrt{P} \sin (h \sin \psi) \sin(S_r \cos \varphi \cos \psi) \qquad (21\text{-}27)$$

$$E_1 = E_0 \sqrt{\frac{R_r}{R_1}} \qquad (21\text{-}28)$$

$$R_1 = R_r + R_a - R_m(2h) - R_m(2S_r) + R_m(2 \sqrt{h^2 + S_r^2}) \qquad (21\text{-}29)$$

For a single-bay curtain with two vertically stacked elements and a reflecting screen,

$$F = 8E_1 f(\varphi') \sqrt{P} \sin (h \sin \psi) \cos \left(\frac{S_v}{2} \sin \psi\right) \sin (S_r \cos \varphi \cos \psi) \qquad (21\text{-}30)$$

$$E_1 = E_0 \sqrt{\frac{R_r}{R_1}} \qquad (21\text{-}31)$$

$$R_t = 2(R_r + R_a) + 2R_m(S_v) - 2R_m(2h) - R_m(2h + S_v) - R_m(2h - S_v)$$
$$- 2R_m(2S_r) - 2R_m(S_1) + 2R_m(S_2) + R_m(S_3) + R_m(S_4) \qquad (21\text{-}32)$$

where h = height to mid-point between radiators
S_v = vertical spacing of radiators
S_r = spacing to reflector

$$S_1 = \sqrt{S_v^2 + (2S_r)^2} \qquad S_2 = \sqrt{(2h)^2 + (2S_r)^2}$$
$$S_3 = \sqrt{(2h + S_v)^2 + (2S_r)^2} \qquad S_4 = \sqrt{(2h - S_v)^2 + (2S_r)^2}$$

As in the case of arrays with tuned reflector elements, the computation of E_1 for two-bay antennas with screen reflectors by the mutual-impedance method becomes quite complex and tedious. A good approximation may be obtained by computing E_1 for a single bay operating with half power by the mutual-impedance method (i.e., neglecting the mutual impedance between bays), or the alternative method of hemispherical integration may be employed.

The size and design of the screen reflector must be adequate to approach the action of an infinite highly conducting plane if the gain and radiation patterns as determined above are to be obtained in practice. Limited quantitative data for establishing minimum reflector dimensions are available; however, current practice for multiple-element curtains is to use screen-type reflectors composed of horizontal wires spaced about one-twentieth wavelength extending well above the highest dipole and beyond the dipole ends. For effective reflector action the screen should be spaced from 45 to 120° from the radiators. For low spacings the radiator currents and also the reflector wire currents increase to large values, resulting in relatively high losses and undesirable impedance-frequency characteristics.

Beam Slewing with Multibay Curtain Arrays. A two-bay curtain antenna offers the designer flexibility since the azimuthal direction of the main radiation beam can be controlled by supplying energy to the bays so that the phase angles of the currents in the radiators of one bay differ from the phase angles of the radiator currents for the
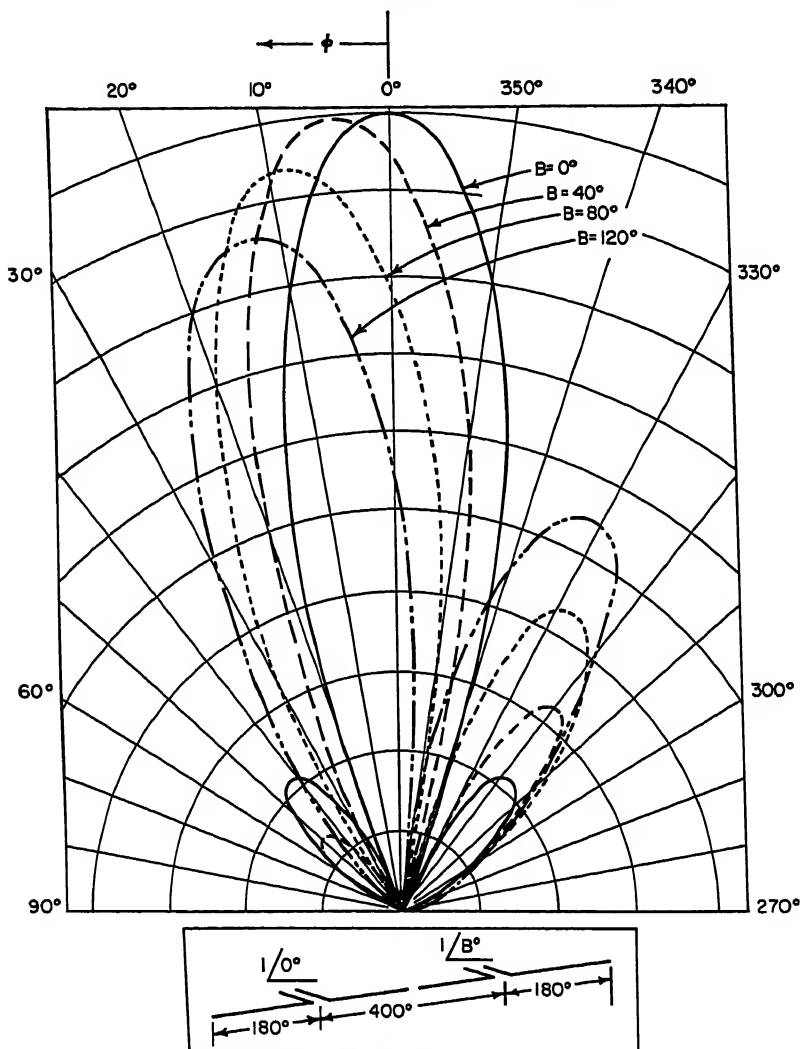
Fig. 21-8. Conical radiation patterns ($\psi = 15°$) for two-bay antenna showing slewing characteristics.

other bay. Thus the beam can be slewed several degrees clockwise or counterclockwise from the equatorial plane. The degree of slewing with good performance is limited because of the formation of a relatively large minor lobe as the slewing angle is increased, which results in a reduction of power gain.

The radiation pattern of a two-bay slewed antenna with the east bay leading the west bay by B degrees (west slew), φ taken counterclockwise, is given by:

For tuned reflector elements,

$$F = 2E_1 \sqrt{P} \, f(\varphi')f(\psi) \cos\left(\frac{S_h}{2} \sin\, \varphi' - \frac{B}{2}\right)$$
$$\sqrt{2M}\left[\frac{1 + M^2}{2M} + \cos\,(A - S_r \cos\,\varphi \cos\,\psi)\right]^{\frac{1}{2}} \quad (21\text{-}33)$$

For a screen-type reflector,

$$F = 4E_1 \sqrt{P} \, f(\varphi')f(\psi) \cos\left(\frac{S_h}{2}\sin\,\varphi' - \frac{B}{2}\right) \sin\,(S_r \cos\,\varphi \cos\,\psi) \quad (21\text{-}34)$$

Figure 21-8 shows some examples of slewed conical radiation patterns for $\psi = 15°$ for a two-bay curtain. The patterns reflect the relative loss in power gain as the degree of slewing is increased because of the formation of the large side lobe.

Currents and Power Losses. The maximum current magnitude on the dipoles for a curtain array of identical elements, based on sinusoidal current distribution, may be determined from:

For radiator elements,

$$I_{max} = \frac{E_1}{37.25(1 - \cos \ell)} \quad (21\text{-}35)$$

For reflector elements,

$$I_{max} = \frac{ME_1}{37.25(1 - \cos \ell)} \quad (21\text{-}36)$$

For a total power input P_0 to n radiator elements, the average no-loss operating resistance per element may be obtained from

$$R_1 = \frac{1,390P_0(1 - \cos \ell)^2}{nE_1^2} \quad (21\text{-}37)$$

The effects of radiator loss may be determined by estimating a lumped-element loss resistance R_a (usually 1 to 2 ohms) and computing the efficiency (power radiated divided by power input) by

$$\text{Effy (\%)} = \frac{R_1 \times 100}{R_1 + R_a + M^2 R_a} \quad (21\text{-}38)$$

This equation is valid for an antenna of n radiator elements with maximum current of I_{max} and n identical reflector elements with maximum current MI_{max}. For screen-type reflectors M may be assumed zero, but an additional loss resistance should be added to the value of R_a to represent losses in the reflector screen.

Feeder and Matching Problems. Figure 21-9 shows two typical feeder systems for curtain-type antenna arrays. Arrangement a is in common use and works well for antiresonant radiators ($\ell = 180°$) over a narrow frequency range. When the vertical spacing is 180° all radiators are excited by equal in-phase voltages and, neglecting the slight difference in feed-point resistances resulting from coupling from other radiators, the radiator currents will be equal and in phase. This arrangement
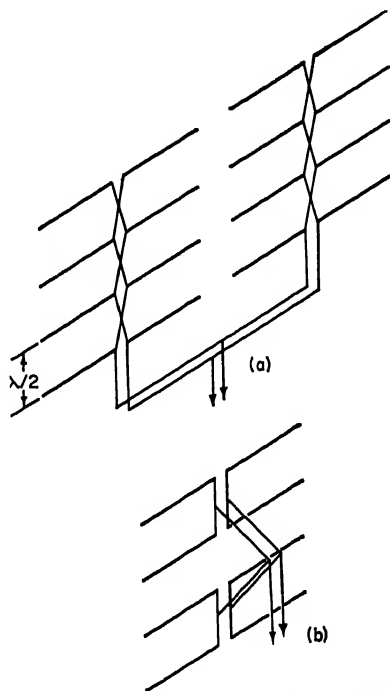
Fig. 21-9. Typical transmission line arrangements for curtain antennas.

also works well with high impedance (e.g., single-wire or closely spaced two-wire elements) since the input impedances of the four elements are effectively placed in parallel, thus lowering the impedance to a value which may be easily matched to an open-wire line and reducing corona problems on unmatched sections of line. For operating frequencies that differ more than a few per cent from the design frequency, the amplitudes and phases of the radiator currents are not properly controlled, making this type of feeder system unsuitable for operating over broad frequency bands.

Arrangement *b* shows a symmetrical feed method which ensures equal in-phase currents in the radiator elements of each bay over a wide frequency range (provided the input impedances are very nearly equal). The element feed lines are all made of equal length, and with careful design in regard to impedance matching, this system will operate satisfactorily over a frequency ratio of 1.5 to 1.0.

Determination of Input Impedance and Current Distribution. The operating resistance of a thin-wire horizontal dipole above ground, assuming sinusoidal current distribution, may be computed by the methods outlined above. The operating resistance R_1 is arbitrarily referred to the maximum current (current loop) along the radiator. For a half-wave radiator ($\ell = 90°$), the maximum current occurs at the input terminals or feed point of the dipole and $R_i = R_1$, where R_i is the input resistance. For sinusoidal current distribution the input resistance for greater lengths may be determined from

$$R_i = \frac{R_1}{\sin^2 \ell} \qquad (21\text{-}39)$$

For radiators of practical dimensions and for half lengths greater than about 120°, the actual current distribution departs considerably from sinusoidal, especially near the input terminals and for antiresonant lengths. For this reason the input impedance of dipole antennas with half lengths other than 90° are best determined by actual measurements or by reference to impedance computations for cylindrical dipoles.[10,11] In the case of single-wire dipoles, the radius of the cylinder is taken as the radius of the wire. For a multiwire cage-type dipole, the effective cylinder radius (a_{eff}) may be determined approximately by[10]

$$a_{eff} = a \left(\frac{n a_0}{a} \right)^{1/n} \qquad (21\text{-}40)$$

where a_0 = radius of each wire
       n = number of wires
       a = radius of cage

For radiators of appreciable effective diameter and half lengths greater than about 150°, the actual current distribution may have a considerable influence on the gain and conical radiation patterns of the complete antenna. In such cases, the radiation patterns should be computed on the basis of individual element directivity factors, $f(\phi')$, determined from integration of the expected current distribution. The current distribution may be predicted on the basis of current distribution data for cylindrical dipoles[10,11] or the current distribution may be measured on a model of the antenna or on the full-scale antenna itself.

Practical Considerations. Half-wave radiators used for transmitter applications are usually constructed as folded dipoles in order to obtain a feed-point resistance of the same order as the surge impedance of the open-wire balanced transmission lines usually employed. A two-wire folded dipole provides a feed-point resistance of approximately 300 ohms and can be easily matched to a 600-ohm line with a simple stub or quarter-wave transformer. A three-wire folded dipole provides an input resistance in the order of 660 ohms and, if properly dimensioned, may be used with a 600-ohm line without further matching.[12] The shunt-fed or delta-matching system may also be employed to obtain an input impedance equal to the surge impedance of

the transmission line.[13] A "Zepp"-type feeder arrangement may also be used with a dipole antenna end connected to a two-wire resonant line.[14] Dipole antennas of half-wave total length are usually used only where broad beamwidth is desired or where extreme simplicity is required or space is at a premium, because dipoles of full wave or slightly greater length provide considerably more radiated signal.

Transmitting dipoles of antiresonant length or optimum length for developing maximum field intensity are generally constructed of two or more appropriately spaced wires in order to improve the impedance-frequency characteristics and reduce voltage gradients at the ends and at other points of low current.

Adjustment and Performance Measurements of Curtain Antennas. After completion of design and construction, careful field adjustment of curtain antennas is required in order to assure optimum performance. Adjustments are usually required to match the input impedance of the antenna to the transmission line, and for tuned reflector types the reflector tuning stubs must be adjusted. Impedance matching should be accomplished by the use of a balanced r-f bridge or by the measurement of standing waves on the input line by other well-known sampling methods.

Reflector tuning may be accomplished by adjusting for maximum forward field intensity or minimum backward field intensity at distances several wavelengths from the antenna. Care must be taken to ensure that only the horizontally polarized component is measured, since at locations near the ground a strong incidental vertically polarized component may be observed and the direct horizontally polarized component is usually largely canceled by the reflected component.

An alternative method is to explore the operating parameters by sampling the currents on the radiators with shielded sampling loops and measuring relative phases and amplitudes of the radiator currents by means of a phase monitor and r-f voltmeters. This method has become standard practice for medium-wave directional antennas and has recently been used with good results for short-wave antenna adjustment. Such measurements permit a thorough check on the variation in amplitude and phase between elements due to second-order effects and show the effect of frequency variations on reflector-element currents and slewing adjustments.

Performance measurements of curtain antennas (or other types) may be obtained by airborne measurements to determine radiation patterns. Another method of establishing the performance is to compare the field intensity measured at a distant location with the field intensity obtained from a simple dipole element. A suitable system for averaging out propagation variations is to switch between the antenna under test and the reference dipole for many alternate periods of several minutes each. The accuracy is less dependent on different propagation modes if the vertical radiation pattern of the reference dipole is made as similar as possible to the vertical pattern of the antenna under test by carefully selecting the height.

Vertical Beam Slewing of Curtain Antennas. For bays composed of two or more vertically stacked radiator elements, the maximum power gain and the lowest vertical angle for maximum radiation for a given height are obtained with all radiator currents of equal amplitude and the same phase angle. Vertical patterns with maximum radiation at higher vertical angles may be obtained by changing the phase angles of one or more of the elements, by employing unequal currents, or by exciting only the lower radiator elements. For example, an antenna with four stacked radiator elements may be designed with separate transmission lines to feed the upper and lower pairs of elements, and the switching as required to obtain vertical beam slewing may be accomplished at ground level.

21.4. HORIZONTAL RHOMBIC ANTENNAS

General. Rhombic antennas are widely used for short-wave transmitting and receiving applications, especially for point-to-point circuits. The use of rhombic

antennas is attractive because of the relatively high gain provided at moderate cost, the broad frequency response from the input-impedance standpoint, and the ease of installation and maintenance. These favorable considerations must be weighed against the limitations of this type of antenna, which include loss of power in the terminating load, relatively large secondary lobes which result in additional power loss, and lack of freedom in independently controlling vertical and horizontal beamwidths.
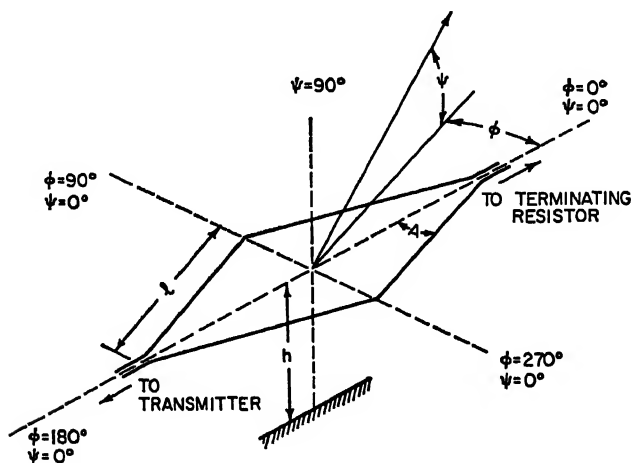
Fig. 21-10. Horizontal rhombic antenna showing symbols used.

Radiation Characteristics. The complete radiation pattern of a horizontal rhombic antenna in free space (Fig. 21-10; Chap. 4), assuming a constant-amplitude traveling wave along the wires, is given by[16–20]

$$F = 468.6 I_0 \ell \sin A \frac{\sin (m_1)}{\sqrt{m_1}} \frac{\sin (m_2)}{\sqrt{m_2}} \qquad (21\text{-}41)$$

$$m_1 = \pi \ell [1 - \cos \psi \cos (\varphi + A)] \qquad (21\text{-}42)$$

$$m_2 = \pi \ell [1 - \cos \psi \cos (\varphi - A)] \qquad (21\text{-}43)$$

where F = field intensity at 1 mile in direction at elevation angle ψ above horizon and horizontal angle φ from principal axis ($\varphi = 0$ for direction of wave travel), mv/meter
  ℓ = side length of rhombic, wavelengths
  A = angle between principal axis and side, degrees
  I_0 = current in rhombic wires, amp

For the case of $\varphi = 0$ (the principal vertical radiation plane) Eq. (21-41) becomes

$$F_{(\varphi=0)} = 74.62 I_0 \sin A \frac{1 - \cos [2\pi \ell (1 - \cos \psi \cos A)]}{1 - \cos \psi \cos A} \qquad (21\text{-}44)$$

The radiation as given by Eq. (21-44) for the principal vertical plane is horizontally polarized, but for the general case where $\varphi \neq 0$ the radiation contains both vertical and horizontal in-phase components and Eq. (21-41) gives the vector sum of these two components. Computations of the separate vertical and horizontally polarized components are not generally required, but the equations for such computations may be found in the literature.[18]

Radiation Resistance. The magnitude of the radiation pattern or power gain may be obtained from the above equations if the current I_0 is known. The value of cur-

rent can be computed from the radiation resistance by

$$I_0 = \sqrt{\frac{P_r}{R_r}} \qquad (21\text{-}45)$$

where P_r = power radiated. An approximate expression for the radiation resistance of an isolated rhombic antenna which provides good accuracy for side lengths greater than 2λ as given by Lewin[20] is

$$R_r \doteq 240(\log_e 4\pi\ell \sin^2 A + 0.577) \qquad (21\text{-}46)$$

The exact equation for computing the radiation resistance involving tabulated functions has also been evaluated by Lewin[20] and confirmed and presented in a different form by Chancy.[21]

Performance Curves. Figure 21-11a shows values of radiation resistance for rhombic antennas in free space with assumed constant-amplitude traveling wave for
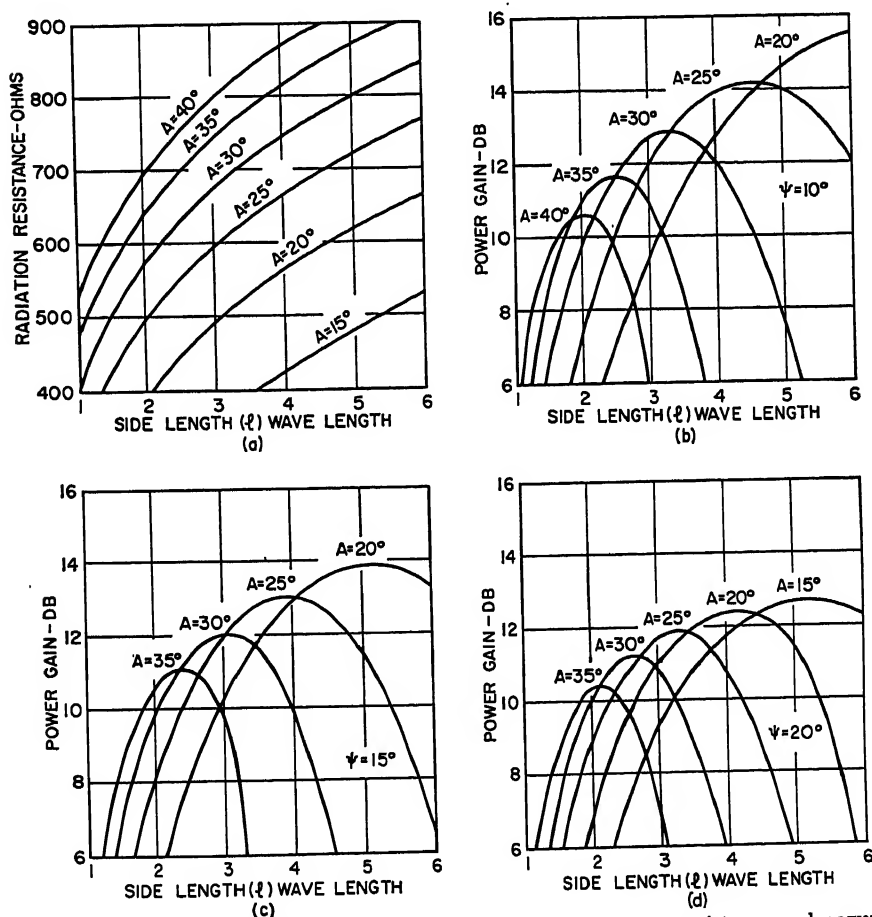
Fig. 21-11. Design curves for rhombic antennas showing radiation resistance and power gain (referred to $\lambda/2$ dipole) of rhombic antenna in free space for principal vertical plane ($\phi = 0$) for vertical angles ψ of 10, 15, and 20° (see Fig. 21-10).

various values of side angles A and length ℓ, expressed in wavelengths. These values were computed by Eq. (21-46).

Figure 21-11 also shows computed gain figures for a free-space rhombic antenna in terms of power radiated compared with a half-wave dipole antenna in free space. Values of power gain are given for vertical-radiation angles ψ of 10, 15, and 20° above the horizon and for the range of side lengths and side angles generally employed. The
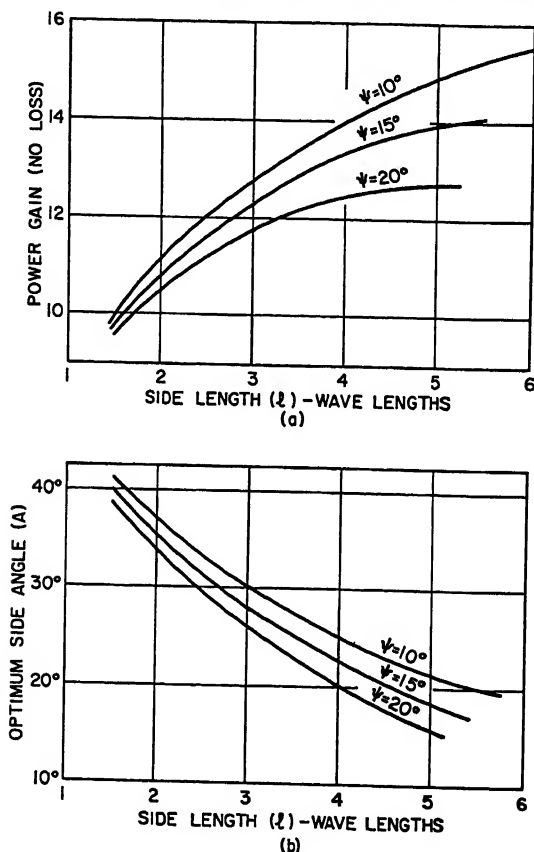
FIG. 21-12. (a) Power gain of free-space rhombic antenna of optimum design for maximum field intensity at vertical angles ψ of 10, 15, and 20°. (b) Side angle A for optimum design.

power gains shown are based on Eq. (21-44), with the current established from radiation-resistance values given by Eq. (21-46). Use of Fig. 21-11 enables a determination of the optimum side angle for a given length to provide maximum radiation at a given vertical-radiation angle. Variations in power gain with frequency can also be established.

Figure 21-12a shows the no-loss power gain over an isolated half-wave dipole for an isolated rhombic antenna with optimum side angle, as given by Fig. 21-12b, for vertical-radiation angles of 10, 15, and 20°.

Figure 21-12b shows the optimum side angle plotted vs. side length on the basis of providing maximum free-space radiation at the specified vertical-radiation angles, as interpolated from Fig. 21-11.

Figure 21-13 shows the conical beamwidths of horizontal rhombic antennas (isolated or above ground) with optimum side angle as given by Fig. 21-12*b*.

Rhombic Antenna above Ground. The radiation pattern for a horizontal rhombic antenna above a perfectly conducting flat ground is given by

$$F = 937.2 I_0 \ell \sin{(h \sin{\psi})} \sin{A} \frac{\sin{(m_1)}}{\sqrt{m_1}} \frac{\sin{(m_2)}}{\sqrt{m_2}} \qquad (21\text{-}47)$$

where h = height expressed in degrees and the other symbols are as defined for Eq. (21-41). Similarly, for the case of the principal vertical plane ($\varphi = 0$), the radiation is given by

$$F_{(\varphi=0)} = 149.2 I_0 \sin{(h \sin{\psi})} \sin{A} \frac{1 - \cos{[2\pi\ell(1 - \cos{\psi} \cos{A})]}}{1 - \cos{\psi} \cos{A}} \qquad (21\text{-}48)$$

An approximate value of field intensity or power gain for a rhombic antenna above ground may be obtained by assuming that the effect of the ground has a negligible
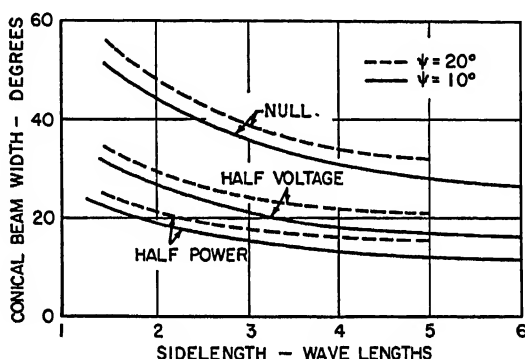
FIG. 21-13. Conical beamwidth of horizontal rhombic antenna of optimum design (side angle A determined from Fig. 21-12) for vertical angles ψ of 10 and 20°.

effect on the radiation resistance as given by Eq. (21-46). The power radiated is determined on the basis of the power input less the estimated power loss in the termination resistance (usually 2 to 3 db). The current can then be determined and substituted in Eq. (21-47) or (21-48) to provide the radiation pattern. This method has been found to provide good accuracy for relatively large antenna heights.

Based on the same assumption, the power gain for a rhombic antenna above ground may be obtained from

$$\text{PG} = \text{PG (no loss, free space)} + 20 \log 2 \sin{(h \sin{\psi})} - P_L \qquad (21\text{-}49)$$

where the PG (no loss, free space), is obtained from Fig. 21-11 for the appropriate vertical angle ψ, and P_L is the termination loss expressed in db.

Suppression of Minor Lobes. In applications where the suppression of minor lobes is important or more detailed pattern information is required, design determination by the methods outlined above involves many lengthy computations. An excellent method of determining the position and relative sizes of the major lobe and the more important minor lobes by means of stereographic charts is given by Laport.[22] Such an analysis of the minor lobes and the height function also permits an evaluation of the performance of the rhombic as influenced by height. Further details may be found in Chap. 4.

Special Types of Rhombic Antennas. Several special types of rhombic antennas have been developed in recent years in order to reduce the power loss dissipated in the terminating load and otherwise improve the performance.

Reentrant rhombics are designed with transmission lines and matching equipment to return the power reaching the "terminated" end of the rhombic back to the input transmission line. The impedance transfer and relative phase angle relationship obtained at the point where the terminating line connects to the input line should satisfy the requirement of low standing-wave ratio on the terminating line. The reentrant rhombic thus has no power loss dissipated in a load resistor, and the efficiency is therefore increased by some 2 to 3 db less losses in the terminating line and matching system. The disadvantage of this type of rhombic is that a given matching and phasing arrangement is effective only for a small range of frequencies, necessitating readjustment for appreciable frequency changes. The matching circuits are also quite critical and are difficult to adjust. A detailed discussion of the reentrant rhombic is given by Christiansen.[19]

Multiple rhombic antennas of various configurations have also been employed to reduce dissipation losses and improve the radiation patterns. Two or more identical rhombic antennas may be connected in tandem so that the output terminals of one connect to the input terminals of the next, with the last rhombic terminated with a resistor. This results in increasing both directivity and over-all radiation efficiency. Details of double rhombic antennas of this type as employed at the new transmitter plant at Wavre-Overijse, Belgium, have been published by Brown-Boveri.[23]

The radiation efficiency of rhombic antennas may also be increased by employing a tier of two identical rhombics installed one above the other so as to reduce the high-angle radiation lobes and increase the vertical directivity. The radiation efficiency of such an arrangement may be further increased by interlacing two or more such sets of tiered rhombics so that the two tiers overlap along the principal axis. Details of such arrangements, including measurements of current distribution and relative gain, are given by Christiansen.[19,44]

Practical Considerations for Rhombic Antennas. The simplest type of rhombic antenna consists of four single wires forming the rhombic sides, and antennas of this type are sometimes employed for receiving or low-cost transmitting installations. For most transmitting and for critical receiving applications "curtain" rhombics are employed, utilizing two or three wires per side, with the wires spread at the side corners and converging at the input and output apexes. Such curtain rhombics provide a substantially constant surge impedance along the length of the antenna, resulting in a lowering of the average surge impedance, a reduction in the termination loss, more constant input-impedance characteristics over a wide frequency band, and a reduction of precipitation static when used for receiving purposes.

Typical rhombic curtains for powers up to 50 kw are constructed of three conductors, each comprised of three twisted strands of No. 12 copper-weld wire. The conductors are separated from 5 to 15 ft in the vertical plane at the side corner suspension points. For low-power applications, an air-cooled resistor load is employed to terminate the end directed toward the transmission direction. For high powers, a shorted dissipation line constructed of stainless steel wire may be employed, provided the dissipation capacity is sufficient and the length is great enough so that the input impedance is very nearly equal to the surge impedance. The shorted end of the line should be grounded for lightning protection.

For transmitter powers of 100 kw or greater, the use of larger conductor size for the rhombic curtains is recommended and insulators must be carefully chosen to avoid corona troubles or excessive heating and power loss.

The input impedance of curtain-type rhombics is of the order of 600 to 800 ohms, so

that usually no matching stubs are required for terminating two-wire open-type transmission lines.

Reversible-direction operation can be obtained by providing a reversing switch to interchange the input-line and dissipation-line connections.

For receiving applications, rhombic antennas may be terminated by a wideband balanced-to-unbalanced shielded transformer for coaxial transmission-line installations. The opposite terminals (end directed toward transmitter) should be terminated in a resistor of about 800 ohms. In cases where bidirectional reception is desired, both ends may be terminated by transformers and connected to separate transmission lines.

21.5. OTHER TYPES OF ANTENNAS

Long Single-wire Antennas. Radiation patterns for single-wire resonant antennas of different lengths are shown by Fig. 21-14. The radiation pattern is given by

$$F = \frac{37.25I \cos\left(\frac{n\pi}{2}\cos\theta\right)}{\sin\theta} \qquad (21\text{-}50)$$

where n = odd integer giving number of half wavelengths for the wire, or

$$F = \frac{37.25I \sin\left(\frac{n\pi}{2}\cos\theta\right)}{\sin\theta} \qquad (21\text{-}51)$$

where n = even number of half wavelengths
  F = field intensity at 1 mile, mv/meter
  I = loop current, amp
  θ = angle of elevation with respect to radiator axis

For a terminated wire assuming constant current with progressive phase,

$$F = 37.25I \cot\frac{\theta}{2} \sin\left[\frac{\pi l}{\lambda}(1 - \cos\theta)\right] \qquad (21\text{-}52)$$

where I is the current in amperes and l is the length expressed in the same units as λ.

Long single-wire antennas can be employed effectively for some applications by adjusting the wire tilt and height above ground for maximum radiation in the desired direction, considering the effect of the image antenna. Vertical polarization may be obtained by tilting the wire in a vertical plane oriented in the direction of transmission, and horizontal polarization may be obtained by tilting the wire with respect to the transmission direction but keeping the wire in a horizontal plane at the appropriate height for the vertical angle of desired transmission.

Horizontal V Antennas. Horizontal resonant and terminated V antennas are shown by Fig. 21-15. The terminated V antenna provides a unidirectional pattern with maximum gain when the radiation lobes for each of the two conductors is aligned. The resonant V antenna has bidirectional characteristics, and hence reduced gain for a given size.

For a resonant V antenna in free space, the field intensity in the vertical plane passing through the bisector of the apex angle is given by

$$F = 74.5I \sin A \left[\frac{\sin\left(\frac{n\pi}{2}\cos A \cos\psi\right)}{1 - \cos^2\psi\cos^2 A}\right] \qquad (21\text{-}53)$$

and for a terminated V antenna,

$$F = 74.5I \sin A \, \frac{\sin\left[\dfrac{\pi \ell}{\lambda}(1 - \cos A \cos \psi)\right]}{1 - \cos \psi \cos A} \qquad (21\text{-}54)$$

where F = field intensity at 1 mile, mv/meter
$\quad\quad n$ = number of half wavelengths in each leg
$\quad\quad A$ = half of angle at apex
$\quad\quad \ell$ = side length in same units as λ
$\quad\quad I$ = current at current loop, amp
$\quad\quad \psi$ = elevation angle above plane of antenna

Optimum design for a given vertical angle ψ and side length requires that the apex angle A be chosen to maximize the above expressions. The vertical pattern for
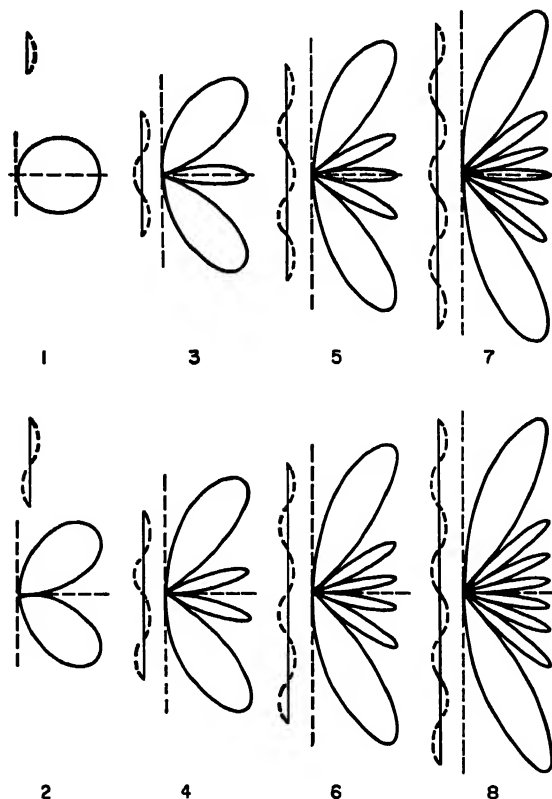
Fig. 21-14. Idealized polar patterns for straight wires with an integral number of half waves of pure standing-wave current distribution. (*Reference 22.*)

horizontal V antennas above a perfectly reflecting ground may be obtained by multiplying the above equation by 2 sin (h sin ψ), where h is the height above ground expressed in degrees.

Inverted-V-type antennas are constructed with the wires in a vertical plane above ground. Such an antenna may be treated as a rhombic antenna in free space by replacing the ground with the image radiators. The radiation resistance for an inverted V antenna is one-half the radiation resistance for the equivalent free-space

rhombic antenna as given by Eq. (21-46). Effective low-angle radiation of such an antenna depends on a highly conductive ground plane. Further details of V-type antennas are given by Kraus[27] and Carter.[28]

Fishbone-type Arrays. The fishbone high-frequency end-fire array is shown in Fig. 21-16a. A two-wire balanced central feeder is terminated at the far end, and half-wave dipole elements are coupled to the transmission line by high-reactance capacitors. Two such antennas may be used in broadside to provide a radiation

RESONANT
V-ANTENNA

(a)

TERMINATED
V-ANTENNA

(b)
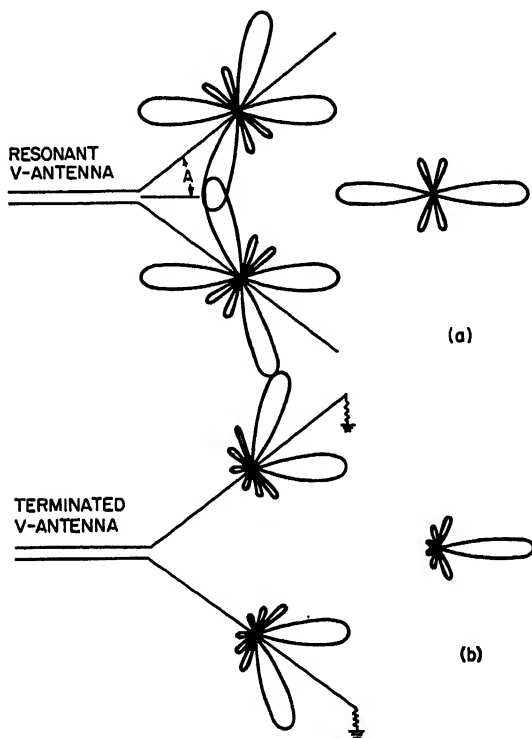
Fig. 21-15. (a) Calculated pattern of two-wavelength resonant V antenna. (b) Terminated V antenna with legs two wavelengths long. (*Reference 7.*)

pattern as shown by Fig. 21-16b. Such antennas provide good radiation-pattern characteristics over a broad frequency range (from 0.5 to 1.2 times the optimum frequency) and are usually employed for receiving applications, especially where space for an effective rhombic antenna is not available. Further details of fishbone-type antennas are given by Laport,[29] by Schelkunoff and Friis,[30] and in Chap. 5.

Parasitic Arrays Using Director and Reflector Elements. Parasitic-type beam arrays, consisting of a dipole radiating element and parallel reflector and director elements, have enjoyed considerable popularity for amateur radio installations operating on the higher-frequency bands and have also been employed for many commercial and military applications. This type of antenna is convenient for use at frequencies above about 14 Mc, where the relatively small physical size permits rotary beam construction so that the direction of maximum gain can be controlled from a remote location. A single half-wave dipole with a parasitic reflector element tuned for optimum forward signal will provide a gain of approximately 4 to 5 db compared with an isolated half-wave dipole antenna. Spacings in the order of 0.15 to 0.25

wavelength provide noncritical operation and high gain, whereas closer spacings involve high currents and resultant losses and unfavorable impedance vs. frequency characteristics.

A dipole with a tuned director element will also provide gains of from 4 to 5 db with optimum spacings ranging from 0.10 to 0.20 wavelength, depending upon the radiator losses. Very close spacings provide high computed gains only if losses are not considered, and experience indicates that the effects of losses, critical tuning, and bandwidth limit the minimum spacing which should be used.
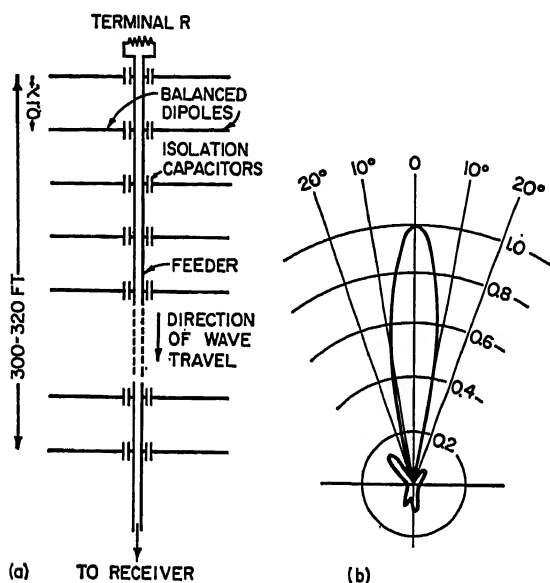
Fig. 21-16. (a) RCA fishbone antenna. (b) Horizontal pattern for two-bay fishbone antenna. (*Reference 22.*)

Three-element parasitic arrays, comprising a half-wave dipole radiator with tuned reflector and director elements, will provide gains of from 5 to 8 db, and additional director elements may be added to form a Yagi array, with a further increase in gain. The adjustment of such arrays is quite critical, especially as the number of elements is increased, because of the high mutual coupling between elements for the close spacings usually employed. Such arrays generally provide optimum performance only over a bandwidth of a few per cent of the center frequency, although greater bandwidth can be achieved at some sacrifice of gain. The input impedance of the driven element is usually quite low, in the vicinity of several ohms. For this reason, folded-dipole, gamma-, or delta-match arrangements are usually employed to increase the input impedance to a reasonable value. Further details of parasitic beam arrays are given in the literature[31,32] and in Chap. 5.

Corner-reflector-type Antennas. The corner-reflector antenna offers interesting possibilities for some high-frequency applications, especially at the higher frequencies. A 90° corner reflector may be formed by utilizing the ground as one reflecting plane and a vertical reflector curtain comprised of closely spaced horizontal wires as the other reflecting plane. This, in effect, is the same as a single horizontal dipole used with a vertical reflecting screen, and the equations and discussions given in Secs. 21.2 and 21.3 may be applied to this type of antenna. Corner reflectors can also be arranged

so that maximum radiation occurs in the horizontal direction, but for horizontal polarization, the effect of the image antenna must be considered in evaluating the radiation pattern. Antennas of this type appear practical to obtain low-radiation angles only for the higher frequencies, where it would be economical to support a corner-reflector antenna at a considerable height above the ground. Vertically polarized corner-reflector-type antennas also have useful applications, especially where a high ground conductivity obtains or a sea-water reflecting plane is available. Discussions of corner-reflector-type antennas are given by Kraus,[33] Moullin,[34] and in Chap. 11.

Flat-top Beam Antennas. Another type of antenna suitable for short-wave use consists of two closely spaced parallel horizontal radiators mounted at the same height above ground carrying equal out-of-phase currents. In free space, such an antenna will provide a figure-eight pattern with maximum radiation in the two horizontal directions at right angles to the radiating elements. The gain of such an array over a half-wave dipole antenna is from 3 to 4 db, depending upon the spacing and the loss resistance. Spacings in the order of 0.1 to 0.2 wavelength provide optimum gain for reasonable loss resistances, but somewhat greater spacings provide more favorable input-impedance characteristics. This type of array, when mounted at a suitable height above ground to obtain maximum radiation at the desired vertical angle, provides an effective antenna system which is relatively simple to erect and is not critical to adjust or maintain. The input impedances of both elements are identical, thus simplifying feeding arrangements.

FIG. 21-17. (a) Sterba curtain array. (b) Chireix-Mesny array. Arrows indicate instantaneous current directions, and dots indicate current minimum points. (*Reference 7.*)

Flat-top arrays may also be designed for equal phasing of the currents in the two elements and with a spacing of approximately one-half wavelength (lazy-H array). Such operation also provides a figure-eight-type pattern with maxima in the horizontal directions at right angles to the radiators and with a power gain of approximately 5 db over an isolated dipole antenna. Further details of flat-top antennas are given by Kraus.[35]

Special Curtain-type Antennas. Figure 21-17 shows examples of two specialized types of curtain arrays. The Sterba type,[36] shown by Fig. 21-17a, provides vertically polarized radiation and can be considered as two sectionalized Franklin-type vertical radiators spaced one-half wavelength and excited in phase.

Figure 21-17b shows the Chireix-Mesny array,[37] a French system for feeding a multi-element curtain which provides the equivalent of several horizontal-dipole elements. The arrows shown on Fig. 21-17b indicate points of maximum current and indicate the instantaneous current direction. The small dots indicate the locations of current minima. Each of the antenna types described above requires that the element lengths be cut or trimmed very carefully in order to obtain in-phase currents in all elements at a given frequency. The bandwidth of such antenna types is therefore quite limited.

New Developments in High-frequency Antenna Design. A new type of high-frequency antenna employing the horn principle has recently been reported by Brueckmann.[38] The surfaces of the horn are formed by a grid-type network of wires and the performance features high gain over a wide frequency range and effective suppression of side lobes.

A new concept in antenna design employing the logarithmic-periodic principle has been applied to high-frequency antenna requirements by DuHamel and Berry.[39] This type of antenna features almost constant beamwidth and gain over a wide range of frequencies. Details of log periodic antennas are given in Chap. 18.

21.6. EXAMPLES OF HIGH-GAIN ANTENNA INSTALLATIONS

Broadband High-power Curtain Array Used by the U.S. Information Agency. Basic information on broadband high-power curtain arrays used by the U.S. Information Agency is shown by Figs. 21-18 to 21-20. These antennas were designed to afford
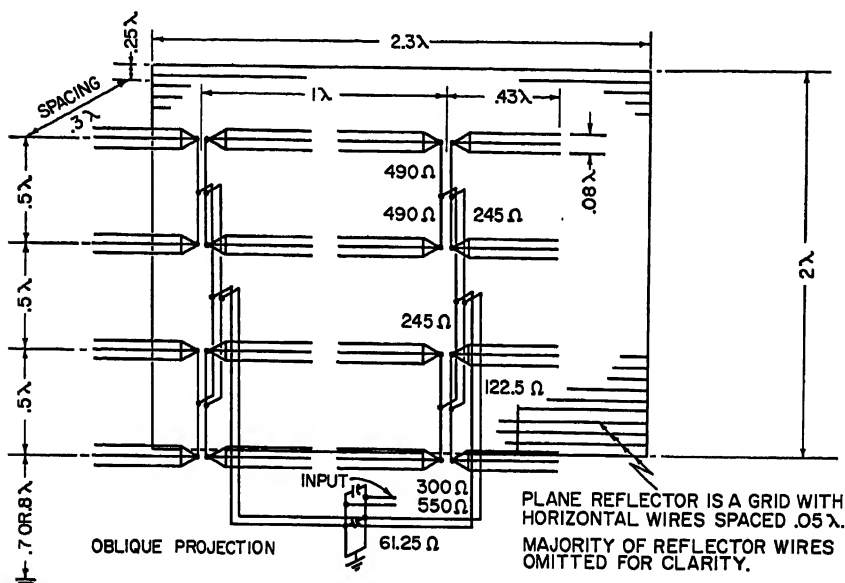
Fig. 21-18. Schematic of broadband high-power curtain array used by the U.S. Information Agency. (*Courtesy of USIA and Weldon & Carr.*)

optimum signal to overseas areas from stations based in the United States, and several installations of this advanced type of antenna have been made at the major United States international broadcasting stations. Each antenna unit consists of two bays of four horizontal full-wave dipole elements and a plane grid reflector. A typical installation includes either four or eight independently operating units supported from two or three common towers. Each antenna unit operates over a frequency range which includes two international broadcast bands and handles 200-kw amplitude modulated 100 per cent.

The desired broadband high-power characteristics are obtained by using in combination:

1. Low-impedance dipole elements
2. Element-to-reflector spacing of 0.3 wavelength

3. Branching type of distribution system with all transmission lines essentially matched

The terminal impedance of each dipole element approximates 490 ohms resistance. Successive line sections of 490, 245, and 122.5 ohms between branching junctions

AZIMUTHAL PATTERNS
VERTICAL ANGLE OF MAXIMUM RADIATION

9 mc BAND

11 mc BAND

VERTICAL PLANE RADIATION
PATTERNS IN PLANE OF MAXIMUM RADIATION

9 mc BAND
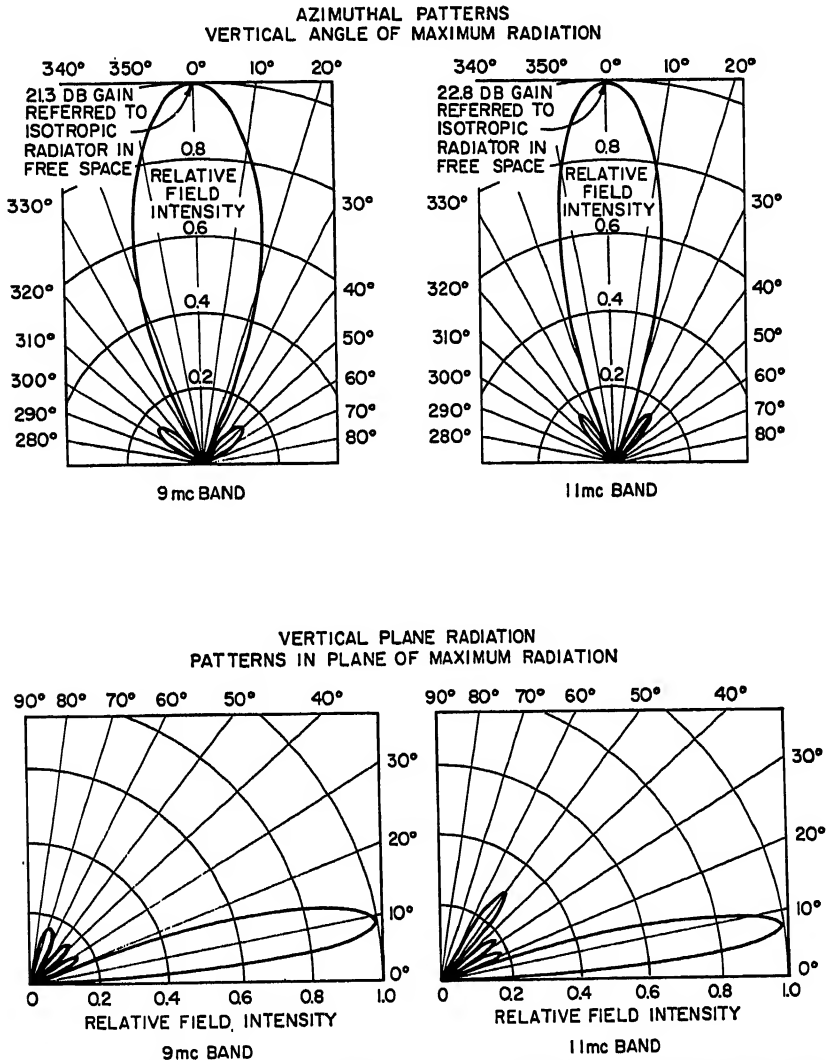
11 mc BAND

FIG. 21-19. Computed radiation patterns for 9- to 11-Mc broadband high-power curtain array used by the U.S. Information Agency. (*Courtesy of USIA and Weldon & Carr.*)

result in uniform phase and amplitude distribution among elements. The 61-ohm impedance resulting at the last branching junction is transformed to either 300 or 550 ohms by a transformer having two fixed line sections one-eighth wavelength long and two variable vacuum capacitors. The capacitors are adjusted to present a match to the transmitter line at the desired broadcast band.

Three-bay Curtain Array with Beam Slewing.　Figures 21-21 to 21-23 show pertinent details of a modern high-gain curtain antenna designed to provide horizontal beam slewing and to operate efficiently over two adjacent international broadcasting frequency bands. This antenna and several others of similar type are employed at the Radio Free Europe short-wave broadcasting station located near Lisbon, Portugal, to provide short-wave radio broadcasting service to central Europe. The antenna is designed for use with two 100-kw transmitters operating simultaneously in different frequency bands.
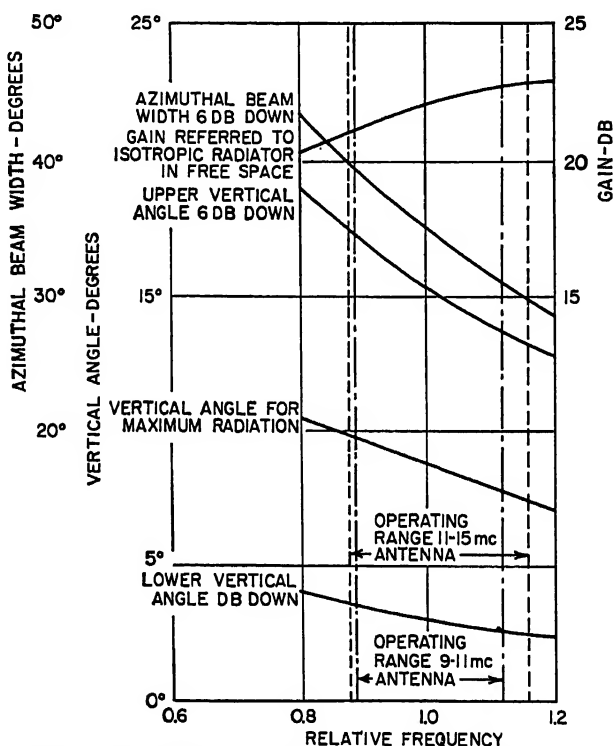
Fig. 21-20. Electrical characteristics of four-tier, two-bay curtain antenna; bottom element 0.7 wavelength above ground. (*Courtesy of USIA and Weldon & Carr.*)

Figure 21-21 shows the arrangement of the four-wire cage-type radiator elements and the parasitically excited reflector elements. Special double-stub tuning elements are used to obtain an impedance match on the bay feed lines over the range of frequencies covered by two adjacent frequency bands. The dimensions shown apply to the center of the higher-frequency band. A remotely controlled slewing switch is employed to insert a delay line in either end bay as required to obtain horizontal slewing of the beam.

Figure 21-22 shows the computed radiation patterns for the antenna, including the effect of actual current distributions (obtained from model measurements) on the patterns of the individual elements. The radiation patterns shown by Fig. 21-22 are plotted in terms of radiated field at 1 mile for an input power of 100 kw. The power gain compared to a half-wave dipole in free space is 22.4 db at 21.6 mc and 21.0 db at 17.8 mc.
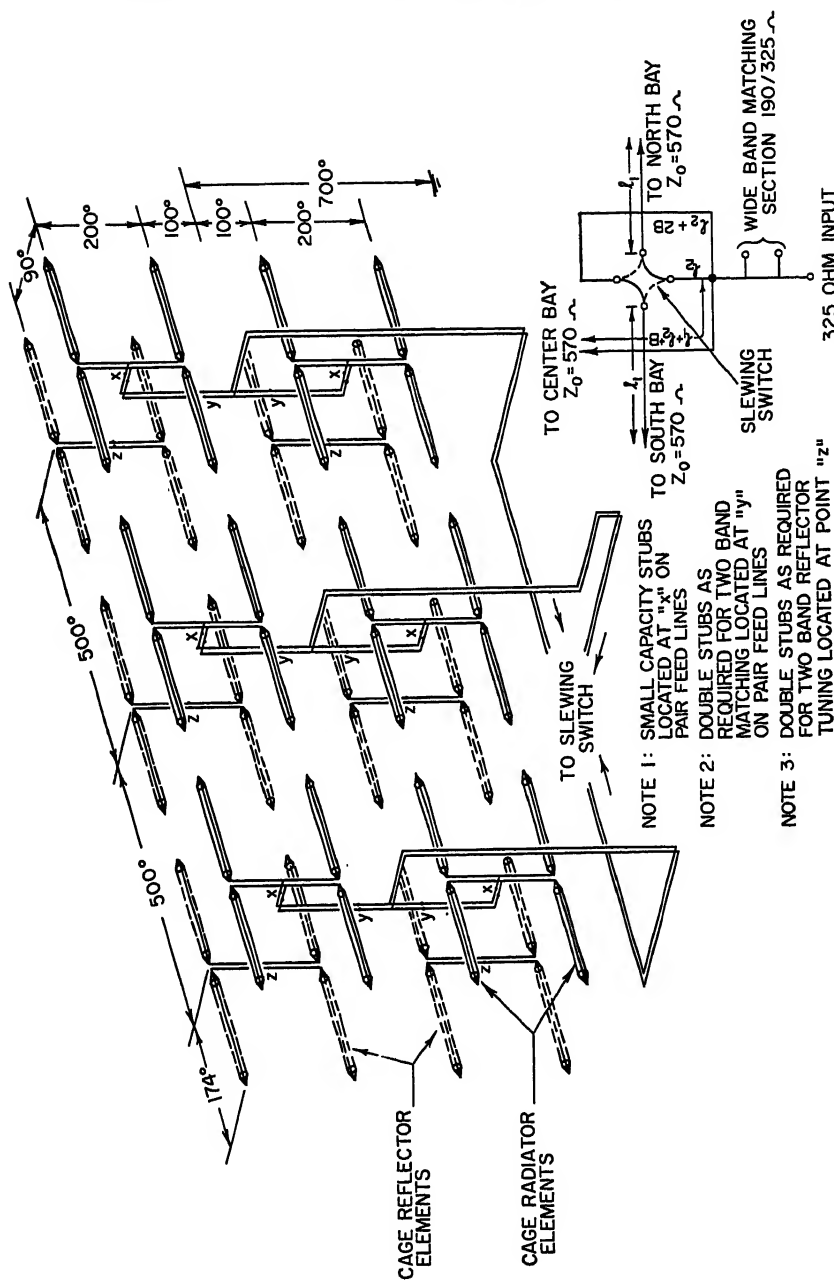
FIG. 21-21. Arrangement of elements and transmission lines: slewable curtain antennas with tuned reflectors installed at Radio Free Europe station near Lisbon, Portugal. (*Courtesy of Radio Free Europe and A. D. Ring & Associates.*)
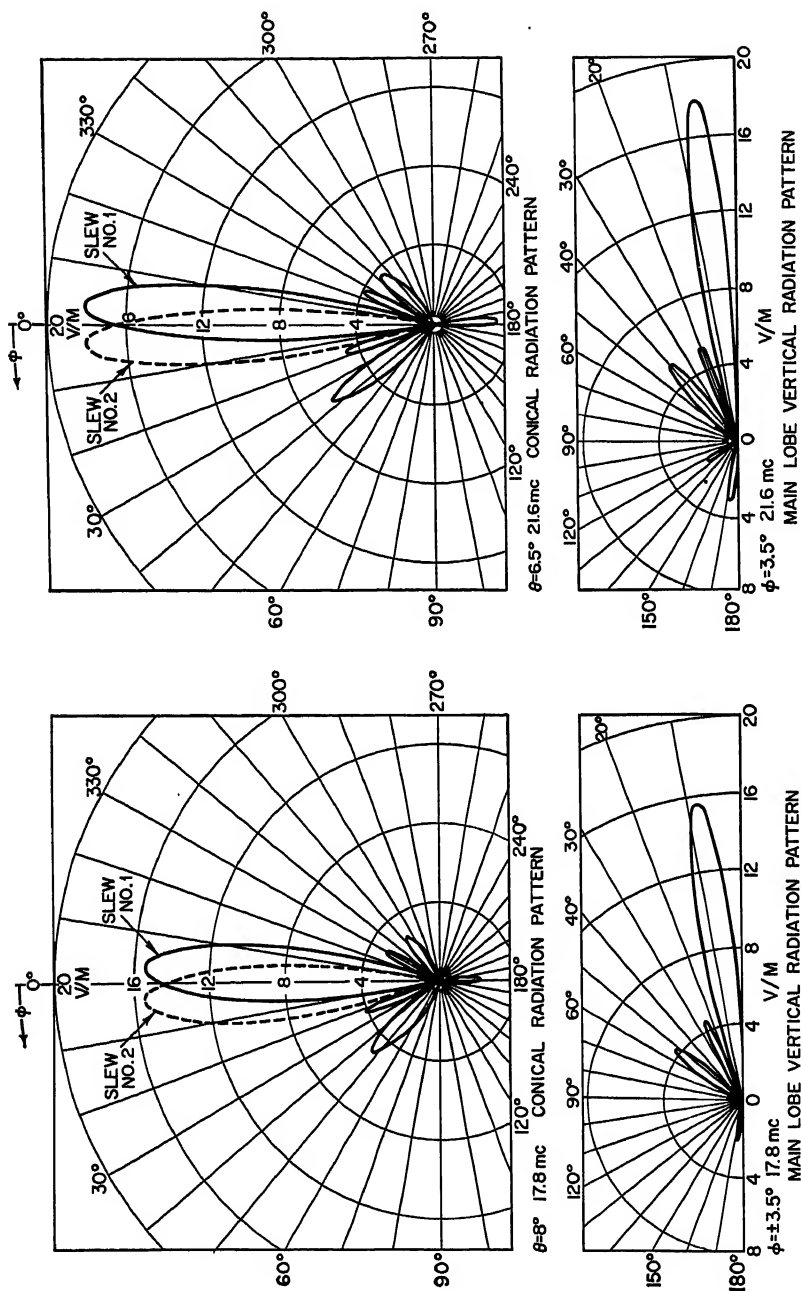
Fig. 21-22. Computed conical and vertical radiation patterns for RFE Lisbon antennas for operation in the 17.8- and 21.6-Mc international broadcasting bands.   (*Courtesy of Radio Free Europe and A. D. Ring & Associates.*)

Figure 21-23 shows the standing-wave-ratio characteristics for the antenna as measured at the input terminals. The tuning adjustments of the antennas were made by employing shielded sampling loops to sample the currents on the radiator and reflector elements. The sampling loops were connected to a phase monitor to permit measurement of the relative amplitude and phase angle on the various elements.
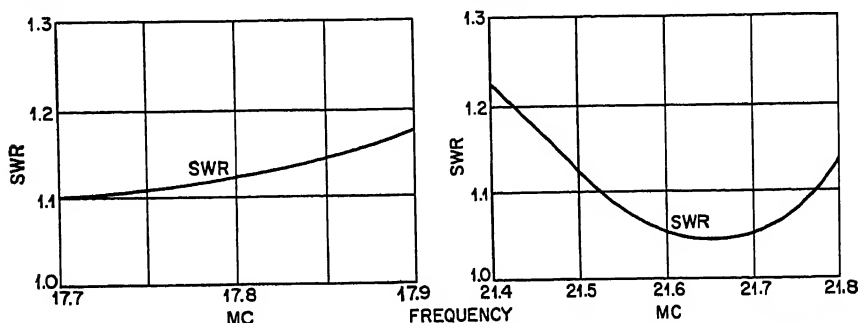
FIG. 21-23. Standing-wave-ratio characteristics: RFE Lisbon antennas. (*Courtesy of Radio Free Europe and A. D. Ring & Associates.*)

21.7. INSULATION REQUIREMENTS AND HIGH-VOLTAGE EFFECTS

For high-power transmitter applications, antennas and transmission lines must be designed so that the critical potential gradient for corona (pluming) will not be exceeded. For an isolated cylindrical conductor, the potential gradient is a function of the voltage and the radius of the conductor.[25,26] Other conductors removed by a distance large compared with the radii have only a small effect on the critical voltage. Measurements at frequencies in the range of 6 to 15 Mc indicate the following corona voltages for practical wire sizes and actual operating conditions, including the effects of rain. Voltages may be minimized by using low-impedance multiwire elements and

AWG wire size	Modulation crest rms voltage to ground, kv
3 strands No. 12 wire..........	7.5
No. 4.......................	12.0
No. 1/0.....................	16.0

low-impedance transmission lines and by maintaining a low standing-wave ratio on the lines.

Insulators should be designed to operate without undue heat loss or surface leakage. High-grade Steatite ceramic-type insulators with a leakage path of 12 in. and rounded end fittings have proved satisfactory for rms carrier voltages with amplitude modulation of 10 to 20 kv. Wire connectors and other hardware exposed to high voltages should be designed with a minimum exposed radius equal to the wire radius. Consistent with these requirements, it is also important to minimize the size of the connectors, insulator end fittings, and other metal objects contacting the wires so as to avoid undue capacity loading. Such loading can cause large impedance transformations, especially where the effects are additive, such as insulators placed at half-wave intervals on a transmission line.

Transmission lines of the open two-wire type with surge impedances in the range of 550 to 600 ohms are commonly employed for connecting antennas to the transmitter. Experience indicates that such lines constructed of conductors of three twisted No. 12 wires are satisfactory for operation with transmitter powers up to 20 to 50 kw (100 per cent amplitude modulation). For higher powers in the range of 50 to 200 kw, larger wire sizes in the order of No. 4 to No. 0 AWG are required to provide a satisfactory corona safety factor, assuming fairly low standing-wave ratios are maintained. Lower impedance lines with four or more conductors are sometimes employed for high-power applications, since the wire size required is less than for a two-wire line.[26]

21.8. RECEIVING ANTENNAS

Receiving antennas may be treated as transmitting antennas, and the radiation patterns computed in accordance with the data outlined in the previous sections of this chapter. For most short-wave applications, either dipole- or rhombic-type receiving antennas are employed. However, for specialized application, other types, including the fishbone-type array, are sometimes used. Diversity receiving-antenna installations are of great value in establishing reliable point-to-point relay circuits for either communications or broadcast relay purposes. It has been found that two rhombic antennas spaced a few hundred feet provide effective space-diversity action. A still further increase in reliability and quality can be obtained by using triple-diversity reception with three antennas, with the antennas spaced along the propagation path, as well as at right angles to the propagation path. Broadband transformers are available for terminating rhombic antennas for receiving purposes. Either closely spaced open-wire transmission lines or coaxial lines may be used, the latter providing better suppression of undesired noise signals which might be picked up by the transmission line. In cases where several receivers are to be operated from one antenna, wideband multicouplers are available to avoid undesirable coupling between receivers and maintain the correct impedance termination of the transmission lines.

REFERENCES

1. "Ionospheric Radio Propagation," *Natl. Bur. Standards* (*U.S.*) *Circ.* 462, June, 1948.
2. CRPL Series D Ionospheric Prediction Reports, issued monthly by the National Bureau of Standards (U.S.), Boulder Laboratories, Boulder, Colo.
3. "Analysis and Prediction of Sky-wave Field Intensities in the High Frequency Band," *Radio Propagation Unit Tech. Rept.* 9, August, 1950, prepared under the direction of the Chief Signal Officer by the Radio Propagation Unit, Baltimore Signal Depot, Baltimore, Md.
4. Donald H. Menzel: "Elementary Manual of Radio Propagation," Prentice-Hall, Inc., Princeton, N.J., 1948.
5. C. B. Feldman: "Deviations of Short Radio Waves from the London–New York Great-circle Path," *Proc. IRE*, vol. 27, p. 635, October, 1939.
6. Frederick Emmons Terman: "Radio Engineers' Handbook," pp. 698–708, McGraw-Hill Book Company, Inc., New York, 1943.
7. J. D. Kraus: "Antennas," p. 271, McGraw-Hill Book Company, Inc., New York, 1950.
8. A. A. Pistolkors: "The Radiation Resistance of Beam Antennas," *Proc. IRE*, vol. 17, pp. 562–579, March, 1929.
9. P. S. Carter: "Circuit Relations in Radiating Systems," *Proc. IRE*, vol. 20, p. 1007, June, 1932.
10. S. A. Schelkunoff and Harald T. Friis: "Antennas: Theory and Practice," John Wiley & Sons, Inc., New York, 1952.
11. R. King and D. Middleton: "The Cylindrical Antenna: Current and Impedance," *Quart. Appl. Math.*, vol. 3, pp. 302–335, June, 1946.
12. W. Van B. Roberts: "Input Impedance of a Folded Dipole," *RCA Rev.*, vol. 8, p. 289, June, 1947.

13. "The ARRL Antenna Book," 7th ed., pp. 102–103, The American Radio Relay League, Inc., West Hartford, Conn., 1955.
14. Reference 13, pp. 93–95.
15. E. Bruce: "Developments in Short-wave Directive Antennas," *Proc. IRE*, vol. 19, pp. 1406–1433, August, 1931.
16. E. Bruce, A. C. Beck, and L. R. Lowry: "Horizontal Rhombic Antennas," *Proc. IRE*, vol. 23, pp. 24–46, January, 1935.
17. Donald Foster: "Radiation from Rhombic Antennas," *Proc. IRE*, vol. 25, pp. 1327–1353, October, 1937.
18. A. E. Harper: "Rhombic Antenna Design," D. Van Nostrand Company, Inc., New York, 1941.
19. W. N. Christiansen: "Rhombic Antenna Arrays," *AWA Tech. Rev.*, vol. 7, no. 4, pp. 361–383, 1947.
20. Leonard Lewin: Discussion on "Radiation from Rhombic Antennas," by Donald Foster, *Proc. IRE*, vol. 29, p. 523, September, 1941.
21. Jesse Gerald Chaney: "Free Space Radiation Impedance of Rhombic Antenna," *J. Appl. Phys.*, vol. 24, pp. 536–540, May, 1953.
22. Edmund A. Laport: "Radio Antenna Engineering," McGraw-Hill Book Company, Inc., New York, 1952.
23. *Brown Boveri Rev.*, vol. 40, no. 10, October, 1953.
24. W. N. Christiansen: "Directional Patterns of Rhombic Antennae," *AWA Tech. Rev.*, vol. 7, no. 1, pp. 33–51, 1946.
25. F. W. Peek, Jr.: "Dielectric Phenomena in High-voltage Engineering," McGraw-Hill Book Company, Inc., New York, 1929.
26. F. C. McLean and F. D. Bolt: "The Design and Use of Radio Frequency Open-wire Transmission Lines and Switchgear for Broadcasting Systems," *J. IEE (London)*, pt. III, vol. 93, pp. 191–210, May, 1946.
27. Reference 7, pp. 407–408.
28. P. S. Carter, C. W. Hansell, and N. E. Lindenblad: "Development of Directive Transmitting Antennas by R.C.A. Communications, Inc.," *Proc. IRE*, vol. 19, p. 1773, October, 1931.
29. Reference 22, pp. 339–341.
30. Reference 10, pp. 479–490.
31. Reference 7, pp. 318–321.
32. Reference 13, Chap. 4, pp. 164–175.
33. Reference 7, pp. 328–336.
34. E. B. Moullin: "Theory and Performance of Corner Reflectors for Aerials," *J. IEE*, pt. III, vol. 92, pp. 58–67, June, 1945.
35. Reference 7, pp. 288–300.
36. E. J. Sterba: "Theoretical and Practical Aspects of Directional Transmitting Systems," *Proc. IRE*, vol. 19, pp. 1184–1215, July, 1931.
37. H. Chireix: "French System of Directional Aerials for Transmission on Short Waves," *Expll. Wireless and Wireless Eng.*, vol. 6, p. 235, May, 1929.
38. H. Brueckmann: "Suppression of Undesired Radiation of Directional HF Antennas and Associated Feed Lines," *Proc. IRE*, vol. 46, p. 1510, August, 1958.
39. R. H. DuHamel and D. G. Berry: "A New Concept in High Frequency Antenna Design," 1959 *IRE Convention Record*, pt. 1, p. 42.

Chapter 22

VHF AND UHF COMMUNICATION ANTENNAS

John F. Byrne

Motorola, Inc.
Riverside, California

and

Edward Bedrosian

The RAND Corporation
Santa Monica, California

22.1. INTRODUCTION

Mobile two-way communication systems present a number of engineering problems because of space, weight, and power limitations. Perhaps the most stringent requirements are placed on the antenna system, which should be small in size, pleasing in appearance, high in gain, rugged in construction, and low in cost. The selection of an

optimum antenna system for a given application requires a design compromise based on a thorough knowledge of the performance of available components. Such antennas are discussed in this section.

22.2. SYSTEM CHARACTERISTICS

The VHF and UHF communication systems considered here find their application in the land mobile service and in the coastwise and inland maritime service. The principal users are in the fields of public safety (fire, police, forestry, etc.), industry, and public communication (radio and telephone). Future development may also be expected in civil use through expansion of activity in the citizens' band.

These services are customarily established between a fixed (base) station and a number of mobile stations.* Since the requirements for base-station antennas and mobile antennas usually differ markedly, they will be treated separately in subsequent sections. Generally speaking, the service radii of most of these communication systems are measured in tens of miles, the range achieved being a function of the antenna heights and types, the transmitted powers, and the local terrain features. The range is further reduced at the higher frequencies because of the more nearly line-of-sight propagation.†

The principal operating frequencies employed in this general class of service are listed in Table 22-1, together with their corresponding channel authorizations and power limitations. The frequency range from 25 to 50 Mc is generally referred to as the "low band," 152 to 162 Mc as the "high band," and 450 to 460 Mc as the "450 band." Commercial assignments of channels in the low and high bands are intermixed with various government and amateur allocations. The technical literature contains a number of references[1-4] to the propagation characteristics of these frequencies and their suitability for mobile use.

Table 22-1

Frequency, Mc	Channel spacing, kc*	Channel bandwidth, kc	Number of channels authorized	Base-station power	Mobile-station power
25–30	20	6	53	To 5 kw	To 100 watts
30–50	40†	30	335	To 5 kw	To 100 watts
152–162	60	30	142	To 250 watts	To 100 watts
450–460	100	30	100	To 250 watts	To 25 watts
460–470‡	50	30	40	To 250 watts	To 25 watts

* Channel spacing is between channel centers.

† Some current operation is with 20-kc channel spacing and 6-kc split-channel bandwidth. Technical development (carrier-frequency stability) will determine the timing of narrow-band authorization in this and higher-frequency bands

‡ Citizens' band: authorizations for commercial use at the band edges depend on the development of citizens' use.

22.3. BASE-STATION ANTENNAS

Vertical antennas are fundamentally omnidirectional in the horizontal plane and are easily made moderately directional by the addition of parallel radiating or parasitic

* For extended range systems, one or more remote auxiliary base stations may be centrally controlled over wire, UHF radio, or microwave facilities.

† In some instances, the almost clearly defined coverage at high frequencies is an advantage when the area of interest is likewise clearly defined, as in the case of a municipality.

elements. Since the coverage desired by base stations is frequently of such a nature, it is not surprising that the resonant vertical radiator is found as the basic element in most systems.

The Vertical Radiator. In its simplest form the vertical radiator appears as a quarter-wave "whip," or monopole, above a ground plane. This is illustrated in Fig. 22-1 together with the equivalent dipole obtained by imaging the monopole in the ground plane. In the presence of an infinite perfectly conducting ground plane the image will mirror the monopole and cause a radiation field in the upper hemisphere which is identical to that which would be obtained from a dipole in free space. Since the monopole radiates only half as much power as the dipole, it follows that its radiation resistance is half that of the corresponding dipole.
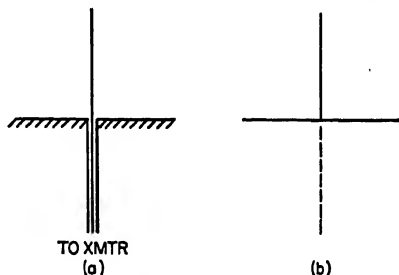
Fig. 22-1. Vertical radiator: (a) Above ground plane. (b) Equivalent dipole due to imaging.

The resonant resistances of a vertical monopole are given in Fig. 22-2 as functions of the length-to-radius ratio.[5] The dashed sections represent extrapolations from Hallén's computations, and the circles give a few experimental points. The significance of Fig. 22-2 lies in its demonstration of the relative constancy of the resonant resistances obtained when the monopole is an odd multiple of a quarter wave in length.
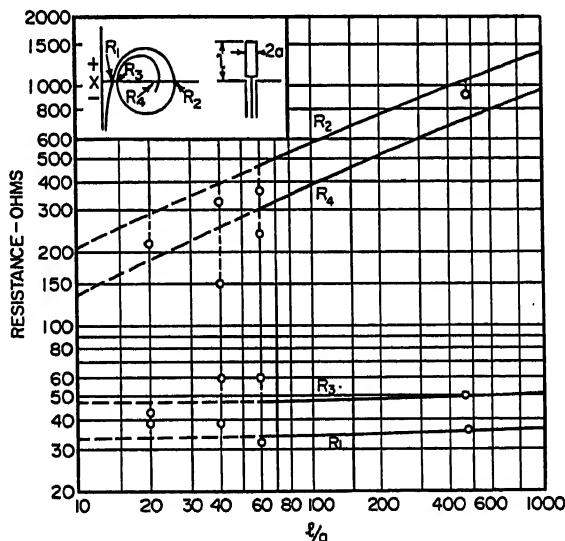
Fig. 22-2. Resonant resistances of vertical monopole above ground plane as functions of length-radius ratio.

(In most mobile applications the 35 to 37 ohms of resonant resistance at a quarter wavelength offer an adequate match to the 50-ohm coaxial cable commonly employed.) Quarter-wave monopoles are strongly favored in the low band because they offer adequate gain at a reasonable cost. Arrays become expensive because of their size; a quarter wave is roughly 8 ft long at 30 Mc. In the high band, a quarter-wave

monopole is only 18 in. long, and hence base-station antennas generally employ arrays because higher gains can be obtained without making the physical size excessive.

The Ground-plane Antenna.   Since base-station monopole antennas are usually mounted on masts atop buildings, a perfect ground plane is not present.   In most cases the ground plane is simulated by wires extending horizontally from the base of the monopole.   Two popular forms of such antennas are shown in Fig. 22-3a and b.   The ground-plane wires are usually four in number and from 0.28λ to 0.30λ in length, where λ is the wavelength; the optimum length is often selected experimentally to produce a
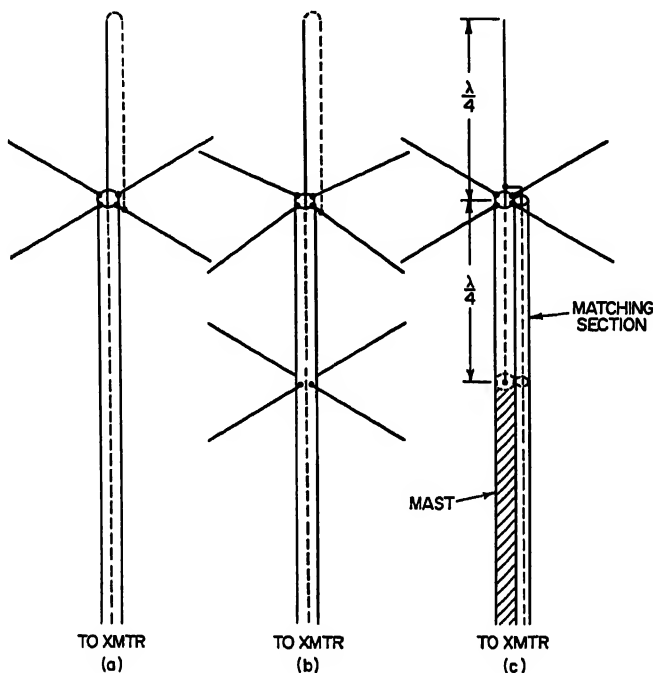
FIG. 22-3. Ground-plane simulation for the mast-mounted vertical antenna.   The folded section is shown in dotted lines, and a modified feed is shown in (c).

maximum of the vertical radiation pattern in the horizontal plane.   When the ground-plane wires are properly adjusted, the entire antenna closely resembles a dipole with respect to its radiation pattern and gain (typically within 0.1 db that of a free-space dipole).

A refinement is obtained by adding a parallel grounded section to the monopole to form a folded monopole.   The d-c path formed to ground affords protection against lightning surges; also the folded configuration is inherently more broadbanded than the single wire.   For equal diameters in the two parts of the fold, the radiation resistance would be quadrupled (nominally 4 × 37.5 = 150 ohms).   The grounded side is made smaller in diameter to lower the resistance to 50 ohms and provide a better impedance match to the conventional line than is obtained from the simple monopole.

An alternative feed is shown in Fig. 22-3c.   Its advantage is that the short-circuited quarter-wave line formed in the upper end of the mast supports the monopole rigidly without loading the feed point since it presents a high impedance.   A quarter-wave matching section is sometimes placed in the transmission line at the feed point to improve the impedance match between the antenna and the line.

The Skirted Antenna. Although the quarter-wave monopole over a ground plane behaves electrically as a half-wave dipole in free space, the radial projections of the ground rods are sometimes objectionable physically. Furthermore, the ground rods shield the mast and prevent the excitation of parasitic elements needed to form high-gain arrays. The coaxial skirted antenna shown in Fig. 22-4 behaves as a half-wave dipole in free space by using a skirt to form the bottom half of the dipole and a choke to isolate the antenna from the mast.
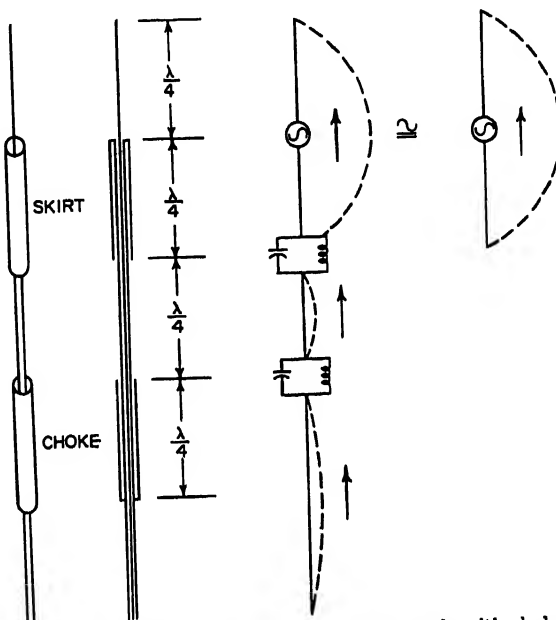
Fig. 22-4. Coaxial, center-fed half-wave dipole with choke.

Fundamentally, the current distribution on any vertical communication antenna should be such as to cause the main lobe of the vertical radiation pattern to lie on the horizon. Referring to Fig. 22-5a, if the center conductor of a coaxial cable is extended a quarter wave beyond the outer conductor, a current distribution is induced on the mast (outer conductor), as indicated by the dotted lines on the equivalent wire antenna. The relative direction of the current in each half-wave section is emphasized by adding arrows to the diagram. It is clear that the alternating phases of this induced current cause a spreading and splitting of the main lobe and the appearance of minor lobes. Of course, the amplitude of the induced current decreases with distance from the feed point, but sections of unfavorably phased current will cause harmful effects. Also, the presence of mast currents causes the entire antenna to become "touchy," i.e., to alter its radiation pattern and input impedance when touched.

Forming a skirt by turning down the outer conductor does not change the current distribution on the upper half wavelength of the antenna (Fig. 22-5b). However, the inside of the skirt becomes a short-circuited quarter-wave line which creates a high impedance at the base of the skirt. The effect of this high impedance is to produce a potential difference across the opening of the skirt and cause the induced current in the next half wavelength to be in phase with the upper section. The effect of the skirt is shown on the equivalent-wire-antenna diagram by inserting an antiresonant circuit at the appropriate point and reversing the phase of the current beneath it.

Two or even three skirts may be added to the mast as shown in Fig. 22–5c, but the reduced excitation of the lower sections diminishes the effectiveness of each additional skirt.[6] Thus, while the multiple-skirt coaxial antenna resembles a collinear array of in-phase half-wave elements, its gain is not as great.   Typical gain values are tabulated in Table 22-2, but since no test data are available for this type of antenna, the values given are merely engineering estimates.

(a)   (b)   (c)
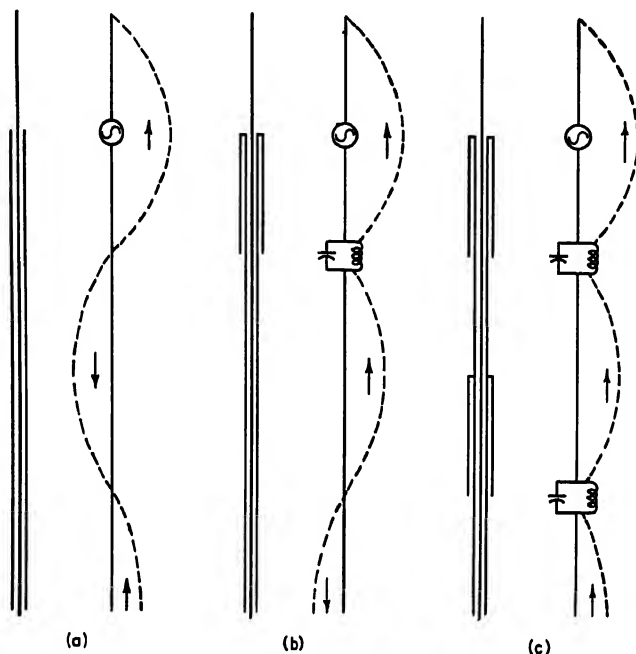
FIG. 22-5. Evolution of multiple-skirt coaxial antenna.

The relatively large diameter-to-length ratio of a practical skirt produces an end effect which requires that the exterior length of the skirt be reduced by a factor of from 0.8 to 0.9 and the interior length by from 0.95 to 0.98.[6] This is accomplished by cutting the skirt to the proper exterior length and inserting a dielectric slug in the skirt to increase its electrical length.

Table 22-2. Gain in Decibels over a Half-wave Dipole for Various Arrays

Antenna	Number of elements					
	2	3	4	6	7	8
Skirted coaxial....................	1–2	2–3				
Modified Franklin.................	...	3.2	4.0	...	7.2	
Series-fed collinear................	...	4.23	...	6.5		
Mast-mounted collinear array.......	...	....	3.1	6.2	...	6.3

Another element used in some coaxial antennas is the choke, which provides increased isolation from the remainder of the mast.   The choke is a skirt which has been inverted

and mounted a quarter wavelength beneath the lowest skirt. This places two high-impedance points a quarter wavelength apart, and since the shortest resonant element is a half wavelength, there is little excitation of this section. This is illustrated in Fig. 22-4 for a single-skirt antenna, showing how it leads to an equivalent free-space half-wave dipole. Although resonant sections can appear beneath the choke, the poorly excited quarter-wave choke section and the increased separation from the upper section usually make further mast currents negligible. In general, skirted coaxial
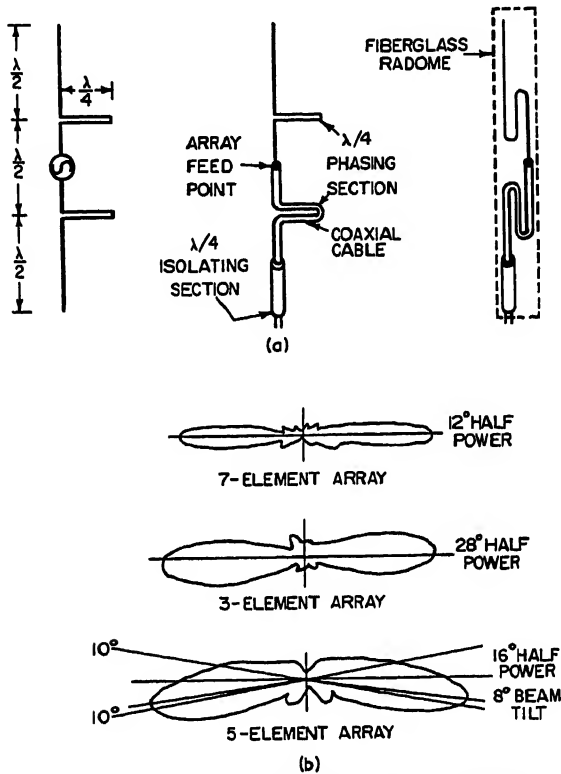
FIG. 22-6. (a) Development of modified Franklin array. (b) 450-Mc vertical radiation patterns.

antennas display increased sensitivity to frequency changes, because of the rapid variation in impedance exhibited by short-circuited lines in the vicinity of antiresonance, and therefore require careful adjustment.

The Vertical Franklin Array. A modification of the Franklin array is illustrated in Fig. 22-6a.[7] The basic Franklin array employs short-circuited quarter-wave lines to perform the same function as the skirts described above. The chief failing of the multiple-skirt coaxial antenna is the poor excitation of the lower skirts The embodiment shown permits center feed, which improves the over-all excitation while maintaining a simple construction. The improved current distribution among the radiating elements permits an increased gain as compared with the skirted coaxial antenna. Also, center feed prevents beam tilting with frequency since the phase variation displayed by the currents induced in the parasitic sections are symmetrical with respect to the principal plane of radiation. The measured gain in decibels over a half-wave

dipole is given in Table 22-2 for a number of elements.   Vertical radiation patterns at 450 Mc for seven- and three-element symmetrical arrays and a five-element tilted array are shown in Fig. 22-6b.

The Collinear Array. The series-fed collinear array shown in Fig. 22-7 employs periodic annular slots in the outer conductor of a coaxial line to excite half-wave dipoles formed by adding skirts symmetrically about the slots.[3]   The slots are spaced 0.7λ apart physically to keep the side lobes 15 to 20 db down.   Dielectric loading of the feed line makes the internal spacing a full wavelength to provide proper phasing.   The
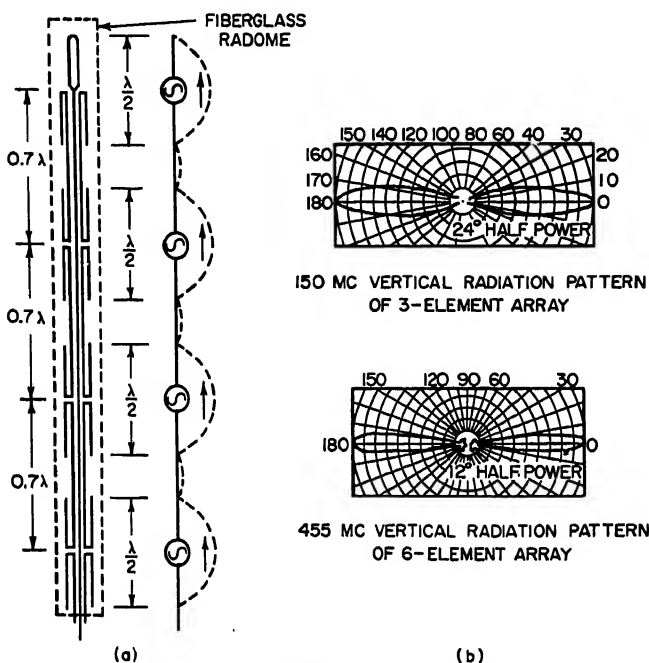
FIG. 22-7. Series-fed, collinear array.

entire antenna is enclosed in a Fiberglas radome for protection and rigidity.   The measured gain in decibels over a half-wave dipole is given in Table 22-2 for arrays of three and six elements   The vertical radiation patterns at 150 Mc for the three-element array and at 455 Mc for the six-element array are shown in Fig. 22-7b.

Another omnidirectional, high-gain array shown in Fig. 22-8a consists of a number of folded half-wave dipoles which are series-fed by a coaxial line.[9]   The dipoles are placed symmetrically on opposite sides of the mast but yield a fairly omnidirectional horizontal pattern by virtue of their shape and their spacing with respect to the mast, the circularity of the pattern being ±1.5 db in the high band and ±0.7 db in the 450 band.   The measured gain in decibels over a half-wave dipole is given in Table 22-2 for arrays of several elements.   A typical vertical radiation pattern and gain plot for the eight-element array are shown in Fig. 22-8b.

Directional Antennas. While omnidirectional coverage is the type most frequently desired, there is an occasional need for a bidirectional pattern when communication is desired along a given path such as a pipeline, a highway, or a railroad.   Coverage resembling a cardioid is desirable when the region to be covered is more or less circular but where the base station must be located at the periphery.   This situation arises

when the local prominence used to hold the antenna is a nearby hill rather than a tall building.   Coastal cities often find their hub near the coast line, again making an off-center, circular pattern desirable, the direction of the pattern being reversed to provide maritime service.   Unidirectional, or beam-type, patterns are the most efficient for point-to-point coverage and constitute another general class of directional antennas.

The most common arrays of antenna types used to form these patterns are illustrated in Fig. 22-9.*   The bidirectional antenna (Fig. 22-9a) consists of a pair of

TYPICAL VERTICAL RADIATION PATTERN
FOR 8-ELEMENT ARRAY

(a)   (b)
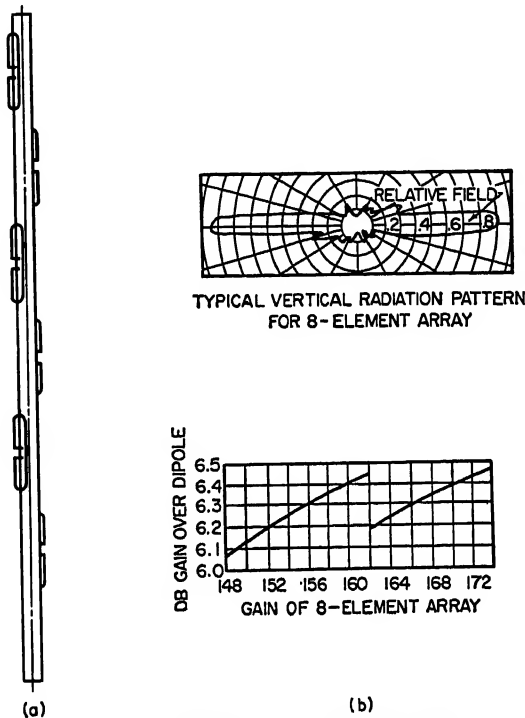
FIG. 22-8. Mast-mounted, collinear array.

dipoles spaced approximately 0.2λ apart and given a 180° phase difference by inserting an additional half-wave section of line between one of the antennas and the junction with the line from the other.   Thus broadside signals arrive in phase at the individual antennas and cancel at the junction, while in-line signals combine nearly in phase in the common line.   The antenna shown exhibits a gain of 3.2 db over a half-wave dipole. Increased directivity and gain can be obtained by combining further properly spaced and phased elements.   A single monopole and reflector can be combined as in Fig. 22-9b to form a cardioidal pattern.

Unidirectional arrays commonly employed in communication systems are illustrated in Fig. 22-9c.   The corner-reflector type usually uses a single half-wave dipole in conjunction with a screen or grid reflector.   The square corner (90°) reflector is the most popular, although 120° reflectors are sometimes used when less directivity is desired. Gains of 7.5 to 8.0 db relative to a half-wave dipole are typical for the former, and

* The radiation patterns shown in Fig. 22-9 were abstracted from the technical literature published by the Andrew Corporation, the Gabriel Company, and the Mark Products Company.

5.2 db for the latter. The spacing of the dipole from the corner is usually 0.25λ to 0.5λ and is selected to give a desirable radiation pattern and radiation resistance. Details of these effects are given in Chap. 11. The reflector itself should have minimum dimensions of $a = 2s$, $b = 0.6λ$, and a grid spacing, if any, of 0.1λ.
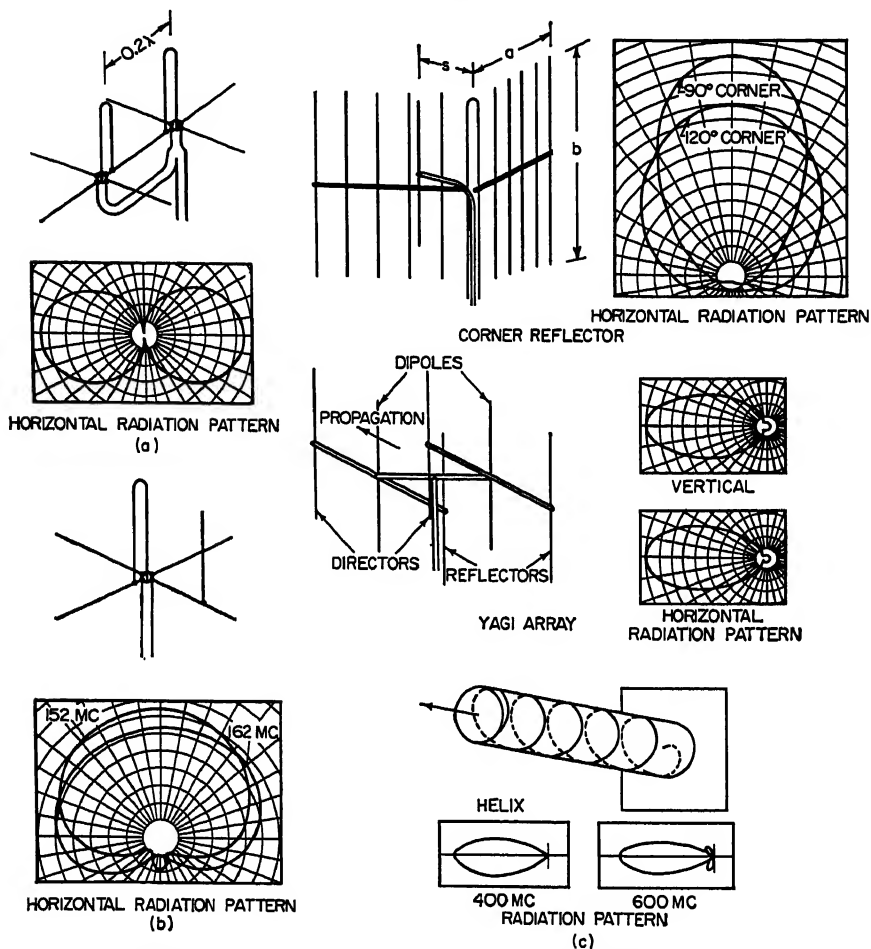
Fig. 22-9. Various types of directional antennas suitable for base-station use: (a) Bidirectional. (b) Cardioidal. (c) Unidirectional.

The Yagi antenna employs a reflector and one or more directors to form a simple but effective directional array. A stacked pair using single directors as illustrated in Fig. 22-9c can display a gain in excess of 15 db.

The only antenna in current use which does not employ vertical polarization is the helical antenna, which is treated in Chap. 7. Its circularly polarized pattern is very nearly symmetrical about its axis, thus giving a "pencil-beam" type of pattern. Compared with the antennas previously discussed, it is quite broadband, showing relatively small variations in impedance or radiation resistance over frequency ranges of as much as 2:1 when radiating in the axial mode. Gains of 10 to 15 db are possible without excessively large structures. Also, the use of right- or left-sense polarization permits

greater decoupling on repeaters. Multiple-helix arrays can combine polarizations of opposite sense to provide linear polarization.

As contrasted with FM and television transmission, mobile and point-to-point communication systems are fortunate in having relatively narrow bandwidths (30 kc maximum), which preclude many difficult broadbanding problems. Even the high-gain arrays described can be tuned by simple matching techniques; of course, they may require retuning if the operating frequency is changed.

22.4. MOBILE ANTENNAS

The requirement that an antenna be capable of operating from a moving vehicle restricts the choice of antenna types markedly. Vertical polarization is virtually a
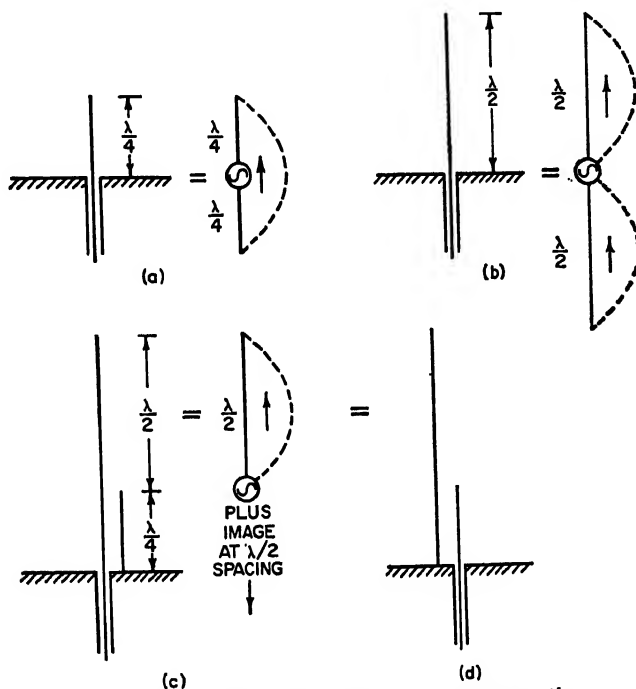
FIG. 22-10. Rooftop antennas of various configurations.

must, and except for rare exceptions an omnidirectional horizontal radiation pattern is desired in order to make communication independent of the orientation of the vehicle. Several possibilities exist for locating the antenna on the vehicle, the location usually determining the suitable antenna type.[10]

The Rooftop Antenna. The designation "rooftop" applies to antennas mounted on a more or less flat surface of a vehicle such as the roof of an automobile or train, the deck of a ship, or the cab or trailer of a truck. Such surfaces provide good ground planes and lead to the quarter-wave rooftop monopole as an ideal choice for an antenna. In the high band a quarter-wave monopole is 18 in. long and makes an excellent antenna, which closely approximates a free-space half-wave dipole. The construction is rugged and simple and is not of an objectionable appearance.

The physical length of 6 in. for the 450-Mc quarter-wave monopole reduces the aperture roughly ninefold, as compared with a high-band monopole, and hence further

aggravates a situation which already suffers from reduced transmitter powers and receiver sensitivities as well as increased line-of-sight limitations. However, an increased gain can be obtained by lengthening the radiating element. Figure 22-10a illustrates the simple quarter-wave rooftop monopole: as pointed out with reference to Fig. 22-2 its resonant resistance is relatively independent of the wire size and the variation in impedance is small in the vicinity of resonance. Extending the radiator to a half wavelength as in Fig. 22-10b leads to an equivalent free-space, full-wave dipole with a theoretical gain of 1.67 db relative to a half-wave dipole. However, the high antiresonant resistance encountered at the feed point makes such an arrangement
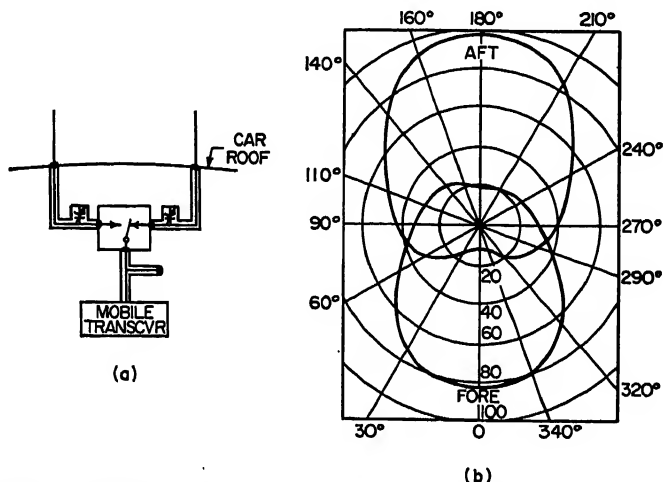
FIG. 22-11. (a) Mobile directive-antenna system. (b) Typical antenna patterns.

impractical to feed from the usual type of coaxial line, and some sort of matching section becomes necessary in the transmission line. The variability of the antenna impedance with wire size and frequency must be accepted as the inevitable consequence of increasing the gain.

The arrangement of Fig. 22-10c uses a two-wire quarter-wave matching section exterior to the coaxial line. The increased separation between the half-wave monopole and its image increases the theoretical gain to 3.26 db relative to a half-wave dipole because of the favorable mutual impedance but introduces a slight matching problem since the fluttering of the wires varies the spacing, and hence the characteristic impedance, of the matching section. A spacer may be placed at the top of the matching line if the feed-point impedance is not too high (i.e., if the length-to-radius ratio of the half-wave radiating section is fairly small), but care must then be exercised to avoid mismatch and degradation of performance in operation due to dirt, moisture, or ice. The antenna of Fig. 22-10d is basically similar but offers some lightning protection by using the grounded wire as the radiating element.

Practical antennas of the foregoing types generally display somewhat less gain than the figures quoted because of the imperfectness of the average rooftop as a ground plane.

When directional mobile antennas are desired, they are most conveniently made of rooftop elements. An interesting example[11] is the antenna evolved to eliminate interference at the vehicle when operating roughly midway between repeater stations on a superhighway. As illustrated in Fig. 22-11a, a pair of quarter-wave monopoles are spaced somewhat less than a quarter wave apart and switched to serve alternately

as the driven and parasitic elements, of a directional array, similar to that depicted in Fig. 22-9b. The resulting cardioidal pattern is reversible and provides a 5:1 field-strength ratio, as shown in Fig. 22-11b.

The Bumper-mount Antenna. Rooftop quarter-wave monopoles are impractical for most land vehicles in the low band because of their height. They are then mounted on the front or rear of the vehicle, usually on the rear bumper in the case of automobiles. The dissymmetrical location of the vehicle with respect to the antenna and the lack of adequate ground plane (there is usually a fairly high impedance from the vehicle to the actual ground) cause a performance which varies with the particular installation.
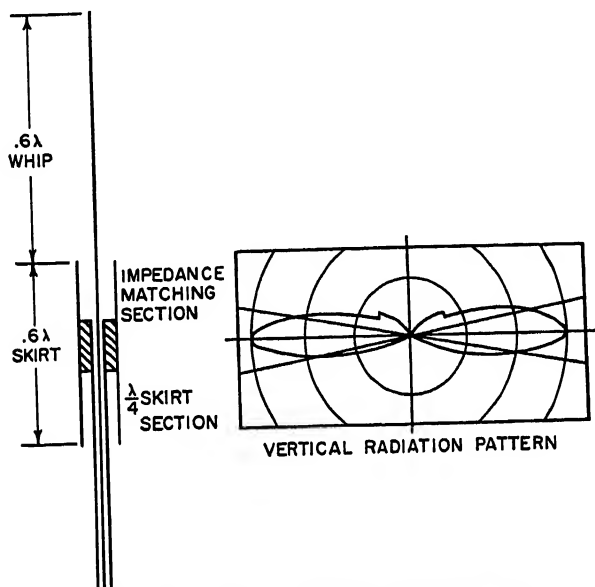
FIG. 22-12. High-gain, 450-Mc coaxial antenna.

The average gain is often near that of a free-space, half-wave dipole, but the influence of the vehicle on the radiation pattern (both horizontal and vertical) is not easily predictable and is best found by measurement.[12]

The coaxial, center-fed half-wave dipole shown in Fig. 22-4 is often used as a high-band, bumper-mount antenna when it is impractical or undesirable to use a rooftop monopole. The performance is not substantially different for the two types, except that the vehicle causes the expected pattern perturbations. Resonances of projections on the vehicle must be considered at the higher frequencies. Objects such as flag supports, brackets, and broadcast-band antennas can seriously distort the radiation pattern.

High-gain antennas for the 450 band are better suited to bumper than to rooftop mounting. The double- and triple-skirt coaxial antennas discussed with respect to Fig. 22-5 work well as bumper-mount antennas. A high-gain, 450-Mc bumper-mount antenna (also suited for base-station use) is shown in Fig. 22-12.[13] The monopole and the skirt are both made 0.6λ in length to give an effective 1.2λ radiator with a subsequent measured gain of 3 db over a free-space half-wave dipole. A matching section couples the coaxial line to the relatively high impedance feed point, while the skirt contains the conventional short-circuited, quarter-wave base section. The matching

section differs from a quarter wave in length since it is necessary to tune out the feed-point reactance which appears for a 1.2λ radiator.

The Cowl-mount Antenna.   Many automobiles mount broadcast-band antennas on the cowl or the rear deck over the fender well.   In some applications it is desirable to mount VHF or UHF communication antennas in the same fashion, even combining their function when possible.   Typical of such use is the disguised antenna shown in Fig. 22-13 for use by law-enforcement agencies that wish to avoid detection by displaying an antenna obviously designed for VHF or UHF communication.   In the low band the disguised antenna is from an eighth- to a quarter-wave long and is tuned by placing short-circuited stubs on the transmission line.   The high-band disguised antenna is ¾λ in length and uses the corner window post of the car body to serve as the second conductor of a two-wire quarter-wave matching section, as in Fig. 22-10c.

FIG. 22-13. Disguised antenna.

Some attention is being directed currently toward developing a high-gain, cowl-mounted, 450-Mc antenna, but no antenna has emerged as yet with a clear-cut superiority over the rooftop antenna.   In general, there is less distortion of the horizontal radiation pattern for a cowl-mount antenna than for a bumper-mount.

Testing.   It may be concluded from the foregoing discussion that the performance of mobile antennas can differ greatly from that which might be expected on the basis of theoretical considerations alone.   The effect of the vehicle on both the radiation pattern and the antenna impedance may be significant, and an experimental procedure is indispensable for successful design.

Electrical similitude permits scale-model testing,[14,15] which is a useful method for simplifying tests.   Unlike aircraft, however, land and water vehicles operate in the vicinity of an imperfect earth, which is not always well simulated by a ground plane.   Furthermore, models do not scale the loss factors, dielectric constants, and current distributions well enough for some purposes.   Hoods, doors, trunk lids, etc., cause impedance discontinuities on the surface of the vehicle and thus affect the current distributions, particularly at the higher frequencies.   For example, full-scale tests[12] indicate that interferences in the radiation pattern are due to high-density currents in the favored paths to ground and that one solution is a modification of the lower extremities of the vehicle by bonding and strapping.   There is a current trend toward full-scale testing on an actual vehicle which gives a more accurate picture of the performance to be expected from various vehicle-antenna combinations.   Minor effects due to varying parameters can then safely be extrapolated from associated model tests.

Polarization Dispersion.   Although vertically polarized antennas are employed in mobile communication systems, operation in mountainous terrain or in metropolitan areas having tall buildings can alter polarization by reflection.   Tests in hilly terrain with antennas of various polarization indicate that substantial improvements can be realized by switching polarization upon encountering fading.[16]

22.5. SYSTEM DESIGN CONSIDERATIONS

The choice of suitable antennas for a VHF or UHF communication system seldom depends solely on the characteristics of the system in question.   This is particularly true of the base-station antenna since the factors which make a particular location desirable as the base-station site for one system usually apply equally well for other

systems and it is not uncommon to find a number of base-station antennas and masts in proximity at the selected site. These and other considerations affecting antenna selection and location are treated in this section.

Pattern Distortion. The radiation patterns of the antennas discussed in Sec. 22.3 are typical of their behavior in free space. In practical cases, such antennas are often mounted alongside building walls, chimneys, masts, or other objects which tend to distort the radiation patterns.[17] In general, the effect is to cast a shadow whose extent depends greatly on the nature of the object. It is not possible to outline procedures which will permit predicting the extent of such effects, but it is clear that their effects can be reduced by increasing their spacing from the antenna as much as possible. A spacing of a half wavelength or more from reasonably sized, nonconducting objects such as chimneys will usually reduce the pattern distortion to a tolerable amount. Larger nonconducting objects such as walls and elevator-shaft housings may cast sizable shadows and should be avoided if possible. If not, the antenna should be oriented so as to direct the shadow away from the main area of interest. Elevating the antenna is often the best solution to the problem.

When the antenna must be located near conducting objects, the resulting pattern distortion can become marked and unpredictable. Masts and other antenna elements, many of which are nearly resonant to the frequency of the system being installed, can act as parasitic elements and reradiate sufficiently to produce nulls and lobes. Tests indicate that a spacing of 0.7λ between a mast and a half-wave dipole gives the most uniform horizontal radiation pattern.[18] (The measured difference between the signal strengths in the most favored and least favored directions was 7 db for mast diameters of both 0.168λ and 0.0773λ.) Small spacings cause large shadows, while spacings in excess of 0.75λ cause the appearance of deep nulls. The excitation of resonant objects can be reduced by raising or lowering the antenna, thereby reducing the coupling, since the principal radiation is generally in the horizontal plane. The resulting radiation pattern must be checked by field test.

Directional antennas such as Yagi arrays, corner reflectors, and helices are usually mounted on walls, chimneys, or masts, since clearance is not required in all directions. In such cases it is simply necessary that the near field be clear of obstructions. The impedance of an antenna is seldom noticeably affected by nearby objects when the antenna is sufficiently isolated from such objects so that their effect on the radiation pattern has been minimized.

Coverage. In the absence of interference, the maximum usable range, or "coverage," is determined by the transmitter power, the receiver sensitivity, the antenna gains and heights, the operating frequency, and the path attenuation. The nomograms presented in Chap. 33 permit the prediction of the received power in dbw between half-wave dipoles for a radiated power of 1 watt as a function of the antenna heights, the operating frequency, the range, and the effective earth's radius.[1] For other antenna types and transmitted powers the received power is increased by the sum of the antenna gains in decibels and the transmitted power in dbw. In particular, it should be noted that the received power is directly proportional to the square of the product of the antenna heights. Accordingly, increased antenna heights are often the most economical means of getting the desired coverage.

At the higher frequencies, notably 450 Mc, the need for increased gain to offset reduced antenna apertures had led to antenna types whose vertical-beam angles have become small enough so that the inclination of the main lobe with respect to the horizon has become important; some antenna types even depress the main lobe a few degrees in order to provide better illumination of the service area (cf. Fig. 22-6b). It is not unlikely that service will soon be extended to the 900-Mc region, where beam alignment will become critical. At the higher frequencies it will be possible to resort to shaped-beam antennas, which can be designed to provide more nearly uniform illumina-

INTERFERING SIGNAL – DBW

RELATIVE FREQUENCY – MC
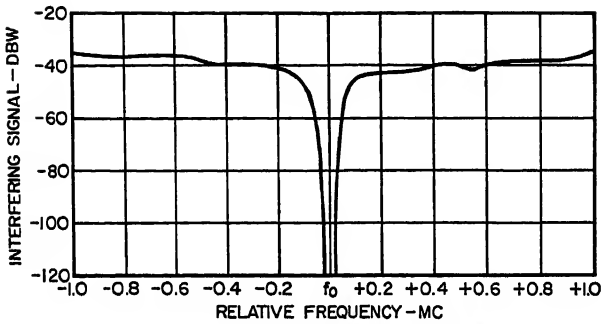
(a) TYPICAL 6 DB RECEIVER DESENSITIZATION CURVE

RELATIVE POWER – DB

CARRIER FREQUENCY

FCC SPECIFICATION

f   8f   16f   24f 32f 40f 48f

HARMONICS OF CRYSTAL FREQUENCY f

(b) TYPICAL TRANSMITTER SPURIOUS EMISSION

INPUT – DBW

IMAGE FREQUENCY

CENTER FREQUENCY

130 134 138 142 146 150 154 158 162 168 170

FREQUENCY – MC
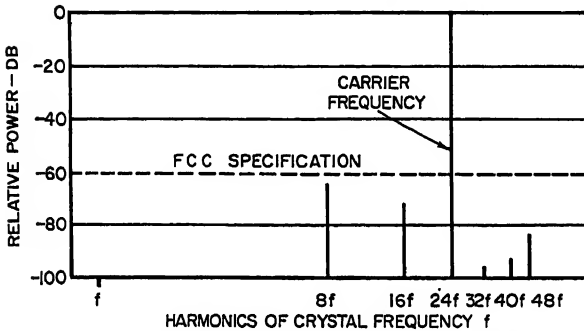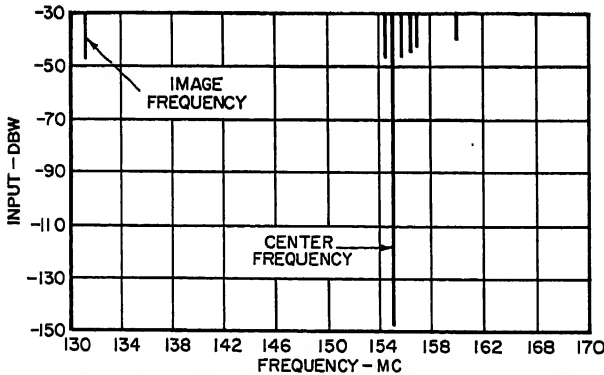
(c) TYPICAL RECEIVER SPURIOUS RESPONSE (10 DB QUIETING)

FIG. 22-14. Typical curves for: (a) Receiver desensitization.   (b) Transmitter spurious emission.   (c) Receiver spurious response.

tion of the service area, as is done in some TV antenna installations.   Fortunately, such techniques are fairly well understood as a result of activity in the radar field and become feasible at the higher frequencies because of the reduced physical sizes of the antenna elements.

Interference.   As mentioned with respect to pattern distortion, base-station antennas for a number of systems may be grouped in proximity with one another.

Under such conditions interference between systems becomes likely and steps must be taken to ensure that the capabilities of the system are not impaired by the operation of other systems on adjacent channels. Studies of the interference problem[19–25] indicate that the following factors are the principal sources of difficulty: (1) receiver desensitization, (2) transmitter spurious emission, and (3) receiver spurious response. These factors are not primarily characteristics of the antenna systems. However, transmitter and receiver imperfections do exist and produce interference by virtue of the coupling between antenna systems. Thus an interference-free system ultimately depends on the design of a good antenna system.
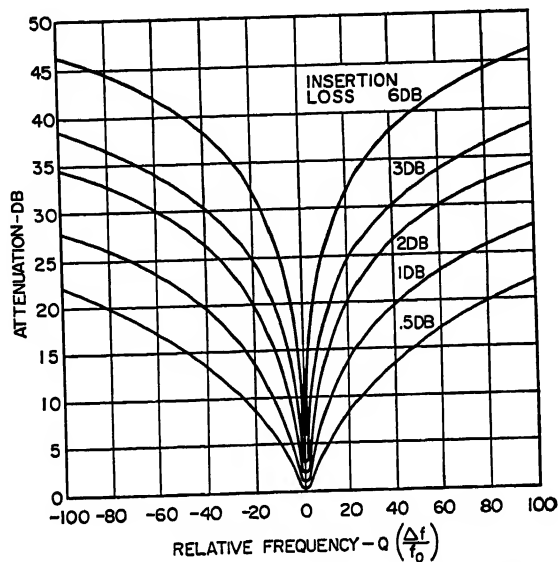
FIG. 22-15. Attenuation curves of resonant cavities.

Receiver desensitization is the reduction in sensitivity caused by the presence of a strong signal in a near or adjacent channel The interfering signal generates a bias which reduces the gain in the early stages. Intermodulation products developed in the converter stage also produce on-channel components which reduce the quieting sensitivity of FM receivers. A typical desensitization curve is given in Fig. 22-14a. Desensitization is described quantitatively by finding that interfering signal-power level which requires a given increase (usually 6 db) in the on-channel signal to restore an initial 20-db quieting.

Transmitter spurious emission results from the appearance at the output of spurious exciter-crystal harmonics. Keeping such emissions 60 db below the carrier as specified by the FCC does not prevent interference in adjacent systems even with well-designed transmitters. Modulation noise and distortion[26,27] produce sidebands which extend to adjacent channels and cause interference. Also present at the transmitter output will be the beat products between the transmitter carrier and other carriers which are fed back through the antenna into the nonlinear amplifying stage. A typical transmitter-spurious-emission plot is shown in Fig. 22-14b.

Receiver spurious response results from the imperfect selectivity of practical tuned circuits and from cross modulation in the converter stage. Adjacent-channel rejection depends strongly on the bandwidth-determining elements in the i-f amplifier.[28]

Strong responses appear in narrow frequency bands wherein the harmonics of the incoming signal and the local oscillator combine to form products in the passband, the most familiar and strongest of these being the image response. A typical receiver-spurious-response plot is shown in Fig. 22-14c. Since most mobile systems employ frequency modulation, the response is shown as a 10-db quieting curve, that is, the signal power required at a given frequency to produce 10 db of noise quieting at the receiver output.

If, using the foregoing as criteria, it is decided that no interfering signal shall cause a densensitization in excess of 6 db or a quieting in excess of 10 db, the isolation which must be obtained between the antennas can be found by comparing Fig. 22-14b with Fig. 22-14a and c and noting that all spurious emissions must fall below the densensitization curve and must avoid the spurious response of the quieting curve.
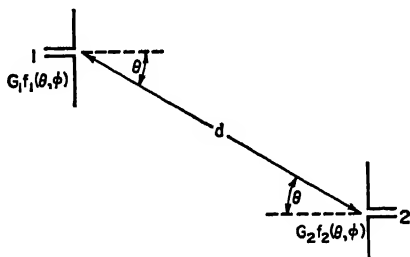
Fig. 22-16. General antenna configuration for computing coupling: G is the gain relative to a half-wave dipole and $f(\theta,\phi)$ is the relative-power-radiation pattern.

If the required isolation cannot be achieved solely by orienting or separating the antennas, additional selectivity can be placed in the receiver input circuit in the form of resonant cavities to discriminate against off-channel signals.[29] A typical set of attenuation curves is shown in Fig. 22-15.

Coupling. The isolation dictated by the preceding considerations is obtained by so orienting the antenna with respect to the other antennas that the coupling is sufficiently reduced. For practical antenna spacings, an estimate of the coupling can be obtained by using the normal propagation formulas.

Referring to Fig. 22-16, the ratio of the received power to the radiated power for antennas operating at a wavelength λ and at a separation d in free space is[1]

$$\frac{P_2}{P_1} = \left(\frac{\lambda}{4\pi d}\right)^2 G_1(\theta,\phi)G_2(\theta,\phi)$$

where $G(\theta,\phi)$ is the antenna gain function relative to an isotropic radiator. Since antenna gain G is frequently given as the maximum directivity relative to a half-wave dipole (which has a gain of 1.64 relative to an isotropic radiator), the gain function can be written

$$G(\theta,\phi) = 1.64 G f(\theta,\phi)$$

where $f(\theta,\phi)$ is the power radiation pattern relative to its maximum. Then the coupling becomes

$$\frac{P_2}{P_1} = \left(\frac{0.13}{d/\lambda}\right)^2 G_1 G_2 f_1(\theta,\phi)f_2(\theta,\phi)$$

As an example, consider the 150-Mc antennas shown in Figs. 22-7 and 22-8 separated by a distance of 10 wavelengths and making an angle of 45°. Then from Table 22-2, $G_1 = 4.23$ db $= 2.65$ and $G_2 = 6.3$ db $= 4.27$, while from Figs. 22-7b and 22-8b (noting

that the patterns are not functions of ϕ since the antennas are omnidirectional), $f_1(-45°) = 0.05$ and $f_2(+45°) = 0.1$, giving

$$\frac{P_2}{P_1} = \left(\frac{0.13}{10}\right)^2 \times 2.65 \times 4.27 \times 0.05 \times 0.1 = 9.56 \times 10^{-6} = -50.2 \text{ db}$$

Differences in polarization may provide additional decoupling.

The steps to be followed in selecting the antennas for a given system are as follows:

1. Select the antenna gain required on the basis of the coverage desired, the available transmitter power, the receiver sensitivity, and the antenna height available, using the nomograms of Chap. 33. (The relative costs of the transmitter power and antenna gain can be compared at this point to select the most economical system. Increased antenna gain often costs less than additional transmitter power. Also, antenna gain increases coverage on reception as well as transmission, an important consideration when a large number of mobile stations are served by a single base station.)

2. Measure the spurious-response characteristics of the receiver and the spurious-emission characteristics of adjacent transmitters. The latter may be done by using a field-strength meter and referring the measurements to the antenna in question. From these data, in accordance with the method described in conjunction with Fig. 22-14, compute the required isolation.

3. Within the limitations of the space available at the antenna site, select locations favorably disposed with respect to pattern distortion or other pertinent considerations and compute the coupling to be expected. If the coupling exceeds the required isolation, cavities may be employed to decrease the coupling further.

REFERENCES

1. K. Bullington: "Radio Propagation at Frequencies above 30 Megacycles," *Proc. IRE*, vol. 35, pp. 1122–1136, October, 1947.
2. A. J. Aikens and L. Y. Lacy: "A Test of 450-megacycle Urban Area Transmission to a Mobile Receiver," *Proc. IRE*, vol. 38, pp. 1317–1319, November, 1950.
3. W. Rae Young, Jr.: "Comparison of Mobile Radio Transmission at 150, 450, 900 and 3700 MC," *Bell System Tech. J.*, vol. 31, pp. 1068–1085, November, 1952.
4. K. Bullington: "Frequency Economy in Mobile Radio Bands," *Bell System Tech. J.*, vol. 32, pp. 42–62, January, 1953.
5. J. D. Kraus: "Antennas," p. 245, McGraw-Hill Book Company, Inc., New York, 1950.
6. R. G. Rowe: "Collinear Coaxial Array for 152 Megacycles," *Tele-Tech*, vol. 60, pp. 34–35, January, 1949.
7. E. F. Harris: "UHF Mobile Antenna," *Electronics*, vol. 26, pp. 181–183, May, 1953.
8. H. J. Rowland: "Antennas for Citizens Radio," *Electronics*, vol. 21, pp. 96–99, May, 1948.
9. *Andrew Corp. Bull.* 65-B.
10. M. R. Freidburg and J. F. Lowenstein: "Selecting Vehicular Antennas," *FM-TV Radio Comm.*, vol. 11, pp. 21–23, December, 1951.
11. P. F. Godley, J. R. Neubauer, and D. R. Marsh: "The New Jersey Turnpike: A Unique Highway Communication System," *Trans. AIEE*, vol. 72, pt. I, pp. 360–369, 1953.
12. R. E. Webster: "20–70 MC Monopole Antennas on Ground-based Vehicles," *IRE Trans.*, vol. AP-5, pp. 363–368, October, 1957.
13. *Mark Products Co. Bull.* 532.
14. G. Sinclair: "Theory of Models of Electromagnetic Systems," *Proc. IRE*, vol. 36, pp. 1364–1370, November, 1948.
15. E. F. Harris: "Investigating Antennas for UHF Mobiles," *Electronics*, vol. 25, pp. 127–129, November, 1952.
16. R. O. Bykerk: "Antennas for VHF Mobile Communications," *IRE Wescon Convention Record*, vol. 1, pt. 8, pp. 103–105, 1957.
17. K. V. Glentzer: "450 MC Coverage Tests at Chicago," *IRE Trans. on Vehicular Communs.*, vol. VC-6, pp. 20–32, July, 1956.
18. W. C. Babcock and H. W. Nylund: "Antenna Systems for Multichannel Mobile Telephony," *Proc. IRE*, vol. 38, pp. 1324–1329, November, 1950.

19. W. Rae Young, Jr.: "Interference between Very-high-frequency Radio Communication Circuits," *Proc. IRE*, vol 36, pp. 923–930, July, 1948.
20. J. G. Schermerhorn: "The Effects of Selectivity, Sensitivity and Linearity in Radio Circuits on Communications Reliability and Coverage," *IRE Convention Record*, pt. 2, pp. 116–122, 1953.
21 P. G. Wulfsberg: "Predicting Interference Levels in the Communication System," *IRE Convention Record*, pt. 8, pp. 74–77, 1954.
22. R. P. Gifford: "The Knee of the Nose," *IRE Trans. on Vehicular Communs.*, vol. VC-4, pp. 40–51, June, 1954.
23. J. R. Neubauer: "Design Problems on VHF Repeater Stations," *IRE Convention Record*, pt. 8, pp. 15–21, 1955.
24. C. Schultz: "Spectrum Compression and Its Problems," *IRE Trans. on Vehicular Communs.*, vol. VC-6, pp. 76–82, July, 1956.
25. M. W. Caquelin: "UHF Communication System Interference Reduction through the Use of Selective Filters," *IRE Trans. on Vehicular Communs.*, vol. VC-7, pp. 16–20, December, 1956.
26. W. C. Babcock: "Intermodulation Interference in Radio Systems," *Bell System Tech. J.*, vol. 32, pp. 63–73, January, 1953.
27. W. L. Firestone: "Evaluation of Sideband Noise and Modulation Splatter," *IRE Convention Record*, pt. 8, pp. 22–28, 1955.
28. H. Magnuski: "Adjacent Channel Rejection Receiver," *Electronics*, vol. 24, pp. 100–104, January, 1951.
29. H. Magnuski: "Cavity Resonators in Mobile Communications," *Communications*, vol. 29, pp. 8–11, August, 1949.

Chapter 23

TV AND FM TRANSMITTING ANTENNAS

DELMER C. PORTS

and

RAYMOND E. ROHRER

Both of
Jansky & Bailey, Inc.
Washington, D.C.

23.1. GENERAL CONSIDERATIONS

Antenna systems for transmitting TV and FM signals are generally broadband devices which are capable of operating over a wide frequency range within the allocated frequency spectrum. The frequencies utilized for the FM broadcast service are from 88 to 108 Mc. The TV broadcast services are located within four bands: 54 to 72, 76 to 88, 174 to 216, and 470 to 890 Mc. The individual channels in the FM band are 200 kc wide, and in the TV band the channels are 6 Mc wide. The basic design of

antennas used for these services must be such that the input impedance remains constant over a frequency range which is 10 per cent of the operating frequency for the lower TV channels and 0.2 per cent of the operating frequency for the FM channels.

The Technical Standards of the Federal Communications Commission specify the maximum effective radiated power (rms power in the horizontal plane) which FM and TV stations can radiate. These Standards do not specifically limit the effective radiated power (ERP) of FM stations, except in the northeastern section of the United States; consequently several stations are operating with radiated power in excess of 300 kw in order to provide wide area coverage. The TV Standards limit the ERP of Channel 2 to 6 stations to 100 kw, Channel 7 to 13 stations to 316 kw, and Channel 14 to 83 stations to 5,000 kw. With the output of present-day transmitters operating in the UHF band limited to 50 kw and with considerable loss in the connecting transmission lines, it is necessary to obtain the ERP by providing antennas having power gains up to 60. Antennas presently in use for these services have power gains ranging from 0.9 to 60.

Under the present system of channel allocation, it is the general practice to employ a horizontal radiation pattern which is essentially circular. The circularity of the horizontal pattern depends on the type of antenna, the gain obtained, and the positioning of the antenna on the supporting structure. At the present time, directional antenna systems may not be used to reduce the minimum mileage separations contemplated in the Standards, but they may be used for the purpose of improving service or utilizing a particular transmitter site. The Standards further limit the radiation in the maximum direction to that value of ERP specified for the particular frequency bands involved. The ratio of minimum to maximum radiation in the horizontal plane cannot exceed 10 db at the present time.

With the advent of high-gain transmitting antennas, the beamwidth in the vertical plane has been reduced to approximately 1° for antennas with a gain of 60. The beamwidth between the half-power points for typical antennas presently used for VHF television installations is approximately 4° and for UHF stations is 2°. An inherent problem associated with high-gain arrays is the existence of nulls in the vertical radiation pattern. These nulls are particularly bothersome especially when the transmitting antenna system is located in or near a residential area. Areas of low signal result from these nulls, and reflections from objects located in contiguous areas of high signal cause ghosting and distortion to the signal received in the low-signal areas. It is necessary to fill in the nulls in the vertical pattern to overcome this difficulty. This is usually done by dividing the power unequally between the various elements of the antenna array. Null fill-in is accomplished with an accompanying reduction in gain in the horizontal plane. With certain combinations of terrain and antenna height, it is desirable to have the maximum radiation occur at an angle other than the horizontal. The required beam tilt can be achieved by several methods. If it is desired to tilt the beam the same amount in all azimuthal directions, the phase relationship between the currents feeding the various elements is modified to give more shift between adjacent elements. If tilt is desired in a certain area and not in others, the antenna can be mechanically tilted in the desired direction. A combination of electrical and mechanical tilt can be utilized to provide the desired amount of tilt in several directions.

It is common practice in television antennas to diplex the visual and aural signals and transmit them from the same antenna. This requires that the interconnecting cables and components used in the antenna must be capable of handling the combined peak power of the visual signal and the average power of the aural transmitter. It is common practice to have the average aural power equal one-half of the peak visual power. In general, most VHF antennas are capable of handling 35 to 50 kw of peak visual power and 17.5 to 25 kw of aural power. The lower-gain UHF antennas will handle 10 kw of peak visual power, and the higher-gain antennas will handle 50 kw.

This power rating is based on the addition of an aural signal having an average value of one-half the peak visual power. The FM antennas presently in use will handle up to 50 kw.

The Technical Standards of the Federal Communications Commission specify certain combinations of maximum ERP and antenna height above average terrain which may be employed by TV and FM stations. The FM Standards specify a maximum ERP of 20 kw and an antenna height of 500 ft above average terrain, except where it can be shown that more power and height are needed in order to provide the desired coverage. The TV Standards presently divide the United States into three zones for the purpose of determining maximum height and power. Zone I consists generally of the heavily populated area east of the Mississippi River and north of the Ohio River, including the entire state of West Virginia and most of the state of Virginia. Zone II consists of the balance of the United States, except for a region along the Gulf coast (defined as Zone III), where abnormal tropospheric propagation conditions are frequently encountered. Table 23-1 contains the data regarding the maximum power and height restrictions for TV.

Table 23-1. Maximum TV Power and Height

Channels	Zone I		Zones II and III	
	Max. ERP, kw	Max. height, ft	Max. ERP, kw	Max. height, ft
2–6	100	1,000	100	2,000
7–13	316	1,000	316	2,000
14–83	5,000	2,000	5,000	2,000

If stations employ antenna heights in excess of those shown in Table 23-1, they are required to reduce their power accordingly. The current trend in TV is to utilize tall towers and obtain as large a coverage area as possible. Another consideration involved when determining the height of the tower and antenna is the desire to have as much of the terrain within the coverage area within radio line of sight. This is a very important consideration in rough terrain, where shadowing is a problem. It is also desirable to have the antenna higher than surrounding buildings or obstructions.

The problem of obtaining a suitable site for the location of TV or FM transmitting installations is complicated by a number of variables. The site should afford a line-of-sight path to the city in which the station is assigned. It should also be situated so that the following minimum field strength in decibels above one microvolt per meter will be provided over the entire principal community to be served: Channels 2 to 6, 74 dbu; Channels 7 to 13, 77 dbu; Channels 14 to 83, 80 dbu. For FM, a median signal strength of 3,000 to 5,000 μv/meter must be provided over the entire community to be served. Care must be taken in selecting a site for a TV or FM antenna so that it will not affect the radiation patterns of any standard broadcast stations which might be in the immediate vicinity. It has been found necessary in certain cases to base-insulate the supporting structure and support the transmission lines and lighting circuits on insulated hangers when the structure is in the immediate vicinity of a standard broadcast station. The base capacity can then be "detuned" to reduce the reradiation from the tower. Several other methods have also been used to "detune" FM and TV towers in order to reduce AM reradiation.

In addition to these problems, care must be taken in locating the tower and antenna structure so that it is not a hazard to air navigation. Part 17 of the Rules of the Federal Communications Commission contains requirements which must be met in

order to obtain approval from the Federal Aviation Agency (FAA) for the erection of a tower.   In general, it is necessary for the site to be outside of established civil airways and also at least 3 miles from any airport.   Coordination with local airport personnel and FAA authorities is a necessity in selecting a site for a tall tower.

FM TRANSMITTING ANTENNAS

23.2. FM SQUARE-LOOP ANTENNA

The square-loop type of antenna has proved to be an efficient means of obtaining high values of effective radiated power without using very high powered transmitters. The square-loop array consists of a number of square loops stacked vertically to provide power gain in the horizontal plane and vertical directivity.   The resulting horizontal radiation pattern is essentially circular.
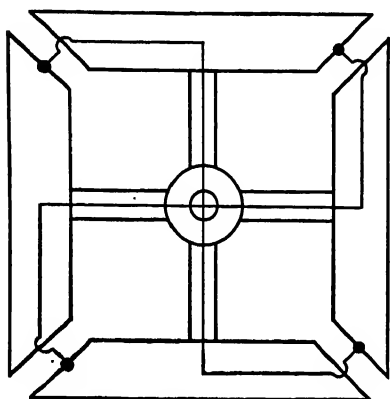
FIG. 23-1. FM square-loop details.   FIG. 23-2. Square-loop multibay feed details.
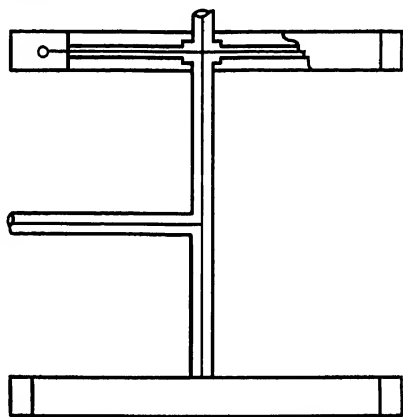
The loops are so designed that the input impedance of each pair of loops is 50 ohms, so they may be fed by standard coaxial transmission lines.   Preliminary impedance matching is achieved within each loop as shown in Fig. 23-1.   The parallel impedance of such a loop has a resistive component which is essentially 100 ohms over the entire FM band.   With the input resistance of each loop equal to 100 ohms, a pair of loops, spaced a half wavelength apart and fed as shown on Fig. 23-2, have an input impedance of 50 ohms.   Thus it is possible to operate the same size loop at any frequency within the FM band and maintain an input impedance of 50 ohms.   The voltage standing-wave ratio measured at the input of a pair of stub-tuned loops can be adjusted to less than 1.2, and the over-all input VSWR to an array will be less than 1.5 at any frequency from 88 to 108 Mc.

It is customary to space adjacent loops 332° apart at 100 Mc in commercial models of this type of array.   It is thus possible to use the same physical structure over the entire FM band since the optimum power gain occurs when the loops are approximately 360° apart.   The loop antenna array is normally available in combinations of 2 loops up to 12 loops.   The power gain* of the array with respect to a dipole varies from 2 for a 2-loop array to 12.4 for a 12-loop array.   In a multiloop array, all loops are fed with equal power and electrically in phase.   Arrangements can be made to feed all loops with a single transmission line from the transmitter, or it is possible to feed them with two lines in order to provide stand-by facilities in the event one line fails.

* All gain figures quoted in this chapter are relative to the gain of a half-wave dipole.

The square-loop array is available as a standard commercial product. The array, including harnesses, feeders, and structural members, ranges in weight from 1,280 lb for the 2-loop array to 15,036 lb for the 12-loop array. The corresponding wind-loading figures are 7,480 and 290,000 lb-ft. The 2-loop array has an over-all height of 18.5 ft, and the 12-loop array is 111 ft over-all.

This antenna has the advantage of providing high gain for a minimum antenna aperture. The array also provides maximum lightning protection, since all-metal parts can be used and the supporting structure is a part of the electrical network. Since the same-sized loops are used for all FM frequencies, it is necessary to change only the matching stubs to change frequency.

A disadvantage of this type of array is the necessity to mount the loops on a square-tower section, which would then mount on the supporting structure. This array has a substantial wind-loading factor, and with the large dead weight, a heavy-duty supporting structure is required.

23.3. FM CLOVERLEAF ANTENNA

The FM cloverleaf antenna is composed of two or more vertically stacked radiating units. Each radiating unit is made up of a cluster of four curved elements, the plan view of which resembles a four-leaf clover. A radio-frequency voltage applied between the common junction of the four elements and their respective ends causes, in effect, a ring of uniform current about their axis, thus producing a circular radiation pattern. The maximum gain of a multi-element array occurs when the instantaneous currents in all radiating elements are equal in phase and magnitude. The individual elements are stacked one-half wavelength apart, and the common point of each element is clamped to a 3-in.-diameter steel conductor, which is centrally located within the antenna structure. The outer conductor of the feed system is the special tower structure. Since there is a phase reversal every half wavelength along such a transmission line, the mounting position of the radiating elements in adjacent units is reversed, as shown in Fig. 23-3. This procedure assures proper current phase-and-magnitude relationship without the use of multiple transmission lines or phase-correcting lines and networks.

It is common to stack any number of elements from 2 to 12 in order to obtain the desired power gain in the horizontal plane. There is no need to stack the elements in multiples of 2 because of the simplicity of

FIG. 23-3. FM cloverleaf multibay feed details.

the feed systems. The power gain for this antenna varies from 1.3 for a two-element array to 4.7 for an eight-element antenna. The existence of a vertical polarized component is minimized by the use of vertical wire members which connect the ends of adjacent bays. At any given instant, the current in two of these members will be

flowing up and the current in the other two will be flowing down, thus canceling out any vertically polarized component.

Since all elements are connected directly to the same feeder, it is necessary to provide impedance transformation only at the base of the antenna to match the feed system to the transmission line. The impedance transformation in this particular antenna is accomplished by the use of a low-loss transformer which utilizes two enlarged sections of the feed line and the antenna structure to provide an impedance match from 50 to 100 ohms. In addition, a quarter-wave stub is inserted at the lower end of the antenna feed line to provide second-harmonic filtering. The antenna can be adjusted for a VSWR of less than 1.5 over three FM channels.

Since all radiating elements are interchangeable, it is relatively simple to replace a damaged element. The simplicity of the feed system and the lack of r-f insulators or dielectric materials minimizes the maintenance and provides full protection against lightning surges. This antenna requires a higher power transmitter to obtain radiated powers in excess of 200 kw, since the maximum power gain is 4.7.

23.4. FM SLOTTED-CYLINDER ANTENNA

The FM slotted-cylinder antenna is based on the principle of a simple loop of wire carrying an electric current. This antenna is merely an infinite number of these loops stacked on top of each other and connected in parallel. This stack of loops takes the form of a cylinder approximately a wavelength long and a half wavelength in circumference. The termination of these loops takes the form of a slot running the full length of the cylindrical element. This slot is fed at the center and shorted at each end, thus taking the form of an open-wire transmission line. The voltage distribution takes the form of the familiar sinusoidal pattern with voltage minimum at the center and each end.
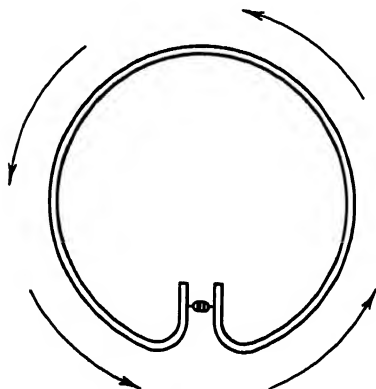
Since the slot is an open-wire transmission line, the currents flowing along the opposite edges of the slot are out of phase and therefore cancel the vertically polarized components of radiation. The slotted-cylinder antenna shown in Fig. 23-4 radiates horizontally polarized waves because of the circumferential currents flowing around the cylinder. A single antenna element produces a moderate power gain because of the fact that the vertical aperture is a wavelength long.

FIG. 23-4. FM slotted cylinder.

It is common to stack a number of these elements to obtain increased horizontal gain since the power gain of a single element is approximately 1.5. An eight-section antenna will have a power gain of 12. When stacking two or more elements, it is necessary to provide interconnecting feed lines to the center of each slot so that voltages equal in phase and magnitude are fed to each slot. The main feed line and all portions of the harness are completely enclosed in the antenna; therefore they are completely protected from the weather since the slot is normally covered with a strip of polyethylene. It is necessary to change the interconnecting harness when using the antenna on a frequency other than the one for which it was designed. The harness contains the necessary matching and dividing stubs so that the input resistance is approximately 50 ohms and the VSWR is less than 1.5 at any desired frequency from 88 to 108 Mc.

The beamwidth of the resulting vertical patterns varies from 24° for a two-element antenna to 6° for an eight-element array. The circularity of the horizontal radiation pattern (radiated field) is within ±2.5 db for all frequencies from 88 to 108 Mc. The maximum radiation occurs in the direction of the slot, and the minima are located approximately 45° from the side opposite the slot.

A slotted-cylinder antenna has the advantage of providing high gain for a minimum aperture with gain figures approaching those obtained from a square-loop array. It has the further advantage of having a smooth outer surface which minimizes wind resistance and loading. The wind loading for an eight-element antenna 108 ft in height is 218,000 lb-ft. All connections to the antenna are made from the inside of the cylinder, where they will be protected from the weather. Icing has a negligible effect on the radiation patterns and the VSWR since the slot is covered.

It is difficult to replace portions of the interconnecting harness in the event of failure of any piece, since this is mounted inside the cylinder and it must be completely removed for servicing. There are no provisions for emergency operation in the event of failure of any portion of the radiating system.

23.5. MULTI-V ANTENNA

The multi-V antenna has been designed especially to mount on the side of existing towers which are used for standard broadcast radiators or TV supporting towers. The multi-V antenna array consists of a number of V elements stacked vertically to provide power gain in the horizontal plane and vertical directivity. The resulting horizontal radiation pattern is essentially omnidirectional. The pattern remains approximately circular when side-mounted on a tower having a uniform cross section with 2 ft on a side.

The bays, or V's, are so designed that the input impedance of each pair is 50 ohms, enabling them to be fed by standard coaxial transmission lines. The feed system enables an even number of bays from two to eight to be employed to obtain power gains ranging from 1.6 to 7.3, with a power rating of 10 kw. The design is such that it is necessary to tune the antenna at the factory for the desired frequency. Two models of each array are necessary to cover the FM band; one model tunes from 88 to 98 Mc, and the second model covers the band from 98 to 108 Mc. It is possible to obtain a VSWR of less than 1.10 at the operating frequency with a VSWR of less than 1.20 over a band of approximately 0.80 Mc.

The multi-V antenna is a lightweight structure ranging in weight from 70 lb for a two-bay array to 365 lb for an eight-bay array. It is very simple, with one feed point per bay and a maximum of four power-dividing elements for an eight-bay array. The radiating elements are grounded for maximum lightning protection.

This array has the disadvantage of requiring tuning when utilized on a frequency other than the one for which it was factory-adjusted. The antenna is not suited for high-power installations since the maximum input power is limited to 10 kw.

23.6. CIRCULAR AND RING ANTENNAS

The circular and ring antennas are different adaptations of half-wave dipoles formed in a circular arrangement. Essentially, the circular antenna is a folded half-wave dipole bent in a circular form with capacitor plates attached to each end as shown in Fig. 23-5. Adjustment of the size of this end capacity serves to provide adjustment to resonance at any frequency within the frequency range of the antenna.

The development of the circular antenna is shown in Fig. 23-6, which shows the current distribution for a standard folded dipole, a folded dipole with concentrated end capacity, and a circular antenna. It is to be noted that the current distribution in the

circular antenna is essentially constant, yielding a very nearly uniform radiation pattern. The antenna is fed at the ground potential point G, without insulation, thus protecting the transmission line from lightning. The adjustable capacitor is constructed of a heavy mycalex plate with conducting plates on each side. This reduces its susceptibility to capacity change due to a collection of snow and ice.

Even numbers of elements can be stacked to obtain increased horizontal gain. Optimum spacing is one wavelength, which also is desirable from the standpoint of phasing of the current in the individual elements. The gain of the circular antenna varies from 0.79 for a one-element antenna to 7.24 for an eight-bay antenna. Low mutual impedances exist between adjacent bays of a multielement array since the radiation is relatively low in a vertical direction. For all practical purposes, matching systems designed for a single bay are usable for multiple-bay systems, and the adjustment of individual elements to resonance becomes a simple matter. The antenna matching system can be tuned so that the VSWR is less than 1.5 over a band of approximately 1.0 Mc.

The radiating elements, matching units, baluns, and supporting pole vary in weight from 810 lb for a two-bay antenna to 6,300 lb for an eight-bay antenna. The two-bay

FOLDED ANTENNA

END CAPACITY ADDED

Fig. 23-5. FM circular-antenna details.

ELEMENTS BENT INTO CIRCLE
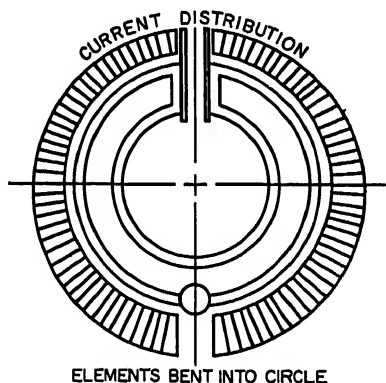
Fig. 23-6. Development of FM circular antenna.

tower-mounted antenna has a length of 32 ft above the top of the tower. An eight-bay antenna would extend 82 ft above the tower top. These antennas are essentially designed for lower power installations since the maximum power-handling capability is 10 kw.

TV TRANSMITTING ANTENNAS

23.7. SUPERTURNSTILE ANTENNA

The antenna which has become the most popular for VHF television broadcasting purposes is the superturnstile, or batwing, antenna. This antenna came into extensive use with the opening of the commercial television broadcasting field in 1948. At the

present time, over 75 per cent of the antennas used for VHF transmitting purposes are superturnstiles.

The superturnstile antenna radiator consists of a welded framework of steel tubes in the form of a batwing. Four of these are mounted around a tubular steel pole at 90° intervals. This configuration is referred to as one-bay. The antenna radiators are a development of the standard dipole, which essentially is a narrow-band device. If
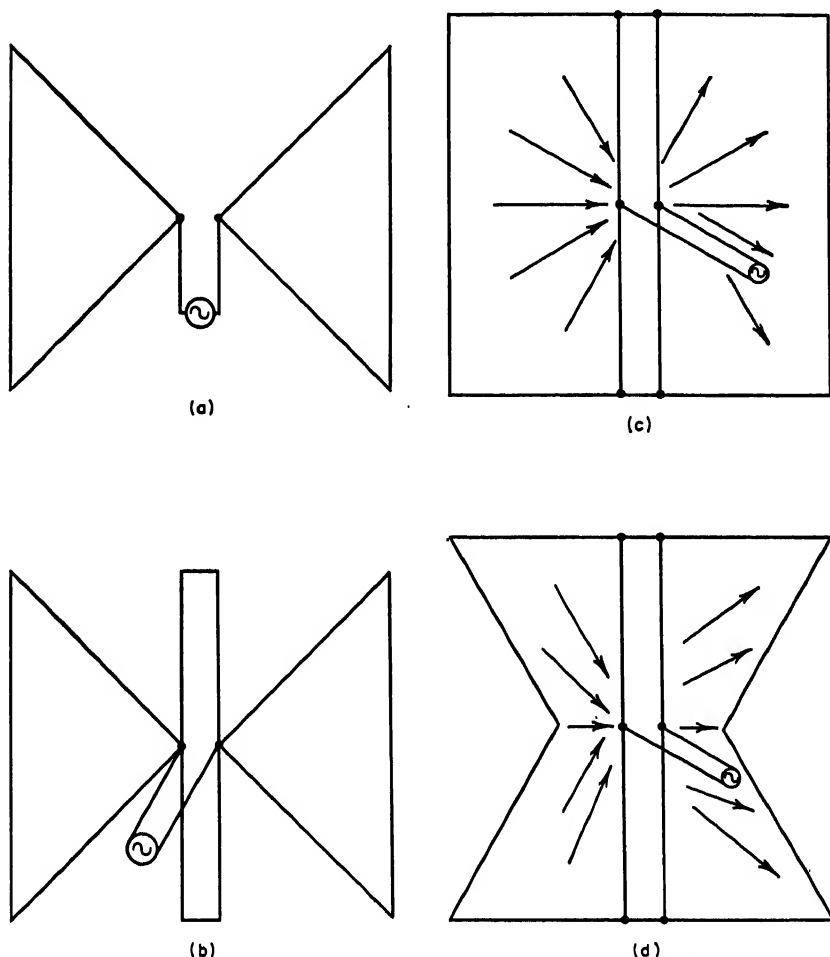
FIG. 23-7. Development of TV superturnstile antenna.

the arms of the dipole are enlarged at the end or made cone-shaped (Fig. 23-7a), the bandwidth is greatly increased, with no sacrifice in the radiation. It is possible to further increase the bandwidth of the antenna by paralleling two quarter-wave stubs at the feed point as shown in Fig. 23-7b. In order to give still better bandwidth characteristics, the cone-shaped arms are changed to solid sheets from the tip of the radiator to the stub, as shown in Fig. 23-7c. This combination yields a bandwidth of 35 per cent, with a VSWR of 1.1 or less. The current distribution expected from this con-

figuration is also shown.   The outside edge of the sheets are notched (Fig. 23-7d), in order to obtain a more uniform current distribution and still retain the desired bandwidth.   An antenna having solid sheets of material for radiators would offer high wind loading and difficulty in mounting.   In order to overcome these difficulties and still maintain the bandwidth, the shape shown in Fig. 23-7d is maintained and a sufficient number of horizontal bars are utilized to provide essentially the same electrical characteristics.

The impedance at the center of the radiator is approximately 75 ohms, thus allowing each radiator to be fed by a standard coaxial line.   This low impedance means that ordinary icing conditions have little effect upon the operation of the antenna.   The radiators are mounted on the pole by clamps at the top and bottom of each radiator, thus affording lightning protection.

The four radiators in each bay are fed in opposite pairs in order to improve the circularity.   In addition, the pairs are fed in phase quadrature, commonly referred to as turnstiling.   This requirement demands that the antenna be fed by two transmission lines, which must be kept electrically similar in order to ensure the proper current-and-phase relationship.

The gain of a single-bay superturnstile antenna is approximately unity in comparison with a dipole.   In order to obtain the effective radiated powers permitted by the Federal Communications Commission, it is necessary to stack bays vertically to obtain vertical directivity and horizontal power gain.   The most commonly used antennas by television broadcast stations are the 6- and 12-bay units.   The 6-bay antennas are commonly used by stations operating on Channels 2 to 6, and the 12-bay antennas by Channels 7 to 13 stations.   Standard 6-bay antennas have a power gain of from 5.9 to 6.6, and the power gain of a standard 12-bay antenna varies from 11.9 to 12.9, depending upon the channel for which the antenna is designed.

It is common practice to feed equal power to all bays for antennas having six bays or less.   The pairs of radiators are referred to as "north-south" and "east-west" to denote the two groups of radiators which are fed by separate transmission lines.   In antennas with six bays or less, in-phase current is fed to each north-south bay.   Likewise, in-phase current is fed to each east-west bay.   The resulting vertical patterns have a first null, which occurs approximately 8° below the horizon.   Generally, this null does not present any problems since the low-signal area resulting from this null falls at a distance of 1.3 miles from the base of a 1,000-ft tower and 2.7 miles from the base of a 2,000-ft tower for a six-bay antenna.   For antennas with fewer numbers of bays, the null area would fall closer to the tower.

Higher-gain antennas with 12 bays present problems because of the deeper nulls in the vertical radiation pattern.   These nulls go to a complete zero if equal power is fed to each bay.   In order to fill in the nulls closer to the horizon, it is common practice to feed 70 per cent of the power to the top six bays and the remaining 30 per cent power to the lower six bays.   The power fed to each half of the antenna is then fed equally to the individual bays.   Null fill-in can be accomplished by further power division and phasing between the various individual bays.   Figure 23-8 contains vertical-plane plots of relative radiated fields from three typical 12-section superturnstile antennas.   The effect of power division and phasing can be seen by examination of the various curves in Fig. 23-8.   Power division and phasing in order to obtain null fill-in serve to lower the gain of the antenna in the horizontal plane.   The typical antenna used as an example in Fig. 23-8 has a power gain of 12.2 for 50:50 power split.   When the power is split 70:30, the power gain is reduced to 11.7.   The gain is further reduced for the third condition shown on Fig. 23-8 and is 9.8.

The depth and position of the nulls in a 12-bay pattern are important since the low-signal areas might possibly fall in areas of heavy population concentration.   For a 12-section antenna mounted on a 1,000-ft tower, the first null area would fall at a distance

of 2.5 miles from the tower base. This distance would increase to 5.2 miles for a 2,000-ft tower.

Six-section antennas have two main feed lines which run from the center of the antenna to the top of the supporting tower. It is possible to connect the transmitter output to the two antenna feed lines by several methods. The standard method is to feed the outputs of the aural and visual transmitters through a bridge diplexer. The output from the diplexer is fed through two transmission lines to the antenna input.

CHANNEL 10
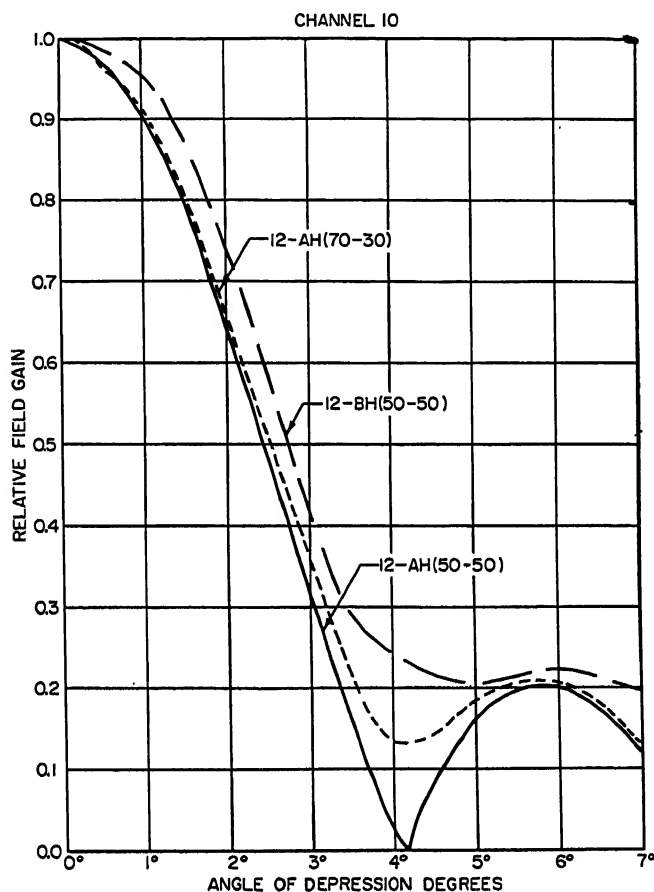
Fig. 23-8. Typical vertical radiation patterns for 12-bay superturnstile antennas.

This method allows for emergency operation in case one of the main feed lines fails, since one feed line is connected to the north-south bays and the other line to the east-west bays. The resulting emergency radiation pattern has a figure-eight shape. A second method of feeding a six-section antenna utilizes a notch-type diplexer. The output from this diplexer is connected to a single transmission line which runs up the tower. This line is then connected to the twin antenna lines through a combining T. This type of feed does not allow for any emergency operation.

The 12-section antenna offers a large number of methods of feeding, since four feed lines are utilized in the antenna. The normal method of feed uses a bridge-type diplexer and two feed lines running up the tower similar to the six-bay antenna. Each

feed line up to the tower is connected to two antenna feed lines through a T. Emergency operation is provided through the use of a single line resulting in a figure-eight radiation pattern. Figure 23-9 shows the details of this method of feeding a 12-section antenna. A further method shown in Fig. 23-9 involves the use of four feed lines running up the tower and a bridge diplexer. In this case, the output from each output terminal of the bridge diplexer is fed to a combining T and two lines run up the tower to the north-south bays and two lines run to the east-west bays. This method of feeding is practical where the length of transmission line is comparatively short. If one transmission fails, the line can be disconnected and replaced by a dummy load. The power fed to one set of bays will be unaffected, since no changes will be made in these lines. One-half of the power fed to the other set of bays will be absorbed in the dummy load, and the remaining power will be fed to the bays. The resulting radiation pattern will be normal in two directions and only slightly reduced in the other two directions.
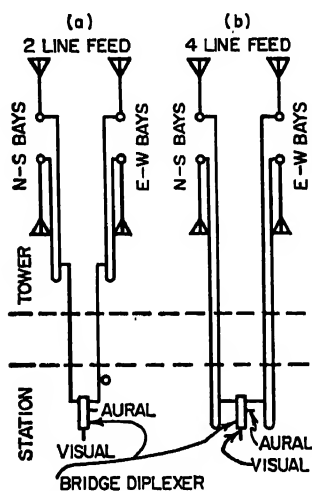
FIG. 23-9. Feed systems for 12-bay super-turnstile antenna using bridge diplexer.
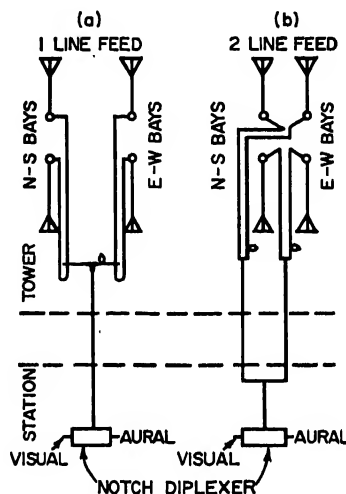
FIG. 23-10. Feed systems for 12-bay super-turnstile antenna using notch diplexer.

It is also possible to feed the 12-section superturnstile antenna using a notch-type diplexer. With this type of diplexer, which has a single-line output, it is possible to feed the antenna with either one or two lines as shown in Fig. 23-10. The first method, employing a notch diplexer, utilizes a single feed line to connect the diplexer to the antenna. This method of feed does not provide for any means of emergency service; therefore a separate antenna and transmission line are necessary if emergency facilities are desired. The second method, using a notch diplexer, employs two feed lines between the diplexer and antenna as shown in Fig. 23-10. This method allows for emergency operation since the upper and lower sections of the antenna are fed by separate lines. In case of emergency, the output of the diplexer is fed through the good transmission line. The resulting radiation pattern has the same shape as the main pattern but with reduced power.

The superturnstile antenna offers a convenient means of obtaining maximum effective radiated power for VHF television broadcast stations. It is possible to obtain the maximum power of 100 kw for stations operating on Channels 2 to 6 with an antenna having five or six bays and a 25-kw transmitter. For the high channels, Channels 7 to 13, it is necessary to utilize a 12-bay antenna and a transmitter having a power output in excess of 25 kw in order to obtain an effective radiated power of 316 kw. These

antennas offer several means of providing emergency operation in case of partial antenna failure or transmission-line failure. The VSWR measured at the antenna is less than 1.1 across the channel for which it is designed.

A disadvantage of the superturnstile antenna is the multiplicity of connections required in the antenna. Four points of connection are required at each bay, one to each batwing. This multiplicity can result in substantial repair time in case of trouble with the antenna.

23.8. "SUPERGAIN" ANTENNA*

Recognizing the need for a high-gain VHF antenna which could be stacked for use by several broadcast stations, the "supergain" antenna was designed and is commercially available for all the VHF channels. This antenna was also designed with the possibility of providing a directional radiation pattern if desired. The supergain antenna was designed to mount directly on the faces of the supporting tower structure.

Since batwings do not have a satisfactory impedance characteristic with frequency when mounted in front of a screen or tower face, a different type of radiator was necessary. The final design consists of dipoles mounted in front of reflecting screens. It is necessary to modify the shape of the conventional dipole in order to obtain a bandwidth so as to match the feed line over the 6-Mc channel. The resulting bandwidth of the supergain antenna is considerably less than that of the superturnstile. The VSWR is less than 1.1 over the channel for which the antenna is designed.

Figure 23-11 is a sketch showing the supergain antenna mounted on the faces of a four-sided supporting structure. The reflecting screens are used to keep radiation out of the tower structure to prevent changes in the impedance over the channel width due to coupling to objects within the structure. The dipoles and associated screens are stacked in layers in order to obtain the desired value of horizontal power gain. The power gain of a single layer is approximately 1.2. The vertical separation of adjacent layers is slightly less than one wavelength from one dipole to the next dipole. In order to reduce the interference between dipoles on adjacent sides of the tower, it is necessary to limit the side dimension to one-half wavelength. A larger side dimension results in difficulty in obtaining an omnidirectional radiation pattern.

FIG. 23-11. TV supergain-antenna details.

The width for a Channel 2 antenna is 9 ft; for a Channel 13 antenna, 2½ ft. Additional screens are placed between adjacent screens and elements in order to reduce the coupling between adjacent dipoles.

For an antenna having an omnidirectional pattern, four dipoles are equally spaced around a square tower section. A number of dipoles are stacked vertically to obtain the desired power gain in the horizontal plane. The north-south and east-west bays are fed in quadrature like the bays of a superturnstile antenna. Equal lengths of feed line are used to connect each junction box to the desired dipole elements. Provision is made to obtain null fill-in and beam tilt by adjusting the magnitude and phase of the

---

* The name "supergain" as used here is a trade name and does not connote the meaning of supergain as discussed in Chap. 2.

current fed to the individual bays.   The use of a bridge-type power equalizer allows the antenna to be fed with a single coaxial feed line.

It is possible to obtain various horizontal radiation patterns using the basic supergain antenna design.   Radiators may be placed on any of the faces of the tower and thus provide several combinations of directional patterns.   Each screen and radiator can be considered to have the same horizontal radiation pattern as that from one side of a dipole antenna.   Different directional patterns can be obtained, depending on the number of radiators placed horizontally around the tower and also upon the amplitude and phase of the current fed to each radiator.

The supergain antenna is adaptable for multiple-antenna installations where it is desired to utilize a single supporting structure.   Since the antenna is mounted around the sides of the tower structure, a number of antennas can be mounted on the same tower and an FM antenna or another television antenna can be mounted on top of the tower structure.

It is possible with this antenna to obtain power gains of the order of 20 for an omnidirectional pattern.   With such a gain, it is possible to obtain the maximum radiated power of 316 kw for Channels 7 to 13 with a 25-kw transmitter.

The supergain antenna offers the advantages of high gain, directional possibilities, and ease of utilization for multi-antenna installations.   With this antenna it is necessary to design the top section of the tower to be part of the antenna. Since only one transmission line is used, there is no provision for emergency operation.

23.9. HELIX ANTENNA

The helix antenna was developed to provide an antenna with a minimum number of feed points and a simple mechanical construction.   The antenna consists of a tubular mast around which are wound helices as shown in Fig. 23-12.   The mast is mainly used as a supporting structure but also acts as a ground plane for the helices.   Two traveling waves are propagated along the helices at the feed point.   Each helix acts like a single wire above a ground plane.   The spacing between the mast and helix was chosen so that there is a considerable amount of radiation per turn.   Each helix is approximately five turns with the diameter and pitch, depending on the frequency.   Each turn is an integral number of wavelengths so that the currents at a given azimuthal angle are in phase.   A high-gain array is achieved by stacking a number of single-bay antennas along a mast.   The power gain per bay is approximately 4.

FEED POINT

FIG. 23-12. TV helical-antenna details.

In order to cancel the vertical radiation component due to the helix pitch angle, a right- and left-hand helix are used in each bay.   The helices are placed end to end and are fed at a common point.   The resulting feed-point impedance is approximately 100 ohms.   The individual bays are coupled to the inner conductor of the feed system by a probe, which is adjusted to give the proper percentage of the power fed to the antenna system.   Stub adjustments and matching sleeves on the inner conductor are available to give the proper impedance match.   The impedance can be adjusted to give a VSWR of less than 1.1 over the desired channel and less than 1.2 over the first adjacent channels.

The antenna is end-fed, requiring a series feed arrangement for multibay systems. The feed system is of the coaxial type, with the supporting mast acting as the outer conductor. The inner conductor is shorted to the mast at a point one-quarter wavelength below the antenna input and at another point one-quarter wavelength above the top bay's feed point. This arrangement gives mechanical stability to the feed system and provides r-f isolation.

This antenna provides a means of obtaining high gain with a minimum vertical aperture. A six-bay helical antenna for Channel 12 would have a gain of approximately 24 with an over-all length of about 100 ft. The antenna can also serve as a support for another television antenna. The present design of this antenna requires a mast having a substantial diameter, which means high wind-loading and dead-weight factors.

23.10. SLOTTED-RING ANTENNA

In an effort to provide high antenna gain on the high VHF Channels 7 to 13, a slotted-ring-type antenna has been developed and used successfully. This antenna provides high gain with a simple feed system and a minimum over-all length.
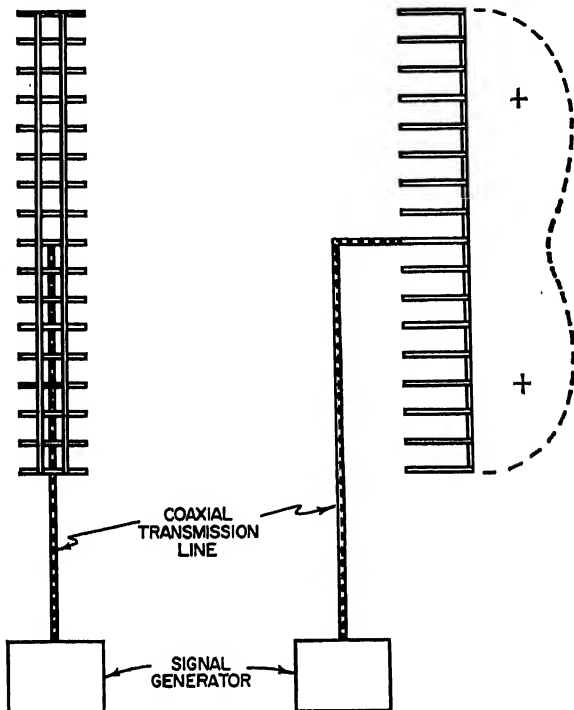
Fig. 23-13. Development of slotted-ring antenna.

The antenna is basically a balanced transmission line shunted by a number of small loops or rings. Consider Fig. 23-13, which is such a line, short-circuited at both ends. The system is center-fed, and a wave propagates from this point toward both ends of the line. Reflection from the short-circuited points sets up standing waves, with the resulting potential difference between the conductors of the balanced line distributed as shown by the dotted line. Since the apparent electrical length from the feed point

to either short circuit is approximately 0.4 wavelength, the phase of the potential difference is substantially constant. The over-all length of this system is 1.5 free-space wavelengths and is known as a half bay.

Circumferential currents are caused to flow in the shunting rings because of the potential difference between the balanced conductors. The resulting currents are cophasal, and the system exhibits characteristics of a stacked-loop array. At a point equidistant from the balanced lines, the currents are a maximum and the potential is essentially zero. These points of zero potential may be joined to a common member without distorting the radiation pattern. This member is used to support the structure.

A novel feed arrangement is used to provide a larger vertical aperture, which could be excited by a single transmission-line feeder. A portion of the balanced conductors or rods and the supporting member are used as an outer conductor to propagate an approximately coaxial TEM mode to the center of the slot in conjunction with an exposed inner conductor. With this method of feeding, it is possible to mechanically join two half bays together and feed them in the center through a coaxial T.

The impedance of each feed point is adjusted by the placement of the feed strap on the center ring of each half bay. If the exposed inner conductor is connected to the center ring at the point of attachment to the mast, the impedance will be zero. On the other hand, if the point of feed is adjacent to the slotted portion, the real component of the impedance will be approximately 70 ohms. The slot impedance can thus be transformed from any desired impedance from a few ohms up to 70 ohms.

Individual bays are stacked vertically in order to achieve higher power gains. A rigid coaxial teflon transmission line is used to make up the interconnecting harness. Provision is made to divide the power unequally between bays and half bays in order to provide null fill-in. The input VSWR of the antenna system, including interconnecting harness, is less than 1.10. Typical power-gain figures for this antenna are 8.0 for a two-bay antenna and 20.0 for a five-bay antenna, both without null fill-in. Null fill-in would lower these figures slightly, depending on the amount of fill desired.

A typical two-bay antenna weighs 3,700 lb and has an overturning moment of 38,700 lb-ft for a 50/33.3 lb/sq ft wind loading. The corresponding figures for a five-bay antenna are 14,800 lb and 288,000 lb-ft.

It is possible to obtain a directional horizontal radiation pattern with this antenna by adding beam-shaping members to each alternate active ring of the antenna. The present design of these members uses small rectangular bar stock of various lengths. Typical directional-antenna arrays have maximum gains which vary from 5.6 to 7.2 per bay, as compared with a gain of 4.0 per bay for an omnidirectional array.

The slotted-ring antenna offers a convenient means of obtaining high power with relatively few feed points and a simple interconnecting harness. It is also relatively insensitive to snow and ice formations due to the low slot impedance. The antenna can handle high power due to the large components and teflon seals. Since the antenna is fed by only one line, there is no provision for emergency operation in case of transmission-line failure.

23.11. TRIANGULAR-LOOP ANTENNA

Another antenna which was specifically designed for high power gain on Channels 7 to 13 is the triangular-loop antenna. Each bay of the antenna is composed of three folded dipoles, each placed on a side of a triangular tower structure. The feed lines to the dipoles are connected to a common junction in the center of the structure. The magnitude of the currents fed to the individual elements is equal, and the currents are in phase. A matching element is inserted between the junction and the common

feed point in order to obtain a constant impedance of 50 ohms to each bay.   This transformer is variable and allows a final adjustment of VSWR of 1.05 or better for each bay.

The gain of a single bay with respect to a dipole is approximately 1, and higher power gains are possible by stacking a number of bays vertically.   The spacing between adjacent bays is 5 ft for Channels 7 to 13.   This antenna presently is not used for Channels 2 to 6.   A steel lattice is used for supporting the various bays.   The size of this structure depends on the number of bays utilized.   As an example, for 2 or 4 bays the structure is 18 in. on a side.   For a 16-bay antenna, four structural sizes are used, ranging from 18 to 12 in. on a side.

In a multiple-bay antenna each bay is fed by a current which is equal in magnitude and phase to the current fed to all other bays.   The feed system is simple and consists of equal-length lines from the main feed point to each loop.   The lines are solid dielectric cables with teflon insulation, or, more recently, styroflex cable has been used. If all the cables of a 16-bay array were tied in parallel at the junction point, the resulting feed impedance would be approximately 3 ohms.   An impedance of this value would be difficult to transform back to 50 ohms and still maintain a satisfactory VSWR over a television channel.   In order to obtain a satisfactory VSWR, the individual lines are connected to a balun transformer which transforms in a ratio of $200/n$, where n is the number of 50-ohm lines.   A simple quarter-wave transformer in the balun transformer is used to obtain an input impedance of 50 ohms and a VSWR of less than 1.10 over a television channel.

In a multiple-bay antenna, it is necessary to insert untuned isolation rings between pairs of loops in order to reduce the coupling effect between adjacent elements.   Without the isolation rings, there would be a variation in impedance over the video bandwidth, resulting in a high VSWR at the antenna input.

As is the case with other high-gain television transmitting antennas, the radiated field in the first null of the vertical radiation pattern is almost zero, and consequently if the antenna is in an urban area, the resulting degraded signal area would be objectionable.   It is possible to fill in this null by changing the phase of the current by 90° in one bay near the center of the antenna.   In order to obtain more null fill-in, more bays near the center may be phased by 90°.   A typical example for a 16-loop antenna involves phasing the seventh, eighth, and ninth loops from the bottom by 90°.   This reduces the horizontal power gain from 12.3 to 10.9 db.   Beam tilt is accomplished by successively advancing the phase of the current in the loops with height.   This is convenient since each feeder is a matched 50-ohm line.   The antenna element and lattice structure range in weight from 430 lb for a two-loop array to 6,400 lb for a 16-loop array.   The over-all height for a two-loop array is 10 ft and for a 16-loop array is 80 ft.   The overturning moment is only 113,000 ft-lb for a 16-loop array.

The triangular loop array is a simple antenna from either the mechanical or electrical viewpoint.   It is relatively light and offers a low wind-loading factor for the power gain obtained.   There is no provision in the antenna for emergency operation since only one transmission line is required from diplexer to antenna and the feed lines for all loops are connected to a single balun.

23.12. CYLINDER WITH MULTIPLE SLOTS

The most popular transmitting antenna for UHF television stations is the slotted-cylinder antenna.   The need in UHF television is for an antenna which has a gain in excess of 25 since the maximum authorized radiated power is 5,000 kw.   The slotted-cylinder antenna is an outgrowth of the FM pylon antenna.

The antenna is of slotted-tubular-steel construction, as shown in Fig. 23-14.   Each

radiating layer consists of three 1-in.-wide slots equally spaced around the circumference of the cylinder. The slots are approximately 1.3 wavelengths long and are parallel to the axis of the antenna. Adjacent layers of slots are spaced vertically approximately one wavelength apart, center to center. The adjacent layers of slots are rotated 60° in order to obtain mechanical strength and to provide essentially an omnidirectional horizontal radiation pattern.

The antenna is made with the number of layers of slots varying from 14 to 32 in order to obtain power gains varying from 20 to 55. The energy to feed the slots is distributed by means of a single coaxial-line feeder system within the slotted cylinder. The slotted cylinder serves as the outer conductor of a coaxial line, the inner conductor being a copper tube within the cylinder. Another coaxial line is installed within the inner conductor to obtain a method of center-feeding the antenna array. Each slot is excited by a tuned loop placed across the face of the slot. The slots are excited with equal in-phase voltages, and the resulting field is assumed to be uniformly distributed across the slot. The radiated field will be essentially horizontally polarized, with a small amount of vertical polarization.

The power to the slotted cylinder is usually fed equally to the slots in the upper and lower halves of the antenna. In order to obtain null fill-in, power would be fed unequally to the various layers of slots. As an example, in an 18-layer antenna the power is normally fed 50:50 to the bottom eight layers and the top eight layers. In order to fill the vertical nulls, 50 per cent of the power could be fed to the top 10 bays and 50 per cent to the lower eight bays. More null fill-in could be obtained by dividing the power equally between the upper 11 bays and the lower 7 bays. It is possible to obtain electrical beam tilt of the main radiation lobe by varying the phase of the current fed to the upper and lower sections of the antenna.
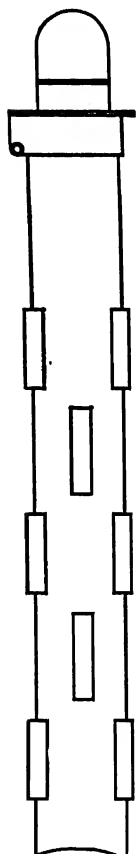
FIG. 23-14. TV slotted-cylinder details.
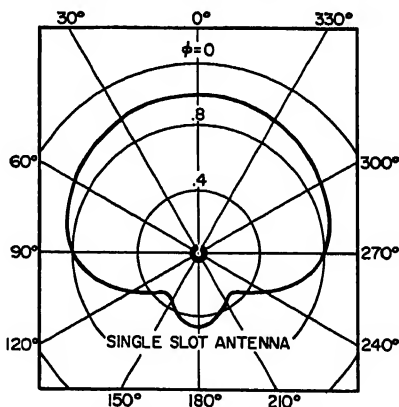
FIG. 23-15. Typical UHF directional-antenna radiation pattern.

The simplicity of the feed system and the low impedance of the slot allow for establishment of a low VSWR across a 6-Mc television channel. A typical slotted-cylinder antenna can be adjusted for a maximum standing-wave ratio of 1.05 over a particular channel. Polyethylene slot covers protect the slots from rain and the accumulation of ice and allow for the maintenance of a low VSWR.

By restricting the slots along certain sides of the cylinder, it is possible to obtain directional horizontal radiation patterns. Figure 23-15 shows a directional horizontal radiation pattern obtained with a slotted-cylinder antenna using one set of collinear slots. Null fill-in and beam tilt can be incorporated in a directional antenna by utilizing the same methods employed for standard antennas.

The slot antenna offers a convenient means of obtaining the high gain required for UHF transmitting antennas. These antennas have been manufactured and used with power gains up to 60. The simplicity of this antenna makes it relatively insensitive to ice accumulation. Since this antenna is fed by one transmission line, there is no provision for emergency operation without the installation of a separate antenna or feed line or both.

23.13. FOUR-SLOT ANTENNA

The four-slot antenna was designed to provide high gain and at the same time provide a fairly uniform signal near the transmitting antenna. The vertical radiation pattern closely approximates a cosecant curve.

The antenna consists of a vertical array of slot radiators propagating horizontally polarized waves. The physical construction of the antenna consists of four structural-steel tubes having an outside diameter of 4 in. arranged in a square with adjacent tube centers 5 in. apart. The tubes are shorted at intervals of one wavelength by welded-steel members. This construction results in a series of rings of resonant slots one wavelength long and spaced one wavelength apart. The physical structure is therefore also the radiation system.

The complete antenna normally comprises two electrically identical sections consisting of 12 slots each. The two sections are center-fed by a standard 3⅛-in. coaxial line which runs up one of the 4-in. vertical tubes. A 1-in. tube runs up the center of the square formed by the vertical tubes. This center tube acts as the center conductor for the feed system for each 12-slot section. The individual slots of each section are tapped across this transmission line. Figure 23-16a is a cross section of the antenna at the feed point of a slot. Normally, each ring of slots is fed in phase. Figure 23-16b shows a cross section of the antenna at a point where the slots are shorted. A dielectric window is placed across the slot openings in order to protect the electrical connections from the weather. The impedance of the slots is adjusted by positioning the point of contact on the slot and the length of the tuning reactance shown on Fig. 23-16a. The impedance is adjusted to be real and to yield the minimum VSWR. The correct tuning is determined on a special test section of the antenna cut to the desired frequency. The actual antenna is constructed without any variable adjustments, and the entire structure welded and then hot-dip-galvanized.

The resulting horizontal radiation pattern is essentially circular. For an antenna in which equal in-phase current is fed to all slots, the power gain is 27.5, with the locus of the maxima in the vertical pattern following a cosecant pattern. In this pattern there are two deep nulls at depression angles of 2.4 and 4.8°. In order to fill in these nulls in the vertical pattern, unequal power distribution between the top and bottom sections is utilized. The second null is filled by reversing the phase of the current fed to one ring of slots. The slot so chosen is near the middle of the structure in order to provide a field in-phase quadrature at the second null. The resulting power gain of such an antenna is 24.

The main radiation beam can be tilted by advancing the phase of the current fed to the top section of 12 slots. With the phase advanced by 60°, the power gain is reduced to 19 and the nulls are filled in.

The four-slot antenna is a simple mechanical and electrical structure, since all electrical connections are made at the time of manufacturing. As there are no append-

ages on the antenna, there is little opportunity for ice formation. The antenna is relatively lightweight, varying in weight from 2,820 lb for a Channel 14 antenna to 1,655 lb for a Channel 83 antenna. The overturning moment is likewise low, having a maximum of 34,700 ft-lb for Channel 14.
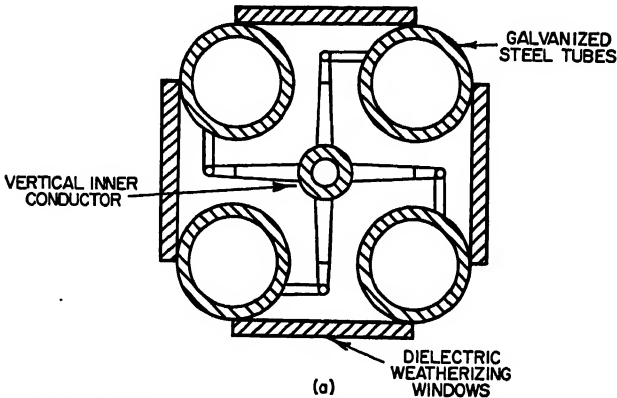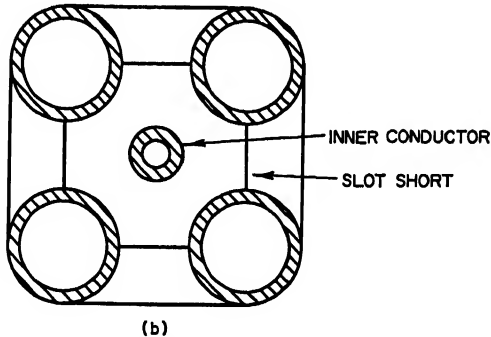
CROSS SECTION OF ANTENNA
FIG. 23-16. Cross sections of four-slot antenna.

Since the antenna is pretuned, it is not possible to use a specific antenna for a frequency other than the one for which it was designed, without considerable expense. It is also difficult to adjust the antenna in the field for various amounts of null fill-in and tilt if it is found necessary to alter these after installation.

23.14. UHF HELICAL ANTENNA

This antenna has the same basic design as the VHF helical antenna described in Sec. 23.9. In UHF installations, it is sometimes desirable to utilize a directional radiation pattern in order to improve service in certain specified areas. A directional pattern can be obtained with a helical antenna by installing horizontal bars on the helices. These bars serve to modify the amplitude and phase characteristics of the

current flowing in the helices and thus result in a noncircular horizontal radiation pattern. This factor is especially important in UHF, where radiated power is presently limited because of equipment limitations.

23.15. PROBLEMS IN MULTIPLE-ANTENNA INSTALLATIONS

It is advantageous to have a number of television stations share the same supporting structure for their transmitting antennas. This results in a saving in the cost of the supporting structure and is also desirable in order to have all the receiving antennas in the area oriented toward only one installation and not several. It is common to utilize an existing building, such as the Empire State Building, or build a tower capable of supporting several antennas, i.e., the "candelabra" installation in Texas.

There are numerous problems raised in connection with a multiple-antenna installation. It is necessary to electrically isolate the various transmitting antennas so that they will not interact and the radiated signals from one antenna will not be picked up by another antenna with such a strength that the signals will provide cross-modulation products. Sometimes it is also desirable to use one of the antennas to transmit both a television signal and an FM signal. A problem which is frequently encountered in a multiple-antenna system is the question as to which station gets what physical position on the structure. Since height is an important consideration, the topmost position is most desirable.

The best example of a multiple-antenna installation is the Empire State Building in New York City. Mounted on the top of the building are the main transmitting antennas of seven television stations, three FM stations, several microwave installations, and a number of communication installations. The television transmitters on the Empire State Building operate on Channels 2, 4, 5, 7, 9, 11, and 13, and the FM transmitters operate on 95.5, 97.1, and 101.1 Mc. In addition to the above antennas, several of the television stations maintain auxiliary antennas at this point.

Originally, the mast on top of the building was built to accommodate the antennas for Channels 2, 4, 5, 7, and 11. The antennas for Channels 2, 5, 7, and 11 are of the supergain type, and the Channel 4 antenna is a superturnstile antenna. The power gain for the low-band antennas is approximately 4 and for the high-band antennas approximately 5. The FM signal for the station operating on 97.1 Mc is triplexed on the Channel 4 superturnstile antenna. The four supergain antennas and the one superturnstile antenna are mounted on a mast which extends 217 ft above the top of the Empire State Building. The Channels 2 and 5 antennas consist of five-bay supergain elements, with the Channel 2 antenna mounted immediately above the top of the building. The Channel 5 antenna is the next highest antenna. The Channels 7 and 11 antennas are mounted next, and they are each six-bay supergain antennas. The Channel 4 four-bay superturnstile antenna is mounted on top of the Channel 11 antenna. These antennas were designed, tested, and mounted as a unit on the Empire State Building.

When designing the multielement installation, it is necessary to consider the coupling between the various antennas. The following specifications were set up for the design of the Empire State antennas:

Coupling: −26 db or less between any two antennas

Input voltage standing-wave ratio: 1.1:1 over the visual band and 1.5:1 over the aural band

Gain: Power gain of 4 relative to a dipole for Channels 2, 4, and 5 antennas and a gain of 5 for Channels 7 and 11 antennas

Circularity: ±2 db

Power handling: Possibility of transmitting 100-kw ERP

It was necessary to test the various antennas completely before they were erected on the building. The various antennas were fabricated and placed on special test towers in order to adjust the impedance and measure the coupling between adjacent antennas. Tests on the antennas showed that the coupling requirement of −26 db was met in all cases. In fact, in most cases the coupling was less than −40 db. The specifications with regard to power-gain circularity and VSWR were all met, with tolerance to spare.

The FM signals for 95.5 and 101.1 Mc are combined and diplexed on a single set of four supergain dipoles. These dipoles are mounted in the middle of the Channel 2 array. This location was chosen because tests showed that it would have the least effect on the impedance and pattern characteristics of the various television antennas. The power gain of this FM antenna is 0.707 compared with a half-wave dipole.

At a later date two more television antennas were added to the Empire State Building. A special antenna was developed for Channel 9 and mounted around the circular parapet immediately below the mast on which are mounted the original five television antennas. This antenna consists of 24 bays of dipoles and parabolic reflectors. Each bay consists of two dipoles and parabolic reflectors stacked vertically. The bays encircle the parapet and provide an essentially nondirectional horizontal radiation pattern. The maximum VSWR at the input of the diplexer is 1.10 and occurs at the high end of the television channel.

After the Channel 9 antenna was installed on the Empire State Building, tests were made to determine the amount of coupling between the Channel 9 antenna and the six other television antennas mounted on the building. The coupling is less than −65.0 db between the main antennas at both the video and aural frequencies of WOR-TV (Channel 9). The coupling between this antenna and the auxiliary antennas for Channels 7 and 4 is less than −45 db.

The seventh television antenna, Channel 13, on the Empire State Building is located on the four corners of the building below the observation platform. This antenna consists of V elements mounted on each corner of the building. Each section of the antenna consists of four sections. The resulting horizontal radiation pattern has a circularity of ±3 db. The coupling between this antenna and other antennas on the building is less than −60 db.

Another method of multiple-antenna mounting consists of mounting several antennas on a triangular platform on top of a tower. This is commonly referred to as the candelabra antenna system. A triangular open-steel framework platform is constructed on top of a tower, and a conventional television transmitting antenna can be mounted on each corner of the platform. The first installation utilized one Channel 4 six-section superturnstile antenna and one Channel 8 twelve-section superturnstile antenna. The third corner of the platform is counterbalanced with scrap steel. In order to make the beacon levels of both antennas the same height, it was necessary to add 10 ft to the Channel 8 antenna length. The platform is 80 ft wide across each side.

Tight specifications were set up with regard to pattern circularity, pattern gain, coupling between antennas, and input VSWR. The entire platform and antenna structure were built to scale, and various measurements were made on this model. The measured horizontal radiation patterns showed a circularity of ±2 db for the Channel 4 antenna and ±3 db for the Channel 8 antenna vs. a specification of ±3 db. The gain of each antenna remained unchanged by the presence of the other antenna since measurements showed the vertical and horizontal patterns to be unaffected by the other antenna. The coupling between antennas was required to be −26 db or less. Measurements on the scale model showed the coupling to be less than −44 db for the Channels 4 and 8 antennas. The input impedance for each antenna showed a VSWR of better than 1.1:1.

23.16. MISCELLANEOUS ACCESSORIES

The standard method of feeding the television signal to the antenna is to diplex the visual and aural carriers and feed them to the same antenna. Several different methods are employed to accomplish this, which result in the utilization of one or more transmission lines to feed the antenna.
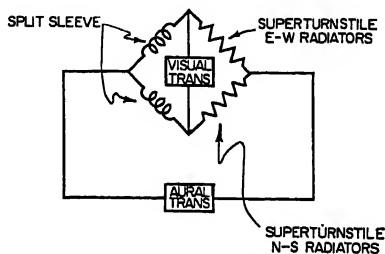
Fig. 23-17. Schematic of typical bridge diplexer.

The most common method of feeding the superturnstile type of antenna utilizes two feed lines and requires a bridge type of diplexer. In this type of diplexer, the visual and aural signals are fed into the diplexer through separate transmission lines and two lines feed the antenna. The diplexer must couple these two signals so that they will be fed correctly to the antenna and must also provide a constant impedance to each transmitter. Figure 23-17 is a schematic of a typical bridge diplexer. The diplexer and the antenna form a Wheatstone bridge with the visual and aural inputs balanced so no cross-coupling exists between the two transmitters. This type of
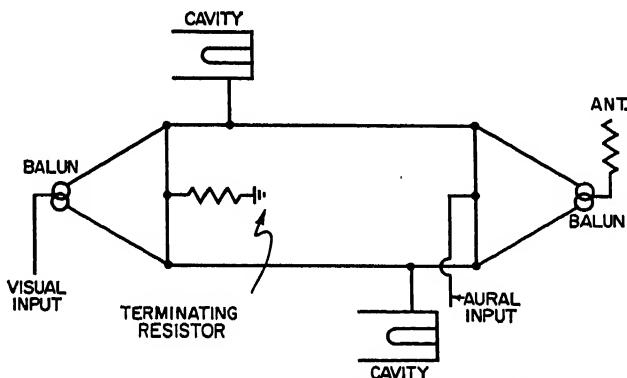
Fig. 23-18. Schematic of typical notch diplexer.

diplexer is easy to construct and has no critical adjustments which must be made in the field and checked regularly.

A second diplexer which is commonly used is the notch type. This diplexer is generally used with UHF antennas and also VHF antennas other than the superturnstile. With the notch diplexer, only one transmission line is needed to feed the antenna, as is shown in Fig. 23-18. The visual input connects through the baluns on either end of the diplexer to the antenna. Aural modulation components which are 4.5 Mc above the visual carrier are fed to the diplexer and are reflected by the two cavities and returned to the terminating resistor which absorbs them. The aural energy cannot go

through the right-hand balun; hence it travels to the left along the two transmission lines and is reflected by the cavities. It then returns to the right-hand balun and goes to the antenna. The physical design of this type of diplexer varies from manufacturer to manufacturer, but the electrical characteristics are similar to those described above. This type of diplexer is usually used with the supergain, triangular-loop, helical, and slotted-ring-type antennas.

It is necessary in the transmission of the visual portion of the television signal to shape the signal to meet the requirements of the Federal Communications Commission. The Technical Standards require the energy radiated at 1.25 Mc below the visual carrier to be 20 db below the amplitude of the visual carrier. Furthermore, with a modulating frequency of 4.5 Mc, the upper sideband amplitude must be at least 20 db below the visual carrier amplitude. Any radiation which is more than 3 Mc above or below the edges of the television channel must be at least 60 db below the visual carrier level. This shaping of the visual signal is accomplished by several means. In transmitters which are modulated at low levels, the shaping takes place in the tuning of the coupling circuits between the various r-f stages. With transmitters where modulation occurs in the last r-f stage, it is necessary to employ a vestigial sideband filter to shape the transmitted visual signal. This filter consists of a number of tuned circuits which provide the necessary attenuation to give the desired radiation.

It is common practice in the UHF band to combine the features of the diplexer and vestigial sideband filter. This piece of equipment has been variously known as a "filterplexer," or "filtrexer."

In order to meet the requirements of the Federal Communications Commission with regard to harmonic and spurious emissions, it is necessary to insert harmonic filters in the output lines of present-day transmitters. The filters for VHF transmitters are generally inserted in the output line of each of the visual and aural transmitters and before the diplexer. The filter is designed to provide a broadband within the desired passband with a sharp high-frequency cutoff and high attenuation of frequencies above the passband. The VHF filter is commonly a series of transmission lines with a uniform-diameter outer conductor, a stepped inner conductor, and a shunt stub.

The UHF harmonic filters are generally inserted in the line after the diplexer, and one filter provides the necessary attenuation for both the visual and aural harmonics. The majority of UHF filters are of the bandpass type, with cavities used instead of the conventional lumped-circuit components. These filters give an attenuation of more than 60 db for all radiation more than 3 Mc above the top limit of the desired channel.

When transmitting color programs, it is necessary to compensate for various distortions introduced in the video signal by the color receiver, vestigial sideband filter, notch diplexer, and various terminal equipment. At the present time, it is necessary to insert special correction networks in the video circuit in order to meet the Federal Communications Commission color specifications. The notch-type diplexer introduces envelope phase distortion due to the high-frequency cutoff in the sound notch filter. The vestigial sideband characteristics cause envelope phase distortion in the low-frequency portion of the transmitted video signal. The distortion is compensated for by a unit which is commonly referred to as a phase equalizer. This unit contains high-frequency and low-frequency phase-equalization circuits, which are adjustable in order to correct for varying amounts of distortion. The individual circuits are controlled individually to obtain the desired amount of correction.

REFERENCES

1. "Federal Communications Commission Rules and Regulations," vol. III, pt. 3, Radio Broadcast Services; Subpart B, FM Broadcast Stations, and Subpart E, Television Broadcast Stations, June, 1959.

2. "Engineering Handbook," National Association of Broadcasters, 4th ed., sec. 2, Notes on Television Antenna Equipment, 1949. Reprinted from RCA "Manual for Television Technical Training Program."

3. RCA "Manual for Television Technical Training Program," General Principles and Theory of TV Antennas· 6th ed., sec. 2, 1951.

4. G. H. Brown: "A Turnstile Antenna for Use at Ultra-high Frequencies," *Electronics,* March, 1936; G. H. Brown: "The Turnstile Antenna," *Electronics*, April, 1936.

5. Armig G. Kandoian: "Three New Antenna Types and Their Applications," *Proc. IRE,* Waves and Electrons Section, vol. 34, no. 2, p. 70w, February, 1946.

6. Philip H. Smith: "Cloverleaf Antenna for FM Broadcasting," *Proc. IRE*, vol. 35, no. 12, p. 1556, December, 1947.

7. George Sinclair: "The Patterns of Slotted-cylinder Antennas," *Proc. IRE*, vol. 36, no. 12, p. 1487, December, 1948.

8. R. W. Masters: "A Power-equalizing Network for Antennas," *Proc. IRE*, vol. 37, no. 7, p. 735, July, 1949.

9. J. B. Dearing, H. E. Gihring, R. F. Guy, and F. G. Kear: "Multiple Television and Frequency-modulation Transmitting Antenna Installation on the Empire State Building," *Proc. IRE*, vol. 41, no. 3, p 324, March, 1953.

10. F. G. Kear and J. G. Preston: "Control of Vertical Radiation Patterns of TV Transmitting Antennas," *Proc. IRE*, vol. 42, p. 402, February, 1954.

11. N. E. Lindenblad: "Antennas at Empire State," *Communications*, vol. 21, May, 1941.

12. L. J. Wolf: "Triplex Antenna for Television and FM," *Electronics*, July, 1947.

13. N. E. Lindenblad: "Slot Antennas," *Proc. IRE*, vol. 35, no. 12, p. 1472, December, 1947.

14. R. W. Masters and C. J. Rauch: "A New Television Transmitting Antenna," *IRE Convention Record*, pt. 7, 1955.

15. G. J. Adams, A. Alford, H. H. Leach, R. Rubin, and F. Abel: "Antenna System for Station WOR-TV Channel 9, Installed on the Empire State Building in New York City," *IRE National Convention Record*, pt. 7, 1954.

16. A. Alford and H. H. Leach: "High Gain Antenna Arrays for Television Broadcast Transmission Using a Slotted Ring Antenna," *IRE National Convention Record*, pt. 7, 1956.

17. C. B. Mayer and P. M. Pan: "Self-diplexing TV Antenna," *IRE National Convention Record*, pt. 4, 1953.

18. H. M. Crosby: "High Power UHF Television Broadcasting Systems," *IRE National Convention Record*, pt. 4, 1953.

19. O. W. B. Reed, Jr.: "Television Allocation Trends," *Electrical Engineering*, June, 1957.

20. Morlock and W. O. Swinyard: "Performance of UHF and VHF Television Transmitting and Receiving Equipment," *Electrical Engineering*, March, 1958.

21. H. G. Smith: "High Gain Side-firing Helical Antennas," *Electrical Engineering*, October, 1954; *AIEE Communs. and Electronics Trans.*, May, 1954.

22. G. B. MacKimmie: "A Quadruplexer Allowing the Simultaneous Transmission of Two Complete Television Stations Using a Common Antenna," *AIEE Communs. and Electronics Trans.*, January, 1959.

23. A. G. Kandoian and R. A. Felsenheld: "Triangular High-band TV Loop Antenna System," *Communications*, August, 1949; A. Alford & A. G. Kandoian: "Ultra-high Frequency Loop Antennas," *AIEE Trans.*, vol. 59, 1940.

24. O. O. Fiet: "8 Bay Pylon Antenna," *FM and Television*, September, 1948.

25. R. F. Holtz: "Super Turnstile Antenna," *Communications*, April, 1946.

26. O. O. Fiet: "Ultra-high-frequency Antenna and System for Television Transmission," *RCA Review*, June, 1950.

27. H. E. Gihring: "Practical Considerations in the Use of Television Super Turnstile and Super-gain Antennas," *RCA Review*, June, 1951.

28. O. O. Fiet: "New UHF-TV Antenna," pt. 1, Construction and Performance Details of TFU-24B UHF Antennas, *FM and Television*, July, 1952; pt. 2, TFU-24B Horizontal and Vertical Radiation Characteristics, *FM and Television*, August, 1952.

29. J. Epstein, D. W. Peterson and O. M. Woodward: "Some Types of Omnidirectional High-gain Antennas for Use at Ultra-high Frequencies," *RCA Review*, vol. 13, June, 1952.

30. L. J. Wolf: "Multiple Antenna System for Television Broadcasting with Antennas of Equal Height," *IRE Trans. on Broadcast Transmission Systems*, January, 1956.

31. R. E. Fisk: "The TV Helical Antenna Adapted to Structural Tower Shapes," *IRE Trans. on Broadcast Transmission Systems*, October, 1957.

32. M. S. Siukola: "The Traveling-wave VHF Television Transmitting Antenna," *IRE Trans. on Broadcast Transmission Systems*, October, 1957.

33. D. W. Peterson: "The Use of Vertical Polarization to Solve UHF Television *Ghosting* Problems in a Shadowed Valley," *RCA Review*, June, 1958.

34. D. W. Peterson: "Post-installation Perfomance Tests of UHF Television Broadcasting Antennas," *RCA Review*, December, 1958.

35. J. B. Sherman: "Circular Loop Antennas at Ultra-high Frequencies," *Proc. IRE*, vol. 32, no. 9, September, 1944.

36. W. Sichak and S. Milazzo: "Antennas for Circular Polarization," *Proc. IRE*, vol. 36, no. 8, p. 997, August, 1948.

37. M. W. Scheldorf: "Multi-V Antenna for FM Broadcasting," *Electronics*, March, 1949.

38. D. G. Fink: "Television Broadcasting in the United States 1927–1950," *Proc. IRE*, vol. 39, no. 2, p. 116, February, 1951.

39. C. E. Smith and R. A. Fouty: "Circular Polarization in FM Broadcasting," *Electronics*, September, 1948.

40. A. Alford: "Long Slot Antennas," *Proc. National Electronics Conf.*, 1946.

41. E. C. Jordan and W. E. Miller: "Slotted Cylinder Antennas," *Electronics*, February, 1947.

42. G. H. Brown and J. Epstein: "A Pretuned Turnstile Antenna," *Electronics*, June, 1945.

Chapter 24

TV RECEIVING ANTENNAS

YUEN T. LO*

*University of Illinois
Urbana, Illinois*

24.1. INTRODUCTION

According to the present FCC frequency allocation for television broadcasting, there are two bands, the high and the low band, in the VHF range and one band in the UHF range. The low band, which covers the frequencies from 54 to 88 Mc, has a bandwidth of 47.8 per cent with respect to a mean frequency of 71 Mc; the high band covers frequencies from 174 to 216 Mc, a bandwidth of 21.4 per cent with respect to 195 Mc; and the UHF band covers frequencies from 470 to 890 Mc, a bandwith of 64.9 per cent with respect to 647 Mc. The frequency allocation of individual VHF channels with their mean wavelength is shown in Table 24-1.

Because of the difference in propagation characteristics of television frequencies as compared with the standard broadcast band and also because of a severe requirement for picture reproduction free from distortion and interference, the receiving antenna for television presents a number of problems.

* Formerly with Channel Master Corp., Ellenville, N.Y.

Table 24-1. Frequency Allocation of VHF Channels

Band	Channel	Frequency, Mc	Carrier Video, Mc	Carrier Audio, Mc	λ_m, in.*	Bandwidth, % of f_m*
VHF:						
Low band	2	54–60	55.25	59.75	207.6	10.5
	3	60–66	61.25	65.75	187.5	9.5
	4	66–72	67.25	71.75	171.2	8.7
	5	76–82	77.25	81.75	149.5	7.6
	6	82–88	83.25	87.75	139.0	7.1
High band	7	174–180	175.25	179.75	66.73	3.39
	8	180–186	181.25	185.75	64.54	3.28
	9	186–192	187.25	191.75	62.49	3.18
	10	192–198	193.25	197.75	60.58	3.08
	11	198–204	199.25	203.75	58.76	2.99
	12	204–210	205.25	209.75	57.06	2.90
	13	210–216	211.25	215.75	55.45	2.82

* λ_m = mean wavelength of a channel. f_m = mean frequency of a channel.

The problems encountered may vary in different localities.   A few of interest are listed below:

1. In the business section of a city, multiple reflections from tall buildings and structures cause ghost images, although signal intensity is generally more than sufficient.

2. In the fringe area, or in the valley, the signal intensity suffers a great deal from propagation attenuation, so that high antenna gain is the main requirement.

3. Most fringe areas are located in between large cities, which usually are the sites of television transmitters; therefore cochannel or adjacent-channel signals may cause considerable interference to the desired picture reception.

4. There are some areas in between large cities where different channels are in different directions.   It is then necessary to rotate the main lobe of the antenna by either mechanical or electrical means.

5. In some areas the channels may be distributed in all bands, or may be in one or two bands.   Since the frequency coverage of an antenna is usually widened at the expense of gain, it is generally desirable to use an antenna with only as much bandwidth as is necessary.

Antennas of different types are manufactured in an attempt to solve some of these problems, but there is no ultimate solution.   For example, an antenna with a very high gain will help to expand the service area and the old problem will be pushed to new areas.

An area of field intensity (at synchronizing pulse peaks) greater than 5,000 μv/meter is considered primary service and 500 μv/meter secondary service; beyond that is the fringe area.   It is difficult to specify a required antenna gain for a given distance since the field intensity varies greatly both with time and terrain.   Therefore an extensive survey of the field strength must be made before it is possible to estimate an average gain needed.   A picture is generally considered acceptable if the signal input is about 25 to 30 db over noise.

A load resistance of 300 ohms is generally accepted as a standard for television receiving antennas.   Since such an antenna usually covers a wideband, a perfect impedance match is impossible.   Therefore it is more meaningful to define the gain of a receiving antenna with reference to the standard load, although the directivity of an

antenna is independent of the load. In other words, the gain of an antenna is the ratio of the power delivered to the standard load by the antenna to that delivered by a certain reference antenna which is matched to the standard load. The standard reference dipole generally used is a tuned $\lambda/2$ folded dipole with an input impedance of 300 ohms.

Table 24-2 lists the dimensions of reference dipoles, for the VHF band, which consist of tuned $\lambda/2$ folded dipoles having a nominal impedance of 300 ohms. The gain figures in this chapter are given with respect to these reference dipoles, unless otherwise stated.

Table 24.2. Length of a Tuned $\lambda/2$ Folded Dipole
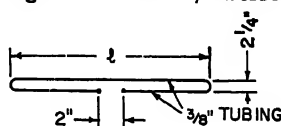
(a) VHF LOW BAND AND FM BAND

CHANNEL	2	3	4	5	6	FM
FREQ. MC	57	63	69	79	85	98
ℓ IN	98.0	88.7	81.0	70.7	65.8	57.0

IN GENERAL: ℓ (IN)= $5.59/f_{mc}$

(b) VHF HIGH BAND

CHANNEL	7	8	9	10	11	12	13
FREQ. MC	177	183	189	195	201	207	213
ℓ IN	30.4	29.4	28.5	27.6	26.8	26.0	25.2

IN GENERAL: ℓ (IN)= $5.38/f_{mc}$

The gain so defined is called "working gain" by some authors. This value of gain is smaller than the gain due to directivity because of the losses due to impedance mismatch and those due to ohmic and dielectric losses.

There is no generally agreed upon tolerance on mismatch, but it has been a practice for some workers to allow about 3:1 VSWR for a high- and low-band antenna and about 2:1 for a single-band antenna. Broadband impedance-compensating techniques may reduce the mismatch loss but usually are not very practical for average home installations.

The radiation pattern of an antenna is actually defined by a three-dimensional plot of the field intensity in every direction in space. For simple antennas the patterns in the principal planes, vertical and horizontal, are sufficient for calculating its directivity. But for some television receiving antennas, particularly those for multiband operation, skew lobes of considerable magnitude can exist and will not be shown in the principal plane patterns. In order to avoid the large effort required for a three-dimensional plot of the radiation pattern, the gain is measured by direct comparison with the standard reference antenna. It is well known that the radiation pattern of an antenna is the same for transmitting and receiving. Also, the radiation impedance of an antenna is equal to its internal impedance when it is used for receiving. For convenience of discussion and measurement, the properties of a receiving antenna are frequently determined from those of a transmitting antenna.

24.2. BROADBAND AND MULTIMODE DIPOLES

A half-wave dipole cut for the low band, say, Channel 4, has a radiation pattern similar to a cosine function, as shown in Fig. 24-1. At the high band, this same dipole

will be approximately $3\lambda/2$ long, and the pattern will be as shown in Fig. 24-2. The relative magnitudes of the front and side lobes depend upon the thickness of the dipole as well as its length. These side lobes indicate a lower forward gain and more stray pickup. Thus provision must be made so that unidirectional radiation can be maintained in both modes.
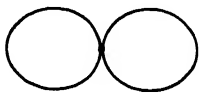
FIG. 24-1. Field pattern of a $\lambda/2$ dipole.
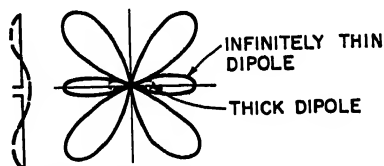
FIG. 24-2. Field pattern of a $3\lambda/2$ dipole.

There are, in general, two approaches to the solution of a high–low-band antenna:

1. *Fat dipole.* The variation of a dipole impedance is closely related to its thickness. It is generally true that the fatter and the longer the dipole, the smaller the VSWR will be over a given bandwidth; on the other hand, for too long a dipole, the higher-mode radiation pattern may split into multilobes. A compromise between impedance and pattern must be reached so that the dipole operates over the whole frequency range, namely, from 54 to 216 Mc, including the FM band.

2. *Multimode dipole system.* Since the ratio of the center frequency of the high band to that of the low band is 3:1, it is possible to design a system which operates efficiently on these two discrete bands.

These principles, in one way or another, have been applied commercially to many TV receiving antennas. Each has its advantages and disadvantages. Although the structure of most commercial antennas makes a rigorous theoretical analysis impossible, it is possible to make a preliminary estimation of the antenna characteristics. The over-all performance remains to be studied and justified by experiments, so that the accuracy of experimental measurements is a decisive factor.

Fan-type Dipole. It is known that as the antenna length increases to more than 1.2λ, the forward radiation begins to diminish rapidly and the side lobes begin to increase. If, however, the dipole is bent forward into a V as in Fig. 24-3, the forward radiation will be restored. The optimum angle θ of the V is a function of leg length in wavelength ℓ/λ, as discussed in Sec. 4.4. For the present case, $\ell = 0.75\lambda$ at the high band, θ should be 114.5°, which gives a gain of 2.67 db over a $\lambda/2$ tuned dipole. At the low band, where $\ell = \lambda/2$, the optimum angle is 180° as expected. If θ is made equal to 180° to favor the low band, the forward gain at the center of the high band will drop to -1.6 db for an infinitely thin dipole, about -3 db for a dipole made of $\frac{3}{8}$-in. tubing, and to -5.5 db for a straight fan-type dipole. On the other hand, if $\theta = 114.5°$, the loss of gain in the low band will be 1.65 db for a very thin dipole, according to the calculation, and from 0.3 to 1.7 db over the whole low band, according to the measurements as in Fig. 24-4. The same figure also shows the tremendous improvement of the high-band gain. From these curves, it is obvious that a fan dipole tilted forward by approximately 33° is a very favorable compromise.
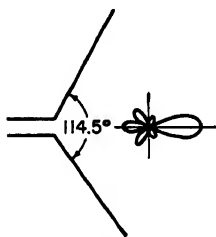
FIG. 24-3. V antenna.

In fact, the fan dipole is essentially a parallel combination of two or more ordinary V dipoles in such a way that at one end they are connected together and at the other end spread out like a fan. It is well known that a strictly parallel combination of two closely spaced dipoles is effectively equivalent to a fat dipole whose radius is the
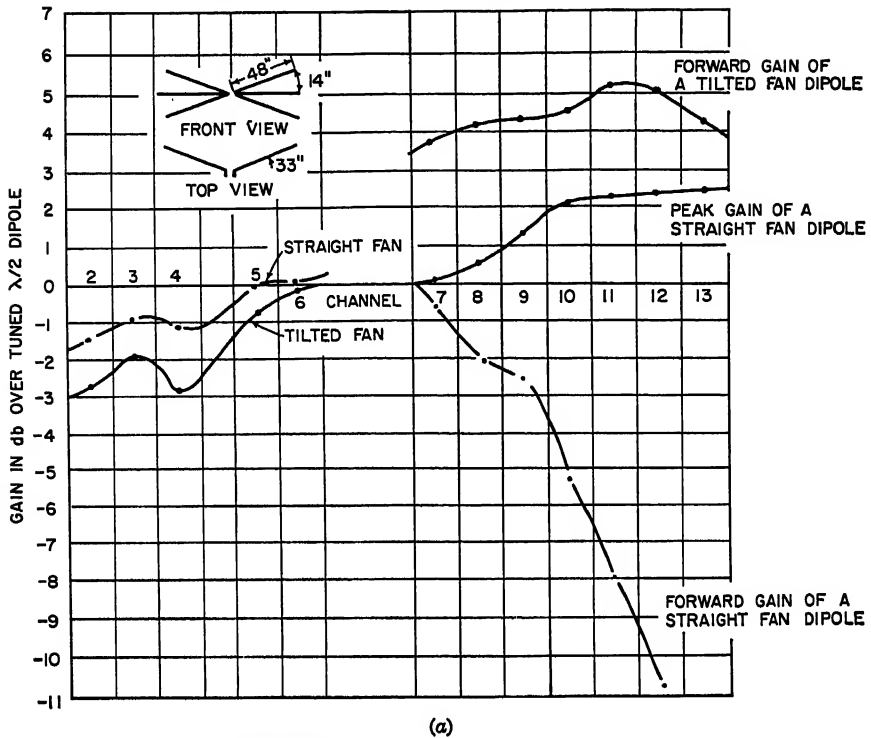
(a)
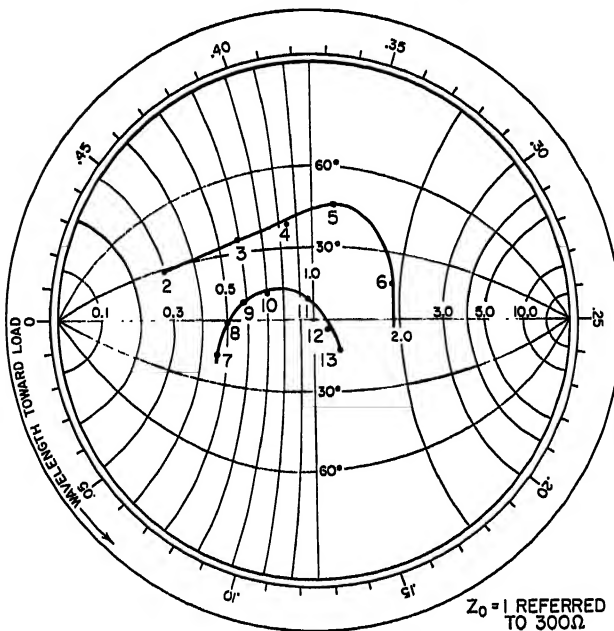
(b)
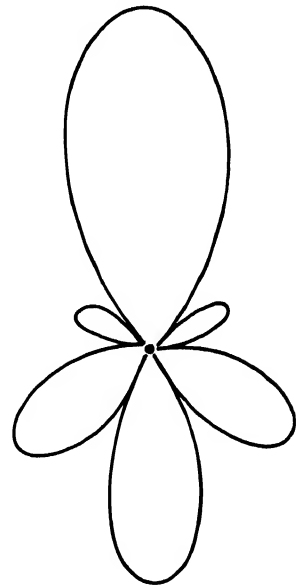
(c)

FIG. 24-4. (a) Gain of a fan dipole. (b) Impedance characteristics of a fan dipole. (c) Field pattern of a fan dipole at Channel 10.

geometrical mean value of the radius of the individual dipole and the spacing between them. Although such a simple relation does not apply to the present fan dipole, the effect is similar. For example, the fan dipole in Fig. 24-4, which consists of ⅜-in. tubing separated by 14 in. at the end tips, is approximately equivalent to a fat dipole made of 2.7-in. tubing. The advantage of using multiple conductors in saving material is evident.

Figure 24-4b and c shows the measured impedance characteristics and field intensity pattern of such a tilted fan dipole. In the low band, the pattern is essentially that of a half-wave dipole as in Fig. 24-1 except that the nulls are filled in.
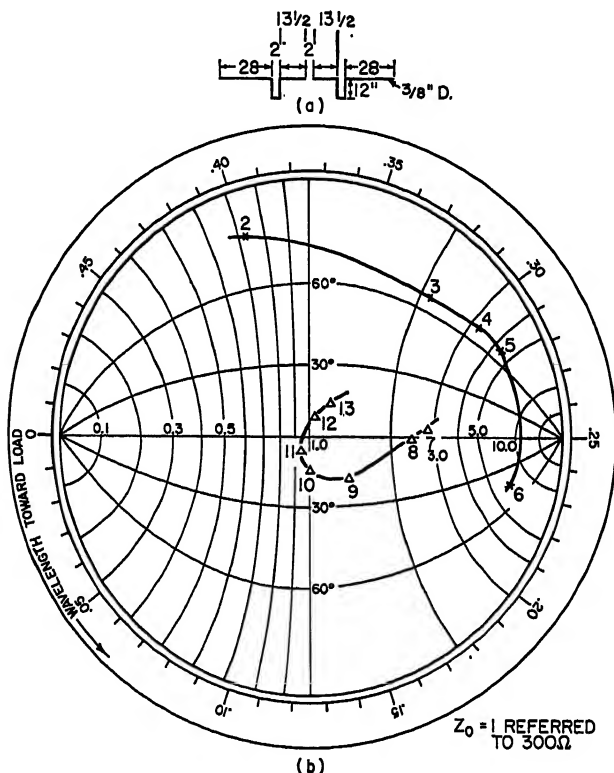
FIG. 24-5. (a) Collinear dipole. (b) Impedance characteristics of collinear dipole.

To improve the gain in the low band, a reflector 107 in. long spaced 30 in. from the dipole can be added. Since the fan dipole itself is unidirectional in the high band, the reflector has negligible effect in this frequency range.

The physical aperture of this dipole is larger than other types, which will be discussed later. Like conventional V-type antennas, in the high band it has few minor lobes.

Collinear Dipole. An array of collinear λ/2 dipoles with phase reversing stubs is known as a Franklin antenna. Since the ratio of the center frequency of the high band to that of the low band is approximately 3:1, three half-wave collinear dipoles with two λ/4 stubs are used, as shown in Fig. 24-5(a). For the low band it will operate approximately as a straight dipole of a length longer than λ/2. A true three-half-wave collinear dipole has excellent gain and directivity, 3.2 db over a tuned λ/2 dipole, a half-power beamwidth of about 34°, and an impedance of 300 ohms. However, in

the present arrangement, the λ/4 line stub for reversing the current in the outside portion is not perfect. In the first place, it is frequency-sensitive; in the second place it is unbalanced, so that it not only radiates but also introduces out-of-phase current in the outside elements; thirdly, there is a coupling between the center and outside elements. All these effects reduce the bandwidth; nevertheless, experiments show that the high-band performance in general is satisfactory. However, in the low band, the performance is rather poor, because, first, the low band has a much wider bandwidth; secondly, the antenna is considerably longer than λ/2; thirdly, and most important of all, it is a very thin antenna even if a ¾-in. rod is used. Measurement shows that the antenna has a VSWR of over 10:1, as seen in Fig. 24-5(b). The impedance characteristics are
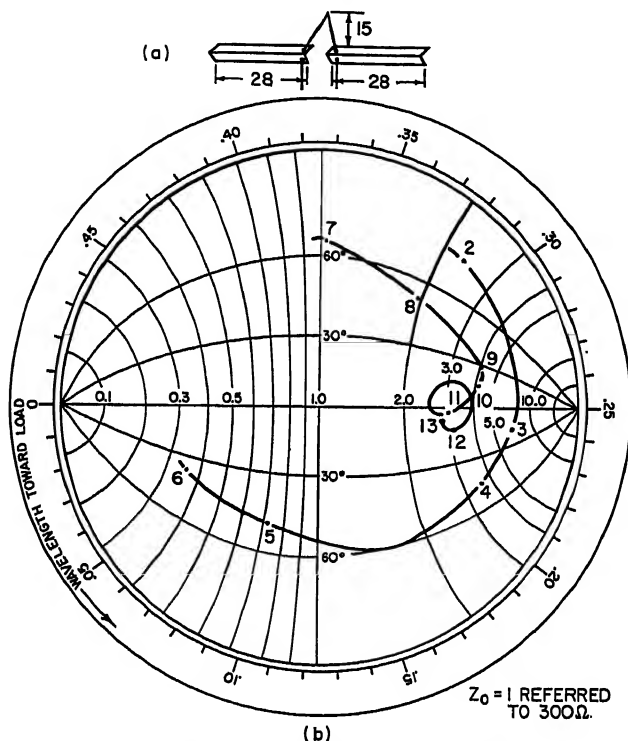
FIG. 24-6. (a) Full-wave dipole. (b) Impedance characteristics of full-wave dipole.

so widely spread that compensation by networks and transmission lines is almost impossible. If two such dipoles are connected in parallel at a close spacing so as to form a fat dipole, it can be expected that the impedance will be greatly improved.

Full-wave Dipole. A full-wave dipole has been used commercially in the high band as a basic element. One advantage of this type of dipole compared with the collinear dipole is that a much thicker conductor can be easily used since it has a straight uninterrupted structure. Thus even in the second mode the impedance is reduced to about 1,000 ohms. As for the low band, it is far less than λ/2, and consequently it is highly capacitive. To compensate this reactance a short-circuit stub can be connected in parallel with the dipole as shown in Fig. 24-6(a). However, the length of the stub must be limited to a quarter of the high-band wavelength, in order to reduce its shunting effect at the high band. Since the length of the stub is almost

fixed and is also a high-Q circuit, it is rather frequency-sensitive.   Because of this and the fact that the dipole is too short, the result is a very poor impedance characteristic even for a rather fat dipole, as shown in Fig. 24-6(b).   The radiation pattern in the high band is essentially that due to a full-wave dipole.

(a)

175 MC

195 MC

215 MC

(b)
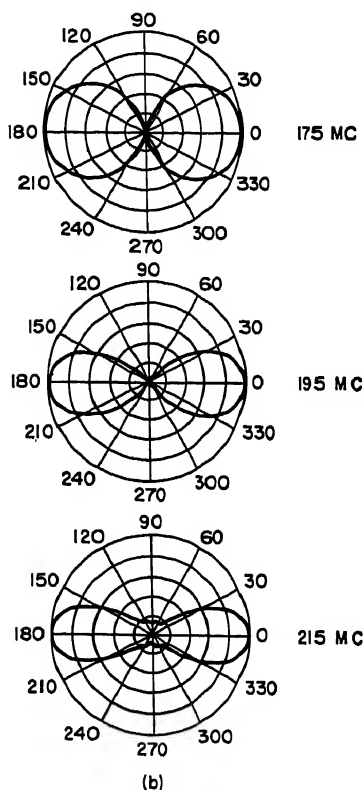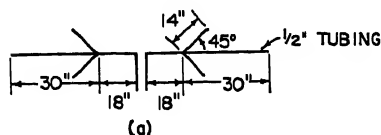
FIG. 24-7. (a) High–low-band dipole with tuning whiskers. (b) Radiation patterns of dipole with whiskers.

Dipole with Whiskers. As mentioned previously, a dipole a half-wave long at the low band will be $3\lambda/2$ at the high band. It is the out-of-phase current in the center portion which causes a split of the radiation pattern. A pair of whiskers[1] can be used to correct such a situation, as shown in Fig. 24-7. It is known that at the junction of a network of wires, not only the continuity of currents is preserved, but also their derivatives with respect to the linear dimension of the wires. If the whisker is cut to $\lambda/4$, the derivative of the current at the junction will be zero. Thus, if the junction is not $\lambda/4$ (or its odd multiple) from the end of the dipole, the current in this portion will be comparatively negligible. In Woodward's original dipole, the whisker is placed at approximately $\lambda/4$ from the feed terminals and $\lambda/2$ from the end; then in the high band it operates close to a full-wave dipole with a VSWR of about 4:1.

As for the low-band operation, the whisker is too short (about $\lambda/16$ to $\lambda/10$ long) to have significant effect, and therefore it is no more than just a simple dipole. One evident drawback of this dipole (as originally suggested) is that the bandwidth in the low-band operation is very much limited. A much thicker conductor may be used to improve the bandwidth, but the effectiveness of the detuning whisker in the high band is reduced.

"Tripole." It is evident that in order to cover the low band properly, a rather fat dipole must be used. A low-band folded dipole is one possibility. Although such a dipole has too high an average impedance as compared with 300 ohms (e.g., a Channel 3 folded dipole made of ⅜-in. tubing with 2-in. spacing has a VSWR of about 1:1 at

Channel 3 and 7:1 at Channel 6 as referred to a 300-ohm line, but less than 3:1 over all the low-band channels if referred to a 740-ohm line), it will be seen later that this situation can be improved.

A folded dipole of a length other than $\lambda/2$ is seldom used.   However, on the three-half-wave mode, the transmission-line mode (or the unbalanced-mode) impedance of the folded dipole is still extremely high and the antenna behaves like an ordinary straight fat dipole on the third mode.

Figure 24-8a shows the radiation pattern of a low-band folded dipole at the high-

(a)

(a)

$Z_0 = 1$ REFERRED
TO 660Ω

(b)

(b)

FIG. 24-8. (a) Field pattern of low-band folded dipole at high-band Channel 10. (b) Impedance characteristics of low-band folded dipole at high-band frequencies.
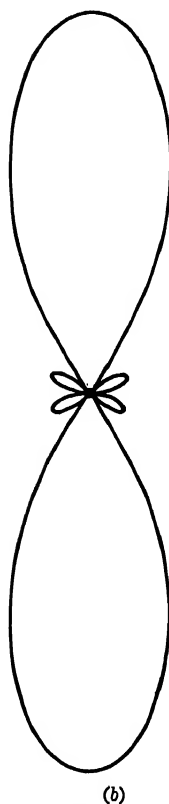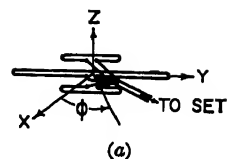
FIG. 24-9. (a) Tripole. (b) Calculated field pattern of tripole.

band Channel 10.   Figure 24-8*b* shows the impedance characteristics, which are very tightly wound within a circle of VSWR 1.8:1 as referred to 660 ohms.

In order to obtain a correct high-band radiation directivity, a closely spaced pair of high-band folded dipoles is added, as in Fig. 24-9*a*.   If the current in this high-band dipole is equal but opposite in phase to that in the center long dipole, the resultant radiation pattern will be the algebraic sum of a $3\lambda/2$ pattern and two $\lambda/2$ patterns as in Figs. 24-8*a* and 24-1.   Based upon this, a theoretical pattern has been calculated and plotted in Fig. 24-9*b*.   The pattern in the plane perpendicular to the dipoles is essentially circular, as one would expect.

The next problem is to obtain equal currents in the three dipoles since the center one is of different length.   To achieve this, an appropriate feed system has been developed.

FIG. 24-10. Feed system for the tripole.

By using a quarter-wave line of characteristic impedance Z_0, a constant-voltage source can be transformed into a constant-current source whose magnitude is equal to the current into a matched load but 90° behind.   Similarly, a constant-current source can be transformed into a constant-voltage source with the same line.
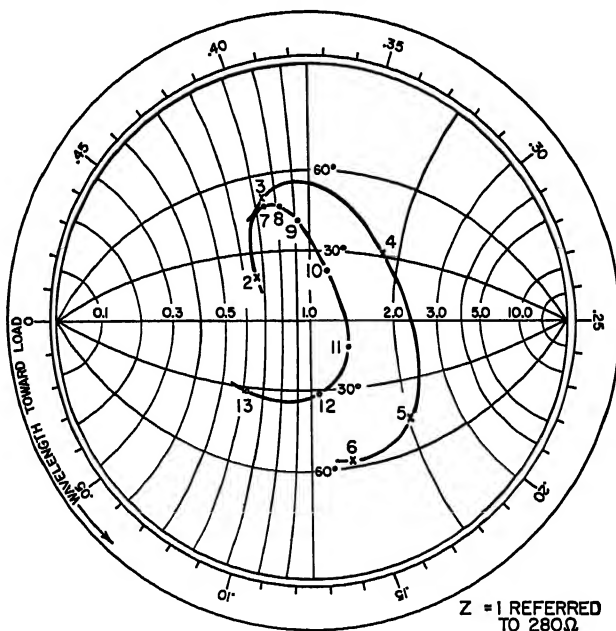
FIG. 24-11. Impedance characteristics of a tripole.

If the three dipoles represented by Z_1, Z_2, and Z_3 in Fig. 24-10 are fed by three identical $\lambda/4$ lines in parallel, the input currents in all dipoles will be of the same magnitude, even if they have different impedances.   Furthermore, by reversing the connections to the long folded dipole Z_2, its input current will be in phase opposition with those in the short dipoles.
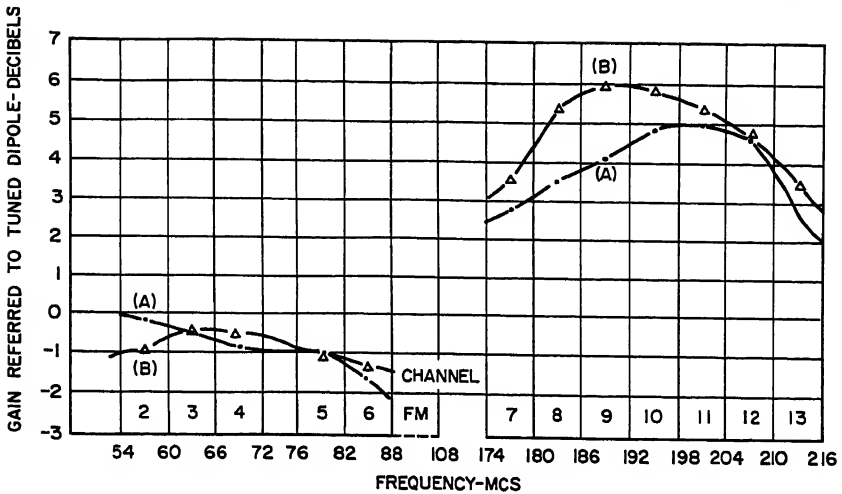
FIG. 24-12. Measured gain for tripole and modified tripole: (a) Tripole. (b) Modified tripole.

The value of the characteristic impedance Z_0 is determined by the input impedance Z_{in}, to be matched. Experiments indicate that a $\lambda/4$ line with a characteristic impedance of about 420 to 450 ohms is very satisfactory for a match to 280 ohms. The resultant impedance characteristics of Z_{in} are shown in Fig. 24-11, indicating a VSWR of about 3:1 over all the high-band channels.

So far only the high-band operation has been considered. At the low band, the short folded dipole is only about one-sixth of the low-band wavelength and is highly inductive. With the transmission line of $\lambda/12$ its measured impedance ranges from $750\underline{/83°}$ on Channel 2 to $6,000\underline{/60°}$ on Channel 6. Its shunting effect upon the low-band folded dipole is therefore not serious. On the contrary, this shunting react-ance tends to tune out the capacitive reactance of the long dipole, which resulted from the $\lambda/12$ line transformation. The measured input impedance of the tripole over all low-band channels is roughly within a VSWR of 3.5:1 as shown in Fig. 24-11, instead of 7:1 for the long folded dipole alone. The measured patterns of the tripole are essentially the same as the theoretical pattern of Fig. 24-9b. The measured gain is shown in curve A of Fig. 24-12.

Figure 24-13 shows another version of the tripole, where only one high-band folded dipole is used. Although the calculated pattern has larger minor lobes, the major lobe is only 28° wide at half-power points. In the plane of these dipoles, the high-band pattern is unidirectional, with two or three rear minor lobes. On the average, its gain is slightly higher than the tripole, as shown in Fig. 24-12.

24.3. SIMPLE ARRAYS

A two-element simple array, either both driven or one driven and one parasitically excited, has a moderate gain of
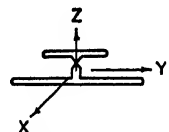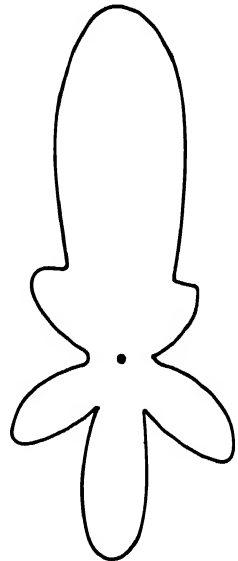
FIG. 24-13. Field pattern of high-low dipole combination at Channel 11.

about 2 to 5 db over a tuned λ/2 dipole and is commonly used in primary areas where either a reduction of the ghosting effect or a higher gain is desirable. A single driven element with either a director or a reflector is the simplest Yagi antenna, for which the theory is well established.[1,3] Its peak gain according to calculation is slightly under 5 db over a tuned λ/2 dipole, but the bandwidth is relatively narrow.

The design of such an array has been discussed in Chap. 5, and Figs. 5-6 and 5-7 can be used for designing the element lengths and spacing. The data in Ref. 2 are also very useful when a detailed design is required.

After choosing the reflector length and spacing, the driven element is made approximately one-half wavelength long. The input reactance is corrected by a minor adjustment of the driven-element length.
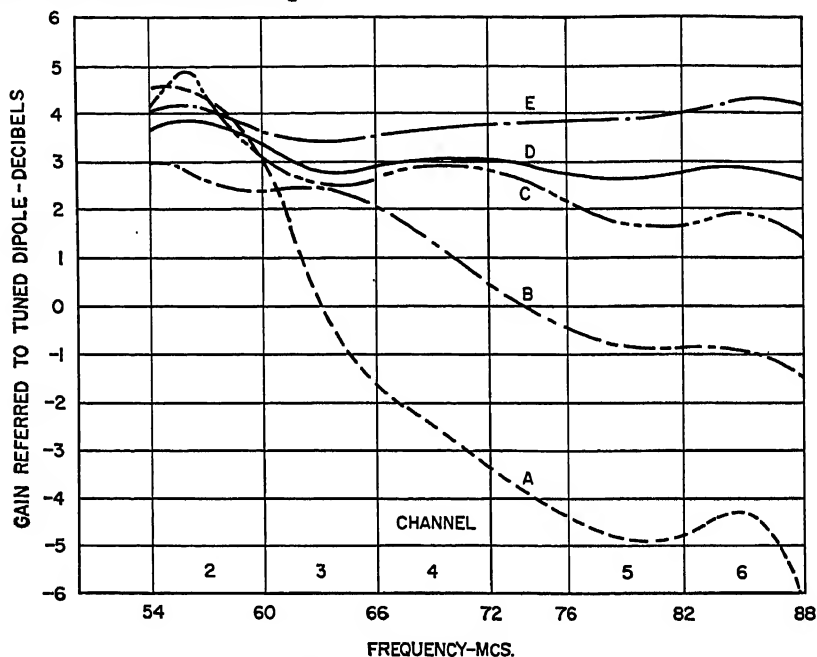
FIG. 24-14. Measured gain of various two-element end-fire arrays.

As 300 ohms is usually chosen as the standard impedance for a receiving antenna, a folded dipole of the proper step-up ratio can be used. However, a simple straight dipole is also widely used because a simplification in construction, and consequently a reduction in cost, can be achieved at the expense of some mismatch loss and a narrower bandwidth. In primary areas of strong signal intensity, both versions will work equally well in so far as the elimination of the ghost due to a reflected wave from the rear is concerned.

A typical design for a two-element array designed for Channel 2 will have the following dimensions:

Reflector element.......................... 103 in., diameter = ⅜ in.
Reflector spacing.......................... 32 in.
Driven element............................ 95 in. long
Diameter of folded dipole conductors....... ½ and ³⁄₁₆ in. with a 2-in.
                                            spacing between them

The measured gain for this antenna is shown as curve *A* in Fig. 24-14. It can be seen that the peak value of the gain agrees with the theoretical calculation but drops

sharply beyond Channel 3. In some commercial wideband Yagis, a greater bandwidth is achieved at the expense of lower peak gain by designing the reflector for the lower edge frequency of Channel 2 and the folded dipole for Channel 4. A typical gain curve is shown as B in Fig. 24-14 for comparison. Evidently the latter is preferable for reception over the entire lower VHF band. Thus the optimum condition for highest gain at one frequency is not always desirable. The gain-bandwidth product would be a better criterion for the wideband application.

It is generally believed that an end-fire array with all elements driven has a wider bandwidth. For a two-element uniform array with a spacing $d < \lambda/2$ and phase difference δ, the calculated gain in decibels over a tuned $\lambda/2$ dipole is shown in the following table:

Table 24-3

d	δ		
	90°	135°	180°
$\lambda/8$	....	4.2 db	3.95 db
$\lambda/4$	3 db	4.5 db	3.6 db
$3\lambda/8$	....	3.43 db	3.0 db

It can be seen that the case ordinarily referred to as an end-fire array with $d = \lambda/4$ and $\delta = 90°$ gives no rearward radiation, but does not give the highest gain. This is a general characteristic of the end-fire arrays, including the Yagi. The maximum gain for d smaller than $\lambda/2$ occurs approximately at $d = 0.2\lambda$, and $\delta = 153.5°$ with a gain over a tuned $\lambda/2$ dipole of 4.91 db.

The feed system of an array is an integral part of the antenna system and plays a role as important as the radiating elements themselves. However, the analysis and design of a feed system required for a given current distribution must take into account the mutual coupling between elements. To illustrate the effect of coupling between elements, let two $\lambda/2$ dipoles be spaced at $\lambda/4$ and fed with a $\lambda/4$ line, as shown in Fig. 24-15. Then the ratio of the currents in two dipoles will be
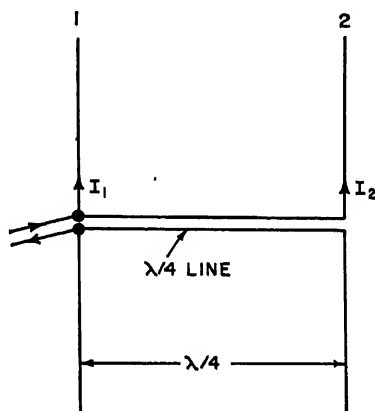
FIG. 24-15. Two-element array with $\lambda/4$ spacing and $\lambda/4$ feeder.

$$\frac{I_2}{I_1} = \frac{Z_{11}/Z_0}{j - Z_{12}/Z_0}$$

where I_1 and I_2 = currents in elements 1 and 2
Z_{11} = self-impedance of each dipole
Z_{12} = mutual impedance between elements 1 and 2
Z_0 = characteristic impedance of $\lambda/4$ line

Suppose $Z_0 = Z_{11} = 70$ ohms for a fat dipole and $Z_{12} = 40 - j40$ at a spacing equal to $\lambda/4$. Then

$$I_2 = 0.599 \underline{/-110°}\, I_1$$

instead of the ideal end-fire case: $I_2 = jI_1$. Therefore a $\lambda/4$ line will not necessarily give a 90° phase shift of the current in the second dipole. In order to obtain such a current, a line other than $\lambda/4$ long or dipoles of different lengths should be used.

Returning to Fig. 24-15, suppose the desired current relation be $I_2 = aI_1$; then the length and the characteristic impedance of the line required will be determined by

$$\cos \beta\ell + j\frac{Z_0}{Z_2}\sin \beta\ell = \pm \frac{Z_1}{aZ_2} \quad (24\text{-}1)$$

where $Z_1 = Z_{11} + aZ_{12}$
$Z_2 = Z_{22} + Z_{12}/a$
Z_{22} = self-impedance of dipole 2
β = wavelength constant of line

and the plus and minus signs are for a straight and for a cross connection respectively, between dipoles. a can be any complex quantity, but for a uniform array with zero rear radiation

$$a = e^{j[(2n-1)\pi - \beta d]} \qquad n = 1, 2, \ldots, n$$

To illustrate this principle, an array is made to consist of two folded dipoles of different lengths and both made of $\frac{3}{8}$-in. tubing with 2-in. spacing between conductors. At Channel 4, the 92-in. dipole has a self-impedance $Z_{11} = 1.8 + j1.2$ and the 75.5-in. one has a self-impedance $Z_{22} = 0.9 + j0.5$, both normalized with respect to 300 ohms. For $d = \lambda/4$, the mutual impedance Z_{12} is equal to $0.534 - j0.466$. For an end-fire array, $a = -j$. Inserting these numbers in Eq. (24-1), the shortest line required for a straight connection will be approximately 54 in. with a characteristic impedance of 380 ohms. A commercial transmission line of nominal impedance of 300 ohms and a velocity factor of about 84 per cent is used. The measured resultant gain is
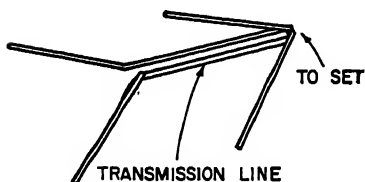
(a) TWIN-DRIVEN VEE
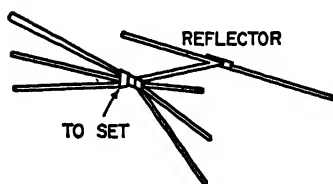
(b) TILTED FAN DIPOLE WITH REFLECTOR
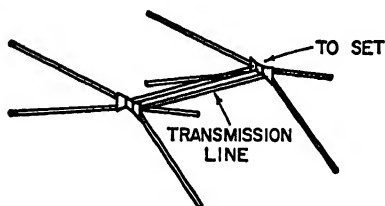
(c) TWIN-DRIVEN TILTED FAN DIPOLE OF TWO ELEMENTS

FIG. 24-16. Various simple end-fire antennas.

shown as curve C of Fig. 24-14, as referred to a 300-ohm load. By some experimental adjustment, it is found that a longer line length will improve the bandwidth even further, as shown in curve D, but with a slight sacrifice of the peak gain in Channel 2. Curve E is the curve D plus the mismatch loss at respective channels, which is determined by the measured input impedance. By comparison of the various curves in Fig. 24-14, it can be seen that this type of end-fire array has almost the same peak gain as the Yagi but with a much wider bandwidth.

So far, the simple array for only one band operation has been considered. For both high- and low-band reception, any type of dipole in the previous section can be used as a basic element of an array. Dipoles such as the fan type and the second version of the tripole are inherently unidirectional in the high band, so that a unidirectional VHF antenna can be obtained by simply adding a low-band reflector, which is found to have only slight effect upon the high-band operation. End-fire arrays of a twin-

driven fan of two elements and simple V dipoles as shown in Fig. 24-16 are also commercially used. The measured gain curves of some typical examples are shown in Fig. 24-17. In the high band, the array has a 3λ/4 spacing in the end-fire mode. If the unit pattern does not have a narrow beam with negligible minor lobes, the array may have high side lobes. Since the high-band wavelength is only one-third of that
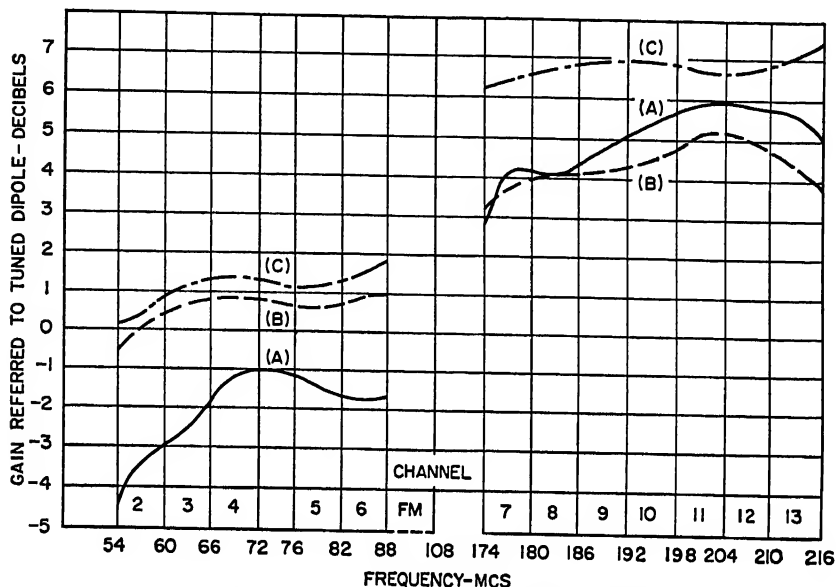
Fig. 24-17. Measured gain for antennas of Fig. 24-16.

of the low band, it is often possible, without substantial effect on the low-band performance, to adjust the spacing for the high-band patterns so that the minima of the unit pattern fall into the minor-lobe maxima of the array pattern.

24.4. SCREEN-REFLECTOR-TYPE ANTENNA

One simple way to improve the directivity of any dipole in Sec. 24.2 is to use a screen reflector. Theoretically, for an infinite perfectly conducting screen, the closer the dipole to the screen the higher the gain, up to a limit of 2.3 relative to a dipole in free space. However, close spacings are not generally used, for the following reasons. First, at this spacing the ohmic loss in the screen, even though small, cuts the gain down drastically. Secondly the impedance at this spacing is not only very low, but changes rapidly, resulting in narrow bandwidth. Thirdly, if the spacing is about 0.1λ to 0.2λ at the low band, then in the high band it will be in the neighborhood of 0.5λ, in which case the forward lobe breaks into two large side lobes. Figure 24-18 is the calculated gain of a λ/2 dipole in front of an infinite lossless sheet reflector as referred to a λ/2 dipole in free space. It can be seen that if the spacing from the reflector is about λ/4 at 67 Mc ($d = 44$ in.), the range of this spacing in wavelength is from 0.2 to 0.33 for the low band and from 0.65 to 0.81 for the high band. The graph shows a gain of about 1.6 to 2 on each band. This spacing not only gives the best compromise in gain between high and low bands but also has a good impedance characteristic. Of course, if the antenna is designed for only one band, the dipole can be as close as 0.15λ from the reflector.

An infinite-sheet reflector is obviously physically impossible. Moullin[4] has investigated both theoretically and experimentally the effectiveness of (1) a finite-sheet reflector and (2) a screen-type reflector made of grid wires. Based upon his calculation, the forward field differs by no more than 1 per cent from what it would have for an infinite sheet if the sheet is about 4λ high (H in Fig. 24-19) and the dipole is no farther than $3\lambda/2$ away from the reflector. A more interesting case in the present application is $d = \lambda/4$. Moullin found no substantial difference between a finite sheet with a height $H = 0.814\lambda$ and an ideal reflector. Figure 24-20, which is derived from Moullin, indicates the front-to-back ratio vs. the height of a sheet reflector as the spacing $d = \lambda/4$. It is seen that it has an F/B ratio of about 38 db when $H = 2\lambda$. Further increase in H yields only a slight improvement in F/B ratio.
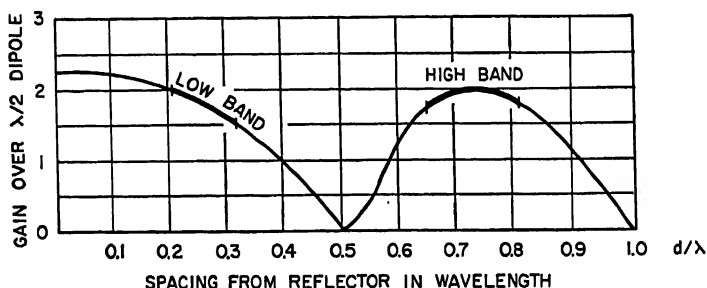
FIG. 24-18. Calculated gain of a $\lambda/2$ dipole in front of an infinite-sheet reflector.
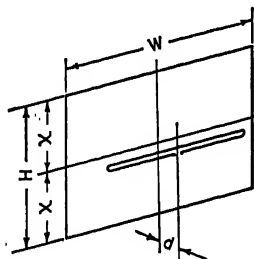
FIG. 24-19. Configuration of a folded dipole in front of a finite-sheet reflector.
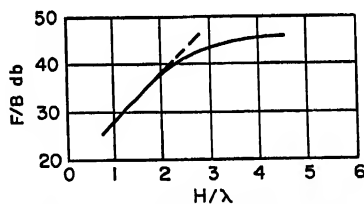
FIG. 24-20. The effect of screen width on front-to-back ratio.

A solid-sheet reflector can be replaced by a screen made of parallel wires if the size of the wire and the spacing between wires are properly chosen. The relation between the radius of the wire b and the spacing g is shown in Fig. 24-21. This calculation is based on the theory that when the self-inductance of the wire is equal and opposite to the mutual inductances between wires, the grid will behave as a solid sheet. Moullin has demonstrated by both calculation and experiment that the size of wire can be much smaller than the curve indicated without substantially reducing the effectiveness of the screen. For example, a $90°$ corner reflector constructed by grid wires of only half the size indicated in the curve has a half-power beamwidth only 10 per cent wider than that of a perfect reflector.

In practice, the size of screen can be even further reduced. The effect of vertical bars for closing up both ends of the grid structure is equivalent to widening the screen. In general, a screen of $\lambda/4$ high and slightly over $\lambda/2$ wide provides a fairly effective reflector.

If a screen is designed for both high and low bands in the VHF range, the over-all size should be determined by the lowest frequency, that is, 54 Mc. The wire size b

and the spacing g should be determined by the highest frequency. It is found experimentally that a closed grid structure of about 4×10 ft, made of $\frac{3}{8}$-in. tubing spaced 8 in. apart (instead of 2-in. tubing at this spacing according to Fig. 24-21) provides a fair reflector unless a very high F/B ratio is sought. Tubing larger than $\frac{1}{2}$-in. diameter is generally too bulky for a receiving antenna. If a better screen is desired, it is more convenient to reduce g/λ than to increase b/λ.

Fig. 24-21. Relation between grid-wire size and spacing.

24.5. SINGLE-CHANNEL YAGIS

For single-channel reception, a Yagi generally is the best solution. Yagis of three or more elements are widely used, although a thorough study is lacking today because of the many parameters, each element having three variables, length, spacing, and the diameter of the conductor. Almost all multielement Yagis are invariably designed empirically. Theoretical calculation has been so far limited to three elements.[5] Figure 24-22b shows the calculated gain vs. the director length ℓ_d and its spacing d_d, as indicated in Fig. 24-22a, for a reflector length $\ell_r = \lambda/2$ and thickness $\rho = \lambda/200$. This

Fig. 24-22. (a) Three-element Yagi antenna. (b) Gain over a half-wave dipole of a three-element Yagi with various director lengths and spacings.

family of curves show that as the spacing d_d decreases, the optimum length of the director increases; however, the maximum optimum gain is about 7db at $\ell_d = 0.45\,\lambda$, $d_d = 0.2\lambda$. This figure is higher than ordinarily obtained with typical three-element Yagis. The reason for this is that the impedance of this combination, with a driving

element length $\ell = \lambda/2$, is about $26 + j59$. Even when stepped up by using an ordinary folded dipole this still represents a VSWR of 2.9:1 referred to 300 ohms. A special folded dipole, with the proper length and a step-up ratio equal to 11.5, will match a 300-ohm load but at an increase in manufacturing cost. Conditions other than the optimum are often used because of economic factors.

Although very little information is available about the bandwidth of a Yagi antenna, experiments show that even in the lowest channel of the television band it is not difficult to maintain the gain within 1 db over the channel without resorting to large-diameter conductors.

For the VHF channels, Yagis with more than 10 elements are rarely used because of their bulky construction and the decrease in gain per element. The number of reflectors is invariably limited to one, because an additional reflector does not improve the performance significantly. However, the use of two parasitic elements stacked vertically or three elements in a trigonal formation,[6] as shown in Fig. 24-23, can improve the gain and bandwidth. In Fig. 24-23a, the reflectors are effectively equal to a thick conductor whose equivalent radius is $\sqrt{A\rho}$, if A is small in wavelengths. This gives more bandwidth, but not necessarily a higher peak gain. In Fig. 24-23b and c the R's are parasitically excited broadside elements rather than reflectors; thus large spacings are necessary to obtain a substantial gain. The gains shown in the figures are measured values referred to that of a dipole without a reflector. In the case of a Yagi antenna with directors, the increase in gain due to these reflectors will be less than the values given.

Experimental results for Yagi antennas with a large number of directors are given in Chap. 5, and the reader is referred to Tables 5-1 and 5-2 for a summary of this information.
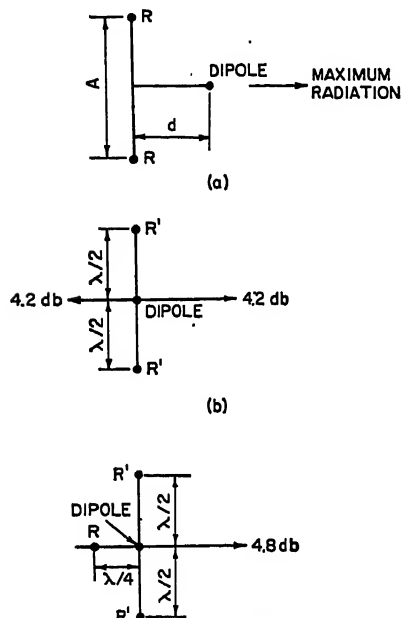
FIG. 24-23. Various arrangements of reflectors.

As mentioned before, the analysis of a Yagi with elements more than three is difficult, but there are a few general properties which may be useful for experimental design.

1. The radiation pattern of a Yagi antenna is almost independent of the length of its driven element. Thus the length and the construction of the driven element are determined only by the impedance characteristics.

2. For the radiation patterns, close spacings will result in a higher front-to-back ratio with a broader main beam. Wider spacings give a sharper beam but more and larger minor lobes. This is particularly true for the spacing of the director next to the driven dipole.

3. The general effect of the length of the parasitic elements on bandwidth is the same as discussed in Sec. 24.3. In order to allow for manufacturing tolerances and for the effect of rain or snow on the antenna, it is preferable to choose directors slightly· shorter and reflectors slightly longer than optimum values.

4. Since the director length decreases very slowly with the increase of the number of directors, it is logical to first adjust the spacing every time a director is added and then to shorten all the lengths slightly.

5. Since a large Yagi antenna has too many parameters to be optimized, it is simpler to design two stacked Yagis, each with few elements, rather than a single Yagi of many elements.

24.6. BROADBAND YAGIS

The Yagi-type antenna is popular for television reception because of its low wind resistance and simple construction. Its chief disadvantage is its narrow bandwidth, since with a conventional Yagi it is impossible to cover several channels. Therefore it is desirable to use a wideband Yagi rather than several single-channel Yagis if provisions can be made to widen the frequency coverage even at some sacrifice in gain.
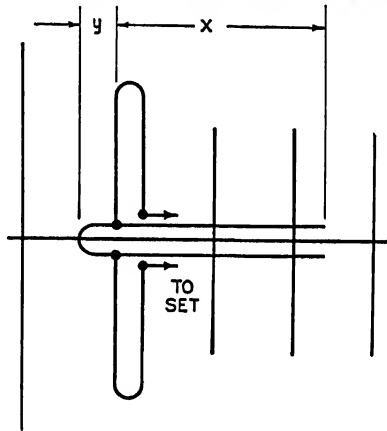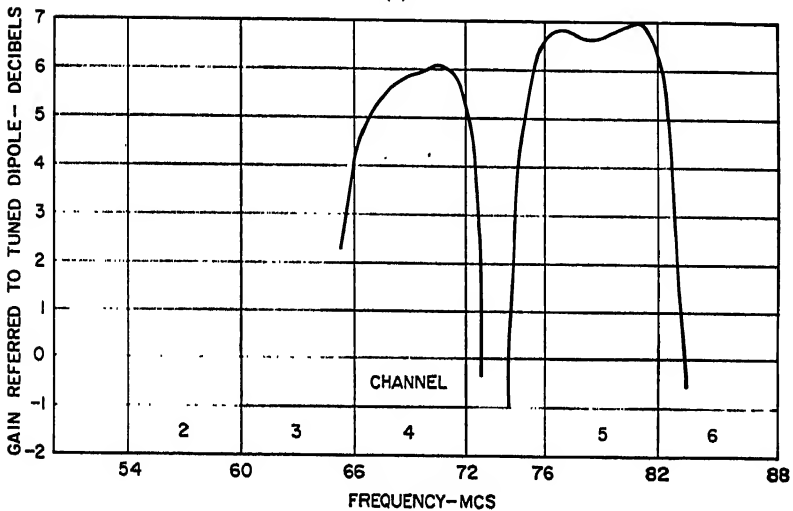
Fig. 24-24. (a) Hairpin-type dual-channel Yagi. (b) Measured gain of hairpin-type dual-channel 10-element Yagi.

The bandwidth of a Yagi is a complex problem to analyze.   Qualitatively, the narrowness of bandwidth is due to the fact that for a given Yagi, as the frequency increases, both the relative spacings and the element lengths in wavelength increase, while the optimum element length decreases with the increase of spacing.   Although a capacitor may be added to effectively shorten the length, there is no passive reactive network with a capacitive reactance increasing with frequency. Therefore the narrow bandwidth is an inherent property of Yagi antennas.

The preceding argument is based upon the optimum gain condition.   If, however, the directors are deliberately made shorter and the reflector is made longer, the bandwidth can be considerably widened with some sacrifice in peak gain.   This can be seen from Fig. 24-14.   There are in general three classes of broadband Yagis: dual-channel, single-band, and high- and low-band Yagis.   A dual-channel Yagi covers two channels, which in most cases are in the same band but are not adjacent.   One type is the so-called hairpin tuned Yagi.   A commercial version of thi is made for Channels 4 and 5,
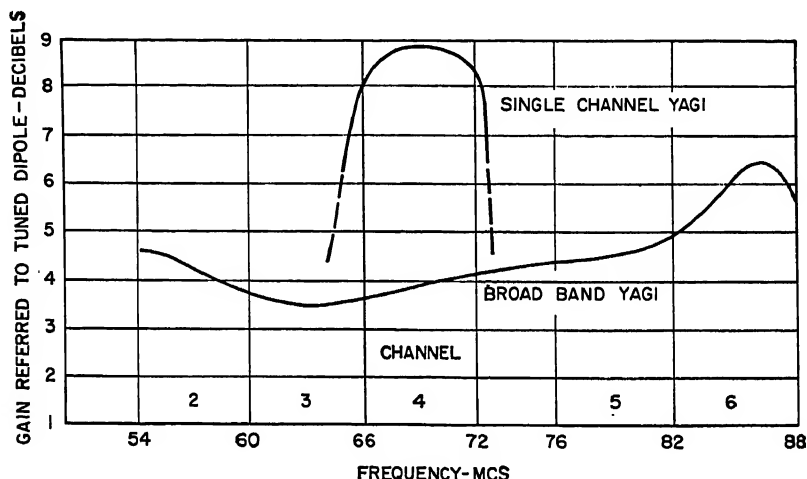
FIG. 24-25. Measured gain of five-element Yagi: (a) Single-channel Yagi.   (b) Broadband Yagi.

since there is a guard band of 4 Mc in between.   In Fig. 24-24a the directors are determined by the upper frequency of Channel 5 and the reflector by the lower frequency of Channel 4.   Acro s the unfed side of the folded dipole is connected a hairpin-shaped line, the open side of which is about λ/4 at Channel 5, so that the folded dipole behaves as if it were a regular dipole cut for Channel 5.   At Channel 4, this dipole is a little short.   This is compensated by the length Y of the short side of the hairpin line, taking into account the capacitive effect of the open side.   It should be noted that one obvious disadvantage with this method is that there always exists a frequency between these two channels for which the hairpin line resonates in its first mode.   When $X + Y$ is approximately equal to λ/4, the hairpin appears as an open circuit to the folded dipole and a sharp drop of gain of 10 to 20 db can be expected, as shown in Fig. 24-24b.

Single-band Yagis include those which receive two or more adjacent channels in one band.   For a Yagi antenna with no more than five or six elements, it is possible to broaden the bandwidth considerably by choosing the element dimensions in the following manner.   The directors are adjusted for the higher frequency, the reflector is adjusted for the lower frequency, and the driven element for the middle frequency. Figure 24-25 shows the measured gain of two five-element Yagis of comparable size Curve A is for a single-channel tuned Yagi, and curve B for a wideband one.   The gain

bandwidth product for curve *A* as referred to a mean frequency of 69 Mc is about 0.76 (roughly 1.0 if the gain in the frequencies outside of Channel 4 is also taken into account), while that of *B* for a bandwidth from Channel 2 to 6 is 2.14. It is evident that the loss of gain in Channel 4 is compensated for by an increase in gain over the other four channels. Also, curve *B* is the antenna directivity gain minus the mismatch loss, which is much more than that of a single-channel Yagi. One minor drawback of this type of Yagi is that there is always a valley in the gain curve somewhere around the mean frequency, in Channels 3 and 4 for the present example. This is particularly true as more directors are added.
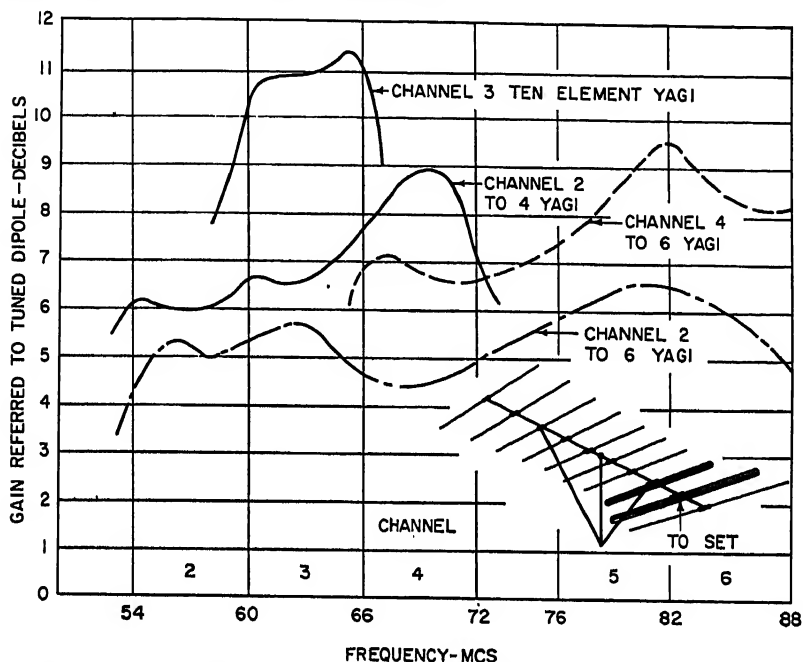
FIG. 24-26. Measured gain of three twin-driven 10-element Yagis and a single-channel 10-element Yagi.

It is known that a properly designed end-fire array of driven elements has a wider bandwidth than an array of parasitic elements. A number of very wide band television receiving antennas use a combination of both driven and parasitic elements. In so doing, the reduction of gain in the middle of the band can be made to a certain extent. One commonly used arrangement is the twin-driven Yagi, which consists of a simple two-driven-element array and a number of parasitic elements. The driven array is designed for the middle of the band, e.g., Channel 3 or 4 for an all-low-band array. Its optimum dimensions may be different from those of the simple driven array alone, because of the mutual coupling of the parasitic elements, but it is a good approximation for the first step in its design. The next step is to add a reflector for the lowest frequency and a few directors for the highest frequency of the band. Further adjustment of the driven elements may then be necessary. Obviously, more than two driven elements can be used for either more uniform gain or a wider bandwidth.

Figure 24-26 shows the gain of several different 10-element twin-driven Yagis, each covering different bandwidths. It should be noted that since there are seven directors, the gain variations would be wider if the array were not twin-driven. All these Yagis

are about 0.91λ to 1.07λ in over-all length at the mean frequency of the band, and all directors are spaced roughly 0.1λ, so that the patterns have relatively few minor lobes. Figure 24-26 also shows the gain of a Channel 3 ten-element Yagi of about the same over-all length for the purpose of the comparison.
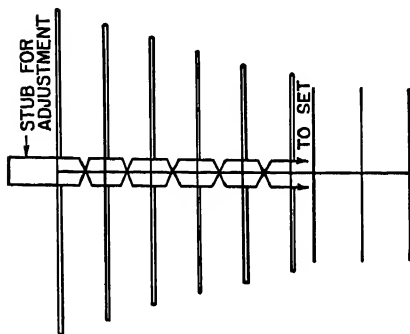
FIG. 24-27. High front-to-back ratio antenna for VHF low band.
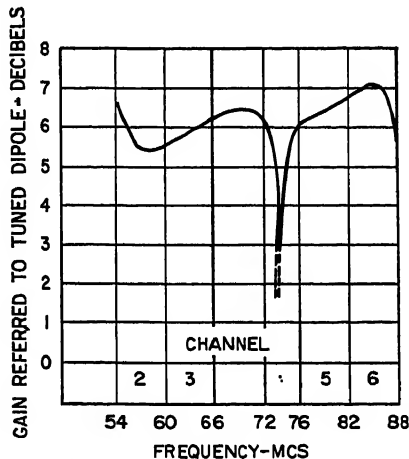
FIG. 24-28. Gain of the antenna shown in Fig. 24-27.

Another example utilizing this principle is an antenna which consists of six cross-fed dipoles tapered in length toward the front of the antenna plus several parasitic elements as shown in Fig. 24-27. This antenna is particularly good for a cochannel interference area because it possesses a very high front-to-side-lobe ratio over the whole low band as shown in Table 24-4. It also has a fairly high gain as shown in Fig. 24-28.

Table 24-4

Channel	2	3	4	5	6
Frequency, Mc	55	61	67	77	83
Front-to-side-lobe ratio, db:					
Single bay	22.5	28.4	26.8	27	21.7
Two-bay stacked at 86 in.	15.3	26	26	23.4	16
Two-bay stacked at 110 in.	19	18	23	21	25

The third type of broadband Yagi is the high- and low-band, or all-VHF-channel, Yagi. It consists of one or several driven elements which are either broadband or multimode dipoles, as described in Sec. 24.2, and a group of interlaced high- and low-band parasitic elements. In the case of a multimode dipole, collinear parasitic elements can be used for higher gain. The construction seems complex, but the elimination of two separate single-band Yagis, two transmission lines, and a switching system plus extra mast length justifies the complexity. The feasibility of such an antenna depends mainly upon the possibility of interlacing the high- and low-band elements. Assume that there are m high-band, n low-band elements interlaced in a certain manner as shown in Fig. 24-29. Let us number them in such a way that from 1 to m they are high-band elements and from $m + 1$ to $m + n$ they are low-band elements. The relation of currents and impedances in the pth low-band element (that is, $m < p \leq m$

$+ n$) at the high-band frequency will be

$$\sum_{q=1}^{m+n} I_q Z_{pq} = 0$$

where Z_{pq} is the mutual impedance between qth and pth elements. For an all-VHF-channel Yagi, the high-band director is slightly shorter than $\lambda/2$ at Channel 13 and the low-band director is about $\lambda/2$ at Channel 6 or in the neighborhood of a full wavelength in the high-band. For ⅜-in. tubing the latter element has a self-impedance in the order of 1,500 ohms at the high-band frequency. As for the mutual impedance, only those elements close to the pth element will have an appreciable effect. The adjacent low-band elements have negligible effect because of (1) their relatively large spacings at high-band wavelengths and (2) the small currents in these elements at high-band frequencies as a result of their high self-impedance. Therefore the current in the pth element can be roughly estimated by

FIG. 24-29. Interlaced high- and low-band Yagi.

$$|I_p| \approx |I_q Z_{qp} + I_{q+1} Z_{(q+1)p}| / |Z_{pp}| \approx 2|I_q Z_{pq}/Z_{pp}|$$

where q and $q + 1$ are two possible nearby high-band elements. For a spacing of $\lambda/10$ between the pth and qth elements, $|Z_{pq}| \approx 120$ ohms. Since $|Z_{pp}| \approx 1,500$ ohms, I_p is only of the order of ⅛ I_q. (Because of the phase difference between I_q and I_{q+1}, I_p may be even smaller.) Therefore the effect of the low-band parasitic elements is not too great at the high-band if the lengths are chosen properly.

The effect of the high-band elements on the low-band operation is negligible, because they are very short in terms of wavelength. A logical experimental design

FIG. 24-30. Measured gain of an all-VHF-channel Yagi antenna.

procedure is to determine the low-band elements first, then the high-band elements. Some readjustment of each set of elements is necessary, since their dimensions are not necessarily the same as those for single-band operation due to coupling effects. As for the reflectors, the high- and low-band elements operate almost independently of each other. Figure 24-30 shows the measured gain of a commercial all-VHF-channel Yagi
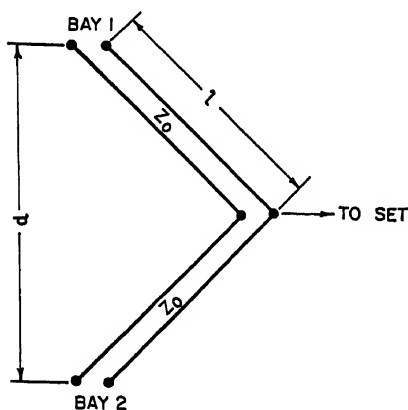
which consists of a tripole as a driven element and five parasitic elements, two for the low-band and three of the collinear type for the high-band. In the low-band, the antenna operates as a three-element Yagi, and in the high-band it operates roughly like three collinear four-element Yagis.

24.7. STACKING PROBLEMS

By stacking, it is meant that two or more single antennas of any type form a broadside array, so that antennas can be stacked horizontally as well as vertically. Vertical stacking is more commonly used because of a higher stacking gain and the elimination of a separate mast. However, stacking more than three or four bays, particularly in the low-band channels, becomes mechanically inconvenient, so that a combination of vertical and horizontal stacking may be used. The optimum stacking spacing for two half-wave dipoles is 0.67λ, but this is not generally true for other single-bay antennas. The general rule is that the group pattern of the array should have a beamwidth at least comparable with that of the unit-bay vertical pattern in order to have an appreciable stacking gain (similarly for horizontal stacking). Thus, in stacking large antennas, large spacing is more fruitful.
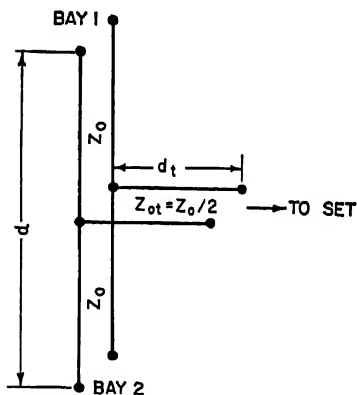
FIG. 24-31. Equivalent-stacking connections.

This procedure often complicates the feeding system, so that half-wave stacking is commonly employed for convenience. Half-wave stacking in the low band (or three-half-wave in the high band) provides a convenient means of impedance matching, since a $\lambda/4$ transformer can be used in each bay to match a 300-ohm load at the feed terminals. A properly designed single-bay antenna will have an impedance-characteristic curve centered around 300 ohms, so that a stacking line 90 in. long of 425 ohms impedance is a good compromise in most cases. For spacing less than $\lambda/2$ (except for very close spacing), the stacking line should still be maintained at approximately $\lambda/2$ in length and 425 ohms impedance. In this case, the stacking rods are longer than the spacing, so that it is necessary to form the rods in V shape. This V-shaped stacking line is equivalent to a T-shaped line as shown in Fig. 24-31, if

$$d_t = \ell - \frac{d}{2} \quad \text{and} \quad Z_{0t} = \frac{Z_0}{2}$$

A slight adjustment of Z_{0t} and d_t may be necessary because of the difference in end effects and coupling between the Z_0 and Z_{0t} lines. The choice of these two alternatives is a matter of mechanical convenience. For four-bay stacking, each pair of adjacent bays is treated as a single bay, after which the same procedure is followed for these two pairs. A second method, shown in Fig. 24-32, uses a straight feeding system with a reversed connection to the outside bays. Since the currents in bays 1 and 4 are a function of the line length, this method is frequency-sensitive and is useful primarily for stacking narrow-band antennas.

24.8. RECEIVING ANTENNAS FOR UHF CHANNELS

The assigned UHF band consists of 70 channels (Channels 14 to 83) and a frequency band from 470 to 890 Mc, or 65 per cent bandwidth with respect to the mean frequency 647 Mc. Since the frequency is approximately ten times that of the VHF low band, UHF antennas of comparable physical size will have considerably higher gain. However, because of greater propagation attenuation in the UHF band, higher values of gain are required.
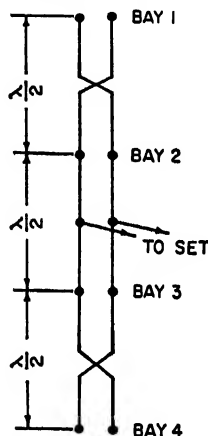
FIG. 24-32. Alternative method of four-bay stacking.
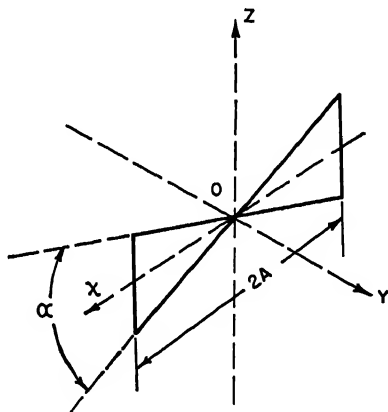
FIG. 24-33. Geometry of the triangular dipole.

Since most types of UHF antennas are relatively small, stacking of four or even eight bays is not too difficult. There is some question as to whether it is desirable to stack too large a number of antennas since the wavefront across a large aperture may be nonuniform, because of the unevenness of the terrain.

Biconical and Triangular Dipoles. To cover the entire UHF band, a fat dipole is almost essential. Theoretical studies on dipoles of certain shapes have been made by various authors. Among them the conical dipole has received considerable attention. Although a biconical antenna is not commonly used in TV reception, yet a few basic dipoles widely used in TV reception are more or less derived from it. The measured resistance and reactance of a conical unipole vs. lengths in electrical degrees for various flare angles are shown in Figs. 3-13 and 3-14. Experimentally, no noticeable difference in impedance has been found whether the ends of the conical dipole are closed with a spherical cap or not. Since all quantities in these figures are referred to a monopole, for a symmetrical dipole the resistance R, the reactance X, and the over-all length should be doubled.

A commonly used UHF dipole is made of triangular sheet metal as shown in Fig. 24-33. It has the advantage of light weight and simple structure and can also be made

of mesh screen instead of solid sheet, provided that the mesh spacing is small in wavelength.

The resistance and reactance of a triangular unipole of length A and flare angle α are shown in Ref. 8 for a wide variation of parameters. The radiation pattern of the triangular dipole is similar to that of a conical dipole except that the vertical pattern (in the YZ plane) is no longer circular because of the dissymmetry of the construction. The larger the values of A and α, the more the pattern in the XZ plane deviates from those in the XY plane and also the more predominant are the side lobes. Based upon the pattern and the impedance characteristics, a compromise value of α of about 60 to 80° may be used for values of A up to 210°. Figure 24-34 shows the measured gain characteristics of a triangular dipole. As with VHF antennas, this dipole can be used in front of a screen to eliminate the rear lobe and increase the directivity and can also be stacked. The measured gain curves for several cases are also shown in Fig. 24-34.
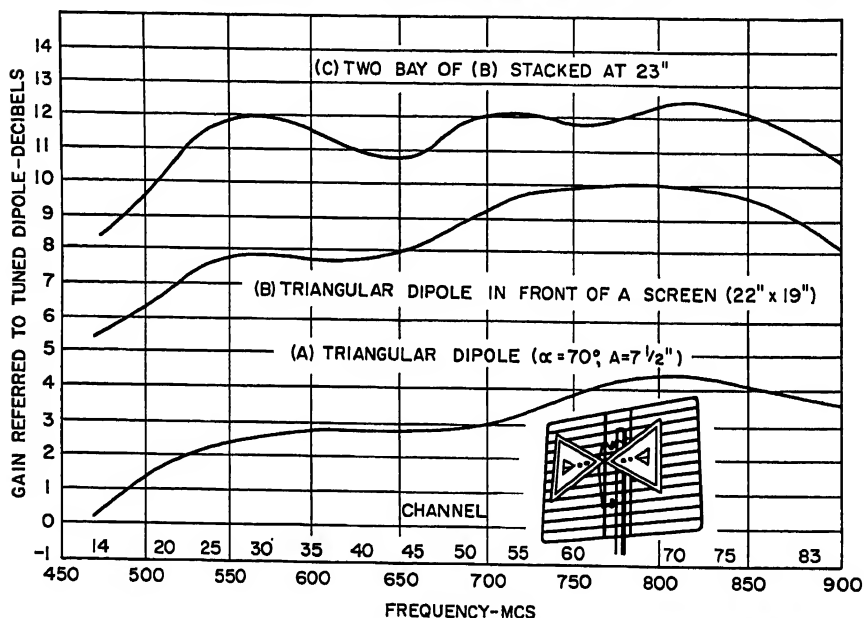
FIG. 24-34. Measured-gain characteristics: (a) Triangular dipole ($\alpha = 70°$, $A = 7\frac{1}{2}$ in.). (b) Triangular dipole in front of screen (22 × 19 in.). (c) Two bays of antenna b stacked 23 in. apart.

V and Rhombic Antennas. A simple UHF antenna is the V antenna, the theory of which has been discussed in Chap. 4. Because of the considerably higher frequency, a V antenna of leg length 2.5λ, at Channel 14 (or 4.5λ at Channel 83), has about the same size as a VHF λ/2 dipole. It is known that the longer the leg, the higher the gain. However, for the simple type of construction used in the average home installation, the V is commonly supported near the vertex. The leg length is then limited to about 55 in., or a length of 2.1λ at 450 Mc and 4.2λ at 900 Mc. For these conditions, the optimum angles are 65 and 50°, respectively, so that a compromise must be reached for the whole band.

One commercial version of simple construction is a two-bay stacked V antenna as shown in Fig. 24-35. Here, two ⅜-in. rods, each 122 in. long, are bent into a U shape approximately 55 in. long and then mounted on two insulators fastened to the mast so as to form a stacked V antenna with an angle of 50° and a built-in stacking line with

2-in. spacing. The feed terminals are at the center of the line. Figure 24-35 also shows the measured gain.

It is possible to use a rhombic antenna for the average home installation at UHF. Figure 24-36 shows the gain of a single-bay rhombic antenna of leg length 55 in. and interior angle 65° and with a termination of 470 ohms. Since it is essentially a traveling-wave antenna, the impedance characteristic is excellent over the whole band.
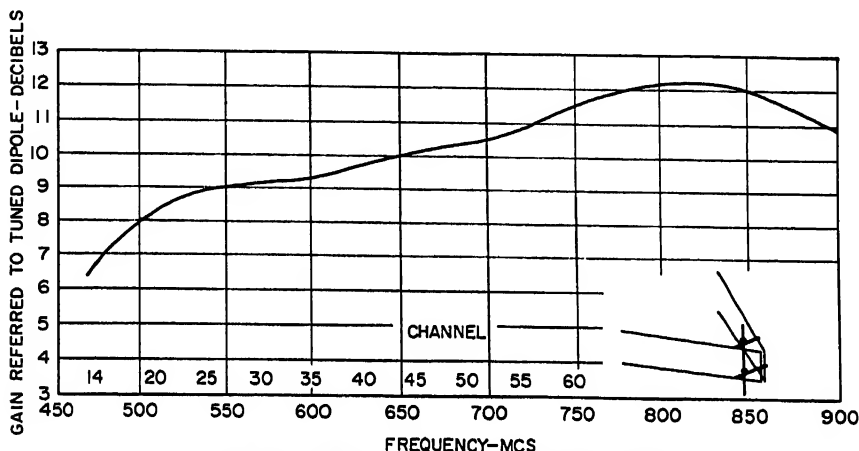
Fig. 24-35. Measured gain of a stacked V antenna.
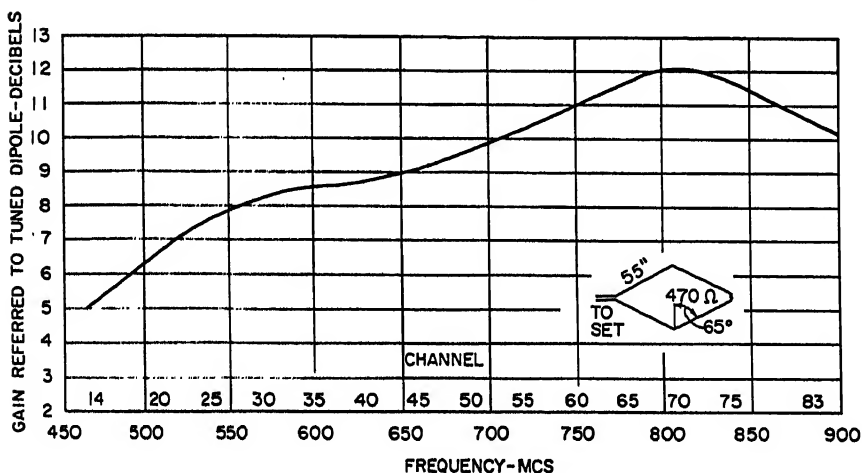
Fig. 24-36. Measured gain of a UHF rhombic antenna.

Corner-reflector-type Antenna. The corner-reflector-type antenna is very useful for UHF reception because of its high gain and large bandwidth. A 90° corner reflector, constructed in grid fashion, is generally used. One typical design is shown in Fig. 24-37. A wide-band triangular dipole discussed in the beginning of this section would be a good choice to use with the corner reflector, except that its dimensions are too large. A modified version is a triangular dipole of flare angle 40°, which is bent 90° along its axis as shown in Fig. 24-37, so that the dipole is parallel to both sides of the reflector. Experimental results indicate that an over-all length of 14¼ in. for the

dipole gave the optimum value of average gain over the band. The dipole has a spacing of about λ/2 at mid-band from the vertex of the corner reflector. Larger spacings would cause a split lobe at the higher edge of the band where the spacing from the vertex becomes equal to a wavelength.

Figures 24-38 to 24-40 are experimental results useful in designing grid-type corner reflectors. Figure 24-38 shows the relation between grid length L and gain at three
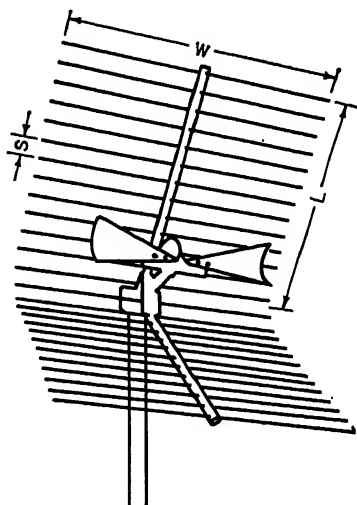
Fig. 24-37. Corner-reflector antenna.
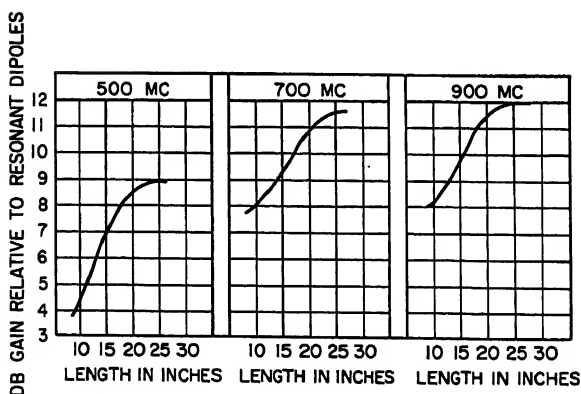
Fig. 24-38. Measured-gain characteristics vs. grid length L.

different frequencies. It is seen that beyond 20 in. of grid length very little is gained. Figure 24-39 shows the relation between gain and grid width W. At 700 and 900 Mc, the improvement in gain for a grid over 20 in. wide is rather insignificant. To reduce the fabrication cost to a minimum, 25 in. is considered a good compromise. In Fig. 24-40 the spacing for grid tubing of ¼-in. diameter can be determined from the allowable level of rear lobe in percentage of the forward lobe at the highest-frequency 900 Mc. If 10 per cent is the allowable value, the spacing should be slightly under 1½ in.

Below 900 Mc, the rear pickup will be less than 10 per cent provided that the grid screen is wide enough. Thus the width is determined by the lowest frequency, while the spacing of the grid tubing is determined by the highest frequency.

Figures 24-41 and 24-42 are the impedance characteristics and field patterns, respectively. Figure 24-43 shows the measured gain over the band.

UHF Yagi Antenna. A Yagi antenna is still the simplest solution in areas where the channels fall within a 10 per cent band about the mean frequency. For example,
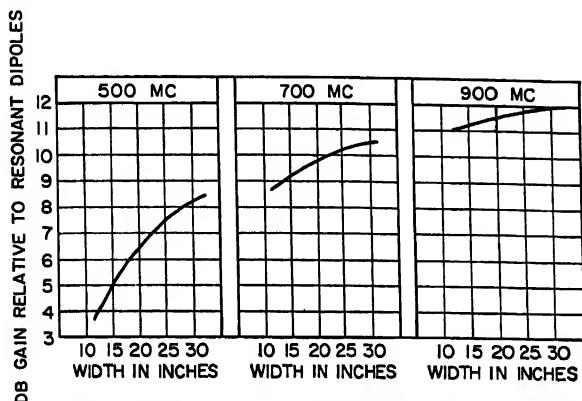
FIG. 24-39. Measured-gain characteristics vs. grid width W.
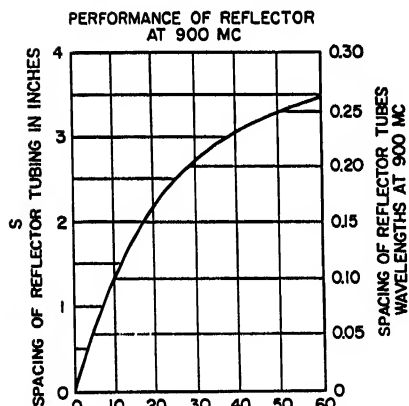
FIG. 24-40. Relation between the rear lobe in per cent of the forward lobe and the grid spacing S at 900 Mc.
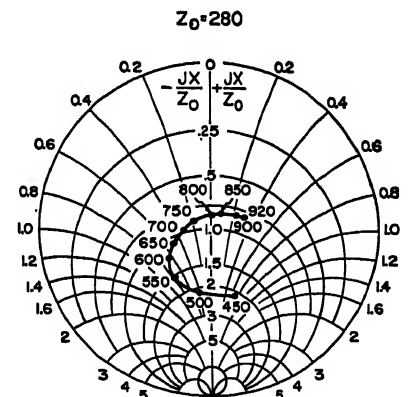
FIG. 24-41. Impedance characteristics of a UHF corner reflector.

a 9 per cent bandwidth Yagi will cover six channels on the low-frequency end and 12 channels on the high end.

The basic principles of designing VHF Yagis are still applicable for UHF Yagis. The dimensions can be obtained approximately by scaling, except for some mechanical parts such as the metal supporting cross arm, which usually does not scale by the same factor. The minor discrepancies due to imperfect scaling can be compensated for by a slight readjustment of element length. Because of short physical wavelength at the UHF channels, Yagis of three or four wavelengths long and up to 16 elements are feasible.

FREQUENCY 450 MC
100%

FREQUENCY 540 MC
100%

FREQUENCY 630 MC
100%

FREQUENCY 720 MC
100%

FREQUENCY 810 MC
100%

FREQUENCY 900 MC
100%

FREQUENCY 450 MC
100%

FREQUENCY 540 MC
100%

FREQUENCY 630 MC
100%

FREQUENCY 720 MC
100%

FREQUENCY 810 MC
100%

FREQUENCY 900 MC
100%

POLAR CHARACTERISTICS
HORIZONTAL ———
VERTICAL ― ― ―
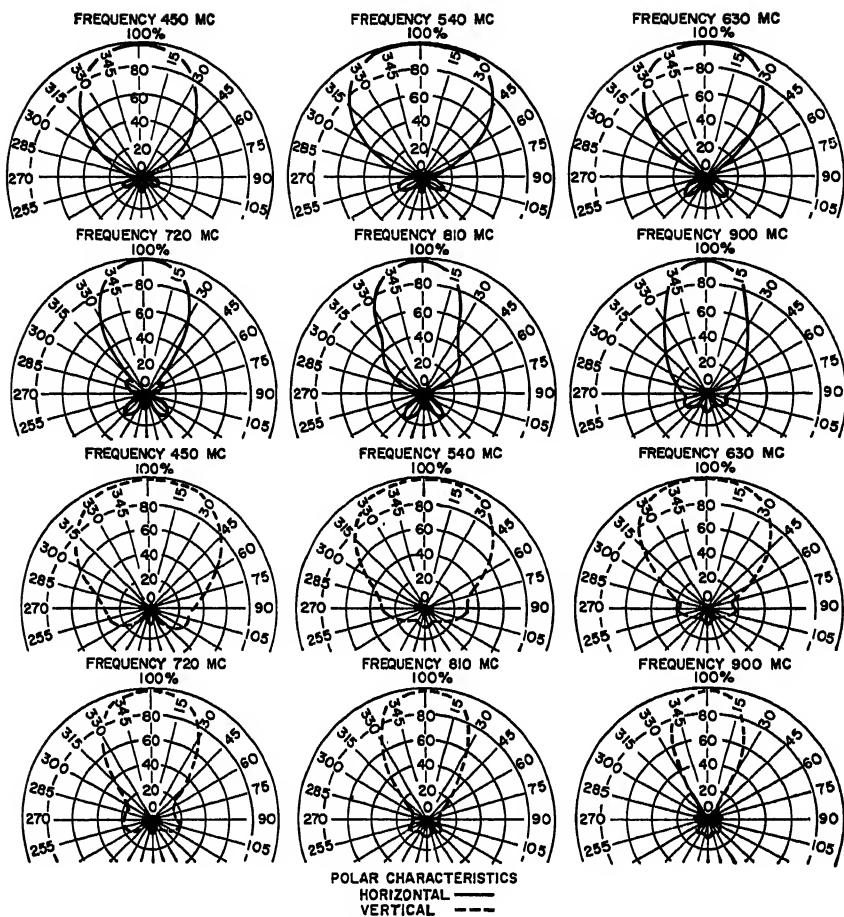
FIG. 24-42. Field patterns of a UHF corner-reflector antenna.
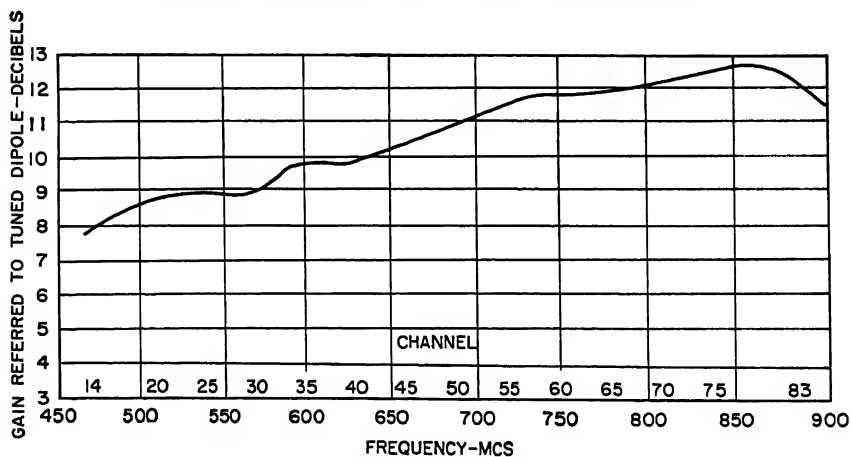
FIG. 24-43. Measured gain of a UHF corner-reflector antenna.

REFERENCES

1. O. M. Woodward, Jr.: "Reversible-beam Antenna for Twelve-channel Television Reception," *RCA Rev.*, vol. 10, p. 230, June, 1949.
2. S. Uda and Y. Mushiake: "Yagi-Uda Antenna," chaps. 7, 8, Sasaki Printing and Publishing Co., Ltd., Sendai, Japan, 1954.
3. R. King: "The Field of a Dipole with a Tuned Parasite at Constant Power," *Proc. IRE*, vol. 36, p. 872, July, 1948.
4. E. B. Moullin: "Radio Aerials," chaps. 5, 11, Oxford University Press, New York, 1949.
5. Reference 2, chap. 9.
6. S. A. Schelkunoff and H. T. Friis: "Antennas: Theory and Practice," p. 570, John Wiley & Sons, Inc., New York, 1952.
7. R. M. Fishenden and E. R. Wiblin: "Design of Yagi Aerials," *Proc. IEE (London)*, pt. III, vol. 96, p. 5, 1949.
8. G. H. Brown and O. M. Woodward, Jr.: "Experimentally Determined Radiation Characteristics of Conical and Triangular Antennas," *RCA Rev.*, vol. 13, p. 425, December, 1952.
9. E. O. Johnson and R. F. Kalor: "Practical TV Antennas for UHF," RCA Victor Division, Home Instrument Dept., Advanced Development Section, Camden, N.J.

OTHER REFERENCES

B. Bailey: "TV and Other Receiving Antennas," John Francis Rider, Publishers, Inc., New York, 1950.

W. A. Cumming: "A Nonresonant End-fire Array for VHF and UHF," *IRE Trans.*, vol. AP-3, p. 52, April, 1955.

W. W. Hansen and J. R. Woodward: "A New Principle in Directional Antenna Design," *Proc. IRE*, vol. 26, p. 333, 1938.

D. G. Reid: "The Gain of an Idealised Yagi Array," *J. IEE*, pt. IIIA, vol. 93, p. 564, 1946.

Y. T. Lo: "Wide Band Antenna," U.S. Patent No. 2,691,730, 1954.

S. A. Schelkunoff and H. T. Friis: "Antennas: Theory and Practice," John Wiley & Sons, Inc., New York, 1952. Pages 499–502 on V antennas; chap. 14 on rhombic antennas; pp. 302–319 on short antennas.

K. Schlesinger: "An Automatic Built-in Antenna for Television Receivers," *Proc. Natl. Electronics Conf.*, vol. 5, p. 292, 1949.

J. Schwartz and Y. T. Lo, "Broad-band End-fire Television Antenna," U.S. Patent No. 2,817,085, 1957.

R. A. Smith: "Aerials for Metre and Decimetre Wavelengths," Cambridge University Press, New York, 1949. Chapter 5 on reflectors and directors; chap. 10 on Yagi antennas.

W. Walkinshaw: "Theoretical Treatment of Short Yagi Aerials," *J. IEE (London)*, pt. IIIA, vol. 93, p. 598, 1946.

H. Yagi: "Beam Transmission of Ultra-short Waves," *Proc. IRE*, vol. 16, p. 715, 1928.

Chapter 25

RADAR ANTENNAS

ROBERT L. MATTINGLY

Bell Telephone Laboratories, Inc
Whippany, New Jersey

25.1. GENERAL DISCUSSION

The antenna is often regarded as the most important single element in the conventional radar system. Justification of this appraisal is explicit in the radar-range equation,[1] which states that radar range varies as the square root of the antenna gain-wavelength product, while the dependence for all other parameters, except two-way transmission loss, enters as a fourth-root factor. These relationships can be underlined by remembering that a fourfold (6-db) increase in antenna gain is required to double the radar range, while a sixteenfold (12-db) increase in transmitter power, or receiver sensitivity, is necessary for the same effect.

Pattern Requirements as Related to Application. The free-space pattern of the antenna is inevitably an important consideration in the radar-system planning. Certain beam shaping is often desirable, whether of the familiar "cosecant" (Sec. 25.4) or some other form. Minor-lobe levels are usually set on a compromise basis after the gain and beam-angle penalties are weighed against other system requirements, which may involve antijamming considerations, the possibility of ambiguous angle information, and the effect of the operating environment, particularly the radome, on the antenna. It is not too early in this discussion to emphasize that it is pointless to impose on an aperture the stringent tolerance requirements and carry out the careful illumination design necessary for a very low side-lobe level when the radome itself, as in streamlined airborne installation, may be the limiting factor in setting the side-lobe intensities.

Gain and Side-lobe Considerations. It can be said in general that the radar antenna never has a high enough gain nor low enough side-lobe levels. Although these desiderata are to some extent mutually exclusive, relative importance can often be assigned. For example, a harbor-navigating radar will usually be better prepared to sacrifice gain than to permit multiple azimuth returns from a single target. Again, a search radar, striving for maximum range, will usually not be misled by azimuth ambiguity and will consequently choose gain over side-lobe suppression. Unfortunately, there are many cases where both high gain and low side lobes are important. A particularly significant example becomes apparent in assessing the vulnerability of a military radar to electronic countermeasures. The signal-to-jamming ratio is directly proportional to the radar antenna gain. However, access to the radar by the jammer is not restricted to the main antenna beam but can also be had through the side lobes. Hence a minimum side-lobe level is an antijamming requirement.

As a guide to a choice of antenna type where either gain or side-lobe suppression is to be emphasized, the following table is presented.

Table 25-1

	Gain	Side-lobe suppression
Doubly curved reflector (including paraboloids)..............	Good	Very good
Metal-plate (acceleration) lens......................	Poor	Good
Two-dimensional array......................................	Very good	Very good
Line feed with cylindrical reflector........................	Very good	Good

Size and Weight Considerations. Antenna size and weight are always factors, particularly in airborne applications where the necessity for restricted physical size often forces the designers into the centimeter and even the millimeter spectrum to attain the requisite directivity. In addition to the obvious airborne demands for minimum weight, the designers of a ground-based antenna are often confronted by the requirement for air transportability of the radar equipment.

25.2. PENCIL-BEAM ANTENNAS

Weight restrictions account in large measure for the popularity of the doubly curved reflector with point or quasi-point feed. This combination almost always represents the lightest weight possible for the production of usual antenna patterns. Special requirements may force the designer to some other antenna type but almost always at the expense of weight. The size and swept-volume advantage of the reflector with point-source feed is not so marked. For most radar frequencies, two-dimensional arrays provide very compact and efficient radiating structures. However, techniques of focal-length folding are possible for the reflector or lens-antenna types which are often effective in reducing size (Sec. 25.2).

Center-fed Paraboloids. A pencil-beam antenna is defined as an antenna in which the main beam is approximately a figure of revolution about the beam axis. A center-fed paraboloidal reflector is the most common antenna of this type. While a center-feed system is simple and quite efficient, it has two associated difficulties: (1) feed-blocking effects and (2) broadband impedance-matching problems produced by direct reflection from the reflector back into the feed system.

Feed-blocking Effects. The effect of feed blocking is to increase the minor-lobe level, to decrease the gain, and to sharpen the beam angle. These latter two effects are negligible for most practical cases where the feed area is much less than the reflector area but the increase in minor-lobe level may be significant.[1] The lobe level with feed-horn blocking can be calculated to a good approximation by the following process. Ignore the blocking effect and calculate the far-field pattern from a knowledge of the feed characteristics and the resulting aperture illumination. The normalized minor-lobe level without feed-horn blocking is then known. Now add to this normalized value twice the ratio of the feed-horn area to the total aperture area. This sum is approximately the normalized minor-lobe level with feed blocking. As an example, a circular aperture with a parabolic aperture illumination has a maximum normalized minor-lobe level of 0.059 (24.6 db). An aperture 10 in. in diameter excited by a feed horn whose area is 2 sq in. will exhibit an approximate minor-lobe level with feed-horn blocking of 0.059 + 4/78.5, or 0.110 (19.2 db). Increasing the feed-horn area to sharpen the taper of aperture illumination will help up to the point where the area ratio is increasing faster than the minor-lobe level of the unblocked aperture is decreasing. From the foregoing we see that feed-horn-blocking effects need be considered only for feed-horn/aperture ratios of the order of 0.01 or greater. It also means that this effect becomes more marked for a given aperture area as the operating frequency goes down, since it is necessary to increase the physical area of the feed horn to maintain a given illumination taper.

Mismatch-improvement Techniques. In the usual pencil-beam antenna, the impedance mismatch produced by direct reflections back into the feed is troublesome if a good impedance match (VSWR $\leq$ 1.1) is required over a frequency band greater than 1 or 2 per cent. This situation comes about in that a reflection-canceling discontinuity placed at or near the feed-horn aperture is usually many wavelengths from the reflector and can be expected to be effective only over a very narrow bandwidth. A completely satisfactory means of circumventing this difficulty is not yet at hand. Partial solutions include polarization rotators, directional couplers by means of

which a compensating discontinuity can be introduced at any desired distance from the feed horn, zone plates placed at the vertex of a paraboloidal reflector, and hybrid feed arrangements. Before beginning a discussion of these stratagems, it is in order to point out that an isolator,[3] when available, is often the best solution to the matching problem. With an isolator, the reflections are absorbed at the expense of some sacrifice in radiated power. This loss of power, exclusive of the isolator insertion loss, is given by

$$\% \text{ power loss } = (\text{voltage-reflection coefficient})^2 \times 100 \qquad (25\text{-}1)$$

As an example, a VSWR of 1.4 corresponds to a loss of only 2.8 per cent. It will be seen that some of the other matching devices imply a power loss as well.

Impedance matching by use of a vertex plate[4] is probably the best known of the various matching techniques, which admit, in principle, good impedance properties (VSWR $\leq$ 1.4) over a fairly wide ($\leq \pm 6$ per cent) frequency band. As shown in Fig. 25-1, a circular plate of radius given by $r = \sqrt{f\lambda/3}$ (where f is the focal length and λ the wavelength) is positioned as shown. The action here is that of cancellation of the reflections over the larger portion of the reflector by correctly phased reflections from the relatively small vertex plate placed in the region of high-illumination intensity. As long as the aperture is fairly large ($>10\lambda$) and the illumination not unusually

(a)

SECTION A-A

3DB
DIRECTIONAL
COUPLER

TO GENERATOR → ← TO ABSORBER

(b)
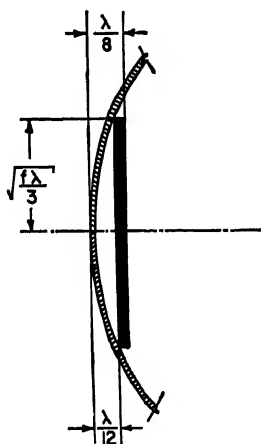
Fɪɢ. 25-1. Vertex plate in paraboloidal reflector.
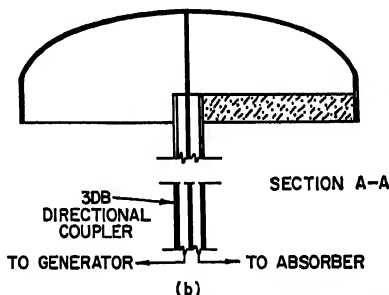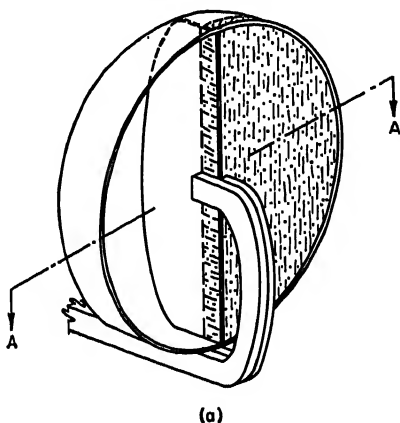
Fɪɢ. 25-2. Compartmented reflector with hybrid feed.

sharply tapered, the dimensions of the vertex plate are independent of the aperture size. The difficulty with this technique lies in the inevitable, and often serious, enhancement of the minor lobes. The phase errors introduced at the center of the aperture typically raise a 20-db lobe level without the vertex plate to a 15-db level with the vertex plate. Effect on gain and beam angle is usually small.

For the compartmented reflector[5] the antenna is split into two sections by a thin conducting plate as shown in Fig. 25-2. Each half is fed by a separate though adjoining feed so that the reflections back into each feed are identical. Note that each feed

must have its electric-field vector perpendicular to the septum. If the feed pair are connected to the transmission line by means of a hybrid, then the identical reflections can be diverted into a power-absorbing arm of the hybrid. This process is shown diagrammatically in Fig. 25-2b. If the hybrid is of the T form, or its equivalent, then the length of line between one feed and the hybrid must be λ/4 longer (or shorter) than the length of line between the other feed and the hybrid. If the hybrid is of directional-coupler form, then the required λ/4-line-length difference is not required. In either case, the results are the same; the reflections, to the extent that the hybrid action is ideal and the reflections from each antenna half are equal, are all absorbed in the load.

This device, so far described, is not yet complete, for the phase difference between each half of the aperture is 90°. This situation, if uncorrected, would produce intolerably high minor lobes. A phase corrector becomes necessary, and it can be either a dielectric slab in one-half of the reflector as indicated in Fig. 25-2a or a parallel-plate phase-advancing arrangement in the other reflector half. The presence of this correction medium disturbs the symmetry upon which reflection cancellation depends. However, the effect is small. Unless the relative dielectric constant is fairly high (>2), matching slots or tapers in the dielectric have not been found to be necessary.

Some corollaries to this general principle should be recognized. The electrical-bore-sight axis can be coincident with the mechanical axis only at the design center frequency. Over a 10 per cent frequency band, the electrical-bore-sight deviation is usually quite small (a few per cent of a beamwidth) and easily calculable. If the media involved are nondispersive over the frequency range of interest, then the bore-sight shift (θ) is given to a good approximation by

$$\theta = \frac{\Delta f}{f} \times \frac{\text{beam angle}}{2} \qquad (25\text{-}2)$$

where f is the frequency. Thus, over a 10 per cent frequency band (± 5 per cent), the electrical-bore-sight direction would deviate from the mechanical axis by $2\frac{1}{2}$ per cent of the beam angle.

As long as the septum is very thin as compared with a wavelength, then the reflector can indeed be simply a paraboloid containing a conducting dividing plate. However, since the focal point for each half lies in the surface of the septum, two paraboloid halves separated by the septum thickness are more exactly used. This is illustrated in Fig. 25-3.

In the split or compartmented reflector, the results are quite similar to that produced by an isolator. In the choice between these two devices (isolator or split reflector), the fragility of the ferrite material, its temperature sensitivity, and the requirement of a magnetic field will be weighed against the complexity of the phase corrector required in the split-reflector assembly and the more elaborate

Fig. 25-3. Separate focal points of compartmented reflector.

feed structure. In both techniques the reflections are absorbed rather than canceled and a power loss occurs as given by Eq. (25-1).

A good impedance match can be obtained through the use of a reflector which simultaneously collimates the beam and rotates the plane of polarization through an angle of 90°. The reflected energy is thus returned in a mode to which the feed is not responsive.

While it is a simple matter to specify a plane structure which will accomplish the desired rotation for normal incidence and at one frequency, the problem in the case of a paraboloidal reflector involves a variety of incidence angles and usually a band of frequencies as well. Silver[6] describes a grating structure consisting of an assembly of plates, with each plate approximately $\lambda/4$ in depth and inclined at an angle of 45° to the direction of polarization. The spacing between these plates is small ($<\lambda/8$) to

(a)

(b)

(c)
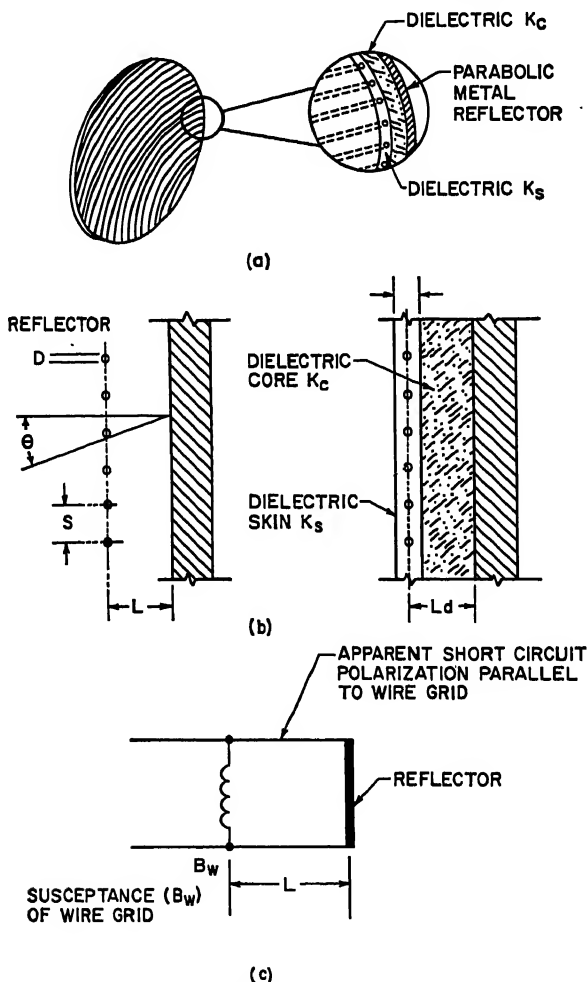
FIG. 25-4. Polarization-rotating paraboloid.

ensure nearly complete reflection of the electric-vector component parallel to plate. This kind of structure has good impedance properties over a narrow band of frequencies. Pattern results are not known, but appreciable degradation over the normal paraboloidal results may be expected.

Hannan[7] has developed a design procedure utilizing a grating of thin wires to produce a very efficient polarization-rotating structure with negligible effect on the pattern. The technique involves the use of a grating which transmits some of the parallel component of the electric vector. This approach makes possible a device

which can be fairly insensitive to frequency changes over at least a 10 per cent bandwidth and to the normal range of incidence angles. The general action can be described in terms of Fig. 25-4. The wire grating, inclined at an angle of 45° to the electric plane of the feed, appears as a negative (inductive) susceptance to the wave component parallel to the grating. Thus the position of the effective short circuit as seen by this wave component will be located between the metal reflector and the grating (Fig. 25-4b). As the frequency increases, the susceptance becomes smaller, but the position of the effective short circuit tends to remain in approximately the same position since the distance between the grating and the reflector becomes a larger portion of the wavelength.

In terms of Fig. 25-4c, where D is the diameter of the wires, S the spacing between the wires, θ the angle of incidence measured from the normal, and L the shortest distance between the wires and the backing metallic reflector, the design equations are

$$\frac{L \cos \theta}{\lambda} = 0.358 \quad (25\text{-}3)$$

$$\frac{\lambda}{S \cos \theta} \frac{1}{\log_e (S/\pi D)} = 2.05 \quad (25\text{-}4)$$

Thus with λ and $\cos \theta$ taken as average values over their range, these equations permit the calculation of various pairs of values for S and D. The spacing S, however, should be less than $\lambda/4$ to ensure that diffraction effects are negligible.

Practically, the wire grating is most easily established in position by embedding it in a dielectric attached to the reflector. Grating protection usually requires that a thin skin of dielectric cover the grating. Introduction of these dielectrics slightly affects the distance between the grating and the reflector. Calling this new distance L_D, assigning K_C and K_S to the values of the relative dielectric constants of the dielectric core and dielectric skin, respectively, and taking T as the skin thickness (Fig. 25-4), then

FIG. 25-5. Directional coupler used in feed system for impedance matching.

$$L_D \simeq L - \frac{L(K_C - 1)}{2 \cos^2 \theta} + \frac{\lambda(K_C - 1)}{8\pi \cos^3 \theta} \sin \frac{4\pi L \cos \theta}{\lambda} - \frac{T(K_S - 1)}{\cos \theta} \sin^2 \frac{2\pi L \cos \theta}{\lambda} \quad (25\text{-}5)$$

The use of this formula is restricted to $T \ll \lambda$ and K_C small (<1.5).

Matching with a directional coupler[8] deserves mention. This technique is most advantageously employed when the mechanical arrangement is such that a matching device cannot be placed at or very near (in terms of a wavelength) the reflection-producing discontinuity. As shown in Fig. 25-5, the compensating discontinuity can be placed as far from the reference plane as the mismatch itself. Thus the frequency dependence usually associated with a separation between a discontinuity and the matching device is largely avoided. All this is done at the cost of some power loss. Assuming that the coupling coefficient in the directional coupler can be adjusted appropriately, then

$$\% \text{ power loss} = (\text{voltage-reflection coefficient}) \times 100 \quad (25\text{-}6)$$

In Eq. (25-6), the voltage-reflection coefficient is the value before the matching process. It is interesting to note that the loss incident to this matching process is greater by a

factor equal to the voltage-reflection coefficient than the loss associated with the use of an isolator [Eq. (25-1)]. It might seem that the problem of compensating for reflections from a paraboloidal reflector back into the feed structure would yield completely to this matching technique. This is not entirely true in that reflections occur from the entire paraboloidal surface rather than just from that small area directly in front of the feed. For the case of the usual paraboloidal reflector ($d/f \simeq 3$) frequency bandwidths of more than ± 3 per cent are difficult to attain.

Feed-horn Design. In the early development of center-fed paraboloids, popular feeds were those for which the waveguide entered through the center of the antenna and the energy was directed back toward the reflector by ingenious arrangements often involving parasitically excited half-wave elements or slots.[9] However, with the
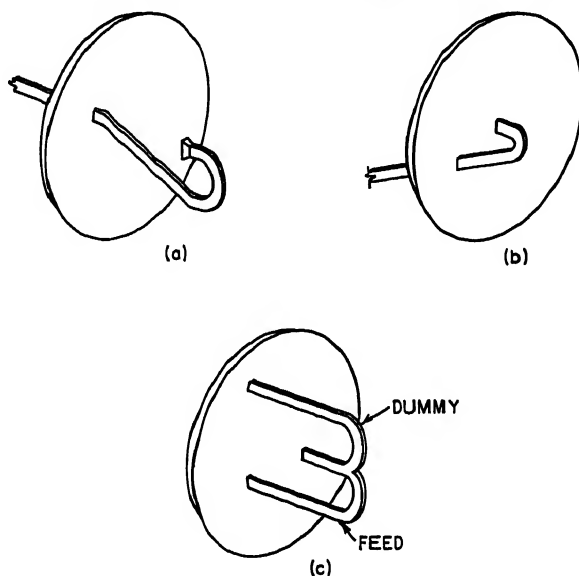
FIG. 25-6. Gooseneck feeds.

emphasis of the modern radar on wide frequency bandwidths and high power, such devices have been largely abandoned in favor of the direct horn feed. The most satisfactory of these direct-feed designs is usually the simplest, a gooseneck feed as shown in Fig. 25-6a, or variants thereof, one of which is shown in Fig. 25-6b. Often a counterpoise (Fig. 25-6c) is used which helps support the feed and, although not an electrical part of the feed system, ensures mechanical, and therefore electrical, symmetry.

A Practical Example. Reasonably good results in predicting the pattern of the complete antenna in the two principal planes result from the procedures as described in Sec. 12.2 in which the free-space feed-horn pattern, the various tapers involving the area variation across the aperture, and the relative areas subtended by constant increments in angle at the feed are taken into account in arriving at the aperture illumination. This sort of calculation of the antenna pattern is often bypassed in radar antenna design. Some useful practical concepts will become apparent in a consideration of the feed-horn–paraboloidal reflector arrangement shown in Fig. 25-7a. Here a feed horn of rectangular aperture with dimensions $d_1 \times d_2$ illuminates a paraboloidal reflector. For $d_1 = 0.455\lambda$ and $d_2 = 0.835\lambda$, low lobes in the xz plane would be expected by reason of the marked illumination taper across the aperture in that plane. Higher side lobes would exist in the yz plane where the shorter horn dimension d_1 makes

for a less sharp illumination taper. Figure 25-8a shows the actual patterns with this geometry. To decrease the lobes in the yz plane, it is necessary to increase dimension d_1. The effect of this is illustrated in Fig. 25-8b, where d_1 has been increased to 0.852λ. However, the lobe level in the xz plane rises as shown. This behavior emphasizes the fact that the patterns in the principal planes can be, in general, considered separately only for very approximate purposes. Here the increased taper in the yz plane has decreased the taper in the xz plane. The shading in Fig. 25-7b and c indicates the taper across the incremental areas for the original and increased d_1. For the larger d_1, it is seen that the center areas are tapered relatively more sharply than the edge areas. Hence the contributions from the edge areas become relatively more effective than before; the over-all taper in the xz plane is less than for $d_1 = 0.455\lambda$, and the lobes go up. Thus it is seen that d_1 must be a minimum to permit the lowest side lobes in the xz plane. One corollary here is that only with the
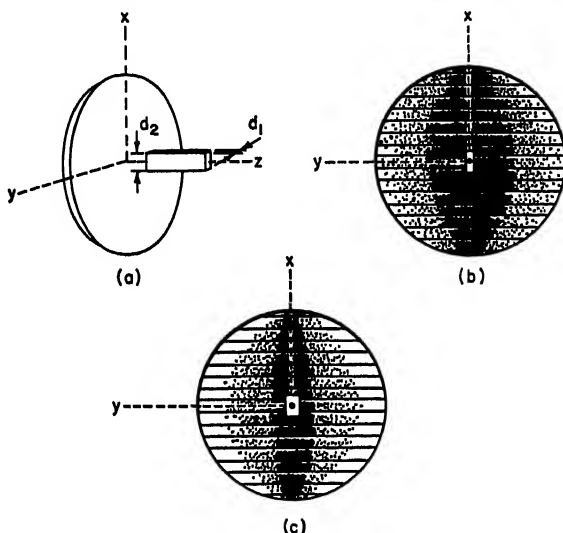
Fig. 25-7. Aperture tapers as affected by feed dimensions.

polarization as shown in Fig. 27-7a (electric-field vector perpendicular to the xz plane) can minimum lobes be obtained in the xz plane with conventional waveguide feeds. Polarization with the E vector perpendicular to the yz plane does not permit the feed dimension in the yz plane to be any smaller than that dictated by cutoff considerations. This effect can be partially overcome through the use of dielectric-loaded or ridge-guide feed types.

Offset Paraboloidal Sections. A very satisfactory method of achieving a wideband impedance match for a pencil-beam antenna utilizes an offset-fed paraboloidal section. This technique is illustrated in Fig. 25-9. The broadband impedance properties arise from (1) the absence of any directly reflected energy back into the feed and (2) the tendency for the back-scattered energy entering the feed system to cancel, since the phase of this energy near its maximum amplitude is rapidly changing with small increments of subtending angle at the feed. This technique is increasingly effective as more "offset" is introduced, although it has the disadvantage of increasing the swept volume of a mechanically scanned antenna. A nonradar example of radical offset is presented by the horn-fed paraboloidal[10] antennas used for radio-relay communication.

Lens Antennas. While the popularity of the parabolic reflector justifies the priority given in this discussion, refractive media (lenses) are also capable of producing
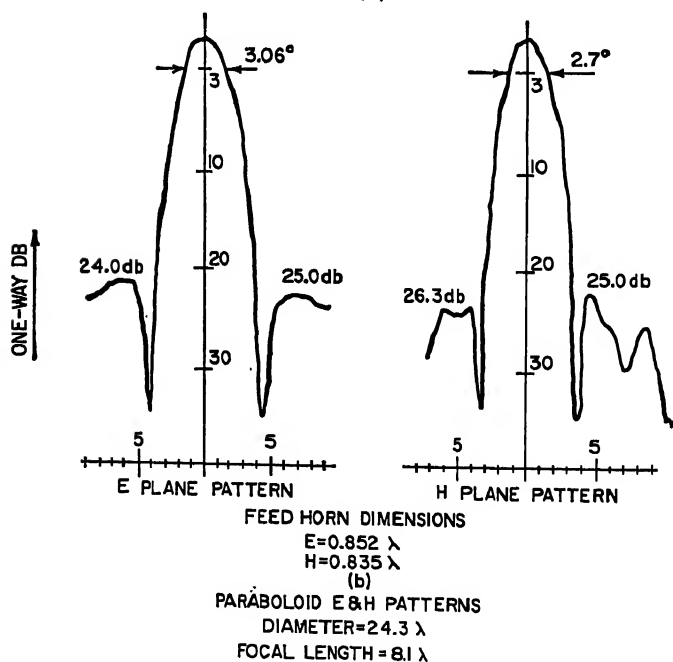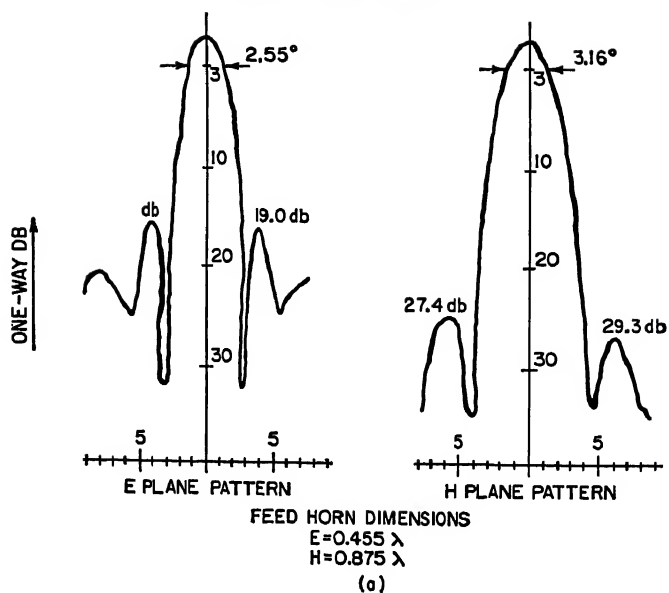
FIG. 25-8. Patterns associated with aperture tapers.

pencil beams. These media fall into one of three classes: (1) dielectric, (2) metal-plate, and (3) artificial-dielectric. Of these the metal-plate lens[11] has found more frequent radar application since the solid dielectrics (e.g., polystyrene, lucite) are quite heavy[12] and artificial dielectric may exhibit unacceptable fragility. Even the metal-plate or acceleration lens has seen only limited use since it has two often serious drawbacks. First, the zone-stepping process necessary to contain its depth to a reasonable dimension significantly diminishes its effective area, so that there is a loss in gain, compared with a reflector of the same size, of between 1 and 2 db. Second, in order to avoid incidence angles near critical values at the air-lens interface, an aperture/focal-length ratio of about 1 is typical. This contrasts with a value of 3 or so for the ordinary paraboloidal reflector and indicates the increase in size of the lens system. However, there are other applications, particularly in scanning by feed displacement, when the metal-plate lens appears to better advantage. In such a case, the good impedance properties and comparatively loose mechanical tolerances of the lens system are corollary benefits.

Cassegrain Antennas.* In a number of radar antennas, the feed system and the associated waveguide circuits become so sophisticated and massive that it is highly desirable to locate these items in the rear of the structure. Although this feature is automatically achieved with a lens antenna, the drawbacks mentioned in the last paragraph often severely reduce the attractiveness of this solution. Another possible type, the offset-fed paraboloidal section, combines a relatively accessible feed location with the simplicity and efficiency of the reflector method of focusing; however, the asymmetry of this configuration creates unacceptable electrical performance in some applications, as well as problems of a mechanical nature. It is due to considerations such as these that the double-reflector or Cassegrain system has in recent years been employed in a wide variety of radar and other microwave antennas.

Fig. 25-9. Offset paraboloidal antennas.

One form of Cassegrain antenna is indicated in Fig. 25-10. The main dish is a paraboloid and the auxiliary reflector, or "subdish," is a hyperboloid. When the feed is located at the near focus of the hyperboloid, and the focus of the paraboloid coincides with the far focus of the hyperboloid,[13] the antenna radiates a collimated beam. As far as the main dish is concerned, there is a virtual feed located at its focus. In the example shown the virtual feed is smaller than the real feed; this property can be used to advantage in the design of certain antenna types, such as those involving a monopulse system.

In order to eliminate what would otherwise be an intolerable amount of aperture blocking by the subdish, one form of Cassegrain antenna employs the polarization-twisting scheme[14] illustrated in Fig. 25-11. A horizontally polarized feed radiates

* Prepared by P. W. Hannan, Wheeler Laboratories.

toward a subdish composed of a horizontal grating of metal slats or wires, and the latter reflects the wave toward the main dish.   On the main dish there is incorporated a polarization-twisting structure, such as that described under mismatch-improvement techniques (Sec. 25.2), which changes the polarization to vertical during the reflection process.   The wave now propagates unhindered through the subdish grating, which is
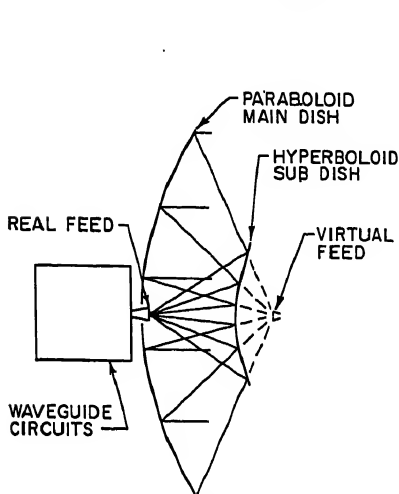
FIG. 25-10. Cassegrain antenna system.
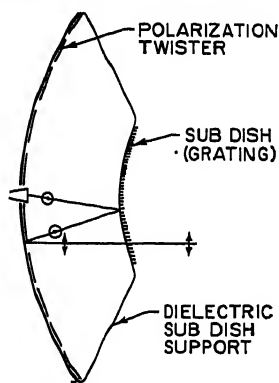
FIG. 25-11. Polarization-twisting scheme.
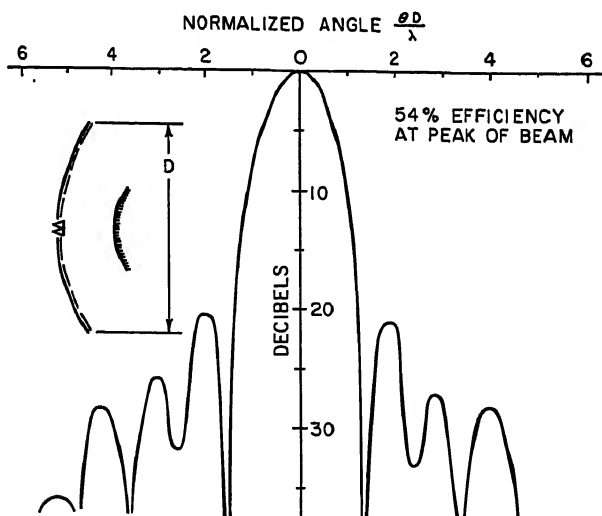
FIG. 25-12. Radiation pattern of a twisting Cassegrain.

designed to be invisible to vertical polarization.   Typically this grating is embedded in a dielectric radomelike structure which extends out to the edge of the main dish to form an ideal support for the subdish.

A radiation pattern for an antenna of this type is shown in Fig. 25-12.   The first side-lobe level of −21 db is consistent with a combination of the −12-db feed-pattern taper used in this case and the contribution from aperture blocking by the feed.   In

spite of a loss associated with the monopulse feeding system employed here, the antenna efficiency is 54 per cent. It is possible from this information alone to conclude that there is practically no loss involved in the polarization operations within this antenna, including even those regions toward the periphery of the aperture.

Several other forms are associated with the polarization-twisting Cassegrain system. One, shown in Fig. 25-13a, has a concave hyperboloidal subdish. This yields a virtual feed which is larger than the real feed. Another form, in Fig. 25-13b, has a flat main dish and a concave paraboloidal subdish. In this case the feed must be small if the axial dimension of the antenna is to be reasonably short. Since all of the focusing is accomplished by the paraboloid, the flat reflector may be tilted without destroying the collimation properties of the assembly. This gives rise to an interesting application[15] in which theoretically perfect wide-angle scanning is obtained by motion of a passive element in a compact system not having circular symmetry.
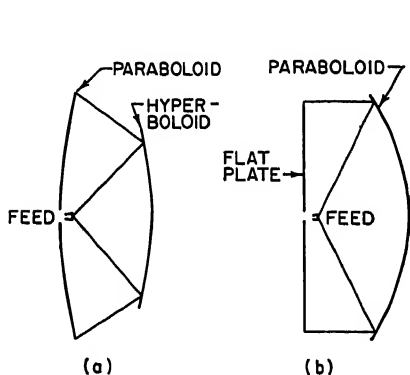
FIG. 25-13. Alternate Cassegrain forms.
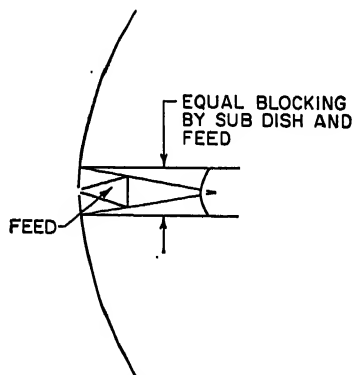
FIG. 25-14. Simple Cassegrain with minimum-blocking geometry.

Although the polarization-twisting technique is available for antennas which need only radiate one polarization, there are applications in the radar field, as well as in the communications and radioastronomy fields, which require polarization diversity. Under certain conditions, it is possible to achieve satisfactory performance in a simple Cassegrain system having ordinary reflecting surfaces that are not limited to any particular polarization. In Fig. 25-14, a system is shown in which the size of the subdish has been reduced by enlarging the feed and extending it forward until the shadows cast by the feed and subdish are equal; this yields the minimum possible amount of aperture blocking. When the geometry is optimized in this way, the proportion of the aperture which is blocked is approximately

$$\frac{\text{aperture-blocking area}}{\text{total aperture area}} = 2 \text{ (beamwidth in radians) } (F/D) \qquad (25\text{-}7)$$

where the beamwidth refers to the angle between half-power points of the antenna pattern and F/D is the focal-length to diameter ratio for the main dish. This result may be applied in the rule discussed under feed-blocking effects (Sec. 25.2) to obtain the approximate effect of this aperture blocking on side-lobe level. It is perhaps instructive to consider the example discussed in that section, a 10-in.-diameter aperture with a 2-sq.-in. feed-blocking area, and to determine the beamwidth of a simple Cassegrain antenna which, if optimized as described above, would have the same relative blocking area. For an F/D of 0.3, this beamwidth would be 2.4°. Consequently, in applications requiring beamwidths narrower than this, a simple Casse-

grain system can provide less relative aperture blocking than that indicated in the example.

A radiation pattern for a simple Cassegrain antenna is shown in Fig. 25-15. Although the feed in this example is appreciably smaller than the optimum size for minimum aperture blocking, the antenna has a beamwidth of 0.6°, which is narrow enough so that a reasonably small amount of blocking is obtained; in this case a relative area of 0.017. However, this blocking is by no means negligible; the first side-lobe level is −19 db, which is higher than that obtained with the previously mentioned twisting Cassegrain, even though the feed pattern is tapered somewhat further in the present case. In spite of the aperture blocking both by the subdish and by the metal struts used in this design to support the subdish, the antenna efficiency is 55 per cent. This compares favorably with the efficiencies of other practical antenna types and is indicative of the rather low-loss performance obtainable with a simple Cassegrain system when the subdish is relatively small.

NORMALIZED ANGLE $\frac{\theta D}{\lambda}$
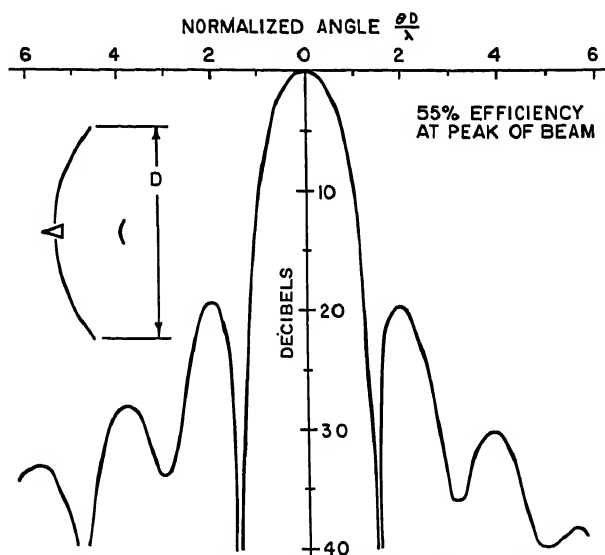
FIG. 25-15. Radiation pattern of a simple Cassegrain.

In concluding this section on Cassegrain antennas, it is perhaps worthwhile to indicate the beamwidth ranges that have been most used for the two types. For the twisting type, although there is no special restriction as to beamwidth, the 1° to 3° range appears to be most popular. With wider beams the applications have usually been such that more conventional types have sufficed, and with narrower beams the Cassegrain with simple reflecting surfaces usually gives sufficiently good performance. For the simple Cassegrain, the beamwidths range from about 2° down to the vicinity of 0.00001°, if in the latter case it is permissible to depart slightly from the field of radar antennas to include the capabilities of the 200-in. telescope on Mount Palomar.

25.3. FAN-BEAM ANTENNAS

The cross section of the main lobe of a fan-beam antenna is markedly elliptical in shape in contrast to the approximate circular cross section of the pencil-beam antenna. The "fan" action is produced by an aperture in which one of the principal dimensions exceeds the other. This ratio is commonly in the range of from 2 to about 5. A

fanned-beam antenna finds frequent application in an unstabilized shipboard radar where the broader vertical-plane pattern ensures against loss of target as the ship pitches and rolls. The vertical-plane half-power beamwidth of such a radiating structure is usually from 15 to 20°.

There are three types of fan-beam antennas: (1) the cut paraboloid, (2) the parabolic cylinder with horn feed, and (3) the parabolic cylinder with line feed.
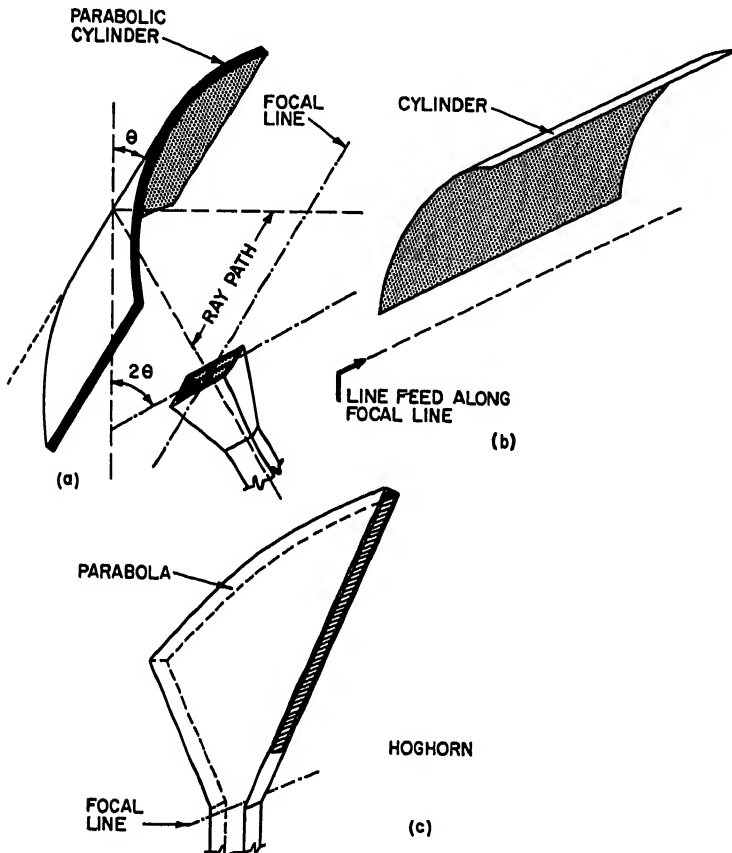
FIG. 25-16. Cylindrical reflectors.

Cut-paraboloidal Sections. In the cut-paraboloidal antenna, offset feeding is almost always used in order to reduce feed-blocking effects. The problems associated with the cut-paraboloid design involve chiefly the selection of the feed horn and the shaping of the reflector edge. If the principal dimensions of the cut reflector are d_1 and d_2 as in Fig. 25-9b, then the ratio of the feed-horn beam angles of the primary radiation patterns in the two principal planes should approximately equal d_1/d_2. Feed-horn flares should be gradual enough to avoid different phase centers for the illumination in the two planes, with the resultant defocusing in one plane or compromise partial focus in both planes.

Contouring of the reflector edge is often carried out on an equal-intensity basis.[16] Equal-intensity contours are calculated from a knowledge of the unobstructed primary feed pattern with inverse-square-distance attenuation taken into account. The

reflector edge is then cut along a particular contour with the 15-db line the usual choice. This produces a quasi-elliptical shape and helps the suppression of minor lobes by the introduction of the corresponding area taper. However, this equal-intensity contouring is more convenient than necessary since only equal spillover levels are maintained. The aperture illumination is not, in general, equal at the edge, nor is maximum efficiency or best gain/side-lobe ratio produced. As for any offset-fed paraboloid, the pattern can exhibit significant cross-polarized lobes even in the principal planes, since the symmetry which minimizes these in the case of the full paraboloid is lost.

The Parabolic Cylinder with Horn Feed. The parabolic cylinder with horn feed usually takes the form shown in Fig. 25-16a. Here the cylinder is tilted forward by an angle θ with the vertical and the feed horn placed on the focal line and inclined upward by an angle of 2θ so that the emergent rays are horizontal. Good results[17] have been produced by this technique with lobe levels in the plane of the parabola as low as 29 db over at least a 3 per cent frequency band. Since the geometrical arrangement to avoid feed obstruc-

FIG. 25-17. The 50-A marine navigational radar antenna. (*Courtesy of the Western Electric Company.*)
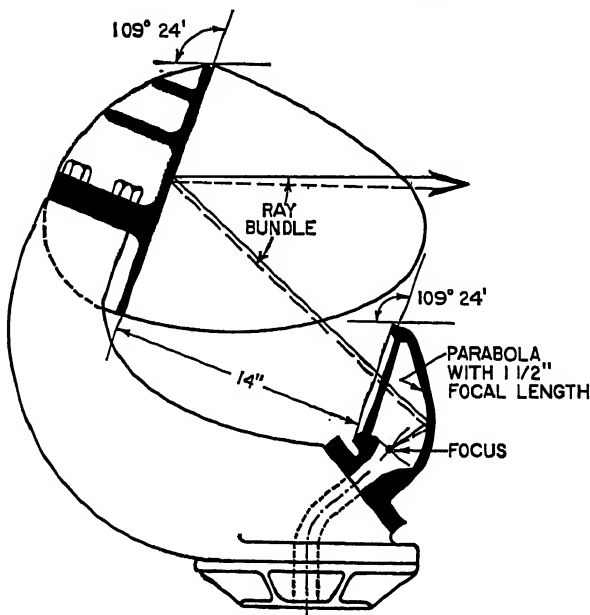
FIG. 25-18. Details of the 50-A antenna.

tion precludes coincidence of the feed plane and focal line of the parabolic cylinder, some, though not significant, defocusing occurs.

The Parabolic Cylinder with Line Feed. A very satisfactory method of producing a fan beam or, for that matter, any special beam shape employs a line feed exciting a cylindrical reflector. It is recognized that the parabolic curvature may be in the plane of the shorter dimension, as in Fig. 25-16b, or in the plane of the larger dimension, as in Fig. 25-16a. While the former arrangement is the more common, effective results have been produced by the use of a "hog-horn" type of line feed,[18] an enlarged view of which is given in Fig. 25-16c. Figures 25-17 and 25-18 show an example of a radar antenna employing an offset hog-horn feed. The reflector is curved in only one plane. Patterns are shown in Fig. 25-19.

Line Feeds. The line feed implied in Fig. 25-16b may take any of a number of forms, of which the pillbox and linear-array types are most common. The pillbox, or cheese,[19] in British parlance, is itself a parabolic cylinder contained between two parallel metal plates separated by a distance somewhat less than one wavelength. Various types are shown in Fig. 25-20. Of these, the single layer (Fig. 25-20a) is simplest, but it has the drawbacks that feed blocking and the effect on impedance of energy reflected directly back into the feed are apt to be troublesome. The effect of feed blocking is much more pronounced with cylindrical symmetry, as for a pillbox, than with circular symmetry, as for a paraboloid. As discussed in Sec. 25.2, twice the feed-to-aperture area ratio is added to the unblocked lobe level to determine the approximate lobe level with feed blocking. This procedure is still valid in the pillbox case, but here the area ratio is proportional to the linear-dimension ratio, since one dimension is common. Typically, feed blocking increases the lobes by 1 to 4 db for a pillbox with a larger dimension of 40 wavelengths with a conventional waveguide feed and with polarization parallel to the pillbox plates.

Fig. 25-19. 50-A antenna patterns.

The effects of energy reflected directly back into the feed can be combated by the various means discussed under center-fed paraboloids (Sec. 25.2), with the pattern penalty associated with the vertex-plate technique especially pronounced. The split-feed procedure (Fig. 25-20b) is simpler to implement than for the paraboloidal case and gives good results.

Both feed blocking and directly reflected energy can be largely avoided by the use of a double-layer,[20] or folded, pillbox. This type is illustrated in Fig. 25-20c. The angle

subtended by the reflector at the feed is typically something less (e.g., 160°) than the usual 180° value for the single-layer box. The fold itself has been made circular (Fig. 25-20d) or squared off (Fig. 25-20e), both with good impedance and pattern performance over at least 10 per cent frequency band. The folded-pillbox type is more difficult to manufacture and to hold tolerances on than the single-layer.

In Fig. 25-20a–c polarization parallel to the metal plates has been implied. Although in principle, either parallel or perpendicular polarization should function satisfactorily, experimental evidence is overwhelmingly in favor of parallel polarization. While parallel polarization imposes more stringent tolerances on plate spacing in that phase velocity is dependent on spacing, at the same time it permits spacers to be

(a) (b)

(c) (d)

(e)

SECTION A–A
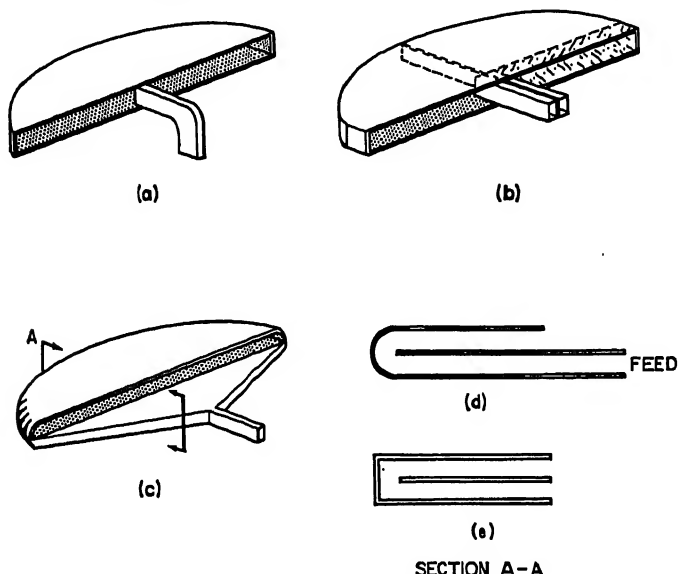
Fig. 25-20. Line feeds of the pillbox type.

used with little electrical difficulty. Also, in the single-layer case, feed-horn scattering is much more pronounced for perpendicular polarization.

25.4. SHAPED-BEAM ANTENNAS

This term describes the general antenna class in which the pattern in one or both of the principal planes exhibits other than a good side-lobe/gain compromise. By far the most common of these is the cosecant (also called cosecant-squared) type or closely related variants thereof.[21] The cosecant designation comes about since for an air-to-ground or ground-to-air radar, constant signal return for a given separation in altitude between the radar and the target requires that the field strength or gain in the vertical plane varies as the cosecant or cosecant squared, respectively, of the angle measured from the horizon. This criterion assumes that the radar cross section of the target is range-independent. This concept is made clear in Fig. 25-21a where it is also evident that the same cosecant requirement obtains for the beacon as well as the two-way radar case. When the range variation of radar cross section and the influence of the cathode-ray-tube presentation are introduced, slight modifiers are introduced to produce, for example, a $csc^2 \sqrt{cos}$ or $csc^2 \sqrt{cot}$ gain-variation specification. The pattern in the azimuth planes is almost always designed for good directivity.

Such special beam shapes can be produced by almost any antenna type, including lenses,[22] dielectric rods,[23] cylindrical-reflector, and doubly curved reflector classes, both with various feed arrangements. In addition, shaped-pattern production is possible in a two-dimensional array.

FIELD STRENGTH

h   R θ

RADAR

SIG. RET. α $\dfrac{G^2}{R^4}$

$R = h \csc\theta$
IF $G \alpha \csc^2\theta$ AND
h = CONSTANT, THEN
SIG. RET = CONSTANT

BEACON

SIG. RET α $\dfrac{G}{R^2}$

AS FOR RADAR, IF $G \alpha \csc^2\theta$
THEN SIG. RET. = CONSTANT

(a)

RELATIVE FIELD
STRENGTH
HIGH ALTITUDE
MEDIUM ALTITUDE
LOW ALTITUDE
θ

(b)

HIGH ANGLE
RADIATION

LOW ANGLE
RADIATION

−12 db

θ_1

PRIMARY
PATTERN

CONTOUR
TO BE
SPECIFIED

ψ_2

ADJUSTABLE
LIP

−15db

LINE
FEED

ψ_1

θ_2

GROUND PLANE

(c)
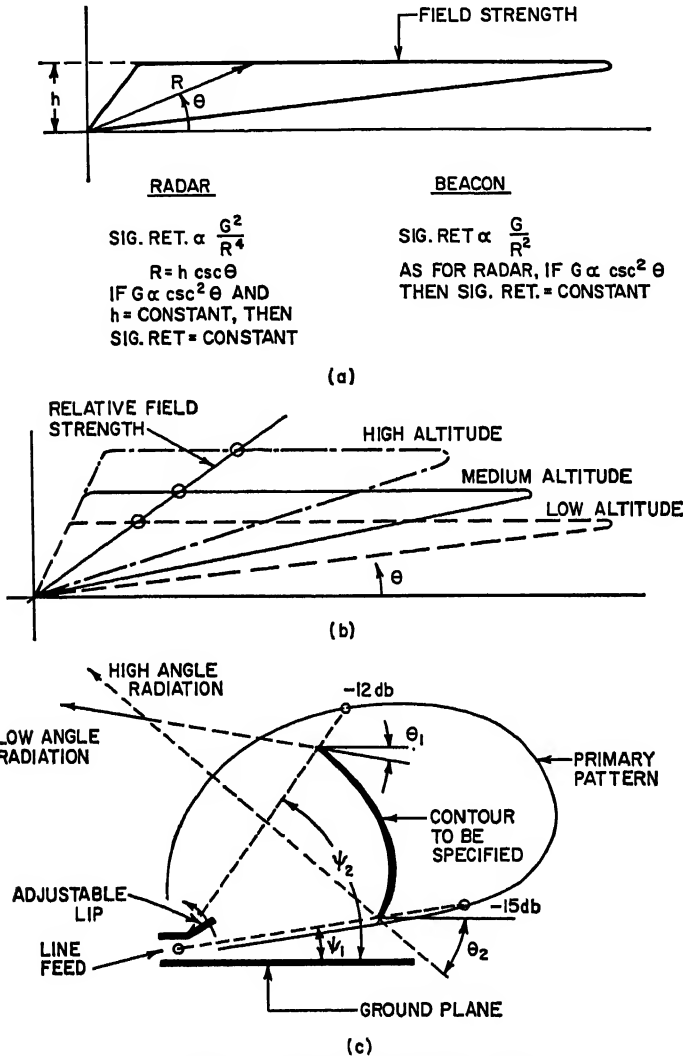
Fig. 25-21. Cosecant antenna geometries.

Historically, the first shaped beams were produced by rather direct modifications to full paraboloidal reflectors.[24] One of these techniques involved multiple feeds, while in another, either (1) part of the paraboloidal contour in the plane of the shaped beam was modified or (2) a "spoiler" was placed along part of the parabolic surface to achieve the desired beam shaping.

To take up the latter case first, Fig. 25-22 shows an interesting application of the spoiler. Here the spoiler takes the form of a grating. For polarization parallel to the grating elements, the grating is opaque and a cosecant-pattern shape is achieved as shown in Fig. 25-23. For the orthogonal polarization, the spoiler is transparent and a pencil-beam pattern results. Polarization rotation is effected by a Faraday rotator in which a magnetic field is applied to a ferrite pencil.

Multiple feeds for paraboloidal reflectors take advantage of the beam tilt produced by lateral shift of feed position away from the focal point to fill in particular angular regions as required by the beam shape desired. A judicious combination of horns fed from a common waveguide is quite effective.

The "barrel" reflector replaces one-half of the normal paraboloid by a figure of revolution produced by rotating the generating parabola about a line through the focal point. The "shovel" reflector replaces the lower third or so of a paraboloid with a parabolic cylinder.

The design procedures involved in all these early techniques were largely empirical. This family has been generally replaced by the optically designed cylinders or doubly curved surfaces.

FIG. 25-22. An antenna whose vertical-plane pattern may be converted to cosecant shape by electrical control. (*Courtesy of the Bendix Aviation Corporation, Eclipse Pioneer Division.*)

The largest number of shaped-beam antennas in use today utilize either the cylindrical reflector with the line feed or the doubly curved reflector with the point or quasi-
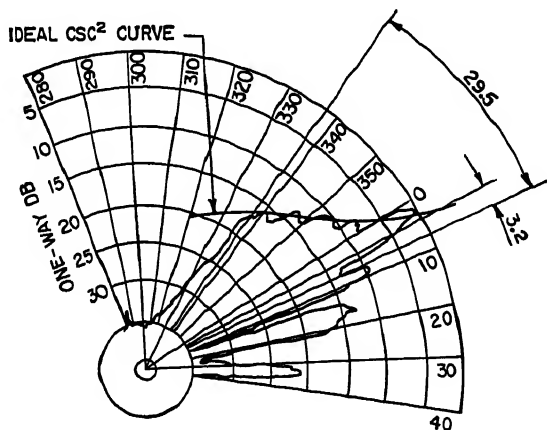
FIG. 25-23. The cosecant vertical-plane pattern of the antenna in Fig. 25-22.

point feed. Lenses are seldom used, for the reasons discussed in Sec. 25.2. The advantage of the cylindrical reflector with line feed includes its relative freedom from cross-polarized response and minimum dependence of azimuth lobes and beam angle on the elevation angle. Its disadvantages are chiefly that the usual line feed makes

it a heavier structure than the doubly curved reflector with its point feed and that it is less amenable to adjustment of the altitude setting of the shaped-beam vertical-plane pattern.

The matter of the "altitude" of a cosecant antenna warrants mention. Clearly, the return from a target at any fixed altitude will be as nearly constant as the adherence of the antenna pattern to the prescribed function dictates. However, as higher and higher altitudes are considered, the nearly constant target return will become too weak to be usable. At this point, it is advantageous to vary the pattern shape to permit useful target returns from higher-altitude targets. Thus Fig. 25-21b shows idealized-cosecant patterns for different altitude settings. Note that the peak gain for each pattern diminishes and the initial angle above the horizon increases as the adjustment is set for a higher altitude. However, for any angle within the common controlled region, the antenna gain is higher for the higher-altitude pattern. While not rigorously correct, it turns out that the areas of the polar plots of field strength (volts per centimeter) are approximately constant for the cases where the azimuth patterns retain their relative shapes as the altitude is varied.

Cylindrical Reflector with Line Feed. The design of the cylindrical reflector for a particular pattern shape follows a procedure developed by Chu.[21,35] In this, the pattern of the line feed in the plane of the curve of the reflector is first determined, usually experimentally, over the full range of adjustment, which often takes the form of a lip over a ground plane as shown in Fig. 25-21c. The illumination intensities at the reflector edges are selected rather arbitrarily, with experience indicating that a value between −12 and −15 db is a reasonable choice. In Fig. 25-21c the lower and upper reflector edges provide the high-angle and low-angle radiation, respectively. These roles could be interchanged, in which case a reversal in curvature would be required, but the situation shown is the normal arrangement and makes for minimum interference between the feed and the outgoing radiation.

The particular pattern of the feed selected within its range of adjustment is tabulated in power density as $I(\phi)$. Details of the computation are then carried out as outlined in Chap. 12 (Sec. 12.5). $P(\theta)$, the required shape of the far-field pattern, is expressed as $P(\theta) = \csc^2 \theta$ for the simple cosecant case.

One typical antenna which has been designed by this method is the APS-23 radar antenna. This particular antenna provides for an adjustable elevation pattern by providing an adjustable lip on the line feed. Typical elevation patterns obtained are shown in Fig. 25-24.

Double Curved Reflector with Point Feed.[26] The production of a shaped beam by this feed-reflector arrangement is also discussed in Sec. 12.5.
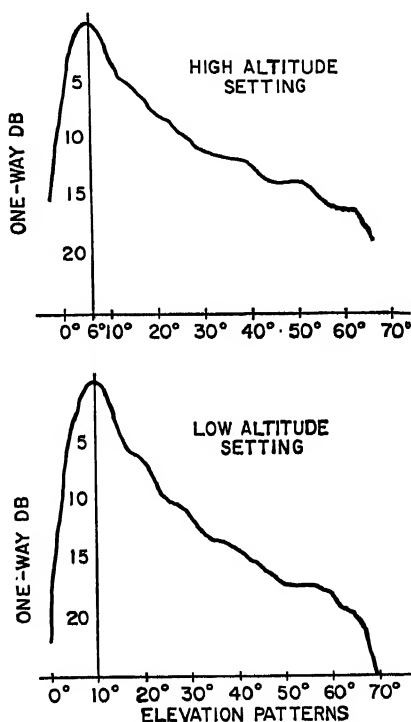
FIG. 25-24. The vertical-plane patterns of the AN/APS-23 antenna.

Figure 25-25 depicts a doubly curved radar antenna with a point feed, and Fig. 25-26 shows representative patterns associated therewith.

Practical Considerations in Shaped-beam Reflector Design. The procedures discussed above and in Sec. 12.5 ignore diffraction and are ray-optical methods producing only a contour to which any proportionality constant may be applied. The far-field pattern may be markedly dependent on the proportionality constant. It can be computed to include most diffraction effects by taking the optically calculated reflector contour together with the known field on the reflector as determined by the feed characteristics.[27] However, this procedure is tedious, and it is not completely satisfactory in that edge diffraction and the effect of mechanical errors are difficult to
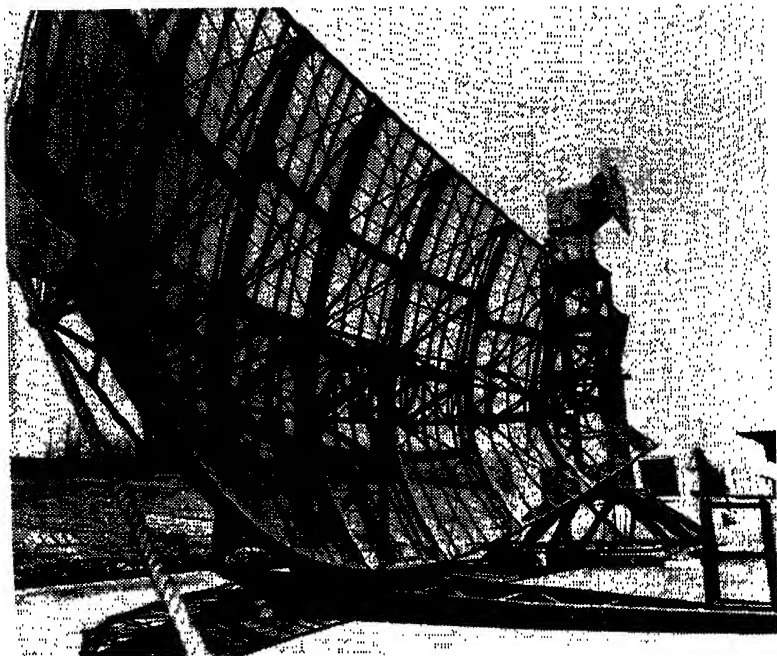
Fɪɢ. 25-25. A doubly curved reflector producing a cosecant beam shape in the vertical plane. (*Courtesy of the General Electric Company*)

include in the computation process. It often turns out that some judicious pre-recognition of diffraction effects can make for a satisfactory pattern.

In general, to exactly obtain a prescribed pattern requires an infinite aperture. Thus, with the usual finite dimensions at the designer's disposal, an "adjusted" design shape can be guessed at which, with diffraction, may be hoped to produce a satisfactory approximation of the desired design shape. This is illustrated in Fig. 25-27, where the desired pattern is of cosecant form between the limits of 10 and 60°. For an aperture of about 10 wavelengths, experience has shown that if the design proceeds on the basis of an "adjusted" requirement of from 6 to 70°, then the actual pattern will usually approximate the desired pattern to acceptably close limits within the required 10 to 60° range. Had the aperture available been larger in size or the desired pattern less sharp, as, for example, a cosecant shape beginning at 15° rather than 10°, then the adjusted requirement could be closer to the actually desired pattern.

In the matter of specifications to impose on a shaped-beam antenna, there is little use in requiring adherence to, say, a cosecant curve when, for example, the entire
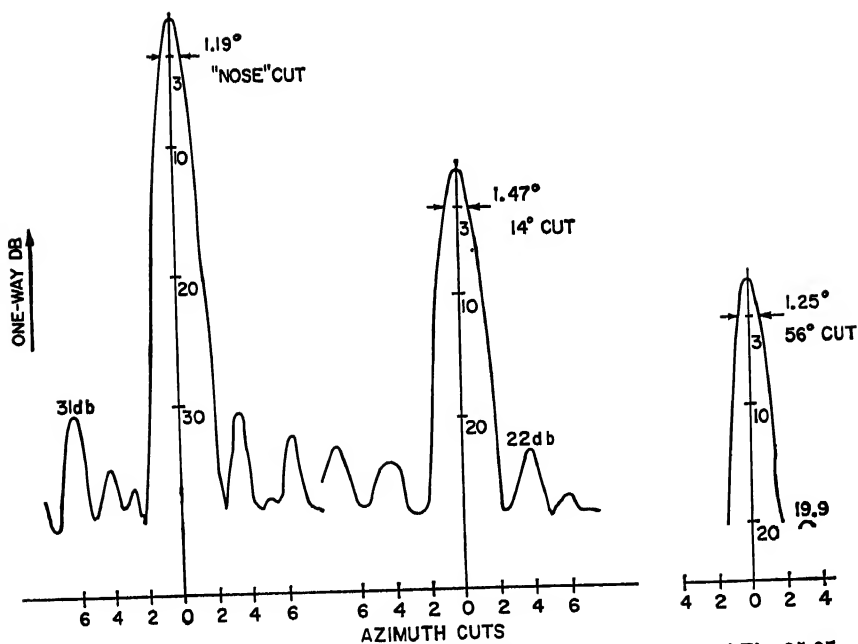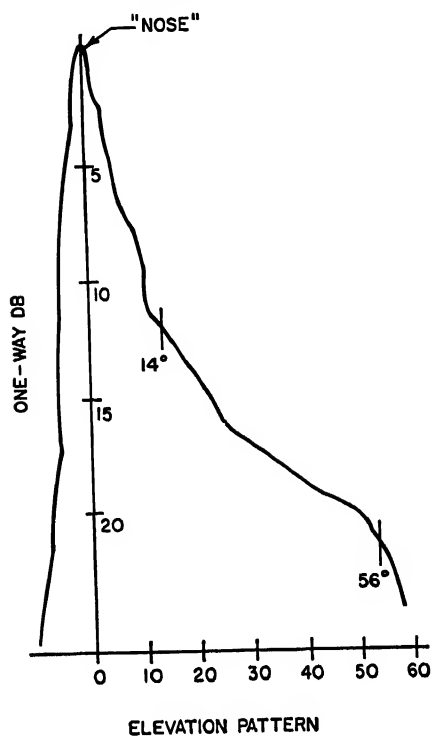
FIG. 25-26. The vertical- and horizontal-plane patterns of the antenna of Fig. 25-25.

reflector, even if parabolic in shape, is not large enough to produce a beam as sharp as that of the cosecant curve at small angles. It is preferable to use the performance of carefully made antenna as a criterion by which subsequent units can be judged.

For the doubly curved reflector, a considerable range of altitude control is possible by appropriate positioning of the feed. This desirable feature is not illustrated in the patterns shown (Fig. 25-26). It may be regarded as offsetting, in many applications, the disadvantage of the slight thickening of the azimuth beamwidth and the tendency for growth of the relative minor-lobe levels as the elevation angle increases. As for the general class of doubly curved reflectors, inevitable, but usually tolerable, cross-polarized lobes with minima on the axis of the main beam of the desired polarization are present, increasing in relative size as the elevation angle increases.

Shaped-beam Arrays. There are several published synthesis techniques[28] that permit the specification of the phase and amplitude of array elements necessary for the production of any special beam shape
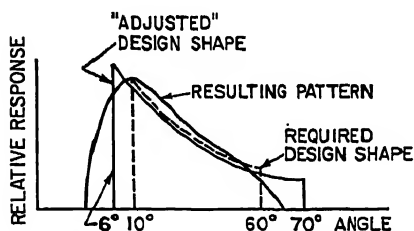
FIG. 25-27. The "adjusting" procedure in cosecant antenna design.
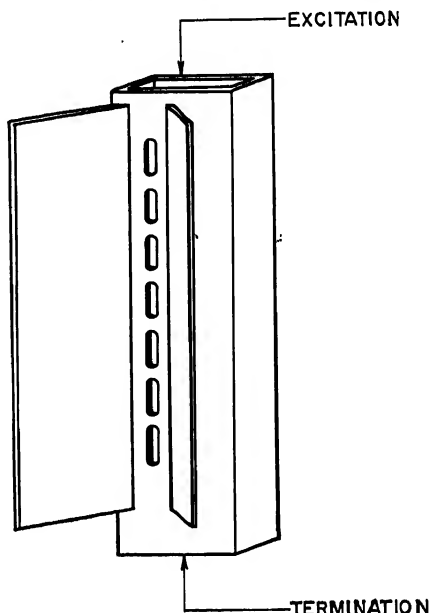
FIG. 25-28. The exponential array in the broad face of a TE_{10} waveguide.

(also see Chap. 2). In addition, it is implied in the literature,[29] though not specifically pointed out, that a linear array, with appropriate exponential amplitude taper and constant phase progression, produces quite an acceptable cosecant approximation when the elements of the array are half-wave, or near half-wave, elements, disposed so that the long dimension lies in the plane of the desired cosecant pattern. Such an arrangement is shown in Fig. 25-28.

For the array structure, in contrast with the situation existing for the reflector antenna, a physical-optical approach is the direct approach and the designer can accurately and simply predict the shape of the final pattern.

A variant of the array is the continuous slot,[30] which is also effective in producing acceptable cosecant approximations. Often special waveguide geometries are required to adequately couple the guided energy to space.

The shaped-beam array does not normally supply the usually necessary directivity in planes perpendicular to the plane of the shaped beam. Aperture size in the required dimension must be obtained either by building up a two-dimensional array by an assemblage of properly phased and excited shaped-beam array units or by utilizing the array to illuminate a parabolic cylinder.[31] This latter technique usually diminishes the angular range over which beam shaping is effective, compared with the array alone.

25.5. LOBING ANTENNAS

In this category are placed the general class of antennas which improve the directivity above that given by usual criteria by variants of the principle illustrated in Fig. 25-29.   In a given plane, two beams are produced, each with equal but opposite displacement from the normal direction (usually along a line of mechanical symmetry). Some process is invoked to mark the equality of the return signals from the two beams;
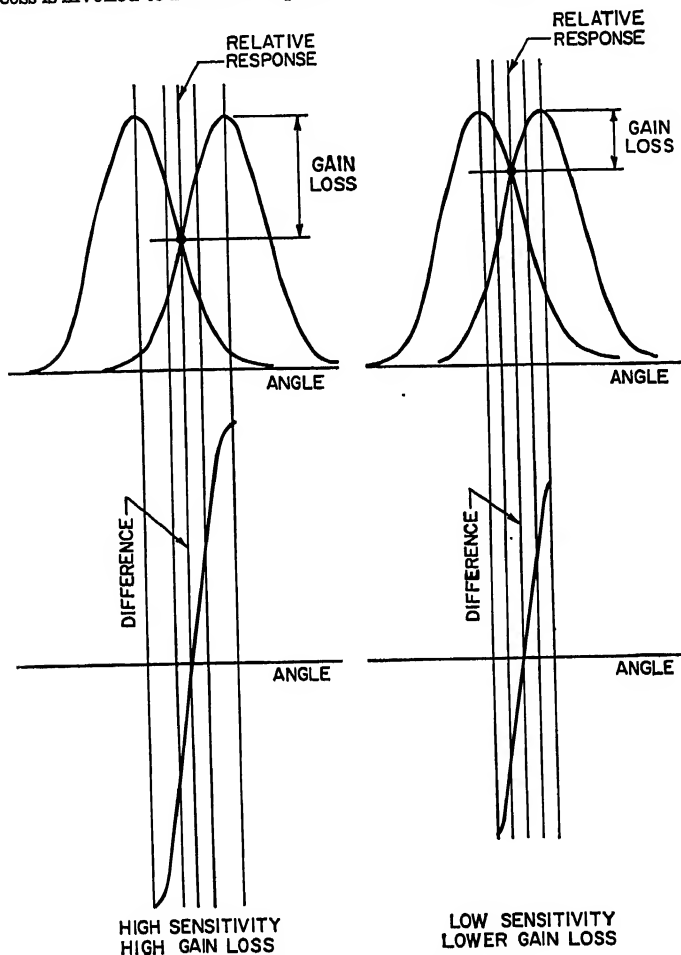
FIG. 25-29. Lobe-switching principle.

or equivalently, the difference between the amplitude of the return signals is made to vanish.   Thus it is possible to make a very accurate determination of the angular coordinates of a target.   The sensitivity of a lobing system increases with the separation between the two beams, as is made clear by the change in slope shown in Fig. 25-29. However, the gain of the system is correspondingly reduced.   The usual compromise places the crossover 1 to 3 db below the peak of either lobe.

It is important to clarify the concept here: *angular resolution* (i.e., the ability to distinguish between two or more targets at the same range) *is not improved.*   Radar

systems employing this technique normally expect a single target as a surface vessel or aircraft. If several targets are actually in the field of view (within a normal beam angle), then these lobing antennas can do no more than indicate the angular position of the instantaneous radar center of gravity.

Mattress Arrays with Split Phasing. These are of interest chiefly for the place they take in the evolution culminating in the modern conical-scan, or monopulse antenna. The SCR-268, the first fire-control radar[12] in the United States, had its elevation and azimuth receiving antenna each divided into two sections. The azimuth antenna arrangement is shown in Fig. 25-30. Two receivers are alternately energized in synchronism with the transmitted pulse so that the receiving beams are alternately skewed to one side or the other of the normal to the array. Equality of signal return is determined by means of oscilloscopes with displaced sweeps. The elevation receiving system utilizes the same principle.

This sort of arrangement is most conveniently exploited with an elevation receiving antenna, an azimuth receiving antenna, and a separate transmitting antenna. The space and volume extravagance thus implied can seldom be tolerated in a modern
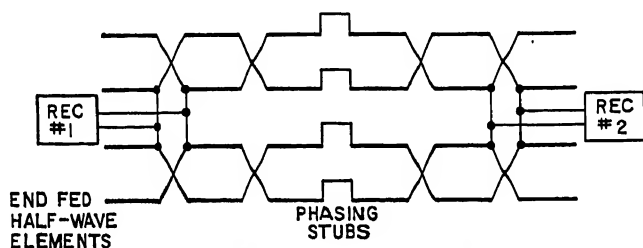
FIG. 25-30. Diagrammatic representation of the SCR-268 azimuth antenna array.

radar. If, however, angular coordinates in a single plane, usually azimuth, are sufficient, then a common transmitting-receiving antenna can be implemented with a mattress array,[33] using either a mechanical or electronic switch to properly phase the antenna feed lines to accomplish the desired lobe switching.

Conical Scanning. The conical-scanning principle[34,35] makes possible the collapse of a complex lobing-antenna system of the SCR-268 type into one antenna which combines the function of transmission and reception and also provides complete angular-coordinate information. This is accomplished by a feed system whose electrical center rotates in a small circle concentric with the focus of a lens or reflector. The antenna beam consequently lies along the surface of a cone whose apex coincides with the center of the aperture and whose included angle increases with the diameter of the feed circle. The energy return from a target situated along the mechanical axis of such a system is independent of the feed position. An off-axis target returns a signal modulated by the feed rotation. The amplitude and phase of this modulation (with respect to some reference as produced by a generator connected to the shaft of the motor driving the feed) define the angular location in space.

The per cent modulation[36] of the return signal voltage is given by

$$M = \frac{4.8\epsilon\Phi}{\beta^2 - 1.2\epsilon^2 - 1.2\Phi^2} \times 100 \qquad (25\text{-}8)$$

where ϵ is the pointing error measured from the scan axis, Φ is the scan angle between the beam axis and the scan axis, and β is the 3-db beamwidth. Equation (25-8) gives good accuracy up to $\epsilon = \Phi$. As for any lobing system, Φ typically lies between 0.2β and 0.5β.

Feeds for conically scanned antennas are usually described as either *nutating* or *rotating*. A feed nutates (or nods) if there is some mechanical asymmetry. Figure 25-31 illustrates a feed of this type in which the feed passes through the center of the drive-motor armature.

Mechanical asymmetry is not necessary to provide an off-axis phase center. In a dipole feed excited from a coaxial line, the unbalance-to-balance skirt can be made only partially effective to permit some current to flow on the outside of the coaxial line, this arrangement produces an off-axis phase center,[34] and the structure is rotated to produce a conical scan.
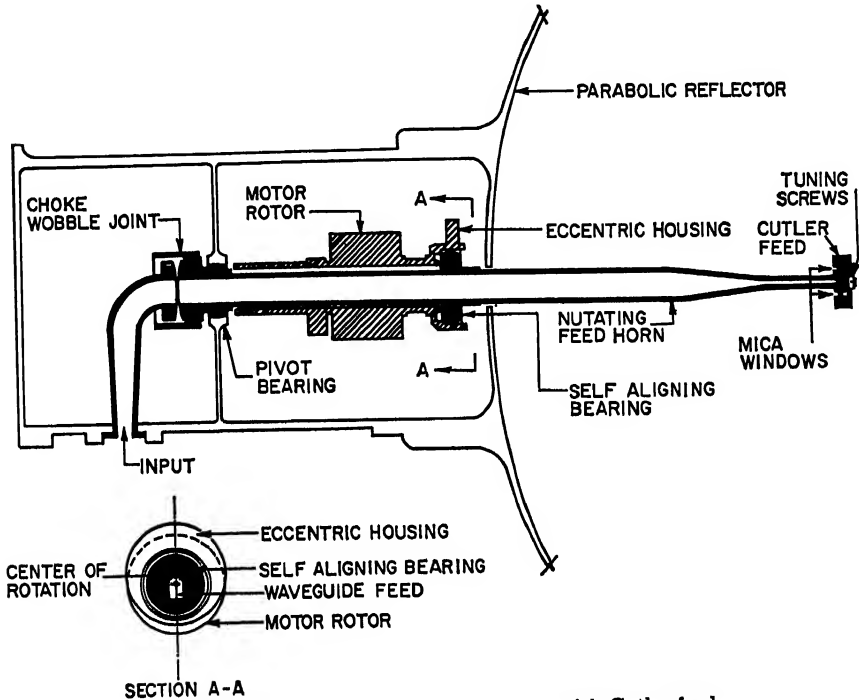
Fɪɢ. 25-31. Nutating conical-scan antenna with Cutler feed.

It is usually preferable that the antenna system retain the same polarization independent of the scanning function as in the case for the nutating feed of Fig. 25-31. A fixed polarization direction avoids unwanted polarization-dependent modulation effects. Conical scan with constant polarization direction can also be achieved by "wobbling" the reflector about a fixed feed. This process is particularly appropriate for small reflectors.

Monopulse System.[37] In the lobing devices so far described, a number of radar pulses are required to define the angular position of the target. In the simple beam switching system, at least two sequential pulses are necessary for either bearing or elevation information, while the conically scanned radar demands one complete, or nearly complete, revolution of the scanning system before angular coordinates may be specified. Consequently, in both the conical-scan and lobing systems, inevitable pulse-to-pulse variations (glinting) in the target return produce an undesirable modulation. Thus the tracking accuracy is affected, particularly in an automatic system

in which target-return variation is equivalent to the introduction of noise in the follow-up system.

It is possible to extract all the necessary information from a single target return and thus avoid glinting effects. Systems so arranged are appropriately designated "monopulse." Actually, it is the waveguide and feed arrangement rather than the antenna that distinguish the monopulse system. The monopulse principle is illus-
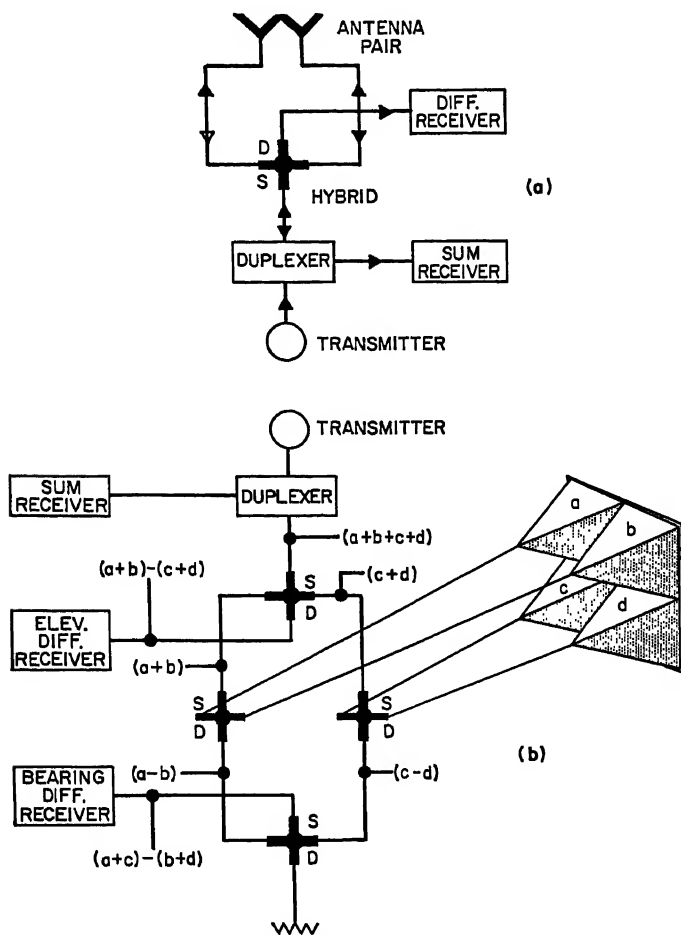
Fig. 25-32. Monopulse principle.

trated in Fig. 25-32a for the two-dimensional case. The hybrids, transmitter, sum receiver, and difference receiver are so connected that the transmitted energy excites the antenna pair in phase and the transmitted beam is broadside to the antenna pair. The system is directed to null the output of the difference receiver, at which orientation the target lies along the normal to the antenna pair. The sum receiver is available for the normal radar display system.

If the two antennas shown in Fig. 25-32a are symmetrically disposed about the focal point of a parabolic reflector or a lens, then the arrangement is categorized as an "amplitude" monopulse system. If the antenna pair radiate and receive directly,

"phase" monopulse is implied. In the amplitude system the amplitude of the excitation of the two feeds by a return signal will be equal only for an on-axis target. In the phase system, the signal return into the two antennas is always equal but there will be phase equality only for an on-axis signal.

Either monopulse system can be extended to solve the three-dimensional problem by a more complicated feed arrangement, an example of which is outlined schematically in Fig. 25-32b. The sum-and-difference arms of the hybrid are designated S and D. Again, the sketch describes either the amplitude or phase monopulse systems, with the distinction only whether the antennas A, B, C, and D excite a reflector or lens (amplitude monopulse) or radiate directly.

The radiating structures shown in Fig. 25-32, while commonly used as feeds for a reflector or lens, are not compatible with good (high gain/low side lobe) sum-and-difference patterns from the antenna systems. The reason for this incompatibility becomes apparent from a consideration of Fig. 25-33, which shows two-dimensional illuminations of a rectangular aperture corresponding to a small and to a large feed-horn pair.[38] The illumination of Fig. 25-33a produces a system sum pattern with an
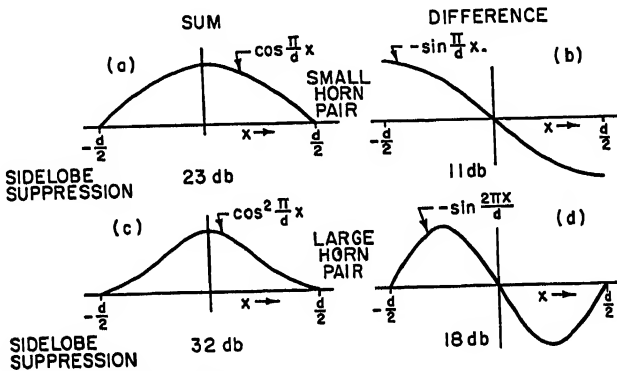
Fig. 25-33. Sum-and-difference illuminations.

acceptable side-lobe level but the corresponding difference pattern (with illumination as in Fig. 25-33b) exhibits side lobes only 11 db below the main lobe. In practice, the gain loss will be high, not only because of the inefficient illumination, but also because of the high spillover implied by the large edge energy. Similarly, the difference system pattern associated with the double-looped illumination of Fig. 25-33d produces a system pattern with a satisfactory level of side-lobe suppression. However, the gain loss of the corresponding sum pattern (with illumination as in Fig. 25-33c) would generally be regarded as excessive. Although the sum-difference correspondence indicated is simplified for the purposes of illustration, the effect is qualitatively as described: (1) a simple feed design for a good sum pattern is, in antiphase excitation, too small to yield a good difference pattern, and (2) a simple feed design for good difference pattern is too large, in in-phase excitation, to yield a good sum pattern.

It follows that essentially independent control of aperture illumination is required for efficient operation in sum-and-difference modes. Such independence can be approached in various ways, perhaps the simplest of which is illustrated in Fig. 25-34, which shows a feed structure to be used for lens or reflector illumination. In the sum mode, only the center four-horn cluster *abcd* is used. However, in the difference mode an illumination approximating a double-looped characteristic (Fig. 25-33d) has been demonstrated to be desirable. Thus a larger feed-horn aperture will be required. Appropriately, the two four-horn clusters *acgh* and *bdef* are operated in phase opposi-

tion for the bearing-difference mode. For the elevation-difference mode, the two four-horn clusters *abjk* and *cdlm* are similarly treated.

This twelve-horn cluster, in itself more complex than the simple four-horn feed, requires a more complicated hybrid structure. However, this complexity can produce a 2–3-db improvement in difference gain and a 3–8-db improvement in difference minor-lobe suppression compared to a four-horn feed with dimensions selected to be optimum for sum operation.
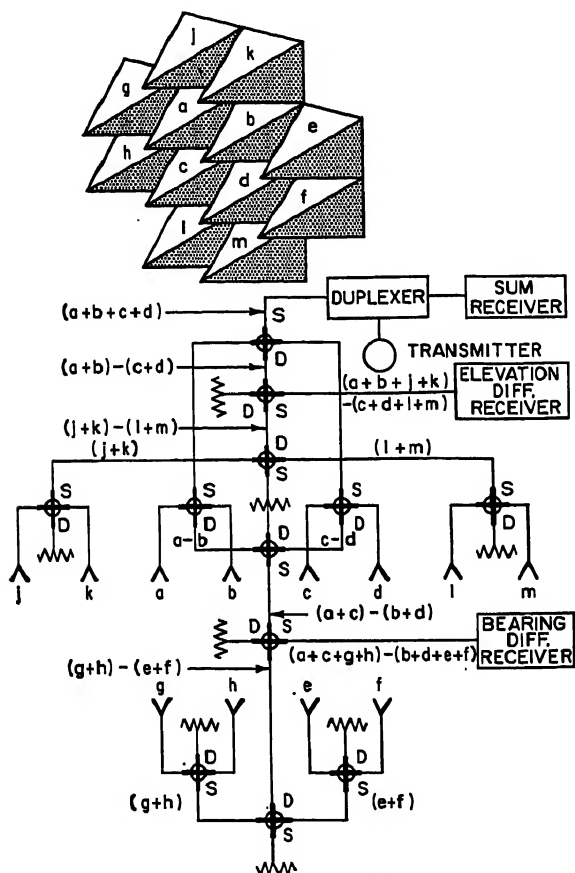
Fig. 25-34. Twelve-horn monopulse cluster and associated hybrid arrangement.

For an array used in a phase-monopulse system, the independent control of sum-and-difference illumination is as necessary for optimum sum-and-difference patterns as in the amplitude-monopulse system just described. Such independence can be achieved but at the cost of a complexity which increases rapidly with the number of array elements.

25.6. FEED-HORN DESIGN PROBLEMS

The usual feed for a reflector or lens antenna is a waveguide exciting a sectoral or pyramidal horn or perhaps simply open-ended. However, for reflector antennas, "rear" feeds find some application. In these, the waveguide enters through the

vertex of the reflector and the radiation is variously directed back toward the reflector by such methods as an arrangement of slots or by the use of a "splash" plate.

Open-ended Waveguides. The simple open-ended rectangular waveguide is not particularly well adapted for use as a paraboloid feed for the reason that the radiation patterns in the two planes (E and H) differ significantly in directivity. For the usual rectangular waveguide dimensions, in the E plane the included angle between the 10-db levels is about 180°. This angle in the H plane is approximately 120°. For a paraboloid diameter/focal-length ratio of 2.5 (a common value), the total included feed angle is 128°, which satisfactorily approximates the H-plane included angle but not the E-plane angle. This does not mean that the simple open-ended rectangular waveguide is useless. As a matter of fact, in a fan-beam antenna, and in a pillbox in particular, the reflector proportions may be such as to make this feed type ideally suited.

The obvious, and in fact effective, means of improving this situation for a paraboloid is to utilize a sectoral horn for which the dimension in the E plane is increased by means of a gradual flare to make the E- and H-plane directivities equal at about the 10-db points. For this situation the H-plane dimension is still greater (by a factor of about 1.4) than the E-plane dimension since there is sinusoidal taper in the H plane. Feed blocking is consequently a little different in the two planes, and the radiation patterns of the reflector system in these places may be expected to differ. Near identity of the patterns in the E and H planes can be approached by lining two

FIG. 25-35. Special feed-horn types: the box horn and the dielectric-lined horn.

walls of the horn with dielectric, as shown in Fig. 25-35. This stratagem can nearly eliminate the H-plane sinusoidal taper and thus make it possible for a square horn to provide almost identical feed patterns.

The radiation pattern of an open-ended circular waveguide[39] operating in the dominant TE_{11} mode is actually better adapted for a feed-horn application than a corresponding rectangular waveguide, since the patterns in the principal planes are more nearly equal. To produce the required directivity for paraboloidal excitation, it is necessary to increase the circular-waveguide diameter to about 0.8λ, which dimension is large enough to support the unwanted TM_{01} mode. Particular care must be taken to escape inadvertent excitation of this higher mode or conversion to an elliptical TE_{11} form. These considerations dictate close mechanical tolerances and gradual tapers. Then, too, long runs of circular waveguides are best avoided through use of rectangular-to-circular transitions.

The Ring-focus Feed. A particularly useful feed-reflector arrangement is that of the ring-focus paraboloid[40] and splash-plate feed combination as given in Fig. 25-36. A rear feed consisting of an open-ended circular waveguide with a reflecting plate has been found to produce a phase center lying along a circle (ring). As a consequence, the simple paraboloid is unsatisfactory for the main reflector and must be replaced by a figure of revolution generated by revolving the parabola given below about the x axis.

$$(y - a)^2 = 4fx \qquad (25\text{-}9)$$

In Eq. (25-9), a is the radius of the circle on which the feed lies. The surface occupying the "hole" in the center of this surface is satisfactorily a plane. The gain of this antenna system is probably better than any other rear feed system. The secondary-lobe discrimination is not quite as good as a conventional system by reason of the hole in the center of the surface.

Cutler Feed.[2] The double-slot, or Cutler (after C. C. Cutler), feed is useful when a compact rear feed is required to operate with acceptable impedance characteristics (VSWR < 1.3) over a 6 per cent frequency band. This is shown in Fig. 25-31. Despite the tapered waveguide, the directivity in the electric plane is a little greater than in the magnetic plane. This feed is not suited to high-power radar application in view of the constricted waveguide and narrow slot widths.
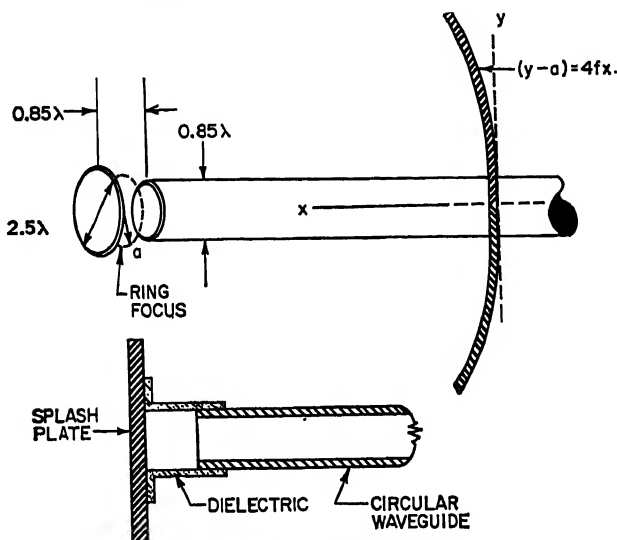
Fig. 25-36. Ring-focus antenna.

The Feed Seal. The antenna feed system is particularly vulnerable to voltage breakdown since (1) the geometry is often complex and (2) the waveguide pressure system usually ends at the feed. For the air-borne application, this latter situation means that the pressures external to the dielectric seal at the feed will be those existing at an altitude of many thousands of feet. Large sealing structures are required in a high-powered radar to ensure that the field strengths in the low-pressure regions are below the breakdown values. Careful design is necessary to avoid adversely affecting (1) the impedance match to the transmission line and (2) the primary feed pattern. Figure 25-37 shows an arrangement successfully used as a feed horn and seal in an X-band pillbox line feed. A word of caution is appropriate regarding testing for breakdown at any altitude. Such tests are virtually meaningless without the inclusion of a radioactive source, such as Cobalt 60 (5 to 15 millicuries), to remove the uncertainty of breakdown as critical values are reached.

Feed Flanges. Some success has been had from the addition of flanges to feed horns to produce special primary-pattern shaping.[41] The currents flowing on the flange surfaces add their contribution to that of the radiating orifice. Since the flanges are necessarily separated by, and are usually as large as or larger than the orifice, the introduction of considerable ripple on the primary pattern is the characteristic effect of flanges. An arrangement in which proportioning is correct to insert a

pronounced dip in the center of the primary pattern is useful in reducing direct reflections back into the feed of a center-fed antenna system.   The minor-lobe enhancement associated with a shadow at the aperture center is not escaped.

The Box Horn.   Another method of approaching a uniform feed-horn aperture in the H plane utilizes the "box horn."[42]   The box horn has its H-plane dimension large enough to support the TE_{30} mode.   The properly phased addition of the TE_{10} and TE_{30} modes combines to produce nearly uniform field intensity along the H-plane dimension. TE_{30} excitation is effected by the abrupt discontinuity shown in Fig.
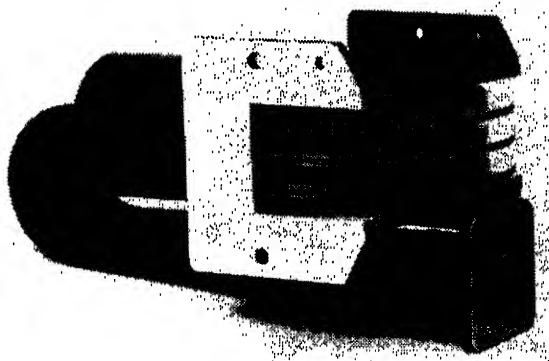
Fig. 25-37. An X-band high-power high-altitude broadband antenna feed seal.

25-35, in which the symmetry avoids even-order modes.   The box horn is somewhat more narrow band in accomplishing a given pattern than the dielectric-lined feed horn.

25.7. LINE SOURCES

A cylindrical reflector requires a line source (line feed) to furnish the beam control in its plane dimension.   By far the most common of the line sources is the pillbox mentioned in Sec. 25.3.   In addition, linear arrays find occasional application and usually represent a volume savings over the pillbox antenna.   However, except for special applications, the pillbox is generally to be preferred for its simpler structure (often even lighter weight).

Pillboxes.   This antenna type is illustrated in Fig. 25-20.   It can be either single-layer or double-layer[20] (folded).   Excitation in either of the two structures can be in the TE_{10} mode, with the electric vector parallel to the pillbox plates (parallel polarization), or in a TEM mode, with electric vector perpendicular to the plates (perpendicular polarization).

Perpendicular polarization has the following advantages over parallel polarization.   It permits attainment of a lower minor-lobe level, and mechanical tolerances are less stringent.   However, its gain will be lower than that of a parallel-polarized pillbox, and spacers, often necessary for maintenance of structural integrity, are likely to be more troublesome.   This last objection is not insuperable for the reasons that (1) metal honeycomb construction can often supply the necessary rigidity without spacers, and (2) as will be seen, resonant spacers can be designed to avoid most electrical difficulties.   In addition, for the perpendicularly polarized pillbox, cracks or gaps between various surfaces, as between the feed and the pillbox, are likely to interrupt lines of current flow, and consequently to radiate.   For the parallel polarization, such gaps are usually not a matter for concern.

The superior minor-lobe discrimination of the perpendicularly polarized pillbox arises from the ease with which the aperture illumination can be sharply tapered and the difficulty, or near impossibility, of such tapers in the parallel-polarization case. In the former, the electric intensity must vanish at the conducting walls of the aperture edge. No such constraint exists for the orthogonal polarization, and a minor-lobe discrimination beyond 20 db is rare.

Metal spacers, when necessary, are troublesome for both pillbox types, though certainly more so for the perpendicular polarization, which aligns the electric vector along the spacer. While a spacer whose diameter is small compared to a wavelength ($<\lambda/8$) is substantially invisible in the parallel-polarized pillbox, such a diameter is often mechanically inadequate especially at X-band and higher frequencies. For this situation and for about any frequency for the perpendicular pillbox, *resonant* spacers are used. Examples are shown in Fig. 25-38. Design proceeds along empirical lines.
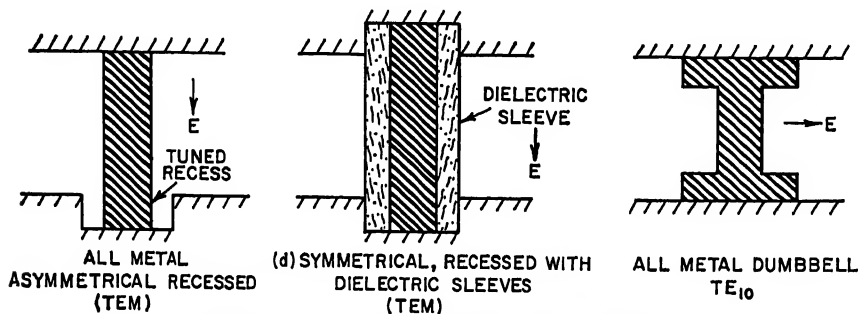
FIG. 25-38. Resonant pillbox posts. (*Reference 20*.)

A particularly significant difference between parallel and perpendicular polarization comes to light in an examination of the relative gains of the two pillbox types. However, for the perpendicularly polarized pillbox, there is some mechanism, possibly feed scattering, producing a gain reduction of about 1 db after all accountable adjustments for spillover, amplitude taper, etc., are made. No such reduction obtains for the parallel-polarized pillbox.

It has already been mentioned that the single-layer pillbox design which places the feed in the radiation path gives rise to difficult impedance-match and feed-shadow problems. Both of these can be overcome by a double-layer pillbox. However, such a pillbox introduces its own set of problems. The septum spacing (a in Fig. 25-39) must be chosen to prevent propagation of unwanted modes inevitably excited in the bend. The criterion means that in the TE_{10} pillbox, $a < \lambda$. In the TEM box, $a < \lambda/2$. The effect of septum thickness, plate spacing, and separation from the parabolic bend is evident principally in the input-impedance characteristic. Rotman[20] reports a relationship as given in Fig. 25-39 for the double-layer TEM pillbox.

Linear Arrays. Perhaps the best-known linear array functioning as a line feed is found in the World War II Eagle antenna[43] of the AN/APQ-7 radar. This X-band antenna consists of an array of 250 half-wave elements probe-excited from a waveguide, with flaps attached to the structure to form a cylinder which produces an approximate cosecant pattern in the vertical plane. Movable waveguide walls which change the phase progression along the array effect a rapid scan (Chap. 15). This antenna admirably fulfilled its design function as a fixed-frequency equipment.

The last statement in the preceding paragraph implies the characteristic of linear arrays which often limits their application. The modern radar is almost always a broadband radar ($\Delta f/f \geq \pm 3$ per cent). A line-feed array of a useful length is

inevitably end-fed if good impedance match and high efficiency are to be maintained over the band of operating frequencies. As the frequency is changed, there is produced a change in interelement phasing which shifts the spatial direction of the radiation peak. This behavior is the more marked if the transmission system is dispersive as for the Eagle antenna or for slots cut in a waveguide.
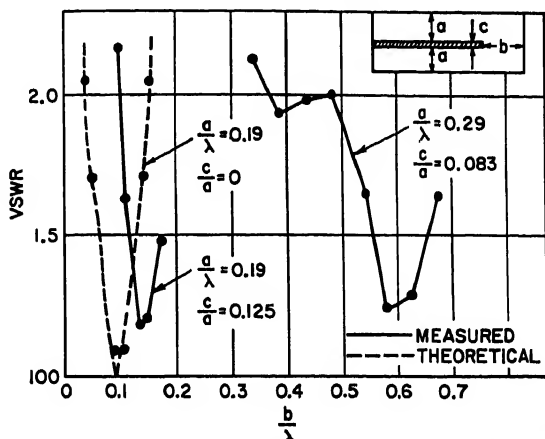
Fig. 25-39. Impedance properties of single-layer TEM pillbox. (*Reference 20.*)

This frequency-beam shift relationship does not per se exclude the end-fed array from consideration as a line feed. It can, in fact, be exploited as a scanning device. Alternatively, the frequency control may be arranged to insert an appropriate bias into the radar indicator, its computer, or into the mechanical positioning of the antenna itself. The complications thus implied must be weighed against the added volume of a pillbox line feed in arriving at a choice between these line-feed types.

25.8. REFLECTOR DESIGN PROBLEMS

In this discussion of radar antennas an antenna reflector has heretofore been assumed to be a continuous conducting sheet whose contour conforms exactly to that prescribed by the mathematics of the design. Certainly the latter is never true. And the continuous sheet may be perforated, replaced by a structure of slats, rods, or even wire embedded in a dielectric, to save weight or minimize windage or sea-water resistance.

Effect of Reflector Errors. Manufacturing processes are never perfect, and reflectors will always deviate from the desired contour. Sometimes such deviations are part of the design for manufacture, as would be the case, for example, with rivet or bolt heads. In general, inadvertent errors increase with the physical size of the antenna. As an example, a 6-ft paraboloidal reflector can, with careful processing, be produced with a surface error of no more than ±0.02 in. For a 60-ft diameter, this tolerance might be expected to increase to ±0.20 in.

The principal result of reflector errors is the increase in the minor-lobe level and pattern minima. Gain is correspondingly reduced, but beam-angle widening, while inevitable, is often not as significant. This effect is likened by Gilbert and Morgan[44] to that produced by a background-noise level which adds in a random way to the nominal pattern. Such a background level would be expected to have its maximum influence on pattern minima and a significant effect on the minor-lobe level and to produce relatively minor change near the peak of the radiation.

The tolerance for paraboloidal reflectors is usually set somewhere in the range of $\pm\lambda/16$ to $\pm\lambda/32$ to produce a deviation in radians between $\pi/8$ to $\pi/16$ from the desired equiphase surface at the aperture. These values are as good as any other arbitrary choices. However, it is desirable to know what penalty accrues when, for example, high-frequency operation or large physical size makes impossible their attainment. Then, too, when more stringent tolerance can be satisfied, it is well to understand what improvements can be thus secured.

There are two ways of approaching the solution to the problem so posed. The first is a statistical attack[45] in which the probability of a certain reduction in gain and enhancement of minor lobes can be determined for a random phase error of a given magnitude. The second involves the computation of the maximum gain loss possible for a given peak-phase error.[46]

Ruze's calculation of the average minor-lobe levels as affected by various amounts of random phase error for a paraboloid is shown in Fig. 2-26. The correlation interval referenced is that separation at which the errors are essentially independent. Figure 2-26 is an example of the statistical approach from which is seen the rapidity of the increase in the minor-lobe level with increasing reflector error.

The "maximum-effect" procedure of Cheng[46] yields

$$\Delta G \leq 20 \log \frac{2}{2 - m^2} \qquad (25\text{-}10)$$

where ΔG is the gain reduction in decibels produced by a maximum phase deviation of m radians. Equation (25-10) is an approximate relationship which gives useful results for values of m up to $\pi/4$. It obtains for either a circular or rectangular aperture and for any amplitude taper. For $m = \pi/8$ and $m = \pi/16$ (corresponding to tolerances of $\pm\lambda/16$ and $\pm\lambda/32$, respectively), the gain reductions are 0.7 and 0.17 db. Although these values represent maxima, it is evident that a $\pm\lambda/32$ tolerance is worth striving for. This is borne out by the fact that the half-power beam-angle increase for a uniformly illuminated circular aperture may be as large as 11.2 per cent for a $\pm\lambda/16$ tolerance. This figure is but 2.8 per cent for a $\pm\lambda/32$ reflector tolerance.

Interrupted-surface Reflectors. All interrupted-surface reflectors (gratings, perforated surfaces, screens) can be regarded as waveguides beyond cutoff. The leakage through these reflectors and the consequent penalty in efficiency diminish as (1) the cutoff-controlling dimension decreases and (2) the length of the equivalent cutoff waveguide increases. For example, a typical perforated reflector has round holes spaced about 0.5λ between centers with a diameter of 0.25λ. Since cutoff for the TE_{11} mode corresponds to a diameter of 0.585λ, skin thicknesses sufficient for structural integrity generally ensure negligible transmission loss.

In addition to the leakage, these reflectors differ in another important particular from the continuous-surface type. Reflections from a continuous surface can admit but one maximum whose direction is given by the optically reflected ray. Reflections from, say, a grating produce the same optically defined maximum, but depending on the spacing and angle of incidence, can form another maximum at an angle such that the contributions from each grating element differ in phase by 2π radians, and consequently reinforce a second time. In order to place the position at which the second maximum appears beyond the range of the real angle, the center-to-center spacing of the elements must be less than $\lambda/(1 + \sin\theta)$, where θ is the angle between the incident ray and the normal to the grating element itself.

Grating formed of edgewise strips are deservedly a popular member of the class of polarization-sensitive interrupted-surface reflectors. Polarization sensitivity dictates that the electric vector of the incident ray lie in a plane determined by the incident ray and the grating element. Silver[47] presents some empirically derived relationship between strip spacing, thickness, and depth.

The grating reflector permits reflector-contour adjustment by the process of sliding one set of strips through a stationary set. The edgewise grating strips for a typical application have a $\lambda/4$ between-center separation and a $\lambda/4$ depth. The thickness is $\lambda/32$. Measured transmission loss is 15 db, corresponding to a gain loss of $\frac{1}{4}$ db.

TRANSMISSION THRU A GRID OF WIRES
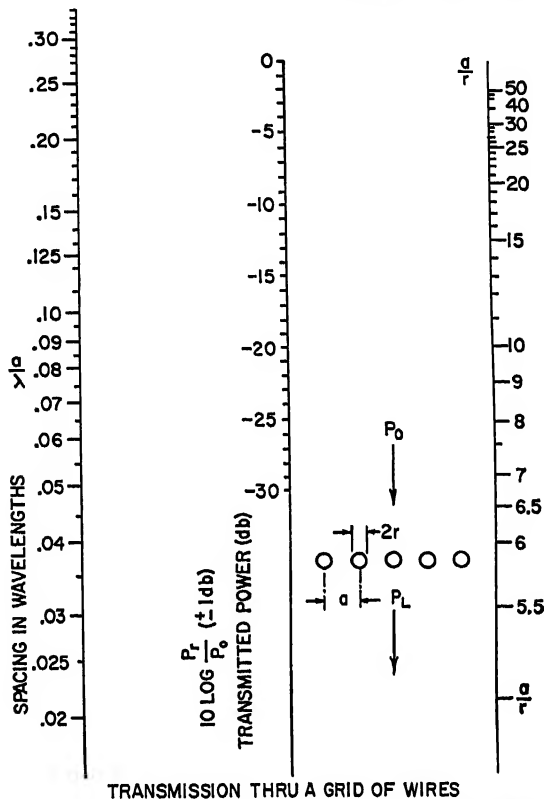
FIG. 25-40. Transmission through a grid of wires. (*Reference 48*.)

Wire reflectors held in position by a dielectric binder usually offer a significant weight saving over the solid-sheet reflector. The requirements on spacing and polarization discussed for gratings obtain for wire reflectors. Mumford[48] has prepared a convenient nomograph relating transmitted power loss, wire spacing, and wire diameter. The accuracy of this nomograph, reproduced in Fig. 25-40, has been established by experimental checks to be slightly better than ±1 db.

REFERENCES

1. L. N. Ridenour (ed.): "Radar Systems Engineering," p. 21, McGraw-Hill Book Company, Inc., New York, 1947.
2. S. Silver: "Microwave Antenna Theory and Design," p. 190, McGraw-Hill Book Company, Inc., New York, 1949; C. C. Cutler: "Parabolic Antenna Design for Microwaves," *Proc. IRE*, vol. 35, no. 11, p. 1284, November, 1947; H. T. Friis and W. D. Lewis: "Radar Antennas," *Bell System Tech. J.*, vol. 26, no. 2, p. 219, April, 1947.
3. P. H. Vartanian, J. L. Melchior, and W. P. Ayres: "Broad-band Ferrite Isolator," *IRE Trans. on Microwave Theory Tech.*, vol. MTT-4, no. 1, p. 8, January, 1956; S. Weisbaum and H. Seidel: "The Field Displacement Isolator," *Bell System Tech. J.*, vol. 35, no. 4, p. 877, July, 1956.

4. A. B. Pippard and N. Elson: "Elimination of Standing-waves in Aerials Employing Paraboloidal Reflectors," *J. IEE (London)*, pt. IIIA, vol. 93, no. 10, p. 1531, 1946; Silver, Ref. 2, p. 443; D. W. Fry and F. K. Goward: "Aerials for Centimeter Wavelengths," p. 60, Cambridge University Press, New York, 1950; A. T. Starr: "Radio and Radar Technique," p. 248, Sir Isaac Pitman & Sons, Ltd., London, 1953.

5. R. L. Mattingly, B. McCabe, and M. J. Traube: "The Split-reflector Technique for Broad-band Impedance Matching of Center Fed Antennas without Pattern Deterioration," *WESCON Convention Record*, 1957.

6. Silver, Ref. 2, p. 447.

7. P. W. Hannan: "Design for a Twistreflector Having Wideband and Wide-angle Performance," ASTIA Report AD 306000, April, 1955.

8. W. C. Jakes: "Broadband Impedance Matching with a Directional Coupler," *Proc. IRE*, vol. 40, no. 10, p. 1216, October, 1952.

9. Cutler, Ref. 2.

10. A. T. Corbin and A. S. May: "Broadband Horn Reflector," *Bell Lab. Record*, vol. 33, no. 11, November, 1955.

11. W. E. Kock: "Metal Lens Antenna," *Proc. IRE*, vol. 34, November, 1946.

12. D. G. Kiely: "Dielectric Lens Aerial for Marine Navigational Radar, *Wireless Eng.*, vol. 28, no. 337, p. 229, October, 1951.

13. J. D. Kraus, "Antennas," p. 325, McGraw-Hill Book Company, Inc., New York, 1950.

14. C. A. Cochrane: "Improvements in or Relating to High Frequency Radio Aerials." British Patent No. 700868, February, 1952-December, 1953; P. W. Hannan: "Principle of the Double-reflector Antenna," available through ASTIA via no. AD 116479, January, 1955.

15. P. F. Mariner and C. A. Cochrane: "Improvements in or Relating to High Frequency Radio Aerials," British Patent No. 716939, August, 1953–October, 1954; R. W. Martin and L. Schwartzman: "A Rapid Wide Angle Scanning Antenna with Minimum Beam Distortion," *Proc. 1958 East Coast Conf. Aeronaut. and Navigational Electronics*, p. 47.

16. Silver, Ref. 2, p. 453.

17. D. G. Kiely: "Parabolic Cylinder Aerials," *Wireless Eng.*, vol. 28, no. 330, p. 73, March, 1951.

18. A. B. Pippard: "The Hoghorn: An Electromagnetic Horn Radiator of Medium Sized Aperture," *JIEE (London)*, pt. IIIA, vol. 93, no. 10, p. 1536, 1946.

19. O. Bohm: "Cheese Aerials," *J. IEE (London)*, pt. IIIA, vol. 93, p. 45; D. G. Kiely, A. E. Collins, and G. S. Evans: "Cheese Aerials for Marine Navigation Radar," *J. IEE (London)*, pt. III, vol. 98, p. 37, 1951.

20. W. Rotman: "A Study of Microwave Double-layer Pillboxes," Air Research and Development Command, Air Force Cambridge Research Center, Electronics Research Directorate, pt. I, AFCRC TR 54-102, July, 1954, and pt. II, AFCRC TR 56-101, January, 1956.

21. Silver, Ref. 2, chap. 13; W. H. Watson: "Waveguide Transmission and Antenna Systems," p. 156, Oxford University Press, New York, 1947.

22. D. W. Fry: "Some Recent Developments in the Design of Centimeter Aerial Systems," *J. IEE (London)*, pt. IIIA, vol. 93, no. 10, p. 1497, 1946.

23. D. G. Kiely: "Dielectric Aerials with Shaped Radiation Patterns," *Wireless Eng.*, vol. 28, no. 333, p. 177, June, 1951.

24. Silver, Ref. 2, Secs. 13.4 and 13.5; C. S. Pao: "Modified Paraboloidal Reflectors for Shaped Beams," *Acta Sci. Sinica*, vol. 1, p. 85, October, 1952.

25. L. J. Chu: "Microwave Beam Shaping Antennas," MIT Research Lab. Electronics Tech. Rept. 40,

26. A. S. Dunbar: "Calculation of Doubly Curved Reflectors for Shaped Beams," *Proc. IRE*, vol. 36, no. 10, p. 1289, October, 1948.

27. Silver, Ref. 2, p. 500.

28. P. M. Woodward: "A Method of Calculating the Field over a Plane Aperture Required to Produce a Given Polar Diagram," *J. IEE (London)*, pt. IIIA, vol. 93, p. 1554, 1946; Silver, Ref. 2, p. 279; A. L. Cullen and F. K. Goward: "The Design of a Waveguide Fed Array," *J. IEE (London)*, pt. IIIA, vol. 93, p. 683, 1946; P. M. Woodward and J. D. Lawson: "The Theoretical Precision with Which an Arbitrary Radiation Pattern May Be Obtained from a Source of Finite Size," *J. IEE (London)*, pt. III, vol. 95, p. 363, 1948; A. S. Dunbar: "On the Theory of Antenna-beam Shaping," *J. Appl. Phys.*, vol. 23, p. 847, August, 1952.

29. G. C. Southworth: "Principles and Applications of Waveguide Transmission," p. 427, D. Van Nostrand Company, Inc., Princeton, N.J., 1950.

30. J. N. Hines, V. H. Rumsey, and C. H. Walter: "Traveling Wave Slot Antennas," *Proc. IRE*, vol. 41, p. 1624, November, 1953.

31. Starr, Ref. 4, p. 268.

32. D. G. Fink: "The SCR-268 Radar," *Electronics*, vol. 18, p. 100, September, 1945.
33. R. V. Alred: "A Switched-beam Directive Aerial on 600 mc.," *J. IEE (London)*, pt. IIIA, vol. 93, p. 411, 1946; Starr, Ref. 4, p. 217.
34. J. F. Reintjes and G. T. Coate: "Principles of Radar," 3d ed., p. 953, McGraw-Hill Book Company, Inc., New York, 1952.
35. J. P. Coales, H. C. Calpine, and D. S. Watson: "Naval Fire Control Radar," *J. IEE (London)*, pt. IIIA, vol. 93, p. 349, March–May, 1946; D. G. Fink: "The SCR-584 Radar, Part I," *Electronics*, vol. 18, no. 4, p. 124, 1945.
36. J. B. Damonte and D. J. Stoddard: "An Analysis of Conical Scan Antennas for Tracking," *IRE Convention Record*, vol. 4, pt. I, p. 39, 1956.
37. R. M. Page: "Monopulse Radar," IRE Convention Record, pt. 8, Communications and Microwave, p. 135, 1955; E. W. Schlieben: "Radomes and Aircraft Design," *Aeronaut. Eng. Rev.*, vol. 11, no. 5, p. 69, May, 1952; D. R. Rhodes: "Introduction to Monopulse," McGraw-Hill Book Company, Inc., New York, 1959.
38. J. F. Ramsay, "Fourier Transforms in Aerial Theory," pts. I and II, *Marconi Review*, vol. 9, p. 139, October–December, 1946; vol. 10, p. 17, January–March, 1947.
39. Reference 34, p. 955.
40. Silver, Ref. 2, p. 348.
41. A. R. G. Owen and L. G. Reynolds: "The Effect of Flanges on the Radiation Patterns of Small Horns," *J. IEE (London)*, pt. IIIA, vol. 93, no. 10, p. 1529.
42. Silver, Ref. 2, p. 377.
43. Friis and Lewis, Ref. 2, p. 315.
44. E. N. Gilbert and S. P. Morgan: "Optimum Design of Directive Arrays Subject to Random Variations," *Bell System Tech. J.*, vol. 34, no. 3, p. 637, May, 1955.
45. J. Ruze: "The Effect of Aperture Errors on the Antenna Radiation Pattern," *Nuovo Cimento*, vol. 9, suppl. 3, p. 304, 1952.
46. D. K. Cheng: "Effect of Arbitrary Phase Errors on the Gain and Beamwidth of Radiation Pattern," *IRE Trans.*, vol. AP-3, no. 3, p. 145, July, 1955.
47. Silver, Ref. 2, p. 450.
48. W. W. Mumford: Bell Telephone Laboratories, Inc., Whippany, N.J., private communication.

Chapter 26

MICROWAVE BEACON ANTENNAS

Henry J. Riblet

Microwave Development Laboratories
Wellesley, Massachusetts

26.1. INTRODUCTION

In many operational uses of radar, it is desirable to reinforce the radar response by means of a beacon system. The beacon transponder, whose response is frequently coded for navigational or homing purposes, operates in conjunction with an antenna system which has an omnidirectional response in the azimuth plane. In order to maximize the response for a given amount of transmitter power, it is usually desirable that the beacon antenna have a nominal amount of antenna gain. This gain can only be obtained by narrowing the vertical plane pattern.

For ground- and ship-borne antennas, the vertical gain is normally obtained by stacking a number of elements in a linear vertical array and feeding the elements so that their contributions combine in phase in the horizontal plane. Depending on the radar with which the beacon is used, the polarization of the beacon antenna may be either vertical or horizontal. For either case, the array consists of a number of linearly polarized elements and a feed system to excite the array elements with energy of the proper amplitude and phase. The preliminary design of a beacon antenna is based on the gain required and its vertical radiation pattern. The effect of aperture

height has been discussed elsewhere in this book and the reader is referred to Chaps. 2 and 5 for details. The following sections treat some of the techniques which have found application in the design of microwave beacon antennas.

26.2. VERTICALLY POLARIZED RADIATOR ELEMENTS

Horizontal Slots. A vertically polarized field can be established by cutting horizontal slots in a vertical waveguide in such a way as to interrupt vertical currents flowing in the waveguide. A suitable radiating element will result if the slots are placed symmetrically on a circular cross section of the waveguide and if the currents exciting them are equal and in phase. This situation is found to hold for the coaxial (TEM) mode and for the TM_{01} mode. As a general rule, it is found that if the slots are placed so that the distance between their effective centers is $\lambda/2$ or less, the azimuth pattern will be reasonably symmetrical. For horizontal slots, this presents a problem, since slots much shorter than $\lambda/2$ may present difficulties in impedance matching. A more serious problem is that of suppressing the higher-order lobes which may appear in the vertical plane if the radiating elements are not sufficiently close together. This requirement ordinarily makes it impractical to use any other than the TEM mode, since the slots are excited directly by the mode currents and no convenient procedure exists for the forced reversal of the exciting current in alternate slots. The use of dielectric loading in coaxial line solves this problem completely, and simultaneously permits the use of a continuous circumferential slot, as shown in Fig. 26-1. This element possesses an exceedingly uniform pattern, and arrays have been constructed with excellent vertical patterns. The problem of impedance matching can be handled by the choice of slot width, since the series impedance of this element can be varied over a wide range. The problems and difficulties with this element are primarily due to the dielectric material which is used in those parts of the antenna where the field distribution is critical. In order to obtain reproducible results, the electrical properties of the dielectric must be very closely controlled and careful consideration given to thermal and mechanical requirements of the antenna.

FIG. 26-1. Vertically polarized slot radiator for coaxial line.

Vertical Dipoles. Another useful radiating element for vertical polarization is shown in Fig. 26-2. It consists of a pair of half-wavelength vertical dipoles supported by a three-wire type of feeder on a small coaxial line. The vertical elements are fed in phase with a spacing of about a quarter of a wavelength. The azimuth pattern which results is oval in shape with a minimum in the plane of the dipoles which is smaller than the maximum by a factor of about 1.6 as a result of the currents flowing on the outer surface of the coaxial line. A two-element array of this type has a VSWR under 1.3 over a 7 per cent frequency band when the feeder is directly connected to the inner conductor of a 50-ohm coaxial line.

Vertical Cylinders. Radiating cylinders such as are shown in Fig. 26-3 are a natural and useful extension of multiple vertical dipole elements, since they yield reasonably uniform azimuth patterns and are inherently more symmetrical and rugged. Two types are used in *S*-band where standard-size ⅞-in. coaxial line permits three feed points to be placed so that azimuth patterns with a threefold symmetry are realized with a ratio of maximum to minimum power of 1.6 to 1. These feed points are excited by three-wire lines of sufficient length so that flexible, reasonably broad

band impedance matching can be achieved.   In one type of element, as used in the array shown in Fig. 26-4, the cylinders are a half wavelength long and are fed from both ends.   This not only permits a rugged construction because the cylinders can be supported at both ends, but yields a more uniform azimuthal pattern since the alternate feed points can be displaced by 60°.

Cylinders slightly less than one-quarter wavelength long as shown in Fig. 26-5 were found to be somewhat easier to match in shorter arrays, and more flexible in that the same unit could be used over a 20 per cent frequency band.   Here scallops were cut in the cylinders to reduce the input capacity at the feed points to tolerable levels.   The elevation patterns of this antenna taken at 9, 10, and 11 cm have a half-width of approximately 50°.   With the exciting probes fastened directly to the inner conductor, the VSWR of this antenna is less than 1.25 over a 20 per cent frequency band.
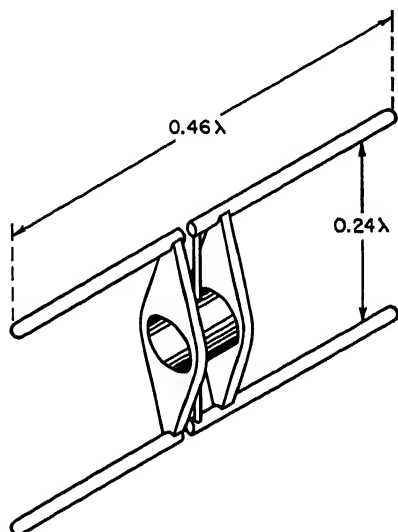
FIG. 26-2. Vertically polarized double dipole element (*H* element).
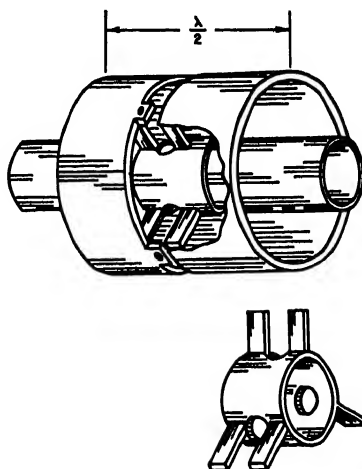
FIG. 26-3. Vertically polarized cylindrical element.

26.3. HORIZONTALLY POLARIZED RADIATOR ELEMENTS

Tridipole Radiators.   For frequencies above 1,000 and below 3,000 Mc, where it is practical to enclose the antenna completely in a plastic cover, and where the standard coaxial line is still large enough to be a reliable structural member, the radiating element shown in Fig. 26-6 has proved to be a very flexible and useful design element. This element consists of three half-wave dipoles arranged on the circumference of a circle.   Each of the dipoles is fed by a three-wire line, where the central line serves as a probe to couple the dipole to the interior of the coaxial line.   When these dipoles are equally coupled to the coaxial line, the azimuth pattern of a single element has a uniformity which is better than 1.7 to 1 in power from 9 to 11 cm.   Actual patterns are shown in Fig. 26-7.   Similar elements constructed for use at longer wavelengths and compressed in size by capacitively loading the ends of the dipoles have even more uniform patterns.   The impedance characteristics of single elements can be controlled by the choice of the length of the dipole lengths, and experience indicates that one, two, or three elements can be directly coupled to the coaxial line with a VSWR less than 1.4 over a 10 per cent frequency band.

Multiple Slots on Circular Guide. Above 3,000 Mc, waveguide is sufficiently small, and the dimensions of dipoles so critical that it is convenient to construct horizontally polarized beacon antennas by locating vertical slots symmetrically on a circular waveguide. The cross section of such a radiating element is shown in Fig. 26-8, where seven slots one half wavelength long are cut symmetrically in a 1¼-in. circular waveguide excited in the TM_{01} mode at X-band. Since the current flow in this mode is

FIG. 26-5. Vertically polarized element with λ/4 cylinders.

FIG. 26-4. Vertically polarized antenna array using λ/2 cylinders.

DIAMETER 0.56 λ
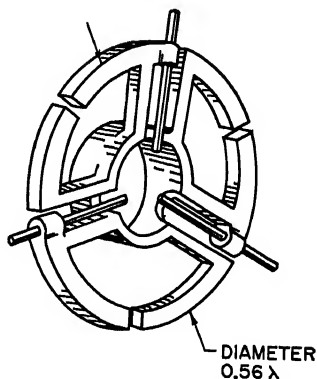
FIG. 26-6. Tridipole radiator.

entirely axial, axial probes must be added to the structure to induce a voltage across each of the slots. On alternate bays, which are spaced by a half wavelength in guide, the position of the probes is reversed so as to maintain in-phase excitation. It should be observed that for the dimensions and frequency chosen, the spacing between the slots along the guide is only slightly less than a half wavelength. For this type of element, the azimuth pattern is essentially uniform within experimental error.

A number of applications of this type of antenna require separate receiving and transmitting antennas. Since these are most conveniently placed one above the other, coaxial line operating above cutoff for some of the lower modes can be used as a feeder. Figure 26-9 shows the azimuth patterns at 3 cm of circular arrays of four and six slots cut in a coaxial line 1 in. diameter. It should be observed that the six slots are very nearly one half wavelength apart circumferentially, and that the pattern deteriorates rapidly with the larger spacings obtained with a smaller number
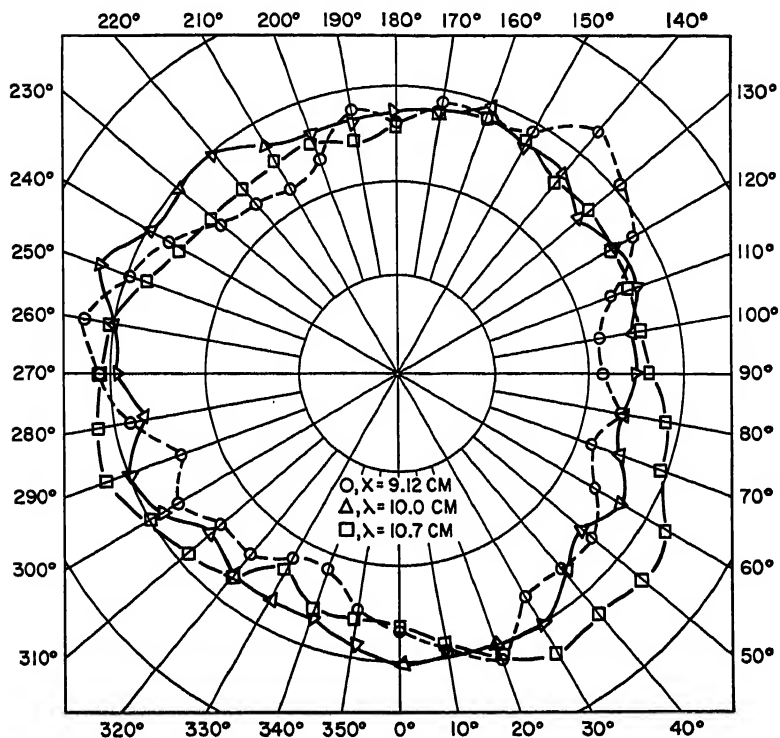
FIG. 26-7. Patterns of a tridipole unit in the plane of the unit.
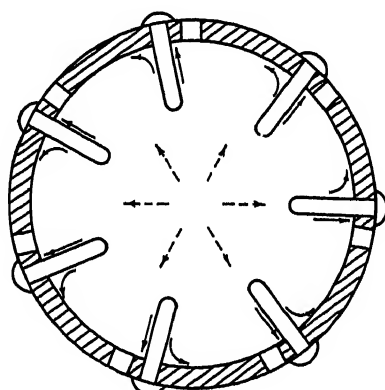
CURRENT FLOW INDUCED BY PROBES.

TRANSVERSE ELECTRIC-FIELD CONFIGURATION OF UNPERTURBED MODE.

FIG. 26-8. Axially symmetrical radiating unit formed by a circular array of slots.

of slots. Attempts to use seven slots in this size line were unsuccessful, this difficulty being attributed to mutual impedance coupling around the cylinder. Both of these antenna feeds are capable of supporting modes other than the symmetrical TM mode required. Providing the desired mode is established in pure form by a suitable rectangular-to-round waveguide transducer, the exciting probes will not establish undesired modes if reasonable care is taken to ensure that the probes are equally coupled to the waveguide.
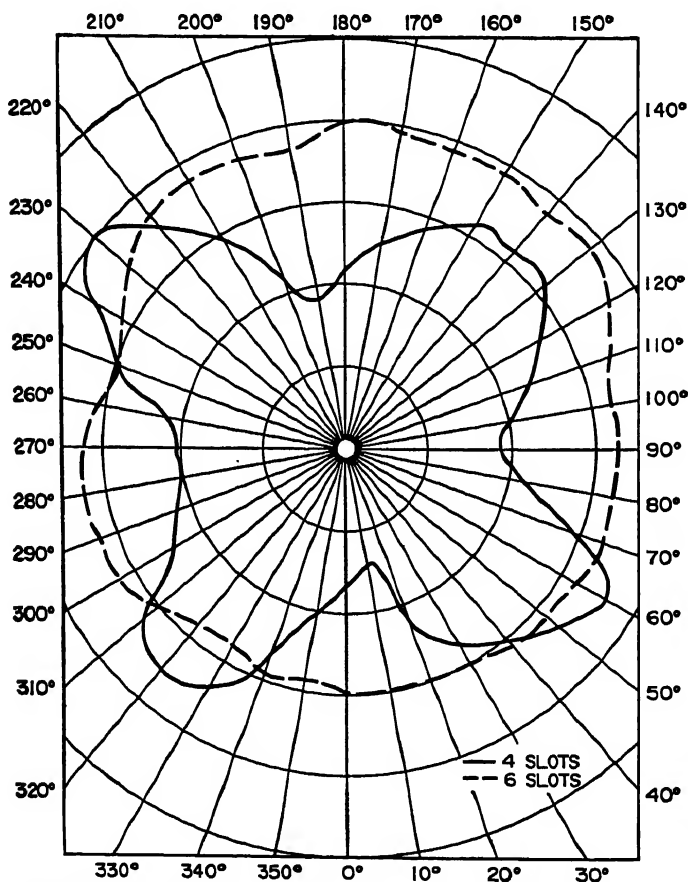
Fig. 26-9. Patterns of circular arrays of four and six slots on coaxial line of 1-in. outside diameter.

26.4. FEED SYSTEM CONSIDERATION

Loaded Line Analysis. The phase of the radiated signal from a single-array element is determined primarily by the phase of the exciting voltage. This in turn is established by the spacing between the elements of the array. Since most practical array designs involve radiating elements which are equally spaced on the feed line, the phase and amplitude of the driving voltages can be determined from the parameters of the loaded line. Consider a line whose characteristic impedance is Z_0 and whose complex propagation constant is $\gamma = \alpha + j\beta$, which is loaded at equal intervals l

by identical radiating elements. The radiator can be regarded, in general, as a symmetrical passive four-terminal network inserted between two equal line segments. Such a network can be replaced by a T or π section equivalent having impedance elements Z_1, Z_2, Z_3, or Z_A, Z_B, Z_C, respectively. For the symmetrical radiating elements assumed, $Z_1 = Z_3$ and $Z_A = Z_C$. Now, as is well known, a section of uniform transmission line of length l also has equivalent T and π section representations. For the T section

$$z_1 = z_3 = Z_0 \tanh\left(\frac{\gamma l}{2}\right) \qquad z_2 = Z_0/\sinh(\gamma l)$$

and for the π section:

$$z_A = z_C = Z_0 \coth\left(\frac{\gamma l}{2}\right) \qquad z_B = Z_0 \sinh(\gamma l)$$

Replacing both the radiators and the line segments by their equivalent T sections, the loaded line is reduced to a cascade of networks as shown in Fig. 26-10a. Here A

(a)

(b)

(c)
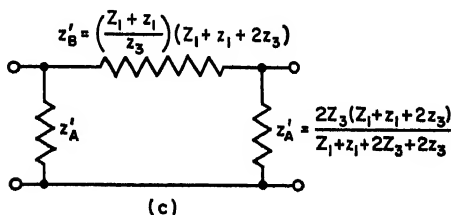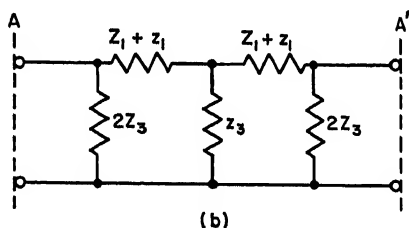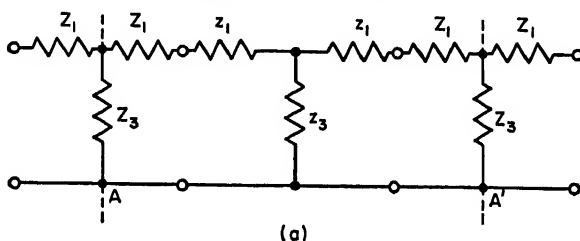
FIG. 26-10. Network system equivalent to a loaded transmission line. (a) T section replacements of radiators and line segments, (b) reduction to symmetrical networks, (c) π section equivalent of the network in (b).

and A' are the mid-points of the radiating elements. By splitting the shunt element Z_3 into a pair of impedances $2Z_3$ in parallel, the line is further reduced to a chain of symmetrical networks, as shown in Fig. 26-10b. The characteristic impedance Z_0' and propagation constant γ' of the loaded line are obtained by reduction of this network to its equivalent π section, as in Fig. 26-10c, and then making the identification

with a uniform line of characteristic impedance Z_0' and propagation constant γ'. If z_A' and z_B' are the elements of the reduced section, then

$$Z_0' \coth\left(\frac{\gamma'\ell}{2}\right) = z_A' \qquad Z_0' \sinh(\gamma'\ell) = z_B'$$

These may be reduced with the help of Fig. 26-10c and the known values of z_A' and z_B' to

$$\cosh(\gamma'\ell) = \left(1 + \frac{Z_1}{Z_3}\right)\cosh(\gamma\ell) + \left(\frac{Z_0}{2Z_3} + \frac{Z_1}{Z_0} + \frac{Z_1^2}{2Z_0Z_3}\right)\sinh(\gamma\ell)$$

and

$$Z_0' \sinh(\gamma'\ell) = \frac{\left[Z_1 + Z_0\tanh\left(\frac{\gamma\ell}{2}\right)\right]^2}{Z_0}\sinh(\gamma\ell) + 2\left[Z_1 + Z_0\tanh\left(\frac{\gamma\ell}{2}\right)\right]$$

For a well-designed waveguide, the conduction losses in the walls of the waveguide are negligible, so that $\gamma = j\beta$ is a pure imaginary. Then the propagation constant of the loaded line is given by

$$\cosh(\gamma'\ell) = \left(1 + \frac{Z_1}{Z_3}\right)\cos(\beta\ell) + j\left(\frac{Z_0}{2Z_3} + \frac{Z_1}{Z_0} + \frac{Z_1^2}{2Z_0Z_3}\right)\sin(\beta\ell)$$

It is evident that the propagation constant γ' of the loaded line is complex and that both the attenuation and phase constants are functions of the loading and spacing of the elements. For half-wavelength spacing, i.e., $\ell = \lambda/2$, this relation becomes

$$\cosh(\gamma'\ell) = -\left(1 + \frac{Z_1}{Z_3}\right)$$

If the radiating element is a pure shunt element so that $Z_1 = 0$, it is found from the above that

$$\gamma' = j\frac{2\pi}{\lambda_g} = \gamma$$

A similar result follows for pure shunt loading, i.e., $Z_3 = \infty$. Thus, there is no change in the propagation constant for a uniform line loaded with pure series or shunt elements at half-wavelength intervals. In particular, there is no attenuation and no change in phase.

For arbitrary spacings, the propagation constant of the shunt-loaded line is given by

$$\cosh(\gamma'\ell) = \cosh(\gamma\ell) + \frac{Z_0}{2Z_3}\sinh(\gamma\ell)$$

and for the series-loaded line

$$\cosh(\gamma'\ell) = \cosh(\gamma\ell) + \frac{Z_1}{Z_0}\sinh(\gamma\ell)$$

The fact that radiating elements, placed exactly a half guide wavelength apart, are excited by voltages exactly 180° out of phase and of equal magnitude is fundamental to the design of most microwave beacon antennas. For equal coupling, one obtains essentially a uniformly illuminated in-phase array, when the line is suitably terminated in a short circuit. This situation can be described somewhat more directly by saying

that for half-wavelength spacing, the radiating elements of pure shunt impedance are simply in parallel with each other, and with the terminating reactance.

The loaded line analysis does not take account of the coupling between the elements by means of external radiation fields. Experience and calculation have both shown that these effects are relatively small, and patterns which closely approximate theoretical patterns, both from the point of view of beamwidth and of side-lobe level, have been achieved on the basis of this simplifying assumption.
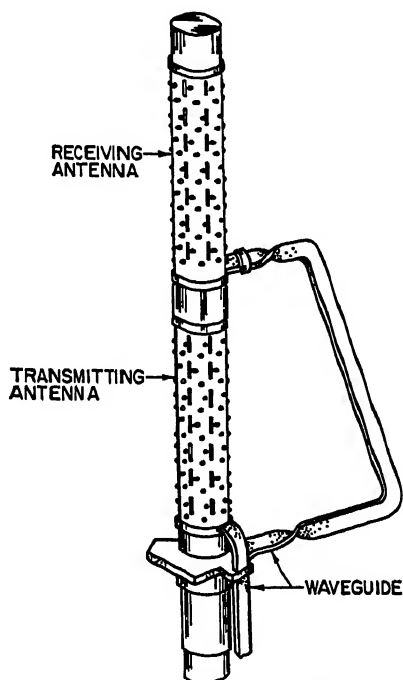
FIG. 26-11. Beacon antenna with an external feed line.

Dual Feed Systems. The feed problem presented by the requirement that a receiving and a transmitting antenna be located one above the other has been solved in a variety of ways. For horizontal polarization, the feed line for the upper antenna can be taken directly past the lower antenna, if care is taken to minimize the total shadow region. How this was accomplished for the slotted X-band waveguide antenna described previously is illustrated in Fig. 26-11. It will be noted that the waveguide feed was twisted where it shadowed the lower antenna, so that its minimum dimension was presented to the radiation from the lower antenna. The waveguide feed was also placed sufficiently far from the antenna, and its axis was tilted with respect to that of the lower antenna to minimize the interference between the two sources.

For antennas employing vertical polarization, and for applications where space is critical, this solution is not practical, and it is necessary to resort to dual coaxial-line arrangements. Such an arrangement is pictured in Fig. 26-4, in which the upper antenna is fed through a stub used in feeding the lower antenna.

A dual coaxial feed involving transitions from waveguide to coaxial line is shown in Fig. 26-12. In this design the inner conductor for the lower antenna is made hollow,
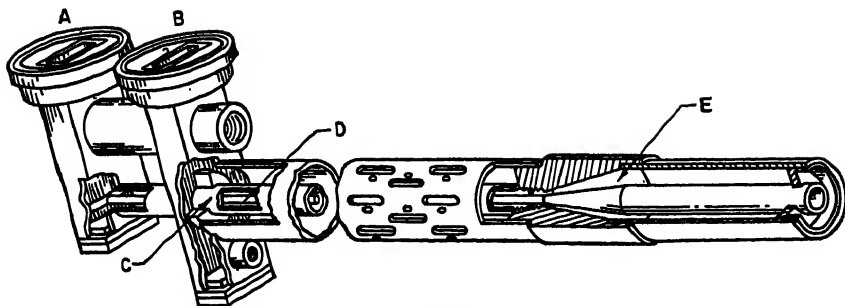
FIG. 26-12. Dual coaxial feed system.

and another conductor runs inside it, forming a coaxial feed line for the upper antenna. This "inner" conductor is then tapered to normal size, as it enters the upper antenna.

26.5. TYPICAL BEACON ANTENNA DESIGN

Vertically Polarized Arrays. A typical low-gain antenna system for *S* band employing quarter-wavelength cylinders is shown in Fig. 26-13. Its patterns and impedance characteristics have already been described in Sec. 26.2. Of interest is the horizontal metallic disk separating the upper and lower antennas. This element serves the
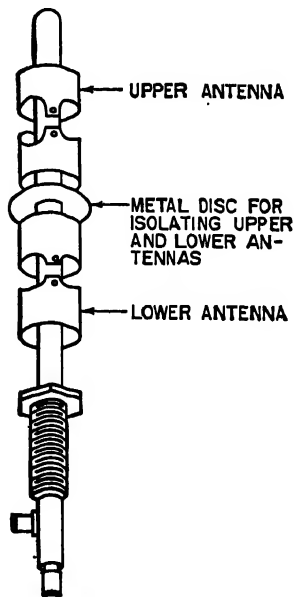
FIG. 26-13. Low-gain vertically polarized antenna system.
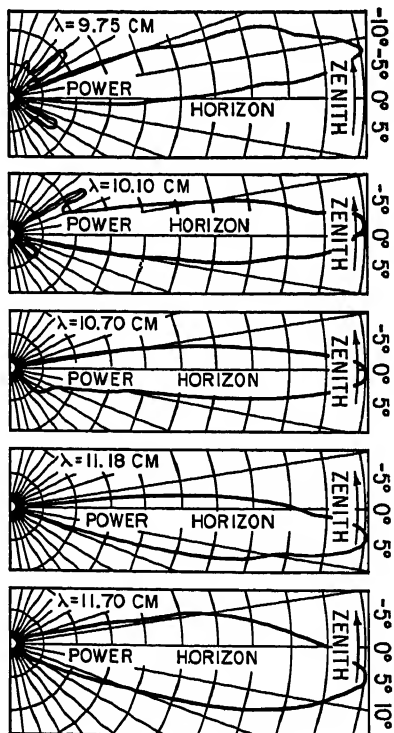
FIG. 26-14. Elevation patterns of a six-element antenna.

Fig. 26-15. An axially symmetric array for horizontal polarization.
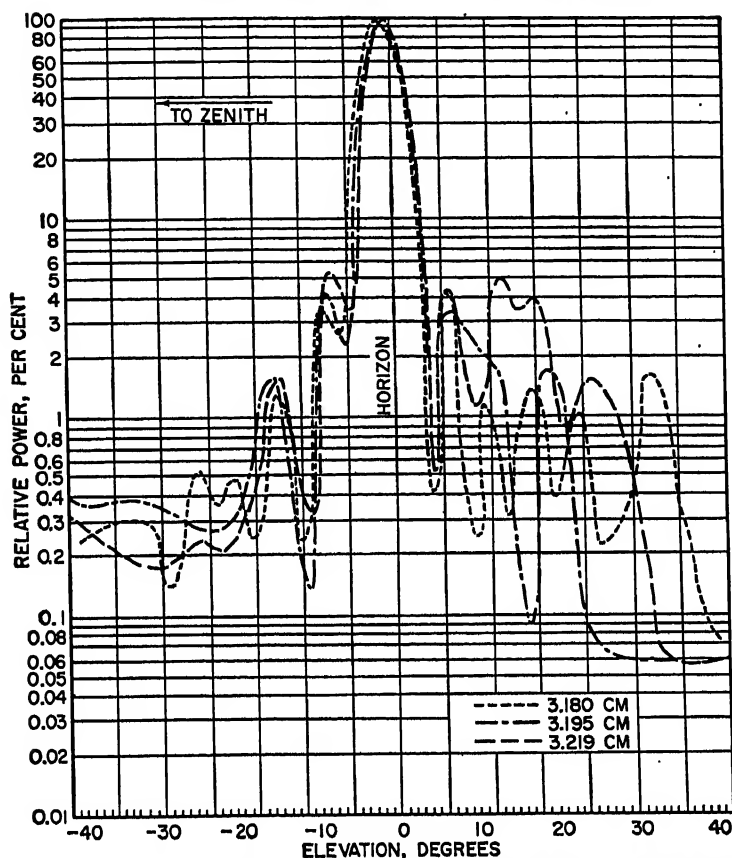
Fig. 26-16. Elevation patterns of an axially symmetric horizontally polarized array.
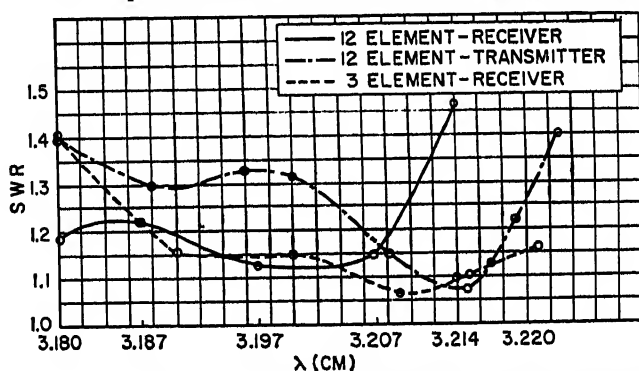
Fig. 26-17. Standing wave ratios of slotted TM$_{01}$ waveguide antennas.

very important function of raising the isolation between the two antennas to acceptable levels. Early introduction of the element into the general design is important, because its effect on the impedance characteristics of the antenna is considerable.

A high-gain antenna system using vertical cylinders is shown in Fig. 26-4. Each antenna of Fig. 26-4 consists of 13 half-wavelength cylinders previously described.

For a six-element antenna of this type having solid cylinders, the VSWR is less than 1.2 from 9.6 to 11 cm. Over this band, the elevation pattern of this antenna varies as shown in Fig. 26-14. Although the elevation angle of the pattern maximum is seen to vary with frequency, no serious splitting of the pattern was observed. Both antennas employed a circular disk to minimize the coupling between antennas

It should be pointed out that elevation patterns of the higher-gain antennas are determined by the ratio of over-all length to wavelength, and are thus nearly independent of polarization and element geometry.

Horizontally Polarized Arrays. One antenna system for horizontal polarization utilizes a dual array of the tridipole elements described previously, each array containing 14 elements.   Over a 2 per cent frequency band, the VSWR of each of these antennas was less than 1.4. The half-power beamwidth was 8° and all side lobes were less than 5 per cent in power.

Figure 26-15 shows an array of vertical slot radiators cut in circular waveguide operating in the TM_{01} mode as described previously. It consists of 12 bays of slots. The excitation of the bays is reversed by alternately placing the pins on different sides of the slots in adjacent bays. An additional set of matching pins is placed midway between the radiating elements for the purpose of increasing the bandwidth of the antenna. The elevation pattern of this antenna over its operating frequency is shown in Fig. 26-16. Figure 26-17 shows the input VSWR for a 12-bay antenna and a 3-bay antenna. A dual coaxially fed antenna using 10 bays of slots on a 1-in.-O.D. coaxial line is pictured in Fig. 26-18.

Fig. 26-18. Dual coaxially fed antenna system.

Antennas having somewhat superior aerodynamic characteristics can be designed by making use of the fact that a pair of axial slots centrally cut in the opposite wide
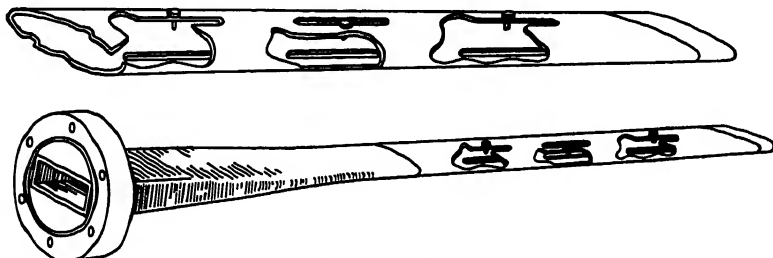
Fig. 26-19. Array of three pairs of slots on streamlined elliptical waveguide.

sides of this waveguide, when excited 180° out of phase, have a rather uniform azimuth pattern. These slots may be excited either by probes extending into the waveguide

as in Fig. 26-19, or by exciting the slots from a coaxial line with a slotted dipole as shown in Fig. 26-20. When the ratio of the minor axis to the major axis of the stream-lined section is at least 4 to 1, and the minor axis is a quarter wavelength or less, then an azimuth pattern can be achieved whose maximum power does not exceed the minimum power by more than 2 to 1. The pattern achieved with a full-length slot, fed
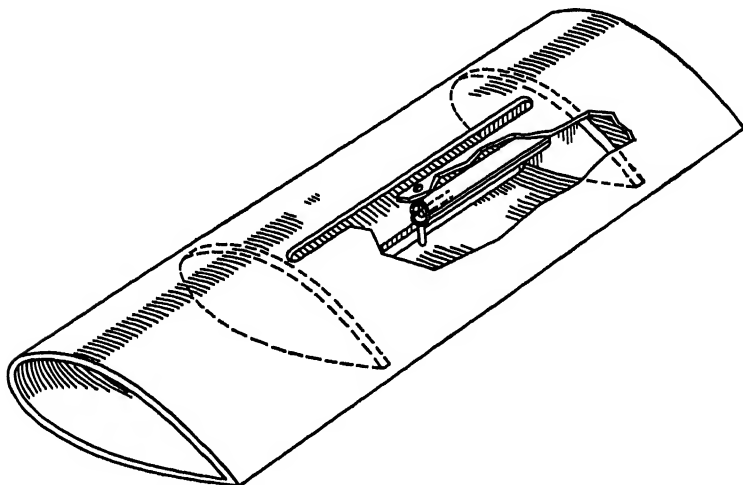
Fig. 26-20. Horizontally polarized streamlined radiator.
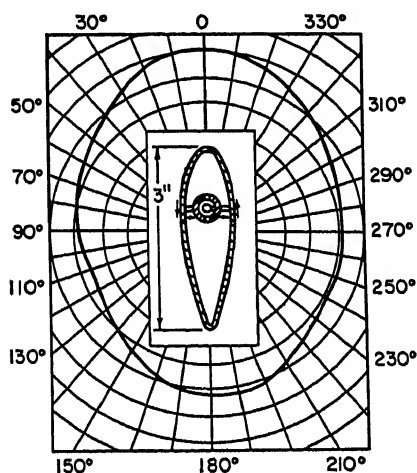
Fig. 26-21. Radiation pattern of a horizontally polarized streamlined radiator.

as shown in Fig. 26-20, is given in Fig. 26-21. The elevation pattern for the full-slot arrangement approximately 0.7 wavelength long had a half-width of 50°, while a half-slot arrangement had a half-width of 80°. For both arrangements the VSWR was under 2 over a 16 per cent frequency band.

REFERENCES

1. H. J. Riblet: "Microwave Omnidirectional Antennas," *Proc. IRE*, vol. 35, no. 5, pp. 474–478, 1947.
2. S. Silver: "Microwave Antenna Theory and Design," McGraw-Hill Book Company, Inc., New York, 1949.
3. A. Roberts: "Radar Beacons," McGraw-Hill Book Company, Inc., 1947.
4. R. E. Plummer: "Surface-wave Beacon Antennas," *IRE Trans. on Antennas and Propagation*, vol. AP-6, no. 1, pp. 105–114, 1958.

Chapter 27

AIRCRAFT ANTENNAS

JOHN T. BOLLJAHN

and

J. V. N. GRANGER

Both of Granger Associates
Palo Alto, California

27.1. INTRODUCTION

The design of antennas for aircraft application differs in two important respects from the analogous problem in other applications: aircraft antennas must be designed to withstand severe static and dynamic mechanical stresses; and, in most instances at least, the size and shape of the airframe play a major role in determining the important electrical characteristics of the antenna. For the latter reason, the type of antenna used in a given system application will often depend on the size of the airframe relative to the wavelength. In the case of propeller-driven aircraft and helicopters, also, the motion of the blades may give rise to modulation of the radiated signal sufficient to produce severe disturbance of system operation. Triboelectric

charging of the airframe surfaces by dust or precipitation particles, known as precipitation static, gives rise to corona discharges, which may produce extreme electrical noise, especially when the location of the antenna element is such that strong electromagnetic coupling to the discharge point exists. In transmitting applications, corona discharge from the antenna element may limit the power-handling capacity of the antenna. Special consideration must frequently be given to the protection of aircraft antennas from damage due to lightning strikes.

27.2. L-F ANTENNAS

The wavelengths corresponding to frequencies below about 2 Mc are considerably larger than the over-all dimensions of most present-day aircraft. Because of the

SECTION AA   SECTION BB
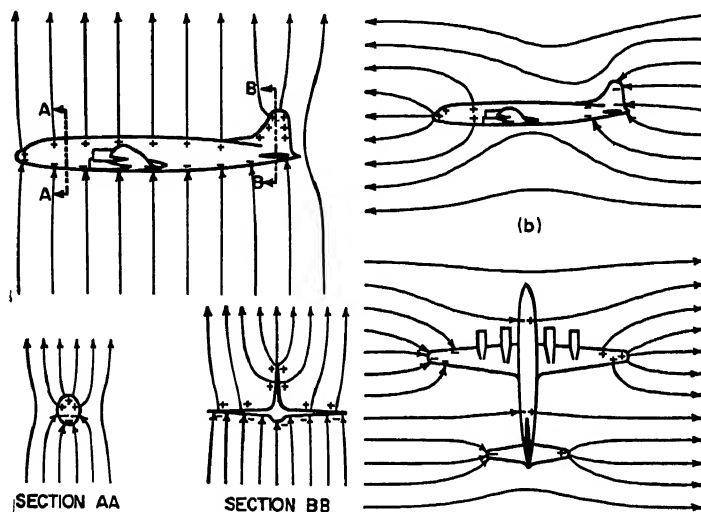
FIG. 27-1. Low-frequency field fringing due to airframe.

inherently low radiation efficiency of antennas which are small relative to the wavelength and the high r-f voltages required in the antennas or their associated matching circuits in order to radiate significant amounts of power, nearly all aircraft radio systems operating at these lower frequencies are designed so that only receiving equipment is required in the aircraft.

Radiation patterns of aircraft antennas in this frequency range are simple electric- or magnetic-dipole patterns, depending upon whether the actual antenna element is a monopole or a loop. Considering first electric-dipole-type antennas, it can be shown with reference to Fig. 27-1 that while the pattern produced by a small monopole antenna placed on the airframe will always be that of a simple dipole regardless of its location, the orientation of the equivalent-dipole axis with respect to the vertical will depend upon the antenna location. In this figure are shown the electric-field fringing produced by an airframe for incident fields polarized in the three principal directions, vertical, longitudinal, and transverse. Clearly, a small antenna element placed on the airframe would respond in general to all three of these principal field components, indicating that the dipole moment of the antenna-airframe combination has projections in all three directions.

Low-frequency antenna sensitivity information is customarily expressed in either of two ways, depending upon whether the antenna location of interest is on a relatively

flat portion of the airframe such as along the top or bottom of the fuselage or at a sharp extremity such as the tip of the vertical stabilizer. In the first case it can be assumed—at least when the antenna element is small relative to the surface radii of curvature—that the antenna performs the same as it would on a flat ground plane except that the apparent incident-field intensity which excites it is greater than the
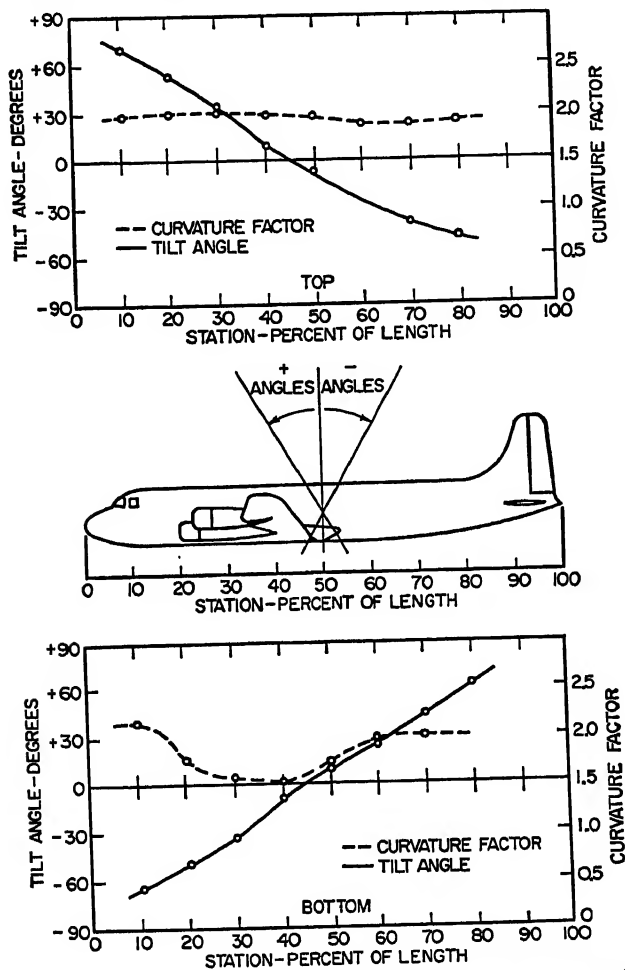
FIG. 27-2. Low-frequency antenna survey data for DC-6 aircraft.

incident free-space field intensity because of the field fringing produced by the airframe (Fig. 27-1). The effect of the airframe on antenna sensitivity is hence expressed by the ratio of the local-field intensity on the airframe surface to the free-space incident-field intensity. For the case of a vertically polarized incident field—which is the case of primary importance in l-f receiving-antenna design—this ratio is designated as F_v and is called the curvature factor for vertical polarization. Survey data giving the equivalent-dipole tilt angle and the factor F_v for top and bottom center-line locations on a typical airframe are shown in Fig. 27-2.

Effective height and capacitance data for antennas to be installed in locations for

which this design procedure is applicable are usually obtained by measurements or calculations for the antenna on a flat ground plane. The effective height (for vertically polarized signals) of the antenna installed on the airframe is then estimated by multiplying the flat-ground-plane effective height by the factor F_v appropriate to the installation location, while the capacitance may be assumed to be the same as that determined with the antenna on a flat ground plane.* The presence of a fixed-
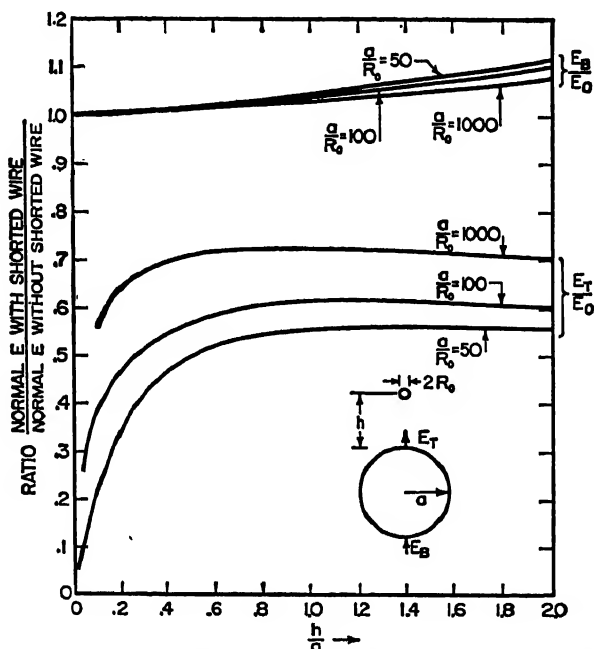
FIG. 27-3. Shielding effect of wire shorted to cylindrical fuselage.

wire antenna on the aircraft may have a significant effect on F_v. Calculated values of the shielding effect of a grounded fixed wire on F_v for an idealized fuselage in the form of a conducting cylinder are shown in Fig. 27-3. If the wire is terminated in an impedance which resonates with the antenna impedance at or near the frequency of interest for the l-f antenna, the effect will be much greater than that shown for the grounded wire. Because of this shielding effect, l-f antennas are seldom located on the top of the fuselage in aircraft which carry fixed-wire antennas.

Flat-ground-plane data for a T antenna are shown in Fig. 27-4. The effective height for such an antenna may be calculated with considerable accuracy from the expression

$$h_e = h \frac{1 + h/2L}{1 + h/L} \tag{27-1}$$

The capacitance curves shown apply to an antenna made with standard polyethylene-coated wire (0.052-in.-diameter conductor and 0.178-in.-diameter polyethylene

---

* In some applications where the antenna capacitance must be held within relatively narrow limits, final adjustments on the installed antenna are required. In most cases, however, the tolerances are made quite wide either through the use of loose coupling between the antenna and the receiver input or by the provision of capacitance trimming adjustments at the receiver input.

sheath). Two antennas of this type are frequently located in close proximity on aircraft having dual automatic direction finder (ADF) installations. The effect of a grounded T antenna on h_s and C_a of a similar nearby antenna are shown in Fig. 27-5. To determine the significance of a given degree of capacitance interaction it is necessary, of course, to consider the Q's of the input circuits to which the antennas are connected and the proximity of the frequencies to which the receivers may be tuned.

Sensitivity data for two flush antennas and a low-silhouette antenna consisting of a relatively large top-loading element and a short downlead are shown in Figs. 27-6 to 27-8, respectively. The antenna dimensions shown in these figures are not indicative of antenna sizes actually in use, but are rather the sizes of the models used in measuring the data. Both h_s and C_a scale linearly with the antenna dimensions.

A simple rule-of-thumb design limit for flush antennas may be derived on the basis of a quasi-static analysis of l-f antenna performance. If any electric-dipole antenna is short-circuited at its feed terminals and placed in a uniform electrostatic field with its equivalent-dipole axis aligned parallel to the field, there will be charges of $+q$ and $-q$ induced on the two elements of the antenna. It may be shown that the product of the low-frequency parameters h_s and C_a is related to the induced charge by the equation

$$h_s C_a = \frac{q}{E} \qquad (27\text{-}2)$$

where h_s and C_a are expressed in meters and micromicrofarads, respectively; q is expressed in micromicrocoulombs, and the incident-field intensity E is expressed in volts per meter. The quantity q/E is readily calculated for a flush, cavity-backed antenna of the type shown in Fig. 27-7, at least for the case where the antenna element virtually fills the cutout

$$\frac{h_e}{h} = \frac{1 + \frac{h}{2L}}{1 + \frac{h}{L}}$$

FIG. 27-4. Effective height and capacitance of T antenna.

in the ground plane. In this case, the shorted antenna element will cause practically no distortion of the normally incident field, and the number of field lines terminating on the element will be the same as the number which would terminate on this area if the ground plane were continuous. The value of q/E is hence equal to $\epsilon_0 a$, where $\epsilon_0 = 8.85 \times 10^{-12}$ farad/meter and a is the area of the antenna aperture in square meters. For the flush antenna with an element which nearly fills the antenna aperture, therefore,

$$h_s C_a = \epsilon_0 a \qquad (27\text{-}3)$$

The line labeled "theoretical maximum $h_s C_a$" in the curves of Figs. 27-6 and 27-7 was calculated from Eq. (27-3). With practical antenna designs, there will be regions

FIG. 27-5. Shielding effect of one T antenna on another.
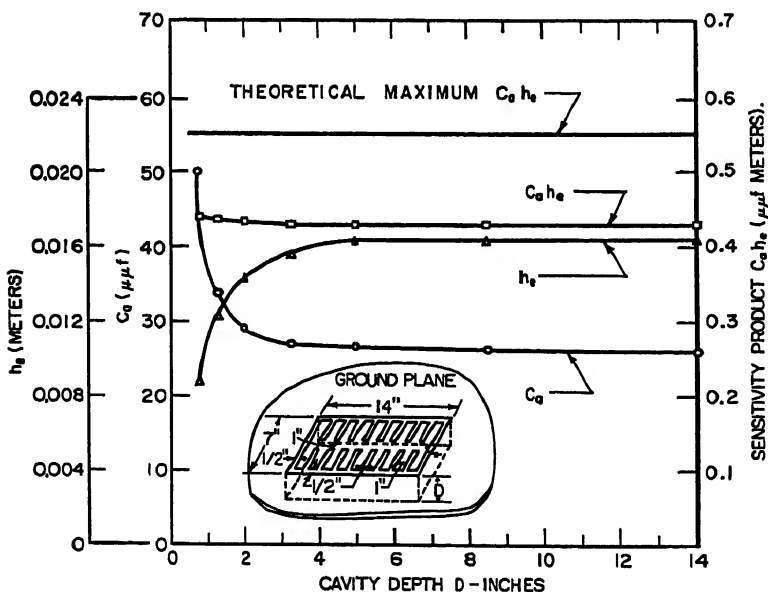
FIG. 27-6. Design data for flush l-f antenna.

of the aperture not covered by the antenna element, so that some of the incident-field lines will penetrate the aperture and terminate inside the cavity. As a result, the induced charge q will be smaller than that calculated above and the product h_eC_a will be smaller than the value estimated from Eq. (27-3).

For antennas located at a sharp extremity of the airframe, such as the tip of the vertical stabilizer, the fringing field is too localized to permit the use of the "curvature-
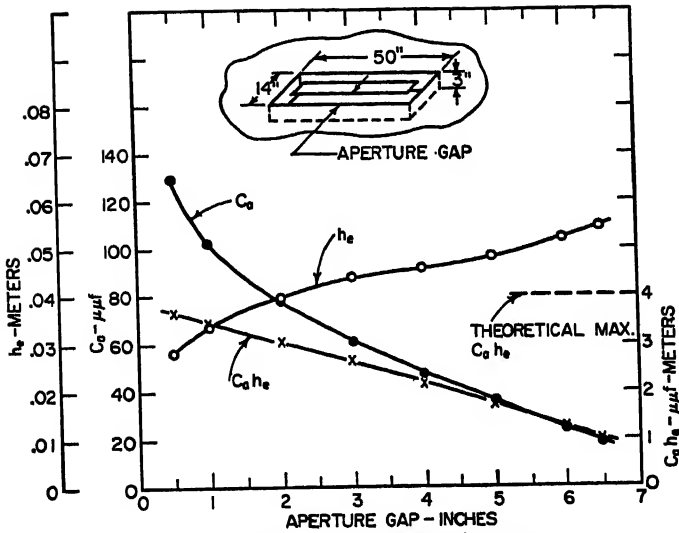
Fig. 27-7. Design data for flush l-f antenna.
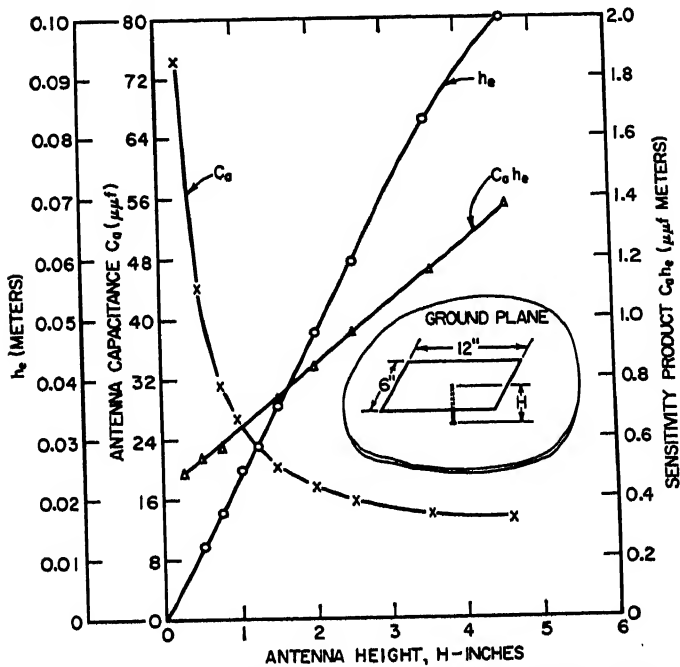
Fig. 27-8. Design data for heavily top-loaded l-f antenna with flat-plate top loading.

factor and flat-ground-plane-data" design approach outlined above, and sensitivity data must be measured with a model of the antenna in the location of interest. Measured design data on a 23-in. stabilizer-cap antenna on a DC-6B aircraft are shown in Fig. 27-9. As a measure of the degree of field fringing produced near the stabilizer tip, it is noted that $h_e C_a$ products of the order of 85 $\mu\mu$f-meters are obtained with this

antenna even though the surface area of the antenna is less than one square meter. To achieve the same sensitivity product with a flush antenna on a flat ground plane, it is seen from Eq. (27-3) that an antenna area of nearly 10 sq meters would be required.

The sensitivity product is a slowly varying function of antenna gap width, at least as long as the gap remains relatively small compared with the total antenna height. This is to be expected from the electrostatic analogy, since the charge induced on the short-circuited element by a vertically polarized field will be concentrated near the extreme tip of the element, and the total quantity of charge will hence not be greatly
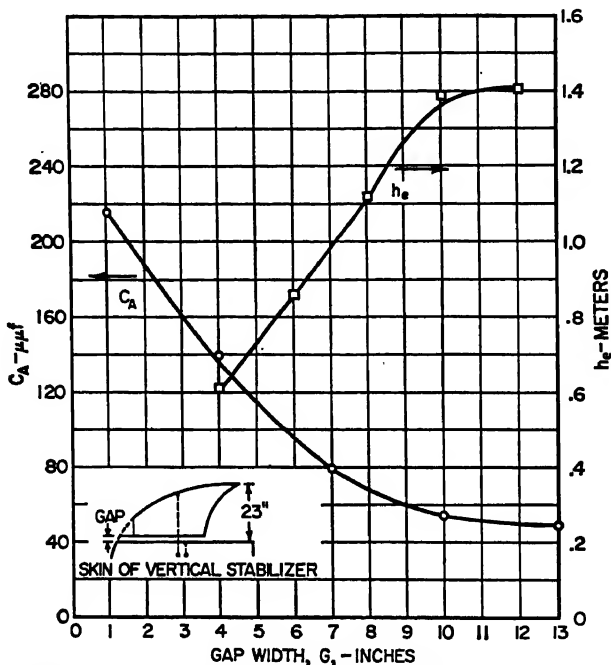
Fɪɢ. 27-9. Tail-tip l-f antenna design parameters for DC-6B aircraft.

affected by changes in the antenna gap width. The individual values of h_e and C_a, on the other hand, are very dependent on the gap width, approaching 0 and ∞, respectively, as the gap width approaches zero. The proper selection of the gap dimension depends upon the characteristics of the system with which the antenna is to work. Generally speaking, if the signal-to-noise ratio of the receiving system is evaluated as a function of antenna gap width—assuming a given incident-field inten-sity—it will be found that there is an optimum value of gap width.

Although, as indicated above, tail-tip antennas have a high sensitivity to vertically polarized signals, their sensitivity to longitudinally polarized signals is usually even greater. In the case of the DC-6B antenna described above, the orientation of the equivalent-dipole axis was found to be tilted approximately 60° from the vertical.

The helicopter presents a special antenna design problem in the l-f range as well as in other frequency ranges because of the shielding and modulation caused by the rotor blades. Measured curves of F_v obtained with an idealized helicopter model to demonstrate the effects of different antenna locations along the top of the simulated fuselage are shown in Fig. 27-10.

It is characteristic of rotor modulation of l-f signals that the modulation envelope
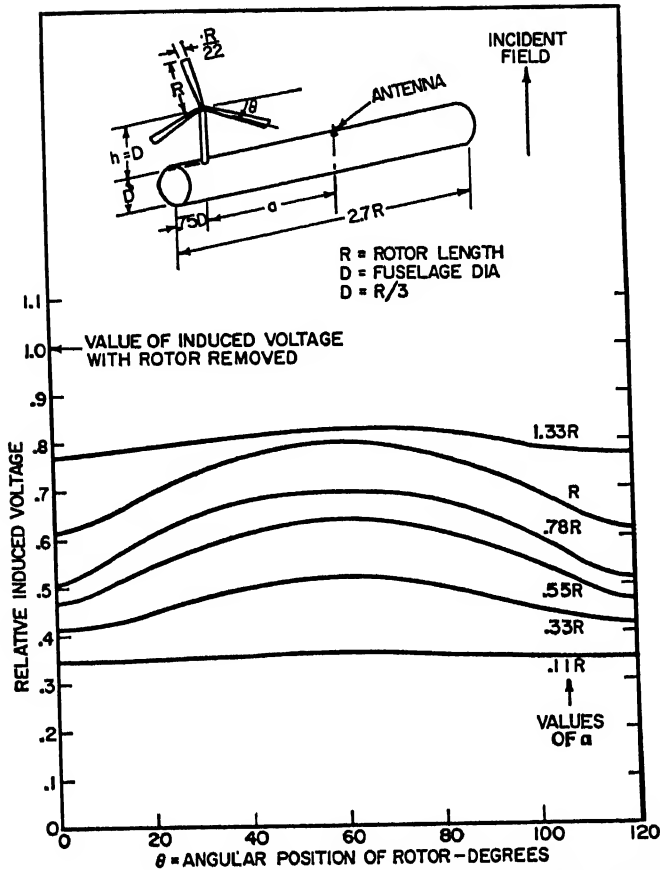
FIG. 27-10. Rotor modulation for l-f receiving antenna on idealized helicopter model.

(a) LONGITUDINAL POLARIZATION

SECTION A-A

(b) TRANSVERSE POLARIZATION
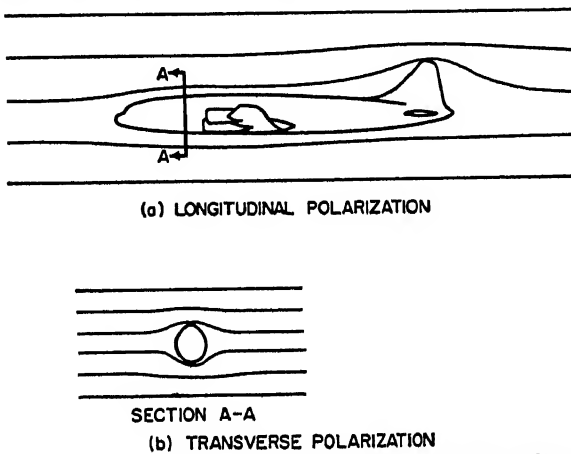
FIG. 27-11. Magnetic-field distortion caused by conducting airframe for: (a) Longitudinal polarization. (b) Transverse polarization.

is smooth, indicating that relatively few modulation components of significant amplitude are produced above the fundamental rotor modulation frequency, which is equal to the number of blade passages over the antenna per second. This fundamental frequency is of the order of 15 cps for typical three-blade single-rotor helicopters. It should be noted that new sidebands with this spacing will be generated about each
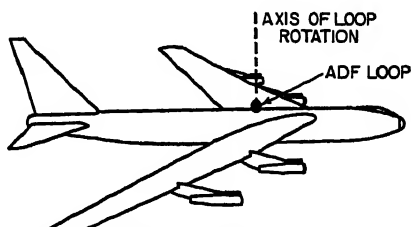
FIG. 27-12. ADF loop antenna on aircraft.

sideband as well as about the carrier of the incoming signal. It is hence not a simple matter to predict the effects of rotor modulation on a particular system unless tests have been made to determine the degree to which the performance of the airborne receiver is degraded by the presence of these extra modulation components.

(a)

(b)
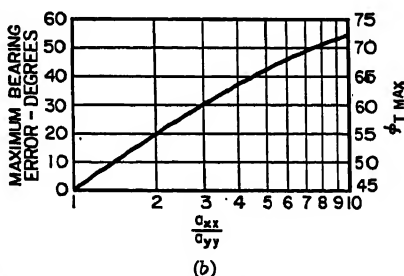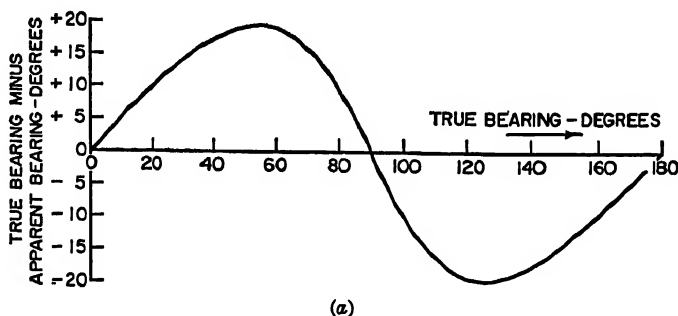
FIG. 27-13. (a) Bearing-error curve for $a_{xx}/a_{yy} = 2$. (b) Maximum bearing error and true bearing at which maximum bearing error occurs as functions of a_{xx}/a_{yy}.

In the case of loop antennas, it is necessary to consider the distortion caused by the airframe in the magnetic-field component of the incident wave. Unlike the electric-field lines, the magnetic-field lines distort in such a way that they avoid entering the conducting airframe. The field-line sketches in Fig. 27-11 illustrate the airframe effect for the two cases in which the ground station is to the side of the aircraft and ahead of the aircraft, respectively. For most locations near the top and bottom

center line the local-field intensity is greater than the incident-field intensity in both cases. This field enhancement is important because it serves to increase the signal induced in a loop antenna and it also affects the bearing accuracy of the direction-finder system. The ratio of local-magnetic-field intensity on the airframe surface to the incident-magnetic-field intensity is designated as a_{xx} for the case in which the incident field is transverse to the line of flight (signal arriving from the front or the rear of the aircraft) and as a_{yy} when the incident field is along the line of flight (signal arriving from the side of the aircraft). These two coefficients give all the essential data for estimating the performance of a direction-finder loop antenna designed to
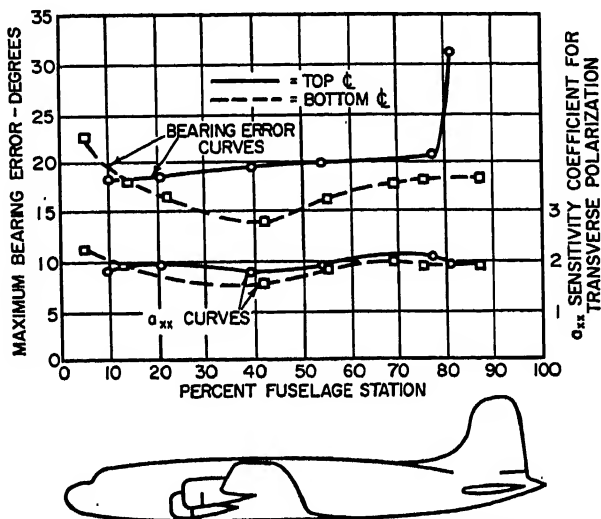
FIG. 27-14. L-F loop-antenna survey data for DC-4 aircraft showing maximum bearing error and sensitivity coefficient for transverse polarization for top and bottom centerline locations.

take bearings on l-f ground-wave signals, provided the loop is placed on the top or bottom center line of the airframe. The amplitude and direction of the local field on the airframe surface may be calculated for any incident-field amplitude and direction (provided the latter is horizontal), once the coefficients a_{xx} and a_{yy} are known, by simply resolving the incident field into x and y components, multiplying these components by a_{xx} and a_{yy}, respectively, and recombining the components.* The ratio of local- to incident-field intensities, which in this case is a function of the angle of arrival of the wave, may be used as a curvature factor for estimating loop-antenna sensitivity in the same way that the factor F_v is used for monopole-antenna calculations.†

The ADF system, which determines the direction of arrival of the signal by rotating its loop antenna about a vertical axis until a null is observed in the loop response (Fig. 27-12), is subject to bearing errors because of the difference in direction of the local and incident magnetic fields. The relationship between the true and the

---

* For locations off the center line, it is readily seen that an incident field polarized in one of the principal directions may cause local-field components in both principal directions (as well as in the z direction), and hence coefficients a_{xy}, a_{yz}, a_{zy}, and a_{zx} are needed in the general case to describe the local-field amplitude and direction in terms of the incident-field amplitude and direction.

† The design of loop-antenna elements is discussed in Chap. 28.

apparent directions of the signal source is given by the equation

$$\tan \phi_t = \frac{a_{xx}}{a_{yy}} \tan \phi_a \qquad (27\text{-}4)$$

where ϕ_t and ϕ_a are the true and apparent bearings of the signal source, respectively. A curve of the bearing error $(\phi_t - \phi_a)$ as a function of ϕ_t with the ratio $a_{xx}/a_{yy} = 2$ is shown in Fig. 27-13a. Figure 27-13b shows graphs of the maximum bearing error $|\phi_t - \phi_a|$ and the value of ϕ_t (in the first quadrant) at which the maximum bearing error occurs as functions of the ratio a_{xx}/a_{yy}. Methods for compensating these so-called quadrantal bearing errors are discussed in a later section.

Survey data showing the coefficient a_{xx} and the maximum bearing error for loop antennas along the top and bottom center line of a DC–4 aircraft are shown in Fig. 27-14.

27.3. H-F COMMUNICATIONS ANTENNAS

Aircraft antennas for use with communications systems in the 2- to 25-Mc range are required to yield radiation patterns which provide useful gain in all directions significant to communications, and impedance and efficiency characteristics such that acceptable power-transfer efficiencies between the air-borne equipment and the radiated field are obtained. An antenna which meets these requirements will, when used in receiving, deliver to the input of a matched receiver atmospheric noise power under noise field conditions prevailing at most locations which is many times greater than the input-circuit noise in any communications receiver of reasonable design. When this is the case, no improvement in signal-to-noise ratio can be achieved by further refinement of the antenna design. Since the transmitting mode of operation poses the more stringent requirements, the remainder of the discussion of h-f antennas will be confined to the transmitting case. Sky-wave propagation is always an important factor at these frequencies, and because of the rotation of polarization which is characteristic of reflection from the ionosphere, polarization characteristics are usually unimportant; the effective antenna gain can be considered in terms of the total power density without regard to polarization. At frequencies below about 6 Mc, ionosphere (and ground) reflections act to make almost all the radiated power useful for communication at least some of the time, so that differences between radiation patterns are relatively unimportant in comparing alternative aircraft antennas for communication applications in the 2- to 6-Mc range. In this range, impedance matching and efficiency considerations dominate. For frequencies above 6 Mc, pattern comparisons are frequently made in terms of the average power gain in an angular sector bounded by cones 30° above and below the horizon.

In the 2- to 25-Mc range, most aircraft have major dimensions of the order of a wavelength and currents flowing on the skin of the aircraft usually dominate the impedance and pattern behavior. Since the airframe is a good radiator in this range, h-f antenna design is aimed at maximizing the electromagnetic coupling to the airframe. The airframe currents exhibit strong resonance phenomena that are important to the impedance behavior of antennas which couple tightly to the airframe.

Wire Antennas. Wire antennas, supported between the vertical fin and an insulated mast on the fuselage or trailed out into the air stream from an insulated reel on the underside of the fuselage, are commonly used and reasonably effective h-f antennas on lower-speed aircraft. Aerodynamic considerations limit the angle between a fixed wire and the air stream to about 15°, so that fixed-wire antennas yield impedance characteristics similar to moderately lossy transmission lines, with resonances and antiresonances at frequencies where the wire length is close to an

integral multiple of λ/4. Figure 27-15 shows the input impedance of an 81-ft fixed-wire antenna on a 1049 Constellation aircraft for two conditions of termination at the vertical fin: open-circuited and short-circuited. Lumped reactances connected between the wire and the fin produce an effect exactly analogous to reactance-terminated lossy transmission lines. The average directive gain of these antennas in the sector ±30° relative to the horizon (i.e., the fraction of the total radiated energy
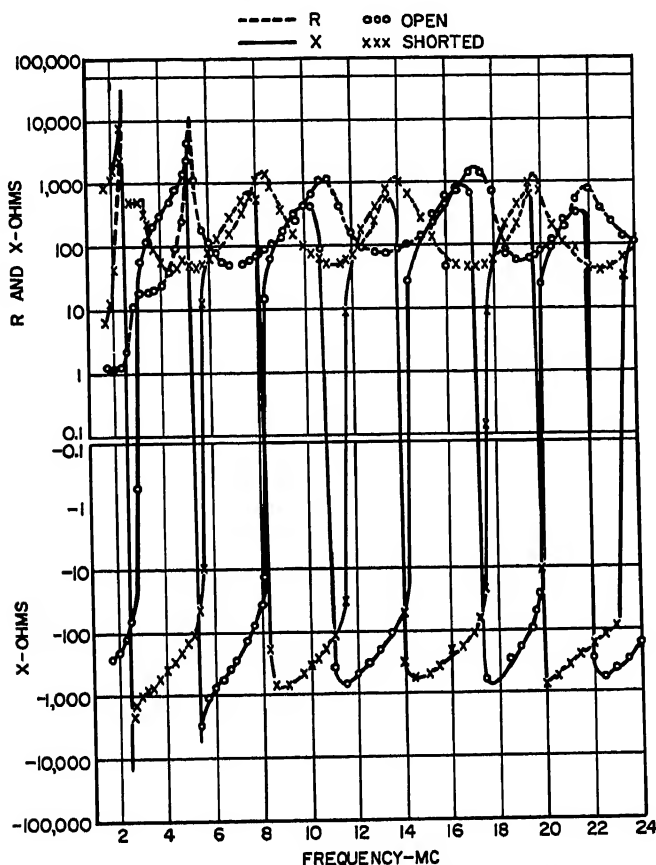
FIG. 27-15. Input impedance of 81-ft open and shorted fixed-wire antennas on 1049 Constellation aircraft.

which goes into the sector bounded by the cones 30° above and below the horizontal plane) remains near 60 per cent from 6 to 24 Mc. The efficiency of wire antennas is not high because of resistance loss in the wire itself and dielectric loss in the supporting insulators and masts. The resistance of commonly used wires is of the order of 0.05 ohm/ft at 4 Mc. The r-f corona breakdown threshold of fixed-wire antennas is a function of the wire diameter and the design of the supporting fittings. To minimize precipitation static a wire coated with a relatively large diameter sheath of polyethylene is frequently used, with special fittings designed to maximize the corona threshold. Even with such precautions, voltage breakdown poses a serious problem with fixed-wire antennas at high altitude. Measurements indicate that standard antistatic strain insulators have an r-f corona threshold of about 11 kv peak at an

altitude of 50,000 ft[1] and a frequency of 2 Mc.   Such an insulator, placed between the vertical stabilizer and the aft end of the open-circuited antenna in Fig. 27-15, would go into corona at this altitude if the antenna were energized with a fully modulated AM carrier of about 150 watts at 2 Mc.   Fixed-wire antennas are usually matched to the transmitter (or transmission line) with an L-section matching unit employing lumped series inductances and shunt capacitances.   At frequencies removed from the series resonance of the wire, the losses in the matching network may be quite high.   For
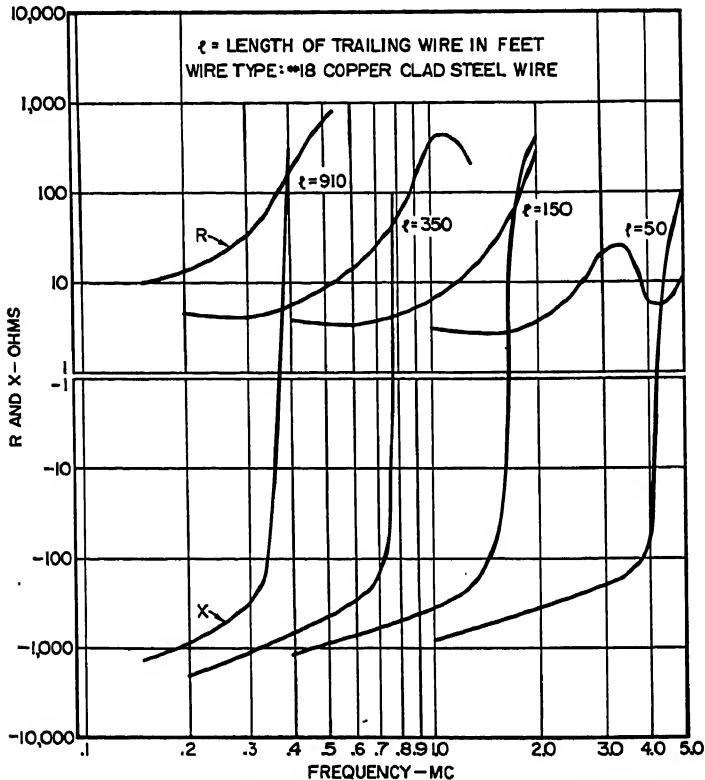
Fig. 27-16. Input impedance of trailing-wire antennas on B-29 aircraft.

example, using a tuning coil with a Q of 100, the matching network efficiency at 2 Mc for the open-circuited antenna of Fig. 27-15 will be less than 30 per cent.

Trailing-wire antennas are usually reeled out in flight to a length corresponding to series resonance in the $\lambda/4$ or $3\lambda/4$ mode at the operating frequency.   At ordinary flight speeds the angle of inclination to the air stream is small ($\sim 6°$) so that the proximity of the wire to the fuselage near the feed point has a marked effect on the physical length of the wire at resonance.   Figure 27-16 gives measured data for the input impedance through the first resonance for trailing wires of different lengths on a B-29 aircraft.[*] In all cases the trailing wire emerged from the fuselage just forward of the empennage, and the measured impedances include the effect of a 10-ft section of No. 10 wire spaced 3 in. from the aircraft skin.   The increase in resistance

* These data were measured by personnel of the Communication and Navigation Laboratory, Wright Air Development Center, United States Air Force.

with decreasing frequency for the shorter wire lengths is caused by losses in the insulating material which supports the trailing wire reel and in the fair-lead which spaces the antenna wire away from the aircraft skin at the point where the wire leaves the fuselage. The hump in the resistance curve for the 50-ft wire is caused by an airframe resonance. Efficient matching to a transmission line can be achieved by combining an adjustable wire length with an adjustable shunting capacitor at the feed point in a manner analogous to an L-section network.
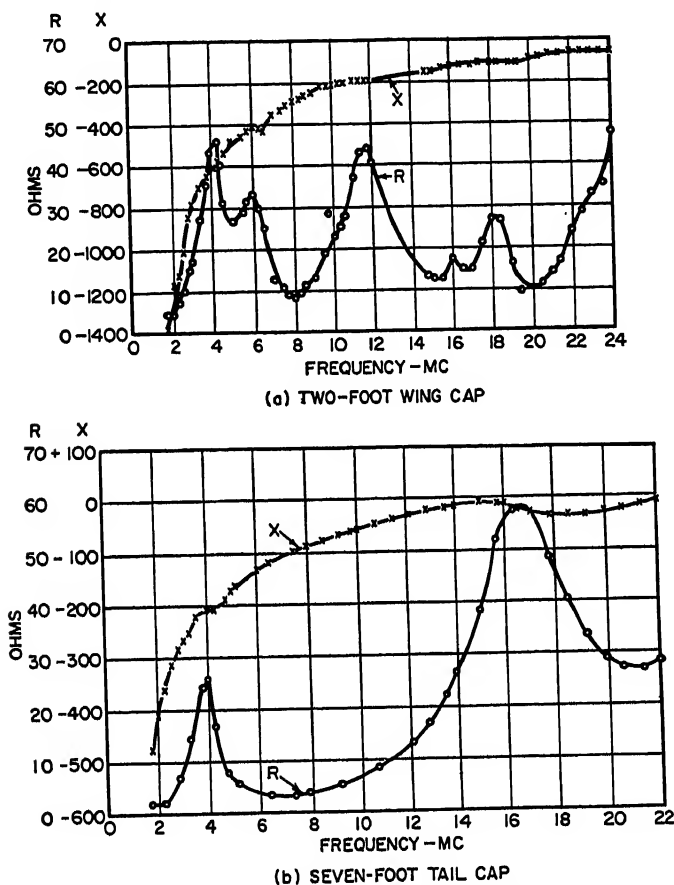
Fig. 27-17. Input impedance of cap antennas on DC-4 aircraft: (a) 2-ft wing cap. (b) 7-ft tail cap.

Isolated Cap Antennas. Effective excitation of the airframe as an h-f antenna can be obtained by electrically isolating a portion of the fin tip or a wing tip to provide antenna terminals. Figure 27-17 shows the impedance curves for a 2-ft wing-cap antenna and a 7-ft tail-cap antenna on a DC-4 aircraft. In each case the isolating gap was cut straight across the aircraft extremity and the gap width was 6 in. for the tail cap and 12 in. for the wing cap. The sharp peak of input resistance at 4 Mc is due to coupling to the λ/2 resonance of the currents on the airframe, which at this frequency flow predominantly along a path extending from the fin tip to the fuselage, thence to the wing root, and along the wings to the tips. This resonance dominates

the lower-frequency impedance characteristics of all cap-type antennas. The resistance peaks at higher frequencies are associated with resonance of other current paths on the wings and fuselage and, in the tail-cap cases, the empennage. The pattern characteristics of the two DC-4 cap antennas and a fixed-wire antenna on the same aircraft are summarized in Fig. 27-18, which shows the average gain over the useful
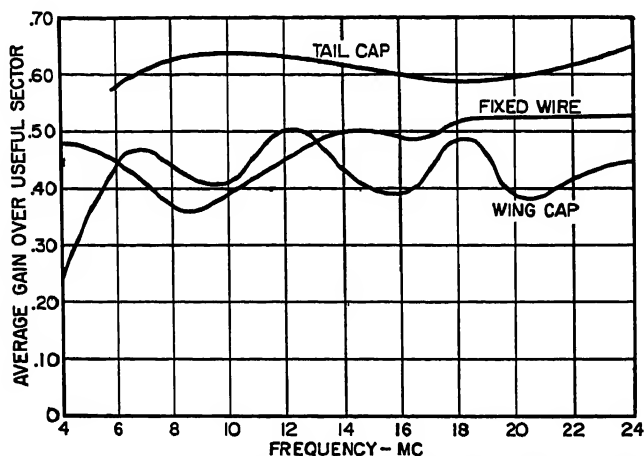
Fig. 27-18. Average gain over useful sector for various antennas on DC-4 aircraft.
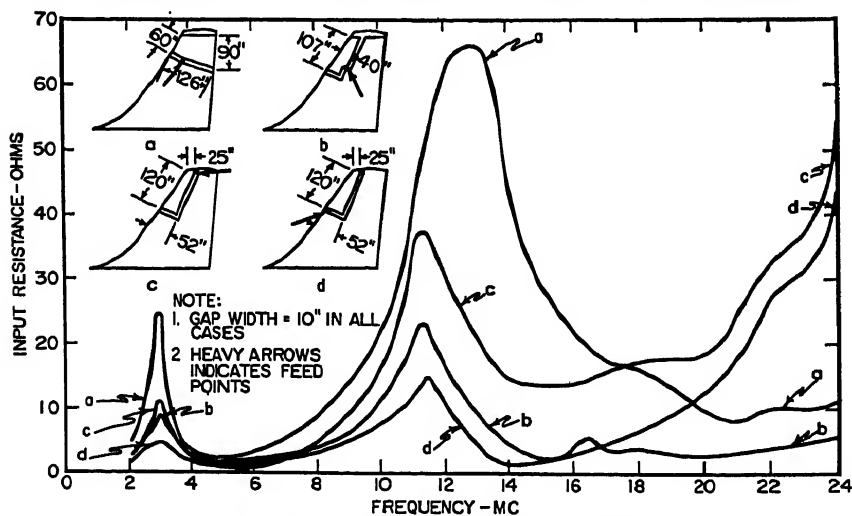
Fig. 27-19. Effect of changing feed configuration on input resistance of tail-cap antenna.

sector for each of these antennas as a function of frequency. The tail-cap patterns are often found to be superior to those for other possible antennas on the same aircraft, as is the case in this example.

The effect on input resistance of changing the feed configuration at a given airframe extremity is illustrated in Fig. 27-19, which shows the input resistance vs. frequency curves for various tail-cap feed configurations on a large jet aircraft.[2] In all cases, the resonant modes of the airframe are seen to govern the behavior of the input

resistance function. Configuration a, in which the isolated cap includes the entire stabilizer extremity, is seen to couple more effectively to the airframe resonant modes than the other configurations, in which only a part of the tip is isolated. The rising resistance values at 24 Mc for configurations c and d are caused by the fact that the isolating gap is approaching $\lambda/2$ in length at this frequency and is being fed near one end in each of these configurations.

The input-reactance curves for these antennas resemble those shown in Fig. 27-17 for the DC-4 tail-cap antenna except that the reactance actually becomes positive at the higher frequencies. Table 27-1 summarizes the salient features of the reactance curves for the configurations shown in Fig. 27-19.

Table 27-1. Summary of Reactance Data for Antennas in Fig. 27-19

Configuration	Reactance at 2 Mc, ohms	Frequency for which $X = 0$, Mc	Reactance at 24 Mc, ohms
a	−405	23.4	+ 2.1
b	−440	22.6	+ 4.6
c	−439	14.7	+112.0
d	−439	16.0	+ 82.1

The result of changing the design parameters of a cap antenna while retaining the same basic configuration may be summarized as follows. Increasing the size of the isolated cap while retaining the same gap width will decrease the low-frequency reactance and lower frequency of zero reactance; such a change will also increase the radiation resistance but will not change the frequencies at which the resonant peaks in the resistance curve occur. The percentage change in radiation resistance caused by a change in cap size is usually much smaller than the corresponding change in reactance. Decreasing the width of the isolating gap while keeping the cap size fixed produces the same result as would be produced by adding a shunt capacitance across the antenna terminals, namely, a reduction in both R and X.

In the design of a cap-type antenna, the choice of cap size, configuration, and gap width is based upon a compromise between electrical and structural factors. The operationally significant electrical factors are the radiation efficiency and the corona threshold of the antenna system. Since both of these quantities pose design problems which rapidly become more difficult as frequency is decreased, the choice of antenna dimensions is almost* invariably based on conditions at 2 Mc (i.e., the low end of the h-f band). The low-frequency equivalent circuit of the antenna and matching unit is shown in Fig. 27-20. The radiation efficiency of the system is given by the product of the matching-circuit efficiency and the antenna efficiency; i.e.,

$$\eta = \eta_A \eta_M$$

where

$$\eta_A = \frac{G_r}{G_r + G_l}$$

and η_M is given by the graph in Fig. 27-21 for the case of a matching circuit with a coil Q of 100 and a capacitor dissipation factor of 0.001. The values of antenna resistance and reactance used to enter the graph in Fig. 27-21 include the effect of the dielectric loss conductance G_l in the antenna. It should be noted, therefore, that

---

* An exception arises in some cases on large aircraft for which the lowest-frequency resonant peak in radiation resistance occurs at or near 2 Mc. In such cases a more stringent design frequency is usually found to occur at the resistance minimum above the first resonant peak.

while increasing G_ℓ will always result in a lower system efficiency, the decrease in system efficiency will not be as great as the decrease in η_A. This follows since an increase in G_ℓ will decrease the matching-circuit losses and hence increase η_M.

The value of G_ℓ is given by the formula

$$G_\ell = \frac{G_0 P}{W}$$

where G_0 is the conductivity of the insulating material in mhos per square, and P and W are the peripheral length and the width of the isolating band, respectively. Minimizing G_ℓ hence requires a careful selection of insulating material as well as

G_r = RADIATION CONDUCTANCE
C_A = ANTENNA CAPACITANCE
G_ℓ = LOSS CONDUCTANCE OF INSULATING BAND
L,Q = INDUCTANCE AND QUALITY FACTOR OF MATCHING
         UNIT INDUCTOR
C,D = CAPACITANCE AND DISSIPATION FACTOR OF
         MATCHING UNIT CAPACITOR.
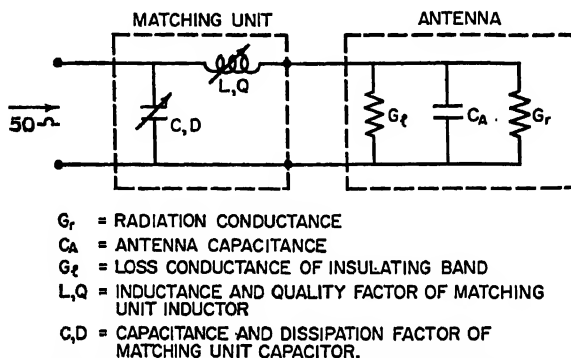
FIG. 27-20. Low-frequency equivalent circuit of cap antenna and matching unit.

control over the dimensions of the insulating band. Extensive studies[8] of the electrical and mechanical properties of Fiberglas-reinforced laminated plastics, particularly with regard to their stability under the severe environmental conditions encountered on aircraft, indicate that such materials may be designed to provide insulating bands with extremely low values of G_0, but only if great care is exercised in controlling their fabrication.

Radio-frequency corona limitations are found to require gap spacings of something less than 12 in. in most cases where power levels of the order of 100 watts and maximum altitudes of the order of 50,000 ft are involved. It is necessary to maintain the radii of curvature of metal contours, particularly near the trailing edge of the airfoil section, at about ⅜ in. or more to avoid corona in these regions. Small sharp points, such as fabricating burrs and the edges of fasteners, usually do not affect the r-f corona breakdown threshold at high altitudes, because of the space-charge shielding that results from the relatively low mobility of the initial ionization.[1]

Shunt-fed Antennas. Various portions of an airframe can be shunt-fed as h-f antennas, using the technique indicated in Fig. 27-22. These arrangements do not require dielectric sections in the main-structure members of the airframe, and thus offer an advantage over cap antennas. However, efficient shunt feed over a wide frequency range requires an auxiliary conductor along a considerable portion of the leading or trailing edge of an airfoil surface, regions which are normally occupied by control surfaces or de-icing equipment. Shunt-feed systems can usually be arranged to present an inductive-input reactance over their entire frequency range, which is useful from the standpoint of minimum matching-circuit loss. Two possible shunt-feed arrangements on a 1049 Super Constellation aircraft are sketched in Fig. 27-23. One arrangement employs a 30-ft conductor along the inboard trailing edge of one wing, and the other a conductor along the entire leading edge of one horizontal

stabilizer. Input-impedance data for the shunt-fed wing antenna are shown in Fig. 27-24. The feed-conductor diameter is 0.875 in., and the width of the dielectric spacer between the feed conductor and the airfoil section is 17 in. The secondary peak in the resistance curve near 4 Mc is due to resonance of the wing-fuselage-fin
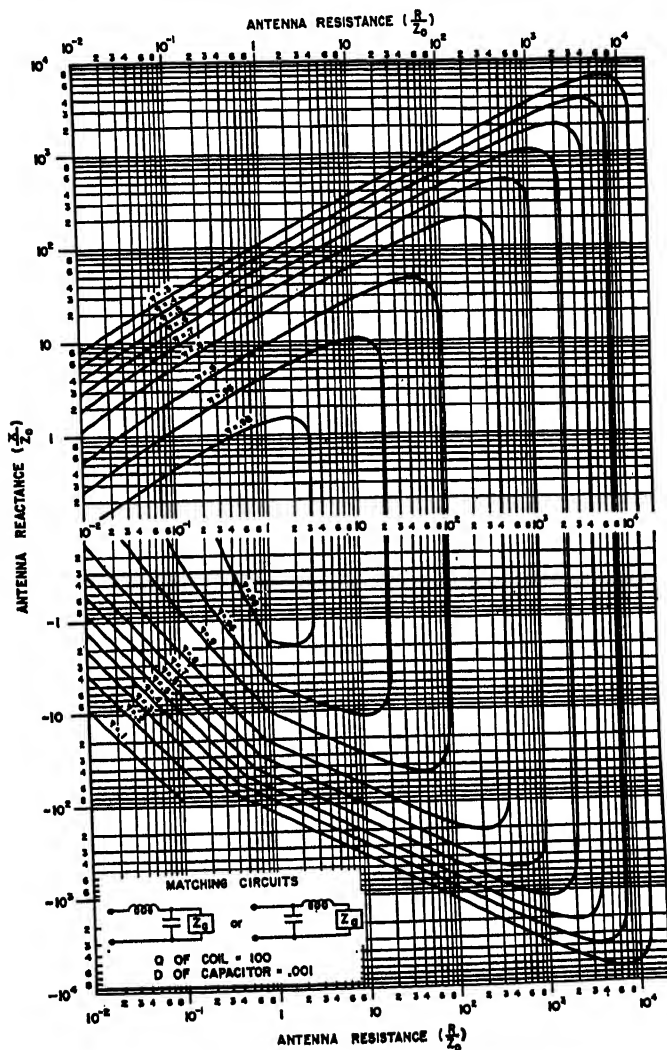
FIG. 27-21. Matching-circuit efficiency.

current mode mentioned in connection with the discussion of cap antennas in the previous section. Changing the feed-conductor diameter from 0.875 to 3.5 in. in the wing installation has a negligible effect on the input impedance. Major changes in the impedance occur with changes in the length of the shunt-feed conductor. By providing one or more shorting relays along the length of the shunt-feed element and suitably interconnecting these with the matching unit, it is possible to achieve the advantage of the strong coupling to the airframe provided by a long conductor at the
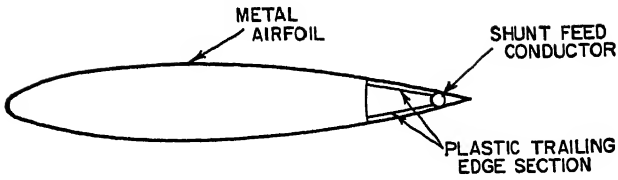
FIG. 27-22. Shunt-feed technique.
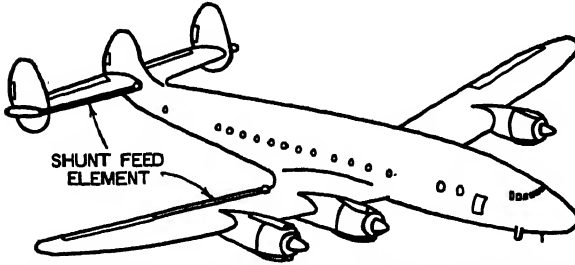
FIG. 27-23. Shunt-feed arrangements on 1049 Constellation aircraft.
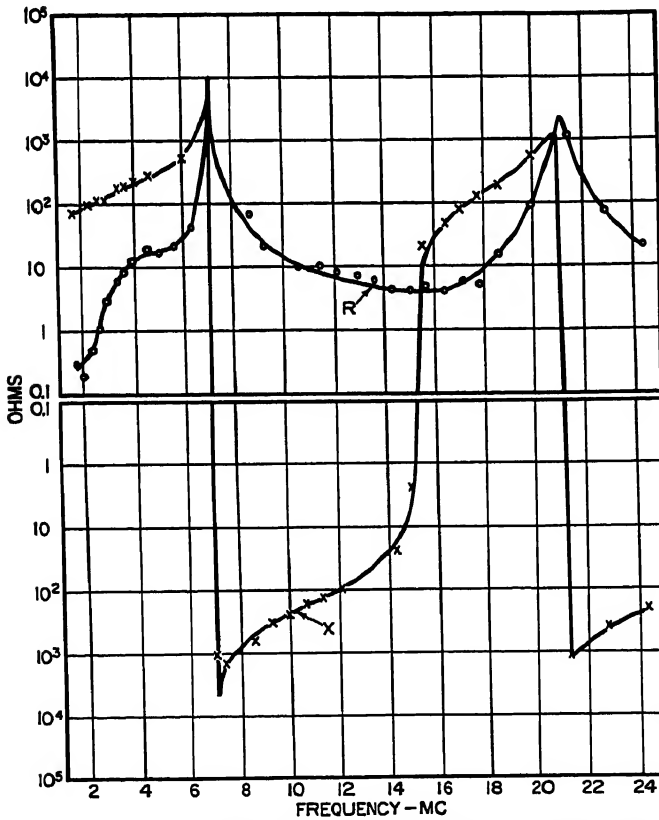
FIG. 27-24. Input–impedance characteristic achieved with 30-ft shunt-feed element at inboard trailing edge of wing in 1049 Constellation aircraft.

lower frequencies while retaining a positive input reactance to the antenna throughout the frequency range.   With a positive input reactance, matching to the feed line can be obtained with an all-capacitance L-section network, a situation favorable to high matching efficiency.

Other possible shunt-feed arrangements adapted to flush mounting employ notches cut into the wing-root or dorsal-fin areas where structural loads are small.   The notch can be fed directly across its open end, or a coupling loop can be mounted in the notch.   Because the coupling of these structures to the radiating airframe currents is relatively low, the input resistance is low compared with the input reactance, which makes efficient impedance matching difficult.   The notch feed appears to offer promise on very large aircraft where the notch can be made quite large and airframe resonances occur near the low end of the frequency band of interest.   The radiation pattern of the notch antenna tends to become rather directional at the higher frequencies of the h-f band, however, particularly when the notch is located at the intersection of the fuselage and the wing trailing edge.

27.4. ADF ANTENNA DESIGN REQUIREMENTS

The ADF loop antenna is normally supplied as a component of the ADF system, and the problem of the aircraft-antenna designer with respect to the loop is to find a suitable location for it on the airframe.   The two restrictions which govern his selection of a location are (1) the cable between the loop antenna and receiver is of fixed length since the loop and cable inductances form a part of the resonant circuit in the loop amplifier input; and (2) the maximum bearing error which the system can compensate is limited to about 20°.   As can be seen from the bearing-error data in Fig. 27-14 positions on the bottom of the fuselage forward of the wing meet the minimum bearing-error requirements on the aircraft type for which the data are applicable (and on other comparable aircraft also).   Such positions are consistent with cable-length restrictions in most cases since the radio-equipment racks are usually just aft of the pilot's cabin.

Bearing-error compensation is accomplished in most ADF systems by means of a mechanical compensating cam which causes the synchro used to transmit angular loop-position information to the bearing indicators in the aircraft to turn at a varying rate as the loop is rotated at a uniform rate.[4,5]   Standard flight-test procedures[4] are generally used in setting the compensating cams, although laboratory tests are sometimes used for this purpose also.[6]   In some loop designs[7] electrical compensation is achieved by means of modifications of the immediate environment of the actual loop element in order to equalize the coefficients a_{xx} and a_{yy}.

Unlike the loop, the sense antenna must be located within a limited region of the airframe for which the equivalent-dipole axis is essentially vertical in order to ensure accurate ADF performance as the aircraft passes over or near the ground station to which the receiver is tuned.[8]   In Fig. 27-25 are shown the regions of confusion which exist above the ground station for an airborne ADF having a nonvertical sense-antenna pattern.   The significance of these confusion zones is that the ADF needle attempts to reverse, and hence to indicate a bearing which is in error by 180° when the aircraft is within the zone.   The intersection of the confusion zone with a surface of constant altitude is a circle; various types of needle behavior for different amounts of course offset at the same altitude are illustrated in Fig. 27-25.   Actually, the needle has a finite reversal time so that the responses to the various reversal signals it receives as the aircraft traverses a flight path near the station become superimposed to an extent which depends upon the aircraft altitude and speed as well as the sense-antenna tilt angle.   As a result, it is virtually impossible for the pilot to make an accurate determination of the time of station passage unless the confusion zone is made quite small.

The size of the zone is dependent upon another parameter also, namely, the phase difference between the loop and sense signals at the point where they are mixed in the receiver. It can be shown[8] that by introducing a controlled phase error of the proper sense at this point, the size of the confusion zone may be reduced very substantially, thereby relaxing the requirement for proper sense antenna placement. Existing ADF receivers do not incorporate this feature, however, and hence a small sense antenna

PLAN VIEW
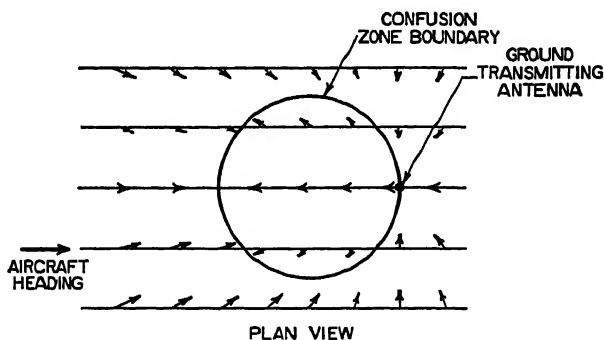
NOTE: SMALL ARROWS SHOW DIRECTIONS WHICH ADF NEEDLE
TRIES TO INDICATE AT VARIOUS POINTS ALONG A GROUP
OF PARALLEL, COPLANAR FLIGHT TRACKS

ELEVATION VIEW
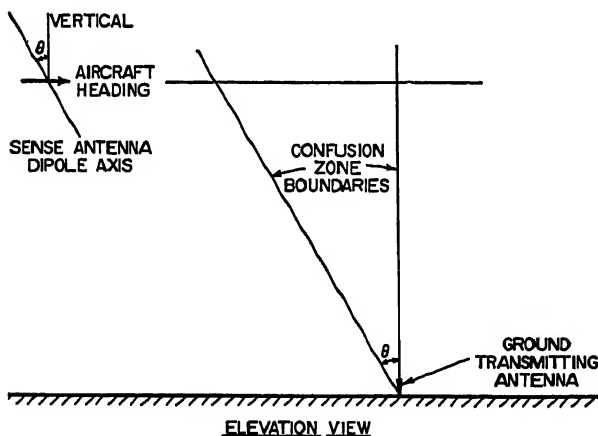
NOTE: ANGLE BETWEEN CONFUSION ZONE BOUNDARIES
IS EQUAL TO SENSE ANTENNA TILT ANGLE

FIG. 27-25. ADF overstation confusion zone.

tilt angle is usually a design requirement. The importance of maintaining sufficient sense signal input to the ADF receiver is illustrated in Fig. 27-26, which shows the estimated operating range of the MN-62 receiver under different conditions as a function of the sense antenna sensitivity product* (product of effective height times antenna capacitance). It is assumed in these estimates that the sum of the sense antenna capacitance and the sense cable capacitance is maintained at 270 $\mu\mu$f, which is the value with which this receiver is designed to operate.

A value for the total capacitance of the antenna and cable is the usual form of

* The sensitivity product is used here as a criterion of performance which correlates roughly with the antenna size.

"impedance" specification on l-f airborne antennas. The reason for this may be seen with reference to Fig. 27-27, which shows the input circuits used in representative l-f airborne receivers, including the sense input circuit of a typical ADF receiver, the susceptiformer input circuit,* and the input circuit of a typical l-f range receiver designed for use in small aircraft where a wide variation in antenna and cable capacitance may be expected from one aircraft type to another. The circuits are analyzed most readily by replacing the various capacitors and transformers to the left of the
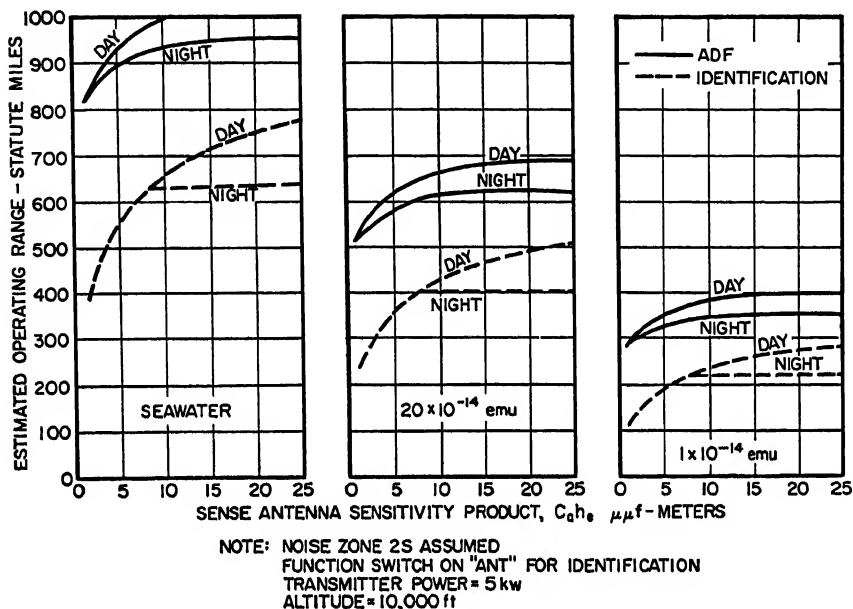
FIG. 27-26. Estimated operating range for ADF and identification functions of MN-62 receiver at 600 kc.

tuning inductance L in each case by an equivalent Thevenin generator as shown in Fig. 22-27d. The object in the design of an l-f input circuit of this type is to make the source capacitance C_R of the Thevenin generator sufficiently high that the frequency range tuned by a given variation in C_T is not greatly reduced and (in the case of the ADF circuits) sufficiently insensitive to variations in C_A and C_C that the circuit is not detuned by normal service variations in these quantities. Values of C_R of the order of 3,000 $\mu\mu f$ are typical with this type of receiver. The relative effectiveness of the different types of input circuits can be shown through a simple graphical construction whereby one may calculate the value of h'_o, the open-circuit voltage of the equivalent Thevenin generator. To do this, one notes that by plotting voltage as ordinate and capacitance as abscissa on a log-log graph, the effect of such elements as series or shunt capacitors or transformers may be represented as straight-line transformations. Figure 27-28 is a plot of the transformations involved in the circuits of Fig. 27-27a-c, assuming an antenna capacitance of 50 $\mu\mu f$ and a value of C_R of 3,000 $\mu\mu f$. To perform such an analysis, one first plots the point corresponding to C_A and Eh_o (taken as unity in this example). Each element in the circuit is considered in sequence, moving to the right in the circuit diagram, and the open-circuit

* Proposed by H. A. Ferris of Trans Canada Air Lines as a means for overcoming the loss of signal due to long sense cables on large aircraft.

voltage and source capacitance which would be obtained for the circuit up to that point are plotted. A shunt capacitor has the property that its addition leaves the produce $h'_s C_R$ unchanged. Addition of a shunt capacitor hence leads to a transformation to the right and downward along a $-45°$ slope on the graph. The length of the straight line is just that required to make the values of C_R at its end points differ by the value of the shunt capacitor. A transformer produces a similar transformation except that in this case the product $h'_s \sqrt{C_R}$ is unchanged by its addition. A
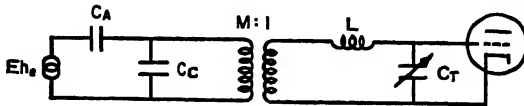
(a) CONVENTIONAL SENSE INPUT CIRCUIT
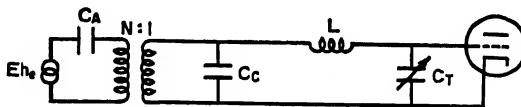
(b) SUSCEPTIFORMER INPUT CIRCUIT
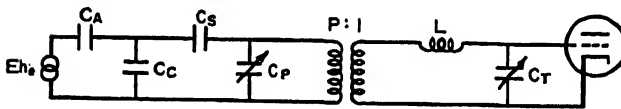
(c) RANGE RECEIVER INPUT CIRCUIT
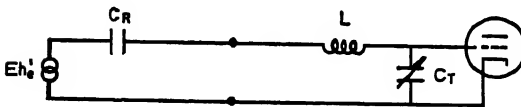
(d) EQUIVALENT CIRCUIT

NOTE: C_A = ANTENNA CAPACITANCE
C_C = CABLE CAPACITANCE
C_T = TUNING CAPACITANCE

FIG. 27-27. Typical input-circuit configuration for airborne l-f receivers.

step-down transformer is hence represented on the graph by a line with a $-22.5°$ slope and having a final value of capacitance which is equal to the square of the turns ratio times the initial capacitance. Finally, a series capacitance causes a transformation to the left along a horizontal line, since the series capacitance does not change the open-circuit voltage but does decrease the source capacitance.

The curves in Fig. 27-28 have been drawn for typical values of the circuit parameters for the three input-circuit configurations discussed above, and they show the superiority of the susceptiformer over the others in delivering signal to the receiver. Of equal significance is the fact that the susceptiformer circuit operates with a total cable capacitance of 1,200 $\mu\mu f$ while the conventional circuit allocates only 220 $\mu\mu f$ to cable capacitance. This means that the susceptiformer can be used with longer
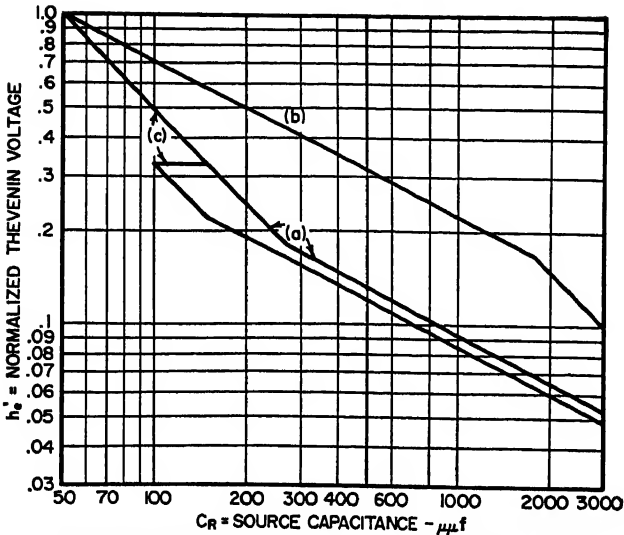
Fig. 27-28. Graphical calculation of circuit performance.
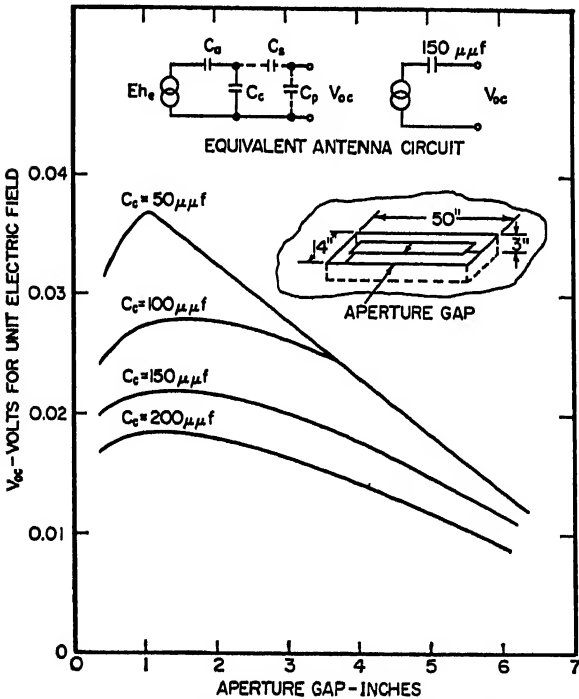
Fig. 27-29. Optimization of antenna dimensions.

cable runs and can employ more rugged cable than does the conventional circuit.* It is of interest to note, however, that the susceptiformer requires greater stability of antenna capacitance than does the conventional circuit.⁹

A knowledge of the characteristics of input circuits is important to the antenna designer since he will wish to optimize the antenna configuration within the space available. For example, Fig. 27-29 shows the relative performance of the antenna in Fig. 27-7 as a function of the aperture gap when this antenna is used in a conventional sense input circuit designed to work with a 150-$\mu\mu f$ value of $C_A + C_C$.

NOTE: C_P ADJUSTED TO MAKE SOURCE CAPACITANCE = C_0
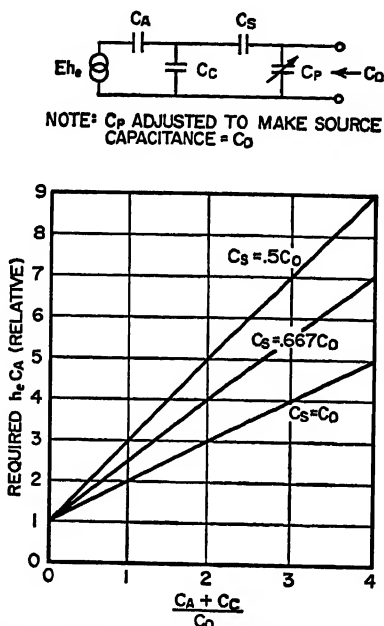
FIG. 27-30. Relative antenna-sensitivity requirement for range receiver.

Since this value is fixed by the receiver design, it is necessary to use either a series or shunt capacitor at the sense cable terminal to achieve proper performance, except when the actual value of $C_A + C_C$ is correct. These curves show that a rather broad maximum exists when the antenna is to be used with a high-capacitance cable but that the maximum is sharply defined when the cable capacitance is low. They also show the substantial price paid with the conventional input circuit when it is necessary to use long, and hence high-capacitance, cable runs.

In the range-receiver input circuit (Fig. 27-27c) the value of C_s and the range of values of C_p are chosen so that the source capacitance of the network feeding the transformer primary can be set to the desired value by adjusting C_s, regardless of the values of C_A and C_C.† The curves in Fig. 27-30 show how the required sensitivity product ($h_e C_A$) of the antenna increases with increasing $C_A + C_C$ for different values of the series capacitor C_s, assuming that the signal delivered to the first tube grid is to be held constant. The reference value of $h_e C_A$ (i.e., the unity value corresponding to

* When long cable runs are to be used, it is necessary to consider the cable as a transmission line rather than as a shunt capacitor as has been done here. The more general solution does not lead to any significant changes in the results discussed here, however.

† This requires simply that $C_{p,max} = C_s + C_{p,min} = C_0$, where C_0 is the required source capacitance.

zero abscissa) is the same as the value which would be required if C_s were short-circuited.   If this were done, it would be possible to adjust the source capacitance to C_0 by means of C_p only if $C_A + C_C < C_0$.   The very considerable increase in $h_e C_A$ requirement to which the addition of C_s leads is apparent from these curves.   Here again it is seen that the use of long high-capacitance cable runs greatly increases the antenna sensitivity requirement.

27.5. UNIDIRECTIONAL VHF ANTENNAS

The marker-beacon, glide-slope, and radio-altimeter equipments require relatively narrow band antennas with simple patterns directed down or forward from the aircraft.   This combination of circumstances makes the design of these antennas a relatively simple problem.   Both flush-mounted and external-mounted designs are available in several forms.
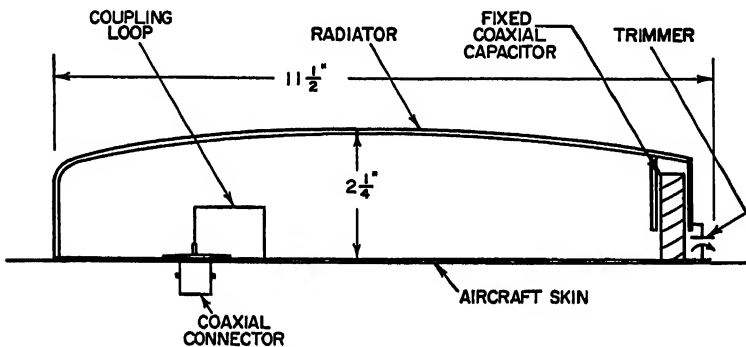
(a) SCHEMATIC OF THE COLLINS 37X-I MARKER BEACON ANTENNA
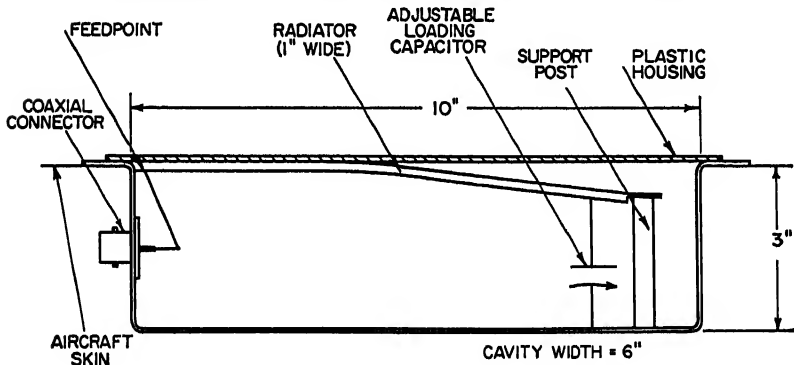
(b) SCHEMATIC OF THE ELECTRONIC RESEARCH INC.
AT-I34/ARN FLUSH MARKER BEACON ANTENNA

FIG. 27-31

Marker-beacon Antennas.   The marker-beacon receiver operates on a fixed frequency of 75 Mc and requires a downward-looking pattern polarized parallel to the axis of the fuselage.   A standard external installation employs a balanced-wire dipole supported by masts.   The masts may be either insulated or conducting.   In some installations one of the masts is the stub used for VHF communications.   Low-drag and flush-mounted designs are sketched in Fig. 27-31.   The low-drag design is a

simple vertical loop oriented in the longitudinal plane of the aircraft, 11.5 in. long by 2.2 in. high. The feed line is inductively coupled to the loop, which is resonated by a series capacitor. The antenna elements are contained in a streamlined plastic housing, yielding a drag of 3.5 oz at 400 mph. The flush design is electrically similar, but in this case the structure takes the form of a conductor set along the longitudinal axis of the open face of a 10- by 6- by 3-in. cavity. To achieve the desired impedance level, the antenna conductor is series resonated by a capacitor and the feed point tapped part way along the antenna element.

Glide-slope Antennas. The glide-slope receiver covers the frequency range 329 to 335 Mc and requires antenna coverage only in an angular sector 60° on either side of the nose and 20° above and below the horizon. This requirement is relatively easily met by horizontal loops or by vertical slots. Because of the narrow bandwidth, the antenna element need not be large compared with the wavelength. Two variations on the loop arrangement are sketched in Fig. 27-32. Configuration *a*, which is the widely used Collins 37-P antenna, can be externally mounted on the nose

FIG. 27-32. Protruding glide-slope antennas.
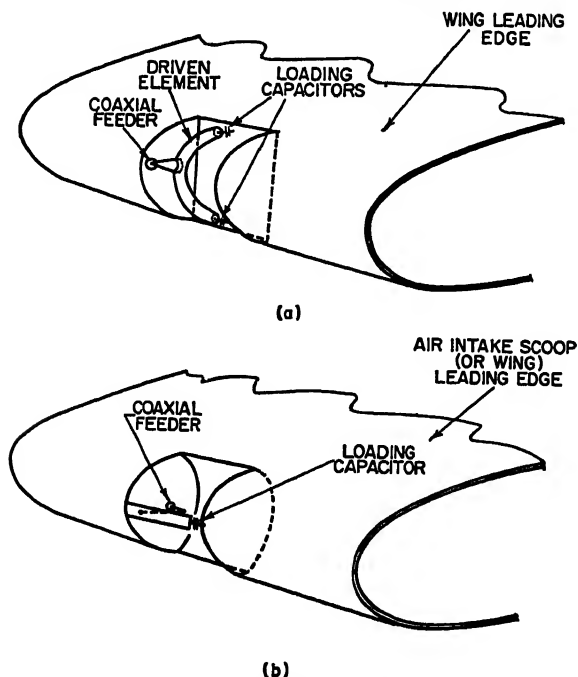
FIG. 27-33. Flush glide-slope antennas.

of the aircraft or, if drag is important, within the nose radome.   It is a simple series-resonant half loop.   Antenna *b* is suitable for either external or flush mounting. Its principle of operation is essentially similar to the cavity-marker-beacon antenna of Fig. 27-31.
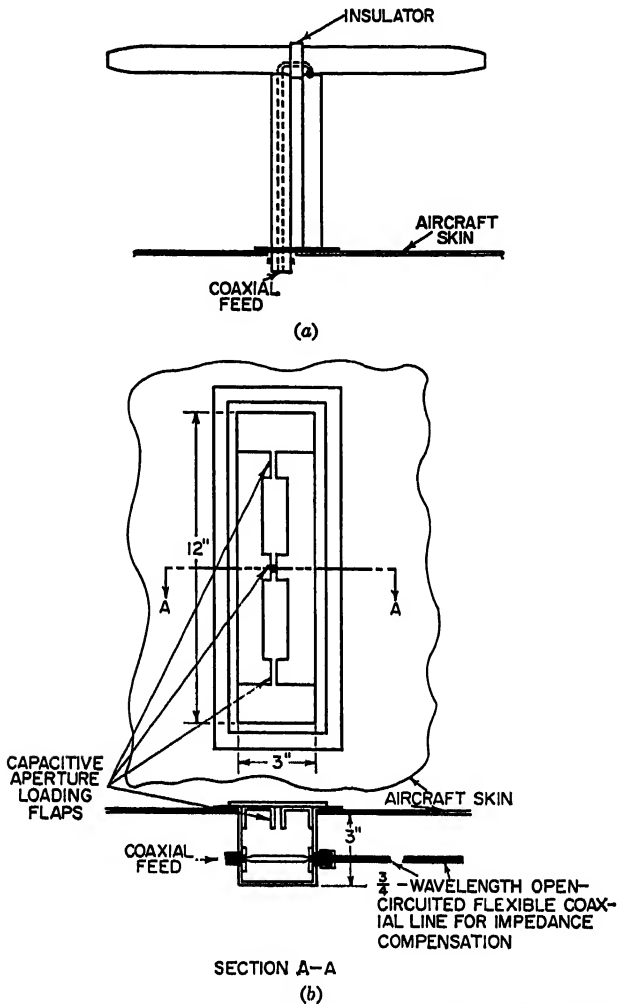
Fig. 27-34. Radio-altimeter antennas: (*a*) Dipole-type element.   (*b*) Loaded-slot element.

Two slot arrangements are sketched in Fig. 27-33.   Antenna *a* employs a simple linear slot wrapped around the leading edge of the wing.   The slot is center-fed through a capacitively loaded bar.   The slot length is adjusted to yield a suitable input resistance, and the resulting positive slot reactance is resonated by the capacitor. Antenna *b* is designed for installation in the edge of the air-intake scoop on a jet fighter and also employs a matching scheme similar to that of the cavity marker-beacon antenna.

Altimeter Antennas. The radio altimeter, which operates in the frequency range 400 to 440 Mc, requires independent downward-looking antennas for transmission and reception. Proper operation requires a high degree of isolation between the transmitting and receiving elements. In the usual installation, externally mounted horizontal dipoles are used, located on the bottom fuselage center line and polarized parallel to it. If the antennas are carefully designed to minimize unbalanced current flow on the supporting vertical structure, center-to-center spacings of several feet will provide the required degree of isolation. A typical dipole unit is illustrated in the sketch of Fig. 27-34a. A downward directive gain of 7.5 db relative to an isotrope is achieved by virtue of the array factor corresponding to the dipole and its image in the surface on which it is mounted.

Figure 27-34b illustrates a loaded slot element useful for this application when flush mounting is required.[10] To achieve directive gain equivalent to the dipole installation, an array using two slots, driven in phase, and spaced 14 in. is required. For minimum coupling, the two-slot arrays are oriented along, and parallel to, the longitudinal axis of the aircraft. Because of the different phasing of the radiating components in the dipole and slot cases, the slot installation requires greater separation for the required isolation. In many installations, the separation required for the slot installation described is impractically large, and it is necessary to locate the arrays so as to take advantage of the additional shielding afforded by some component of the airframe, e.g., the fuselage, when the antennas are mounted on the underside of the horizontal stabilizer on either side of the airframe.

27.6. OMNIDIRECTIONAL VHF AND UHF ANTENNAS

In the frequency range where the principal dimensions of the airframe are many times the wavelength, the design of antennas requiring omnidirectional patterns,

such as those used for short-range communications, is enormously complicated by effects due to the airframe. Since antennas of resonant size are small enough to be structurally feasible, the required impedance characteristics can usually be achieved with fixed matching networks without serious difficulty. Shadowing and reflection by the airframe, on the other hand, result in major distortions of the primary pattern of the radiating element.

Airframe Effects on VHF and UHF Patterns. The tip of the vertical fin is a preferred location for omnidirectional antennas in the VHF and UHF range because antennas located there have a relatively unobstructed "view" of the surrounding sphere. Figure 27-35 shows the principal plane patterns of a $\lambda/4$ stub on the fin tip of a B-50 aircraft at 1,000 Mc. At this frequency, where the mean chord of the fin is 10 wavelengths, the principal effect of the airframe on the radiation patterns is a sharply defined shadow region, indicated by the dashed lines in the figure. At the lower end of this frequency range, and on smaller aircraft, the effect of

FIG. 27-35. Principal-plane patterns of 1,000-Mc stub antenna on tip of vertical stabilizer of B-50 aircraft.

the airframe on the patterns is more complicated. Figure 27-36 shows the principal plane patterns of a $\lambda/4$ stub on the fin tip of an F-86 aircraft at 300 Mc. The deep nulls in the forward quadrants are due to the destructive interference between direct radiation and radiation reflected from the fuselage and wings. The latter contribution

is more important than in the case of Fig. 27-35 since the ground plane formed by the surface of the fin tip is now sufficiently small to permit strong "spillover" of the primary

VERTICAL STUB ON
TAIL OF TYPICAL FIGHTER
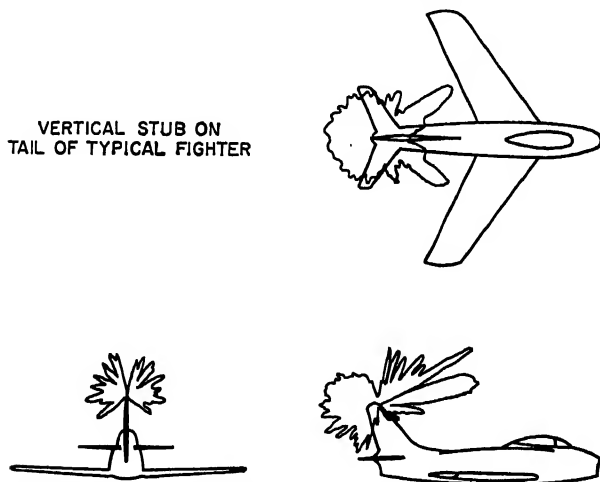
FIG. 27-36. Principal-plane patterns of 300-Mc stub antenna on tip of vertical stabilizer of fighter aircraft.

pattern, which accounts also for the lobing in the transverse-plane pattern. In this part of the frequency range the null structure is strongly influenced by the position of the radiating element along the chord of the fin, and careful location of the antenna along the chord may result in improvements in the signal strength at the forward horizon by 10 to 15 db. Chokes designed to minimize current flow on the fin have been used successfully to minimize pattern degradation of this type. Such measures are limited to relatively narrow bandwidth systems, however.

Most external antennas are located on the top or bottom center line of the fuselage in order to maintain symmetry of the radiation patterns. Pattern coverage in such locations is sharply limited by the shadows cast by the airframe. Figure 27-37 shows the patterns of a 1,000-Mc monopole on the bottom center line of a B-50 aircraft. It is apparent that coverage is limited to the hemisphere below the aircraft. UHF antennas on the top of the fuselage yield patterns confined to the upper hemisphere, with a null aft due to the shadow cast by the vertical fin. In many applications, as for example in scheduled airline operations, these pattern limitations are acceptable and fuselage locations are frequently used.

The deep lobing in the transverse-plane pattern of Fig. 27-37 is due to reflections from the strongly illuminated engine nacelles. In some locations similar difficulties are encountered because of reflection from the wing flaps when they are extended. Shadows and lobing due to the land-

FIG. 27-37. Principal-plane patterns of 1,000-Mc stub antenna on belly of B-50 aircraft.

ing gear, when extended, are frequently troublesome for bottom-mounted antennas. One of the most serious of the airframe effects is propeller modulation. Over wide

portions of the VHF and UHF, spectrum signals reradiated from the propellers will combine with the direct signal to produce a modulation of the received signal at the various harmonics of the blade-passage frequency (i.e., the rotational frequency of the propeller times the number of blades). An example of rotor-modulation effects on helicopters is discussed later in this section.

Antennas for Vertical Polarization. The simple monopole is the most commonly used vertically polarized VHF and UHF antenna for aircraft. For the 100- to 156-Mc range, the AN-104B is widely used. This is a simple tapered vertical mast with an airfoil cross section to minimize drag. The radiating element is 21 in. long, 1.25 in. wide, and 3.5 in. deep and is formed by copper plating over resin-impregnated wood. The drag is 2.75 lb at 350 knots. A simple shunt-stub matching network yields a VSWR below 2:1 from 100 to 150 Mc.

Figure 27-38 shows a modified mast developed by the late J. P. Shanklin. This configuration is formed as if the upper portion of the AN-104B blade just described
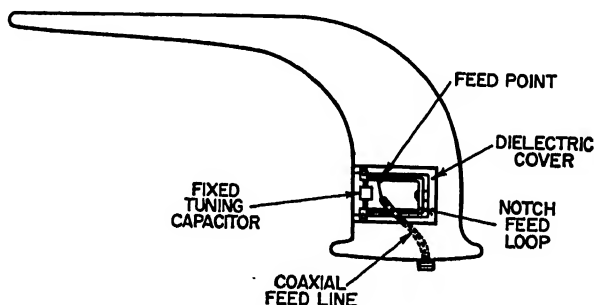
FIG. 27-38. Construction of Collins 37-R-1 antenna.

had been drawn back until it lay parallel to the airframe. This reduces the aerodynamic drag. The structure shown differs from the AN-104B also in that it is shunt-fed; that is, the main body of the antenna is bonded directly to the aircraft at the base, and excitation is by way of a notch, cut approximately halfway through the base of the antenna and resonated with a fixed capacitor. The feed cable is tapped across the notch feed loop at an appropriate point. The VSWR is below 1.4:1 over the 118- to 136-Mc band. The shunt-feed arrangement yields a structure which is very strong mechanically and is virtually impervious to damage by lightning strikes. The bent arrangement reduces the drag but gives an omnidirectional vertically polarized pattern with a low (0.6-db) cross-polarized component.

Figure 27-39 shows a sleeve monopole for the 225- to 400-Mc UHF communications system, which is designed to yield a low aerodynamic drag. The cross section is diamond-shaped, with a thickness ratio of 5:1. A unique feature of this antenna[11] is the introduction of a shunt stub into the impedance-compensating network in such a fashion that the inner conductor of the stub serves as a tension member to draw the two halves of the antenna together. In addition to providing mechanical strength, this inner conductor also forms a d-c path from the upper portion of the antenna to the aircraft skin, thereby protecting the radio equipment with which it is used from lightning strikes.

A number of monopole designs have been developed for the fin-tip location, intended for installation on a fin in which the top portion of the metal structure has been removed and replaced by a suitable dielectric housing. Figures 27-40 and 27-41 show two forms of the "partial-sleeve" monopole, consisting of a driven element and two short parasites, which provide excellent impedance characteristics in a simple lightweight structure.[12] Figure 27-40 gives some basic design data for this type of

antenna, and Fig. 27-41 shows a UHF antenna of this type* which provides a VSWR of less than 1.8 between about 200 and 420 Mc. Various other forms of vertically polarized UHF and VHF radiators have been designed for tail-cap installation. The pickax antenna, consisting of a heavily top-loaded vertical element, has been designed
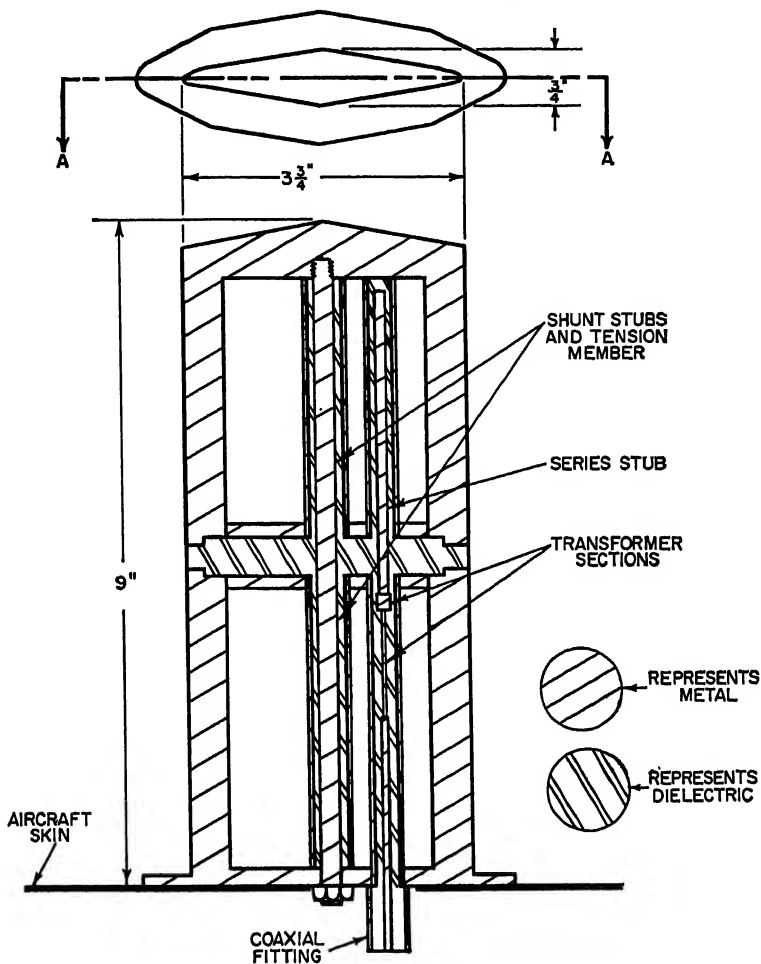
SECTION A–A
Fig. 27-39. AT-256A antenna.

to provide a VSWR of less than 3 from 110 to 155 Mc with an over-all height of 15½ in. and a length of 14 in. Very broadband tail-cap antennas which will cover both the VHF and UHF communication bands have been designed also. Such antennas, which are usually adaptations of the biconical antenna configuration modified to fit into a relatively long and narrow plastic housing, normally suffer from a degradation in their primary radiation pattern at the higher frequencies in their band.

* Designed by the Boeing Airplane Company.
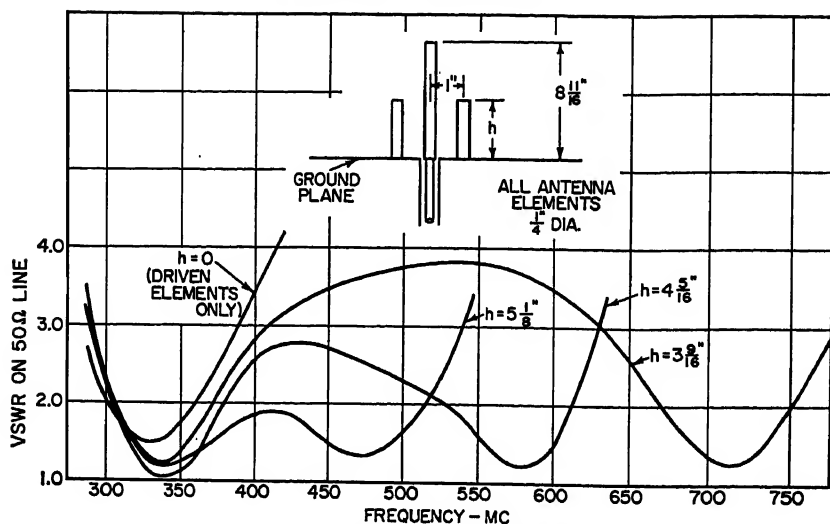
FIG. 27-40. Design data for simple open-sleeve antenna.
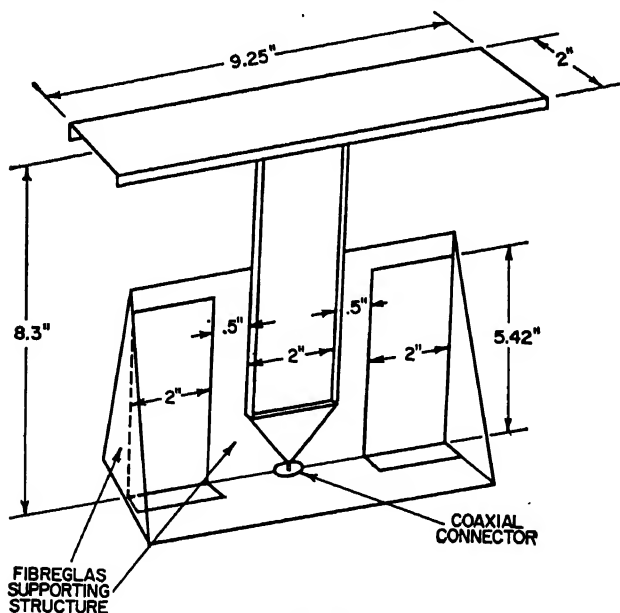
FIG. 27-41. Open-sleeve antenna.

The basic flush-mounted vertically polarized element for fuselage mounting is the annular slot,[13] which can be visualized as the open end of a large-diameter, low-characteristic-impedance coaxial line. As can be seen from the impedance curve of Fig. 27-42, such a structure becomes an effective radiator only when the circumference of the slot approaches a wavelength. The radiation patterns, on the other hand, have their maximum gain in the plane of the slot only for very small slot
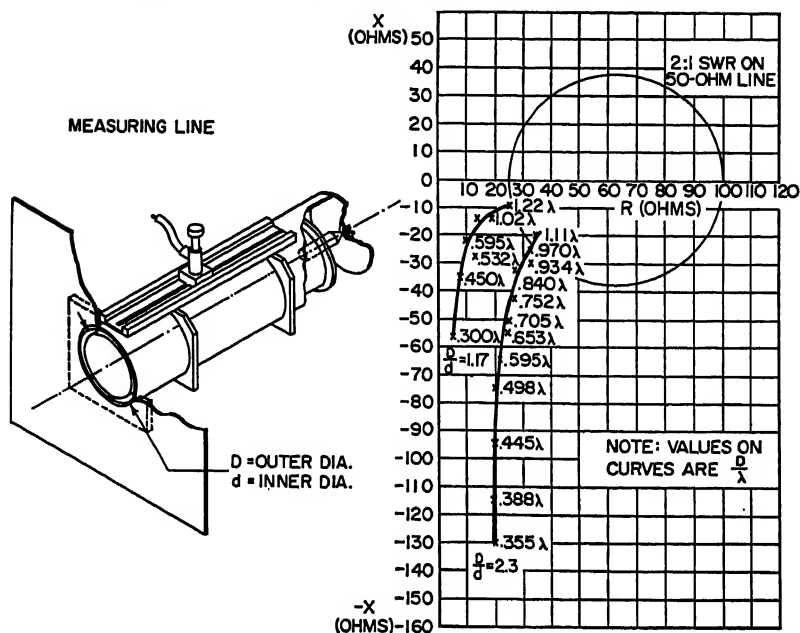
FIG. 27-42. Impedance of annular-slot antenna.
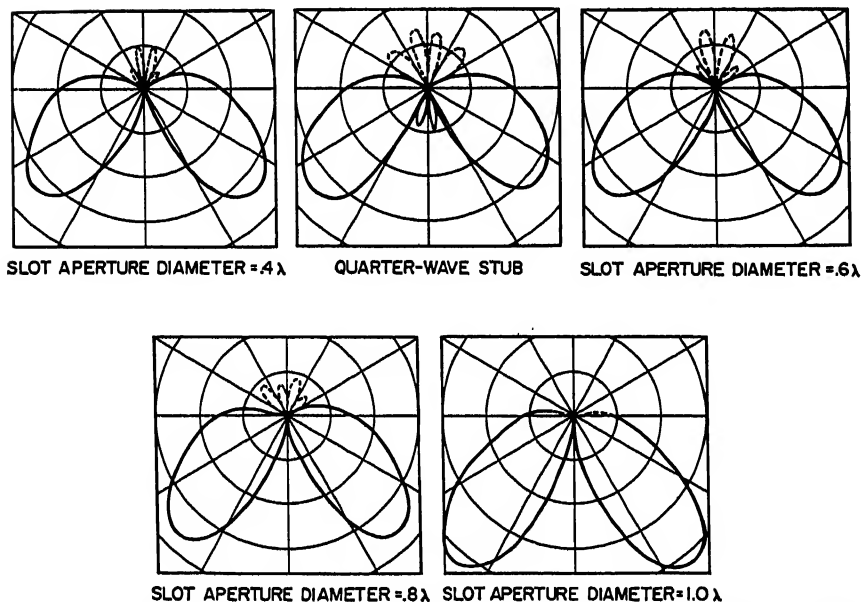
FIG. 27-43. Radiation patterns of annular-slot antenna and quarter-wave stub on a 2½-wavelength-diameter circular ground plane.

diameters and yield a horizon gain of zero for a slot diameter of 1.22λ.[14]   This pattern variation is illustrated in Fig. 27-43.   For these reasons, and to minimize the structural difficulty of installing the antenna in an aircraft, the smallest possible diameter yielding the required bandwidth is desirable.   For the 225- to 400-Mc band, the minimum practical diameter, considering constructional tolerances and the effect of the airframe on the impedance, is about 24 in.   A VSWR under 2:1 can be obtained with this diameter and a cavity depth of 4.5 in.   Figure 27-44 shows a design by A. Dorne, together with its approximate equivalent circuit.   In the equivalent
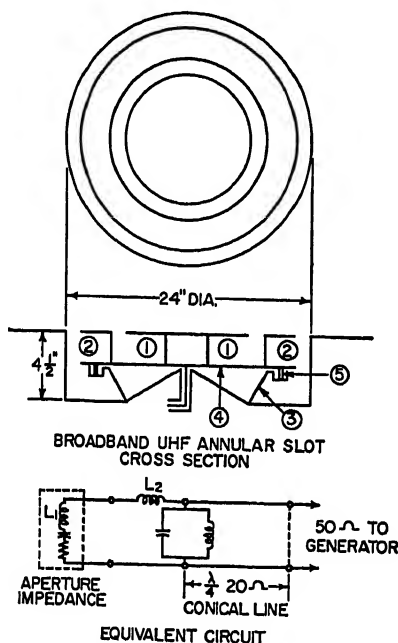
FIG. 27-44. Annular-slot antenna for the 225- to 400-Mc band and equivalent circuit.

circuit the net aperture impedance of the driven annular slot and the inner parasitic annular slot is shown as a series RC circuit.   The annular region 1, which is coupled to the radiating aperture through the mutual impedance between the two slots, and the annular region 2, which is part of the feed system, are so positioned and proportioned that they store primarily magnetic energy when the antenna is driven.   The inductances associated with the energy storage in these regions are designated as L_1 and L_2 in the equivalent circuit.   The parallel-tuned circuit indicated in the equivalent circuit is formed by the shunt capacitance between the vane 3 and the horizontal disk 4, together with the shunt inductance provided by four conducting posts, 5, equally spaced about the periphery of 4, which also serve to support 4 above 3.   From this element inward to the coaxial line, the base plate is cambered upward to form a conical transmission-line region of low characteristic impedance.   A short additional section of low-impedance line is added external to the cavity to complete the required impedance transformation.

Antennas for Horizontal Polarization.   There are three basic antenna elements which yield omnidirectional horizontally polarized patterns: the loop, the turnstile, and the longitudinal slot in a vertical cylinder of small diameter.   All three are used on aircraft (the turnstile largely for special military applications[15]), and all suffer

from a basic defect. Because they must be mounted near a horizontal conducting surface of rather large extent (i.e., the top or bottom surface of the aircraft), their gain at angles near the horizon is low. The greater the spacing from the conducting surface, the higher is the horizontal gain. For this reason, locations at, or near, the top of the vertical fin are popular for horizontally polarized applications, particularly for the VHF navigation system (VOR) which covers the 108- to 122-Mc range. Figure 27-45 shows a folded-dipole loop design developed by W. A. Cumming suitable
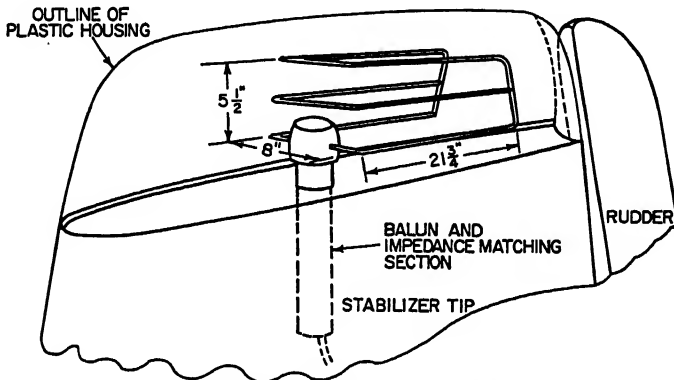
Fig. 27-45. Folded-dipole VOR antenna.
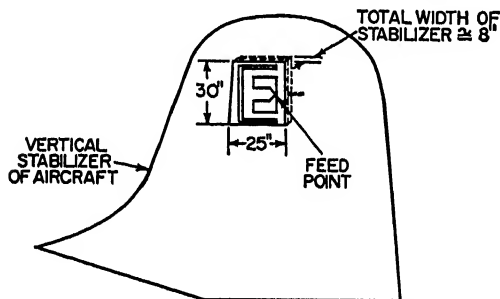
NOTE: ANTENNA CONSISTS OF IDENTICAL CAVITIES ON BOTH SIDES OF STABILIZER, DRIVEN WITH 180 DEGREE PHASE RELATION

Fig. 27-46. E-fed cavity VOR antenna.

for this application on aircraft large enough to provide the required space in a tail-tip radome. When the tip section is not sufficiently large to accommodate a structure of adequate size for the VHF navigation antenna, it is frequently possible to employ a flush cavity design located in the vertical fin itself. Figure 27-46 shows a design by I. J. Stampalia, which employs two loaded vertical slots, suitably phased, located in the faces of a 30- by 25-in. cavity extending through the vertical fin. The radiation patterns for this antenna are usually quite satisfactory. Principal plane patterns of such an antenna on a DC-6B aircraft are shown in Fig. 27-47a. For comparison, the corresponding patterns produced by a ram's-horn VOR antenna (discussed below), mounted above the pilot's cabin on the same aircraft, are shown in Fig. 27-47b. The superiority of the cavity in the horizontal plane is evident from this comparison. The E-shaped radiating elements are properly proportioned to provide a folded-dipole
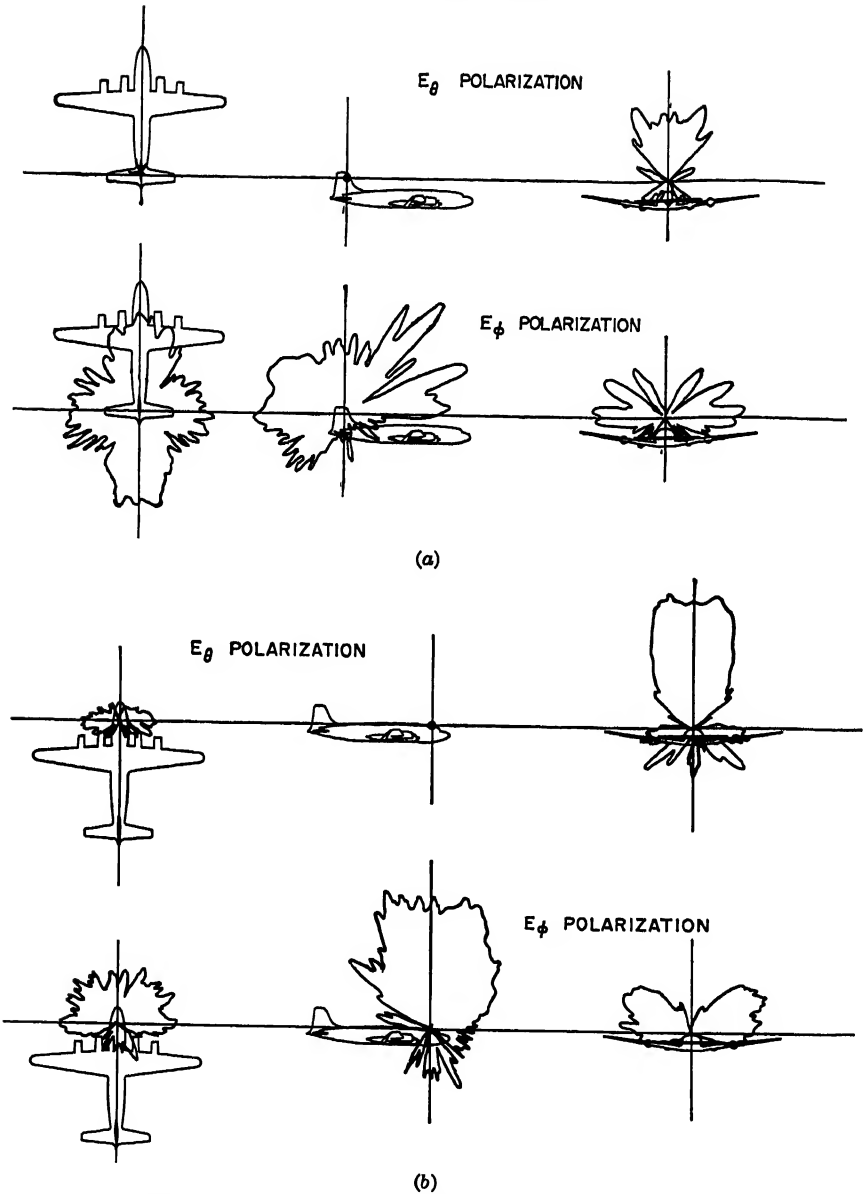
FIG. 27-47. Radiation patterns of VOR antennas on DC-6B aircraft: (a) E-fed cavity antenna. (b) Ram's-horn antenna.

form of impedance transformation which provides a portion of the matching network. When the average thickness of the fin at the location of the cavity is less than 8 in., impedance matching is extremely critical unless the matching elements introduce considerable loss resistance.

The question of whether a given antenna impedance can be matched over the

required band to a stated VSWR limitation[16] is discussed in Sec. 2.14 and can be resolved through the use of the chart of Fig. 2-37.

When a fuselage location is necessary, the U dipole, supported by a vertical mast, is commonly employed.[17] Figure 27-48 shows the arrangement of a shunt-fed U-dipole or ram's-horn antenna, which is basically similar to the bent stub described in Sec. 27.5.* This design, with a shunt-feeding arrangement similar to that described
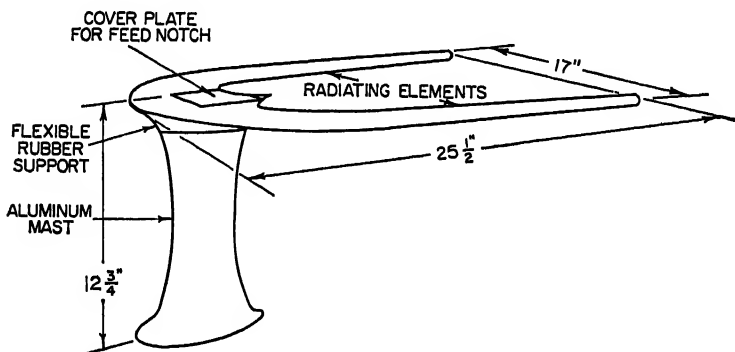
Fig. 27-48. Collins 37-J VOR antenna.
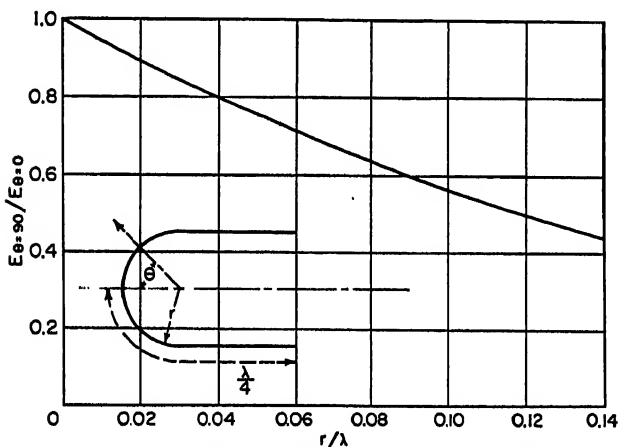
Fig. 27-49. Departure from circularity of U-dipole antenna pattern.

earlier, yields a VSWR of less than 4.8:1 over the 108- to 122-Mc band. Increasing the mast height above the 12 in. shown will improve the low angle gain and lower the peak VSWR but rapidly increase the dynamic mechanical loads on the supporting structure. Increasing the width of the U will lower the peak VSWR but deteriorate the uniformity of the pattern, as shown in Fig. 27-49.

The VOR navigation system is one which is particularly vulnerable to helicopter rotor-modulation effects since, with this system, angular-position information is contained in a 30-cycle modulation tone which corresponds closely to the third harmonic of the fundamental blade-passage frequency on typical helicopters. In Fig. 27-50 are shown two VOR antenna installations on an H-19 helicopter and the

* The Collins Radio Company Type 37J-3.

horizontal-plane radiation patterns of each. The fine structure on those patterns shows the peak-to-peak variation in signal amplitude due to passage of the rotor blades. The percentage of modulation of the signal received on the horizontal loop antenna is seen to be lower than that received on the ram's-horn antenna. This is due partly to the shielding afforded the loop by the tail boom and partly to the fact that the loop has inherently less response to scattered signals from the blades because
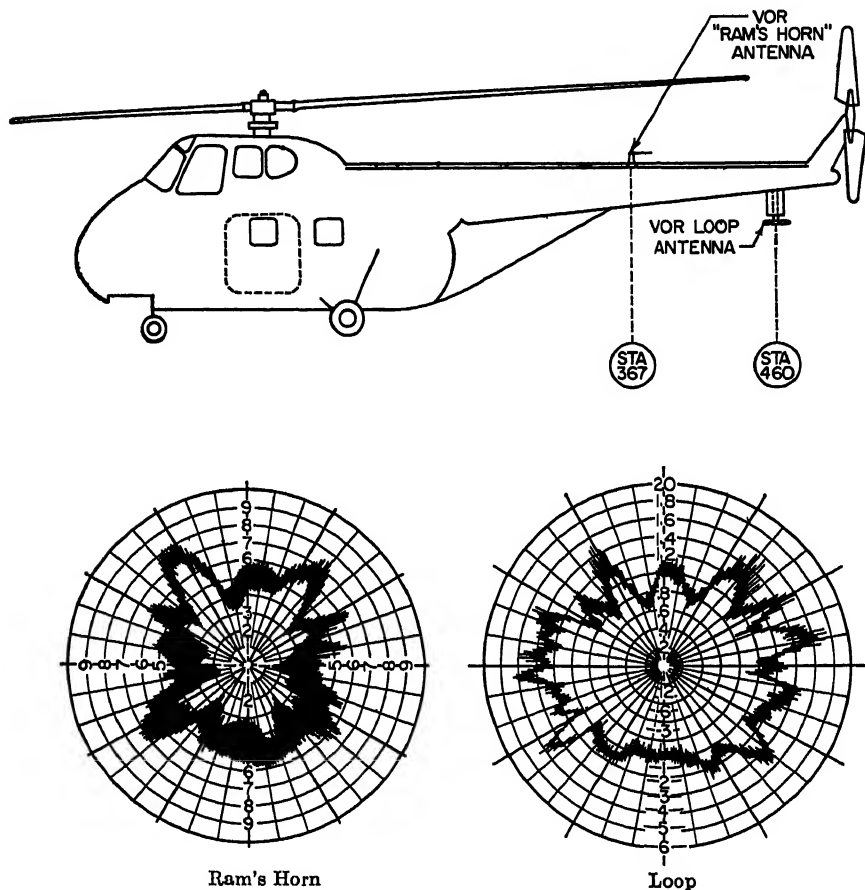
Fig. 27-50. Two VOR-antenna locations on the H-19 helicopter and horizontal-plane radiation patterns.

its pattern has a null along its axis while the ram's-horn receives signals from directly above it very effectively.

Multiple-antenna Systems. The limitations on omnidirectional coverage due to shadowing by the airframe described in Sec. 27.5 can be overcome by the use of two or more antennas. A variety of diversity schemes are possible. If the pattern coverage of the two antennas is complementary, or at least approximately so, and if the separation between the two is a large number of wavelengths, the antennas can be connected directly together without the use of diversity techniques.[18] The resultant pattern is characterized by a large number of narrow lobes, with deep nulls only at those angles where the patterns of the two antennas have nearly equal amplitudes,

as shown in Fig. 27-51. Considering the dynamic nature of the air-to-ground communications problem, it is easy to see that the time interval in which a given ground station is within one of the nulls is small, especially if the two patterns overlap in the
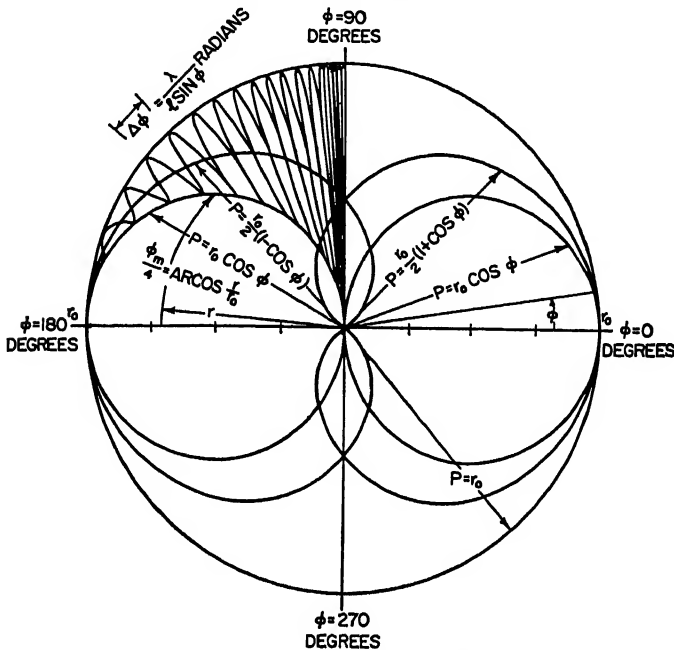
FIG. 27-51. Resultant of two cardioid patterns connected in parallel. r_0 = maximum range, ℓ = spacing between antennas, ϕ_m = total angle for which the range $\geq r$.

directions broadside to the airplane. Sichak and Nail have described many experiments with this approach.[19]

27.7. HOMING ANTENNAS

Airborne homing systems have been devised for various frequency bands to permit the pilot to fly directly toward a signal source. Although the navigational data supplied by a homing system are rudimentary, in the sense that it indicates only the direction and not the amount of course correction required to orient the aircraft toward the signal source, it is a self-contained system which does not require special cooperating equipment on the ground. Because of the symmetry of most airframes, it is possible to design satisfactory homing antennas in frequency ranges where direction-finder antennas are unusable because of airframe resonances or scattering effects.

The principle of operation used in airborne homing systems is illustrated in Fig. 27-52. Two patterns, which are symmetrical with respect to the line of flight and which are ideally in the form of cardioids, are generated alternately in time either by switching between separate antennas or by alternately feeding a symmetrical antenna array in two modes.

The homing system compares the signals received under these two conditions and presents to the pilot an indication either that he is flying a homing course or, if not, in which direction he should turn to come into the homing course. The equisignal condition which leads to the on-course indication will arise for a reciprocal course

leading directly away from the signal source as well as for the true homing course. The pilot can resolve this ambiguity by making an intentional turn after he has obtained the on-course indication and noting whether the direction of the required course correction shown by his instrument is opposite the direction of his intentional
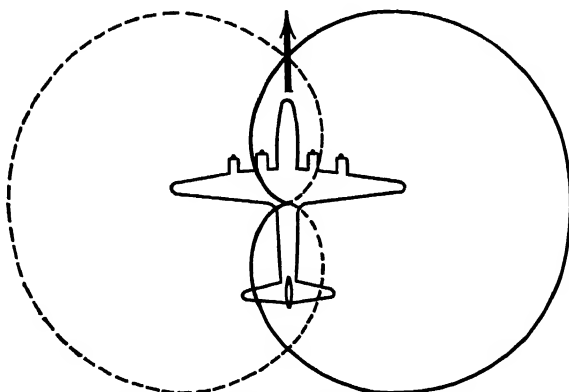
Fig. 27-52. Cardioid homing patterns.

ANTENNA ELEMENTS

MATCHED
ATTENUATORS

A B

TRANSMISSION LINE HAVING
ELECTRICAL LENGTH EQUAL
TO SPACING BETWEEN
ANTENNA ELEMENTS
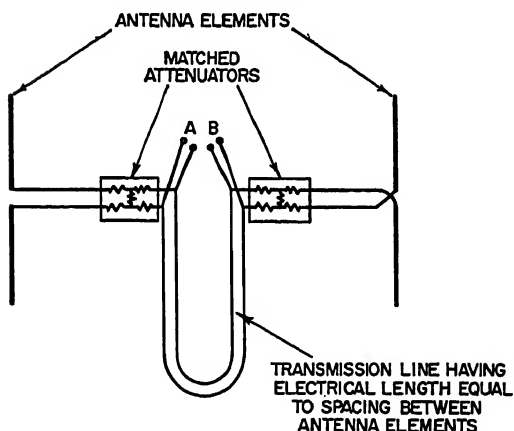
NOTE: FEEDING TERMINAL A GIVES CARDIOID
PATTERN POINTING TO LEFT
FEEDING TERMINAL B GIVES CARDIOID
PATTERN POINTING TO RIGHT

Fig. 27-53. Homing array.

turn (in which case he is operating about the correct equisignal heading) or in the same direction (in which case he is operating about the reciprocal heading).

One of the basic problems in the design of a homing-antenna system is the selection of the proper compromise between directivity patterns and system sensitivity. Consider the idealized homing array shown in Fig. 27-53, which is assumed to be in free space, and hence free of airframe scattering effects. Neglecting mutual impedance between the two elements, it is readily shown that by arranging the feed system as indicated, the array will have a null in one direction along the line joining the midpoints of the two elements and that the null direction reverses as the feed is switched between the two sets of feed terminals. In Fig. 27-54 are shown the horizontal-

plane patterns for such an array with various values of element spacing. For small values of spacing, the pattern becomes a cardioid and is hence well suited for homing applications. The pattern quality, as determined by the pattern slope at the on-course heading (a steep slope is desirable since this will lead to a clear indication of course error due to a small deviation from the homing course) and by the difference in response between the left-hand and right-hand patterns for courses other than the homing course and the reciprocal course, is seen to become poorer as the spacing is increased. The relative system sensitivity for the homing-course direction, on the
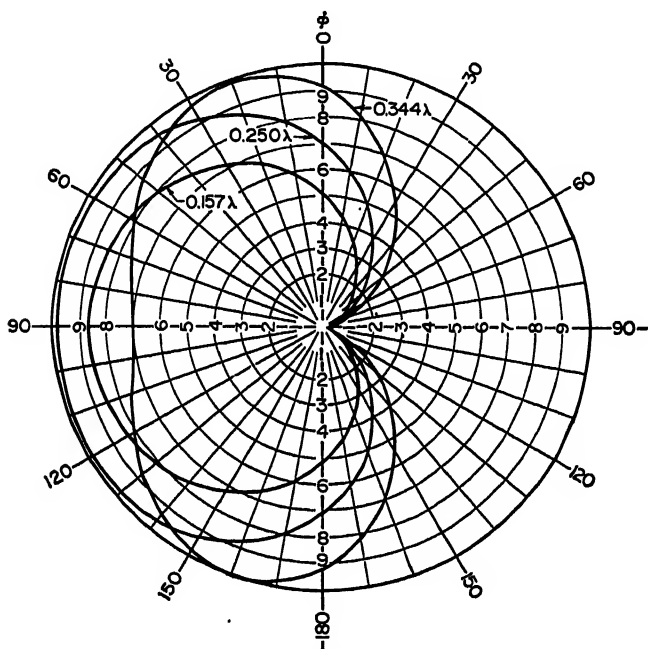
FIG. 27–54. The effect of dipole spacing on the pattern of a homing array.

other hand, is seen to increase as the element spacing is increased, being proportional to the sin $(\pi s/\lambda)$, where s/λ is the spacing between elements in wavelengths. Since most homing systems are designed to cover a relatively wide band of frequencies, the element spacing must be chosen as a compromise value which will avoid excessive pattern deterioration at the high-frequency end while retaining as much system sensitivity as possible at the low-frequency end. The sensitivity of the system is increased by increasing the receiving cross section of the individual elements also, and hence broadband elements of resonant size are used wherever possible. At the lower frequencies, when resonant-size elements are too large from the standpoint of aerodynamic drag or for other reasons, the largest elements considered feasible are usually employed.

Since it is not possible to predict accurately the effect of the airframe on the patterns of a homing-antenna system, the design of such a system is usually a step-by-step process in which experimental data obtained through model measurements are used to supplement the free-space antenna design concepts.

At sufficiently low frequencies, it is possible to use a symmetrical pair of balanced vertical elements as illustrated in Fig. 27–55 to achieve essentially free-space antenna

characteristics. The elements are decoupled from currents and charges induced in the wings by virtue of the balanced construction of the elements and from fuselage effects by virtue of their spacing from the fuselage.

The application of this technique is limited at low frequencies by the increasing difficulty of maintaining the degree of symmetry between the upper and lower halves of each element necessary to isolate the antenna from airframe resonance effects[20] and at high frequencies due to scattering from the fuselage and empennage. For
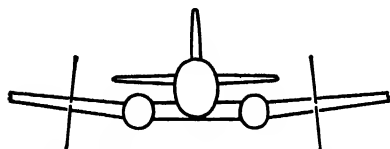
FIG. 27-55. Aircraft homing array.
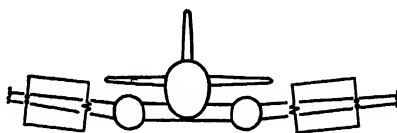
FIG. 27-56. Homing system using resistance-loaded loops to generate separate cardioid patterns.

HOMING
ARRAY

24 mc   38 mc   52 mc
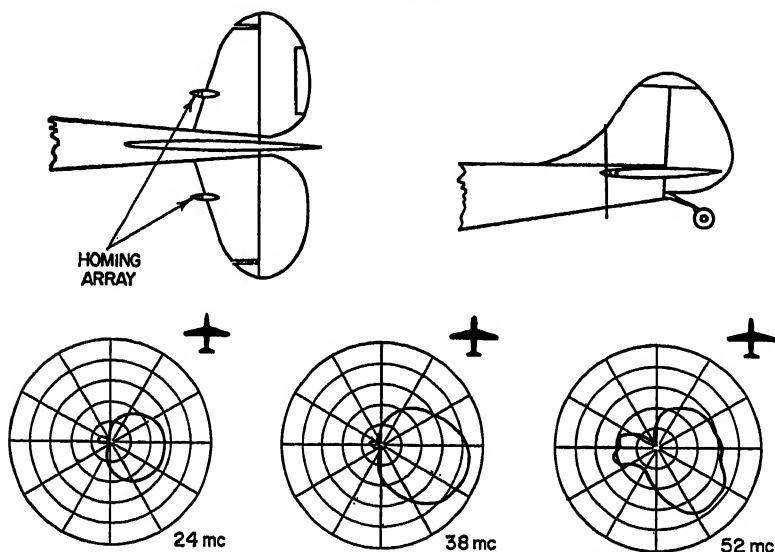
FIG. 27-57. Horizontal-plane patterns of homing array on horizontal stabilizer on L-19 aircraft.

frequencies as high as 10 Mc, balanced dipoles of this type on a DC-3 aircraft have been found to provide patterns which are remarkably close to the free-space dipole pattern. The design problem is made difficult at the higher frequencies because of the necessity for decreasing the antenna spacing, thereby placing the elements in close proximity to the fuselage where airframe scattering effects become more pronounced.

The use of separate antennas to generate the right- and left-hand cardioids is a sound design procedure for frequencies that are above the range for which the homing-array technique is applicable. A homing system using two resistance-loaded loop antennas is illustrated in Fig. 27-56. Here again, the balanced configuration is used to isolate the antennas from airframe resonance effects, and the elements may be placed well outboard to separate them from the fuselage. Since the low-signal portions of the cardioid patterns are oriented toward the scattering sources on the airframe, this technique is capable of providing quite clean homing patterns.

The upper frequency limit of the array technique may be extended in some cases

by mounting the elements on the horizontal stabilizer as shown in Fig. 27-57. This installation was designed for a homing system covering the frequency range 24 to 52 Mc on the L-19 aircraft. The radiation patterns show considerable departure from the free-square array patterns, particularly at the high-frequency end of the band, because of the presence of the vertical stabilizer, but they are adequate for homing purposes.
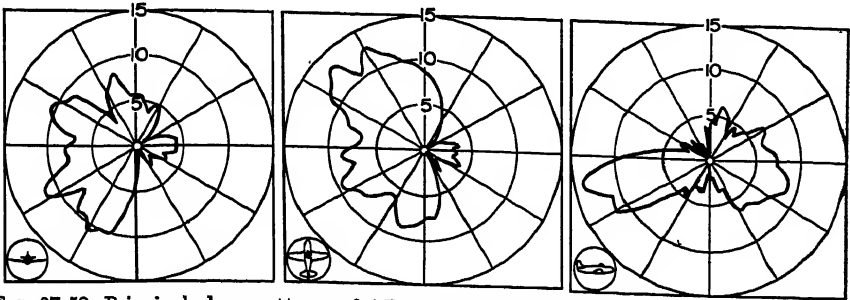
FIG. 27-58. Principal-plane patterns of ARA-8 homing array on bottom center line of B-26 aircraft; fuselage station 50, frequency = 130 Mc.

Radiation patterns for the AN/ARA-8 VHF homing array are shown in Fig. 27-58. This system operates in the frequency range of 100 to 156 Mc, which is too high to permit the effective use of balanced elements; the AN/ARA-8 antenna system consists of a pair of monopole elements which are located on the top or bottom center line of the aircraft. The patterns show the scalloping usually found in this frequency range because of the simultaneous arrival at the antenna of signals scattered from various parts of the airframe, in addition to the direct signal. These effects are not serious provided that they do not so deform the patterns that equisignal indications occur for courses other than the homing course or the reciprocal course.

REFERENCES

1. R. L. Tanner: "High Voltage Problems in Flush and External Aircraft HF Antennas," *IRE Trans. on Aeronaut. Navigational Electronics*, vol. AN-1, no. 4, pp. 16–19, December, 1954.
2. O. C. Boileau, Jr.: "An Evaluation of High-frequency Antennas for a Large Jet Airplane," *IRE Trans. on Aeronaut. Navigational Electronics*, vol. AN-3, no. 1, pp. 28–32, March, 1956.
3. H. J. Sang, D. M. Coulson, and B. M. Sifford: "High-strength Plastic Laminates for Use in Aircraft H-F Antennas," Final Report, Stanford Research Institute, Project 1252-1, U.S. Air Force Contract AF33(616)-2750, Menlo Park, Calif., June, 1956.
4. Instruction Book for Type NA-1 Aircraft Navigation System, Bendix Aviation Corp., Bendix Radio Division, Baltimore, Md.
5. L. R. Mullen: "The Marconi AD 7092 Series of ADF Receivers," *IRE Trans. on Aeronaut. Navigational Electronics*, vol. AN-2, December, 1955.
6. J. T. Bolljahn and R. F. Reese: "Electrically Small Antennas and the Low-frequency Aircraft Antenna Problem," *IRE Trans. on Antennas and Propagation*, vol. AP-1, no. 2, pp. 46–54, October, 1953.
7. A. A. Hemphill: "A Magnetic Radio Compass Antenna Having Zero Drag," *IRE Trans. on Aeronaut. Navigational Electronics*, vol. AN-2, December, 1955.
8. H. H. Ward, 3rd: "Analysis of the Over-station Behavior of Aircraft Low-frequency ADF Systems," *IRE Trans. on Aeronaut. Navigational Electronics*, vol. AN-2, no. 4, pp. 31–41, December, 1955.
9. J. T. Bolljahn: "ADF Sense Antenna Requirements and Design," *IRE Trans. on Aeronaut. Navigational Electronics*, vol. AN-2, no. 4, pp. 23–30, December, 1955.
10. N. E. Lindenblad: "Slot Antennas," *Proc. IRE*, vol. 35, no. 12, pp. 1472–1479, December, 1947.
11. H. Jasik: U.S. Patent No. 2,700,112.
12. J. T. Bolljahn: U.S. Patent No. 2,505,751.

13. A. Dorne: U.S. Patent No. 2,644,090.
14. A. A. Pistolkors: "Theory of the Circular Diffraction Antenna," *Proc. IRE*, vol. 36, no. 1, p. 56, January, 1948.
15. Radio Research Laboratory Staff: "Very High Frequency Techniques," McGraw-Hill Book Company, Inc., New York, pp. 131ff., 1947.
16. R. L. Tanner: "Theoretical Limitations on Broad-band Impedance Matching," *Electronics*, vol. 2, February, 1951.
17. B. E. Montgomery: "A VHF Aircraft Antenna for the Reception of 109 Mc Localizer Signals," *Proc. IRE*, vol. 33, pp. 762–772, November, 1945.
18. A. G. Kandoian: "The Aircraft Omnidirectional Antenna Problem for UHF Navigational Systems," *Aeronaut. Eng. Rev.*, vol. 12, pp. 75–80, May, 1953.
19. W. Sichak and J. J. Nail: "UHF Omnidirectional Antenna Systems for Large Aircraft," *IRE Trans. on Antennas and Propagation*, vol. AP-2, no. 1, pp. 6–14, January, 1954.
20. P. S. Carter, Jr.: "Study of the Feasibility of Airborne HF Direction Finding Antenna Systems," *IRE Trans. on Aeronaut. Navigational Electronics*, vol. AN-4, no. 1, pp. 19–23, March, 1957.

GENERAL REFERENCES

F. D. Bennett, P. D. Coleman, and A. S. Meier: "The Design of Broadband Aircraft Antenna Systems," *Proc. IRE*, vol. 33, pp. 671–700, October, 1945.
J. T. Bolljahn and J. V. N. Granger: "The Use of Complementary Slots in Aircraft Antenna Impedance Measurements," *Proc. IRE*, vol. 39, no. 11, pp. 1445–1448, November, 1951.
R. C. Borden, C. C. Trout, and E. C. Williams: "Description and Evaluation of 100-channel Distance Measuring Equipment," *Proc. IRE*, vol. 39, no. 6, pp. 612–618, June, 1951.
R. H. J. Cary: "The Slot Aerial and Its Application to Aircraft," *Proc. IEE (London)*, Pt. III, vol. 99, pp. 187–196, July, 1952.
R. H. J. Cary: "A Survey of External and Suppressed Aircraft Aerials for Use in the High-frequency Band," *Proc. IEE, (London)*, Pt. III, vol. 99, pp. 197–210, July, 1952.
H. Diamond and G. L. Davies: "Characteristics of Airplane Antennas for Radio Beacon Reception," *Proc. IRE*, pp. 346, February, 1932.
J. V. N. Granger: "Designing Flush Antennas for High-speed Aircraft," *Electronics*, vol. 11, March, 1954.
J. V. N. Granger: "Design Limitations on Aircraft Antenna Systems," *Aeronaut. Eng. Rev.*, vol. 11, no. 5, pp. 82–87, May, 1952.
J. V. N. Granger: "Shunt Excited Flat Plate Antennas with Applications to Aircraft Structures," *Proc. IRE*, vol. 38, no. 3, pp. 280–287, March, 1950.
J. V. N. Granger and T. Morita: "Radio-frequency Current Distributions on Aircraft Structures," *Proc. IRE*, vol. 39, no. 8, pp. 932–938, August, 1951.
George L. Haller: "Aircraft Antennas," *Proc. IRE*, vol. 30, no. 8, pp. 357–362, August, 1942.
H. C. Hurley, S. R. Anderson, and H. F. Keary: "The Civil Aeronautics Administration VHF Omnirange," *Proc. IRE*, vol. 39, no. 12, pp. 1506–1520, December, 1951.
H. Kees and F. Gehres: "Cavity Aircraft Antennas," *Electronics*, vol. 20, pp. 78–79, January, 1947.
E. J. Moore: "Factor of Merit for Aircraft Antenna Systems in the Frequency Range 3–30 Mc," *IRE Trans. on Antennas and Propagation*, vol. AP-3, pp. 67–73, August, 1952.
K. A. Norton and P. L. Rice: "Gapless Coverage in Air-to-ground Communications at Frequencies above 50 Mc," *Proc. IRE*, vol. 40, no. 4, pp. 470–474, April, 1952.
L. E. Raburn: "Faired-in ADF Antennas," *IRE Convention Record*, vol. 1, part 1, pp. 31–38, March, 1953.
L. E. Raburn: "A VHF-UHF Tail-cap Antenna," *Proc. IRE*, vol. 39, no. 6, pp. 656–659, June, 1951.
O. H. Schmitt and W. P. Payser: "Aircraft Antenna Pattern Plotter," *Electronics*, vol. 20, pp. 88–91, May, 1947.
G. Sinclair, E. C. Jordan, and E. W. Vaughan: "Measurement of Aircraft Antenna Patterns Using Models," *Proc. IRE*, vol. 35, no. 12, pp. 1451–1462, December, 1947.
R. L. Tanner: "Shunt-notch-fed HF Aircraft Antennas," *IRE Trans. on Antennas and Propagation*, vol. AP-6, no. 1, pp. 35–43, January, 1958.
H. H. Ward, 3rd: "Phase Shift Cleans up ADF Confusion," *Aviation Week*, vol. 62, no. 22, pp. 73–76, May 30, 1955.
A. Weisfloch and C. Ancona: "Utilisation de la cage électrostatique pour l'étude de certains antennes d'Avion," *L'Onde Électrique*, no. 363, pp. 1–6, June, 1957.

Chapter 28

DIRECTION-FINDING ANTENNAS

Avery G. Richardson

ITT Laboratories
Nutley, New Jersey

28.1. SCOPE AND DESCRIPTIONS

Purpose of Direction Finder. A radio direction finder (DF) is used to determine the direction of arrival of a radio signal. Because signal sources of practical interest are many wavelengths distant, the received signal is assumed to have a plane wavefront at right angles to the direction of travel. The angle of elevation may vary, and the polarization may be vertical, horizontal, circular or elliptical. There may be two or more signals which arrive by slightly different paths because of ionospheric irregularities, particularly in the 1- to 30-Mc region. These variations are responsible for much of the complexity of DF systems.

Direction finders comprise a directional antenna or antenna system, a receiver, and a directional indicating means, but only the antenna portion will be considered herein. All the goniometric or switching circuitry prior to the receiver is defined as part of the antenna system.

All direction finding is based on the knowledge that the signal is a wave motion traveling in some given direction at substantially the speed of light, and two concepts of this fact are used. The first is that the signal arrives at successive points in its path at later and later times, and the second and more usual concept is that the phase of the signal is progressively varying along its path.

To determine the direction of signal travel from time or phase differences, DF antennas must consist of two or more elements which are physically displaced from each other. Since it is difficult to measure radio-frequency phase differences directly, the signals from the elements are usually combined so that the response of the antenna system varies with the direction of arrival of the signal.

It is well known that all realizable antennas have directional characteristics in certain directions. It is the use of these characteristics and the special precautions necessary to DF which are to be covered here. The phase concept is introduced for later use with sense antennas.

(a) LOOP   (b) ADCOCK   (c) ROTATING
                                    REFLECTOR
FIG. 28-1. Rotatable antenna systems.

Types of Direction Finder Covered. *Rotatable Antenna Systems.* Systems like Fig. 28-1 are those in which the entire antenna system and its directional pattern are rotated about the usually vertical axis of the system. In manually operated devices,

the system is often positioned to produce a null output from the receiver and the direction is read from a scale on the antenna positioning shaft. Automatic versions employ a servo to position the antenna system to a null or other usable position. In continuously rotated motor-driven antenna systems, the receiver output may be displayed on a cathode-ray tube and either the null points or maximum response points may be read from an azimuth scale around the face of the tube. A variation may employ a motor-driven loop whose output is combined with a sense antenna to produce a cardioid pattern giving a sinusoidal modulation of the signal. This sine-wave modulation can be detected and compared in phase with a sinusoidal reference signal derived from the antenna rotation means.

DIRECTION OF SIGNAL θ	FIELD IN GONIOMETER-TOP VIEW				LOOP PLANE NULL°
	DUE TO STATOR A	DUE TO STATOR B	RESULT ANT=1	RESULT ANGLE	
0°	→ 1	0	→	0	90
45	→ .7	↑ .7	↗	45	135
90	0	↑ 1	↑	90	180
135	← .7	↑ .7	↖	135	225
180	← 1	0	←	180	270
225	← .7	↓ .7	↙	225	315
270	0	↓ 1	↓	270	0
315	→ .7	↓ .7	↘	315	45
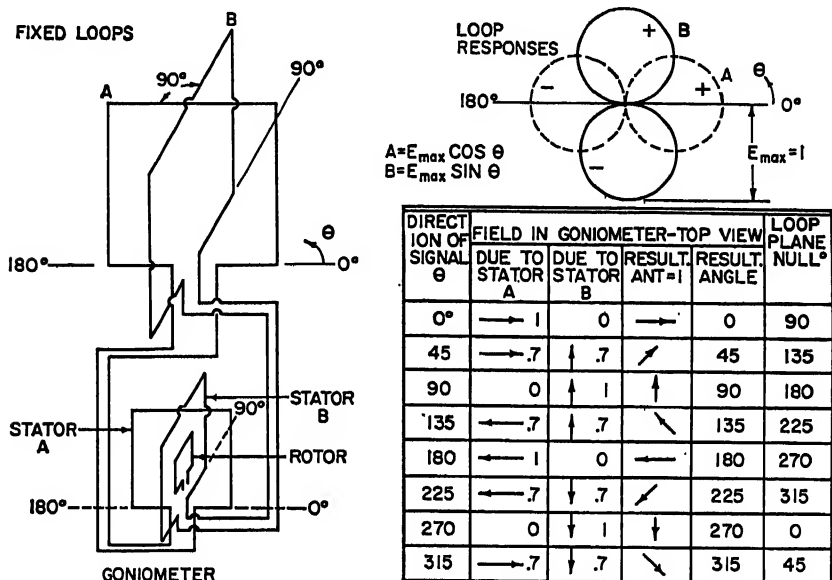
FIG. 28-2. Rotatable pattern-fixed system using crossed loops and goniometer.

Rotatable-pattern Fixed Systems. These systems are used where the antenna system is too large to be physically rotated at the desired rate. In a common version, the radio-frequency field present in the antenna system is simulated in miniature within a goniometer. A search coil may be rotated in this simulated field to produce a signal like that of a rotatable loop located at the antenna site. Such a system is shown in Fig. 28-2.

A second type called Wullenweber employs a circle of moderately directive antennas and a switching type of goniometer including phase delay networks. Several antenna outputs are combined to form a sharp pattern which appears to rotate with the goniometer rotation (Fig. 28-3).

Quasi-instantaneous Systems. These systems employ two antennas and two receivers connected to a common indicator for simultaneous comparison of the signals received by the two antennas. In the Watson-Watt device,[5] the antennas have directional overlapping patterns and the bearing is displayed as a function of the relative instantaneous amplitude of the signals in the two channels. Alternative systems have been proposed[62] using omnidirectional antennas spaced several wavelengths apart, the bearing being determined by measuring the relative phase of the received signals (usually at the i-f portion of the system).

Special Direction-finder Requirements. *Undesired-signal Error.* Since direction finding generally employs either a null indication or a sharp-beam display, and since these indications are secured by taking the difference or sum of radio-frequency voltages, severe requirements obtain for close similarity between the r-f voltages and phases of the antenna outputs. Similar precautions are needed in connection with transmission lines, transformers, goniometers, ground systems, and ground conductivity.

Particularly with null systems, the introduction of small unwanted signals is damaging. Balanced circuitry is usually employed; transformers require electrostatic shielding; transmission lines must be double-shielded; and the receiver itself must not pick up signals.
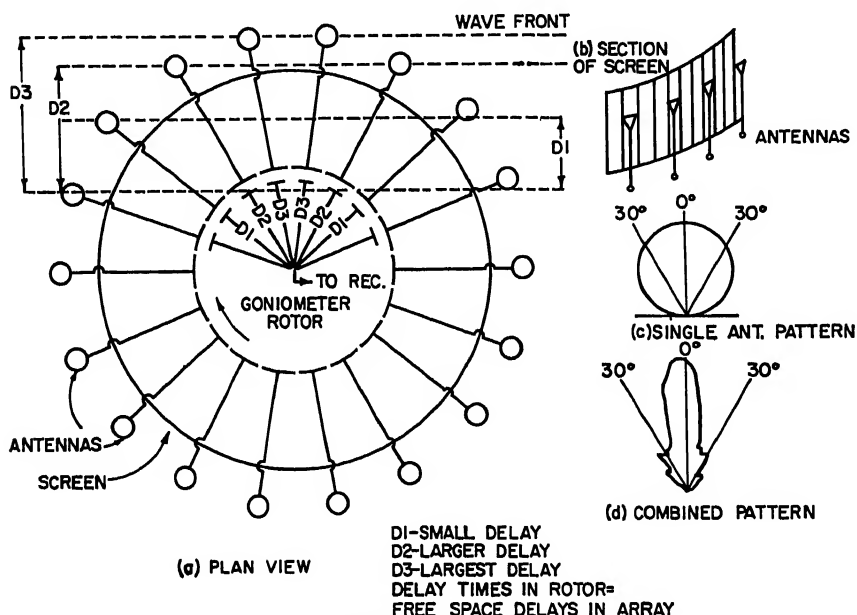
FIG. 28-3. Rotatable pattern-fixed system using capacitive switching as in Wullenweber.

Polarization Error. Many DF systems employ a null or minimum response as an indication of direction and are designed for a specific polarization which is most frequently vertical. Signals of undesired polarization may produce signals when the antenna system is at the null position for desired polarization, either blurring the null or causing it to be displaced. This effect may be inherent in an antenna such as a loop or dependent upon transmission-line placement or electrical length, ground conditions, current in supporting members, or improper electrostatic shielding. Precautions are discussed in connection with the various antenna systems subsequently described.

Standard Wave Error. In vertically polarized systems this was originally described[13] as the error due to a signal polarized at 45° and arriving from an elevation angle of 45°. It was later modified to correct for ground reflections by requiring test-transmitter adjustment to produce equal intensities of horizontally and vertically polarized fields at the antenna system under test. In practice, the intensities may be varied to produce the greatest error.

28.2. ROTATABLE ANTENNA SYSTEMS

The first class to be described consists of loops, Adcocks, and various other arrangements which combine the energy from various parts of the antenna system at the carrier frequency so that a variation of amplitude with respect to direction of arrival results. Usually a null point exists which is useful for direction finding.
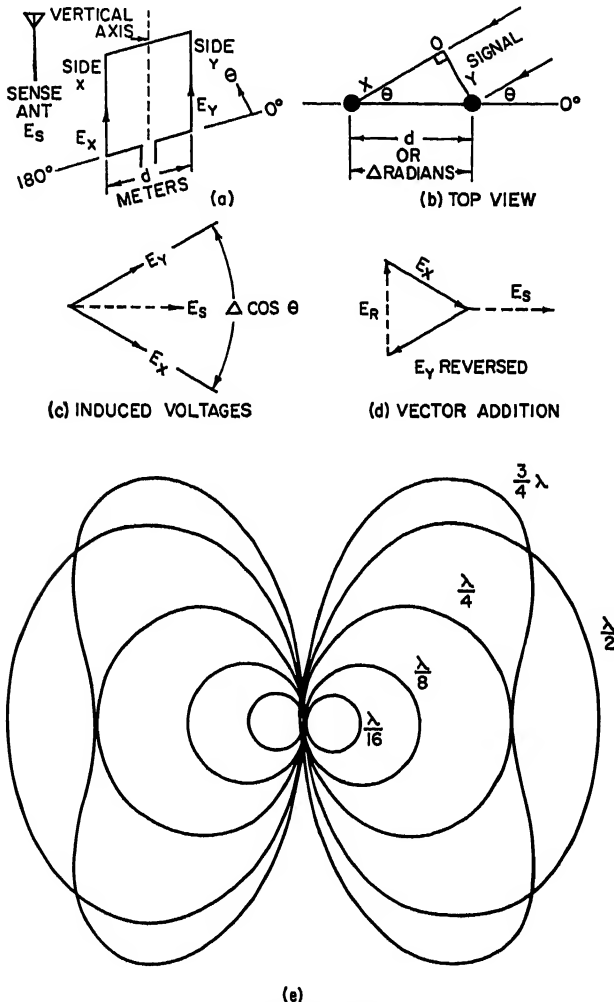
Fig. 28-4. Loop response for varying angles of signal arrival and spacing of vertical sides.

Single Loops. *Single-loop Response.* The response pattern of a vertical-axis loop as in Fig. 28-4(a) relative to a vertically polarized signal of specified frequency arriving horizontally at an angle θ to the plane of the loop is

$$E_R = 2E \sin \frac{\Delta \cos \theta}{2}$$

which is the general expression for a one-turn loop with any spacing Δ radians, where E is the voltage induced in one vertical side.

The response patterns are plotted for convenience against fractions of a wavelength d/λ in Fig. 28-4e, where d is loop width in meters.

For small spacings ($d < \lambda/4$) between loop sides, $\sin [(\Delta \cos \theta)/2]$ in radians closely approximates $(\Delta \cos \theta)/2$, and we may write

$$E_R = E \Delta \cos \theta$$

Introducing loop turns N and expressing Δ as a function of d, we write

$$E_R = NE \frac{2\pi d}{\lambda} \cos \theta$$

where E_R is the voltage induced in the loop.

For single rotatable loops using the null, the departure of the pattern shape from the exact cosine function is of no consequence up to spacings of about $\frac{3}{4}\lambda$. Its effect in a crossed-loop rotated-pattern system can be appreciable and is considered later under rotated-pattern systems.

Note that in Fig. 28-4d, E_R has a phase of 90° with respect to the mean of the voltages induced in each side of the loop. E_R is also 90° out of phase with the voltage induced in a vertical antenna used for sense purposes. This is important in combinations of loop and sense antennas.

Loop Effective Height (h). This is expressed in meters as a factor which, multiplied by the field strength in microvolts per meter, gives the induced voltage in the loop in microvolts.

$$h = \frac{2\pi NA}{\lambda}$$

where $d/\lambda \ll 1$

　　N = number of turns

　　A = area of each turn, sq meters

The effective height above is for signals arriving horizontally at a loop oriented for *maximum* response.

Radiation Resistance of a Loop. A loop, small with respect to wavelength and remote from earth, has

$$\text{Radiation resistance, ohms} = 31,200 \left(N \frac{A}{\lambda^2} \right)^2$$

where N = number of turns

　　A = area of loop, sq meters

　　λ = wavelength, meters

Shielded Loop. When a loop is used in practical circuits, it is generally near grounded surfaces, as shown in Fig. 28-5a, and is often connected to the receiver through a center-tapped transformer T. If the distributed capacities C_1 and C_2 between ground and opposite sides of the loop are unequal, the voltages of the loop sides with respect to ground will cause unequal currents to flow through C_1, C_2, and transformer T primary, with a resulting distortion of the pattern. To avoid this condition, the loop is enclosed with a metal shield as in Fig. 28-5b, thus providing equal capacities to ground. The gap prevents the shield from behaving as a short-circuited turn. The shield also reduces effects of electrostatic induction fields due to precipitation static or nearby conductors.

Balanced Loops. Even though a shielded loop may be used, its connection to a receiving circuit may introduce unsymmetrical capacity to ground, as in Fig. 28-6a. Numerous corrective measures exist; the use of a balanced amplifier as in part b or a

shielded transformer as in part *c* is common. The shield ground must be symmetrically located, not as in part *d*.
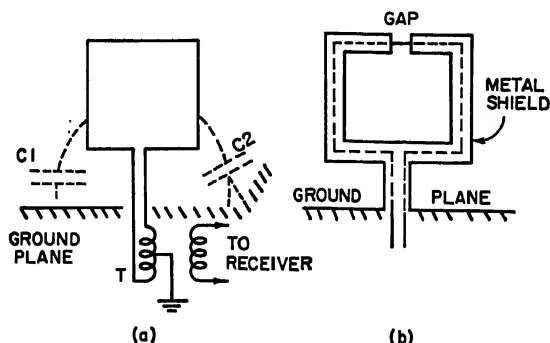
FIG. 28-5. Corrective effect of loop shielding.

(a) UNBALANCE DUE TO UNSYMMETRICAL CONNECTION

(b) CORRECT CONNECTION

(c) CORRECT CONNECTION

(d) IMPROPER TRANSFORMER ELECTROSTATIC SHIELD
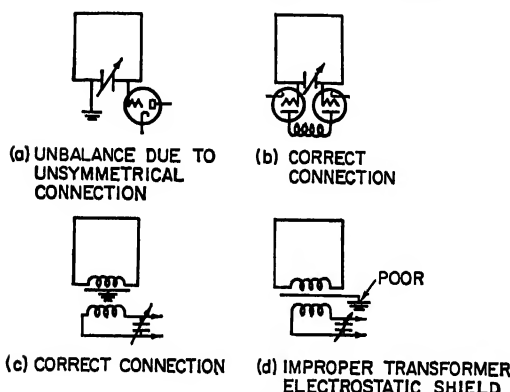
FIG. 28-6. Balanced loops.

Tuned Loops. When a loop is tuned and connected to a vacuum-tube grid, the voltage E_{VT} at the grid is

$$E_{VT} = E_L \frac{\omega L_L}{R_L} = E_L Q_L$$

where E_L = voltage induced in loop
ω = frequency
L_L = loop inductance
R_L = loop r-f resistance
Q_L = loop circuit Q

Such tuning produces the best possible sensitivity, provided the loop does not have to be resistively loaded to secure sufficient bandwidth. An alternative expression is

$$E_{VT} = E_F h Q_L$$

where E_F = field, mv/meter
h = loop effective height, meters
Q_L = loop circuit Q

Loop with Transformer Having Tuned Secondary-maximum Gain.[31,43] The equivalent circuit is shown in Fig. 28-7, where

E_L = induced voltage in loop
L_L = loop inductance
R_L = loop resistance
m = transformer turns ratio
R_{VT} = loading resistance of vacuum tube circuits

$$m^2 R_L = R_{VT} \quad \text{for maximum gain (matched condition)}$$

Loop Sensitivity with Receiver of Known Noise Factor.   When a small loop is reso-
nated by a condenser and connected to a receiver, the field strength E_F in microvolts
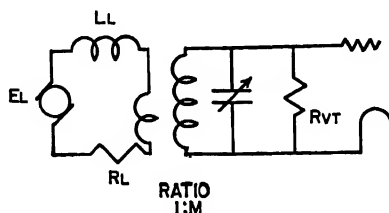
Fig 28-7. Equivalent circuit of loop with transformer having tuned secondary-maximum gain

per meter necessary to produce a 1.1 carrier to thermal-noise ratio at detector output
of receiver is

$$E_F = \frac{30N}{D^{3/2}} \sqrt{\frac{B}{QF}}$$

where N = receiver-voltage noise factor
   D = diameter of loop, meters
   B = receiver bandwidth, cps
   Q = Q of loop resonant circuit
   F = r-f mid-frequency, cps

Loops with Iron-rod Cores.   When a low-loss core or rod of magnetic material having
a high permeability for the applied radio-frequency field is inserted in a small coil
used as a loop, the flux threading the loop is increased.   Figure 28-8 shows the para-
bolic nature of the flux paths in a "rod antenna" immersed in a uniform field.[61]
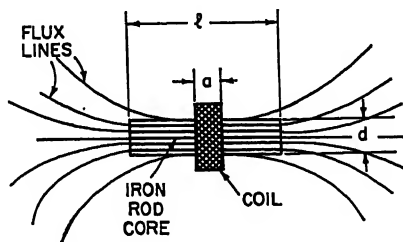
Fig. 28-8. Flux distribution in coil with magnetic rod.

The magnetic core increases the flux, the coil inductance, and the coil Q in varying
amounts, so that it is necessary to consider these variations together in order to
determine optimum performance.

The increase in flux in a narrow coil at the rod center may be defined as due to the
apparent permeability of the rod (μ_{rod}).   This depends on the rod dimensions and the
intrinsic permeability of the rod material when measured in a toroid (μ_{toroid}).

Figure 28-9 shows μ_{rod} for rods and hollow cylinders with various l/d ratios and different values of μ_{toroid} (or intrinsic permeabilities). Induced voltage is proportional to μ_{rod}.

The increase in inductance may be expressed as an increase in the coil permeability (μ_{coil}). This is greater for longer coils, as shown in Fig. 28-10, curve a. The Q, however, decreases as the coil is lengthened, as in curve b.
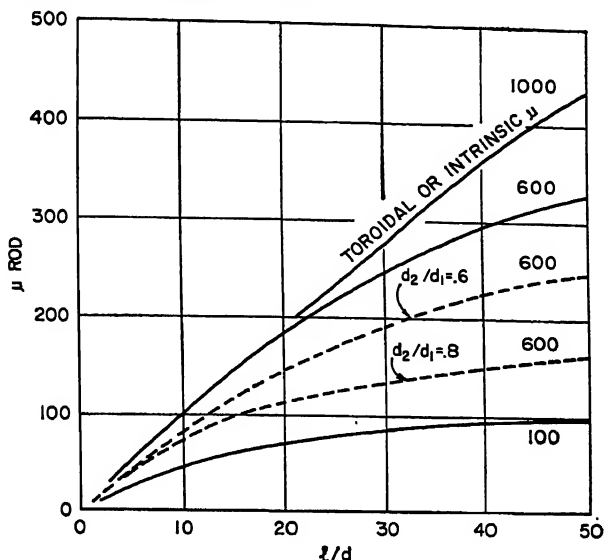
FIG. 28-9. Apparent permeability of rod (increase of flux in the coil) with respect to rod-length diameter ratio for various toroidal permeabilities of rod material. d_2 and d_1 are, respectively, inside and outside diameters of hollow rods.
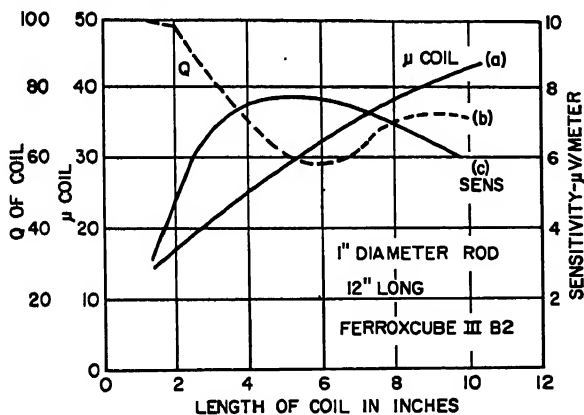
FIG. 28-10. Effect of coil/rod-length ratio on Q, sensitivity, and apparent μ of coil.

The sensitivity of a rod-and-coil antenna varies with coil length, as in curve c of Fig. 28-10. It is expressed as the field strength necessary to produce a 10-db signal-to-noise ratio. Since loop antennas must generally be tuned with a specified condenser, the number of turns was adjusted to produce the same coil inductance for each different length. It is clear that short coils are most desirable.

The displacement of a short coil from the rod center increases Q and decreases μ_{coil} as in Fig. 28-11, but does not markedly increase the sensitivity as might be expected because μ_{rod}, or the flux within the coil, decreases toward the end of the rod.

Loops with Iron Spheroidal Cores.[53] In Fig. 28-12 the long axis $2b$ of the prolate spheroid iron core is shown perpendicular to the plane of the loop L_1, with the magnetic field H_1 in the direction of the long axis. The ratio of the induced voltage with
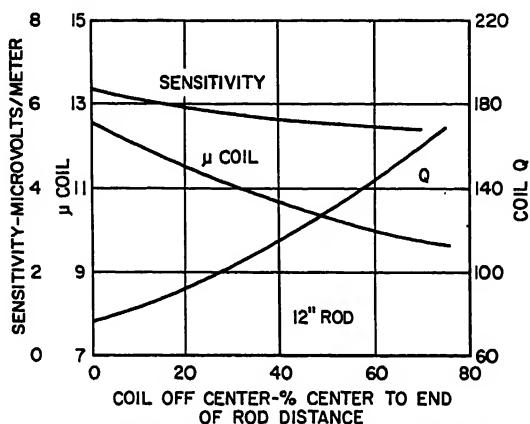
FIG. 28-11. Displacement of coil from rod center versus μ coil, Q, and relative sensitivity.
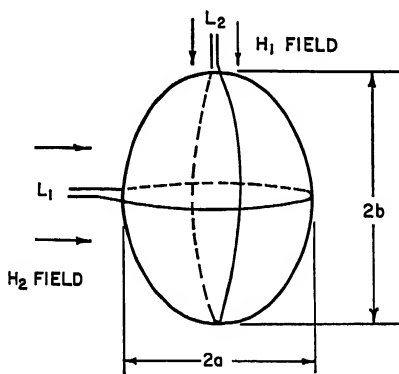
FIG. 28-12. Prolate spheroidal core with loop coils around major and minor axes.

the core to that without the core is shown in Fig. 28-13 for various μ_{toroid} (intrinsic permeabilities) of the core and increasing ratios of b/a.

When the loop is wound as an ellipse (shown in Fig. 28-12 as L_2) and the field is H_2, the induced voltage with core divided by the voltage less core is plotted in Fig. 28-14.

Loop Rotatable Transformers. These may be used with loops in place of slip rings, as shown in Fig. 28-15.

Ferrite cores and close spacing yield a coupling coefficient greater than 0.9 for low frequencies, resulting in losses less than 1 db. Because of close spacing, an electrostatic shield is necessary. It is shown in the sectional and developed views as a number of wires forming a cylinder between the windings. The common ground must be at the center and broken at one point to avoid short-circuited turn effect.
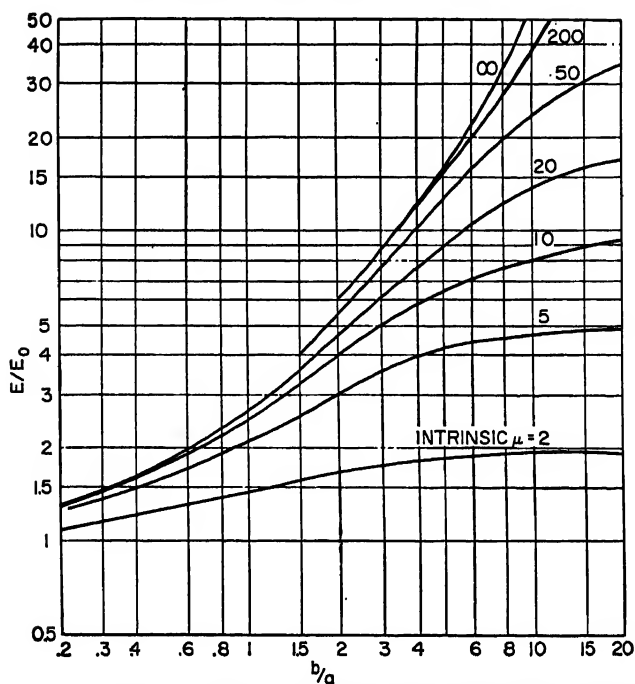
FIG. 28-13. Increase of induced voltage due to prolate spheroid magnetic core in minor-axis loop coil.
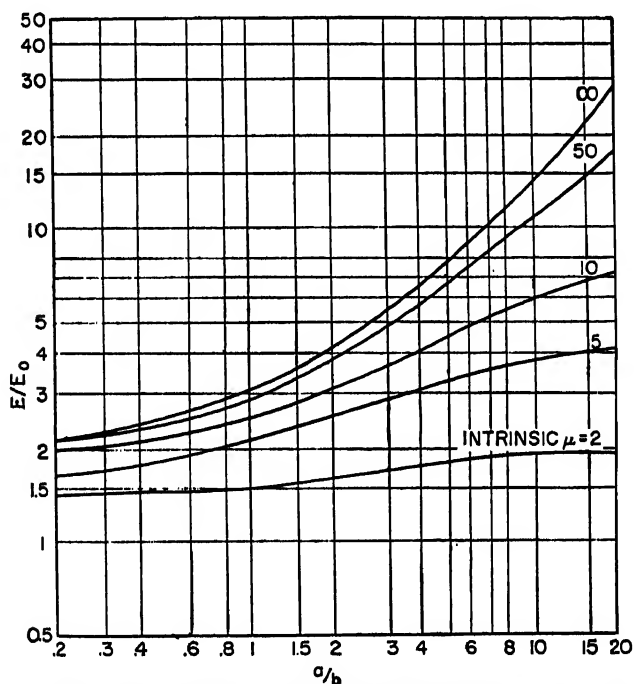
FIG. 28-14. Increase of induced voltage due to prolate spheroid magnetic core in major-axis loop coil.
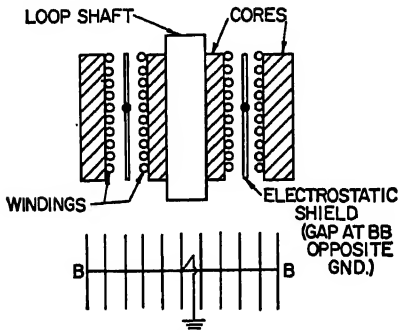
Fig. 28-15. Rotatable transformer.

Fig. 28-16. Loop and vertical-antenna combination.

Loop and Vertical Antenna. The voltage induced in a vertical antenna at the center of a loop is nearly in phase with the induced voltage in a loop side and therefore 90° out of phase with the loop open-circuit voltage. This antenna voltage may be combined with the loop voltage in quadrature or be shifted into phase and combined. Figure 28-16 shows effects on the pattern where K equals the fractional relationship

of antenna to loop-maximum voltage. In part a, $K = 1$, and in-phase relation gives a cardioid pattern. Part b shows $K = 0.5$ for in-phase combination. Part c shows $K = 0.2$ for quadrature mixing. Response for in-phase conditions is given by $E = K + \cos \theta$.

Loop Sense of Direction. Which of the two loop nulls indicates the correct bearing is usually determined by switching in some vertical-antenna voltage and noting which direction loop must be rotated to secure a null.
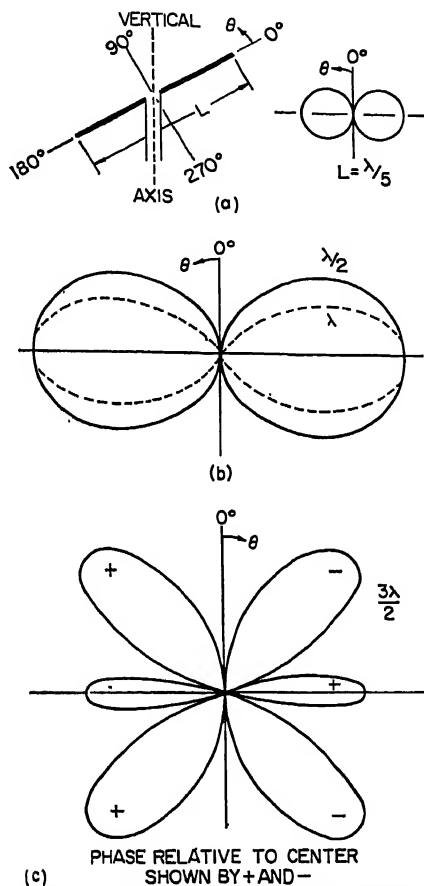
Fig. 28-17. Response patterns of horizontal dipoles of $\frac{1}{5}$, $\frac{1}{2}$, 1, and $1\frac{1}{2}$ wavelengths.

Loop Errors. For signals of zero elevation, the loop shows no error as the polarization is rotated from vertical to horizontal, but the induced voltage (at maximum response position) is proportional to the cosine of this angle of polarization rotation from the vertical.

Downcoming pure vertically polarized signals produce neither error nor reduction in maximum response, but any horizontally polarized component induces voltage at the normal null position. The *standard wave error* for a loop is 37° (45° polarization, 45° elevation angle).

Note that both tilting and rotating the loop to produce a null cannot indicate the direction of arrival. It can only determine the direction of the magnetic field, which

is not sufficient, because such an inclined magnetic field may be produced by many combinations of direction, elevation angle, and polarization rotation.

Horizontal Dipole. The horizontal patterns in free space for center-fed dipoles of length $L = \lambda/5$, $\lambda/2$, λ, and $3\lambda/2$ are shown in Fig. 28-17.

Length	Pattern factor
$< \dfrac{\lambda}{10}$	$\sin \theta$
$\dfrac{\lambda}{2}$	$\dfrac{\cos\,(\pi/2\,\cos\,\theta)}{\sin\,\theta}$
λ	$\dfrac{\cos\,(\pi\,\cos\,\theta)\,+\,1}{\sin\,\theta}$
$\dfrac{3\lambda}{2}$	$\dfrac{\cos\left(\dfrac{3\pi}{2}\,\cos\,\theta\right)}{\sin\,\theta}$

The three-dimensional patterns are all solids of revolution of the horizontal pattern around the long axis of the dipole. Thus for $L = \lambda/10$ the shape is that of a doughnut with zero-diameter center hole.
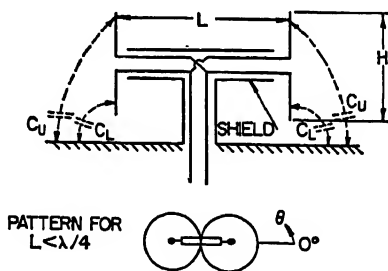
FIG. 28-18. Elevated-H-Adcock antenna.

For direction finding on horizontally polarized signals the horizontal dipole may be used as a manually rotated device with aural null indication. It is generally restricted to the VHF and UHF regions.

Errors due to downcoming signals having some vertical polarization are negligible, since the pattern of the horizontal dipole is unaffected by elevation angle. Any currents in the vertical support, however, may induce voltages affecting the null.

Elevated H Adcock. For frequencies in the 2- to 30-Mc region, a loop is unsatisfactory because of its large errors on downcoming sky-wave signals containing some horizontally polarized energy.

To minimize these errors, the arrangement of Fig. 28-18 is used. Two vertical dipoles are spaced by a horizontal support which carries balanced transmission lines cross-connected at the center to a line feeding the receiver.

The pattern for vertically polarized signals in the horizontal plane appears in Fig 28-4e and is similar to that of a loop. The induced voltage of the system for-spacing L less than $\lambda/4$ is

E_{IND} = field strength (μv/meter) $\times$ 0.635$H \times L$ (electrical degrees) cos θ

where H = height of a dipole, meters

θ = angle of arrival

0.635 = effective height of a 1-meter dipole

For downcoming signals arriving at angle ϕ to the ground, the above response E_{IND} is multiplied by $\cos^2 \phi$, since both the phase difference between dipoles and their induced voltages decrease with cos ϕ.

Since the capacities to ground C_U and C_L of the upper and lower halves of the dipoles are unequal, some shortening of the lower halves is required to secure balanced output.

Elevated-H-Adcock systems are usually manually rotated to secure a null. For UHF, the smaller size (L = 18 in.) allows high-speed motor rotation and a cathoderay-tube indication.

Standard wave error for an H Adcock without artificial balancing has been given[41] as 4° for 10 Mc and 3° for 1 Mc. At VHF, the errors vary with frequency and are greatest when (1) the product of aerial length and spacing equals $\lambda/20$; (2) the spacing is $\lambda/2$; and (3) aerial length and spacing = 0.8λ.[50]

FIG. 28-19. Vertical coplanar spaced loops rotated about vertical axis A-A.

Spaced Loops. These are useful for sky-wave signals. At the null, downcoming horizontally polarized energy (which causes errors in single loops) produces identical signals in each loop, which are canceled by the cross connection. In addition, the
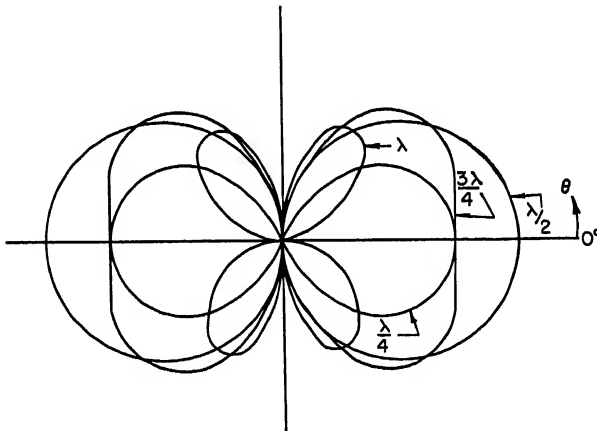
FIG. 28-20. Response patterns of vertical coplanar spaced loops for center-to-center loop spacings in wavelengths.

induced voltage of downcoming signals is not reduced as with Adcock antennas. Two types of spaced-loop systems are used as follows:

Vertical Coplanar Loops. Connections are as in Fig. 28-19, and patterns in Fig. 28-20. The open-circuit voltage is

$$E_{INDISIDE} \, L \cos \theta \, \sqrt{2[1 - \cos (S° \cos \theta)]}$$

where E_{IND} = voltage induced per loop side

$\quad\quad S°$ = electrical degrees between center of loops

$\quad\quad \theta$ = angle of arrival

$\quad\quad L$ = loop side to side spacing, electrical degrees. $L < \lambda/4$

Vertical Coaxial Loops.   Although coplanar loops reduce sky-wave error, there may still be some coupling between loops and the horizontal support.   Coaxial loops

(a)

(b)
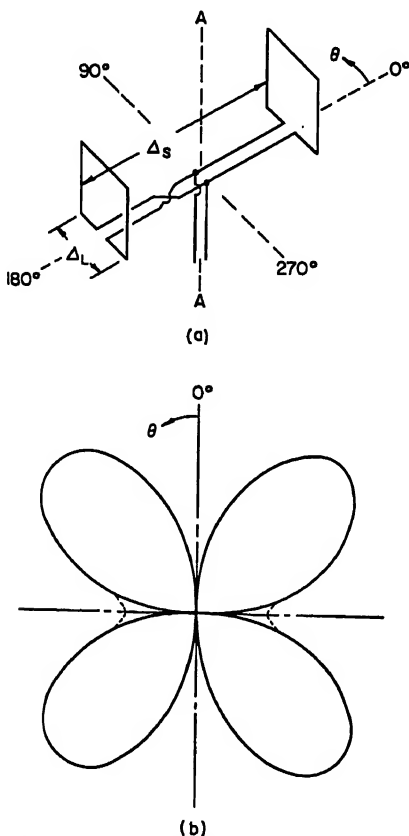
FIG. 28-21. Vertical coaxial spaced loops and response pattern.   Dotted lines indicate effect of undesired horizontally polarized signal.

as in Fig. 28-21a decrease this coupling and improve the null quality, but at the expense of a 4-null-per-revolution pattern as in Fig. 28-21b, which is described by

$$E_R = \frac{E_L\,\Delta_L\,\Delta_S}{2}\sin 2\theta$$

where E_L = induced voltage one side of a loop

$\quad\quad \Delta_L$ = loop side-to-side spacing, electrical degrees

$\quad\quad \Delta_S$ = loop center-to-center spacing, electrical degrees

$\quad\quad \theta$ = angle of arrival measured from line through center of loops

The null in the 0 to 180° direction will be clear under all conditions, while the 90 to 270° null will be blurred as shown in the dotted lines when horizontally polarized downcoming signals are present.

Horizontal Coplanar Loops. When spaced loops are arranged as in Fig. 28-22 so as to lie in the horizontal plane, the pattern for horizontally polarized signals is the same as for the elevated *H* Adcock with vertical polarization, i.e., a simple figure of eight for spacings below λ/4. As in the Adcock, the polarization error is small and response to downcoming signals is proportional to $\cos^2 \phi$, where ϕ = angle of elevation of the signal.

A second class of DF rotatable arrays includes the following.

Amplitude-comparison Systems. These employ two directive-antenna arrays whose relative amplitude is examined to determine direction. The advantages are
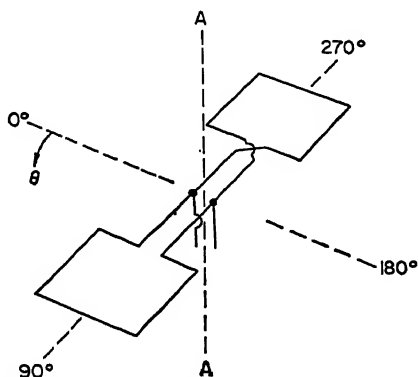
Fig. 28-22. Horizontally polarized spaced loops.

PATTERNS   RECEIVER   IND.
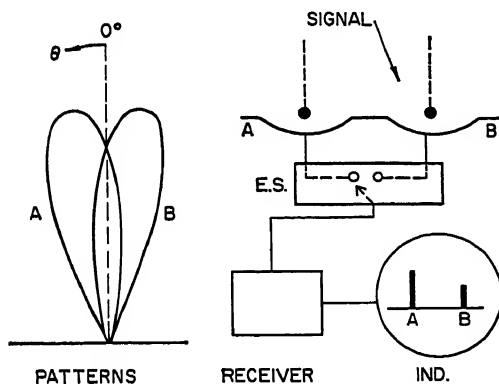
Fig. 28-23. Switching of overlapping directive patterns.

increased gain, resistance to interfering signals from the rear, and occasionally dual-polarization response. Two directive elements are generally arranged with identical overlapping patterns as in Fig. 28-23 and are alternately switched into the receiver input. The receiver output is synchronously switched to two positions on a cathode-ray tube to allow comparison of the two signal levels, which are made to be equal by rotation of the entire system.

A wide variety of antenna types may be used with amplitude-comparison systems. Virtually any antenna with unidirectional properties may be used, and the reader is referred to the other chapters of this book for the characteristics of suitable antenna types.

Airborne Automatic DF (ADF). This is a special case of a vertically polarized rotatable system which avoids ambiguity by using both a loop and a vertical sense antenna. The combination pattern of the two antennas is a cardioid whose broad null is unsuitable for DF. By the ingenious expedient of modulating the loop with a low audio frequency, the sharp loop null is used without the masking effect of the sense antenna or of noise. The modulation detected and delivered by the receiver is then proportional to the RF voltage induced in the loop.
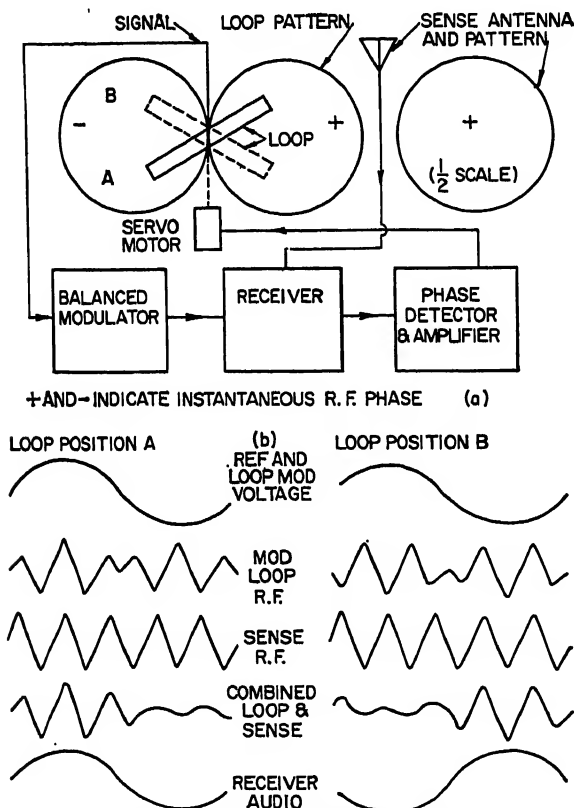
Fig. 28-24. L-F automatic-direction-finder block diagram with modulating and demodulating voltages.

In Fig. 28-24 is seen a loop in two possible positions A and B on opposite sides of a null for the signal. This loop voltage is fed to a balanced modulator driven by a reference audio oscillator of, say, 90 cycles. This kind of modulator suppresses the carrier and delivers the two sidebands to the receiver. The instantaneous r-f phase of these sidebands differs by 180° for conditions A and B, since the loop phase reverses when passing through a null.

When the sidebands are recombined with the constant-phase sense-antenna energy, the resulting audio envelope and demodulated signal change phase 180° (with respect to the reference) as the loop r-f voltage changes 180° in passing through a null. A phase detector and servo rotate the loop in the right direction to approach the null giving the correct direction. The opposite null is theoretically a point at which the servo could also come to rest but in practice is unstable.

28.3. FIXED ANTENNA SYSTEMS WITH ROTATABLE PATTERNS

Principles. These systems are used to simulate the rotation of a directional antenna which is too large to be physically rotated conveniently. As an example of the principle, Fig. 28-2 shows a crossed-loop arrangement feeding a goniometer having two stator coils at right angles to each other and enclosing a small rotor coil. It is desired to simulate the radio-frequency field (exciting the antennas) within the goniometer, so the rotor may be treated as if it were a real rotating loop.

It is necessary that the antenna patterns be proportional to sin θ and cos θ and be identical in maximum response. In addition, the coupling law between rotor and
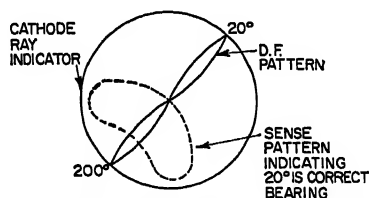
FIG. 28-25. Propeller pattern CRT display and sense pattern as used in high-frequency direction finder.
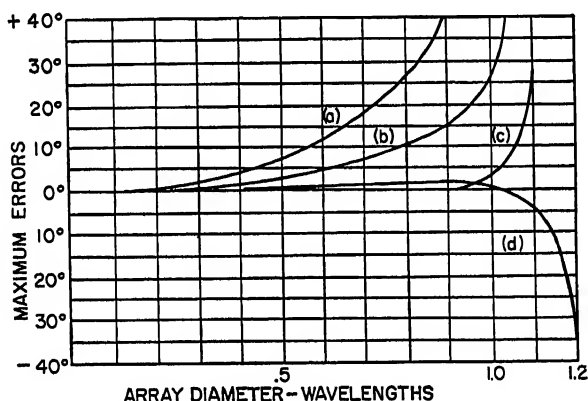
FIG. 28-26. Spacing (octantal) errors in Adcock systems: (a) 4-element, 2-phase. (b) 8-element, 2-phase, 45° between parallel antennas. (c) 8-element, 4-phase. (d) 8-element, 2-phase, 55° between parallel antennas.

stators must vary in a sinusoidal manner. Remembering that loop phase reverses as signal passes through a null, the individual vectors representing the separate stator fields and their resultant are shown in the figure.

The rotor may be turned manually to secure an aural null or motor-rotated in synchronism with a circle on a cathode-ray tube which is displaced inward for increasing signal. Figure 28-25 shows the type of display together with a sense pattern.

Limitations and Errors. If the loop width or Adcock element spacing exceeds $\lambda/5$, the response patterns depart from the true cosine law (Fig. 28-4e). For two crossed pairs (as a four-element Adcock) no errors occur at 0, 45, 90°, etc., but at $22\frac{1}{2}$, $67\frac{1}{2}°$, etc., the relative energy fed to the stator coils differs from $\lambda/5$ conditions and the resultant field is displaced toward the greater response. The error so produced is octantal in nature and alternately positive and negative. The form and magnitude of such maximum errors for various fractional wavelength spacings are

shown in Fig. 28-26 for four- and eight-element Adcocks. The error is about 1° maximum for a four-element spaced λ/5 or an eight-element spaced 0.95λ and, because it increases with frequency, cannot be compensated for in the goniometer. The spacing error for a given four-element Adcock decreases with angle of elevation of arriving signal, as in Fig. 28-27.

Quadrantal Error. This occurs when the gain of the north-south pair of antennas, or its transmission-line loss, or its stator-to-rotor transfer differs from corresponding characteristics in the east-west. On ships the loop whose plane lies fore and aft
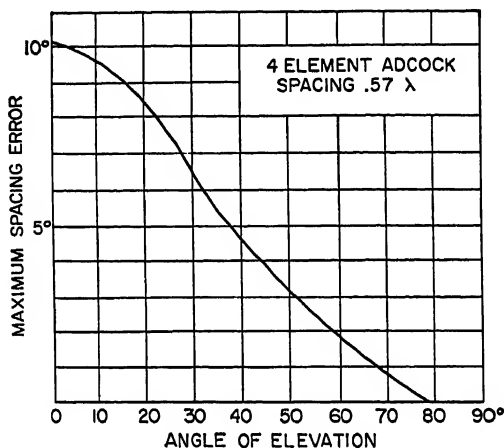
FIG. 28-27. Decrease of spacing errors with increase in elevation angle of signal.
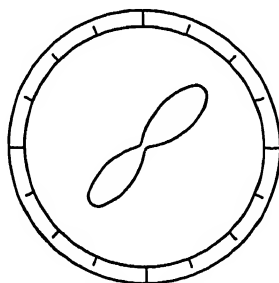
FIG. 28-28. Poor CRT DF pattern due to phase difference in antenna circuits.

receives more signal because of hull currents, and compensation is required. An amplitude difference of 3 per cent produces about 1° error at the 45° points.

Tuning Errors. Tuning of each pair of antennas requires that each circuit has the same Q and be tuned to exactly the same frequency. Reference to universal resonance curves[66] will show that if the resonant frequencies of the two pairs differ by as little as 0.2 per cent the amplitude responses (for circuit Q's of 100) will differ by 6 per cent, with a consequent error of about 1½°. In addition, the phase difference will be about 24° and will produce a poor CRT minimum pattern as in Fig. 28-28. For these reasons tuned circuits are not in practical use except in very special circumstances.

Crossed Loops. These are generally used for vertical polarization at frequencies below 1.5 Mc where small size of the antennas is necessary and where errors due to sky-wave reception are small. The arrangement appears as previously shown in Fig. 28-2. The performance is similar to that of a single rotated loop of the same

size, except that the coefficient of coupling of the goniometer (which may be 50 to 60 per cent) reduces the energy transfer. Because of space requirements, the loops are usually much less than 1λ in diameter, and negligible spacing error results.

Crossed Horizontal Dipoles. These can be used for horizontal polarization. λ/2 dipoles provide a convenient 73-ohm radiation resistance for matching purposes but introduce an octantal error of about 3½°. λ/4 dipoles reduce the error to 1°, with a radiation resistance of approximately 20 ohms. Since dipoles are usually employed at frequencies above 50 Mc, a capacity goniometer is frequently used to avoid the necessity of shielding an inductive goniometer.
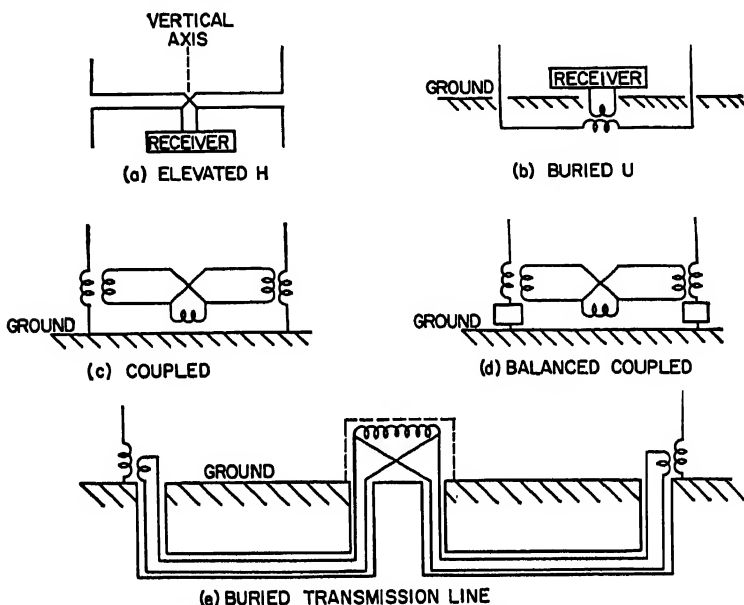
FIG. 28-29. Adcock antenna variations: elevated, buried, balanced.

Fixed Adcock Arrays with Goniometer. The basic Adcock building block consists of a pair of antenna elements spaced and cross-connected to produce a figure-of-eight pattern and providing the very useful characteristic of being relatively insensitive to the undesired (usually horizontal) polarization. One form consists of two vertical dipoles elevated above ground; the other form employs monopole antennas working against ground. Various arrangements are shown in Fig. 28-29. The monopole types are most frequently used, particularly the one employing buried transmission lines.

Four or eight separate antennas combined as in Fig. 28-30a and b are generally used. Eight antennas allow greater spacing and more gain for a given error, the limit of spacing being 1.22λ for an infinite number of antennas. In part c a simpler goniometer may be used, provided 2° of spacing error may be tolerated. Errors due to nonsymmetrical mutual coupling have not been evaluated.[38]

Spacing of greater than ¾λ requires a separate sense antenna.

The spacing errors of four antennas (two pairs) and eight antennas (four-phase goniometer) are shown relative to spacing in Fig. 28-26.

Wullenweber. Wullenweber consists of a number of vertical antennas symmetrically located around a cylindrical screen as shown in Fig. 28-3. Each antenna is connected to a capacity stator segment of a rotating switch. The rotor segments

span about 100° of arc and feed delay lines D_1, D_2, and D_3, whose values are equivalent to the like-marked free-space delays of the signal. The signals from all antennas arrive at the receiver in phase to produce the sharp beam due to a broadside array.

The system pattern has maximum gain on its axis of symmetry, but the side-lobe level is only 12 db down. Introduction of loss into the off-center antenna circuits can modify the pattern as described in Chap. 2 for fixed broadside arrays.

(a) 4 ELEMENT- 2 PHASE

(b) 8 ELEMENT- 4 PHASE

PLAN VIEW ADCOCK ARRAYS
WITH GONIOMETER. STATOR
COILS ARE CONNECTED
DIAMETRICALLY ACROSS
CENTER, AS 1 TO 1, 2 TO 2

(c) 8 ELEMENT- 2 PHASE
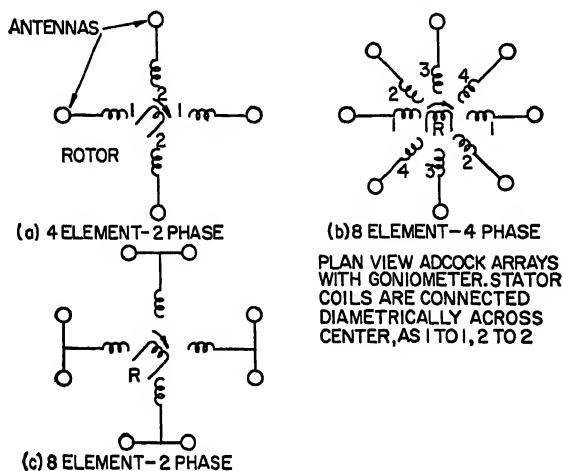
FIG. 28-30. Adcock array and goniometer connections.

PLAN VIEW

DOPPLER PRINCIPLE
ANTENNA MOVED IN CIRCLE
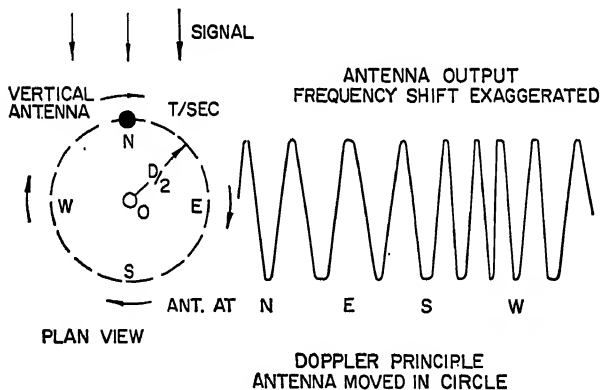
FIG. 28-31. Doppler principle.

Doppler. The basic principle depends on moving an antenna in a circular path and comparing the resulting phase or frequency modulation of a receiver signal with the antenna rotational position. In Fig. 28-31 a single vertical antenna is moved about point O at T revolutions per second. The frequency of the received signal is unchanged at N and S, but is decreased at E and increased at W. The antenna output is phase-modulated at rate T. The receiver is usually arranged to multiply the signal to produce frequency modulation, after which the signal is heterodyned to a convenient intermediate frequency and detected in a discriminator to produce an audio output whose phase can be compared with a reference signal derived from the antenna rotation. The radius of the antenna circle is limited to $\lambda/2$ at the highest usable frequency in order to avoid ambiguities.

In practical systems, a circular fixed array of vertical antennas is used and the phase modulation secured by connecting the receiver to successive antennas by means of a capacity switch.

The antenna requirements are relatively moderate, since amplitude variations are removed by limiting. Dipoles or monopoles may be used, provided they are similar, but equal electrical length of transmission lines must be maintained.
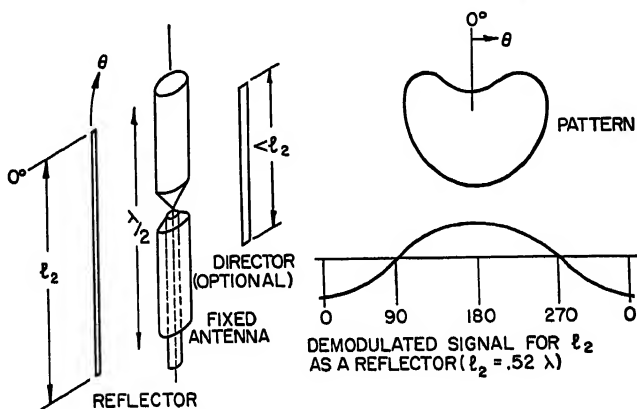
FIG. 28-32. Rotated reflector and vertical antenna with resultant modulation.
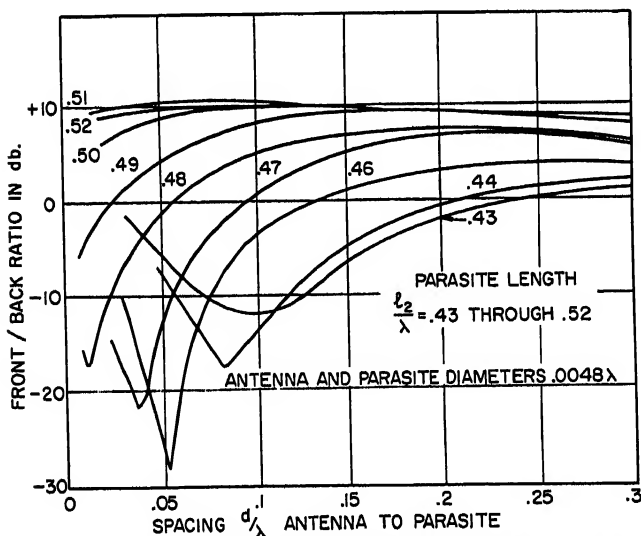
FIG. 28-33. Reflective effect of parasitic antenna 0.5λ and less.

Circuitry involved in use of arrays over 1λ in diameter and depending on cyclical phase difference between adjacent antennas is covered in Refs. 35 and 57.

Fixed Antenna with Rotating Reflector. When the wavelengths of interest are sufficiently short (say, 3 meters) to permit mechanical rotation of a reflector, the signal received by a fixed vertical antenna may be modulated with a rotated reflector as in Fig. 28-32. The pattern is approximately cardioid in shape and because of symmetry can contain only odd harmonics and fundamental when demodulated. The

phase meter used to compare the receiver output with the reference voltage must respond to the fundamental component only. Additional depth of modulation can be secured by use of a director less than $\lambda/2$ for the highest frequency used.

Experimental curves showing the front-to-back ratio of a $\lambda/2$ antenna with various lengths of parasitic antennas at different spacings are shown in Fig. 28-33. Note that the parasitic antenna is a reflector when over $\lambda/2$ long and becomes a director as the length and spacing decrease.
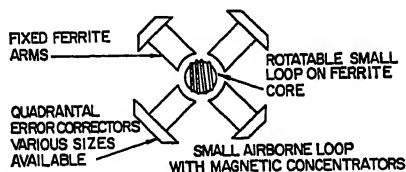
FIG. 28-34. Airborne ADF loop with magnetic concentrators.

Airborne Loop with Magnetic Concentrators. To avoid moving large masses of iron in an airborne servo-driven loop, the loop is made small and placed in the field of four fixed ferrite bars as in Fig. 28-34. Various length-corrector bars are attached to adjust for quadrantal error caused by the airplane structure. The principle of operation is the same as for standard DF.

28.4. SPECIAL QUASI-INSTANTANEOUS TYPES

Watson-Watt. The Watson-Watt DF employs two loops or Adcocks at right angles as in goniometer (Bellini-Tosi) systems (Fig. 28-35). The output of each
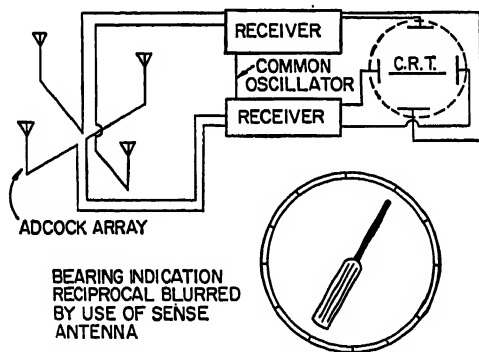
FIG. 28-35. Watson-Watt dual-channel instantaneous-DF block diagram and pattern.

antenna pair is amplified by a separate receiver and applied to one pair of deflection plates of a CRT indicator. The bidirectional pattern may be modified by sense-antenna energy so as to blur the reciprocal-bearing direction. A test signal is required to allow the receivers to be adjusted for equality of gain and phase. The Watson-Watt system is useful for the reception of short-duration signals since it produces a practically instantaneous display.

Phase Comparison.[62] These systems have been proposed using two omnidirectional antennas spaced several wavelengths apart with each connected through a receiver to a phase detector and indicator. In this case the separate channels require excellent phase stability.

28.5. SENSE ANTENNAS

The various systems which employ a figure-of-eight antenna pattern have a 180° ambiguity. To resolve this, energy from a vertical sense antenna with omnidirectional pattern is combined with the figure-of-eight voltage to produce a cardioidlike pattern as in Fig. 28-5a. If the loop is then rotated from one null position (say, 0°) toward 90°, the signal will decrease. If rotation in the same direction starts from 180°, the signal will increase. Hence the direct and reciprocal bearings may be determined.
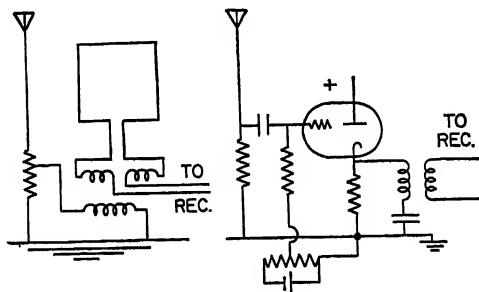
Fig. 28-36. Sense-antenna circuits using resistance.
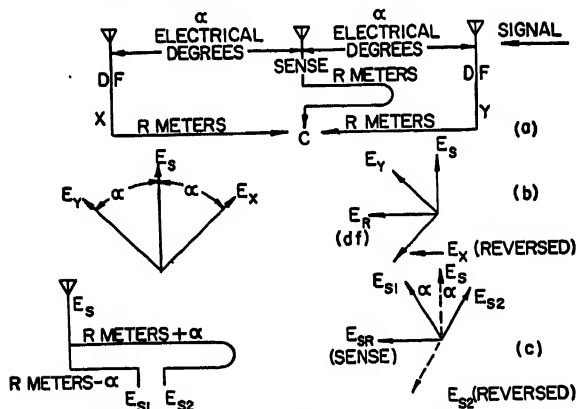
Fig. 28-37. Dual-delay sense-circuit principles.

From Fig. 28-4d, the sense-antenna induced voltage is 90° out of phase with respect to the loop resultant induced voltage E_R. E_S must be shifted 90° to allow combination with the loop voltage to produce a cardioid.

Sense phase shift may be secured by resistance-loading the sense antenna with 2,000 to 5,000 ohms or using an amplifier with gain control as in Fig. 28-36. For relatively narrow bands, a length of transmission line may often be inserted in the sense circuit and adjusted experimentally.

For broadband applications, and in Adcocks where the loss due to a resistance in the sense-antenna circuit cannot be tolerated but where coupling amplifiers are permitted, another scheme is possible.

Consider a four-element Adcock with a sense antenna at the center. Assume a signal arriving in line with a pair of DF antennas; the other pair is at a null and can be neglected. In Fig. 28-37a are seen DF antennas X and Y spaced R meters from

the sense antenna and connected to a common point C by R meters of transmission line. For discussion, insert R meters of line in a sense-antenna circuit.

The vector conditions at C before combination are shown in part b, where E_x and E_y lead and lag E_s by α electrical degrees, which is the free-space delay due to R meters. After combination, E_x is shown reversed as in actual practice and the DF resultant voltage E_R is seen to be 90° out of phase with E_s.

Suppose that in part c we modify the connection from E_S to C by providing two paths in which the delays are R meters $-\alpha$ electrical degrees and $R + \alpha$ electrical degrees. Consider the two output voltages now delivered to C as E_{S1} and E_{S2}. They appear vectorially as leading and lagging the original E_S (at C) by α. Now reverse E_{S2} and combine with E_{S1} to produce the resultant sense voltage E_{SR} which is in phase with E_R.
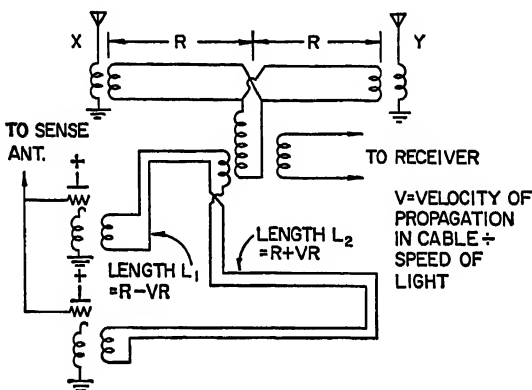
Fig. 28-38. Dual-delay practical sense circuit.

The amount of transmission line to be removed or added to R must have the same delay as α. Hence

$$L_1 = R - VR \quad \text{and} \quad L_2 = R + VR$$

where R = radius of array

V = velocity of propagation of transmission line used expressed as fraction of speed of light

A practical circuit appears in Fig. 28-38.

REFERENCES

1. R. H. Marriott: "An Electrical Method for Guiding Aerial and Marine Craft," *Proc. IRE*, October, 1920.
2. L. W. Austin: "Loop Uni-directional Receiving Circuits for Detecting Direction of Arrival of Atmospheric Disturbances," *Proc. IRE*, August, 1923.
3. R. H. Barfield: "Shielded Loop," *J. IEE (London)*, vol. 62, p. 249, 1924.
4. H. T. Friis: "New Directional Receiving System," *Proc. IRE*, December, 1925.
5. R. A. Watson-Watt and J. F. Herd: "An Instantaneous Direct Reading Goniometer," *J. IEE (London)*, vol. 64, p. 11, 1926; also *Wireless World*, vol. 18, p. 366, 1926.
6. H. Pratt: "Night Variations in Cross Coil Radio Beacons," *Proc. IRE*, May, 1928.
7. J. H. Dellinger and H. Pratt: "Development Radio Aids to Air Navigation," *Proc. IRE*, July, 1928.
8. R. L. Smith-Rose: "Radio DF Transmitters and Receivers," *Proc. IRE*, March, 1929.
9. H. Pratt: "Field Intensity Characteristics Double Modulation Directional Radio Beacon," *Proc. IRE*, May, 1929.
10. H. A. Chinn: "Radio Beacon without Night Effect," *Proc. IRE*, June, 1933.

11. R. H. Barfield: "Principles Underlying the Design of Spaced Aerial DF," *J. IEE (London)*, vol. 76, p. 423, April, 1935.
12. P. B. Taylor: "Theory of Loop Antenna with Leakage between Turns," *Proc. IRE*, December, 1937.
13. R. H. Barfield: "Elevated Transmitter for Testing Direction Finders," *Wireless Eng.*, vol. 15, p. 495, September, 1938.
14. R. E. Burgess: "Screened Loop Aerials," *Wireless Eng.*, vol. 16, p. 492 (October), 1939.
15. H. Pigge: "New Type DF Antenna," *Hochfrequenztech u. Electroakustik*, vol. 54, December, 1939.
16. J. D. Kraus: "Antenna Arrays with Closely Spaced Elements," *Proc. IRE*, February, 1940.
17. R. H. Barfield: "Compensated Loop Direction Finder," *J. IEE (London)*, vol. 86, April, 1940.
18. R. L. Smith-Rose and H. G. Hopkins: "Radio Direction Finders," *J. IEE (London)*, vol. 87, August, 1940.
19. J. A. McGillivray: "Direct Reading DF," *Wireless World*, vol. 46, October, 1940.
20. E. M. Williams: "Radiating Characteristics of S. W. Loops," *Proc. IRE*, October, 1940.
21. Breuninger: "Three Mast Adock," *Hochfrequenztech u. Electroakustik*, February, 1941.
22. R. E. Burgess: "Signal to Noise in Receiving Aerials," *Proc. Phys. Soc.*, May, 1941.
23. G. F. Levy: "Loop Antennas for Aircraft," *Proc. IRE*, February, 1943.
24. D. E. Foster and C. W. Finnegan: "Method of Measuring Loop Shielding," *Proc. IRE*, June, 1943.
25. F. S. Howes and F. M. Wood: "Loop Errors in Abnormally Polarized Fields," *Proc. IRE*, April, 1944.
26. R. E. Burgess: "Reactance and Effective Height of Screened Loop Aerials," *Wireless Eng.*, May, 1944.
27. J. Sherman: "Circular Loops for UHF," *Proc. IRE*, September, 1944.
28. D. Foster: "Loop Antennas with Uniform Current," *Proc. IRE*, October, 1944.
29. F. E. Terman and J. M. Pettit: "Compensated-loop Direction Finder," *Proc. IRE*, May, 1945.
30. C. C. Pine: "New Type Direction Finder," *Proc. IRE*, August, 1945.
31. W. S. Bachman: "Loop Antenna Coupling Transformer Design," *Proc. IRE*, December, 1945.
32. L. L. Libby: "Shielded Loops," *Proc. IRE*, September, 1946.
33. R. Keen: "Wireless Direction Finding," 4th ed., Iliffe & Sons, London, 1947.
34. J. H. Moon: "Design of Electromagnetic Goniometers for Use in Medium Frequency Direction Finding," *J. IEE (London)*, vol. 94, p. 69, January, 1947.
35. C. W. Earp and R. M. Godfrey: "Radio Direction Finding by Measurement of the Cyclical Difference of Phase," *J. IEE (London)*, pt. IIIA, vol. 94, p. 705, March, 1947.
36. F. Horner: "Experimental Spaced Loop VHF DF," *J. IEE (London)*, pt. IIIA, vol. 94, March, 1947.
37. Pearce: "Conductive Screens: U-type Spaced Aerials," *J. IEE (London)*, pt. III, vol. 94, March, 1947.
38. P. G. Redgment, W. Struszynski, and G. J. Phillips: "An Analysis of the Performance of Multi-aerial Adcock Direction-finding Systems," *J. IEE (London)*, pt. IIIA, vol. 94, no. 15, March, 1947.
39. W. Ross: "Use of Earth Mats to Reduce Polarization Errors in U Type Adcocks," *J. IEE (London)*, pt. III, vol. 94, no. 28, March, 1947.
40. W. Ross: "Development and Study of Practical H.F. Spaced Loops," *J. IEE (London)*, pt. IIIA, vol. 94, March, 1947.
41. W. Ross: "Site and Polarization Errors in H.F. D.F.," *J. IEE (London)*, pt. III, vol. 94, March, 1947.
42. J. E. Browder and V. J. Young: "Design Values for Loop-antenna Input Circuits," *Proc. IRE*, May, 1947.
43. J. Kobilsky: "Loop Antenna Coupling Transformers," *Proc. IRE*, September, 1947.
44. H. A. Wheeler: "Fundamental Limitation of Small Antennas," *Proc. IRE*, December, 1947.
45. L. J. Giacolletto and S. Stiber: "Medium Frequency Crossed-loop Direction Finder," *Proc. IRE*, September, 1949.
46. M. Joachim: "Theory of the Double-frame Radiogoniometer," *Časopis Pěst. Mat. Fis.*, vol. 75, no. 1, 1950. In Czech.
47. W. R. LePage, C. S. Roys, and S. Seely: "Radiation from Circular Current Sheets," *Proc. IRE*, September, 1950.
48. J. H. Moon: "The Development of the Aircraft Automatic Radio Compass," *J. Inst. Navigation*, vol. 3, October, 1950.

49. J. E. Walsh: "Radiation Pattern of Arrays on Reflective Cylinder," *Proc. IRE*, September, 1951.

50. H. G. Hopkins and F. Horner: "Rotating H-type Adcock Direction-finders for Metre and Decimetre Wavelengths," *IEE Monograph* 11, *Proc. IEE (London)*, pt. IV, vol. 98, October, 1951.

51. W. R. LePage and R. F. Harrington: "D.F. Array Elements about Cylindrical Reflector," *Proc. IRE*, January, 1952.

52. F. Horner: "An Investigation of Polarization Errors in an H Adcock Direction Finder," *IEE Monograph Proc. IEE (London)*, pt. IV, vol. 99, April, 1952.

53. J. R. Wait: "Receiving Properties of a Wire Loop with a Spheroidal Core," *Can. J. Technol.*, vol. 31, January, 1953.

54. L. A. Raburn: "Faired-in A.D.F. Antennas," IRE Convention Record, 1953.

55. J. G. Holbrook: "Null Characteristics of the Rotating Adcock Antenna System," *J. Appl. Phys.*, vol. 24, pp. 530–532, May, 1953.

56. J. R. Wait: "Radiation Resistance of a Small Circular Loop in the Presence of a Conducting Ground," *J. Appl. Phys.*, vol. 24, May, 1953.

57. M. G. Hopkins and E. N. Bramley: "Practical Measurements of Relative Performance of a Cyclical Phase-comparison and U Adcock DF," *J. IEE (London)*, pt. III, vol. 100, no. 67, September, 1953.

58. H. Meinke: "Wide-band Directional Aerials with High Radiating Efficiency," *FTZ, Fernmeldetech. Z.*, vol. 7, April, 1954.

59. A. Kohler: "V.H.F. Direction-finding Aerials," *Funk u. Ton*, vol. 8, June, 1954. In German.

60. Fred Haber: "Generation of Standard Fields in Shielded Enclosures," *Proc. IRE*, November, 1954.

61. J. S. Belrose: "Ferromagnetic Loop Aerials for Kilometric Waves," *Wireless Eng.*, vol. 32, no. 2, February, 1955.

62. Friedland and Marchand: "AFMTC Technical Note: Phase Comparison DF," MTLG-152-1, Sept. 1, 1952.

63. F. E. Terman: "Radio Engineer's Handbook," p. 136, McGraw-Hill Book Company, Inc., New York, 1943.

Chapter 29

RADIO-TELESCOPE ANTENNAS

John D. Kraus

The Ohio State University
Columbus, Ohio

29.1. DEFINITION OF RADIO TELESCOPE

A radio telescope consists of an antenna for collecting celestial radio signals and a sensitive receiver for detecting and recording them. The antenna is analogous to the objective lens or mirror of an optical telescope, while the receiver-recorder is analogous to the eye or photographic plate (Fig. 29-1). By analogy the entire antenna-receiver-recorder system may be referred to as a "radio telescope," although it may bear little resemblance to its optical counterpart.[19,20]

Radio telescopes are used in much the same manner as ordinary astronomical telescopes, that is, for the observation and study of extraterrestrial emitting bodies. However, at radio wavelengths the sky has a strangely different appearance. With a radio telescope the sun is much less bright, while the Milky Way shines with tremendous brilliance, and hundreds of new objects called radio "stars" or localized sources dot the sky, forming totally unfamiliar constellations.[4,20,22,28]

The earth's atmosphere and ionosphere are opaque to electromagnetic waves with two principal exceptions, a band or window in the visual and infrared region and a wider window in the radio part of the spectrum. This radio window extends from *at least* 1 cm to 20 meters wavelength, being limited on the short-wavelength side by molecular absorption and on the long-wavelength side by ionospheric reflection. Radio telescopes observe through this radio window, and any antenna employed for

such celestial observation may be called a "radio-telescope antenna." Since the wavelength range in radio astronomy is at least 2,000 to 1, many different forms of antennas are used.[20]

There are several reasons for the different appearance of the sky at radio and visual wavelengths. Radio waves are immensely longer than light, and a celestial object that is an intense light source may be a very weak radio emitter, and vice versa. Also radio waves easily penetrate the huge clouds of dust in space that hide many objects from visual observation. Furthermore, radio telescopes have potentially a greater range than optical telescopes (see Sec. 29.8).

It should be noted that radio telescopes are entirely passive; that is, they receive only, depending on natural phenomena in the sources for the generation of the radio
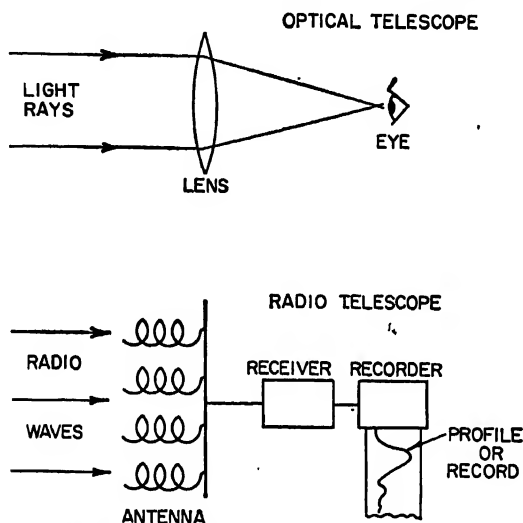
FIG. 29-1. Analogy between radio telescope and optical telescope.

waves. Many radio objects are so distant that it would take millions of years to receive a radar echo. Regardless of other considerations, such as the power required, this long echo interval is quite sufficient to make radar impractical. There are, however, two important exceptions. Radar can be employed to track meteors and also to measure the distance to nearby celestial objects, such as the moon and, probably in the near future, also some of the planets. Radar systems for such applications may be appropriately referred to as "radar telescopes."[22] Although radar telescopes, as such, are not discussed in this section, much of the material applies to them as well as to radio telescopes.

29.2. FUNCTIONS OF RADIO TELESCOPES

The purpose of a radio telescope is to detect and study celestial radio sources. In general, the ideal radio telescope should be able to provide as accurate and complete information as possible concerning each of the following source parameters:

1. The position of the source in the sky
2. The total power flux of the source and, in case the source has appreciable angular extent, the manner in which this power flux per unit solid angle (brightness) is distributed

3. The polarization and, in case the source is extended, the manner in which it varies with position

4. The modulation of the signal, if any

5. The dependence of the power flux (also its distribution, polarization, and modulation) on frequency, that is, the spectrum

6. The variation of position, power flux, polarization, and modulation with time, as could be produced by motion and variability in strength of the source

29.3. POSITION AND COORDINATES

The accurate position of the source is necessary to distinguish the source from others and to assist in its identification with optical objects where possible. The position is conveniently expressed in celestial equatorial coordinates,[10] *right ascension* (α) and *declination* (δ). The poles of this coordinate system occur at the two points where the earth's axis, extended, intersects the celestial sphere. Midway between these poles is the *celestial equator*, coinciding with the earth's equator, expanded.

The *declination* of an object is expressed in degrees and is the angle included between the object and the celestial equator. It is designated as a positive angle if the object is north of the equator and negative if south. For example, at the earth's equator a point directly overhead (the zenith) has a declination of 0° while at a north latitude of 40° the declination of the zenith is +40°.

The *meridian* is a great circle passing through the poles and a point directly overhead (the zenith). The *hour circle* of an object is the great circle passing through the object and the poles. The *hour angle* of the object is then the arc of the celestial equator included between the meridian and the object's hour circle. This angle is usually measured in hours.

A reference point has been chosen on the celestial equator. It is called the *vernal equinox*. The arc of the celestial equator included between the vernal equinox and the object's hour circle is termed the *right ascension* of the object. It is measured eastward from the vernal equinox and is usually expressed in hours, minutes, and seconds of time. It can also be expressed in degrees (°), minutes ('), and seconds (") of arc since:

$$1 \text{ hour} = 15° \qquad 1 \text{ min} = 15' \qquad 1 \text{ sec} = 15''$$

The right ascension and declination of an object define the position in the sky, independent of the earth's diurnal rotation. However, because of the earth's precession, there is a gradual change in these coordinates for a fixed object in the sky, the change completing one cycle in 26,000 years. Thus the right ascension and declination of an object will again be the same as they are now in 26,000 years. To be explicit, it is necessary to specify the date to which the right ascension and declination refer. This date is called the *epoch*. At present the epoch 1950.0 is most commonly used; that is, the right ascension and declination are those of Jan. 1, 1950.

Sometimes the positions of celestial objects are given in *galactic coordinates* which are based on the geometry of our galaxy.[26a] These coordinates are independent of the earth and hence require no date or epoch.

By placing an antenna on an *equatorial mounting*, that is, on axes one of which is parallel to the earth's axis and the other perpendicular to it, measurements of the right ascension and declination are greatly facilitated. However, if the antenna is mounted on vertical and horizontal axes, a coordinate conversion is required to obtain the right ascension and declination. The coordinates of antenna motion in this case are the *altitude* (or elevation) and the *azimuth* (horizontal angle), and hence this type of mounting is often called an *altazimuth* mounting.

For a more complete discussion of astronomical terms reference should be made to a book on astronomy.[1,2,10,15,21,26,29,33]

29.4. POWER FLUX DENSITY AND OTHER UNITS

Radiation over an extended area of the sky is conveniently specified in terms of its *brightness*, that is, the power per unit area per unit bandwidth per unit solid angle of sky. The symbol B is used for *brightness*, and in mksc units it is expressed in janskys* per steradian. Thus

$$B = \text{brightness (janskys rad}^{-2})$$

where 1 jansky = 1 watt per square meter per cycle per second
or   jan = w m^{-2} cps^{-1}
Solid angle is sometimes expressed in square degrees. Thus

$$1 \text{ steradian} = 57.3^2 \text{ square degrees} = 3{,}283 \text{ square degrees}$$

The integral of the brightness B over a given solid angle of sky yields the power per unit area per unit bandwidth received from that solid angle. This quantity is called the *power flux density*.† The symbol S is used for power flux density, and in mksc units it is expressed in janskys. Thus

$$S = \iint B \, d\Omega = \text{power flux density (jan} = \text{w m}^{-2} \text{ cps}^{-1}) \qquad (29\text{-}1)$$

where B = brightness (jan rad^{-2})
      $d\Omega$ = element of solid angle (rad^2)
The power flux density is also sometimes called the *intensity*.

In general, the celestial radio radiation has a continuous spectrum and, integrating the power flux density from a radio source with respect to frequency, yields the *total power flux density* S_T in the frequency band over which the integration is made. Thus

$$S_T = \int S \, df = \text{total power flux density (w m}^{-2}) \qquad (29\text{-}2)$$

where S = power flux density (w m^{-2} cps^{-1})
      df = element of bandwidth (cps)
There is a continuous background of radio radiation extending over the entire sky. This background radiation is a function of position in the sky and is conveniently specified by the brightness B, that is, the power flux density per square degree. Integrating B over a solid angle of sky yields the power flux density S from that solid angle. The power flux density is power per unit area per unit bandwidth at a particular frequency. As mentioned above, integrating this over a frequency band Δf yields the total power flux density S_T from that band of frequencies and solid angle Ω. Thus

$$S_T = \int_{\Delta f} \iint_{\Omega} B \, d\Omega \, df = B_{\text{avg}} \Omega \, \Delta f \qquad (29\text{-}3)$$

where B = brightness (jan rad^{-2})
      Ω = solid angle (rad^2)
      Δf = band of frequencies (cps)
      B_{avg} = average brightness (jan rad^{-2}) over Ω and Δf

* The jansky is named for Karl G. Jansky, pioneer American radio astronomer, who was the first to detect radio waves of extraterrestrial origin. However, the unit has not yet been adopted officially.[35]
† In optical astronomy the power flux density from a star is sometimes called its brightness. When this is done, the *brightness* B as defined above is called the *surface brightness*.

Whereas the brightness B is convenient for specifying the strength of radiation from extended regions of the sky, the power flux density S or total power flux density S_T is used for indicating the strength of localized sources or small areas of the sky.

Table 29-1

Source	Level	Unit
Cassiopeia A....................	57×10^{-24}	jansky
Cygnus A......................	38×10^{-24}	jansky
Taurus A......................	8×10^{-24}	jansky
Virgo A.......................	6×10^{-24}	jansky
Sky near galactic north pole.....	5×10^{-25}	jansky per square degree

As examples, the power flux density of four prominent localized radio sources as measured at 250 Mc/sec with the Ohio State University radio telescope is given in Table 29-1. The brightness of the sky background is also included for the region near the north galactic pole. The brightness here is nearly a minimum for the entire sky.

It is to be noted in Table 29-1 that the power levels are very low. For example, all the power from the strongest radio source, Cassiopeia A, falling on the entire earth's surface at 250 Mc/sec, amounts to less than one one-hundredth of a microwatt per cycle per second. It is evident that large antennas and sensitive receivers are essential in radio astronomy.

In general, celestial radio radiation is of an incoherent, unpolarized nature. A radio-telescope antenna, whether linearly or circularly polarized, will accept only half of the power available from such radiation. Accordingly, the powers listed in Table 29-1 are twice those observed so as to include the polarization component to which the antenna is insensitive.

29.5. EQUIVALENT TEMPERATURE AND CALIBRATION

A resistor of resistance R and temperature T matched to a receiver by means of a lossless transmission line as in Fig. 29-2a delivers a power to the receiver given by

$$P = kT \Delta f \qquad (29\text{-}4)$$

where P = power received (watts)

k = Boltzmann's constant ($= 1.38 \times 10^{-23}$ joule per degree Kelvin)

T = absolute temperature of resistor (degrees Kelvin)

Δf = bandwidth (cps)

If the resistor is replaced by an antenna of radiation resistance R, Eq. (29-4) still applies. However, the radiation resistance is not at the temperature of the antenna structure but at the effective temperature T of that part of the sky toward which the antenna is directed, as in Fig. 29-2b. In effect, the radiation resistance is distributed over that part of the sky included within the antenna acceptance pattern. From this point of view the antenna and receiver of a radio telescope may be regarded as a bolometer (or heat-measuring device) for determining the effective temperature of distant regions of space coupled to the system through the radiation resistance of the antenna.

It may be shown that the power received per unit bandwidth is related to the sky brightness by[28,36]

$$\frac{P}{\Delta f} = kT_b = \frac{1}{2} B\lambda^2 \tag{29-5}$$

since

$$T_b = \frac{B\lambda^2}{2k} \tag{29-6}$$

where T_b = brightness temperature or equivalent temperature of celestial object (deg Kelvin)

B = brightness of celestial object (including both polarizations), (jan rad^{-2})

λ = wavelength (meters)

k = Boltzmann's constant (1.38 $\times$ 10^{-23} joule per degree Kelvin)

It should be noted that the celestial object is not necessarily at the thermal temperature T_b. Rather, T_b is the temperature a black-body radiator would need to have in order to emit an amount of radiation equal to that actually emitted by the object at the wavelength λ. Hence, T_b is often called the *equivalent temperature* of
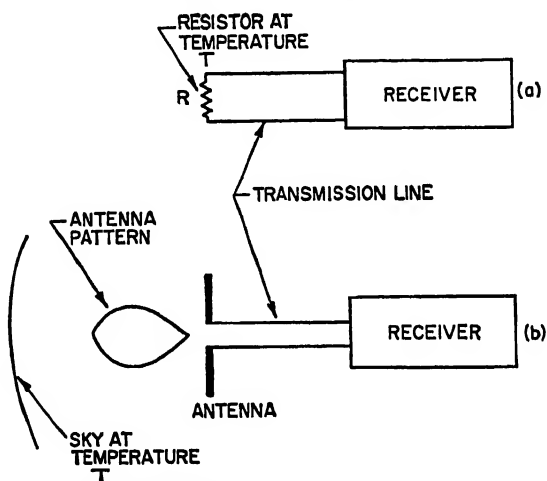
FIG. 29-2. Receiver connected to matched resistor and to antenna.

the object. For example, at a wavelength λ, a turbulent gas cloud at a thermal temperature T_0 may emit radiation equal to that from a black-body radiator at a much higher temperature T_b. It is then said that the gas cloud has an equivalent temperature T_b.

Referring to Table 29-1, the sky brightness near the north galactic pole is measured to be about 5 $\times$ 10^{-25} jansky per square degree at 250 Mc/sec (1.2-meter wavelength). This is equal to 1.64 $\times$ 10^{-21} jansky per steradian (square radian). From Eq. (29-6) the equivalent temperature of this part of sky at this frequency is then

$$T_b = \frac{1.64 \times 10^{-21} \times 1.2^2}{2 \times 1.38 \times 10^{-23}} = 86°\text{Kelvin}$$

By way of comparison, normal room temperature is about 295°Kelvin.

Temperature equations are not only of interest astronomically but they also form a convenient basis for the calibration of a radio telescope. Thus the power flux density from a celestial radio source is

$$S = \frac{2k \Delta T}{A} \tag{29-7}$$

where S = power flux density of celestial source (including both polarizations), (jan)

k = Boltzmann's constant [see Eq. (29-4)]

A = effective antenna aperture (including effect of cable losses)

ΔT = temperature change required in matched resistor (substituted for antenna) to give deflection equal to that for celestial source (deg Kelvin)

If the solid angle ω subtended by the source is known, the average source brightness is given by Eq. (29-7) divided by ω.

The average brightness of the sky over the beam area of the antenna is

$$B = \frac{2k\Delta T}{A\beta} \qquad (29\text{-}8)$$

where B = average brightness (jan rad^{-2})

k = Boltzmann's constant

A = effective aperture of antenna [as in Eq. (29-7)]

β = beam area of antenna (rad^2)

ΔT = temperature change of matched resistor (substituted for antenna) that gives deflection equal to that for sky (deg Kelvin)

Table 29-2. Units Used in Radio Astronomy

Dimension or quantity	Symbol	Description	Equation no.	Equivalent terms	Unit	Equivalent units
Brightness.......	B	$\dfrac{\text{Power flux density}}{\text{Solid angle}}$		Surface brightness	$\dfrac{\text{jan}}{\text{rad}^2}$	w m^{-2} cps^{-1} rad^{-1}
Power flux density	S	$= \iint B \, d\Omega$	(29-1)		jan	w m^{-2} cps^{-1}
Total power flux density........	S_T	$= \int S \, df$	(29-2)		w m^{-2}	
Power (in terms of temperature)...	P	$= kT \, \Delta f$	(29-4)		watts	
Brightness temperature....	T_b	$= \dfrac{B\lambda^2}{2k}$	(29-6)	Surface brightness temperature	deg. K	
Power flux density (in terms of temperature)...	S	$= \dfrac{2k \, \Delta T}{A}$	(29-7)		jan	w m^{-2} cps^{-1}
Average brightness (in terms of temperature)	B	$= \dfrac{2kT}{A\beta}$	(29-8)		$\dfrac{\text{jan}}{\text{rad}^2}$	

29.6. OBSERVED BRIGHTNESS DISTRIBUTION AND EFFECT OF ANTENNA SMOOTHING

The true response pattern of an antenna is obtained when the radiator is a point source situated at a sufficient distance from the antenna. The distance is sufficient if an increase in the distance produces no detectable change in the pattern. Let the true pattern of a receiving antenna be as shown in Fig. 29-3a. If the point source is replaced by an extended source at the same distance, the observed pattern is modified as suggested in Fig. 29-3b.[23] The extended source results in a broadened pattern with reduced minor lobes.

The patterns in Fig. 29-3 are in polar coordinates. In rectangular coordinates, the antenna pattern is as shown in Fig. 29-4a and the extended source distribution as in Fig. 29-4b. The observed pattern is then as shown in Fig. 29-4c. These three patterns are superposed in Fig. 29-4d to facilitate intercomparison.

It is to be noted that the observed pattern is only an approximation to the actual source pattern or distribution, the sharp shoulders of the source distribution being rounded off. It is said that the source distribution has been smoothed or blurred by the observing technique. The broader the antenna beamwidth compared with the source pattern, the greater is the smoothing effect. On the other hand, the narrower the antenna beamwidth compared with the source pattern, the more nearly is the observed pattern an exact reproduction of the source distribution. However, there is always some smoothing, and one of the important problems of radio astronomy

Fig. 29-3. Antenna patterns in polar coordinates for a point source and for an extended source.

is to reconstruct, in so far as possible, the source distribution from the observed pattern. It turns out that it is not possible to reconstruct the exact source distribution since certain of the finer source details have no effect on the observed pattern and are irretrievably lost.[6,20a] However, partial reconstruction is usually possible, so that a source distribution can be obtained that is more nearly like the exact source distribution than the observed pattern.

Fig. 29-4. Pattern in rectangular coordinates for antenna (a) with uniform source distribution (b). The resultant observed pattern is at (c). The three patterns are superposed for comparison in (d).

Referring to Fig. 29-5, the general problem of the effect of antenna smoothing may be stated as follows

$$G(\phi_0) = \int F(\phi + \phi_0) B(\phi) \, d\phi \qquad (29\text{-}9)$$

where $G(\phi_0)$ = observed pattern (jan)

     $F(\phi + \phi_0)$ = true antenna pattern (dimensionless)

         $B(\phi)$ = source brightness distribution (jan rad^{-1})

           ϕ_0 = hour angle (angle between maximum of antenna pattern and center of source) (rad)

The function $B(\phi)$ is the same as the brightness B referred to earlier, and it is convenient to assume that the power flux density of the source (integral of the brightness over the source) is a constant.

In Eq. (29-9) the more general (two-dimensional) problem has been simplified to the one-dimensional case where the patterns are functions only of one coordinate (ϕ). This has the advantage that the basic problem is retained intact but the analysis is greatly simplified. The simplified situation stated in Eq. (29-9) often occurs in prac-tice, as, for example, when the antenna pattern in the direction normal to ϕ is sufficiently broad compared with the source extent in this direction. In Eq. (29-9) the antenna pattern $F(\phi + \phi_0)$ and the observed pattern $G(\phi_0)$ are usually known, while the source brightness distribution $B(\phi)$ is unknown and is the function whose value is sought.

The function $B(\phi)$ in Eq. (29-9) is the brightness, with dimensions in this case of power flux density per unit angle instead of unit solid angle. The function $F(\phi + \phi_0)$ is the normalized antenna pattern. It is dimensionless and has a maximum value of unity. The observed pattern $G(\phi_0)$ has the dimensions of power flux density, being the

FIG. 29-5. Antenna pattern, source distribution, and observed distribution.

brightness function integrated over the extent of the antenna pattern for a particular value ϕ_0 of the hour angle.

For the case of a point source the brightness distribution becomes an infinitely high peak of zero width but of constant power flux density or integrated brightness (like an impulse function). In this case the observed pattern has the same shape as the true antenna pattern, or

$$G(\phi) = SF(\phi) \qquad (29\text{-}10)$$

where S = power flux density of source (jan)

At the maximum of the antenna pattern ($F(\phi) = 1$) the observed pattern $G(\phi)$ equals S.

For the case of a very extended source, with variations in brightness that are gradual compared with the antenna beamwidth, the observed pattern approximates closely the shape of the source distribution, or

$$G(\phi) = \beta B(\phi) \qquad (29\text{-}11)$$

where β = beam area (integral of antenna pattern) (rad or rad^2)

Although there are an infinite number of source distributions which will yield the same observed distribution, they differ only in the finer details. For example, the observed pattern will be the same for a continuous brightness distribution and a distribution of discrete point sources provided the separation of the sources is less than the half-power beamwidth. However, for larger spacings the observed pattern will differ for a continuous distribution and for a distribution of discrete point sources.

Although the exact brightness distribution of a source is not known, it is often very convenient in practice to assume that it is a uniform distribution. The width of such a uniform distribution required to yield the observed pattern broadening at the half-power level is called the *equivalent width* of the source. For example, calculated observed distributions are shown in Fig. 29-6 for the 40-wavelength uniform broadside array of the Ohio State University radio telescope for assumed uniform source distributions of various widths α. The patterns are symmetrical, only the right half being shown. By comparing an actual observed pattern with the curves of Fig. 29-6 the equivalent width of the source may be determined.[23]
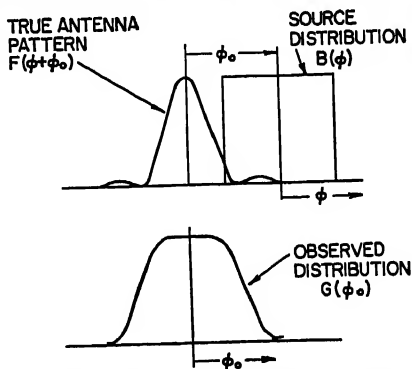
It is to be noted from Fig. 29-6 that the amount of observed pattern broadening is very slight when the source is much narrower than the antenna half-power beamwidth. In such cases the precision attainable in determining the equivalent width of a source depends largely on the source brightness, but even for bright sources one can usually only state the maximum possible extent of the source if the broadening amounts to less than a few per cent. Thus, if the broadening observed with a 40-wavelength antenna (Fig. 29-6) is less than 1 per cent, it is possible to state merely that the equivalent width of the source is less than $\frac{1}{10}$ degree. The relation between source extent and pattern broadening is shown explicitly in Fig. 29-7 for a 40-wavelength uniform broadside array.

FIG. 29-6. Patterns which would be observed with a uniform 40-wavelength broadside antenna for uniform sources of various width α. The patterns are symmetrical, only the right half being shown.

Although most sources may not have an exactly uniform distribution, as has been assumed for convenience, it should be mentioned that precisely this type of distribution does occur for spherical sources with uniform surface emission, as observed with a fan beam considerably broader in its wide dimension than the source.

As an illustration of the extent to which a source brightness distribution can be determined from an observed pattern, there is shown at the left in Fig. 29-8a a profile of the Cygnus region observed with the Ohio State University radio telescope at a
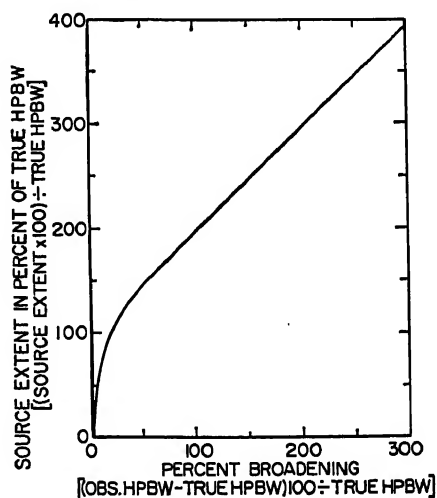
FIG. 29-7. Pattern broadening at half power as a function of uniform source extent for a 40-wavelength uniform broadside antenna.

declination of +40.5°. This profile, obtained by H. C. Ko and D. V. Stoutenburg on Nov. 27, 1954, shows structure caused by a number of localized and extended radio sources. No detectable broadening is observed for the Cygnus A source, but there is appreciable broadening for the sources designated Cygnus X and Cygnus B.

In Fig. 29-8*b* is shown the equivalent source brightness distribution which can be deduced from the observed profile. The ordinate is brightness. The Cygnus A width is known from other observations to be less than that shown, but the width in Fig. 29-8*b* is an upper limit as based on the observed profile. The brightness of Cygnus A in Fig. 29-8*b* should be 2½ times that shown. The weak source near right ascension 21 hr is due to the North American nebula. The removal of the four discrete sources from the profile leaves the smooth background level which peaks at the
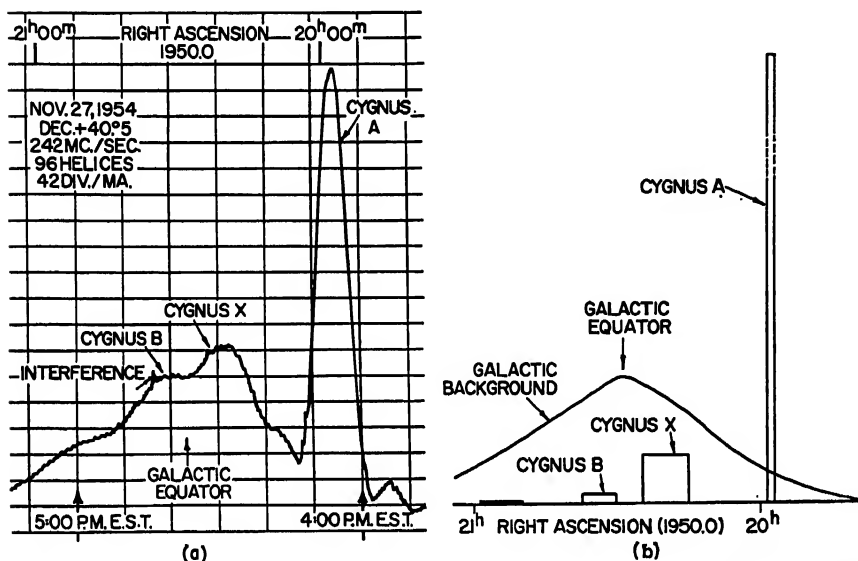
FIG. 29-8. Signature or profile taken with the Ohio State University radio telescope in the Cygnus region (*a*) and its resolution into four discrete sources and residual background radiation (*b*).

galactic equator. This background could probably be resolved into more discrete sources with an antenna of narrower beamwidth.

29.7. RESOLUTION

The limiting resolution of an optical device is usually given by *Rayleigh's criterion*.[32] According to this criterion, two identical point sources can be just resolved if the maximum of the diffraction pattern of source 1 coincides with the first minimum of the pattern of source 2.

Assuming a symmetrical antenna pattern as in Fig. 29-9*a*, Rayleigh's criterion applied to antennas states that the resolution of the antenna is equal to one-half the beamwidth between first nulls; that is,

$$R = \frac{\text{BWFN}}{2} \qquad (29\text{-}12)$$

where R = Rayleigh resolution or Rayleigh angle
  BWFN = Beam Width between First Nulls

An antenna pattern for a single point source is shown in Fig. 29-9*a*. The pattern for two identical point sources separated by the Rayleigh angle is given by the solid curve in Fig. 29-9*b*, with the pattern for each source when observed individually

shown by the dashed curves. It is to be noted that the two sources will be resolved provided the half-power beamwidth is less than one-half of the beamwidth between first nulls, as is usually the case.

It may be shown[17] that the beamwidth between first nulls for a broadside antenna with a uniform aperture many wavelengths long is given by

$$\text{BWFN} = \frac{114.6}{L_\lambda} \quad \text{degrees} \tag{29-13}$$

where BWFN = beamwidth between first nulls

L_λ = length of aperture in wavelengths

It is assumed that $L_\lambda \gg 1$. It may also be shown that the half-power beamwidth for such an antenna is

$$\text{HPBW} = \frac{50.8}{L_\lambda} \quad \text{degrees} \tag{29-14}$$

These results are summarized in Table 29-3, which also gives the beamwidths for uniform circular apertures. It is to be noted that the half-power beamwidths are
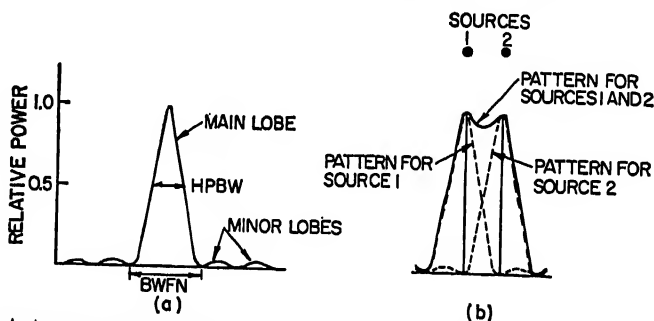
FIG. 29-9. Antenna power pattern (a) and power patterns for two identical point sources separated by the Rayleigh angle as observed individually (dashed) and together (solid).

some 15 per cent less than the resolution angles for both rectangular and circular apertures. Since two identical sources could just be resolved if separated by slightly more than the half-power beamwidth instead of the Rayleigh angle, one could define the resolution as equal to the half-power beamwidth. However, the Rayleigh angle is a slightly more conservative value. For this reason, and also in the interests of consistency with the optical definition, the term *resolution* will here be understood to refer to the *Rayleigh angle*.

Table 29-3

Uniform apertures	Resolution (BWFN/2)	Half-power beamwidth HPBW
Rectangular (length L_λ wavelengths)	$\dfrac{57.3°}{L_\lambda}$	$\dfrac{50.3°}{L_\lambda}$
Circular (diameter D_λ wavelengths)	$\dfrac{70°}{D_\lambda}$	$\dfrac{59°}{D_\lambda}$

A graph of the resolution or Rayleigh angle of radio and optical telescopes as a function of the telescope aperture is presented in Fig. 29-10.[20] The fact that radio

waves are so much longer than light is evident in this figure from the lower resolutions of the radio telescopes, even though these telescopes have much bigger physical apertures than the optical types. To obtain the resolution of the human eye at a wavelength of 1 meter would require a radio antenna with an aperture nearly 4 miles across. The pioneer radio telescopes of Jansky[16] and Reber[30] were 100 and 31 ft in aperture and operated at 15 and 1.9 meters wavelength, respectively. The Ohio
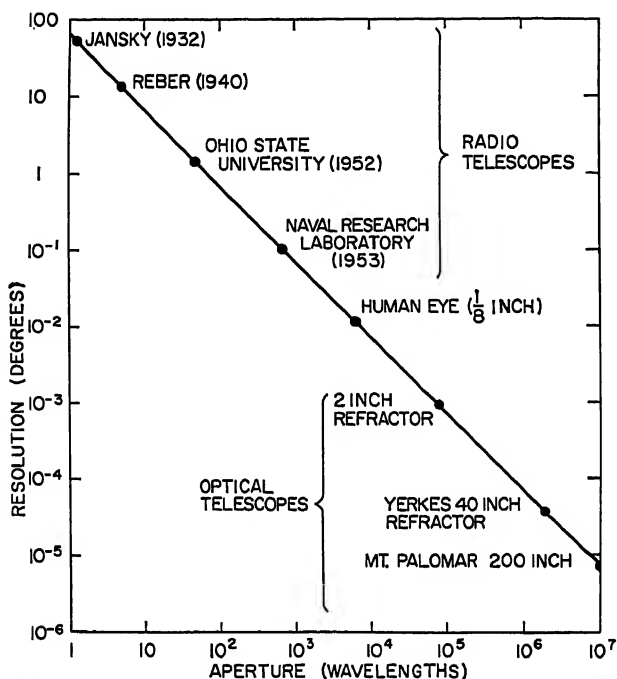
FIG. 29-10. Resolution of radio and optical telescopes as a function of telescope aperture in wavelengths.

State University radio telescope has an aperture of 160 ft and operates at 1.2 meters, while the U.S. Naval Ordnance Laboratory antenna is 50 ft in diameter with operation possible at 2 cm or even somewhat less[12,13] (Fig. 29-15).

29.8. SENSITIVITY AND RANGE

The range of a radio telescope is of much interest since it gives some indication of how big a sample of the universe the telescope is capable of observing. The range is a function not only of the telescope but also of the celestial sources. The celestial source having the largest known radio-power output is Cygnus A, which has been identified as two entire galaxies in collision at a distance of some 200 million light years.[3] It is of interest to consider the maximum distance at which this source or ones like it might be observed since this would set something of an upper limit for the telescope range.

The minimum power flux density that can be detected with a radio telescope is given by

$$S_{\min} = \frac{2kTN}{A\sqrt{ni\,\Delta f}} \qquad (29\text{-}15)$$

where S_{min} = minimum detectable power flux density (janskys)

k = Boltzmann's constant $(1.38 \times 10^{-23}$ joules per degree Kelvin)

T = receiver ambient temperature (degrees Kelvin)

N = noise figure of receiver (dimensionless)

A = effective aperture of antenna (square meters)(includes effect of cable losses)

n = number of records or profiles averaged (dimensionless)

t = time constant of output integrating circuit (seconds)

Δf = radio-frequency bandwidth of receiver (cps)

The factor 2 is included since the telescope is responsive to only one polarization component of the incident radiation, which is assumed to be of an incoherent nature. Calculating S_{min} for the Ohio State University radio telescope operating at 250 Mc, with $T = 300°K$, $N = 1.5$, $A = 208$ sq meters, $t = 60$ sec, $\Delta f = 4$ Mc, and for the case where four records or profiles are averaged $(n = 4)$, we obtain

$$S_{min} = 1.9 \times 10^{-27} \text{ jansky} \qquad (29\text{-}16)$$

The measured power flux density of Cygnus A at this frequency is 38×10^{-24} jansky, so that the maximum range at which a stationary source of this type could be detected with the present Ohio State University radio telescope is given by

$$r_{max} = r_0 \sqrt{\frac{S_0}{S_{min}}} = 28 \times 10^9 \text{ light years} \qquad (29\text{-}17)$$

where r_{max} = maximum range (light years)(1 light year = 6,000,000,000,000 miles)

r_0 = range of Cygnus A $(= 200 \times 10^6$ light years)

S_0 = power flux density of Cygnus A $(= 38 \times 10^{-24}$ jansky)

S_{min} = minimum detectable power flux density as in Eq. (29-15)

Because of receiver instability and interference, the minimum detectable power flux density will be somewhat more than given in Eq. (29-16), and because of this effect and also any absorption, the range will be less than in Eq. (29-17). However, the values given in Eqs. (29-16) and (29-17) may be regarded as the ultimate that might be approached under the assumed conditions.

It should be mentioned that the significance of such a large range as given in Eq. (29-17) is questionable. This is because it is believed that distant galaxies are receding from us and the more distant the galaxy the greater its rate of recession.[14b] At a distance of 4 billion light years* the rate of recession equals the velocity of light and objects further away are beyond the range of observation. This limit to the detectable universe may be called the "celestial horizon."[14a]

The "range" given in Eq. (29-17) is seven times the horizon distance, whereas the range of the largest optical telescope, the 200-in. on Mt. Palomar, is one-half the horizon distance. Regardless of the complete significance of the range given in Eq. (29-17), it is at least apparent that radio telescopes are potentially able to detect celestial sources well beyond the range of the largest optical telescope, thus opening to exploration for the first time vast new regions of space. Although Eq. (29-17) gives the "range" for a particular radio telescope, at the Ohio State University, other telescopes of the same size would have comparable "ranges" and larger telescopes even greater "ranges."

Sufficient sensitivity does not necessarily imply ability to detect a source since because of the proximity of other sources, the antenna may not be able to resolve it. Thus a radio telescope may be limited in its ability to detect a source by insufficient sensitivity or insufficient resolution or both. At the longer radio wavelengths, where

---

* All extra galactic distances in this section are on the "new scale," equal to 1.9 times the old scale.

the receiver noise figure is low, the sensitivity of the radio telescope may be adequate but the antenna resolution may be insufficient, and in the case of most sources it may be said that this telescope is *resolution-limited*. On the other hand, at the shorter radio wavelengths an antenna of the same physical aperture may have adequate resolution but the higher receiver noise figure may result in insufficient sensitivity, and in the case of most sources it may be said that this telescope is *sensitivity-limited*. Likewise, a radio telescope at a given wavelength may be resolution-limited for some of the stronger sources but sensitivity-limited for some of the weaker sources.

Assuming that a radio telescope can resolve a maximum of one source per beam area, the ultimate number N_S of celestial sources that the telescope can resolve is given by *Ko's criterion* as equal numerically to the directivity of the antenna.[20a] Thus

$$N_S = \frac{4\pi}{\beta} = \frac{41,253}{\beta^\circ} = D \qquad (29\text{-}18)$$

where N_S = ultimate number of sources telescope can resolve
β = beam area of antenna (steradians)
β° = beam area of antenna (square degrees)
D = directivity of antenna
In Eq. (29-18) the beam area is given by

$$\beta = \iint F(\phi,\theta)\, d\Omega \qquad (29\text{-}19)$$

where $F(\phi,\theta)$ = normalized true antenna pattern (dimensionless)
$d\Omega = \sin\theta\, d\theta\, d\phi$ = element of solid angle (rad²)
The assumption of one source per beam area neglects the fact that if there is a background of extended sources, each occupying several beam areas, the ultimate number could be somewhat larger. On the other hand, less than the entire sky is observable at most observatories (because of latitude and obstructions near the horizon) so that N_S will be reduced. However, the correct order of magnitude is given by the directivity.

It is sometimes convenient to express the telescope sensitivity in terms of the minimum detectable temperature instead of the minimum detectable power flux density. This can be done from the equation

$$T_{\min} = \frac{NT}{\sqrt{nt\,\Delta f}} \qquad (29\text{-}20)$$

where $T_{\min}$ = minimum detectable temperature (deg Kelvin)
N = noise figure of receiver (dimensionless)
T = receiver ambient temperature (deg Kelvin)
n = number of records averaged (dimensionless)
t = time constant of output integrating circuit (seconds)
Δf = radio-frequency bandwidth of receiver (cps)

29.9. TYPES OF RADIO TELESCOPES

In this subsection the different ways in which radio telescopes can be classified are discussed. The various designs are described, and many of their important characteristics are pointed out. A table is included listing many of the larger radio telescopes with their characteristics.

Radio telescopes may be classified in several ways. For example, they may be classified according to their *application* (search or tracking), according to the *beam shape* (fan or pencil beam), or according to the *antenna design*. The type of *mounting* of the antenna might also be used as a basis for the classification.

A *search type* of radio telescope is used to scan the sky in order to locate radio sources or to map the background radiation. For this application it is simplest to observe on the meridian and to let the earth's rotation sweep the beam across the sky in right ascension. Steerability is then required only in declination, and to provide this the antenna is mounted on a single horizontal east-west axis. This mounting is referred to as a *meridian transit type,* since observations are made of an object as it crosses or transits the meridian.

In order to study particular celestial sources or sky regions more continuously, a *tracking type* of radio telescope is desirable. In this type the antenna is mounted so that a celestial source can be tracked or followed in its motion across the sky. To do this either an equatorial or an altazimuth mounting is used. Since motion is required in two coordinates, the cost of a tracking radio telescope is much greater than for a search type of the same size. For observations of the 21-cm hydrogen line a tracking type of radio telescope is almost essential in order to keep the object or sky region in the antenna beam sufficiently long for the receiver to sweep through the desired band of frequencies.

Fɪɢ. 29-11. Pencil beam and fan beam of same beam area (and directivity).

The antenna *beam shapes* used in radio astronomy are either fan or pencil types. A pencil beam has approximately the same beamwidth in declination and right ascension, while a fan beam has different beamwidths. A pencil and fan beam of the same directivity (or beam area) are compared in Fig. 29-11
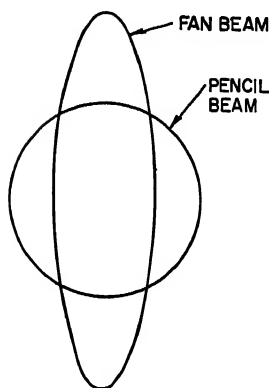
A fan beam is commonly used for search-type telescopes with the narrow dimension of the beam horizontal (in right ascension). A fan beam of this kind has two important advantages over a pencil beam for a search telescope: (1) the aperture and directivity can be much greater for the same cost; and (2) the time required to scan the entire sky is less.

The larger the aperture of a radio telescope the greater its sensitivity and resolution, and accordingly it is desirable in many cases to obtain the largest possible aperture

(a)

(b)
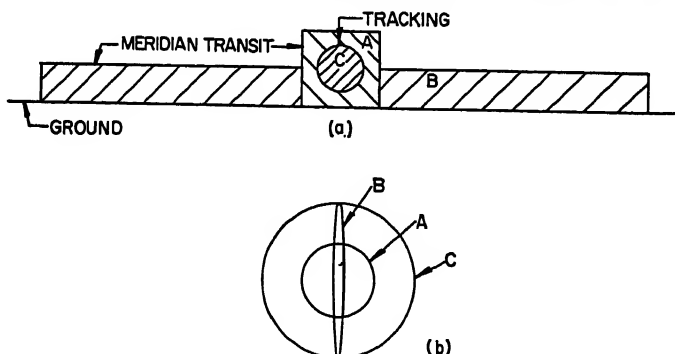
Fɪɢ. 29-12. Comparison of meridian transit telescopes with antennas of square aperture A and rectangular aperture B and tracking telescope with aperture C, all having the same cost. The beams of the three antennas are compared at (b).

for a given cost. Three antennas of different aperture but of the same cost are compared in Fig. 29-12a. Aperture A is a square structure pivoted on an axis at the ground level. It operates as a meridian transit telescope, and its beam is pencil-

shaped as indicated by beam A in Fig. 29-12b. Aperture B is also a meridian transit type pivoted on an axis at the ground level. However, it is half the height of A and eight times as wide, it being assumed that the cost of the structures is proportional to the cube of their height. Aperture B has four times the area of aperture A and four times the directivity. The beam of aperture B is fan-shaped, being twice as wide as for aperture A in declination but one-eighth the width in right ascension. The fact that the ground acts as the supporting structure for one edge of aperture B, and also of A, results in considerable economy. In a completely steerable antenna
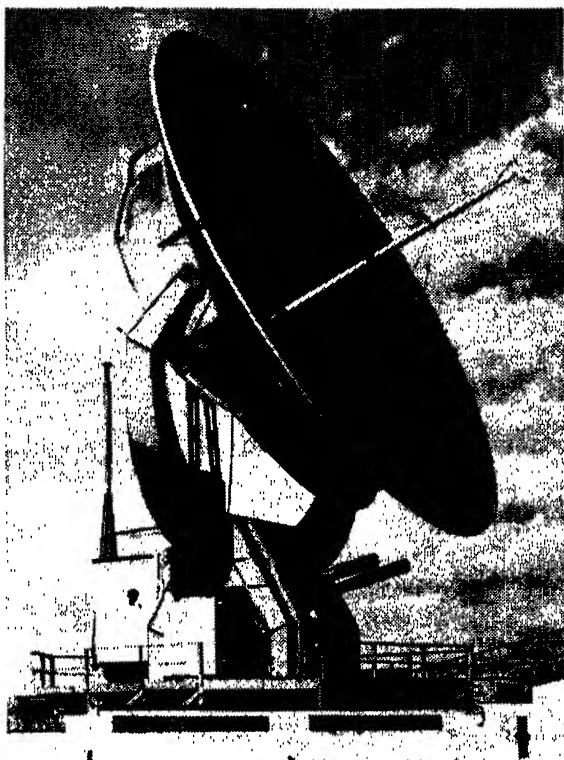
FIG. 29-13. Fifty-foot-diameter altazimuth-mounted radio-telescope antenna at the Naval Research Laboratory, Washington, D.C. The parabola is a cast aluminum dish machined to an accuracy permitting operation at wavelengths down to 1 cm.

this advantage is lost and the required stiffness must be built into the movable antenna structure at increased cost. Or for the same cost the aperture must be reduced. Accordingly, a completely steerable antenna of the same cost as apertures A and B would have an aperture about the size of aperture C in Fig. 29-12a. Aperture C has a pencil beam about twice the beamwidth and one-quarter the directivity of aperture A. It is to be noted that the beam for aperture B has a resolution in declination equal to that for aperture C but 16 times the resolution of C in right ascension. The characteristics of the three apertures are compared in Table 29-4.

The principal mountings for radio telescopes have already been mentioned. These are meridian transit, equatorial, and altazimuth. Although the altazimuth mounting is ordinarily less expensive, a coordinate conversion is required. This is conveniently provided by an analog computer. Usually the antenna is turned physically. How-

Table 29-4. Three Antennas of Different Aperture but Same Cost Compared

Aperture	Shape	Mounting	Aperture area*	Directivity*
A	Square	Meridian transit	1	1
B	Rectangular	Meridian transit	4	4
C	Circular	Equatorial or altazimuth	¼	¼

* Values for A taken as unity.

ever, in some cases the antenna structure is physically fixed and the beam is tilted electrically to obtain the equivalent effect of a mounting.

Turning next to the antenna design, there are many types which lend themselves to use in radio telescopes. Paraboloidal reflector antennas are among the most
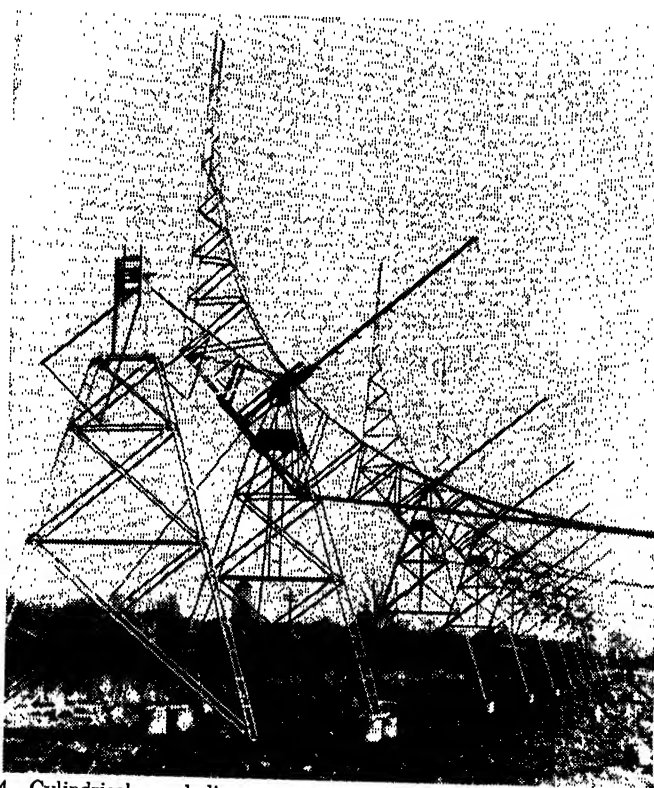
Fig. 29-14. Cylindrical parabolic antenna at Cambridge University, England. This meridian transit antenna is 300 ft long by 40 ft wide and is one of four units forming an interferometer.

common types because of their usefulness over a large frequency range. One typical example shown in Fig. 29-13 is the 50-ft-diameter reflector at the Naval Research Laboratory. The largest steerable reflector currently in use is the 250-ft paraboloid at Manchester, England.

A cylindrical parabolic reflector with a line feed is well adapted as a meridian transit type. An example of this design is shown in Fig. 29-14, being the radio telescope at Cambridge, England.
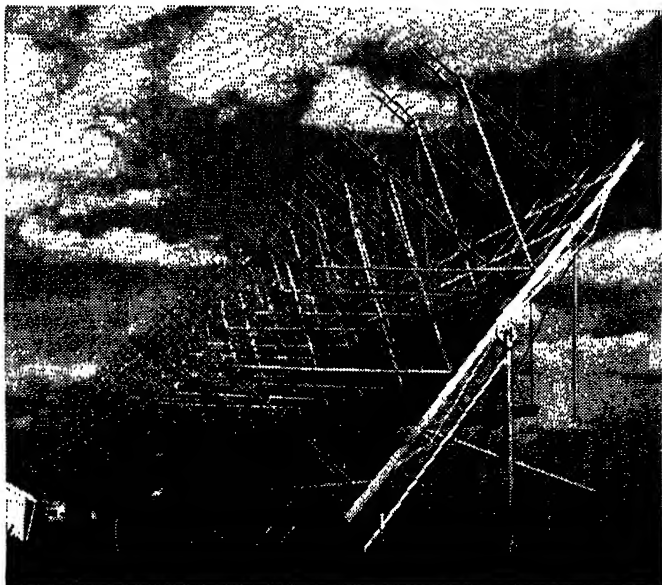
FIG. 29-15. Radio-telescope antenna at the Ohio State University consisting of array of 96 helices mounted on steel ground plane 160 ft long by 22 ft wide.
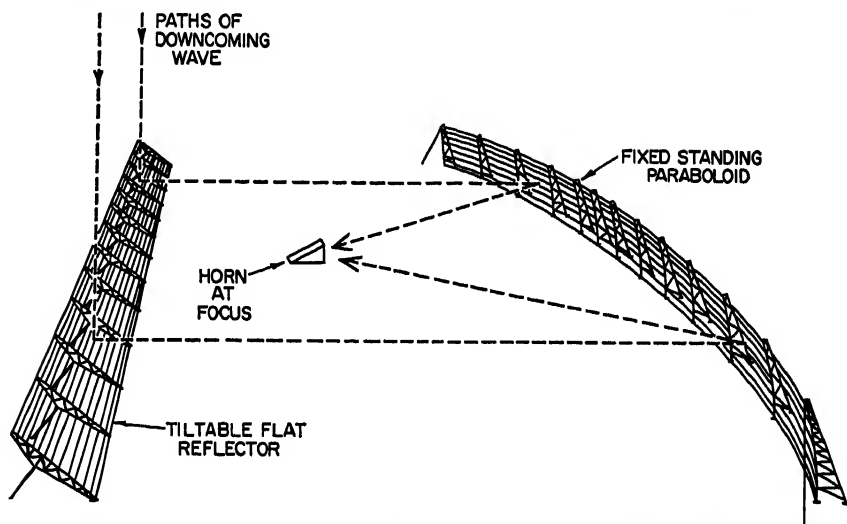
FIG. 29-16. Sketch of proposed Ohio State University radio telescope 700 ft across by 70 ft high.

Flat ground planes with arrays of dipoles are also well suited for meridian transit telescopes. By using helices instead of dipoles, the number of individual elements can be reduced. In the radio telescope at the Ohio State University, shown in Fig. 29-15, 96 helices give the same directivity as 1,000 dipoles.

Whereas dipoles are linearly polarized, the helical beam antenna is circularly polarized. A right-handed helix receives only the right circularly polarized component of the incoming radiation (IRE definition), while a left-handed helix receives

only the left circularly polarized component of the incoming radiation.[17] By using a left- and a right-handed helical beam antenna and comparing the outputs, the amount and rotation direction of the wave polarization can be determined.

In order to obtain the largest possible antenna aperture per dollar of cost a design has been developed at the Ohio State University which uses a fixed standing paraboloid with a tiltable flat-sheet reflector.[20] A sketch of a proposed antenna of this design 700 ft across by 70 ft high is presented in Fig. 29-16. The antenna is a meridian-transit type built relatively close to the ground and using the ground as an integral part of the structure both mechanically and electrically. Vertical polarization is used, and the ground, covered with a conducting screen, acts as an image plane. A downcoming wave is deflected by the large flat sheet into the paraboloid, and thence to a horn antenna at the prime focus. The only movable structure is the tiltable flat reflector. This reflector is nonrigid, which is an important factor in the low cost of the design. By raising or lowering the flat reflector supports individually, its surface can be readily adjusted to the desired degree of flatness.

29.10. INTERFEROMETERS

Although merely another type of radio telescope, the interferometer is so widely used as to warrant a separate subsection. The principal advantage is that in certain
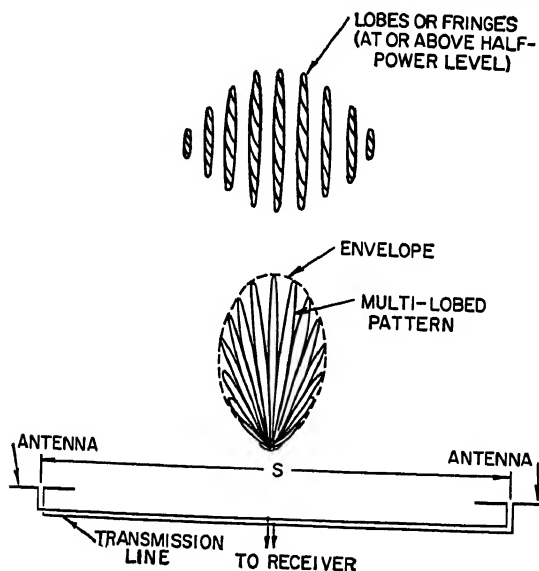
FIG. 29-17. Two-unit Michelson interferometer with patterns.

situations high resolution may be obtained by using two small antennas of low resolution separated many wavelengths. The general arrangement is shown in Fig. 29-17. There are two identical antennas, each with the pattern shown by the envelope. By the principle of pattern multiplication[17] the resultant pattern is equal to the pattern of the individual antenna multiplied by the pattern of two isotropic point sources having a separation S equal to the spacing between the antennas. The resultant pattern, as shown in Fig. 29-17, is multilobed, the number of lobes being proportional to the separation distance S in wavelengths. Each lobe has the shape of a narrow fan beam. In optics these would be referred to as *fringes*. The uppermost diagram

in Fig. 29-17 shows the pattern in two dimensions, the shaded areas, or fringes, being at or above the half-power level.

The antenna at Cambridge, England, shown in Fig. 29-14, is one of four identical units placed at the corners of a rectangle 1,800 by 158 ft and operating as an interferometer.

For angles near the center lobe, the *lobe width between first nulls* is given by

$$\text{LWFN} = \frac{57.3}{S_\lambda} \quad \text{degrees} \tag{29-21}$$

where LWFN = lobe width between first nulls (deg)

S_λ = spacing between interferometer antennas in wavelengths

This lobe width is one-half the beamwidth obtained with a continuous broadside array of length S_λ (Table 29-3). However, the side lobes in the interferometer pattern are nearly equal in magnitude to the center or main lobe, and the directivity is only about twice that for a single unit of the interferometer.
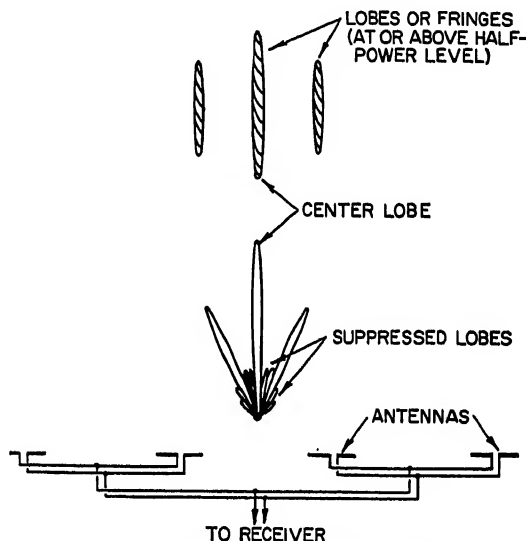
Fig. 29-18. Multiunit interferometer.

The true interferometer pattern described above is obtained if the object being observed is a point source. If the source has appreciable angular width, the nulls of the pattern will tend to fill in, and if the source width equals the lobe width between first nulls, the pattern will be smoothed out to the shape of the envelope. The envelope is the same as the pattern of a single unit. This property is useful for determining the equivalent width of the source. For example, if the spacing S_λ between the interferometer units is increased until the pattern is smoothed out to the envelope, the source width (assuming a uniform source distribution) is equal to the lobe width between first nulls as given by Eq. (29-21). The interferometer can also be very conveniently used to study sources with nonuniform brightness distributions since the Fourier transform of the observed pattern is equal to the source distribution.[24,25]

In certain applications it is desirable to suppress some of the lobes of the interferometer pattern so that the angle between the large lobes is increased. This can be done by using additional antenna units as suggested in Fig. 29-18. This multi-

unit or suppressed-lobe interferometer is a compromise between a two-unit type and a continuous array of the same over-all extent. The photograph (Fig. 29-19) is of a 32-unit interferometer of this type at Sydney, Australia. Operating at 21 cm, each main lobe has a half-power width of 0.05°, but the lobe spacing is nearly 2°, so that in observations of the sun only one fringe or lobe is on the sun's disk at a time.[7,28]

FIG. 29-19. Thirty-two-unit interferometer of the Commonwealth Scientific and Industrial Research Organization at Sydney, Australia.
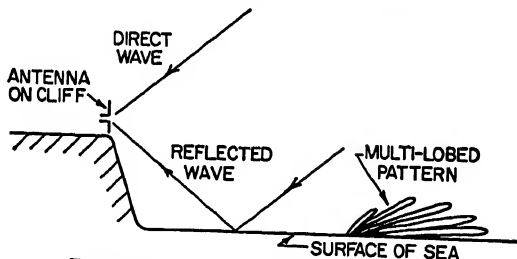
FIG. 29-20. Lloyd's mirror interferometer.

PLAN VIEWS
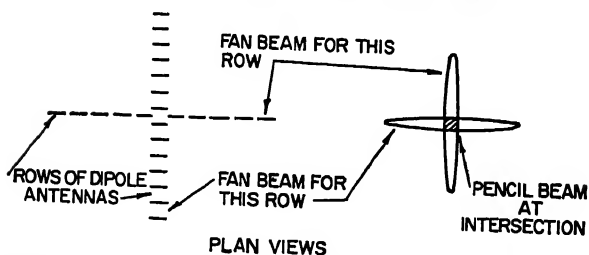
FIG. 29-21. Phase-switching crossed-fan-beam arrangement (Mills Cross) giving effectively a pencil beam.

For studying source extent and distribution in right ascension, the interferometers described above have their units mounted along a horizontal east-west line and at least 2 units are required. It is also possible to construct an interferometer with a single antenna unit by using a flat reflector such as the surface of the sea. As suggested in Fig. 29-20, the antenna, mounted on a cliff overlooking the sea, combines with its image to produce a multilobed pattern in the vertical plane.[5] This kind of interferometer is often called a *Lloyd's mirror* type, while the two-unit variety is called a Michelson interferometer.

A phase-switching method originated by Ryle[31] has been applied by Mills[25] to an interferometer having the form of a fixed horizontal cross. This type of interferometer, often called a Mills cross, is usually constructed of two rows of dipole antennas, one east-west and the other north-south. The dipoles are fixed and at the same height above a level ground. Each row produces a fan beam as shown in Fig. 29-21. By suitably combining the outputs of the two rows, the effective antenna beam is of a pencil type formed where the two fan beams intersect. By electrical phase shifting, one or both of the fan beams can be tilted and the pencil beam moved to different positions of the sky. The Mills cross antenna near Sydney, Australia, has legs 1,500 ft in length.

REFERENCES

1. L. H. Aller: "Nuclear Transformations, Stellar Interiors, and Nebulae," The Ronald Press Co., New York, 1954.
2. "American Ephemeris and Nautical Almanac," issued yearly by the U.S. Government Printing Office, Washington, D.C. Gives positions of sun, moon, planets, and many stars. Tables are useful in converting local time of observation into celestial coordinates.
3. W. Baade and R. Minkowski: "Identification of the Radio Sources in Cassiopeia, Cygnus A, and Puppis A," *Astrophys. J.*, vol. 119, no. 1, p. 206, January, 1954.
4. B. J. Bok: "New Science of Radio Astronomy," *Sci. Monthly*, vol. 80, no. 6, pp. 333, June, 1955.
5. J. G. Bolton and G. J. Stanley: "Observations on the Variable Source of Cosmic Radio-frequency Radiation in the Constellation of Cygnus," *Australian J. Sci. Research*, vol. A1, p. 58, 1948.
6. R. N. Bracewell and J. A. Roberts: "Aerial Smoothing in Radio Astronomy," *Australian J. Phys.*, vol. 7, no. 4, p. 615, December, 1954.
   Bracewell (see also Pawsey).
   Broten (see Covington).
7. W. N. Christiansen: "A High Resolution Aerial for Radio Astronomy," *Nature (London)*, vol. 171, p. 831, May 9, 1953.
7a. W. N. Christiansen and J. V. Hindman: "A Long-period Change in Radio-frequency Radiation from the Quiet Sun at Decimeter Wavelengths," *Nature*, vol. 167, p. 635, 1951.
   Clegg (see Lovell).
8. A. E. Covington and N. W. Broten: "Brightness of the Solar Disc at a Wavelength of 10.3 Cm," *Astrophys. J.*, vol. 119, no. 3, p. 569, May, 1954.
9. R. D. Davies and D. R. W. Williams: *Nature (London)*, vol. 173, p. 1182, 1954.
9a. R. H. Dicke: "Measurement of Thermal Radiation at Microwave Frequencies," *Rev. Sci. Inst.*, vol. 17, no. 7, p. 268, July, 1946.
10. J. C. Duncan: "Astronomy," Harper & Brothers, New York, 1926. An introductory textbook.
11. H. I. Ewen: "Radio Waves from Interstellar Hydrogen," *Sci. American*, vol. 189, no. 6, p. 42, December, 1953.
12. F. T. Haddock, C. H. Mayer, and R. M. Sloanaker: "Radio Emission from the Orion Nebula and Other Sources at 9.4 Cm," *Astrophys. J.*, vol. 119, no. 2, p. 456, March, 1954.
13. J. P. Hagen, A. E. Lilley, and E. F. McLain: "Absorption of 21 Cm Radiation by Interstellar Hydrogen," Naval Research Lab. Rept. 4448, Oct. 18, 1954.
14. R. Hanbury Brown and C. Hazard: "Radio Emission from the Andromeda Nebula," *Monthly Notices Roy. Astron. Soc.*, vol. 3, no. 4, p. 357, 1951.
   Hazard (see Hanbury Brown).
   Hindman (see Christiansen).
14a. Fred Hoyle: "The Nature of the Universe," Harper & Brothers, New York, 1950.
14b. Edwin Hubble: "The Realm of the Nebulae," Yale University Press, New Haven, Conn., 1936. Discusses expanding universe.
15. J. A. Hynek (ed.): "Astrophysics," McGraw-Hill Book Company, Inc., New York, 1951.
16. K. G. Jansky: "Electrical Disturbances Apparently of Extraterrestrial Origin," *Proc. IRE*, vol. 21, no. 10, p. 1387, October, 1933.
17. J. D. Kraus: "Antennas," McGraw-Hill Book Company, Inc., New York, 1950. Textbook on antennas of all types and for all frequency ranges.

18. J. D. Kraus: "Electromagnetics," McGraw-Hill Book Company, Inc., New York, 1953. Textbook on basic theory of electricity, waves, and antennas.
19. J. D. Kraus and E. Ksiazek: "New Techniques in Radio Astronomy," *Electronics*, vol. 26, no. 9, p. 148, September, 1953.
20. J. D. Kraus: "Radio Telescopes," *Sci. American*, vol. 192, p. 36, March, 1955.
20a. J. D. Kraus: "Resolution, Pattern Effects, and Range of Radio Telescopes," *IRE Trans.*, vol. AP-4, p. 445, July, 1956.
    Kraus (see also Matt).
    Ksiazek (see Kraus).
21. G. P. Kuiper (ed.): "The Solar System," University of Chicago Press, Chicago, 1953.
    Lilley (see Hagen).
22. B. Lovell and J. A. Clegg: "Radio Astronomy," John Wiley & Sons, Inc., New York, 1952. Elementary text on radio and radar astronomy.
23. S. Matt and J. D. Kraus: "The Effect of the Source Distribution on Antenna Patterns," *Proc. IRE*, vol. 43, no. 7, p. 821, July, 1955.
    Mayer (see Haddock).
    McClain (see Hagen).
24. L. L. McCready, J. L. Pawsey, and R. Payne-Scott: "Solar Radiation at Radio Frequencies and Its Relation to Sunspots," *Proc. Roy. Soc.*, vol. A190, p. 357, August, 1947.
25. B. Y. Mills: "The Radio Brightness Distributions over Four Discrete Sources of Cosmic Noise," *Australian J. Phys.*, vol. 6, p. 452, 1953.
    Muller (see van de Hulst).
26. J. J. Nassau: "Textbook of Practical Astronomy," McGraw-Hill Book Company, Inc., New York, 1948. Text on basic astronomical calculations.
26a. John Ohlsson: "The Conversion of Equatorial Coordinates into Galactic Coordinates," *Ann. Observatory of Lund (Sweden)*, no. 3, 1932.
27. J. L. Pawsey: "A Catalogue of Reliably Known Discrete Sources of Cosmic Radio Waves," *Astrophys. J.*, vol. 121, no. 1, p. 1, January, 1955.
28. J. L. Pawsey and R. N. Bracewell: "Radio Astronomy," Oxford University Press, London, 1955. Comprehensive textbook on radio astronomy.
    Pawsey (see also McCready).
29. C. Payne-Gaposchkin: "Introduction to Astronomy," Prentice-Hall, Inc., Englewood Cliffs, N.J., 1954. Introductory text on astronomy.
    Payne-Scott (see McCready).
30. Grote Reber: "Cosmic Static," *Astrophys. J.*, vol. 100, no. 3, p. 279, November, 1944.
    Roberts (see Bracewell).
31. M. Ryle: "A New Radio Interferometer and Its Application to the Observation of Weak Radio Stars," *Proc. Roy. Soc.*, vol. A211, p. 351, March, 1952.
32. F. W. Sears: "Principles of Physics, III. Optics," p. 257, Addison-Wesley Publishing Company, Reading, Mass., 1948.
    Sloanaker (see Haddock).
33. W. M. Smart: "Textbook on Spherical Astronomy," Cambridge University Press, New York, 1944.
34. R. C. Spencer: "Antennas for Radio Astronomy," U.S. Air Force, Cambridge Research Center, Rept. TR-55-101, April, 1955.
    Stanley (see Bolton).
35. URSI (International Scientific Radio Union), Sub-Commission 5b, Report on Terminology and Units, Mar. 15, 1954.
36. H. C. van de Hulst: "A Course in Radio Astronomy," Leiden Observatory, Holland, 1951. Mimeographed lecture notes.
37. H. C. van de Hulst, C. A. Muller, and J. H. Oort: "The Spiral Structure of the Outer Part of the Galactic System Derived from the Hydrogen Emission at 21 Cm Wavelength," *Bull. Astron. Inst. Netherlands*, vol. 12, no. 452, p. 117, May 14, 1954.
    Williams (see Davies).

Chapter 30

TRANSMISSION LINES AND WAVEGUIDES

KARLE S. PACKARD

and

RODERIC V. LOWMAN

Both of Airborne Instruments Laboratory
Melville, Long Island, New York

30.1. GENERAL*

In the applications of antennas, it becomes necessary to use some form of transmission line to connect the antenna to a transmitter or receiver. It therefore is essential to know the propagation characteristics of the more common forms of line and the properties of some of the devices constructed from transmission-line elements.

The transmission lines considered in Secs. 30.2 to 30.6 are almost always used in the transverse electromagnetic (TEM) mode of propagation and therefore possess a unique characteristic impedance. In air, the guide wavelength λ_g is equal to the free-space wavelength λ. Propagation in this mode exists at any frequency, although above a certain frequency higher modes may also exist. It is assumed that the line loss is small and may be neglected in calculating the characteristic impedance.

The waveguides considered in Secs. 30.7 and 30.8 use modes of propagation having a longitudinal component and do not possess a unique characteristic impedance.[1] Propagation may only take place above a certain unique cutoff frequency defined by the mechanical dimensions. The guide wavelength λ_g is related to the free-space wavelength λ by $1/\lambda_g{}^2 = 1/\lambda^2 - 1/\lambda_c{}^2$, where λ_c is the cutoff wavelength.

In all cases, it will be assumed that the skin depth is small compared with the dimensions of the conductors and that these conductors are nonmagnetic. The medium surrounding the conductors is often air, but for other dielectrics, a loss will be introduced and this is independent of the line dimensions. In the case of TEM modes this loss is

$$\alpha_D = \frac{\pi}{\lambda_D} \tan \delta \qquad \text{nepers/meter}$$

where $\lambda_D \ (= \lambda/\sqrt{\epsilon})$ is the intrinsic wavelength in the medium and $\tan \delta$ is the loss tangent of the dielectric. ϵ is the relative dielectric constant. For waveguide modes, the wavelength in the guide must be considered, and the dielectric loss becomes

$$\alpha_D = \frac{\pi \lambda_g}{(\lambda_D)^2} \tan \delta \qquad \text{nepers/meter}$$

It should be pointed out that in circuits having discontinuities, such as bends, the open types of line will have additional loss because of radiation at these points, and therefore shielded types should generally be used for complex circuits.

The power-handling capacity of transmission lines in the following sections is given in terms of the maximum allowable field intensity E_a in the dielectric, whereas for waveguides the power is given directly for air dielectric. For such calculations, $E_a = 3 \times 10^6$ volts/meter is the theoretical maximum for air dielectric, at normal temperature and atmospheric pressure, but for proper derating a value of 2×10^6 volts/meter is more practical. Other dielectrics having a higher dielectric strength may be used to increase the power limit, but in the case of solid dielectrics, the increased field strength in air pockets, which are very likely to exist, imposes a serious limitation. A common method of increasing the power limit is to use pressurized air, the maximum power being proportional to the square of the absolute pressure.

The conditions discussed above apply to a matched line. The maximum power is inversely proportional to the standing-wave ratio.

30.2. OPEN-WIRE TRANSMISSION LINES

Open-wire transmission lines comprise an arrangement of wires generally having diameters small compared with the spacings involved. This arrangement is sometimes used in conjunction with a ground plane to which the wires are parallel. Such

* A list of symbols used in this chapter will be found on p. 30–41.
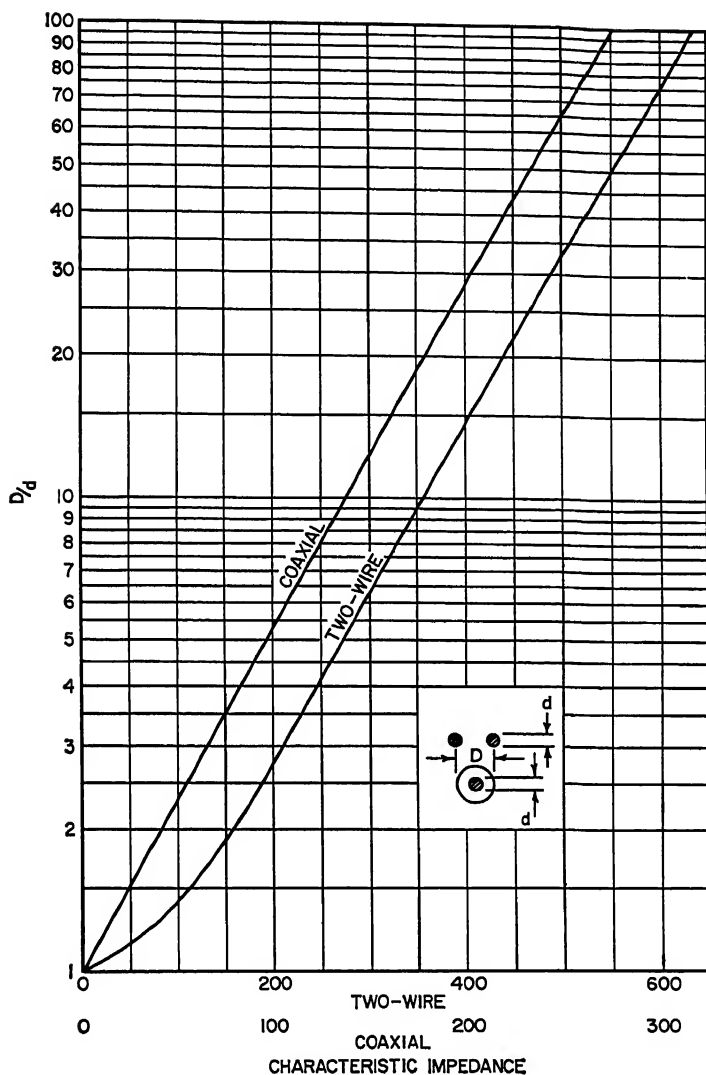
FIG. 30-1. Characteristic impedance of common lines.

transmission lines have the advantage of simplicity and economy. The spacing between the wires and between the wires and the ground plane is very much less than a wavelength.

The most common of the open-wire lines is the two-wire line. For two wires of diameter d, spaced at a center-to-center distance D, the characteristic impedance is

$$Z_0 = \frac{120}{\sqrt{\epsilon}} \cosh^{-1} \frac{D}{d} \qquad \text{ohms}$$

This relation is plotted in Fig. 30-1. In the case of unequal wire diameters d_1 and d_2, d is replaced by $\sqrt{d_1 d_2}$.

The conductor loss is

$$\alpha_e = 2.29 \times 10^{-8} \sqrt{\frac{f\epsilon}{\sigma}} \frac{1}{d \log_{10}(2D/d)} \quad \text{nepers/meter}$$

The power-handling capacity is

$$P = \frac{E_a^2 d^2 \sqrt{\epsilon}}{240} \cosh^{-1} \frac{D}{d} \quad \text{watts}$$

where E_a is the maximum allowable field intensity in the dielectric (Sec. 30.1).

Other configurations of open-wire lines are shown in Fig. 30-2, together with formulas for the characteristic impedance. Lines near a ground plane are also included. Other types of open-wire lines can be found in the literature.
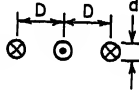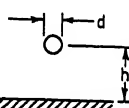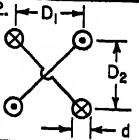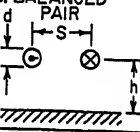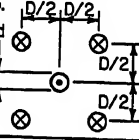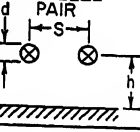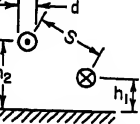
WIRES IN SPACE	CHARACTERISTIC IMPEDANCE	WIRES NEAR GROUND	CHARACTERISTIC IMPEDANCE
1.	$Z_0 = \dfrac{207}{\sqrt{\epsilon}} \log_{10} 1.59 \dfrac{D}{d}$	4.	$Z_0 = \dfrac{138}{\sqrt{\epsilon}} \log_{10} \dfrac{4h}{d}$
2.	$Z_0 = \dfrac{138}{\sqrt{\epsilon}} \log_{10} \dfrac{2D_2}{d\sqrt{1+(D_2/D_1)^2}}$	5. BALANCED PAIR	$Z_0 = \dfrac{276}{\sqrt{\epsilon}} \log_{10} \dfrac{4h}{d\sqrt{1+(2h/S)^2}}$
3.	$Z_0 = \dfrac{173}{\sqrt{\epsilon}} \log_{10} 1.14 \dfrac{D}{d}$	6. PARALLEL PAIR	$Z_0 = \dfrac{69}{\sqrt{\epsilon}} \log_{10} \dfrac{4h}{d}\sqrt{1+(2h/S)^2}$
		7.	$Z_0 = \dfrac{276}{\sqrt{\epsilon}} \log_{10} \dfrac{2S}{d\sqrt{1+S^2/4h_1 h_2}}$

FIG. 30-2. Open-wire lines. *Note:* d is small compared to other dimensions.

30.3. COAXIAL LINES, SOLID CONDUCTOR

Coaxial transmission lines using a cylindrical center conductor within a cylindrical tubular outer conductor are widely used for the propagation of microwave power. Although more costly than open-wire transmission lines, they have the advantage that they completely enclose the electromagnetic fields, thereby preventing radiation losses and providing shielding from nearby circuits.

Coaxial-line Parameters. For a coaxial line with inner-conductor diameter $2a$ and outer conductor diameter $2b$, the characteristic impedance is

$$Z_0 = \frac{138}{\sqrt{\epsilon}} \log_{10} \frac{b}{a} \quad \text{ohms}$$

which is plotted in Fig. 30-1.

The cutoff wavelength of the first higher mode is[1]

$$\lambda_c = F\pi \sqrt{\epsilon}\,(a + b) \qquad F \cong 1$$

The conductor loss for the dominant mode is

$$\alpha_c = 1.14 \times 10^{-6} \sqrt{\frac{f\epsilon}{\sigma}}\left(\frac{1}{a} + \frac{1}{b}\right)\frac{1}{\log_{10}\dfrac{b}{a}} \qquad \text{nepers/meter}$$

The minimum conductor loss occurs at the limiting size for the first higher mode, in which case $\sqrt{\epsilon}\,Z_0 = 92.6$ ohms and

$$\alpha_c = 0.637\,\frac{\epsilon}{\lambda_c^{3/2}\sqrt{\sigma}} \qquad \text{nepers/meter}$$

For a fixed outer-conductor size, the minimum conductor loss occurs for $\sqrt{\epsilon}\,Z_0 = 77$ ohms and is

$$\alpha_c = 0.164\,\frac{1}{b}\sqrt{\frac{\epsilon}{\sigma\lambda}} \qquad \text{nepers/meter}$$

The power transmitted by the line is

$$P = \frac{E_a{}^2 a^2 \sqrt{\epsilon}}{52.2}\log_{10}\frac{b}{a} \qquad \text{watts}$$

where E_a is the electric field intensity at the center conductor (Sec. 30.1). The maximum power-handling capacity occurs for a 44.4-ohm line operating at the limit of the first higher mode and is

$$P_{\max} = 6.53 \times 10^{-5}\frac{E_a{}^2\lambda_c{}^2}{\sqrt{\epsilon}} \qquad \text{watts}$$

For a fixed outer-conductor size, the maximum power-handling capacity occurs for $\sqrt{\epsilon}\,Z_0 = 30$ ohms and is

$$P'_{\max} = 1.53 \times 10^{-3}E_a{}^2 b^2 \sqrt{\epsilon} \qquad \text{watts}$$

The effect of dimensional tolerances on the characteristic impedance may be found from

$$\frac{\Delta Z_0}{Z_0} = \frac{60}{Z_0\sqrt{\epsilon}}\left(\frac{\Delta b}{b} - \frac{\Delta a}{a}\right)$$

while the effect of eccentricity is to change the characteristic impedance to

$$Z_0 = \frac{138}{\sqrt{\epsilon}}\log_{10}\left[\frac{b}{a}\left(1 - \frac{e^2}{b^2}\right)\right] \text{ ohms}; \qquad \frac{e}{b} < \log_{10}\frac{b}{a} < 0.7$$

where e is the off-center distance.

For a balanced coaxial line (sheathed two-wire line) having two center conductors spaced at a distance s within a single outer conductor, the characteristic impedance is given by

$$Z_0 = \frac{276}{\sqrt{\epsilon}}\log_{10}\left(\frac{s}{a}\frac{4b^2 - s^2}{4b^2 + s^2}\right) \qquad \text{ohms}$$

Coaxial Line with Helical Center Conductor. Coaxial lines with a helical inner conductor[2] are often useful to obtain a high characteristic impedance or slow propagation velocity. The diameter of the outer conductor will be assumed small compared with a wavelength *in the line,* and the following symbols will be used:

D = diameter of outer conductor

d = mean helix diameter

a = diameter of helix wire

N = turns per unit length

The characteristic impedance is given by

$$Z_0 = \frac{202Nd}{\sqrt{\epsilon}} \sqrt{\left(1 - \frac{d^2}{D^2}\right) \log_{10} \frac{D}{d}} \quad \text{ohms}$$

The relative velocity of propagation is given by

$$\frac{v}{c} = \frac{0.683}{Nd\sqrt{\epsilon}} \sqrt{\frac{\log_{10}(D/d)}{1 - (d/D)^2}}$$
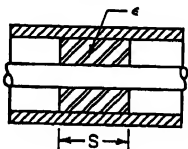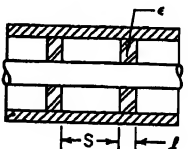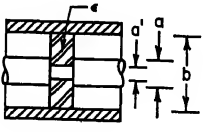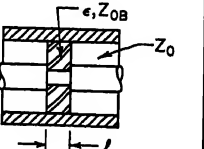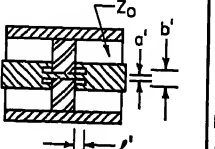
TYPE	CONFIGURATION	DESIGN FORMULAS	REMARKS
1. HALF WAVE		$S = \dfrac{\lambda}{2\sqrt{\epsilon}}$	FREQUENCY SENSITIVE
2. SPACED PAIR		$S = \dfrac{1}{\beta} \arctan\left[\dfrac{2\sqrt{\epsilon}}{1+\epsilon} \cot \beta \ell \sqrt{\epsilon}\right]$ $\beta = \dfrac{2\pi}{\lambda}$	FREQUENCY SENSITIVE
3. SIMPLE UNDERCUT		$a' = b\left(\dfrac{b}{a}\right)^{-\sqrt{\epsilon}}$	GOOD AT LOW FREQUENCY. NEGLECTS FRINGING CAPACITANCE AT UNDERCUT
4. COMPENSATED UNDERCUT		$\ell = \dfrac{1}{\beta} \arctan\left[\dfrac{2\omega C Z_{OB}}{(\omega C Z_{OB})^2 + \left(\dfrac{Z_{OB}}{Z_0}\right)^2 - 1}\right]$ $\beta = \dfrac{2\pi\sqrt{\epsilon}}{\lambda}$ FIND C AS IN SECTION 30.10	COMPENSATES FRINGING CAPACITANCE AT UNDERCUT. MATCH AT $f = \omega/2\pi$, LOW REFLECTION AT LOWER FREQUENCIES
5. COMPOUND UNDERCUT (REF. 4)		$\sqrt{L/C} = Z_0$ FIND C AS IN SECTION 30.10 $L = \dfrac{138\ell'}{v} \log_{10} \dfrac{b'}{a'}$ FIND a' AS IN 3) ABOVE $v = 3 \times 10^8$ m/sec.	VERY LOW REFLECTION IF DISCONTINUITIES ARE OF INFINITESIMAL EXTENT ($\ell' < \lambda/20$). GOOD WHERE MANY BEADS MUST BE USED

FIG. 30-3. Coaxial-line beads.

The attenuation, for copper conductors, is given approximately by

$$\alpha_c = 1.64 \times 10^{-5} \frac{(Nd)^2 \sqrt{f}}{Z_0} \left(\frac{1}{\pi N a} + \frac{d^3}{D^3} \right) \quad \text{nepers/meter}$$

Coaxial Line, Bead-supported. In order to support the center conductor of an air-dielectric coaxial line, insulating beads are often used. These beads will introduce discontinuities and, if not properly designed, produce large reflection losses. The design procedure for these support beads depends upon the frequency range of application, a broad range requiring a more complex design. The more common procedures are summarized in Fig. 30-3, and others can be found in the references.[3]

In the bead-supported line, the cutoff wavelength in the bead section should be kept below the operating wavelength. The power-handling capacity is about 0.033 times that of the theoretical maximum for the unsupported line.

Coaxial Line, Stub-supported. In many applications, particularly where high power is to be transmitted, it is desirable to support the center conductor of an air-dielectric coaxial line by means of stubs. The power-handling capacity of a stub-supported line is about 0.15 times that of the theoretical maximum for the unsupported line. Such stubs take the form of a short length of short-circuited transmission line in shunt with the main transmission line. For frequencies at which the stub is an odd number of quarter wavelengths long, it presents zero admittance and therefore does not affect the main line. Obviously, it is often necessary to maintain a low stub admittance over a broad range of frequencies, and this may be effected by using an impedance transformer on the main line at the junction with the stub. The design of stubs and transformers can be found in the literature.[3]

Semiflexible Coaxial Lines. There are several commercially available coaxial lines having a limited permissible bending radius but exhibiting a loss only slightly greater than rigid coaxial lines. They are characterized by a helical- or foamed-dielectric support for a copper center conductor and a solid aluminum tube for the outer conductor. These lines go under the names Styroflex,* Foamflex,* and Styrafil* and are available in 50-, 70-, and 77.5-ohm impedances and in a variety of outer-conductor sizes. In the smaller sizes they are usable up to about 10 kmc.

An analysis of the propagation characteristics of this type of line may be found in the literature.[5]

30.4. FLEXIBLE COAXIAL LINES

Flexible coaxial line using a solid or stranded inner conductor, a plastic-dielectric support, and a braided outer conductor is probably the most common means of connecting together many separated components of an r-f system. Although the transmission loss is relatively high, because of the dielectric loss, the convenience often outweighs this factor in applications where some loss is tolerable. Such lines are commercially available in a wide variety of size and impedance.

Table 30-1 summarizes the characteristics of the more common lines. The attenuation is shown in Fig. 30-4, and the power-handling capacity in Fig. 30-5.

Leakage of electrical energy through the braided outer conductor is often a problem and, although the work on this problem has been scant, results have been obtained for RG-8/U, a widely used single-braid cable.[6] The energy leakage may be considered in terms of the coupling impedance between two concentric coaxial lines in which the braid forms the inner conductor of the outer line and the outer conductor of the inner line. The results for RG-8/U show this coupling impedance to be primarily a series mutual inductance of approximately 150 $\mu\mu$h/ft from 100 to 5,500 Mc/sec.

* Manufactured by Phelps Dodge Copper Products Corp., New York.

Table 30-1. Flexible Coaxial Lines

Type	Inner conductor	Dielectric material*	Nominal diameter of dielectric, in.	Number and type of shielding braids	Protective covering	Nominal over-all diameter, in.	Weight, lb/ft	Nominal impedance, ohms	Nominal capacitance, μμf/ft	Maximum operating voltage, volts(rms)	Engineering data
RG-58/U	0.053-in. silver-covered copper	A-1	0.185	Silver-coated copper, double braid	Noncontaminating synthetic resin	0.332	0.087	50.0	28.5	3,000	
RG-6A/U	0.0285-in. copper-covered steel	A-1	0.185	Double braids, inner, silver-covered copper, outer, copper	Noncontaminating synthetic resin	0.332	0.082	75.0	20.0	2,700	
RG-8A/U	7/0.0296-in. copper	A-1	0.285	Copper, single braid	Noncontaminating synthetic resin	0.405	0.106	50.0	29.5	5,000	
RG-9B/U	7/0.0296-in. silvered copper	A-1	0.285	Silver-coated copper double braid	Noncontaminating synthetic resin	0.425	0.150	50.0	30.0	5,000	
RG-10A/U	7/0.0296-in. copper	A-1	0.285	Copper, single braid	Noncontaminating synthetic resin with armor	0.475 (max.)	0.146	50.0	29.5	5,000	RG-8A/U with armor
RG-11A/U	7/0.0159-in. tinned copper	A-1	0.285	Copper, single braid	Noncontaminating synthetic resin	0.405	0.096	75.0	20.5	5,000	
RG-12A/U	7/0.0159-in. tinned copper	A-1	0.285	Copper, single braid	Noncontaminating synthetic resin with armor	0.475 (max.)	0.141	75.0	20.5	5,000	RG-11A/U with armor
RG-13A/U	7/0.0159-in. tinned copper	A-1	0.285	Copper, double braid	Noncontaminating synthetic resin	0.425	0.126	75.0	20.5	5,000	Same as RG-11A/U except has double braid
RG-14A/U	0.108-in. copper	A-1	0.370	Copper, double braid	Noncontaminating synthetic resin	0.545	0.216	50.0	29.5	7,000	
RG-17A/U	0.195-in. copper	A-1	0.680	Copper, single braid	Noncontaminating synthetic resin	0.870	0.460	50.0	29.5	11,000	
RG-18A/U	0.195-in. copper	A-1	0.680	Copper, single braid	Noncontaminating synthetic resin with armor	0.945 (max.)	0.585	50.0	29.5	11,000	RG-17A/U with armor

Type	Inner conductor			Outer conductor	Insulation						Remarks
RG-19A/U	0.260-in. copper	A-1	0.910	Copper, single braid	Noncontaminating synthetic resin	1.120	0 740	50.0	29.5	14,000	
RG-20A/U	0.260-in. copper	A-1	0.910	Copper, single braid	Noncontaminating synthetic resin with armor	1.195 (max.)	0.925	50.0	29.5	14,000	RG-19A/U with armor
RG-21A/U	0.0533-in. high-resistance wire	A-1	0.185	Silver-coated copper, double braid	Noncontaminating synthetic resin	0.332	0.087	50 0	29.0	2,700	
RG-22B/U	2-conductor 7/0.0152-in. copper	A-1	0.285	Tinned copper, double braid	Noncontaminating synthetic resin	0.420	0.151	95.0	16.0	1,000	Dual-coaxial balanced cable, twisted conductors
RG-34A/U	7/0.0249-in. copper	A-1	0.460	Copper, single braid	Noncontaminating synthetic resin	0.630	0.224	75.0	21.5	6,500	
RG-35A/U	0.1045-in. copper	A-1	0.680	Copper, single braid	Synthetic resin with armor	0.945 (max.)	0.525	75.0	21.5	10,000	
RG-55A/U	0.035-in. silver-covered copper	A-1	0.116	Silver-covered copper, double braid	Noncontaminating synthetic resin	0.216 (max.)		50.0	21.5	1,900	
RG-58C/U	19/0.0071-in. tinned copper	A-1	0.116	Tinned copper, single braid	Noncontaminating synthetic resin	0.195	0 029	50.0	28.5	1,900	
RG-59A/U	0.0230-in. copper-covered steel wire	A-1	0.146	Copper, single braid	Noncontaminating synthetic resin	0.242	0.032	75.0	21.0	2,300	
RG-62A/U	0.0253-in. copper-covered steel wire	A-2	0.146	Copper, single braid	Noncontaminating synthetic resin	0.242	0.0382	93 0	14.5 (max.)	750	
RG-63B/U	0.0253-in. copper-covered steel wire	A-2	0.285	Copper, single braid	Noncontaminating synthetic resin	0.405	0.0832	125.0	11.0 (max.)	1,000	Low capacitance
RG-65A/U	#32 Formex F, 0.128-in. diameter (helix)	A-1	0.285	Copper, single braid	Synthetic resin	0.405	0.086	950.0	44.0	1,000	
RG-71A/U	22 AWG copper-covered steel	A-2		Tinned copper, double braid	Synthetic resin	0.250		93.0	13.5	750	Similar to RG-17/U except jacket is synthetic resin

Table 30-1. Flexible Coaxial Lines (Continued)

Type	Inner conductor	Dielectric material*	Nominal diameter of dielectric, in.	Number and type of shielding braids	Protective covering	Nominal over-all diameter, in.	Weight, lb/ft	Nominal impedance, ohms	Nominal capacitance, μμf/ft	Maximum operating voltage, volts(rms)	Engineering data
RG-74A/U	0.106-in. copper	A-1	0.370	Copper, double braid	Noncontaminating synthetic resin with armor	0.615 (max.)	0.310	50.0	29.5	7,000	RG-14/U with armor
RG-86/U	2 conductors 7/0.0285-in. soft copper	A-1	0.650 × 0.300	None	None	0.650 × 0.300		200.0	7.8		Twin lead
RG-87A/U	7/0.0312-in. silver-covered copper	F-1	0.285	Silver-coated copper, double braid	Teflon-tape, moisture seal, two braids, Fiberglas, silicone-varnish-impregnated	0.430		50.0	29.5	5,000	High temperature, similar to RG-9B/U
RG-116/U	7/0.0312 silver-covered copper	F-1	0.285	Silver-coated copper, double braid	Teflon-tape, moisture seal, two braids, Fiberglas, silicone-varnish-impregnated, with armor	0.490 (max.)		50.0	29.5	5,000	RG-87A/U with armor
RG-117/U	0.190-in. copper	F-1	0.620	Copper, single braid	Teflon-tape, moisture seal, two braids, Fiberglas, silicone-varnish-impregnated	0.730		50.0	29.0	7 kv	High temperature
RG-118/U	0.190-in. copper	F-1	0.620	Copper, single braid	Teflon-tape moisture seal, two braids, Fiberglas, silicone-varnish-impregnated, with armor	0.795 (max.)	0.610	50.0	29.0	7 kv	R-G117/U with armor
RG-122/U	27/38 AWG tinned copper	A-1	0.096	Tinned copper, single braid	Synthetic resin	0.160		50.0	29.3	1,900	Same as RG-58A/U except smaller in size and lighter in weight

Type	Inner conductor	Dielectric	Dielectric dia.	Outer conductor	Protective covering	Overall dia.	Impedance	Capacitance	Max. voltage	Remarks
RG-126/U	7/0.0203-in. karma wire	F-1	0.185	Karma wire, single braid	Teflon-tape, moisture seal, two braids, Fiberglas, silicone-varnish-impregnated	0.280	50.0	29.0	3,000	High attenuation
RG-130/U	2 conductors, 7/0.0285-in. copper	A-1	0.472	Tinned copper, single braid	Synthetic resin	0.625	95.0	17.0	8,000	Same as RG-57A/U except inner conductors are twisted for improved flexibility
RG-131/U	2 conductors, 7/0.0285-in. copper	A-1	0.472	Tinned copper, single braid	Synthetic resin, with aluminum armor	0.710	95.0	17.0	8,000	Same as RG-130/U except for armor
RG-140/U	0.025-in. silver-covered, copper-covered, steel wire	F-1	0.140	Silver-coated copper, single braid	Teflon-tape moisture seal, single Fiberglas braid, silicone-varnish-impregnated	0.233	75.0	21.0	2,300	High temperature, similar to RG-59A/U
RG-141/U	0.0359-in. silver-covered, copper-covered, steel wire	F-1	0.116	Silver-coated copper, single braid	Teflon-tape moisture seal, single Fiberglas braid, silicone-varnish-impregnated	0.190	50.0	28.5	1,900	High temperature, similar to RG-58C/U
RG-142/U	0.0359-in. silver-covered, copper-covered, steel wire	F-1	0.116	Silver-coated copper, double braid	Teflon-tape moisture seal, single Fiberglas braid, silicone-varnish-impregnated	0.206	50.0	28.5	1,900	High temperature, similar to RG-55A/U
RG-143/U	0.057-in. silver-covered, copper-covered, steel wire	F-1	0.185	Silver-coated copper double braid	Teflon-tape moisture seal, double Fiber-glas braid, silicone-varnish-impregnated	0.325	50.0	28.5	3,000	High temperature, similar to RG-5B/U
RG-144/U	7/0.0179-in. silver-covered, copper-covered, steel wire	F-1	0.285	Silver-covered copper, single braid	Teflon-tape moisture seal, double Fiber-glas braid, silicone-varnish-impregnated	0.410	75.0	20.5	5,000	High temperature, similar to RG-11/U

Table 30-1. Flexible Coaxial Lines (*Continued*)

Type	Inner conductor	Dielectric material*	Nominal diameter of dielectric, in.	Number and type of shielding braids	Protective covering	Nominal over-all diameter, in.	Weight, lb/ft	Nominal impedance, ohms	Nominal capacitance, μμf/ft	Maximum operating voltage, volts(rms)	Engineering data
RG-164/U	0.1045-in. copper	A-1	0.680	Copper, single braid	Noncontaminating synthetic resin	0.870		75.0		10,000	
RG-165/U	7/0.032-in. silver-covered copper	F-1	0.285	Silver-covered copper, single braid	Type V double braid	0.410		50.0		5,000	
RG-166/U	7/0.032-in. silver-covered copper	F-1	0.285	Silver-covered copper, single braid	Type V double braid with armor	0.460		50.0		5,000	
RG-174/U	7/34 AWG copper-weld	A-1	0.060	Copper, single braid	Polyvinyl (black)	0.100		50.0	30.4	1,500	
RG-177/U	0.195-in. copper	A-1	0.680	Silver-covered copper, double braid	Noncontaminating synthetic resin	0.895		50.0		11,000	
RG-178/U	7/38 AWG silver-covered copper	F-1	0.036	Silver-plated copper, single braid	Extruded KEL-F or equal	0.075		50.0	27.9	750.0	
RG-179/U	7/38 AWG silver-plated copper	F-1	0.057	Silver-plated copper, single braid	Extruded KEL-F or equal	0.090		70.0	2.4	750.0	
RG-180/U	7/38 AWG silver-covered copper	F-1	0.103	Silver-plated copper, single braid	Extruded KEL-F or equal	0.137		93.0	14.5	750.0	

* Dielectric materials: A-1—solid polyethylene; A-2—air-spaced polyethylene; F-1—solid tetrafluoroethylene (Teflon).
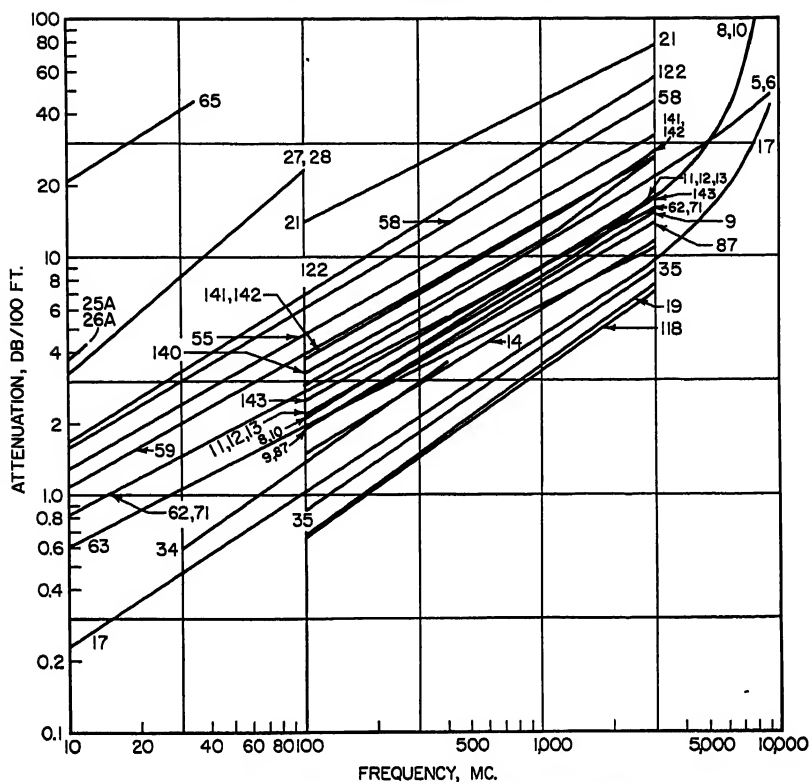
FIG. 30-4. Attenuation of flexible coaxial lines.
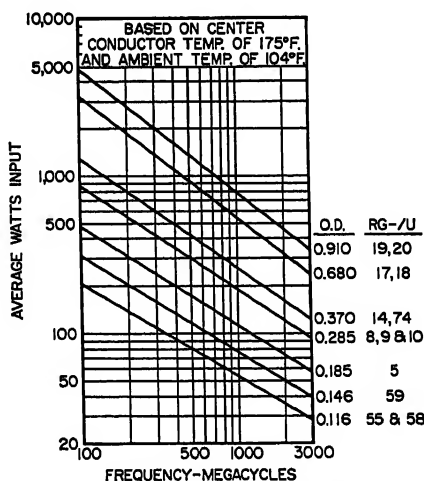
FIG. 30-5. Power-handling capacity of flexible coaxial lines.

30.5. WIRES IN VARIOUS ENCLOSURES

It is often advantageous to tailor a transmission line to fit a specific application where one of the more common forms is not convenient. Furthermore, with many antenna configurations, a nonstandard form of line has definite advantages.

Various forms of transmission line comprising wires in different-shaped enclosures are shown in Fig. 30-6, together with formulas for characteristic impedance. It should be noted that these lines are shielded, with the exception of the corner enclosure, provided that those that are physically open have an opening less than one-half wavelength across, extend beyond the wire at least one-half wavelength, and have opposing surfaces that are maintained at the same potential.
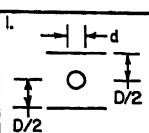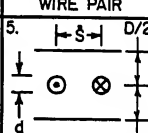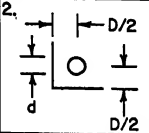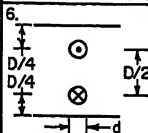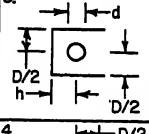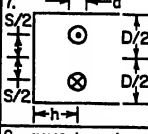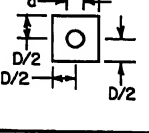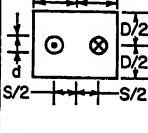
SINGLE WIRE	CHARACTERISTIC IMPEDANCE	BALANCED WIRE PAIR	CHARACTERISTIC IMPEDANCE
1.	$Z_0 = \dfrac{138}{\sqrt{\epsilon}}\left[\log_{10}\dfrac{4D}{\pi d} - \dfrac{0.0367\left(\frac{d}{D}\right)^4}{1-0.355\left(\frac{d}{D}\right)^4}\right]$	5.	$Z_0 = \dfrac{276}{\sqrt{\epsilon}}\log_{10}\dfrac{4D}{\pi d}\tanh\dfrac{\pi S}{2D}$
2.	$Z_0 = \dfrac{138}{\sqrt{\epsilon}}\log_{10}\dfrac{\sqrt{2}D}{d}$	6.	$Z_0 = \dfrac{276}{\sqrt{\epsilon}}\log_{10}\dfrac{2D}{\pi d}$
3.	$Z_0 = \dfrac{138}{\sqrt{\epsilon}}\log_{10}\dfrac{4D}{\pi d}\tanh\dfrac{\pi h}{D}$ FOR EXACT FORMULA SEE REFERENCE 7	7.	$Z_0 = \dfrac{276}{\sqrt{\epsilon}}\log_{10}\dfrac{2D}{\pi d\sqrt{A}}$ $A = \csc^2\left(\dfrac{\pi S}{d}\right) + \operatorname{csch}^2\left(\dfrac{2\pi h}{d}\right)$
4.	$Z_0 = \dfrac{138}{\sqrt{\epsilon}}\log_{10}1.08\,\dfrac{D}{d}$	8.	$Z_0 = \dfrac{276}{\sqrt{\epsilon}}\left(\log_{10}\dfrac{4D}{\pi d}\tanh\dfrac{\pi S}{2D} - \sum_{n=1}^{\infty}\log_{10}\dfrac{1+u_n^2}{1-v_n^2}\right)$ $u_n = \dfrac{\sinh\frac{\pi S}{2D}}{\cosh\frac{n\pi W}{2D}}$, $v_n = \dfrac{\sinh\frac{\pi S}{2D}}{\sinh\frac{n\pi W}{2D}}$

FIG. 30-6. Wires in various enclosures. *Note: d* is small compared to other dimensions except in case 1.
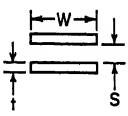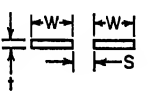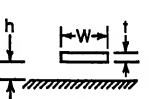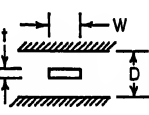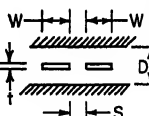
30.6. STRIP TRANSMISSION LINES

Strip transmission lines are those in which the conductors have the form of flat strips or plates. In terms of relative simplicity and cost, these types might be ranked between open-wire lines and coaxial lines. Both open and shielded types exist, the choice depending upon the application. The more common forms of strip lines utilize one or two ground planes, the strip circuit in itself being essentially two-dimensional. This fact permits use of economical fabrication methods such as photo-etching. This type of line is particularly suited for feeding essentially planar antennas such as printed arrays and slots. It is also useful for auxiliary circuits such as power splitters and hybrid ring junctions.

Formulas for the characteristic impedance of the more common forms of strip transmission lines are given in Fig. 30-7. The most widely used forms are the strip above a ground plane and the strip between ground planes. The former, termed microstrip,[9] usually consists of a dielectric sheet clad on one side with a copper-foil

ground plane and on the other with a copper-foil strip. The latter type may have the strip supported by full dielectric sheets,[10] beads, or by a thin dielectric sheet splitting the strip in the median plane,[11] thereby approximating an air-dielectric line. More complete data on these types of strip transmission lines are given below.

Microstrip Lines. The characteristic impedance for microstrip line is shown in Fig. 30-8.[12,13] It should be pointed out that the theoretical curve is for a uniform

	CHARACTERISTIC IMPEDANCE	
	EXACT FOR t=0*	APPROXIMATE
	$Z_0 = \dfrac{377}{\sqrt{\epsilon}} \dfrac{K}{K'}$ MAX $zn(u,k) = \dfrac{\pi W}{2KS}$	$Z_0 \approx \dfrac{377}{\sqrt{\epsilon}} \dfrac{S}{W}$, $S \ll W$ $Z_0 \approx \dfrac{276}{\sqrt{\epsilon}} \log_{10} \dfrac{4S}{W}$, $S \gg W$
	$Z_0 = \dfrac{377}{\sqrt{\epsilon}} \dfrac{K}{K'}$ $k = \dfrac{S}{S+2W}$	$Z_0 \approx \dfrac{257}{\sqrt{\epsilon}\, \log_{10}\left(4+\frac{8W}{S}\right)}$, $S \ll W$, $t=0$ $Z_0 \approx \dfrac{276}{\sqrt{\epsilon}} \log_{10}\left(8+\dfrac{4S}{W}\right)$, $S \gg W$, $t=0$
	$Z_0 = \dfrac{189}{\sqrt{\epsilon}} \dfrac{K}{K'}$ MAX $zn(u,k) = \dfrac{\pi W}{4Kh}$	$Z_0 \approx \dfrac{377}{\sqrt{\epsilon}} \dfrac{h}{W}$, $h \ll W$ $Z_0 \approx \dfrac{138}{\sqrt{\epsilon}} \log_{10} \dfrac{8h}{W}$, $h \gg W$
	$Z_0 = \dfrac{94}{\sqrt{\epsilon}} \dfrac{K}{K'}$ $k = \text{sech}\, \dfrac{\pi W}{2D}$	$Z_0 \approx \dfrac{94}{\sqrt{\epsilon}} \dfrac{1-\frac{t}{D}}{\frac{W}{D}+0.47+0.65\frac{t}{D}-1.12\left(\frac{t}{D}\right)^2}$, $t \le .5D$, $W \ge .35(D-t)$ $Z_0 \approx \dfrac{138}{\sqrt{\epsilon}} \log_{10}\left(\dfrac{\frac{8}{\pi}}{\frac{W}{D}+1.4\frac{t}{D}}\right)$, $t \le .25D$, $W \le .35(D-t)$
	BALANCED $Z_0 = \dfrac{189}{\sqrt{\epsilon}} \dfrac{K'}{K}$ $k = \tanh\left(\dfrac{\pi W}{2D}\right) \cdot \coth\left(\dfrac{\pi[W+S]}{2D}\right)$	FOR APPROXIMATE FORMULAS IN THE CASE t>0, SEE REFERENCE 8
*K(k) IS THE COMPLETE ELLIPTIC INTEGRAL OF THE FIRST KIND, K'=K(k') WHERE $k'^2=1-k^2$. zn(u,k) IS THE JACOBI ZETA-FUNCTION.		

FIG. 30-7. Strip transmission lines.

dielectric, whereas usually in practice, the dielectric is air above the strip and a solid dielectric between the strip and ground plane. The experimental curve shows the departure from theory due to this cause.

Whereas microstrip lines have conductor losses on the same order as other lines of the same size, a practical line has rather high loss because of the dielectric. A typical value being $1.6 \times 10^{-6} \sqrt{f}$ neper/meter for Fiberglas G-6 dielectric $\frac{1}{16}$ in. thick and a characteristic impedance of 37 ohms.

When the dielectric above the strip differs from that below, the propagation velocity is not readily calculated and depends on the characteristic impedance and relative

dielectric constants.   In this case, the propagation is not pure TEM, the amount of energy in higher modes depending upon the physical constants of the line.

Symmetrical Strip Lines.   The characteristic impedance for symmetrical strip line comprising a strip centered between two ground planes is shown in Fig. 30-9.[14]   For
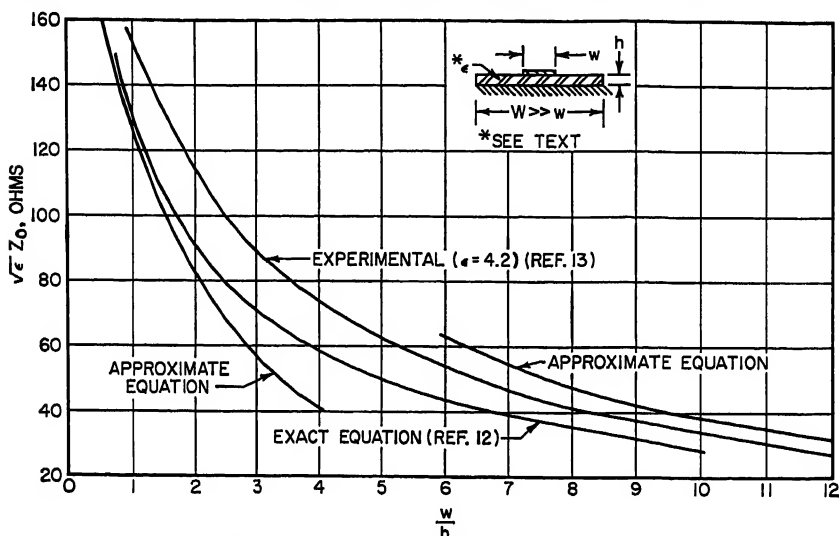
FIG. 30-8. Characteristic impedance of microstrip line.
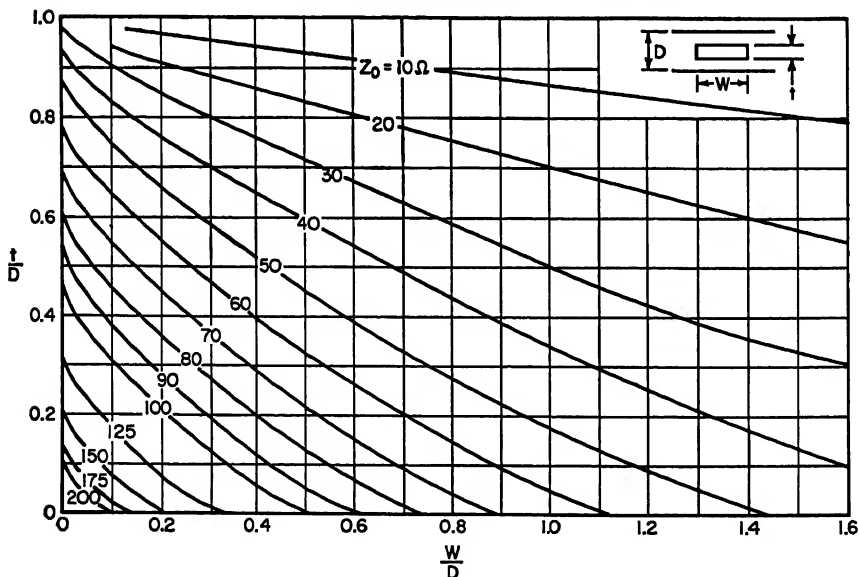
FIG. 30-9. Characteristic impedance of symmetrical strip line.

the type wherein the center strip is made in two layers supported by a thin dielectric sheet, these curves may be used with negligible error up to 75 ohms for Teflon-bonded Fiberglas when $t/D \leq 0.15$. For higher impedances and thicker strips, the fringing field will cause a gradual departure from the curves.
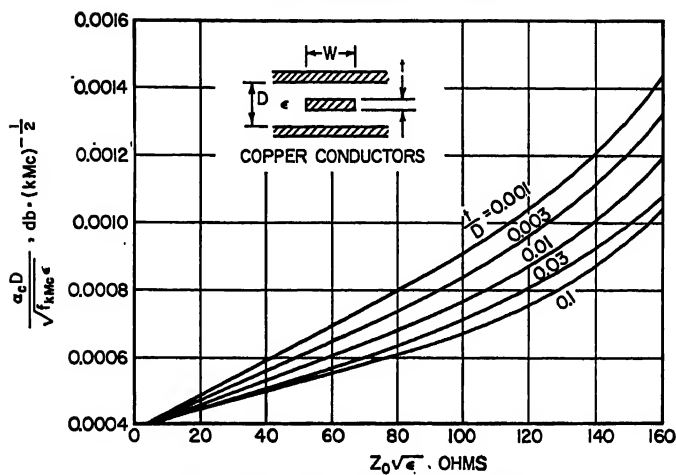
FIG. 30-10. Attenuation of symmetrical strip line.
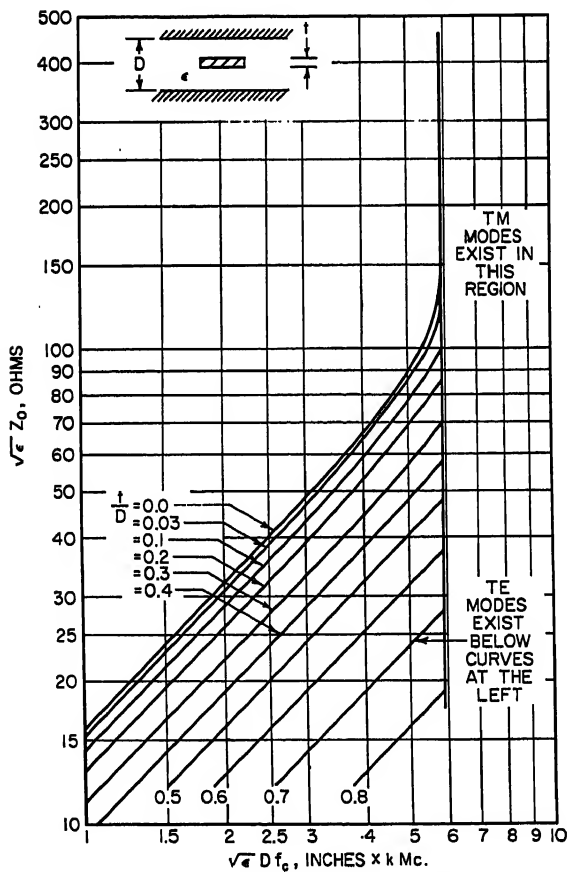
FIG. 30-11. Higher modes in symmetrical strip line.

The attenuation of symmetrical strip line is shown in Fig. 30-10 for a solid-strip center conductor. In the case of the sheet-supported split center conductor using Teflon-bonded fiberglas, the attenuation is about two times this and the velocity of propagation is about 98 per cent of the velocity in free space.

There are two types of higher-order mode which can exist in this type of line. The cutoff wavelength for the lowest TM mode is given by

$$\lambda_c = 2D$$

and these modes will radiate. The cutoff frequency for the lowest TE mode may be found from the curves in Fig. 30-11,[15] and these modes will radiate only when they fulfill the same condition as the TM modes.

The maximum power-handling capacity of symmetrical strip line has been found experimentally to occur for $t/D = 0.175$ when the center strip has semicircular edges. For $Z_0 \leq 50$ ohms, the maximum power for this value of t/D can be found from the empirical formula

$$P_{max} = \frac{E_a^2 D^2}{65 Z_0} \qquad \text{watts}$$

For bead- and stub-supported lines, the same general methods may be used as described in Sec. 30.3 for coaxial line.

The effect of dimensional tolerances can be found from the slope of the characteristic-impedance curves in Fig. 30-9. The effect of off centering will be approximately the same as in the coaxial-line case. If the strip is not parallel to the ground planes, an unbalanced parallel-plate TEM mode may result. This can be suppressed by using metallic spacers to ensure that the ground planes are at the same potential. In the case of high-Q circuits where the losses associated with this mode, even though suppressed, cannot be tolerated, the strip should be held parallel to the ground planes to within 0.5°, thereby preventing generation of this mode.

Discontinuities in this type of line are discussed in Sec. 30.10.

30.7. HOLLOW-TUBE WAVEGUIDES

Propagation in Hollow-tube Waveguides. Electromagnetic energy can be propagated down hollow metal tubes if the tubes are of sufficient size and are properly excited. The size of the tubes required usually limits their use to the VHF region or above.

The energy can be propagated in a number of different types of waves as described below. In the usual case, waveguide devices are designed for transmission of a single wave type (most often the dominant wave or that having the lowest cutoff frequency) because the design problems are very greatly simplified.

TE_{mn} waves: In the transverse-electric waves, sometimes called H_{mn} waves, the electric vector is always perpendicular to the direction of propagation.

TM_{mn} waves: In the transverse magnetic waves, sometimes called the E_{mn} waves, the magnetic vector is always perpendicular to the direction of propagation.

The propagation constant γ_{mn} determines the amplitude and phase of each component of a wave as it is propagated along the waveguide. Each component may be represented by $A \exp(jwt - \gamma_{mn} z)$, where A is a constant, z is the distance along the direction of propagation, and $\omega = 2\pi f$. When γ_{mn} is real, there is no phase shift along the waveguide but there is high attenuation. In fact, no propagation takes place, and the waveguide is considered below cutoff. The reactive attenuation L along the waveguide under these conditions is given by

$$L = \frac{54.58S}{\lambda_c} \left[1 - \left(\frac{\lambda_c}{\lambda} \right)^2 \right]^{1/2} \text{db/unit length}$$

where λ is the wavelength in the unbounded medium, and λ_c is the cutoff wavelength of that wave (a function of waveguide dimensions only). Waveguides are often used at frequencies far below cutoff as calibrated attenuators, since the rate of attenuation is determined by cross-section dimensions of the waveguide and the total attenuation in db is a linear function of the displacement of the output from the input.[16]

When γ_{mn} is imaginary, the amplitude of the wave remains constant but the phase changes with z and propagation takes place. γ_{mn} is a pure imaginary quantity only for lossless waveguide. In a practical case, γ_{mn} has both a real part α_{mn}, which is the attenuation constant, and an imaginary part β_{mn}, which is the phase constant; that is, $\gamma_{mn} = \alpha_{mn} + j\beta_{mn}$.

The wavelength in a uniform waveguide is always greater than the wavelength in the unbounded medium and is given by

$$\lambda_g = \frac{\lambda}{[1 - (\lambda/\lambda_c)^2]^{1/2}}$$

The phase velocity is the apparent velocity, judging by the phase shift along the guide. Phase velocity, $v = c\,(\lambda_g/\lambda)$, is always greater than that in an unbounded medium.

E LINES FOR TE MODES   H LINES FOR TM MODES
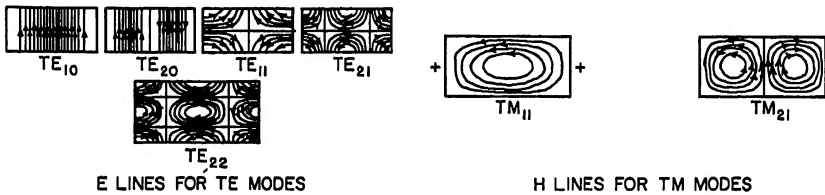
FIG. 30-12. Field configurations for rectangular waveguide.

The group velocity is the velocity of energy propagation down the guide. Group velocity, $u = c\,(\lambda/\lambda_g)$, is always less than that in an unbounded medium.

For air-filled guide and those filled with dielectric having very low loss, the attenuation is mainly due to conductor losses in the walls. For any particular type of wave, the loss is high near cutoff and decreases as the frequency is increased. For all excepting the TE_{0n} waves in circular waveguide, the attenuation reaches a minimum value for that wave and that waveguide, then increases with frequency. For most waves, this minimum is slightly above $2f_c$. To avoid high loss near cutoff and the complexity of multiwave transmission, the useful band is usually considered to lie between $1.3f_c$ of the desired mode and $0.9f_c$ of the next higher mode. For rectangular waveguides having a width equal to twice the height, the useful range is about 1.5:1.

Rectangular Waveguides. For TE_{mn} waves in rectangular waveguides, m and n may take any integer value from 0 to infinity, except the case $m = n = 0$. For the TM_{mn} waves, m and n may take any value from 1 to infinity. The m and n denote the number of half-period variations of the electric field for TE waves or magnetic field for TM waves in the direction of the small and large dimensions of the waveguide, respectively. Field patterns for some of the simpler waves are shown in Fig. 30-12.

The propagation constant for rectangular guides is given by

$$\gamma_{mn} = \sqrt{\left(\frac{m\pi}{a}\right)^2 + \left(\frac{n\pi}{b}\right)^2 - \omega^2\mu\epsilon} = \frac{2\pi}{\lambda_g}$$

where a is the wide dimension, b is the narrow dimension, ϵ is the relative dielectric constant, and μ is the relative permeability of the dielectric in the waveguide. Since propagation takes place only when the propagation constant is imaginary, the cutoff

frequency for rectangular waveguide is

$$f_o = \frac{c}{2\sqrt{\mu\epsilon}} \sqrt{\left(\frac{m}{a}\right)^2 + \left(\frac{n}{b}\right)^2}$$

and

$$\lambda_c = \frac{2\sqrt{\mu\epsilon}}{\sqrt{(m/a)^2 + (n/b)^2}}$$

Most frequently, operation is limited to the TE_{10} or dominant wave in rectangular waveguide. For this simplified case, the important formulas reduce to

$$\lambda_c = 2a\sqrt{\mu\epsilon}$$
$$\gamma = 2\pi\sqrt{(1/4a) - f^2\mu\epsilon}$$

In order to relate the waveguide properties to similar properties of low-frequency circuits, the impedance concept has been developed. Three characteristic impedances can be defined, differing from each other by a constant:[33]

$$Z_{VI} = \frac{V}{I} = 377\frac{\pi}{2}\frac{b}{a}\frac{\lambda_g}{\lambda}$$

$$Z_{PV} = \frac{V^2}{2P} = 754\frac{b}{a}\frac{\lambda_g}{\lambda}$$

$$Z_{PI} = \frac{2P}{I^2} = 377\frac{\pi^2}{8}\frac{b}{a}\frac{\lambda_g}{\lambda}$$

Any one of the three is reasonably satisfactory if used consistently throughout, since the most frequent use is in determining mismatch at waveguide junctions and
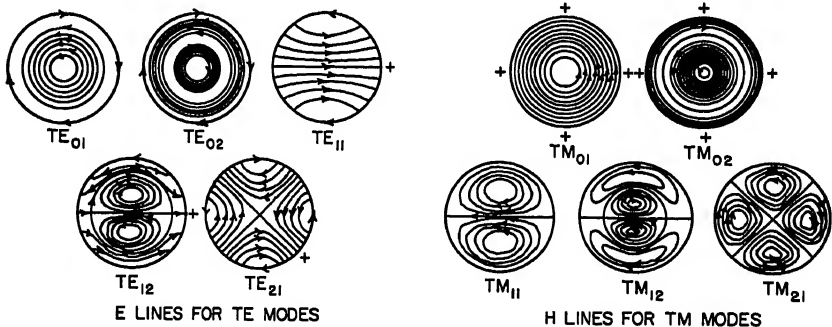
FIG. 30-13. Field configurations for circular waveguide.

it is the ratio of impedance that matters. Ratios involving only different values of b give accurate indication of impedance mismatch. Differences in a give ratios nearly correct for small changes in a from the usual cross-section dimensions of rectangular waveguide, but errors are appreciable for large differences in a. Z_{PV} is most widely used, but Z_{VI} is found to be more nearly correct in matching coaxial line to waveguide.

Circular Waveguides. The usual coordinate system is ρ, θ, z, where ρ is in the radial direction, θ is the angle, and z is the longitudinal direction.

For TE_{mn} waves in circular waveguides m denotes the number of axial planes along which the normal component of electric field vanishes and n the number of cylinders including the boundary of the guide along which the tangential component of electric field vanishes. The number m may take any integral value from 0 to infinity, and n may take any integral value from 1 to infinity. The dominant wave in circular waveguide is the TE_{11}. For TM_{mn} waves, m denotes the number of axial planes along

which the magnetic field vanishes and n the number of cylinders to which the electric field is normal. The number m may take any integral value from 0 to ∞, and n may take any integral value from 1 to ∞. Of the circularly symmetrical waves, the TM_{01} has the lowest cutoff frequency.

Field patterns for some of the simpler waves in circular guides are shown in Fig. 30-13.

The cutoff wavelength in lossless circular guide is given by

$$\lambda_c = \sqrt{\mu\epsilon}\, D_{mn}a$$

where a is the radius, ϵ the relative dielectric constant, μ the relative permeability of the dielectric, and the constant D_{mn} is as shown in Table 30-2.
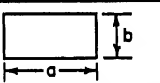
Table 30-2. Cutoff Constants for Circular Waveguide

D_{mn} for TE_{mn} Waves

n \ m	0	1	2	3
1	1.640	3.412	2.057	1.496
2	0.896	1.178	0.937	0.764
3	0.618	0.736	0.631	0.554
4	0.475	0.54	0.48	0.44

D_{mn} for TM_{mn} Waves

n \ m	0	1	2	3
1	2.613	1.640	1.224	0.966
2	1.139	0.896	0.747	0.644
3	0.726	0.618	0.541	0.482
4	0.534	0.475	0.425	0.388

A summary of the cutoff and attenuation constant formulas for circular and rectangular waveguides is given in Table 30-3.

Table 30-3. Summary of Cutoff and Attenuation Constant Formulas*

TYPE OF GUIDE	RECTANGULAR TE_{MO}	TM_{OI}	TE_{II}	TE_{OI}
CUTOFF WAVELENGTH	$\dfrac{2a}{m}$	$2.613a$	$3.412a$	$1.640a$
ATTENUATION CONSTANT NEPERS/METER DUE TO CONDUCTION LOSSES ONLY	$\dfrac{4a_0 A}{a}\left(\dfrac{a}{2b}+\dfrac{\lambda^2}{\lambda_c^2}\right)$	$2\dfrac{a_0 A}{a}$	$2\dfrac{a_0}{a}A\left(0.415+\dfrac{\lambda^2}{\lambda_c^2}\right)$	$2\dfrac{a_0}{a}A\dfrac{\lambda^2}{\lambda_c^2}$
ATTENUATION FAR BELOW CUTOFF	27.28 DB PER GUIDE WIDTH	41.78 DB PER DIAMETER	31.98 DB PER DIAMETER	66.56 DB PER DIAMETER

*See page 30 24 for definitions.

Table 30-4. Standard Rectangular Waveguides and Flanges

RETMA designation WR	Army-Navy No. RG-	Material	Inside dimensions	Tolerance	Wall thickness	Frequency range, kmc for TE$_{10}$	f_c, kmc, TE$_{10}$	λ_c, cm, TE$_{10}$	Attenuation, db/100 ft highest and lowest frequency	Theoretical power, megawatts	Cover UG-	Choke UG-	Rubber flange gasket
1500			15.000 × 7.500	±.015	.125	.47-.75	0.393	76.3					
1150			11.500 × 5.750	±.015	.125	.64-.96	0.514	58.4					
975			9.750 × 4.875	±.010	.125	.75-1.12	0.605	49.6					
770			7.700 × 3.850	±.005	.125	.96-1.45	0.767	39.1					
650	69/U 103/U	B A	6.500 × 3.250	±.005	.080	1.12-1.70	0.908	33.0	.424-.284 .269-.178	11.9-17.2	417A/U 418A/U		MS90065-2
510			5.100 × 2.550	±.005	.080	1.45-2.20	1.16	25.9					
430	104/U 105/U	B A	4.300 × 2.150	±.005	.080	1.70-2.60	1.375	21.8	.788-.516 .501-.330	5.2-7.5	435A/U 437A/U		MS90065-3
340	112/U 113/U	B A	3.400 × 1.700	±.005	.080	2.20-3.30	1.735	17.3			553/U 554/U		MS90065-1
284	48/U 75/U	B A	2.840 × 1.340	±.005	.080	2.60-3.95	2.08	14.2	1.47-1.01 .940-.641	2.2-3.2	66/U* 53/U 584/U	54A/U 585/U	MS90064-9
229			2.290 × 1.145	±.005	.064	3.30-4.90	2.59	11.6					
187	49/U 95/U	B A	1.872 × 0.872	±.005	.064	3.95-5.85	3.16	9.50	2.79-1.93 1.77-1.22	1.4-2.0	149A/U 407/U	148B/U 406A/U	MS90064-8

WR	JAN Type	Material	Dimensions, in. (±tol)	Wall	Freq. Range, GHz			Power	Atten.	Flanges		MS Flange
159			1.590 × 0.795 ±.004	.064	4.90–7.05	3.71	8.09	3.85–3.08 / 2.45–1.94	.56–.71	150/U* 344/U 441/U	343A/U 440A/U	MS90064-7
137	50/U 106/U	B A	1.372 × 0.622 ±.004	.064	5.85–8.20	4.29	6.98					
112	51/U 68/U	B A	1.122 × 0.497 ±.004	.064	7.05–10.00	5.26	5.70	5.51–4.31 / 3.50–2.74	.35–.46	51/U 138/U	52A/U 137A/U	MS90064-6
90	52/U 67/U	B A	0.900 × 0.400 ±.003	.050	8.20–12.40	6.56	4.57	8.04–6.02 / 5.49–3.83	.20–.29	39/U 135/U	40A/U 136A/U	MS90064-5
75			0.750 × 0.375 ±.003	.050	10.00–15.00	7.88	3.81					
62	91/U 107/U	B A	0.622 × 0.311 ±.003	.040	12.40–18.00	9.49	3.16	12.7–11.1 / 6.14–5.36	.12–.16	419/U	541/U	MS90064-4
51			0.510 × 0.255 ±.0025	.040	15.00–22.00	11.6	2.59					
42	53/U 66/U 12/U	B S A	0.420 × 0.170 ±.002	.040	18.00–26.50	14.1	2.13	27.7–19.8 / 13.3–9.5 / 17.6–12.6	.043–.058	595/U 597/U	596/U 598/U	MS90064-2
34			0.340 × 0.170 ±.002	.040	22.00–33.00	17.3	1.73					
28	96/U	S	0.280 × 0.140 ±.0015	.040	26.50–40.00	21.2	1.42	21.9–15.0	.022–.031	599/U	600/U	MS90064-1
22	97/U	S	0.224 × 0.112 ±.001	.040	33.0–50.0	26.35	1.14	31.0–20.9	.014–.020	383/U*		MS90064-3
19		S	0.188 × 0.094 ±.001	.040	40.0–60.0	31.4	.955					
15	98/U	S	0.148 × 0.074 ±.001	.040	50.0–75.0	39.9	.753	52.9–39.1	.0063–.0090	385/U*		MS90064-3
12	99/U	S	0.122 × 0.061 ±.0005	.040	60.0–90.0	48.4	.620	93.3–52.2	.0042–.0060	387/U*		MS90064-3
10		S	0.100 × 0.050 ±.0005	.040	75.0–110.0	59.0	.509					

* Indicates a contact flange.

For attenuation—resistivity of brass = 7.0×10^{-8} ohm-meter
silver = 1.62×10^{-8} ohm-meter
aluminum = 2.83×10^{-8} ohm-meter

Power computed using breakdown strength of air of 15,000 volts/cm. A safety factor of about 2 at sea level has been allowed.

where $A = \dfrac{\sqrt{c/\lambda}}{\sqrt{1 - (\lambda/\lambda_c)^2}}$

c = velocity of light in free space $\approx 3 \times 10^8$ meters/sec

For copper and air, $\alpha_0 = 3.5 \times 10^{-8}$ neper/meter. To convert nepers per meter to decibels per 100 ft, multiply by 264.

Standard Waveguide Sizes. The waveguide sizes which have become standardized are listed in Table 30-4, together with the flanges used in connecting them together.

Hollow-tube Waveguides with Other Cross Sections. One of the most useful of the many cross sections that might be used is the ridged waveguide as shown in Fig. 30-14, which is useful in wideband transmission. For ridged waveguide[17-19] (and others of arbitrary cross section), the best method of obtaining cutoff wavelength is by resonance in the cross section. A convenient longitudinal plane is chosen.

At cutoff, the susceptance looking into the shorted parallel-plate guide to the right of this plane is equal in amplitude and opposite in phase to that looking to the left. If the guide is symmetrical, only half the guide need be used since Y at the center is zero. For the ridged guide this gives

$$\cot \frac{2\pi l}{\lambda_c} - \frac{B}{Y_{01}} = \frac{b}{a} \tan \frac{2\pi S}{\lambda_c 2}$$

where B is the capacitive discontinuity at the height change. A plot of cutoff frequency and a plot of admittance defined as power/(voltage)^2 of ridged guide of different shapes are given in Figs. 30-15 to 30-17.
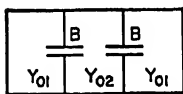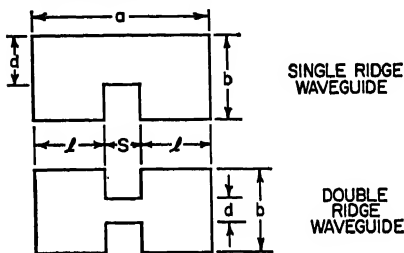
FIG. 30-14. Ridged-waveguide configurations.

The loading in the center of the guide lowers the cutoff frequency of the dominant mode so that a useful bandwidth of over 4:1 may be obtained with single-mode transmission. The impedance is reduced by the loading and can be adjusted by proportioning the ridges for impedance matching of waveguides to coaxial line, for example.

The ridged guide for a given frequency band is smaller than the regular guide, but the losses are higher.

Flexible Waveguides. Flexible rectangular waveguides to match most of the Army-Navy type of waveguides are made by several manufacturers. These differ primarily in the mechanical construction. Waveguides using seamless corrugations, spiral-wound strip with adjacent edges crimped and soft-soldered, spiral-wound strip with heavier crimping to provide sliding contact, and vertebra type (consisting of cover-choke wafers held in place by a rubber jacket) are all available. The first two will bend in either plane, stretch, or compress, but will not twist. The last two twist as well as bend and stretch. Where the guide is flexed during operation, or pressurized, the guide is nearly always covered with a molded-rubber jacket. When unjacketed, all are subject to a minimum bending radius (of the guide center line) of two to three times the outer guide dimension in the plane of the bend, and when jacketed to about four to six times the outer dimensions. The mismatch between rigid and flexible guide is small when straight and designed for lower frequencies. Mismatch increases as the waveguide size decreases since the depth of convolutions cannot be decreased as fast as the waveguide dimensions (mismatch also increases as the bending radius is decreased). Similarly, attenuation which is only slightly
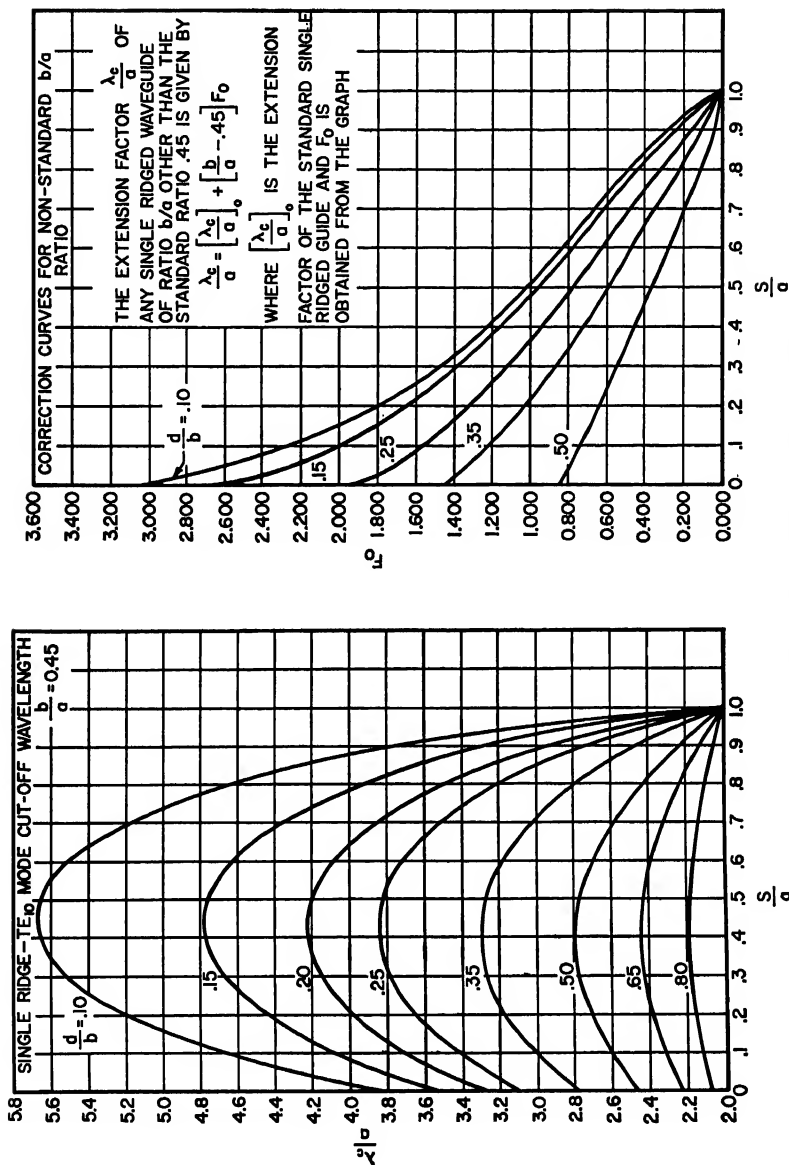
FIG. 30-15. Cutoff wavelength of single ridged waveguide.
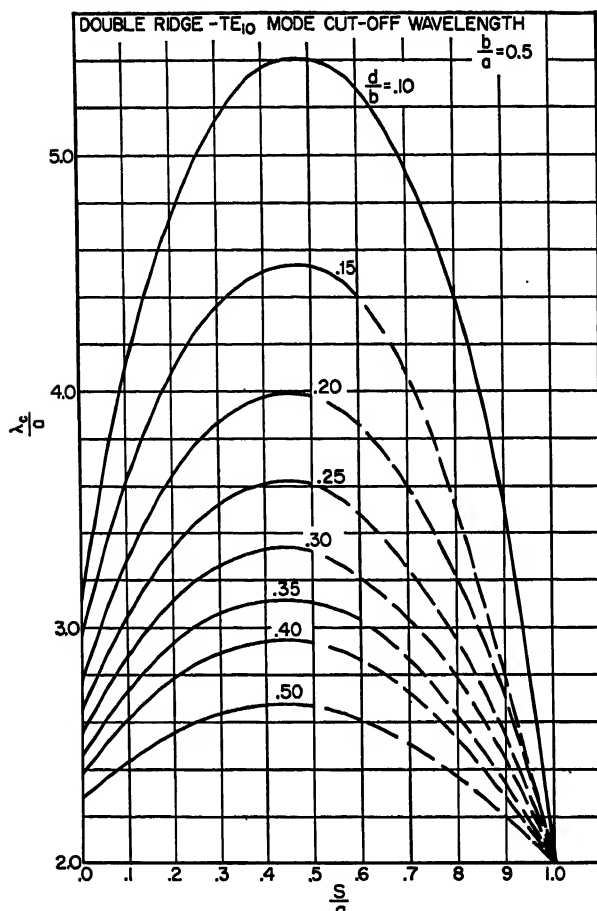
FIG. 30-16. Cutoff wavelength of double ridged waveguide.

greater than that in rigid guide for low frequencies becomes about twice as great at 40 kmc. Power capacity is nearly equal to that of rigid guide.

30.8. MISCELLANEOUS TYPES OF WAVEGUIDES

Trough Waveguide.[20] Trough waveguide having the cross section shown in Fig. 30-18 is derived from the lowest TE mode on symmetrical strip line by inserting a longitudinal electric wall at the center of the strip. Energy is transmitted in the TE modes in which the electric fields are symmetrical about the center vane. The cross section is such that probes, tuning, or attenuating devices may easily be inserted and moved from the open side, with a minimum of electrical disturbance. Trough waveguide is a broadband transmission device since the cutoff of the second propagating mode is three times that of the dominant mode, instead of twice as in rectangular waveguide. It is easily fed from an end-on transition from coaxial or symmetrical strip line. The outer conductor of the TEM line is connected to the outer walls of the trough guide. The inner conductor of the line is connected at a point on the center vane of the trough guide at a distance S up from the bottom of the center

vane, as determined from the relation for the power-voltage characteristic impedance at that point,

$$Z_{\text{PV}}(S) = 754 \frac{D}{\lambda_c} \frac{\lambda_g}{\lambda} \sin^2\left(\frac{2\pi S}{\lambda_c}\right)$$

Similarly, a crystal may be attached at an appropriate point to provide a crystal mount. The cutoff wavelength of the dominant mode in trough waveguide may be determined from the graph in Fig. 30-18.
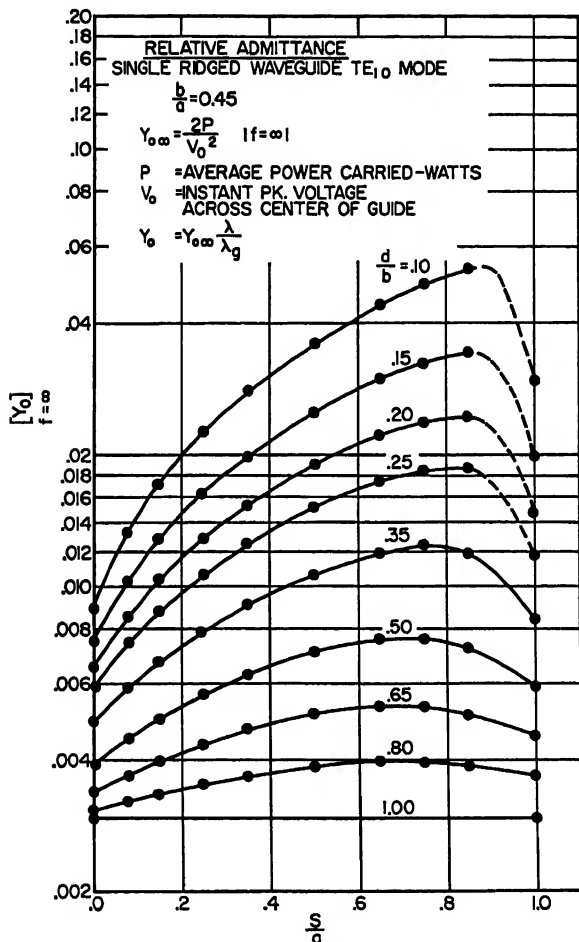
FIG. 30-17. Admittance of single ridged waveguide.

Radial Line and Biconical Guide. Two circular parallel conducting plates, separated by a dielectric and fed at the center or outer edge, form a line in which the transmission is radial. This type of line is frequently used in choke junctions and resonant cavities such as microwave oscillator tubes. The simplest wave transmitted by this type of line is a TEM wave. The phase front of this wave is a circle of ever increasing or decreasing radius. The radial current in one plate returns radially through the other plate. With radial lines it is very useful to know the input impedance with
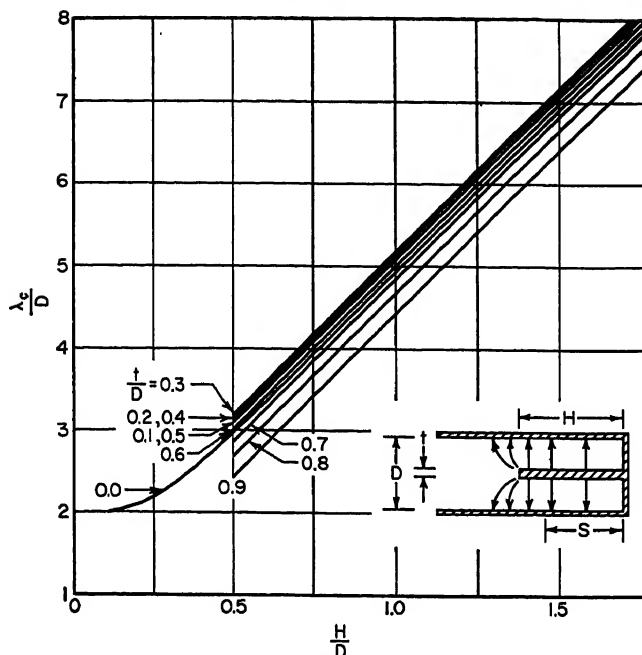
Fig. 30-18. Cutoff wavelength of trough waveguide.
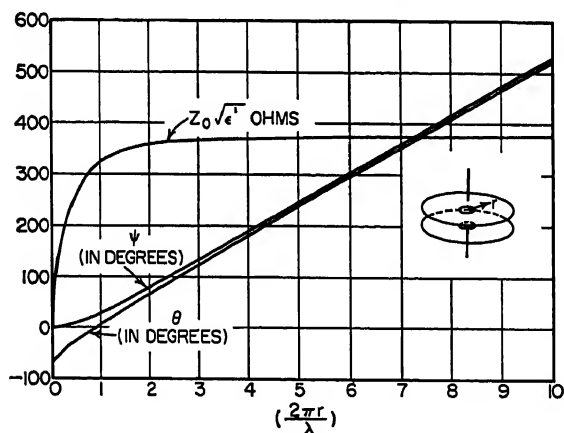
Fig. 30-19. Radial transmission-line quantities.

(1) known termination, (2) output shorted, and (3) output open.   Input impedance is

$$Z_i = Z_{0i} \left[\frac{Z_L \cos (\theta_i - \psi_L) + jZ_{0L} \sin (\theta_i - \theta_L)}{Z_{0L} \cos (\psi_i - \theta_L) + jZ_L \sin (\psi_i - \psi_L)} \right]$$

where Z_i = input impedance, ohms
   Z_{0i} = characteristic impedance, ohms, at input (Z_0 of Fig. 30-19 at $r = r_i$)
   Z_{0L} = characteristic impedance at output (Z_0 of Fig. 30-19 at $r = r_L$)
   Z_L = terminating impedance, ohms
θ_i, θ_L, ψ_i, ψ_L = angles as plotted in Fig. 30-19

In one special case of this, $Z_L = 0$; then

$$Z_i = jZ_{0i} \frac{\sin(\theta_i - \theta_L)}{\cos(\psi_i - \theta_L)}$$

In another $Z_L = \infty$; then

$$Z_i = -jZ_{0i} \frac{\cos(\theta_i - \psi_L)}{\sin(\psi_i - \psi_L)}$$

There are many higher-order modes possible. Those with variations in ϕ only will propagate with any spacing of plates. Those having variations in z propagate only if the plate separation is greater than a half wavelength. More complete descriptions can be found in Refs. 1, 21, and 22.

Two cones with their apices facing and fed by a balanced input at the center as shown in Fig. 30-20 form a biconical waveguide. This structure also simulates a dipole antenna and certain classes of cavity resonators.

One important wave transmitted by this type of guide has no radial components and propagates with the velocity of light along the cones. It is analogous to the TEM wave in cylindrical systems. The ratio of voltage to current or characteristic impedance, is
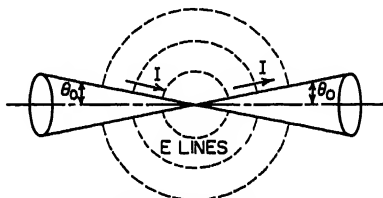
FIG. 30-20. Biconical waveguide.

$$Z_0 = 120 \log_e \cot \frac{\theta}{2} \text{ ohms}$$

where θ is the conical angle. From this it is seen that the characteristic impedance is independent of radius, and not variable as in the radial line.

Many higher modes can propagate on this system. These will all propagate at a velocity different from that of light. For transmission of higher modes, see Refs. 1 and 22.

Surface Wave Transmission Lines. The surface wave transmission line[23] is a single wire having a relatively thick dielectric sheath. The sheath diameter is often three or more times the diameter of the conductor. A mode of propagation which is practically nonradiating is excited on the wire from a coaxial line by means of a conical horn at each end as shown in Fig. 30-21. The mouth of the horn is roughly one-quarter to one wavelength in diameter. Losses are about half those of a two-wire line. The surface wave line has a practical lower-frequency limit of about 50 Mc.

FIG. 30-21. Surface wave transmission line with launchers from coaxial line.

Loss in the two launchers combined varies from less than 0.5 db to a little more than 1 db according to their design. Conductor loss for copper can be calculated by the formula below and Fig. 30-22. Loss for other nonmagnetic materials may be found by multiplying by $(\rho_{conductor}/\rho_{copper})^{\frac{1}{2}}$. Dielectric loss can be determined by the second formula and Figs. 30-23 and 30-24.

$$L_c = 0.455 \frac{\sqrt{f}}{Z_0} d_i$$

$$L_i = \frac{26 f F_p L_p}{\epsilon_r - 1}$$

$$= \frac{L_p f}{100} \quad \text{(for brown polyethylene)}$$

where F_p = power factor of dielectric

L_c = conductor loss, db/100 ft

L_t = dielectric loss, db/100 ft

L_p = dielectric loss in brown polyethylene at 100 Mc (Fig. 30-23)

f = frequency, Mc

ϵ_r = relative dielectric constant

Dielectric Waveguide. Electromagnetic waves will propagate along a dielectric rod[24] if the rod is of sufficient size. At low frequencies, there is little advantage to
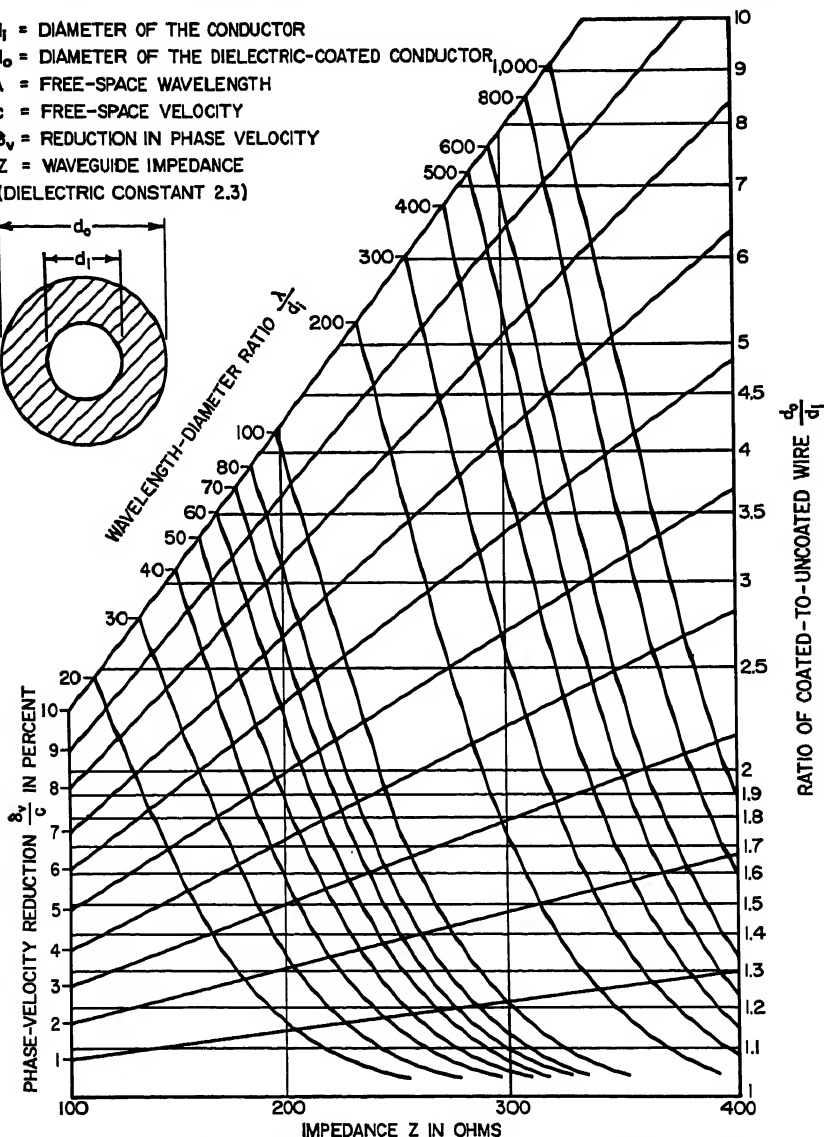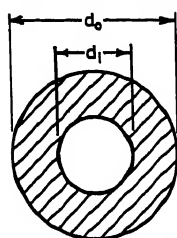
FIG. 30-22. Relationship among wire diameter, dielectric layer, phase-velocity reduction, and impedance for brown polyethylene.

dielectric waveguide since low loss in metal waveguide makes them a convenient shielded carrier of microwave energy. At frequencies above 20 kmc, the lower loss possible with dielectric waveguides makes their use attractive. For lossless dielectric waveguides, the propagation constant can never be real, so there is no cutoff frequency as with metal waveguides. For a given waveguide, very high frequency energy is
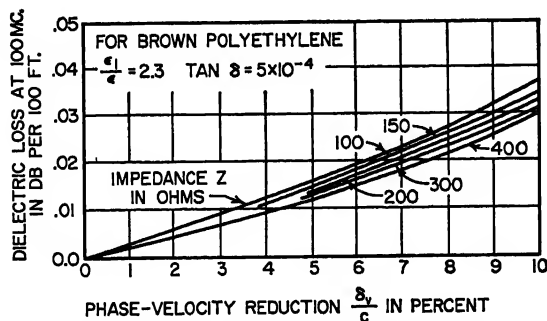
FIG. 30-23. Dielectric loss as a function of phase-velocity reduction.
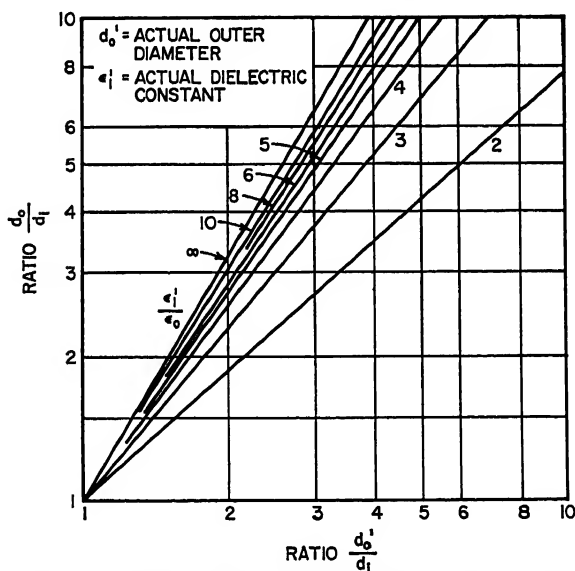
FIG. 30-24. Conversion chart for dielectrics other than polyethylene.

confined entirely within the dielectric. The velocity of propagation and the loss correspond to that in the waveguide dielectric. As the frequency is reduced, more of the field is outside the waveguide and the velocity and loss approach that of the surrounding air, but the dielectric ceases to guide the wave. The only TE and TM modes possible in a circular rod are those having axial symmetry. One hybrid mode, the HE_{11} (hybrid because it has both E_z and H_z components), is particularly well adapted for microwave transmission. It can be small (it is the only mode which can be propagated when the ratio of diameter to wavelength is low; less than 0.6 for polystyrene). It can be launched from the dominant TE metallic waveguide mode,

and it has low loss. The approximate field configuration of this mode is shown in Fig. 30-25.
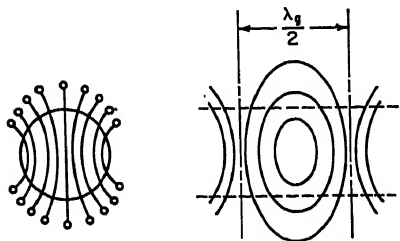
FIG. 30-25. Approximate E-field configuration of HE_{11} mode on a dielectric rod waveguide.

Figures 30-26 to 30-28 show variation of guide wavelength with diameter, loss as a function of diameter, and a waveguide launcher for the HE_{11} hybrid mode. The polarization of the hybrid mode in circular rod is subject to rotation because of internal stresses, dimensional nonuniformity, and bends. A rectangular or oval cross section prevents this depolarization. Measurements of loss and radius of field extent (radius at which field decreases to $1/e$ times that at surface) for cross sections of the oval type are shown in Table 30-5 for 24 and 48 kmc.

Transmission with dielectric tubes as well as rods is possible. Tubes can have lower loss than rods, and theoretical calculations indicate[25] that, with a polystyrene tube with diameter ratios of 0.9, attenuation at 30 kmc compares with TE_{01} guide.
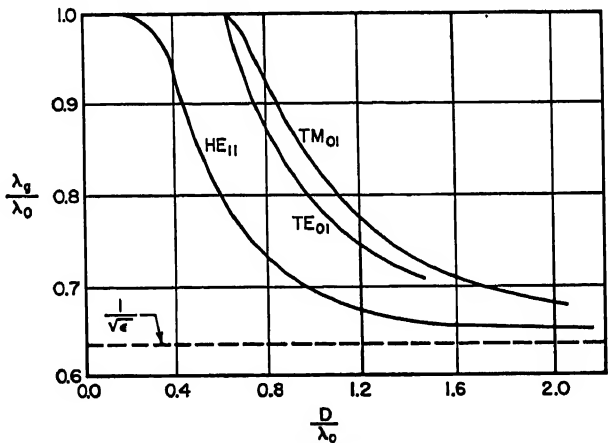
FIG. 30-26. Guide wavelength vs. diameter for polystyrene waveguide.

Table 30-5. Loss for HE_{11} Mode in Dielectric Waveguide

MATERIAL POLYSTYRENE	DIMENSIONS INCHES	E DIRECTION	RADIUS OF FIELD EXTENT (INCHES)	LOSS DB/FT	FREQ. KMC.
SHEET STOCK	.095 × .156		1.5	.05	
EXTRUDED	.086 × .155		4	.05	24
EXTRUDED	.086 × .155		7	.025	
	.056 × .142		.4	1.0	
	.056 × .142		.8	.27	
	.038 × .114		1.5	.045	48
	.032 × .096		3	.007	

FIG. 30-27. Loss vs. diameter for polystyrene waveguide.
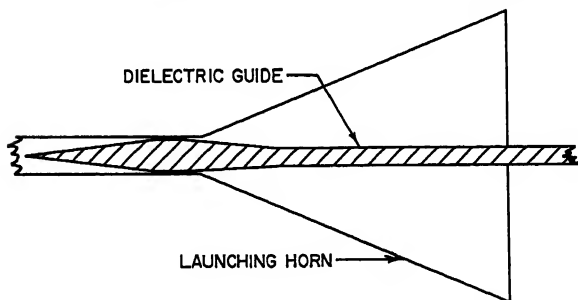
FIG. 30-28. Waveguide launcher for HE_{11} mode.

For a loss of 6 db/mile at 30 kmc, the dielectric tube is 1 cm radius with an 8-cm radius of field extent while the TE_{01} guide would have a radius of 4.5 cm.

Large-radius bends must be used to minimize power loss due to radiation. If sharp bends are necessary, loss can be minimized by using a plane metallic reflector outside the convex band to make equal angles with each leg of the bend.

For good operation, low-loss supports for the guide and a good shield to protect it from cross talk, rain, snow, and absorbing moist atmospheres are required. Nylon thread has been used satisfactorily for support. A lossy tube outside the field is believed to be the best shield.

The image line[26,27] is a variation of the dielectric guide which simplifies the support problem. The HE_{11} mode, being symmetrical, can be split longitudinally and one-

half replaced by a metal plate as shown in Fig. 30-29. Losses at bends are lower for concave bends than for convex. Losses in the image plane are lower than those in the dielectric for all commonly used materials.

FIG. 30-29. Image line using HE_{11} mode.

30.9. CONNECTORS

Coaxial Connectors. The standard connectors used in joining lengths of coaxial cables and connecting such cables to other devices are listed in Table 30-6.

Chokes and Flanges. A list of chokes and flanges used in joining standard waveguides is given in Table 30-4. A choke flange is usually mated with a cover flange to provide a waveguide junction which is weathertight, low-loss, and more tolerant of misalignment than a junction of two cover flanges. The object of the choke junction is to present a low impedance at the inner-wall break in the waveguide.

30.10. DISCONTINUITIES

Coaxial-line Discontinuities. The most frequently occurring coaxial-line discontinuity is an abrupt change in the diameter of either the inner or outer conductor. A change in either or both diameters causes a capacitive discontinuity, and unless
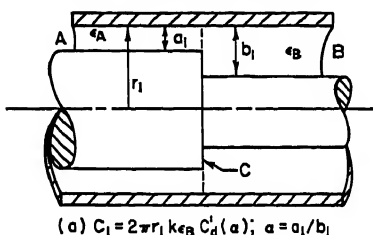
(a) $C_1 = 2\pi r_1 k \epsilon_B C_d'(\alpha)$; $\alpha = a_1/b_1$
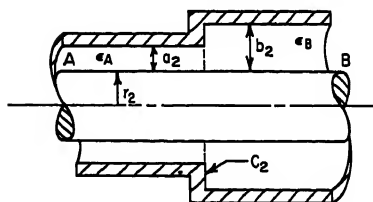
(b) $C_2 = 2\pi r_2 k \epsilon_B C_d'(\alpha)$; $\alpha = a_2/b_2$
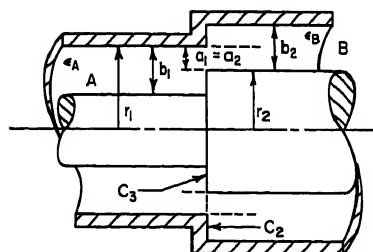
(c) $C_3 = 2\pi r_1 k \epsilon_A C_d'(\alpha)$; $\alpha = a_1/b_1$
TOTAL CAPACITY IS $C_c = C_2 + C_3$
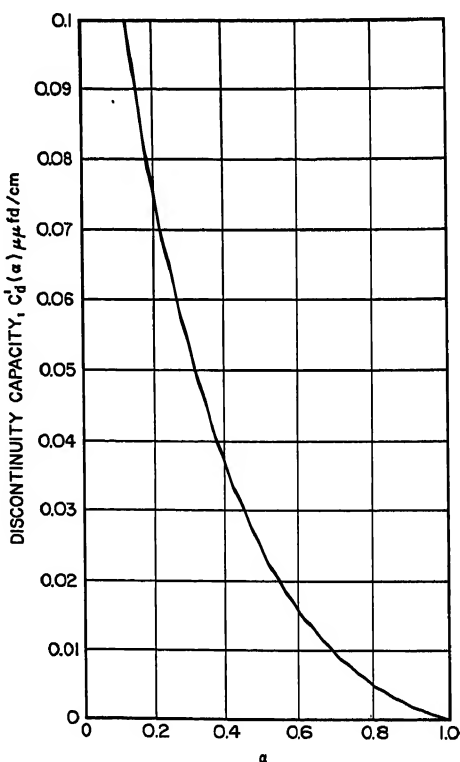
FIG. 30-30. Capacitive discontinuity in coaxial line.

Table 30-6. Frequently Used Cable Connectors

Type	Description	z, ohms	For use with cables
	BNC Type		
UG-88C/U	Plug		
UG-89B/U	Jack	50	R6-55, 58,
UG-909/U	Panel jack, $\frac{1}{2}''$-diam. mounting		141, 142/U
UG-913/U	Plug, right-angle		
UG-306A/U	Right-angle adapter (F-M)		
UG-491/U	Straight adapter (M-M)		
UG-914/U	Straight adapter (F-F)		
UG-274A/U	T adapter (F-M-F)		
UG-1094/U	Receptacle $\frac{3}{8}''$-diam. hole mount		
UG-1098/U	Right-angle receptacle $\frac{3}{8}''$-diam. hole mount		

Notes:
1. General-purpose weatherproof coaxial connectors for small size r-f cables.
2. Bayonet-lock coupling (quick disconnect).
3. Rated at 500 volts peak.
4. VSWR less than 1.35 to 10 kmc.
5. Operate to 250°C.

	Type C		
UG-626A/U	Plug		RG-5, 6, 21,
UG-630/U	Panel jack $\frac{3}{4}''$-diam. hole mount	50	143/U
UG-633/U	Jack		
UG-570/U	Panel jack $\frac{3}{4}''$-diam. hole mount		RG-8, 9, 11,
UG-572/U	Jack	50	13, 41, 63,
UG-573A/U	Plug		144/U
UG-710A/U	Right-angle plug		
UG-942A/U	Plug		RG,10, 12
UG-943A/U	Plug	50	79/U
UG-944/U	Jack		
UG-945A/U	Right-angle plug		
UG-709A/U	Plug	50	RG-55, 58
UG-704/U	Panel jack $\frac{5}{8}''$-diam. hole mount		141, 142/U
UG-707A/U	Plug	50	RG-14/U
UG-708A/U	Plug	50	RG-17, 35/U
UG-567A/U	Right-angle adapter (M-F)		
UG-642A/U	Straight adapter (M-M)		
UG-643/U	Straight adapter (F-F)		
UG-566A/U	T-adapter (F-M-F)		
UG-569/U	Receptacle $\frac{3}{4}''$-diam. hole mount		
UG-701/U	Pressurized bulkhead adapter $\frac{3}{4}''$-diam. hole mount		

Notes:
1. General-purpose weatherproof coaxial connectors.
2. Bayonet-lock coupling (quick disconnect).
3. Rated at 1,000 volts peak.
4. VSWR less than 1.35 to 10 kmc.

Underlined cables are not electrically matched with connectors listed. Cables include improved versions.

Table 30-6. Frequently Used Cable Connectors (*Continued*)

Type	Description	z, ohms	For use with cables
	Type N		
UG-18C/U UG-20C/U UG-159B/U	Plug Jack Bulkhead jack ⅝″-diam. hole mount	50	RG-5, 6 21, 143/U
UG-21D/U UG-23D/U UG-160C/U UG-594/U	Plug Jack Bulkhead jack ⅝″-in. hole mount Right-angle plug	50	RG-8, 9, 11, 13, 41, 63, 114, 144/U
UG-536A/U UG-556/U UG-1095/U	Plug Bulkhead jack ⅝″-diam. hole mount Panel jack	50	RG-55, 58/U
UG-27C/U UG-29B/U UG-57B/U UG-680/U UG-997A/U UG-107B/U	Right-angle adapter (M-F) Straight adapter (F-F) Straight adapter (M-M) Pressurized receptacle Right-angle receptacle T adapter (F-M-F)		

Notes:
1. General-purpose weatherproof coaxial connectors for medium-size r-f cables.
2. Screw-lock coupling.
3. Rated at 1,000 volts peak.
4. VSWR less than 1.35 to 10 kmc.

Type	Description	z, ohms	For use with cables
	Type HN		
UG-333B/U UG-334B/U UG-495B/U	Jack Panel jack Plug	50	RG-17/U
UG-494A/U	Plug	50	RG-14/U
UG-926A/U	Plug	50	RG-118/U
UG-1021/U	Plug	50	RG-74/U
UG-1041/U UG-1102/U UG-1103/U	Plug Jack Panel jack	50	RG-18/U
UG-212C/U UG-413/U UG-1019/U UG-496/U MX-564A/U TL-612/U	Right-angle adapter (M-F) T adapter (F-F-F) Straight adapter (F-F) Receptacle Armor clamp Cable dresser		

Notes:
1. Special high-voltage connectors.
2. 4,000 volts peak at 50,000 ft.
3. Good performance to 3 kmc.
4. Requires special cable-tapering tool MX-10317.

Type	Description	z, ohms	For use with cables
	Straight adapters between series		
UG-201A/U UG-349A/U UG-564/U UG-565A/U UG-635/U UG-636A/U UG-702/U UG-703A/U	Type N(F) to BNC(M) Type N(M) to BNC(F) Type C(M) to N(F) Type C(F) to N(M) Type C(M) to BNC(F) Type C(F) to BNC(F) Type C(M) to HN(M) Type C(F) to HN(M)	50	

All adapters are weatherproof.

PLAN VIEW OF STRIP	EQUIVALENT CIRCUIT	CIRCUIT PARAMETERS*
	B_b, B_a, B_a	$\dfrac{B_a}{Y_0} = -\dfrac{2D}{\lambda}\ln\cosh\dfrac{\pi d}{2D}$ $\dfrac{B_b}{Y_0} = \dfrac{D}{\lambda}\ln\coth\dfrac{\pi d}{2D}$
	B_B, B_A, B_A	$\dfrac{B_A}{Y_0} = \dfrac{1 + \dfrac{B_a}{Y_0}\cot\dfrac{\pi d}{\lambda}}{\cot\dfrac{\pi d}{\lambda} - \dfrac{B_a}{Y_0}}$ $\dfrac{B_B}{Y_0} = \dfrac{1}{2}\left[\dfrac{1 + \left(2\dfrac{B_b}{Y_0} + \dfrac{B_a}{Y_0}\right)\cot\dfrac{\pi d}{\lambda}}{\cot\dfrac{\pi d}{\lambda} - \left(2\dfrac{B_b}{Y_0} + \dfrac{B_a}{Y_0}\right)} - \dfrac{B_A}{Y_0}\right]$
	B_b, B_a, B_a	$\dfrac{B_a}{Y_0} = \dfrac{1}{4\dfrac{B_b}{Y_0}}$ $\dfrac{B_b}{Y_0} = -\dfrac{3}{4\pi}\dfrac{\lambda D W}{d^3}$
	B_B, B_A, B_A	$\dfrac{B_A}{Y_0} = \dfrac{1 + \dfrac{B_a}{Y_0}\cot\dfrac{\pi d}{\lambda}}{\cot\dfrac{\pi d}{\lambda} - \dfrac{B_a}{Y_0}}$ $\dfrac{B_B}{Y_0} = \dfrac{1}{2}\left[\dfrac{1 + 2\dfrac{B_b}{Y_0}\cot\dfrac{\pi d}{\lambda}}{\cot\dfrac{\pi d}{\lambda} - 2\dfrac{B_b}{Y_0}} - \dfrac{B_A}{Y_0}\right]$
	X	$\dfrac{X}{Z_0} = \dfrac{2W}{\lambda}\ln\csc\dfrac{\pi W'}{2W}$
	X_a, X_a, X_b	$\dfrac{X_a}{Z_0} = \dfrac{2W}{\lambda}\left\{\Psi\left[-\dfrac{1}{2}\left(1-\dfrac{\theta}{\pi}\right)\right] - \Psi\left[-\dfrac{1}{2}\right]\right\}$ $\dfrac{X_b}{Z_0} = -\dfrac{\lambda}{4\pi W}\cot\dfrac{\theta}{2}$

*D IS THE GROUND–PLANE SPACING. $\Psi(X)$ IS THE LOGARITHMIC DERIVATIVE OF $X!$

$W = D\dfrac{K(k)}{K(k')}$, $k = \tanh\left(\dfrac{\pi w}{2W}\right)$, $k' = \sqrt{1-k^2}$, $K(k)$ IS COMPLETE ELLIPTIC INTEGRAL OF FIRST KIND.

$W \approx w + \dfrac{2D}{\pi}\ln 2$ FOR $\dfrac{w}{D} > 0.5$

Fig. 30-31. Discontinuities in symmetrical strip line.

the ratio of diameters remains constant, a change in Z_0. If neither the line before nor the line after the discontinuity will propagate the higher modes and if the discontinuities are separated from each other by at least the space between inner and outer conductors in the line between discontinuities, the capacitance at each step can be obtained by using the relations and curves in Fig. 30-30. If the ratio of outer to inner diameter of neither the line before nor the line after the discontinuity is greater than 5, the results are accurate to better than 20 per cent for all values of a plotted. In all cases, only the dielectric of the line having the largest ratio of outer to inner diameter is considered since the field distortion in the other is little affected. Greater accuracy can be obtained by use of Refs. 28 and 29.

POLYSTYRENE
$D_1 = .034$
$D_2 = .335$

TEFLON
$D_1 = .028$
$D_2 = .335$

.406
D_1
D_2 .397
.120

FIG. 30-32. Grooved bead for connector.

If the spacing between two discontinuities is less than the spacing between inner and outer diameters in the intervening line, then the capacitance of the combination will be less than the sum of the two, as calculated by this method. The curves of Ref. 28 may be used to obtain greater accuracy in this case.

Discontinuities in Strip Transmission Line. A variety of discontinuities in symmetrical strip transmission line have been analyzed, and a method given for obtaining

TYPE N
CONNECTOR

.4" x .9" X-BAND
WAVEGUIDE

.291 D
.075 D
.605
.200
.185

PROBE TRANSITION

CROSSBAR TRANSITION

2.840 x 1.34
WAVEGUIDE

.178
.834
1.000
6.750
.750
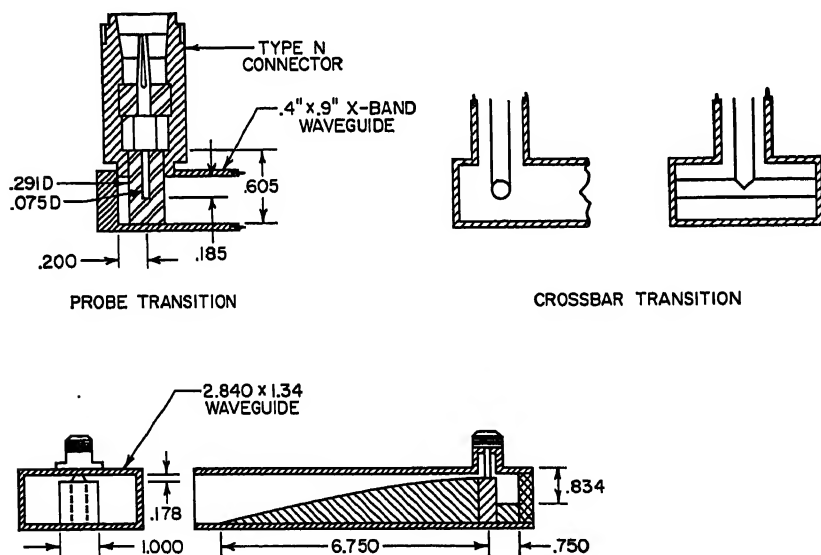
RIDGED GUIDE TRANSITION

FIG. 30-33. Waveguide to coaxial-line transitions.

the equivalent circuit from that of analogous discontinuities in rectangular waveguide.[30] These include (1) transverse slot in ground plane, (2) gap in center conductor, (3) round hole in center conductor, (4) change in width of center conductor, (5) H-plane bend in center conductor, and (6) H-plane T junction and are shown in Fig. 30-31. An abrupt change in the thickness of the center conductor or ground-plane spacing causes a shunt-capacitive discontinuity which can be evaluated by the method used for coaxial lines.

Compensation and Connector Design. In air-dielectric line, some support of the center conductor is required. A similar problem exists in coaxial-line connectors. Beads are generally used to provide this support. Line diameters in the bead section are usually changed to provide nearly the same impedance in the bead section as in the line to avoid an impedance discontinuity. There still remains a capacitive discontinuity at each end of the bead. This may be minimized by use of the lowest
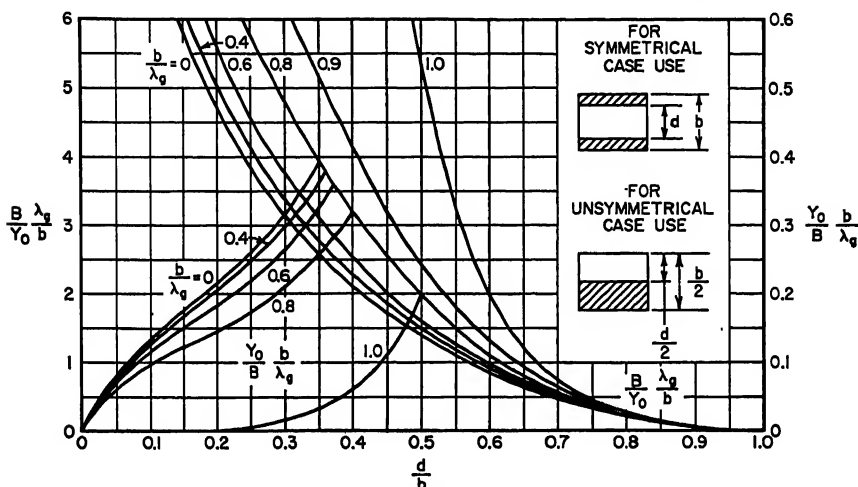
FIG. 30-34. Susceptance of a capacitive iris in rectangular waveguide.
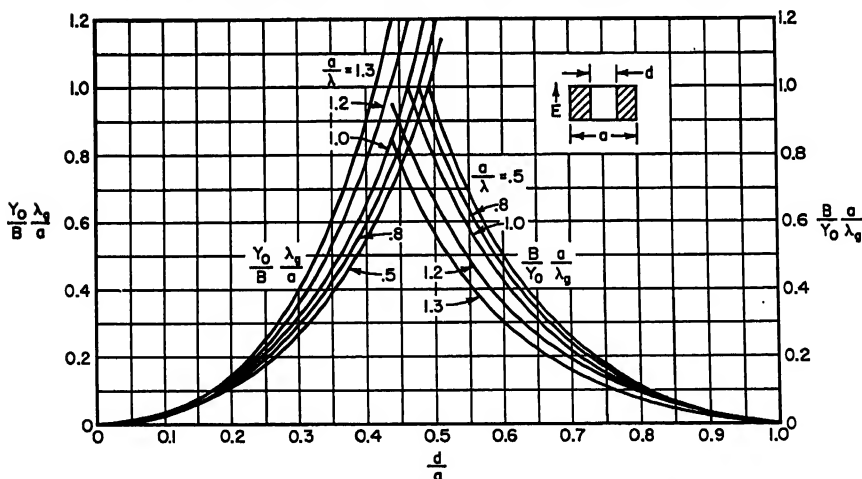
FIG. 30-35. Susceptance of a symmetrical inductive iris in rectangular waveguide.

possible dielectric-constant bead. The discontinuity can be further compensated by one of the methods described in Sec. 30.3. A combination of methods is often used for further compensation. In connectors, the grooved bead is an example of this method. The bead has an enlarged hole at each end to provide the required high-impedance section. Figure 30-32 shows dimensions for a bead for a ⅜-in. line which has VSWR of 1.08 or less up to 10 kmc. More detailed design information will be found in Ref. 31.

Dominant-mode Transitions in Unbalanced Line.   In order to excite the dominant mode in waveguide, it is necessary to set up an electric field which is parallel to the desired one in the waveguide.   This is most frequently done with a waveguide-to-coaxial or strip-line transition.   Transitions into rectangular guide are usually probe type, cross-bar type, or ridged-waveguide type.   These are shown in Fig. 30-33.   The ridged-waveguide type can be built to give the lowest SWR over a given bandwidth,
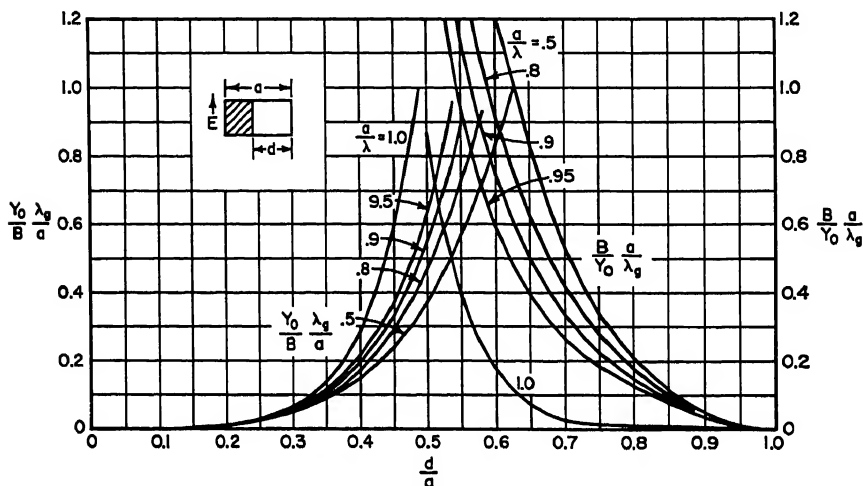
FIG. 30-36. Susceptance of an asymmetrical inductive iris in rectangular waveguide.
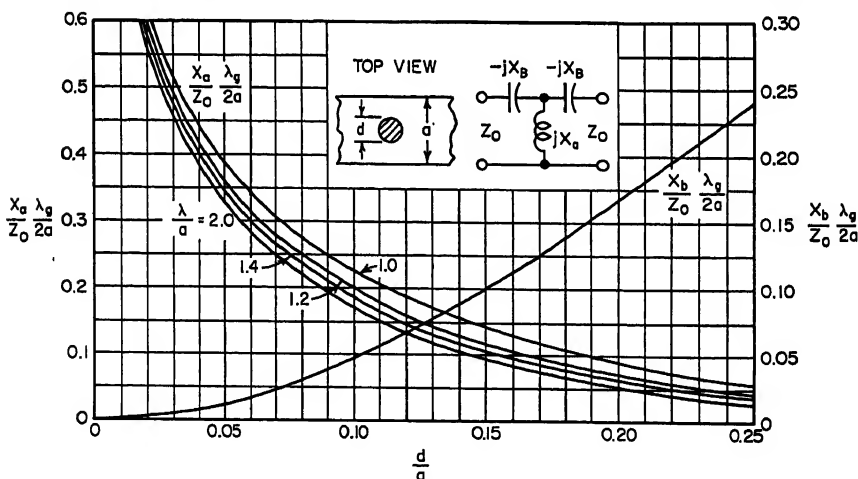
FIG. 30-37. Circuit parameters of centered inductive post in rectangular waveguide.

but the probe type, which is extremely simple, is usually adequate.   Transitions of the probe type[3,32] are available which provide an SWR of less than 1.25 over a 1.5:1 bandwidth.

Data on Waveguide Irises and Posts.   Certain discontinuities in waveguides provide reactance which approximates a lumped capacitance, a lumped inductance, or a combination of the two.

In general, discontinuities which constrict the guide in the direction of the electric field act as capacitance (*E*-plane iris, tuning screws, etc.). Discontinuities which constrict the guide in the direction of the magnetic field act as an inductance (*H*-plane iris, posts, etc.). Thin metal irises are widely used as matching elements since the reactance they provide is readily calculable.

The normalized susceptance of an infinitely thin capacitive iris is plotted in Fig. 30-34. Thick irises have higher susceptances than those shown. The capacitive iris reduces the power breakdown below that of normal guide.

The normalized susceptance of an infinitely thin inductive iris is plotted in Fig. 30-35 and 30-36. Finite thickness increases the susceptance. If *d* is 0.8*a* or greater, the breakdown is little affected by the inductive iris.

A post across the narrow dimension of the guide also acts as an inductance and is mechanically simple to construct. The normalized susceptance of this structure is shown in Fig. 30-37.

LIST OF SYMBOLS

f = frequency in cycles per second

ω = $2\pi f$

c = velocity of light $\approx 3 \times 10^8$ meters/second

λ = wavelength

ϵ = relative dielectric constant

μ = relative permeability

σ = conductivity, mhos per meter

α = attenuation constant, nepers per meter (note: 1 neper = 8.686 decibels)

E_a = breakdown of air expressed in volts per meter (see p. 30-2)

P = power, watts

tan δ = loss tangent or dissipation factor

The properties of some commonly used metals will be found in Table 35-1 (Chap. 35). The conductivity, σ, can be found from the resistivity values by the relationship

$$\sigma \text{ (mhos per meter)} = \frac{10^8}{\text{resistivity (microohm-cm)}}$$

Values for ϵ and tan δ of some commonly used dielectrics will be found in Table 35-2.

REFERENCES

1. C. G. Montgomery, R. H. Dicke, and E. M. Purcell (eds.): "Principles of Microwave Circuits," McGraw-Hill Book Company, Inc., New York, 1948. A good general reference work for theoretical background.
2. W. Sichak: "Coaxial Line with Helical Conductor," *Proc. IRE*, vol. 42, pp. 1315–1319, August, 1954. Also correction: *Proc. IRE*, vol. 43, p. 148, February, 1955.
3. G. L. Ragan (ed.): "Microwave Transmission Circuits," McGraw-Hill Book Company Inc., New York, 1948. A good general reference for applications.
4. D. W. Peterson: "Notes on a Coaxial Line Bead," *Proc. IRE*, vol. 37, p. 1294, November, 1949.
5. J. W. E. Griemsmann: "An Approximate Analysis of Coaxial Line with Helical Dielectric Support," *IRE Trans. on Microwave Theory Tech.*, vol. MTT-4, pp. 13–23, January, 1956.
6. S. Greenblatt, J. W. E. Griemsmann, and L. Birenbaum: "Measurement of Energy Leakage from Cables at VHF and Microwave Frequencies," *AIEE Conf. Paper*, Winter General Meeting, 1956.
7. R. M. Chisholm: "The Characteristic Impedance of Trough and Slab Lines," *IRE Trans. on Microwave Theory Tech.*, vol. MTT-4, pp. 166–172, July, 1956.
8. S. B. Cohn: "Shielded Coupled-strip Transmission Line," *IRE Trans. on Microwave Theory Tech.*, vol. MTT-3, pp. 29–38, October, 1955.

9. D. D. Greig and H. F. Engelmann: "Microstrip: A New Transmission Technique for the Kilomegacycle Range," *Proc IRE*, vol. 40, pp. 1644–1650, December, 1952.
10. R. M. Barrett: "Etched Sheets Serve as Microwave Components," *Electronics*, vol. 25, pp. 114–118, June, 1952.
11. E. G. Fubini, W. E. Fromm, and H. S. Keen: "New Technique for High-Q Strip Microwave Components," *IRE Convention Record*, pp. 91–97, Mar. 22, 1954.
12. K. G. Black and T. J. Higgins: "Rigorous Determination of Microstrip Transmission Lines," *IRE Trans. on Microwave Theory Tech.*, vol. MTT-3, pp. 93–113, March, 1955.
13. M. Arditi: "Characteristics and Applications of Microstrip for Microwave Wiring," *IRE Trans. on Microwave Theory Tech.*, vol. MTT-3, pp. 31–56, March, 1955.
14. R. H. T. Bates: "The Characteristic Impedance of the Shielded Strip Lines," *IRE Trans. on Microwave Theory Tech.*, vol. MTT-4, pp. 28–33, January, 1956.
15. K. S. Packard: "Optimum Impedance and Dimensions for Strip Transmission Line," *IRE Trans. on Microwave Theory Tech.*, vol. MTT-5, pp. 244–247, October, 1957.
16. H. A. Wheeler: "The Piston Attenuator in a Waveguide below Cutoff," Wheeler Monograph 8, Wheeler Laboratories, Inc., Great Neck, N.Y., 1949.
17. Radio Research Laboratory Staff: "Very High Frequency Techniques," McGraw-Hill Book Company, Inc., New York, 1947.
18. Samuel Hopfer: "The Design of Ridged Waveguides," *IRE Trans. on Microwave Theory Tech.*, vol. MTT-3, pp. 20–29, October, 1955.
19. Tsung-Shan Chen: "Calculation of the Parameters of Ridge Waveguides," *IRE Trans. on Microwave Theory Tech.*, vol. MTT-5, pp. 12–17, January, 1957.
20. K. S. Packard: "The Cutoff Wavelength of Trough Waveguide," *Trans. IRE on Microwave Theory Tech.*, vol. MTT-6, no. 4, pp. 455–456, October, 1958.
21. N. Marcuvitz (ed.): Waveguide Handbook, McGraw-Hill Book Company, Inc., New York, 1951.
22. S. Ramo and J. R. Whinnery: "Fields and Waves in Modern Radio," John Wiley & Sons, Inc., New York, 1953.
23. George Goubau: "Designing Surface-wave Transmission Lines," *Electronics*, vol. 27, pp. 180–184, April, 1954.
24. M. T. Weiss and E. M. Gyorgy: "Low Loss Dielectric Waveguides," *IRE Trans. on Microwave Theory Tech.* vol. MTT-2, pp. 38–44, September, 1954.
25. *Arch. der Elektrischen Übertragang*, vol. 8, no. 6, June, 1954.
26. D. D. King: "Circuit Components in Dielectric Image Lines," *IRE Trans. on Microwave Theory Tech.*, vol. MTT-3, pp. 35–39, December, 1955.
27. D. D. King: "Properties of Dielectric Image Lines," *IRE Trans. on Microwave Theory Tech.*, vol. MTT-3, pp. 75–81, March, 1955.
28. J. R. Whinnery and H. W. Jamieson: "Equivalent Circuits for Discontinuities in Transmission Lines," *Proc. IRE*, vol. 32, pp. 98–114, February, 1944.
29. J. R. Whinnery, H. W. Jamieson, and T. E. Robbins: "Coaxial Line Discontinuities," *Proc. IRE*, vol. 32, pp. 695–709, November, 1944.
30. A. A. Oliner: "Equivalent Circuits for Discontinuities in Balanced Strip Transmission Lines," *IRE Trans. on Microwave Theory Tech.*, vol. MTT-3, pp. 134–143, March, 1955.
31. J. W. E. Griemsmann: "Handbook of Design Data on Cable Connectors for Microwave Use," Report No. R-520-56, PIB-450, Polytechnic Institute of Brooklyn, Microwave Research Institute, New York, May, 1956.
32. W. W. Mumford: "The Optimum Piston Position for Wide-band Coaxial-to-waveguide Transducers," *Proc. IRE*, vol. 41, pp. 256–261, February, 1953.
33. S. A. Schelkunoff: "Electromagnetic Waves," p. 319, D. Van Nostrand Company, Inc., Princeton, N.J., 1943.

Chapter 31

IMPEDANCE MATCHING AND BROADBANDING

David F. Bowman

I-T-E Circuit Breaker Company
Philadelphia, Pennsylvania

31.1. GENERAL

Impedance matching is the control of impedance for the purpose of obtaining maximum power transfer or minimum reflection. This chapter describes circuits and

techniques used for impedance matching with special emphasis on those most suitable for broadband operation.

Impedance Matching for Maximum Power Transfer. A variable load impedance connected to a source will receive the maximum possible power from the source when it is adjusted to equal the complex conjugate of the impedance of the source (Fig. 31-1a). The load impedance and source impedance are then matched on a conjugate impedance basis.†

$$Z_G = R + jX$$
$$Z_G^* = R - jX$$
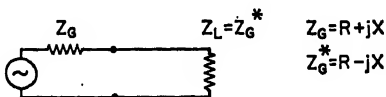
A. A SOURCE AND A LOAD MATCHED ON A CONJUGATE-IMPEDANCE BASIS
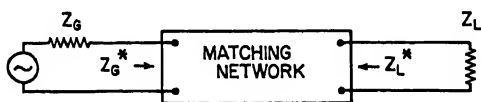
B. A SOURCE AND A LOAD MATCHED ON A CONJUGATE-IMPEDANCE BASIS BY A MATCHING NETWORK
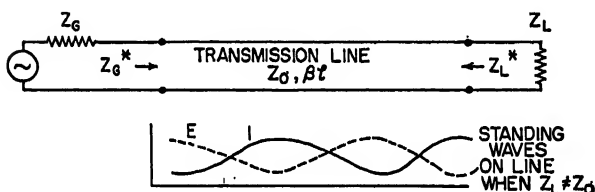
C. A SOURCE, LOSSLESS LINE AND A LOAD MATCHED ON A CONJUGATE-IMPEDANCE BASIS
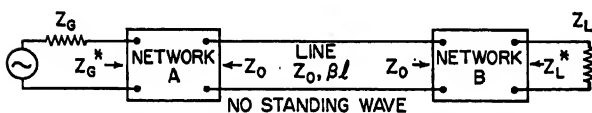
D. A SOURCE, A LINE AND A LOAD MATCHED ON A CONJUGATE IMPEDANCE AND CHARACTERISTIC IMPEDANCE BASIS BY NETWORKS

FIG. 31-1. Impedance matching of transmission circuits.

It is not necessary to vary either the load impedance or the source impedance. A fixed source impedance and a fixed load impedance may be coupled for maximum power transfer by a properly proportioned network (Fig. 31-1b) interposed between them. This "matching" network transforms the source impedance to the conjugate of the load impedance, and vice versa. Thus a conjugate-impedance match occurs at the input to the network and at the output of the network. It is true of any lossless transmission circuit that if a conjugate-impedance match is obtained at any

† This is distinct from impedance matching on an image-impedance basis in which the source and load impedances are equal. Image-impedance matching is sometimes used for convenience, often when the impedances are nearly resistive. However, it does not result in the maximum-power transfer condition unless the impedances are purely resistive. See Ref. 8.

point along the transmission path, then a conjugate-impedance match is obtained at all other points along the path.

Impedance Matching for Minimum Reflection. A length of lossless transmission line may form one link in a lossless transmission circuit. Maximum power transfer will occur when the circuit is adjusted for a conjugate-impedance match (Fig. 31-1c). However, in general, the line will be subject to two waves, a direct and a reflected wave, propagating in opposite directions. The interference between these waves creates standing-wave patterns of voltage and current. These effects may be tolerable, but usually they are undesirable.

If the line has finite attenuation, maximum power transfer from the source to the load is obtained only when the following conditions are met:

1. The generator is loaded by the conjugate of its internal impedance.
2. The line is terminated in its characteristic impedance.

The first condition provides maximum power delivery from the source. The second condition provides minimum power dissipation in the line by eliminating the reflected wave on the line.

Figure 31-1d shows a "matched" system, that is, a system matched both on a conjugate-impedance basis and on a characteristic-impedance basis. This represents an ideal condition.

The importance of matching can be seen by an examination of the detrimental effects of a mismatch. A measure of mismatch at the load junction is the voltage reflection coefficient.

$$\rho = \frac{Z_L - Z_0}{Z_L + Z_0}$$

This defines vectorially the reflected voltage wave for a unit wave incident on the junction. The power in the load is thus reduced from the maximum available power by the ratio of $1 - |\rho|^2$.

FIG. 31-2. Reflection loss.

The transmission coefficient $\tau = \sqrt{1 - |\rho|^2}$ defines the transmitted wave for a unit incident wave. The reduction in transmission is called a reflection loss or transition loss. Reflection loss expressed in decibels is shown as a function of SWR in Fig. 31-2. The reflected wave combines with the incident wave on the line to form a standing wave having a standing-wave ratio (maximum to minimum) of

$$S = \frac{1 + |\rho|}{1 - |\rho|}$$

The presence of the standing wave increases the maximum voltage and current limits on the line for the same delivered power by the ratio $\sqrt{S}$. The efficiency η of the line may be expressed by

$$\eta = \frac{S_2 - 1/S_2}{S_1 - 1/S_1}$$

$$= \frac{4S_1}{10^{0.14}(S_1 + 1)^2 - 10^{-0.14}(S_1 - 1)^2}$$

where subscripts 1 and 2 refer to output and input of line, respectively, and A is the normal line attenuation in decibels.
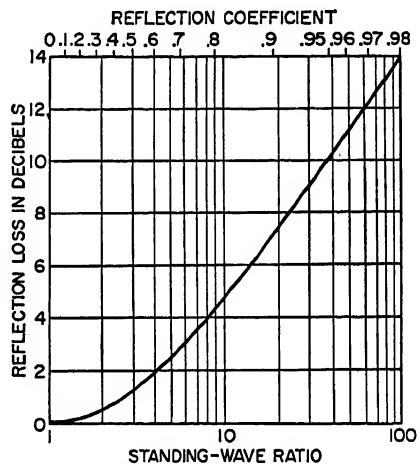
In addition to the relationships discussed above for steady-state conditions, impaired operation of a modulated system is frequently encountered because of a delayed reflection or echo caused by a mismatch.

Reflection-coefficient Charts. The reflection coefficient is a vector quantity related directly to impedance ratio and mismatch. Its magnitude does not exceed unity, so a plot of all possible reflection ratios for passive impedances may be charted within a circle of unit radius. Furthermore, the representations of a mismatch referred to different distances along the length of a line lie at a constant radius from
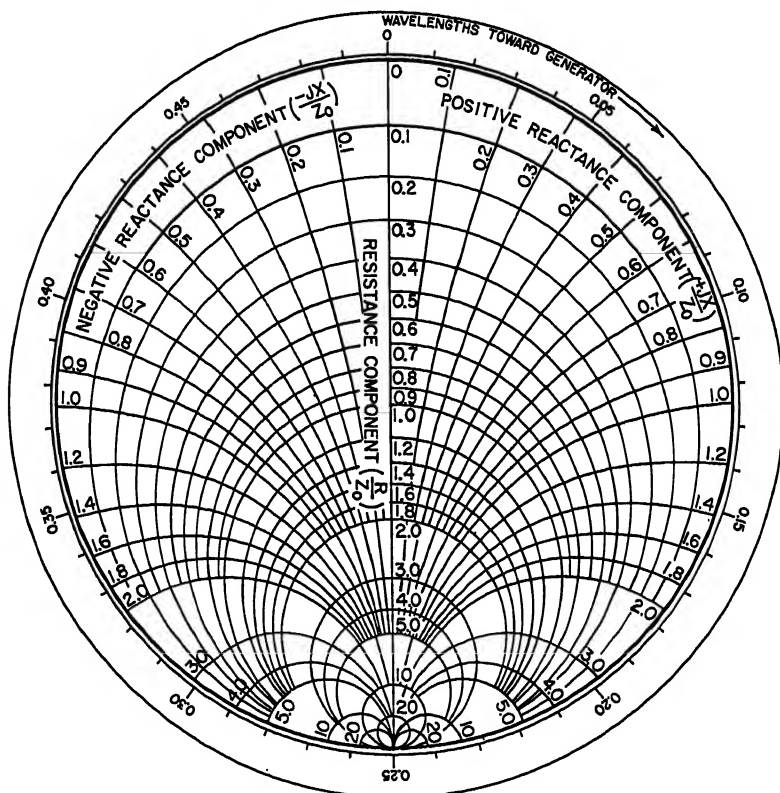
Fig. 31-3. The Smith chart.

the center of the chart at angles proportional to the distances. Coordinates of impedance ratio or admittance ratio may be superimposed on the chart in either real and imaginary components (Smith chart, Fig. 31-3) or magnitude and phase angle (Carter chart, Fig. 34-14). The convenience of the resulting charts for dealing with matching problems, especially those involving transmission lines, has led to their use almost to the exclusion of other forms. Certain related specialized charts are treated in Refs. 19 to 21.

31.2. IMPEDANCE MATCHING WITH LUMPED ELEMENTS

Throughout the lower range of radio frequencies, it is convenient to use lumped reactance elements such as coils and capacitors in impedance-matching networks. In higher frequency ranges, pure inductance or capacitance may not always be

obtained from practical coils and capacitors. However, it is convenient to analyze circuits in terms of their lumped reactance (and resistance) elements.

Any two complex impedances may be matched by a simple L section of two reactance elements. If, in addition to matching, it is necessary to maintain given phase relationships between the source and load voltages and currents, a third element must be used to form a T or π section. A lattice section using four elements is more convenient for some applications. The primary use of the simple sections is for matching at a single frequency, although it is possible to obtain matching at two or more separate frequencies by replacing each reactance element of the basic network with a

$$X_P = \pm R_2 \sqrt{\frac{R_1}{R_2 - R_1}} = -\frac{1}{B_P}$$

$$X_s = \mp \sqrt{R_1 R_2 - R_1^2}$$

NOTE: X_P AND X_S MUST BE OF OPPOSITE SIGN

$$\theta = \cos^{-1}\left(\frac{R_1}{R_2}\right)^{1/2}$$

A. L SECTION FOR MATCHING BETWEEN RESISTANCES

$Z_1 = R_1 + jX_1$

$Z_2 = \frac{1}{Y_2} = \frac{1}{G_2 + jB}$

$X_s' = X_s - X_1$

$B_P' = B_P - B_2$
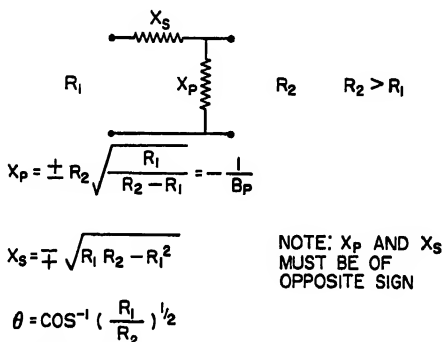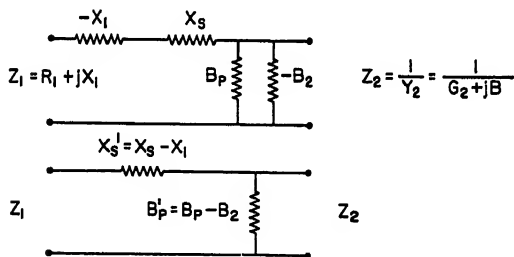
B. L SECTION FOR MATCHING BETWEEN COMPLEX IMPEDANCES

FIG. 31-4. Impedance matching with reactive L sections.

more complex combination giving the required reactance at each specified frequency. Harmonic reduction can be effected in a similar manner by introducing high series reactances or low shunt reactances at the harmonic frequencies.

L Section. The expressions for the required reactance values for an L section providing a match between pure resistances is shown in Fig. 31-4a. (Here and in the remainder of this chapter, X and B will designate reactance and susceptance values respectively.) If X_s is positive, the network will delay the phase of the wave by angle θ. If X_s is negative, it will advance the phase by the same angle.

If two complex terminations are to be matched, the series reactance X_s' is made to include a compensation for the series reactance of the right-hand termination and the shunt susceptance B_p' is made to include the susceptance of the left-hand termination as shown in Fig. 31-4b. For this case θ represents the phase between the current in the left- to the voltage on the right-hand termination.

T and π Sections. Design expressions are given in Fig. 31-5 for T and π sections matching between resistive terminations. If the terminations contain reactive or susceptive components, it is necessary to include an appropriate compensating component in the end elements as in the case of the L section.

L, T, and π sections may be used in unbalanced circuits as shown or in balanced circuits by moving one-half of each series element to the opposite conductor of the line. The lattice section is inherently balanced. It is also useful to convert from a

$$X_3 = \frac{(R_1 R_2)^{1/2}}{\sin \theta}$$

$$X_1 = -\frac{R_1}{\tan \theta} - X_3$$

$$X_2 = -\frac{R_2}{\tan \theta} - X_3$$

A. T SECTION FOR MATCHING BETWEEN RESISTANCES

$$G_1 = \frac{1}{R_1} \qquad G_2 = \frac{1}{R_2}$$

$$B_3 = -\frac{(G_1 G_2)^{1/2}}{\sin \theta}$$

$$B_1 = -\frac{G_1}{\tan \theta} - B_3$$

$$B_2 = -\frac{G_2}{\tan \theta} - B_3$$
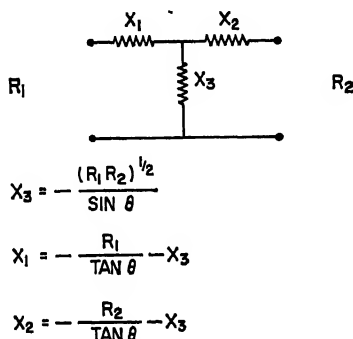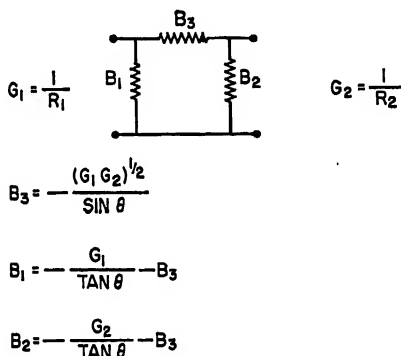
B. π SECTION FOR MATCHING BETWEEN RESISTANCES

FIG. 31-5. Impedance matching with reactive T and π sections.

balanced termination to an unbalanced termination, as discussed in Sec. 31.6 on Baluns.

Lattice Section. The elements of a lattice section as well as T and π sections are given in Fig. 31-6 in terms of an equivalent transmission line having the same characteristic impedance and phase shift. The required equivalent line may be determined as described in latter parts of this section.

Inductive Coupling. A pair of inductively coupled coils is useful in a wide variety of impedance-matching circuits. Figure 31-7 shows two possible equivalent circuits of lossless coupled coils. The first is expressed in terms of reactance elements, including the mutual reactance X_m. The second is in terms of susceptance elements, including the transfer susceptance B_T. (The transfer susceptance is the susceptance component of the transfer admittance, which is the ratio of the current induced in

the short-circuited secondary to the voltage applied to the primary.)   If capacitive tuning reactances are added, the equivalent circuits can be proportioned in accordance with the T and π matching sections described above.   The required capacitive
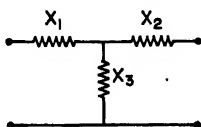
REACTANCES:

$$X_1 = X_2 = Z_0 \, \mathrm{TAN} \left(\frac{\theta}{2} \right)$$

$$X_3 = \frac{-Z_0}{\mathrm{SIN} \, \theta}$$
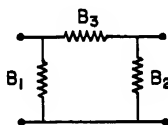
A.   T SECTION

SUSCEPTANCES:

$$B_1 = B_2 = \frac{1}{Z_0} \, \mathrm{TAN} \left(\frac{\theta}{2} \right)$$

$$B_3 = -\frac{1}{Z_0 \, \mathrm{SIN} \, \theta}$$
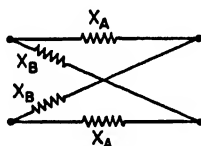
B. π SECTION

REACTANCES:

$$X_A = Z_0 \, \mathrm{TAN} \left(\frac{\theta}{2} \right)$$

$$X_B = -Z_0 \, \mathrm{COT} \left(\frac{\theta}{2} \right)$$

C.   LATTICE SECTION

FIG. 31-6. T, π, and lattice equivalents of transmission-line section of characteristic impedance Z_0 and electrical length, θ.
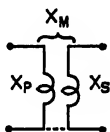
A.   IN REACTANCE TERMS
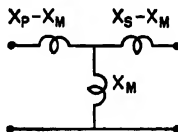
B.   IN SUSCEPTANCE TERMS

FIG. 31-7. Inductively coupled circuits and equivalent T and π sections.

reactances required for (1) series tuning and (2) parallel tuning are given in Fig. 31-8 for matching from R_1 to R_2.

The series and parallel capacitors may be used for tuning out the series reactance or shunt susceptance, respectively, of a complex termination.

Lumped Matching Reactance.   The standing wave on a transmission line may be eliminated on the source side of a matching reactance that is properly proportioned

and positioned, as shown in Fig. 31-9.   The choice of series or parallel connections, inductive or capacitive element, may be determined by the position of the standing-wave pattern and other practical considerations.

$$X_{C1} = -X_P - R_1 \left(\frac{X_M}{R_1 R_2} - 1 \right)^{1/2}$$

$$X_{C2} = -X_P - R_2 \left(\frac{X_M}{R_1 R_2} - 1 \right)^{1/2}$$

$$\theta = \sin^{-1} \left(-\frac{\sqrt{R_1 R_2}}{X_M} \right)$$

A.   SERIES TUNING

$$X_{C1} = -1/B_{C1} \qquad B_{C1} = -B_P - G_1 \left(\frac{B_M}{G_1 G_2} - 1 \right)^{1/2}$$

$$X_{C2} = -1/B_{C2} \qquad B_{C2} = -B_S - G_2 \left(\frac{B_M}{G_1 G_2} - 1 \right)^{1/2}$$

$$G_1 = 1/R_1 \qquad B_P = 1/X_P$$

$$G_2 = 1/R_2 \qquad B_S = 1/X_S$$

$$\theta = \sin^{-1} \left(-\frac{\sqrt{G_1 G_2}}{B_M} \right) \qquad B_M = \frac{X_M}{X_M^2 - X_P X_S}$$
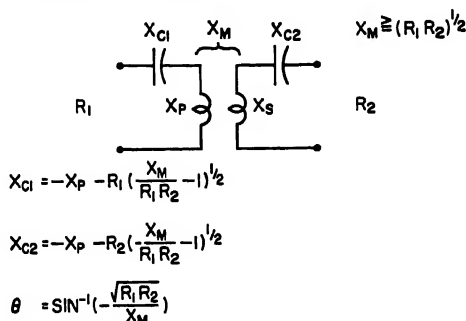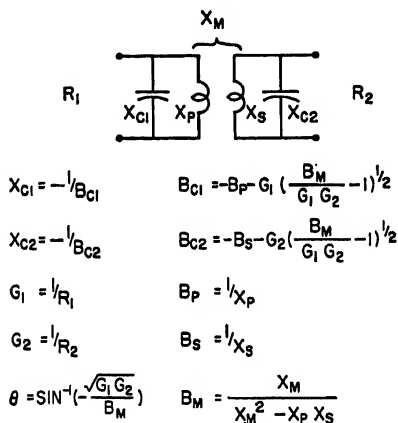
B.   PARALLEL TUNING

FIG. 31-8. Tuned inductively coupled circuits for matching between resistances.

31.3. IMPEDANCE MATCHING WITH DISTRIBUTED ELEMENTS

In much of the higher frequency range, it is desirable to use sections of transmission line having distributed reactances rather than lumped reactances in the form of coils and capacitors.   The lines are usually proportioned to yield negligible loss so that the following expressions for impedance relationships in lossless lines apply:

$$Z_{\text{in}} = Z_0 \frac{Z_L \cos \beta \ell + j Z_0 \sin \beta \ell}{Z_0 \cos \beta \ell + j Z_L \sin \beta \ell} \qquad (31\text{-}1)$$

= input impedance of line Z_0, $\beta \ell$ terminated in Z_L

For a short-circuited line, $Z_L = 0$, so that

$$Z_{\text{in}} = Z_{so} = j Z_0 \tan \beta \ell \qquad (31\text{-}2)$$

For an open-circuited line, $Z_L = \infty$, so that

$$Z_{\text{in}} = Z_{oo} = -j Z_0 \cot \beta \ell \qquad (31\text{-}3)$$

Transmission-line Stubs. Lengths of transmission line short-circuited or open-circuited at one end are often used as reactors in impedance-matching circuits. Inspection of Eqs. (31-2) and (31-3) will show that the designer by choice of characteristic impedance and line length has control of reactance value and slope (with respect to frequency) at any given frequency. Alternatively, he has control of the value of reactance at any two frequencies. The available slope of reactance is always greater than unity, the value obtained from a single lumped reactance element. Unfortunately, the available slope of reactance is always positive, although a negative slope would be ideal in many applications. However, an effect similar to that of a
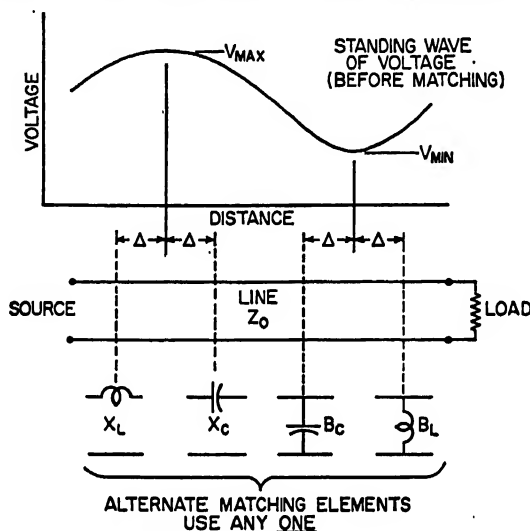
$$\frac{X}{Z_0} = \frac{B}{Y_0} = BZ_0 = \sqrt{S} - \frac{1}{\sqrt{S}}$$

$$S = \frac{V_{MAX}}{V_{MIN}}$$

$$\Delta = \frac{\lambda}{2\pi} \cos^{-1}\left[\frac{4S}{(S+1)^2}\right]$$

FIG. 31-9. Determination of lumped reactance to match a transmission line.

series-connected or parallel-connected reactance having the unattainable negative slope may often be obtained over a limited frequency range by the use of a parallel-connected or series-connected reactance, respectively.

General Line Transformer. The expression for Z_{in} [Eq. (31-1)] may be recast to relate generator and load impedances $(Z_G = R_G + jX_G, \; Z_L = R_L + jX_L)$ to the characteristic impedance and electrical length of a line section, providing a perfect match between them. The new expressions are

$$Z_0 = \sqrt{\frac{R_L|Z_G|^2 - R_G|Z_L|^2}{R_G - R_L}}$$

$$= \sqrt{|Z_G Z_L| \frac{\dfrac{R_L}{R_G}\left|\dfrac{Z_G}{Z_L}\right| - \left|\dfrac{Z_L}{Z_G}\right|}{1 - \dfrac{R_L}{R_G}}}$$

$$\tan \beta \ell = \frac{Z_0(R_L - R_G)}{R_L X_G - R_G X_L}$$

$$= \frac{Z_0(X_G - X_L)}{R_L R_G + X_L X_G - Z_0^2}$$

For Z_0 to be a positive finite real number, it is necessary that

$$\frac{1}{2} < \frac{\log\left|\dfrac{Z_L}{Z_G}\right|}{\log\left(\dfrac{R_L}{R_G}\right)} < \infty$$

Instead of using the above expression for $\tan \beta l$, one may determine βl from a plot of Z_L/Z_0 and Z_G^*/Z_0 on a Carter chart (or a Smith chart) once Z_0 has been determined. The two points will be at the same radius. The electrical angle measured clockwise from Z_L/Z_0 to Z_G^*/Z_0 is βl. (Note that $Z_G^* = R_G - jX_G$.)
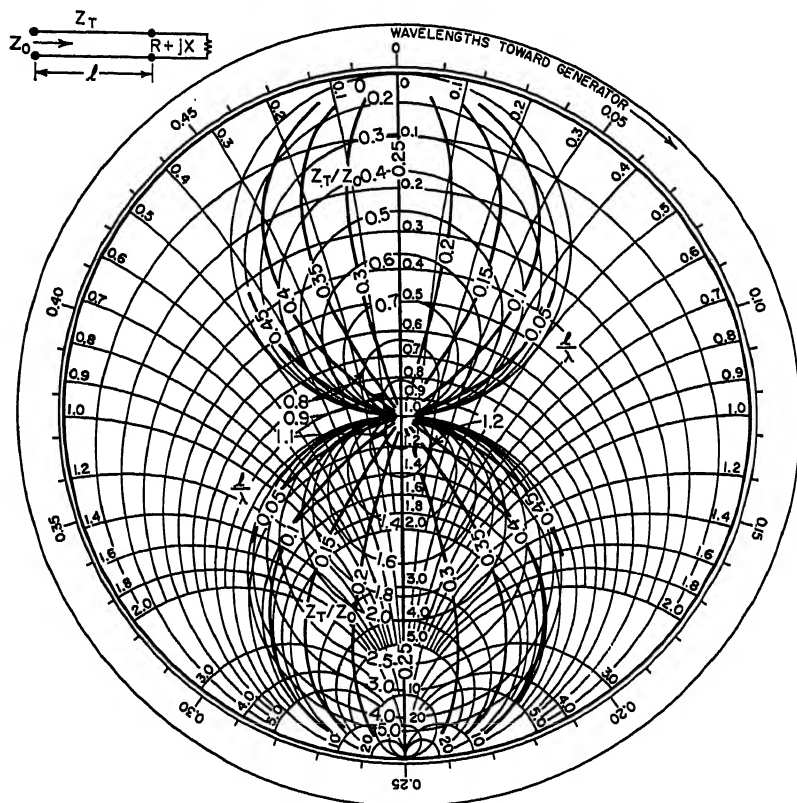
FIG. 31-10. Line transformer to match to a resistance.

The Z_0 and βl quantities for the required line section may be used to compute T', π, and lattice sections of lumped reactances to perform the same function using expressions given in Fig. 31-6.

Line Transformer for Matching to Resistance. For the frequently encountered case in which either the load impedance or the source impedance is a pure resistance, a solution for the required matching line may be obtained from Fig. 31-10. The complex impedance $R + jX$ is located on the Smith chart in terms of its normalized components R/Z_0 and X/Z_0, where Z_0 is the resistance to which a match is desired. The point so found is located within an area having a second set of coordinates if a solution is possible. These coordinates Z_T/Z_0 and l/λ give the characteristic impedance and length of the required line.

Quarter-wave Transformer. The useful quarter-wave transformer results from the general line transformer when $\beta \ell = \pi/2$. It has an impedance-inverting property, as seen from an inspection of

$$Z_{\text{in}} = \frac{Z_0{}^2}{Z_L}$$

The input impedance is thus proportional to the reciprocal of the load impedance. The phase angle of the input impedance is the negative of that of the load impedance.

DIAGRAM FOR B_C TRIMMER

$$A = \text{SIN}^{-1}\left[\frac{R_1 R_2 + Z_0{}^2}{(R_1 + R_2) Z_0}\right]$$
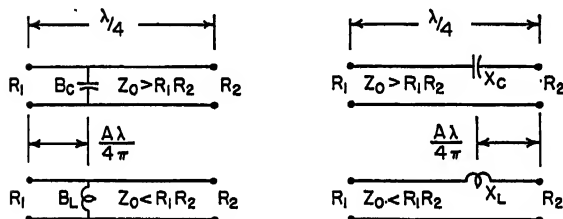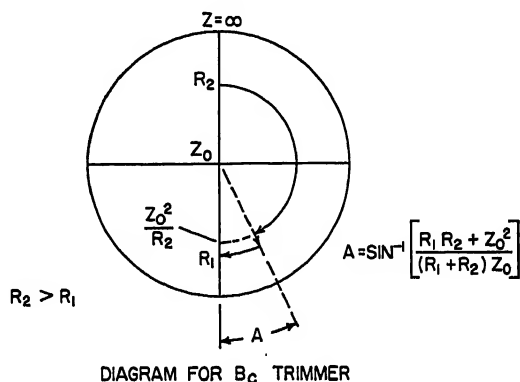
ALTERNATE FORMS OF TRIMMER

Fig. 31-11. Reactive transformation trimmer for quarter-wave transformer.

The quarter-wave line can be used, for example, to transform an inductive low impedance to a capacitive high impedance.

The quarter-wave transformer is often used to match between different resistance levels. In this case

$$Z_0 = \sqrt{R_1 R_2}$$

In a mismatched coaxial line a quarter-wave transformer formed by a simple sleeve can be used to tune out the reflection. The sleeve forms an enlargement of the inner conductor or a constriction of the outer conductor which may be stationed where required. The characteristic impedance of the line is reduced over the quarter-wave length by the sleeve to a value of

$$\frac{Z_0}{\sqrt{S}}$$

where S is the initial SWR of the line. The load end of the sleeve is positioned at a voltage minimum on the standing-wave pattern. The impedance, here looking toward the load, is Z_0/S. The transformer transforms this to Z_0 so the line on the source side is perfectly matched.

The transformation ratio of a quarter-wave transformer can be changed for fine-adjustment purposes by the addition of a lumped reactive element, as shown in Fig. 31-11. This is a convenient way of trimming to obtain an exact match when close control of the transformer Z_0 is not practical. The placement of the adjuster element is such as to provide substantially pure radial effect on the reflection-coefficient plane. The magnitude of the required reactance may be determined graphically or experimentally.

Frequency Sensitivity of Line Transformer. The mismatching effect of a departure from the design frequency for the general line transformer (and hence the quarter-wave transformer) can be estimated from Fig. 31-12.
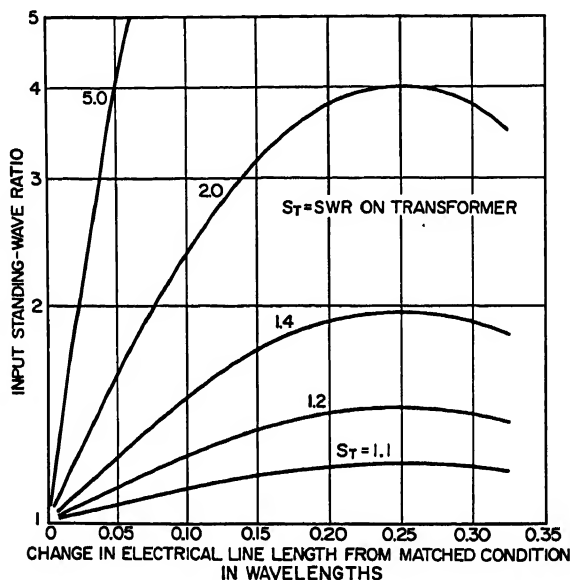
FIG. 31-12. Frequency sensitivity of a transmission-line transformer.

Cascaded Quarter-wave Transformers. A number of quarter-wave transmission-line sections may be arrayed in cascade to realize great improvement in wideband performance over a single-section transformer. The characteristic impedances of the successive sections are proportioned to divide the over-all transformation systematically. Figure 31-13 defines the terms that will be used in the discussion below.

Binomial Transformer. The binomial (or binomial-coefficient) distribution gives almost maximally flat performance. In this distribution the logarithms of the impedance ratios of the steps between sections are made to be in the ratio of the binomial coefficients.

Table 31-1 may be used to determine the characteristic impedance Z_n of the nth section in an N-section transformer as a function of R_2/R_1.

The input standing-wave ratio of an N-section binomial transformer can be expressed by

$$S = 1 + (\cos \theta)^N \ln \frac{R_2}{R_1}$$

where θ is the electrical length of each section. This expression is subject to the assumptions of small steps, zero discontinuity capacitance[41,42], and equal lengths of the sections.

N=1 R_1 •——$Z_1 = R_0$——• R_2

N=2 R_1 •——Z_1——Z_2——• R_2

N=3 R_1 •——Z_1——$Z_2 = R_0$——Z_3——• R_2

N=4 R_1 •——Z_1——Z_2——Z_3——Z_4——• R_2

N=5 R_1 •——Z_1——Z_2——$Z_3 = R_0$——Z_4——Z_5——• R_2

N=6 R_1 •——Z_1——Z_2——Z_3——Z_4——Z_5——Z_6——• R_2
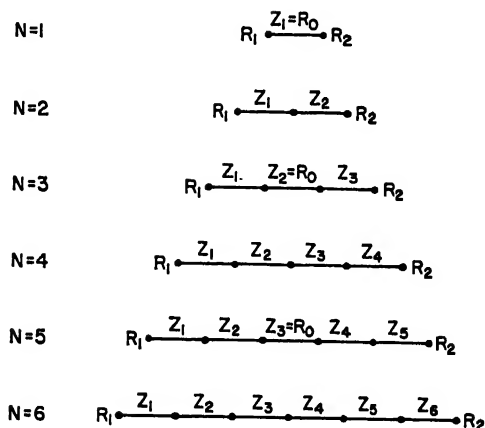
R_1, R_2 = TERMINATING RESISTANCES

$R_1 < R_2$

$R_0 = \sqrt{R_1 R_2}$ = MEAN IMPEDANCE

SECTIONS ARE EACH A QUARTERWAVE AT f_0

f_0 = DESIGN FREQUENCY = $\dfrac{f_+ + f_-}{2}$

f_+ = UPPER FREQUENCY LIMIT

f_- = LOWER FREQUENCY LIMIT

f_+/f_- = FREQUENCY RATIO = $\dfrac{1+F}{1-F}$

F = FREQUENCY COEFFICIENT = $\dfrac{f_+/f_- - 1}{f_+/f_- + 1}$

FIG. 31-13. Cascaded quarter-wave transformers.

Table 31-1. Design Ratios for Binomial Transformer

N = \ n =	1	2	3	4	5	6	7
1	½						
2	¼	¾					
3	⅛	4/8	⅞				
4	1/16	5/16	11/16	15/16			
5	1/32	6/32	16/32	26/32	31/32		
6	1/64	7/64	22/64	42/64	57/64	63/64	
7	1/128	8/128	29/128	64/128	99/128	120/128	127/128

$$\text{Ratios} = \frac{\log (Z_n/R_1)}{\log (R_2/R_1)} = 1 - \frac{\log (R_2/Z_n)}{\log (R_2/R_1)}$$

The two-section transformer has maximally flat bandwidth curve for all transformation ratios. For other values of N the performance approximates the maximally flat curve for transformation ratios near unity.

Tchebyscheff Transformer. If a certain maximum reflection coefficient ρ_m may be tolerated within the operating band, an optimum design is possible which allows the reflection coefficient to cycle between 0 and ρ_m within the band and to increase sharply outside of the band. This is called the Tchebyscheff transformer, since Tchebyscheff polynomials are used in its design.

The input standing-wave ratio of the Tchebyscheff transformer has been given by

$$S = 1 + \ln\left(\frac{R_2}{R_1}\right) \frac{T_N\left(\dfrac{\cos\theta}{\cos\theta_-}\right)}{T_N\left(\dfrac{1}{\cos\theta_-}\right)}$$

where $T_N(x)$ is the Tchebyscheff polynomial of mth degree defined by

$$T_0(x) = 1$$
$$T_1(x) = x$$
$$T_2(x) = 2x^2 - 1$$
$$T_3(x) = 4x^3 - 3x$$
$$\cdot$$
$$\cdot$$
$$\cdot$$
$$T_{m+1}(x) = 2xT_m(x) - T_{m-1}(x)$$

and where θ is the electrical length of each section and θ_- is the length at f_-. The expression is subject to the same assumptions as were made in the binomial case.

Another expression of Tchebyscheff transformer performance, which does not require the assumption of small steps, is

$$P_L = 1 + \frac{\left(\dfrac{R_2}{R_1} - 1\right)^2}{\dfrac{4R_2}{R_1}} \frac{T_N{}^2\left(\dfrac{\cos\theta}{\cos\theta_-}\right)}{T_N{}^2\left(\dfrac{1}{\cos\theta_-}\right)}$$

where P_L is the power-loss ratio defined by $1/(1 - |p|^2)$.

The above equation may be converted to an implicit relationship between four principal quantities, namely,

R_2/R_1, the transformation ratio

ρ_m, the maximum tolerable reflection coefficient within the band

N, the number of sections

F, the frequency coefficient

Any one of these may be determined by reference to Fig. 31-14 if the other three are known. Design constant C of Fig. 31-14 can be used as a measure of difficulty of transformation. It may be expressed as a function of R_2/R_1 and ρ_m or as a function of N and F.

$$C\left(\frac{R_2}{R_1}, \rho_m\right) = \frac{\dfrac{R_2}{R_1} - 1}{2\sqrt{\dfrac{R_2}{R_1}\left(\dfrac{1}{\rho_m{}^2} - 1\right)}}$$

$$C(N,F) = T_N\left\{\frac{1}{\cos\left[\dfrac{\pi}{2}(1 - F)\right]}\right\}$$
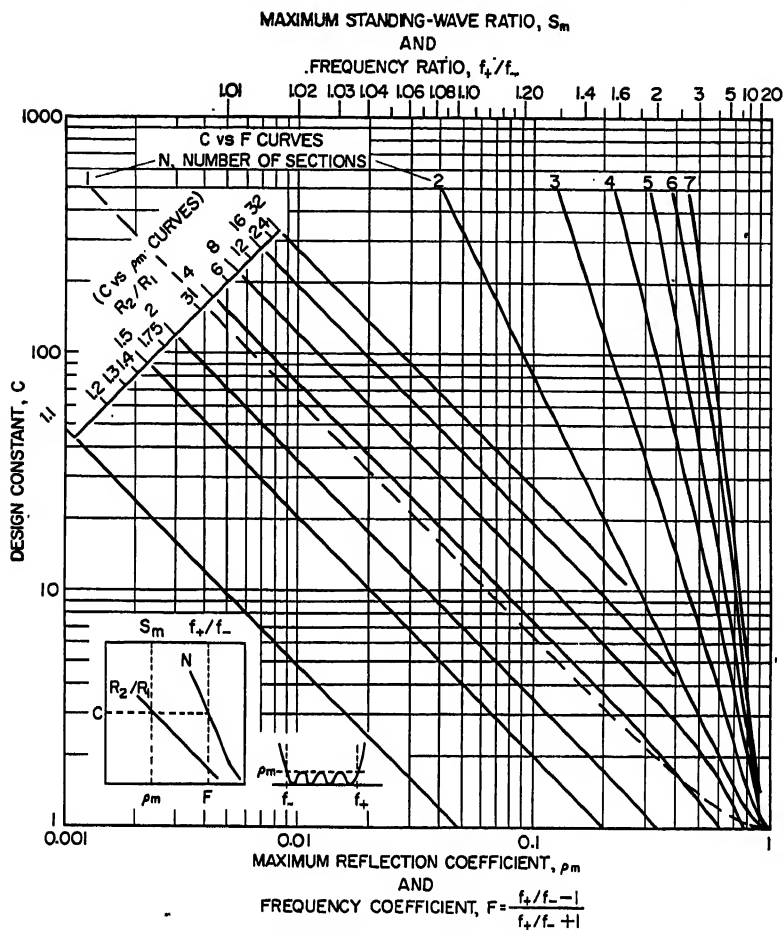
FIG. 31-14. Performance of Tchebyscheff transformer.
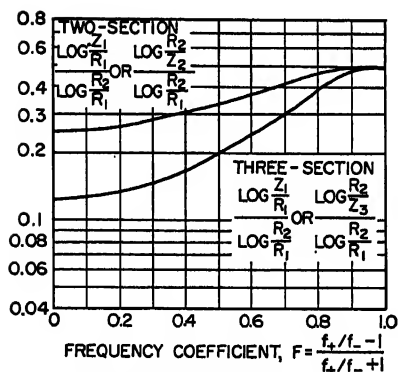
FIG. 31-15. Design chart for two- and three-section Tchebyscheff transformers.
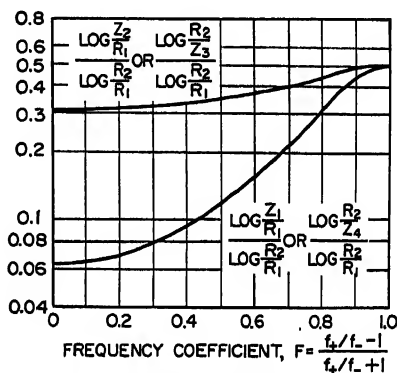
FIG. 31-16. Design chart for four-section Tchebyscheff transformers.

For a working condition, it is necessary that

$$C\left(\frac{R_2}{R_1}, \rho_m\right) \lesseqgtr C(N,F)$$

Figure 31-14 has an auxiliary scale at the top which permits conversion of ρ_m to S_m and F to f_+/f_-.
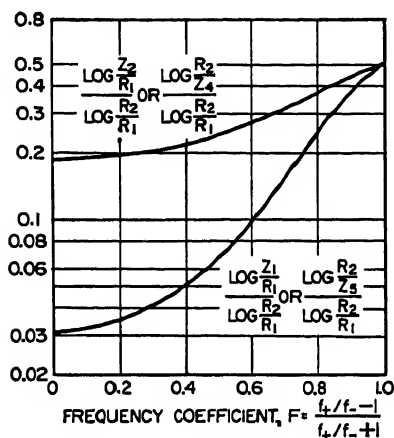
FIG. 31-17. Design chart for five-section Tchebyscheff transformers.
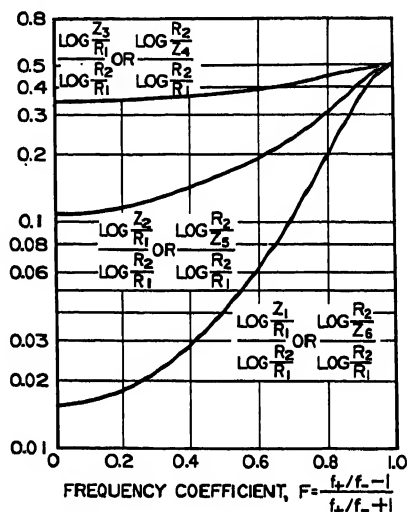
FIG. 31-18. Design chart for six-section Tchebyscheff transformers.
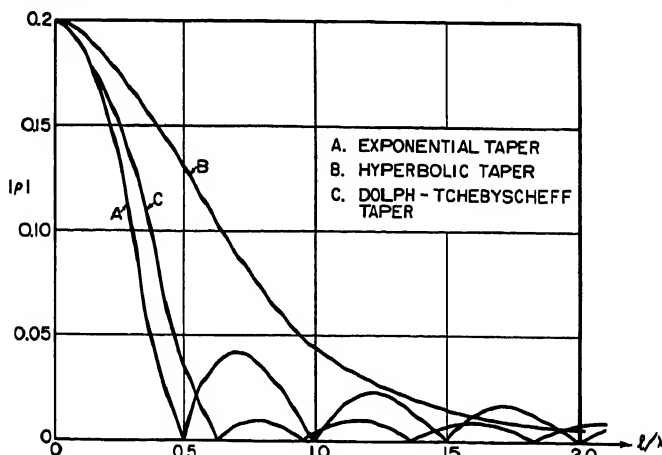
FIG. 31-19. Performance of 50- to 75-ohm Dolph-Tchebyscheff tapered transition.

The C versus F curve for $N = 1$ (the dashed curve) corresponds to the common quarter-wave transformer. For this case $Z_1 = \sqrt{R_1 R_2}$, so it is, in fact, identical to the binomial transformer for $N = 1$.

The characteristic impedances may be determined at least approximately from the charts shown in Figs. 31-15 to 31-18. For applications in which C is large or where greater accuracy is needed, the values should be calculated directly from func-

tions given in Table 31-2.   The impedance of the center section when N is odd is simply $\sqrt{R_1 R_2}$ and is independent of F.

Table 31-2. Design Ratios for Tchebyscheff Transformer

$$N = 2 \qquad \frac{\log\,(R_2/R_1)}{\log\,(Z_1/R_1)} = 4 - 2\cos^2\theta_-$$

$$N = 3 \qquad \frac{\log\,(R_2/R_1)}{\log\,(Z_1/R_1)} = 8 - 6\cos^2\theta_-$$

$$N = 4 \qquad \frac{\log\,(R_2/R_1)}{\log\,(Z_1/R_1)} = 16 - 16\cos^2\theta_- + 2\cos^4\theta_-$$

$$\frac{\log\,(Z_2/R_1)}{\log\,(Z_1/R_1)} = 5 - 4\cos^2\theta_-$$

$$N = 5 \qquad \frac{\log\,(R_2/R_1)}{\log\,(Z_1/R_1)} = 32 - 40\cos^2\theta_- + 10\cos^4\theta_-$$

$$\frac{\log\,(Z_2/R_1)}{\log\,(Z_1/R_1)} = 6 - 5\cos^2\theta_-$$

$$N = 6 \qquad \frac{\log\,(R_2/R_1)}{\log\,(Z_1/R_1)} = 64 - 96\cos^2\theta_- + 36\cos^4\theta_- - 2\cos^6\theta_-$$

$$\frac{\log\,(Z_2/R_1)}{\log\,(Z_1/R_1)} = 7 - 6\cos^2\theta_-$$

$$\frac{\log\,(Z_3/R_1)}{\log\,(Z_2/R_1)} = 1 + 21\sin^2\theta_- - 9\sin^2\theta_-\cos^2\theta_-$$

where $\theta_- = \dfrac{(1 - F)\pi}{2}$

31.4. TAPERED LINES

If the characteristic impedance of a long section of transmission line varies extremely slowly with distance along the line, a nearly perfect match between resistive terminations may be obtained.   Since a line of such length and such small taper can seldom be afforded, much attention has been directed toward the design of tapered lines giving acceptable performance over short lengths.

Exponential Line.   An exponential line is one simple form of tapered line.   For an exponential line tapering from R_1 to R_2 in an over-all length ℓ, the characteristic impedance Z_0 of any short section of line (so that the taper may be neglected) at distance x from the R_1 end of the line is

$$Z_0 = \sqrt{\frac{L_x}{C_x}} = R_1 \exp\frac{x \ln\,(R_2/R_1)}{\ell}$$

where L_x and C_x are the distributed constants of the line.   The line performs similarly to a low-pass filter having a cutoff wavelength

$$\lambda_c = \frac{4\pi\ell}{\ln\,(R_2/R_1)}$$

The wavelength in the line λ_g is related to λ_c by the familiar equation

$$\frac{1}{\lambda_c{}^2} + \frac{1}{\lambda_g{}^2} = \frac{1}{\lambda_0{}^2}$$

where λ_0 is the wavelength in a nontapered line that has the same product of distributed constants as the exponential line.

For an infinite length of exponential line in which no reflected wave can occur, the input impedance Z_{i1} at the low-impedance end is related to R_1 for $\lambda_0 \leqq \lambda_c$ by

$$Z_{i1} = \sqrt{1 - \left(\frac{\lambda_0}{\lambda_c}\right)^2} - j\frac{\lambda_0}{\lambda_c}$$
$$= \exp\left(-j\sin^{-1}\frac{\lambda_0}{\lambda_c}\right)$$
$$= \exp(-j\phi)$$

where $\phi = \sin^{-1}(\lambda_0/\lambda_c)$. Similarly, the input impedance Z_{i2} at the high-impedance end is related to R_2 by

$$Z_{i2} = \sqrt{1 - \left(\frac{\lambda_0}{\lambda_c}\right)^2} + j\frac{\lambda_0}{\lambda_c}$$
$$= \exp\left(j\sin^{-1}\frac{\lambda_0}{\lambda_c}\right)$$
$$= \exp j\phi$$

Conjugate-impedance matching to these impedances can be approximated over a considerable band so that the line may be operated on a quasi-nonresonant basis.[53]

If the line is terminated in a resistance equal in magnitude to the output-characteristic impedance, the line is not matched. The reflection coefficient at each end is

$$\rho = \pm j \tan\frac{\phi}{2}$$

The sign depends on the direction of viewing.

1. When $4\ell/\lambda_g$ is an even integer, the reflections at opposite ends of the line cancel and the line acts as a perfect transformer.

2. When $4\ell/\lambda_g$ is an odd integer, the reflections at opposite ends of the line combine to give an input-reflection-coefficient magnitude of

$$\rho = \pm j \sin\phi$$
$$= \pm j\frac{\lambda_0}{\lambda_c}$$

Nonexponential Tapered Lines. Tapered lines having other than a simple exponential taper are more complex to handle analytically. Of the several recent treatments of tapered lines, the one by Klopfenstein[52] promises to have the most general application. In this treatment the proportions of an optimum taper are given. The taper is optimum in the sense that for a given taper length, the input reflection coefficient has a minimum magnitude through the passband, and for a specified tolerance of the reflection-coefficient magnitude, the taper has minimum length. The method of obtaining the design consists of allowing the number of sections of the multisection Tchebyscheff transformer to increase without limit. As the length of sections decreases without limit, the upper cutoff frequency is increased without limit.

The expression for the input reflection coefficient of the optimum tapered line is

$$\rho \exp j\beta\ell = \rho_0 \frac{\cos\left(\sqrt{(\beta\ell)^2 - A^2}\right)}{\cosh A}$$

where $\beta\ell$ is the electrical line length and ρ_0 is the reflection coefficient without the transformer. At the lower end of the passband $\beta\ell = A$. Maximum reflection coefficient in the passband $|\rho_m|$ is $|\rho_0|/\cosh A$.

The variation of impedances along the taper is given by

$$\ln Z_0 = \frac{1}{2}\ln(Z_1 Z_2) + \frac{\rho_0}{\cosh A}\left[A^2\phi\left(\frac{2x}{\ell}, A\right)\right.$$
$$\left. + U\left(x - \frac{\ell}{2}\right) - U\left(-x - \frac{\ell}{2}\right)\right] \qquad |x| \leq \frac{\ell}{2}$$

$$= \ln Z_2 \qquad x > \frac{\ell}{2}$$

$$= \ln Z_1 \qquad x < -\frac{\ell}{2}$$

U is the step function defined by

$$U(z) = 0 \qquad z < 0$$
$$U(z) = 1 \qquad z \geq 0$$

and ϕ is defined by

$$\phi(z,A) = -\phi(-z,A) = \int_0^z \frac{I_1(A\sqrt{1-y^2})}{A\sqrt{1-y^2}}\, dy \qquad |z| \leq 1$$

where I_1 is the first kind of modified Bessel function of the first order.

The function $\phi(z,A)$ cannot be expressed in closed form except for special values of the parameters. It may be determined from computed Table 31-3. It should be noted that because of a design approximation, the value of ρ_0 to be used for best accuracy is $[\ln(R_2/R_1)]/2$ instead of the usual $(R_2 - R_1)/(R_2 + R_1)$.

Table 31-3. Values of the Function $\phi(z,A)$ for $z = 0(0.05)1.00$
and $20\log_{10}(\cosh A) = 0(5)40$*

$$\phi(z,A)$$

z	20 $\log_{10}(\cosh A)$								
	0	5	10	15	20	25	30	35	40
0.00	0.000000	0.000000	0.000000	0.000000	0.000000	0.000000	0.000000	0.000000	0.000000
0.05	0.025000	0.029593	0.036848	0.048140	0.065590	0.092539	0.134313	0.199460	0.301772
0.10	0.050000	0.059101	0.073629	0.096137	0.130902	0.184564	0.267098	0.397208	0.600025
0.15	0.075000	0.088681	0.110276	0.143848	0.195661	0.275507	0.399242	0.591802	0.893707
0.20	0.100000	0.118128	0.146721	0.191132	0.259507	0.365055	0.528062	0.781511	1.178306
0.25	0.125000	0.147479	0.182899	0.237850	0.322448	0.452552	0.653321	0.964936	1.451913
0.30	0.150000	0.176708	0.218746	0.283869	0.383062	0.537610	0.774237	1.140744	1.712272
0.35	0.175000	0.205794	0.254197	0.329059	0.443899	0.619809	0.890101	1.307751	1.957437
0.40	0.200000	0.234711	0.289191	0.373296	0.502035	0.698767	1.000282	1.464942	2.185803
0.45	0.225000	0.263438	0.323607	0.416400	0.558103	0.774142	1.104238	1.611487	2.390134
0.50	0.250000	0.291950	0.357508	0.458441	0.612094	0.845635	1.201523	1.746753	2.587582
0.55	0.275000	0.320226	0.390837	0.499134	0.663658	0.912094	1.291792	1.870306	2.759684
0.60	0.300000	0.348244	0.423420	0.538444	0.712709	0.970019	1.374800	1.981918	2.912359
0.65	0.325000	0.375982	0.455266	0.576284	0.759120	1.034555	1.450409	2.081555	3.045886
0.70	0.350000	0.403418	0.486328	0.612574	0.802790	1.088504	1.518582	2.169376	3.160575
0.75	0.375000	0.430533	0.516559	0.647248	0.843641	1.137814	1.579377	2.245710	3.258228
0.80	0.400000	0.457305	0.545918	0.680245	0.881619	1.182484	1.632947	2.311049	3.339098
0.85	0.425000	0.483716	0.574365	0.711518	0.916692	1.222564	1.679531	2.366019	3.404835
0.90	0.450000	0.509746	0.601805	0.741027	0.948855	1.258145	1.719443	2.411361	3.456938
0.95	0.475000	0.535377	0.628386	0.768745	0.978123	1.289303	1.753005	2.447905	3.497000
1.00	0.500000	0.560591	0.653899	0.794653	1.004533	1.316391	1.780835	2.476547	3.526658

* Reference 52, by permission.

A comparison between the optimum taper, the exponential taper,[45] and the hyperbolic taper[55] is shown in Fig. 31-19 for a specific example.

31.5. COMBINATIONS OF TRANSFORMERS AND STUBS

Transformer with Two Compensating Stubs. The simple quarter-wave transformer has rather poor performance over a wide band. Its wideband performance
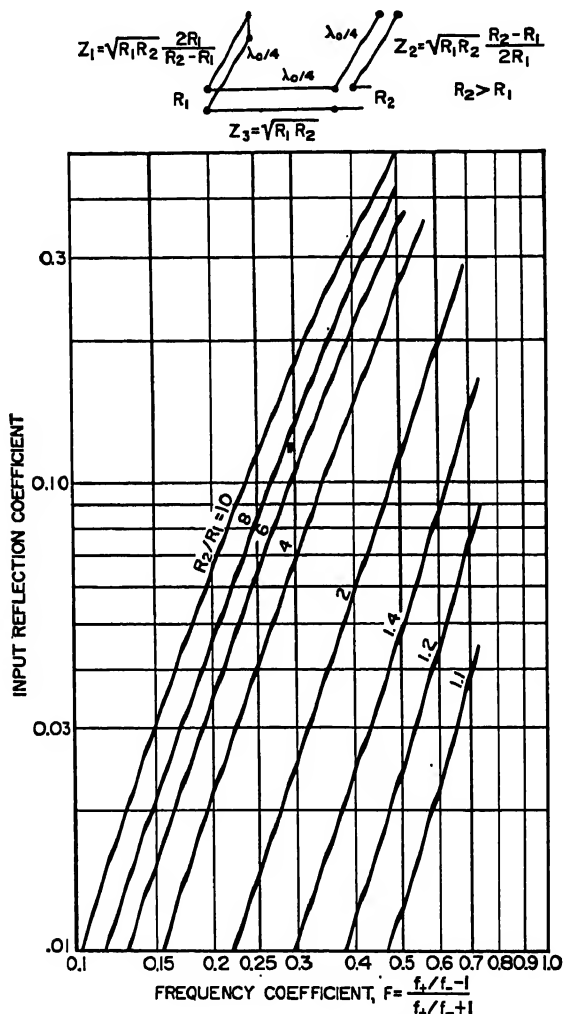
Fig. 31-20. Transformer with two compensating stubs.

may be improved greatly by the addition of a compensating stub at each end, as shown in Fig. 31-20. The reactance introduced by each stub counteracts the variation with frequency of one-half of the transformer length at and near the design frequency. For the impedance proportions shown, the wideband performance is comparable with that of a three-section binomial transformer. For values of R_2/R_1

below 3, the performance is better than that of the binomial transformer.   Above this value of R_2/R_1, the opposite is true.   The difference in performance is small, however, so considerations of over-all length, adaptability to available space, etc., may govern the choice of method.

Modifications may be made to the basic proportions to suit particular applications. The lengths and impedances of the stubs may sometimes be altered to compensate for reactance variation in the terminations. Stub lengths of half wave and three-quarter wave may be used where R_2/R_1 is high and F is 0.25 or less, for the purposes of giving

FIG. 31-21. Transformer with two-section compensating stubs.

more moderate values of Z_1 and Z_2.   More nearly exact reactance compensation at the band limits may be obtained by using two-section stubs as shown in Fig. 31-21. The values of Z_1 and Z_2 are chosen close to the ones given in the previous figure, while the ratio $Z_4/Z_2 = Z_1/Z_5$ is selected for the best compensation at the edge of the
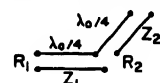
SERIES STUB:

$$Z_1 = \sqrt{S_m R_1 R_2}$$

$$Z_2 = Z_1\left(\frac{R_2}{S_m R_1} - 1\right)$$
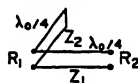
SHUNT STUB:

$$Z_1 = \sqrt{S_m R_1 R_2}, \quad R_2 > R_1$$

$$Z_2 = Z_1/\left(\frac{R_2}{S_m R_1} - 1\right)$$

BANDWIDTH (EITHER TYPE):

$$\cos[\pi(1-F)] = \frac{2S_m \dfrac{R_2}{R_1} - \dfrac{1}{S_m}}{\dfrac{R_2}{R_1} - \dfrac{1}{S_m}}$$
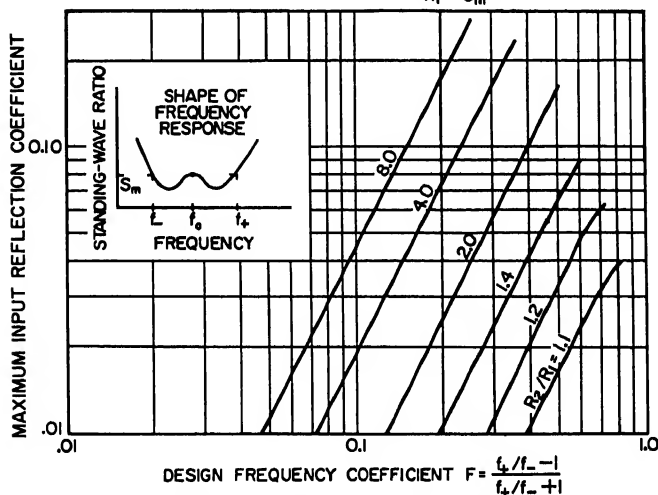
FIG. 31-22. Transformer with single compensating stub.

required band.   Simple series and parallel-resonant lumped-constant circuits may be used to replace the stubs at low frequencies.   It is always necessary to have a series-connected, series-resonant circuit at the R_2 end and a parallel-connected, parallel-resonant circuit at the R_1 end.

Transformer with Single Compensating Stub.   If it is convenient to use only one compensating stub with the transformer, one of the circuits shown in Fig. 31-22 may be used.   In this design the allowable maximum standing-wave ratio S_m affects the choice of Z_1 and Z_2.

Tapped Stub Transformer.   The tapped stub transformer, shown in Fig. 31-23, is a useful circuit for matching between two widely different resistive terminations for single-frequency or narrow-band operation.   The design chart shows the relationship existing between R_2/R_1, Z_0^2/R_1R_2, and the two line lengths L_1 and L_2 for the matched
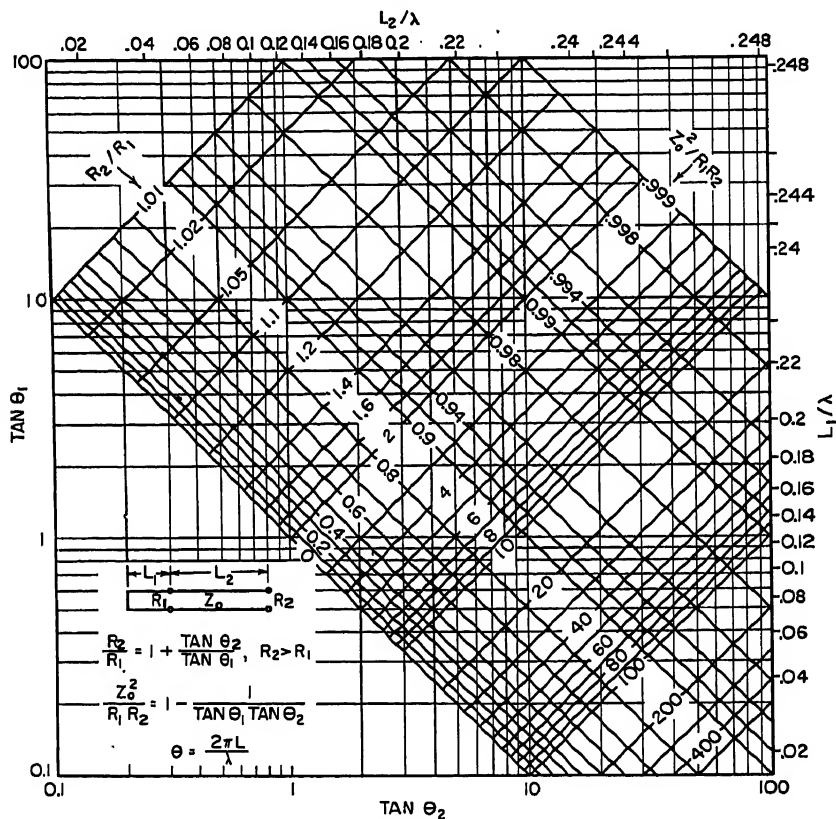
Fig. 31-23. Tapped-stub transformer.

condition.   The total stub length is a minimum of one-quarter wavelength and increases with increasing Z_0.   The chart is based on a lossless transmission line.   For very high transformation ratios the effect of even a small loss is appreciable and must be accounted for separately.

31.6. BALUNS

A balun is an impedance transformer designed to couple a balanced transmission circuit and an unbalanced transmission circuit.   The impedance transformation may be accomplished usually with conventional techniques.   The conversion between a balanced mode and an unbalanced mode, however, requires special techniques. Several basic techniques are exemplified by the balun types shown in Fig. 31-24.
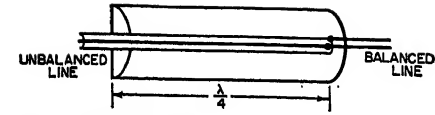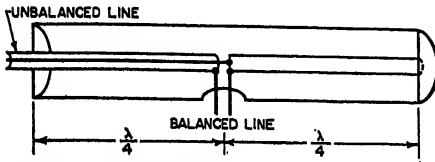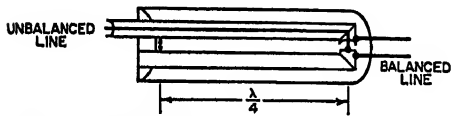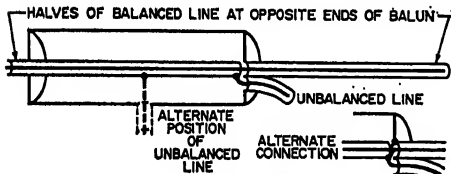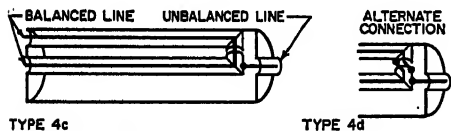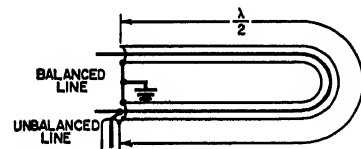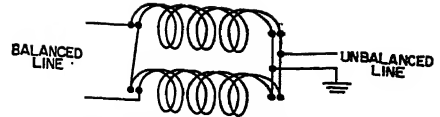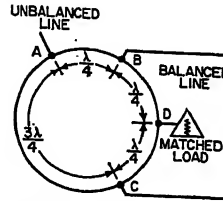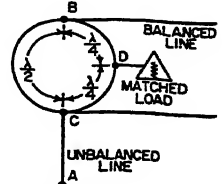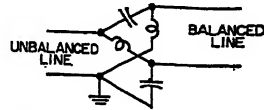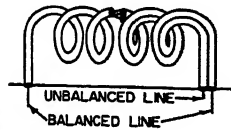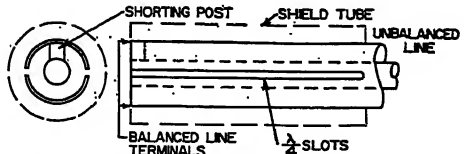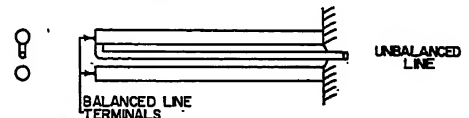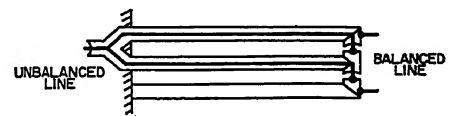
FIG. 31-24. Basic types of baluns.

A balanced circuit is obtained in type 1 by introducing a high impedance of a resonant coaxial-choke structure between the outer conductor of the unbalanced coaxial circuit and ground. There is no counterpart of the choke impedance in the other side of the balanced circuit. Hence the balun does not present a well-balanced impedance at any frequency for which the choke impedance is not high.

The shortcoming of type 1 is overcome in types 2 and 3. Symmetry of the balanced circuit is maintained independently of frequency by a two-conductor choke (type 3) or by two identical opposed coaxial-choke cavities (type 2). The first three types have been widely used because of their simplicity and mechanical adaptability. The impedance bandwidth is limited by the shunting effect of the choke. Thus it is advantageous to keep the characteristic impedance of the choke lines as high as possible for wideband operation.

Type 4 represents an improvement for many applications, particularly those involving impedance-level transformation. Unlike types 2 and 3, type 4 has the balanced circuit in the innermost line. Coupling is attained through a gap between line sections, as before. The necessary choke cavity, however, is around this gap in the unbalanced side of the structure. An unbalanced or single-ended cavity can be used without disturbing the perfect balance. The connections at the gap may be either the series type, as in types 4a and 4c, or of a parallel type, as in types 4b and 4d. The parallel connection results in a balanced-to-unbalanced impedance ratio of 4.

An additional impedance control is available in any of the type 4 baluns at some expense of bandwidth by application of the principle of the tapped-stub transformer. This is illustrated by the alternate position of the unbalanced line in the drawing of type 4a. The desired impedance transformation ratio determines the length of coaxial-choke line on each side of the unbalanced-line tap position in accordance with Fig. 31-23.

The type 5 balun employs a half-wave delay line. It is connected between the two balanced-line terminals as shown, forcing the potentials to ground to be equal and opposite at the design frequency. A balanced-to-unbalanced impedance ratio of 4 is obtained.

Type 6 employs helically wound two-wire transmission lines. At the unbalanced end, they are connected in parallel. Enough line length is used to develop high impedances to ground at the opposite ends. There the lines are connected in series to form the balanced terminals. A balanced-to-unbalanced impedance ratio of 4 is obtained.

Type 7a is a conventional $6\lambda/4$ hybrid ring which operates similarly to type 5. The path length from A to C is one-half wave longer than from A to B. Each path is an odd number of quarter waves long so that impedance transformation may be incorporated by proper selection of wave impedances. Furthermore, a load resistor at D is connected to terminals B and C by quarter-wave lines. This arrangement tends to dissipate the energy in an unbalanced wave without affecting a balanced wave.

Type 7b is a $4\lambda/4$ hybrid ring that operates similarly, except that the impedance-matching function is performed by the separate quarter-wave line AC.

Type 8 is the familiar lattice circuit. In it the incoming unbalanced wave energy is divided equally between two channels, one providing a 45° lead, the other a 45° lag. The output voltage is balanced with respect to ground and is in quadrature with the input voltage. The lattice may be proportioned to match any two resistance values.

Type 9 is similar in principle to type 6. It is most suitable for operation at the longer wavelengths where the size of a type 4 tends to become excessive. It may be connected for an impedance ratio of 1 or of 4.

Type 10a is a convenient balun type for feeding balanced dipoles. The slotted

portion of transmission line supports two modes of transmission simultaneously. Energy in a coaxial mode from the unbalanced input is substantially unchanged by the presence of the slots. The field of this mode is almost completely confined within the outer conductor. A balanced mode also exists in which the halves of the slotted cylinder are at opposite potentials and the center conductor is at zero potential. The field is not confined to the space within the slotted cylinder. (If leakage and radiation are to be minimized, another cylinder may be added over-all for shielding.) The connection strap between the inner conductor and one-half of the slotted cylinder requires that the coaxial-mode voltage be equal and opposite to that half of the balanced-mode voltage. Thus a balanced-to-unbalanced impedance ratio of 4 is obtained.

Type 10a will give almost perfect balance over a wide frequency range if the slot width is kept small and symmetry is maintained at the strap end. A variation of this basic type of balun is the three-wire balun shown in type 10b. It is sufficiently well balanced for use in noncritical applications.

Type 11 illustrates another method by which an impedance transformation may be obtained by a connection independently of frequency. Two coaxial lines are connected in parallel at the unbalanced terminal and in series at the balanced terminal. A third cylinder is added to preserve symmetry. The impedance transformation ratio for this structure having two lines is 2^2, or 4. More coaxial lines could be added to give impedance transformation ratios of 9, 16, etc. Practical limits are soon reached in this direction, however. Bifilar coils can also be used in a balun operating on this principle.

Balun action can be obtained by the use of a pair of inductively coupled coils. Leakage reactance interferes with wideband performance, although its effect may be tuned out for narrow-band operation. When the coils are closely spaced to reduce the leakage reactance, intercoil capacitance is increased. Its effect toward unbalancing the balanced end of the circuit must be minimized.

31.7. BROADBANDING

The most general problem of broadbanding is that of synthesizing a circuit to match one arbitrary impedance to another arbitrary impedance over a prescribed frequency range to within a prescribed tolerance. Fortunately, the broadbanding problems found in practice involve impedances that are not completely arbitrary, inasmuch as they are composed of a combination of physically realizable inductances, capacitances, and resistances.

Nevertheless, the combinations are usually too complex for the impedances to be treated as simple functions of frequency for which theoretical solutions[66,67] are available. As a result, graphical representations of the transcendental impedance functions are frequently relied upon.

A further simplification of the broadbanding problem often occurs because at least one of the impedances to be matched usually is the characteristic impedance of a transmission line and thus is either constant and resistive or nearly so. The problem of matching two resistive impedances is treated in earlier parts of this section. The problem of matching a load of frequency-varying impedance to a constant resistance is so common that the following discussion will be limited to this case.

Several broad rules that apply to broadbanding practice are given, as follows:

1. The difficulty of obtaining a prescribed tolerance of match increases with the required bandwidth. Refer to performance charts of a Tchebyscheff transformer for an example of this and of the following rule.

2. The difficulty increases with transformation ratio (expressed as a quantity greater than 1).

3. The difficulty increases with the electrical length of the transmission circuit between the load and the first point of control.

4. Improvement of match throughout one sector of the frequency range will generally be accompanied by an increase in mismatch in other sectors of the frequency range.

5. Any physically realizable passive impedance plotted on the reflection-coefficient plane displays a circular or spiral motion having a clockwise sense of rotation with frequency.
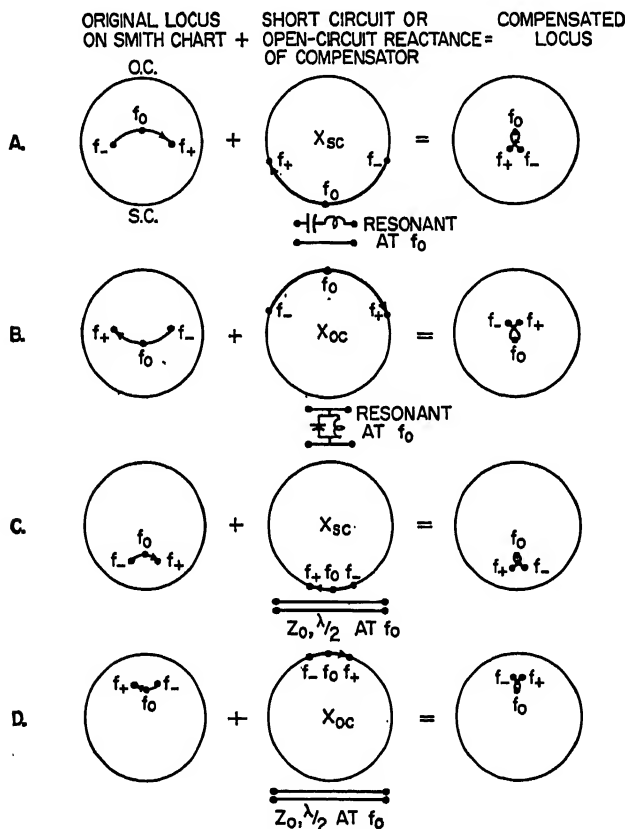
Fig. 31-25. Broadband compensation methods.

The effect of a length of mismatched transmission line between the load terminals and the first impedance-matching control is to introduce an additional variation with frequency that is seldom favorable over an appreciable bandwidth (rule 3). For this reason it is advantageous to conduct impedance-matching control at a position close to the load terminals. In fact, if control of the load impedance is available from within the load itself, advantage should be taken of this to select the most suitable shape and position of the impedance locus on the reflection-coefficient plane.

Transformation of the given impedance locus on the chart to one that is compactly situated about the desired impedance point requires, first, a method of moving the impedance locus and, second, a method of compensating for the variation with frequency inherent in the original impedance locus and that introduced by the moving
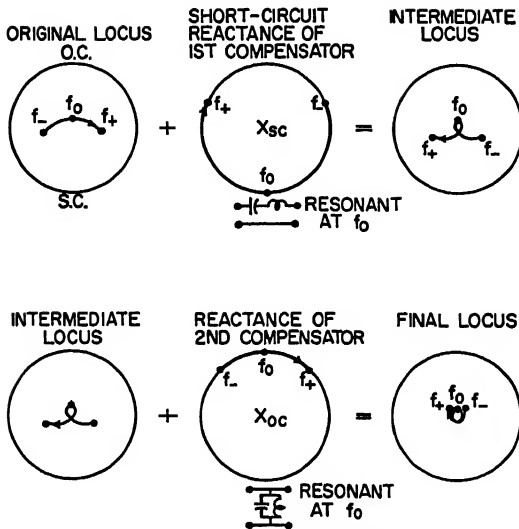
FIG. 31-26. A two-stage compensation method.
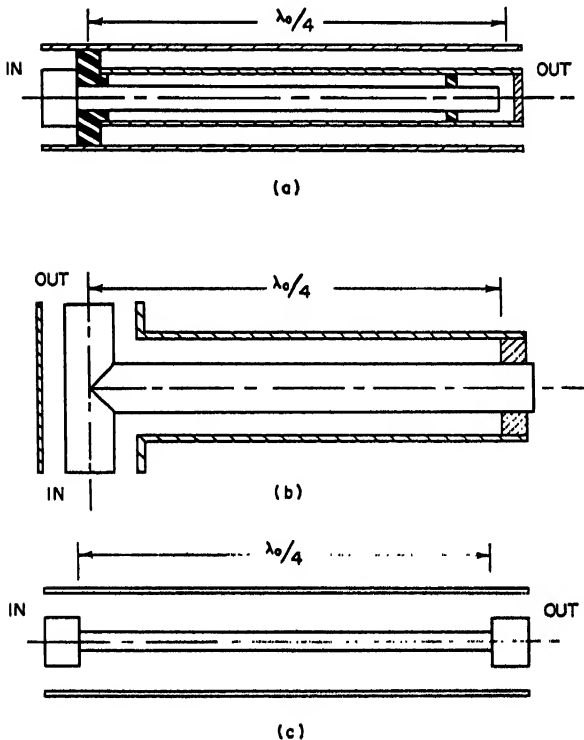
FIG. 31-27. Possible physical embodiments of compensation methods of Fig. 31-25.

process. Means for moving the impedance locus may include lumped or distributed constant elements forming shunt or series reactances, cascade transformers, or a combination of these. Selection is made to introduce as little adverse variation of impedance with frequency as possible.

Compensation of variation of impedance with frequency is usually limited to a band including less than one complete convolution of the original impedance locus if a high degree of compensation is required. Typically, a sector of the original impedance locus is selected which may be made to appear similar to those shown in Fig. 31-25. Then a matching circuit having a variation of reactance of opposite sense (and of the proper magnitude) is added to yield the tightly knotted transformed locus as shown. Essentially all the reactance variation may be eliminated; however, a small reactance variation and a larger resistance variation remain. In certain instances it may be advantageous to utilize two stages of compensation, as illustrated in Fig. 31-26, in order to accomplish a doubly knotted transformed locus. Note that the orientation of the Smith charts as shown in Figs. 31-25 and 31-26 is rotated 180° from the usual orientation of the Smith chart as shown in Fig. 31-3.
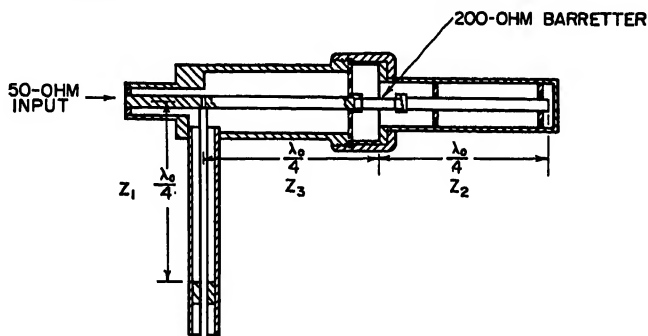
FIG. 31-28. Structure to match barretter to 50-ohm impedance.

There are many ways of forming these matching circuits into physical structures. A few simple examples are shown in Fig. 31-27. A more complex structure utilizing a transformer with two compensating stubs in a circuit described earlier in this chapter is shown in Fig. 31-28.

Resonant lengths of the transmission line may be used in place of the lumped-constant resonant circuits. The LC product or the length of the line is selected for resonance at f_0, the mid-frequency of the sector. The L/C ratio or the characteristic impedance of the line section is selected to give the proper amount of compensating reactance at f_+ and f_-, the edge-band frequencies.

31.8. DISSIPATIVE AND NONRECIPROCAL DEVICES

The methods for impedance matching described elsewhere in this chapter all employ means to introduce controlled nondissipative reflections to cancel or reduce the original reflection. By these methods the energy from the source is channeled efficiently to the load, with little or none allowed to reflect into the source. If it is of more importance to reduce the effect of the reflection upon the source than it is to maintain a high efficiency, it may be advantageous to use either a dissipative network or a nonreciprocal network and to accept a loss in the transmitted energy.

A dissipative network having a power ratio of attenuation k introduced between the source and load will cause a reduction in the reflection coefficient (at the source end, referred to the characteristic impedance of the network) by the factor k. Thus an attenuation of 1 db is required for each 2-db reduction of the reflection coefficient.

Nonreciprocal microwave devices are available as isolator units employing ferrite materials. In these the path of the reflected wave is made to terminate in a dissipative load rather than in the source itself. A typical design may give a reduction in the reflected wave at the source of 20 db or more with only a $\frac{1}{2}$- or $\frac{1}{4}$-db increase in attenuation for a matched load. The attenuation loss for a nonmatched load is increased by the reflection loss given by Fig. 31-2.

REFERENCES

General

1. R. W. Beatty and A. C. MacPherson: "Mismatch Errors," *Proc. IRE*, vol. 41, pp. 1112–1119, September, 1953.
2. W. L. Everitt and G. E. Anner: "Communication Engineering," 3d ed., McGraw-Hill Book Company, Inc., New York, 1956.
3. W. Jackson: "High Frequency Transmission Lines," 3d ed., John Wiley & Sons, Inc., New York, 1951.
4. N. Marcuvitz (ed.): Waveguide Handbook, McGraw-Hill Book Company, Inc., New York, 1951.
5. C. G. Montgomery, R. H. Dicke, and E. M. Purcell (eds.): "Microwave Circuits," McGraw-Hill Book Company, Inc., New York, 1948.
6. T. Moreno: "Microwave Transmission Design Data," McGraw-Hill Book Company, Inc., New York, 1948.
7. G. L. Ragan: "Microwave Transmission Circuits," McGraw-Hill Book Company, Inc., New York, 1948.
8. S. Roberts: "Conjugate-image Impedances," *Proc. IRE*, vol. 34, pp. 198–204, April, 1946.
9. S. A. Schelkunoff: "The Impedance Concept," *Bell System Tech. J.*, vol. 17, pp. 17–48, January, 1938.
10. S. A. Schelkunoff: "Electromagnetic Waves," D. Van Nostrand Company, Inc., Princeton, N.J., 1943.
11. Samuel Silver (ed.): "Microwave Antenna Theory and Design," McGraw-Hill Book Company, Inc., New York, 1949.
12. J. C. Slater: "Microwave Transmission," McGraw-Hill Book Company, Inc., New York, 1942.
13. C. G. Southworth: "Principles and Application of Waveguide Transmission," D. Van Nostrand Company, Inc., Princeton, N.J., 1950.
14. F. E. Terman: Radio Engineers' Handbook, McGraw-Hill Book Company, Inc., New York, 1943.
15. H. P. Westman: "Reference Data for Radio Engineers," 4th ed., International Telephone and Telegraph Corporation, New York, 1956.
16. M. Wind and H. Rappaport: "Handbook of Microwave Measurements," vols. I and II, Polytechnic Institute of Brooklyn, New York, 1954.
17. Radio Research Laboratory Staff: "Very High Frequency Techniques," vols. 1 and 2, McGraw-Hill Book Company, Inc., New York, 1947.
18. J. F. Reintjes and G. F. Coate: "Principles of Radar," 3d ed., McGraw-Hill Book Company, Inc., New York, 1946.

Transmission-line Impedance Charts

19. H. N. Dawirs: "A Chart for Analysing Transmission-line Filters from Input Impedance Characteristics," *Proc. IRE*, vol. 43, pp. 436–443, April, 1955.
20. H. N. Dawirs: "Application of the Smith Chart to General Impedance Transformations," *Proc. IRE*, vol. 45, pp. 954–956, July, 1957.
21. G. A. Deschamps: "A Hyperbolic Protractor for Microwave Impedance Measurements and Other Purposes," Federal Telecommunication Laboratories, Nutley, N.J., 1953.
22. W. Jackson and L. G. H. Huxley: "The Solution of Transmission-line Problems by the Use of the Circle Diagram of Impedance," *J. IEE* (London), pt. III, vol. 91, p. 105, 1944.
23. P. H. Smith: "An Improved Transmission Line Calculator," *Electronics*, vol. 17, pp. 130–133, January, 1944.
24. H. A. Wheeler: "Geometric Relations in Circle Diagrams of Transmission-line Impedance," Wheeler Monographs, vol. I, no. 4, Wheeler Laboratories, Great Neck, N.Y., 1953.

Lumped-constant-element Applications

25. W. A. Edson: "The Single-layer Solenoid as an RF Transformer," *Proc. IRE*, vol. 43, pp. 932–936, August, 1955.
26. R. G. Fellers and R. T. Weidner: "Broad-band Wave-guide Admittance Matching by Use of Irises," *Proc. IRE*, vol. 35, pp. 1080–1085, October, 1947.
27. L. Storch: "Design Procedures for Pi-network Antenna Couplers," *Proc. IRE*, vol. 37, p. 1427, December, 1949.
28. R. L. Tanner: "Antenna-matching Network Efficiency," *Electronics*, vol. 26, pp. 142–143, November, 1953.

Uniform Transmission-line-element Applications

29. S. B. Cohn: "Optimum Design of Stepped Transmission Line Transformers," *IRE Trans. on Microwave Theory Tech.*, vol. MTT-3, pp. 16–21, April, 1955.
30. R. E. Collin: "Theory and Design of Wide-band Multisection Quarter-wave Transformers," *Proc. IRE*, vol. 43, pp. 179–185, February, 1955.
31. R. E. Collin and J. Brown: "Transmission Line Matching System," *Wireless Eng.*, vol. 31, pp. 31–35, February, 1954.
32. E. G. Fubini and F. H. Rockett: "Bandwidth of Quarter-wave Sections," *Electronics*, vol. 25, p. 138, 1952.
33. S. Hopfer: "The Design of Ridged Waveguides," *IRE Trans. on Microwave Theory Tech.*, vol. MTT-3, pp. 20–29, October, 1955.
34. R. W. Klopfenstein: "The Design of Transmission-line Tuning Elements for Minimum Dissipation," *Proc. IRE*, vol. 39, pp. 1089–1094, September, 1951.
35. A. A. Meyerhoff and R. Graham, Jr.: "Fixed Length Lines as Circuit Elements," *Proc. IRE*, vol. 41, p. 262, February, 1953.
36. H. J. Riblet: "General Synthesis of Quarter-wave Impedance Transformers," *IRE Trans. on Microwave Theory Tech.*, vol. MTT-5, pp. 36–43, January, 1957.
37. H. J. Rowland: "The Series Reactance in Coaxial Lines," *Proc. IRE*, vol. 36, pp. 65–69, January, 1948.
38. H. Salinger: "The Quarter-wave Step-up Transformer," *Proc. IRE*, vol. 32, pp. 553–556, September, 1944.
39. H. A. Wheeler: "Transmission Lines and Equivalent Circuits," Wheeler Monographs, vol. I, no. 1, Wheeler Laboratories, Great Neck, N.Y., 1953.
40. M. S. Wheeler: "Two-section Transmission-line Transformer," *Wireless Eng.*, vol. 32, pp. 15–18, January, 1955.
41. J. R. Whinnery and H. W. Jamieson: "Equivalent Circuits for Discontinuities in Transmission Lines," *Proc. IRE*, vol. 32, pp. 98–116, February, 1944.
42. J. R. Whinnery, H. W. Jamieson, and T. E. Robbins: "Coaxial-line Discontinuities," *Proc. IRE*, vol. 32, pp. 695–709, November, 1944.

Tapered Transmission Lines

43. E. F. Bolinder: "Fourier Transforms and Tapered Transmission Lines," *Proc, IRE*, vol. 44, p. 557, April, 1956.
44. E. F. Bolinder: "Fourier Transforms in the Theory of Inhomogeneous Transmission Lines," *Proc. IRE*, vol. 38, p. 1354, November, 1950.
45. C. R. Burrows: "The Exponential Transmission Line," *Bell System Tech. J.*, vol. 17, pp. 555–573, October, 1938.
46. A. Chlavin: "Matching Non-standard Waveguide Sections," *Electronics*, vol. 26, pp. 192–193, November, 1953.
47. W. N. Christiansen: "An Exponential Transmission Line Employing Straight Conductors," *Proc. IRE*, vol. 35, p. 576, June, 1947.
48. S. B. Cohn: "Wave-guide-to-coaxial-line Junctions," *Proc. IRE*, vol. 35, pp. 920–926, September, 1947.
49. R. E. Collin: "The Optimum Tapered Transmission Line Matching Section," *Proc. IRE*, vol. 44, pp. 539–547, April, 1956.
50. N. Ghose: "Exponential Transmission Lines as Resonators and Transformers," *IRE Trans. on Microwave Theory Tech.*, vol. MTT-5, no. 3, pp. 213–217, July, 1957.
51. J. G. Gurley: "Impedance Matching by Means of Nonuniform Transmission Lines," *IRE Trans.*, vol. PGAP-4, pp. 107–109, December, 1952.
52. R. W. Klopfenstein: "A Transmission Line Taper of Improved Design," *Proc. IRE*, vol. 44, pp. 31–35, January, 1956.
53. B. J. Migliaro: "Designing Tapered Waveguide Transitions," *Electronics*, vol. 30, pp. 183–185, November, 1957.

54. J. R. Pierce: "A Note on the Transmission Line Equation in Terms of Impedance," *Bell System Tech. J.*, vol. 22, pp. 263–265, 1943.
55. H. J. Scott: "The Hyperbolic Transmission Line as a Matching Section," *Proc. IRE*, vol. 41, pp. 1654–1657, November, 1953.
56. L. Solymar: "On Higher Order Approximations to the Solution of Nonuniform Transmission Lines," *Proc. IRE*, vol. 43, pp. 1547–1548, November, 1957.
57. L. R. Walker and N. Wax: "Nonuniform Transmission Lines and Reflection Coefficients," *J. Appl. Phys.*, vol. 17, pp. 1043–1045, December, 1946.
58. H. A. Wheeler: "Transmission Lines with Exponential Taper," *Proc. IRE*, vol. 27, pp. 65–71, January, 1939.
59. J. Willis and N. K. Sinha: "Nonuniform Transmission Lines as Impedance Matching Sections," *Proc. IRE*, vol. 43, p. 1975, December, 1955.
60. R. F. H. Yang: "Parabolic Transmission Line," *Proc. IRE*, vol. 43, p. 1010, August, 1955.

Baluns

61. L. J. Cutrona: "Biconjugate Networks," *Proc. IRE*, vol. 39, pp. 827–832, July, 1951.
62. E. G. Fubini and P. J. Sutro: "A Wide-band Transformer from an Unbalanced to a Balanced Line," *Proc. IRE*, vol. 35, pp. 1153–1155, October, 1947.
63. W. K. Roberts: "A New Wide-band Balun," *Proc. IRE*, vol. 45, pp. 1628–1631, December, 1957.
64. O. M. Woodward, Jr.: "Balance Measurements on Balun Transformers," *Electronics*, vol. 26, pp. 188–191, September, 1953.

Broadbanding

65. F. D. Bennett, P. D. Coleman, and A. S. Meier: "The Design of Broad-band Aircraft-Antenna Systems," *Proc. IRE*, vol. 32, pp. 671–700, October, 1945.
66. R. M. Fano: "Theoretical Limitations on the Broad-band Matching of Arbitrary Impedance," *J. Franklin Inst.*, vol. 249, no. 1, p. 57, January, 1950, and no. 2, February, 1950.
67. E. Green: "Amplitude-frequency Characteristics of Ladder Networks," Marconi's Wireless Telegraph Co., Essex, England, 1954.
68. W. C. Jakes, Jr.: "Broad-band Matching with a Directional Coupler," *Proc. IRE*, vol. 40, pp. 1216–1218, October, 1952.
69. W. W. Mumford: "The Optimum Piston Position for Wide-band Coaxial-to-waveguide Transducers," *Proc. IRE*, vol. 41, p. 256, February, 1953.
70. V. H. Rumsey: "The Design of Frequency-compensating Matching Sections," *Proc. IRE*, vol. 38, pp. 1191–1196, October, 1950.
71. A. Vassiliadis and R. L. Tanner: "Evaluating the Impedance Broadbanding Potential of Antennas," *IRE Nat. Convention Record*, pt. 1, pp. 108–113, 1957.

Chapter 32

RADOMES AND ABSORBERS

ALAN F. KAY

Technical Research Group
Somerville, Massachusetts

32.1. GENERAL DISCUSSION

Functions of a Radome. Many microwave antennas and some UHF antennas require a housing, or radome, to fill one or more of the following requirements:

1. Protection against weather, including wind, rain, and icing.

2. Proper incorporation into the streamlined structure of an airplane or guided missile.

3. Provision for pressurizing.

4. Reduction of scanning-power requirements.

5. Matching of feed horns.

Apart from requirement 5, these are mechanical needs which must be met without impairment of the performance of the antenna electrically. Radomes are generally
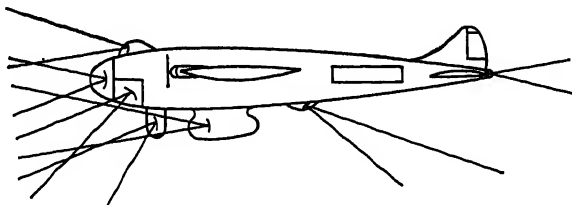
Fɪɢ. 32-1. Possible airborne radome shapes.

low-loss dielectrics of thickness comparable to a wavelength which are shaped to cover the antenna and, if necessary, conform to aerodynamic streamlining (Fig. 32-1). Radomes are used with virtually all aperture-type airborne antennas and many ground-based and shipboard aperture antennas which must withstand severe weather conditions or have a rapid scan rate. Gridded or perforated reflectors, which are not airborne, are less likely to need radomes.

Electrical Problems. Radomes can distort the fields of antennas in many ways. They may change the phase and amplitude of the incident wave, and this change may be a function of the position of the radome with respect to the beam cross section. This in general produces an error in gain, beamwidth, side-lobe level, and other pattern characteristics, all of which may be appreciable (Fig. 32-2). The radome may cause depolarization or rotation of polarization. Radomes may also reflect or absorb an appreciable portion of the energy from the beam, which may reduce the range, cause magnetron pulling, or change the effective impedance of the antenna. Radome distortion may be sufficiently bad to cause disappearance of signals by magnetron pulling, signals from spurious directions by reflection, or slight shifting of the apparent signal direction by refraction and diffraction.

In an analysis of these effects, it is often sufficient to replace the curved radome wall locally by a plane wall of the same cross section. The reflected and transmitted waves may then be determined from plane-sheet theory, and if these are a sufficiently good approximation, the results can be translated into estimates of the electrical effects, for which the radome is responsible. With the exception of feed-matching radomes, an ideal radome wall acts electrically like free space. This would be true if the radome were totally transmitting and its transmission insert phase were constant independent of incidence angle and polarization. Achievement of transmission close to 100 per cent (or of reflection and absorption close to zero) and of nearly constant insert phase are thus measures of the excellence of any radome.

Mechanical Problems. Radome mechanical problems may be quite mild, as in the case of a beacon in a small cylindrical radome; or as in the case of a supersonic nose radome, they may be so severe that the electrical requirements must be modified.

Ordinary solutions to mechanical-strength problems are not satisfactory. Only certain wall cross sections are permissible, and supporting ribs generally may not be placed on that part of the radome through which energy is transmitted.

Strength. All operational radomes must be able to withstand rough handling. Airborne radomes have to meet aerodynamic loading requirements and, if possible, the ditching load requirements in the case of a forced landing. Ground and shipboard radomes may have to withstand hurricane-force winds. In some systems, pressurizing the radome instead of only the r-f transmission line places a tensile stress on the radome.

Stiffness. Some deformation of the radome in operation may be tolerated; radome electrical performance is generally not as sensitive to shape changes as to dimensionally comparable wall cross-section errors. Deformation inhibiting the motion

DETAILS
9375 MC
12-INCH DISH
———— WITHOUT RADOME
– – – – WITH RADOME
10° GIMBAL ANGLE
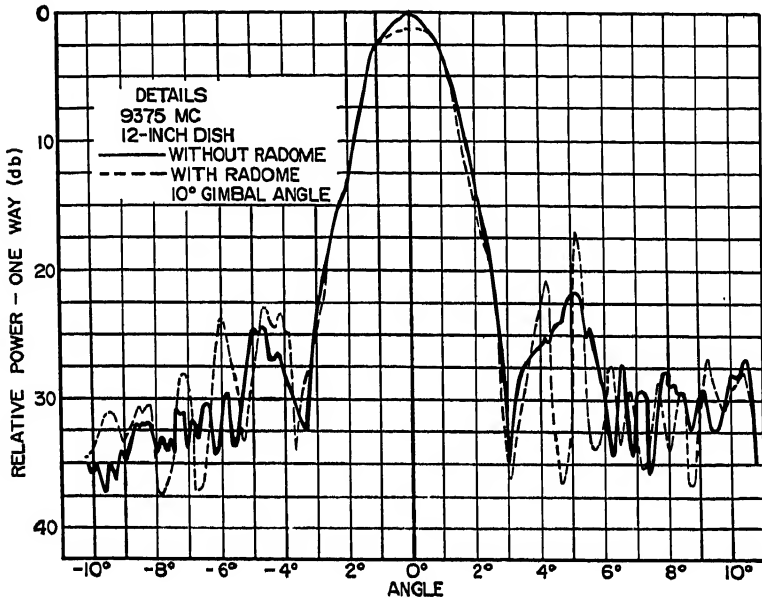
Fig. 32-2. Typical radiation patterns showing the effect of the radome.

of a scanning antenna or inelastic deformations which lead to permanent impairment of electrical properties and structural breakdown cannot be permitted.

Heating. High-speed airborne radomes may encounter extremely high temperatures due to aerodynamic heating. Other radomes encounter high temperature from the direct heat of the sun. Most common radome materials deteriorate both structurally and electrically in the temperature range 175 to 500°F.

Absorption of Water. Absorbed water increases the dielectric constant and loss tangent of the radome wall. Hygroscopic radome materials should be avoided. Materials which absorb water on immersion because of pores or voids require a protective coating. A weight increase of less than 6 per cent at equilibrium in an atmosphere at 100 per cent relative humidity and 125°F is generally acceptable.

Abrasion and Erosion. Dust and small stones may cause wear to aircraft radomes, especially at take-off and landing. Pitting due to raindrops can cause damage to aircraft nose radomes at speeds over 350 mph. Up to 600 mph, elastomeric coatings of neoprene compounds are used to inhibit erosion.

Weight. Weight considerations are very important for medium-size or large airborne radomes and for the very large ground-based radomes. Thin-wall radomes ranging in weight from 0.2 to 2 psf and A-sandwich radomes weighing 1 to 3 psf are employed for these applications.

Icing. Ground, ship, and aircraft radomes may gather ice during unfavorable weather conditions. Even a thin ice coating may impair the electrical performance of the radome and must be removed by the application of heat or de-icing sprays. Mechanical removal by de-icing boots is electrically unsatisfactory.

Gun Blast. Radomes for gun-laying radar may have to withstand sudden pressure from gun blast. A 20-mm gun muzzle should not be closer than about 10 in. from a radome. Radome blast resistance is relatively independent of wall construction, but a spherical shape stands up considerably better than a flat panel of the same construction.

Common Radome Classifications. *Wall Structures.* The simplest type is the single homogeneous layer whose thickness is electrically a multiple of a half wavelength: $d = n\lambda/2(\epsilon/\epsilon_0 - \sin^2 \theta)^{1/2}$, where d is thickness, n is an integer, ϵ/ϵ_0 is relative dielectric constant, θ is incidence angle, and λ is wavelength. If ohmic wall losses may be neglected, as is usually the case, such a wall is nonreflecting at the specified incidence angle and wavelength and any polarization. The two most common types are the *half-wave wall*, when $n = 1$, and the *thin wall*, when $d \ll \lambda/2(\epsilon/\epsilon_0 - \sin^2 \theta)^{1/2}$, which is the practical approximation to the $n = 0$ case.

Multilayered walls are employed for structural reasons. Apart from surface-finish treatments, they are almost always symmetrical with respect to the cross-section center line, and hence consist of an odd number of layers. By far the most common is the ordinary, or A sandwich (Fig. 32–24). This is a three-layered wall whose core has a low dielectric constant relative to the outer layers, or skins. The core is approximately a quarter wavelength thick, and the skins are thin compared with a wavelength. The B sandwich is also three-layered with a thin core of high-dielectric material and quarter-wavelength skins. Five-, seven-, and even nine-layer walls are sometimes used when great strength is required, coupled with some weight limitations. The simplest of these is the C sandwich: two A sandwiches back to back.

Shape. Radome problems are considerably aggravated if the radome must be streamlined. If the radome need not be streamlined, then a shape is generally chosen so that the maximum incidence angle of the rays from the antenna is less than 30°. The reflection and transmission formulas (Sec. 32.2) are substantially independent of incidence angle and polarization in the range 0 to 30°, so that these radomes are classified as *normal-incidence* radomes and the normal-incidence formulas are applied. All other radomes are considered *streamlined.* Normal-incidence radomes are sometimes called cylindrical radomes, although some radomes of this type are flat, spherical, parabolic, etc. Common streamlined radome shapes are ogive, ellipsoidal, conical, and log-spiral.

Application. Large *ground-based* radomes are used for early-warning radar. They may be rigid or flexible. *Airborne* radomes are lightweight, strong, and often streamlined. *Pressure seals* for antenna feeds are small normal-incidence radomes.

32.2. SINGLE-WALL RADOMES

Single-wall radomes are frequently used in ground and shipboard applications and less frequently with airborne antennas where large strength-weight-ratio requirements call for a sandwich construction.

General formulas for the complex reflection and transmission coefficients of the single wall are as follows:

$$\rho = \frac{r[1 - \exp(-2\varphi L_0 - 2j\varphi)]}{1 - r^2 \exp(-2\varphi L_0 - 2j\varphi)} \tag{32-1}$$

$$\tau = \frac{(1 - r^2)\exp(-\varphi L_0 - j\varphi)}{1 - r^2 \exp(-2\varphi L_0 - 2j\varphi)} \tag{32-2}$$

Here φ is 2π times the electrical thickness.*

$$\varphi = \frac{2\pi d}{\lambda}\left(\frac{\epsilon}{\epsilon_0} - \sin^2\theta\right)^{\frac{1}{2}} \qquad \text{radians} \tag{32-3}$$

where θ = incidence angle (measured from normal)

d/λ = thickness, wavelengths

L_0 is the attenuation due to loss given by

$$L_0 = \frac{(\epsilon/\epsilon_0)\tan\delta}{2(\epsilon/\epsilon_0 - \sin^2\theta)}$$

and r is the Fresnel (interface) reflection coefficient given by

$$r = \frac{1 - \sqrt{\epsilon_e} + jL_1}{1 + \sqrt{\epsilon_e} - jL_1} \tag{32-4}$$

where ϵ_e is the equivalent relative dielectric constant (Figs. 32-3 and 32-4) given by

$$\epsilon_e = \begin{cases} \dfrac{(\epsilon/\epsilon_0) - \sin^2\theta}{\cos^2\theta} & \text{(perpendicular polarization)}\dagger \\[3mm] \dfrac{(\epsilon/\epsilon_0)^2\cos^2\theta}{(\epsilon/\epsilon_0) - \sin^2\theta} & \text{(parallel polarization)}\dagger \end{cases} \tag{32-5}$$

and L_1 is the reactance due to loss:

$$L_1 = \begin{cases} \dfrac{(\epsilon/\epsilon_0)\tan\delta}{2\cos\theta[(\epsilon/\epsilon_0) - \sin^2\theta]^{\frac{1}{2}}} & \text{(perpendicular polarization)} \\[3mm] \dfrac{(\epsilon/\epsilon_0)\tan\delta[(\epsilon/\epsilon_0) - 2\sin^2\theta]\cos\theta}{2[(\epsilon/\epsilon_0) - \sin^2\theta)]^{\frac{3}{2}}} & \text{(parallel polarization)} \end{cases}$$

In these and later formulas we observe the customary radome convention of considering the negative of the actual reflection coefficient for parallel polarization. Under this convention the reflection or transmission formulas for perpendicular and parallel polarization are equal when $\theta = 0$.

The preceding formulas neglect loss terms of order $\tan^2\delta$. This approximation is satisfactory for all usable radome materials, except at very oblique incidence angles.

Lossless Case. If we neglect loss entirely, the power reflection and transmission coefficients reduce to

$$|\rho|^2 = \frac{4r^2\sin^2\varphi}{(1 - r^2)^2 + 4r^2\sin^2\varphi} = \frac{1}{\dfrac{4\epsilon_e}{(1 - \epsilon_e)^2\sin^2\varphi} + 1} \tag{32-6a}$$

$$|\tau|^2 = \frac{(1 - r^2)^2}{(1 - r^2)^2 + 4r^2\sin^2\varphi} = \frac{1}{1 + \dfrac{(1 - \epsilon_e)^2\sin^2\varphi}{4\epsilon_e}} \tag{32-6b}$$

and we obtain the conservation of energy:

$$|\rho|^2 + |\tau|^2 = 1 \tag{32-7a}$$

* Also known as the optical path length, in geometrical optics.

† For perpendicular polarization, the electric vector is perpendicular to the plane of incidence. For parallel polarization, the electric vector is in the plane of incidence. (*Note:* The plane of incidence is defined as the plane containing a ray and the normal to the surface that it intersects.)
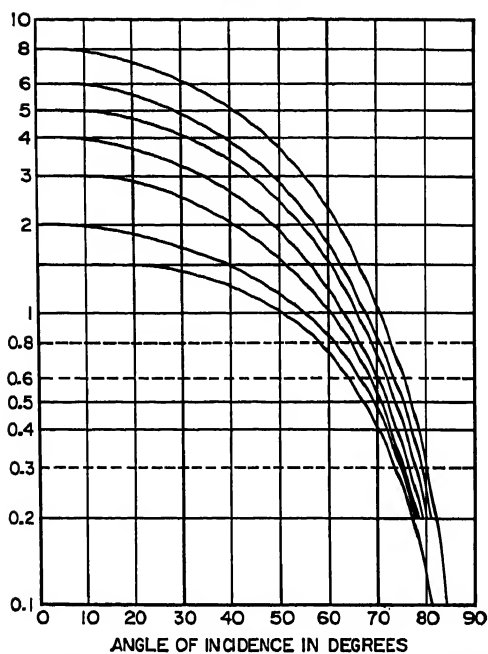
FIG. 32-3. Effective dielectric constants (parallel polarization).
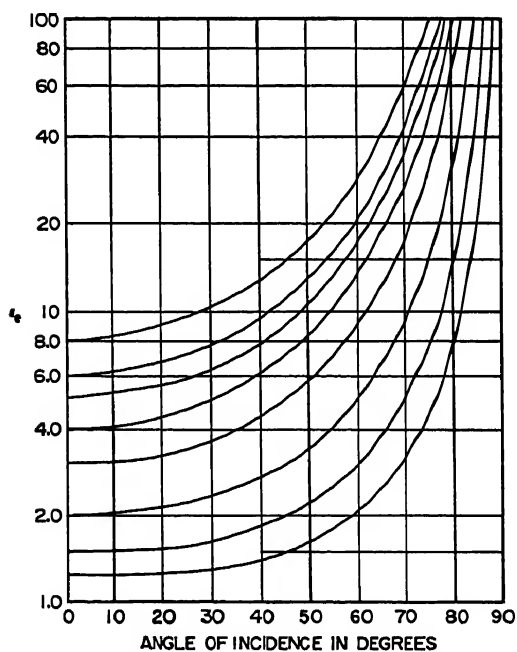
FIG. 32-4. Effective dielectric constants (perpendicular polarization).

Since the phase of the reflection coefficient and the phase of the transmission coefficient are related by

$$\angle \tau - \angle \rho = \pm \frac{\pi}{2} \qquad (32\text{-}7b)$$

either coefficient serves to determine the other (apart from the sign ambiguity) by means of Eqs. (32-7a) and (32-7b). From Eqs. (32-6) it follows that $\rho = 0$ if φ is a multiple of π or if

$$d = \frac{n\lambda}{2[(\epsilon/\epsilon_0) - \sin^2 \theta]^{\frac{1}{2}}} \qquad (32\text{-}8)$$

Here n is an integer called the order of the radome. The case $n = 1$ is the "half-wave wall." The value of θ for which Eq. (32-8) holds is called the *design angle*.
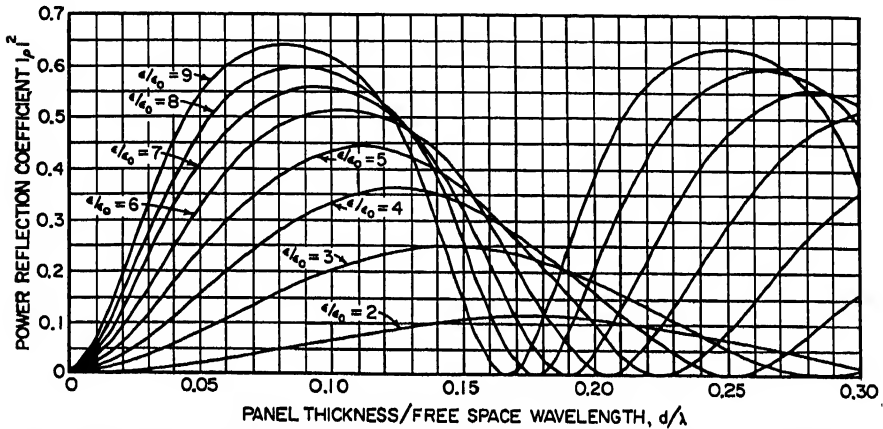
FIG. 32-5. Power-reflection coefficient of a lossless dielectric sheet at normal incidence.

Reflection will be exactly zero at the design angle. ρ is also zero when $r = 0$; this occurs only with parallel polarization at Brewster's angle θ_B.

$$\theta_B = \tan^{-1} \sqrt{\frac{\epsilon}{\epsilon_0}} \qquad (32\text{-}9)$$

As a function of thickness or frequency the power reflection and transmission alternate through maxima and minima. Maximum reflection, and hence minimum transmission, occurs at odd multiples of the quarter-wavelength thickness. These values are

$$|\rho|^2_{\min} = 0 \qquad |\rho|^2_{\max} = \left(\frac{2r}{1 + r^2}\right)^2 \qquad (32\text{-}10a)$$

$$|\tau|^2_{\max} = 1 \qquad |\tau|^2_{\min} = \left(\frac{1 - r^2}{1 + r^2}\right)^2 \qquad (32\text{-}10b)$$

This behavior is illustrated in Fig. 32-5. Figure 32-6 offers a convenient method for obtaining $|\rho|^2$ in terms of $(d/\lambda)[(\epsilon/\epsilon_0) - \sin^2 \theta]^{\frac{1}{2}}$ and r. A useful type of plot for design purposes shows contours of constant power reflection vs. wall thickness in wavelengths and incidence angle, as shown in Figs. 32-7 to 32-10. These graphs show that while the horizontal zero reflection contours* are independent of polarization, the reflection coefficient otherwise is very much polarization-dependent. In particular, the contour which occurs at Brewster's angle for parallel polarization does

---

* These are the curves defined by Eqs. (32-6).

not appear at perpendicular polarization. The transverse zero reflection contours are steeper at higher orders (only orders $n = 0$, 1, and 2 are shown), but this behavior is general. For a given thickness and incidence angle, reflection at parallel polarization is always less than at perpendicular polarization.

We observe that as ϵ increases, the nonzero reflection contours hug the horizontal zero reflection contours more closely and the latter become flatter. This shows that at high values of ϵ, low reflection may be obtained over a wider range of high-incidence angles but that small thickness tolerances must be maintained.
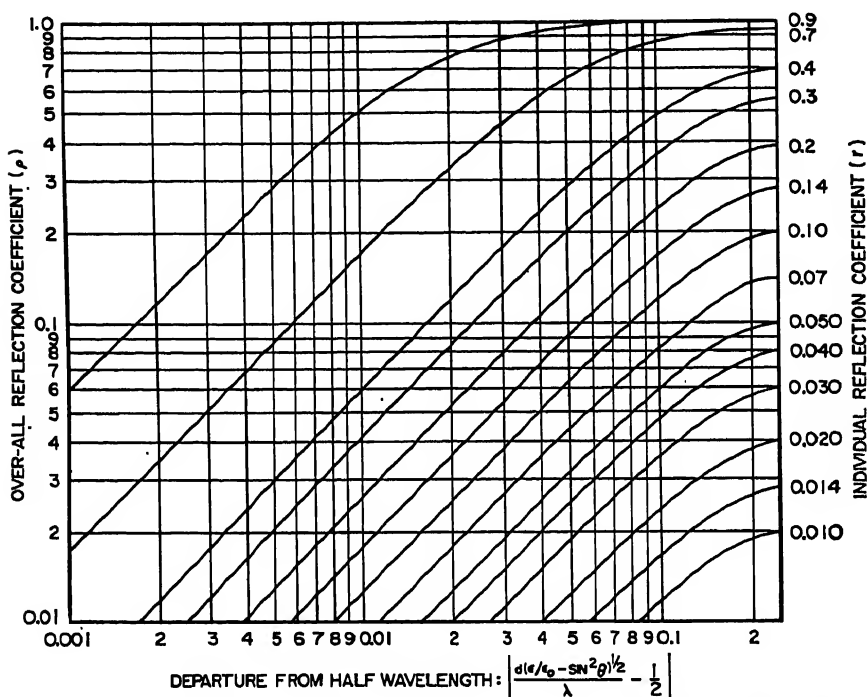
FIG. 32-6. Over-all reflection coefficient (ρ) for a symmetrical configuration of zero absorption plotted as a function of the departure from electrical half-wave thickness and the skin reflection coefficient r.

The insert phase Φ, which is the quantity of interest in radome phase-distortion considerations, is given by

$$\Phi = -\angle\tau - \frac{2\pi d \cos \theta}{\lambda}$$

$$= \tan^{-1}(A \tan \varphi) - \frac{2\pi d \cos \theta}{\lambda} \qquad \text{radians} \qquad (32\text{-}11)$$

where

$$A = \frac{1+r^2}{1-r^2} = \begin{cases} \dfrac{(\epsilon/\epsilon_0) + 1 - 2 \sin^2 \theta}{2 \cos \theta[(\epsilon/\epsilon_0) - \sin^2 \theta]^{1/2}} & \text{(perpendicular polarization)} \\ \dfrac{(\epsilon/\epsilon_0)^2 \cos^2 \theta + \epsilon/\epsilon_0 - \sin^2 \theta}{2(\epsilon/\epsilon_0) \cos \theta[(\epsilon/\epsilon_0) - \sin^2 \theta]^{1/2}} & \text{(parallel polarization)} \end{cases} \qquad (32\text{-}12)$$

The factor A is a correction which takes account of multiple reflections between the interfaces of the panel. When this may be neglected (i.e., taken equal to unity),
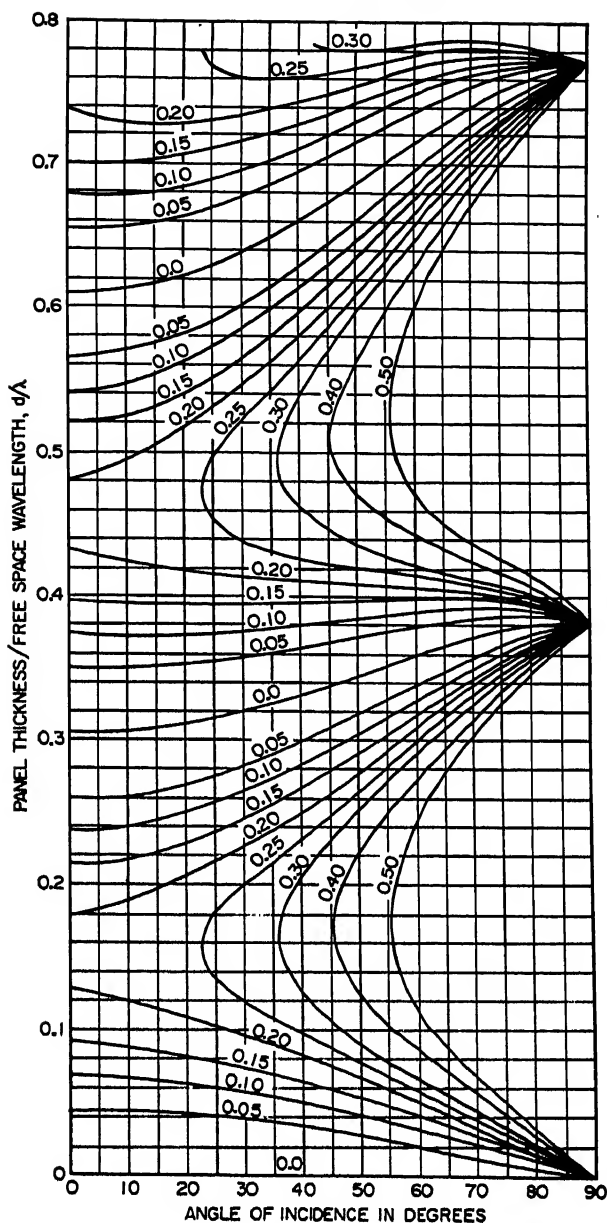
FIG. 32-7. Contours of constant power reflection (perpendicular polarization, dielectric constant = 2.7 ϵ_0).

the insert phase Φ is simply the difference between the electrical thickness of the panel φ and that of free space. The inverse tangent in Eq. (32-11) must be taken in the same quadrant as φ. Figure 32-11 shows a plot of insert phase vs. incidence angle of a ¼-inch K-band panel for various values of ϵ at parallel polarization. The behavior is typical: insert phase is always an increasing function both with respect
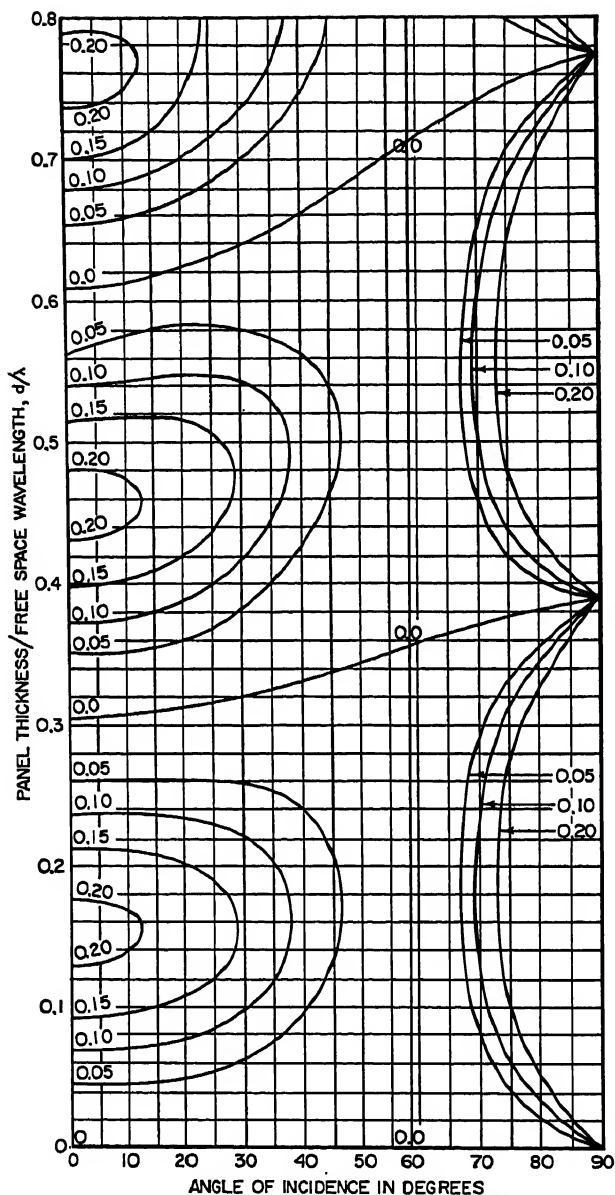
Fig. 32-8. Contours of constant power reflection (parallel polarization, dielectric constant $= 2.7 \, \epsilon_0$).

to ϵ and d for any fixed incidence angle and either polarization. Insert phase is also an increasing function of θ except at oblique angles. If the curves of Fig. 32-11 were continued to $\theta = 90°$, all of them would pass through one of a sequence of nodal points $\varphi = (2n + 1)\pi/2$, where $n = 0, 1, 2$, etc. Some would turn down in order to do so. For these, therefore, the insert phase decreases with θ at oblique angles.

Figures 32-12 and 32-13 show the dependence of insert phase at perpendicular polarization on the thickness-to-wavelength ratio for various incidence angles and for values of $\epsilon = 2\epsilon_0$ and $6\epsilon_0$, respectively. Figures 32-14 and 32-15 show the same quantities at parallel polarization. The variation V of insert phase with incidence angle, which is defined by $V = \partial\Phi/\partial\theta$, is a quantity of interest for streamlined radome design. From these figures we observe that, while not particularly sensitive to ϵ, V is proportional to d/λ, modified by a modulation of half-wave periodicity which causes a relative decrease in V near multiples of the electrical half-wave thickness and a relative increase in V near odd multiples of the electrical quarter-wave thickness.
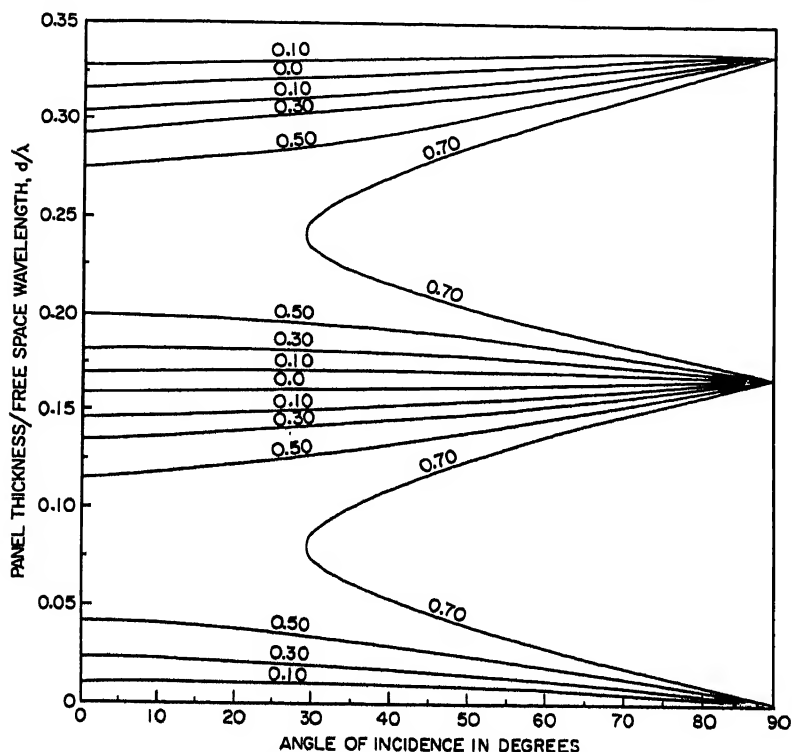
FIG. 32-9. Contours of constant power reflection (perpendicular polarization, dielectric constant = 10 ϵ_0).

Thin Radomes. Whenever it is structurally permissible, a sufficiently thin radome offers the most satisfactory electrical wall. The possibility of using a thin radome depends on the minimum thickness structurally tolerable (Sec. 32.4) and the required transmission properties. The maximum thickness for 90 and 95 per cent power transmission is shown in Fig. 32-16 as a function of incidence angle and dielectric constant. Suppose 90 per cent transmission is desired with a dielectric constant of 4 and an angle of incidence of 56°. From the figure, d/λ cannot exceed 0.02. If $\lambda = 12$ in. (L band), d cannot exceed 0.24 in. This may be structurally sufficient. But if $\lambda = 0.5$ in. (K band), d cannot exceed 0.01 in. and such a wall would not be structurally satisfactory for a rigid radome.

Approximate formulas for the power reflection and transmission coefficient valid if the electrical thickness is less than an eighth wavelength and if the amplitude
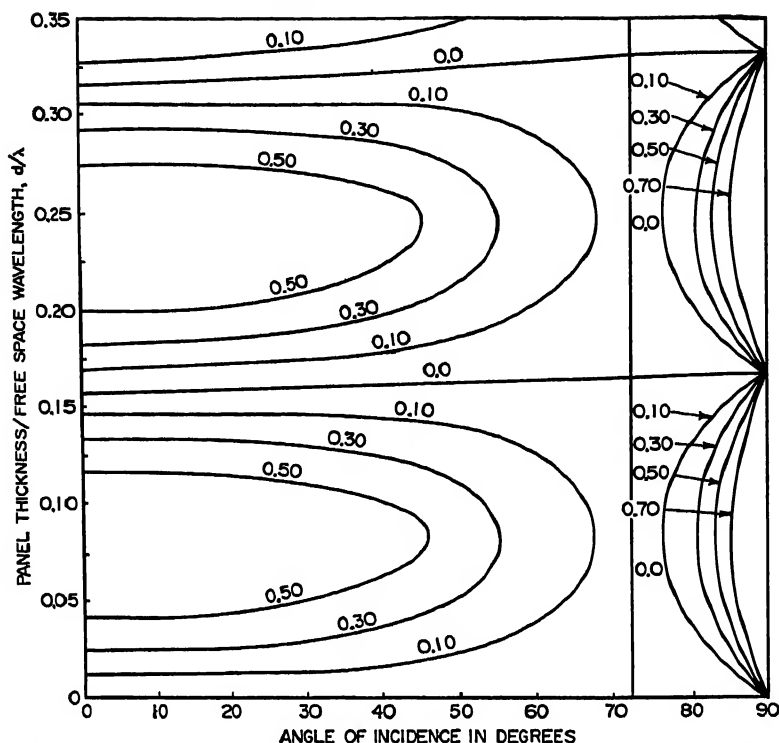
FIG. 32-10. Contours of constant power reflection (parallel polarization, dielectric constant = 10 ϵ_0).

reflection is small are

$$|\rho|^2 = \frac{(\epsilon_e - 1)^2}{\epsilon_e}\left(\frac{\pi d}{\lambda}\right)^2\left(\frac{\epsilon}{\epsilon_0} - \sin^2\theta\right) \tag{32-13}$$

$$|\tau|^2 = 1 - \frac{(\epsilon_e - 1)^2}{\epsilon_e}\left(\frac{\pi d}{\lambda}\right)^2\left(\frac{\epsilon}{\epsilon_0} - \sin^2\theta\right) \tag{32-14}$$

If the electrical thickness is less than an eighth wavelength and if the interface reflection coefficient r is not large, the insert phase becomes approximately

$$\Phi = \begin{cases} \dfrac{\pi d[(\epsilon/\epsilon_0) - 1]}{\lambda\cos\theta} & \text{(perpendicular polarization)} \\[2ex] \dfrac{\pi d[(\epsilon/\epsilon_0)\cos^2\theta + \sin^2\theta][(\epsilon/\epsilon_0) - 1]}{\lambda\epsilon\cos\theta/\epsilon_0} & \text{(parallel polarization *)} \end{cases} \tag{32-15}$$

Design for Normal Incidence. A normal-incidence radome is used whenever streamlining is not required. If the angles of incidence of rays transporting appreciable energy from the antenna to the radome wall are all less than 30°, the radome is considered a normal-incidence radome even though it may appear quite streamlined

---

* Formulas (32-13) to (32-15) also give the approximate power reflection and transmission coefficients and insert phase for panels nearly n half waves thick if d is interpreted as the difference between the actual thickness and the n half-wave thickness, the latter given by Eq. (32-8). Thus these formulas also give the effect of thickness tolerances for thick single-wall radomes.
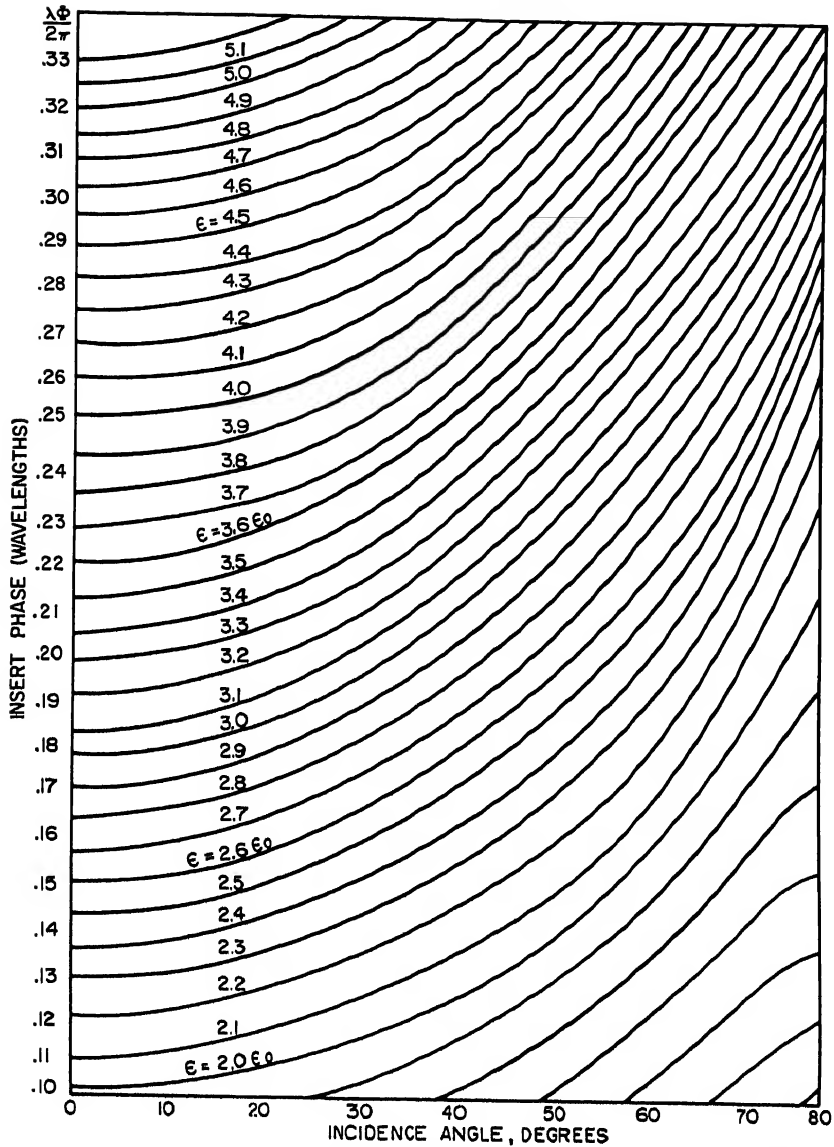
Fig. 32-11. Insert phase vs. dielectric constant and incidence angle ($d/\lambda = 0.508$).

because of fairing or because the electrical area of the radome does not include the highly curved regions (Fig. 32-17).

The shape of the radome is not critical to its electrical performance; any smooth surface is satisfactory in which the curvature is kept uniformly low and which fairs into the mounting structure properly, provided sufficient clearance with regard to the antenna is maintained.

A low-loss dielectric material with satisfactory mechanical properties such as a Fiberglas and polyester resin laminate is used for the wall itself. Normal-incidence
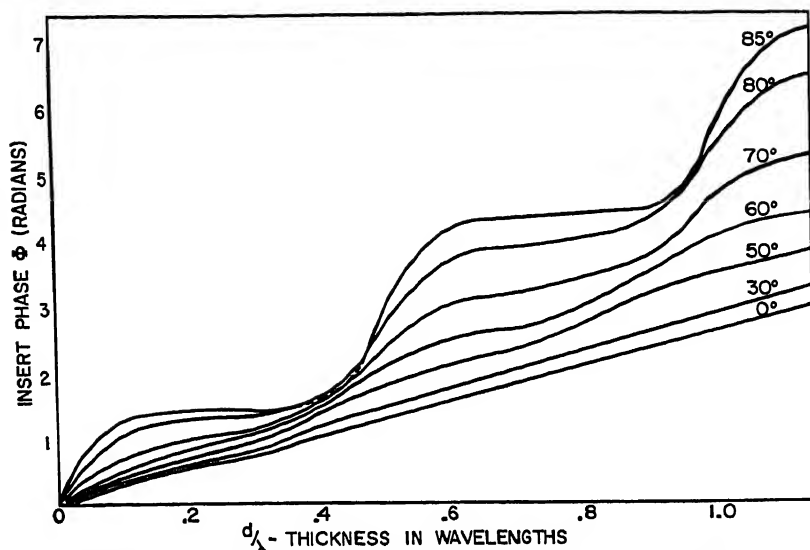
FIG. 32-12. Insert phase of plane sheet, $\epsilon = 2\epsilon_0$, perpendicular polarization.
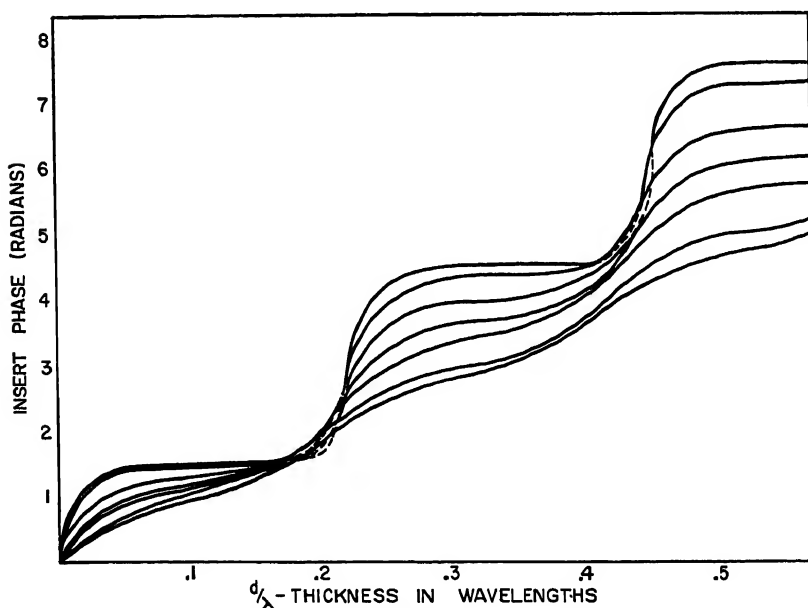
FIG. 32-13. Insert phase of plane sheet, $\epsilon = 6\epsilon_0$, perpendicular polarization.

radomes do not have the problem of minimization of reflection or transmission-insert-phase variation over a wide range of angles such as streamlined radomes do. The dielectric constant is generally chosen lower than in the case of streamlined radomes. The lower dielectric constant yields larger thickness tolerances. This is demonstrated for the half-wave wall in Table 32-1 where the maximum error in thickness Δd divided by wavelength λ is shown for various maximum permissible power-reflec-
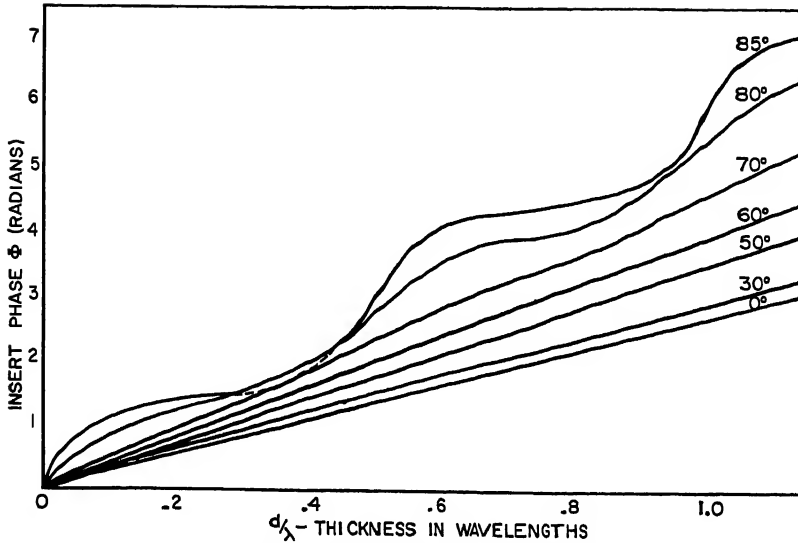
FIG. 32-14. Insert phase of plane sheet, $\epsilon = 2\epsilon_0$, parallel polarization.
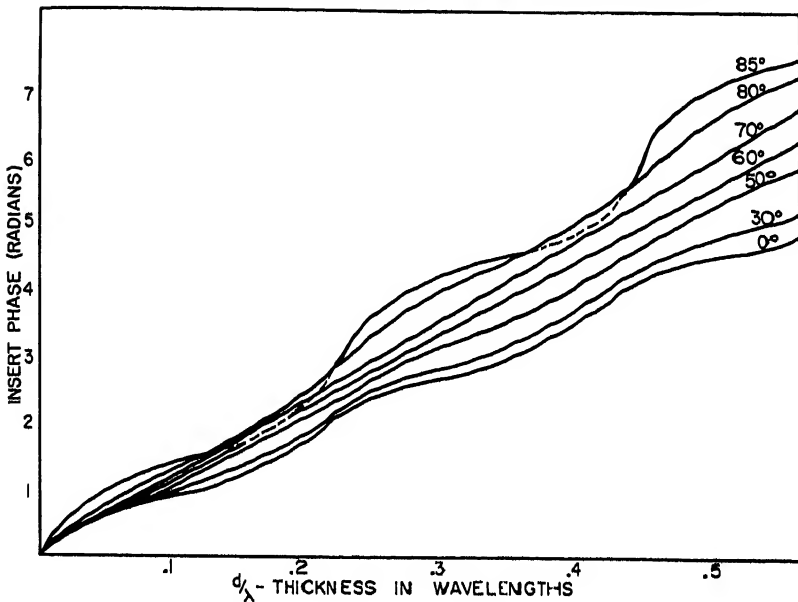
FIG. 32-15. Insert phase of plane sheet, $\epsilon = 6\epsilon_0$, parallel polarization.

tion coefficients and values of dielectric constant. Transmission loss due to absorption is also less for low values of ϵ (Fig. 32-18) and a fixed loss tangent.

If the radome is to be made of a single layer, an optimum thickness is chosen. The amplitude reflection coefficient is made as small as possible in order to minimize transmitted power losses and to reduce reflection back into the antenna transmission line. For the half-wave wall, the optimum thickness will be slightly less than the

Table 32-1. Tolerances in Half-wavelength Thicknesses of Homogeneous Panels

$\dfrac{\epsilon}{\epsilon_0}$	Values of $\dfrac{\Delta d}{\lambda_0}$		
	$\lvert\rho\rvert^2 = 0.01$	$\lvert\rho\rvert^2 = 0.02$	$\lvert\rho\rvert^2 = 0.04$
2	0.033	0.047	0.069
4	0.011	0.015	0.022
10	0.004	0.005	0.007

value given by Eq. (32-8), if loss is taken into consideration. This is indicated in Fig. 32-19, where the first maxima after $d = 0$ are seen to occur for values of $(d/\lambda)(\epsilon/\epsilon_0)^{1/2}$ less than 0.5. If a thin wall is structurally permissible, a thickness which is the best compromise between strength and transmission requirements is chosen.

The effect on the antenna gain may be approximately computed as follows. If P_R and P_0 are the power radiated per unit solid angle with and without the radome,
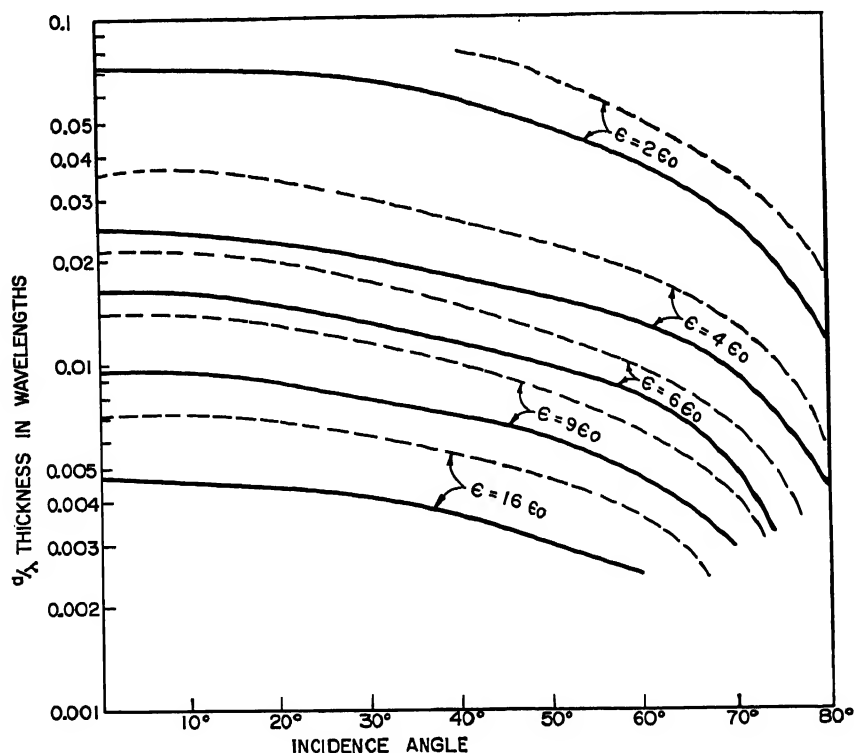
FIG. 32-16. Maximum permissible thickness as a function of incidence angle and dielectric constant for:

———95 per cent power transmission.
– – – –90 per cent power transmission.

respectively, then

$$P_R = |\tau|^2 P_0$$

when $|\tau|^2$ is the power transmission coefficient of the radome wall. In a well-designed normal-incidence radome, phase errors and the accompanying changes in beamwidth and the direction of peak power are generally negligible. Side-lobe level may increase slightly and more so for low side-lobe antennas. The normal-incidence
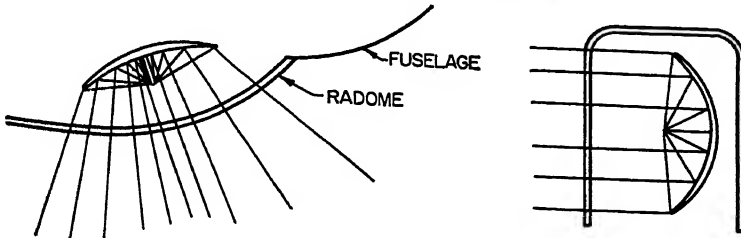
FIG. 32-17. Normal-incidence radomes.
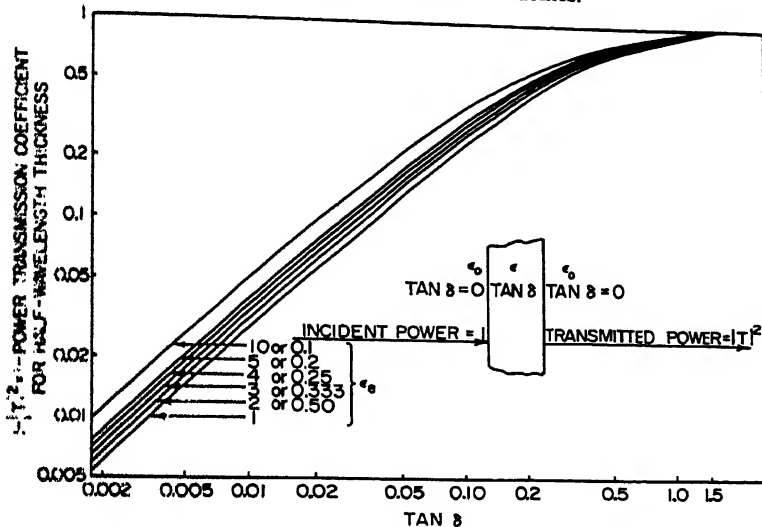
FIG. 32-18. Transmission loss of a lossy sheet of half-wavelength thickness.

radome introduces reflection into the r-f line and effectively modifies the antenna impedance. The latter effect is virtually absent in streamlined radomes. The reflection into the line is proportional to the amplitude reflection coefficient of the radome wall. For a dish antenna in a cylindrical radome, the line reflection is given by

$$\rho_L = \frac{7|\rho|\sqrt{\lambda p}}{19a} 2^{-2(\phi/\psi)^2} \qquad (32\text{-}16)$$

where $|\rho|$ = amplitude reflection coefficient of radome wall, assumed to be a plane sheet at normal incidence

λ = free-space wavelength

p = radius of cylindrical radome

a = radius of antenna aperture

ϕ = angle between axis of antenna and a plane transverse to cylinder

ψ = half-power width of antenna beam

Equation (32-16) is valid for small ϕ provided the aperture center coincides with the cylinder center and $\sqrt{\lambda p}$ is less than a.

A step-by-step method of normal-incidence radome design is given in Ref. 22, pp. 538 and 539.

Design of Streamlined Radomes. In a streamlined radome the variation of incidence angle and polarization angle among the various rays in the beam causes pattern distortion of all types: beam widening, loss of gain, peak power directional shift, etc.
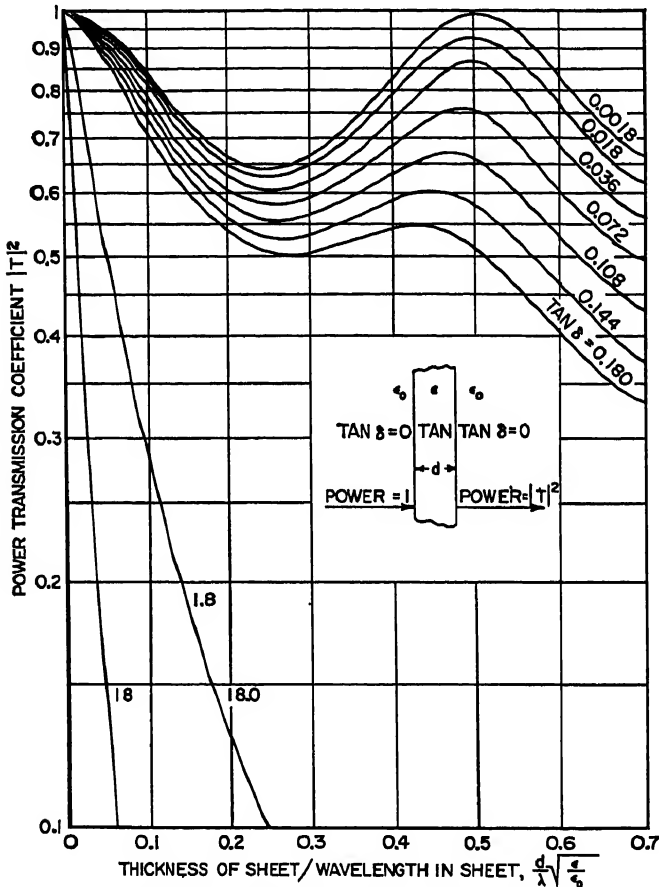
Fig. 32-19. Transmission of a plane lossy sheet. The dielectric constant is $4\epsilon_0$.

If the antenna scans, pattern distortion is a function of the scan position. Crossover shift is introduced into conical scanning and monopulse systems. All antenna systems in which beam directional accuracy of the order of a fraction of a degree is required can expect appreciable radome errors.

The pattern distortion to be expected from a proposed radome design can be predicted with the aid of an incidence-angle study. For a representative set of positions of the antenna, rays are drawn from the antenna to the interior of the radome wall following the paths of energy propagation. The effect of the radome is represented by the local transmission coefficient. The local transmission coefficient is the plane-sheet complex transmission coefficient for a wall of the same cross section

(i.e., values of dielectric constant and thickness) as the radome wall with the incidence angle taken equal to the angle between the ray at the point of contact with the wall and the normal to the wall at this point.

If Fraunhofer diffraction is not important, the far-field pattern as distorted by the radome is obtained from

$$P_R(\theta, \varphi) = |\tau(\theta', \varphi')|^2 P_0(\theta', \varphi') \qquad (32\text{-}17)$$

In this formula $P_0(\theta', \varphi')$ is the far-field pattern of the antenna in direction (θ', φ'), the direction of the ray leaving the antenna, and $\tau(\theta', \varphi')$ is the local transmission coefficient associated with this ray. Fraunhofer diffraction may be neglected if the antenna does not have a pencil beam and if the radome is smooth and does not have ribbing, a sharp nose, or other diffracting features. If refraction may be neglected,

POWER IN THIS CONE OF RAYS IS THAT OF ANTENNA WITHOUT RADOME MULTIPLIED BY POWER TRANSMISSION COEFFICIENT OF WALL AT INCIDENCE ANGLE θ —
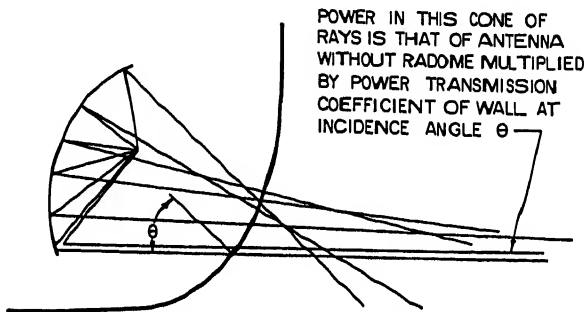
FIG. 32-20. Paths of rays for a csc² antenna.

as is usually the case, the directions (θ, φ) and (θ', φ') coincide. Figure 32-20 illustrates the procedure with a csc² antenna.

If we are dealing with a pencil-beam antenna, the prediction of pattern distortion by radomes has several new features. In this case the rays are extended to a plane just exterior to the radome and parallel to the aperture. The intersection of the beam of rays with this plane determines a new effective aperture. The field values in this aperture are those associated with the rays. The phase must take due account of the ray path length and the phase delay of transmission through the radome. Let $f_0(x, y)$ be the principal component of the E field in the aperture of the antenna. The antenna axis is assumed to coincide with the z axis, so that all rays are initially parallel to the z axis. Let $|\tau(\theta)|$ be the amplitude of the local transmission coefficient, with θ the angle of incidence of that ray passing through the point (x, y) (Fig. 32-21).

Apart from a constant-phase factor, which is omitted, since it does not affect the pattern, the field in the effective aperture is given by

$$f(x, y) = f_0(x, y)|\tau(\theta)|e^{i\Phi} \qquad (32\text{-}18)$$

where Φ is the insert phase as defined by Eq. (32-11). The far-field pattern with the radome in place is then obtained by the usual Fourier transform [see Eqs. (6-16) and (6-9) in Ref. 22].

$$P(\theta, \varphi) = \left(\frac{\epsilon_0}{\mu_0}\right)^{1/2} \frac{1}{2\lambda^2} \left| \iint f(x, y) e^{j(k_x x + k_y y)} \, dx \, dy \right|^2 \qquad (32\text{-}19)$$

where $k_x = k \sin \theta \cos \varphi$

$k_y = k \sin \theta \sin \varphi$

and the integration is performed over the effective aperture.*

* Here, θ and φ are spherical coordinates with the polar axis coincident with the $+z$ axis.

The presence of ribs or a sharp-pointed nose may be taken into account by this method by using the appropriate local transmission coefficient.   Because of the ray-optics assumptions, formulas (32-18) and (32-19) can be considered only semi-quantitative in general and only qualitative if the aperture has a diameter less than five wave-lengths or if diffraction effects are very severe.
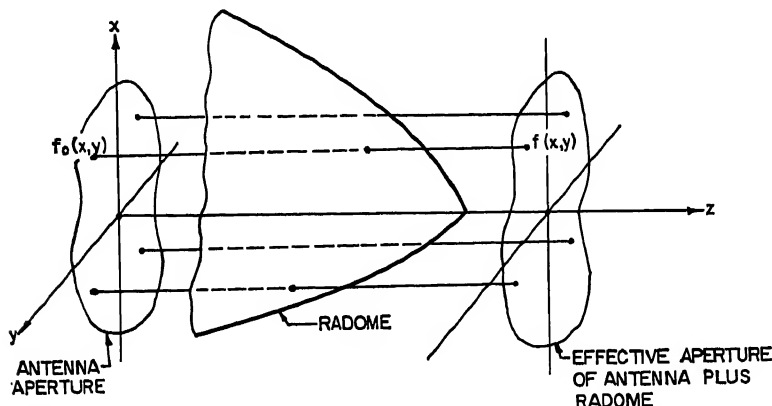
FIG. 32-21. Ray tracing of a pencil-beam antenna through a radome to determine radome pattern distortion.

If polarization effects are to be considered, the above procedure must be modified. If $f_0(x,y)$ represents the main polarization component of a linearly polarized antenna, then $|\tau(\theta)|$ in Eq. (32-18) must be replaced by

$$|\tau'(\theta)| = [|\tau_\perp|^2 \sin^4 \alpha + |\tau_\parallel|^2 \cos^4 \alpha + 2|\tau_\perp \tau_\parallel| \sin^2 \alpha \cos^2 \alpha \cos \delta]^{1/2} \quad (32\text{-}20)$$

and Φ in Eq. (32-18) must be replaced by

$$\Phi = \Phi_\perp - \sin^{-1} \left(\frac{\tau_\parallel \cos^2 \alpha \sin \delta}{|\tau'(\theta)|} \right) \quad (32\text{-}21)$$

where α = polarizing angle
        $\delta = \angle\tau_\perp - \angle\tau_\parallel$ = difference in transmission phase between polarizations
$|\tau_\perp|$ and $|\tau_\parallel|$ = perpendicular and parallel amplitude transmission coefficients, respectively, at incidence angle θ

Pattern distortion analyses based on the above formulas may be very complicated, especially if the analysis is three-dimensional or includes refraction errors, cross-polarization effects, or other refinements.   If such a complete analysis is not warranted but some estimate of pattern distortion is required, ray diagrams may be made for one or two positions of the antenna, in which the worst pattern distortion by the radome is expected.   For this purpose one or more two-dimensional analyses may be sufficient.   In a streamlined radome which does not possess even an approximate symmetry axis, elevation and plan views may be required and incidence and polarizing angles for skew rays may have to be estimated numerically or from a three-dimensional model.

From these formulas it follows that if the amplitude transmission coefficients and insert phase are as independent of incidence angle and polarization as possible over the ranges of these angles which are encountered, the antenna pattern will be as little distorted as possible.   In addition, if the amplitude transmission coefficient is as large as possible, loss of gain will be minimized.   With a linearly polarized antenna, whose polarization direction is independent of scan, the polarizing angle will often

vary from 0 to 90°, so that at some point in the scan the situations of pure perpendicular or pure parallel polarization are encountered. For moderately streamlined radomes, the incidence angle often varies from 0 to 60°. For highly streamlined radomes, incidence angles up to 90° are encountered while near-normal incidence may or may not be encountered in the same radome. The extreme grazing angles are more often due to the proximity of the wall to the edge of the antenna rather than extreme fineness ratios (Fig. 32-22).

From curves of the transmission and phase quantities prepared for a variety of dielectric constants, wall thicknesses, and other radome parameters, the best wall

(a)

VERTICAL PLANE
DISH LOOKING DOWN
PURE PERPENDICULAR POLARIZATION
$\alpha = 90°$

HORIZONTAL PLANE
DISH LOOKING TO SIDE
PURE PARALLEL POLARIZATION
$\alpha = 0°$

(b)
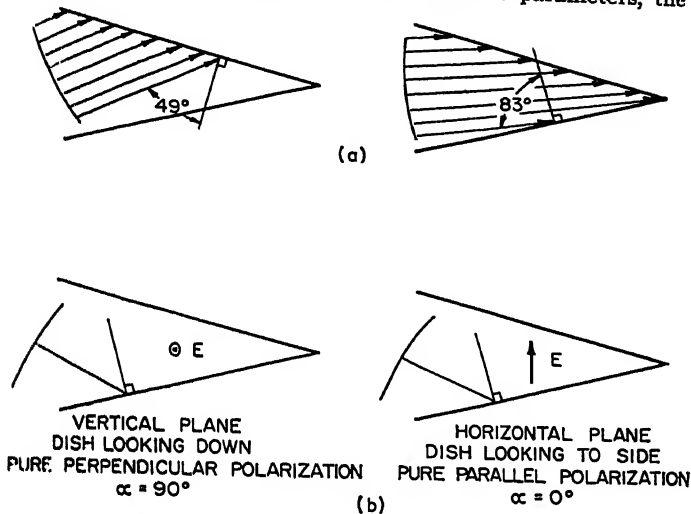
FIG. 32-22. (a) Occurrence of grazing incidence in conical radome with 30° vertex angle. (b) Illustrating the extreme polarizing angles which are often encountered in one radome.

construction to employ to minimize pattern distortion or loss of gain can be determined. For a half-wave wall, a high relative dielectric constant in the neighborhood of 6 to 9 is generally desirable. The upper limit is fixed by material tolerances, bandwidth, and the lossiness of available high-dielectric materials. An optimum thickness to minimize the transmission loss and variation of phase as well as the effect of tolerances can also be determined from these graphs.

Refraction. The directions (θ', φ') and (θ, φ) of the rays before and after passing through the radome will not be coincident if refraction takes place. This effect can occur either because of the curvature of the wall or because of the presence of a taper or gradual thickness variation in the wall.

The incident and refracted rays will not generally be coplanar. However, for rays in the bore-sight plane of an axially symmetric radome, the angular deviation due to curvature of the wall can be determined from

$$\delta_0 = \frac{d \sin \theta}{r} \left[\sec \theta - \left(\frac{\epsilon}{\epsilon_0} - \sin^2 \theta \right)^{-\frac{1}{2}} \right] \quad \text{radians} \quad (32\text{-}22)$$

where d = wall thickness
$\quad r$ = radius of curvature of wall
$\quad \theta$ = incidence angle (measured from normal)
$\quad \epsilon/\epsilon_0$ = relative dielectric constant

This formula applies if $d/r \ll 1$ and $\theta < 80°$. Refraction due to curvature always causes a ray which is initially on the concave side to deflect toward the surface normal

on passing through the radome, and thus tends to produce a divergent error in beam direction with axially symmetric radomes. For walls which are a half wavelength thick at angle θ, the deviation δ_0 can be read from Fig. 32–23a. The angular deviation or refraction due to a variation in thickness is given by

$$\delta_1 = \left[\left(\frac{\epsilon}{\epsilon_0} - \sin^2 \theta \right)^{1/2} - \cos \theta \right] \gamma \sec \theta \qquad (32\text{--}23)$$

where γ is the average taper, in the same units as δ_1.

Tapers of the order of 1 to 5 angular mils are often introduced into radome walls to correct for radome error. Equation (32–23) will give a rough estimate of the
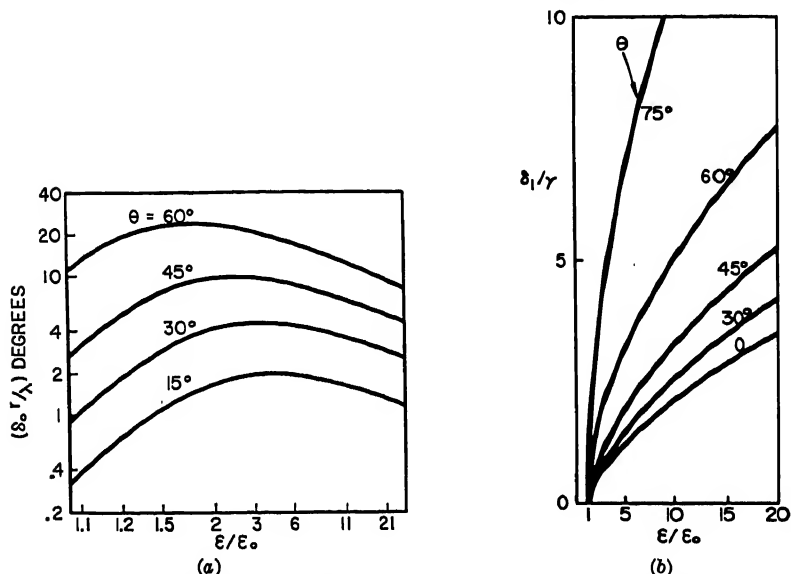
Fig. 32-23. (a) Refraction δ_0 for half-wave radomes due to radius of curvature r/λ in wavelengths. (b) refraction δ_1 due to taper γ in radome wall.

effect of such a taper if δ_1 is interpreted directly as the change in error due to the taper (Fig. 32–23b).

Radome Losses. A usable radome material generally has a loss tangent under 0.015. Such a material is said to be low-loss. When the loss tangent is 0.015 in a half-wave wall, the power-transmission loss ranges from 4 to 7.5 per cent, corresponding to dielectric constants from ϵ_0 to $10\epsilon_0$. For a thin-wall low-loss radome, transmission loss due to absorption is negligible. The effect of loss on insert-phase variation or on the amplitude reflection coefficient is also negligible both for thin and half-wave walls for values of ϵ less than $10\epsilon_0$.

Loss is the chief limiting factor in the use of very high dielectric materials because of the reduction of transmission. At normal incidence for dielectric constants of $6\epsilon_0$ and above, power transmission for a low-loss wall is approximately

$$|\tau|^2 = 1 - 1.5 \sqrt{\frac{\epsilon}{\epsilon_0}} \tan \delta \qquad (32\text{--}24)$$

The Use of Small Radomes for Matching Feed Horns. It is often desired to pressurize, or at least weatherproof, a feed horn with a small radome, which may also be used for matching. The radome is generally cylindrical, with its axis approxi-

mately in the aperture plane and is faired into a supporting flange just behind the aperture. An external inclosure of this type is superior to a diaphragm in the aperture plane, for it reduces the likelihood of power breakdown and is less critical to tolerances. The thickness d of the radome wall is chosen to make the amplitude reflection coefficient equal to that of the measured reflection coefficient of the unmatched aperture; the spacing x between the aperture and the radome inner surface is then chosen to complete the match. If $\Gamma = |\Gamma|e^{j\angle\Gamma}$ is the measured complex reflection coefficient of the horn referred to the aperture plane and $\rho = |\rho|e^{j\angle\rho}$ is the reflection coefficient of the radome, we have the following conditions for a match:

$$|\rho| = |\Gamma|$$

$$\angle\rho - \angle\Gamma - \frac{4\pi x}{\lambda} = (2m + 1)\pi$$

where m is an integer. From Eqs. (32-3) and (32-6) we obtain the required thickness:

$$d = \frac{\lambda|\Gamma|}{\pi[(\epsilon/\epsilon_0) - 1](1 - |\Gamma|^2)^{\frac{1}{2}}} \qquad (32\text{-}25)$$

The spacing x follows from Eqs. (32-8) and (32-11):

$$x = \frac{\lambda}{4\pi}\left\{ -\tan^{-1}\left[\frac{(\epsilon/\epsilon_0) + 1}{2\sqrt{\epsilon/\epsilon_0}}\tan\left(\frac{2\pi d}{\lambda}\sqrt{\frac{\epsilon}{\epsilon_0}}\right)\right] - \angle\Gamma + \left(2m + \frac{1}{2}\right)\pi\right\} \qquad (32\text{-}26)$$

Because the plane-sheet, plane-wave theory used to derive Eqs. (32-25) and (32-26) only approximates the actual geometry, empirical corrections will be required in thickness and spacing for an optimum match. The experimental optimum x is generally larger than that calculated from Eq. (32-26). When the feed mismatch is small or the wavelength very short, the thickness d_0 calculated from Eq. (32-25) may be impractically small. In these cases, a thickness $d_0 + \lambda/(2\sqrt{\epsilon/\epsilon_0})$ may be used without affecting x or the match.

Plexiglas, polystyrene, Teflon, or Rexolite may be used for wavelengths above 3 cm. At 1.25 cm Corning 707 glass has been used for flat pressurizing enclosures. It necessitates building the feed of metals with low coefficients of expansion such as Invar and Covar. Plastic enclosures are sealed by means of gaskets; glass by platinizing or bonding metal to the edges and soft-soldering.

32.3. SANDWICH RADOMES

If a half-wave wall of a suitable dielectric material is too heavy and if the thin wall is structurally unsatisfactory, a three-layered sandwich construction is employed. In the ordinary, or A, sandwich (Fig. 32-24), the outer layers, or skins, are thin compared with a wavelength with dielectric constant about $4\epsilon_0$, and the middle layer, or core, is a low dielectric (about $1.2\epsilon_0$).

Fig. 32-24. Ordinary sandwich wall.

If loss is neglected, the complex reflection and transmission coefficients for such a structure may be determined from the following formulas:

$$\rho = \frac{\rho_1 - \rho_2\exp[j(\angle\rho_1 + \angle\rho_2 - 2X)]}{1 - \rho_2^2 e^{-2jX}} \qquad (32\text{-}27)$$

$$\tau = \frac{\rho_1\rho_2(1 - |\rho_1\rho_2|^{-1})e^{-jX}}{1 - \rho_2^2 e^{-2jX}} \qquad (32\text{-}28)$$

where X is 2π times the electrical thickness of the core.

$$X = \frac{2\pi x}{\lambda}(\beta - \sin^2\theta)^{1/2} \tag{32-29}$$

where β = relative dielectric constant of core

x/λ = core thickness/wavelength

θ = incidence angle (measured from normal)

and where ρ_1 and ρ_2 are the so-called left and right skin reflection coefficients (Fig. 32-25) defined by

$$\rho_1 = -\frac{r_1 + r_2 e^{-2j\varphi}}{1 + r_1 r_2 e^{-2j\varphi}}$$
$$\rho_2 = \frac{r_2 + r_1 e^{-2j\varphi}}{1 + r_1 r_2 e^{-2j\varphi}} \tag{32-30}$$

φ is 2π times the electrical thickness of the skin:

$$\varphi = \frac{2\pi d}{\lambda}(\alpha - \sin^2\theta)^{1/2} \tag{32-31}$$

where α = relative dielectric constant of skin

r_1 and r_2 = Fresnel interface reflection coefficients for an $(\alpha{:}1)$ interface and a $(\beta{:}\alpha)$ interface, respectively
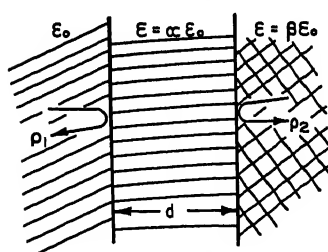
FIG. 32-25. The skin-reflection coefficients.

These are given by

$$r_1 = \frac{\sqrt{\alpha_e} - 1}{\sqrt{\alpha_e} + 1} \qquad r_2 = \frac{\sqrt{\beta_e} - \sqrt{\alpha_e}}{\sqrt{\beta_e} + \sqrt{\alpha_e}} \tag{32-32}$$

where α_e and β_e are the equivalent relative dielectric constants of the skin and core, respectively, at incidence angle θ. These are given by

$$\alpha_e = \begin{cases} \dfrac{\alpha - \sin^2\theta}{\cos^2\theta} & \text{(perpendicular polarization)} \\[2mm] \dfrac{\alpha^2 \cos^2\theta}{\alpha - \sin^2\theta} & \text{(parallel polarization)} \end{cases}$$
$$\beta_e = \begin{cases} \dfrac{\beta - \sin^2\theta}{\cos^2\theta} & \text{(perpendicular polarization)} \\[2mm] \dfrac{\beta^2\cos^2\theta}{\beta - \sin^2\theta} & \text{(parallel polarization)} \end{cases} \tag{32-33}$$

and β is the relative dielectric constant of the core.

The value of d, to be used in Eq. (32-31), is the effective skin thickness, which may be larger than the actual thickness if an adhesive layer bonding skin to core is present. The power reflection and transmission coefficients are

$$|\rho|^2 = \frac{4|\rho_1|^2 \sin^2(\angle\rho_2 - X)}{(1 - |\rho_1|^2)^2 + 4|\rho_1|^2 \sin^2(\angle\rho_2 - X)}$$
$$|\tau|^2 = \frac{(1 - |\rho_2|^2)^2}{(1 - |\rho_1|^2)^2 + 4|\rho_1|^2 \sin^2(\angle\rho_2 - X)} \tag{32-34}$$

where

$$|\rho_1|^2 = |\rho_2|^2 = \frac{\alpha_e(\sqrt{\beta_e} - 1)^2 - (\alpha_e - 1)(\beta_e - \alpha_e)\sin^2\varphi}{\alpha_e(\sqrt{\beta_e} + 1)^2 - (\alpha_e - 1)(\beta_e - \alpha_e)\sin^2\varphi} \tag{32-35}$$

Reflection will be absent if $\angle\rho_2 - X$ is a multiple of π or if the core thickness satisfies

$$x = \frac{\lambda}{2\pi(\beta - \sin^2\theta)^{1/2}}\left\{ n\pi - \tan^{-1}\left[\frac{2(\alpha_e - 1)\sqrt{\alpha_e\beta_e}\sin 2\varphi}{(\beta_e - \alpha_e)(1 + \alpha_e) + (\alpha_e - 1)(\beta_e + \alpha_e)\cos 2\varphi}\right]\right\} \tag{32-36}$$

where n is any integer such that x is positive. The particular angle θ at which Eq. (32-36) holds is called the core design angle. The least value of x satisfying Eq.

(32-36) is the first-order spacing.   Reflection will also be zero if $|\rho_1|$ is zero.   The latter can occur only if (1), $\beta_e = 1$ and φ is a multiple of π or (2), $\beta_e = \alpha_e{}^2$ and φ is an odd multiple of $\pi/2$.   These conditions can hold only for a particular value of θ, the skin-design angle.   The former corresponds to a core of free space and skins which are half-wave walls (or multiples thereof) and is called "double wall."   The latter is known as the B sandwich; the skins are electrically a quarter wavelength thick, and the equivalent skin dielectric constant is the geometric mean between that of the core and free space.   The B sandwich is the microwave analogue of matching

DATA:

SKIN DIELECTRIC CONSTANT	4 ε_0
CORE DIELECTRIC CONSTANT	1.2 ε_0
SKIN THICKNESS	.020 IN.
CORE THICKNESS	.651 IN.
SKIN LOSS TANGENT	.02
CORE LOSS TANGENT	.005
DESIGN ANGLE	70°
WAVELENGTH	3.2 CM
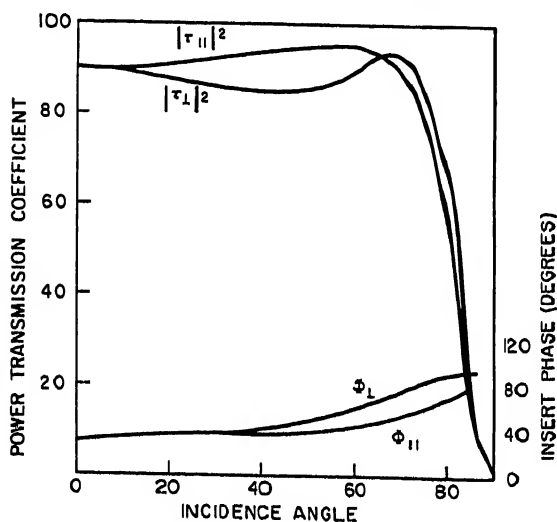
Fig. 32-26. A-sandwich design curves.

coatings used in optical lenses.   Observe that at the skin design angle the reflection is zero independent of core thickness for the double wall or B sandwich.   The skin design angle thus corresponds to Brewster's angle.

Sandwiches for the 10-cm band can be made with skins that are electrically thin compared with the wavelength.   Such sandwiches have good mechanical properties and are low-reflecting for a wide range of incidence angles at either polarization.   In the 3-cm band the skins that are required for mechanical reasons are thicker electrically.   Only the first-order spacing can be used for low reflection.   In the 1-cm band it is often structurally necessary to abandon the thin skins in favor of a half-wavelength skin construction.   For a thin-skinned sandwich, the skins are chosen as thin as mechanically feasible for good electrical performance.   This is especially important for a high core design angle, as Figs. 32-26 and 32-27 illustrate.

For customary design values, reflection at perpendicular polarization for either the A or B sandwich generally exceeds that at parallel polarization so that if both polariza-

DATA:

SAME AS FIG. 32-26 EXCEPT
SKIN THICKNESS .040 IN.
CORE THICKNESS .444 IN.
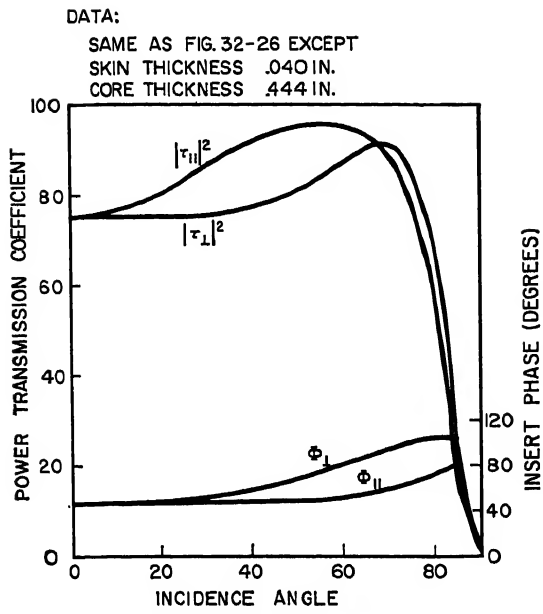
FIG. 32-27. A-sandwich design curves.

tions are to be encountered in a streamlined radome, the radome is often designed for the perpendicular polarization component.

The relative skin dielectric constant is chosen at a moderate value in the range $\alpha = 4$, corresponding to a suitable material. High values are undesirable. The relative core dielectric constant should be kept low, although this is not critical. For example, if $\alpha = 4$ and the design angle is 50°, then power transmission and total insert phase variation for various values of β are given in Table 32-2. The design angle is chosen to maximize transmission and (if pattern distortion by the radome is

Table 32-2

	Polarization	$\theta = 0°$		$\theta = 60°$		
		$\perp$	$\parallel$	$\perp$	$\parallel$	
Per cent power transmission	$\beta = 1.2$	91	91	91	96	Design angle 50°
	$\beta = 1.4$	91	91	91	94	$\tan \delta = \begin{cases} 0.005 \text{ (core)} \\ 0.020 \text{ (skin)} \end{cases}$
	$\beta = 1.6$	91	91	90	94	Skin thickness = .030 in.
						$\lambda = 3.2$ cm
	Polarization	$\perp$		$\parallel$		
Total insert phase variation in range 0–60°, degrees	$\beta = 1.2$	20		6		
	$\beta = 1.4$	23		10		
	$\beta = 1.6$	25		15		

DATA:

$\alpha = 4$

$\beta = 1.2$

TAN $\delta = \begin{cases} .020, \text{ SKIN} \\ .005, \text{ CORE} \end{cases}$

$d = .030$ IN.

$\lambda = 3.2$ CM
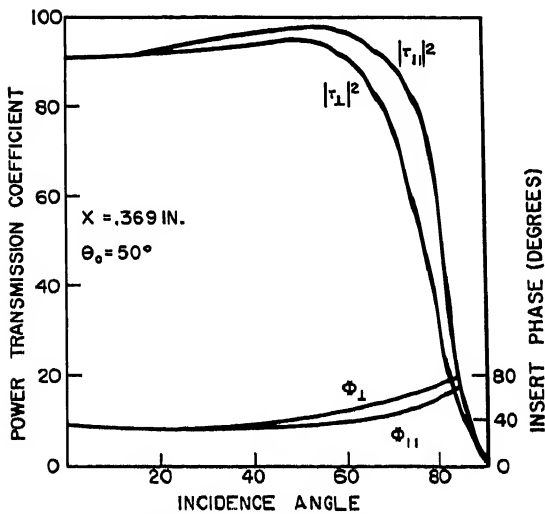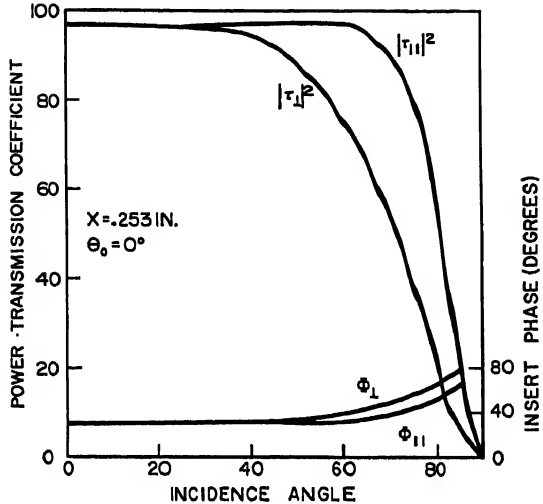
Fig. 32-28. A-sandwich design curves.

important) to minimize insert phase variation over the range of incidence and polarizing angles encountered in the radome. This information may be obtained from plots such as those of Figs. 32-28 and 32-29.

If the ordinary sandwich is unsatisfactory because of insufficient strength, a five-layered construction called the double, or C, sandwich may be used: this consists of

DATA:
α = 4
β = 1.2
TAN δ = { .020, SKIN
           .005, CORE
d = .030 IN.
λ = 3.2 CM

FIG. 32-29. A-sandwich design curves.

two identical A sandwiches back to back.   The complex reflection and transmission coefficients of the C sandwich are given by

$$\rho_c = \rho + \frac{\tau^2 \rho}{1 - \rho^2} \qquad (32\text{-}37)$$

$$\tau_c = \frac{\tau^2}{1 - \rho^2} \qquad (32\text{-}38)$$

where ρ and τ are the reflection and transmission coefficients of either of the A sandwiches.

32.4. RADOME MATERIALS

Most solid-wall, rigid radomes and radome sandwich skins are made of a plastic base with glass fibers as a reinforcing agent. The glass fibers give excellent strength, stiffness, low moisture absorption, and satisfactory electrical properties. The individual glass filaments are about 0.00025 in. in diameter and yield very high tensile strengths. The filaments are gathered into twisted strands which are either used in short lengths or woven into a glass-cloth fabric. Starch and oil lubricants used in the handling and weaving of the glass are replaced by moisture-repellant compounds in a finishing process which ensures good adhesion of the plastic and moisture resistance of the finished radome.

The basic plastic materials are polyester and phenolic resins. The polyesters are thick liquids which harden (i.e., polymerize, or cure) with little or no pressure on the application of catalysts and heat (generally around 240°F, although curing at room temperature is possible). The phenolics are solids at room temperature and usually require considerably more pressure and heat for curing. They are dissolved in a solvent which is later removed from the fabric by drying. The phenolics can withstand higher temperatures, but the polyesters are better electrically, more easily fabricated, and less brittle.

A common technique for manufacturing solid-wall radomes or radome sandwich skins out of polyester resin and glass-fiber cloth is as follows. A precision machined mandrel of the proper shape is covered with a sheet of cellophane or silicone grease to act as a parting medium. The fabric is dipped in resin with catalyst added in precut pieces that will fit the mandrel shape (if this is highly curved). The excess resin and trapped air are squeezed out by hand. When sufficient thickness has been attained, a second sheet of cellophane is placed over the laminate, and the mandrel with laminate is placed in a rubber bag which is evacuated. Heat is applied in an oven or autoclave. After curing, if the wall is thick, machining with a lathe is generally required to obtain the correct thickness.

Thin flexible ground-based radomes are made from one- or two-ply glass–fiber cloth, nylon, dacron, or fortisan rayon, with a neoprene or hypolon coating of about 10 mils for weathering and the prevention of water absorption. Impregnation with polyethylene has also been used for this purpose.

The cores of ordinary sandwiches are generally made of foamed plastic or a glass-fabric honeycomb construction. In a "foamed-in-place" radome, the inner and outer skins are laid up and cured on male and female molds in the manner of thin-wall radomes. The two molds are positioned so that the cavity between skins represents the desired core dimensions (Fig. 32–30). A foaming mixture made of an alkyd resin and an isocyanate is poured into the cavity. The foaming takes place either with the application of heat (e.g., steam) or at room temperature with an exothermic reaction. In the latter case, a postcure at elevated temperatures is required. If a honeycomb core is used, the procedure is modified. The outer skin is fabricated as previously. Its inner surface is then roughened, and a single-ply glass fabric wet with resin is applied. The honeycomb core, which is supplied in large blocks, has been previously sliced into strips of perhaps 4 by 18 in., of the proper thickness. The pieces are then laid in place one by one against the wet ply. The inner skin is then built upon the honeycomb, ply by ply, the vacuum bag added, and heat curing applied.

Table 32-3 gives the dielectric constant and loss tangent of a number of materials in the microwave region which have been used for radomes. All are low-loss and,
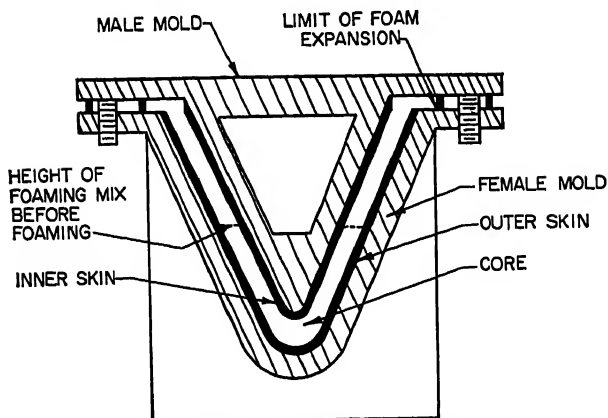
FIG. 32-30. Foamed-in-place radome construction.

except for the glass, have relative dielectric constants close to 3. Fiberglas cloth and resin laminates have dielectric constants between the extremes of the constituents, generally yielding a value about $\epsilon = 4\epsilon_0$. Data for laminates are quite variable, depending on the method of fabrication and the resin used. Commercial resins do not meet precision electrical specifications. If much air is trapped in the lay-up, the dielectric constant may be considerably reduced.

Table 32-3. Dielectric Constants and Loss Tangents of Radome Materials

Material	Relative dielectric constant, $\frac{\epsilon}{\epsilon_0}$	tan δ (approx.)
Polystyrene	2.56	
Polymethyl methacrylate	2.66	0.01
Poly 2, 5 dichlorostyrene	2.57	0.0003
Bakelite BRS 16631, cast	2.09	0.019
Selectron 5003, cast	2.87	0.010
Plaskon 911, cast	3.06	0.020
Owens-Corning "E" glass	6.24	0.007
Penacolite G1131	3.86	0.10-0.15

The dielectric constant of a mixture of two materials is given empirically by

$$\frac{\epsilon}{\epsilon_0} = \left(\frac{\epsilon_a}{\epsilon_0}\right)^a \left(\frac{\epsilon_b}{\epsilon_0}\right)^b \tag{32-39}$$

where a and b are the volume fractions of the two components, and ϵ_a/ϵ_0 and ϵ_b/ϵ_0 are their respective dielectric constants. Higher dielectric constants may be obtained, according to this rule, by loading the resin to be used with titanium dioxide or barium and strontium titanate mixtures. The relative dielectric constants of some of these titanates are up in the hundreds or thousands, but these values generally drop rapidly, with increasing frequency in the microwave region accompanied by a rapid rise in loss tangent.[24]

The low dielectric constants of foams come from the incorporation of air into a plastic base. The dielectric constant of a foam is given by

$$\log \frac{\epsilon}{\epsilon_0} = \frac{\rho}{\rho_0} \log \frac{\epsilon^0}{\epsilon_0} \tag{32-40}$$

where ρ = density of foam

ρ_0 = density of solid, unexpanded plastic with dielectric constant ϵ^0/ϵ_0

A 6 lb/cu ft polystyrene foam has a modulus of rupture of about 200 psi, a Young's modulus of about 10,000 psi, and a dielectric constant of $1.1\epsilon_0$. Low-loss foams of dielectric constants and densities in the range $2\epsilon_0$ to $3\epsilon_0$ and 10 to 20 lb/cu ft have been made by loading resin with metallic particles of an appropriate size. Walls which are mechanically sandwiches with foam cores can be made of a uniform dielectric constant and half-wavelength electrical construction by this means with a considerable weight saving. For operating temperatures above about 500°F, organic resins are not suitable. For these extremely high temperatures molded glass, Pyroceram, or ceramics have been used.

FIG. 32–31. Simple bending test.

Mechanical Properties. The two principal mechanical radome requirements are strength and stiffness. They may both be determined from a simple bending test made on a flat panel of the radome wall material.

Single Walls. If W_m is the load per unit transverse direction that just causes failure of the test sample in Fig. 32–31, then the modulus of rupture f_r is given by

$$f_r = \frac{3 W_m l}{2 d^2} \qquad (32\text{-}41)$$

where d = sample thickness

l = separation of supports

The modulus of rupture (or flexural strength) approximately equals the lesser of the maximum tensile stress and the maximum compressive stress that the material can withstand. If l/d exceeds 16, the error in Eq. (32-41) due to the presence of shearing force is generally negligible. The flexural strength of the panel itself is given by the maximum bending moment M_m the panel can withstand.

$$M_m = \frac{W_m l}{4} \qquad (32\text{-}42)$$

If W is the load per unit transverse direction and if W is sufficiently less than W_m so that the vertical deflection δ of the panel is proportional to W, then Young's modulus is given by

$$E = \frac{W l^3}{4 \delta d^3} \qquad (32\text{-}43)$$

and is a measure of the stiffness of the material. The flexural stiffness of the panel is given by

$$EI = \frac{W l^3}{48 \delta} \qquad (32\text{-}44)$$

where $I = d^3/12$ is the normalized moment of inertia about the neutral axis.

For glass cloth and polyester resin laminates of the type discussed above, Young's modulus ranges between 1.3 and 2.6 million psi at room temperature, and the modulus of rupture ranges between 25,000 and 80,000 psi. The variation is due to orientation of the fibers and methods of fabrication, including heat treatment, number of plies, thickness of each ply, and resin content. Both the strength and stiffness are somewhat less in directions which are 45° to the strand orientation rather than parallel to the warp or filling. For a standard polyester resin, the modulus of rupture drops rapidly, with rising temperatures reaching 2,000 psi at 500°F. The drop over the same temperature range is less for heat-resistant polyester or silicone resins; a special heat-resistant phenolic resin maintains a modulus of rupture of 25,000 psi at 500°F.
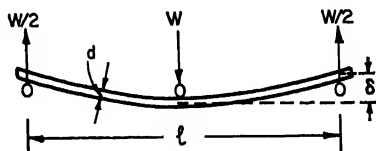
Sandwiches. For low-density core sandwiches, most of the strength comes from the skins even if these are thin. In this case the flexural strength in bending is given by

$$f_r = \frac{W_m \ell}{4dx} \tag{32-45}$$

where W_m and ℓ = as defined in Eq. (32-41)
$\qquad d$ = thickness of one skin
$\qquad x$ = thickness of core

Eq. (32-45) holds only if ℓ is above a critical length ℓ_c, so that shear may be neglected. Below ℓ_c, W_m is independent of ℓ, and failure is due to shear in the core. If τ_{cm} is the value of the shearing stress in the core at which failure occurs, then

$$\tau_{cm} = \frac{W_m - 2\tau_s d}{x} \tag{32-46}$$

where τ_s is the average shear stress in the skins. Eq. (32-46) holds if ℓ is below ℓ_c. If the maximum dimension of a radome is below

$$\ell_c = \frac{4xdf_r}{2\tau_s d + \tau_{cm} x} \tag{32-47}$$

failure will generally occur because of shear in the core. Above ℓ_c, failure generally results from longitudinal stresses in the skins.

In the determination of the apparent stiffness of a low-density, thin-skin sandwich, deflection due to shear can no longer generally be neglected. The ratio of deflection δ to load per unit transverse direction is given by

$$\frac{\delta}{W} = \frac{\ell^3}{24E_s x^2 d} + \frac{5\ell}{8E_c x} \tag{32-48}$$

where the first term is due to the bending moment and the second is due to shear. If $\delta/W\ell$ is plotted versus ℓ, the extrapolated value of $\delta/W\ell$ when ℓ is zero is $5/8xE_c$. This determines E_c. When ℓ is large compared with $\sqrt{150xd}$, the second term may be neglected and E_s is given by

$$E_s = \frac{W\ell^3}{24\delta x^2 d} \tag{32-49}$$

The apparent flexural stiffness of the sandwich is given by

$$\frac{\ell^3 W}{48\delta} \tag{32-50}$$

and may vary over wide limits, depending on the details of fabrication.

Edgewise compression and normal tension tests are also used for evaluation of the sandwich, particularly the skin-core bond. The compressive strength of the skin determined by the former test is generally 25 to 40 per cent lower than that determined from the flexure test.

Table 32-4 may be considered representative mechanical data for an ordinary sandwich designed for high transmission at perpendicular polarization over the range of incidence angles of 0 to 70° at a wavelength of 3.2 cm and a half-wave radome designed for the same conditions.

Table 32-4

	Sandwich	Half-wave radome
Skin thickness, d	0.030 in.	0.363 in.
Skin dielectric constant, α	3.7 or {4.1	3.7
Core thickness, x	0.385 in. {0.360 in.	
Core dielectric constant, β	1.4	
Flexural strength, M_m	200–350 lb	780 lb
Flexural stiffness, EI	6,000–8,000 lb in.	8,000 lb in.
Computed Young's modulus of skin, E_s	2.5–3.2 × 10⁶ psi	
Computed Young's modulus of core, E_c	1.5–2.5 × 10⁴ psi	
Average weight per unit area	1.1 psf	3.3 psf

Radome Testing. It is important to test the dielectric constant of the wall material employed in the radome. This is particularly true in the usual resin and glass laminate solid wall and low-density-core sandwich constructions because the dielectric constant, and hence the radome performance, depend upon the details of
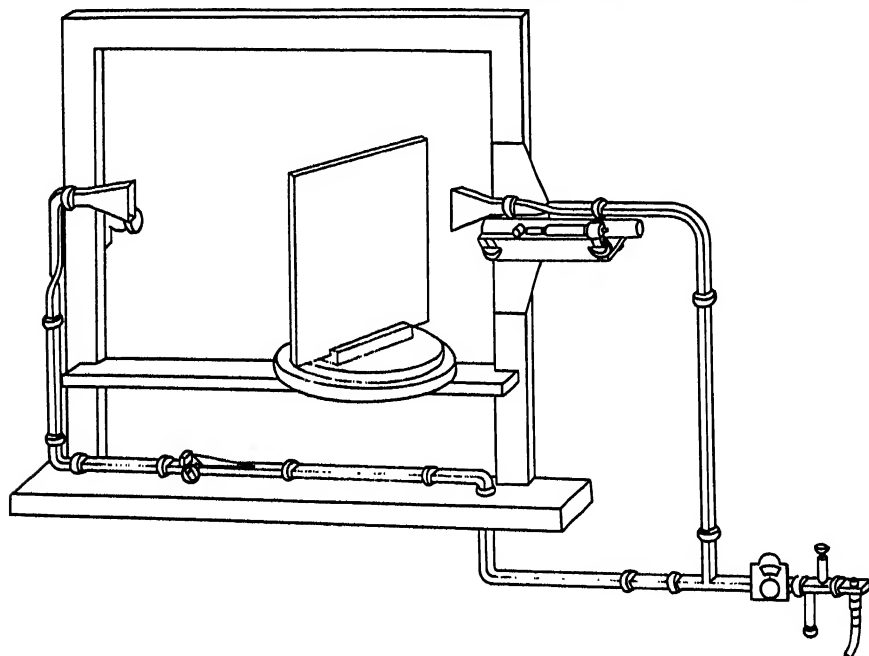
Fig. 32-32. Equipment for measurement of a phase in free space.

the fabrication process as well as the proportion of ingredients. This test may be made in waveguide by resonant-cavity, short-circuited line, reflection, or transmission methods as described in Ref. 25.

A free-space measurement is also commonly used. If D_1 is the separation of the horn aperture in Fig. 32-32 for a null reading without the panel and D_2 is the same quantity when the panel is present, the measured insert phase is given by

$$\Phi = \frac{2\pi|D_1 - D_2|}{\lambda} \qquad (32\text{-}51)$$

For incidence angles less than 30° it is necessary first to repeat the measurements with the panel a distance $\lambda/4$ closer to the transmitter and then to average the two values of Φ obtained. This type of measurement yields an average value of the dielectric constant over a large panel area and introduces the extra parameters of incidence angle and polarization which may be used for checking. If only a limited number of measurements are to be made, Eq. (32-11) may be solved for ϵ from the measured value of Φ by a trial-and-error process, which is facilitated by the knowledge that Φ is an increasing function of ϵ. If many determinations are to be made, it is best to prepare graphs of Φ versus ϵ (Ref. 26) for a direct reading of ϵ as a function of Φ and the parameters d, λ, and θ.

The finished radome will require some electrical testing. A general rule is that whatever performance tests are required of the antenna should also be duplicated with the radome present, unless, as often happens in certain cases, the effect of the radome is safely known to be negligible.

The following precautions should be noted.

1. *Antenna pattern measurements with radome present.* The geometry of the antenna and radome should duplicate actual conditions. Other nearby parts of the installation such as aircraft fuselage or projecting gun barrels may also be simulated in the same test. If the antenna scans, a representative member of patterns should be taken for all positions of the antenna with respect to the radome and polarization orientations. For example, an airplane nose radome and a linearly polarized pencil-beam antenna may require pattern measurements at every 5 or 10° azimuth and elevation gimbal angle throughout the antenna's scanning range. More patterns may be required in the immediate neighborhood of the nose if the radome is highly streamlined and incidence angles over 70° are encountered.

2. *VSWR measurements.* These may ordinarily be omitted with streamlined radomes where the line reflection due to the radome is generally down 30 db or more. With normal-incidence radomes in a standing-wave determination, reflection from room objects must be avoided. Multiple reflections between antenna and radome may be averaged out of either the VSWR or the radome reflection-coefficient determination by averaging values for a sequence of separations of antenna and radome. In principle, two separations differing by $\lambda/4$ are sufficient.

3. *Radome error.* The error produced by the radome in the crossover-point direction of a conical scanning or monopulse antenna may be tested on an antenna pattern range which has facility for mounting and rotating the radome independently of the housed antenna. The radome error, which is the change of beam direction in space produced by the radome, and hence a vector quantity, is described by its bore-sight and cross-talk components. The former is the component in the plane of offset which contains the antenna and radome axes. The latter is the component in a plane perpendicular to the plane of offset. These angles are customarily measured as functions of scanning antenna azimuth angle over the complete range of azimuth angles and representative elevation angles, or alternatively in the case of a symmetrical radome and linearly polarized antenna for a complete range of gimbal angles at various polarizing angles.

If difficulty is encountered with the electrical performance of a radome, it may be desirable to test small portions of the wall area at a time with small dipole or horn transmitting and receiving antennas, both located close to the radome wall. These are substituted for the full-size service antenna and a distant source. Such a measurement may be one of two types. If the energy traverses only the path in space between transmitter and receiver, the local power-transmission coefficient of the wall may be determined as the ratio of energy received with and without the radome present. If a microwave bridge and phase comparison device is used (as in the interferometer of Fig. 32-32), the insert phase may be read for a part of the radome wall with a pro-

cedure analogous to the dielectric-constant determination of a panel. These measurements serve to determine where the wall is electrically too thick or too thin. Small changes may then be made by hand-sanding of the radome wall where it is too thick or adding patches of plastic film with a thermosetting resin where it is too thin. By this method an electrically unsatisfactory radome may be brought up to par.

Radome error curves are plots of bore-sight and cross-talk error vs. gimbal, azimuth, or elevation angle. Typically, the bore-sight error component is the greater and the bore-sight error curve has an absolute maximum near the zero gimbal angle in a streamlined nose radome. Several other maxima often occur, although it is rare that these should appear more closely spaced than 2° gimbal angle and on large radomes tend to disappear altogether. A typical maximum radome error in degrees is in the range of one to five times the ratio of the wavelength to the antenna aperture diameter. The more streamlined radomes approach the upper figure.

Structural Tests. The strength and stiffness of the radome material may be determined from flexural tests as described previously. For tests of the completed radome, simple dead-weight loading in either the transverse or longitudinal direction will give an estimate of the deflection of the radome at the rated load, and the maximum load before failure. The former gives an estimate of structural stability and the allowable clearance for the motion of the antenna.

If an attempt is made to simulate operational loading conditions, both negative and positive pressures will be required. Loading pads and hydraulic jacks may be used.

Other tests that may be required are water absorption under total immersion, surface hardness, and flammability.

Aerodynamic Problems. Radomes for airplanes should be streamlined and fair smoothly into the vehicle surface with discontinuities in slope avoided whenever possible. Streamlining of the radome is very important at high speeds for reducing drag. The fineness ratio, which is the ratio of length to base diameter of a nose radome, is a measure of its streamlining. Fineness ratios as high as 3:1 may be required at supersonic speeds. The exact shape of a radome for a particular application is generally not critical either electrically or aerodynamically. For both purposes smoothness and smooth variation in curvature are desirable. For radomes which are not located in the nose, reduction in drag of the radome is obtained by a reduction of its frontal area and by installation of the antenna if possible at a location where the air is already turbulent, such as in the middle or aft. A low-drag radome has lower pressure, and hence lower structural requirements, and thus may be made better electrically.

32.5. ABSORBING MATERIALS

Absorbing materials for use in microwave measurements are commercially available in 2- to 4-sq-ft pieces ranging in thickness from ½ to 8 in. They are rated in decibels absorption relative to total reflection at stated frequencies, incidence angles, and polarization. Some of the thinner material is flexible and can be cut and conformed to antenna mounts and supporting jigs. The rigid material may be bonded to wood-frame supports to form a large continuous absorbing surface which, if properly placed, will reduce specular reflection which interferes with antenna impedance and pattern measurements in confined indoor areas. If one room is to have continuous use for this purpose, it may be advantageous to completely and permanently cover the walls, floors, ceilings, and in so far as possible, measuring instruments. If such a free-space room is contemplated, ray diagrams should be sketched showing the energy paths in the room for the typical measurements which are to be performed there. Estimates of the absorption required to make satisfactory measurements possible should

then be made. It may be found, for example, that immediately behind the test antenna 30 db absorption is required, with 20 db satisfactory elsewhere, or it may be found that the measurements contemplated are not feasible in a particularly small place with the absorbing material available. Rearrangement of the test equipment or test procedures may reduce the requirements. We may illustrate this procedure with the case of pattern measurements of directive antennas. The greatest error from wall reflection in this case occurs when the antenna whose pattern is being measured points at a spot on the wall midway between the receiving and transmitting antennas. The ratio of reflected to direct-path signal strength is

$$\left|\frac{E_R}{E_D}\right| = \frac{r_1|R|}{r_2}\left(\frac{G_{TR}G_{RR}}{G_{TD}G_{RD}}\right)^{\frac{1}{2}} \tag{32-52}$$

where r_1 = direct-path distance between antennas

r_2 = reflected path distance between antennas

$|R|$ = amplitude reflection coefficient of wall at angle of incidence of reflected path

G_{TD}, G_{RD} = transmitter and receiver gains in direct-path direction

G_{TR}, G_{RR} = transmitter and receiver gains in reflected-path direction

If the two antennas have the same gain, the radical in Eq. (32-52) is unity. As an example in this case, if $r_1/r_2 = \frac{1}{2}$ and $|R| = 0.10$, then

$$\left|\frac{E_R}{E_D}\right| = 0.05$$

and the pattern could be in error by $\pm\frac{1}{2}$ db at this angle. If this error is tolerable, then 20 db absorber is satisfactory for this application. If the probe antenna is less directive than the test antenna, then absorber with higher absorption rating is required.

The absorber to be used should be judged on its reliability, wearing qualities, and absorption rating at the frequencies, incidence angles, and polarizations which are to be encountered. Some expensive free-space rooms have been built and found unsatisfactory because insufficient attention was paid to these factors.

Absorbing materials are used in small pieces in waveguide attenuators and dummy loads and in some antenna feeds such as the Robinson scanner to replace part of the metal feed surface with an energy dissipating medium which reduces mismatch. Glass-fiber cloth impregnated with resin loaded with a lossy material such as conducting carbon black may be used. If thermal shock is not a problem, Polyiron has satisfactory absorption. A material made of 40 parts silicon carbide and 100 parts porcelain is electrically satisfactory and has an adequate resistance to thermal shock. Absorbers are also used as military camouflage and are sometimes employed behind or to the side of operational antennas for improved performance.

The following classification is according to design principle.

1. *Salisbury screen.* A thin screen of material (such as Uskon cloth or canvas impregnated with graphite) whose resistance R_0 is 377 ohms per square if placed at a distance which is an odd multiple of $\lambda_0/4$ (λ_0 = design wavelength) from a metal surface will produce total absorption at normal incidence. The power reflection coefficient $|\rho|^2$ at other incidence angles θ, wavelengths λ, and screen resistances R_0 for this type of absorber is obtained from the formula

$$|\rho|^2 = \frac{(1-M)^2 + \cot^2\dfrac{\pi\lambda_0\cos\theta}{2\lambda}}{(1+M)^2 + \cot^2\dfrac{\pi\lambda_0\cos\theta}{2\lambda}} \tag{32-53}$$

$$\text{where} \qquad M = \begin{cases} \dfrac{377 \cos \theta}{R_0} & \text{(parallel polarization)} \\[2mm] \dfrac{377 \sec \theta}{R_0} & \text{(perpendicular polarization)} \end{cases} \qquad (32\text{-}54)$$

Equation (32-53) is valid under the assumptions that the screen is thin compared with λ_0 and λ, that the loss tangent of the screen is large compared with unity, and

FOAM OR
SPONGE RUBBER

METAL $R_0 = 377$ OHMS/SQUARE

$\dfrac{\lambda_0}{4}$
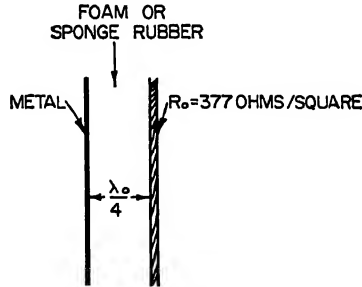
FIG. 32-33. Salisbury screen.

DIELECTRIC SPACERS

METAL

5.9mm 9mm 9mm 9mm 9mm 9mm 9mm
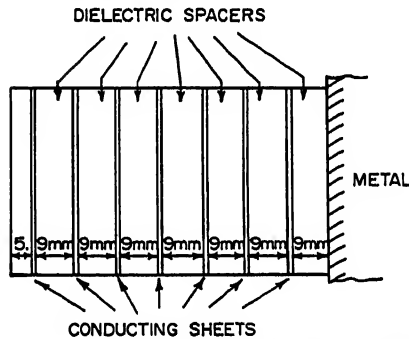
CONDUCTING SHEETS

Surface Resistivities of Conducting Sheets of Multilayer Absorber

Sheet number (from front surface)	1	2	3	4	5	6	7
Surface resistivity, ohms per square	30,000	14,000	6,500	3,000	1,400	650	300
Equivalent conductance relative to dielectric line	0.011	0.024	0.051	0.110	0.24	0.51	1.10

FIG. 32-34. Construction of absorbing sheet containing conducting layers.

that the spacing material which maintains the quarter-wave separation of metal and screen has a low dielectric constant such as provided by polyfoam or sponge rubber (Fig. 32-33).

2. *Tapered line.* Lossy dielectric materials are built up to form a thick wall in such a way that the impedance varies slowly with respect to the longest operational wavelength from a value of zero at the absorber's back face to that of free space at the front face. The variation is often exponential and may be accomplished by a multilayer approximation (Fig. 32-34) or by indentations (Fig. 32-35).

3. *Balanced μ and ϵ.* If a material has both magnetic and dielectric losses and the additional property that ϵ/ϵ_0 and μ/μ_0 are approximately equal, the attenuation constant may be large and the wave impedance almost unity. When energy enters this material, absorption takes place continuously and without reflection at any point. Efforts to find such a material among the ferromagnetics have not produced commercially available absorbers as satisfactory as the preceding types.[1]

Frequency Dependence. Salisbury screens are totally absorbing at frequencies which are an odd multiple of the fundamental, but since they are also totally reflecting at the even harmonics, they are useless over a wideband. The theoretical full
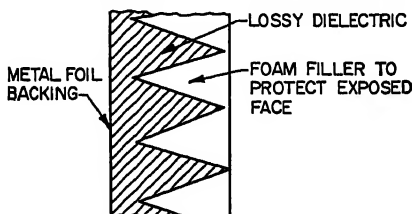
Fig. 32-35. Section of thick absorber with tapered ϵ and μ achieved by conical or pyramidal indentations in surface of lossy dielectric.

bandwidth for 10 per cent reflected power at normal incidence is 74 per cent of the central frequency.

Typical tapered-line absorbers are excellent throughout the upper microwave band (2,500 to 50,000 Mc) with less than 1 per cent reflection in the incidence range 0–60°. Performance at lower frequencies is limited only by thickness; the following figures may be considered representative:

Thickness, in.	Frequency (Mc) below which more than $|\rho|^2$ power is reflected at normal incidence	
	$|\rho|^2 = 2\%$	$|\rho|^2 = 10\%$
2	1,600	1,400
4	800	600
8	400	300

Materials and Performance. One type of absorber is presently made commercially by impregnating a mat of curled animal hair with a mixture of aluminum flake, graphite, or conducting carbon black in a rubber solution. The animal-hair mat is commercially available, inexpensive, and superior to vegetable-fiber door mat, packing material, or excelsior, which may be substituted for it. The following are examples.[18]

NRL Type I. Made of two layers of curled-animal-hair mat, each 1 in. thick, density 3.5 oz/sq ft. Top layer dipped twice in a mixture of 60 per cent graphite, 40 per cent neoprene, made up to 20 per cent solids in xylene. Bottom layer dipped three times in a mixture of 75 per cent graphite, 25 per cent neoprene, made up to 30 per cent solids in xylene. After each dip, layer drains in horizontal position with outer face up, to give a taper.

NRL Type II. Made of a single 1-in. layer of curled animal hair dipped twice in a mixture of 45 per cent Statex A, 55 per cent neoprene made up to 20 per cent solids in xylene. Drains and dries horizontally after each dip with outer face up. Final density 9 oz/sq ft.

NRL Type III. Made of a single half-inch layer of curled animal hair dipped three times as in type II. Initial density 3.5 oz/sq ft; final density 8 oz/sq ft. Performance is as follows:

λ	Per cent power reflection at parallel polarization, 10° incidence angle			
	1.25 cm	3.2 cm	9 cm	12 cm
Type I: *·†·‡				
Top layer alone...............	0.15	4.0	12.0	36.0
Bottom layer alone...........	0.0	1.5	3.0	3.0
Combination.................	0.0	0.8	0.1	0.5
Type II: †·§				
Dry.........................	0.0	0.8		
Wet.........................	0.0	0.4		
Type III: †·§				
Dry.........................	0.2	0.6		
Wet.........................	0.2	4.8		

* A reflection peak may occur near 6 cm.

† Results are not uniform, vary from sample to sample.

‡ Dentating surface gives more reliability and slightly better performance especially when wet.

§ For K- and X-band use only.

Other processes for making tapered-line absorbers include loading of polystyrene foam or cement with fine iron or aluminum particles. Because of their smooth surface, these absorbers do not catch dust and may wear better than the hair type.

Each piece of absorber should be individually tested under conditions corresponding to actual use. Large variations are often found among different pieces in a single batch. There is also some tendency among the poorer commercial grades to absorb moisture and deteriorate with age.

A variety of types of absorbers are currently available commercially from Emerson and Cuming, Inc., Canton, Mass.; McMillan Laboratory, Ipswich, Mass., and B. F. Goodrich Sponge Products Division, Shelton, Conn.

REFERENCES

1. C. G. Montgomery, R. H. Dicke, and E. M. Purcell (eds.): "Principles of Microwave Circuits," MIT Radiation Laboratory Series, vol. 8, pp. 396 400, McGraw-Hill Book Company, Inc., New York, 1948. Contains a theoretical description of the various aborber types.
2. W. M. Cady, M. B. Karelitz, and L. A. Turner (eds.): "Radar Scanners and Radomes," pp. 241-462, Radiation Laboratory Series, vol. 26, McGraw-Hill Book Company, Inc., New York, 1948. Contains a complete survey of radome problems except for recent developments in highly streamlined, high-accuracy radomes and very large radomes.
3. "Graphs of Transmission and Phase Data of Plane Dielectric Sheets for Radome Design," July 1, 1953, and "Supplementary Graphs of Transmission and Phase Delay of Plane Dielectric Sheets and Sandwich Constructions for Radome Design," June 10, 1954, Bureau of Aeronautics TED Project ADCEL-800 and 41026, Report NADC-EL-5313, Johnsville, Pa.
4. "Tables of Transmission and Reflection Coefficients of Lossy, Symmetrical, Dielectric Radome Sandwiches," NADC-EL-52188, Oct. 22, 1953, and "Tables of Transmission and Reflection Coefficients of Lossy, Homogeneous Dielectric Sheets," vol. I, NADC-EL-52195, Feb. 11, 1954, Bureau of Aeronautics TED Project NADC EL-800.
5. "Notes on Electric Design of Radomes," Naval Air Material Center, Rev., February, 1947.
6. "Radome Engineering Manual," AMC Manual 80-4, NAVAER 16-45-502, Oct. 1, 1948.

7. "Fabrication and Repair of Reinforced Plastic," NAVAER 01-1A-501, Bureau of Aeronautics, Jan. 15, 1952.
8. Samuel Wolin: "Ray Deflection through a Homogeneous Dielectric Radome," Report NADC-EL-5272, Aug. 6, 1952.
9. Martin H. Paiss: "Phase Report, Electronic Correction of Boresight Shift in Symmetrical Antenna-radome Systems," Report NADC-EL-52122, Jan. 21, 1953.
10. Paul J. Carroll: "Angular Error and Miss Distance Due to Radome Error in Airborne Radar Turret Fire Control," Report NADC-EL-5461, 1954.
11. Martin H. Paiss: "Phase Report, Investigation of Metal-ribbed Radomes," Report NADC-EL-L5315, Apr. 27, 1953.
12. Samuel S. Oleesky: "Repairing Reinforced Plastics," *Modern Plastics*, February, 1952.
13. Ernest W. Schlieben: "Radomes and Aircraft Design," *Aeronaut. Eng. Rev.*, vol. 11, no. 5, pp. 69–81, May, 1952.
14. Samuel S. Oleesky: "Designing Radomes for Supersonic Speeds," *Electronics*, January, 1954.
15. M. C. Horton, W. E. L. Boyce, and E. O. Hartig: "Optical Theory for Microwave Transmission through Dielectric Wall Structures," Goodyear Aircraft Corp., Akron, Ohio, Aug. 4, 1953.
16. W. W. Salisbury: "Absorbent Body for Electromagnetic Waves," U.S. Patent No. 2,599,944, June 10, 1952.
17. A. J. Simmons and W. H. Emerson: "Anechoic Chamber for Microwaves," *Tele-Tech*, July, 1953.
18. H. A. Tanner, A. G. Sands, and M. V. McDowell: "Darkflex: A Fibrous Microwave Absorber," Naval Research Laboratory AD-10220, Washington, D.C., Apr. 20, 1953.
19. R. M. Redheffer: "The Theory of the McMillan Absorber," McMillan Laboratory, Ipswich, Mass., 1953.
20. H. Bremmer: "The W.K.B. Approximation as the First Term of a Geometric-optical Series," published in "The Theory of Electromagnetic Waves, Proceedings of a Symposium," New York University, Interscience Publishers, Inc., New York, 1951.
21. "Calculated Electrical Transmission Characteristics of (a) Half-wavelength Thick Solid Plane Sheets," D-13622, Oct. 24, 1952, and "(b) Symmetric Sandwich Flat Sheets," D-13643, Oct. 30, 1952, Boeing Airplane Company, Seattle, Wash.
22. S. Silver. (ed.): "Microwave Antenna Theory and Design," MIT Radiation Laboratory Series, vol. 12, pp. 537–542 and 383–387, McGraw-Hill Book Company, Inc., New York, 1949.
23. B. D. Raffel and E. Duploga: "Techniques for Fabricating Plastic Radomes," Goodyear Aircraft Corp., Aerophysics Dept., Akron, Ohio, June, 1953.
24. A. R. Von Hippel: "Dielectric Materials and Applications," John Wiley & Sons, Inc., New York, 1954. Contains the most complete published table of dielectric constants and loss tangents in all frequency bands as well as an extensive theory of dielectrics.
25. C. G. Montgomery (ed.): "Technique of Microwave Measurements," MIT Radiation Laboratory Series, vol. 11, pp. 560–676, McGraw-Hill Book Company, Inc., New York, 1948. Contains a description of measurement techniques of dielectric constant and loss tangent.
26. R. B. Barrar, A. F. Kay, and R. M. Redheffer: "A Graphical Procedure for Accurate Determination of the Dielectric Constant of a Panel from the Measurement of Its Transmission Phase," McMillan Laboratory, AF33(038)-12283, Ipswich, Mass., June 23, 1953.
27. Proceedings of the Ohio State University Symposiums on Radomes, unclassified volumes for June, 1955–1958, Ohio State University, Columbus, Ohio. Contains description of many recent radome developments.

Chapter 33

RADIO PROPAGATION FUNDAMENTALS

Kenneth Bullington

Bell Telephone Laboratories, Incorporated
Murray Hill, New Jersey

33.1. INTRODUCTION

The power radiated from a transmitting antenna is ordinarily spread over a relatively large area. As a result the power available at most receiving antennas is only a small fraction of the radiated power. This ratio of radiated power to received power is called the radio transmission loss, and its magnitude in some cases may be as large as 10^{15} to 10^{20} (150 to 200 db).

The transmission loss between the transmitting and receiving antennas determines whether the received signal will be useful. Each radio system has a maximum allowable transmission loss, which, if exceeded, results in either poor quality or poor reliability. Reasonably accurate predictions of transmission loss can be made on paths that approximate the ideals of either free space or plane earth. On many paths of interest, however, the path geometry or atmospheric conditions differ so much from the basic assumptions that absolute accuracy cannot be expected; nevertheless, worthwhile results can be obtained by using two or more different methods of analysis to "box in" the answer.
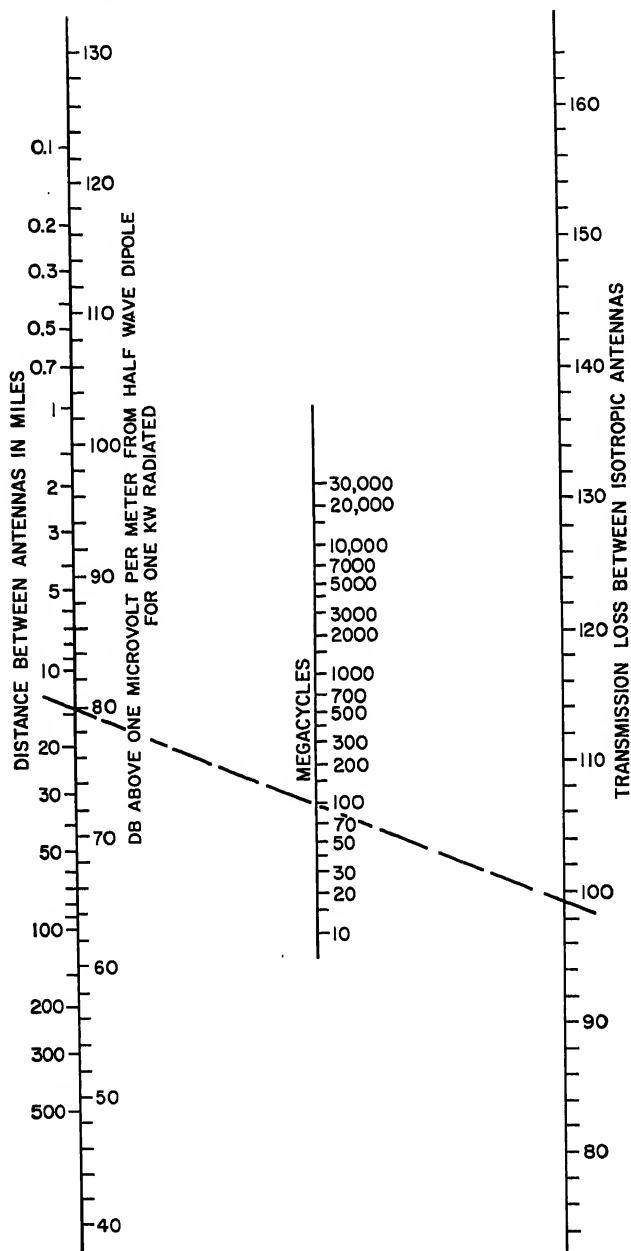
Fig. 33-1. Free-space transmission.

The basic concept in estimating radio transmission loss is the loss expected in free space, that is, in a region free of all objects that might absorb or reflect radio energy. This concept is essentially the inverse square law in optics applied to radio transmission. For a one-wavelength separation between nondirective (isotropic) antennas, the free-space loss is 22 db, and it increases by 6 db each time the distance is doubled. The free-space transmission ratio at a distance d is given by

$$\frac{P_r}{P_t} = \left(\frac{\lambda}{4\pi d}\right)^2 g_t g_r \qquad (33\text{-}1a)$$

where P_r, P_t = received power and radiated power, respectively, measured in same units

λ = wavelength, in same units as d

g_t (or g_r) = power gain of transmitting (or receiving) antenna

The power gain of an ideal isotropic antenna that radiates power uniformly in all directions is unity by definition. A small doublet whose over-all physical length is short compared with one-half wavelength has a gain of $g = 1.5$ (1.76 db), and a one-half-wave dipole has a gain of 2.15 db in the direction of maximum radiation. A nomogram for the free-space transmission loss between isotropic antennas is given in Fig. 33-1.

When antenna dimensions are large compared with the wavelength, a more convenient form of the free-space ratio is given by[1]

$$\frac{P_r}{P_t} = \frac{A_t A_r}{(\lambda d)^2} \qquad (33\text{-}1b)$$

where $A_{t,r}$ = effective area of transmitting or receiving antennas.

Another form of expressing free-space transmission is the concept of the free-space field intensity E_0, which is given by

$$E_0 = \frac{\sqrt{30 P_t g_t}}{d} \qquad \text{volts/meter} \qquad (33\text{-}2)$$

where d is in meters and P_t in watts.

The use of the field-intensity concept is frequently more convenient than the transmission-loss concept at frequencies below about 30 Mc, where external noise is generally controlling and where antenna dimensions and heights are comparable to or less than a wavelength. The free-space field intensity is independent of frequency, and its magnitude for 1 kw radiated from a half-wave dipole is shown on the left-hand scale on Fig. 33-1.

The concept of free-space transmission assumes that the atmosphere is perfectly uniform and nonabsorbing and that the earth is either infinitely far away or its reflection coefficient is negligible. In practice, the modifying effects of the earth, the atmosphere, and the ionosphere need to be considered. Both theoretical and experimental values on these effects are described in the following sections.

33.2. TRANSMISSION WITHIN LINE OF SIGHT

The presence of the ground modifies the generation and the propagation of radio waves so that the received power or field intensity is ordinarily less than would be expected in free space.[2] The effect of plane earth on the propagation of radio waves is given by

$$\frac{E}{E_0} = 1 + Re^{j\Delta} + (1 - R)Ae^{j\Delta} + \cdots \qquad (33\text{-}3)$$

| Direct wave | Reflected waves | "Surface wave" | Induction field and secondary effects of the ground |

where R = reflection coefficient of ground

A = "surface-wave" attenuation factor

$\Delta = \dfrac{4\pi h_1 h_2}{\lambda d}$

$h_{1,2}$ = antenna heights measured in same units as wavelength and distance

The parameters R and A depend to some extent on polarization and ground constants. In addition, the term "surface wave" has led to considerable confusion since it has been used in the literature to stand for entirely different concepts. These factors are discussed more completely in Sec. 33.4. However, the important point to note in this section is that considerable simplification is possible in most practical cases and that the variations with polarization and ground constants and the confusion about the surface wave can often be neglected. For near-grazing paths, R is approximately equal to -1 and the factor A can be neglected as long as both antennas are elevated more than a wavelength above the ground (or more than 5 to 10 wavelengths above sea water). Under these conditions the effect of the earth is independent of polarization and ground constants and Eq. (33-3) reduces to

$$\left| \frac{E}{E_0} \right| = \sqrt{\frac{P_r}{P_0}} = 2 \sin \frac{\Delta}{2} = 2 \sin \frac{2\pi h_1 h_2}{\lambda d} \qquad (33\text{-}4)$$

where P_0 is the received power expected in free space.

The above expression is the sum of the direct and ground reflected rays and shows the lobe structure of the signal as it oscillates around the free-space value. In most radio applications (except air to ground) the principal interest is in the lower part of the first lobe, that is, where $\Delta/2 < \pi/4$. In this case, $\sin \Delta/2 \approx \Delta/2$, and the transmission loss over plane earth is given by

$$\frac{P_r}{P_t} = \left(\frac{\lambda}{4\pi d} \right)^2 \left(\frac{4\pi h_1 h_2}{\lambda d} \right)^2 g_t g_r$$

$$= \left(\frac{h_1 h_2}{d^2} \right)^2 g_t g_r \qquad (33\text{-}5)$$

It will be noted that this relation is independent of frequency, and it is shown in decibels in Fig. 33-2 for isotropic antennas. Figure 33-2 is not valid when the indicated transmission loss is less than the free-space loss shown in Fig. 33-1, because this means that Δ is too large for this approximation.

Although the transmission loss shown in Eq. (33-5) and in Fig. 33-2 has been derived from optical concepts that are not strictly valid for antenna heights less than a few wavelengths, approximate results can be obtained for lower heights by using h_1 (or h_2) as the larger of either the actual antenna height or the minimum effective antenna height shown in Fig. 33-3. The concept of minimum effective antenna height is discussed further in Sec. 33.4. The error that can result from the use of this artifice does not exceed ± 3 db and occurs where the actual antenna height is approximately equal to the minimum effective antenna height.

The sine function in Eq. (33-4) shows that the received field intensity oscillates around the free-space value as the antenna heights are increased. The first maximum occurs when the difference between the direct- and ground-reflected waves is a half wavelength. The signal maxima have a magnitude $1 + |R|$, and the signal minima have a magnitude of $1 - |R|$.

Frequently the amount of clearance (or obstruction) is described in terms of Fresnel zones. All points from which a wave could be reflected with a path difference of one-half wavelength form the boundary of the first Fresnel zone; similarly, the boundary of the nth Fresnel zone consists of all points from which the path difference is $n/2$
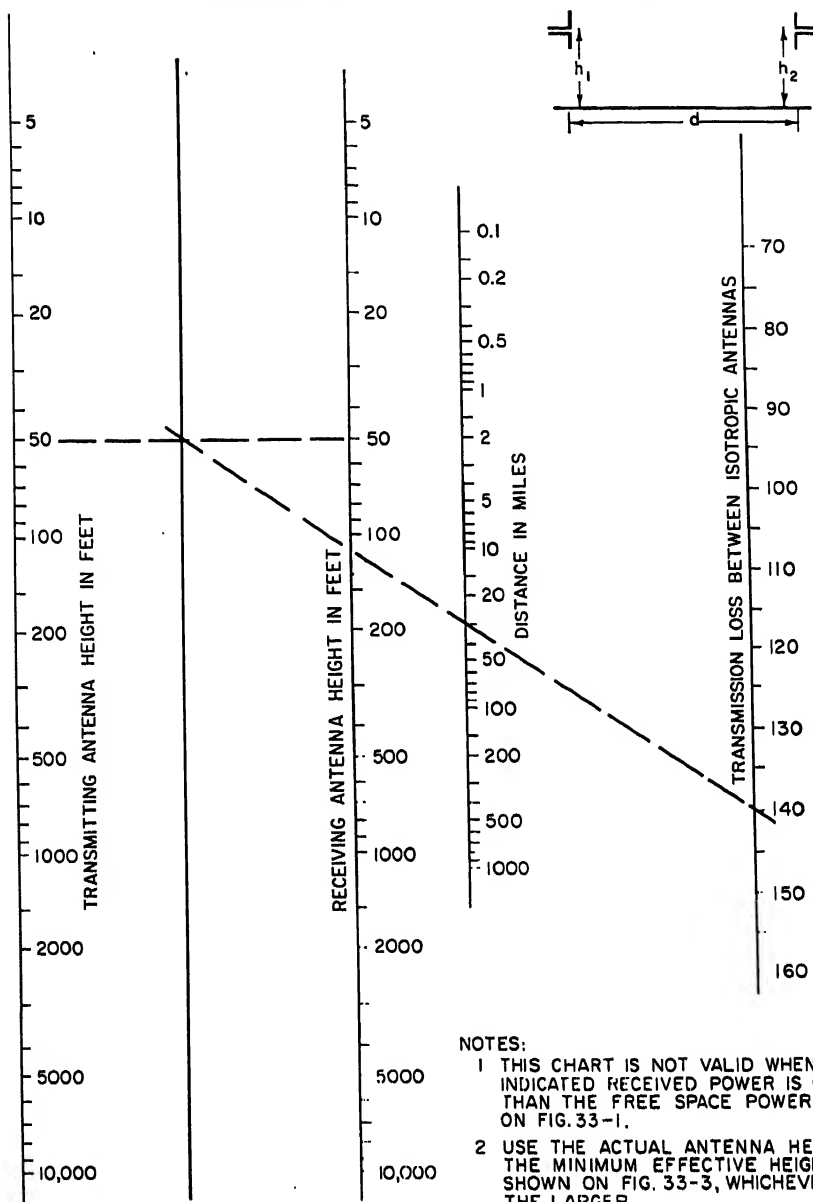
FIG. 33-2. Transmission loss over plane earth.

wavelengths. The nth-Fresnel-zone clearance H_n at any distance d_1 is given by

$$H_n = \sqrt{\frac{n\lambda d_1(d - d_1)}{d}} \qquad (33\text{-}6)$$

Although the reflection coefficient is very nearly equal to -1 for grazing angles over smooth surfaces, its magnitude may be less than unity when the terrain is rough.

The classical Rayleigh criterion of roughness indicates that specular reflection occurs when the phase deviations are less than about $\pm\pi/2$ and that the reflection coefficient will be substantially less than unity when the phase deviations are greater than $\pm\pi/2$. In most cases this theoretical boundary between specular and diffuse reflection occurs when the variations in terrain exceed one-eighth to one-fourth of the first Fresnel-zone clearance. Experimental results with microwave transmission have
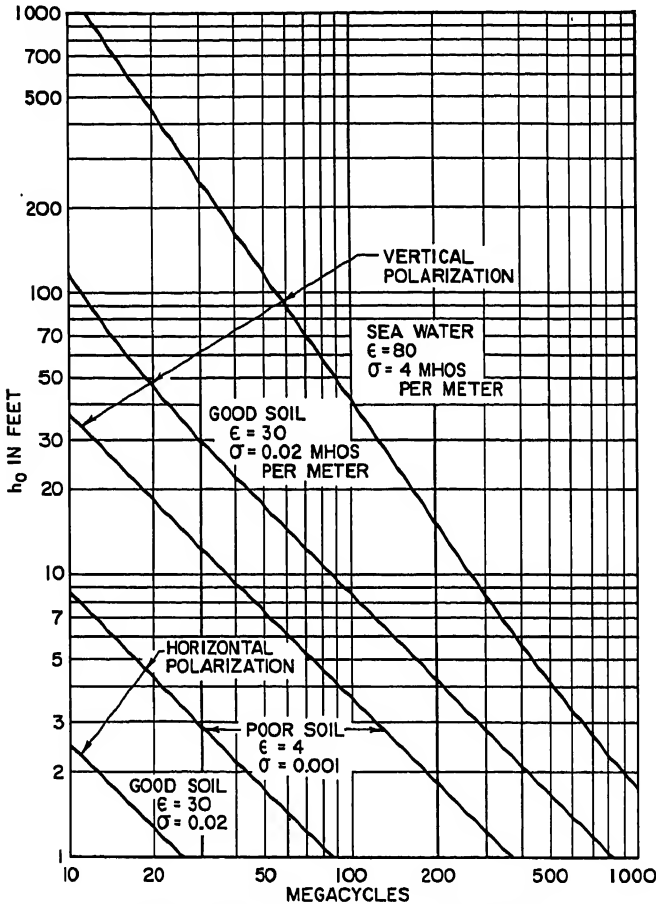
FIG. 33-3. Minimum effective antenna height.

shown that most practical paths are "rough" and ordinarily have a reflection coefficient in the range of 0.2 to 0.4. In addition, experience has shown that the reflection coefficient is a statistical problem and cannot be predicted accurately from the path profile.[3]

Fading Phenomena. Variations in signal level occur on line-of-sight paths as the result of changing atmospheric conditions. The severity of the fading usually increases as either the frequency or path length increases. Fading cannot be predicted accurately, but it is important to distinguish between two general types: (1) inverse bending and (2) multipath effects. The latter includes the fading caused by interference between direct- and ground-reflected waves as well as interference

between two or more separate paths in the atmosphere. Ordinarily, fading is a temporary diversion of energy to some other than the desired location; fading caused by absorption of energy is discussed in a later paragraph.

The path of a radio wave is not a straight line except for the ideal case of a uniform atmosphere. The transmission path may be bent up or down, depending on atmospheric conditions. This bending may either increase or decrease the effective path clearance, and inverse bending may have the effect of transforming a line-of-sight path into an obstructed one. This type of fading may last for several hours. The frequency of its occurrence and its depth can be reduced by increasing the path clearance, particularly in the middle of the path.

Severe fading may occur on over-water or other smooth paths because the phase difference between the direct and reflected rays varies with atmospheric conditions. The result is that the two rays sometimes add and sometimes tend to cancel. This type of fading can be minimized, if the terrain permits, by locating one end of the circuit high, while the other end is very low. In this way the point of reflection is placed near the low antenna and the phase difference between direct and reflected rays is kept relatively steady.

Most of the fading that occurs on rough paths with adequate clearance is the result of interference between two or more rays traveling slightly different routes in the atmosphere. This multipath type of fading is relatively independent of path clearance, and its extreme condition approaches the Rayleigh distribution. In the Rayleigh distribution, the probability that the instantaneous value of the field is greater than the value R is $\exp[-(R/R_0)^2]$ where R_0 is the rms value.

Representative values of fading on a path with adequate clearance are shown on Fig. 33-4. After the multipath fading has reached the Rayleigh distribution, a further increase in either distance or frequency increases the number of fades of a given depth, but decreases the duration so that the product is the constant indicated by the Rayleigh distribution.

Miscellaneous Effects. The remainder of this section describes some miscellaneous effects of line-of-sight transmission that may be important at frequencies above about 1,000 Mc. These effects include variation in angles of arrival, maximum useful antenna gain, useful bandwidth, the use of frequency or space diversity, and atmospheric absorption.

On line-of-sight paths with adequate clearance, some components of the signal may arrive with variations in angle of arrival of as much as $\frac{1}{2}$ to $\frac{3}{4}°$ in the vertical plane, but the variations in the horizontal plane are less than $0.1°$.[4,5] Consequently, if antennas with beamwidths less than about $0.5°$ are used, there may occasionally be some loss in received signal because most of the incoming energy arrives outside the antenna beamwidth. Signal variations due to this effect are usually small compared with the multipath fading.

Multipath fading is selective fading, and it limits both the maximum useful bandwidth and the frequency separation needed for adequate frequency diversity. For 40-db antennas on a 30-mile path the fading on frequencies separated by 100 to 200 Mc is essentially uncorrelated regardless of the absolute frequency. With less directive antennas, uncorrelated fading can occur at frequencies separated by less than 100 Mc.[6,7] Larger antennas (more narrow beamwidths) will decrease the fast multipath fading and widen the frequency separation between uncorrelated fading, but at the risk of increasing the long-term fading associated with the variations in the angle of arrival.

Optimum space diversity, when ground reflections are controlling, requires that the separation between antennas be sufficient to place one antenna on a field-intensity maximum while the other is in a field-intensity minimum. In practice, the best spacing is usually not known because the principal fading is caused by multipath

variations in the atmosphere. However, adequate diversity can usually be achieved with a vertical separation of 100 to 200 wavelengths.

At frequencies above 5,000 to 10,000 Mc, the presence of rain, snow, or fog introduces an absorption in the atmosphere which depends on the amount of moisture and on the frequency. During a rain of cloudburst proportions, the attenuation at 10,000 Mc may reach 5 db/mile and at 25,000 Mc it may be in excess of 25 db/mile.[8] In addition to the effect of rainfall, some selective absorption may result from the oxygen and water vapor in the atmosphere. The first absorption peak due to water
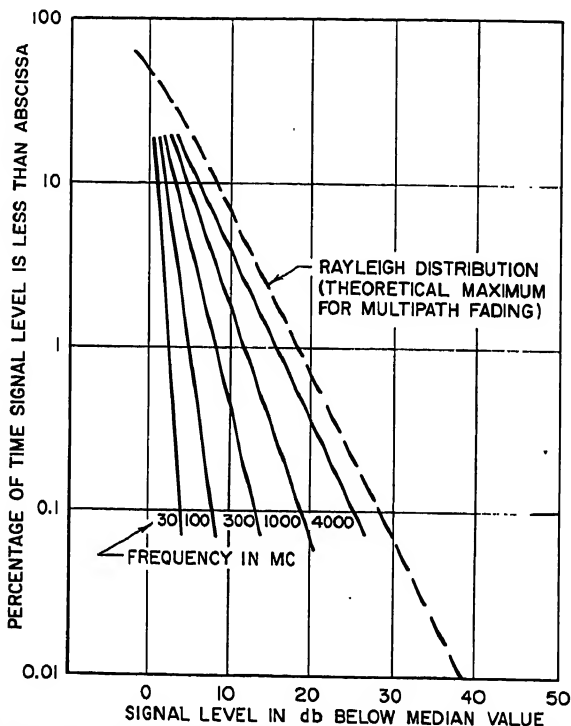
FIG. 33-4. Typical fading characteristics in the worst month on 30- to 40-mile line-of-sight paths with 50- to 100-ft clearance.

vapor occurs at about 24,000 Mc and the first absorption peak for oxygen occurs at about 60,000 Mc.

33.3. TROPOSPHERIC TRANSMISSION BEYOND LINE OF SIGHT

A basic characteristic of electromagnetic waves is that the energy is propagated in a direction perpendicular to the surface of uniform phase. Radio waves travel in a straight line only as long as the phase front is plane and is infinite in extent.

Energy can be transmitted beyond the horizon by three principal methods: reflection, refraction, and diffraction. Reflection and refraction are associated with either sudden or gradual changes in the direction of the phase front, while diffraction is an edge effect that occurs because the phase surface is not infinite. When the resulting phase front at the receiving antenna is irregular in either amplitude or position, the distinctions between reflection, refraction, and diffraction tend to break down. In this case the energy is said to be scattered. Scattering is frequently pictured as a

result of irregular reflections, although irregular refraction plus diffraction may be equally important.

The following paragraphs describe first the theories of refraction and of diffraction over a smooth sphere and a knife edge. This is followed by empirical data derived from experimental results on the transmission to points far beyond the horizon, on the effects of hills and trees, and on fading phenomena.

Refraction. The dielectric constant of the atmosphere normally decreases gradually with increasing altitude. The result is that the velocity of transmission increases with the height above the ground, and, on the average, the radio energy is bent or refracted toward the earth. As long as the change in dielectric constant is linear with height, the net effect of refraction is the same as if the radio waves continued to travel in a straight line but over an earth whose modified radius is

$$ka = \frac{a}{1 + \frac{a}{2}\frac{d\epsilon}{dh}} \tag{33-7}$$

where a = true radius of earth

$d\epsilon/dh$ = rate of change of dielectric constant with height.

Under certain atmospheric conditions the dielectric constant may increase ($0 < k < 1$) over a reasonable height, thereby causing the radio waves in this region to bend away from the earth. This is the cause of the inverse bending type of fading mentioned in the preceding section. It is sometimes called substandard refraction. Since the earth's radius is about 2.1×10^7 ft, a decrease in dielectric constant of only 2.4×10^{-8} per foot of height results in a value of $k = \frac{4}{3}$, which is commonly assumed to be a good average value.[9] When the dielectric constant decreases about four times as rapidly (or by about 10^{-7} per foot of height), the value of $k = \infty$. Under such a condition, as far as radio propagation is concerned, the earth can then be considered flat, since any ray that starts parallel to the earth will remain parallel.

When the dielectric constant decreases more rapidly than 10^{-7} per foot of height, radio waves that are radiated parallel to or at an angle above the earth's surface may be bent downward sufficiently to be reflected from the earth. After reflection the ray is again bent toward the earth, and the path of a typical ray is similar to the path of a bouncing tennis ball. The radio energy appears to be trapped in a duct or waveguide between the earth and the maximum height of the radio path. This phenomenon is variously known as trapping, duct transmission, anomalous propagation, or guided propagation.[10,11] It will be noted that in this case the path of a typical guided wave is similar in form to the path of sky waves, which are lower-frequency waves trapped between the earth and the ionosphere. However, there is little or no similarity between the virtual heights, the critical frequencies, or the causes of refraction in the two cases.

Duct transmission is important because it can cause long-distance interference with another station operating on the same frequency; however, it does not occur often enough nor can its occurrence be predicted with enough accuracy to make it useful for radio services requiring high reliability.

Diffraction over a Smooth Spherical Earth and Ridges. Radio waves are also transmitted around the earth by the phenomenon of diffraction. Diffraction is a fundamental property of wave motion, and in optics it is the correction to apply to geometrical optics (ray theory) to obtain the more accurate wave optics. In other words, all shadows are somewhat "fuzzy" on the edges, and the transition from "light" to "dark" areas is gradual, rather than infinitely sharp. Our common experience is that light travels in straight lines and that shadows are sharp, but this is only because the diffraction effects for these very short wavelengths are too small to be noticed without the aid of special laboratory equipment. The order of mag-

nitude of the diffraction at radio frequencies may be obtained by recalling that a 1,000-Mc radio wave has about the same wavelength as a 1,000-cycle sound wave in air, so that these two types of waves may be expected to bend around absorbing obstacles with approximately equal facility.

The effect of diffraction around the earth's curvature is to make possible transmission beyond the line of sight. The magnitude of the loss caused by the obstruction increases as either the distance or the frequency is increased, and it depends to some
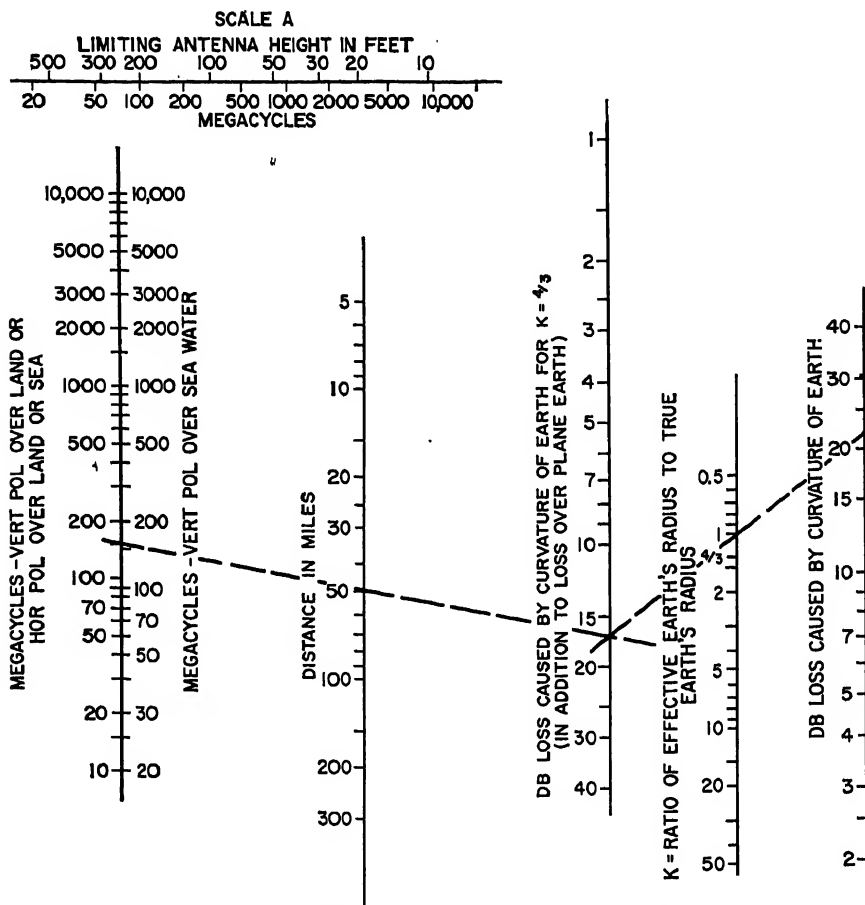
Fig. 33-5. Diffraction loss around a perfect sphere.

extent on the antenna height.[11] The loss resulting from the curvature of the earth is indicated by Fig. 33-5 as long as neither antenna is higher than the limiting value shown at the top of the chart. This loss is in addition to the transmission loss over plane earth obtained from Fig. 33-2.

When either antenna is as much as twice as high as the limiting value shown on Fig. 33-5, this method of correcting for the curvature of the earth indicates a loss that is too great by about 2 db, with the error increasing as the antenna height increases. An alternative method of determining the effect of the earth's curvature is given by Fig. 33-6. The latter method is approximately correct for any antenna height, but

it is theoretically limited in distance to points at or beyond the line of sight, assuming that the curved earth is the only obstruction. Figure 33-6 gives the loss relative to free-space transmission (and hence is used with Fig. 33-1) as a function of three distances: d_1 is the distance to the horizon from the lower antenna; d_2 is the distance
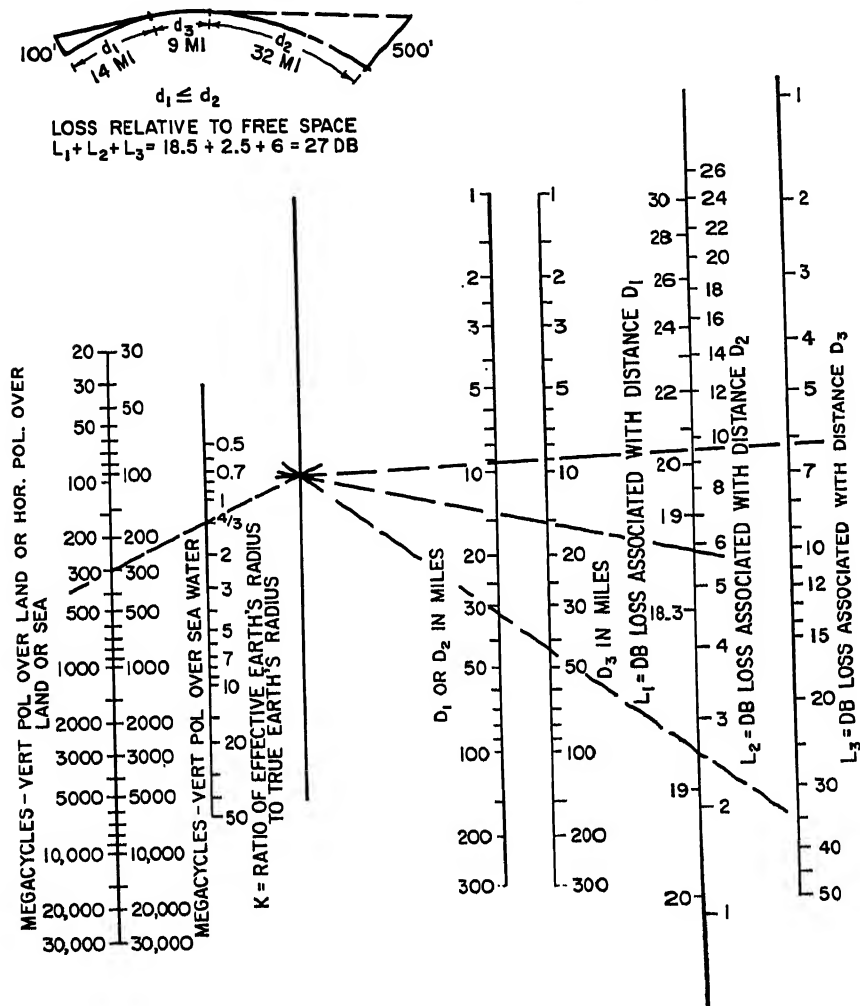
FIG. 33-6. Diffraction loss relative to free-space transmission at points beyond line of sight over a smooth sphere.

to the horizon from the higher antenna; and d_3 is the distance beyond the line of sight. In other words, the total distance between antennas is $d = d_1 + d_2 + d_3$. The distance to the horizon over smooth earth is given by

$$d_{1,2} = \sqrt{2kah_{1,2}} \tag{33-8}$$

where $h_{1,2}$ = the appropriate antenna height
ka = effective earth's radius

The preceding discussion assumes that the earth is a perfectly smooth sphere, and the results are critically dependent on a smooth surface and a uniform atmosphere. The modification in these results caused by the presence of hills, trees, and buildings is difficult or impossible to compute, but the order of magnitude of these effects may be obtained from a consideration of the other extreme case, which is propagation over a perfectly absorbing knife edge.
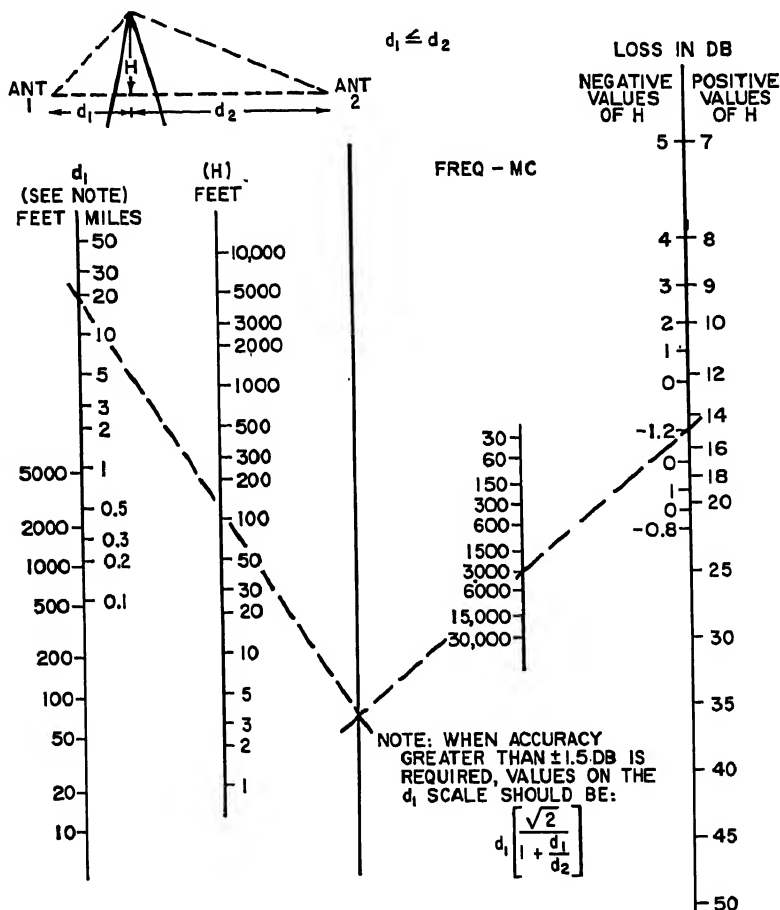
FIG. 33-7. Knife-edge diffraction loss relative to free space.

The diffraction of plane waves over a knife edge or screen causes a shadow loss whose magnitude is shown on Fig. 33-7. The height of the obstruction H is measured from the line joining the two antennas to the top of the ridge. It will be noted that the shadow loss approaches 6 db as H approaches 0 (grazing incidence) and that it increases with increasing positive values of H. When the direct ray clears the obstruction, H is negative, and the shadow loss approaches 0 db in an oscillatory manner as the clearance is increased. In other words, a substantial clearance is required over line-of-sight paths in order to obtain "free-space" transmission. The knife-edge diffraction calculation is substantially independent of polarization as long as the distance from the edge is more than a few wavelengths.
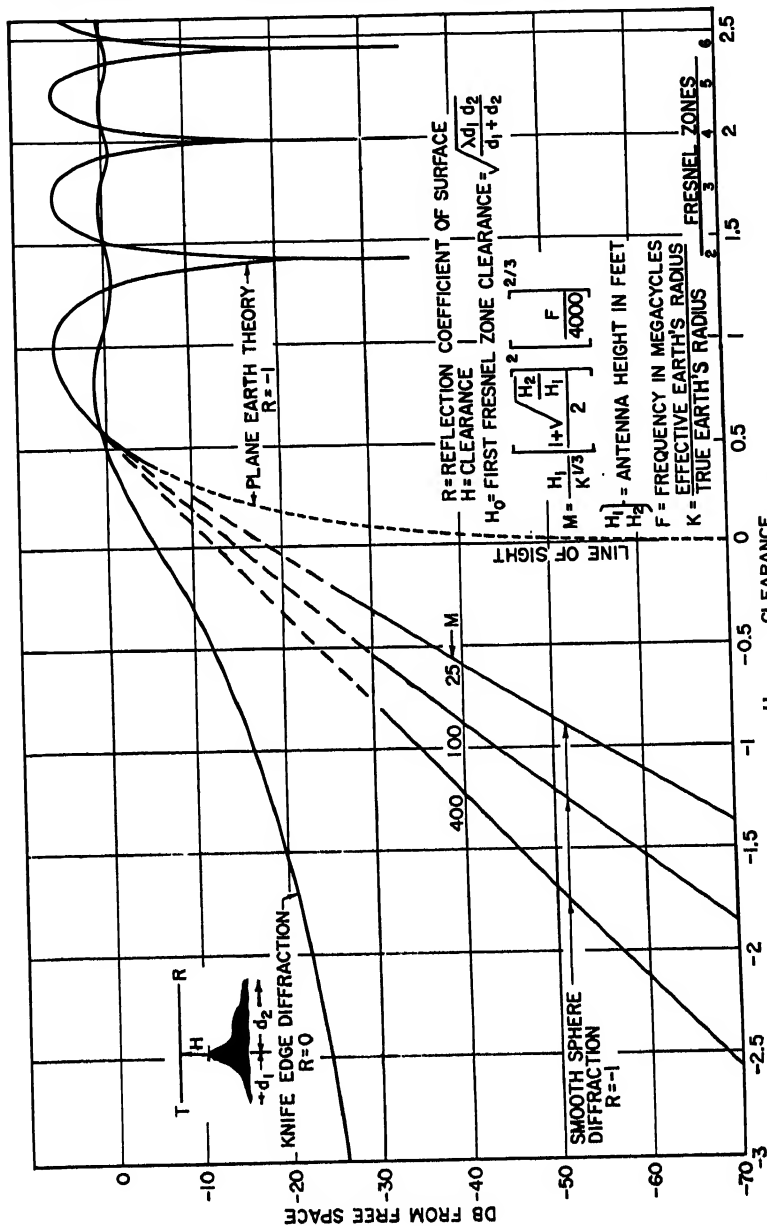
Fig. 33-8. Transmission loss vs. clearance.

At grazing incidence the expected loss over a ridge is 6 db (Fig. 33-7), while, over a smooth spherical earth, Fig. 33-6 indicates a loss of about 20 db. More accurate results in the vicinity of the horizon can be obtained by expressing radio transmission in terms of path clearance measured in Fresnel zones, as shown in Fig. 33-8. In this representation the plane-earth theory and the ridge diffraction can be represented by single lines; but the smooth-sphere theory requires a family of curves with a parameter M that depends primarily on antenna heights and frequency. The big difference in the losses predicted by diffraction around a perfect sphere and by diffraction over a knife edge indicates that diffraction losses depend critically on the assumed type of profile. A suitable solution for the intermediate problem of diffraction over a rough earth has not yet been obtained.

Experimental Data Far beyond the Horizon. Most of the experimental data at points far beyond the horizon fall in between the theoretical curves for diffraction over a smooth sphere and for diffraction over a knife-edge obstruction. Various theories have been advanced to explain these effects, but none has been reduced to a
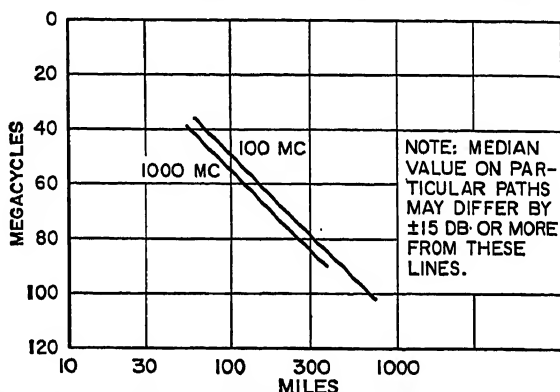
FIG. 33-9. Beyond-horizon transmission—median signal level vs. distance.

simple form for everyday use.[13] The explanation most commonly accepted is that energy is reflected or scattered from turbulent air masses in the volume of air that is enclosed by the intersection of the beamwidths of the transmitting and receiving antennas.[14]

The variations in the long-term median signals with distance have been derived from experimental results and are shown in Fig. 33-9 for two frequencies.[15] The ordinate is in decibels below the signal that would have been expected at the same distance in free space with the same power and the same antennas. The strongest signals are obtained by pointing the antennas at the horizon along the great-circle route. The values shown on Fig. 33-9 are essentially annual averages taken from a large number of paths, and substantial variations are to be expected with terrain, climate, and season as well as from day-to-day fading.

Antenna sites with sufficient clearance so that the horizon is several miles away will, on the average, provide a higher median signal (less loss) than shown on Fig. 33-9. Conversely, sites for which the antenna must be pointed upward to clear the horizon will ordinarily result in appreciably more loss than shown on Fig. 33-9. In many cases the effects of path length and angles to the horizon can be combined by plotting the experimental results as a function of the angle between the lines drawn tangent to the horizon from the transmitting and receiving sites.[16]

When the path profile consists of a single sharp obstruction that can be seen from both terminals, the signal level may approach the value predicted by the knife-edge-

diffraction theory.[17]   While several interesting and unusual cases have been recorded, the knife-edge, or "obstacle-gain," theory is not applicable to the typical but only to the exceptional paths.

As in the case of line-of-sight transmission, the fading of radio signals beyond the horizon can be divided into fast fading and slow fading.   The fast fading is caused by multipath transmission in the atmosphere, and for a given size antenna the rate of fading increases as either the frequency or the distance is increased.   This type of fading is much faster than the maximum fast fading observed on line-of-sight paths, but the two are similar in principle.   The magnitude of the fades is described by the Rayleigh distribution.
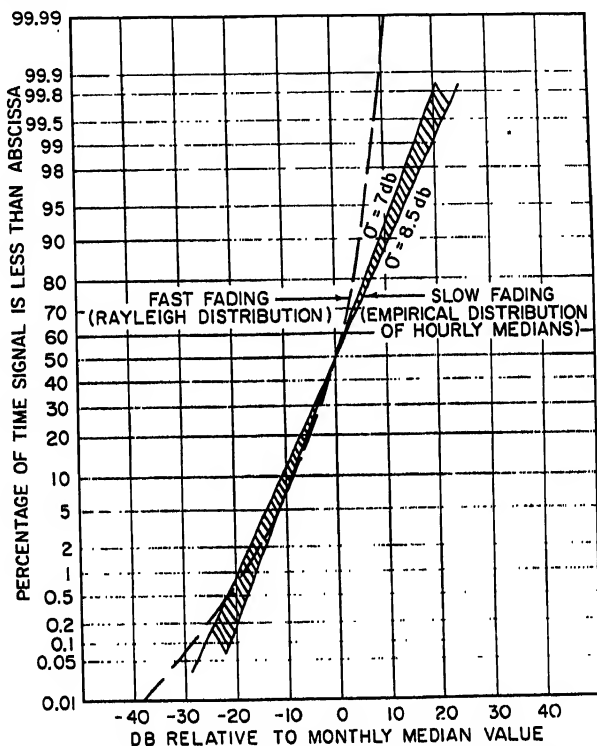
Fig. 33-10. Typical fading characteristics at points far beyond the horizon.

Slow fading means variations in average signal level over a period of hours or days, and it is greater on beyond-horizon paths than on line-of-sight paths.   This type of fading is almost independent of frequency and seems to be associated with changes in the average refraction of the atmosphere.   At distances of 150 to 200 miles the variations in hourly median value around the annual median seem to follow a normal-probability law in decibels with a standard deviation of about 8 db.   Typical fading distributions are shown on Fig. 33-10.

The median signal levels are higher in warm humid climates than in cold dry climates, and seasonal variations of as much as ±10 db or more from the annual median have been observed.[18]

Since the scattered signals arrive with considerable phase irregularities in the plane of the receiving antenna, narrow-beamed (high-gain) antennas do not yield power outputs proportional to their theoretical area gains.   This effect has sometimes

been called loss in antenna gain, but it is a propagation effect and not an antenna effect.   On 150 to 200 miles this loss in received power may amount to 1 or 2 db for a 40-db gain antenna and perhaps 6 db for a 50-db antenna.   These extra losses vary with time, but the variations seem to be uncorrelated with the actual signal level.

The bandwidth that can be used on a single radio carrier is frequently limited by the selective fading caused by multipath or echo effects.   Echoes are not troublesome as long as the echo time delays are very short compared with one cycle of the highest baseband frequency.   The probability of long-delayed echoes can be reduced (and the rate of fast fading can be decreased) by the use of narrow-beam antennas both

* REFERRED TO PLANE
  EARTH VALUES
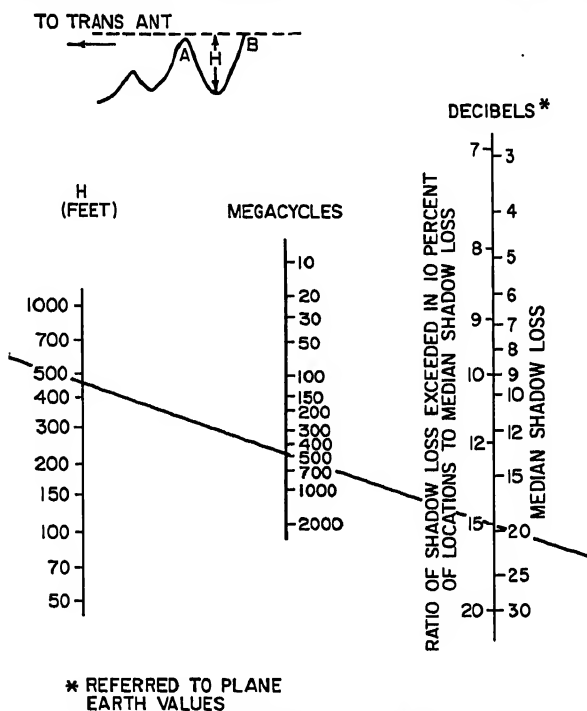
FIG. 33-11. Estimated distribution of shadow losses.

within and beyond the horizon.[13-19]   Useful bandwidths of several megacycles appear to be feasible with the antennas that are needed to provide adequate signal-to-noise margins.   Successful tests of television and of multichannel telephone transmission have been reported on a 188-mile path at 5,000 Mc.[20]

The effects of fast fading can be reduced substantially by the use of either frequency or space diversity.   The frequency or space separation required for diversity varies with time and with the degree of correlation that can be tolerated.   A horizontal (or vertical) separation of about 100 wavelengths is ordinarily adequate for space diversity on 100- to 200-mile paths.   The corresponding figure for the required frequency separation for adequate diversity seems likely to be more than 20 Mc.

Effects of Nearby Hills, Particularly on Short Paths.   The experimental results on the effects of hills indicate that the shadow losses increase with the frequency and with the roughness of the terrain.[21]

An empirical summary of the available data is shown on Fig. 33-11.   The roughness of the terrain is represented by the height H shown on the profile at the top of the

chart. This height is the difference in elevation between the bottom of the valley and the elevation necessary to obtain line of sight from the transmitting antenna. The right-hand scale in Fig. 33-11 indicates the additional loss above that expected over plane earth. Both the median loss and the difference between the median and the 10 per cent values are shown. For example, with variations in terrain of 500 ft, the estimated median shadow loss at 450 Mc is about 20 db and the shadow loss exceeded in only 10 per cent of the possible locations between points A and B is about $20 + 15 = 35$ db. It will be recognized that this analysis is based on large-scale variations in field intensity and does not include the standing-wave effects which sometimes cause the field intensity to vary considerably within a few feet.

Effects of Buildings and Trees. The shadow losses resulting from buildings and trees follow somewhat different laws from those caused by hills. Buildings may be more transparent to radio waves than the solid earth, and there is ordinarily much more back scatter in the city than in the open country. Both of these factors tend to reduce the shadow losses caused by the buildings, but, on the other hand, the angles of diffraction over or around the buildings are usually greater than for natural terrain. In other words, the artificial canyons caused by buildings are considerably narrower than natural valleys, and this factor tends to increase the loss resulting from the presence of buildings. The available quantitative data on the effects of buildings are confined primarily to New York City. These data indicate that in the range of 40 to 450 Mc there is no significant change with frequency, or at least the variation with frequency is somewhat less than that noted in the case of hills.[22] The median field intensity at street level for random locations in Manhattan (New York City) is about 25 db below the corresponding plane-earth value. The corresponding values for the 10 and 90 per cent points are about 15 and 35 db, respectively.

Typical values of attenuation through a brick wall are from 2 to 5 db at 30 Mc and 10 to 40 db at 3,000 Mc, depending on whether the wall is dry or wet. Consequently, most buildings are rather opaque at frequencies of the order of thousands of megacycles.

When an antenna is surrounded by moderately thick trees and below treetop level, the average loss at 30 Mc resulting from the trees is usually 2 or 3 db for vertical polarization and is negligible with horizontal polarization. However, large and rapid variations in the received field intensity may exist within a small area, resulting from the standing-wave pattern set up by reflections from trees located at a distance of several wavelengths from the antenna. Consequently, several nearby locations should be investigated for best results. At 100 Mc the average loss from surrounding trees may be 5 to 10 db for vertical polarization and 2 or 3 db for horizontal polarization. The tree losses continue to increase as the frequency increases, and above 300 to 500 Mc they tend to be independent of the type of polarization. Above 1,000 Mc, trees that are thick enough to block vision are roughly equivalent to a solid obstruction of the same over-all size.

33.4. MEDIUM- AND LOW-FREQUENCY GROUND-WAVE TRANSMISSION

Wherever the antenna heights are small compared with the wavelength, the received field intensity is ordinarily stronger with vertical polarization than with horizontal and is stronger over sea water than over poor soil. In these cases the "surface-wave" term in Eq. (33-3) cannot be neglected. This use of the term "surface wave" follows Norton's usage and is not equivalent to the Sommerfeld or Zenneck "surface waves."

The parameter A is the plane-earth attenuation factor for antennas at ground level. It depends upon the frequency, ground constants, and type of polarization. It is never greater than unity and decreases with increasing distance and frequency, as indicated by the following approximate equation:[1,23]

$$A \approx \frac{-1}{1 + j\frac{2\pi d}{\lambda}(\sin\theta + z)^2} \tag{33-9}$$

where $z = \dfrac{\sqrt{\epsilon_0 - \cos^2\theta}}{\epsilon\theta}$ for vertical polarization

$z = \sqrt{\epsilon_0 - \cos^2\theta}$ for horizontal polarization

$\epsilon_0 = \epsilon - j60\sigma\lambda$

θ = angle between reflected ray and ground

 = 0 for antennas at ground level

ϵ = dielectric constant of ground relative to unity in free space

σ = conductivity of ground, mhos/meter

λ = wavelength, meters

In terms of these same parameters the reflection coefficient of the ground is given by[25]

$$R = \frac{\sin\theta - z}{\sin\theta + z} \tag{33-10}$$

When $\theta \ll |z|$ the reflection coefficient approaches -1; when $\theta \gg |z|$ (which can happen only with vertical polarization) the reflection coefficient approaches $+1$. The angle for which the reflection coefficient is a minimum is called the pseudo-Brewster angle, and it occurs when $\sin\theta = |z|$.

For antennas approaching ground level, the first two terms in Eq. (33-3) cancel each other (h_1 and h_2 approach zero, and R approaches -1) and the magnitude of the third term becomes

$$|(1 - R)A| \approx \frac{2}{(2\pi d/\lambda)z^2} = \frac{4\pi h_0^2}{\lambda d} \tag{33-11}$$

where h_0 = minimum effective antenna height shown in Fig. 33-3

 $= \left|\dfrac{\lambda}{2\pi z}\right|$

The surface-wave term arises because the earth is not a perfect reflector. Some energy is transmitted into the ground and sets up ground currents, which are distorted relative to what would have been the case in an ideal, perfectly reflecting surface. The surface wave is defined as the vertical electric field for vertical polarization, or the horizontal electric field for horizontal polarization, that is associated with the extra components of the ground currents caused by lack of perfect reflection. Another component of the electric field associated with the ground currents is in the direction of propagation. It accounts for the success of the wave antenna at lower frequencies, but it is always smaller in magnitude than the surface wave as defined above. The components of the electric vector in three mutually perpendicular coordinates are given by Norton.[26]

In addition to the effect of the earth on the propagation of radio waves, the presence of the ground may also affect the impedance of low antennas and thereby may have an effect on the generation and reception of radio waves.[25] As the antenna height varies, the impedance oscillates around the free-space value, but the variations in impedance are usually unimportant as long as the center of the antenna is more than a quarter wavelength above the ground. For vertical grounded antennas (such as are used in standard AM broadcasting), the impedance is doubled and the net effect is that the maximum field intensity is 3 db above the free-space value instead of 6 db as indicated in Eq. (33-4) for elevated antennas.

Typical values of the field intensity to be expected from a grounded quarter-wave vertical antenna are shown in Fig. 33-12 for transmission over poor soil and in Fig.
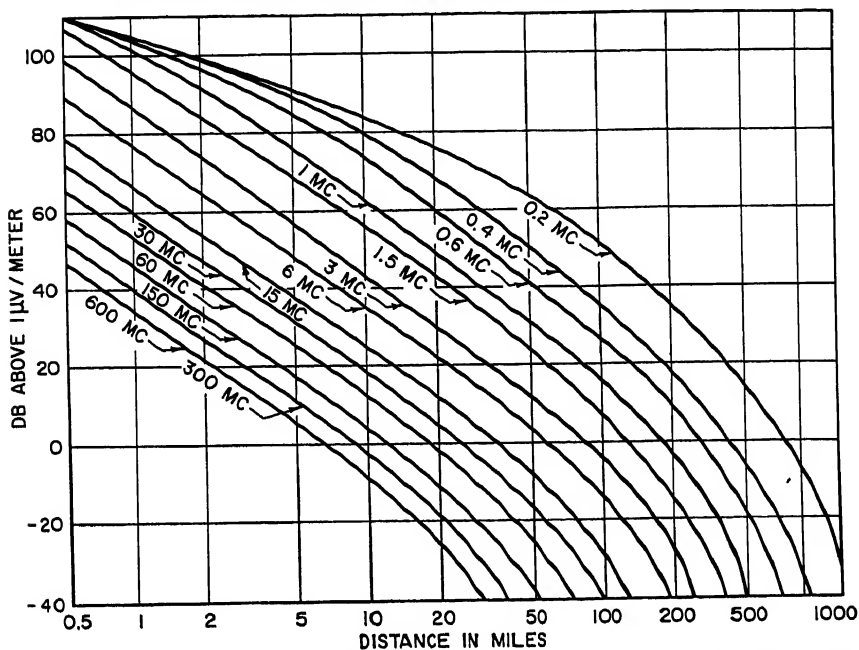
FIG. 33-12. Field intensity for vertical polarization over poor soil for 1 kw radiated power from a grounded whip antenna.
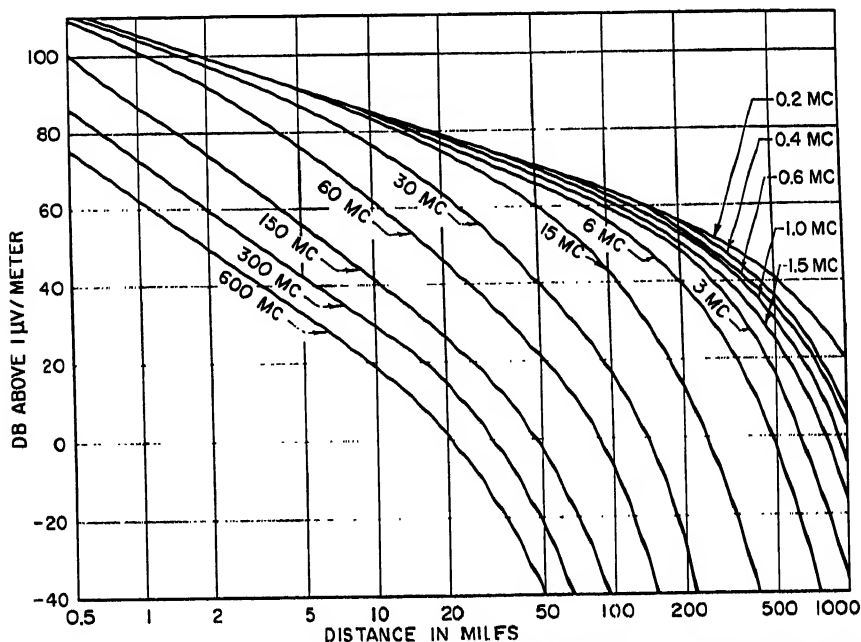
FIG. 33-13. Field intensity for vertical polarization over sea water for 1 kw radiated power from a grounded whip antenna.
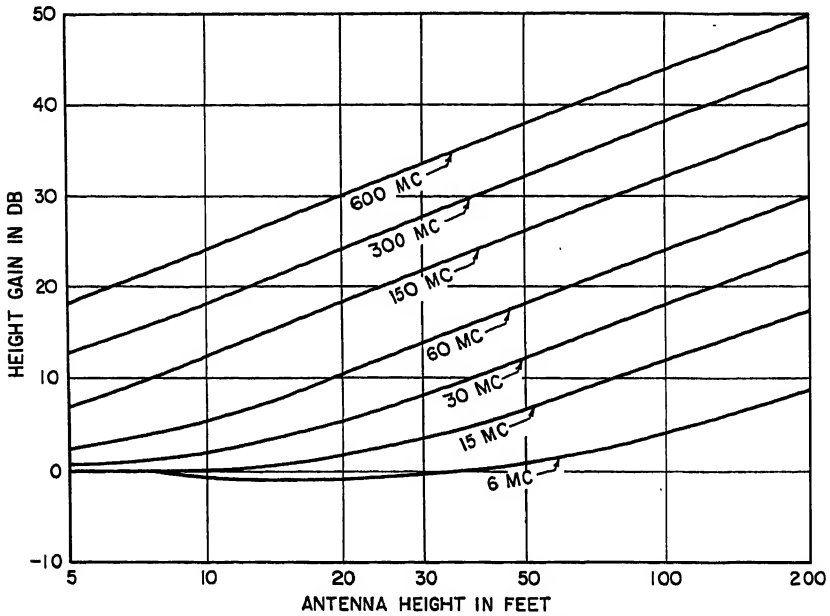
FIG. 33-14. Antenna height-gain factor for vertical polarization over poor soil.
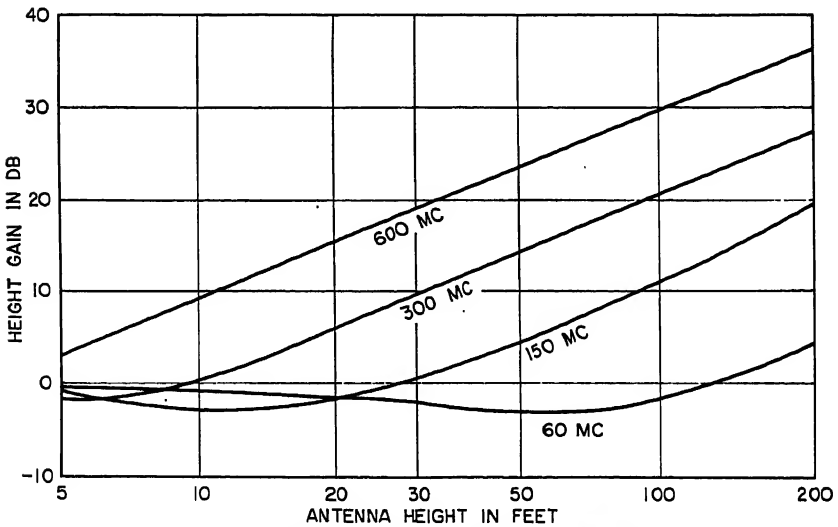
FIG. 33-15. Antenna height-gain factor for vertical polarization over sea water.

33-13 for transmission over sea water. These charts include the effect of diffraction and average refraction around a smooth spherical earth as discussed in Sec. 33.3, but do not include the ionospheric effects described in the next section. The increase in signal obtained by raising either antenna height is shown in Fig. 33-14 for poor soil and Fig. 33-15 for sea water.

33.5. IONOSPHERIC TRANSMISSION

In addition to the tropospheric or ground-wave transmission discussed in the preceding sections, useful radio energy at frequencies below about 25 to 100 Mc may be returned to the earth by reflection from the ionosphere, which consists of several ionized layers located 50 to 200 miles above the earth.   The relatively high density of ions and free electrons in this region provides an effective index of refraction of less than 1, and the resulting transmission path is similar to that in the well-known optical phenomenon of total internal reflection.   The primary mechanism is refraction in the ionosphere, but for convenience it is generally spoken of as reflection from certain virtual heights.[27]   Polarization is not maintained in ionospheric transmission, and the choice depends on the antenna design that is most efficient at the desired elevation angles.
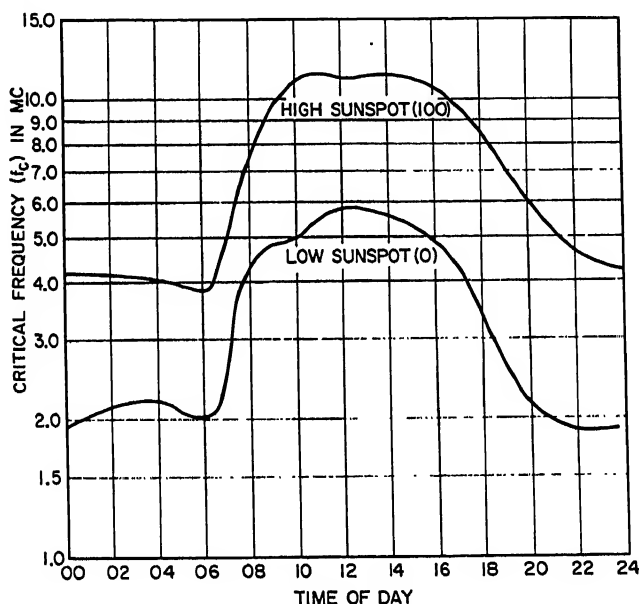
Fig. 33-16. Typical diurnal variation of critical frequency for January at latitude 40°.

Regular Ionospheric Transmission.   The ionosphere consists of three or more distinct layers.   This does not mean that the space between layers is free of ionization but rather that the curve of ion density vs. height has several distinct peaks.   The E, F_1, and F_2 layers are present during the daytime, but the F_1 and F_2 combine to form a single layer at night.   A lower layer called the D layer is also present during the day, but its principal effect is to absorb rather than reflect.

Information about the nature of the ionosphere has been obtained by transmitting pulsed radio signals directly overhead and by recording the signal intensity and the time delay of the echoes returned from these layers.   At night all frequencies below the critical frequency f_c are returned to earth with an average signal intensity that is about 3 to 6 db below the free-space signal that would be expected for the round-trip distance.   At frequencies higher than the critical frequency the signal intensity is very weak or undetectable.   Typical values of the critical frequency for Washington, D.C., are shown in Fig. 33-16.

During the daytime, the critical frequency is increased two to three times over the corresponding nighttime value. This apparent increase in the useful frequency range for ionospheric transmission is largely offset by the heavy daytime absorption, which reaches a maximum in the 1- to 2-Mc range. This absorption is caused by interaction between free electrons and the earth's magnetic field. The absence of appreciable absorption at night indicates that most of the free electrons disappear when the sun goes down. Charged particles traveling in a magnetic field have a resonant or gyromagnetic frequency, and for electrons in the earth's magnetic field of about 0.5 gauss, this resonance occurs at about 1.4 Mc. The magnitude of the absorption varies with the angle of the sun above the horizon and is a maximum about noon. The approximate midday absorption is shown on Fig. 33-17 in terms of decibels per 100 miles of path length. (On short paths this length is the actual path traveled, not the distance along the earth's surface.)

FIG. 33-17. Typical values of midday iono-spheric absorption.

Long-distance transmission requires that the signal be reflected from the ionosphere at a small angle instead of the perpendicular incidence used in obtaining the critical frequency. For angles other than directly overhead an assumption which seems to be borne out in practice is that the highest frequency for which essentially free-space transmission is obtained is $f_c/\sin \alpha$ where α is the angle between the radio ray and ionospheric layer. This limiting frequency is greater than the critical frequency and is called the "maximum usable frequency" (MUF). The curved geometry limits the distance that can be obtained with one-hop transmission to about 2,500 miles, and the MUF at the longer distances does not exceed 3 to 3.5 times the critical frequency.

The difference between day and night effects means that most sky-wave paths require at least two frequencies. A relatively low frequency is needed to get under the nighttime MUF, and a higher frequency is needed that is below the daytime MUF, but above the region of high absorption. This lower limit depends on the available signal-to-noise margin and is commonly called the lowest useful high frequency.

Frequencies most suitable for transmission over 1,000 miles or over will ordinarily not be reflected at the high angles needed for much shorter distances. As a result, the range of sky-wave transmission ordinarily does not overlap the range of ground-wave transmission, and the intermediate region is called the skip zone because the signal is too weak to be useful. At frequencies of a few megacycles the ground-wave and sky-wave ranges may overlap, with the result that severe fading occurs when the two signals are comparable in amplitude.

In addition to the diurnal variations in frequency and in absorption, there are systematic changes with season, latitude, and with the nominally 11-year sunspot cycle. Random changes in the critical frequency of about ± 15 per cent from the monthly median value are also to be expected from day to day.

The F layer is the principal contributor to transmission beyond 1,000 to 1,500 miles, and typical values of the maximum usable frequency can be summarized as follows. The median nighttime critical frequency for F-layer transmission at the latitude at Washington, D.C., is about 2 Mc in the month of June during a period of low sunspot activity. All frequencies below about 2 Mc are strongly reflected to earth, while the higher frequencies are either greatly attenuated or are lost in outer space. The

approximate maximum usable frequency for other conditions is greater than 2 Mc by the ratios shown in Table 33-1.

Table 33-1

Variation with:	*Multiplying factor*
Time of day:	
Midnight......................	1 (reference)
Early afternoon:	
June........................	2
December....................	3
Path length:	
Less than 200 miles.............	1 (reference)
Approximately 1,000 miles........	2
More than 2,500 miles...........	3.5
Sunspot cycle	
Minimum......................	1 (reference)
For 1 year in 5:	
June........................	1.5
December....................	2
For 1 year in 50:	
June........................	2
December....................	3

When all the above variations add "in phase," transmission for distances of 2,500 miles or more is possible at frequencies up to 40 to 60 Mc. For example, using the above table, 2,500-mile transmission on an early December afternoon in 1 year out of 5 can be expected on a frequency of about 42 Mc, which is $3 \times 3.5 \times 2 = 21$ times the reference critical frequency of 2 Mc. Peaks of the sunspot cycle occurred in 1937 and in 1947–1948, so another peak is expected in 1958–1959.

The maximum usable frequency also varies with the geomagnetic latitude, but as a first approximation, the above values are typical of continental United States. Forecasts of the MUF to be expected throughout the world are issued monthly by the National Bureau of Standards.[28,29] These estimates include the diurnal, seasonal, and sunspot effects.

Another type of absorption, over and above the usual daytime absorption, occurs both day and night on transmission paths that travel through the auroral zone. The auroral zones are centered on the north and south magnetic poles at about the same distance as the Arctic Circle is from the geographical North Pole. During periods of magnetic storms these auroral zones expand over an area much larger than normal and thereby disrupt communication by introducing unexpected absorption. These conditions of poor transmission can last for hours and sometimes even for days. These periods of increased absorption are more common in the polar regions than in the Temperate Zones or the tropics because of the proximity of the auroral zones and are frequently called h-f "blackouts." During a blackout, the signal level is decreased considerably but the signal does not drop out completely. The outage time normally associated with h-f transmission could be greatly reduced by the use of transmitter power and antenna size comparable with that needed in the ionospheric scatter method described below.

In addition to the auroral-zone absorption, there are shorter periods of severe absorption over the entire hemisphere facing the sun. These erratic and unpredictable effects, which seem to be associated with eruptions on the sun, are called "sudden ionospheric disturbances" (SID's), or the "Dellinger effect."

The preceding information is based primarily on F-layer transmission. The E layer is located closer to the earth than the F layer, and the maximum transmission distance for a single reflection is about 1,200 miles.

Reflections from the E layer sometimes occur at frequencies above about 20 Mc but are erratic in both time and space. This phenomenon has been explained by

assuming that the E layer contains clouds of ionization that are variable in size, density, and location. The maximum frequency returned to earth may at times be as high as 70 or 80 Mc.[30] The high values are more likely to occur during the summer and during the minimum of the sunspot cycle.

Rapid multipath fading exists on ionospheric circuits and is superimposed on the longer-term variations discussed above. The amplitude of the fast fading follows the Rayleigh distribution, and echo delays up to several milliseconds are observed. These delays are 10^4 to 10^5 times as long as for tropospheric transmission. As a result of these relatively long delays, uncorrelated selective fading can occur within a few hundred cycles. This produces the distortion on voice circuits that is characteristic of "short-wave" transmission.

Ionospheric Scatter. The concept of maximum usable frequency used in conventional sky-wave transmission is defined as the highest frequency returned to earth for which the average transmission is within a few decibels of free space. As the frequency increases above the MUF, the signal level decreases rapidly but does not drop out completely. Although the signal level is low, reliable transmission can be obtained at frequencies up to 50 Mc or higher and to distances up to at least 1,200 to 1,500 miles.[31] In this case the signal is 80 to 100 db below the free-space value, and its satisfactory use requires much higher power and larger antennas than are ordinarily used in ionospheric transmission. The approximate variation in median signal level with frequency is shown in Fig. 33-18.

FIG. 33-18. Median signal levels for ionospheric-scatter transmission.

Ionospheric scatter is apparently the result of reflections from many patches of ionization in the E layer. It is suspected that meteors are important in establishing and in maintaining this ionization, but this has not been clearly determined.

In common with other types of transmission, the fast fading follows a Rayleigh distribution. The distribution of hourly median values relative to the long-term median (after the high signals resulting from sporadic E transmission have been removed) is approximately a normal-probability law with a standard deviation of about 6 to 8 db.

Ionospheric-scatter transmission is suitable for several telegraph channels, but the useful bandwidth is limited by the severe selective fading that is characteristic of all ionospheric transmission.

33.6. NOISE LEVELS

The usefulness of a radio signal is limited by the "noise" in the receiver. This noise may be either unwanted external interference or the first circuit noise in the receiver itself.

Atmospheric static is ordinarily controlling at frequencies below a few megacycles, while set noise is the primary limitation at frequencies above 200 to 500 Mc. In the 10- to 200-Mc band the controlling factor depends on the location, time of day, etc., and may be either atmospheric static, man-made noise, cosmic noise, or set noise.

The theoretical minimum circuit noise caused by the thermal agitation of the electrons at usual atmospheric temperatures is 204 db below 1 watt/cycle of bandwidth; that is, the thermal noise power in decibels below 1 watt is $-204 + 10 \log$ (bandwidth). The first circuit or set noise is usually higher than the theoretical minimum by a factor known as the noise figure. For example, the set noise in a receiver

with a 6-kc noise bandwidth and an 8-db noise figure is 158 db below 1 watt, which is equivalent to 0.12 μv across 100 ohms. Variations in thermal noise and set noise follow the Rayleigh distribution, but the quantitative reference is usually the rms value (63.2 per cent point), which is 1.6 db higher than the median value shown on Figs. 33-4 and 33-10. Momentary thermal noise peaks more than 10 to 12 db above the median value occur for a small percentage of the time.

Atmospheric static is caused by lightning and other natural electrical disturbances and is propagated over the earth by ionospheric transmission. Static levels are generally stronger at night than in the daytime. Atmospheric static is more noticeable in the warm tropical areas where the storms are most frequent than it is in the colder northern regions which are far removed from the lightning storms,

Typical average values of noise in a 6-kc band are shown on Fig. 33-19. The atmospheric static data are rough yearly averages for a latitude of 40°. Typical
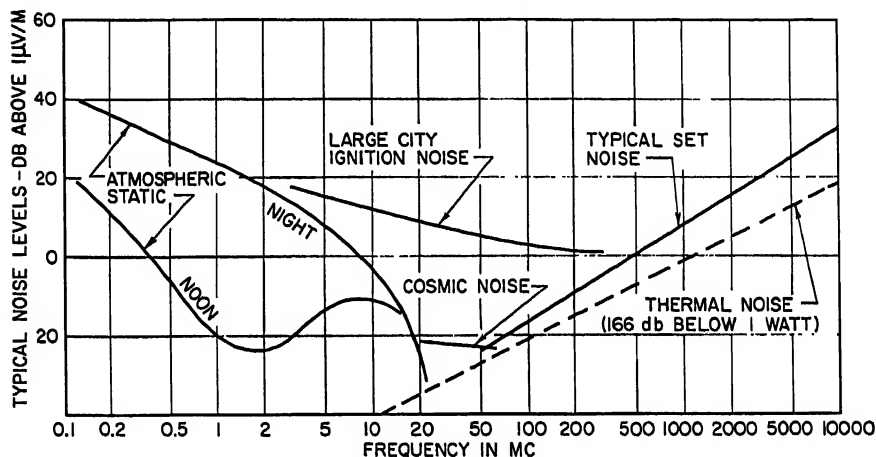
Fig. 33-19. Typical average noise level in a 6-kc band.

summer averages are a few decibels higher than the value on Fig. 33-19, and the corresponding winter values are a few decibels lower. The average noise levels in the tropics may be as much as 15 db higher than for latitudes of 40°, while in the arctic region the noise may be 15 to 25 db lower. The corresponding values for other bandwidths can be obtained by adding 10 db for each tenfold increase in bandwidth. More complete estimates of atmospheric noise on a world-wide basis are given in the *National Bureau of Standards Bulletin* 462.[27] These noise data are based on measurements with a time constant of 100 to 200 msec. Noise peaks, as measured on a cathode-ray tube, may be considerably higher.

The man-made noise shown in Fig. 33-19 is caused primarily by operation of electric switches, ignition noise, etc., and may be a controlling factor at frequencies below 200 to 400 Mc. Since radio transmission in this frequency range is primarily tropospheric (ground-wave), man-made noise can be relatively unimportant beyond 10 to 20 miles from the source. In rural areas, the controlling factor can be either set noise or cosmic noise.

Cosmic and solar noise are thermal-type interference of extraterrestrial origin.[32] Its practical importance as a limitation on communication circuits seems to be in the 20- to 80-Mc range. Cosmic noise has been found at much higher frequencies, but its magnitude is not significantly above set noise. On the other hand, noise from the sun increases as the frequency increases and may become the controlling

noise source when high-gain antennas are used. The rapidly expanding science of radio astronomy is investigating the variations in both time and frequency of these extraterrestrial sources of radio energy.

REFERENCES

1. H. T. Friis: "A Note on a Simple Transmission Formula," *Proc. IRE*, vol. 34, pp. 254–256, May, 1946.
2. K. Bullington: "Radio Propagation at Frequencies above 30 Megacycles," *Proc. IRE*, vol. 35, pp. 1122–1136, October, 1947.
3. K. Bullington: "Reflection Coefficients of Irregular Terrain," *Proc. IRE*, vol. 42, pp. 1258–1262, August, 1954.
4. W. M. Sharpless: "Measurements of the Angle of Arrival of Microwaves," *Proc. IRE*, vol. 34, no. 11, pp. 837–845, November, 1946.
5. A. B. Crawford and W. M. Sharpless: "Further Observations of the Angle of Arrival of Microwaves," *Proc. IRE*, vol. 34, no. 11, pp. 845–848, November, 1946.
6. A. B. Crawford and W. C. Jakes: "Selective Fading of Microwaves," *Bell System Tech. J.*, pp. 68–90, January, 1952.
7. R. L. Kaylor: "A Statistical Study of Selective Fading of Super High Frequency Radio Signals," *Bell System Tech. J.*, pp. 1187–1202, September, 1953.
8. H. E. Bussey: "Microwave Attenuation Statistics Estimated from Rainfall and Water Vapor Statistics," *Proc. IRE*, vol. 38, pp. 781–785, July, 1950.
9. J. C. Shelleng, C. R. Burrows, and E. B. Ferrel: "Ultra-short Wave Propagation," *Bell System Tech. J.*, vol. 12, pp. 125–161, April, 1933.
10. D. E. Kerr (ed.): "Propagation of Short Radio Waves," MIT Radiation Laboratory Series, vol. 13, McGraw-Hill Book Company, Inc., New York, 1951.
11. Stephen S. Attwood (ed.): Summary Technical Report of the Committee on Propagation, vol. 1, "Historical and Technical Survey," vol. 2, "Wave Propagation Experiments," vol. 3, "Propagation of Radio Waves," National Defense Research Committee, Washington, D.C., 1946.
12. C. W. Burrows and M. C. Gray: "The Effect of the Earth's Curvature on Ground Wave Propagation," *Proc. IRE*, vol. 29, pp. 16–24, January, 1941.
13. K. Bullington: "Characteristics of Beyond-horizon Radio Transmission," *Proc. IRE.*, vol. 43, no. 10, p. 1175, October, 1955.
14. W. E. Gordon: "Radio Scattering in the Troposphere," *Proc. IRE*, vol. 43, no. 1, p. 23, January, 1955.
15. K. Bullington: "Radio Transmission beyond the Horizon in the 40–4000 Mc Band," *Proc. IRE*, vol. 41, no. 1, pp. 132–135, January, 1953.
16. K. A. Norton, P. L. Rice, and L. E. Vogler: "The Use of Angular Distance in Estimating Transmission Loss and Fading Range for Propagation through a Turbulent Atmosphere over Irregular Terrain," *Proc. IRE*, vol. 43, no. 10, pp. 1488–1526, October, 1955.
17. F. H. Dickson, J. J. Egli, J. W. Herbstreit, and G. S. Wickizer: "Large Reductions of VHF Transmission Loss and Fading by Presence of Mountain Obstacle in Beyond-line-of-sight Paths," *Proc. IRE*, vol. 41, no. 8, pp. 967–969, August, 1953.
18. K. Bullington, W. J. Inkster, and A. L. Durkee: "Results of Propagation Tests at 505 Mc and 4090 Mc on Beyond-horizon Paths," *Proc. IRE*, vol. 43, no. 10, pp. 1306–1316, October, 1955.
19. H. G. Booker and J. T. deBettencourt: "Theory of Radio Transmission by Tropospheric Scattering Using Very Narrow Beams," *Proc. IRE*, vol. 43, no. 3, pp. 281–290, March, 1955.
20. W. H. Tidd: "Demonstration of Bandwidth Capabilities of Beyond-horizon Tropospheric Radio Propagation," *Proc. IRE*, vol. 43, no. 10, pp. 1297–1299, October, 1955.
21. K. Bullington: "Radio Propagation Variations at VHF and UHF," *Proc. IRE*, vol. 38, no. 1, pp. 27–32, January, 1950.
22. W. R. Young: "Comparison of Mobile Radio Transmission at 150, 450, 900 and 3700 Mc," *Bell System Tech. J.*, vol. 31, pp. 1068–1085, November, 1952.
23. K. A. Norton: "The Physical Reality of Space and Surface Waves in the Radiation Field of Radio Antennas," *Proc. IRE*, vol. 25, no. 9, pp. 1192–1202, September, 1937.
24. Reference 1.
25. C. R. Burrows: "Radio Propagation over Plane Earth: Field Strength Curves," *Bell System Tech. J.*, vol. 16, pp. 45–75, January, 1937.
26. K. A. Norton: "The Propagation of Radio Waves over the Surface of the Earth and in the Upper Atmosphere," pt. II, *Proc. IRE*, vol. 25, pp. 1203–1236, September, 1937.
27. "Ionospheric Radio Propagation," Natl. Bur. Standards (U.S.) Circ. 462, 1948.

28. *Basic Radio Propagation Predictions*, National Bureau of Standards CRPL Series D, issued monthly, U.S. Government Printing Office, Washington.
29. "Instructions for Use of Basic Radio Propagation Predictions," Natl. Bur. Standards (U.S.) Circ. 465.
30. E. W. Allen, "Very-high Frequency and Ultra-high Frequency Signal Ranges as Limited by Noise and Co-channel Interference," *Proc. IRE*, vol. 35, pp. 128–136. February, 1947.
31. D. K. Bailey, R. Bateman, and R. C. Kirby: "Radio Transmission at VHF by Scattering and Other Processes in the Lower Ionosphere," *Proc. IRE*, vol. 43, no. 11, pp. 1181–1230, October, 1955.
32. J. W. Herbstreit: *Advances in Electronics*, vol. 1, pp. 347–380, 1948.

Chapter 34

ANTENNA MEASUREMENTS

RICHARD RUBIN

Sylvania Electric Products, Inc.
Waltham, Massachusetts

34.1. GENERAL DISCUSSION

This volume so far has provided much of the information which the design engineer requires when designing antennas to meet particular requirements. These requirements or specifications may be expressed in various terms, but in most instances may be resolved into a fairly small number of well-defined characteristics, which are:

1. Input impedance and mutual impedance
2. Radiation patterns
3. Gain
4. Phase front
5. Polarization

In order to prove that an antenna, which is designed to meet specific requirements, does indeed conform to these specifications, it is necessary to perform measurements which will determine the appropriate characteristics of the antenna. It is the purpose of this chapter to discuss methods of obtaining the information listed in items 1 to 5 above. The problem of power-handling abilities has already been discussed in Chap. 30 for transmission lines, and it applies equally well for antennas.

Before going into the detail required in describing the measurements and measurement techniques, it is advisable to insert a word of caution. Antennas are radiating elements and are subject to radio-frequency interference from outside sources and from reflecting objects. Care must be exercised to avoid unreliable results. Appropriate reminders and suggestions will be used throughout this chapter. Where applicable, the use of microwave-absorbing material will be discussed and recommended as part of the continuous effort to obtain reliable and repeatable data.

34.2. INPUT- AND MUTUAL-IMPEDANCE MEASUREMENTS

There are three general methods which may be used in the measurement of impedance. For radio frequencies below 30 Mc, it is quite practical, if not essential, to use bridge measurements. For frequencies above 1,000 Mc, the use of the slotted line is almost universal. In the frequency range from 30 to 1,000 Mc, either method may be used, depending on the application and on equipment availability. A reflection method may also be used to determine the relative radiation resistance of a short-circuited resonant element, such as a parasitic element which has no terminals available.

Bridge Measurements for Low Frequencies. Adaptations of the fundamental Wheatstone-bridge circuit have been used for many years for the measurement of impedance. These bridge measurements, which utilize a null method, have proved most useful for the determination of impedance, resistive or reactive (inductive or capacitive), from direct current through the lower UHF band. The null method provides great convenience in addition to its high precision. Bridges derived from the basic Wheatstone bridge generally contain a number of fixed known resistors, inductors, or capacitors and one or more variable calibrated elements. The measurements usually are preceded by a calibration in which the bridge is balanced with the unknown impedance terminals short-circuited or open-circuited. The short is then removed, and the unknown impedance is inserted. The bridge is rebalanced, and the measured impedance is determined. Table 34-1 gives some examples of commercially available bridges, their operating frequency ranges, basic circuit diagrams, and impedance equations.

In using any of the bridges described above or any others, a number of additional pieces of equipment are required. The signal source which is used should provide at least 1 mv output, and the detector should be an extremely well shielded receiver having a sensitivity of approximately 5 μv. Depending on the particular bridge

Table 34-1. Commercially Available Bridges.

FREQUENCY RANGE	COMPANY AND MODEL NUMBER	CIRCUIT DIAGRAM	CHARACTERISTIC EQUATIONS
50 KC TO 5 MC	*GR-916-AL		$R_X = R_B \dfrac{(C_{A2} - C_{A1})}{C_N}$
400 KC TO 60MC	*GR-916-A		$X_X = \dfrac{1}{\omega}\left(\dfrac{1}{C_{P2}} - \dfrac{1}{C_{P1}}\right)$
460 KC TO 40MC	*GR-821-A		$G_X = \omega^2 K \Delta C_G$ $B_X = \omega \Delta C_B$ $K = \dfrac{C' \, C'' \, R}{C'''}$
10 MC TO 165 MC	*GR-1601-A	SIMILAR TO GR-916-A	
41 MC TO 1000 MC	*GR-1602-A		DIRECT READING
52 MC TO 500MC	**HP-803-A		DIRECT READING
100 MC-1000 MC	***PRD-219		DIRECT READING

*GR-GENERAL RADIO

**HP-HEWLETT PACKARD

***PRD-POLYTECHNIC RESEARCH AND DEVELOPMENT CORP.

which is used, additional accessories may be conveniently used, as specified by the bridge manufacturers.

Slotted-line Measurements. The measurement of input impedance utilizing a slotted line makes use of well-known and often-discussed characteristics of traveling waves; that is, input impedance may be uniquely determined from a knowledge of the standing-wave ratio of voltage or current (VSWR) and the distance between the voltage or current minimum and the reference point at which the impedance is desired. The slotted line permits one to measure these two parameters in an extremely simple manner.
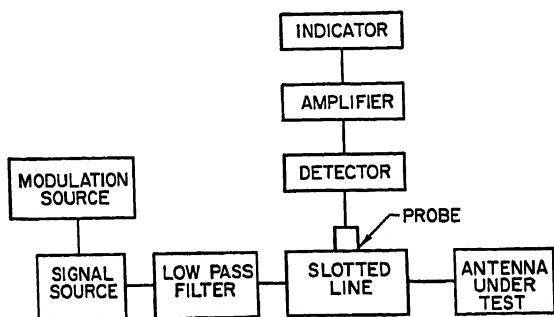
Fig. 34-1. Setup for slotted-line impedance measurement.
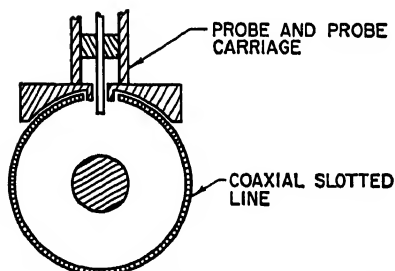
Fig. 34-2. Cross section of voltage probe.
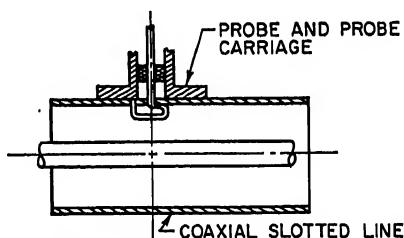
Fig. 34-3. Cross section of current (loop) probe.

Slotted lines which may be purchased commercially fall into three categories:
1. Coaxial slotted lines
2. Slab lines
3. Waveguide slotted lines

The characteristic impedance of the coaxial slotted lines and the slab lines is generally 50 ohms, although there are some 46-ohm lines available. Because of construction and connector compensation it is generally difficult to modify the characteristic impedance of the lines by changing the size of the inner conductor if a different impedance line is required. Waveguide slotted lines are available commercially in sizes corresponding to standard waveguide dimensions.

A typical block diagram indicating the type of equipment used in making slotted-line measurements is shown in Fig. 34-1. A transmission-line system which is terminated in an antenna that is not perfectly matched to the feeding transmission line contains an incident traveling wave and a wave which is reflected from the mismatched load. The amplitude of the reflected wave is proportional to the mismatch of the load. These waves will alternately cancel and add, resulting in a stand-

ing wave on the feed transmission line.   In the VSWR or impedance-measuring setup, part of the transmission line is replaced by a slotted section.   A traveling probe inserted in the slotted line and connected to a detector will allow the standing-wave pattern to be measured.   The probe may be a voltage probe as illustrated in Fig. 34-2 or a current probe as shown in Fig. 34-3.   The latter is not recommended for use at frequencies over 2,000 Mc.   The detector may be a receiver tuned to the frequency being used, or it may be a crystal or a bolometer detector connected to a voltmeter or VSWR indicator.   The signal source is usually amplitude-modulated with a square wave or pulse.

In general, two sets of measurements are taken.   During the first set of measurements the antenna to be tested is connected to the load end of the slotted line.   At
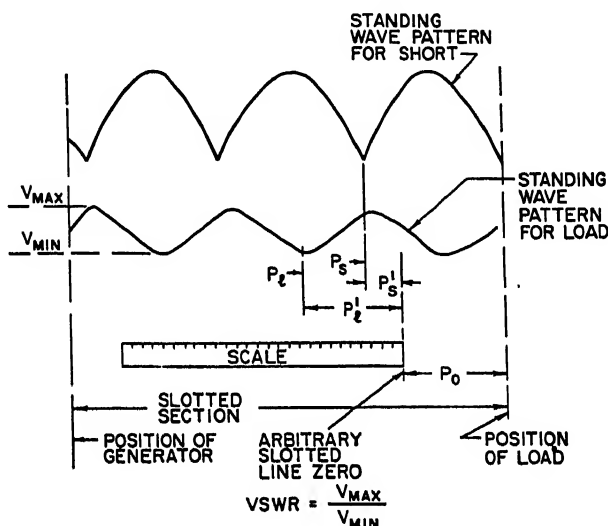
Fig. 34-4. Standing-wave patterns and minima determination.

each frequency of interest the VSWR is measured by moving the probe along the line and noting the reading on the standing-wave indicator or by determining the difference between the voltage minimum and maximum using a calibrated attenuator.   The "load" minimum position P_ℓ is also determined at each frequency (Fig. 34-4).   Standing-wave ratio (SWR) is usually specified in decibels or as a voltage ratio (VSWR). This is expressed as follows:

$$\text{SWR(db)} = 20 \log \text{VSWR} = 20 \log \frac{V_{\max}}{V_{\min}}$$

The second set of measurements is used to determine the location of the reference point for the impedance.   The reference point is generally the end of the slotted line. The slotted line is short-circuited at the load end, and the "short" minimum positions P_s are determined at the same frequencies.

The input impedance may be determined analytically by use of the following equation:

$$Z_L = Z_0 \left\{ \frac{S}{\cos^2 \beta\ell + S^2 \sin^2 \beta\ell} + j \left[\frac{(S^2 - 1) \sin \beta\ell \cos \beta\ell}{\cos^2 \beta\ell + S^2 \sin^2 \beta\ell} \right] \right\}$$

where S = VSWR

$\beta = 2\pi/\lambda_g$

λ_g = guide wavelength

Z_0 = characteristic impedance of measuring line

Z_L = load input impedance

Also

$$|P'_l - P'_s| = |\ell|$$

Note: If P_l is closer to the load than P_s, then consider ℓ as positive. If P_l is closer to the generator than P_s, then consider ℓ as negative. However, it is much simpler to use a Smith chart for determining this impedance. The Smith chart is discussed along with other impedance charts later in this chapter.

When making slotted-line impedance measurements, a number of sources of error are possible. Proper technique and awareness of the causes of these errors can eliminate or minimize most of them. Some of the causes for error are:

1. Probe loading of slotted line
2. Mismatch of signal source
3. Nonuniformity of detector characteristics
4. Harmonics, frequency modulation, spurious signal sources, received signals, etc.
5. Reflections from nearby objects
6. Coupling from antenna into detector

The probe must be inserted into the slotted line in order to sample the standing-wave patterns. If the probe penetration is too deep, the probe acts as a reflection point, which produces an impedance in shunt with the line. As the probe moves, the disturbance moves with it, upsetting the standing-wave pattern. This results in a VSWR value which is lower than the actual VSWR being measured.

Reflections from the probe return to the signal source. If the source is poorly matched, the reflected wave will be partially returned toward the load. This would result in both phase and amplitude errors. Padding may be used between sources having VSWR's greater than 2 (such as klystrons) and the line, in order to reduce this effect. In addition to this, an even more important consideration is that probe penetration should be made as small as possible.

When crystals are used as the detecting element, they should be operated at power levels less than 20 μw in order to retain their square-law characteristics. Barretters should be operated at less than 200 μw. When the signal-source output is 1 mw, these conditions will generally be met if the probe penetration is adjusted so that the output is 5 to 10 db above noise level at the load minimum position for a VSWR of 10:1 or less.

To avoid harmonics, spurious signal sources, and unwanted received signals, it is necessary to make use of high- and low-pass filters when using commercial standing-wave indicators. The use of a superheterodyne receiver will also eliminate these difficulties.

Most signal generators are fairly low in their frequency-modulation content. However, klystron sources not modulated with a good square wave will produce frequency modulation which will tend to broaden the null in the standing-wave pattern, making position determination quite impossible. Klystron outputs should be monitored with an oscilloscope to be sure that no frequency modulation exists. This procedure also helps in tuning the klystron.

If the antenna under test is not located in a clear area, it is possible that reflections from various objects will reenter the slotted line through the antenna. This will cause false measurements. This type of difficulty can be detected by moving the antenna a quarter wavelength and noting the change in VSWR and minimum position. In order to eliminate these reflections, the antenna should be tested in a clear area,

or alternatively, the reflecting objects should be removed or covered with low-reflecting absorbing material, which is available commercially.

Coupling of energy from the antenna into the detector occurs mainly at the lower frequencies. Although easily detected by its effect (an irregular standing-wave pattern), it is quite difficult to eliminate. In this condition everything appears to be "hot." Just moving the cable between probe and detector can cause a change in the reading. One solution is to move the antenna farther away from the slotted line by using longer feed cable, remembering that there is additional cable attenuation to be accounted for in the VSWR. Surrounding the suspected part of the antenna with absorbing material may also help. If this type of condition is found at the higher frequencies, loose cable connections should be suspected.

Impedance Charts. A formula for determining antenna impedance from slotted-line measurements was previously given. For informational purposes and for use in modifying existing impedance characteristics it is desirable to plot impedance vs. frequency in an easily used form. It is also desirable to dispense with the calculations required by the load-impedance equation and go directly to an impedance plot. A large number of charts have been developed for this purpose. Some that are more widely used are the impedance circle diagram, the Smith chart, and the Carter chart.

Impedance Circle Diagram. The input impedance of a transmission line terminated in an impedance is given by the following equation:

$$Z_L = Z_0 \frac{Z_R + jZ_0 \tan \beta \ell}{Z_0 + jZ_R \tan \beta \ell}$$

Also

$$Z_L = R_L + jX_L$$

and normalizing,

$$\frac{Z_L}{Z_0} = \frac{R_L}{Z_0} + j\frac{X_L}{Z_0}$$

or

$$\frac{Z_L}{Z_0} = R + jX$$

A rectangular plot of R and jX, with circles of constant position and circles of constant VSWR superimposed, is known as an impedance circle diagram. A basic
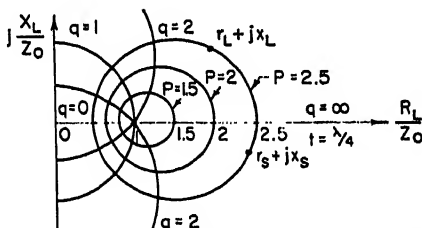
Fig. 34-5. Basic form of impedance circle diagram.

form of this chart is shown in Fig. 34-5. A known impedance may be plotted on this chart after normalizing. The chart coordinates are

$$R = \frac{R_L}{Z_0} = r_L$$

and

$$X = \frac{X_L}{Z_0} = x_L$$

as shown in Fig. 34-5. If it is desired to transfer this impedance to another point farther toward the generator, then the point is moved along a constant p circle the required amount in terms of q. The p circles are VSWR circles (p = VSWR); the q circles are constant ℓ circles (q = tan $\beta \ell$). The new normalized impedance point is

shown in Fig. 34–5 as $r_s + jx_s$. The actual impedance is

$$Z_s = Z_0(r_s + jx_s)$$

One of the most serious disadvantages of this type of chart is that it does not contain all impedance values. Infinite VSWR values and values approaching infinity ($R_L/Z_0 \to \infty$, $X_L/Z_0 \to \infty$) are not found on the chart. Also high VSWR's with low values of R_L/Z_0 are difficult to handle because of the compressed scale involved.

Smith Chart. The most commonly used impedance chart is the Smith chart (Figs. 34–6 and 34–7). The Smith chart is derived by using a bilinear transformation.
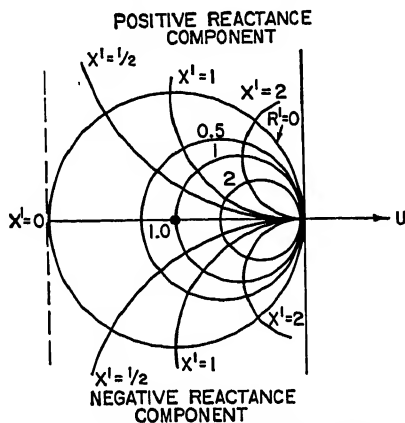
FIG. 34–6. Basic form of Smith chart.

It consists of orthogonal families of circles. One family consists of constant resistance circles. The second family consists of constant reactance circles. Circles of constant VSWR are concentric with the center of the chart. The point of zero reflection coefficient (VSWR = 1) is at the center of this circular chart. The locus of unity reflection coefficient (VSWR = ∞) is the limiting circle of the chart, which also coincides with the position circle.

The Smith chart is used almost universally for plotting impedances from the information obtained from slotted-line measurements. As an example of how the load input impedance may be determined by use of the Smith chart, the following representative slotted-line values will be used:

P_s = 25 cm = short position
P_ℓ = 17 cm = load position
VSWR = 4 = voltage-standing-wave ratio
λ_g = 26 cm wavelength

Then $\Delta P = |P_\ell - P_s| = |\ell| = 8$

and $\dfrac{\Delta P}{\lambda_g} = \dfrac{8}{26} = 0.308$ wavelength

Assuming that P_s is closer to the load end of the line than P_ℓ, the value $\Delta P/\lambda_g$ is plotted using the position scale on the Smith chart which reads "wavelengths toward load." If P_s is closer to the generator than P_ℓ, then $\Delta P/\lambda_g$ is plotted using the scale which reads "wavelengths toward generator." The resulting impedance (normalized value) is shown in Fig. 34–7. Further use of the Smith chart is described in the references.

Carter Chart. The Carter chart, which is pictured in Fig. 34–8, gives a representation of magnitude and phase angle of an impedance. This chart may be derived

directly from the Smith chart by connecting points of equal impedance magnitude together and connecting points of equal phase together. The chart may be used in the same manner as the Smith chart and has some special applications when used in connection with circularly polarized antenna measurements (Sec. 34.6).
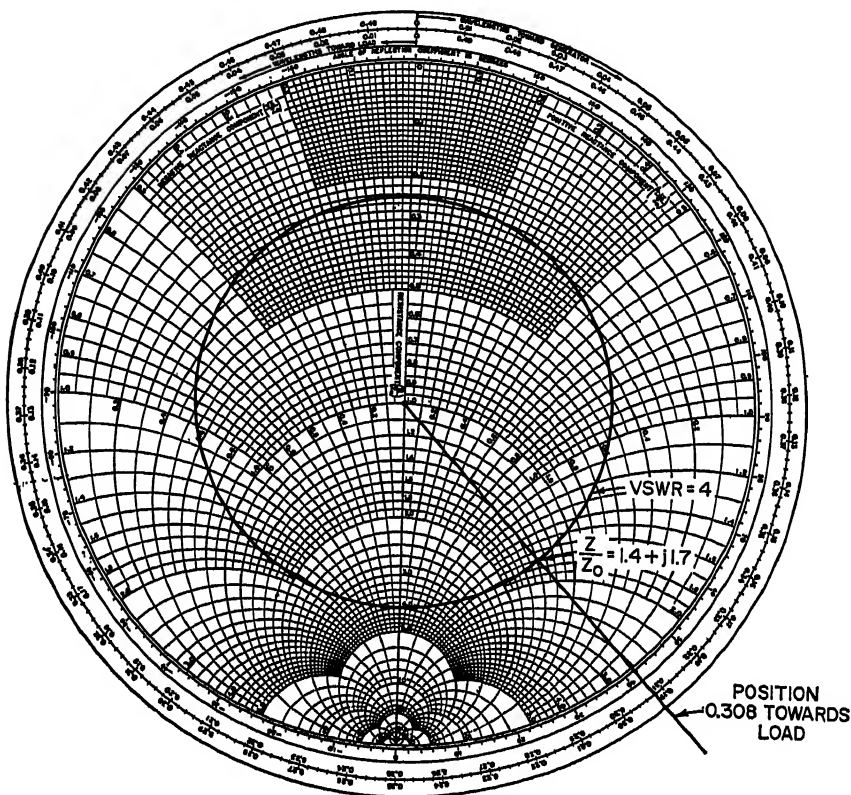
FIG. 34-7. Smith chart.

Measurement of Very High VSWR. When using crystal detectors for the measurement of VSWR, it should be remembered that the square-law characteristic of the crystal holds only for low power levels. If high standing waves are involved, it is possible to overload the crystal and obtain incorrect readings. The use of an indicating device which has only a limited dynamic range may prevent the accurate measurement of high VSWR in the usual way. If either one of these situations exists, the method described below is extremely useful.

In Fig. 34-9 the actual VSWR is $S = V_{max}/V_{min}$. Instead of measuring V_{max}, an intermediate value is chosen, say, V_I. The ratio $S_I = V_I/V_{min}$ and the distance $d = |x_2 - x_1|$ are used in the equation below to determine the actual VSWR.

Thus
$$S = \frac{\sqrt{S_I^2 - \cos^2 (\pi d/\lambda_g)}}{\sin (\pi d/\lambda_g)}$$

where $\lambda_g =$ guide wavelength.

For accurate results the measurements of x_2 and x_1 must be carefully made and the value of λ_g must be known.

Measurement of Mutual Impedance. In an antenna array in which the phase difference between elements remains constant with time, the mutual-impedance
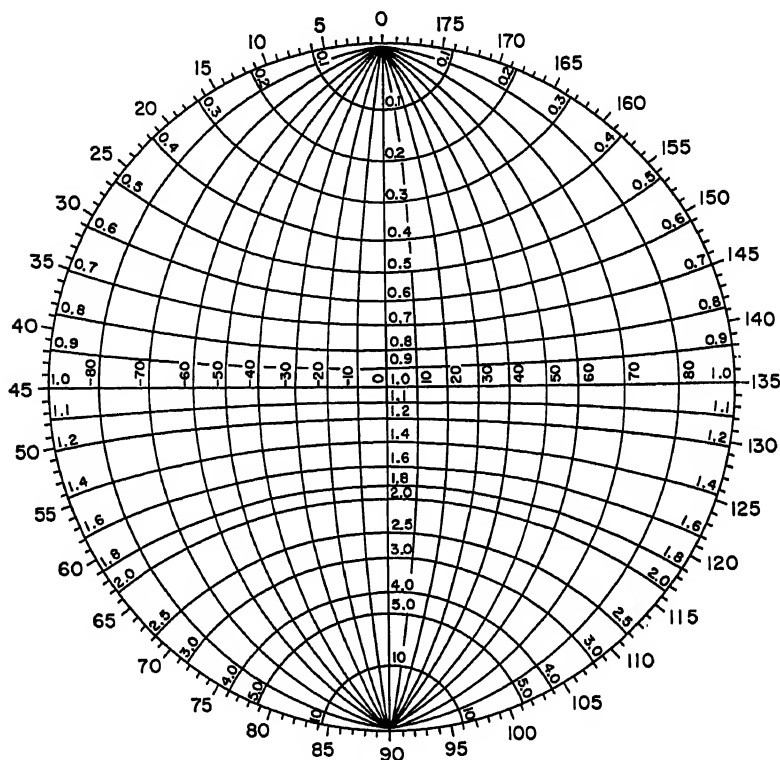
CARTER CHART

FIG. 34–8. Carter chart.
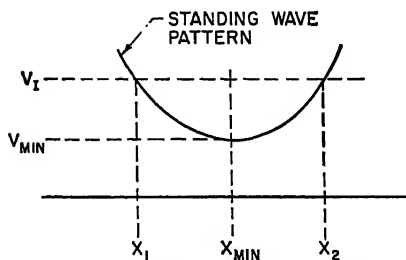
FIG. 34–9. Determination of high VSWR and accurate location of minimum position.

problem resolves itself into one of compensating each antenna element in the presence of other nearby elements which may affect its impedance. In an antenna array in which the phase difference between elements varies with time, the mutual-impedance problem is more complex. For a particular spacing between elements, the mutual

impedance between two elements remains fixed. However, the variation in phase difference between mutually coupled elements has a large effect on input impedance.

The measurement of mutual impedance, for the purpose of reducing its effect on input impedance, is important in some applications. Referring to Fig. 34-10, the terminal impedances of two identical antennas are

$$Z_1 = Z_{self} + \frac{I_2}{I_1} Z_{mutual}$$

and

$$Z_2 = Z_{self} + \frac{I_1}{I_2} Z_{mutual}$$

where Z_{self} = self-impedance of element 1 or element 2
$\quad\quad Z_1$ = terminal impedance of antenna 1
$\quad\quad Z_2$ = terminal impedance of antenna 2
$\quad\quad I_1$ = current in antenna 1
$\quad\quad I_2$ = current in antenna 2

Z_{self} is defined as the limit of Z_1 as the current I_2 approaches zero at the reference terminals of the second antenna. Z_{self} will in general depend on the spacing between the antennas since the current is not necessarily zero everywhere in the second antenna when the current is zero at its reference terminals. An open circuit at the reference terminals satisfies this requirement.

Z_{mutual} may be obtained by short-circuiting antenna 2 and measuring the terminal impedance Z_1 of antenna 1. Thus

$$Z_1 = Z_{self} + \frac{I_2}{I_1} Z_{mutual}$$

and

$$0 = Z_{self} + \frac{I_1}{I_2} Z_{mutual}$$

Then $\quad\quad (Z_{mutual})^2 = Z_{self}(Z_{self} - Z_1)$
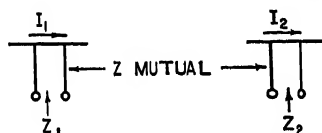
Fig. 34-10. Terminal impedances of two identical antennas.

Using the method of measurement implied here, it is found that for small values of Z_{mutual}, the values of Z_{self} and Z_1 are so close together that their difference cannot be measured accurately.

A second method may be used for more precise results. It will be noted that if Z_1 is measured for some known current ratio I_2/I_1, then

$$Z_{mutual} = \frac{I_1}{I_2}(Z_1 - Z_{self})$$

If an image plane is used to replace the second antenna as in Fig. 34-11, then the current ratio will be equal to the following:

$$\frac{I_1}{I_2} = +1 \quad\quad \text{for collinear dipoles}$$

and

$$\frac{I_1}{I_2} = -1 \quad\quad \text{for parallel dipoles}$$

For the same Z_{mutual} value as used in the first method, the difference measured between Z_1 and Z_{self} is now considerably greater and can be measured more accurately by using this second method of measurement.

For collinear dipoles mounted over a reflecting ground plane as shown in Fig. 34-12, the values of Z_{self} and Z_{mutual} are determined by the following equations:

$$Z_1 = (Z_{11} - Z_{11'}) + (Z_{12} - Z_{12'})$$
$$Z_{11} - Z_{11'} = Z_{self}$$

and

$$Z_{12} - Z_{12'} = Z_{mutual}$$

Miscellaneous Techniques. *Location of Minima.* In order accurately to determine impedance, a precise location of voltage or current minima in the standing-wave pattern is required. It is especially important in this case that the signal source be free of frequency modulation or spurious frequency sources. Accurate location of minima is obtained by averaging. A convenient standing-wave pattern level S_I is
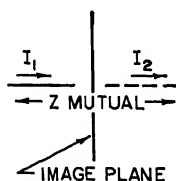
FIG. 34-11. Image-plane method of measuring self-impedance and mutual impedance.
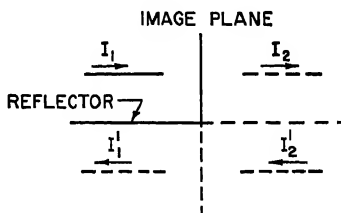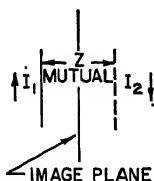
FIG. 34-12. Collinear dipoles over reflecting ground plane.

chosen, and the slotted-line scale reading corresponding to S_I on each side of the minimum is recorded. The actual minimum is

$$x_{\min} = \frac{x_2 + x_1}{2}$$

This is illustrated in Fig. 34-9.

Measurement of Impedance Using an Image Plane. Very often, when a balanced antenna such as a sleeve dipole is being investigated, it is necessary for design purposes to optimize the impedance curve of the dipole without the additional complication of a balun or parallel line feed being involved in the measurement. Half
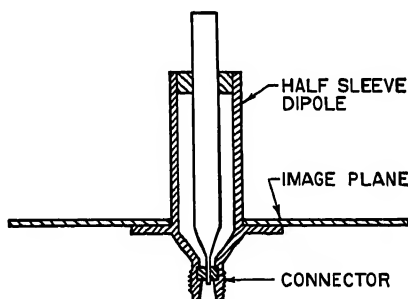
FIG. 34-13. Image-plane method for measuring impedance.

the dipole can be replaced by an image plane (Fig. 34-13), and convenient measurements may then be made on one-half of the dipole. The impedance of the full dipole is twice the impedance of the half which was measured.

34.3. RADIATION PATTERN MEASUREMENTS

Conical, Vertical, *E*-plane, and *H*-plane Patterns. The radiation pattern of an antenna is three-dimensional and requires field-intensity measurements over all angles of space. In taking radiation patterns it is therefore necessary to specify various space angles with respect to the antenna under test. Figure 34-14 describes the coordinate system in general use. The xy plane is the horizontal plane. Radiation patterns may be taken either along latitude or polar angle as a function of azimuth angle (these are conical cut patterns), or they may be taken along azimuth

angle as a function of polar angle (these are vertical cut patterns), depending on the application and information desired.   The orientation in space of the E vector is arbitrary, depending on the polarization of the radiated field.   For elliptical polarization, more than one orientation of the E vector is desirable.
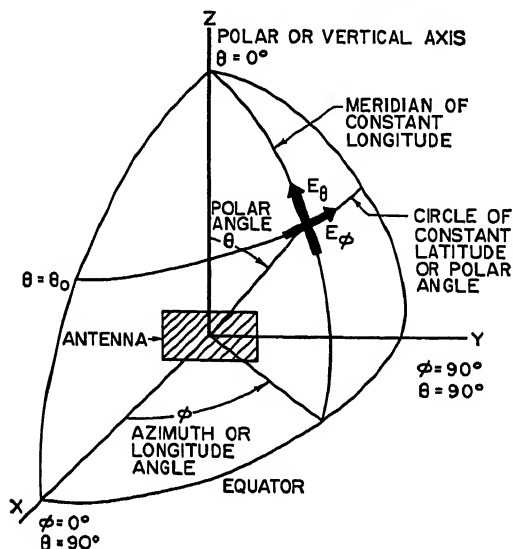
Fig. 34-14. Coordinate system for radiation-pattern measurements.

A complete set of measurements obtained by the above methods is often necessary for describing the radiation pattern of an antenna mounted on an aircraft or other irregularly shaped objects.

For most antennas with simply shaped radiation patterns, it is often necessary only to take radiation patterns in the xy and xz planes as shown in Fig. 34-15.   In part a, the E_ϕ $(\theta, \phi = 0)$ pattern is the H-plane pattern; the E_ϕ $(\theta = 90°, \phi)$ pattern is the E-plane pattern.   In part b, the E_θ $(\theta, \phi = 0)$ pattern is the E-plane pattern while the E_θ $(\theta = 90°, \phi)$ pattern is the H-plane pattern.
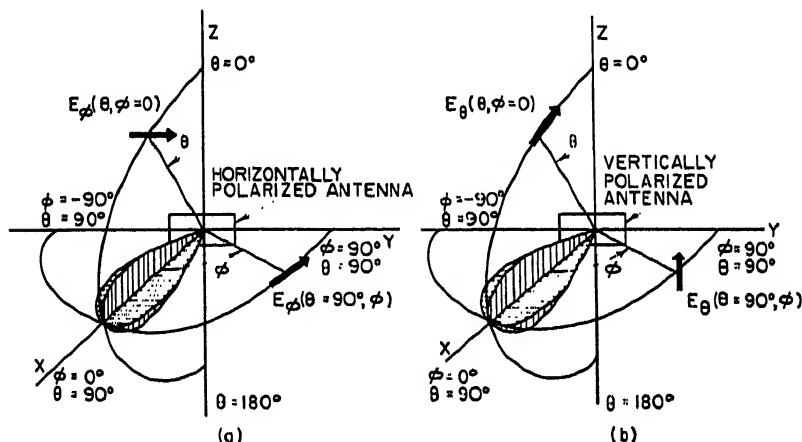
Fig. 34-15. Radiation patterns in the horizontal and vertical planes.

Antenna Radiation Pattern Range Requirements. In its simplest form, a pattern range will contain a transmitting source, an antenna under test, a mount for turning the antenna under test, and a detector for indicating the relative magnitude of received field. A setup of this kind is shown in Fig. 34-16. The equipment used may be completely automatic, may require a point-by-point plot, or may have many variations between these two extremes. In any case a number of important factors
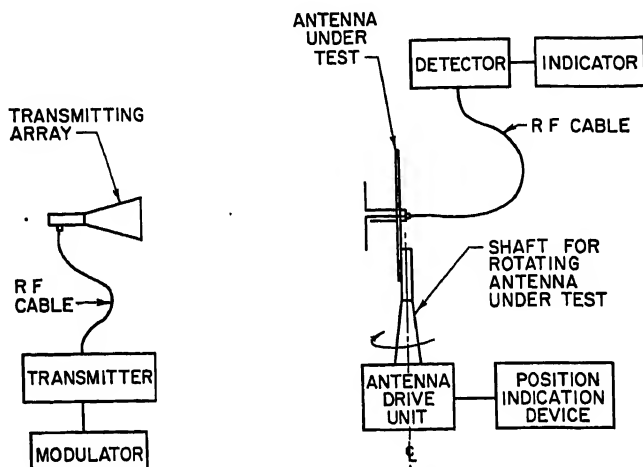
FIG. 34-16. Radiation-pattern-measuring setup.

should be considered in order to be sure that the radiation patterns obtained are valid and accurate.

Distance. In order to obtain accurate far-field, or Fraunhofer, radiation patterns it is necessary that the distance between the transmitting antenna and the antenna under test be sufficiently large. If this distance is too small, then the near-field, or Fresnel, pattern is obtained. The Fresnel pattern is a function of the distance at

PHASE DIFFERENCE $= \dfrac{45d^2}{\lambda R}$ DEGREES $= \delta°$
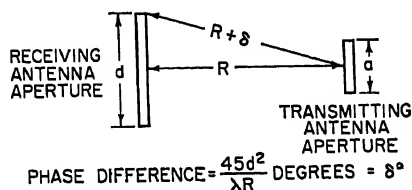
FIG. 34-17. Phase difference between center and edges of receiving array.

which it is measured. For accurate far-field measurements the antenna under test should be illuminated with a plane wavefront. Since plane wavefronts are obtainable only at infinite distances, some limits must be specified. A commonly specified criterion is that the phase difference between the center and edge of the antenna under test shall be no greater than $\lambda/16$. If this is the case, the distance shown for R in Fig. 34-17 is given by the equation

$$R \geq \frac{2d^2}{\lambda}$$

The distance R is obtained in terms of d and δ from geometric relations:

$$(R + \delta)^2 = R^2 + \left(\frac{d}{2}\right)^2$$

and
$$R^2 + 2R\delta + \delta^2 = R^2 + \frac{d^2}{4}$$

For $R \gg \delta \ll d$, δ^2 may be neglected, and

$$R \cong \frac{d^2}{8\delta}$$

By replacing δ with the allowable phase difference the required R may be obtained. Reducing the distance R tends to give broader radiation patterns, higher minor lobes,
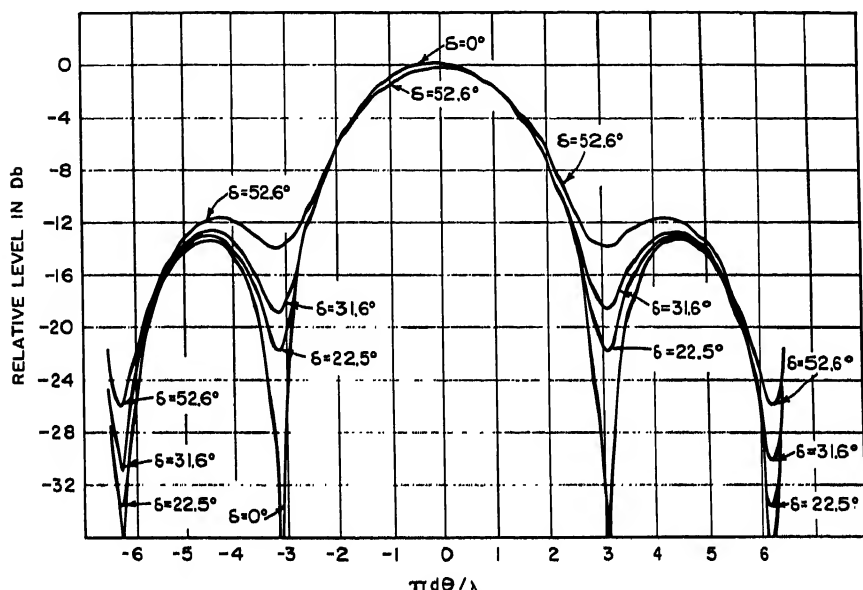
Fig. 34-18. Distortion of antenna pattern for four different phase errors δ.

and shallower nulls between lobes, as shown in Fig. 34-18 for four different phase errors δ.

Uniform Illumination. A number of site conditions can contribute to a nonuniform field at the antenna under test. In almost all cases the site condition results in a reflection of energy which causes cyclic or irregular variations in field intensity. Figure 34-19 shows the type of field variation that can occur in the vertical plane because of ground reflections.

These measurements were taken at the Waltham Laboratories of Sylvania Electric Products, Inc., on the 87-ft pattern range pictured in Fig. 34-20.

If an antenna with a large vertical aperture were to be illuminated in this manner, erratic and incorrect results would be obtained. Vertical-plane pattern taking is almost impossible with such a setup. Ground reflection can sometimes be avoided by mounting the antennas high above the ground on towers or making the transmitting antenna more highly directional in the vertical plane so as to reduce the
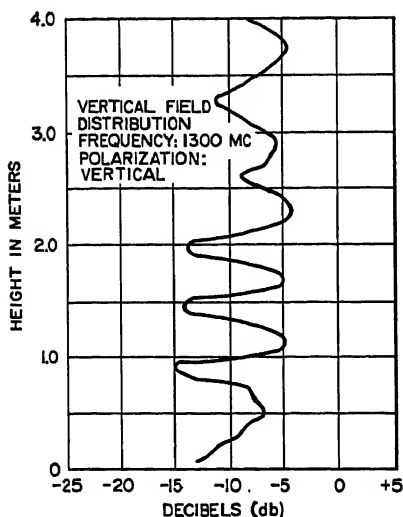
FIG. 34-19. Vertical-field distribution due to ground reflections.
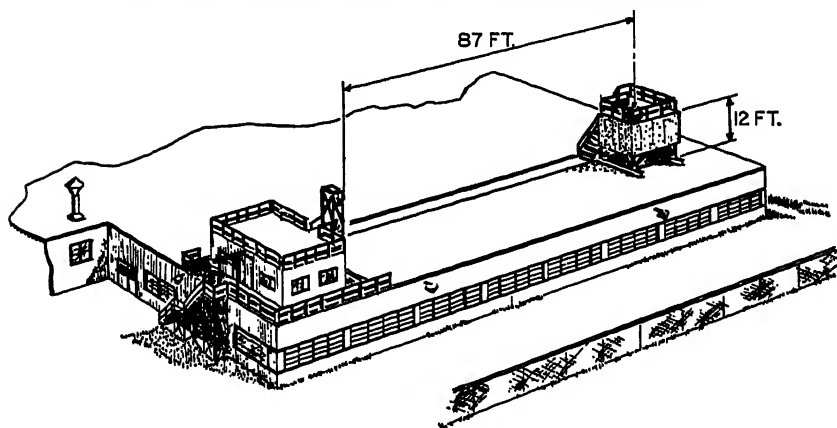
FIG. 34-20. Layout of antenna pattern range on roof of Sylvania Waltham Laboratories.
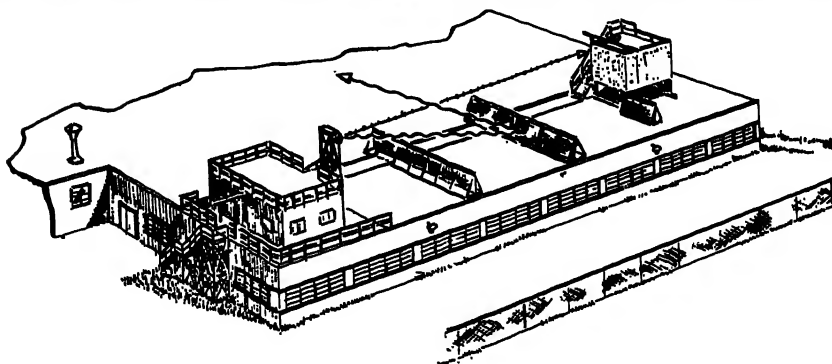
FIG. 34-21. Conducting fences for shielding antenna from ground reflections.

amplitude of the reflection from the ground.   Three other methods have been used with some success in overcoming the ground-reflection difficulty.

One method utilizes a conducting fence essentially to shield the antenna under test from any radiation reflected from the ground.   Care must be observed when using this type of fence that diffraction fields from the edge of the fence will not affect the uniformity of the field at the antenna under test.   The diffraction effect may be reduced by covering the top of the fence with microwave-absorbing material such as that manufactured by Emerson and Cuming, Inc., McMillan Laboratory, B. F. Goodrich Sponge Products Division, and others.   The diffraction effect may be calculated using Fresnel's diffraction theory.
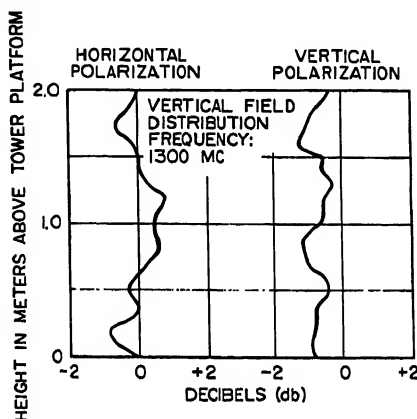
Fig. 34-22. Field variation after installation of fences.

Fences of this type were used to correct erratic field distribution at the Sylvania Waltham Laboratories.   The fences are pictured in Fig. 34-21.   The field variation after the fences were installed is plotted in Fig. 34-22.

A second method which has been employed with some success at the Whippany and Holmdel test sites of the Bell Telephone Laboratories is to use a flat range in order to utilize the ground reflection.   A typical range would be 1,400 ft long and 200 ft wide.   It should be graded to a flatness of ±3 in. and kept neat with grass, which is clipped short.   Measurements taken at 11.5 kmc at the Holmdel range indicate that with the transmitting antennas 41 in. above the ground, the field is uniform within ± ½ db over a 5½-ft aperture, which has its lower end at a 6-ft height above ground.

A third method of avoiding the deleterious effect of ground reflections is to have the range cover a length of irregular or rough terrain.   The random reflections tend to give a somewhat uniform illumination over larger vertical apertures.   Rayleigh suggested a method for formulating a relationship between wavelength, surface roughness, and grazing angle.   Using the Rayleigh criterion, a surface is considered rough if the following relationship is true:

$$h \sin \psi_2 > \frac{\lambda}{8}$$

where h = height of surface irregularities
  ψ_2 = grazing angle
  λ = wavelength of incident wave
Other sources of reflections such as buildings, power and telephone lines, and

fences should be eliminated by careful choice of site and beamwidth of the illuminating antenna.

In any event, it should be considered axiomatic to explore the test site to determine the field uniformity over the test-antenna aperture. Variations of 5 per cent are not considered serious for most applications.

12CM TYPE ABSORBER PRODUCTION SAMPLE

PERFORMANCE VS. ANGLE OF INCIDENCE
POLARIZATION AND WAVELENGTH

ABSORPTION PERFORMANCE VS. FREQUENCY
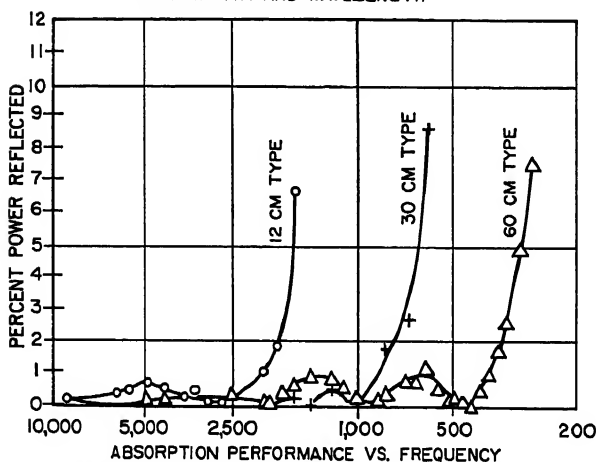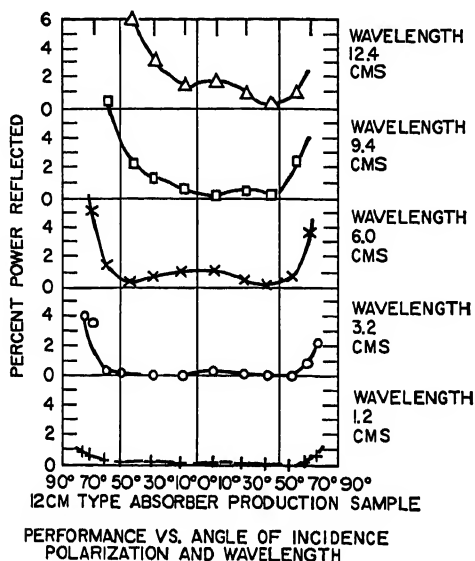
FIG. 34–23. Characteristics of microwave-absorbent material.

Antenna Darkrooms. A great amount of radiation-pattern work is performed on antennas which are small enough to satisfy the $R \geq 2d^2/\lambda$ requirement when R is of the order of 20 ft or less. It is very convenient in this case to have use of one or more indoor ranges. All problems previously discussed are repeated many times for the indoor operation. The solution that has proved most satisfactory involves the construction of anechoic rooms using microwave-absorbing material for the walls,

ceiling, and floor. This material, which has less than 1 per cent reflection, will provide excellent results for many radiation-pattern problems. A room 16 ft high by 20 ft long by 16 ft wide will accommodate a wide range of antenna sizes and cover a broad band of frequencies. Typical characteristics of one type of absorbing material are shown in Fig. 34-23.

Automatic Pattern Range Equipment. In order to make the most effective use of facilities and manpower, semiautomatic equipment is very often used in the instrumentation of radiation-pattern ranges. The mount which is used for rotating the antenna under test may be driven by means of a variable-speed d-c motor which can be controlled by utilizing a variable-voltage rectifier unit. The output shaft of the test mount is geared 1:1 and 36:1 to two synchro generators. The output of these generators is connected to a 1:1 and a 36:1 synchro-control transformer in the recording equipment. The control transformer provides the servo system in the recorder with the information required to position the recorder turntable and to follow the rotation of the test mount.

A number of recorders specifically designed for use in taking radiation patterns may be purchased commercially.

Some of these recorders are supplied with integral chart-positioning servos which will operate when supplied with synchro information; others have constant-speed motor drives; others are positioned by means of an input d-c voltage proportional to angular position; and so on. The recorder which best suits a particular application will depend on many factors, in addition to consideration of positioning methods. These factors include pen speed, chart angular scale, recorder dynamic range, type of presentation desired, i.e., field units (linear plot), power units (square-law plot), or decibel scales (logarithmic plot). For examining narrow-beam radiation patterns and their minor-lobe structures, a 40-db logarithmic scale with an expanded chart display on a rectangular recorder gives a very satisfactory result. For conical-cut radiation patterns of broad-beam or aircraft antennas, a polar recorder with a linear scale is desirable.

Examples of broad-beam radiation patterns taken with a rectangular recorder with a 40-db logarithmic scale and the same pattern with a polar recorder with a linear scale are shown in Fig. 34-24. It is noted that the minor-lobe structure is clearly visible on the logarithmic recording, while on the linear recording very little accuracy can be obtained below 12 db or so.

Transmitting-antenna Requirements. The requirements for transmitting antennas which are used for taking radiation patterns will depend to some extent on the particular application, but some generalities can be given. In order to minimize the phase error of the antenna under test, the transmitting antenna or array should have as uniform a phase front as possible. This in turn implies that it should have as high a gain as possible for the particular physical aperture that is used. The antenna should be linearly polarized and should be singly lobed with a minimum number of minor lobes. The minor lobes should be sufficiently less than the major lobe so that their reflections from the ground and from other objects have a negligible effect on the field at the antenna under test. Minor lobes which are 20 db less than the major lobe generally will give satisfactory results if care is exercised to reduce reflections to a minimum.

The beamwidth of the transmitting antennas should be sufficiently wide and uniform so that the variation in field strength over the aperture and circle of rotation of the antenna under test is no more than about 5 per cent.

For long pattern ranges where high gain is desirable, narrow-beam transmitting-antenna parabolic dishes are very popular. For shorter ranges where broader beams are necessary, arrays of dipoles and horns are commonly used. For convenience and versatility, broadband ridge horns have been designed for transmitting needs.
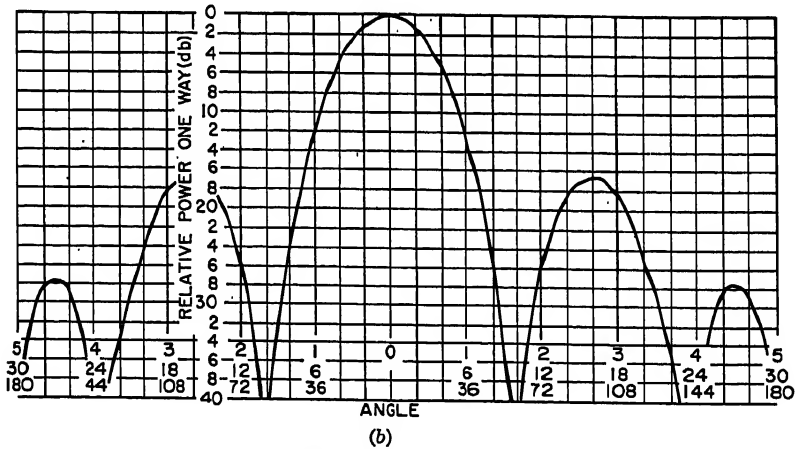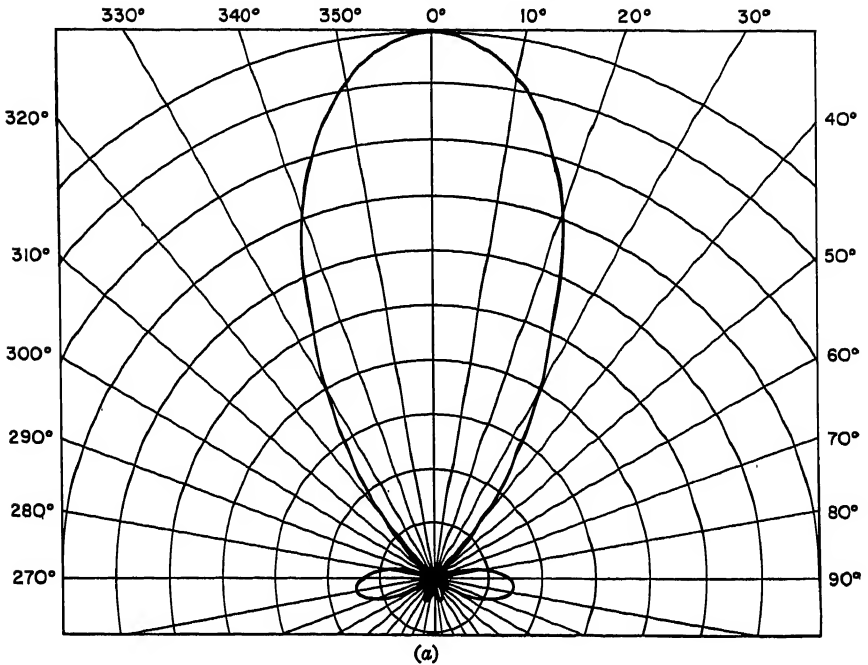
Fig. 34-24. (a) Radiation pattern taken on a polar recorder. (b) Radiation pattern taken on a 40-db rectangular recorder.

34.4. GAIN MEASUREMENTS

Definitions of Gain and Directivity. It is easy to visualize the difference between gain and directivity if one remembers that directivity is concerned only with the comparison of a lossless test antenna with a fictitious isotropic lossless source while gain compares an actual test antenna with any particular reference antenna. The

actual defining relationships are

$$\text{Gain} = \frac{\text{maximum radiation intensity (test antenna)}}{\text{maximum radiation intensity (reference antenna)}}$$

$$\text{Directivity} = \frac{\text{maximum radiation intensity}}{\text{average radiation intensity}}$$

It is assumed that in the equation for gain, both antennas have the same input power. Also, in this equation the values of radiation intensity are generally obtained by a measurement of field intensity or power density. In the equation for directivity, the values of radiation intensity are obtained only in a relative manner from radiation patterns. Since the gain of an antenna is always equal to or less than its directivity, then[6]

$$G_0 = \alpha D$$

where G_0 = gain with respect to isotropic source
D = directivity
α = effectiveness ratio ($0 \leq \alpha \leq 1$)

Also $$G_0 = \gamma G$$

where G = gain of subject antenna over arbitrary reference antenna
γ = gain of arbitrary reference antenna over isotropic antenna ($1 \leq \gamma$ for lossless antennas)

Direct-comparison Method. Since gain is defined as a comparison of two antennas, a comparison method of measurement is a logical approach. Figure 34-25 shows a

ANTENNA UNDER TEST
OR STANDARD ANTENNA

ARBITRARY TRANSMITTING
ANTENNA

FIXED
ATTENUATOR
PAD·

PRECISION CALIBRATED
VARIABLE ATTENUATOR

SIGNAL
SOURCE

R

RECEIVER
DETECTOR

MODULATOR

DETECTOR

INDICATOR

POWER
BRIDGE
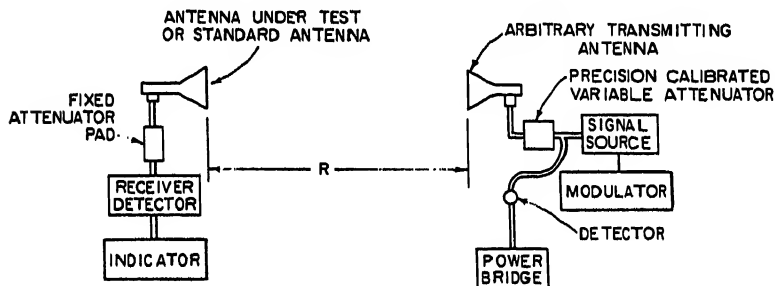
NOTE: WHEN CALIBRATING TWO IDENTICAL ANTENNAS, THE RECEIVING AND
TRANSMITTING ANTENNAS SHOWN ARE REPLACED BY TWO IDENTICAL ANTENNAS.

Fig. 34-25. Setup for measurement of gain by comparison method.

typical setup for the measurement of gain. The method for determining the gain of the standard which is used in the measurement is given later in this section. In order to be sure of the validity of the results, it is necessary to separate the standard from the subject antenna by an appropriate distance in order to prevent interaction. The distance between transmitting and receiving antennas should satisfy the $R \geq 2d^2/\lambda$ relationship. Reflections from nearby objects should be reduced to a minimum through care and the use of absorbing materials.

The attenuator pads should be inserted at the input to the receiver so that both of the antennas work into a matched load and the receiver sees a constant matched load. The power bridge or other power-level indicating device is used as a check on the stability of the transmitter. Corrections may easily be made if the power level changes, provided it is monitored. Gain is obtained in the following manner.

With the standard antenna connected to the receiver, the antenna is pointed in the direction of maximum signal intensity. The input to the transmitting antenna is adjusted to a convenient level, and the reading at the receiver for this level is noted. The attenuator-dial setting and the power-bridge reading are recorded as W_1 and P_1, respectively. The antenna under test now replaces the standard antenna. The attenuator dial is adjusted until the receiver reads the same previous level. The attenuator-dial setting and the power-bridge reading are recorded as W_2 and P_2, respectively. If $P_1 = P_2$, then no correction need be applied and the gain of the test antenna relative to the standard antenna is

$$\text{Power gain} = G_i = \frac{W_2}{W_1}$$

that is, if W_2 and W_1 are relative power levels.

Also

$$\text{Decibel gain} = G_{id} = W_2 - W_1$$

where W_1, W_2, and G_{id} have values in decibels. If the power level has changed between measurements and $P_2 \neq P_1$, then the actual power gain is obtained by multiplying G_i by the ratio of P_1/P_2. Thus

$$\text{Power gain} = G = G_i \frac{P_1}{P_2} = \frac{W_2 P_1}{W_1 P_2}$$

if W_2 and W_1 are relative power levels.

Converting P_1/P_2 to decibels, the following is obtained:

$$P_d = 10 \log \frac{P_1}{P_2}$$

and

$$\text{Decibel gain} = G_d = G_{id} + P_d = W_2 - W_1 + P_d$$

where W_1 and W_2 have values in decibels.

Errors in measurements of this type are due mainly to the following factors:

1. Receiving and transmitting antennas are too close together and thus are not in the "far zone."

2. Reflections from ground and nearby objects interfere with direct radiation.

3. The antennas involved are not oriented for maximum reception.

4. The equipment may drift off frequency, or if a nonselective detector such as a bolometer is used, there is the possibility of receiving more than a single frequency.

5. The antenna under test is badly mismatched. (Note that inherent antenna mismatch losses affect the operational gain figure. External matching devices can reduce the mismatch loss, but if not used in actual operation, an optimistic value of gain will result.)

Use and Calibration of Gain "Standards." In the previous section use was made of a standard antenna for determining gain by the comparison method. However, the standard referred merely to an antenna with known or calibrated gain. The standard antenna could have been any other antenna with which the test antenna could be compared. It must be remembered that the precision of the results is determined to a large degree by the precision with which the gain of the standard is known or can be obtained.

The calibration of a standard-gain antenna may be accomplished by one of the two methods described below. The first method involves the use of only two antennas; these antennas, however, must be identical. The second method involves three arbitrary antennas and provides a method by which the gain of each may be determined without prior knowledge of the gain of any of them.

First method. Two identical antennas (Fig. 34-25) are separated by a distance R. The distance R should be sufficiently large so that small errors in its measurement have a negligible effect on the result. In addition to this, R must be large enough to satisfy far-zone requirements. W_t is the transmitted power, and W_r is the received power, with the receiver approximately padded for impedance-matching purposes. A_{er} and A_{et} are the effective apertures of the two antennas, and $A_{er} = A_{et}$.

Then

$$A_{et} = A_{er} = \frac{G_0 \lambda^2}{4\pi}$$

and from Friis's transmission equation,

$$\frac{W_r}{W_t} = \frac{A_{er} A_{et}}{\lambda^2 R^2}$$

so

$$\frac{W_r}{W_t} = \frac{G_0^2 \lambda^2}{(4\pi R)^2}$$

and

$$G_0 = \frac{4\pi R}{\lambda} \sqrt{\frac{W_r}{W_t}}$$

The procedure for obtaining W_r and W_t is described below.

With the antennas oriented for maximum signal, the input to the transmitting antenna is adjusted to a convenient level and the receiver reading is noted for this level. The attenuator-dial setting and the power-bridge reading are recorded as W_t and P_{t1}. The transmitter is now disconnected from the antenna and is connected to the receiver through the pads. The attenuator dial is adjusted until the receiver reads the same previous level. The attenuator-dial setting and the power-bridge reading are recorded as W_r and P_{t2}. If $P_{t1} = P_{t2}$, then no correction due to transmitter-power-level fluctuation need be applied. The gain may then be obtained from the equation for G_0 above. If the power has drifted, an appropriate correction must be made.

Second Method. If two identical antennas are not available, the three-antenna method for gain determination may be used. In the first set of measurements, since $G_{01} \neq G_{02}$, the following is obtained:

$$A_{er} = G_{01} \frac{\lambda^2}{4\pi}$$

and

$$A_{et} = G_{02} \frac{\lambda^2}{4\pi}$$

Proceeding with the measurements in the same manner as in the above paragraph, the following expression results:

$$\frac{W_r}{W_t} = \frac{G_{01} G_{02} \lambda^2}{(4\pi R)^2}$$

and

$$\sqrt{G_{01} G_{02}} = \frac{4\pi R}{\lambda} \sqrt{\frac{W_r}{W_t}}$$

The third unknown antenna with gain G_{03} is used to obtain the ratio of gain between antenna 1 and antenna 2. Letting G_1 and G_2 be the gain of antennas 1 and 2 over antenna 3, obtained by using the comparison method, then

$$G' = \frac{G_1}{G_2}$$

and

$$G' = \frac{G_{01}}{G_{02}}$$

Also
$$G_{01} = G'G_{02} = \frac{G_1}{G_2} G_{02}$$

Substituting,
$$\sqrt{\frac{G_1}{G_2} G_{02}{}^2} = \frac{4\pi R}{\lambda} \sqrt{\frac{W_r}{W_t}}$$

Therefore
$$G_{02} = \frac{4\pi R}{\lambda} \sqrt{\frac{W_r}{W_t} \frac{G_2}{G_1}}$$

Also
$$G_{01} = \frac{4\pi R}{\lambda} \sqrt{\frac{W_r}{W_t} \frac{G_1}{G_2}}$$

and
$$G_{03} = \frac{G_{01}}{G_1} = \frac{G_{02}}{G_2}$$

Thus the gain of three antennas is obtained without previous knowledge of the gain of any of them.

Sensitivity. The sensitivity of a system which utilizes an antenna for its input is of interest especially in those situations in which detection occurs at the antenna
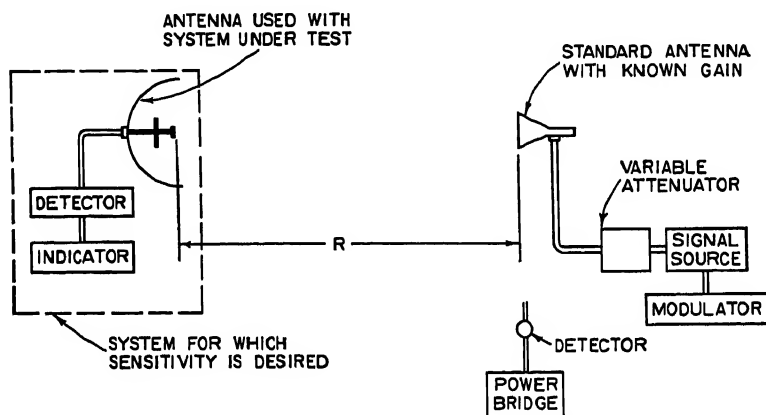
Fig. 34-26. System sensitivity measurement.

terminals. In this case, however, the impedance of the antenna and its gain are actually without meaning, since in performing gain or impedance measurements the detector characteristics are missing from the measurements.

It is more direct to determine the field strength at the antenna for a particular system indication. The result would be system sensitivity in terms of power density. Assume that an antenna of known gain G_0 is separated from the antenna under test by a distance R. The antenna under test is connected to its detector and indicating system as shown in Fig. 34-26. The appropriate far-zone and reflection precautions must be taken. The input to the transmitting antenna is increased or decreased, depending upon system operation, until the desired indication appears in the system under test. At this point the power P_t into the transmitting antenna is determined by measurement, and then P_0 is equal to the following:

$$P_0 = \frac{P_t G_0}{4\pi R^2}$$

where P_0 is in watts per square meter if R is in meters. For the particular system operation performed, P_0 is system sensitivity.

Directivity. Directivity was previously defined as follows:

$$\text{Directivity} = \frac{\text{maximum radiation intensity}}{\text{average radiation intensity}}$$

or

$$D = \frac{U_m}{U_0}$$

Also

$$D = \frac{4\pi U_m}{\text{total power radiated}}$$

where

$$W = 4\pi U_0 = \text{total power radiated}$$

Although many references give only a theoretical approach to the problem, directivity may be obtained from an examination and integration of antenna radiation
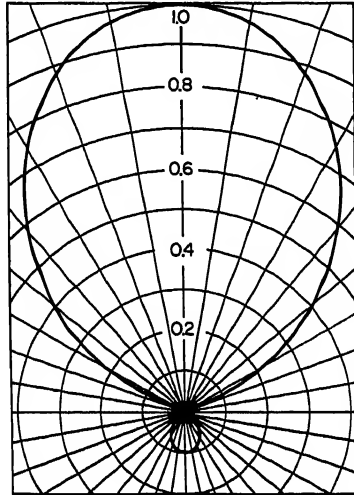
Fig. 34-27. Radiation pattern (linear-field plot).

patterns which have been taken (a lossless antenna is assumed). Relative values of maximum radiation intensity and total power radiated are required rather than absolute values.

Figure 34-27 indicates one cut of the radiation pattern from a particular antenna. In order to determine W, an infinite number of cuts are required unless an assumption is made with regard to the maximum radiation intensity discussed below.

Since

$$W = k\iint F^2(\theta,\phi) \sin \theta \, d\theta \, d\phi$$

where F = relative field intensity

θ = polar angle

ϕ = azimuth angle

k = proportionality constant

if it is assumed that the maximum radiation intensity is equal to 1, then

$$W = \iint F^2(\theta,\phi) \sin \theta \, d\theta \, d\phi$$

For simplicity, it is also assumed that there is no variation with respect to ϕ. Then

$$D = \frac{4\pi}{2\pi \int_0^\pi F^2(\theta) \sin \theta \, d\theta} = \frac{2}{\int_0^\pi F^2(\theta) \sin \theta \, d\theta}$$

The integration indicated in the denominator may be performed numerically or graphically. The graphical procedure necessitates a plot of $F^2(\theta) \sin \theta$ versus θ. This is shown in Fig. 34-28. The area of this plot may be obtained by using a planim-
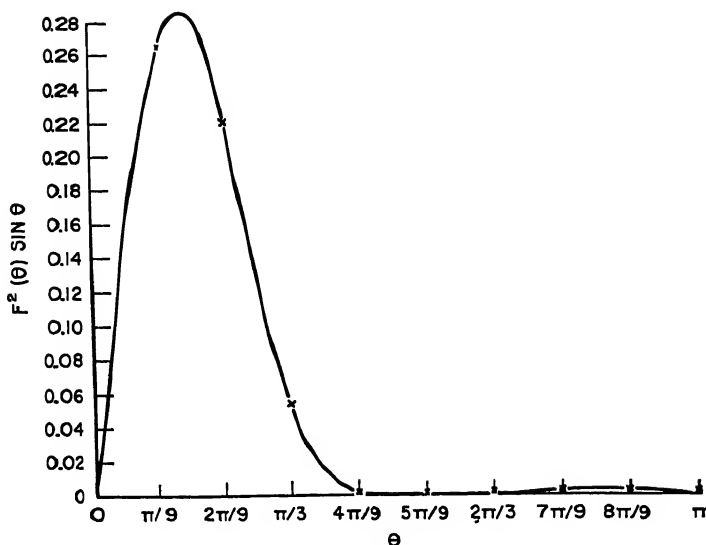
FIG. 34-28. Plot of $F^2(\theta)$ sin θ vs. θ.

eter or by any other applicable method.   The resulting area is equal to 0.064π, and

$$D = \frac{2}{0.064\pi} = 9.94$$

34.5. PHASE-FRONT MEASUREMENTS

For proper performance of certain types of antennas, especially those which are used to illuminate reflectors, it is desirable to determine contours of constant phase. From the contour information it is generally possible to determine the effective center of radiation of the antenna.   This information is of importance in work with lenses and shaped reflectors.   There are numerous variations of the basic method which are used for phase-contour determination.

In its most rudimentary form the measurement involves the sampling of the radiated field of the antenna of interest and comparing the phase of this sample with a reference signal which is obtained directly from the signal source.   By providing a means for varying the amplitude and phase of either the reference or the sampled signal, it is possible to mix the two signals and produce an easily recognizable interference condition between them.   The interference may be either a maximum or a null.   A simple apparatus for performing this type of measurement is shown in Fig. 34-29.   Modulated radio-frequency power is fed into the transmitting antenna. A sample of this power is fed through a matching pad and a variable attenuator to a crystal or bolometer detector.   The transmitted energy is picked up by the dipole-probe antenna at a convenient distance.   For most applications the distance should be sufficiently large so that the center of radiation may be determined with satisfactory accuracy.   The level of the reference signal is adjusted so that it is approximately equal to that picked up by the probe.   The output of the probe is fed into the same detector.   The probe carriage is moved radially with respect to the transmitting antenna until a null is obtained.   This location is recorded.   The probe is then moved a wavelength toward the antenna, to obtain another null, and a wavelength away from the antenna, to obtain a third null.   These locations are also recorded.   Moving

the probe slowly and carefully, one may follow the constant phase contour by following the course of the nulls.

The above situation requires the use of a length of coaxial line for flexibility in performing the measurement. If waveguide must be used or if only a limited amount
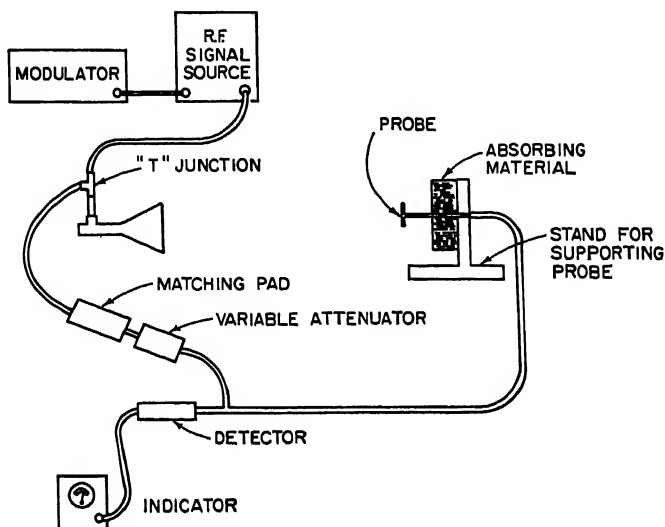
FIG. 34-29. Apparatus for phase-front measurements using null detection method.
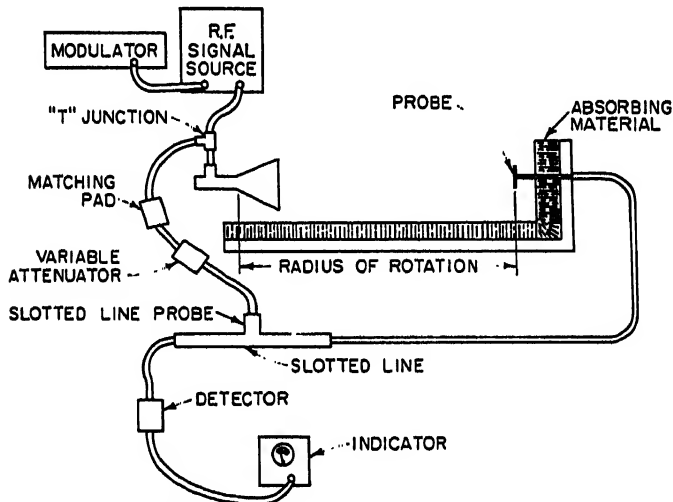
FIG. 34-30. Slotted-line phase-front measurements using null detection method.

of freedom of probe movement is available, the phase contour may be obtained with the aid of a slotted section. In this case the reference signal is applied to the detector by means of a slotted-line probe as shown in Fig. 34-30. The field probe is allowed to move only in a circular path, with the center of the circle at the transmitting antenna. The null position is obtained at the initial position of the field probe by moving the slotted-line probe along the line. The field probe is then moved in the prescribed path. At each point the slotted-line probe is moved to a new null position.

In terms of the slotted-line probe shift, the phase change is given by

$$\Delta\phi = \frac{2\pi\,\Delta S}{\lambda_g}$$

The result of these measurements properly interpreted will give the constant phase contour.

In all these measurements it is necessary to ensure well-matched lines in order to prevent phase errors due to reflected energy. It is considered good practice to use attenuator pads and/or well-matched components in order to satisfy the matching requirements.
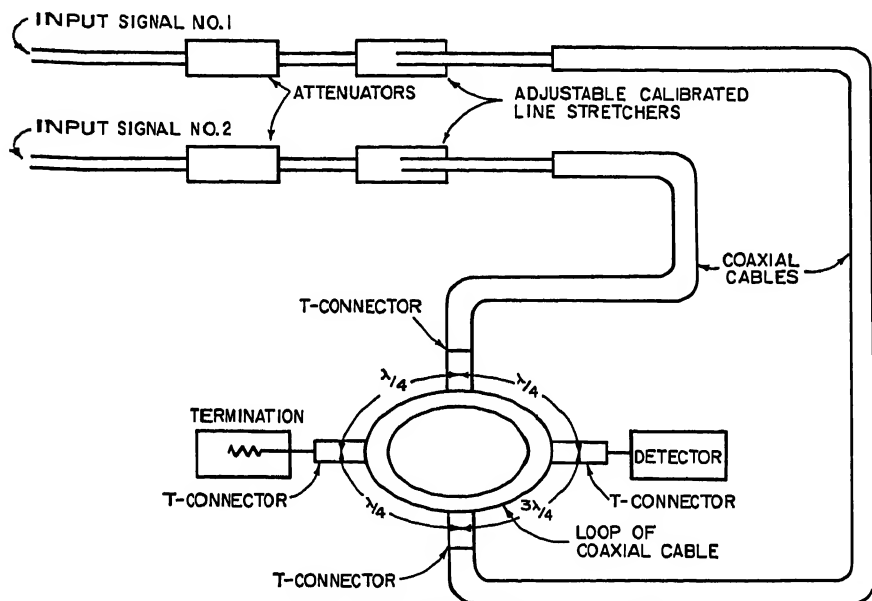
FIG. 34-31. Phase measurements using hybrid.

Another method which has been used with a great deal of success, especially when highly accurate measurements are desired, makes use of a coaxial bridge, or "hybrid" (Fig. 34-31). The signals to be compared are attenuated to comparable levels and fed into the bridge arms through a calibrated phase shifter. The outputs of the bridge will depend on the phase of the two signals. Specifically, if the balanced output is terminated in a matched load, the remaining output will exhibit minimum signal for an in-phase condition at the input and maximum signal for an out-of-phase condition at the input. By adjusting the calibrated phase shifter, either of these conditions may be obtained and the phase difference between the input signals may be determined. The detector to be used should be a tunable receiver with good sensitivity, for best results.

A null detection method results in higher accuracy than a peak detection method, although either may be used.

34.6. POLARIZATION MEASUREMENTS

For convenience the polarization of an electromagnetic wave, whether linear, elliptical, or circular, can be considered to be some form of elliptical polarization.

Elliptical polarization can be considered the resultant of two linearly polarized waves of the same frequency. Using the coordinate axes shown in Fig. 34-32, with the positive z coordinate being the direction of wave propagation, the two linear waves can be specified as

$$E_z = E_1 \sin (\omega t - \beta z)$$
and $$E_y = E_2 \sin (\omega t - \beta z + \delta)$$

where δ is the phase angle between E_z and E_y.

Combining E_z and E_y into the resultant total field $\bar{E}$, we have

$$\bar{E} = iE_1 \sin (\omega t - \beta z) + jE_2 \sin (\omega t - \beta z + \delta)$$

If any particular value of z is specified and if the value of $\bar{E}$ is then calculated versus time at the specified z, it is found that $\bar{E}$ will describe an ellipse for $E_1 \neq E_2$, $\bar{E}$ will describe a circle for $E_1 = E_2$ with $\delta = 90°$, and $\bar{E}$ will describe a straight line for either $E_1 = 0$ or $E_2 = 0$, or $\delta = 0°$ or $\delta = 180°$.

Fig. 34-32. Perpendicular linear components of an elliptically polarized wave.

Elliptical polarization can also be considered to be produced by two circularly polarized waves, as shown intuitively in Fig. 34-33. If the vectors for the two circularly polarized fields are specified as

$$E_{ccw} = E_3 e^{j(\omega t - \beta z)}$$
and $$E_{cw} = E_4 e^{-j(\omega t - \beta z + \delta')}$$

then the components in the principal planes can be shown to be

$$E_z = E_3 \cos (\omega t - \beta z) + E_4 \cos (\omega t - \beta z + \delta')$$
$$E_y = E_3 \sin (\omega t - \beta z) - E_4 \sin (\omega t - \beta z + \delta')$$

COMPONENT WAVES   RESULTANT WAVE

E_{CCW} + E_{CW} =   LINEAR POLARIZATION (POLARIZED PARALLEL TO y PLANE)

E_{CCW} + $\frac{1}{2} E_{CW}$ =   ELLIPTICAL POLARIZATION

E_{CCW} + $E_{CW} = 0$ =   CIRCULAR POLARIZATION

Fig. 34-33. Two circularly polarized waves resulting in elliptical polarization.

For a particular value of βz it can be shown that $\bar{E}$ will describe an ellipse for $E_3 \neq E_4$, $\bar{E}$ will describe a circle for $E_1 = E_2$ with $\delta' = 90°$, and $\bar{E}$ will describe a straight line for $E_1 = 0$ or $E_2 = 0$, or $\delta' = 0°$ or $\delta' = 180°$.

In general, the polarization ellipse is tilted in space with respect to the coordinate axes. This tilt angle, defined by Fig. 34-34, may be calculated by using the following equation:

$$\tan 2\tau = \frac{2E_1 E_2 \cos \delta}{E_1{}^2 - E_2{}^2}$$

A quantity which is very often of interest when dealing with elliptical polarization is the "axial ratio," or "ellipticity" of the radiated energy. Another quantity that
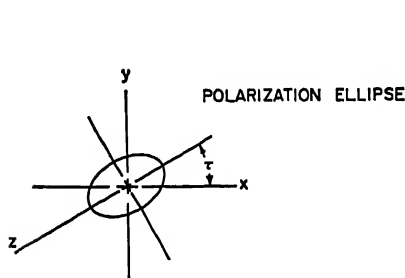
FIG. 34-34. Tilted polarization ellipse.
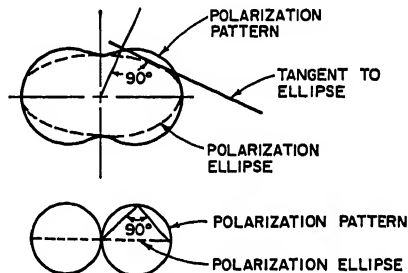
FIG. 34-35. Polarization pattern and ellipse.

is less common but desirable, especially in broad-beam work, is the "polarization ratio." Axial ratio and ellipticity refer to the ratio of the major axis to the minor axis of the polarization ellipse taken on the axis of the beam in question. Under some specific conditions of antenna configuration this same ratio will apply over the entire beam. Generally, however, in the design of elliptically polarized radiators, it is necessary to form a resultant elliptically polarized wave from two linearly polarized waves oriented at 90° to each other in space. Unless the E-plane radiation pattern of each linearly polarized radiator is the same as its H-plane pattern, the axial ratio will in general apply only to the "on-axis" part of the beam. The polarization ratio, which is defined as the ratio of the major axis to the minor axis of the polarization ellipse at any angle in the beam of the antenna, can be used to describe the elliptical-polarization characteristics of an antenna very completely.

Antennas in which this type of treatment is necessary for a complete description include the following: helical antennas, crossed-dipole antennas, double-ridge horns, crossed-loop antennas, and so on.

In order to make the fullest use of any polarization measurements that are made, it is necessary that the results be shown in an easily usable form. By means of polarization measurements of the radiated wave, it is possible to determine what changes have to be effected on the antenna in order to obtain more perfect circular polarization. The method of plotting polarization measurements which utilizes the Carter transmission-line chart is highly recommended. This is described later in this section.

The three methods which are used for measuring the polarization characteristics of a wave are:

1. Polarization-pattern method, in which the polarization and direction of rotation of E are determined

2. Linear-component method, in which the amplitude and relative phase of two perpendicular linearly polarized components of the wave are measured

3. Circular-component method, in which the amplitude and relative phase of two circularly polarized components (of opposite rotation) of the wave are measured

Polarization-pattern Method. A linearly polarized directional antenna, mounted so that it can be rotated, is connected to a detector which is calibrated to read relative field intensity. As the linearly polarized antenna is rotated, the signal received from the elliptically polarized antenna traces out a polarization pattern of the type shown in Fig. 34–35 in the solid line. The dotted line represents the polarization ellipse.

The direction of polarization may be obtained quite simply by comparing the signal received by two circularly polarized antennas, one being polarized clockwise, the other being polarized counterclockwise. The antenna with the larger response would be the one with the proper polarization rotation.

In the limiting cases of circular and linear polarization, the polarization pattern would degenerate into a circle and figure of eight, respectively, and the polarization ellipse would become a circle and a straight line, respectively.

Linear-component Method. The linear-component method utilizes two linearly polarized antennas which are identical. One of these antennas is horizontally polarized, and the other antenna is vertically polarized. The ratio of these two received signals is E_2/E_1 or E_1/E_2, where

$$E_x = E_1 \sin (\omega t - \beta z)$$

and

$$E_y = E_2 \sin (\omega t - \beta z + \delta)$$

The phase difference δ between these two waves may be obtained by using a slotted-line phase measurement of the type described in Sec. 34.5. The direction of rotation is clockwise for $0 < \delta < 180°$ and is counterclockwise for $0 > \delta > -180°$.

The angle of tilt of the ellipse may be determined from the following equation:

$$\tau = \frac{1}{2} \arctan \frac{2E_1E_2 \cos \delta}{E_1{}^2 - E_2{}^2}$$

Circular-component Method. In order to utilize this method, one must have available two circularly polarized antennas of opposite polarization rotation but otherwise identical. Left- and right-hand helical antennas with multiple turns may be used.

The relative signal received by the counterclockwise-polarization-rotation antenna E_L and that received by the clockwise-polarization-rotation antenna E_R are substituted in the following equation to obtain the axial ratio:

$$\text{AR} = \frac{E_R + E_L}{E_R - E_L}$$

If the value of AR is positive, then the wave is polarized clockwise; if negative, the wave is polarized counterclockwise. The angle of tilt of the polarization ellipse may be determined by using a linearly polarized antenna.

Comments on the Three Methods of Measuring Polarization. Of the various methods proposed for measuring elliptical polarization, the last one described is actually the most difficult to perform accurately. The need for two circularly polarized antennas which are identical, especially when it is necessary to cover a broad frequency band, is the primary difficulty. Then there is the necessity of going to a linear element to determine the value of τ.

The first and second methods are actually quite similar to each other and are recommended for general use. Another method, making use of a continuously rotating linearly polarized antenna for complete polarization information, cannot be surpassed.

In general, it is much simpler and quicker when axial ratio is desired to combine the polarization-pattern method and the linear-component method to obtain polarization information. The following procedure is used: with a single linearly polarized directional antenna mounted so that it may be rotated about its axis, determine the relative magnitudes of the vertically and horizontally polarized received signals and

obtain the angle of tilt above the horizontal of the polarization ellipse. Thus E_1, E_2, and τ are obtained. It is now quite a simple matter to determine the phase difference from the following equation:

$$\cos \delta = \frac{(E_1{}^2 - E_2{}^2) \tan 2\tau}{2E_1 E_2}$$

Plotting of Polarization Information. A number of charts are available for use in plotting polarization information. The Carter chart is one of the best for this purpose provided that the proper identification is used for the scales.

The chart (Fig. 34-8) is a transmission-line chart on which are plotted lines of constant phase indicated by the horizontal scale which reads from -90 to 0 to $+90°$, lines of constant impedance magnitude indicated by the vertical scale which reads from 0 to ∞, and line length toward the load indicated by the outside scale which reads from 0 to $180°$ in a counterclockwise direction.

The chart may be used for circular or elliptical polarization plotting by using the scales for counterclockwise-approaching elliptical polarization as follows:

1. The outside scale reading from 0 to 180° gives the angle of tilt of the polarization ellipse; 0° is vertical (linear) polarization, 90° is horizontal (linear) polarization; any point located at the outer circle is linearly polarized at the particular angle specified by the point.

2. The angle of tilt of the polarization ellipse measures counterclockwise from the position where the major axis is vertical.

3. The vertical scale is the ratio of the horizontally polarized signal to the vertically polarized signal.

4. Calling E_y the vertically polarized component and E_x the horizontally polarized component, then for counterclockwise-approaching circular polarization, if E_y lags E_x by 90°, then $\delta = -90°$, and if E_x leads E_y by 90°, then $\delta = -90°$ (δ is positive for E_x lagging and negative for E_x leading), δ being the phase difference between E_x and E_y.

5. If the horizontal scale is called θ, then $\delta = \theta - 90°$ and E_x leads E_y by the resultant of $\delta = \theta - 90°$.

6. The axial ratio, or ellipticity ratio, is given by circles of radius equal to the lower half of the vertical scale.

7. When a plot is made of polarization vs. frequency, the chart may be used to compensate the antenna in order to obtain the required axial ratio, or ellipticity ratio.

REFERENCES

1. Edwin Istvanffy: "Antenna Impedance Measurement by Reflection Method," *Proc. IRE*, vol. 37, pp. 604–608, June, 1949.
2. F. A. Jenkins and H. E. White: "Fundamentals of Optics," McGraw-Hill Book Company, Inc., New York, 1957.
3. D. E. Kerr (ed.): "Propagation of Short Radio Waves," MIT Radiation Laboratory Series, vol. 13, McGraw-Hill Book Company, Inc., New York, 1951.
4. D. D. King: "Measurements at Centimeter Wavelength," D. Van Nostrand Company, Inc., Princeton, N.J., 1952.
5. R. W. P. King: "The Theory of Linear Antennas," Harvard University Press, Cambridge, Mass., 1956.
6. J. D. Kraus: "Antennas," McGraw-Hill Book Company, Inc., New York, 1950.
7. C. G. Montgomery (ed.): "Technique of Microwave Measurements," MIT Radiation Laboratory Series, vol. 11, McGraw-Hill Book Company, Inc., New York, 1948.
8. Radio Research Laboratory Staff: "Very High Frequency Techniques," McGraw-Hill Book Company, Inc., New York, 1947.
9. Reich, H. J.: "Microwave Theory and Techniques," D. Van Nostrand Company, Inc., Princeton, N.J., 1953.
10. M. Wind and H. Rapaport: Handbook of Microwave Measurements, Polytechnic Institute of Brooklyn, Microwave Research Institute, New York, 1954.
11. E. L. Ginzton: "Microwave Measurements," McGraw-Hill Book Company, Inc., New York, 1957.

Chapter 35

MECHANICAL CONSIDERATIONS IN ANTENNA DESIGN

Roger Avery

Airborne Instruments Laboratory
Melville, Long Island, New York

35.1. INTRODUCTION

Antenna systems cover a wide range of sizes, varying from low-frequency antenna systems which require many acres of ground to millimeter-wave antennas which are small enough to be held in one's hand. Regardless of size, it is invariably true that the mechanical design of an antenna is closely linked with its electrical design. While the antenna engineer need not be a mechanical engineer, he should have some appreciation of mechanical problems if he expects his electrical design to be translated into a workmanlike structure which will withstand the environment in which it is placed.

Tall antenna towers and large reflector systems are generally erected by construction firms which specialize in these structures, so that the average antenna engineer will not be concerned with their mechanical design.

However, many antennas and feed systems which operate in the VHF range and

upward are constructed as packaged units. For this type of structure, the electrical and mechanical designs are often so closely interlocked that the mechanical requirements play an important role in the electrical design. Here it is essential that the antenna engineer be familiar with materials and methods of fabrication. This chapter will review some of the recent advances in these areas with the hope that the antenna engineer will look more deeply into these problems in order to improve the effectiveness of his designs.

A treatment of stress computations has not been given here because this topic has been treated at great length in a number of handbooks and texts on strength of materials. It should be mentioned, however, that the mechanical forces to which
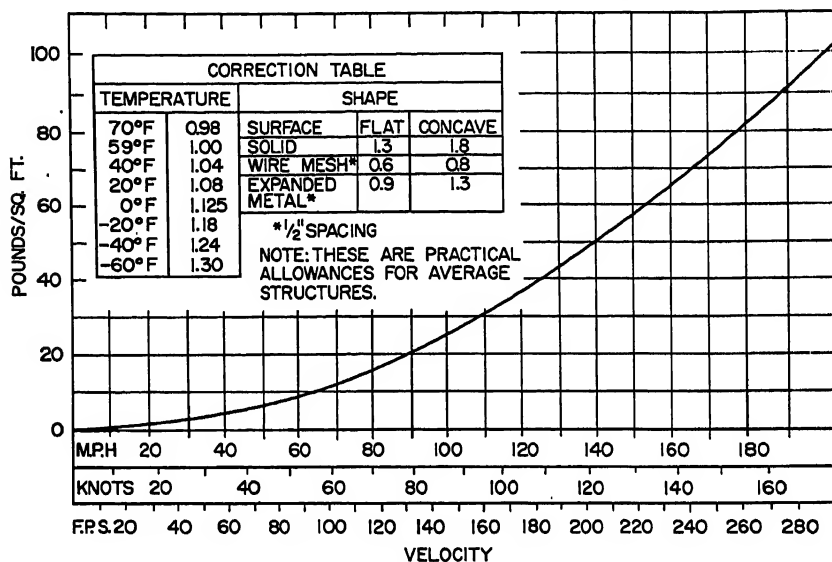
Fig. 35-1. Wind-loading data.

an antenna is subjected in use are primarily wind loading, ice loading, and vibration stresses. Some idea of the magnitude of wind-loading forces can be obtained from Fig. 35-1. Forces on a cylindrical tube can be estimated by using the correction factor for a flat plate. Ice loading increases the stress on a structure because of the increase in area presented to the wind and because of the additional weight due to the ice loading (approximately 57 lb/cu ft).

35.2. MATERIALS

The use of any material is conditional on the environmental and mechanical stresses to which it will be subjected. The military specifications pertaining to environmental use are without question the most exacting, but one should be doubly careful of the phrase "commercial use." The air around us is filled with fumes from the stacks of industry, the chimneys of homes, and the exhausts of automobiles loaded with corrosive gases and dirt. These fumes plus the forces of nature will complete the speedy deterioration of any improperly chosen material or finish. The pressure of competition has forced most of the suppliers of materials and processing services to equate their products and services to known standards of serviceability under a wide range of environmental conditions. Laboratories are maintained by both manu-

facturers and buyers to evaluate, under specific environmental conditions, services and products and to seek out means of improving them. In the exploration of outer space entirely new environmental conditions have been encountered. Belts of radiation that lie in the weightless, heatless void beyond our atmosphere will adversely affect materials and finishes. It will be years before the full extent of these changes to material and finishes will be known. The effects of total vacuum and high-intensity ultraviolet radiation will in due time become known. Simulated conditions in the laboratory plus information from our space probes will provide the basis for present material choice.

The most common chart, found in textbooks and manufacturers' literature and prepared by private and governmental testing laboratories, is known as a "properties chart." On the basis of information contained in these charts, better than 95 per cent of materials used in antenna design are chosen. We have reproduced only a limited number of these charts for use in this Handbook. The availability of such charts plus the continual changes being made in them make it desirable to acquire the latest charts as they are released. We shall attempt to highlight, in the following description of the various materials, their properties suitable to antenna construction.

Metals. The number of new metals available in recent years has increased steadily. New methods of extraction and processing have brought the rare metal into greater use.[1] The push to develop stronger heat- and corrosion-resistant materials has brought about the superalloys, ultrastrength steels, and special alloys of some of the well-known metals.[2] Most of these metals fit into the design of outer-space vehicles or nuclear reactors rather than in a conventional structure. A number of new or special alloys do, however, fit into antenna design. The most promising is titanium, 120,000 to 180,000 psi in tensile, weighing half as much as steel. It can be integrated into an aluminum structure at discrete points, providing high strength and stiffness without serious increase of mass. Titanium has a high relative resistance of 47.8, but can be plated successfully for use in r-f transmission lines, etc. The new beryllium coppers[3] and heat-treating techniques have improved the design of sliding contacts or fingers of all kinds.

Copper, brass, and aluminum[4] are still the most important metals in antenna construction today. Where weight is not of prime importance, brass and copper are used extensively. These two metals machine, solder, and plate so easily, with little or no special equipment, that they are the favorites of the model shop and production shop alike. Complicated assemblies can be built with practically no r-f discontinuities due to contact between parts. Aluminum equals or surpasses both copper and brass in all counts except plating. Although it requires special equipment to weld aluminum, the versatility and quality of the technique are comparable with that of steel. Special care must be taken in the choice of some alloys when welding is contemplated. The weldability is given in Table 35-1 along with some other important properties of some commonly used metals.

Plastics. The increased use of reinforced plastics[5] in antennas as a structural material is a result of the improved techniques of laminating and the use of complex resin systems. The designer should be cautioned that critical structures, fabricated by hand lay-up using vacuum, pressure-bag, or matched-die techniques, must be type-tested. They should be given tests to determine their strength throughout the entire molding. This can best be accomplished by cutting the molded part into many pieces and testing it piece by piece. In the case of a radome, the part must be checked for loss tangent (dissipation factor) and its effect on the transmission characteristics of the antenna. Two molded parts of the exact same shape, cloth, resin, and weight, but using different techniques of lay-up and pressure, can have both electrical and structural properties that vary by 40 to 50 per cent. With the use of reinforced plastics, it is now possible to cut weight, maintain greater surface tolerances for a

Table 35-1. Typical Properties of Some

Type or class	Name	Composition, per cent	Density, lb/cu in.	Melting point, °F	Thermal conductivity, Btu/(hr)(sq ft)/(°F)(ft)	Coefficient of thermal expansion per °F	Electrical resistivity (68°F), microhm-cm
					Physical properties		
25	Gray iron, cast	....	0.26	....	24–34	6×10^{-6}	50–200
Standard 32510	Malleable iron, cast	C 2.3–2.7, Si 1.5–0.8, Mn 0.55 max, P 0.18 max, S 0.2 max	0.259–0.263	....	20.5 at 80°F	6.6×10^{-6}	32.0
	Wrought iron, hot-rolled	C < 0.02, Mn < 0.02, Si trace, P 0.005, S 0.02	0.278	2750	34.5	7.4×10^{-6}	....
AISI C1020	Low-carbon steel Hot-rolled Cold-worked	C 0.18–0.23, Mn 0.30–0.60, P 0.040 max, S 0.050 max	0.283	2750–2775	27	8.4×10^{-6}	14.3
AISI C1040	Medium-carbon steel Hot-rolled Cold-worked Hard and tempered	C 0.37–0.44, Mn 0.60–0.90, P 0.040 max, S 0.050 max	0.283	2700–2750	27	8.3×10^{-6}	19
AISI C1060	High-carbon steel Annealed Hot-rolled Hard and tempered	C 0.55–0.65, Mn 0.60–0.90, P 0.40 max, S 0.50 max	0.283	....	27	8.1×10^{-6}	18
AISI B1112, C1212	Free-cutting steel, 1-in.-diam.	C 0.13 max, Mn 0.70–1.00, P 0.07–0.12, S 0.17–0.23	0.283	....	27	8.4×10^{-6}	14.3
AISI 303	Austenitic stainless steel Annealed Cold-worked	C 0.15 max, Mn 2 max, P, S, Se 0.07 min, S 11 max, Cr 17–19, N 18–10, Mo or Zr 0.60 max	0.29	2550–2590	9.4	9.9×10^{-6}	72
AISI 430	Ferritic stainless steel Annealed Cold-worked	C 0.12, Mn 1.00, Si 1.00, P 0.04, S 0.03, CR 14.0–18.0	0.28	2600–2750	15.1	5.8×10^{-6}	60
AISI 416	Martensitic stainless steel Annealed Hard and tempered	C 0.15 max, CR 12–14, P, S, or Se 0.07 min, Mo or Zr 0.06 max	0.28	2700–2790	14.4	5.8×10^{-6}	70
1100	Aluminum alloy, wrought Annealed Half-hard Hard	Al 99.0 min	0.098	1190–1215	128	13.1×10^{-6}	2.92 .... 3.02

Commonly Used Metals

Mechanical properties					Fabricating properties				Corrosion resistance
						Weldability			
Modulus of elasticity in tension, psi	Tensile strength, 1,000 psi	Elongation (in 2 in.), %	Hardness (Brinell)	Shear strength, 1,000 psi	Machinability	Torch	Inert arc	Electrical resistivity	
14 × 10⁶ 13 × 10⁶ 11.5 × 10⁶	27-33 25-30 20-24	....	205 190 175	37	40-110	Yes	Yes	Yes	Resistant to strong sulfuric acid, cold concentrated phosphoric and nitric acids. Attacked by dilute sulfuric, phosphoric, and nitric acids. Resistant to sodium hydroxide, soda ash, and ammonia.
25 × 10⁶	50-52	10-18	110-145	45-48	120ᵃ	No	No	No	Resistant to atmospheric corrosion in rural, industrial, and marine atmospheres; fresh and salt waters.
29.5 × 10⁶	48	30	....	40	50ᵈ	Yes	Yes	Yes	Current improved wrought iron has at least 25 per cent greater corrosion resistance than former grade.
29-30 × 10⁶	65 78	36 20	143 156	45	50ᵃ 60ᵃ	Yes	Yes	Yes	Rusted by oxygen and water at room temperature, rate of attack increasing sharply as pH goes above 4 and decreasing below a pH of 8. Dilute salt
29-30 × 10⁶	91 100 113ᵇ	27 17 23ᵇ	201 207 235ᵇ	....	.... 65ᵃ 55ᵃ	Yes	Yes	Yes	solutions increase corrosion rate. Attacked by acids in general, but satisfactorily resistant to alkalis at normal temperature. Corrosion rate in ordinary rusting not appreciably affected by carbon or alloy content or by cold-working.
29-30 × 10⁶	105 116 160ᶜ	20 17 12	192 241 321	....	53	No	No	No	Rust when brought into contact with moisture and air at room temperature; rates not appreciably affected by carbon content. If salts are present, corrosion rate is increased. Attacked readily by acids, but resistant to alkalis at room temperature.
29 × 10⁶	80-105	12-22	163-229	......	100	Yes	Yes	Yes	
28 × 10⁶	90 110	50 30	160 240	....	Fair	Yes	Yes	Yes	Very good atmosphere resistance; some resistance sacrificed for better machinability.
29 × 10⁶	75 75-90	25-30 15-25	B 80ᵈ B 95ᵈ	... .	Fair	Yes	Yes	Yes	Excellent resistance to weather, water; good resistance to most chemicals.
29 × 10⁶	115-120 120-200	15-20	235 250-410	..	Fair	Yes	Yes	Yes	Good resistance to weather and water; also good resistance to some chemicals.
10 × 10⁶	13 18 24	35-45 9-20 5-15	23 32 44	9 11 13	Good	A	A	A	High resistance to rural, industrial, and marine atmosphere. Good resistance to most neutral or nearly neutral fresh waters; sea water, organic acids, and anhydrides. Alcohols, aldehydes; esters; ketones; oils; gasoline; greases, waxes, and

Table 35-1. Typical Properties of Some

Type or class	Name	Composition, per cent	Physical properties				
			Density, lb/cu in.	Melting point, °F	Thermal conductivity, Btu/(hr)(sq ft)/(°F)(ft)	Coefficient of thermal expansion per °F	Electrical resistivity (68°F), microhm-cm
2024	Aluminum alloy, wrought Annealed Heat-treated	Cu 3.8-4.9, Mn 0.3-0.9, Mg 1.2-1.8	0.100	935-1180	111.0	12.6×10^{-6}	3.45 5.75
5052	Aluminum alloy, wrought Annealed Half-hard Hard	Mg 2.2-2.8, Cr 0.15-0.35	0.097	1100-1200	79.2	13.2×10^{-6}	4.93 ...... 4.93
6061	Aluminum alloy, wrought Annealed Heat-treated	Mg 0.8-1.2, Si 0.4-0.8, Cr 0.15-0.35, Cu 0.15-0.40	0.098	1080-1200	99	13.0×10^{-6}	3.8 ......
7075	Aluminum alloy, wrought Annealed Heat-treated	Zn 5.1-6.1, Mg 2.1-2.9, Cu 1.2-2.0, Cr 0.18-0.40	0.101	890-1180	...... 70 (T6)	12.9×10^{-6}	...... 5.7 (T6)
356-T6	Aluminum alloy, sand-cast	Si 6.5-7.5, Mg 0.20-0.40	0.097	1035-1135	39	11.9×10^{-6}	
	Electrolytic tough-pitch copper Annealed Hard	Cu 99.9 min, O about 0.04	0.321-0.323	1949-1981	226	9.8×10^{-6}	1.71
	Deoxidized copper Annealed Hard	Cu 99.9 min, P 0.015-0.040	0.323	1981	196	9.8×10^{-6}	2.03
	Beryllium copper Annealed Hard	Be 1.90-2.15, Co 0.20-0.35, Cu bal	0.296-0.298	1600-1800	100 110	9.3×10^{-6}	4.82 5.82
	Common bronze, 90% Annealed Hard	Cu 89.0-91.0, Zn bal	0.318	1870-1910	109	10.2×10^{-6}	3.9
	Yellow brass Annealed Hard	Cu 63.0-68.5, Zn bal	0.306	1660-1710	67	11.3×10^{-6}	6.4

Commonly Used Metals (*Continued*)

Mechanical properties					Fabricating properties				Corrosion resistance
						Weldability			
Modulus of elasticity in tension, psi	Tensile strength, 1,000 psi	Elongation (in 2 in.), %	Hardness (Brinell)	Shear strength, 1,000 psi	Machinability	Torch	Inert arc.	Electrical resistivity	
									other petroleum derivatives; ammonia and ammonium compounds; nitric acid above 82%; essential oils; amides; nitro paraffins; coal-tar derivatives. Hydrogen peroxide; and many neutral aqueous inorganic salt solutions.
10.6×10^6	27 70 (T3)	20 18 (T3)	47 120 (T3)	18 41 (T3)	A (T3)	D	B	B	High resistance to rural atmospheres, fairly good resistance to industrial atmospheres and poor resistance to marine atmospheres and sea water. More susceptible to corrosive attack than other aluminum alloys. Both degree and nature of the attack are greatly influenced by thermal treatment.
10.2×10^6	28 38 42	25-30 10 14 7 8	47 68 77	18 21 24	Good	B	A	A	See 1100 Aluminum Alloy.
10.0×10^6	18 35 (T4) 45 (T6)	25 22 (T4) 12 (T6)	30 65 (T4) 95 (T6)	12 24 (T4) 30 (T6)	B (T4, T6)	A	A	A	High resistance to rural atmospheres, good resistance to industrial and marine atmospheres. Degree and nature of attack in other environments are greatly influenced by heat-treatment.
10.4×10^6	33 83 (T6)	17 11 (T6)	60 150 (T6)	22 48 (T6)	A (T6)	D	C	C	Good resistance to rural atmospheres but attacked by industrial and marine atmospheres. In other environments generally less corrosion-resistant than other wrought aluminum alloys and frequently clad.
10.3×10^6	33	3, 5	70	26	B	B	B	.....	Generally good resistance to industrial rural and marine atmospheres, also gasolines, fuel oils, and lacquers. Generally poor resistance to ammonia, ferric and ammonium compounds, and cyanides. Good resistance to weak acids and bases; some resistance to strong acids and bases.
17×10^6	32 35 50 55	45 35 6 1.5	F 40d B 55d	22 21 28 29	20d	Poor	Fair	Poor	
17×10^6	32 50	45 8	F 40d B 55d	22 28	20d	Fair	Good	Poor	
19×10^6	60 80 165 185	35 50 3 12	B 60d C 36d	50 90	20d	Poor	Excellent	Excellent	
17×10^6	37 40 51 71	45 50 5 4	F 53d B 70d	28 30 38 12	20d	Good	Good	Poor	
15×10^6	46 50 74 110	65 00 8	F 58d B 80d	32 34 43 55	30d	Good	..	Fair	Generally good resistance to industrial rural and marine atmospheres; also gasolines, fuel oils, and lacquers. Poor resistance to ammonia, ferric and ammonium compounds, and cyanides. Susceptible to dezincification and stress-corrosion cracking. Some resistance to weak acids and bases. Poor resistance to strong acids and bases, soft and high-salinity water.

Table 35-1. Typical Properties of Some

Type or class	Name	Composition, per cent	Density, lb/cu in.	Melting point, °F	Thermal conductivity, Btu/(hr)(sq ft)/(°F)(ft)	Coefficient of thermal expansion per °F	Electrical resistivity (68°F), microhm-cm
	Naval brass Annealed Quarter-hard Half-hard	Cu 59.0–62.0, Sn 0.5–1.0, Zn bal	0.304	1630–1650	67	11.8×10^{-6}	6.6
65-12	Nickel silver, wrought Annealed Hard	Cu 65.0, Ni 12.0, Zn 23.0	0.314	1830–1900	23	9.0×10^{-6}	8
	Phosphor bronze, 8% (Grade C) Half-hard Spring	Cu 90.5 min, Sn 7.0–9.0, P 0.03–0.35	0.318	1620–1880	36	10.1×10^{-6}	13
	Common lead, soft Rolled Sand-cast	Pb 99.73+	0.41	621	19.6	16.3×10^{-6}	20.6
ASTM AZ61A-F	Magnesium alloy, wrought Extruded Forged	Al 2.5–3.5, Zn 0.6–1.4, Mn 0.20 min	0.065	950–1140	33.8	14×10^{-6}	12.5
AZ92A	Magnesium alloy, cast As cast Solution-treated Solution-treated and aged	Al 8.3–9.7, Zn 1.6–2.4, Mn 0.10 min	0.066	830–1100	26.6–33.8	14×10^{-6}	12.4 16.8 ....
Monel	Nickel alloy, wrought Annealed Spring	Ni 66, C 0.12, Mn 0.9, Fe 1.35, S 0.005, Si 0.15, Cu 31.5	0.315	2370–2460	15	7.8×10^{-6}	48.2
Monel	Nickel alloy, cast As cast	Ni 63, Cu 32, Fe 1.5, Si 1.6, Mn 0.75, C 0.15, S 0.015	0.312	2400–2450	15.5	9.0×10^{-6}	53.2
	Gold Annealed Cold-worked As cast	....	0.698	1945	172	7.9×10^{-6}	2.35
	Silver Annealed Cold-worked As cast	....	0.379	1761	242	10.9×10^{-6}	1.59
	Rhodium Annealed Cold-worked	....	0.447	3571	50	46×10^{-6}	4.5

Commonly Used Metals (*Continued*)

Mechanical properties					Fabricating properties				Corrosion resistance
						Weldability			
Modulus of elasticity in tension, psi	Tensile strength, 1,000 psi	Elongation (in 2 in.), %	Hardness (Brinell)	Shear strength, 1,000 psi	Machinability	Torch	Inert arc.	Electrical resistivity	
15×10^6	57 69 75	47 27 20	B 55ᵈ B 78ᵈ B 82ᵈ	40 43 44	30ᵉ	Good	.....	Fair	Good resistance to industrial rural and marine atmospheres; petroleum products; alcohols; dry gases and sea water; fairly good resistance to weak bases. Resistance to some weak bases and weak organic acids, but generally poor resistance to most acids and strong bases. Poor resistance to solutions of cyanides and ammonium compounds. Resistance to dezincification.
18×10^6	52–61 85	35–48 4	B 22–55ᵈ B 89ᵈ	41 52	20ᵉ	Good	Fair	Excellent	Attacked rapidly by oxidizing acids. Resistant to sodium and potassium hydroxide but attacked rapidly by ammonium hydroxide and moist ammonia. Good resistance to rural and marine atmospheres and to fresh and salt waters. Subject to stress corrosion.
16×10^6	76–105 112	32 3	B 84ᵈ B 98ᵈ	.....	20ᵉ	Good	.....	Excellent	Generally good resistance to atmosphere, water, salt water, and salt solutions. Some resistance to alkaline solutions and inorganic acids. Poor resistance to organic acids, cyanides, and ferric and ammonium compounds.
2×10^6	20.9 18	43 30	3.2–4.5	1820					Resistant to sulfuric, sulfurous, phosphoric, and chromic acids. Attacked by acetic, formic, and nitric acids. Resistant to atmosphere and fresh and salt water.
6.5×10^6	40–45 43	15–16 12	55–60 55	21 21	500ᵉ	G	A	A	High resistance to atmosphere.
6.5×10^6	24 40 40	2 10 2	65 63 83	19 20 21	500ᵉ	D	A	A	Good resistance to atmosphere and salt water.
26×10^6	70–85 100–140	50–35 15–2	B 68 maxᵈ B 98 minᵈ			Yes	Yes	Yes	Good resistance to flowing salt water, dilute acids, hydrochloric, hydrofluoric, sulfuric, phosphoric, and most organic acids and strong caustic soda. Not resistant to strongly oxidizing solutions such as nitric acid and ferric chloride.
23.0×10^6	65–90	20–50	125–150						
12×10^6	19 32 18	45 4 30	25 58 33			Yes		Yes	Does not oxidize when heated in air. Resists alkalis, salts, and most acids. Not attacked by oxygen or sulfur. Rapidly attacked by chlorine and bromine.
11×10^6	22 54 15	48 2.5 60	25–35 42					Yes	Does not oxidize when heated in air. Resists most dilute mineral acids and alkalis. Attacked rapidly by nitric and hot sulfuric acids. Attacked rapidly by sulfur-bearing gases.
42×10^6	73 300		55–156 260–390					Yes	Oxidizes slowly when heated in air. Resistant to most acids, including aqua regia at room temperature.

Table 35-1. Typical Properties of Some

Type or class	Name	Composition, per cent	Physical properties				
			Density, lb/cu in.	Melting point, °F	Thermal conductivity, Btu/(hr)(sq ft)/(°F)(ft)	Coefficient of thermal expansion per °F	Electrical resistivity (68°F), microhm-cm
	Grade A tin Annealed sheet Cold-rolled sheet As cast	Sn 99.8 min	0.264	449.4	37	13×10^{-6}	11.5
	Tin foil Cold-rolled sheet	Sn 32, Zn 8	......	390	34	......	12
Grade 8	Tin-lead-antimony Cast	Sn 5, Sb 15, Pb 80	0.361	522–459	14	13×10^{-6}	28.2
	Commercial rolled zinc Hot-rolled Cold-rolled	Pb 0.05–0.10, Cd 0.05–0.08, Zn bal	0.258	786	62.2	18.1×10^{-6}	6.06 6.10
Alloy XXV	Zinc alloy, cast Die-cast	Al 3.5–4.3, Cu 0.75–1.25, Mg 0.03–0.08, Zn bal	0.24	727	62.9	15.2×10^{-6}	6.54
	Tungsten, cold-worked	....	0.70	6152	96.6	2.2×10^{-6}	5.48[j]
	Molybdenum Annealed Cold-worked	....	0.37	4760	84.5	3.0×10^{-6}	5.17[j]
	Beryllium, annealed	....	0.067	2341	87	6.4×10^{-6}	5
Unalloyed	Titanium	Ti 99.0	0.163	3135	9.8	5.8×10^{-6}	55.0

NOTES.
[a] AISI B1112 Steel = 100.
[b] 1-in. round, water-quenched 1525°F, drawn at 1000°F.
[c] 1-in. round, normalized 1650°F, reheated to 1475°F.
[d] Rockwell hardness.
[e] Based on free-cutting brass = 100.
[f] 32°F.
[g] Difficult even with special tools and methods; grinding recommended.
[h] From powder.
[i] Like cast iron, but tool life is shorter.
[j] Warm-extruded and annealed at 1400°F. The mechanical properties of beryllium are greatly influenced by the method of fabrication.
[k] Difficult because of low ductility.

Commonly Used Metals (*Continued*)

Mechanical properties					Fabricating properties				Corrosion resistance
						Weldability			
Modulus of elasticity in tension, psi	Tensile strength, 1,000 psi	Elonga-tion (in 2 in.), %	Hardness (Brinell)	Shear strength, 1,000 psi	Machin-ability	Torch	Inert arc.	Elec-trical resis-tivity	
6–6.5×10^6	2.2 2.8 2.1	45 35 55	7 8 5–6	......	....	....	. ...	Yes	Resists distilled, sea, and soft tap water. Attacked by strong acids, alkalis, and acid salts. Oxygen in solution accelerates rate of attack.
....	8.7	6.0							
4.2×10^6	10	5	20	. . ...	. . ...	....	.....	... ..	Resistant to corrosion by the usual lubricants.
	21 25 22–29	52–30 40–30	43	. . .	Good	Poor	. . ...	Fair	Excellent resistance to both metropolitan and rural atmos-pheric corrosion, also hot soapy water, printing inks, trichloro-
									ethylene, carbon tetrachloride,
	47.6	7	91	38	Good	Poor	.... .	Fair	dry illuminating gas, and mois-ture- and acid-free hydrocar-bons. Fair resistance to pure ethyl and methyl alcohols, glycerine, water, and petroleum products. Poor resistance to steam, spray insecticides, ani-mal oils, strong acids, bases, and mixtures of glycerine or alcohol and water.
50×10^6	70–300	0	(* 37*d* –(* 47)	......	*g*	No	Yes	Yes	Resists most acids and alkalis to 212°F., attacked by nitric-hydrofluoric mixture at room temperature, by aqua regia at 212°F.
42×10^6	85–130*h* 120 175*h*	4.7*h* 1*h*	B 95*d,h* (* 22 27*d,h*)	. ....	*i*	No	Yes	Yes	Moderately resistant to acids and alkalis up to 212°F; at-tacked by nitric-hydrofluoric mixture at room temperature, by aqua regia at 212°F.
44×10^6	60–90*j*	2 5*j*	....	......	*k*	No	No	No	Resistant to air at room tem-perature; attacked by both oxygen and nitrogen at elevated temperature; resistance to sea water. Rate of attack in fresh water varies with air content.
15 15.5×10^6	89 100	15 22	(* 30*l*	. ....	......	Yes	Yes	Yes	Superior resistance to nitric acid, most chlorine, chlorine solutions, chlorinated organic compounds, and inorganic chlo-ride solutions. Excellent re-sistance to corrosive attack by sea water and most chloride salt solutions. Unchallenged by other structural metals. Resists impingement, pitting attack.

A D are arbitrary relative ratings in decreasing order of merit.

Table 35-2. Typical Properties of Some

Class	Name	Description	Physical properties		
			Specific gravity gm/cc	Coefficient of thermal expansion, per °F	Moisture absorption, %
Ceramics..............	Alsimag A-196	Magnesium silicate	2.6	8.6 × 10⁻⁶	0 to 0.02
	Alsimag 243	Magnesium silicate	2.8	11.2 × 10⁻⁶	0 to 0.02
	Alsimag 576-L5A	Cordierite	3.4	7.5 × 10⁻⁶	0 to 0.00
	Alumina	90% A10	3.6 (approx.)		
	Alumina	Sapphire	3.6 (approx.)		
	Alumina, Coors A1-200	Aluminum oxide	3.61		
	Boron-silicon-nitride McMillan 2-6	M.P. 2500°C	ca. 1.7		
	Steatite 228	Cordierite	2.7	8.0 × 10⁻⁶	0 to 0.02
	Steatite 410				
	Zircon	ZrSiO₄	ca. 3.7		
Epoxy laminates........	Araldite 6020		1.16		0.05
	Epon RN-48			1.7 × 10⁻⁵	0.6
Glasses...............	Corning 0120	Soda–potash–lead silicate	3.05	87 × 10⁻⁷	
	Corning 7060 (pyrex)	Soda–borosilicate		50 × 10⁻⁷	
	Corning 7070	Potash-lithia-borosilicate	2.13	31 × 10⁻⁷	
	Corning 7740	Borosilicate	2.23		
	Corning 7900	96% silicon dioxide	2.18	8 × 10⁻⁷	
	Corning 7911	96% silicon dioxide	2.18	8 × 10⁻⁷	
	Fused Silica 915C	Silicon dioxide			
	Quartz (fused)	100% silicon dioxide		5.7 × 10⁻⁷	
Low-density materials: Honeycomb or similar.	Glass fiber, 0.0065″ wall, ¼″ cell (a) E Vector ⊥ double cell walls (b) E Vector ∥ double cell walls (c) E Vector ⊥ sample McMillan isotropic core	40% AL	0.06　　　　　0.10		
Mineral..............	Emerson and Cuming, sodium silicate		0.38		
	Foamglass		0.71		
	Owens-Illinois, integrated wallastonite, same converted at 1,700°F		0.28		
	Pittsburgh-Corning, foamed silica		0.16		
Resin................	McMillan, polyurethane	13% AL	0.23		
		22% AL	0.23		
		30% AL	0.10		
	Silicon XR 544		0.17		
	NOPCO Lockfoam A-206				
	NOPCO Lockfoam A-210				0.9
	NOPCO Lockfoam A-216				0.8
	Emerson & Cuming Eccofoam S,	*bulk density* Sheet stock..... 3 lb/cu ft 25 lb/cu ft		(40 × 10⁻⁶ cm/cm/°C)	1.3 0.1
	Eccofoam S4	Sheet stock..... 2 lb/cu ft		(30 × 10⁻⁶ cm/cm/°C)	1.4
	Eccofoam FP	Foamed in place			
Mica................	Mycalex 400	Mica, glass			
	Supramica 500	Glass-synthetic fluor-phlogopite			
	Supramica 555	Mica, glass	4.13		

Commonly Used Dielectrics

| Mechanical properties | | | | Dielectric properties | | | | | |
| Impact strength, Ft-lb/in. | Tensile strength, 1,000 psi | Compression strength, 1,000 psi | Flexural strength, 1,000 psi | Temperature, °C | Frequency, mc | Dielectric constant | | Dissipation factor | |
						Dry	Soaked	Dry	Soaked
5.0	10	90	20		10,000	5.24		0.0026	
4.0	10	85	20		10,000	5.76		0.00085	
6.3	20	140	40		10,000	8.5		0.0023	
	27	280	50	Room	9,375	8.5		0.001	
				25	1.0	8.25		0.001	
				500	10,000	9.03		0.0021	
				70	5,000	4.8		0.04	
				25	10,000	9.65		0.0003	
4.0	10	90	20		10,000	5.95		0.0019	
				25	10,000	5.7		0.0022	
				800	5,000	7.0		0.005	
0.46	8.5	22	16	25	10,000	3.10		0.0263	
				25	10,000	2.91		0.0184	
				25	10,000	6 6		0.0063	
				25	10,000	4.8		0.0098	
				25	10,000	4.0		0.0021	
				25	10,000	4.52		0.0085	
				20	10,000	3.82		0.00094	
				25	10,000	3.82		0.0006	
				25	10,000	3.78		0.00017	
				25	10,000	3.78		0.0001	
				25	8,500	1.10			
				25	8,500	1.15			
				25	8,500	1.20			
				25	9,300	4.03		0.0146	
				25	8,500	1.65		0.005	
				25	9,300	1.14		0.025	
				250	8,500	1.41		0.001	
				25	8,500	1 15		0.002	
				25	9,300	2 4			
				25	9,300	4.5			
				25	9,300	3 6		0.008	
				25	8,500	1 18			
	0.19	0 15	5 6			1 12			
	0 39	0 40	14		9,375	1 08			
	0.66	0.80	23		9,375	1 31			
	55	65			10,000	1 04			
	1,100	1,200			10,000	1 47			
		50				1 04			
Same as Eccofoam S									
				25	10,000	7.12		0.0033	
				25	9,375	7.0			
				25	8,500	9.32		0.007	

Table 35-2. Typical Properties of Some

Class	Name	Description	Physical properties		
			Specific gravity gm/cc	Coefficient of thermal expansion, per °F	Moisture absorption, %
Neoprene............	Antistatic coating, Goodyear No. R-14-123-252 Erosion coating, Goodyear No. 1801C				
Phenolic resin........	CTL-91LD	ECC 181-114 glass laminate	1.87		
Polyester resin........	Laminac 4323	ECC 181-114 glass laminate	1.68		
	Paraplex P-43	ECC 181-112 Garan glass laminate	1.78		
	Paraplex P-43	Fiberglas material	1.75		
	Selectron 5003	ECC-181			
	Selectron 5065	ECC-181	1.99		
	Sunform A-1	ECC-181 } glass laminate	1.8		
	Stypol 16B	ECC-181	1.75		
	Stypol 25	ECC-181	1.79		
	Vibrin 135	ECC-181, Volan glass laminate	2.15		
	Vibrin 135	Borosilicate 181 Volan A fabric, glass laminate			
	Marco Resin MR-25C	Unsaturated polyester			
Silicone resin........	DC-2104	181, 80°F ½ hr 500°F	1.93		0.10
Silicone laminate......	30% DC 2106 250 Final cure	ECC-181 Heat-cleaned	1.93		0.1
Polyethylene.........	DuPont	Extruded	0.92		0.005-0.01
Polystyrene..........	Polystyrene		1.04–1.07	$0-8 \times 10^{5}$	0.05
	Rexolite 1422		1.045–1.050	$0 7.6 \times 10^{5}$	0.05
	Mylar		1.39	15×10^{5}	0.5
Polyvinyl chloride.....	Geon 2046	59% polyvinyl-chloride 30% dioctyl phosphate 6% stabilizer 5% filler			0.5
	Plasticell	Expanded polyvinyl-chloride			
	Polyvinyl chloride, W-174	65% Geon 101, 35% Paraplex G-25			
Teflon...............	Teflon	Polytetrafluoroethylene	2.1–2.3	5.5×10^{5}	0
	KEL-F Grade 300P25	Plasticized polychloro-trifluoroethylene			
	Teflon Laminate	ECC-112			
Woods..............	Balsawood				2-24
	Douglas fir	⊥ to grain	0.48–0.55		
	Mahogany	⊥ to grain	0.56–0.85		
	Yellow poplar	⊥ to grain	0.43		
Miscellaneous materials.	Soil, sandy, dry				
	Soil, loamy, dry		1.5		
	Ice	Pure distilled water	0.88–0.92		
	Snow	Freshly fallen snow	0.125		
	Snow	Hard-packed snow followed by light rain	0.5-0.6		
	Water	Distilled	1.0		

Commonly Used Dielectrics (*Continued*)

	Mechanical properties					Dielectric properties			
Impact strength, Ft-lb/in.	Tensile strength, 1,000 psi	Compression strength, 1,000 psi	Flexural strength, 1,000 psi	Temperature, °C	Frequency, mc	Dielectric constant Dry	Dielectric constant Soaked	Dissipation factor Dry	Dissipation factor Soaked
				23	8,500	13.31		0.031	
				23	8,500	2.99		0.35	
			62.5	70	16,100	5.25		0.006	
			39.8	−73.3	16,100	4.4		0.012	
			47.8	23	8,500	4.25	4.27	0.011	0.011
			89.2						
				23	8,500	4.21	4.15	0.023	0.016
				23	8,500	4.21	4.22	0.0115	0.012
				70	9,370	4.79		0.040	
				23	8,500	4.27	4.20	0.017	0.016
				23	8,500	4.11	4.31	0.018	0.030
				23	8,500	4.24	4.26	0.021	0.021
				24	9,600	4.16	4.39	0.006	0.008
				25	8,500	3.5		0.015	
				25		3.24		0.0072	
	53.9	23.8	41						
	31.1	6.3	15.5						
	53	23	41	20	8.6	4.35		0.0058	
				300	8.6	4.31		0.0063	
3.0	1.7		1.5	25	10,000	2.25		0.0004	
0.25–0 35	5 8	11.5 16	8·15	25	10,000	2.54		0.00043	
0.3–0.4	7·9	14–15	14·16	25	10,000	2.54		0.00048	
(60 Kg-cm)	17·25			25	1	2.98		0.016	
				23	10,000	2 83		0.0116	
				25	3,000	1.04		0.0055	
				25	100	3.00		0.0415	
2.5 4.0	1.5 3 0	0 7 1.8	1.6	22	10,000	2 08		0.00037	
				25	10,000	2 26		0.0093	
				23	8.5	2.97	3 00	0.0046	0.006
				26	10,000	1 2		0.00083	
	15.9			25	10,000	1 8		0.0200	
				25	10,000	1 7		0.021	
				25	10,000	1 42		0.020	
				25	3,000	2 55		0.0062	
				25	3,000	2 44		0.0011	
				12	3,000	3 20		0.0009	
				·20	3,000	1 20		0.0003	
				·6	3,000	1.50		0.0009	
				25	3,000	76 7		0.157	

given shaped reflector or feed unit, and at the same time provide a structure impervious to its environmental surroundings.

Sandwich construction, which consists of two or more thin laminates stabilized against buckling with a lightweight core, can be used in all three areas of antenna design: the antenna, the radome, and the mount system. It is possible to cut more than half to two-thirds of the weight from some present-day antenna systems with proper use of reinforced-plastic materials. The cost of special tooling has deterred its use in small-quantity production, but where extreme tolerances and light weight are the goal, its cost may be far outweighed by its repeatable accuracy. Table 35-2 gives data covering the typical mechanical and electrical properties of dielectrics in use today. Table 35-3 covers various techniques in radome construction, most of which are adaptable to antennas, feeds, or mount construction.

Table 35–3. Methods of Fabricating Radomes

Radome type	Method	Materials
Solid:		
Thin..................	Bag	Glass-cloth or nylon laminate
Half-wave.............	Bag or matched die	Glass cloth with heat-resistant resin
Type B...............	Bag, matched die, lathe-turned	Glass cloth with heat-resistant resin and pigments
"A" sandwich:		
Foam-in-place..........	Matched die	Glass-cloth laminate, polyurethane foam core
Honeycomb............	Bag	Glass-cloth laminate, glass-cloth phenolic-core cell walls
Preformed core........	Bag or press	Glass-cloth laminate, foam core
Multiple "A":		
Heat de-iced	Bag	Glass-cloth laminate, fluted-glass-cloth core
Broadband............	Matched die or bag	Foam or honeycomb core
Half-wave sandwich	Bag or matched die	Glass-cloth laminate, loaded foam with or without honeycomb partitions

It is now possible to fabricate a radome that meets the most rigid environmental specification and to tailor the sandwich to meet a complicated beam shape. The highly specialized techniques involved in the fabrication and testing of such a radome require exceptional quality control over skin and core material and very elaborate r-f pattern-measuring equipment (Ref. 6; see also Chap. 32).

Foamed-in-place materials (Table 35-2) offer a wide range of uses, for example, core material for sandwich-construction support and sealer for strip-line or printed-antenna circuitry. Specially loaded foams can be used in beam-forming lenses. One such system in wide use is the Luneberg lens. Where the power is not too great and a small loss can be tolerated, many of the previously sealed systems using gas or dry air can be designed to be filled with foam. The resulting unit will not be affected by the presence of moisture and will not break down at moderate vacuum. Most foams are limited in use to low-temperature systems (200 to 300°F); however, the recent developments in silicone foams[7] have brought the useful range to better than 700°F. A ceramic foam[8] is available in stock forms to be machined that can be used at temperatures in excess of 1200°F. Dissipative losses of the ceramic foam remain low at the elevated temperatures. Techniques for molding the ceramic foam are being perfected.

The high-speed missiles with their high surface and internal temperature have promoted the use of ceramics in radome design.   The use of some of these materials in some of the more conventional systems may be warranted.   The megawatt peak power and resulting high average power of many transmitters rule out all known dielectrics except ceramics.   Table 35-2 covers many materials in use today.   Materials can be tailored to fit special needs by a number of manufacturers.

Simple effective checks of loss and dielectric constant of any plastic or ceramic material can be made by resonant element techniques, one of which is described below.

Figure 35-2 shows a loosely coupled, full-wavelength, strip-line resonator.   The resonator strip is held in place by very thin dielectric supports, located at voltage nodes of the resonant section.
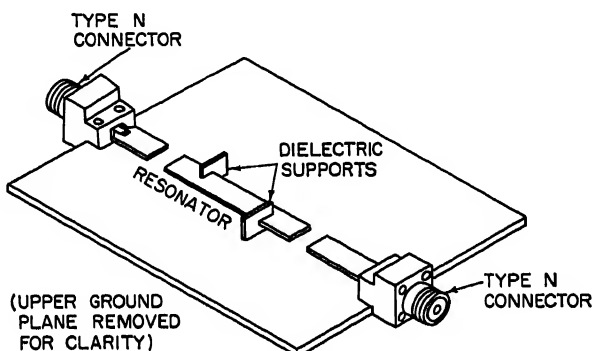
Fig. 35-2. Setup for checking dielectric constant.

The loaded Q, which is designated as Q_{Lo}, is determined by measuring the frequency of greatest transmission, F_0 and the 3-db bandwidth of the transmission response ΔF_0. The loaded Q is given by

$$Q_{Lo} = \frac{F_0}{\Delta F_0}$$

The insertion loss of the resonator is measured by direct substitution.   The transmission coefficient T_0 is calculated from

$$\text{Insertion loss (db)} = 10 \log T_0$$

The unloaded Q of the resonator, Q_{uo} is calculated from:

$$Q_{uo} = \frac{Q_{Lo}}{1 - \sqrt{T_0}}$$

The dielectric supports of the strip resonator are removed, and the prepared sheets of the dielectric material to be tested replace the original air dielectric, completely filling the space between the ground planes and the resonator strip.

The dielectric will reduce the velocity of propagation in the resonator, so that a new (and lower) resonator frequency, F_1, will result.

The dielectric constant of the material is expressed as ϵ and is computed from

$$\epsilon = \left(\frac{F_0}{F_1}\right)^2$$

The 3-db bandwidth of the dielectric-loaded resonator and the insertion loss can now be measured, and the new unloaded Q, Q_u, can be calculated.

The effective Q of the dielectric material will be expressed as Q_d and can be calculated from the expression

$$\frac{1}{Q_d} = \frac{1}{Q_u} - \frac{1}{Q_{u0}}$$

This reciprocal form of Q_d represents the power factor of the dielectric.

Special Products. The number of special products used as materials for antenna fabrication is formidable. The highly complex and imaginative nature of antennas seems capable of finding a place for almost any item the chemist or process engineer can dream up. The difficulty seems to be finding time to read the scores of trade journals, catalogues, laboratory reports, etc., in order to become acquainted with what is available. What has been included in the following paragraphs in no way covers the field, but it does indicate how necessary such a literature search is.
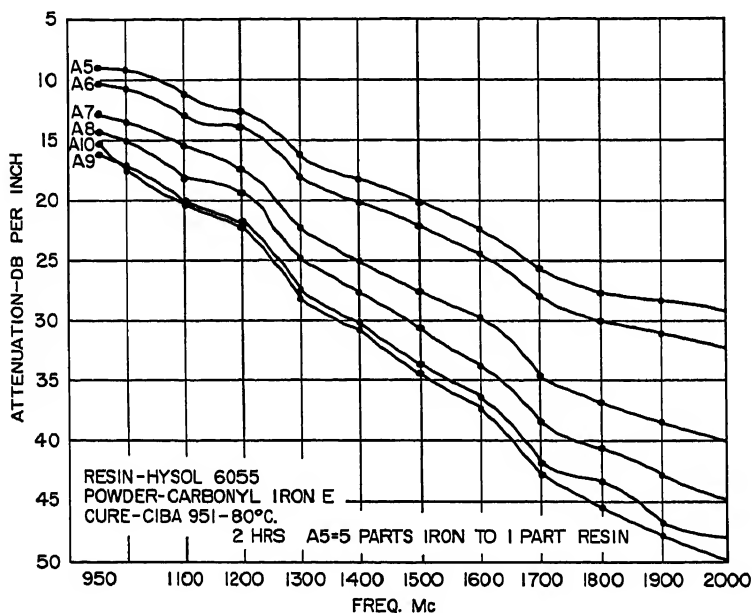
FIG. 35-3. Attenuation characteristics of some epoxy-iron mixtures.

Whole families of conductive paints[9], resistive coatings, and even conductive rubbers are available. Special load materials used in attenuators or terminations are supplied mixed or can be formulated on the job. Some of the resistive materials[10] brushed on to shaped forms provide matched terminations with an SWR of 1.02 or better. Molded or cast shapes can provide the same match and will operate as high-power loads at temperatures up to 800 to 900°F. Fig. 35-3 is based on special development work by Airborne Instruments Laboratory in the formulation of epoxy-iron materials. Referring to the figure, it can be seen that a number of combinations of epoxy-iron materials can be tailored to suit design needs.

There are many conductive paints, but they have been limited in usefulness because the carrier was soluble and easily washed away by thinners or plating solutions. Paints have recently been improved so that they are usable as cured or can be built up by plating without harm to the base coat. All types and shapes of plastics have been sensitized and successfully plated and used as part or whole of an antenna.

These paints have stood up under the most exacting environmental conditions and are accepted by the military services.

Conductive rubber has been greatly improved by Du Pont Fabrics Development, Fairfield, Connecticut. It can be obtained in sheet form or uncured stock to be molded in place by any fabricator. Its use in waveguide gaskets and equipment covers has been very successful in providing gas- and watertight seals as well as providing excellent r-f shielding. The base material is silicone and can be used in ambients above 500°F.

The elements have long played havoc with standard types of gaskets, including O rings. The silicone rubbers[11] are being used in practically every form of gasket in use today. The extreme temperature range of silicone (−70 to 500°F for standard stock and −130 to 500°F for special stocks) is one good reason for its popular use. There are potting, caulking, and sealing compounds of silicone base.[11] The difficulties of sealing radomes, covers, and cables have all been eased by the use of these materials.

35.3. FABRICATION TECHNIQUES

Before any serious thought can be given to a final design of an antenna, the environmental conditions under which it will operate must be known. The life expectancy may vary from a few minutes to many years. These conditions provide the basis for material choice as well as techniques in fabrication. Often, the final design must be a compromise between the desired electrical performance and some difficult structural problem due to environment. The designer may find it necessary to provide some form of radome protection for an antenna unable, by itself, to meet severe environmental conditions. While this Handbook is not greatly concerned with military specifications, some of these could well be used as design guides, where the environment is known to be difficult.

Another factor greatly affecting design as well as cost is the degree of dimensional tolerances and surface finish vs. frequency required in reflector construction (Fig. 35-4). The graph indicates that at about 25 kmc, the tolerances required are standard machine tolerances of ±0.005 in. Surface finishes become extremely important above 1 kmc, affecting both the Q and losses.

Antennas are highly complex structures involving a number of materials having widely different physical characteristics and temperature coefficients of expansion. The design must be integrated to counteract or remove forces caused by unequal expansion of materials.

Since much is known of the strictly conventional fabrication techniques, more detailed information will be given on nonconventional fabrication and assembly techniques. The required antenna size will, to some extent, limit some of the following techniques.

Casting Techniques. Special casting techniques now available can provide parts requiring little or no machining with a 60-microinch finish and better than ±0.005 in. tolerance on all dimensions. While it is true that some of these techniques require very special tooling and are expensive, a careful study of the process, machining, and assembly time of a fabricated part may indicate that the special casting may be cheaper in the end.

A common fault of designers is to require such tolerances over the entire casting, so that the cost of the pattern equipment is prohibitive. It is possible, with the help of a foundry engineer, to design a casting that will have all the advantages of a precision casting but will permit machining on some surfaces and, by so doing, cut the cost in half. Shell molding, french sand, frozen mercury, and various plaster techniques, of which the Antioch technique is the most interesting,[12] use carefully machined metal masters of core boxes or molds or both.

Shell molding, or "C" process, is accomplished by spreading a mixture of fine sand mixed with a plastic binder over the metal mold. The shell is about ¼ in. thick and is cured in an oven. The thin shells are stripped from the metal masters and mounted in cope and drag backed up by chilled steel shot or coarse sand. Very fine detail and dimensional accuracy are easily held. The porosity of the plastic shell permits the gases to escape and does not affect the surface finishes that are between 50 to 100 microinches.

The french-sand process is similar except that as a rule it is made up full thickness over the metal master and needs no other backing during processing. The mercury
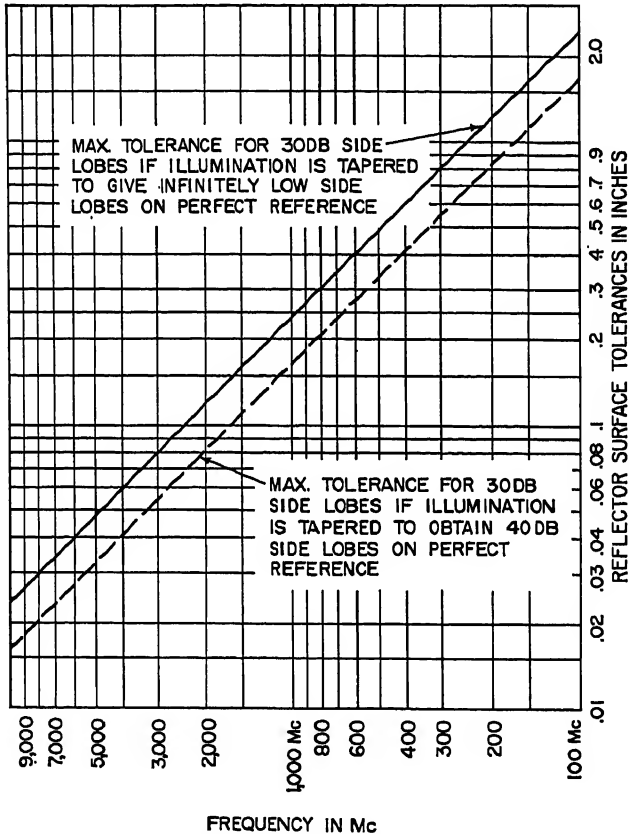
FREQUENCY IN Mc
FIG. 35-4. Reflector surface tolerances.

process permits the molding of fine detail in complicated cores with great accuracy. The Antioch process centers around a treatment of the green-plaster molds and cores that renders them microscopically porous. The high strength and stability of the molds have provided dimensional accuracies of ±0.040 in. over 80 in. and surface finishes of 60 to 80 microinches.

Machining. Machining, or the art of shaping materials by cutting, milling, turning, or drilling, is commonplace except as it applies to a few special metals or plastics. Carbide tools and cutters are a must for all reinforced plastics. Ceramics must be ground to shape.

Spinning and Stretching. Metal spinning is commonly used in antenna fabrication. Parabolic dishes and feed sections have been spun from aluminum or copper for many years. These same shapes can be spun from titanium and titanium alloys except that they require more power and must be sandwiched between two thin sheets of stainless steel. Stretch forming[2] is accomplished by gripping the edges of a sheet of metal, then drawing it down over a male die, stretching the metal to fit. Practically all metals in common use for antennas can be formed in this way.

Another useful process is hydroforming. The metal is placed over a female die and sealed. Oil under high pressure is instantly released above the metal, forcing
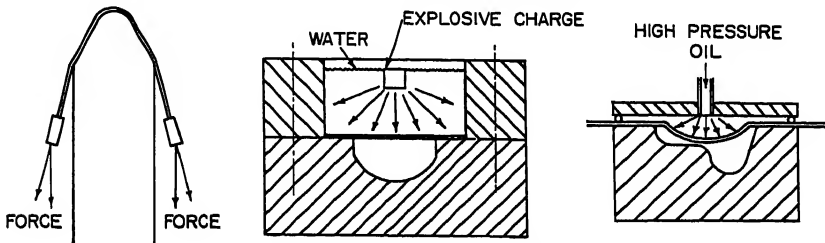
Fig. 35-5. Forming methods.
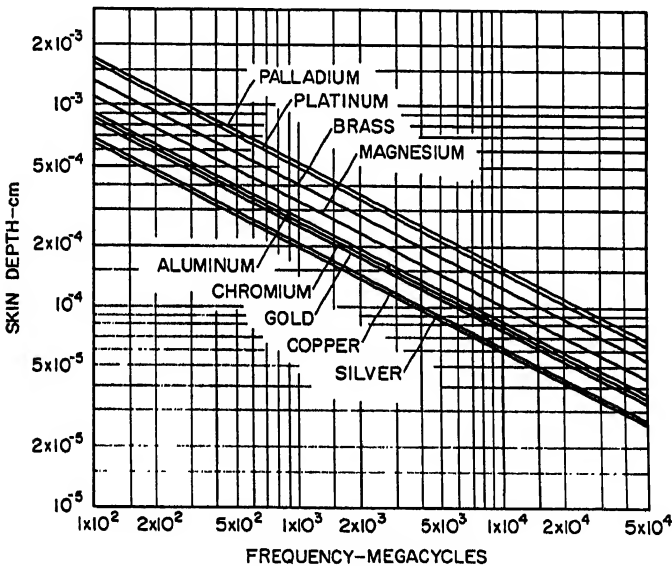
Fig. 35-6. Variation in skin depth with frequency for different metals.

it into the die. This method can be used for highly complex shapes and deep draws. Real deep draws are best done in two steps, with stress-relieving treatment between draws. Because only half of a die set has to be made, considerable savings can be realized.

A similar technique known as explosive forming[2,13] is used for some of the new very tough alloys. The blank is placed above the female die and locked in large metal rings. Using a plastic sheet, a container is formed for water, of considerable head, in contact with the blank. A carefully placed charge of explosive is set off. The tremendous pressure developed in the water forces the metal into the die. The

method will see a lot of use in forming large parts without the expense of big presses. A diagram showing some of the forming methods is given in Fig. 35-5.

Electroforming. The art of electroforming is extremely useful in duplicating complicated horns, feeds, and waveguide sections, because the duplicating accuracy of electroforming is greater than that of any other technique. Matrices can be cast

HORN ASSEMBLY

HIGH TEMP FOAM

FIBERGLASS OUTER SHELL

PRECISION ELECTRO- FORMED HORN AND PHASER
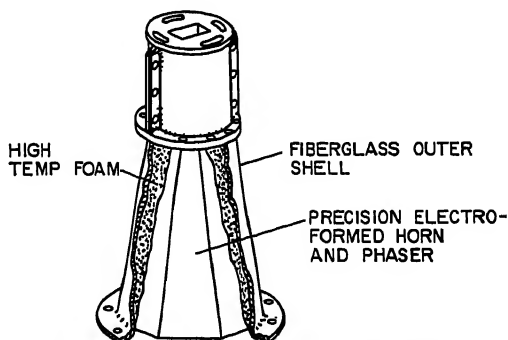
FIG. 35-7. Electroformed horn supported by fiberglass shell and foam.

SLOT TOLERANCES WITHIN ±.001

GRIND FLUSH

FINISH LINE (SURFACE A)

SOLUBLE MATRIX
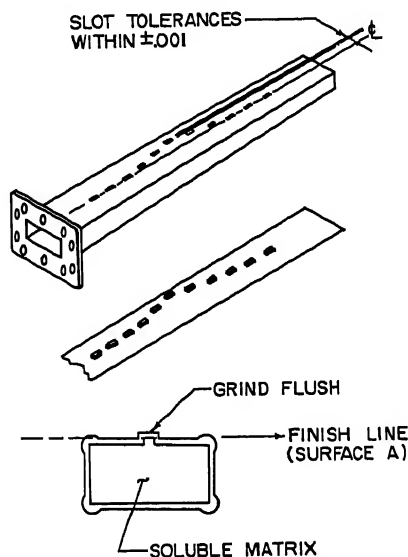
FIG. 35-8. Slot array produced by electroforming.

of low-melting alloys[14]; they can be machined out of expendable aluminum and dissolved out of the interior of the part; or they can consist of permanent stainless-steel mandrels which are usable many hundreds of times. The r-f current-carrying surface can be copper, silver, or gold. Laminates of these metals are frequently used to provide special properties such as reduced bulk, weight, corrosion resistance, electrical conductivity, and strength. The surface plating must be at least as thick as the skin

depth at the operating frequency (Fig. 35-6). A typical surface and back-up for 1,000 mc is 0.0002 in. silver plus 0.006 in. copper. At this point it can be backed up with copper or nickel deposited to any desired thickness.

The thin precision electroformed part can be molded into plastic or cast in one of the foams (Fig. 35-7). The composite structure will be lighter and more accurate than any other type of fabrication. A number of feed horns requiring an adjustable

WOOD MOCKUP
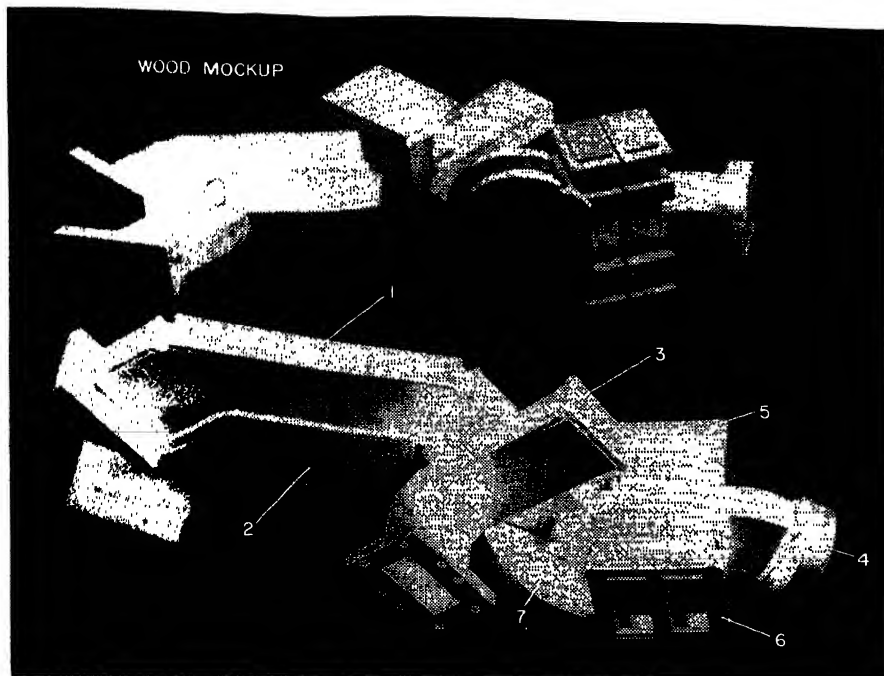
FIG. 35-9. Assembly by electroplating.
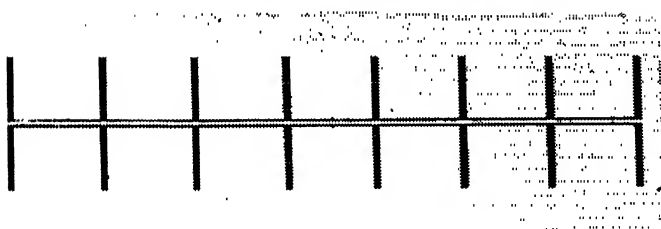
FIG. 35-10. Examples of photo-etched circuits.

phasing unit were built by this method. The phasing stubs were grown in place and were not adjustable. The accuracy of reproduction was such that correction adjustments were unnecessary.

An array of slots can be electroformed with extremely tight tolerances (Fig. 35-8). The part when set up and ground on surface *A* will produce a slot array that is cheaper to produce and more accurate than machining. Figure 35-9 is a complex assembly of electroformed sections grown together by plating. The wood mock-up was used by the platers to determine the techniques in the assembly of the part.

Etched Circuits. Etching of intricate arrays and feed systems on plastic-backed copper foil has been in wide use for some years. Improvements in the technique have been in materials and adhesives. Many of the early difficulties were caused by the poor peel strength of the copper foil to the base sheet and high dielectric constant of the plastic. With the advent of foil on Teflon sheet, printed feeds are now successful at X band and up. Briefly, the foil surfaces are photo-sensitized and direct-printed with extreme copy accuracy. The photo-sensitive area is subjected to light. The area subjected to light washes clean upon development, leaving the rest of the surfaces coated with an acid-resistant film that is ready for etching. There are two etching fluids in use today, ferric chloride and ammonium persulfate. The latter is the newest and cleanest to handle, but both are about even on a production basis as to speed of etching. Figure 35-10 shows an example of a strip feed and antenna made by this process.

35.4. FASTENING METHODS

The knowledge of how to fasten parts together is the most important factor in product design and the key to mass production. A screw is the most common fastener in use today and probably the most abused. Failure in screw fasteners can be traced to a number of conditions such as wrong type, unsatisfactory layout and number of screws, and improper prestress.[2,15] The choice of a screw fastener must be made on the basis of requirements of the job, backed up by sound engineering practices. Table 35-4 covers most of the standard machine screw sizes in use today. The data on torque and stress are included as a guide and must be modified whenever there are changes in the materials of the parts or the screws. A simple way of determining both torque and tension is to bolt a rigid joint close to the breaking point of the bolt. The degree of tightness can be determined by tightening a few bolts to their breaking point and then specifying the torque as 75 per cent of that loading. In a gasketed joint, the bolts can be tightened to a point that does not leak, and then the torque is specified as 10 per cent above that. No shop or laboratory should be without a good torque wrench and some means of checking it.

The riveted joint when compared with the screwed or bolted joints is by far the cheaper. Its versatility and simplicity are very well known. The need for a truly blind rivet in small complicated structures has been a stumbling block for many years. Now it is possible to choose from a number of types.

Another valuable type of rivet is the eyelet. Eyelets are available in all standard materials and sizes. Whenever shear and pressure tightness are not the prime consideration, the eyelet is simple and easy to use.

Welding. The antenna designer can use a diverse number of welding methods and techniques. It is therefore difficult to comment on any particular welding procedure. The properties chart (Table 35-1) contains information concerning the weldability of most metals considered in antenna construction. Each method has inherent difficulties, and where the design is particularly complicated, a great deal of consideration must be given to distortion due to welding. The preliminary design when reviewed by a good welder will save many headaches later on. The inert arc in the hands of a skilled welder can accomplish satisfactory welds and hold very tight tolerances. A great deal of consideration should be given to those tolerances that are important. To meet these tolerances, as great a deviation as possible in the less important dimensions should be permitted. With this knowledge the welder can design his tools and fixtures to ensure meeting the critical dimensions. It is possible, with good tooling, to hold ±0.010 in., and with better-than-average tooling, ±0.005 in.

Dip brazing of aluminum is accomplished by assembling in a holding fixture a number of carefully machined parts that have been fluxed and a preform of filler

Table 35-4. Machine Screws

Screw		Threads/in.		Clearance drill		Tap drill		Head Round Max OD	Head Round Max height	Head Flat Max OD	Head Socket Max OD	Head Socket Max height	Hex nut Across flat	Hex nut Across corner	Hex nut Thickness	Washer OD	Washer ID	Washer Thickness	Torque,* in.-lb Steel	Torque,* in.-lb Brass
No.	Diam.	Coarse	Fine	No.	Diam.	No.	Diam.													
0	0.060	...	80	52	0.064	56	0.047	0.113	0.053	0.119	......	......	0.156	0.171	0.046			0.046		
1	0.073	64	72	47	0.079	53	0.060	0.138	0.061	0.146	......	......	0.156	0.171	0.046					
2	0.086	56	64	42	0.094	50	0.070	0.162	0.070	0.172	0.140	0.086	0.187	0.205	0.082	¼	0.093	0.032	4.5	3
3	0.099	48	56	37	0.104	47 / 45	0.079 / 0.082	0.187	0.078	0.199	0.161	0.099	0.187	0.205	0.062	¼	0.105	0.020		
4	0.112	40	48	31	0.120	43 / 42	0.089 / 0.094	0.211	0.086	0.225	0.183	0.112	0.250	0.275	0.093	5⁄16	0.125	0.032	8	5.5
5	0.125	40	44	29	0.136	38 / 37	0.102 / 0.104	0.236	0.095	0.252	0.205	0.125	0.312	0.344	0.100	3⁄8	0.140	0.032		
6	0.138	32	40	27	0.144	36 / 33	0.107 / 0.113	0.260	0.103	0.279	0.220	0.138	0.312	0.344	0.100	5⁄16 / 3⁄8	0.166	0.026 / 0.046	15	10.5
8	0.164	32	36	18	0.170	29 / 29	0.136 / 0.136	0.309	0.119	0.332	0.270	0.164	0.344	0.373	0.125	3⁄8 / 7⁄16	0.186	0.032 / 0.046	30	21
10	0.190	24	32	9	0.196	25 / 21	0.150 / 0.159	0.359	0.136	0.385	5⁄16	0.190	0.375	0.413	0.125	7⁄16 / ½	0.218	0.036 / 0.063	53	37
12	0.216	24	28	2	0.221	16 / 14	0.177 / 0.182	0.408	0.152	0.438	11⁄32	0.216	0.437	0.488	0.156	½ / 9⁄16	0.250	0.063	70 / 80	49 / 56
¼	0.250	20	28	17⁄64	0.266	7 / 3	0.201 / 0.213	0.472	0.174	0.507	3⁄8	¼	0.437 / 0.500	0.488 / 0.577	0.203 / 0.250	9⁄16 / 5⁄8	0.281	0.040 / 0.063	99 / 133	
5⁄16	0.3125	18	24	P	0.323	F / I	0.257 / 0.272	0.562	0.246	0.625	7⁄16	5⁄16	0.593	0.686	0.297	7⁄8	0.375	0.083	215 / 270	

Table 35-4. Machine Screws (*Continued*)

Screw		Threads/in.		Clearance drill		Tap drill		Head						Hex nut			Washer			Torque,* in.-lb	
								Round		Flat	Socket head										
No.	Diam.	Coarse	Fine	No.	Diam.	No.	Diam.	Max OD	Max height	Max OD	Max OD	Max height		Across flat	Across corner	Thickness	OD	ID	Thickness	Steel	Brass
3⁄8	0.3750	16	24	W	0.386	5⁄16 Q	0.312 0.332	0.625	0.273	0.750	9⁄16	3⁄8		0.687	0.794	0.344	1	0.437	0.083	398 519	
7⁄16	0.4375	14	20	15⁄32	0.469	U 25⁄64	0.368 0.390	0.760	0.328	0.812	5⁄8	7⁄16		0.781	0.902	0.390	1¼	0.500	0.083	649 814	
1⁄2	0.5000	13	20	17⁄32	0.531	27⁄64 29⁄64	0.422 0.453	0.812	0.355	0.875	3⁄4	1⁄2		0.875	1.011	0.437	1⅜	0.562	0.109	1,004 1,290	
9⁄16	0.5625	12	18	19⁄32	0.594	31⁄64 33⁄64	0.484 0.516	0.937	0.410	1.000	13⁄16	9⁄16		0.968	1.110	0.484	1½	0.625	0.109	1,468 1,844	
5⁄8	0.6250	11	18	21⁄32	0.656	17⁄32 37⁄64	0.531 0.578	1.000	0.438	1.125	7⁄8	5⁄8		1.062	1.227	0.531	1¾	0.687	0.134	2,043 2,650	

* Approximate inch-pounds required to twist of screws at root diameter made of materials with tensile strength of 100,000 psi for steel, 70,000 for brass. To provide proper safety factor use two-thirds listed value for safe torque.

Table 35-5. Properties of Adhesives
Materials approved and in general use

Commercial designation	Source	Applicable specification	Application	Remarks
3M Adhesive EC-776	Minnesota Mining & Mfg.	3M Data Sheet EC-776	Bonds Nearly all materials include synthetic rubber, metal, glass, and plastics	General-purpose
3M Adhesive EC-870 or equivalent	QPL-5092	MIL-A-5092, Type 2	Bonds Rubber to metal Rubber to rubber Laminations	General-purpose
3M Adhesive EC-1022	Minnesota Mining & Mfg.	3M Data Sheet EC-1022	Bonds Steel, aluminum, vinyl, and rubber	Also phenolic to rubber
Adhesive Bondmaster M692	Rubber & Asbestos Co.	Bondmaster Data Sheet M692	Bonds Metal to metal Metal to phenolics Structural applications	(M692, formerly N92B) Bonds, transistors, and transformers to phenolics Gaskets to bases
Adhesive Bondmaster M693	Rubber & Asbestos Co.	Bondmaster Data Sheet M693	Bonds Metal to metal Metal to phenolics Structural applications	Bonds, transistors, and transformers to phenolics Gaskets to bases
Adhesive Bondmaster M688	Rubber & Asbestos Co.	Bondmaster Data Sheet M688	Bonds Metal to metal Metal to phenolics Structural applications	Bond transistors and transformers to phenolics Gaskets to bases
Adhesive Glyptal #1276	General Electric Co.		Bonds Metal, glass, rubber, and plastics	
Adhesive Acryloid B-7	Rohm & Haas Co.	Rohm & Haas Bulletin 7b	Bonds Plexiglass to metal Plexiglass to rubber	
Adhesive silicone rubber	QPL-25457	MIL-A-25457	Bonds Silicone Rubber to same Silicone rubber to aluminum	Air-curing
Adhesive Armstrong X-12	Armstrong Product Co.	Armstrong X-12	Bonds Aluminum to aluminum Steel to steel Polyester laminate to to same	Air-curing (color: amber)
Adhesive Armstrong C-7 + "W" Activator	Armstrong Product Co.	Armstrong C-7 + "W" Activator	Bonds Same as X-12 above	Same as X-12 except filler material omitted. Heat-cure preferred. Color clear
Sealer, synthetic rubber	QPL-8516	MIL-S-8516B	Sealing compound	For electrical connections and electrical systems
Sealer, DC-4 or equivalent	QPL-8660	MIL-I-8660	Insulating and sealing compound	Electrical (supersedes AN-C-128)
Impregnant, Pelron Resin 9403 or equivalent	QPL-6869	MIL-I-6869A	Porosity seal for aluminum and magnesium castings	
Compound, 3M Scotchcast 1A or equivalent	QPL-16923	MIL-I-16923B	Insulating compound imbedding	Electrical
Compound, Silastic RTV	Dow Corning Corp.	Dow Corning Data Sheet RTV	Sealing and potting compound	Electrical connectors and components

alloy that has been added in the area to be joined. The assembly is preheated to about 1000°F, then dipped into the salt bath at 1100°F for 15 to 30 sec. The brazed assembly is cooled to 200°F and washed in hot water. The unit can then be removed from the fixture and finished by anodizing or iriditing. Complicated assemblies with proper fixtures can be expected to hold tolerances of better than ±0.005 in. The technique is limited only by the size of the vendor's ovens and salt baths.

Oven brazing and soldering are similar to the previous techniques, except that the complete operation is accomplished in an oven. The oven can be fed an inert gas to prevent oxidation of some materials. The salt bath can be controlled to uniform temperatures of about ±2°C so that the melting point of the filler alloys can be within a few degrees of the melting point of the base materials. Even with excellent temperature control, this is difficult in an air- or gas-filled oven because of nonuniform heat transfer to the part to be brazed. To be safe, the melting point of the filler alloys is always substantially lower in the oven-brazing technique than in dip brazing. Again, the success of the brazing can be ensured when the preliminary design of the finished part is discussed with a reliable vendor and his recommendations are incorporated in the final design.

Bonding. High-strength adhesives have been developed for bonding metal, plastic, rubber, wood, and paper or combinations of these materials. Many times, this is accomplished at considerably lower cost and is compatible with other techniques of fastening. The uniform coating of adhesive in the bond area distributes the load and eliminates the local stress concentration found in other types of fasteners such as rivets, screws, staples, etc. Adhesives provide a complete seal against air or fluids and are in general resistant to salt spray, humidity, and a wide range of temperatures. The problem of joining lightweight metals less than 0.060 in. thick was almost impossible before the advent of adhesive bonding. Bonded thin sheets of aluminum develop their full tensile strength and seldom, if ever, fail in the bond even under fatigue. It is difficult to join dissimilar metals using standard metal fasteners. The very source of galvanic corrosion is prevented in a bonded joint since the adhesive separates the two metals. This separation in some ways limits or restricts the use of adhesives in areas where d-c or r-f paths over the surfaces are important. Antennas can be partially or wholly assembled with adhesives, provided care is taken to provide adequate r-f and d-c paths. Typical of some of the uses of adhesives are attachment of supporting structures to lightweight dishes and special waveguide components, positioning dielectric parts within coaxial or waveguide assemblies, and assembly of radomes to horns or slot arrays.

The selection of the proper adhesives for a particular bonding problem can be difficult. If no previous experience with adhesives is available, competent help should be obtained. All the reputable manufacturers maintain a staff of consultants or technical sales people backed up by a laboratory staff. They are prepared to assist in the choice of a particular adhesive to suit specific needs plus type testing to satisfy service requirements. The properties (Table 35-5) are very limited in scope and should be used only as a reference. The continued use of adhesive will in time familiarize and extend the scope of its application. Many of the difficult or impossible assembly operations can be made so simple with the proper adhesive that the saving in time and actual cost is almost unbelievable.

35.5. FINISHES

Exposed surfaces can be treated by chemical, electrochemical, and organic coatings to enhance their looks or extend their service life. The successful choice of a surface finish requires a thorough knowledge of the environment to which it will be exposed and the compatibility of the metal in assembly (Table 35-6). Practically all finishes

Table 35-6. Compatibility of Metals
COMPATIBLE COUPLES

GROUP NO.	METALLURGICAL CATEGORY	E.M.F (VOLT)	ANODIC INDEX (.01 VOLT)	COMPATIBLE COUPLES
1	Gold, solid, and plated; Gold-platinum alloys; Wrought platinum	+0.15	0	
2	Rhodium plated on silver-plated copper	+0.05	10	
3	Silver, solid or plated; High silver alloys	0	15	
4	Nickel, solid or plated; Monel metal, High nickel-copper alloys	−0.15	30	
5	Copper, solid or plated; low brasses or bronzes; Silver solder; German silver; High copper-nickel alloys; Nickel-Chromium alloys; Austenitic stainless steels	−0.20	35	
6	Commercial yellow brasses and bronzes	−0.25	40	
7	High brasses and bronzes; Naval brass; Muntz metal	−0.30	45	
8	18% chromium type corrosion-resistant steels	−0.35	50	
9	Chromium, plated; Tin, plated; 12% chromium type corrosion-resistant steels	−0.45	60	
10	Tin plate; Terne-plate; Tin-Lead solders	−0.50	65	
11	Lead, solid or plated; High lead alloys	−0.55	70	
12	Aluminum, wrought alloys of the Duralumin type	−0.60	75	
13	Iron, wrought, gray, or malleable; Plain carbon and low alloy steels; armco iron	−0.70	85	
14	Aluminum, wrought alloys other than Duralumin type; Aluminum, cast alloys of the silicon type	−0.75	90	
15	Aluminum, cast alloys other than silicon type; Cadmium, plated and chromated	−0.80	95	
16	Hot-dip-zinc plate; Galvanized steel	−1.05	120	
17	Zinc, wrought; Zinc-base die-casting alloys; Zinc, plated	−1.10	125	
18	Magnesium and magnesium-base alloys, cast or wrought	−1.60	175	

Note: O indicates the most cathodic member of the series, ● An anodic member, and the arrows the anodic direction.

NOTES: *Compatibility graphs.* Permissible-couple series are shown in Table 35-6 by the graphs at the right. Members of groups connected by lines will form permissible couples. O indicates the most cathodic member of each series; ● an anodic member; the arrow, the anodic direction.

Selection of compatible couples. Proper selection of metals in the design of equipment will result in fewer intermetallic contact problems. For example, for Type II exposure, neither silver nor tin requires protective finishes. However, since silver has an anodic index of 15 and tin 65, the emf generated as a couple is 0.50 volt, which is not allowable by Table 35-6. In this case, other metals or plates will be required. It should be noted that in intermetallic couples, the member with the higher anodic index is anodic to the member with the lower anodic index and will be susceptible to corrosion in the presence of an electrolytic medium. If the surface area of the cathodic part is significantly greater than that of the anodic part, the corrosive attack on the contact area of the anodic part may be greatly intensified. Therefore material selection for intermetallic contact parts should strive to make the smaller part the cathodic member of the couple.

in use today have been thoroughly tested under all environmental extremes; thus their characteristics under all conditions are well known. Failure of a surface treatment can usually be traced to the mismatch of the finish to either the environment or the material or both. There are a number of sources that are available to determine the climatic and service conditions of most geographical locations throughout the world.

In general, climatic elements include temperature extremes, humidity extremes, rain, hail, snow, sleet, salt-laden air, industrial atmospheres, direct solar radiation, dust, and the scouring action of wind-blown sand. An appraisal of the climatic condition under which the equipment must operate is of prime importance in terms of cost and reliability. The best antenna design is of little use when the equipment falls apart because it was improperly treated. To assist the engineer, most makers of raw materials have specified certain finishes for each alloy or type of alloy over a wide range of climatic conditions. However, information concerning finishes in regard to r-f transmission cannot easily be specified.

The following is an attempt to cover a few examples of this problem. Chemical treatments are either conductive or nonconductive. The conductive treatments, such as alodine or iridite, become basically poor when permitted to stay in the bath up to 5 min as specified by their manufacturers. Where good radio-frequency grounds between the treated parts are required, the length of the treatment must be limited to 1 min maximum. To ensure its being done, a special note must be added to the drawings. This also applies to the treatment of iridite 15 for magnesium, since the magnesium is so active that it may be necessary to reduce the time to 10 to 15 sec. It would be wise to run a few samples to obtain the correct timing when the contact resistance is critical.

Electroless-nickel treatment of metals is not new. However, until recently, there have been only a limited number of vendors that were equipped to handle this process. A number of years ago the process was not used since it was not reliable. The high quality of the chemically deposited nickel on aluminum has made it a desirable finish for feed systems and welded reflectors. The size of the welded reflectors was limited only by the size of the vendors' tanks. This treatment performed well under those climatic conditions of humidity and salt spray in accordance with military specifications.

A new plating technique for aluminum that is showing great promise is a hot tin dip. The assembly to be plated is dipped in a tin bath. The thin tin coating becomes the base for standard plating of copper, silver, gold, etc. Early samples showed no signs of deterioration even after full salt-spray and humidity tests. The problem of porosity in castings has been the cause of at least 75 per cent of the failures in plating. There is hope that this technique will work equally well for magnesium.

Organic coatings have become highly specialized, and surface preparation has become a carefully controlled part of the operation. Wet blasting a fine abrasive in some fluid carrier and a special chemical-etching bath provide a surface that is free of oil or grease and an excellent base for any paint. Special ovens with close temperature control bake the coating to a porcelainlike finish. The new finishes that are of special interest include two-part-cure epoxies and the special low-loss radome coating and silicones that meet most temperature extremes. The two-part epoxy coatings are simple to handle and apply, producing results that meet the environmental conditions as specified by military specification for Type 1 exposure.

Product evaluation is possibly the most important part of fabrication and assembly. Properly handled, it can be a source of valuable design criteria for future work, as well as guaranteeing the quality of a product. Testing laboratories will help to set up a test specification based on the environment within which the equipment will operate and conduct these tests in accordance with NEMA or military standards.

REFERENCES

1. Hampel, "Rare Metals Handbook," Reinhold Publishing Corp., New York.
2. "Metals Engineering—Design" and "Metals Engineering—Processes," ASME Handbooks, McGraw-Hill Book Company, Inc., New York, 1953 and 1958.
3. Beryllium Corporation, Reading, Pa.
4. "Alcoa Structural Handbook," Aluminum Company of America, Pittsburgh, Pa, 1959.
5. Encyclopedia Issue for 1960, *Modern Plastics*, Modern Plastics Publishing Co., New York.
6. "Techniques for Airborne Radome Design," Wright Air Development Center, TR 57-67, ASTIA AD 142001. (Classified.)
7. Foaming Resins, Ref. 7-511, Adhesives, Refs. 4-612 and 4-605b, Dow Corning Corp., Midland, Mich.
8. Emerson and Cuming, Inc., Canton, Mass.
9. Hysol 6280-6281, Houghton Laboratories, Inc., Olean, N.Y.
10. Aqua Dag, Acheson Colloids Co., Pt. Huron, Mich.
11. 1959 Guide to Silicones, Dow Corning Corp., Midland, Mich.
12. Antioch Process, Morris Bean and Company, Yellow Springs, Ohio.
13. Materials Selector, 1959-1960, Materials in Design Engineering, New York.
14. Low Melting Alloy, Cerro De Pasco Sales Corp., New York.
15. "Handbook of Fastening and Joining Metal Parts," McGraw-Hill Book Company, Inc., New York, 1956.
16. "Welding Alcoa Aluminum," Aluminum Company of America, Pittsburgh, Pa., 1956.
17. Kanogen Process, "Electro-less Nickel Process," General American Transportation, Chicago, Ill.
18. Hexcel Technical Brochure D, Hexcel Products, Inc., Oakland, Calif.
19. Garforming Brochure, Gar Precision Parts, Inc., Stamford, Conn.
20. "Dielectric Materials and Applications," edited by A. R. Von Hippel, John Wiley and Sons, Inc., New York, 1954.

INDEX